Northern Sierra Historical Range of Variability and Current Landscape Departure

Kevin McGarigal Becky Estes[1] Scott Conway Danielle Perrot
Marilyn Tierney Terri Walsh Christina Liang Laurie Perrot
Edward Smith

August, 2022

Abstract

This report describes modeling historical range of variability (HRV) and current departure for landscapes within the Northern Sierra ecoregion in California and Nevada. We discuss the need for this study with respect to the historical and contemporary context of the ecoregion, including background on the natural range of variability concept and the use of simulation modeling to quantify it. For several focal landscapes within the Northern Sierra ecoregion, we simulated wildfire disturbance and succession processes under historical reference period conditions (circa 1550-1850) at the 5 m spatial resolution. Based on the output, we quantified the mean Fire Return Interval (FRI) under historical dynamic equilibrium conditions and estimated departure of the contemporary fire interval from the historical FRI for each cell. We also quantified the FRI for high-mortality wildfire (i.e., complete overstory mortality) as a proxy for vegetation persistence under historical reference period conditions, in which short return intervals represented locations where early-seral vegetation would be expected to predominate over time and, conversely, in which long return intervals represented locations where late-seral vegetation would be expected to predominate over time. Lastly, we quantified the HRV in forest vegetation patterns and compared the results to the patterns present in the current landscape to quantify departure at three scales or levels: Sites, Geophysical Units (GPUs) and Subbasins.

We defined Sites as 40-m radius plots (1.25 acre) centered on each focal cell, which corresponds to the predominant ecological neighborhood of a single mature tree. We further classified each Site to one of four Biophysical Classes (BPCs) that discriminated Sites on the basis of simulated tree productivity (from low to high) under historical dynamic equilibrium conditions. We quantified HRV as the range of variation across Sites and over time under historical dynamic equilibrium conditions for three different vegetation metrics. We quantified the current range of variability (CRV) as the range of variation across Sites in the current landscape and compared it to HRV to estimate current departure for Sites in each BPC. We illustrate the use of the Site-level metrics to inform unit- and project-level planning and management, as well as their use for monitoring vegetation changes over time across the landscape.

We defined Geophysical Units (GPUs) as contiguous spatial units discriminated on the basis of relative homogeneity in 10 geophysical variables and averaging 50 acres in extent. We quantified HRV for each GPU independently for a suite of 11 vegetation composition and configuration metrics, and compared the current condition to HRV for each metric separately and in combination to estimate current departure for

1 Corresponding author. Becky Estes, USDA Forest Service, becky.estes@usda.gov

each GPU. We illustrate the use of the GPU-level metrics to identify and prioritize local areas for treatments designed to restore historical reference conditions, as well as their use in monitoring treatment implementation.

We defined Subbasins based on Hydrologic Unit Code (HUC) level 12 watersheds, which averaged approximately 15,000 acres in size. We further partitioned each Subbasin into BPCs. We quantified HRV for each Subbasin-by-BPC partition independently for a suite of 6 vegetation composition and configuration metrics, and compared the current condition to HRV for each metric separately and in combination to estimate current departure for each landscape partition. We illustrate the use of the Subbasin-level metrics to identify and prioritize broad areas for projects designed to restore historical reference conditions.

Keywords: range of variability; historical range of variability; natural range of variability; range of natural variability; current landscape departure; landscape disturbance-succession modeling; Landscape Disturbance Simulator; northern Sierra Nevada

Authors

- Kevin McGarigal is a landscape ecologist with Vibrant Planet, proprietor of LandEco Consulting and retired professor of landscape ecology at the University of Massachusetts, Amherst. He received a B.S. in Forestry and Wildlife from Virginia Tech, an M.S. in Wildlife Science from Oregon State University, and a Ph.D. in Forest Science from Oregon State University.
- Becky Estes is the Central Sierra Province Ecologist (Tahoe, Eldorado, Stanislaus, and Lake Tahoe Basin Management Unit), Pacific Southwest Region, USDA Forest Service. She received a Ph.D. in Forestry from Auburn University and is a Certified Ecologist with the Ecological Society of America.
- Scott Conway is the Chief Resilience Officer with Vibrant Planet and former forest ecologist with Pacific Southwest Region, USDA Forest Service Remote Sensing Lab and Truckee District Ranger, Tahoe National Forest, Pacific Southwest Region, USDA Forest Service. He received a B.S. in Natural Resources Management from Colorado State University.
- Danielle Perrot is an applied ecologist with Vibrant Planet. She received a B.S. in Environmental Science from University of California, Los Angeles and an M.A. in Geography with a Graduate Certificate in Hydrologic Sciences from University of Colorado, Boulder.
- Marilyn Tierney is retired District Biologist for the Yuba River Ranger District, Tahoe National Forest, Pacific Southwest Region, USDA Forest Service. She received a B.S. in Biology and an M.A. in Biology with an emphasis in Ecology and Systematics from San Francisco State University.
- Terri Walsh is retired silviculturist for the Tahoe National Forest, Pacific Southwest Region, USDA Forest Service. She is a certified silviculturist and studied Forestry at Cal Poly San Luis Obispo.
- Christina Liang is Forest Biologist for the Tahoe National Forest, Pacific Southwest Region, USDA Forest Service. She received a Ph.D. in Ecology from University of California, Davis.
- Laurie Perrot is Forest Environmental Coordinator for the Tahoe National Forest, Pacific Southwest Region, USDA Forest Service. She received a B.S. in forestry from the University of California, Berkeley.
- Edward Smith is Senior Forest Ecologist and Fire Manager for The Nature Conservancy in California. He received a B.A. in Biology from the University of California, San Diego and a M.S. in Forestry from Northern Arizona University.

Acknowledgments

We appreciate the comments and suggestions of the many participants at multiple workshops during which this project evolved. We especially appreciate the contributions of Dana Walsh and Roger Brown for their regular participation throughout the project and their contributions to the many decisions made along the way. We also thank the Tahoe National Forest staff and leadership for their support of this project. Eduard Ene served as a programmer and helped to develop the landscape disturbance-succession model used in this application.

Preface

This assessment replaces the earlier assessment published by McGarigal et al. (2018) for the Yuba River watershed. Specifically, the previous assessment was based on 30 m resolution input data and the Landscape Disturbance-Succession Model (LDSM), RMLands, was parameterized accordingly. This assessment was based on 5 m resolution data (essentially the scale of a single mature tree canopy), which led to an entirely different conceptualization and parameterization of a new LDSM (LDSim). In addition, the assessment of current departure (i.e., the deviation of the current landscape structure from its simulated HRV) in this report was based on more accurate and higher spatial resolution Lidar data, which led to a much improved assessment of current landscape departure. Lastly, the previous assessment was limited to the Yuba River watershed. Here, we expand our modeling to several focal landscapes within the Northern Sierra ecoregion, specifically those encompassing the Tahoe Central Sierra Initiative (TCSI) area of interest. Importantly, this document serves as the technical background for modeling all landscapes within the Northern Sierra ecoregion.

This General Technical Report (GTR) provides the necessary background material and detailed methods for modeling historical range of variability (HRV) and current departure for any of the focal landscapes within the northern Sierra ecoregion. Results for specific focal landscapes are included as separate appendices and cannot be understood completely or interpreted correctly without the background presented in this GTR.

Contents

Abstract . . . 1
Authors . . . 2
Acknowledgments . . . 3
Preface . . . 3

INTRODUCTION **8**
Purpose and need . . . 8
Why Natural Range of Variability? . . . 10
Why Historical Range of Variability? . . . 11
The Choice of Historical Reference Period . . . 12
Is HRV relevant today? . . . 13
Are there sufficient data for generating a reliable reconstruction of HRV? . . . 13
Is HRV practical for managing dynamic, especially non-equilibrium, systems in today's society? . . . 14
Alternatives to HRV . . . 14
Why Simulation Modeling? . . . 15
The Challenge of Scale . . . 15
Scope & Limitations . . . 16

PROJECT AREA **18**
Post Euro-American Settlement Land Use . . . 18
Vegetation . . . 19

LANDSCAPE DISTURBANCE-SUCCESSION MODEL **21**
Model Structure . . . 21
Succession . . . 22
Disturbance . . . 22

GEOSPATIAL DATA **23**

MODEL PARAMETERIZATION **27**
Wildfire Climate . . . 27
Wildfire Susceptibility . . . 29
Wildfire Initiation . . . 31
Wildfire Spread . . . 33
Wildfire Termination . . . 38
Wildfire Mortality . . . 39
Wildfire Disturbance Transitions . . . 44

Succession Climate . . . 44
Succession Transitions . . . 45
Shrublands . . . 45
Forests . . . 46

MODEL CALIBRATION **69**
Fire Rotation Period . . . 70
Fire Mortality Rate . . . 71
Fire Size Distribution . . . 71
Variability in Total Area Burned . . . 71
Relationship Between Total Area Burned and Climate . . . 72

MODEL EXECUTION **73**

HISTORICAL RANGE OF VARIABILITY and CURRENT DEPARTURE **74**
Scales of Analysis . . . 74
Biophysical Classes and Units . . . 75
Model Calibration Context . . . 78
Fire Return Interval and Departure . . . 79
Management applications . . . 82
Vegetation Persistence . . . 83
Management applications . . . 84
Site Level HRV and Departure . . . 85
Metric 1: Developmental Stage . . . 87
Metric 2: Tree Size . . . 90
Metric 3: Tree Cover . . . 93
Management Applications . . . 96
Geophysical Unit Level Departure . . . 98
Metric 1: Basal Area Departure . . . 102
Metric 2: Percent Open Forest . . . 102
Metric 3: Developmental Stage Diversity . . . 103
Metric 4: Coefficient of Variation in Open Patch Size . . . 104
Metric 5: Coefficient of Variation in Developmental Stage Patch Size . . . 104
Metric 6: Percent Large Trees . . . 105
Metric 7: Tree Size Class Diversity . . . 106
Metric 8: Coefficient of Variation in Large Tree Patch Size . . . 107
Metric 9: Coefficient of Variation in Tree Size Class Patch Size . . . 108
Metric 10: Coefficient of Variation in Quadratic Mean Diameter . . . 109

Metric 11: Coefficient of Variation in Percent Tree Cover . . . 110
Composite Departure Scores . . . 111
Management Applications . . . 113
Subbasin Level Departure . . . 119
Metric 1: Percent Large Forest Openings . . . 123
Metric 2: Large Forest Openings Patch Size Distribution . . . 124
Metric 3: Developmental Stage Patch Size Distribution . . . 125
Metric 4: Percent Large Trees . . . 126
Metric 5: Large Tree Patch Size Distribution . . . 127
Metric 6: Tree Size Class Patch Size Distribution . . . 128
Composite Departure Score . . . 129
Management Applications . . . 130

BIBLIOGRAPHY **135**

GLOSSARY of TERMS and ACRONYMS **142**

APPENDICES **144**
APPENDIX A . . . 144
Age . . . 145
Aspect . . . 148
Available Water Storage . . . 150
Biophysical Classes . . . 151
Buffer . . . 153
Cover . . . 154
Developmental Stage . . . 160
Elevation . . . 162
Energy Index . . . 164
Geophysical Units . . . 166
Growing Degree Days . . . 168
Heat Load Index . . . 170
Mesic Index . . . 171
Precipitation . . . 173
Site Index . . . 174
Slope . . . 175
Solar Radiation Index . . . 176
Streams . . . 178
Tau Index . . . 180

Topographic Position Index 182
Topographic Wetness Index 183
Tree Cover and Tree Cover Class 184
Tree Diameter 186
Tree Height 188
Tree Size (QMD) and Tree Size Class 190
Vegetation State 192
Vegetation State Age 194
Water Balance Deficit 197

APPENDIX B: Yuba River Landscape Historic Range of Variability 198
APPENDIX C: Truckee River Landscape Historic Range of Variability 276
APPENDIX D: Lake Tahoe Basin Management Unit Landscape Historic Range of Variability . . .347
APPENDIX E: Bear River Landscape Historic Range of Variability. 417
APPENDIX F: American North Fork River Landscape Historic Range of Variability 493
APPENDIX G: American South Fork River Landscape Historic Range of Variability 568

INTRODUCTION

The purpose and need for this assessment was described in detail in McGarigal et al. (2018), along with a discussion of the historical and contemporary context of the northern Sierra Nevada landscape, justification for the choice of historical reference period, background on the range of variability concept and the use of simulation modeling to quantify it, and the scope and major limitations of the assessment, with particular attention to the limitations of the simulation modeling. In this introduction, we repeat much of this material for completeness of this document. Importantly, this introduction provides the necessary conceptual background and context for this assessment and is prerequisite to understanding our choice of analytical methods.

Purpose and need

The Northern Sierra ecoregion (2.1 million hectares) in northern California (**Figure 1**) is a spatially and temporally dynamic mosaic of ecological systems. This dynamic stems from a complex natural and human land use history, much of which is driven by the interplay of disturbance regimes, especially fire, and vegetation succession, in which cycles of fire and vegetation recovery occur variably over large extents, as well as over long periods of time, and produce a constantly shifting mosaic of ecosystem conditions. Understanding this dynamic is essential to the management of this landscape.

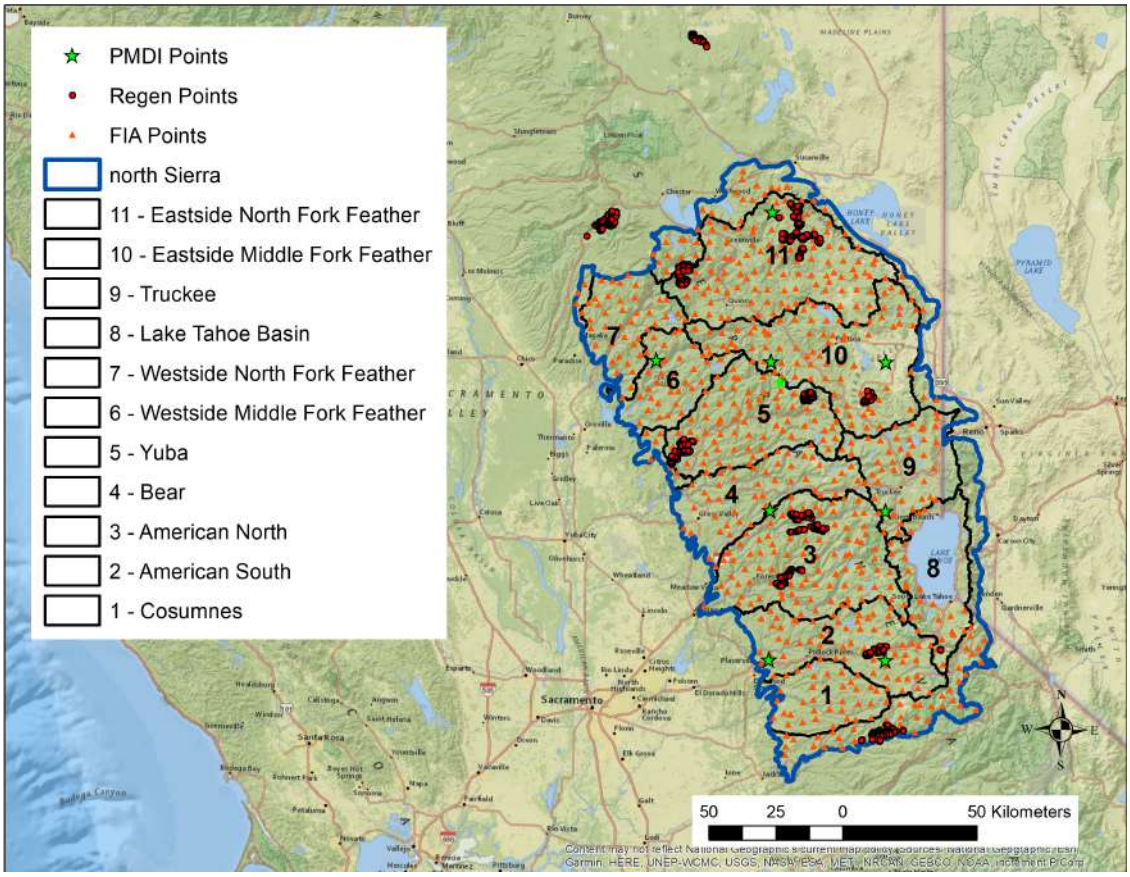

Figure 1: The Northern Sierra ecoregion (based on CalVeg Mapping zones) and the seven westside (1 - 7) and four eastside (8 - 11) landscapes (based on watersheds within the region) defined for the purpose of simulating wildfire disturbance and vegetation succession. Also depicted are the eight sample point locations for the Palmer Modified Drought Severity Index (PMDI Points) used to model historical climate

conditions, the 1,022 tree regeneration plot locations from the Shive et al. (2018) study on post-fire forest regeneration (Regen Points) used to model the probability of tree establishment following high mortality wildfire, and the 574 Forest Inventory and Analysis (FIA) plots used to model Site index and tree height growth.

It is generally believed that prior to Euro-American settlement in the mid-1800s the Sierra Nevada landscape had been shaped by a set of environmental conditions – including climate, topography, vegetation, and Native American management – that over thousands of years had led to high resilience to major ecological change (Van Wagtendonk and Fites-Kaufman 2006). Although climate is always changing, for approximately the last 4,000 years, the general outlines of modern Sierra Nevada ecosystems have been in place (Millar and Woolfenden 1999). Prior to Euro-American settlement, fire was the major source of disturbance in Sierran forests, shaping the composition and spatial configuration of vegetation communities (Safford and Stevens 2017). Fires were primarily lightning-caused, although indigenous peoples set fires for a variety of purposes, especially at lower elevations (Safford and Stevens 2017). Fires during this period were exceptionally frequent, resulting in an overall fire rotation period (i.e. the time it takes to burn an area equivalent to the total area under consideration, Agee 1993) of roughly 30 years, although fire rotation varied considerably among vegetation types in relation to moisture and elevation gradients (Mallek et al. 2013). In general, regardless of vegetation type, fires during the pre-settlement period are thought to have burned primarily at low intensities. High mortality ($>$ 75 % overstory canopy mortality) fire was relatively uncommon (Collins et al. 2007; Safford and Stevens 2017) and, when it did occur, it likely occurred as relatively small ($<$ 1 to several hectares) patches embedded within a mosaic of lower severity and unburned areas (Collins et al. 2007). When stand-replacing fire did occur, it initiated early-development conditions on the landscape. Most fires, however, were surface fires only removing understory fuels and tree regeneration. In some cases, moderate overstory mortality opened forest canopies without resetting stand development, especially in more xeric parts of the forest or areas of dense patches of trees (Mallek et al. 2013; Safford and Van de Water 2014; SNEP 1996a,b). Where fires did not recur frequently or only occurred at very low severity levels, succession processes such as infilling and overstory growth led to a gradual closing of the canopy. For most of the ecological communities, high-severity fire rates were low enough to allow most stands to succeed into late-development and old-growth conditions characterized by a variety of (mostly open) canopy structures (Mallek et al. 2013; Safford and Van de Water 2014; SNEP 1996a,b). Thus, it is generally believed that during the pre-settlement period the landscape was in a dynamic equilibrium — a relatively stable shifting mosaic of vegetation conditions — and highly resilient to permanent change (Hessburg et al. 2005; North et al. 2009).

Since Euro-American settlement, grazing, logging, mining, and fire exclusion have interacted to greatly and rapidly alter the historical fire regime and vegetation patterns (Knapp et al. 2013; Stephens et al. 2015). Heavy grazing in the late 19th and early 20th century altered fine fuels and likely reduced understory flammability (Hessburg et al. 2005). Widespread timber harvest in the past, especially of fire-tolerant species such as ponderosa pine (*Pinus ponderosa*) and sugar pine (*P. lambertiana*), accelerated the increased cover of fire-intolerant species such as white fir (*Abies concolor*) and incense cedar (*Calocedrus decurrens*) and selectively removed most of the late-seral forests (Hessburg et al. 2005; McKelvey et al. 1996; McKelvey and Johnston 1992). Timber harvesting continues today but the emphasis has switched from commercial timber production to fuels management. Hydraulic mining in the past had a long-lasting effect on fire through the local removal of both vegetation (i.e., fuels) and soils, which prevented or dramatically altered the potential for vegetation development after the cessation of mining (Storer and Usinger 1963). For oak woodlands, yellow pine and mixed conifer forest types, frequent fires (usually having low mortality) were historically common (Mallek et al. 2013; Safford and Van de Water 2014; Van de Water and Safford 2001). After large-scale fire exclusion in the second half of the 19th century, less fire-tolerant species such as white fir, incense cedar and Douglas fir (*Pseudotsuga menziesii*) have become more dominant in areas where they were once a minor part of the vegetation community (Beaty and Taylor 2007; Knapp et al. 2013; Safford and Stevens 2017; Stephens et al. 2015). In addition, fire exclusion has allowed the buildup of surface fuels and ladder fuels, which promotes larger and hotter fires when they do occur (Knapp 2015). Moreover, the lack of natural fires has increased the contiguity in fuel loading that allows fires to spread over very large areas under the right conditions (Beaty and Taylor 2007; Hessburg et al. 2005; Meyer et al. 2008). Thus, the current landscape is now dominated by fuel-rich, early- to mid-seral

stage, overstocked forests comprised disproportionately of less fire-tolerant species (Hessburg et al. 2005; Knapp et al. 2013; Stephens et al. 2015; Storer and Usinger 1963). Given the uncharacteristically high canopy cover, tree density, and continuity of abundant surface fuels, it is believed that the landscape has become less resilient to the occurrence of future fires and other disturbance agents and is especially susceptible to extensive and uncharacteristically severe fires (Beaty and Taylor 2007; Hessburg et al. 2005; Meyer et al. 2008).

Triggered by recent large and uncharacteristically severe wildfires within the region, land managers have determined that to better guide resiliency planning efforts it is prudent to gain a better understanding of the natural range of variability (NRV, a.k.a. range of natural variability, RNV) in vegetation composition and configuration. For example, the U.S. Forest Service, the largest public land manager in the region, pursuant to the 2012 Forest Planning Rule (36 CFR 219), has decided to develop a quantitative assessment of the NRV in landscape structure to serve as a reference against which to evaluate current landscape conditions and provide a framework for deriving potential desired future conditions and planning future management. The National Forests decided to use the historical (i.e., pre-Euro-American settlement) range of variability (HRV) as the measure of NRV because it offered the best reference for evaluating the current and future landscapes (Keane et al. 2009), and because the historical data were deemed sufficient to reliably characterize landscape conditions during the historical reference period.

In this context, it is important to understand that responsible land management is ultimately about planning and managing for desired conditions that are detailed, specific and quantitative in order to meet multiple goals and, often competing, objectives based on many ecological and socio-economic considerations. Natural Range of Variability (and thus HRV) is merely one of many factors that contribute to this endeavor. It is not the purpose of this assessment to suggest where and when NRV, or more specifically HRV, should be used, but rather to provide a detailed, specific and quantitative assessment of HRV and current departure across the entire landscape so it is available for use in establishing desired conditions. To this end, this assessment is based on the following specific objectives:

1. Synthesize empirical and expert knowledge on disturbance and succession processes characteristic of the pre-Euro-American settlement period in the Northern Sierra ecoregion.
2. Quantify HRV in landscape structure (i.e., vegetation land cover composition and configuration) in Northern Sierra landscapes using a landscape disturbance-succession model (LDSM).
3. Quantify current departure of Northern Sierra landscapes from their HRV at multiple spatial scales or levels.

Why Natural Range of Variability?

Since the late 1970s, ecologists have increasingly focused on community and ecosystem dynamics rather than static endpoints such as the climax. Disturbance and response to disturbance are now recognized as natural processes that lay at the core of ecosystem dynamics, a concept that plant ecologists have variously expressed as "patch dynamics" (Pickett and Thompson 1978), the "shifting mosaic" (Bormann and Liken 1979), and the "mosaic cycle" (Remmert 1991). This is more generally known as the "dynamic view", reflecting the increasing recognition that disturbances and other factors mitigate against ecological communities attaining a lasting constancy in species composition and structure. This dynamic view of ecosystems and landscapes has had a tremendous impact on land management. It is now universally accepted that ecosystems and landscapes are dynamic in space and time; that disturbance and succession processes interact to affect the range of variability in ecosystem structure, composition, and function.

- *Axiom 1: Ecological systems and landscapes are spatially and temporally dynamic* - The "dynamic view" of ecosystems and landscapes is the key ecological axiom underpinning NRV as a scientific and management framework. The primary implication for NRV is that variability rather than central tendencies is the appropriate way to characterize natural systems.

Although the notion of "natural" in ecological systems is equivocal (Sprugel 1991), many scientists and land managers believe that NRV can provide a useful framework for managing dynamic ecosystems/landscapes, especially as human activity is increasingly seen as the causal agent of large-scale environmental changes resulting in departure of the ecosystem/landscape from its "natural" range of variability. For our purposes, NRV can be defined as: "The ecological conditions, and the spatial and temporal variation in these conditions, that are relatively unaffected by people, within a period of time and geographical area appropriate to an expressed goal" (Landres et al. 1999). Management use of NRV concepts began in earnest out of a search for a legally defensible strategy for maintaining biological diversity and sustaining the viability of threatened and endangered species, pursuant to the requirements of laws such as the National Forest Management Act of 1976 and Endangered Species Act of 1973. Eventually, it was realized that incorporating ecological variability into management is key to maintaining ecosystem integrity because it: 1) ensures optimal biodiversity, 2) recognizes the roles of disturbance, 3) widens the options for management, and 4) maintains resilience. Consequently, the NRV concept gradually evolved and expanded into a general "coarse filter" strategy for sustaining ecological integrity and as a benchmark for evaluating the impacts of human activities on ecosystems and landscapes (Christensen et al. 1996). In fact, by 2000, the Forest Service Planning Rule explicitly called for the agency to estimate and describe the range of variability under natural disturbance regimes, and manage for those characteristics (36 CFR §219 2000). Decisions were to be grounded in the context of "maintain[ing] or restor[ing] ecological conditions that are similar to the biological and physical range of expected variability" (36 CFR §219.4). The need to consider the natural range of variability was maintained through various amendments to the Rule, and is prominent in the current 2012 Planning Rule (finalized in early 2015): "Plan decisions affecting ecosystem diversity must provide for maintenance or restoration of the characteristics of ecosystem composition and structure within the range of variability that would be expected to occur under natural disturbance regimes of the current climatic period" (36 CFR §219 2012). Consequently, NRV concepts guide most current land management activities on National Forests and other public lands.

Why Historical Range of Variability?

The NRV approach required a baseline or reference, and historical ecology appeared to provide the best reference, so HRV quickly became the standard for applying NRV concepts (Swetnam et al. 1999; Keane et al. 2009). Prerequisite to the use of HRV, however, is the ability to define a meaningful historical reference period during which human activities had relatively minor effects on overall landscape structure and function, and the ability to examine the range of variation in key landscape attributes during this period, which can then be used as a benchmark for comparison with contemporary or potential future conditions. Assuming the prerequisites can be met, HRV can be a useful tool for understanding and evaluating change and communicating the concept that landscapes are dynamic to the public. Moreover, a quantitative characterization of HRV can help determine whether the current landscape is "outside" its natural range of variability and provide detailed, specific and quantitative criteria for establishing desired future conditions that seek to emulate natural disturbance patterns. HRV can also help to develop hypotheses about the drivers and mechanisms of ecosystem change that can then be tested with spatial and temporal data, and the understanding obtained from these analyses can help predict how ecosystems might change in the future (i.e., future range of variability, FRV) in response to novel structures and processes (e.g., accelerated climate change)(Romme et al. 2012).

Perhaps the most important rationale for choosing HRV as the approach to NRV stems from one of the first laws of ecology: that the strength of ecological relationships weakens with distance in both space in time (e.g., Nekola and White 1999). In other words, the farther apart in space (and time) the more likely that the ecological patterns and processes will differ. The corollary in landscape ecology is that no two landscapes are alike (at any scale) and are in fact somewhat idiosyncratic due to the unique ecological setting of each landscape. This is also referred to as "non-stationarity"; i.e., that ecological patterns and processes vary over space (and time). Consequently, the best (and perhaps only) way to control for landscape idiosyncrasies is to compare a landscape only to itself by using historical snapshots of the landscape to characterize NRV, but this approach is not without its own challenges, as discussed below.

- *Axiom 2: Ecological similarity decreases with distance in space and time* - Increasing ecological dissimilarity between locations with increasing distance is the key ecological axiom underpinning the choice of HRV as the ideal approach to NRV. The primary implication for NRV is that temporal variability rather than spatial variability is the best way to account for landscape idiosyncrasies.

The Choice of Historical Reference Period

Despite the appeal of HRV, it too is not without some major challenges that should be addressed up front, the first of which is the choice of historical reference period. We defined the historical reference period as the 300 years prior to Euro-American settlement (circa 1550 - 1850). This is because our understanding of past climate and vegetation patterns becomes less clear as we move back in time, but 300 years is sufficient to capture notable variability (Meyer 2013a; Safford and Stevens 2017; Van de Water and Safford 2011). Because this reference period captures landscape changes over hundreds of years, far longer than the typical forest planning cycle, the HRV results allow managers to develop near-term plans and expectations within a broader temporal context. Indeed, in restoration planning efforts, it is logical to look back to the last known period during which a dynamic but resilient landscape existed. The arrival of Euro-American settlers in the Sierra Nevada led to sweeping ecological changes that now have greatly altered many Sierran landscapes through fire exclusion, grazing, road-building, timber cutting, recreation, and other activities (Storer and Usinger 1963; Stephens et al. 2015; Knapp et al. 2013; Hessburg et al. 2005). The period prior to Euro-American settlement, then, is a suitable reference condition against which we can compare current landscape structure and dynamics. Moreover, it is frequently used in the western United States as the historical reference period for restoration planning (Meyer 2013a; Safford and Stevens 2017; Van de Water and Safford 2011). This reference period is also several times the length of fire rotation periods identified for well-understood cover types within the region. Finally, it is a time frame for which we have sufficient information to reasonably calibrate the disturbance and succession model.

We are mindful of the fact that this reference period overlaps the "Little Ice Age" (circa 1300 - 1850), which may temper the utility of the results as specific management targets, but does not diminish their usefulness in other ways (Minnich 2007; Safford and Stevens 2017). The chosen reference period was not a time of stasis, climatically, ecologically, or culturally. The oscillation of the Palmer Drought Severity Index, a measure of climate variability in terms of precipitation and temperature, over time illustrates this (see Results). Although the Late Holocene was characterized by general cooling and gradual increases in precipitation, multi-year droughts and El Nino/La Nina events also occurred over this time frame (Minnich 2007). The "Medieval Warm Period" (circa 900 - 1300) was extremely dry and warm and is postulated to be climatic analogues to a warmer, drier future (Safford and Stevens 2017). Even though fire frequencies moderated during the Little Ice Age, frequencies were still much higher than today, permitting fire- and drought-tolerant species to dominate much of the landscape (Safford and Stevens 2017). Culturally, several Native American tribes were living in the region during the reference period. Debate continues among scientists and researchers as to the extent to which those peoples managed vegetation through setting fires (Anderson and Morrato 1996). Because we lack empirical evidence to distinguish between lightning-caused and human-caused fires during the reference period, we decided not to exclude any fire frequency or rotation data on the basis of not being reflective of "natural" conditions.

We emphasize that our choice of reference periods does not suggest that it should be our goal in management to recreate all of the ecological conditions and dynamics of this period. Such a goal may not be possible, nor potentially desirable in light of current climate change, ecological shifts, and social realities. However, the chosen reference period allows us to compare current conditions to a baseline set of data on ecosystem conditions (composition, configuration, and disturbance processes) to develop an idea of the level of departure of altered ecosystems from their "natural' state" (Safford and Stevens 2017). The results of this study complement the NRV assessments compiled by the Forest Service, U. S. Department of Agriculture, Pacific Southwest Region Ecology group for the Bioregional Assessment process necessary for forest planning (e.g., Safford and Stevens 2017; Merriam 2013; Meyer 2013a,b; Estes 2013a,b; Gross and Coppoletta 2013), and provides a basis for forest management policies and associated actions that seek to emulate natural disturbance patterns (Romme et al. 2000; Buse and Perera 2002).

Is HRV relevant today?

Perhaps the most common criticism of HRV involves questioning the relevance of using the past to guide management today and in the future given the following:

- Native and contemporary people have so altered natural systems that there are no pristine natural areas left on our planet, making information derived from the past difficult to interpret or irrelevant.
- Each point in time and space is unique, and dominant climate patterns are continually changing, therefore a description of past patterns and processes may be largely irrelevant today or in the future.
- Management goals based on HRV may seek to recreate past environments and then maintain those environments in a static condition.

We submit that the use of HRV does not require pristine conditions during the reference period, nor does it suggest that it should be our goal in management to recreate all of the ecological conditions and dynamics of the historical reference period. Complete achievement of such a goal would be impractical in many cases given the current and future ecological, socio-cultural, economic and political climate. In general, understanding past conditions and the natural processes that influenced those conditions, regardless of the level of human impact, yields insight into why and how current conditions developed, and what changes might be expected in the future. In addition, the use of HRV is not necessarily an attempt to simply mimic or recreate the processes that occurred on a site long ago, or to return managed landscapes to a single and unchanging past condition. Rather, it is an attempt to improve understanding about the ecological context of an area and the landscape-scale effects of disturbance in an effort to make existing and future conditions more ecologically sustainable.

Are there sufficient data for generating a reliable reconstruction of HRV?

Another common criticism of HRV revolves around generating enough reliable data and understanding to model historical conditions given the following:

- Site-specific data may be lacking, requiring extrapolation from other areas and a great deal of expert opinion to fill the knowledge gaps.
- There may be insufficient temporal depth of data, precluding a reconstruction of historical conditions for a sufficiently long reference period, and the estimates derived from paleo-reconstructions become more uncertain further back in time for several reasons, making the analysis of long-term trends difficult.
- The spatial configuration and severity of disturbances may not be identified with confidence from historical data, resulting in a general lack of information about the spatial variation of past conditions.

Our understanding of spatial and temporal dynamics in ecological systems will never be complete and will always be based on imperfect data. Consequently, in applying HRV concepts, multiple sources of information are needed, ranging from site-specific data and simulation models, to expert opinions and judgments. These disparate types of information allow for the forming and testing of hypotheses about how HRV concepts can best be applied to managing ecological systems. Of course, HRV results must be interpreted within the scope and limitations of the information sources, but the ultimate issue is whether we are able to make more informed decisions with or without an HRV based on the incomplete and imperfect data.

Is HRV practical for managing dynamic, especially non-equilibrium, systems in today's society?

Another criticism of HRV involves the practicality of using NRV in general to manage dynamic systems given the following:

- Management systems are not geared for managing moving targets or coping with the uncertainty and surprise that are inherent and fundamental aspects of dynamic ecological systems. Consequently, managing dynamic systems will always be difficult and fraught with surprises.
- Even in those cases where there is sufficient ecological understanding of how to manage the processes that drive dynamic systems, there may be insufficient social or political will to maintain or restore these processes given people's unwillingness to accept high uncertainty in the protection of life and property.
- Even if there is sufficient ecological understanding and socio-political will to manage for variability, how does HRV derived under dynamic equilibrium conditions help us manage future landscapes under non-equilibrium conditions being driven by rapidly changing climate and human land use?

HRV is not a panacea for dealing with uncertainty and surprises, but nor is there any other approach that will eliminate the uncertainties and surprises that are inherent to all dynamic systems. HRV merely helps to understand and communicate these uncertainties as "normal" behavior of the system. Moreover, using the concept of HRV to communicate and contextualize planned forest management to the public can help them to understand and expect the changes brought about by disturbance events and to view them as important and integral to the resiliency of the system. Lastly, despite the possibility of novel and non-equilibrium conditions in the future, characterizing HRV can nonetheless help determine when those future conditions might be forcing the system to operate outside its natural range of variability. This knowledge can help to build expectations for different future outcomes and/or serve as a "call to arms" for proactive management to promote greater resiliency.

Alternatives to HRV

It should be noted that although HRV generally has become the preferred reference framework for NRV, there are alternative frameworks that have received some attention, briefly as follows:

- *Historical Snapshot* — In this approach, a single historical snapshot of the focal landscape is used to establish NRV. Briefly, vegetation patterns based on evidences remaining in the contemporary landscape (e.g., stumps and logs) are used to "recreate" the conditions that occurred during this previous point in time (typically, just prior to Euro-American settlement), and the NRV is inferred by quantifying the variation across space at that point in time. This approach has been used frequently in the arid southwestern U.S. where dry conditions favor the preservation of stumps and logs for long periods of time (e.g., Abella and Denton 2009; Rodman et al. 2017; Sanchez Meador et al. 2009). The primary advantage of this approach is that the historical conditions are site-specific and thus accurately reflect the site-specific idiosyncrasies that determine realized vegetation patterns; i.e. there is no need to extrapolate findings from other locations with different site-specific conditions. The primary limitations of this approach are that it is only feasible where historical vegetation evidences are preserved (e.g., in arid regions), is limited to the few vegetation attributes represented in the evidences (e.g., stem density and spacing), and represents NRV based on a single snapshot in time using "space for time" substitution (i.e., assuming the variation across space is representative of the variation across time at a single location). Because of these limitations, this framework has not received widespread attention outside of the southwestern U.S. Nevertheless, the use of historical evidences in the contemporary landscape, such as fire scars in low- and mixed-severity fire regimes, is widely used to supplement other approaches.

- *Contemporary Reference Landscape/Sites* — In this approach, a reference landscape, or a suite of reference sites, deemed to reflect the NRV of the focal landscape is used to characterize NRV (e.g., Jeronimo et al. 2019). In this approach, as in the historical snapshot approach, "space" is substituted for "time" under the assumption that the contemporary range of variation across space adequately represents the expected variation across time in one location. Not surprisingly, there are pros and cons to this approach as well. The most important advantage of this approach is the ability to quantify detailed and specific attributes of the vegetation with relative accuracy and precision, since the entire assessment is based on empirical data derived from the current landscape. This often allows for the quantitative characterization of detailed vegetation composition and structure attributes such as stem density and basal area, which are of obvious interest to forest management. Another advantage of this approach is that it does not require the acquisition of historical data and understanding sufficient to parameterize and calibrate an LDSM. The most important limitations of this approach are the assumption that "space" is a reliable substitute for "time" given the idiosyncrasies of ecological patterns and processes across space (Axiom 2) and that a single snapshot in time (i.e., the current landscape), despite the variation across space, is an adequate representation of the full temporal range of variation given the dynamic view of ecosystems and landscapes. An equally important practical limitation is the difficulty in finding sites that are sufficiently free of anthropogenic influences to deem them suitable "reference" sites, and the nearly impossible task in most locations of finding a suitable reference "landscape" at the scale of the focal landscape. Despite these limitations, this approach has received considerable attention in the Northern Sierra and elsewhere (Jeronimo et al. 2017).

Why Simulation Modeling?

Natural range of variability analyses have been conducted by using literature searches exclusively, including within the Sierra Nevada (e.g., Safford and Stevens 2017). Results of such analyses depend on the assumption that an aggregation of many small studies is sufficient to address long-term, broad-scale questions, and require researchers to accept many unknowns about research methodologies. Moreover, in landscapes severely impacted by European settlement, such as those of the northern Sierra Nevada, we can never observe trajectories in which fire suppression is not part of the equation (Keane 2012). In the absence of consistent and complete data, simulations can be used to incorporate the data that do exist and generate new datasets of otherwise unobservable landscape trajectories (Swetnam et al. 1999; Mladenoff and Baker 1999; Keane et al. 2009). From these new datasets, statistical analyses can be used to describe the landscape quantitatively and subsequently make inferences about the HRV of an area, as well as compare current conditions to the HRV. Within the western US, the Rocky Mountains and Oregon Coast Range in particular have been the focus of several simulated HRV studies, while only one has been conducted in the Sierra Nevada that we are aware of, which took place in Sequoia National Park in the southern Sierra (Miller and Urban 1999).

Models for simulating HRV (and NRV in general), as well as future range of variability (FRV), have proliferated since the early 1990's. By 2004, some 45 LDSMs alone had been developed (Keane et al. 2004). Many of these, such as SAFE-FORESTS (Sessions et al. 1997), LANDIS (He and Mladeno 1999), ZELIG-L (Miller and Urban 1999), BFOLDS (Perera et al. 2003), SIMPPLLE (Chew et al. 2004), LANDSUM (Keane 2012), and RMLands (McGarigal and Romme 2005; McGarigal and Romme 2012) are still in use today. LDSMs are used to create spatially-explicit simulations of both of these key forest processes, typically outputting a set of GIS layers for each timestep of the model that can then be analyzed to quantify trajectories and patterns in the disturbance regime and vegetation over time (Keane et al. 2004; Gustafson et al. 2010).

The Challenge of Scale

One of the principal axioms of landscape ecology is that patterns and processes are scale-dependent. In other words, the measured variability in any ecological attribute is a function of the scale (in both space

and time) at which it is measured. For example, the temporal range of variability in landscape composition (e.g., the proportion of the landscape in each vegetation seral stage) decreases with increasing landscape extent. This happens because, all other things being equal, larger areas are able to buffer smaller disturbance effects. Thus, at the scale of a single forest stand, the range of variability in the proportion of the stand in an early seral stage will often vary from 0 to 1 because the scale of a single disturbance event may exceed that of a single stand. However, as the landscape extent increases beyond the scale of single disturbance events, the proportion of the landscape in an early seral stage will likely be considerably less, because while some areas may be recently disturbed, other areas will likely be in a state of recovery, and the two will balance each other out to some degree thereby dampening the variability over time. Indeed, if the landscape extent becomes large enough there may be little or no variability over time observed. In this respect, there is no single "right" scale for characterizing NRV (or HRV), since each scale uniquely characterizes variability at that scale. The challenge then becomes choosing a set of scales that capture the most relevant ecological patterns and processes and that are relevant to land management.

- *Axiom 3: Ecological variability is scale-dependent* - The dependence of measured ecological variability on the scale of the system is axiomatic. The key implication for NRV/HRV is that all range of variability and departure estimates are scale-dependent, and thus the choice of scale(s) or level(s) must be clearly justified on both ecological and anthropogenic grounds, and begs for a multi-scale/level approach to NRV/HRV.

Scope & Limitations

Because this project relies on the use of computer models, is is paramount to understand the scope and limitations of the modeling up front.

- We use a phenomenological modeling approach; therefore, we limit our simulations of wildfire disturbance to reflect the historical and modern fire record. This contrasts with a "mechanistic" modeling approach that tries to simulate the actual physical, chemical or biological mechanism of the process, such that the outcomes are emergent properties of the mechanism governing the process (Gustafson et al. 2013). Of course, there are advantages and disadvantages to both approaches. The major advantage of the phenomenological approach is that it does not require a complete understanding of the mechanisms associated with the processes, requires far fewer model parameters, and can be more easily parameterized to reflect the limited observations of real-world behavior (that are more often statistical rather than mechanical). The major disadvantage is that the algorithms can be somewhat arbitrary, and thus may not have an intuitive ecological interpretation or can be viewed as somewhat of a "black box". The major advantage of the mechanistic approach is that, if the mechanisms are well understood and parameterized correctly, it allows for the projection of landscape changes under novel environmental conditions (e.g., future climate) for which we have no observational data. However, if the mechanics are poorly understood or parameterized incorrectly, the projections will be inaccurate and can be grossly misleading. Because we use a phenomenological modeling approach, we limited our simulations of wildfire disturbance to reflect the historical and modern fire record. In particular, we do not project wildfire disturbance under future climate conditions.
- Model results should be viewed as "fuzzy" estimates, not as exact answers. While models have many uses and advantages over strictly empirical studies, they are fundamentally abstract and simplified representations of reality. This is especially true for LDSMs. The processes that drive real landscapes to change are far too many and complex to model comprehensively and accurately. Therefore, our goal in modeling these systems is to capture the most important drivers well enough that our results, in a very general sense, reflect our real world expectations. Although it is tempting to view the results as exact, given their quantitative nature and apparent numerical precision, we should strongly resist over-interpreting them. Moreover, because the results may not be accurate in an absolute sense, they may nonetheless be reliable in a relative sense, especially when the focus is on

comparisons. Specifically, whereas the absolute predictions may not be accurate, if the processes are parameterized and calibrated well, and implemented consistently in the model, then the relative results may still be reliable, especially when used to compare among scenarios. For example, in the context of this application, the estimate of absolute departure for a unit of ground may not be accurate, but the relative degree of departure of one unit compared to another may be quite reliable.

- As long as the model gets it right most of the time, it still can have great utility. The results of our model, as with any model, are constrained by the quality of input data, which are not perfect. For example, the vegetation cover layer is subject to human interpretation errors and objective classification errors, and is further limited by the spatial resolution of the grid. Consequently, there will be places where the model gets it wrong, not necessarily because the model itself is wrong, but rather because the input data are wrong. Getting it wrong in some places, however, should not undermine the utility of the results as a whole. In the end, the results should be used and interpreted with the appropriate degree of caution and an appreciation for the limits of the available data.
- Model results are subject to change as new scientific understanding or better data become available. The LDSM we used here (LDSim), like all landscape disturbance-succession models, requires substantial parameterization before it can be applied to a particular landscape. To the extent possible, we utilize local empirical data. However, we also draw on relevant scientific studies, often from other geographic locations, and rely heavily on expert opinion when scientific studies and local empirical data are not available. Despite our best efforts to incorporate the most relevant data and scientific findings, it is clear that we have a very limited understanding of the disturbance and succession processes being modeled. This does not undermine the utility of the results. The key question is whether the results lead to more informed and thus better decisions. Moreover, the model should lead to new insights that might at first seem counter-intuitive or inconsistent with our limited observations, because the model is able to integrate a large amount of data over broad spatial scales and long time frames in a consistent manner and thus provide a perspective not easily obtained via direct observation.
- Model results reflect landscape dynamics as driven by the selected succession and disturbance processes — in our case, wildfire. In this application, the results do not reflect the influence of other disturbance processes (e.g., insects and pathogens, wind-throw, ungulate and beaver herbivory, avalanches, and other forms of soil movement, etc.) or all of the complex interactions among them that characterize real landscapes and drive the full range of variability. Other kinds of natural disturbances also occur in the region, as noted above, but the impacts of these other natural disturbances tend to be localized in time or space and have far less impact on vegetation patterns over broad spatial and temporal scales than does fire. Thus, while the model is incomplete in the strict sense, it can still provide useful results because it reflects the dominant landscape change process.
- Model results pertaining to individual cover types should be interpreted with caution for cover types having limited extent within the focal landscape. The Sierra Nevada vegetation is extremely diverse and complex in its spatial arrangement of ecological settings and conditions; accordingly, the accuracy of mapping each unique ecological setting (i.e., cover type) and condition varies considerably. In general, because the model results are statistical in nature, confidence in the model results should decline as the extent of a cover type declines. Consequently, we limit our interpretation of the results to cover types that extend across $>$ 1,000 ha of the focal landscape.
- Lastly, extrapolating model results from one landscape to another should be done with extreme caution. As noted above (Axiom 2), landscapes are idiosyncratic; in other words, they have a unique internal structure and history, such that no two landscapes are the same. Thus, extrapolating our findings for, say, the Yuba River watershed to other landscapes should be done with caution. Our general findings certainly pertain to other similar surrounding landscapes and can probably be safely extrapolated to neighboring landscapes to some extent. However, to the extent that detailed quantitative results are desired for other geographies or ecoregions, a separate modeling exercise should be undertaken.

PROJECT AREA

The Sierra Nevada is a major North American mountain range and ecological region, located east of California's Central Valley and extending from Fredonyer Pass in the north to southern Kern County in the south. Much of the Sierra Nevada is reserved as federally-held public land, managed by the Forest Service, Bureau of Land Management, and National Park Service. The Northern Sierra ecoregion is located in the northern portion of the Sierra Nevada and encompasses ~ 2.1 million hectares. It is comprised of several major Hydrologic Unit Code (HUC) 8th-level watersheds, including the upper portions of seven watersheds west of the Sierra crest (Cosumnes, American South, American North, Bear, Yuba, Westside Middle Fork Feather, and Westside North Fork Feather) and four watersheds east of the Sierra crest (Lake Tahoe Basin, Truckee, Eastside Middle Fork Feather, and Eastside North Fork Feather)(**Figure 1**). Note, we divided the Middle and North Forks of the Feather River watersheds into "westside" and "eastside" watersheds based on physiographic differences, despite the fact that the entire Feather River watershed flows westward.

The topography of the region consists of rugged mountains incised by several major and numerous minor river drainages. Elevation ranges from roughly 300 - 3,000 meters. The area receives 30 - 260 cm of precipitation annually, with snow exceeding rain above about 1,750 m elevation (Storer and Usinger 1963). A summer drought typically persists from May to September, increasing the importance of developing a significant snowpack during the winter months, since snowmelt runoff is a key source of soil moisture during the late spring and summer months (Minnich 2007). In the Sierra Nevada, the heaviest precipitation occurs to the east and north of the San Francisco Bay area (Van Wagtendonk and Fites-Kaufmann 2006). Datasets of the 30-year normal (1981 - 2010) precipitation at 800 m resolution for the northern Sierra illustrate that particularly high amounts of precipitation fall across the middle elevations of the region (PRISM Climate Group 2014). This increased moisture contributes to the occurrence of exceptionally productive patches of forest (Littell et al. 2012; Alan Doerr, personal communication).

For purposes of simulation modeling, we divided the Northern Sierra ecoregion into 11 landscapes corresponding to the watersheds defined above. For the current project, we focused on six of these landscapes comprising the Tahoe Central Sierra Initiative (TCSI) area of interest, including: American South, American North, Bear, Yuba, Truckee and Lake Tahoe Basin. Each of these focal landscapes was assessed separately; specifically, we simulated wildfire disturbance and vegetation succession under historical dynamic equilibrium conditions and quantified the historical range of variation in landscape structure and current landscape departure, as described in detail below.

Post Euro-American Settlement Land Use

The arrival of Euro-American in the 1850s sparked a transformation of this landscape as people harvested timber, extracted gold using hydraulic mining techniques, and suppressed wildfires (Storer and Usinger 1963). Forestry, mining, grazing, and dozens of recreational activities, including hunting, mountain biking, and hiking, are all important uses taking place in the region. Numerous cattle and sheep grazing allotments exist within the region. In addition, a significant portion of the region in private ownership. Many of these lands were held by timber companies before the National Forests were created. In addition, many public lands were given to the Central Pacific Railroad in the late 19th century and subsequently returned to the public land system under the Bureau of Land Management, resulting in "checkerboard" ownership pattern persisting today. Mining of gold and other minerals also continues. These activities affect and interact with ongoing vegetation succession and disturbance processes in the area (USDA Forest Service 2014).

Although many uses of the forest led to changes in vegetation structure and composition, early century logging and wildfire suppression in combination have altered the historical fire regime and vegetation patterns the most (Hessburg et al. 2005; Knapp et al. 2013; McKelvey et al. 1996; Stephens et al. 2015; Safford and Stevens 2017). The National Forests have active timber and fire management programs. Clearcutting, shelterwood, salvage cutting, and plantation management have been major components of timber management on the Forests in the past. Between 1988 and 2002, timber sales in the Sierra Nevada dropped drastically, but on the National Forests timber sale levels have fluctuated both up and down,

although annual sawtimber sold has steadily decreased (USDA Forest Service 2004). Although the acreage burned in the Sierra Nevada has been increasing over the past several decades (Miller et al. 2009), relatively few large fires have impacted the region in the last 100 years until recently (USDA Forest Service 1990). The low total burned acreage until recently is despite fairly high fire starts (both human- and lightning-caused), indicating that suppression efforts have been very successful (USDA Forest Service 1990).

Vegetation

Vegetation in the region is tremendously diverse and changes slowly along an elevation gradient and in response to local changes in microclimate and soils, and includes the following major ecological zone groupings (Van Wagtendonk and Fites-Kaufmann 2006)(see also Appendices A and B). Note, while we treat vegetation structure (e.g. canopy height, tree cover, seral stage, etc.) as dynamic in response to wildfire disturbance and succession, we treat the distribution of broad cover types as static (i.e., unchanging over time):

- *Foothill shrubland and woodland* — This zone lies directly adjacent and to the west of the region, and generally is found below 914 m (3,000 ft) on the westside of the Sierras and below 2,103 m (6,900 ft) on the eastside of the Sierras (Sierra Nevada Framework Project 2001). A small part of the buffers we used around the focal landscapes includes this zone, which is represented predominantly by the oak woodland cover type on the westside and pinyon-juniper woodland and shrubland types on the eastside. This type is characterized by savannas, woodlands, or forests of either monospecific or mixed stands of various broadleaf species, including: blue oak (*Quercus douglasii*), valley oak (*Q. lobata*), interior live oak (*Q. wislizenii*), canyon live oak (*Q. chrysolepis*), madrone (*Arbutus menziesii*), California buckeye (*Aesculus californica*), and big-leaf maple (*Acer macrophyllum*). Foothill pine (*Pinus sabiniana*) is also an important tree in this zone, and chaparral shrubland stands are common as well.

- *Lower montane forest* — This ecological zone includes oak-conifer forests and woodlands and mixed evergreen forests at lower elevations, developing into Sierran mixed conifer forests with increasing elevation, and generally is found between 914-2,134 m (3,000-7,000 ft) on the westside of the Sierras and between 2,103-2,682 m (6,900-8,800 ft) on the eastside of the Sierras (Sierra Nevada Framework Project 2001). All three of these cover types are typified by a combination of both coniferous and broadleaved trees.

  Mixed evergreen is characterized on very moist sites by dense stands of tanoak (*Notholithocarpus densflorus*) and madrone with a variable component of Douglas fir. In mesic sites, Douglas-fir will often dominate, and broadleaf species are dominated by canyon live oak and black oak (*Q. kelloggii*). In dry sites Douglas-fir is less common, and is replaced by patchy stands of foothill pine and (mostly evergreen) oaks (canyon live oak and interior live oak), interspersed with chaparral and occasional stands of knobcone pine (*P. attenuata*). Historically, low- and mixed-severity fires were fairly common in this cover type (mean Fire Return Interval, FRI = ~ 30 years), and vegetation would quickly recover even from severe fires, since the hardwood dominants resprout after fire.

  Oak-conifer forests and woodlands are characterized by ponderosa pine and one or more oaks, such as California black oak, interior live oak, or canyon live oak. Lower amounts of incense cedar, Douglas-fir and sugar pine are also found in these forests. Historically, low severity fires were extremely common. Fire is integral to the ecology of yellow pines, and this cover type is one of the most altered by fire suppression and urban development.

  Sierran mixed conifer forests are characterized by multiple conifer and hardwood species, including: ponderosa pine, Jeffrey pine (in higher, colder or drier sites and on the east side of the Sierra crest), sugar pine, white fir, Douglas fir, incense cedar, California black oak, canyon live oak, and other broadleaf species. At least three conifers are typically present in any given stand. Today white fir and Douglas fir tend to be the most ubiquitous species, especially on moister aspects and drainages. Pines were historically the dominant species under the previous frequent low severity fire regime and are

still common on south slopes. Pines (primarily ponderosa pine) are present continuously from the oak-conifer forest and woodland zone below it in elevation. Historically, low- to- moderate severity fires were very frequent in this forest type (mean FRI = ~ 11 - 16 years), and fire suppression and widespread logging have greatly altered forest structure and composition (Safford and Stevens 2017).

- *Upper montane forest* — This zone is defined by the presence of red fir forests, which occur within and above the level of maximum precipitation and maximum snowfall on the Sierra Nevada westslope (Potter 1998; Safford and Van de Water 2014), and generally is found between 2,134-2,743 m (7,000-9,000 ft) on the westside of the Sierras and between 2,682-3,322 m (8,800-10,900 ft) on the eastside of the Sierras (Sierra Nevada Framework Project 2001). The red fir cover type is dominated by red fir (*A. magnifica*), but other species do co-occur, for example western white pine (*P. monticola*) and lodgepole pine (*P. contorta ssp. murrayana*). On xeric sites, Jeffrey pine can occur. Historically, wildfires were less common in these forests than those of the lower montane zone (mean FRI = ~ 40 years), and stands were characterized by complex patches of even-aged trees within a single stand arising from localized disturbance events. The boundaries between Sierran mixed conifer and red fir are fuzzy, and the types tend to co-occur, particularly in the ecotones. Similarly, red fir forests of the upper montane zone blend into the lodgepole pine and subalpine conifers of the subalpine forest zone.

- *Subalpine forest* — This zone is extremely heterogeneous, and comprised of patches of dense trees, rock outcrops, meadows and lakes, and open forest, and generally is found above 2,743 m (9,000 ft) on the westside of the Sierras and above 3,322 m (10,900 ft) on the eastside of the Sierras (Sierra Nevada Framework Project 2001). This zone includes two major cover types: Lodgepole pine and western white pine. Lodgepole pine is found throughout the subalpine zone in a variety of habitats, including in wetter soils, such as along meadow edges, or in very rocky soils. Unlike the subspecies of lodgepole pine found in the Rocky Mountains, the lodgepole pine subspecies found here does not have serotinous cones. Wildfires in lodgepole pine occur in a mix of severities, from low severity underburning in drier subalpine stands, to high severity in dense stands in drainages. Mountain hemlock (*Tsuga mertensiana*) is common on north slopes where heavy snows accumulate. Red fir is often an associate. Drier slopes support western white pine at lower elevations and whitebark pine (*P. albicaulis*) at higher elevations. Trees often grow as krummholz forms at the highest elevations. Wildfire is relatively rare in this cover type (mean FRI > ~ 100 years).

  Western white pine sometimes occurs in sufficiently continuous patches to be classified as its own type, separate from the Subalpine Conifer group. Typified by western white pine, species from the Subalpine Conifer and Red Fir cover types sometimes co-occur as well. This cover type tends to occur on drier soils. Most fires are low severity that promote the development of late-successional forests.

- *Eastside Pine and woodland* — For purposes of the simulation (see below), we classified and described the Eastside Yellow Pine cover type, characterized by Jeffrey pine (with some ponderosa pine), but other conifers and oaks, as well as western juniper (*Juniperus occidentalis*) may occur. Under historical conditions, wildfires were extremely common and were almost always low severity; fire is integral to the ecology of yellow pines. Oak-conifer forests and woodlands, as described above, are also present in this zone. Also east of the crest are two shrub community types typified by either big sagebrush (*Artemisia tridentata*) or mixture of black sagebrush (*A. arbuscula*) or low sagebrush (*A. nova*).

- *Other cover types and variants* — Some cover types not listed above can be found in any zone. Montane riparian vegetation occurs throughout the region and is usually dominated by willow (*Salix spp.*), alder (*Alnus spp.*) and cottonwood (*Populus spp.*). Curl-leaf mountain mahogany (*Cercocarpus ledifolius*), a shrubland cover type, is most common in the upper montane zone and above, but may occur in the lower montane zone as well. Several of the major forest cover types described above include variants growing on ultramafic ("serpentine") soils, which are characterized by low levels of macronutrients and high levels of toxic heavy metals (Alexander et al. 2006). Vegetation on ultramafic soils is almost always more open than on neighboring, more fertile substrates and therefore supports a more diverse understory. Chaparral stands are common on ultramafic sites, but open forests are also found, dominated by Jeffrey pine, incense cedar, and other conifers usually at low

density. Many endemic species grow on ultramafic soils (Safford et al. 2005), and biomass and fuels accumulation is lower than on other soil types (DeSiervo et al. 2015). Several of the major forest cover types include an aspen (*Populus tremuloides*) variant that is seral to corresponding conifer forest type in the absence of fire to maintain the aspen component.

LANDSCAPE DISTURBANCE-SUCCESSION MODEL

To simulate disturbance and succession processes representative of the historical reference period within the region, we developed a landscape disturbance-succession simulator (LDSim). LDSim was developed based on the framework implemented in RMLands (Rocky Mountain Landscape Simulator, McGarigal and Romme 2005a,b; McGarigal and Romme 2012) that was originally developed to simulate HRV of forests in the Rocky Mountains (e.g., Cushman et al. 2011). LDSim adopted the overall structure of RMLands but greatly expanded the flexibility of the software to model any heterogeneous landscape and any suite of disturbance processes. It is beyond the scope of this document to fully describe the inner workings of LDSim. Here, we provide only a brief overview of the model structure and a brief description of the major components pertaining to the simulation of natural disturbance and succession processes.

Model Structure

The overall structure of LDSim can be characterized as follows:

- *Raster-based* - The data format is a raster in geotiff format. Each cell or pixel has a suite of attributes that record its biophysical condition and disturbance history over time. Disturbance and succession act to change these attributes over time. The grain (cell size) and extent of the grid is only limited by computer memory. For this application we used a 5 m cell resolution representing the average footprint of a single mature tree.
- *Spatially-explicit* - Location matters, particularly in the disturbance model in which disturbance events are modeled as a contagious process; i.e., one that spreads from cell to cell. For example, the location of a cell will affect whether it gets disturbed during an event because the disturbance may spread faster uphill, in the direction of the prevailing wind, or through more susceptible vegetation.
- *Stochastic* - Each step of the disturbance and succession processes have a stochastic component that adds variability to the outcome. Consequently, the model outcomes from replicate simulations will never be exactly the same. As a result, the specific outcomes are not intended to be predictive of what will actually happen in any particular place at any point in time. Rather, the outcomes are intended to be representative, in a statistical sense, of the kinds of outcomes that could happen.
- *Phenomenological* - The model seeks to emulate the statistical properties of disturbance and succession processes; i.e., produce simulated behavior that is consistent with the statistical properties of real-world observations (e.g., mean disturbance patch size, mean return interval, etc.). In this statistical or phenomenological modeling approach, the mechanics of the process are deemed unimportant so long as the observed statistical properties of the phenomenon are emulated well. For example, the actual mechanism by which a fire of a given intensity determines whether a tree is killed (i.e., severity) is not represented explicitly in the algorithm. Instead, the algorithm is designed to produce the desired result of, say, a 20 % chance of high severity under particular conditions.

Succession

Succession occurs at the beginning of each timestep in the simulation and represents the establishment, gradual growth and/or development, and eventual senescence of vegetation over time. Succession is implemented as a completely unconstrained process in which the user defines a function for changing any of the cell attributes. Typically, a function is written to cause changes in one or more discrete vegetation attributes, such as the vegetation state, in what is referred to as a stochastic state-and-transition approach. In this case, vegetation cover types transition probabilistically between discrete states (e.g., seral stages). Transitions can be defined uniquely for each cover type and can be conditioned on any of the cell attributes. Alternatively, and in this application, a function is written to cause continuous changes in one or more vegetation attributes, such as canopy height growth, in which case there are no transitions between discrete states but rather continuous change in the vegetation attribute(s), and affected by climate conditions. In addition, succession transitions can occur either at the cell level in which each cell undergoes succession independently or at the patch level (defined as spatially contiguous cells having the same cell attributes, as defined) in which each patch rather yhan each cell undergoes succession independently. Succession patches might represent something akin to forest stands. However, in this application we apply succession at the 5m cell level - essentially at the scale of a single mature tree.

Disturbance

Disturbance follows succession in each timestep in the simulation. LDSim uses a generic disturbance algorithm that can be meaningfully parameterized to represent a variety of natural disturbances, including fire, insects/pathogens and wind, although only fire was simulated in this project. Each disturbance process is implemented separately using the same generic algorithm (albeit parameterized separately), but affects and is affected by other disturbance processes operating concurrently to produce changes in landscape conditions. The common disturbance algorithm consists of the following key components:

- *Climate* - Climate can play a significant role in determining the temporal and spatial characteristics of the disturbance regime. The disturbance climate is specified as an optional global parameter that optionally can affect initiation, spread, and/or mortality of all disturbance events within a timestep. Climate can be specified as constant with a user-specified level of temporal variability, a trend over time (with variability), or as a user-defined trajectory reflecting the climate conditions during a specific reference period. The climate parameter can play a major role in producing temporal variability in the disturbance regime and in the temporal dynamics of the landscape structure outcomes.
- *Susceptibility* - Prior to the initiation of a disturbance event each cell is evaluated for its susceptibility to the disturbance. Each cell has a probability of disturbance (i.e., susceptibility) that can be defined as a simple or complex function of any of the cell attributes or global parameters. For example, susceptibility to wildfire may be given as a function of the cell's vegetation type (e.g., cover type), vegetation condition (e.g., age), time since the last disturbance, and/or physical site conditions (e.g., topographic position), and as a function of the current climate. Susceptibility affects the probability of a cell initiating a disturbance event and the probability of a disturbance spreading to the cell from an adjacent cell.
- *Initiation* - Disturbance events are initiated at the cell level. Each cell has a relative probability of initiation in each timestep that is a function of its susceptibility to the disturbance (as defined above) and the overall rate of disturbance. The rate of disturbance is a function of the current climate and a single global parameter that determines the baseline number of disturbance attempts per unit area per timestep. The realized number of disturbance events initiated in any given timestep will be a function of the global initiation rate, which remains constant over time, the current climate, which varies over time, and the susceptibility of the cell, which varies over both space and time.

- *Spread* - Once initiated, disturbance spreads to adjacent cells (or nearby cells via "spotting") in a probabilistic fashion. Each cell has a probability of spread during each iteration of the spread process that is a function of its susceptibility to disturbance (as defined above), which can be further modified in a variety of ways including, for example, its relative position (e.g., relative elevation or wind direction), the influence of potential barriers (e.g., roads and streams), and the maximum size of the event (reflecting the propensity for the weather to impede or facilitate spread).
- *Termination* - An event terminates either due to the probabilistic spread (i.e., fails to spread further by chance due to the low spread probabilities in adjacent cells) or because of a limit placed on spread to reflect variable weather conditions at the time of the event. This event modifier limits the final size of the disturbance and is specified as a user-defined size distribution.
- *Mortality* - Following spread, each cell is evaluated to determine the magnitude of ecological effect of the disturbance. Each cell can exhibit either high mortality or low mortality. The interpretation of high versus low mortality will depend on the spatial resolution (i.e., cell size) of the simulation, because at very high resolutions (e.g., 5 m cell size) a mature tree either dies or does not, hence the use of only two severity levels (high or low).
- *Transition* - Following mortality, each cell is evaluated for potential immediate changes to any of the spatail attributes of a cell, including the transition to a different vegetation state as defined. Transitions can be defined uniquely for each cover type and can involve any attributes of the cell. Note, these immediate disturbance-induced transitions are differentiated from the successional transitions that occur at the end of each timestep in response to gradual growth and development of vegetation over time.

GEOSPATIAL DATA

We compiled and derived several geospatial data layers for the region as a whole (and resampled for the focal landscape) and/or separately for each focal landscape to support the HRV simulation. As noted in **Table 1**, only some of these layers serve as direct input to LDSim; many of the layers are needed for deriving other layers. All layers are represented as 5 m rasters (in a geotiff data format) with a common projection (California Albers). In **Table 1** we provide only a brief description of each layer; see **Appendix A** for additional details.

Table 1: Geospatial data layers developed for the Northern Sierra Historical Range of Variability assessment (See Appendix A for a detailed description of each layer). Layers are listed in alphebetical order.

Spatial Layer	**Description**	**Source**
Age	Estimate of vegetation Age (yrs) predicted from canopy height and site index (see below) based on developed growth equations for forests within the region core (i.e., extent of the Lidar data), and classified based on canopy cover from above for all shrublands and tree diameter for forests within the region buffer based on Eveg data. [LDSim model input]	EcObjects: Tahoe National Forest, nominal date of data: June 2014; Eveg: USDA Forest Service FSGeodata Clearinghouse, https://data.fs.usda.gov/geodata/edw/datasets.php, nominal date of data: March 22 - Jan 18, 2018.

(continued)

Spatial Layer	Description	Source
Aspect	Aspect (degrees) derived from the elevation raster (see below) using the R terrain() function in the Raster package, and then classified into nine bins (eight 45 degree bins plus flat). [LDSim model input]	Elevation layer
Available Water Storage (AWS)	Estimate of potential soil water storage (ml) to a depth of 150cm, which served as an input to the mesic index layer (see below).	USGS NRCS gSSURGO soil data, Geospatial data gateway (https://gdg.sc.egov.usda.gov/)
Biophysical Class (BPC) and unit (BPU)	Categorical clasification of predicted cumulative tree biomass (Biomass) under historical dynamic equilibrium conditions, but spatially simplified to create more practical management units. Predicted Biomass was derived from a Random Forest model based on simulated cumulative tree biomass and a suite of ten geophysical predictor variables at the cell level. BPCs were derived largely for the purpose of summarizing and describing the historical range of variability metrics (i.e., as a means of packaging the results) at the Site and Subbasin levels. Contiguous areas of the same BPC were organized into discrete Biophysical Units (BPUs) and represented as individual polygons.	Precipitation, Water balance deficit, Available water storage, Topographic wetness index, Heat load index, Growing degree days, Topographic position index, Solar radiation index, Slope, and Elevation layers
Buffer	Categorical dstinction between the focal landscape "core" and a 5 km wide "buffer", which served to distinguish the broader simulation landscape from the target core landscape for which all results were computed and reported. [LDSim model input]	Derived
Cover	Categorical cover types representing relatively stable biophysical settings that support characteristic vegetation communities under a natural disturbance regime. [LDSim model input]	EcObjects: From a variety of sources, nominal date of data: June 2014 - 2018; Eveg: USDA Forest Service FSGeodata Clearinghouse, https://data.fs.usda.gov/geodata/edw/datasets.php, nominal date of data: March 22 - Jan 18, 2018; several other secondary sources as listed in Appendix A.

(continued)

Spatial Layer	Description	Source
Developmental Stage	Categorical successional stages of vegetation development following a high-mortality disturbance used to classify cells into vegetation states for the purpose of characterizing landscape structure.	Age, Cover and Site Index layers
Elevation	Elevation (m) derived from a digital elevation model. [LDSim model input]	Lidar: 1 m surface elevation, nominal date of data: June 2014; USGS Digital Elevation Model (DEM) 1/3 arc (~ 10 m) data, National Geospatial Program (https://viewer.nationalmap.gov/basic/), date of data access: January 16, 2019.
Energy Index	Potential site productivity index based on physical site attributes pertaining to light and heat energy.	Growing Degree Days and Heat Load Index layers
Geophysical Unit (GPU)	Multivariate, spatially-constrained clustering of cells into spatial units based on similarity in 10 geophysical layers for the purpose of summarizing and describing the historical range of variability metrics (i.e., as a means of packaging the results).	Precipitation, Water balance deficit, Available water storage, Topographic wetness index, Heat load index, Growing degree days, Topographic position index, Solar radiation index, Elevation, and Slope layers
Growing Degree Days (GDD)	Estimate of the number of growing degree days above 0 degrees Celsius based on downscaled climate 30-year summary data for the period 1981 - 2010.	California BCM (Basin Characterization Model) Downscaled Climate 30-year Summaries (http://climate.calcommons.org/dataset/2014-CA-BCM)
Heat Load Index (HLI)	Unitless index of heat load based on potential direct incident solar radiation adjusted to reflect the maximum temperature gradient along the southwest-northeast axis. [LDSim model input]	Elevation layer
Precipitation	Estimate of precipitation (mm) based on downscaled climate 30-year summary data for the period 1981 - 2010.	California BCM (Basin Characterization Model) Downscaled Climate 30-year Summaries (http://climate.calcommons.org/dataset/2014-CA-BCM)
Mesic Index	Potential site productivity index based on physical site attributes pertaining to available moisture. [LDSim model input]	Precipitation, Topographic Wetness Index, Heat Load Index, Water Balance Deficit, and Available Water Storage layers

(continued)

Spatial Layer	Description	Source
Site Index	Potential site productivity index based on physical site attributes derived from a combination of mesic and energy site indices. [LDSim model input]	Energy Index and Mesic Index layers
Slope	Percent slope.	Elevation layer
Solar Radiation Index	Unitless index of direct solar radiation during the growing season based on latitude, longitude and a digital elevation model that accounts for sun angle and azimuth during the solar period of representative days during the growing season as well as the affect of topographic shading.	Elevation layer
Streams	Categorical representation of rivers and streams based on size. [LDSim model input]	Elevation layer
Tau Index	Index randomly assigned to groups of cells (based on site index) for the purpose of assigning tree height growth trajectories above or below the average determined by site index. [LDSim model input]	Site Index layer
Topographic Position Index (TPI)	Unitless index of topographic position based on mean deviations in the elevation surface. [LDSim model input]	Elevation layer
Topographic Wetness Index (TWI)	Unitless index of topographic wetness based on the potential for water to accumulate resulting from the predicted quantity of water flowing to a site and the predicted rate of drainage from the site (i.e., water balance).	Elevation and Precipitation layers
Tree Cover	Percent established tree cover within a local neighborhood for the purpose of characterizing landscape structure, along with a classified version into several classes.	Cover and Developmental Stage layers
Tree Diameter	Diameter at breast height (in) of forested cells with established trees used to classify cells into tree size classes for the purpose of characterizing landscape structure.	Cover, Developmental Stage and Tree Height layers
Tree Height	Height (ft) forested cells with established trees used to classify cells into developmental stages for the purpose of characterizing landscape structure.	Cover, Developmental Stage, Site Index and Age layers

(continued)

Spatial Layer	Description	Source
Tree Size	Quadratic mean diameter (QMD) of neighboring forested cells with established trees for the purpose of characterizing landscape structure, along with a classified version into several size classes.	Cover, Developmental Stage and Tree Diameter layers
Vegetation State	Categorical representation of the discrete vegetation "states" that a cover type could exist in during the simulation based on a combination of developmental stage and tree cover. [LDSim model input]	Cover, Developmental Stage and Tree Cover Class layers
Vegetation State Age	Number of years in the current Vegetation Sate. [LDSim model input]	Age, Cover, Developmental Stage and Site Index layers
Water Balance Deficit (WBD)	Estimate of climatic water balance deficit (mm), computed as the difference between an Potential Evapotranspiration (PET) and Actual Evapotranspiration (AET), based on downscaled climate 30-year summary data for the period 1981 - 2010.	California BCM (Basin Characterization Model) Downscaled Climate 30-year Summaries (http://climate.calcommons.org/dataset/2014-CA-BCM)

MODEL PARAMETERIZATION

LDSim has a user-defined set of model parameters that govern the disturbance and succession processes for any particular user-defined application and scenario. Importantly, the parameterization of the disturbance and succession processes represents the set of user assumptions about the system being modeled, and the results are only meaningful in reference to this set of assumptions. In addition, the parameterization of the model is application- and scenario-specific. For example, one application might involve wildfire disturbances, while another application might involve a combination of wind and insect disturbances, and the model parameterization would vary accordingly. Similarly, for the wildfire application, one scenario might involve natural wildfires under historical climate conditions, while another scenario might involve future climate conditions, and the model parameterization would vary among scenarios. Importantly, the parameterization represents a user-defined objective and LDSim has a relatively open architecture that allows for the disturbance and succession processes to be defined uniquely for every application. For the HRV scenario in this project, we parameterized the model to reflect our best understanding of the succession and wildfire disturbance processes characteristic of the historical reference period in the region. In the following sections, we briefly describe the model parameterization for this application.

Wildfire Climate

Climate conditions affecting wildfire disturbance during each timestep of the simulation is governed by a single global forcing variable, the Wildfire Climate Index, in which a single coefficient is assigned to each timestep. The Wildfire Climate Index is incorporated into several stages of the wildfire disturbance process, including: 1) susceptibility, 2) initiation, 3) spread, and 4) mortality, as described below.

The Wildfire Climate Index is based on the Palmer Modified Drought Severity Index (PMDI), which is a long-term measure of drought, on the scale of months to years, that is based on precipitation and temperature and incorporates soil moisture. PMDI data is obtained from NOAA's Living Blended Drought Atlas (LBDA) Version 2 (https://www.ncdc.noaa.gov/paleo-search/study/22454). As described by NOAA, "the half degree gridded Jun - Aug PMDI reconstructions from Cook et al. (2010) were recalibrated using the Global Historical Climatology Network (GHCN) 5 km grid PMDI data (for the years 0 to 2017). The 5 km data were first upscaled to match the original half-degree grid. The recalibration was performed using a kernel density distribution mapping (KDDM) technique outlined in McGinnis et al. (2015) using an R package provided by Seth McGinnis. LBDA used a 50-year recalibration period covering 1929 - 1978 CE. They also adjusted each grid point's mean PMDI value for the recalibration period to be zero to avoid importing wet or dry bias into the recalibration. The recalibrated data set covers the continental United States just as the GHCN instrumental data does. Since instrumental data were used for 1979 - 2005 CE in the Cook dataset, recalibration applied only to the years 0 - 1978 CE. The 1979 - 2017 instrumental years were filled in using the post-recalibration period values from the GHCN PMDI data."

We extract the PMDI data from the LBDA dataset for the point locations falling within the Northern Sierra ecoregion (**Figure 1**) and process it as follows:

- First, we compute the inverse distance-weighted average PMDI value for each year based on the distance between the PMDI sample point locations and the centroid of the focal landscape.
- Next, we select these data for the years corresponding to our designated historical reference period (1550 - 1850, n = 300) and then use a bootstrap procedure to expand this record to 2,500 observations. Specifically, our procedure for simulating HRV involves running LDSim for 500 5-year timesteps (or 2,500 years) as described below, which our previous work (McGarigal et al. 2018) indicated was sufficient to effectively characterize the HRV in landscape structure. Thus, we require a climate trajectory of equal length. Rather than use the observed PMDI data for the past 2,000 years, we restrict the climate record to our chosen historical reference period (1550 - 1850). The bootstrap procedure involves randomly selecting a 10-year period from the historical reference period, appending this data to the historical reference period data, and repeating this process until we derive the desired record length of 2,500. This procedure produces a PMDI record of the desired length but one in which the observed variability over time is representative of the 300-year historical reference period.
- Next, we compute the 5-year average PMDI to align with the five-year timesteps in our model, resulting in a total of 500 observations.
- Next, we invert the 5-year average PMDI by multiplying by -1 so that positive values represent drier conditions and negative values represent wetter conditions for a more intuitive use in the LDSM (i.e., increasing values result in increasing wildfire).
- Lastly, we shift and rescale the index to accommodate the wildfire spread function described below. Specifically, we shift the index so that its neutral value is 1 instead of 0 (by adding 1 to all values). Thus, values > 1 are drier than average and values < 1 are wetter than average. We also adjust the spread of the distribution to have a standard deviation of 0.2, although this is arbitrary and resulted from model calibration (see below).

The final Wildfire Climate Index trajectory represents a vector of 500 coefficients, one for each 5-year timestep of the simulation, as shown in **Figure 2** for the Yuba River landscape.

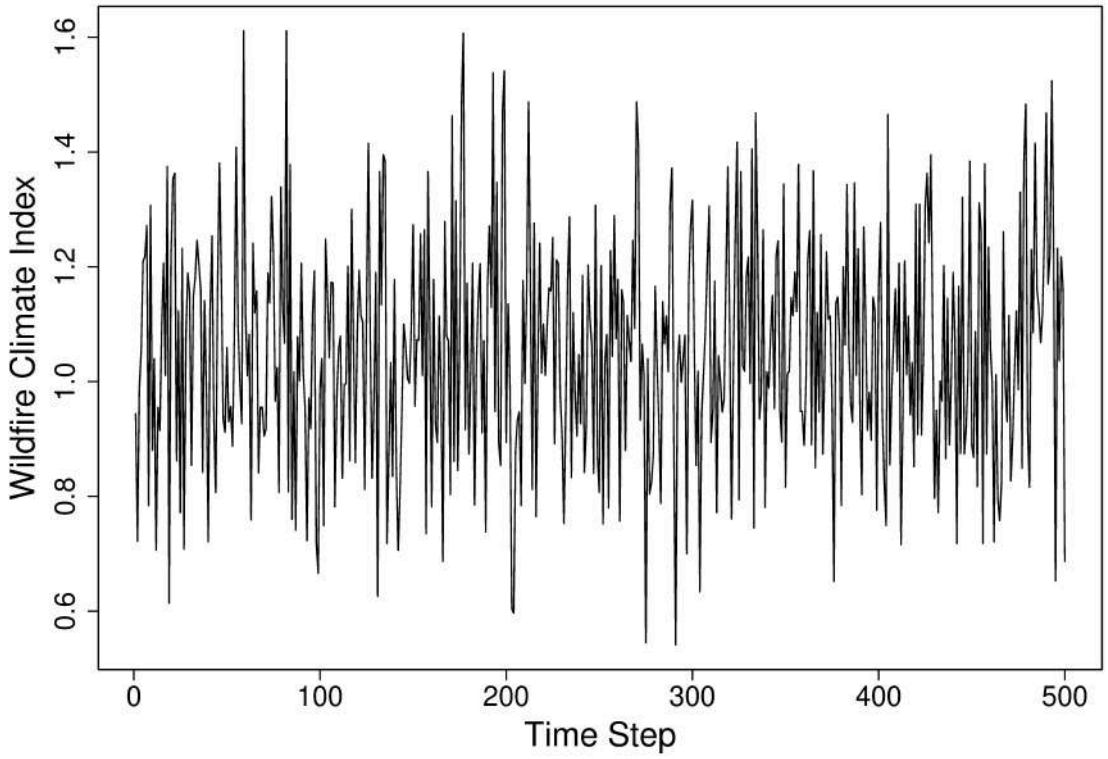

Figure 2: Wildfire Climate Index trajectory for the Yuba River landscape corresponding to 500 5-year timesteps in the simulation. The Climate Index was based on the inverted and rescaled 5-year averaged, inverse-distance weighted mean Palmer Modified Drought Severity Index (PMDI) for the sample point locations within the Northern Sierra ecoregion relative to the focal landscape (Yuba River watershed in this case). Note, here we inverted PMDI so that positive values represented drier conditions and negative values represented wetter conditions, and we also rescaled the index to have a standard deviation of 0.2 (see text for details).

Wildfire Susceptibility

Wildfire susceptibility for any given cell in the current timestep is modeled as a function of fuels and climate for most cover types (exceptions noted below). Specifically, the fuels component (F) is modeled as a Logistic function of the number of years since the last fire, reflecting the build up of fuels over time, and the Heat Load Index (hli), reflecting the expected flammability of the fuels based on topographically-influenced fuel moisture. The climate component (M) is modeled as a Logistic function of the Wildfire Climate Index, reflecting the expected flammability of fuels based on climate conditions during the timestep. The fuels and climate components are combined with a geometric mean to produce the final Wildfire Susceptibility Index (V). Specifically, the Wildfire Susceptibility Index for any given cell in any given timestep is determined as follows:

$$F_{it} = \frac{e^{(b_0+b_1 A_{it}+b_2 H_i)}}{(1+e^{(b_0+b_1 A_{it}+b_2 H_i)})}$$

$$M_t = \frac{e^{(b_3+b_4 C_t)}}{(1+e^{(b_3+b_4 C_t)})}$$

$$V_{it} = \sqrt{F_{it} M_t}$$

where: b_0 - b_4 = user-specified Logistic parameters that could vary among cover types; A_{it} = Age since the last fire of the i^{th} cell in the t^{th} timestep; H_i = Heat Load Index of the i^{th} cell; C_t = Wildfire Climate Index in the t^{th} timestep; F_{it} = Fuels Index of the i^{th} cell in the t^{th} timestep; M_{it} = Climate Index of the i^{th} cell in the t^{th} timestep; and V_{it} = Wildfire Susceptibility Index of the i^{th} cell in the t^{th} timestep.

Given this function, the final Wildfire Susceptibility Index is on the probability scale (0 - 1) and used in the wildfire initiation and spread functions (see below) such that a value of 0 would prevent wildfires from initiating in or spreading into the cell, and as the value increases to 1 the probability of initiating a wildfire would increase as would the probability of a wildfire spreading to the focal cell from an adjacent burning cell, all other things being equal.

We use expert opinion to specify the starting beta coefficients for each cover type. However, we then vary the b_0 and b_1 coefficients among cover types to reflect differences in reported historical mean fire return intervals among cover types within each landscape (see Model Calibration) - shifting the response curves left or right so that the inflection point (Wildfire Susceptibility Index = 0.5) roughly equals the target mean return interval - and hold the Heat Load Index coefficient (b_2) and Climate coefficients (b_3 and b_4) the same across all cover types and landscapes to reflect the global affect of topography and climate on wildfire susceptibility. As an example, the wildfire susceptibility function for Sierra Mixed Conifer (SMC) forest in the Yuba River landscape is depicted in **Figure 3**. Note that the Wildfire Susceptibility Index is close to 0 for several years following a fire and then rises rapidly as the fire-free period increases, reflecting the gradual build up of fuels. Also note that for any particular number of years since fire, the Wildfire Susceptibility Index increases with increasing Heat Load Index, reflecting drier fuels on ridgetops and southwest facing slopes, but that the effect is greatest during the period of rapid build up of fuels. Lastly, note that climate exerts a major influence on susceptibility after the initial build up of fuels. Under very wet climate conditions susceptibility to wildfire remains low regardless of fuel conditions, and as the climate conditions increasingly became drier the susceptibility increases dramatically.

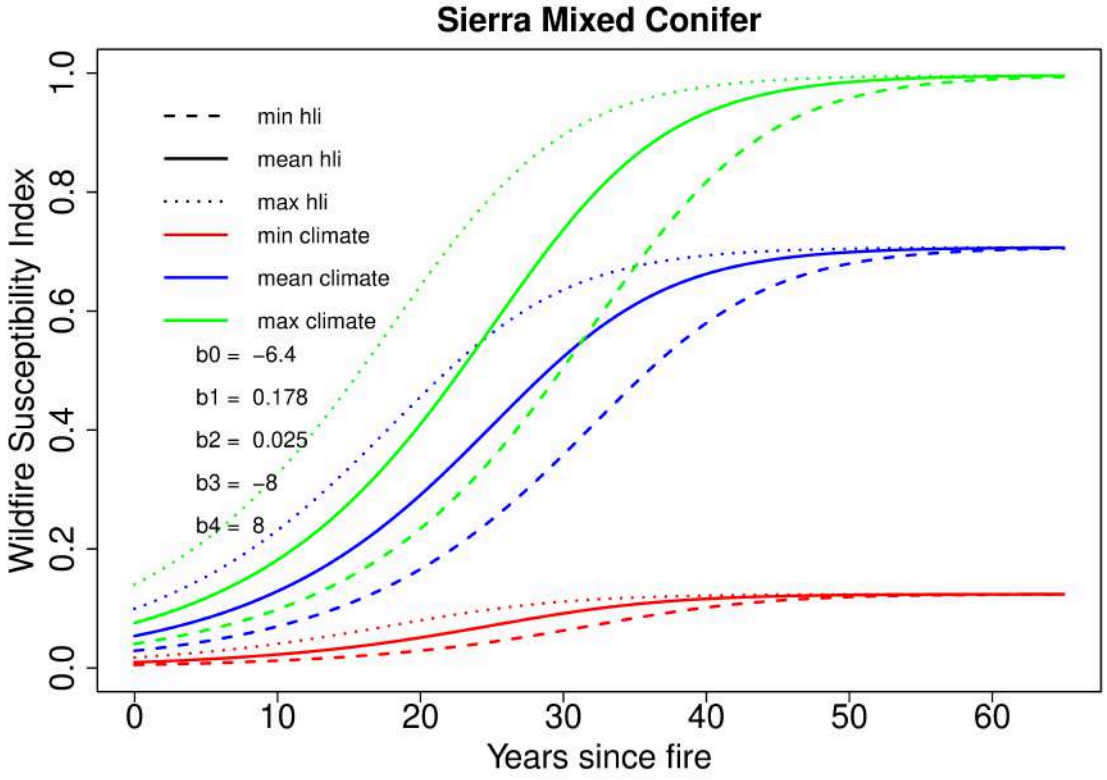

Figure 3: Wildfire Susceptibilty Index as a Logistic function of the number of years since the last fire (Years since fire) for Sierra Mixed Conifer forest in the Yuba River landscape in the Northern Sierra

ecoregion. The dashed, solid and dotted lines depict the response functions for the minimum, mean and maximum Heat Load Index (hli), and the red, blue and green sets of lines depict the response functions for the minimum, mean and maximum wildfire Climate Index. The values of the Logistic parameters (b_0 - b_4) for this cover type are shown as well.

There are a few exceptions to the wildfire susceptibility function, as follows:

- *Wetland* - Susceptibility to wildfire is modeled as a simple Logistic function of climate, reflecting the observation that wetlands generally are almost never fuel limited and topography is relatively unimportant, as follows:

$$V_{it} = \frac{e^{(b_0+b_1 C_t)}}{(1+e^{(b_0+b_1 C_t)})}$$

where: b_0 - b_1 = user-specified Logistic parameters; C_t = Wildfire Climate Index in the t^{th} timestep; and V_{it} = Wildfire Susceptibility Index of the i^{th} cell in the t^{th} timestep.

We parameterize the function so that susceptibility remains ~ 0 until the climate conditions become extremely dry, for example as depicted in **Figure 4** for the Yuba River landscape.

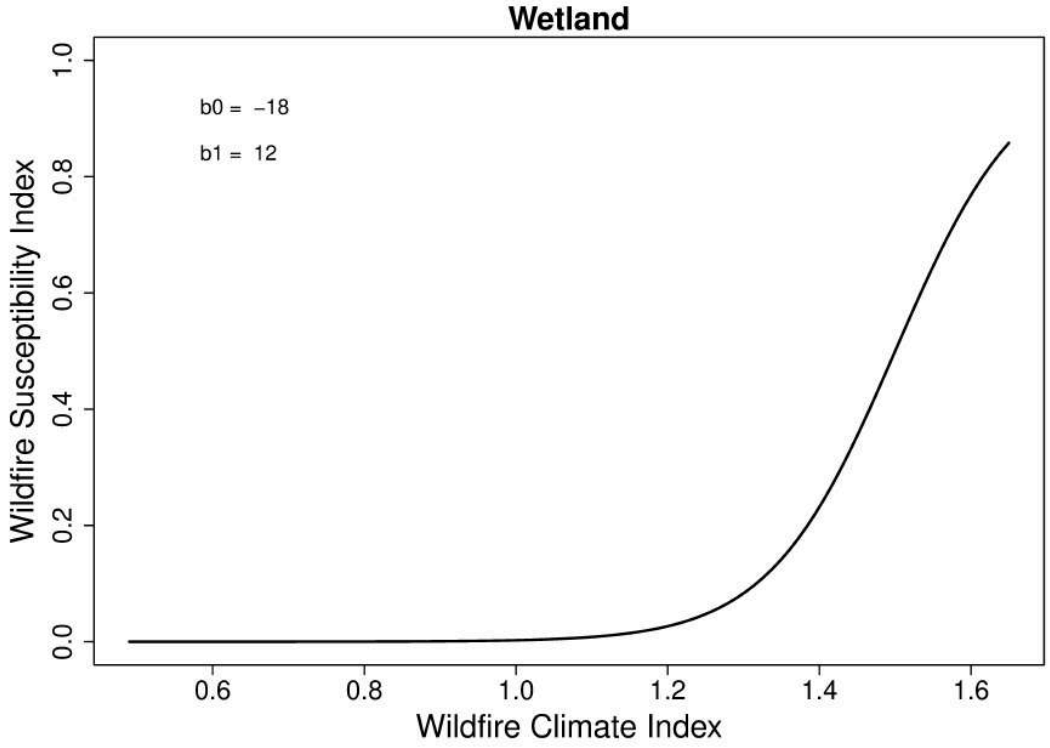

Figure 4: Wildfire Susceptibilty Index as a Logistic function of the wildfire Climate Index (inverted and rescaled 5-year mean Palmer Modified Drought Severity Index, see text for details) for wetlands in the Yuba River watershed in the Northern Sierra ecoregion. The values of the Logistic parameters (b_0, b_1) for this cover type are shown as well.

- *Water and Barren* - Susceptibility to wildlife is set to 0 for these cover types, reflecting the lack of fuel in these cover types.

Wildfire Initiation

The number and spatial distribution of wildfire initiations in any given timestep is governed by: 1) a global wildfire initiation rate parameter that controls the number of initiation attempts per unit area and remains

constant over time, 2) the current climate conditions as represented by the Wildfire Climate Index, that varies over time but not space, and 3) the susceptibility to wildfire as represented by the Wildfire Susceptibility Index, that varies over both space and time. The relative probability of wildfire initiation in any given cell in the current timestep is determined by the Wildfire Susceptibility Index (wfireSusc). Thus, as the susceptibility to wildfire in a cell increases, the relative probability of initiating a wildfire increases as well. However, the number of attempted wildfire initiations per unit area in any given timestep is determined by the product of the global wildfire initiation rate parameter and the Wildfire Climate Index, as follows:

$$A_t = IC_t$$

where: I = global wildfire initiation rate parameter; C_t = Wildfire Climate Index in the t^{th} timestep; and A_t = number of attempted wildfire initiations in the t^{th} timestep.

Thus, the number of *attempted* wildfire initiations per unit area varies over time with the Wildfire Climate Index. When the Wildfire Climate Index is relatively high, say, 1.5 (indicative of very dry conditions), the number of attempts per unit area is 50 % greater than the number given by the global wildfire initiation rate; conversely, when the index is relatively low, say, 0.5 (indicative of very wet conditions), the number of attempts is 50 % less than the baseline number.

The *realized* number of wildfire initiations in any given timestep is governed by the number of attempts (A_t) and the distribution of the Wildfire Susceptibility Index, which determines whether any cell chosen at random actually initiates a wildfire event. The number of attempted wildfire initiations determine how many cells are chosen at random and the Wildfire Susceptibility Index determines the probability of the chosen cells initiating an event. Thus, the realized number of wildfire events varies over time with the changing climate and with the changing susceptibility of the landscape to wildfire, for example as depicted in **Figure 5** for the Yuba River landscape. The global wildfire initiation rate parameter is used as a calibration parameter to raise or lower the average realized number of wildfire events to achieve the target wildfire rotation period for the focal landscape (see Model Calibration below).

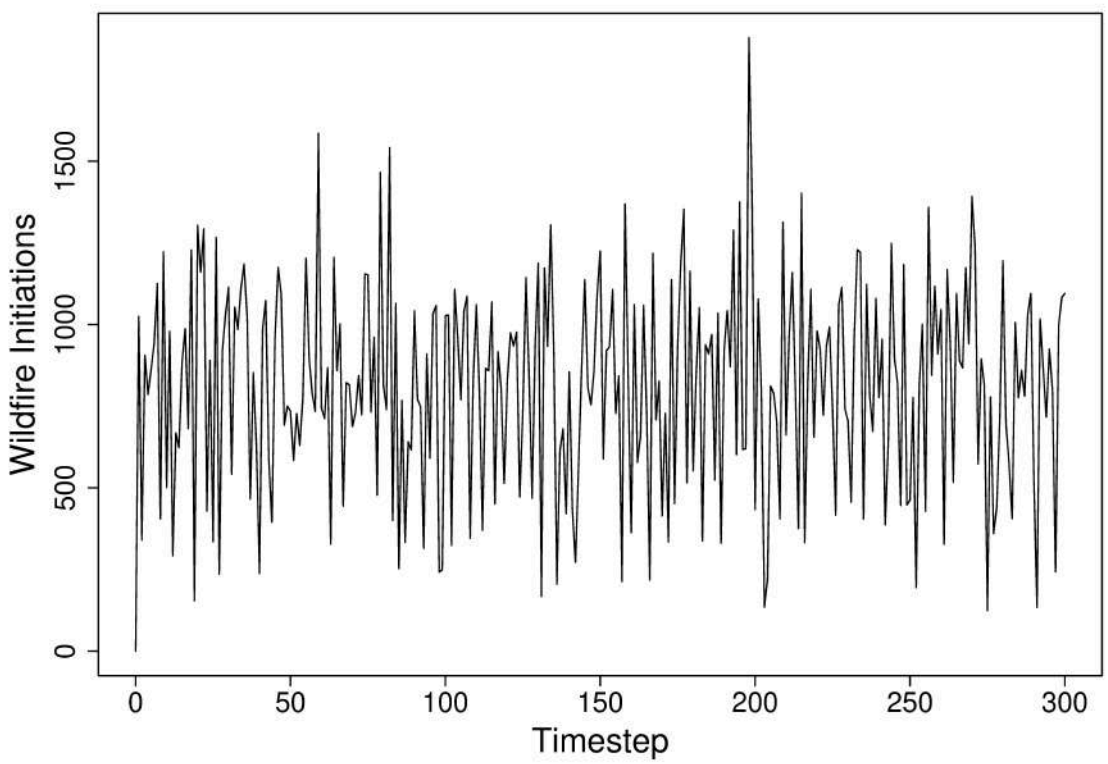

Figure 5: Number of realized simulated wildfire initiations per 5-year timestep for the Yuba River watershed in the Northern Sierra ecoregion.

Wildfire Spread

The probability of wildfire spread to a focal cell from an adjacent burning cell during an individual disturbance event is determined by several factors, including the Wildfire Susceptibility Index, wind direction and strength, relative slope, the presence of streams, and climate, and the spread coefficients are held constant across all focal landscapes. The relative weight of the Wildfire Susceptibility Index, wind, and relative elevation, as well as the strength of the stream impediment effect, varies with the size of the event. These factors are combined in a complex function as follows:

$$Z_{ijt} = max[\frac{max[V_{ijt}, (w^v_{jt}V_{ijt} + w^w_{jt}W_{ijt} + w^e_{jt}E_{ijt})]S_i)}{d}C_t, 1]$$

where: Z_{ijt} = probability of spread from an adjacent burning cell to the i^{th} cell during the j^{th} wildfire event in the t^{th} timestep; V_{ijt} = Wildfire Susceptibility Index of the i^{th} cell during the j^{th} wildfire event in the t^{th} timestep; W_{ijt} = Wind Index (direction and strength) of the i^{th} cell during the j^{th} wildfire event in the t^{th} timestep; E_{ijt} = Relative Slope Index of the i^{th} cell during the j^th wildfire event in the t^{th} timestep; $w_{jt}{}^{v}$ = weight of the Wildfire Susceptibility Index during the j^th wildfire event in the t^{th} timestep; $w_j{}^{w}$ = weight of the Wind Index during the j^th wildfire event in the t^{th} timestep; $w_j{}^{e}$ = weight of the Relative Slope Index during the j^th wildfire event in the t^{th} timestep; S_i = Stream Impediment Index for the i^{th} cell; d = distance between adjacent cells adjustment: d = 1 for the spread to an orthogonal neighboring cell (i.e., shares a full side) and d = 1.4 for the spread to a diagonal neighboring cell; C_t = Wildfire Climate Index in the t^th timestep.

Wildfire Susceptibility Index (V) is scaled as a probability (0 - 1) and was described previously.

Wind (W) is incorporated in two parts. First, a prevailing wind direction for an individual wildfire event is selected probabilistically from the eight cardinal directions. To derive the wind distribution values, we summarize all available historical wind direction data from 6 local weather stations (Rice Canyon, Saddleback, Downieville, White Cloud, Emigrant Gap, and Blue Canyon) for the fire season (May 15 to October 15) and burning period times (1000 to 1800 hours)(**Figure 6**). Data from all weather stations is weighted equally. After the wind direction (i.e., the direction the wind is blowing from) is selected for the particular event, the fire is able to grow in all directions, but is relatively more likely to spread with the wind than against it (i.e., directional bias). We use expert opinion to parameterize the strength of this directional bias, which causes a reduction in the probability of spread as the angle increases from the direction the wind is blowing (**Figure 6**). Note, the realized effect of wind on the probability of spread depends on the weight assigned to wind and the maximum size of the fire (see below).

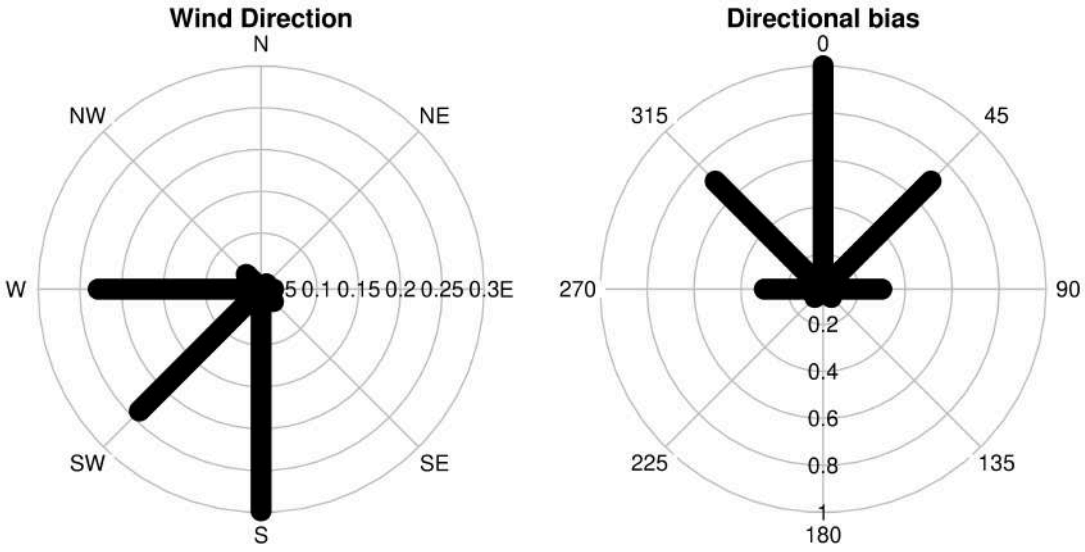

Figure 6: Probability of the wind direction (i.e., the direction the wind is blowing from) for a wildfire event and the relative probability of wildfire spreading to a cell from an adjacent burning cell based on its direction relative to the chosen wind direction. With a southwest wind, for example, a cell that was Northeast of a burning cell would have 0 degree directional bias and a relative probability of 1, whereas a cell that was East of a burning cell would have a 45 degree directional bias and a relative probability of 0.75 (see text for details).

Relative slope (E) is defined as the percent slope uphill or downhill from an adjacent "burning" cell to the focal cell. A positive relative slope means that the focal cell is uphill of the burning cell. Conversely, a negative relative slope means that the focal cell is downhill of the burning cell. We use expert opinion to parameterize the strength of the relative slope effect, which causes a reduction in the probability of spread from the maximum (1) when the focal cell is uphill at > 50 % slope from the burning cell (**Figure 7**). Probability of spread decreases for shallower slopes and cells downhill of the burning cell. Note, as with wind, the realized effect of relative slope on the probability of spread depends on the weight assigned to relative elevation and the maximum size of the fire (see below).

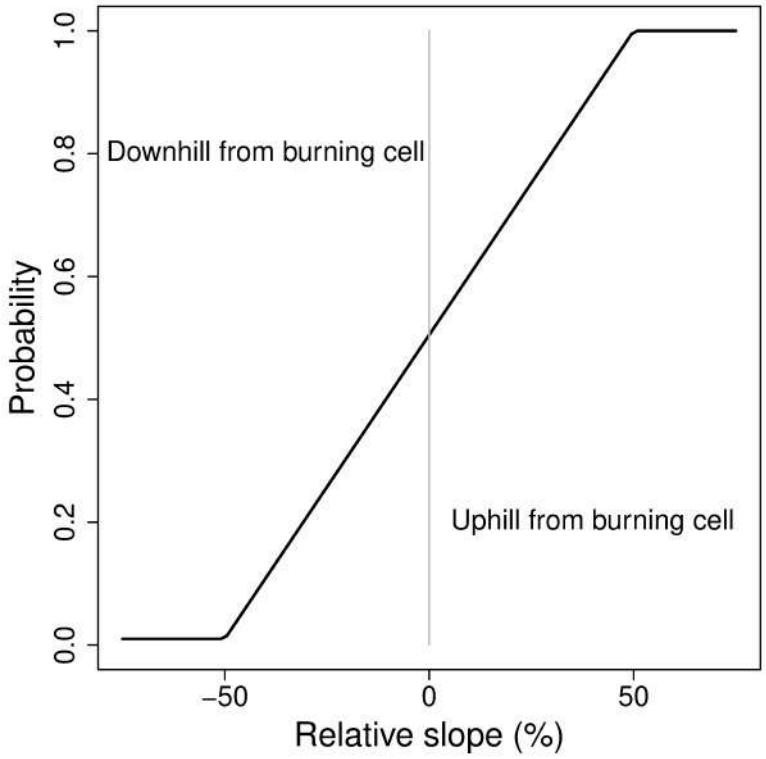

Figure 7: Relative probability of wildfire spreading to a cell from an adjacent burning cell based on its relative percent slope. Probability increased with increasing slope uphill of a burning cell and decreased with increasing slope downhill of a burning cell (see text for details).

Streams (S) are treated as a potential impediment to spread, depending on stream size and maximum fire size. We use expert opinion to parameterize the magnitude of the effect, which causes a reduction in the probability of spread. Regardless of size, streams have no effect on spread for the largest fires (i.e., probability = 1) but their effect increases as the fire size decreases and stream size increases (**Figure 8**). Consequently, large streams are usually an effective barrier for the smallest fires, whereas small streams have almost no effect even on the smallest fires.

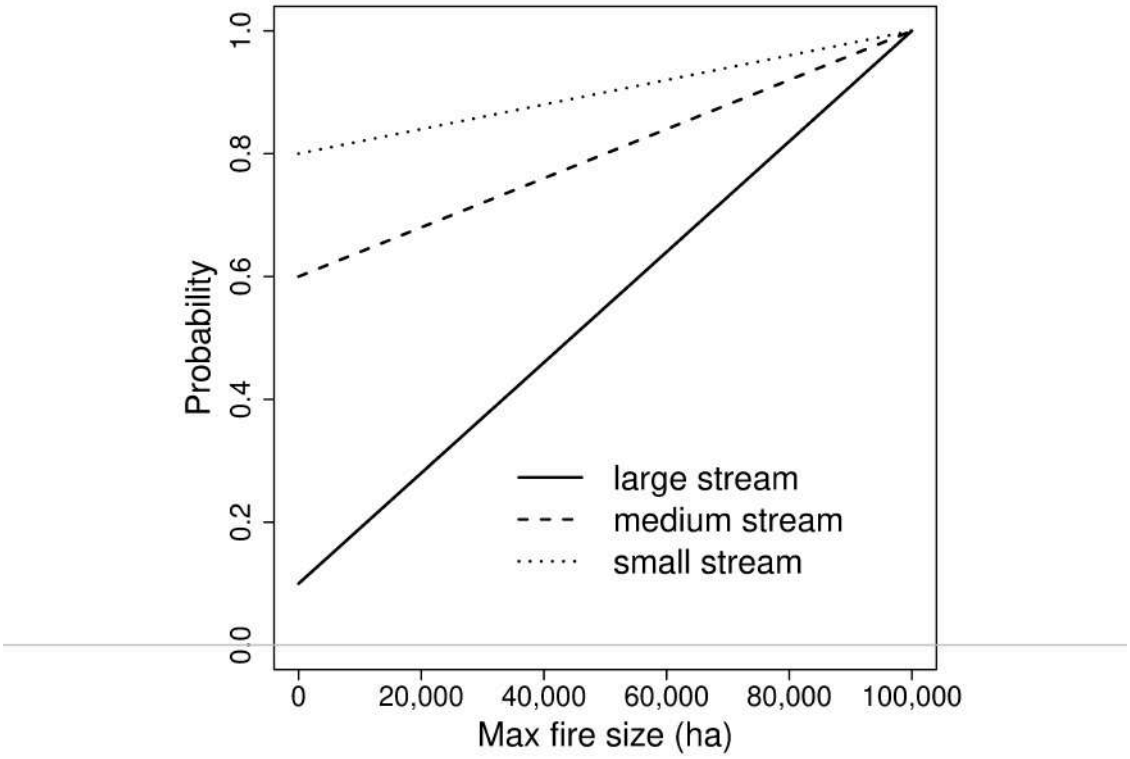

Figure 8: Relative probability of wildfire spreading through a stream cell as function of stream size class and the maximum size (ha) of the fire.

Climate (C) is based on the Wildfire Climate Index described previously. The Wildfire Climate Index, as described previously, varies over time within the range of ~ 0.5 - 1.5. Thus, as used in the spread function, when the Index is < 1 (indicative of wetter conditions) climate acts to reduce the probability of spread; whereas, when the Index is > 1 (indicative of drier conditions) climate acts to increase the probability of spread.

We also allow for "spotting" during wildfire spread; i.e., the fire leaping ahead and initiating in cells ahead of the advancing front. Specifically, during each iteration of the fire spread there is a Bernoulli probability of spotting (i.e., yes or no) that varies with fire size (**Figure 9**). If the Bernoulli trial is successful, a cell on the fire front is selected at random to serve as the source of the spotting. Next, a spotting distance is selected at random from a Uniform distribution between 1 and a maximum spotting distance that also varies with fire size (**Figure 9**). Next, the cell at the randomly selected distance from the source cell and in the direction the wind is blowing for this particular event is subjected to a Bernoulli trial based on its probability of initiation (see above). If successful, the cell becomes part of the active fire front for the next spread iteration. We use expert opinion to parameterize spotting so that as fires become larger, their probability of spotting and spotting distance increases, as depicted in **Figure 9**. Thus, spotting is only important for the largest fires where its main effect is to facilitate fire spread past potential barriers such as large rivers, barren areas and water bodies.

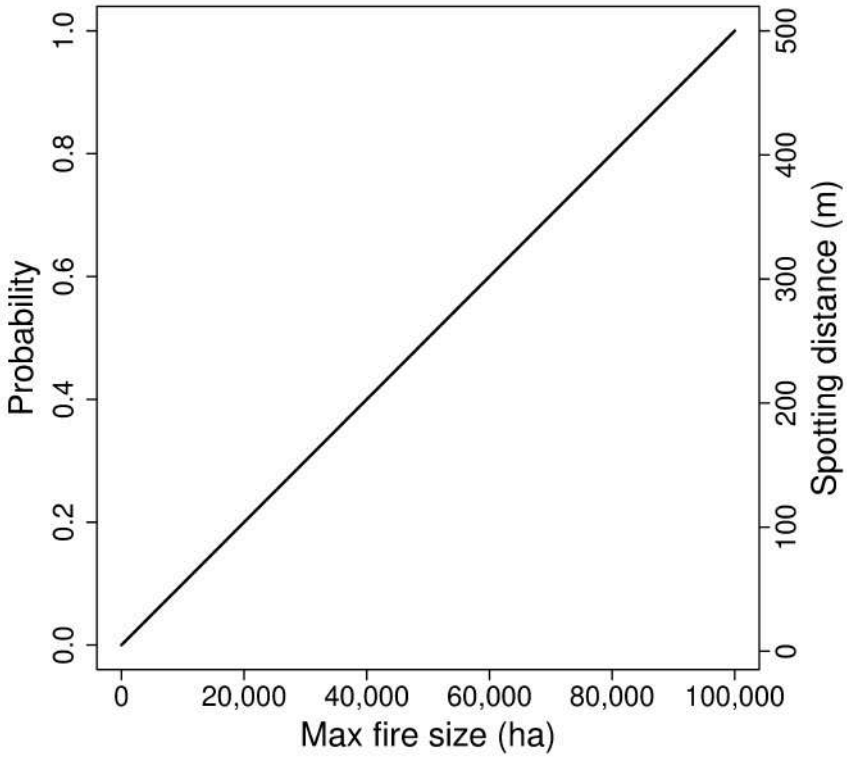

Figure 9: Relative probability of wildfire spreading via "spotting" to a cell ahead of the active burning front. Probability of spotting and the maximum spotting distance (m) increased with the maximum size (ha) of the fire (see text for details).

A complete description of the spread algorithm is beyond the scope of this document. Briefly, based on the parameterization described above, after a successful wildfire initiation, fire spreads contagiously to adjacent cells based on their probability of spread (Z_{ijt}) and occasionally spots ahead of the burning front. Fire continues to spread in an iterative manner outward from all "burning" cells until either it stopped by chance due to low spread probabilities or it reaches the randomly selected maximum fire size (see wildfire Termination below). As given in the spread equation above, the probability of spreading from a "burning" cell to an adjacent cell is largely determined by the maximum of the cell's current Wildfire Susceptibility Index (V_{ijt})(which is largely a function of its fuel load and condition based on topographic position) and a weighted combination of the cell's current Wildfire Susceptibility Index, Wind Index and Relative Slope Index ($w^v_{jt}V_{ijt} + w^w_{jt}W_{ijt} + w^e_{jt}E_{ijt}$), where the weights vary as a function of the randomly selected maximum fire size for the current event (see wildfire Termination below). We parameterize these spread weights such that the larger the selected maximum fire size, the more weight that is given to wind and relative elevation (**Figure 10**). For the largest fires (~ 100,000 ha), wind is the dominant factor determining the local probability of spread. Streams (S_i) are incorporated as a multiplier such that they act to suppress the probability of spread across a stream, but with the strength of the effect decreasing with increasing fire size and decreasing stream size (**Figure 8**). Next, the Wildfire Climate Index (C_t) is incorporated as a multiplier such that it acts to increase (to a ceiling of 1) or decrease the probability of spread for all cells and all wildfire events within the current timestep (t).

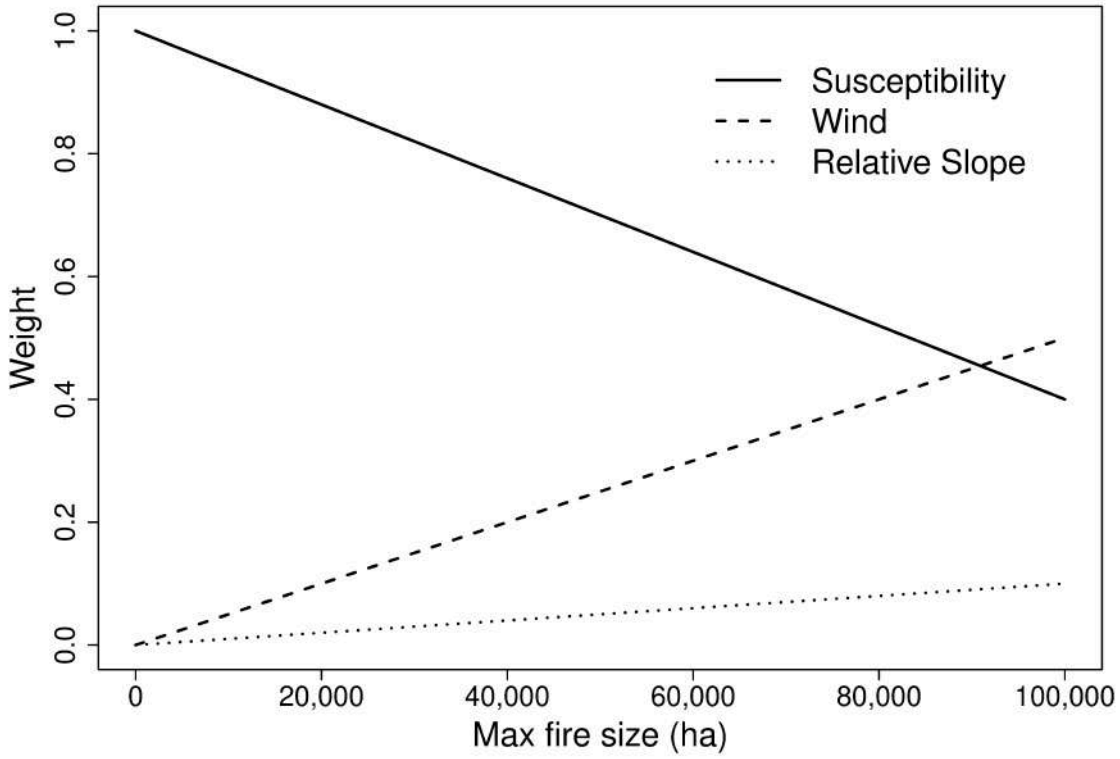

Figure 10: Relative weights assigned to the wildfire Susceptibility Index, Wind Index, and Relative Slope Index in the wildfire spread function. As maximum fire size (ha) increases, the relative importance of susceptibility decreases and the importance of wind and relative slope increases. At the largest fires, wind becomes the dominant factor; whereas, at the smallest fires only susceptiblity has an effect (see text for details).

Wildfire Termination

The spread of an individual wildfire event is terminated when either it stopped by chance due to low spread probabilities or it reaches a randomly selected maximum fire size. In this regard, maximum fire size functions as a surrogate for random weather conditions (e.g., rain event) that can limit the spread of a fire regardless of the underlying fuel conditions. We determine the maximum fire size distribution by analyzing the size distribution of all mapped fires (N = 32,497) that occurred between 1908 - 1979 in the Northern Sierra ecoregion (data from the USDA Forest Service, Pacific Southwest Region, Fire Return Interval Departure (FRID) dataset,
https://www.fs.usda.gov/detail/r5/landmanagement/gis/%3Fcid%3Dstelprdb5361974)(**Figure 11**). We limit the fire record to those prior to 1980 to reflect conditions prior to major changes in the fire regime resulting from accumulated fuels and climate change. In addition, although these data do not stem from the historical reference period, we deemed that they are an acceptable representation of the expected fire size distribution for the reference period, with the exception that they don't contain the largest fires that may have occurred episodically during the historical reference period. The maximum wildfire size distribution is held constant across all focal landscapes.

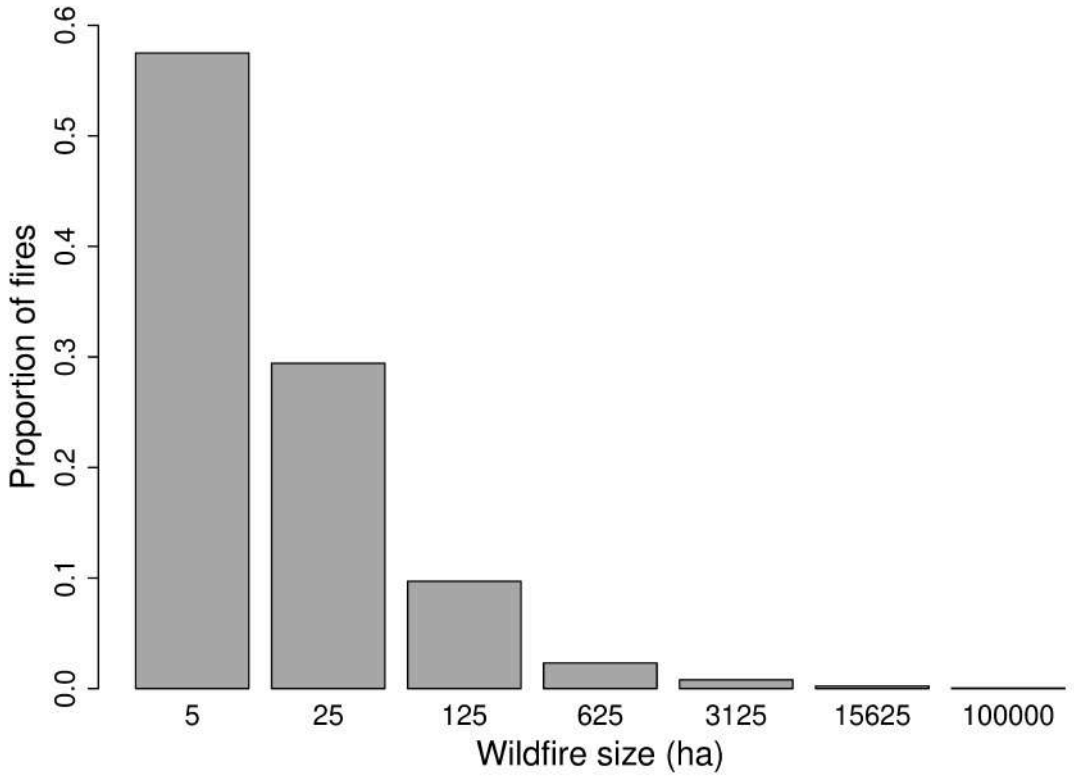

Figure 11: Maximum wildfire size distribution used a surrogate for individual wildfire event factors such as weather conditions that can limit the spread of fire regardless of the underlying fuel conditions. Data represent 32,497 mapped fires that occurred between 1908 - 1979 in the Northern Sierra ecoregion, available from the USDA Forest Service, Pacific Southwest Region, Fire Return Interval Departure (FRID) dataset.

Wildfire Mortality

Following the termination of a wildfire event the probability of high versus low mortality of the overstory vegetation in each 5 m cell that burned is determined by two major factors: 1) fire intensity, which is a function of fuel loads in the neighborhood of the focal cell (proxied by the age of the vegetation and time since the last fire), the topographic position of the focal cell, and the climate conditions of the current timestep; and 2) the resistance of the focal cell, which is a function of the age of the vegetation in the focal cell, as described below. High mortality is interpreted as the death of all overstory vegetation in the cell, whereas a low mortality response is interpreted as partial or no overstory mortality in the cell.

Fire Intensity - Fire intensity for any given cell in any given timestep is modeled as a Logistic function of fuel loads in the neighborhood of the focal cell, topographic position and climate, as follows and as shown in **Figure 12**:

$$I_{it} = \frac{1}{(1 + e^{-(b_0 + b_1 F_{it} + b_2 T_i + b_3 C_t)})}$$

where: b_0 - b_3 = user-specified Logistic parameters that is held constant across all cover types (b_0 = -12, b_1 = 0.08, b_2 = 0.035, b_3 = 4); F_{it} = Fuel Load Index of the i^{th} cell in the t^{th} timestep (see below); T_i = Topographic Position Index (tpi) of the i^{th} cell; C_t = Wildfire Climate Index in the t^{th} timestep; and I_{it} = Fire Intensity Index of the i^{th} cell in the t^{th} timestep.

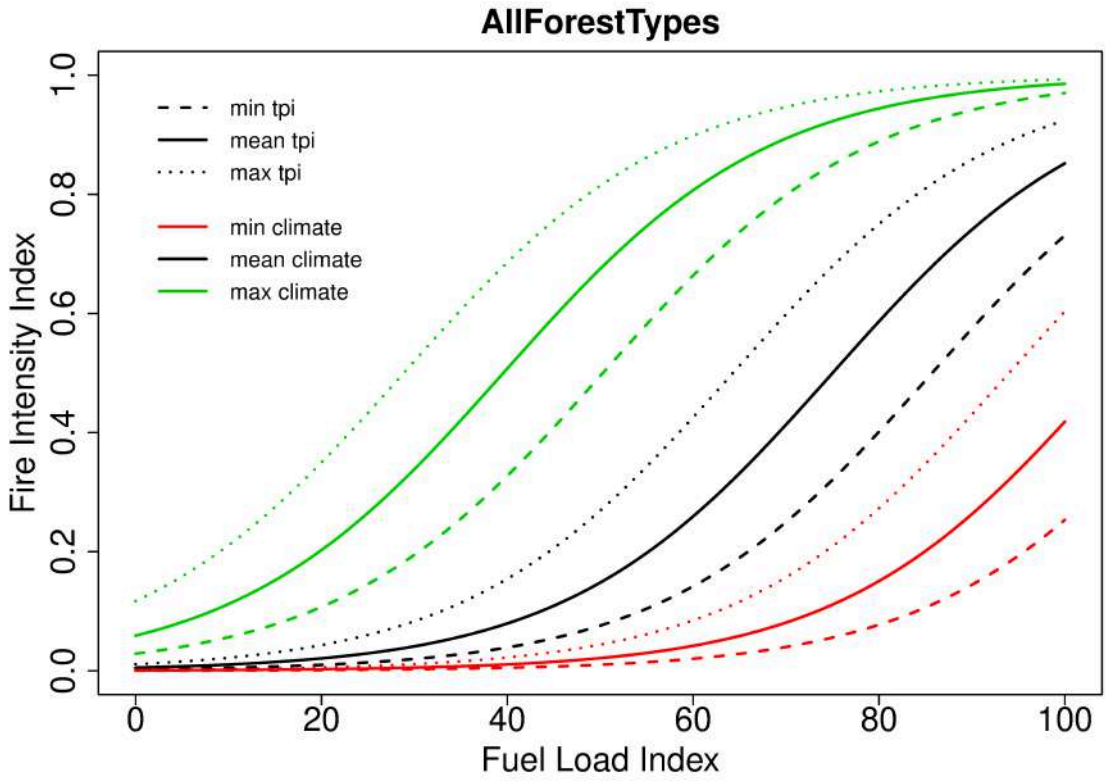

Figure 12: Fire Intensity Index (0 - 1), which served as one of the components of the wildfire mortality function to determine the probability of a high mortality response (i.e., death of all overstory vegetation) in a cell after burning. Fire intensity was a Logistic function of the Fuel Load Index of the focal cell, the Topographic Position Index (tpi) of the focal cell and the wildfire Climate Index for the current timestep, as depicted.

The Fuel Load Index (F) of a focal cell is derived by computing the Gaussian kernel intensity of coarse and fine fuels in the ecological neighborhood of the focal cell, as follows. First, a Gaussian kernel with a bandwidth (standard deviation) of 30 m (98 ft) is placed over each neighboring cell within 90 m (295 ft) of the focal cell. To compute the intensity of coarse fuels, the height of the Gaussian kernel, which serves as the weight of the cell, is based on a cumulative Weibull function of tree breast height Age (as a proxy for coarse fuel loads), as follows and as shown in **Figure 13**:

$$W_{jt} = 1 - e^{-(\frac{A_{jt}}{56.41896})^2}$$

where: A_{jt} = breast height Age (yrs) of the j^{th} neighboring cell in the t^{th} timestep; and W_{jt} = Weight assigned to the j^{th} neighboring cell in the t^{th} timestep.

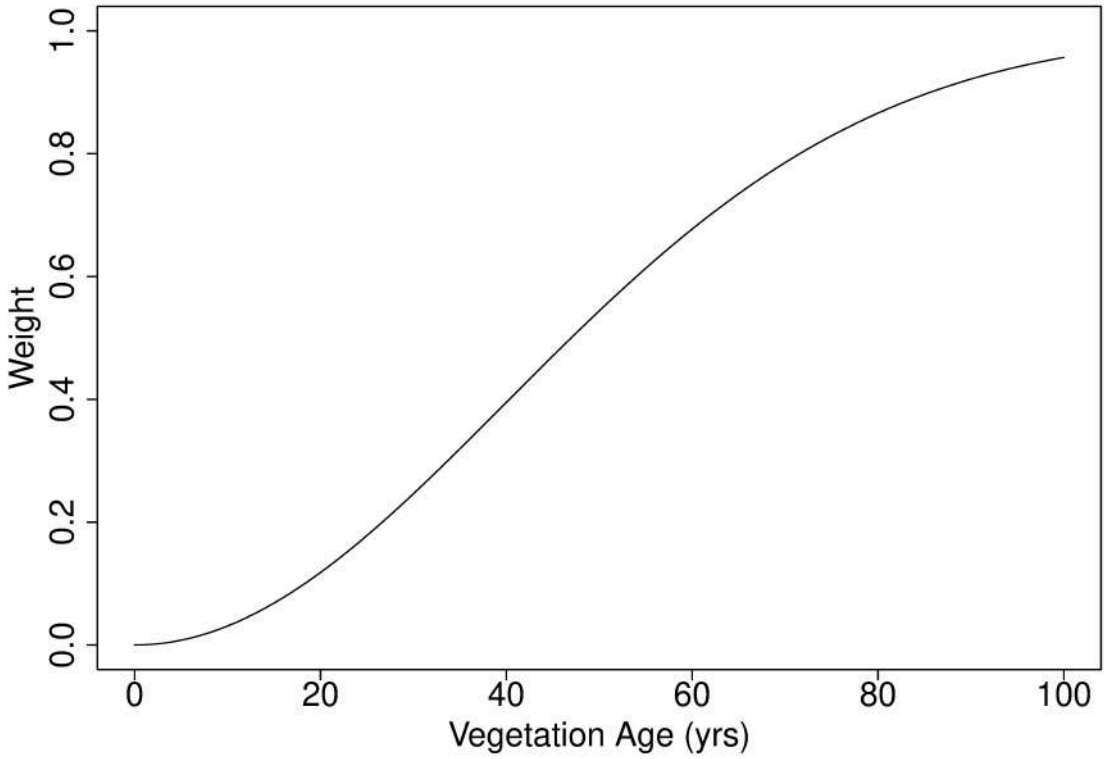

Figure 13: Weight of a cell given as a cumulative Weibull function of breast height Age (yrs) to determine the intensity of coarse fuels in the neighborhood of a focal cell based on a Gaussian kernel. The kernel intensity of coarse fuels was combined with the kernel intensity of fine fuels (see below) to determine the intensity of fuels for a focal cell, which combined with other factors to determine the probability of a high mortality response (i.e., death of all overstory vegetation) in a cell after burning (see text for details).

Thus, once a cell reaches ~ 100 years breast height Age it is assigned the maximum weight (i.e., full coarse fuel load production).

Next, to compute the intensity of fine fuels, the height of the Gaussian kernel is based on a cumulative Weibull function of the time (years) since the last fire (as a proxy for fine fuel loads), as follows and as shown in **Figure 14**:

$$W_{jt} = 1 - e^{-(\frac{Y_{jt}}{10})}$$

where: Y_{jt} = time (yrs) since the last fire of the j^{th} neighboring cell in the t^{th} timestep; and W_{jt} = Weight assigned to the j^{th} neighboring cell in the t^{th} timestep.

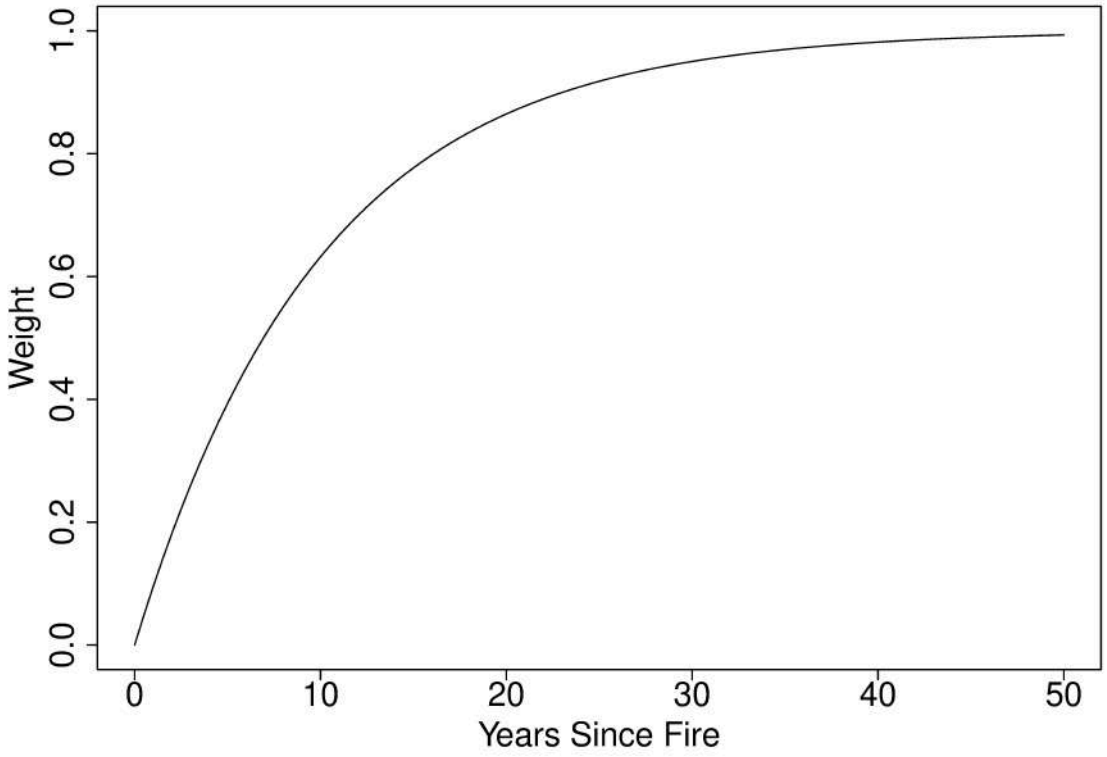

Figure 14: Weight of a cell given as a cumulative Weibull function of the time (yrs) since the last fire to determine the intensity of fine fuels in the neighborhood of a focal cell based on a Gaussian kernel. The kernel intensity of fine fuels was combined with the kernel intensity of coarse fuels (see above) to determine the intensity of fuels for a focal cell, which combined with other factors to determine the probability of a high mortality response (i.e., death of all overstory vegetation) in a cell after burning (see text for details).

Thus, once a cell reaches ~ 30 years since the last fire it is assigned the maximum weight (i.e., full fine fuel load production).

The bandwidth (standard deviation) of the Gaussian kernel is 30 m; thus, 95 % of the Fuel Load Index of a focal cell is determined by the breast height Age (coarse fuels) and time since the last fire (fine fuels) of neighboring cells within 2 standard deviations or 60 m of the focal cell.

Lastly, the final Fuel Load Index (F) of the focal cell is computed as the average of the coarse and fine Fuel Load indices and then standardized (by dividing by the maximum theoretical value) to range from 0 - 100. The index is 0 when all cells within ~ 90 m of the focal cell have breast height age equal to 0 years and time since last fire equal to 0 years, and approaches 100 when the entire neighborhood is comprised of cells with breast height age > 100 years and time since last fire > 30 years. Note, the Fuel Load Index is computed independent of cover type and focal landscape.

Resistance - Resistance to high mortality fire (i.e., the ability to survive burning) for any given cell in any given timestep is modeled as a negative exponential function of vegetation breast height Age (yrs), such that the rate of exponential decline with age decreases with fire intensity, as follows, and for example as shown for Sierra Mixed Conifer in the Yuba River landscape in **Figure 15**:

$$r_{jt} = b_5 + b_6 I_{it}$$

$$M_{it} = b_4 e^{(r_{it} A_{it})}$$

where: b_4 - b_6 = user-specified parameters that can vary among cover types (see below); I_{it} = Fire Intensity Index of the i^{th} cell in the t^{th} timestep (as defined above); r_{it} = rate of exponential decline in the

probability of high mortality with vegetation age; A_{it} = vegetation breast height Age (yrs) of the i^{th} cell in the t^{th} timestep; and M_{it} = probability of high mortality after burning of the i^{th} cell in the t^{th} timestep.

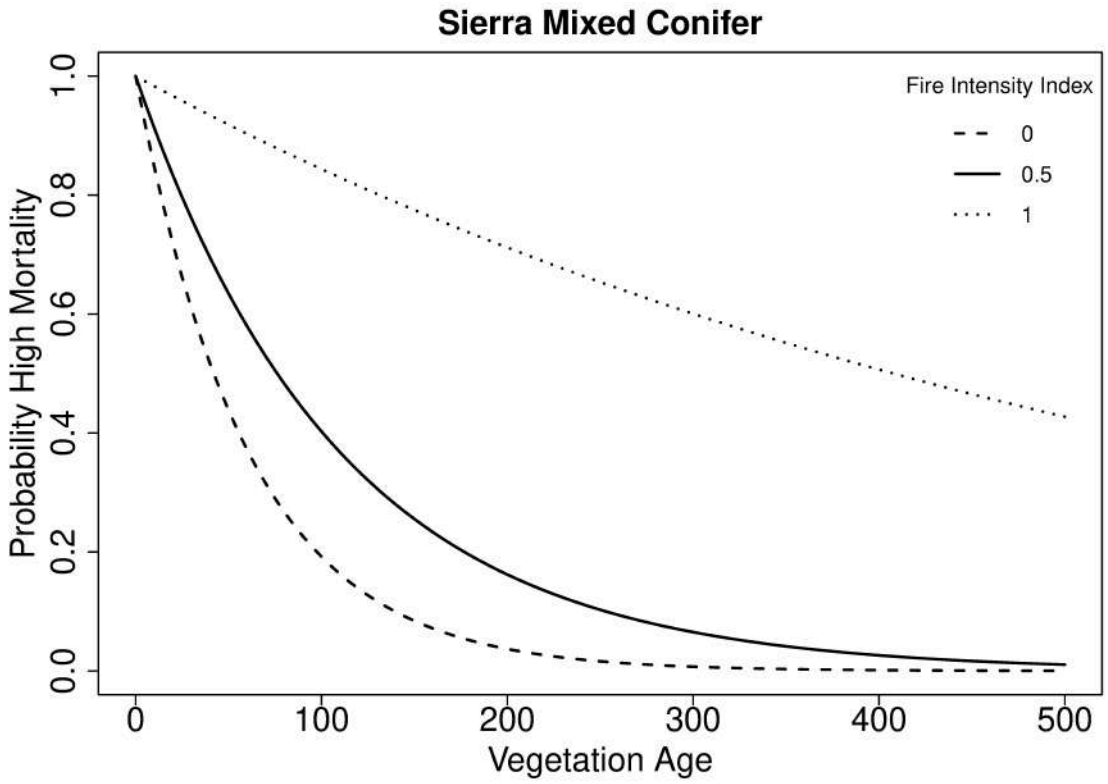

Figure 15: Probability of high mortality (i.e., death of overstory vegetation) in a cell after burning as negative exponential function of vegetation breast height Age (yrs) and fire intensity (see text for details), shown here for the Sierra Mixed Conifer forest cover type in the Yuba River landscape in the Northern Sierra ecoregion. Probability of high mortality decreased with increasing vegetation Age, but the rate of exponential decline decreased (i.e.,shallower slope) with increasing fire intensity, such that for any given Age the probability of high mortality increased with increasing fire intensity.

Given this function, the final wildfire Mortality Index is on the probability scale (0 - 1) such that a value of 0 results in a low mortality response to fire, and as the value increases to 1 the probability of a high mortality response (i.e., complete overstory mortality) increases accordingly.

We use expert opinion to specify the initial beta coefficients for each cover type, but these are subsequently modified as necessary during model calibration for each focal landscape (see Model Calibration). We hold b_4 constant at 1 across all cover types and landscapes so that the probability of high mortality is always 1 when the vegetation Age is 0. We vary the b_5 and b_6 coefficients among cover types and landscapes to reflect differences in reported historical mean fire return intervals and high mortality rates among cover types (see Model Calibration) - increasing or decreasing the rate of exponential decline in high mortality with increasing vegetation Age as a function of fire intensity to reflect differences among cover types in their propensity for high mortality following fire of any given intensity. Note, there is no empirical basis for assigning these coefficients to each cover type or landscape, so we use these coefficients as calibration parameters (see Model Calibration), increasing or decreasing them as necessary to achieve the target high mortality rates that we assigned to each cover type in each landscape. As an example, the probability of high mortality wildfire assigned for Sierra Mixed Conifer (SMC) forest in the Yuba River landscape is depicted in **Figure 15**. Note that the probability of high mortality following fire is 1 when the vegetation Age (yrs) is 0 and then decreases rapidly with increasing vegetation Age, reflecting the increasing

resistance to fire with tree age. Also note that for very young cells fire intensity has almost no effect on the probability of high mortality, and that the effect of fire intensity is greatest during the early to mid seral stages of successional development.

Wildfire Disturbance Transitions

Following each wildfire disturbance event, each cell that suffers a high mortality response (i.e., death of all overstory vegetation) immediately transitions to the Open vegetation state. Forested cells remain in the Open state until successful tree regeneration occurs as part of forest succession, and shrubland cells immediately began regrowth via sprouting as part of shrubland succession, as described below. Each cell that suffers a low mortality response remains in its current developmental stage and vegetation state.

Succession Climate

Climate conditions affecting succession during each timestep of the simulation are governed by a single global forcing variable that operates across all cover types within a single timestep; thus, a single Succession Climate Index coefficient is assigned to each timestep. The Index is incorporated into the probability of tree regeneration function, as described below.

Like the Wildfire Climate Index, the Succession Climate Index is based on the inverted 5-year average Palmer Modified Drought Severity Index (PMDI), as described above. The only difference is that for the Succession Climate Index we do not shift and rescale the index (the last step in the derivation of the Wildfire Climate Index) as it is not necessary to do so given how we use it in the functions below. Thus, as in the original PMDI, positive values still represent drier conditions and negative values represent wetter conditions and the range of values is greater. The final Succession Climate Index trajectory represents a vector of coefficients, one for each 5-year timestep of the simulation for each focal landscape, as shown in **Figure 16** for the Yuba River landscape.

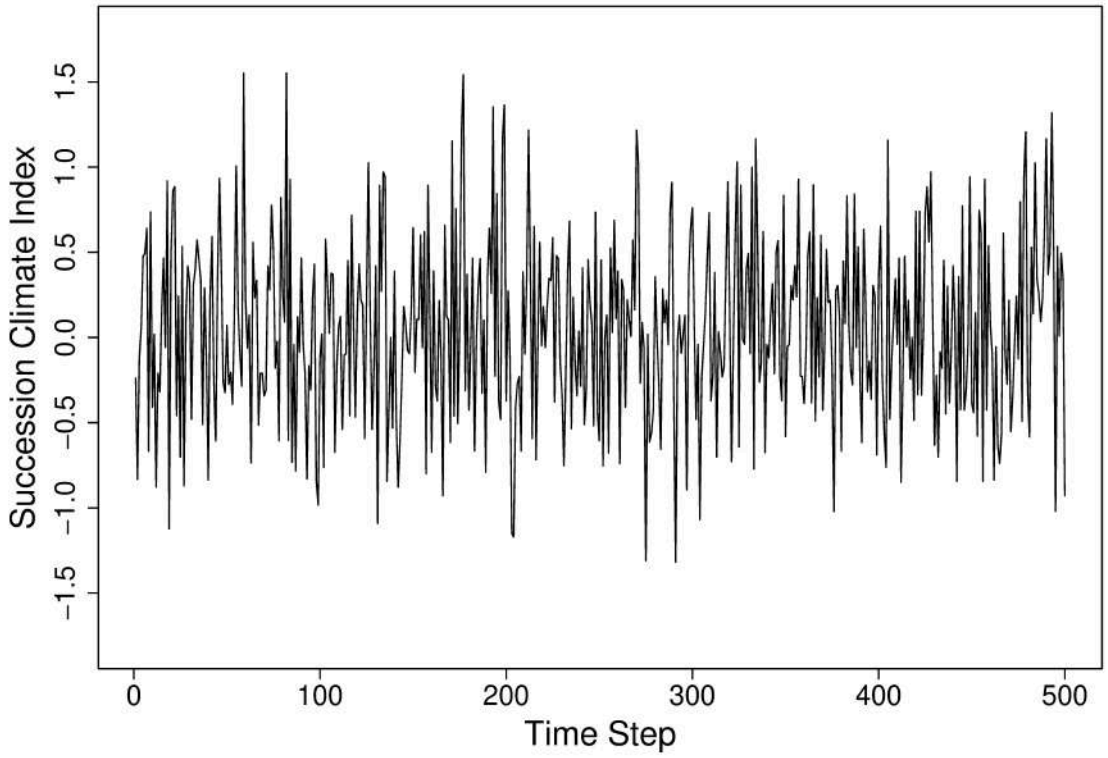

Figure 16: Succession Climate Index trajectory for the Yuba River landscape corresponding to 500 5-year timesteps in the simulation. The Climate Index was based on the inverted 5-year averaged, inverse-distance weighted mean Palmer Modified Drought Severity Index (PMDI) for the sample point locations within the Northern Sierra ecoregion relative to the focal landscape (Yuba River watershed in this case). Note, here we inverted PMDI so that positive values represented drier conditions and negative values represented wetter conditions (see text for details).

Succession Transitions

Succession transitions are modeled separately for shrublands and forests; all other cover types are treated as non-seral and consist of a single state that remains constant over the duration of the simulation.

Shrublands

Shrubland succession is modeled probabilistically as a Logistic function of Developmental Stage Age (years in current developmental stage) and Site Index. Following high-mortality disturbance, shrublands transition immediately to the *Early-shrub* Developmental Stage (and Vegetation State) and initiate secondary succession. Transitions to subsequent Developmental Stages or Vegetation States are determined as follows:

$$P_{it} = \frac{1}{1 + e^{-(b_0 + b_1 A_{it} + b_2 S_i)}}$$

where: b_0 - b_2 are user-specified Logistic parameters that can vary among state transitions and among shrubland cover types; A_{it} = Developmental Stage Age of the i^{th} cell in the t^{th} timestep; S_i = Site Index of the i^{th} cell; and P_{it} = probability of Developmental Stage transition of the i^{th} cell in the t^{th} timestep.

We use expert opinion guided by the corresponding LandFire Biophysical Setting (BPS) models to parameterize Logistic functions for each transition for each cover type, and these are held constant across landscapes. For example, the *Early-shrub* to *Mid-shrub* transition for Chaparral is as shown in **Figure 17**.

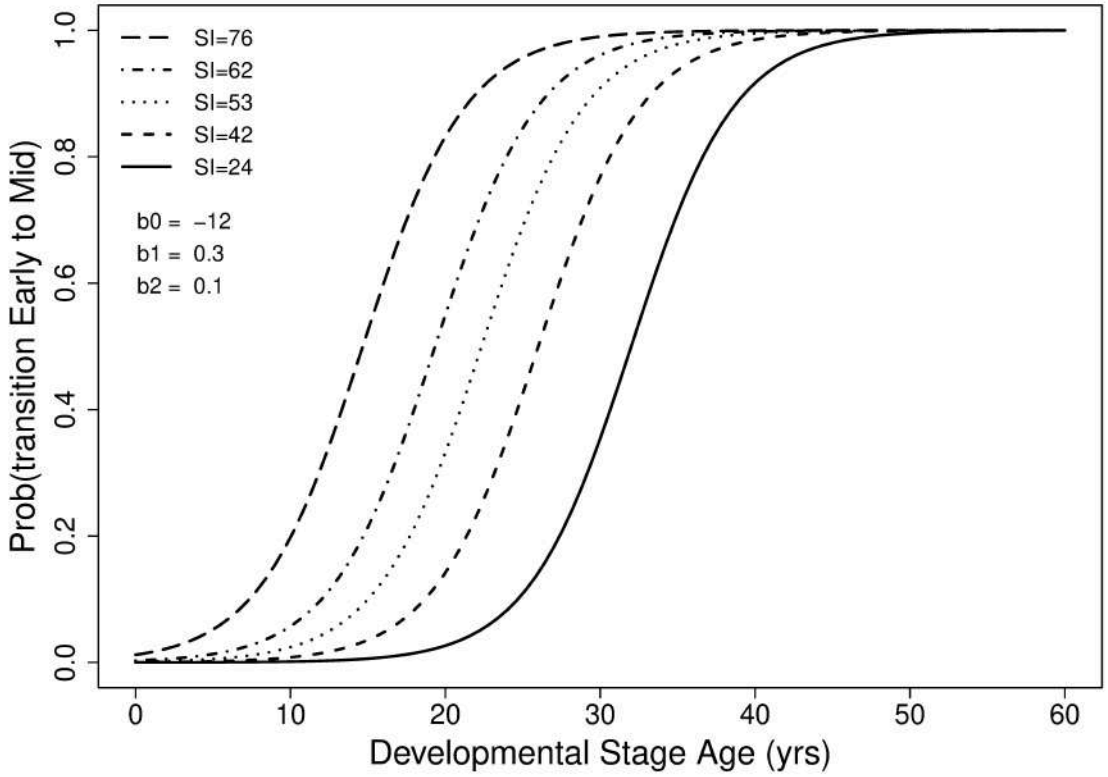

Figure 17: Probability of vegetation succession transition from the Early-shrub Developmental Stage (or Vegetation State) to the Mid-shrub Developmental Stage (or Vegetation Stage) for Chaparral shrublands as a function of Developmental Stage Age (years) and Site Index (SI). Note, Developmental Stage Age is equal to the number of years since transitioning to the current stage.

The *Mid-shrub* to *Late-shrub* transition for Chaparral is as shown in **Figure 18**. Note, Developmental Stage Age represents the number of years since transitioning to the current stage, which is the *Mid-shrub* stage in this case.

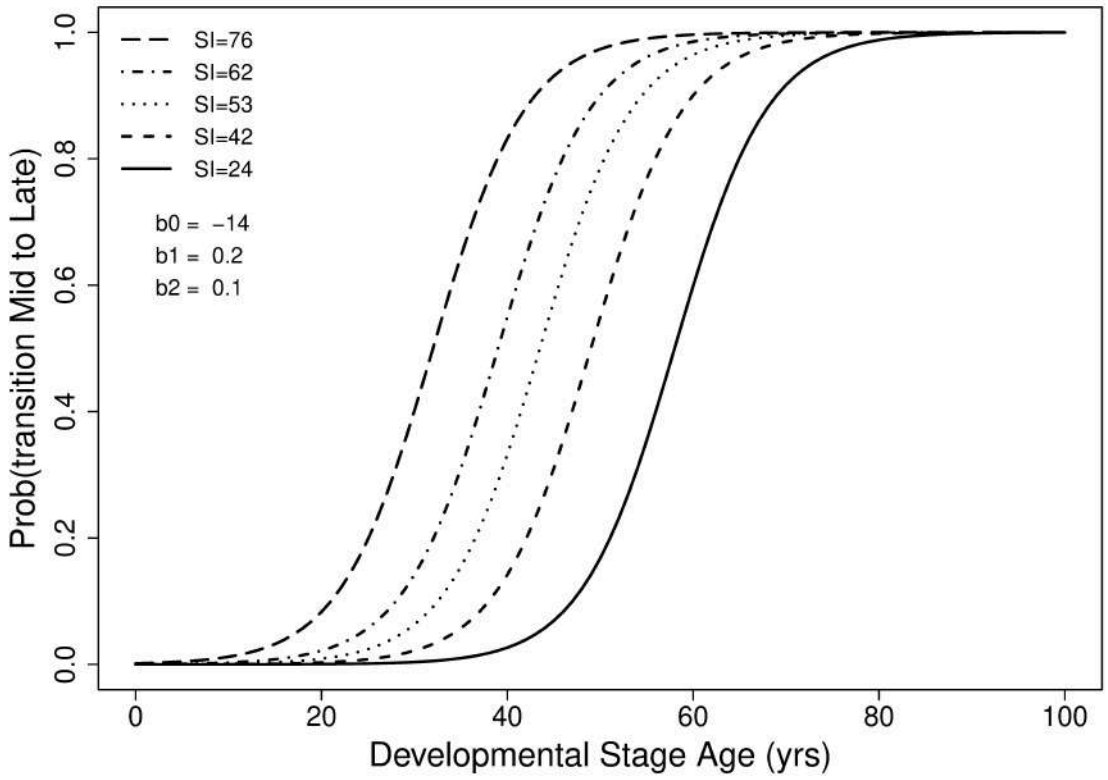

Figure 18: Probability of vegetation succession transition from the Mid-shrub Developmental Stage (or Vegetation State) to the Late-shrub Developmental Stage (or Vegetation Stage) for Chaparral shrublands as a function of Developmental Stage Age (years) and Site Index (SI). Note, Developmental Stage Age is equal to the number of years since transitioning to the current stage.

Note, shrublands in the Late-shrub stage remain in that stage indefinitely until the next high-mortality wildfire disturbance.

Forests

Forest succession is modeled in three stages: 1) tree establishment, 2) tree growth, and 3) state transitions. However, for organizational purposes it is convenient to describe forest succession has having seven steps, as follows:

1. Tree establishment: First, we model the probability of successful tree regeneration (defined as achieving breast height or 4.5 ft tall and 1 inch diameter at breast height) in an unoccupied forest cell.

2. Tree Height Growth: Following tree establishment, we model continuous tree height growth over time.

3. Tree Diameter Growth: Following tree establishment, we also model continuous tree diameter at breast height (dbh) over time.
4. Quadratic Mean Diameter: Following tree growth at the cell level, we compute the quadratic mean diameter (QMD) of established trees within a 40-m radius window centered on each forested cell.
5. Tree Cover: Following tree growth at the cell level, we also compute the percent established tree cover within a 40-m radius window centered on each forested cell.
6. Senescence: Following tree establishment, we also model the probability of senescence and tree death over time.
7. Vegetation States: Lastly, we classify cells into several discrete States, including: 1) Developmental Stage based on tree height bins, 2) Size Class based on QMD bins, and 3) Tree Cover Class based on percent tree cover bins.

Tree Establishment

Tree establishment in an unoccupied forested cell (i.e., a cell in the *Open* Developmental Stage or Vegetation State) is modeled probabilistically as a Logistic function of Burn Severity, number of years post-fire, Mesic Index, Seed Proximity Index, and Succession Climate Index as follows:

$$P_{it} = \frac{1}{1 + e^{-(b_0 + b_1 B_{it} + b_2 Y_{it} + b_3 M_i + b_4 X_{it} + b_5 C_t)}}$$

where: b_0 - b_5 are estimated Logistic parameters that can vary among forest cover types; B_{it} = burn severity of the i^{th} cell in the t^{th} timestep, which is always equal to 1 (high mortality) in this application; Y_{it} = number of years post-fire of the i^{th} cell in the t^{th} timestep; M_i = Mesic Index of the i^{th} cell; X_{it} = Seed Proximity Index of the i^{th} cell in the t^{th} timestep; C_t = Succession Climate Index in the t^{th} timestep; and P_{it} = probability of successful tree establishment in the i^{th} cell in the t^{th} timestep.

The choice of this "regen" function and the covariates is based largely on the work of Shive et al. (2018), with modifications. We estimate the Logistic parameters of the regen function (except for the Succession Climate Index, see below) based on the empirical data used in Shive et al. (2018). Specifically, we limit the plot data analyzed by Shive et al. (2018) to the fires occurring primarily in the Northern Sierra ecoregion, as shown in **Figure 1** and listed in **Table 2**.

Table 2: Wildfires sampled by Shive et al. 2018 that we included to model post-fire tree regeneration following high mortality wildfire.

Fire	**Fire Year**
PENDOLA	1999
SHOWERS	2002
POWER	2004
FREDS	2004
STRAYLOR	2004
HARDING	2005
BASSETTS	2006
RALSTON	2006
ANTELOPE	2007
MOONLIGHT	2007
CUB	2008
AMERICAN RIVER	2008
RICH	2008

This includes a set of 1,022 60-m^2 plots ranging in elevation from 1,000 - 2,300 m. It is worth noting that there are no observations of sites > 2,300 m in elevation; therefore, the fitted relationships may not predict

regeneration accurately at the highest elevations where upper montane forests (e.g., red fir, lodgepole pine, and subalpine conifer) predominate. Indeed, given the often harsh microclimate conditions at these higher elevations it is quite possible that the fitted relationships may over-predict regeneration rates at these higher elevations. Unfortunately, no empirical data from these higher elevations exists at this time, nor is there consistent expert opinion on how to model regeneration at these sites in the absence of empirical data. Thus, until addition empirical data becomes available, we are compelled to use the fitted relationships at these higher elevation sites and simply acknowledge the potential bias.

Similarly, there are no observations on ultramafic soils (a.k.a. serpentine); therefore, the fitted relationships may not predict regeneration accurately on these sites. However, results from the DeSiervo et al. (2015) study of serpentine versus non-serpentine sites in the Northern Sierra indicate roughly a 33% reduction in tree basal area and above-ground tree biomass and a 60% reduction in tree density on serpentine (i.e., ultramafic) sites, suggesting that the primary affect of serpentine is to reduce tree establishment. Consequently, we reduce the probability of tree establishment, all other things being equal, by an amount determined through model calibration to achieve an average 33 % reduction in our cumulative tree biomass index (see below). Specifically, we multiply the probability of tree establishment derived from the fitted relationship by 0.2 (i.e., 80% reduction).

For each plot, we extract the binary regeneration value (CONbnJP) from the Shive et al. (2018) dataset as provided, in which the response is coded as either 0 (no conifer regeneration) or 1 (successful conifer regeneration). This variable serves as the response variable in the binary logistic regression. For the predictors, we derive values for the first four covariates in the Logistic function above, as follows:

- *Burn Severity* - We extract the burn severity value (IA_Filt) from the Shive et al. (2018) dataset as provided, which is based on the Initial Assessment (IA) of burn severity immediately post-fire. As described by Shive et al. (2018), burn severity (IA_Filt) was generated from 30 m pixel Landsat imagery, using the Relativized differenced Normalized Burn Ratio (RdNBR; Miller and Thode 2007). RdNBR was derived by calculating the Normalized Burn Ratio (NBR) that is sensitive to chlorophyll and moisture (using the near- and mid-infrared, Landsat bands 4 and 7) for both pre- and post-fire imagery, which were then differenced (dNBR) and relativized (RdNBR) to account for variation in pre-fire cover. Based on the threshold value of 700 reported by Shive et al. (2018), we transform burn severity (IA_Filt) to a binary variable ($< 700 = 0$ or low severity, $\geq 700 = 1$ or high severity) to align with how we treat burn severity (i.e., mortality) in LDSim.

- *Years Post-Fire* - We extract the number of years post-fire (yrsPost) from the Shive et al. (2018) dataset as provided, which ranges from 3 to 12 years.

- *Mesic Index* - We extract the value of our Mesic Index layer, which is derived as the average of five variables: Annual Precipitation, Topographic Wetness Index, Heat Load Index, Water Balance Deficit, and Available Water Storage (see **Appendix A** for details). Note, for consistency with the LDSim model structure and for simplicity, we substitute the Mesic Index variable for the suite of variables associated with site productivity analyzed by Shive et al. (2018), which included Aspect, Slope, Actual Evapotranspiration, Annual Precipitation, Climatic Water Deficit and Snow water Equivalent.

- *Seed Proximity Index* - We extract the value of the Gaussian kernel-based seed availability proxy (SAP) for the 150-m kernel bandwidth (A6_SP_1) from the Shive et al. (2018) dataset as provided, rescale this index to range 0 - 100 (for consistency with our Seed Proximity Index described below), and use this rescaled value for estimating the model parameters (see below). For consistency with the LDSim model structure and for simplicity, we substitute our own Seed Proximity Index variable for the Shive et al. (2018) SAP variable, which are conceptually similar.

  Briefly, our Seed Proximity Index layer is derived by computing the Gaussian kernel intensity of mature trees in the ecological neighborhood of the focal cell, as follows. First, a Gaussian kernel is placed over each neighboring cell within 180 m (591 ft) of the focal cell. The height of the Gaussian kernel is based on a Logistic function of tree breast height Age (as a proxy for seed production), as

follows and as shown in **Figure 19**:

$$W_{jt} = \frac{1}{e^{((-A_{jt}+50)/10)} + 1}$$

where: A_{jt} = breast height Age (yrs) of the j^{th} neighboring cell in the t^{th} timestep; and W_{jt} = Weight assigned to the j^{th} neighboring cell in the t^{th} timestep.

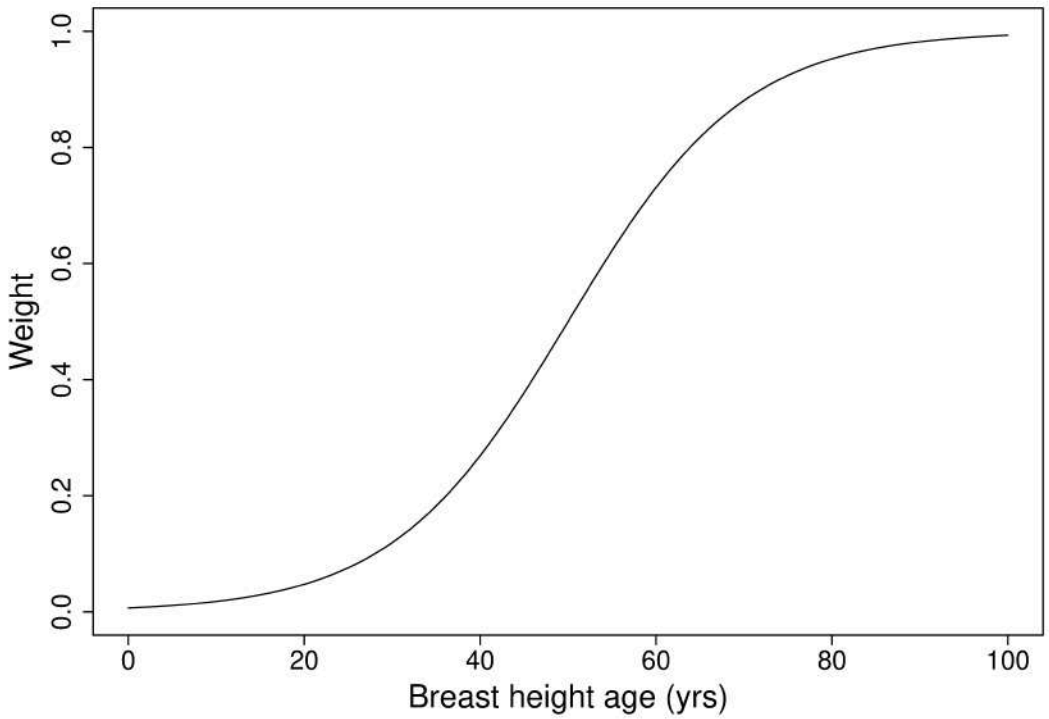

Figure 19: Cell weight as a Logistic function of Age as used in the Seed Proximity Index function. Note, cell weight represents the weight of each cell in the Gaussian kernel intensity of seed production in the ecological neighborhood of the focal cell.

Thus, a tree < 20 years in breast height Age has almost no weight, but once a tree reaches 100 years of breast height Age it is assigned the maximum weight (i.e., full seed production). The standard deviation (bandwidth) of the Gaussian kernel is based on its estimated tree height, which is a function of Cover type, breast height Age and Site Index, as described in **Appendix A** for the Age layer. Thus, a tree 30.5 m (100 ft) tall has a bandwidth of 30.5 m, which results in 95 % of its seed dispersing within 2 standard deviations or 61 m (200 ft) and > 99 % of its seed dispersing within 3 standard deviations or 91.5 m (300 ft). Essentially, seed dispersal occurs up to a maximum of 3 tree heights from the cell. Lastly, the Gaussian kernels are summed across all neighboring cells and the value at the focal cell is divided by the maximum theoretical value. Thus, the final index ranges from 0 - 100. It is 0 when there are no trees of seed-bearing age within a distance of roughly 180 m (591 ft) and approaches 100 when the entire neighborhood is comprised of trees > 100 years and reaching maximum tree heights on the highest Site Index.

The final dataset consists of 1,022 observations. We analyze the data using a Generalized Linear Mixed Effects (GLMM) model with a Binomial error and Logit link. The response variable is binary presence/absence of conifer regeneration. The four covariates described above are treated as independent covariates and have the distributions shown in **Figure 20**. Fire as a categorical factor is included as random effect to account for variation among individual fires. We fit the model using the R glmer()

function in the lme4 package. Note, the dataset is not sufficient to allow us to model regeneration separately for each forest cover type, nor did Shive et al. (2018) account for the variation among cover types, so we fit a single global model and applied it to all forest cover types.

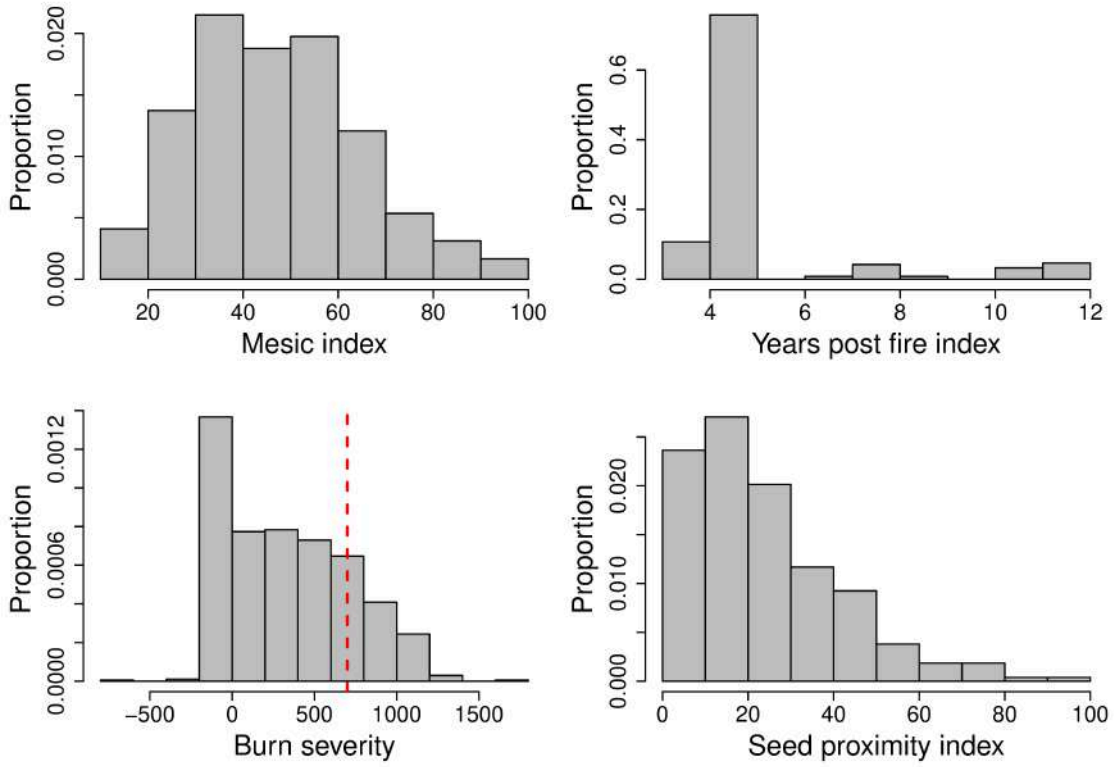

Figure 20: Distribution of the four predictors across 1,022 plots from Shive et al. (2018) used to model the probability of tree regeneration in an unoccupied forest cell.

The fitted model results in a probability of successful tree regeneration to breast height for any combination of values of the four covariates in the model. Unfortunately, there is no simple empirical way to incorporate climate into the Logistic Regression model based on these data. In part, this is because we have no way of knowing in which years after the fire regeneration of conifer trees occurred so that we could associate it with the climate of that year; all we know is that regeneration occurred by the time of the sampling, which was anywhere between 3 - 12 years after the fire. Moreover, successful tree establishment is likely affected by climate conditions over several years following disturbance, since it may take 7-12 years post-fire, or longer, to establish to breast height. Unfortunately, while it is possible to summarize the average climate conditions during the 12-year post-fire period, we would have no way of modeling how variation in climate affected regeneration since we would have only a single observation of climate. Thus, we add the Succession Climate Index variable to the Logistic model post-hoc by subjectively assigning a beta coefficient such that the probability of regeneration due to the Succession Climate Index roughly matches the variability observed among fires due to the random Fire effect.

The final model includes five covariates. As such, there is no single figure that can display the fitted relationships, noting that burn severity is effectively a constant in the model (i.e., we apply the model only to cells having experienced a high-mortality wildfire) and thus can be excluded from consideration here. Instead, the following figures display the relationship between three of the predictors and the probability of regeneration, holding the fourth predictor constant at either its maximum or minimum value in order to show the range of results. The first figure **Figure 21** depicts the relationships for Years Post-Fire, Mesic Index, and Succession Climate Index while holding Seed Proximity Index constant at its maximum value.

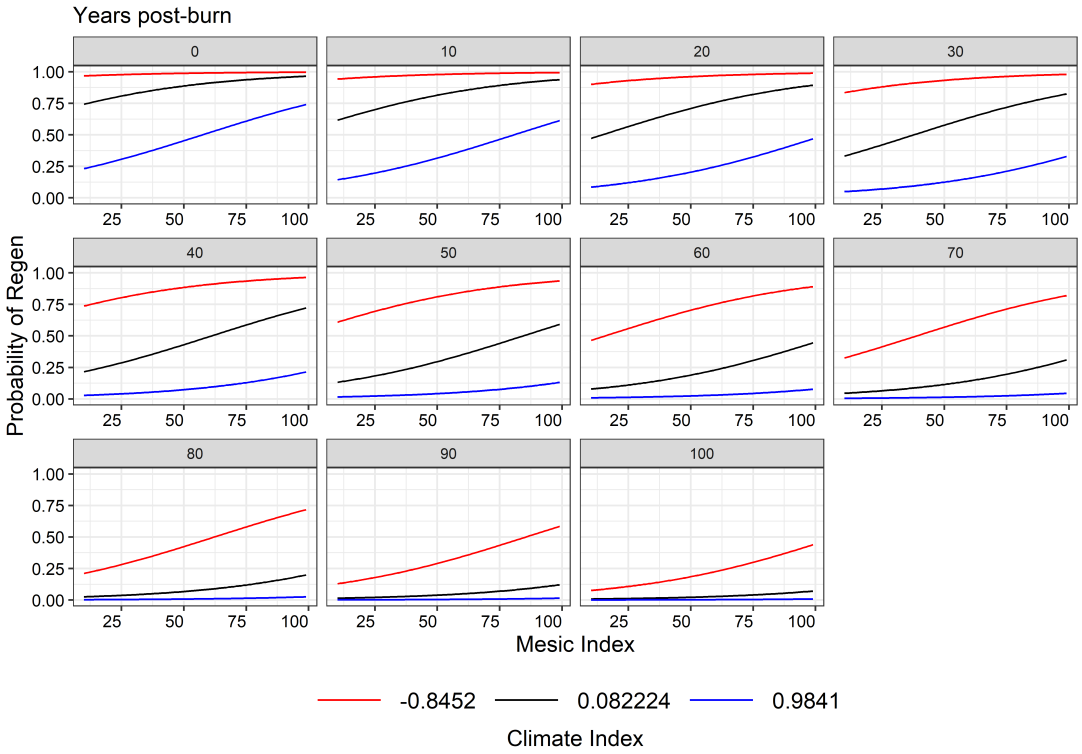

Figure 21: Probability of successful tree regeneration to breast height as a function of the number of years post fire (shown in the facets from 0 to 100 years), Site Index (x-axis), and succession Climate Index (colored lines shown for the minimum, mean and maximum values) when the Seed Proximity Index is maximum.

The next figure **Figure 22** depicts the relationships for Years Post-Fire, Mesic Index, and Succession Climate Index while holding Seed Proximity Index constant at its minimum value.

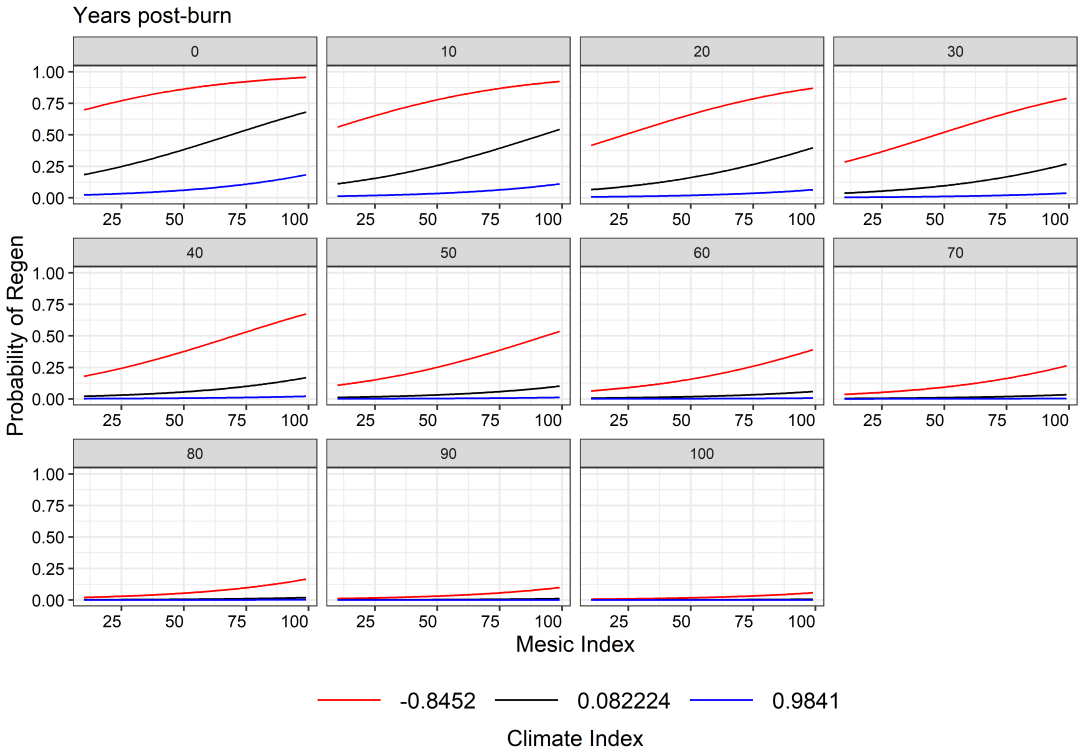

Figure 22: Probability of successful tree regeneration to breast height as a function of the number of years post fire (shown in the facets from 0 to 100 years), Site Index (x-axis), and succession Climate Index (colored lines shown for the minimum, mean and maximum values) when the Seed Proximity Index is minimum.

The next figure **Figure 23** depicts the relationships for Years Post-Fire, Mesic Index, and Seed Proximity Index while holding Succession Climate Index constant at its maximum (i.e., driest) value.

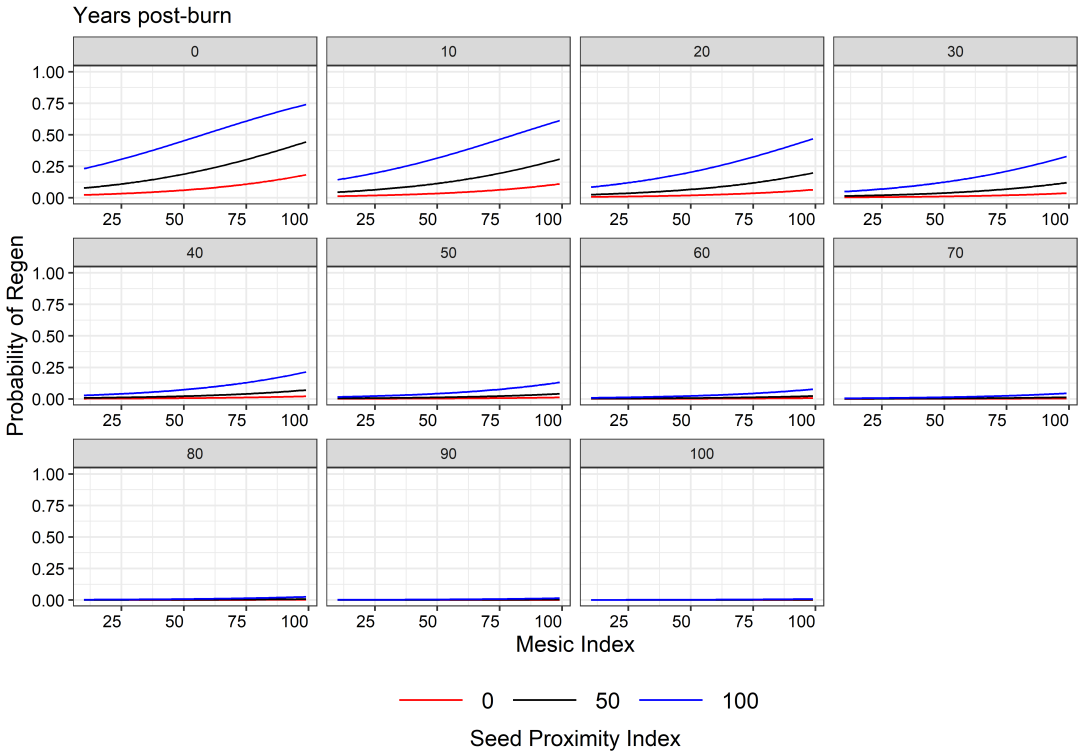

Figure 23: Probability of successful tree regeneration to breast height as a function of the number of years post fire (shown in the facets from 0 to 100 years), Site Index (x-axis), and Seed Proximity Index (colored lines shown for the minimum, mean and maximum values) when the succession Climate Index is maximum (i.e., driest).

The last figure **Figure 24** depicts the relationships for Years Post-Fire, Mesic Index, and Seed Proximity Index while holding Succession Climate Index constant at its minimum (i.e., wettest) value.

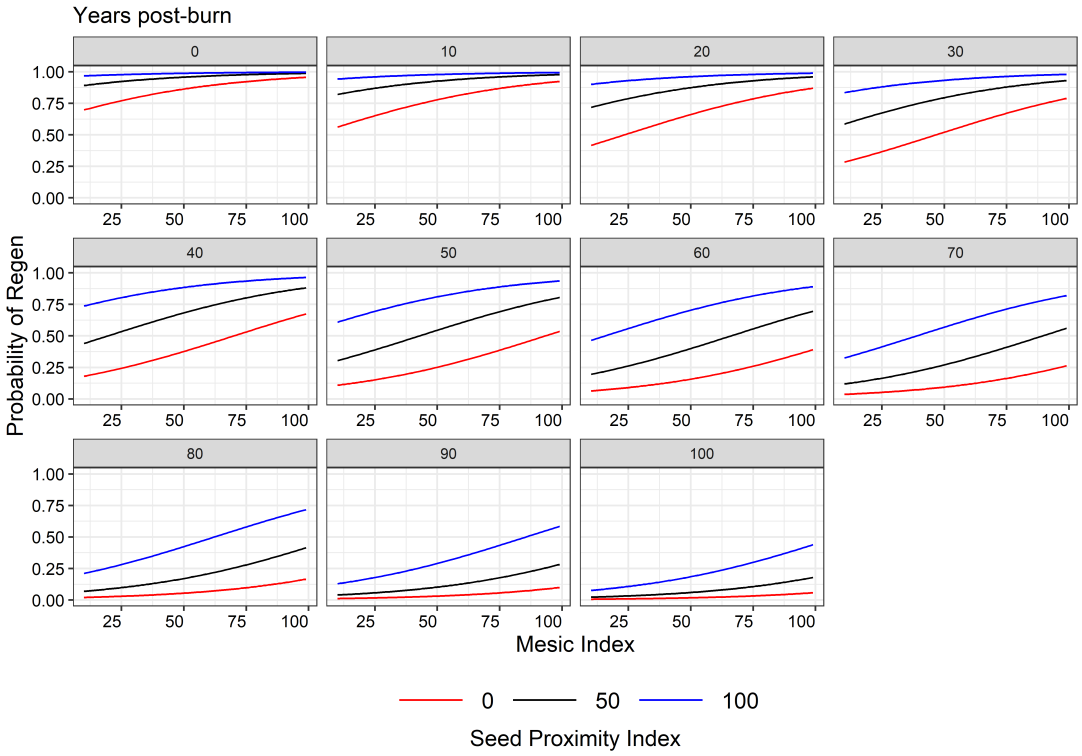

Figure 24: Probability of successful tree regeneration to breast height as a function of the number of years post fire (shown in the facets from 0 to 100 years), Site Index (x-axis), and Seed Proximity Index (colored lines shown for the minimum, mean and maximum values) when the succession Climate Index is minimum (i.e., wettest).

The final set of Logistic model parameters (beta coefficients) for the probability of tree regeneration function are listed in **Table 3**, noting that in the simulation Burn Severity (burnSev) is always equal to 1, reflecting the fact that the cell has experienced high mortality from wildfire (and thus is in the *Open* Developmental Stage or Vegetation State).

Table 3: Logistic model parameters (beta coefficients) for the probability of tree regeneration function used to model tree regeneration following high mortality wildfire, based on data from Shive et al. 2018.

Parameter	**Beta coefficient**
intercept	-0.9282727
burnSeverity	-0.6003258
yrsPost	-0.0586678
mesicIndex	0.0251890
seedProximity	0.0254282
climate	-2.5000000

Tree Height Growth

Following tree establishment in a forested cell, we model continuous tree height growth over time in the absence of a high-mortality disturbance as a function of breast height Age and Site Index. To establish the tree height growth function, we use FIA plot data from within the Northern Sierra ecoregion, consisting of 714 plots uniformly distributed across the ecoregion (**Figure 1**), containing 24,288 trees with breast height age (yrs) and tree height (ft) data, although we reduce this to 597 plots containing 21,898 trees on areas we

map as forest cover. For modeling purposes, we convert breast height age to total tree age by adding 7 years to breast height age for non-mafic sites and 10 years for ultramafic sites. We recognize that many other local factors such as tree species and tree spacing affect real-world tree height growth, and thus using total tree Age and Site Index alone provides only an approximation of expected tree height, but we deem this sufficient for the purposes of this model application.

After evaluating several alternative functions and estimators, we use Non-Linear Least Squares (NLS) estimation to fit the following Monomolecular function to closely approximate the site index curves used in the Forest Vegetation Simulator (FVS) based on Dunning and Reineke (1933), Dunning (1942), Dolph (1987 and 1991), and Long and Shaw (2012).

$$H_{it} = (b_0 + b_2 SI_i)(1 - e^{-b_1 TA_{it}})$$

where: b_0 - b_2 are estimated parameters; SI_i = site index of the i^{th} cell; TA_{it} = total tree age of the i^{th} cell in the t^{th} timestep; and H_{it} = predicted tree height (ft) of the i^{th} cell in the t^{th} timestep;.

Note, in the function above we substitute our custom Site Index variable (as described below) for the conventional site index used in the references cited above because we are able to derive the former from several geospatial layers that we develop for the region (see **Appendix A**), whereas the latter requires age and height data for every location (which is not available).

We develop our custom Site Index variable based on several geospatial layers that we develop for the region that represent variables known to affect site productivity. Specifically, we develop two separate site productivity indices representing two major factors affecting site productivity and then combine them into a single composite site index for use in the function above, as follows:

First, we develop a site index based on moisture availability, which we term the Mesic Index, because moisture limitation is likely the principal driver of tree establishment and growth across much of the region. We derive the Mesic Index by combining the following variables, each of which either directly or indirectly affects the availability of moisture at a site:

- Precipitation
- Topographic Wetness Index
- Heat Load Index
- Water Balance Deficit
- Available Water Storage

Each of these variables are described briefly in **Table 1** and in more detail in **Appendix A**. Briefly, we standardize each of these variables based on benchmarks derived for the Northern Sierra ecoregion, compute the average standardized value, and standardize the result based on ecoregional benchmarks to serve as the Mesic Index.

Next, we develop a site index based on light and heat energy input, which we term the Energy Index, because energy limitation is likely a contributing driver of tree growth in the higher-elevation upper montane forests of the region and potentially on steep northeasterly aspects receiving relatively low solar radiation input. We derive the Energy Index by combining the following variables, each of which directly affects the availability of energy to support tree growth at a site:

- Growing Degree Days
- Heat Load Index
- Solar Radiation Index

Again, each of these variables are described briefly in **Table 1** and in more detail in **Appendix A**. Briefly, we standardize each of these variables based on benchmarks derived for the Northern Sierra ecoregion, compute the average standardized value, and standardized the result based on ecoregional benchmarks to serve as the Energy Index. It is worth noting that the Head Load Index, as an indirect measure of direct

incident solar radiation, is included in both the Mesic Index and the Energy Index because while the magnitude of direct incident solar radiation at a site indirectly affects moisture availability (i.e., sites with more solar radiation exhibit higher rates of evapo-transpiration and thus greater moisture limitation), it is a direct measure of light and heat energy available at a site.

We recognize that both moisture and energy limitation potentially play a role in tree height growth (as well as tree establishment), but that the relative importance of these two factors likely varies with elevation in the montane forests of the northern Sierras. At lower elevations moisture limitation likely predominates, but at higher elevations and on steep northeasterly aspects energy limitation likely becomes more important. Indeed, it is common to conceptualize forested systems as either moisture-limited or energy-limited, and it is commonly understood that lower-montane systems are best characterized as moisture-limited and that upper-montane systems are best characterized as energy-limited. We sought to account for the varying importance of these two factors along the elevation gradient. Moreover, we posit that this relationship differs between westside and eastside forests, owing to major orographic effects of the High Sierra crest that may not be fully captured in the geospatial variables at our disposal (i.e., those listed above).

Lastly, we combine the Moisture and Energy Indices into a composite Site Index by taking a weighted average of the two component indices, such that the relative weights vary with elevation, and we do so separately for westside and eastside forests. To determine the relative weighting as a function of elevation, we fit the Monomolecular function above, but substituting for Site Index (SI) a weighted combination of the Mesic and Energy Indices such that the relative weights vary with elevation according to the following weighted Logistic function:

$$SI_i = (\frac{1}{1 + e^{-(b_0 + b_1 E_i)}})EI_i + (1 - (\frac{1}{1 + e^{-(b_0 + b_1 E_i)}})MI_i)$$

where: b_0 and b_1 are estimated Logistic parameters; E_i = elevation (m) of the i^{th} cell; EI_i = Energy Index of the i^{th} cell; MI_i = Mesic Index of the i^{th} cell; and SI_i = Site Index of the i^{th} cell.

Note, this weighted Logistic function is substituted in the Monomolecular function above for the Site Index variable (SI) and the Logistic parameters b_0 and b_1 are estimated along with the Monomolecular parameters a, b and c simultaneously via NLS.

The estimated Logistic parameters support a gradual decrease in the relative weight of the Mesic Index and gradual increase in the relative weight of the Energy Index for westside forests, as depicted in **Figure 25**, which also depicts a Generalized Linear Model (GLM) fit of red fir forest presence along the same elevation gradient for reference purposes.

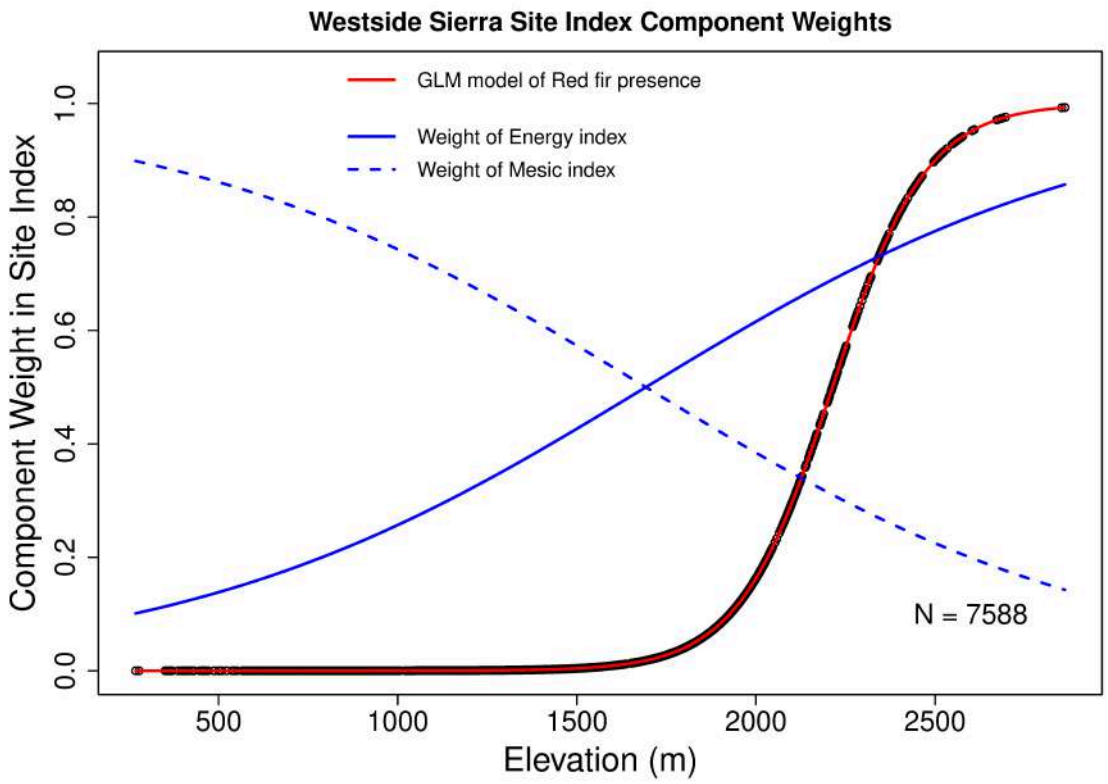

Figure 25: Relative component weights of the Mesic and Energy Indices as a function of Elevation in the composite Site Index to predict tree Height (ft) as a function of total tree Age (yrs) and Site Index for sites on the westside of the Northern Sierra ecoregion, based on the fit of a Nonlinear Least Squares (NLS) model to Forest Inventory and Analysis (FIA) data (see text for details). Note, total tree Age equaled breast height Age plus 7 years. Also shown is the distribution of FIA tree data along the elevation gradient and the fit of a Generalized Linear Model (GLM) of red fir presence.

The estimated Logistic parameters support an abrupt change in the relative weights of the Mesic and Energy Indices between 2,000 - 2,500 m in elevation for eastside forests, as depicted in **Figure 26**, which also depicts a GLM fit of red fir forest presence along the same elevation gradient for reference purposes.

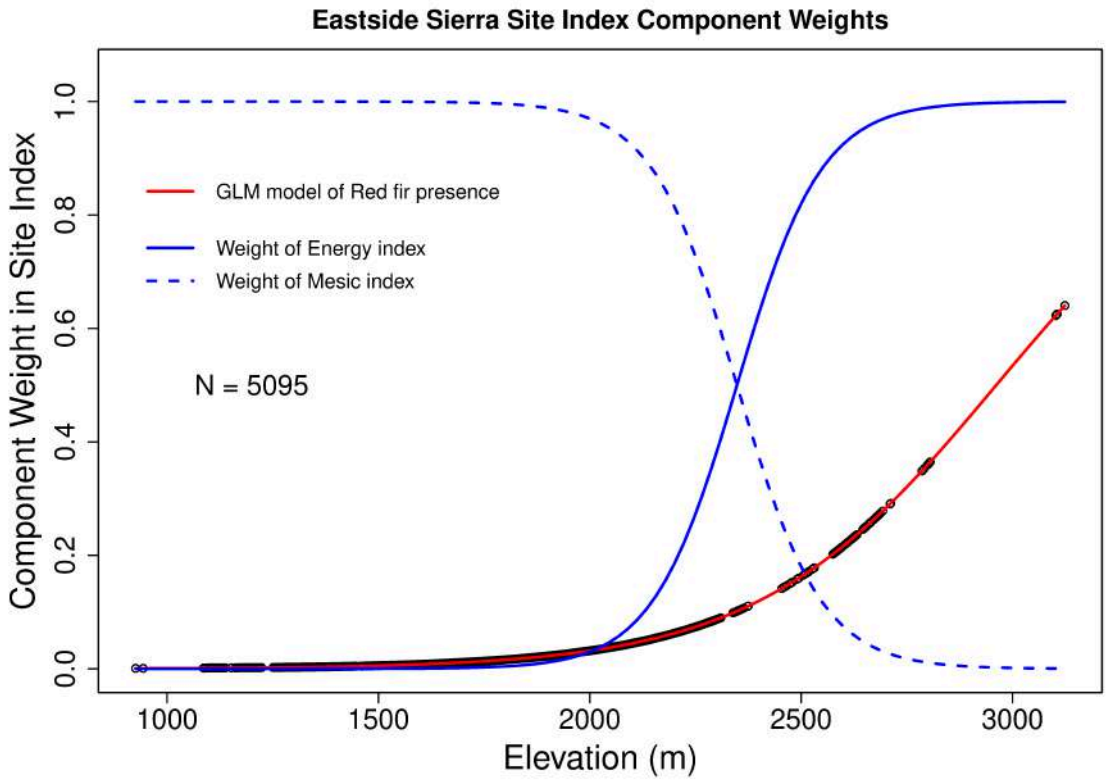

Figure 26: Relative component weights of the Mesic and Energy Indices as a function of Elevation in the composite Site Index to predict tree Height (ft) as a function of total tree Age (yrs) and Site Index for sites on the eastside of the Northern Sierra ecoregion, based on the fit of a Nonlinear Least Squares (NLS) model to Forest Inventory and Analysis (FIA) data (see text for details). Note, total tree Age equaled breast height Age plus 7 years. Also shown is the distribution of FIA tree data along the elevation gradient and the fit of a Generalized Linear Model (GLM) of red fir presence.

In addition to expected or average tree height growth for a given Site Index, we are also interested in accounting for the deviations from expected; i.e., trees/sites that grow better or worse than the average for their Site Index, e.g., due to tree spacing or intra-specific competition for resources. For this purpose, we use Non-Linear Quantile Regression (NLQR) estimation to fit the Monomolecular function above, but with the newly derived composite Site Index, to a range of quantiles (referred to as Tau in NLQR). Specifically, we fit the Monomolecular function to Tau values ranging from 0.01 - 0.99 at intervals of 0.01. A Tau of 0.01 fits the model to the data but weighs observations such that it estimates the fit that best describes the 1^{st} quantile of data; i.e., the observations that fall well below the expected or average for a given Age and Site Index. Similarly, a Tau of 0.99 estimates the fit that best describes the 99^{th} quantile of data; i.e., the observations that fall well above the expected or average for a given Age and Site Index. Each Tau value produces a unique set of estimates for the parameters of the Monomolecular function, and thus produces a site index curve that varies slightly in shape as the Tau value increases. The result is a set of polymorphic site index curves that captures the full range of the observed height growth relationships. In addition, after preliminary analyses, we opted to model trees on non-mafic sites separately from ultramafic sites. The bulk of the data are from non-mafic sites, which includes 583 plots and 21,408 trees. The results are depicted in **Figure 27**, which for simplicity only shows site index curves for the minimum, mean and maximum Site Index values in the FIA data and Tau values of 0.05 and 0.95 for each.

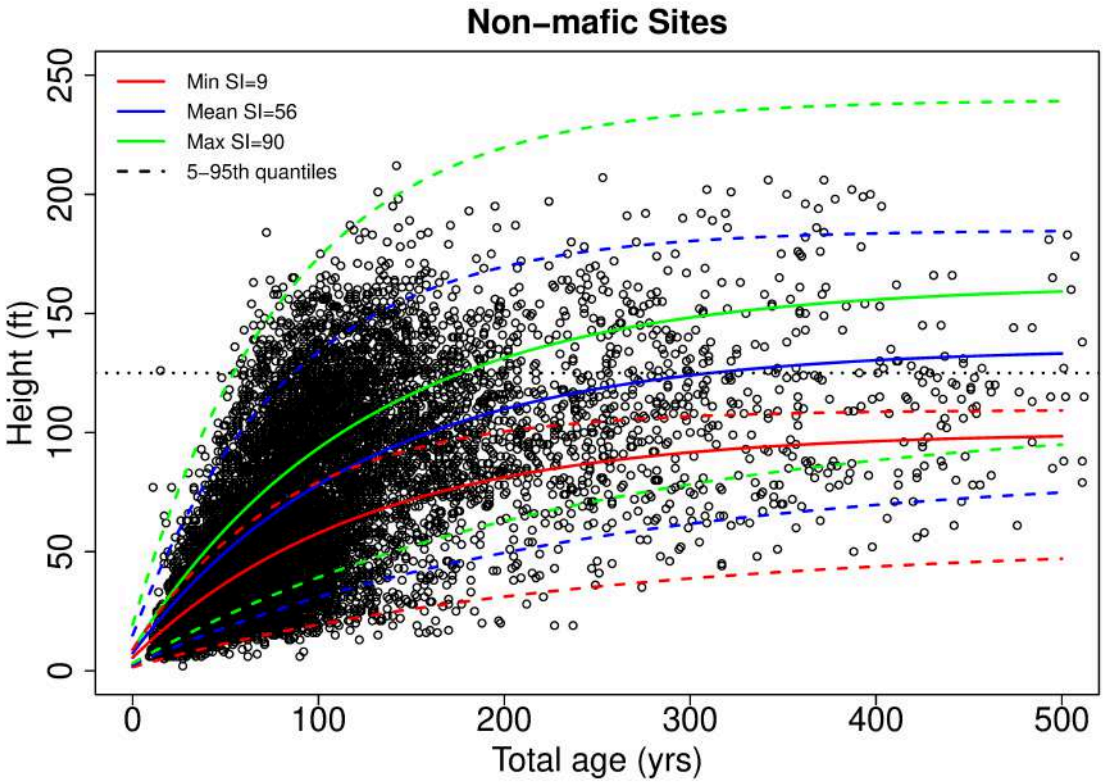

Figure 27: Expected or average tree Height (ft) as a nonlinear function of total tree Age (yrs) and Site Index for non-mafic forest cover types estimated from 21,408 trees on 583 Forest Inventory and Analysis (FIA) plots distributed across the Northern Sierra ecoregion. Note, total tree Age equaled breast height Age plus 7 years.

A minority of the data are from ultramafic sites, which includes only 14 plots and 490 trees. We fit the model above to the ultramafic data but decided that the data is not robust enough to ensure confidence in the reliability of the fit. Instead, we assessed the average difference between non-mafic and ultramafic sites in predicted height for trees of the same Age and Site Index and determined that trees on ultramafic sites had height growth reduced by ~ 5 - 20 %, depending on Age and Site Index. Consequently, for the purpose of modeling height growth in LDSim, we use the fitted growth equations for non-mafic sites but reduce the height by 15 % across all Ages and Site Indices.

To implement the fitted polymorphic site index curves in LDSim, we need a mechanism to determine whether a given cell should exhibit tree height growth based on the expected or average for its Site Index or instead should exhibit tree height growth less than or greater than expected based on the variation we model with NLQR. To do this, first we fit a normal distribution to the residuals of the fitted Monomolecular function above. Each residual represents the deviation of the observed tree height from the expected or average tree height given the tree's total Age and Site Index. We rescale the residuals to range 0 - 1 prior to fitting a normal distribution, and save the estimated standard deviation to quantify the spread of observed tree heights (i.e., variation) around the expected or average value. In effect, the standard deviation provides a quantitative measure of the "noise" or uncertainty in the fitted site index curve, as depicted in **Figure 27** by the 5 - 95th quantiles (i.e., Tau = 0.05 - 0.95). The residual distribution is approximately normally distributed with a mean of 0.469 and standard deviation (SD) of 0.12, as depicted in **Figure 28**

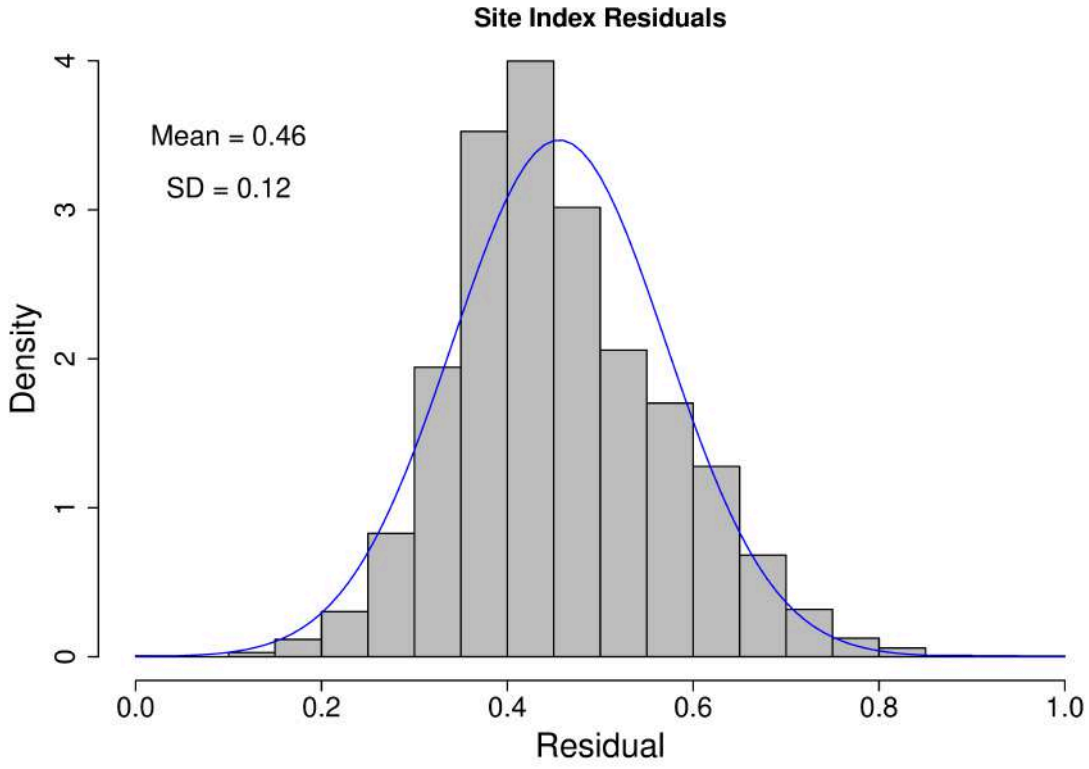

Figure 28: Standardized residuals of the fit of tree Height (ft) as a nonlinear function of total tree Age (yrs) and Site Index for non-mafic forest cover types estimated from 20,678 trees on 561 Forest Inventory and Analysis (FIA) plots distributed across the Northern Sierra ecoregion. The residuals represent the observed deviation from the expected or average tree Height given the total tree Age and Site Index.

Lastly, we assign a Tau value to each cell that determines the site index curve to apply to the cell for the duration of the simulation. The assigned Tau value determines whether the cell adopts a site index curve above or below the average for the cell's Site Index. For example, a cell assigned a Tau of 0.5 realizes the expected or average site index curve for that cell's Site Index, whereas a cell assigned a Tau of, say, 0.9, realizes a site index curve much higher than the expected or average for that cell's Site Index. For this purpose, we do not randomly assign a Tau value to each cell, as this would not preserve the observed spatial autocorrelation in tree height growth. Instead, we posit that the spatial autocorrelation in tree height growth is largely driven by the spatial autocorrelation in underlying physical site conditions (e.g., terrain, soils). Exploratory analyses indicate that tree height growth is weakly related to topographic position and aspect. Consequently, we model Tau as a Logistic function of Topographic Position Index (TPI) and a linear transformation of Aspect along the NE - SW axis, as follows:

$$Tau_i = \frac{1}{1 + e^{-(b_1 T_i + b_2 A_i)}}$$

where: b_1 and b_2 are assigned Logistic parameters; T_i = TPI of the i^{th} cell; A_i = Aspect (linearly transformed along the NE - SW axis) of the i^{th} cell; and Tau_i = Tau Index of the i^{th}.

Note, there is no empirical data from which to estimate the Logistic parameters, so we assign them manually so as to give equal weight to the two predictors. Specifically, we assign b_1 = -0.05 and b_2 = 0.05 to reflect a negative relationship between height growth and TPI (i.e., decreasing height growth with increasing topographic position) and a positive relationship between height growth and the linear transformation of Aspect (i.e., increasing height growth on northeasterly aspects), respectively. Note, the absolute value of the parameters has no effect on the final result given the normal transformation described below, so all that matters is the relative weight given to the two predictors.

We derive the value of Tau for each cell based on the Logistic function above. However, the realized distribution of Tau values for a focal landscape does not have the target distribution based on the residual analysis described above - because of the irregular distribution of topographic positions and aspects within any focal landscape. Therefore, we transform the Tau distribution for each focal landscape into a Normal distribution with a mean and standard deviation equal to that of the residual distribution described above, for example as shown in **Figure 29** for the Yuba River landscape.

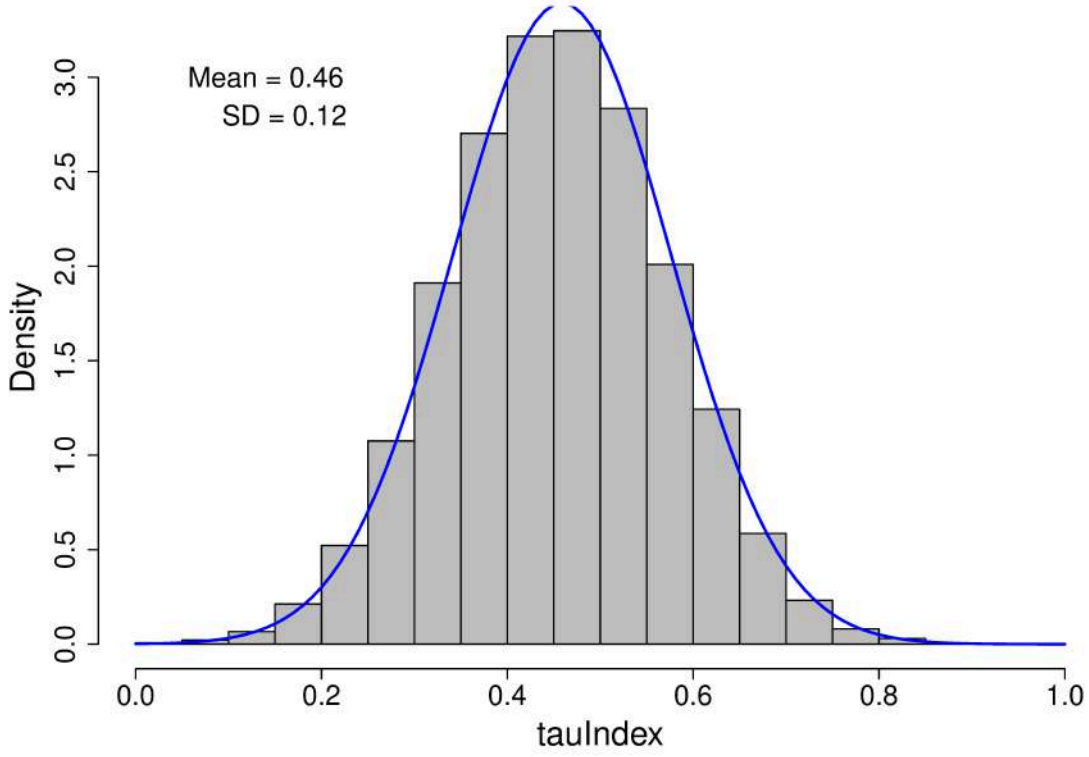

Figure 29: Distribution of Tau Index values in the Yuba River landscape, and a fitted Guassian or Normal distribution with a mean = 0.5 and standard deviation (SD) = 0.13.

To evaluate this procedure as a means of representing the range of height growth relationships observed in the FIA data, we constructed a simulation as follows. First, we used the distribution of Site Index values in the FIA data set as representative of what we would be realized across the region in LDSim, which is depicted in **Figure 30**.

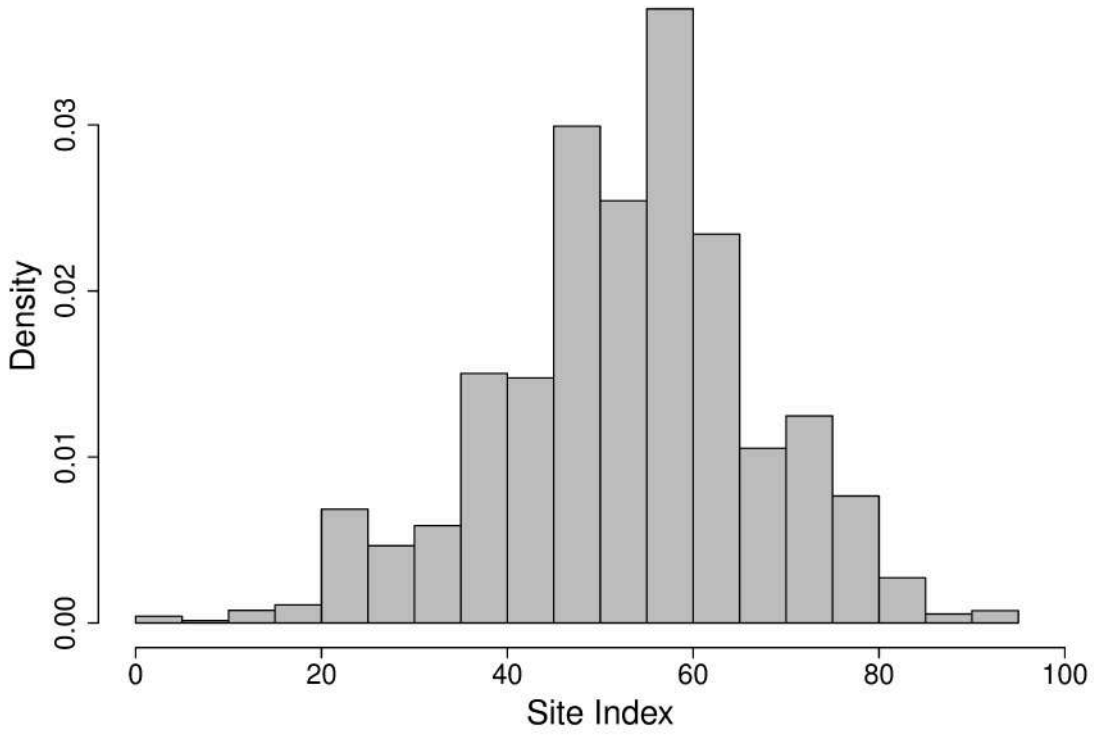

Figure 30: Distribution of Site Index values for 21,408 trees on 583 Forest Inventory and Analysis (FIA) plots distributed across the Northern Sierra ecoregion.

Next, we randomly assigned a Tau value to each of the 21,408 trees based on the distribution of residuals from the fitted growth equation (**Figure 28**).

Next, we used the polymorphic site index curves to predict the height growth of each tree based on its Site Index and assigned Tau over a period 0 - 500 years. Thus, each tree produced a simulated height growth trajectory, and the collection of simulated height growth trajectories represented the distribution of trajectories we would expect in the LDSim application. We summarized the simulated trajectories by computing select quantiles of the simulated distribution for each year and plotted the result in **Figure 31**:

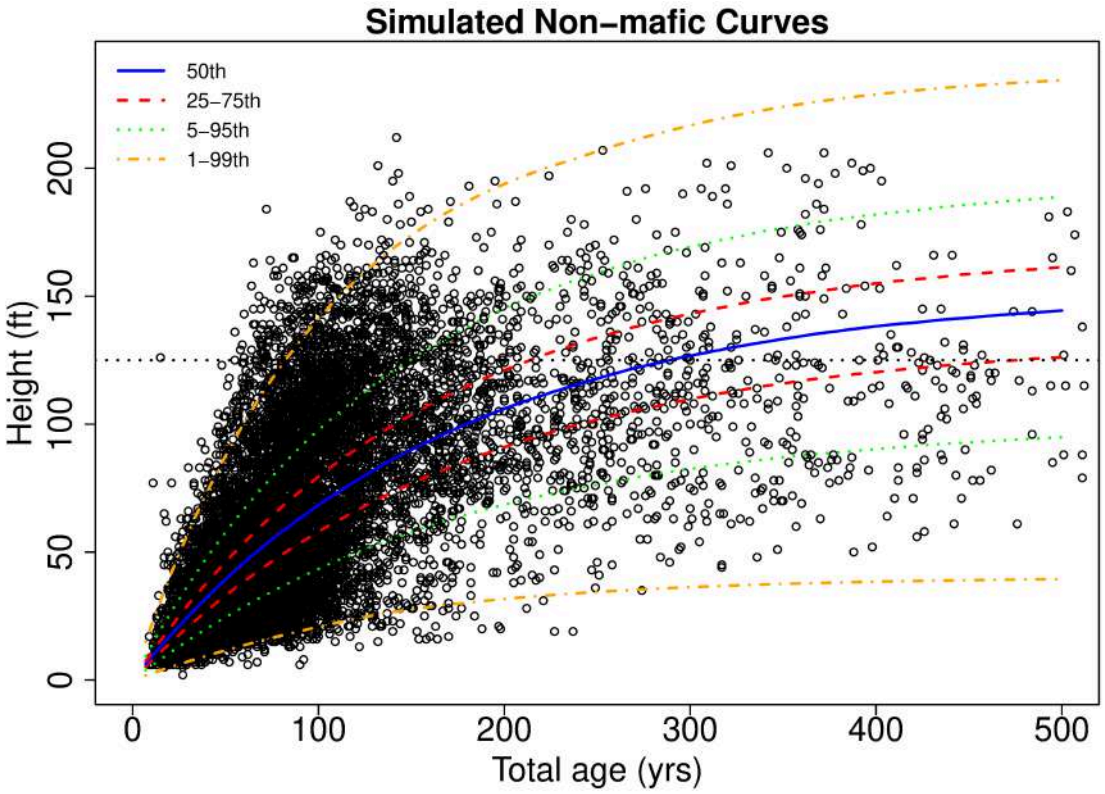

Figure 31: Simulated tree Height (ft) as a nonlinear function of total tree Age (yrs) and Site Index for non-mafic forest cover types estimated from 21,408 trees on 583 Forest Inventory and Analysis (FIA) plots distributed across the Northern Sierra ecoregion. Note, total tree Age equaled breast height Age plus 7 years.

As is evident in the figure, the simulated distribution of site index curves captured the distribution of FIA data well. We concluded that our implementation of tree height growth trajectories would be effective in capturing the range of variation observed in the FIA data set.

Tree Diameter Growth

Following tree establishment in a forested cell, we also model continuous tree diameter growth over time in the absence of a high-mortality disturbance as a function of tree height and cover type. To establish the tree diameter growth function, we use the same FIA plot data from the Northern Sierra ecoregion as before, consisting of 597 plots containing 21,898 trees (pooled across mafic and non-mafic sites) with tree height (ft) and diameter at breast height (DBH in inches) data recorded. We recognize that many other local factors such as tree species and tree spacing affect real-world tree diameter growth, and thus using tree height and cover type alone provides only an approximation of expected tree diameter, but we deem this sufficient for the purposes of this application.

After preliminary inspection of the data and the evaluation of alternative linear and non-linear models, we opted for the following. We use Ordinary Least Squares (OLS) estimation to fit the following no-intercept simple linear regression model separately for each major cover type:

$$D_{it} = b_{0[k]} H_{it}$$

where: $b_{0[k]}$ is an estimated slope parameter representing the rate at which tree diameter increases per unit increase in tree height for the k^{th} cover type; H_{it} = tree height (ft) the i^{th} cell in the t^{th} timestep; and D_{it} = tree diameter (in) of the i^{th} cell in the t^{th} timestep.

The fitted equations give the predicted tree diameter for any given tree height and cover type, as depicted in **Figure 32**:

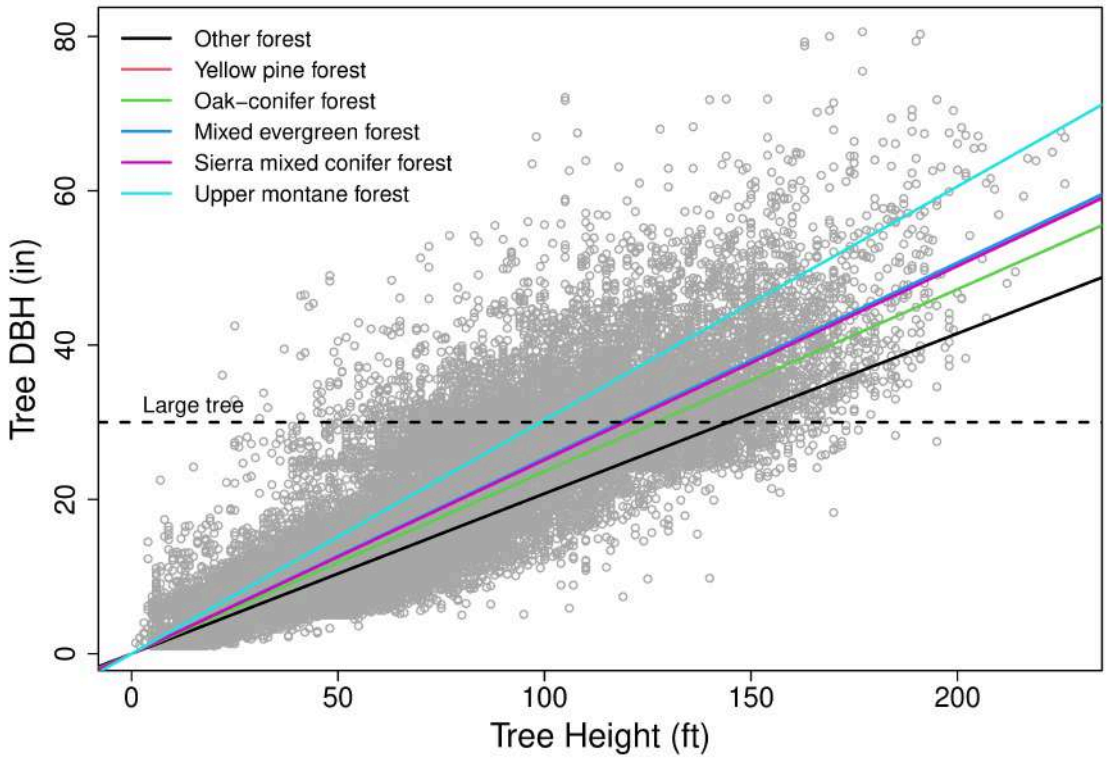

Figure 32: Expected or average tree Diameter at breast height (in) as a function of tree Height (ft) and Cover type for several major cover types estimated from 21,408 trees on 583 Forest Inventory and Analysis (FIA) plots distributed across the Northern Sierra ecoregion. Note, total tree Age equaled breast height Age plus 7 years.

In addition to expected or average tree diameter growth for a given tree height and cover type, we are also interested in accounting for the deviations from expected; i.e., trees that grow better or worse than the average for their height and cover type; e.g., due to tree spacing or intra-specific competition for resources. For this purpose, we use Quantile Regression (QR) estimation to fit quadratic polynomial functions to a range of quantiles (referred to as Tau in QR) separately for each cover type. Specifically, we fit the following quadratic polynomial function to Tau values ranging from 0.01 - 0.99 at intervals of 0.01:

$$D_{it} = b_{0[k]}H_{it} + b_{1[k]}H_{it}^2$$

where: $b_{0[k]}$ and $b_{1[k]}$ are estimated slope parameters representing the rate at which tree diameter increases nonlinearly per unit increase in tree height for the k^{th} cover type; H_{it} = tree height (ft) the i^{th} cell in the t^{th} times step; and D_{it} = tree diameter (in) of the i^{th} cell in the t^{th} timestep.

Recall, a Tau of 0.01 fits the model to the data but weights observations such that it estimates the fit that best describes the 1^{st} quantile of data; i.e., the observations that fall well below the expected or average for a given tree height and cover type. Similarly, a Tau of 0.99 estimates the fit that best describes the 99^{th} quantile of data; i.e., the observations that fall well above the expected or average for a given tree height and cover type. Each Tau value produces a unique set of estimates for the parameters of the quadratic polynomial function, and thus produces curves that vary slightly in shape as the Tau value increases. The result is a set of polymorphic curves that capture the full range of the observed diameter growth relationships. For example, the fitted growth curves for the 1^{st}, 50^{th} and 99^{th} quantiles for the Sierra Mixed Conifer forest cover type is depicted in **Figure 33**.

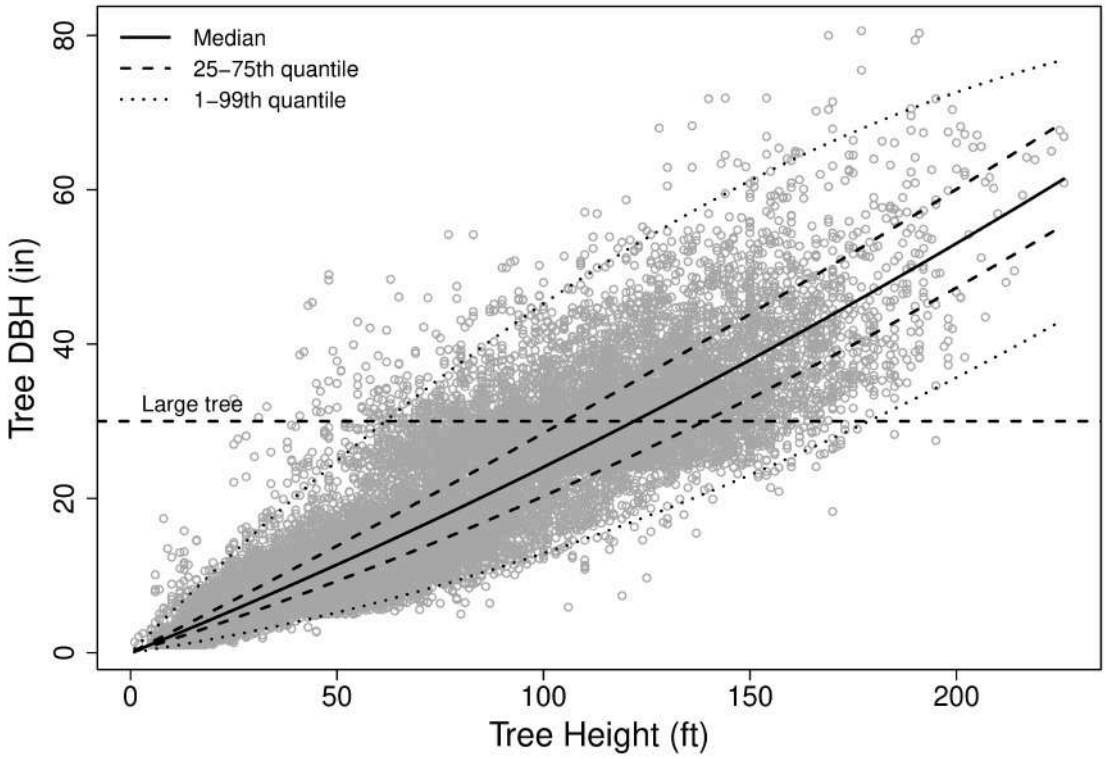

Figure 33: Predicted tree Diameter at breast height (in) as a function of tree Height (ft) for Sierra Mixed Conifer forest estimated from 16,029 trees on 394 Forest Inventory and Analysis (FIA) plots distributed across the Northern Sierra ecoregion. Note, total tree Age equaled breast height Age plus 7 years.

To implement the fitted polymorphic diameter growth curves in LDSim, we need a mechanism to determine whether a given cell exhibits tree diameter growth based on the expected or average for its tree height and cover type or instead exhibits tree diameter growth less than or greater than expected based on the variation we model with QR. To do this, first we fit a normal distribution to the residuals of the fitted simple linear regression model above, pooled across cover types. Each residual represents the deviation of the observed tree diameter from the expected or average tree diameter given the tree's height and cover type. We rescale the pooled residuals to range 0 - 1 prior to fitting a normal distribution, and save the estimated standard deviation to quantify the spread of observed tree diameters (i.e., variation) around the expected or average value. In effect, the standard deviation provides a quantitative measure of the "noise" or uncertainty in the fitted diameter growth curves, for example as depicted in **Figure 33** for the Sierra Mixed Conifer forest cover type. The pooled residual distribution is approximately normally distributed with a mean of 0.5 and standard deviation (SD) of 0.16, as depicted in **Figure 34**

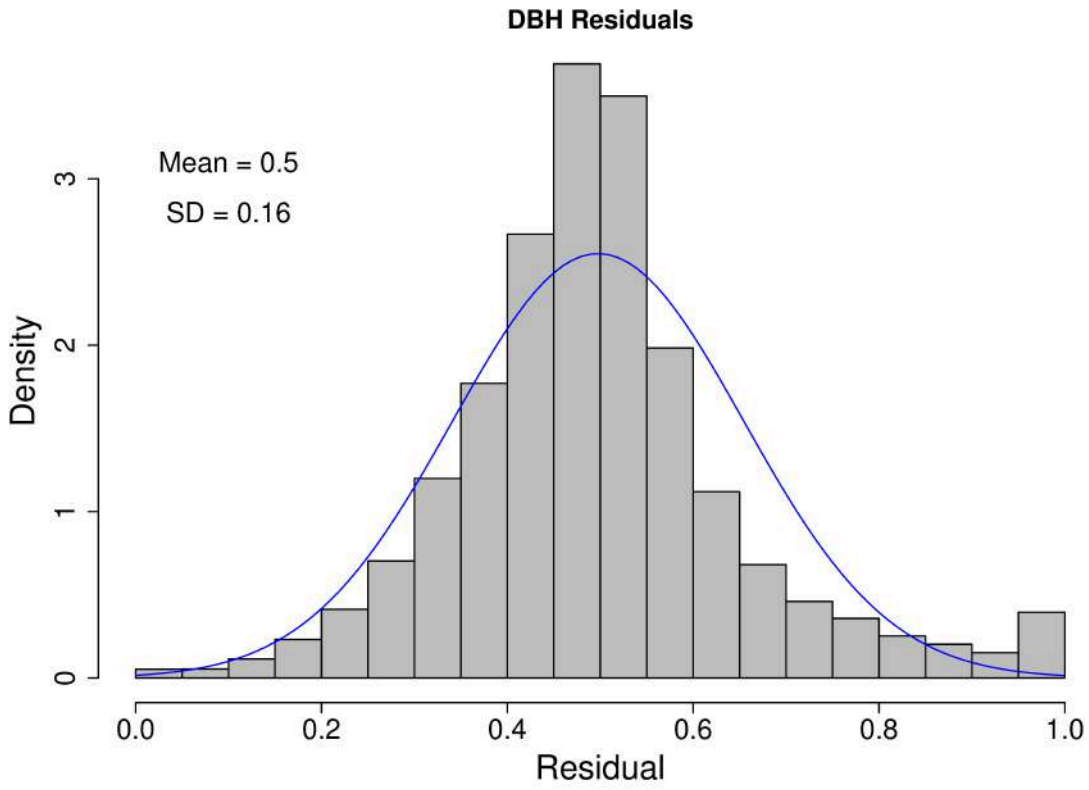

Figure 34: Standardized residuals of the fit of tree Diameter (in) as a linear function of tree Height (ft) and Cover type estimated from 21,408 trees on 583 Forest Inventory and Analysis (FIA) plots distributed across the Northern Sierra ecoregion. The residuals represent the observed deviation from the expected or average tree Diameter given the tree Height and Cover type.

Lastly, we randomly assign a Tau value to each cell to indicate whether the cell realizes a diameter growth curve above or below the average for the cell's cover type. For example, a cell assigned a Tau of 0.5 realizes the expected or average tree diameter curve for the cell's cover type, whereas a cell assigned a Tau of, say, 0.9, realizes a diameter growth curve much higher than the expected or average for the cell's cover type. For this purpose, we randomly assign a Tau value to each cell. We opted not to model Tau as a contagious function because we posit that diameter growth is largely determined by the distance to neighboring trees at a very fine scale, which we are unable to account for in our model. Thus, we simply assign a random Tau value drawn from a normal distribution with a mean of 0.5 and a standard deviation equal to that observed in the normalized residuals above (i.e., 0.16) to each cell, ensuring that the random Tau values fall within the range 0.01 - 0.99 corresponding to the range of Tau values fit with QR, and the assigned Tau value is held constant for the duration of the simulation to ensure that diameter growth over time follows a single fitted curve.

Quadratic Mean Diameter

Following tree diameter growth at the cell level, we compute the quadratic mean diameter (QMD) of established trees within a 40-m radius window centered on each forested cell. QMD is computed as follows:

$$Q_{it} = \sqrt{\frac{\sum d_{ijk}^2}{n_{it}}}$$

where: $d_{ijk}{}^2$ = diameter at breast height of the k^{th} cell with an established tree within the window of the i^{th} cell in the t^{th} timestep; n_{it} = number of cells with an established tree within the window of the i^{th} cell in the t^{th} timestep; and Q_{it} = QMD (in) of the i^{th} cell in the t^{th} timestep. Note, QMD is computed for all

forested cells regardless of whether the focal cell has an established tree or not; thus, it is a measure of the neighborhood QMD centered on the forested focal cell. All non-forest cells are assigned a QMD of 0.

Tree Cover

Following tree height and diameter growth at the cell level, we also compute the percent established tree cover within a 40-m radius window centered on each forested cell. Tree cover is computed as follows:

$$T_{it} = \frac{\sum (I|s_{ijk} > 4|)}{\sum I|s_{ijt}|} * 100$$

where: I = indicator (i.e., 1 if condition met, 0 if not); s_{ijk} = developmental stage of the k^{th} cell within the window of the i^{th} cell in the t^{th} timestep; and T_{it} = percent tree cover of the i^{th} cell in the t^{th} timestep. Note, the numerator on the right side of the equation is simply a count of the number of forested cells with established trees (i.e., developmental stage > 4) within the window of the i^{th} cell in the t^{th} timestep, and the denominator is a count of the number of forested cells; thus, the ratio times 100 represents the percentage of the forested window with established trees.

Importantly, we recognize that our measure of percent tree cover is not a true measure of actual canopy cover. Technically, it is a measure of the percent of the 5 m cells within the neighborhood with at least one established tree. Recognizing that during early successional stages the percent canopy cover of a cell with an established tree is likely much less than 100 % and realistically can vary widely from near 0 to 100 %, our percent tree cover estimate is likely much higher than percent canopy cover. Indeed, we conducted a detailed analysis that revealed that our percent tree cover is on average 16 % higher than true canopy cover. Thus, it is imperative to understand the distinction between percent tree cover as we measure it and true canopy cover when interpreting our results. Tree cover is computed for all forested cells regardless of whether the focal cell has an established tree or not; thus, it was a measure of the neighborhood percent tree cover centered on the forested focal cell. All non-forest cells are assigned a percent tree cover of 0.

Senescence

Following tree establishment at the cell level, we model the probability of tree death via senescence in the absence of disturbance based on the cumulative Weibull Function, as shown in **Figure 35**

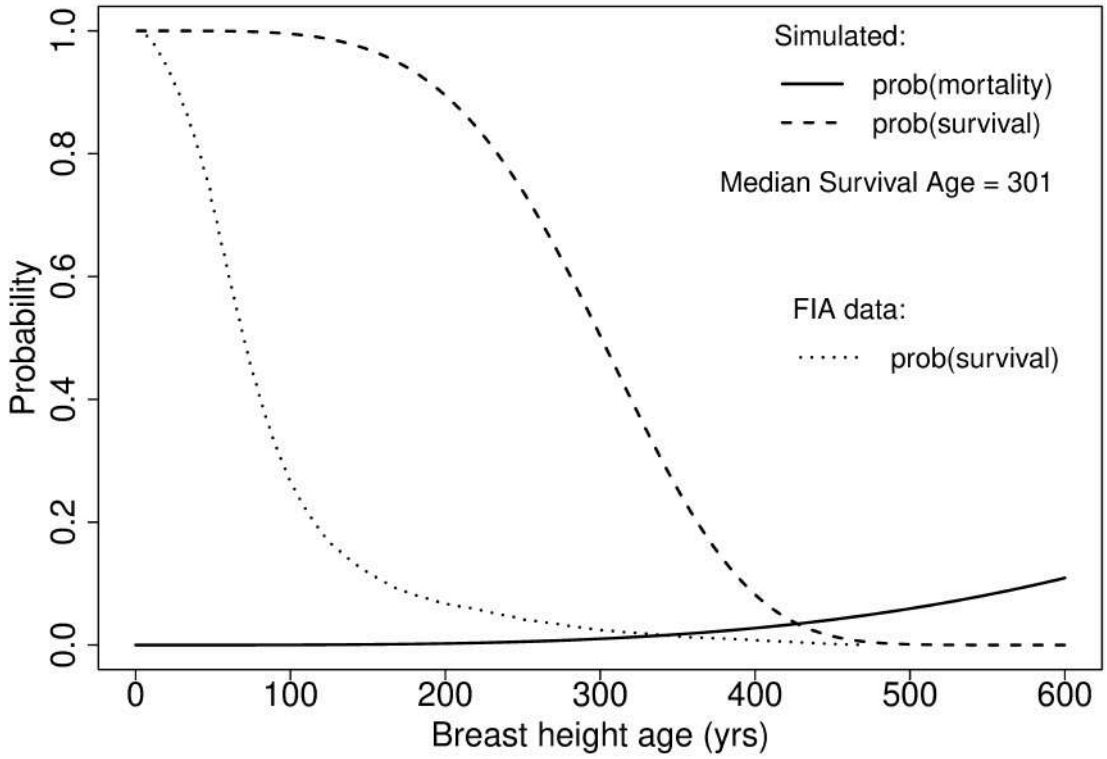

Figure 35: Probability of tree senescence and death (solid line) and the corresponding probability of survival to any given age (dashed line) at the cell, applied to all forest cover types.

In the corresponding figure, the solid line depicts the instantaneous probability of tree death as a function of tree age and the dashed line depicts the corresponding probability of tree survival to any given age in the absence of disturbance. As parameterized, this results in a median survival age of 301 years, barring mortality caused by wildfire. Note, we apply this common senescence function to all forest cover types due to the lack of sufficient data on senescence for each cover type separately. The parameters of the senescence function are subjectively assigned based on expert opinion and a cursory review of the literature regarding tree species longevity for the dominant tree species in the Northern Sierra ecoregion. For comparative purposes, **Figure 35** also depicts the probability of survival derived from the FIA data (dotted line). Note the disparity between the FIA survival curve and the Weibull curve, as parameterized. The marked lower survival of the FIA trees is a direct result of land use practices such as timber harvest that have removed many of the older trees on the FIA plots, resulting in a much younger age distribution of residual trees than we would expect to occur naturally due to senescence.

Vegetation States

The last stage of forest succession involves classifying cells into several discrete States, including: 1) Developmental Stages based on tree height bins, 2) Size Classes based on QMD bins, and 3) Tree Cover Classes based on percent tree cover bins.

- *Developmental Stage* - We classify forested cells into the following Developmental Stages based on user-specified thresholds in tree height, applying the same thresholds for all forest cover types, as follows. Note, shrublands are assigned a Developmental Stage as described previously and all other cover types are assigned a class of zero:
  - Tree Height $<$ 4.5 ft = Open
  - Tree Height 4.5 - 24 ft = Sapling

  - Tree Height 25 - 49 ft = Pole
  - Tree Height 50 - 74 ft = Short-tree
  - Tree Height 75 - 124 ft = Medium-tree
  - Tree Height $\geq$ 125 ft = Tall-tree

- *Tree Size Class* - We classify forested cells into the following Tree Size Classes based on user-specified thresholds in QMD within a 40-m radius neighborhood, applying the same thresholds for all forest cover types, plus a zero class for all non-forest cells, as follows:

  - QMD $\leq$ 1 in = no trees or seedlings
  - QMD 1.1 - 5.9 in = Saplings
  - QMD 6 - 10.9 in = Poles
  - QMD 11 - 23.9 in = Small-trees
  - QMD 24 - 29.9 in = Medium-trees
  - QMD $\geq$ 30 in = Large-trees

- *Tree Cover Class* - We classify forested cells into the following Tree Cover Classes based on user-specified thresholds in percent Tree Cover within a 40-m radius neighborhood, applying the same thresholds for all forest cover types, plus a zero class for all non-forest cells, as follows:

  - Tree Cover $\leq$ 10 % = Isolated
  - Tree Cover 10 - 24.9 % = Sparse
  - Tree Cover 25 - 39.9 % = Scattered
  - Tree Cover 40 - 59.9 % = Clump
  - Tree Cover $\geq$ 60 % = Dense

MODEL CALIBRATION

Although LDSim is a process-oriented model with individual parameters sourced either from data, literature, or expert opinion, the model outcomes reflect the complex spatio-temporal interactions of the various stochastic disturbance and succession processes. Consequently, it is necessary to calibrate the model by tuning (i.e., adjusting up or down) one or more of the model parameters to produce selected outcomes that are consistent with the data, literature and expert opinion. Importantly, in this context, we consider the parameters associated with the disturbance process to be "independent" variables and the vegetation conditions (e.g., seral stage distribution, spatial patterns of vegetation states, etc.) to be "dependent" outcomes. We calibrate selected disturbance parameters (i.e., independent variables) to achieve the target disturbance regime without any attention to the vegetation response, which we treat as the dependent outcome of the disturbance regime. Importantly, we do not tune disturbance regime parameters to achieve desired vegetation outcomes.

We focus model calibration on the following five disturbance regime attributes that we consider emergent properties of the disturbance regime:

1. Fire rotation period (FRP) by cover type, which is the number of years required to burn a cumulative area equal to the extent of the cover type;
2. Fire mortality rate (FMR) by cover type, which is the percentage of burned cells of the corresponding cover type that exhibit a high-mortality response (i.e., complete overstory mortality);
3. Fire size distribution, which is the percentage of realized fire sizes across bins of increasing fire size;
4. Variability in the total area burned over time; and

5. Strength of the relationship between total area burned and the Wildfire Climate Index over time.

Importantly, these "emergent" attributes are quantitative aspects of the disturbance regime that arise (i.e., emerge) out of the complex spatio-temporal interactions of the stochastic processes in the model and are not themselves dictated directly by model parameters. In other words, we have no means of ensuring specific outcomes via model parameterization, but instead have the option to tune one or more parameters through trial and error to achieve the desired outcomes. In addition, this is not a comprehensive suite of emergent disturbance regime attributes, but rather represents those emergent aspects of the disturbance regime for which we have some confidence that our targets accurately represent the historical reference period. In this regard, however, not all of the chosen calibration metrics are deemed equal, as noted below. For example, we have the most confidence in the FRP metrics by cover type, since this is strongly based on empirical studies of the pre-settlement wildfire disturbance regime. Thus, we use this metric as our primary means of calibrating the model. We have much less confidence in FMR by cover type during the historical reference period as this relies more heavily on expert opinion and contemporary observations. Similarly, the fire size distribution is only partially emergent as it is more directly affected by the specified maximum fire size distribution parameters in the model, although the final realized size distribution is affected by other factors as well. Lastly, the variability in total area burned and relationship to the climate index are entirely empirically based, although the data derive from the post-settlement period of 1908 - 1979 from which we have an empirical record and not the historical reference period of 1550 - 1850. Thus, each of the calibration metrics have to be interpreted in the context of their reliability.

Fire Rotation Period

Fire Rotation Period (FRP) is the number of years required to burn a cumulative area equal to the extent under consideration. FRP combines fire frequency and fire size into a single integrated measure of how much fire occurs. Regardless of whether there are more smaller fires or fewer larger fires, FRP provides an effective measure of how much fire is actually applied to a unit of ground. FRP is equivalent to the "point-specific" or "population" mean fire return interval (FRI); i.e., the average number of years between fires to a single point on the ground (or cell), and is roughly equivalent to the oft reported "grand mean" FRI computed from a large sample of point-specific intervals (e.g., from a set of fire-scarred trees). Importantly, FRP is not equivalent to the oft reported "composite" FRI, which is computed based on the average interval between fires to an area of some specified size larger than a single point or cell (e.g., a forest stand). The FRP or point-specific FRI is generally much longer than the composite FRI, because the interval between fires to a single point is generally much greater than the interval between fires to anywhere within an arbitrarily defined larger site. A major limitation with composite FRI is that the unit area is arbitrary and varies considerably from one study to the next, making comparisons of published composite FRIs very difficult. In our assessment, we use FRP to describe the amount of fire applied to the landscape, in part because it is unambiguous in meaning and well understood by managers, but also because the simulation modeling gives us a complete census of simulated wildfires, which lends itself well to the calculation of FRP.

We tune the global wildfire initiation rate parameter, which controls the number of wildfire initiation attempts per unit area within each timestep and remains constant over time (see Wildfire Initiation above), and two of the wildfire susceptibility coefficients (b_0 and b_1) for each cover type, which affect the susceptibility of fire initiation and spread in each cover type (see Wildfire Susceptibility above), and measure calibration success based on agreement with the pre-specified target FRP for each cover type. We set our calibration goal as within 10 % of the target FRP for forested cover types with $>$ 1,000 ha in the focal landscape. Target values are based on empirically-based published values (Van de Water and Safford 2011 and Mallek et al. 2013) and expert input from H. Safford and B. Estes. Because of the strong empirical basis for pre-settlement FRPs, we deem FRPs our most reliable calibration metric and strive to achieve these targets first and foremost, even at the cost of not meeting the targets set for the other calibration metrics as well.

Fire Mortality Rate

Fire mortality rate (FMR) is the percentage of burned cells that exhibit a high-mortality response (i.e., complete overstory mortality). For the purpose of model calibration, we consider the FMR only for cells in the "short", "medium" and "tall" tree developmental stages (i.e., "mature" trees) since this is the basis for specifying the target values.

We tune two of the wildfire mortality coefficients (b_5 and b_6) for each cover type, which affect the probability of high mortality fire as a function of age and fire intensity in each cover type (see Wildfire Mortality above), and measure calibration success based on conformity to pre-specified fire mortality targets for each cover type. We set our calibration goal as within 10 % of the targets for forested cover types with > 1,000 ha in the focal landscapes. Target values are based on LANDFIRE estimates, as modified by H. Safford and B. Estes. Because of the relatively weak empirical basis for pre-settlement FMRs and the heavy reliance on observations of contemporary wildfires to establish the targets, we deem FMRs as a comparatively weak calibration metric. However, because FMR has a strong affect on the vegetation developmental stage distribution and represents an important user assumption of the model, we deem it an important calibration metric nonetheless.

Fire Size Distribution

Fire size distribution (FSD) is the percentage of realized fire sizes across bins of increasing fire size. As noted above, the realized fire size distribution is only partially an emergent property of the model, as it is more directly affected by the specified maximum fire size distribution parameters in the model (see Wildfire Termination above). However, the final realized size distribution is affected by other factors as well (e.g., fuels, climate, etc.) and thus we consider it a useful calibration metric nonetheless.

We opted not to tune the maximum fire size distribution parameters, which affect the probability of a fire growing to a particular size (see Wildfire Termination above) and are empirically based. Instead, we treat the realized fire size distribution as an emergent outcome of the model and measure calibration success based on agreement with the pre-specified fire distribution derived from the post-settlement period of 1908 - 1979 from which we have an empirical record. We set our calibration goal as a subjective evaluation of the realized fire size distribution compared to the target fire size distribution. Because the target fire size distribution, although empirically derived from historical data, is not based on data from the pre-settlement reference period, we deem this a comparatively weak calibration metric and secondary to FRP and FMR.

Variability in Total Area Burned

Variability in total area burned over time is a measure of the temporal variability in the wildfire disturbance regime. Although the total area burned over time is strongly determined by the user-specified Wildfire Climate Index (see Wildfire Climate above), the realized variability in total area burned over time is truly an emergent property of the model, as it depends on the spatio-temporal interactions of the disturbance process and the vegetation, and thus we consider it a useful calibration metric.

We opted not to tune the Wildfire Climate Index, as it is empirically based. Instead, we treat the variability in total area burned as an emergent outcome of the model and measure calibration success based on agreement with the observed variability in total area burned for the post-settlement period of 1908 - 1979 from which we have an empirical record (**Figure 36**).

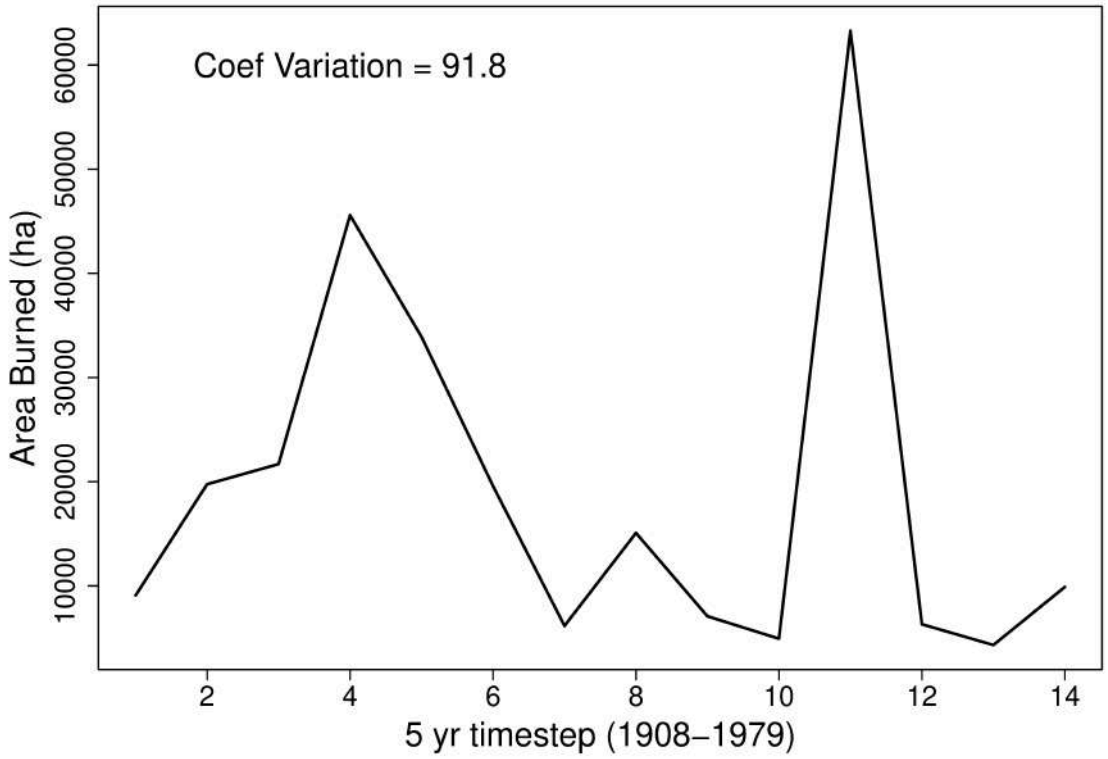

Figure 36: Total area burned per 5 years in the Northern Sierra ecoregion during the post-settlement period of 1908 - 1979 and the computed Coefficient of Variation (CV).

We set our calibration goal as within 10 % of the target coefficient of variation (CV) in total area burned per timestep. Because the target CV in total area burned, although empirically derived from historical data, is not based on data from the pre-settlement reference period, we deem this a comparatively weak calibration metric and secondary to FRP and FMR.

Relationship Between Total Area Burned and Climate

The relationship between total area burned and climate is a measure of the degree to which the simulated total area burned is affected by variability in the specified Wildfire Climate Index. Some relationship between total area burned and climate is guaranteed, because the Wildfire Climate Index is incorporated into both wildfire initiation and wildfire spread processes in the model (see Wildfire Initiation and Wildfire Spread above); however, the nature and magnitude of the relationship is truly an emergent property of the model as it depends on the spatio-temporal interactions of the disturbance process and the vegetation, and thus we consider it a useful calibration metric.

We opted not to tune the Wildfire Climate Index, in particular, or any parameter associated with the wildfire disturbance process with regards to this calibration metric. Instead, we treat the observed relationship between total area burned and the climate index as an emergent outcome of the model and measure calibration success based on agreement with the strength of the relationship for the post-settlement period of 1908 - 1979 from which we have an empirical record (**Figure 37**).

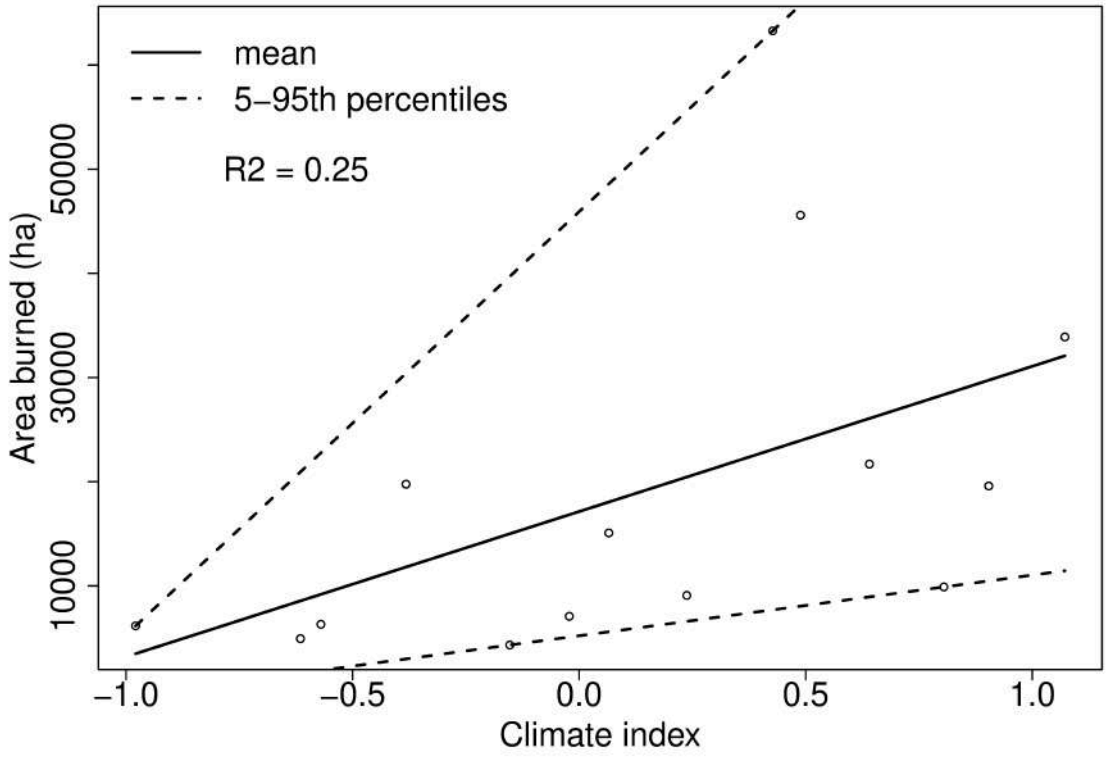

Figure 37: Scatterplot of the unmodified wildfire Climate Index based on the modified Palmer Drought Severity Index (see text for details) and the log of total area burned per 5 years in the Northern Sierra ecoregion during the post-settlement period of 1908 - 1979 and the fitted linear regression for the mean and 5 - 95th quantiles (see text for details) along with the Coefficient of Determination (R2) of the fit.

We set our calibration goal as within 10 % of the target coefficient of determination (R2) in the fit of a log-linear regression to the target data. R2 measures the percentage of variation in the log of total area burned explained by the climate index. Because the target R2 in the fitted relationship, although empirically derived from historical data, is not based on data from the pre-settlement reference period, as noted above, we deem this a comparatively weak calibration metric and secondary to FRP and FMR.

MODEL EXECUTION

For each focal landscape (see Project Area), we use the landscape disturbance-succession model LDSim to simulate succession and wildfire disturbance under historical reference period conditions (circa 1550 - 1850) for a 1,500-year period with a 5-year timestep (i.e., 300 timesteps) and output several spatial data layers representing disturbance and vegetation attributes at each timestep. We drop the first 500 years or 100 timesteps as a liberal estimate of the model equilibration period (i.e., the time to reach dynamic equilibrium) and retain the remaining 1,000 years or 200 timesteps to quantify the range of variability in various landscape attributes (see below). However, for some landscape metrics at some levels, as noted below, it is necessary to sample the outputs from the last 200 timesteps due to size of the data sets generated. In addition, recall that we include a 5-km buffer around the focal landscape for purposes of the simulation to avoid landscape boundary effects, resulting in a much larger landscape for the simulation. Wildfire disturbances are allowed to spread across the focal landscape boundary unimpeded, but we restrict the analysis of landscape structure to the core of the focal landscape.

Although we simulate landscape dynamics for 1,500 years and retain the last 1,000 years for the analysis of landscape dynamics under equilibrium, it is important to recognize that this does not conflict with our ~ 300-year historical reference period. We parameterize LDSim to represent disturbance processes characteristic of the 300-year historical reference period; the longer simulation merely allows us to produce a larger sample of landscape snapshots that are characteristic of this historical disturbance regime. Preliminary simulations revealed that 1,000 years or 200 snapshots was sufficient to quantify a stable range of variation in landscape characteristics.

HISTORICAL RANGE OF VARIABILITY and CURRENT DEPARTURE

Scales of Analysis

It is absolutely essential to interpret the model results in the context of the model parameterization, which is essentially a set of assumptions about how disturbance and succession processes operate at a particular scale in the focal landscape under historical reference period conditions. The choice of scale in representing the landscape is a user assumption that is especially important, as the simulated range of variability and current departure in landscape structure is highly scale-dependent (Axiom 3). In other words, the measured variability and current departure depends on the grain and extent of the assessment in both the spatial and temporal domains. Thus, it is imperative that both the spatial and temporal scale, in terms of both grain and extent, of the assessment be made explicit. In this regard, we fixed by design the spatial grain of our assessment at 5 m – the approximate scale of a single mature tree – and the temporal grain at 5 years. In addition, we fixed by design the temporal extent of our assessment at the ~ 300-year historical reference period (circa 1550 - 1850). The spatial extent of our assessment, however, was not fixed by design, and we chose to describe HRV and current departure at a few different scales, or rather "levels" in the hierarchical organization of landscape mosaics, as described below. Importantly, any attempt to compare our results to those generated at a different scale should be done with extreme caution or, preferably, not at all. Moreover, it is important to note that we chose our scales to ensure minimal inherent bias in the computation of HRV and current departure. In particular, at none of our chosen scales is the historical or current vegetation conditions considered in delineating the spatial units; i.e., the spatial units are agnostic to past or present vegetation conditions. Thus, the measured HRV and current departure is truly an emergent property of the simulation.

We measure HRV and current departure at the following three levels, which are briefly described below (greater detail in subsequent sections):

- *Site level* - We quantify HRV and compute several departure metrics at the "Site" level, which we define as a 40-m radius window around each focal cell corresponding to the height and ecological neighborhood of a single "tall" tree in our classification of developmental stages. Thus, Sites represent moving windows (i.e., overlapping windows) across focal cells. We further classify each Site into one of several Biophysical Classes (BPCs), as described below, to better distinguish among Sites varying in overall forest productivity. Importantly, we consider the Site to be the finest scale for which we can reliably compute many vegetation characteristic. It is essentially analogous to a local "plot" scale for characterizing vegetation. However, we deem it unreliable to compare the current condition of a Site to its own HRV because of the small size of a Site, given the stochastic nature of disturbance and succession processes. Thus, we do not derive an HRV or compute departure for each individual Site. Rather, we define HRV at the Site level as the variation in the landscape metrics across Sites and over time under historical dynamic equilibrium conditions, thus representing spatio-temporal variability in vegetation conditions across Sites over the full extent of the focal landscape, rather than for each Site individually. Here, departure is based on a comparison of the current range of variation (CRV) across Sites to the HRV across Sites and time.

- *Geophysical Unit level* - We quantify HRV and compute several departure metrics at the "Geophysical Unit" (GPU) level. We derive GPUs through a series of geoprocessing steps to create meaningful spatial units that differ in one or more geophysical attributes from adjacent units so as to be distinguishable in terms of geophysical characteristics and presumably different enough to potentially affect disturbance and succession processes (and thus resulting vegetation patterns), and also be meaningful for management purposes (i.e., roughly corresponding to the scale of potential treatment units). Vegetation conditions are not considered in delineating GPUs so as to not bias the HRV and current departure results. Importantly, we deem it reliable to compare the current condition of a GPU to its own HRV because it is sufficiently large enough to do so. Thus, we derive an HRV and compute departure for each GPU independently (in contrast to the Site-level HRV and departure).

- *Subbasin level* - We quantify HRV and compute several departure metrics at the "Subbasin" level, which we define by Hydrologic Unit (HUC) level 12 watersheds. We further partition each Subbasin into BPCs, as described below, to better distinguish among sites varying in overall forest productivity. Importantly, we consider the Subbasin to be a meaningful "landscape" for characterizing vegetation dynamics; it is large enough to capture coarse-scale patterns resulting from disturbance and succession processes, yet small enough to capture the idiosyncrasies of non-stationary landscape processes. In lieu of having a comprehensive suite of designated project areas for the region, we deem HUC12 Subbasins as a practical surrogate and an appropriate scale for project-level planning and management, since HUC12 Subbasins generally encompass 10,000 - 25,000 acres - roughly the scale of most National Forest NEPA projects. Note, because some of the delineated Subbasins in the source dataset (USGS Watershed Boundary Dataset) exceed 25,000 acres, we manually split these larger Subbasins roughly in half based on logical drainage boundaries. Thus, all final subsasins are less than 25,000 acres. Like the GPU level assessment, here we compare the current condition of a Subbasin-by-BPC partition to its own HRV and compute departure for each partition independently.

Biophysical Classes and Units

To summarize HRV and current departure in landscape structure at the Site and Subbasin levels (see below), we subdivide the landscape into a set of Biophysical Classes (BPCs) based on estimated site productivity. It is important to recognize that BPCs are defined within each focal landscape; thus, the BPC classes are relative to the site productivity gradient within each focal landscape. We create BPCs as a means of "packaging" the results in a manner that will be most relevant to management at the project level and will best discriminate differences in the landscape metrics, given the assumption that tree productivity relates to vegetation characteristics of major interest to land management (e.g., tree cover). We also seek a parsimonious suite of BPCs; i.e., the fewest number of BPCs that will best characterize meaningful differences in the landscape metrics. After consideration of many alternative approaches, we opted for the following approach.

- First, we derive a proxy for cumulative tree biomass production under historical dynamic equilibrium conditions (i.e., HRV) at the cell level for all forested cells by summing Tree Height (ft) values every 20 years between simulation years 500 - 1,500, for example as depicted in **Figure 38** for the Bear River landscape.

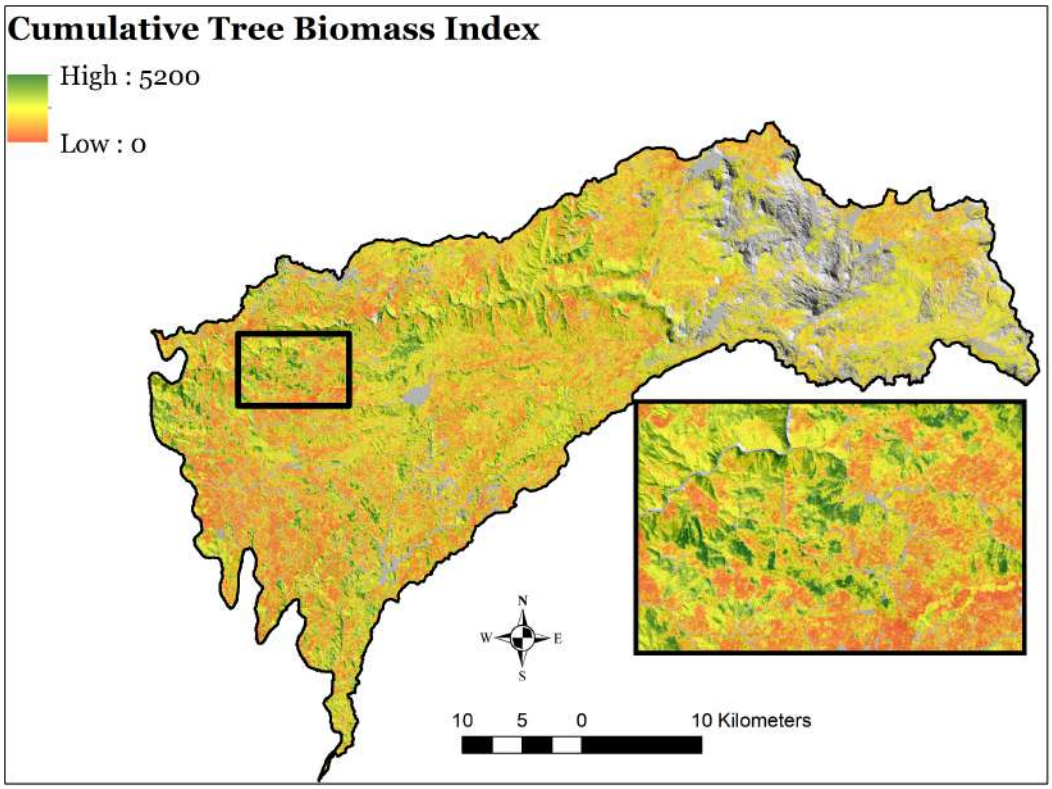

Figure 38: Simulated Cumulative Biomass Index derived by summing Tree Height (ft) at the cell level every 20 years over a period of 1,000 years under simulated historical (i.e., pre-settlement) dynamic equilibrium conditions, shown here for the Bear River landscape.

We posit that the cumulative sum of Tree Height (hereafter, "Biomass") under historical dynamic equilibrium condtions represents an index of realized site productivity that effectively integrates the net effects of all the disturbance and succession processes in LDSim, including, in particular, the frequency and severity of wildfire, the rate of tree establishment and the rate of tree growth after establishment. To reduce the "noise" in the data owing to pixelation, we apply a 25x25 m focal mean smoothing of the cumulative tree biomass layer. Thus, each 5 m cell value is replaced with the mean of the cell values within a 5x5 cell window centered on the focal cell.

- Next, we randomly sample one million cells and extract the values of Biomass and the following 10 geophysical variables (see **Appendix A** for a detailed description of each variable):

  - Precipitation
  - Water balance deficit
  - Available water storage
  - Topographic wetness index
  - Heat load index
  - Growing degree days
  - Topographic position index
  - Solar radiation index
  - Elevation
  - Slope

  Note, each of these geophysical variables is involved either directly or indirectly (e.g., combined with other variables into a composite index such as the site index) in one or more of the processes affecting cumulative tree biomass.

- Next, we use a Random Forest analytical framework (Breiman 2001) to predict Biomass from the 10 geophysical site variables. Random Forest is a non-parametric machine learning technique that allows for non-linear and heterogeneous responses (e.g., biomass may respond differently to precipitation as elevation increases) and thus can account for complex interactions among the predictors. The predicted value at each cell is in effect a "site index" of sorts as it is an index of the likely long-term realized productivity of the site under historical dynamic equilibrium conditions. Random Forest does not produce a single equation for predicting Biomass that can be reported here; rather, it builds 500 regression trees, each of which is a hierarchical, tree-like partitioning of the data based on the predictors (i.e., a decision tree), and takes the average predicted Biomass value across the 500 trees as the final predicted value. In general, the Random Forest is able to explain roughly 70 - 80 % of the variation in Biomass, depending on the focal landscape; the remaining 20 - 30 % of variation is "noise" that can not be explained by the 10 predictors (at least by this technique).

- Next, we classify predicted Biomass into 4 equal-area classes based on quartiles of the data, plus a zero class for all non-forest cells. Thus, this output layer includes 4 classes ranging from the least productive to most productive forest sites; i.e., supporting on average low to high cumulative tree Biomass under historical dynamic equilibrium conditions (as simulated), plus an "unknown" class representing non-forest areas (as mapped).

- Next, we apply a forest/nonforest mask based on the "existing" cover layer (as opposed to the estimated "historical" cover layer which is used in the simulation), and assign all nonforest cells in the existing cover layer to the zero Biophysical Class. We did this because the BPC layer is purposed to evaluate current departure, which is only feasible for cells mapped as forest in the current (or existing) landscape. The final BPC layer for the Bear River landscape, as an example, is depicted in **Figure 39**. It is important to recognize that the BPCs are artificial classes derived from an inherently continuous surface; i.e., they are categorical constructs derived solely to help with the visualization and packaging of results; they are not "real" in the sense that the depicted boundaries are not discrete nor are they recognizable as features on the ground.

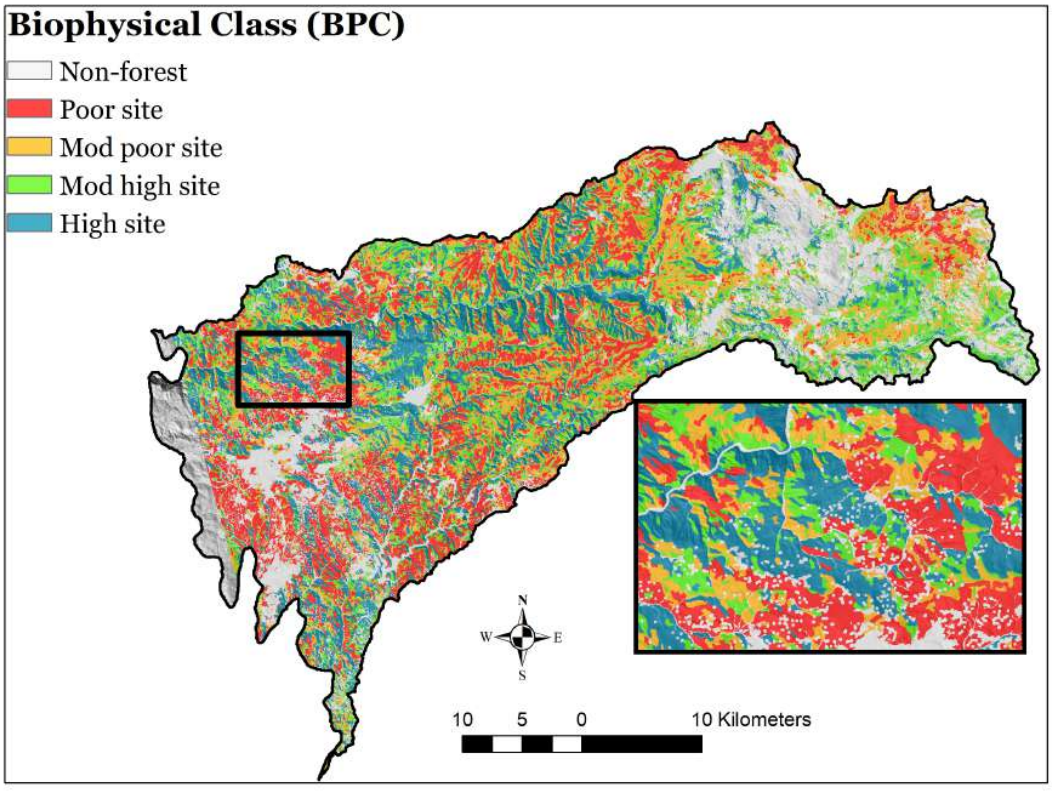

Figure 39: Biophysical Classes (BPCs) based on quartiles of predicted cumulative tree biomass derived from a Random Forest model to predict cumulative tree biomass under historical (i.e., pre-settlement) dynamic equilbrium conditions, as simulated, from 10 biophysical variables, shown here for the Bear River landscape. The Random Forest model explains roughly 70 - 80 % of the variation in Biomass under simulated historical dynamic equilibrium conditions, depending on the landscape.

- Lastly, we use a custom algorithm to simplify the BPC raster by dissolving patches < 1 ha in size (and replacing each patch with the neighboring patch having the longest shared edge) and trimming narrow appendages or "arms" < 30 m in width. Thus, the final BPC raster is comprised of patches, or Biophysical Units (BPUs), with a minimum size of 1 ha and minimum width at its narrowest of 30 m.

Model Calibration Context

It is essential to interpret the model results in the context of the model calibration, which is the means by which certain parameters are adjusted to produce certain output targets. As noted previously, we calibrate a few key disturbance regime parameters to achieve a suite of disturbance regime targets, without attention to the effects on the vegetation attributes, which we deem the dependent outcomes of interest. Together, model parameterization and calibration ultimately determine the outputs of the simulation and thus are critical to understand before judging the reliability and usability of the results. In particular, there are a few key processes that govern the production and maintenance of forest openings (i.e., cells classified as forest but without established trees to breast height), which is a critical aspect of the landscape composition and configuration with respect to the simulated range of variation in percent tree cover and the spatial distribution of developmental stages. Understanding the parameterization and calibration of these key processes is paramount to understanding and interpreting the results.

- *Forest regeneration* - The probability of tree establishment (i.e., forest regeneration) after high-mortality disturbance determines how quickly cells re-establish tree cover after canopy-replacing disturbance and thus how long cells remain in the Open developmental stage without tree cover. Lower probability of regeneration results in a greater percentage of the forest being in an Open developmental stage with reduced tree cover. Conversely, higher probability of regeneration results in a decrease in Open area and thus increase in tree cover.

  As described previously, we parameterize the probability of regeneration based on a statistical model derived from a large empirical dataset (Shive et al. 2018), and thus it is as objective as possible. Consequently, we deem the parameterization of the tree regeneration process extremely reliable, with the following caveats. The model and the empirical data set are not perfect of course, and thus any biases in the model assumptions or data will affect the outcome. In particular, the dataset does not contain observations from sites above ~ 2300 m in elevation, yet we apply the fitted model to all elevations, including those above 2300 m for lack of a better alternative. Given the unknown reliability of this extrapolation to higher elevations, it is possible that we over- (or under-) estimate the probability of regeneration on higher elevation sites, which would affect the estimated composition of the landscape with respect to the proportion in an Open canopy condition. Indeed, it is possible that due to the often harsh microclimate conditions and poorer soils at these higher elevations that tree regeneration in reality is less than we predict based on the empirical model. If, for example, our model over-estimates the probability of regeneration on these higher elevation sites our estimated proportion of the forest in an Open condition will be biased low (i.e., we will simulate less Open area than in the real world).

- *Wildfire Frequency and Severity* - The frequency and severity of wildfire together largely drive the production of forest in Open areas. Shorter fire return intervals and higher probability of high-mortality response together result in a greater proportion of the forest maintained in Open areas. Conversely, longer fire return intervals and lower probability of high-mortality response result in a decrease in Open areas.

As described previously, we parameterize and calibrate the wildfire susceptibility function by cover type to achieve the target FRP for each cover type. The targets are based largely on published scientific studies and thus represent our best estimates of FRP under historical reference period conditions. Nevertheless, if the published FRP estimates are inaccurate then the proportion of the landscape maintained in an Open condition in the simulation will also be inaccurate. Similarly, we parameterize and calibrate the wildfire mortality function by cover type to achieve the target percent mortality rates for each cover type. The targets are based on a combination of published scientific studies and expert opinion and thus do represent our best estimates of mortality rates under historical reference period conditions. However, as it is exceedingly difficult to estimate wildfire mortality rates for the historical reference period, the degree of uncertainty in our model calibration is much greater for wildfire mortality than FRP. For example, if we increase the wildfire mortality rate for mature trees from, say, 5 %, to, say, 10 %, for a common cover type such as Sierra Mixed-Conifer, this would have a significant affect on the proportion of the landscape maintained in an Open condition. Thus, it behooves the reader to review the model calibration pertaining to wildfire mortality before interpreting the results. This factor more than anything else drives the proportion of the forest in an Open condition and, in particular, in large forest openings. Therefore, it is paramount to consider the results in the context of this model calibration.

- *Senescence* - The probability of tree senescence as it ages also contributes to the production of forest Open areas, but the contribution from senescence is much less than that of high-mortality wildfire given the relative short FRPs. Although there is a random chance of mortality from senescence at any age, the probability is extremely low until trees reach an age of 200 years, at which point the probability of survival decreases steadily until 400+ years. Thus, most trees live > 200 years but few survive beyond 400 years. Given that FRPs are between 28 - 62 years for the common forest types, the probability of mortality from wildfire generally assumes a greater importance than the probability of mortality from senescence. Nevertheless, it behooves the reader to review the senescence parameterization before interpreting the results.

Fire Return Interval and Departure

Mean point-specific Fire Return Interval (FRI) represents the average number of years between fire events at the 5 m cell level. We compute mean FRI for the historical reference period by summarizing the interval between fires after model equilibration; i.e., under historical dynamic equilibrium, as simulated (N = 200 timesteps). The mean FRI layer for the Yuba River landscape, as an example, is depicted in **Figure 40**. We interpret the observed mean FRI after model equilibration at the cell level as a single integrated (albeit not comprehensive) summary of the historical wildfire disturbance regime.

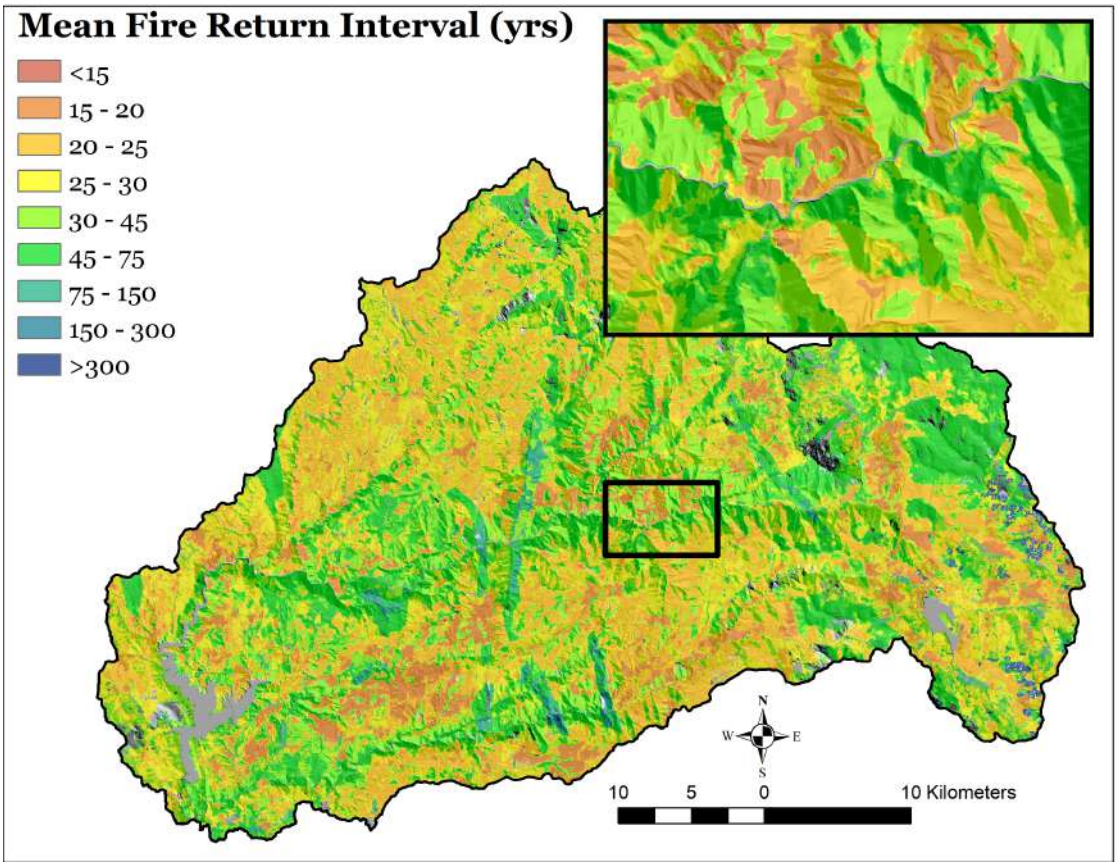

Figure 40: Mean Fire Return Interval (FRI) (yrs) at the 5 m cell level under historical (i.e., pre-settlement) dynamic equilibrium conditions, as simulated, shown here for the Yuba River landscape.

In addition to the map of cell-level FRI, we also quantify the variation among cells in FRI by BPC. Here, the emphasis is on the *spatio-temporal* range of variability in fire occurrence at the spatial extent of the individual *cell*. The "spatio-temporal" variability stems from the fact that we measure the variability both across cells (i.e., spatial variability) and over time as represent by FRI (i.e., temporal variability). The measured variability is specific to this particular landscape and landscape extent owing to the idiosyncrasies of landscapes. Importantly, the variability would likely differ if the landscape features that affect wildfire were to differ or if we were to change the spatial grain of the assessment from 5 m to, say, 30 m. For this purpose, we compute select quantiles (Q) of the FRI distribution for each BPC, in which the range in values between the 2.5^{th} and 97.5^{th} quantiles represents the 95 % range of variability in FRI, analogous to a 95 % confidence interval. The corresponding table for the Yuba River landscape, as an example, is shown in **Table 4**.

Table 4: Mean Fire Return Interval (FRI)(yrs) historical range of variability (HRV) by Biophysical Class (BPC) for the Yuba River landscape. HRV is given as select quantiles of the simulated range of variability in cell-level FRI under historical dynamic equilibrium conditions

BPC	Q2.5	Q25	Q50	Q75	Q97.5
Low	16	21	23	26	52
ModLow	17	23	26	38	97
ModHigh	18	25	30	44	107
High	20	28	35	50	99

Fire Return Interval Departure (FRID) represents the percentage deviation of the contemporary

(post-settlement) mean point-specific FRI and the mean point-specific FRI under historical (i.e., pre-settlement) dynamic equilibrium conditions. We compute FRID based on one of the metrics reported in Safford and Van de Water (2014), but substitute our simulated mean point-specific FRI under pre-settlement conditions for their mean FRI by cover type, as follows:

$$for\ (cFRI_i \geq pFRI_i):\ FRID_i = (1 - \frac{pFRI_i}{cFRI_i}) * 100$$

$$for\ (pFRI_i < cFRI_i):\ FRID_i = -(1 - \frac{pFRI_i}{cFRI_i}) * 100$$

where: $cFRI_i$ = contemporary FRI for the i^{th} cell; and $pFRI_i$ = pre-settlement FRI for the i^{th} cell. Thus, if the contemporary FRI is > the pre-settlement FRI, the departure is positive and increases asymptotically to 100 % as the difference between the two FRIs increases. Conversely, if the contemporary FRI is < the pre-settlement FRI, the departure is negative and increases asymptotically to -100 % as the difference between the two FRIs increases. cFRI is computed as the length of the contemporary period (1909 - 2019 = 110 years, in this case) divided by the frequency of wildfires and prescribed fires plus one. Thus, if there have been no contemporary fires, cFRI equals the length of the contemporary period (110 years in this case). As such, FRID is a conservative estimate of actual departure; i.e., true departure could be greater than calculated since the true fire-free period could be longer than the length of the contemporary record of 110 years. It follows that for cells with a pre-settlement FRI longer than 110 years, the negative departure estimates should be interpreted with caution, and perhaps not at all to be safe.

The FRID layer for the Yuba River landscape, as an example, is depicted in **Figure 41**. Like the metrics reported by Safford and Van de Water (2014), our FRID metric quantifies the extent in percent to which contemporary fires (i.e., since 1909) are burning at frequencies similar to the frequencies that occurred prior to significant Euro-American settlement, as simulated. However, our FRID metric differs from Safford and Van de Water (2014) in two important ways. First, Safford and Van de Water computed four different FRID metrics based on the equation above, but substitute the mean, median, minimum and maximum reported pre-settlement FRIs for each cover type. We use only our mean point-specific FRI under pre-settlement conditions because at the cell-level the variation in simulated FRI captures the range reported by cover type that Safford and Van de Water used. In other words, the use of our cell-level FRI eliminates the need to compute several different FRID metrics based on the mean and range, since the complete variation within a cover type is captured by our cell-level mean FRI. Second, and more importantly, Safford and Van de Water (2014) used pre-settlement FRIs by cover type, whereas we use pre-settlement FRIs at the 5 m cell level. Hence, our reference FRIs for comparison against the contemporary record is highly refined and spatially resolved, making it much more useful for unit and project-level planning and management.

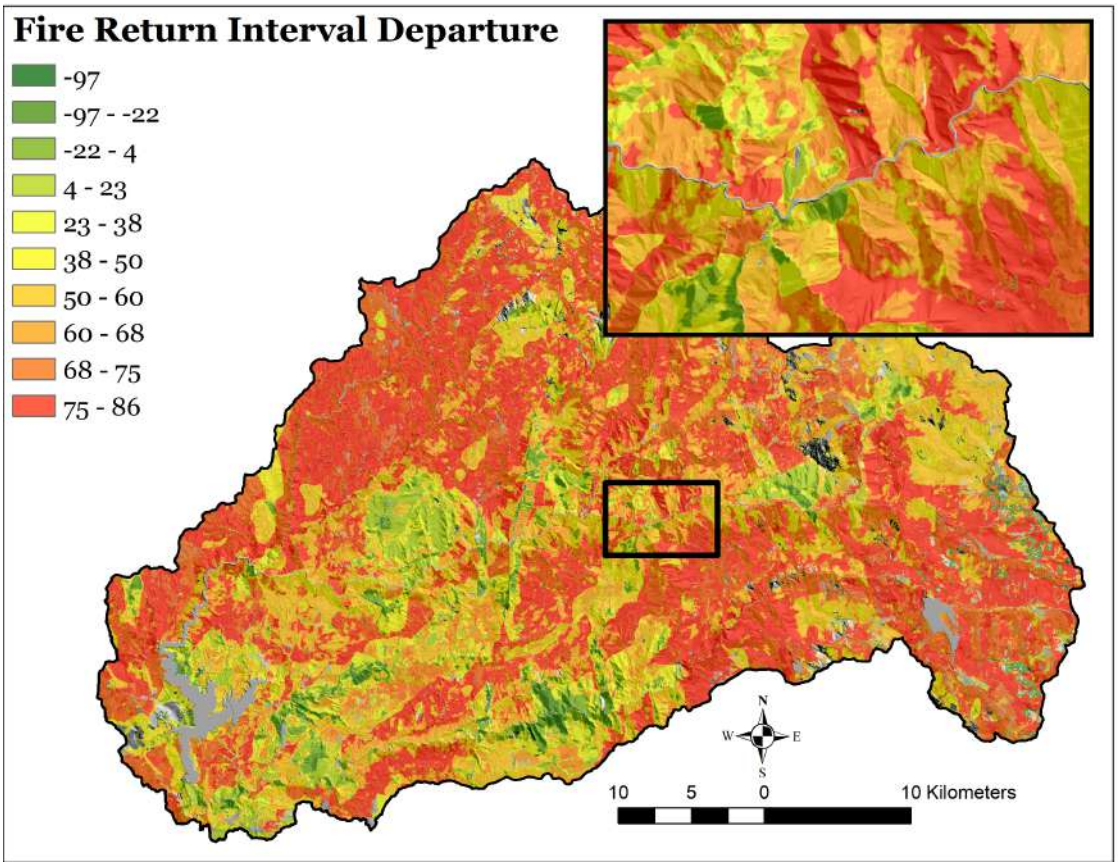

Figure 41: Fire Return Interval (FRI) Departure (FRID) index at the 5 m cell level, representing the percent to which contemporary fires (i.e., since 1909) are burning at frequencies similar to the frequencies that occurred prior to significant Euro-American settlement, as simulated, shown here for the Yuba River landscape. Positive values represent a contemporary FRI > the pre-settlement FRI and, conversely, negative values represent a contemporary FRI < the pre-settlement FRI.

Management applications

Mean FRI and FRID at the cell level can be used for unit- and project-level planning and management; i.e., the scale at which individual treatments and collections of treatments (projects) are planned and implemented. Indeed, FRI and FRID are often major considerations in the choice of fuels treatments applied to individual units within projects, although we acknowledge that many other factors will likely play an important role in fuels management at the unit level.

Mean FRI and FRID at the cell level have the following specific management applications:

- The map of FRI at the cell level can suggest where and how frequently prescribed fire treatments should be applied to restore the historical fire frequency, recognizing that many areas may not be in a current condition to receive stand-alone fire treatments due to constraints or concerns such as high levels of surface and ladder fuels, proximity to homes, sensitive cultural or natural resources, or plantations.
- The map of FRID provides a single integrated summary of departure in the fire regime at the cell level that can be used as a stand-alone product to aid in the spatial planning and management of fire. For example, given a practical limit on the number of acres that can be treated with prescribed fire

over some period of years, the map of FRID can suggest priorities for where fire is most urgently needed to restore the historical fire frequency – should that be the goal. For example, **Figure 42** identifies the top 10 % of the Yuba River landscape in terms of FRID cells. Of course, the top 10 % cells would simply serve as the "seeds" for creating practical treatment units. Note that any number of spatial filters could be applied before determining the priority cells, such as excluding private lands, sensitive soils, vulnerable wildlife habitat, etc.

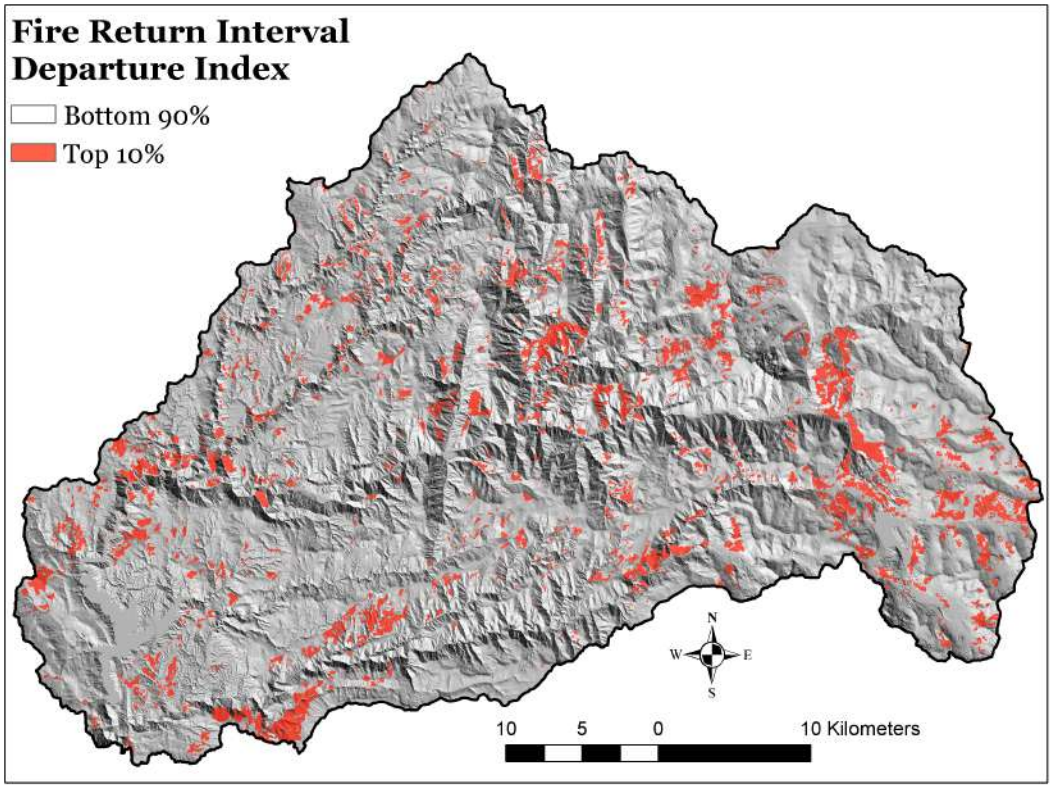

Figure 42: Fire Return Interval Departure (FRID) index at the 5 m cell level, representing the percent to which contemporary fires (i.e., since 1909) are burning at frequencies similar to the frequencies that occurred prior to significant Euro-American settlement, as simulated, shown here for the Yuba River landscape and the top 10 % of the landscape with respect to FRID.

Vegetation Persistence

We define vegetation persistence as the likelihood of persisting in either an early- or late-seral condition at the 5 m cell level. We interpret the observed mean FRI of high-mortality wildfires after model equilibration (N = 200 timesteps) at the cell level as a proxy for vegetation persistence, under the assumption that locations with shorter high-mortality FRIs would likely persist longer in early-seral stages and, conversely, locations with longer high-mortality FRIs would likely persist longer in late-seral stages. The corresponding layer for the Yuba River landscape, as an example, is depicted in **Figure 43**.

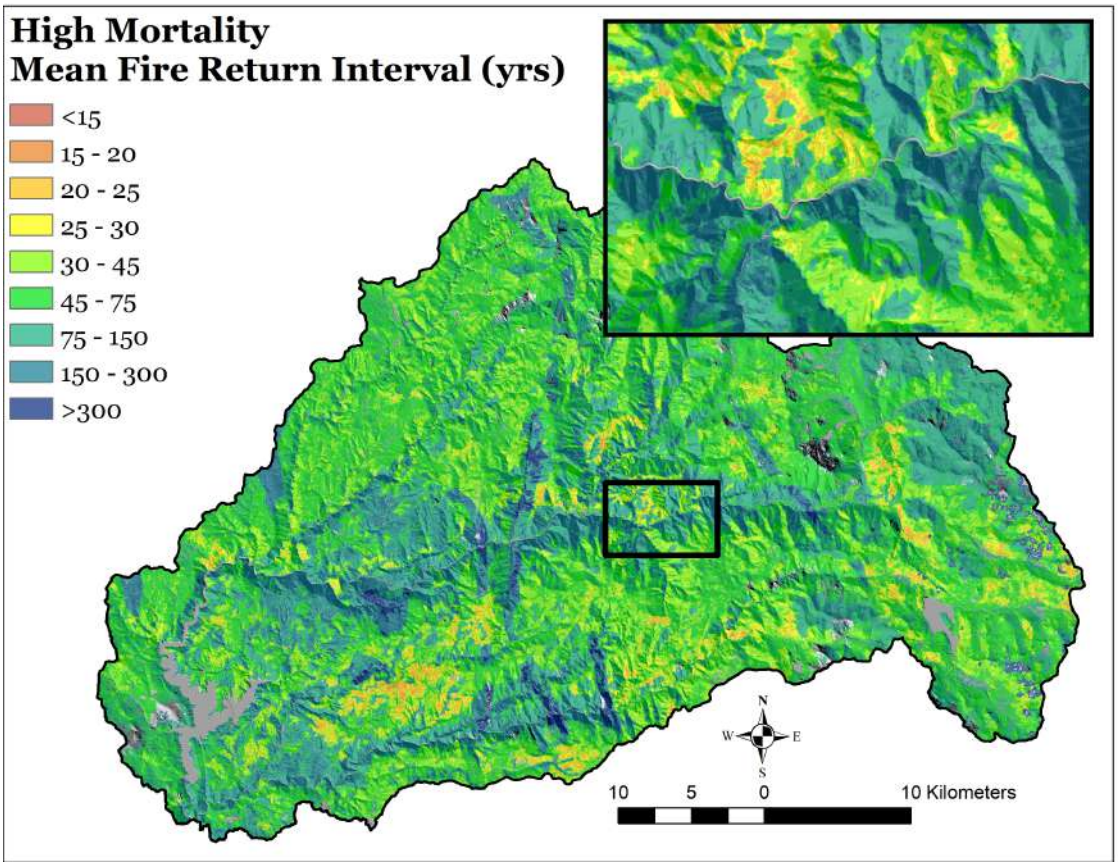

Figure 43: Mean High-mortality Fire Return Interval (FRI) (yrs) at the 5 m cell level under historical (i.e., pre-settlement) dynamic equilibrium conditions, as simulated, shown here for the Yuba River landscape.

Management applications

The map of high-mortality FRI provides a proxy for vegetation persistence that can be used as a stand-alone product to aid in the spatial planning and management of vegetation treatments.

The high-mortality FRI map has the following specific management applications:

- Areas with a longer high-mortality FRI have a greater likelihood of persisting in late-seral forest conditions under the forcings of natural wildfire disturbance, all other things being equal. Such areas might be logical priorities for managing habitat for late-seral dependent species such as the California spotted owl (*Strix occidentalis occidentalis*). For example, **Figure 44** identifies the 10 % of the Yuba River landscape with the longest high-mortality FRIs. If there were a management objective to maintain, say, 10 % of the landscape in late-successional reserves, these areas would be logical choices since they would have low risk of high mortality wildfire under natural forcings. Of course, these areas would logically be considered in combination with those areas in the current landscape that have low risk of high mortality fire. Indeed, the intersection of these two layers would make the best choices for late-successional reserves from a fire risk perspective, and could be combined with other spatial filters to identify the final priorities.

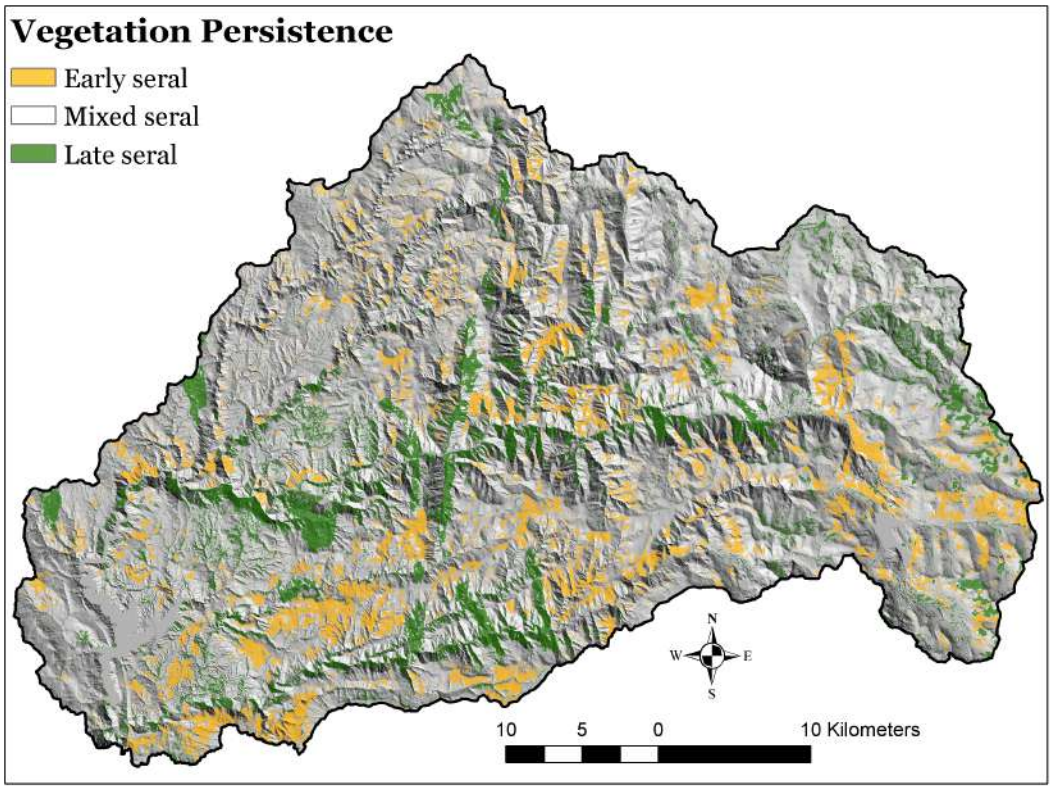

Figure 44: Mean High-mortality Fire Return Interval (FRI) (yrs) at the 5 m cell level under historical (i.e., pre-settlement) dynamic equilibrium conditions, as simulated, for the Yuba River landscape, highlighting the 10 % of the landscape with the shortest FRI (Early seral) and the 10 % of the landscape with the longest FRI (Late seral).

- Areas with a shorter high-mortality FRI have a greater likelihood of persisting in early-seral forest conditions under the forcings of natural wildfire disturbance, all other things being equal. Such areas might be logical priorities for creating and maintaining large forest openings that provide habitat for numerous early-seral dependent species (e.g., Dellasala et al. 204; Swanson et al. 2014). For example, **Figure 44** identifies the 10 % of the Yuba River landscape with the shortest high-mortality FRIs. If there were a management objective to maintain, say, 10 % of the landscape in early-successional reserves or large forest openings, these areas would be logical choices since they would have high risk of high mortality wildfire under natural forcings. Of course, these areas would logically be considered in combination with those areas in the current landscape that have high risk of high mortality fire. Indeed, the intersection of these two layers would make the best choices for early-successional reserves from a fire risk perspective, and could be combined with other spatial filters to identify the final priorities.

Site Level HRV and Departure

We quantify HRV and current departure at the spatial extent of a "Site"; i.e., a 40-m radius window around each focal cell, primarily for the purpose of monitoring current vegetation conditions compared to historical reference conditions across the entire focal landscape. In addition, because each Site also falls within a single BPC based on the location of the focal cell, we are able to characterize HRV and current departure separately for each BPC. We also restrict our assessment of Site-level HRV and departure to cells mapped as forest and where we have Lidar-derived vegetation attributes for the current landscape.

At the Site level, HRV represents the variation in the landscape metric across all Sites within each BPC and over time under historical dynamic equilibrium conditions. Specifically, the landscape at each timestep of the simulation after model equilibration (N = 200) represents a single snapshot of what the landscape condition could have been like at any point in time under historical dynamic equilibrium conditions, and here we focus on the conditions at the Site level in each snapshot. Because of the enormous size of the data sets being generated, we evaluate every cell as the focal cell (i.e., center) of a Site, but only at 100-year (or 20 timestep) intervals after model equilibration, for a total of 11 landscape snapshots and millions of Site-level observations. In addition, the current landscape also has a range of values across Sites (CRV), rather than a single value. Thus, a comparison of HRV and CRV involves comparing two distributions, and current departure represents the degree to which the CRV distribution deviates from the HRV distribution. Moreover, because each Site falls within a single BPC, we can describe the HRV and CRV distributions for each metric separately by BPC.

At the Site level, we include only those landscape metrics that we deem appropriate for use in guiding unit and project-level planning and management. We present the results in both tabular and graphical form. The template for the output is illustrated in **Figure 45**. What is important to note in the tabular output is that the HRV is presented as a select set of quantiles (Q), in which the Q2.5 - Q97.5 range represents the 95 % range of variability in the metric under historical dynamic equilibrium conditions, and that the current condition also has a quantile distribution representing the variation among Sites in the current landscape (CRV). Again, here the emphasis is on the differences between these two distributions: HRV versus CRV. The tabular data is also presented graphically as a box-and-whisker plot, in which the median value is represented as a solid black horizontal line, the 25 - 75th quantiles as the box, and the 2.5 - 97.5th quantiles as solid black lines (a.k.a. whiskers) extending outward from the box. Both the CRV and HRV have box-and-whisker distributions and are thus presented beside each other as a pair.

Metric	Scenario	Q2.5%	Q25%	Q50%	Q75%	Q97.5%
Landscape metric	CRV	value of the landscape metric corresponding to each of the specified quantiles (Q) of the current range of variability (CRV)				
	HRV	value of the landscape metric corresponding to each of the specified quantiles (Q) of the historical range of variability (HRV)				

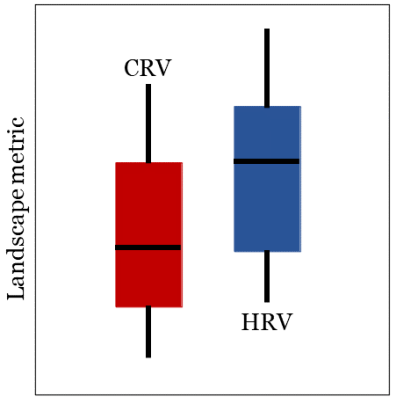

Figure 45: Tabular and graphical template for summarizing the Current Range of Variation (CRV) and Historical Range of Variation (HRV) in a landscape metric at the Site level (40-m radius window centered on a 5 m focal cell).

At the Site level, we derive a departure index for each metric by BPC based on the Percentage Dissimilarity Index (also known as the Bray-Curtis or Sorensen Dissimilarity Index), as follows:

$$DI_i = 100 * \left(\frac{\sum_{j=1}^{5} abs(H_{ij} - C_{ij})}{\sum_{j=1}^{5} (H_{ij} + C_{ij})} \right)$$

where: C_{ij} = current condition of the corresponding metric for the i^{th} BPC and the j^{th} quantile (for the set Q2.5, Q25, Q50, Q75, Q97.5); H_{ij} = historical reference period condition of the corresponding metric for the i^{th} BPC and j^{th} quantile; j = quantile bin index {1:5}; abs = absolute value; and DI_i = departure index for the corresponding metric for the i^{th} BPC. Note, in the numerator we are taking the absolute value of the difference between the current and HRV values for each of the five quantile, and then summing across quantiles; thus, we are not distinguishing whether the current landscape has more or less than the HRV for any quantile, simply that it differs and by how much. In the denominator we are summing the current and HRV values for each of the five quantiles, and then summing across quantiles. After multiplying by 100, the quotient of these two quantities represents the percentage of non-overlap between the two distributions. Equivalently, this index represents the compliment of the overlap between the two distributions. As such, if the current and HRV distributions are identical, the percentage dissimilarity (i.e., departure) will be zero, and if the two distributions do not overlap at all the percentage dissimilarity (or departure) will be 100 %. In other words, the departure index computed this way represents the percentage of maximum departure of the current landscape relative to the HRV, and it therefore has an intuitive interpretation.

Metric 1: Developmental Stage

Developmental stage at the Site level is based on discrete stages of canopy height development: Open, Sapling, Pole, Small Tree, Medium Tree, and Tall Tree. We quantify the *composition* of forest developmental stages at the Site level based on the percentage of the forested portion of the Site in each developmental stage. Specifically, for each developmental stage we compute the percentage of each Site in that developmental stage and summarize the distribution across Sites in the current landscape to generate the CRV. We do the same for the historical snapshots of the landscape under dynamic equilibrium conditions to generate the HRV. The pairwise comparison of the CRV and HRV distributions for each developmental stage indicate the nature and degree of current departure in the Site-level prevalence of each developmental stage across the landscape.

Table 5 and **Figure 46** provide an example of the pairwise CRV and HRV distributions for forest developmental stages on High productivity Sites in one of the focal landscapes. In this example, departure in the Open and Tall Tree stages is most notable. Specifically, there is a disproportionate number of Sites with too little area in the Open and the Tall Tree stages relative to HRV. More generally, the figure suggests that the current landscape has a distinctly unimodal distribution in developmental stages, with the majority of Sites having a preponderance of Poles and Small Trees and a paucity of Open areas and Tall Trees. In contrast, the HRV distribution suggests a much more even distribution of area among developmental stages.

Table 5: Current Range of Variation (CRV) and Historical Range of Variation (HRV) in the percentage of a Site (40-m radius window centered on a 5 m focal cell) in each forest developmental stage on High productivity Sites in one of the focal landscapes.

Tile	Class	Scenario	Q2.5	Q25	Q50	Q75	Q97.5
High	Open	CRV	0	0	0	7	53
High	Open	HRV	1	4	8	17	66
High	Sapling	CRV	0	3	13	31	68
High	Sapling	HRV	0	5	18	37	72
High	Pole	CRV	1	13	23	35	68
High	Pole	HRV	0	4	11	24	58
High	ShortTree	CRV	0	11	21	34	64
High	ShortTree	HRV	0	2	6	13	41
High	MedTree	CRV	0	1	12	35	70
High	MedTree	HRV	0	7	16	28	57
High	TallTree	CRV	0	0	0	1	26
High	TallTree	HRV	0	5	12	22	46

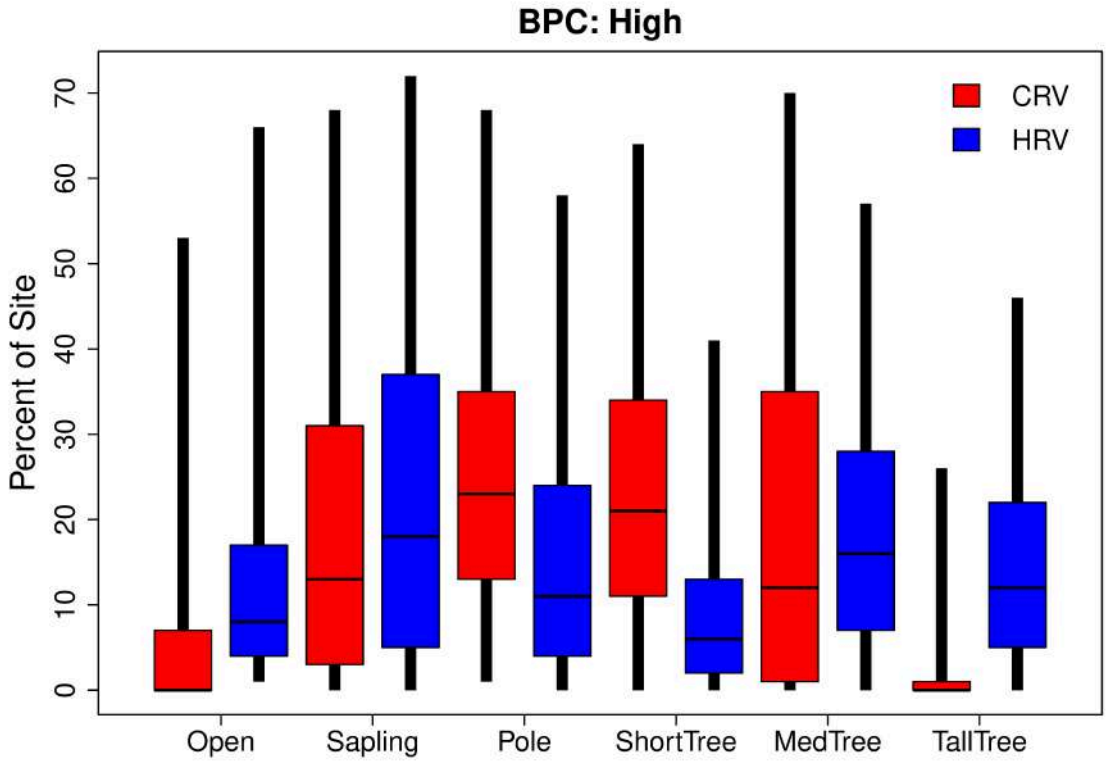

Figure 46: Current Range of Variation (CRV) and Historical Range of Variation (HRV) in the percentage of a Site (40-m radius window centered on a 5 m focal cell) in each forest developmental stage on High productivity Sites in one of the focal landscapes.

The departure index for this example, based on Percentage Dissimilarity defined above, is ~ 23 %, which is the average across the six developmental stages. Note, this means that the developmental stage distribution on High productivity sites in this focal landscape has ~ 77 % overlap between the CRV and HRV distributions or, conversely, ~ 23 % non-overlap of the two distributions. The departure index for all four BPCs and all three Site-level metrics is shown in **Figure 47**. In this particular example, the departure in developmental stage distribution is greatest on Low productivity sites and roughly similar on the other BPCs.

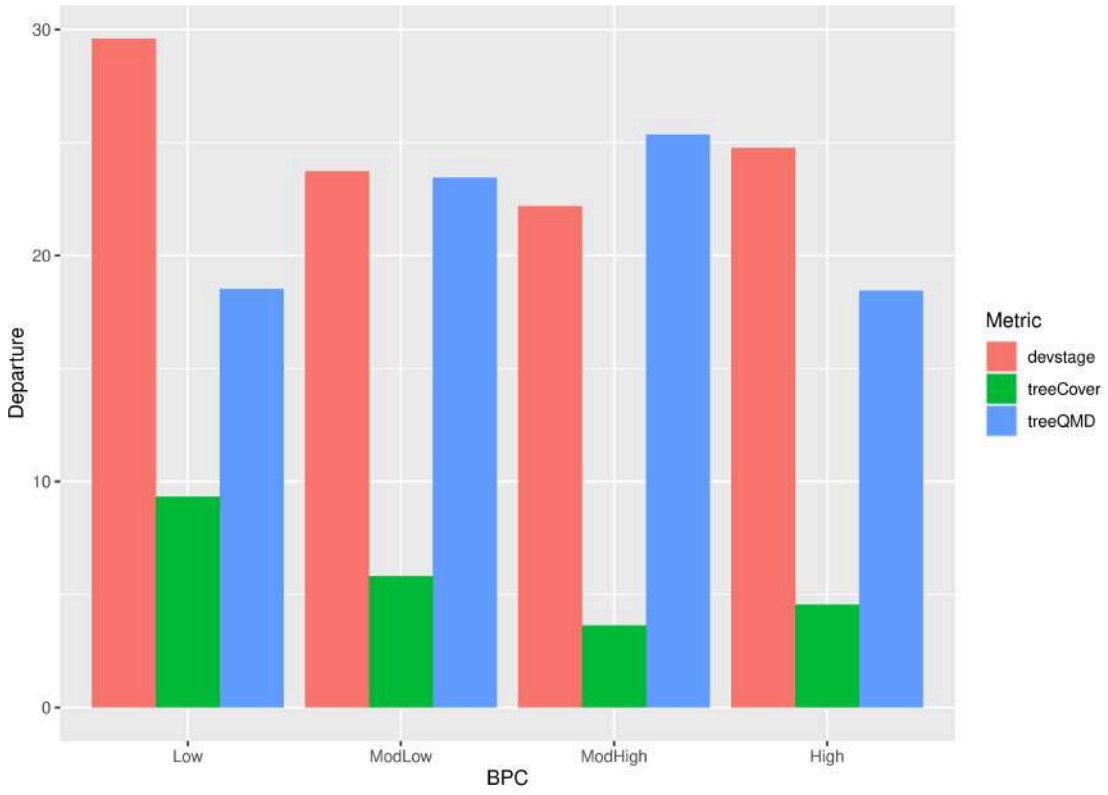

Figure 47: Site-level Departure Index based on Percentage Dissimilarity between the Current Range of Variation (CRV) and Historical Range of Variation (HRV) for Sites (40-m radius window centered on a 5 m focal cell) on four Biophysical Classes (BPCs) in one of the focal landscapes for three different Site-level metrics: Developmental Stage, Quadratic Mean Diameter of trees, and Percentage Tree Cover.

Departure in developmental stage composition at the Site level can also be visualized as illustrated in **Figure 48** for a randomly selected area in one of the focal landscapes. The figure depicts vegetation Developmental Stage in the unit for the current landscape and three random snapshots under historical dynamic equilibrium conditions. For reference purposes, the figure also depicts three randomly selected 40-m radius Sites within the unit. The figure illustrates several things. First, within this single unit there is considerable variability in developmental stage composition across Sites at every point in time. In other words, within the unit the vegetation is maintained as a spatially heterogeneous mosaic of developmental stages and, moreover, the patches of like developmental stages are quite small, suggesting a markedly heterogeneous seral stage distribution at the Site level, and this pattern is consistent across most of the landscape. Second, the fine-grained mosaic of developmental stages behaves as a shifting mosaic; i.e., the patches of like developmental stage shift in space over time, reflecting the fine-scale interplay of disturbance and succession processes operating on individual trees, clumps of trees, and openings. Lastly, current departure is visually evident in the figure. The current unit has a majority of area (> 60 %) in the sapling and pole stages of development, whereas the historical snapshots have a preponderance of medium and tall tree stages of development interspersed with larger openings.

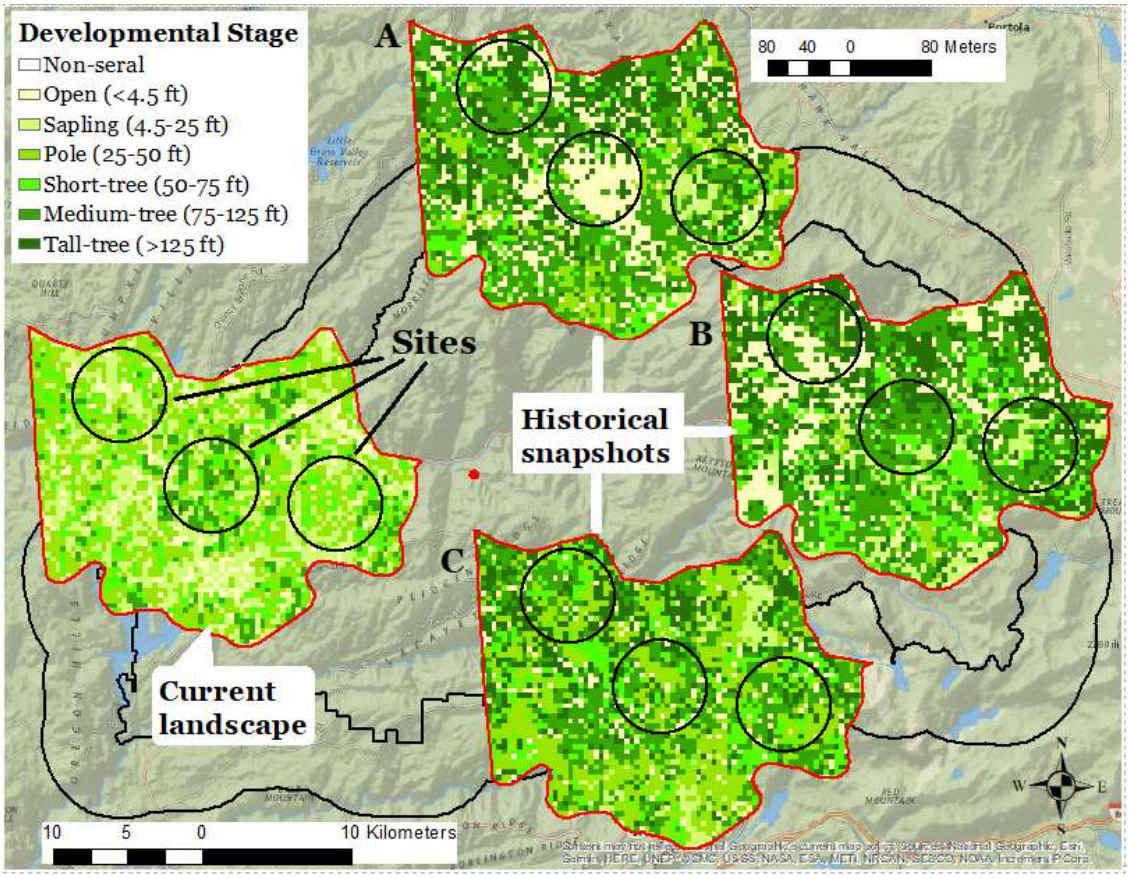

Figure 48: Vegetation developmental stages (based on canopy height classes) for a single randomly selected 8-ha (20-acre) forest unit, depicting the current vegetation condition and three random snapshots (A-C) under historical dynamic equilibrium conditions. For comparative purposes, three random 40-m radius Sites are also depicted.

Metric 2: Tree Size

Tree Size at the Site level is based on the Quadratic Mean Diameter (QMD) of established trees within a 40-m radius of the focal cell. Thus, even a cell in the Open developmental stage (i.e., forest cell without an established tree to breast height, and thus no diameter at breast height) is likely to have a QMD > 1 inch so long as there is a single established tree within 40 m of the focal cell. Moreover, QMD is based on only the cells with established trees; therefore, any cell in the Open developmental stage (i.e., no established tree) is not considered in the computation – only cells with established trees are tallied. Thus, if there is a single cell with an established tree in the window, then QMD is based on that single tree and equals the tree's diameter at breast height (DBH). Accordingly, QMD can be quite high even in relatively open areas if the few neighboring trees are large in diameter. Also, note that at the Site level, we report the range of variation in QMD as a continuous variable, not tree size classes derived from QMD.

Table 6 and **Figure 49** provide an example of the pairwise CRV and HRV distributions for Tree Size (QMD) on High productivity Sites in one of the focal landscapes. In this example, departure is quite apparent. Specifically, the HRV in QMD is shifted about 6 - 8 inches greater than in the CRV. Not surprisingly, this suggests that the current landscape contains too few Sites with a preponderance of larger diameter trees relative to the HRV.

Table 6: Current Range of Variation (CRV) and Historical Range of Variation (HRV) in the quadratic mean diameter (QMD) of trees on a Site (40-m radius window centered on a 5 m focal cell) on High

productivity Sites in one of the focal landscapes.

Tile	Scenario	Q2.5	Q25	Q50	Q75	Q97.5
High	CRV	3	9	13	18	30
High	HRV	10	17	21	25	33

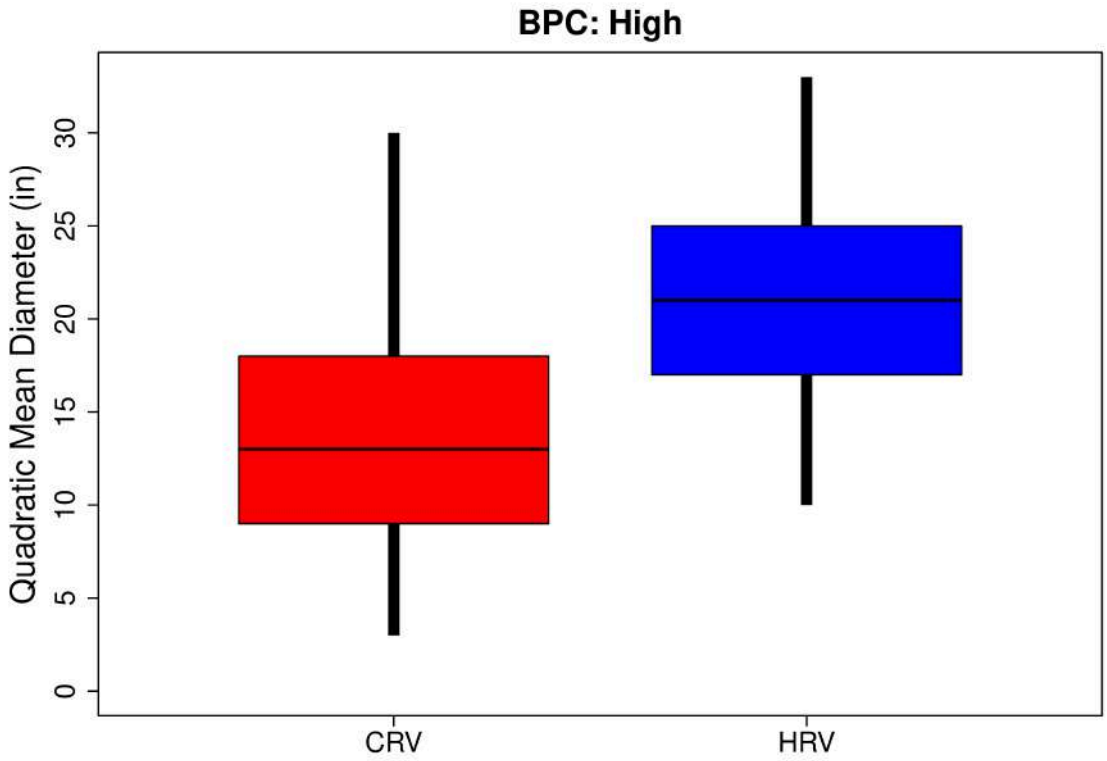

Figure 49: Current Range of Variation (CRV) and Historical Range of Variation (HRV) in Quadratic Mean Diameter (QMD)(inches) of trees within a 40-m radius Site centered on each 5 m focal cell on High Productivity Sites in one of the focal landscapes.

The departure index for this example, based on Percentage Dissimilarity defined above, is ~ 18 %. Note, this means that the QMD distribution on High productivity sites in this focal landscape has ~ 82 % overlap between the CRV and HRV distributions or, conversely, 18 % non-overlap of the two distributions. The departure index for all four BPCs and all three Site-level metrics is shown in **Figure 47**. In this particular example, the departure in QMD distribution is slightly greater on moderate productivity sites than either Low or High productivity sites.

Departure in Tree Size at the Site level can also be visualized as illustrated in **Figure 50** for a randomly selected area in one of the focal landscapes. As before, the figure depicts Site-level QMD in the unit for the current landscape and three random snapshots under historical dynamic equilibrium conditions. For reference purposes, the figure also depicts three randomly selected 40-m radius Sites within the unit. The figure illustrates several things. First, similar to the Site-level variability in Developmental Stage, there is considerable variability in QMD across Sites at every point in time. In other words, within the unit there is spatial variability in tree sizes at the Site level. Second, despite there being a strong shifting mosaic in developmental stage composition within this unit over time (as described above), the spatial distribution of QMD is much more stable. In other words, even though there are fine-scale shifting patches of trees in different Developmental Stages over time, the QMD for any particular Site tends to remain relatively more

stable. Lastly, current departure is quite evident in the figure. The current unit has a mean Site-level QMD of ~ 12 inches and no Sites above 19 inches, whereas the historical snapshots all have mean QMDs > 20 inches and no Sites < 11 inches, as further depicted in **Figure 51**.

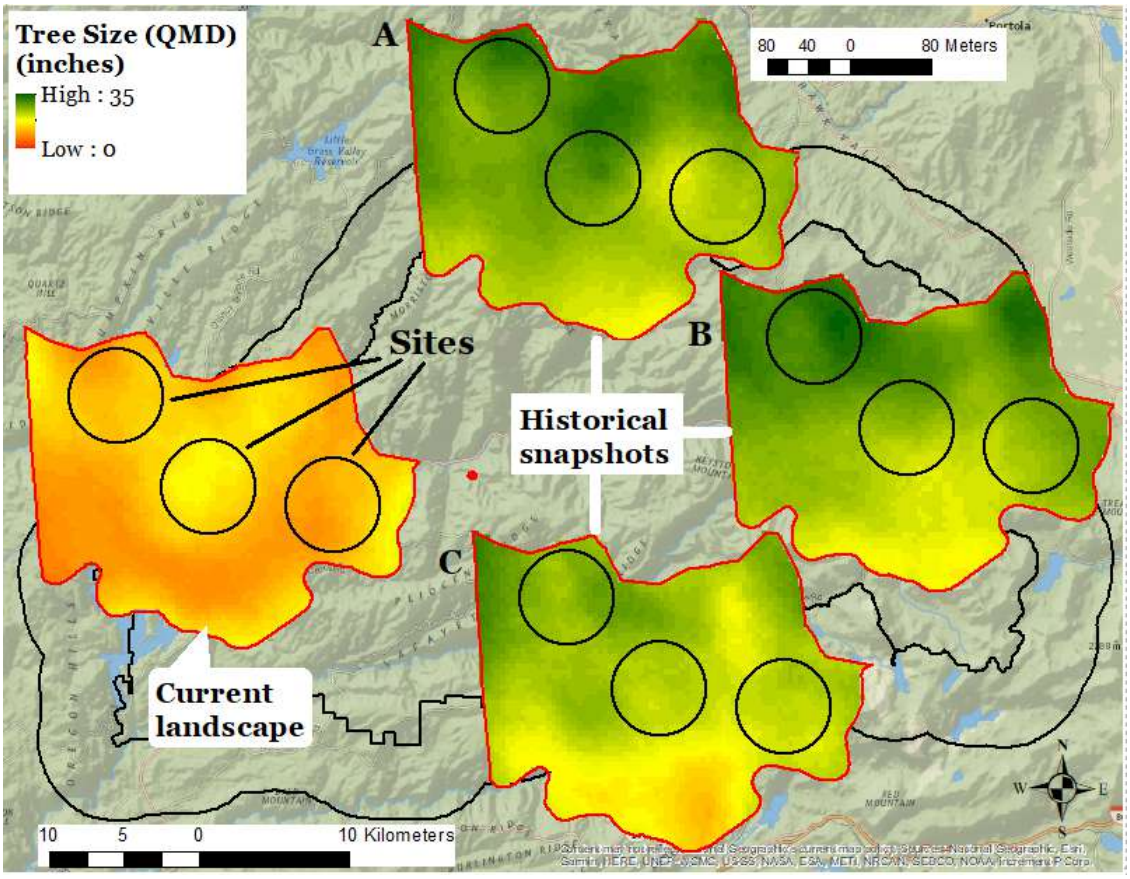

Figure 50: Tree size based on Quadratic Mean Diameter (QMD)(inches) within a 40-m radius Site centered on each focal cell for a single randomly selected 8-ha (20-acre) forest unit, depicting the current vegetation condition and three random snapshots (A-C)under historical dynamic equilibrium conditions. For comparative purposes, three random 40-m radius Sites are also depicted.

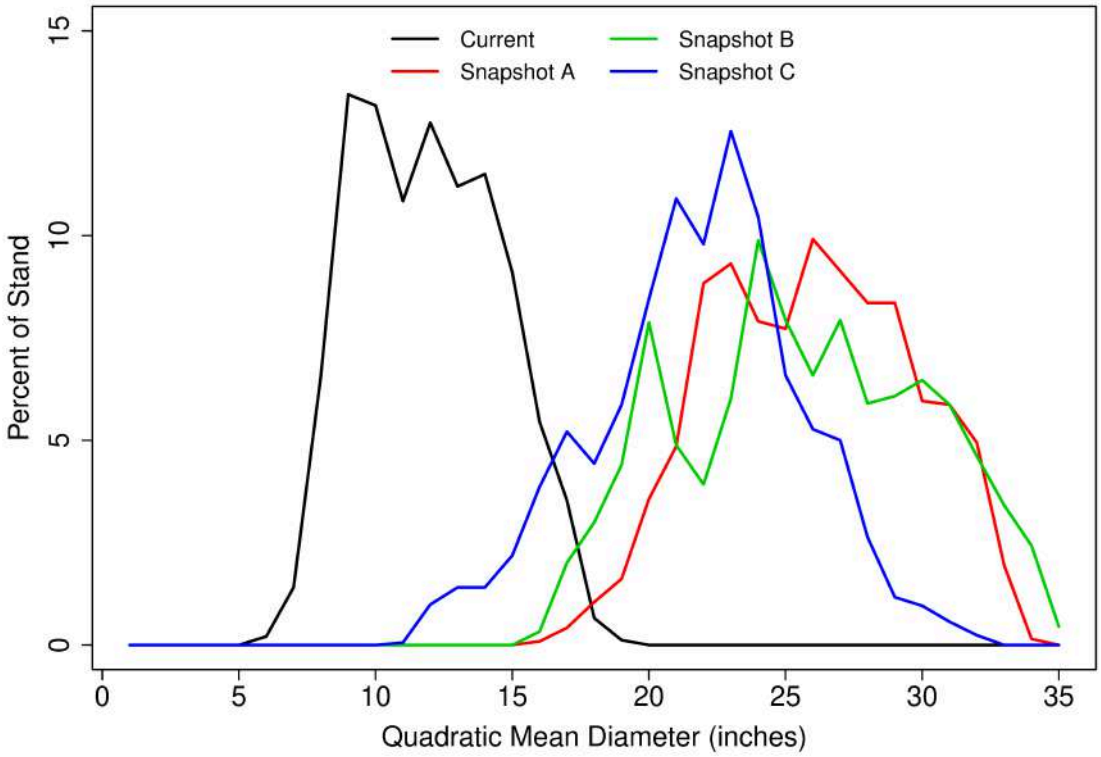

Figure 51: Distribution of tree size based on Quadratic Mean Diameter (QMD)(inches) within 40-m radius Sites centered on each 5 m focal cell within a single randomly selected 8-ha (20-acre) forest unit for the current landscape and three random snapshots (A-C, corresponding to the images in the previous figure) under historical dynamic equilibrium conditions.

Metric 3: Tree Cover

Tree Cover at the Site level is based on the percentage of 5-m cells with established trees to breast height within a 40-m radius of the focal cell. Thus, even a cell in the Open developmental stage (i.e., forest cell without an established tree to breast height) has a percent tree cover > 0 % so long as there is a single established tree within 40 m of the focal cell. In addition, as computed here, Tree Cover represents the percentage of cells within 40 m containing one or more established trees to breast height, not actual tree canopy cover, and as such is a biased (high) index of actual tree canopy cover (i.e., actual tree canopy cover will be less than reported here). We compared our estimates of percent tree cover to Lidar-based estimates of percent canopy cover for the Yuba River landscape and found a 16 % average positive bias; i.e., our percent tree cover is on average ~ 16 % higher than actual percent tree canopy cover. Consequently, to convert our Tree Cover estimates to canopy cover, simply subtract 16 %. Also, note that at the Site level we report the range of variation in percent tree cover (as a continuous variable), not tree cover classes.

Table 7 and **Figure 52** provide an example of the pairwise CRV and HRV distributions for percent tree cover on High productivity Sites in one of the focal landscapes. In this example, departure is apparent, as the CRV in percent tree cover is shifted about 5 - 10 percent greater than the HRV. Not surprisingly, this suggests that the current landscape contains too many Sites with exceptionally high percent tree cover and, conversely, too few Sites with relatively low percent tree cover. Recall, to interpret these tables and figures with respect to tree canopy cover, subtract 16.

Table 7: Current Range of Variation (CRV) and Historical Range of Variation (HRV) in the percent tree cover of a Site (40-m radius window centered on a 5 m focal cell) on High productivity Sites in one of the

focal landscapes.

Tile	Scenario	Q2.5	Q25	Q50	Q75	Q97.5
High	CRV	46	92	99	100	100
High	HRV	33	82	91	95	98

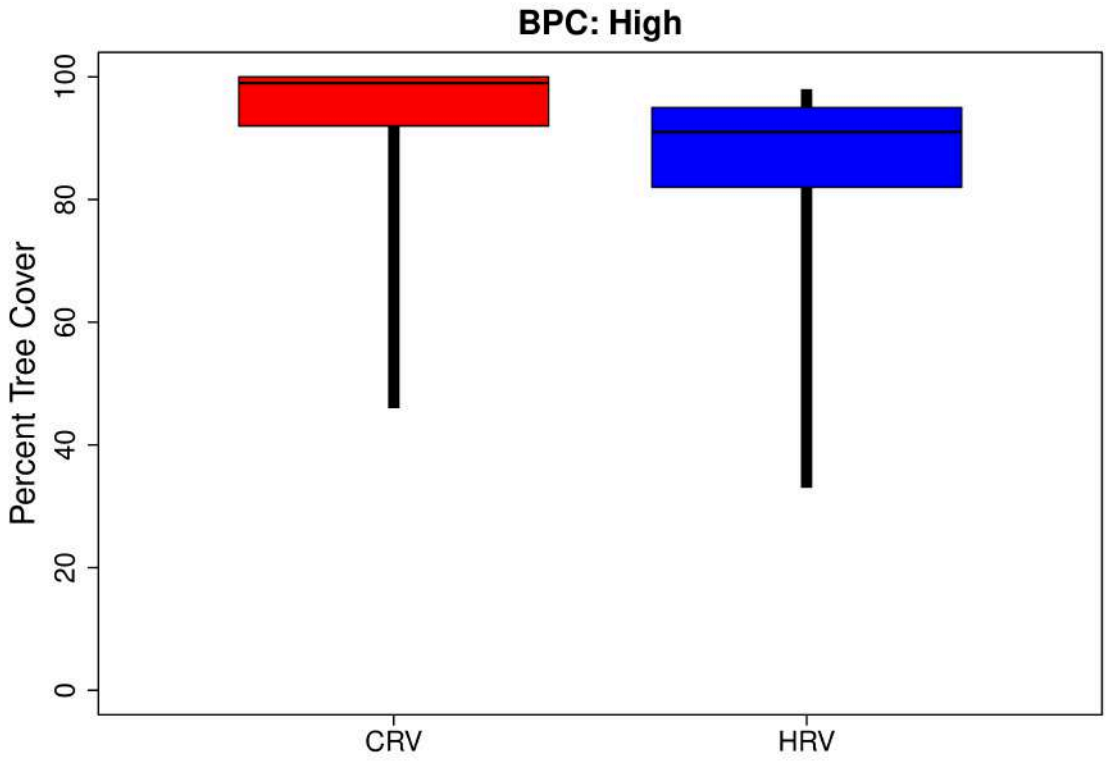

Figure 52: Current Range of Variation (CRV) and Historical Range of Variation (HRV) in percent Tree Cover (as defined) within a 40-m radius Site centered on each 5 m focal cell on High Productivity Sites in one of the focal landscapes.

The departure index for this example, based on Percentage Dissimilarity defined above, is ~ 4 %. Note, this means that the percent tree cover distribution on High productivity sites in this focal landscape has ~ 96 % overlap between the CRV and HRV distributions or, conversely, 4 % non-overlap of the two distributions. The departure index for all four BPCs and all three Site-level metrics is shown in **Figure 47**. In this particular example, the departure in percent tree cover distribution is greatest on Low productivity sites.

Departure in percent tree cover at the Site level can also be visualized as illustrated in **Figure 53** for a randomly selected area in one of the focal landscapes. As before, the figure depicts Site-level percent tree cover within the unit for the current landscape and three random snapshots under historical dynamic equilibrium conditions. For reference purposes, the figure also depicts three randomly selected 40-m radius Sites within the unit. The figure illustrates several things. First, consistent with the previous metrics, there is considerable variability in percent tree cover across Sites at most points in time, although Snapshot C depicts relatively little Site-level variability, and this pattern is consistent across most of the landscape. This is also evident in **Figure 54**. Sites vary from ~ 25 - 99 percent tree cover in two of the three historical snapshots. Second, consistent with the shifting mosaic of developmental stages discussed above, percent tree cover also exhibits a shifting distribution of high and low cover over time, reflecting the fine-scale interplay of disturbance and succession processes operating on individual trees, small clumps of trees, and

openings. Lastly, in contrast to findings for Developmental Stage and Tree Size, this unit appears to be well within the HRV in percent tree cover, and is in fact relatively similar to Snapshot C in having most of the area in high percent tree cover.

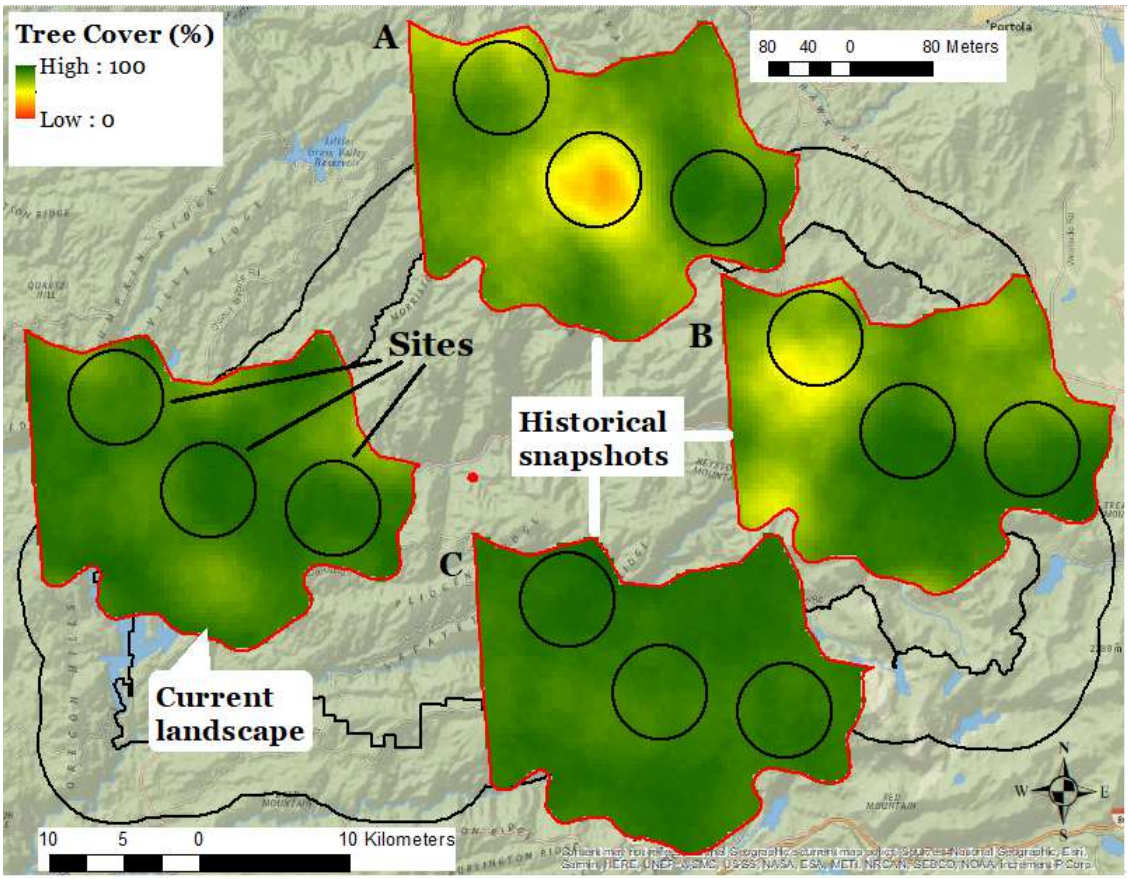

Figure 53: Tree cover based on percent of cells with established trees to breast height within a 40-m radius Site centered on each focal cell for a single randomly selected 8-ha (20-acre) forest unit, depicting the current vegetation condition and three random snapshots (A-C) under historical dynamic equilibrium conditions. For comparative purposes, three random 40-m radius Sites are also depicted.

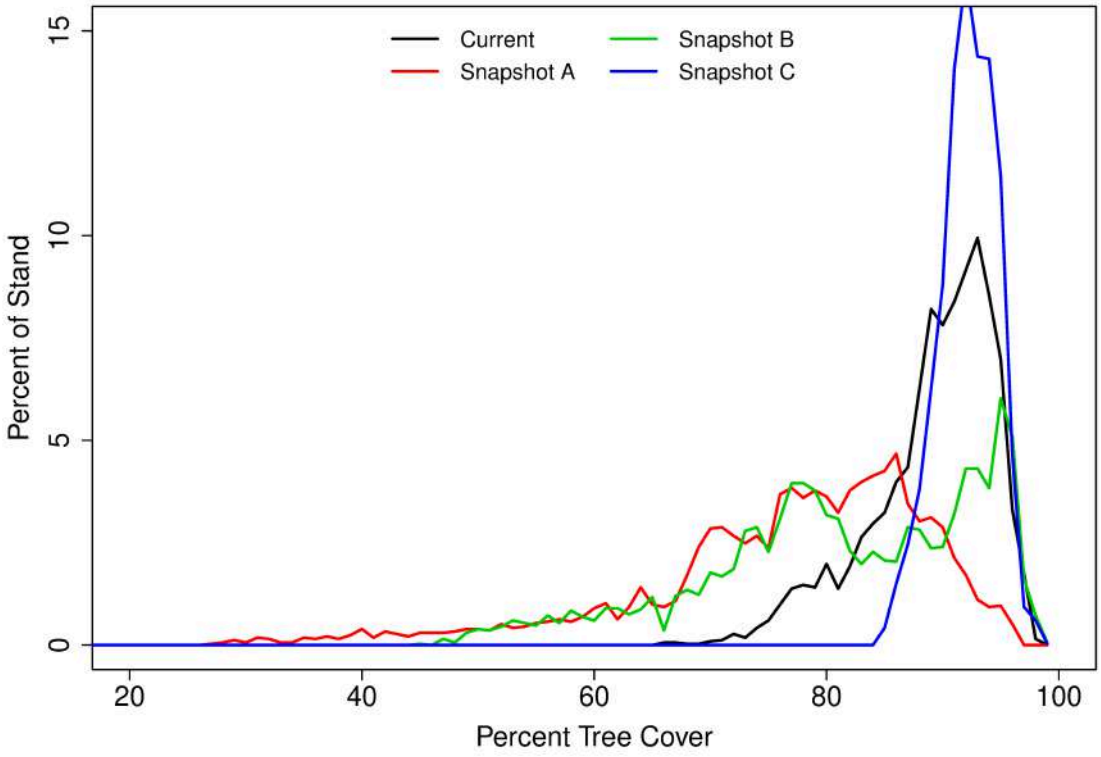

Figure 54: Distribution of tree cover based on percent of cells with established trees within 40-m radius Sites centered on each focal cell within a single randomly selected 8-ha (20-acre) forest unit for the current landscape and three random snapshots (A-C, corresponding to the images in the previous figure) under historical dynamic equilibrium conditions.

Management Applications

Site-level results can aid unit and project-level planning and management as well as watershed-level monitoring of vegetation conditions over time. More specifically, Site-level HRV can provide a detailed, specific and quantitative basis for establishing desired conditions across the landscape based on a goal of ecological restoration of historical reference conditions, and Site-level CRV can provide a quantitative benchmark for determining the direction and magnitude of change needed to move the current landscape towards HRV – should that be the goal. Of course, we acknowledge that current departure from historical reference conditions is only one consideration in evaluating vegetation conditions across the landscape.

Specific management applications of Site-level results, as described below, should be interpreted with the following considerations in mind:

- First, it is important to recognize that at the Site level the emphasis is on the *spatio-temporal* range of variability in landscape structure at the spatial extent of an individual *Site* - the 40-m radius neighborhood around each focal cell. The "spatio-temporal" variability stems from the fact that the variability is across Sites within a single timestep (i.e., spatial variability) and over time (i.e., temporal variability) for HRV. Importantly, the measured HRV is still specific to the focal landscape and landscape extent owing to the idiosyncrasies of landscapes. Importantly, the HRV would likely differ if we were to define "Site" at a different scale.
- Second, it is important to recognize that *Site-level* variation is likely to be considerably greater than *Geophysical Unit-level* or *Subbasin-level* variation, for the simple reason that small areas have the

potential to take on the full range of potential conditions (e.g., from no canopy cover to complete canopy cover), whereas larger areas are less likely to exhibit the extreme conditions because local changes in vegetation conditions are likely to be subsumed within the much larger landscape. Importantly, the wider range of variation in landscape structure at the Site level does not mean that "anything goes" and that management has license to promote any landscape condition (given that desired conditions are based on HRV). Rather, it is the distribution of landscape conditions across Sites (and over time under HRV) that can serve as the target for desired conditions across the landscape. The "distribution" of Site-level conditions, not any particular Site condition, is the appropriate use of the Site-level HRV.

- Third, it is important to distinguish between "Site" and "Geophysical Unit". Here, we choose to summarize HRV and CRV at the Site level using a fixed 40-m radius plot so as to maintain constancy in the spatial scale of a Site. Thus, every Site has the same spatial extent – a 40-m radius window around the focal cell. This facilitates comparison of metrics across space (i.e., from one Site to another) and over time. In contrast, as described previously, a GPU is defined based on geophysical criteria and can vary widely in size and shape from one location to another due to differences in terrain, soils and microclimate. Thus, a GPU does not have an explicitly defined single spatial scale. Thus, while a GPU is a useful concept and provides an unbiased means of assessing local HRV and departure at the approximate scale of potential treatment units, it serves poorly for comparing the HRV of one place to another – although it can be useful to compare itself in its current condition to its own HRV (see below).

- Fourth, we chose the scale of a Site (40-m radius neighborhood) based on two major factors. First, many important ecological processes such as tree establishment, growth and competition are affected by environmental conditions within the distance of a single mature tree. In other words, the ecological neighborhood within which a tree significantly affects its surroundings and is significantly affected by its surroundings is often considered to be that of a single tree height. This may be especially true for processes affected by light levels, which is often a limiting factor for tree establishment and growth. We considered a tree ~ 40 m tall to be a "tall" tree in our classification of developmental stages, and thus we used this distance to define the ecological neighborhood corresponding to a "Site". Second, we chose a scale that was practical for management in the field; i.e., the scale at which a forester or biologist in the field could easily assess vegetation conditions. We considered 40 m to be a reasonable compromise in this regard; small enough to be able to effectively "see" the vegetation conditions from a single location, and yet large enough to account for ecological conditions of importance. However, we recognize that there is "no one size to fit all" in this regard. Nevertheless, we deemed the advantages of a single scale for "Site" to outweigh the disadvantages of defining Site at multiple scales. In particular, given the scale-dependent nature of landscape metrics, having a single and consistent scale for measuring HRV makes the interpretation of the results unambiguous.

- Lastly, it is important to recognize that Site-level departure reflects the deviation between the CRV across Sites and the HRV across Sites and over time within the focal landscape. Thus, departure for a Site is not based on a comparison of the current Site condition to its own HRV (as is the case with GPU and Subbasin departure, see below); rather it is the distribution of current Site conditions across the entire landscape compared to the historical distribution across Sites and over time that forms the basis for Site-level departure.

Subject to the considerations above, Site-level results have the following specific management applications:

- Site-level results do not provide a single quantitative target for vegetation condition – should restoration of HRV conditions be the objective – for any individual Site within a treatment unit. Instead, the results can provide loose quantitative targets for the distribution of vegetation conditions to be achieved across all Sites over the full extent of the landscape (albeit within BPCs).

  Let's take the example presented above for percent tree cover on High productivity Sites for one of the focal landscapes (**Table 7**) and work through how these results can provide management

direction at the unit and project levels. The HRV distribution reveals a range in the percent tree cover of a Site between 34 - 99 % and a median condition of 92 %. Note, this is the 95 % range of variation and does not include the extremes, which extend between 0 - 100 %. Recall, this would equate to a range in percent tree canopy cover of 18 - 83 % and a median of 76 % because of the average bias in our 5 m resolution-based estimate of percent canopy cover. This means that at the Site level, percent tree cover (and by extension, percent tree canopy cover) can and should vary widely; there is no single "right" target condition. Instead, it is the comparative distribution across Sites between CRV and HRV that provides some management direction. In this example, the CRV distribution has on average 7 % greater percent tree cover (and by extension, 7 % greater percent tree canopy cover). Thus, if vegetation treatments were to reduce tree canopy cover on average by 7 % across all High productivity Sites (and thereby maintain the variability across Sites), the CRV and HRV distributions would align and the departure index would shrink to zero.

- As note above, Site-level results can provide loose quantitative targets for the distribution of vegetation conditions to be achieved across all Sites over the full extent of the landscape (albeit within BPCs) – should restoration of HRV conditions be the objective. Specifically, comparing the CRV distribution to the HRV distribution provides a quantitative basis for estimating current departure. In this regard, our departure index provides a single quantitative summary of the deviation between these two distributions that can serve as a benchmark for measuring where we are today. Recomputing the departure index after some period of vegetation treatments (real or simulated) could be used to determine the magnitude and rate of change resulting from the treatments, and thus serve as the quantitative basis for monitoring landscape changes under the auspices of adaptive management.

Geophysical Unit Level Departure

We quantify HRV and current departure at the spatial extent of a Geophysical Unit (GPU), primarily for the purpose of identifying and prioritizing local areas for restoration treatments – should that be the goal. After considering many alternative approaches for defining GPUs, we opted for the following:

- First, we resample the following 10 geophysical layers (see **Appendix A** for a detailed description of each variable) to a 40 m spatial resolution and extract the values of the variables for each cell (note, the 40 m resolution is necessary for computational purposes):

  - Precipitation
  - Water balance deficit
  - Available water storage
  - Topographic wetness index
  - Heat load index
  - Growing degree days
  - Topographic position index
  - Solar radiation index
  - Elevation
  - Slope

  Note, each of these geophysical variables is involved either directly or indirectly (e.g., through complex interactions) in one or more of the ecological processes affecting vegetation conditions over space and time.

- Next, we use a Spatially-Constrained Multivariate Clustering analytical framework to cluster cells into GPUs within each HUC12 Subbasin. Specifically, we use the Rgeoda package in R and the RedCap (Regionalization with dynamically constrained agglomerative clustering and partitioning) function developed by Guo (2008) to perform the clustering. Briefly, RedCap starts by agglomerating neighboring cells hierarchically into larger and larger clusters until they are all combined into one

large cluster, in our case using z-score standardized variables (i.e., raw variables converted to z-scores by subtracting the mean and dividing by the standard deviation) and Ward's minimum variance linkage. Ward's linkage fuses the neighboring cells and/or clusters at each step based on the linkage that minimizes the overall within-cluster variance in the 10-dimensional geophysical space. Note, RedCap is similar to other agglomerative hierarchical clustering methods except that it enforces a spatial contiguity constraint such that the clusters always form spatially contiguous units. Then, RedCap prunes the tree back to find the final set of clusters based on user-supplied criteria. In our case, we impose a minimum cluster area of 4 hectares (~ 10 acres) and a target final number of clusters based on an average cluster area of 20 hectares (~ 50 acres). Thus, RedCap prunes the tree back from the top down, at each step choosing the partition (i.e., cutting a subtree into two) resulting in the largest decrease in overall within-cluster variance (i.e., the most homogeneous resulting clusters), until the target number of clusters is achieved and without splitting a cluster such that either of the resulting sub-clusters falls below the minimum area specified.

- Next, after deriving the GPUs above, we apply a spatial filter to remove mapped non-forested areas based on our existing cover layer (Ecover), since we are focused exclusively on HRV and current departure in forests. We apply a second spatial filter to remove areas without Lidar coverage, since we rely on Lidar to produce an accurate assessment of current vegetation conditions, and thus departure. After applying these spatial filters, we use custom software to dissolve residual GPUs $<$ 4.04 ha (~ 10 acres); i.e., merge them with an adjacent GPU having the longest border, and to eliminate residual appendages $<$ 40 m in width.
- Next, we resample the final GPU layer to 5 m for consistency with other spatial layers.
- Lastly, we describe each GPU based on each of the 10 geophysical variables (plus Aspect) to assist in the interpretation of the GPUs and to facilitate queries of the GPU database (e.g., to evaluate departure for a subset of GPUs that meet a set of descriptive geophysical conditions). Specifically, we classify each of the geophysical variables into 3 - 5 classes (see **Appendix A**). The Method field denotes the classification method: literature = derived from literature; expert = based on logical break points; quantiles = based on breakpoints of 0.2 and 0.8 quantiles of the data (i.e., values corresponding to the lower 20 % and upper 20 % of the observations). Note, the values given for the aspect variable represent class values previously derived from aspect in degrees and corresponding to the Labels given. Also, the variable elevation is divided between westside (elevWest) and eastside (elevEast) based on the Sierra Nevada Framework Project (2001). The Class field is a numeric representation of the class. The Value field corresponds to break point values for the corresponding variable, such that the first class has values $<$ the break point value given, the second class has values $\geq$ the first break point and $<$ the break point value given, and so on. Lastly, the Label field gives the descriptive label for each class. After classifying each of the geophysical layers, we determine which, if any class, comprises $\geq$ 80 % of the unit and assign that descriptive label to the GPU. If no class comprises $\geq$ 80 % of the unit, we assign 'mixed' as the descriptive label.

At the GPU level, we use a large but parsimonious suite of landscape metrics (see below) that we deem meaningful for estimating departure and appropriate given the available data, again solely for the purpose of prioritizing units for treatments aimed at restoring HRV conditions. However, we acknowledge that there may be other potentially meaningful metrics for this purpose, as our chosen suite of metrics is not exhaustive. Specifically, we selected metrics that measure vegetation composition and configuration with respect to tree cover, tree size (dbh) and developmental stage (or tree height). Stem density is another important and complementary attribute of GPU condition, but we do not have the data from our simulation model to assess this directly. However, the Tahoe Central Sierra Initiative (TCSI) project developed a basal area departure metric based on a remote sensing derived product (for the current condition) in comparison to reference HRV conditions based on a suite of reference sites deemed to reflect pre-settlement vegetation conditions. We have chosen to include the TCSI basal departure metric in our suite of LDSim-derived metrics for the purpose of creating a more comprehensive composite departure index (see below).

For each landscape metric, the current condition of the GPU is given by the value of the landscape metric computed for the current landscape. The HRV of the GPU is based on the variability in the landscape metric under historical dynamic equilibrium conditions. To compute HRV for each landscape metric, the GPU at each timestep of the simulation after model equilibration (N = 200 timesteps) is considered a single snapshot of what the GPU condition could have been like at any point in time under historical dynamic equilibrium conditions. Because of the enormous size of the data sets being generated and the computational requirements, we evaluate snapshots of each GPU at 20-year (or 4 timestep) intervals after model equilibration for a total of 51 snapshots of each GPU. We define HRV as the range in values between the 2.5^{th} and 97.5^{th} quantiles, which represents the 95 % range of variability in the metric under historical dynamic equilibrium conditions, analogous to a 95 % confidence interval.

To compute current departure for each landscape metric (except as noted below), we compare the current condition value to the HRV distribution and derive a Departure Index and Score for each GPU, as follows:

- First, we compute the value of the metric for the current GPU condition.
- Next, we derive the HRV for the GPU by computing quantiles of the simulated distribution of values for the metric (based on the 51 snapshots). Here we are primarily interested in the values corresponding to the 2.5^{th} (Q2.5), 50^{th} (Q50) and 97.5^{th} (Q97.5) quantiles, as described next.
- Next, we derive a departure index for the GPU, as follows:

$$for\ (C_i \geq Q50_i) : DI_i = \frac{C_i - Q50_i}{Q97.5_i - Q50_i}$$

$$for\ (C_i < Q50_i) : DI_i = \frac{C_i - Q50_i}{Q50_i - Q2.5_i}$$

where: C_i = current condition for the i^{th} GPU; Q_i = specified quantiles of the simulated distribution under historical dynamic equilibrium conditions for the i^{th} GPU; and DI_i is the departure index for the i^{th} GPU. Thus, if the current condition is greater than the 50^{th} quantile of the HRV (i.e., the median of the HRV), the departure index will be positive. Conversely, if the current condition is less than the 50^{th} quantile of the HRV, the departure index will be negative. Moreover, if the current condition is equal to the 97.5^{th} quantile of the HRV (i.e., the upper range of the HRV), the departure index will equal 1. Similarly, if the current condition is equal to the 2.5^{th} quantile of the HRV (i.e., the lower range of the HRV), the departure index will equal -1. Accordingly, if the current condition is, say, twice the distance from the median HRV as the upper range of the HRV, the departure index will be 2, and so on. Thus, the departure index is unbounded on both sides and any values between -1 and 1 can be considered within the HRV, and values less than -1 or greater than 1 can be considered degrees of departure, with more negative numbers indicating greater negative departure and more positive numbers indicating greater positive departure.

Figure 55 illustrates the computation of the departure index. The horizontal box-and-whisker plot depicts the HRV distribution. Actually, the box itself, which represents the range in the metric from the 2.5^{th} to 97.5^{th} quantiles, is how we define the HRV – the whiskers here represent the extremes of the simulated range (0 - 100 quantiles). The current landscape has a value that falls somewhere along the continuum in relation to the HRV distribution. If the current value is less than the 2.5^{th} quantile it is considered "negative" departure (depicted in blue). Conversely, if the current value is greater than the 97.5^{th} quantile it is considered "positive" departure (depicted in green). The departure index is computed as the quotient of: 1) the difference between the current landscape value and the median HRV value, and 2) the difference between the 2.5^{th} and 50^{th} quantiles for negative departure (Ref-) or the difference between the 97.5^{th} and 50^{th} quantiles for positive departure (Ref+). Hence, if the current value is equal to the 2.5^{th} quantile, the departure index will be -1. Similarly, if the current value is equal to the 97.5^{th} quantile the departure index will be +1. A departure index between -1 and +1 is considered within the HRV.

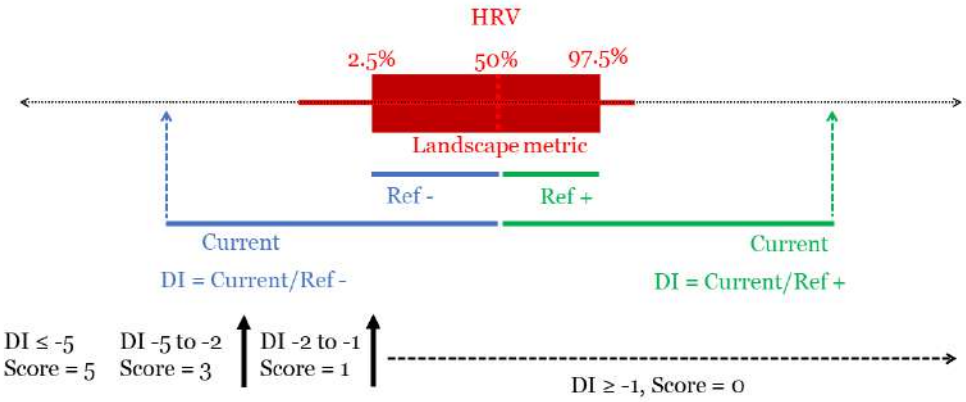

Figure 55: Illustration of the derivation of the departure index and departure score as applied to the Geophysical Unit (GPU) level departure metrics and the Subbasin level departure metrics representing landscape composition.

- Next, we assign a "negative" departure score to the GPU by classifying the departure index, as follows:

$$if\ DI_i \leq -5,\ DSN_i = 5$$
$$elseif\ DI_i \leq -1,\ DSN_i = -1 * DI_i$$
$$else\ DSN_i = 0$$

where: DI_i = departure index, as defined above, for the i^{th} GPU; and DSN_i = negative departure score for the i^{th} GPU. Thus, if the current condition is within the HRV or greater than the HRV (i.e., departure index > -1) the departure score equals 0; otherwise, if the current condition is less than the HRV the departure index will be less than -1 and the departure score will be 1 to 5 depending on the magnitude of negative departure. Note the difference between the departure "index" and departure "score". The departure index represents degrees of departure in either direction from the median HRV value, whereas the departure score is always positive and represents degrees of negative departure in this case. This negative departure scoring scheme reflects our principle concern for GPUs in which the current condition has a value for the metric that is less than the HRV for that metric, which makes sense in the context of the specific metrics described below. In addition, the departure score was created to standardize the departure indices across metrics (i.e., putting them all on a 0 - 5 scale) so as to be able to combine them meaningfully into a composite departure score, as described below.

- Lastly, we assign an "absolute" departure score to the GPU by classifying the departure index, as follows:

$$if\ abs(DI_i) \geq 5,\ DSA_i = 5$$
$$elseif\ abs(DI_i) \geq 1,\ DSA_i = DI_i$$
$$else\ DSA_i = 0$$

where: $abs(DI_i)$ = absolute value of the departure index, as defined above, for the i^{th} GPU; and DSA_i = absolute departure score for the i^{th} GPU. Thus, if the current condition is within the HRV (i.e., departure index -1 to 1) the departure score equals 0; otherwise, if the current condition differs from the HRV by more than 1 in either direction the departure score will be 1 to 5 depending on the magnitude of absolute departure. Again, note the difference between the departure "index" and departure "score". The departure index represents degrees of departure in either direction from the median HRV value, whereas the departure score is always positive and represents degrees of departure in either direction (positive or negative) in this case. Note, this absolute departure scoring scheme reflects concern for GPUs that simply differ from HRV in either direction, which may or may

not suggest practical management options for moving the current condition closer to HRV, depending on the metric. In addition, as with the negative departure score, the absolute departure score was created to standardize the departure indices across metrics (i.e., putting them all on a 0 - 5 scale) so as to be able to combine them meaningfully into a composite departure score, as described below.

Given the above algorithm, it is important to recognize that each GPU is evaluated independently for departure; i.e., the departure index and score reflect the deviation of each GPU's current condition to its own unique HRV.

Metric 1: Basal Area Departure

We measure departure in basal area of trees within the GPU, which is a measure of landscape *composition*. We chose this departure metric because of the importance of basal area as an integrator of stem density and stem diameter and the important role this metric plays in the design of silvicultural treatments. As noted previously, the TCSI project developed a basal area departure metric for the extent of the TCSI area of interest, which is contained within the Northern Sierra ecoregion. Briefly, they first characterized current basal area for each 1-hectare pixel across the TCSI landscape as well as for a suite of contemporary reference sites located in the south Sierra ecoregion (see Jeronimo et al. 2019) based on 2018 Silvia-Terra modeled vegetation. Next, they summarized basal area within spatial units defined and delineated on the basis of biophysical setting, primarily based on a suite of climate and land management unit (LMU) classes but with a minimum and maximum size constraint. Lastly, they used a set of heuristic rules to assign each polygon to one of five departure classes (1-below reference, 2-within reference, 3-low departure, 4-medium departure, and 5-high departure) based on a comparison of the current basal area to an expected basal area under pre-settlement conditions derived from the reference sites (Jeronimo et al. 2019) in which the current condition was assumed to reflect pre-settlement conditions.

We assign a negative departure score to each polygon as follows:

- Below reference = 0
- Within reference = 0
- Low departure = 1
- Medium departure = 3
- High departure = 5

Next, we rasterize the vector layer based on the negative departure score using our 5 m reference raster for the focal landscape. Lastly, we compute the average negative departure score for each GPU. Note, this is the only departure metric reported here that is NOT based on the LDSim products. In addition, note that this departure metric is given only as a "score" from 0 - 5 and not also as an index, and only reflects "negative" departure, whereas all the other departure metrics are given first as an index that ranges negative to positive on a standardized scale before converting to a score from 0 - 5 to reflect either negative departure or absolute departure.

Metric 2: Percent Open Forest

We measure departure in the percentage of cells in the Open developmental stage within the GPU, which is a measure of landscape *composition*. We chose this departure metric because of the importance of Open canopy conditions in the restoration of forest vegetation and the dominant role this metric plays in the design of silvicultural treatments. GPUs with a departure index less than -1 have less area in the Open developmental stage than under HRV.

For example, the focal GPU depicted in **Figure 56** illustrates a GPU with a percent Open forest that is currently well below the HRV for this GPU, as depicted by the reference condition under historical dynamic equilibrium conditions for the sample shown here. This results in a departure index of -2.23 and thus a corresponding departure score of 3.

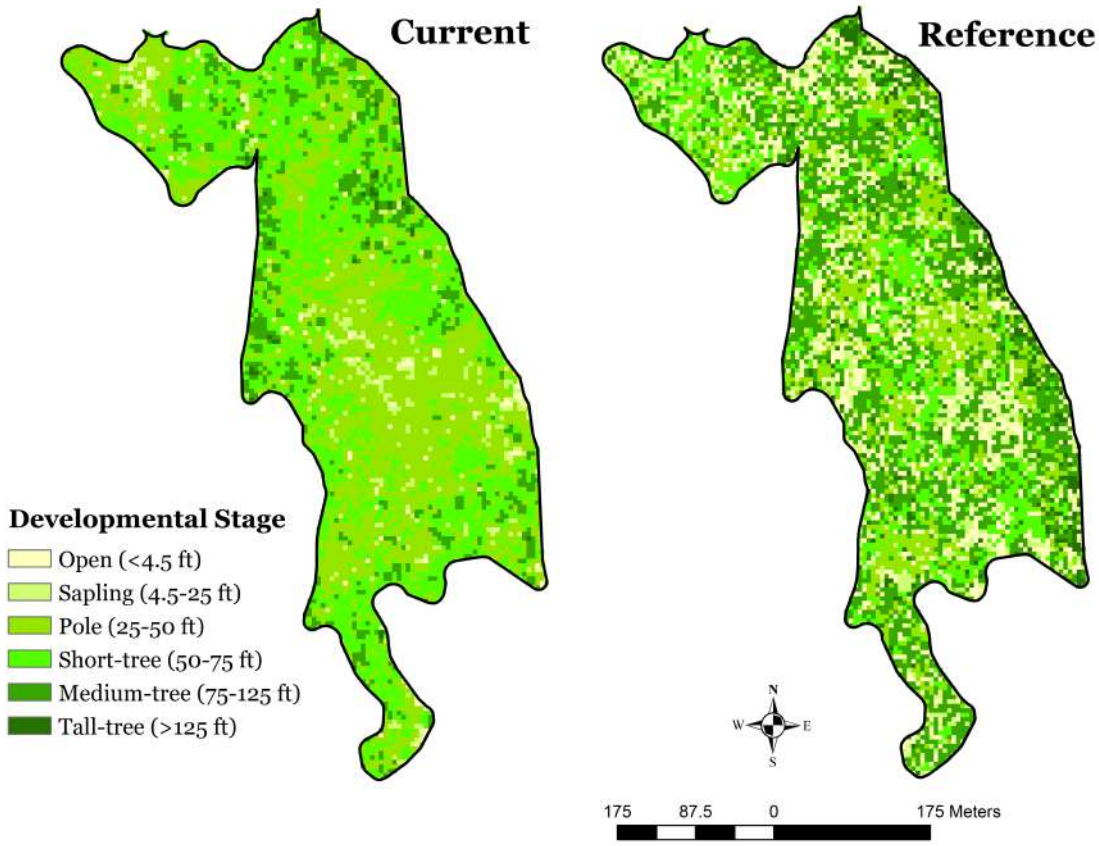

Figure 56: Focal Geophysical Unit (GPU) depicting developmental stage at the 5 m cell level for the current GPU condition and a sample reference condition under historical dynamic equilibrium conditions.

Metric 3: Developmental Stage Diversity

We measure departure in the diversity of developmental stages within the GPU based on the Simpson's Diversity index, which is a measure of landscape *composition*. Here, Simpson's Diversity is defined as the probability that any two cells selected at random would be different developmental stages, given as follows:

$$SIDI_i = 1 - \sum P_j^2$$

where: P_j = proportion of forested cells in the j^{th} developmental stage; and $SIDI_i$ = Simpson's Diversity index for the i^{th} cell. SIDI = 0 if the GPU contains a single developmental stage and approaches 1 as the number of developmental stages increases and the proportional distribution of area among developmental stages becomes more equitable. We chose this metric to capture GPUs in which there is too little diversity in developmental stage composition relative to HRV. The departure index for Simpson's Diversity is less than -1 if the current GPU has a diversity of developmental stages that is less than HRV.

For example, the focal GPU depicted in **Figure 56** illustrates a GPU currently with a relatively low Simpson's diversity index due to the preponderance of area in the Pole and Short-tree developmental stages and a paucity of area in the remaining stages. In contrast, the reference condition under historical dynamic equilibrium conditions for the sample shown here has a relatively even distribution of area among all six developmental stages. This results in a departure index of -3 and thus a corresponding departure score of 3.

Metric 4: Coefficient of Variation in Open Patch Size

We measure departure in the Coefficient of Variation (CV) in the size of all Open patches, including single cell patches, in which forest openings are defined by contiguous cells in the Open developmental stage based on the 4-neighbor rule (i.e., adjacent cells of the same class must share a full side to be considered in the same patch). Note, Open patches here are not the same as "large" openings, which we define later for use at the Subbasin-level. CV is defined as the standard deviation divided by the mean times 100; here it is a measure of relative variability in Open patch size and thus serves as a measure of landscape *configuration*. We chose this metric to capture GPUs in which there is too little heterogeneity in the size of Open patches relative to HRV. The departure index is less than -1 if the current GPU has relatively invariant Open patch sizes compared to HRV.

For example, the focal GPU depicted in **Figure 57** illustrates a GPU currently with no variation in Open patch size, as all of the Open patches are 1 cell in size; hence a CV of zero. In contrast, the reference condition under historical dynamic equilibrium conditions for the sample shown here has a wide variety of Open patch sizes; hence, a relatively large CV. This results in a departure index of -2.64 and thus a corresponding departure score of 3.

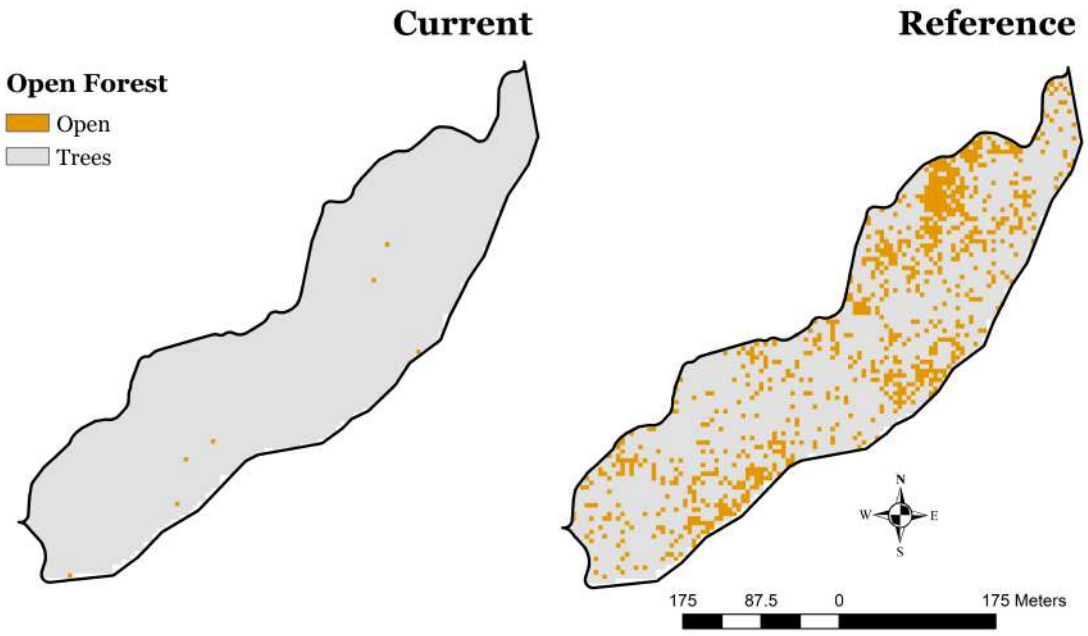

Figure 57: Focal Geophysical Unit (GPU) depicting forest in the Open developmental stage versus established tree stages at the 5 m cell level for the current GPU condition and a sample reference condition under historical dynamic equilibrium conditions.

Metric 5: Coefficient of Variation in Developmental Stage Patch Size

We measure departure in the CV in the size of all developmental stage patches, including single cell patches, in which patches are defined by contiguous cells in the same developmental stage based on the 4-neighbor rule (i.e., orthogonal neighbors). CV is defined as the standard deviation divided by the mean times 100; here it is a measure of relative variability in developmental stage patch size and thus serves as a measure of landscape *configuration*. We chose this metric to capture GPUs in which there is too little heterogeneity in the size of developmental stage (or canopy height) patches relative to HRV. The departure index is less than -1 if the current GPU has relatively invariant developmental stage patch sizes compared to HRV.

For example, the focal GPU depicted in **Figure 58** illustrates a GPU currently with a mean developmental stage patch size of 64.75 m^2 and a standard deviation of 190.75 m^2, amounting to a CV of 295 %. In contrast, the reference condition under historical dynamic equilibrium conditions for the sample shown here has a mean patch size of 72.5 m^2 and a standard deviation of 307.25 m^2, amounting to a CV of 424 %. In this case, the current GPU and the sample reference GPU both have roughly the same small mean patch size, reflecting a high degree of canopy height heterogeneity. However, the reference GPU has a much greater standard deviation in patch size than the current GPU, resulting in a greater CV. Thus, the reference GPU has greater "relative" variation in patch size. This results in a departure index of -4.28 and thus a corresponding departure score of 3.

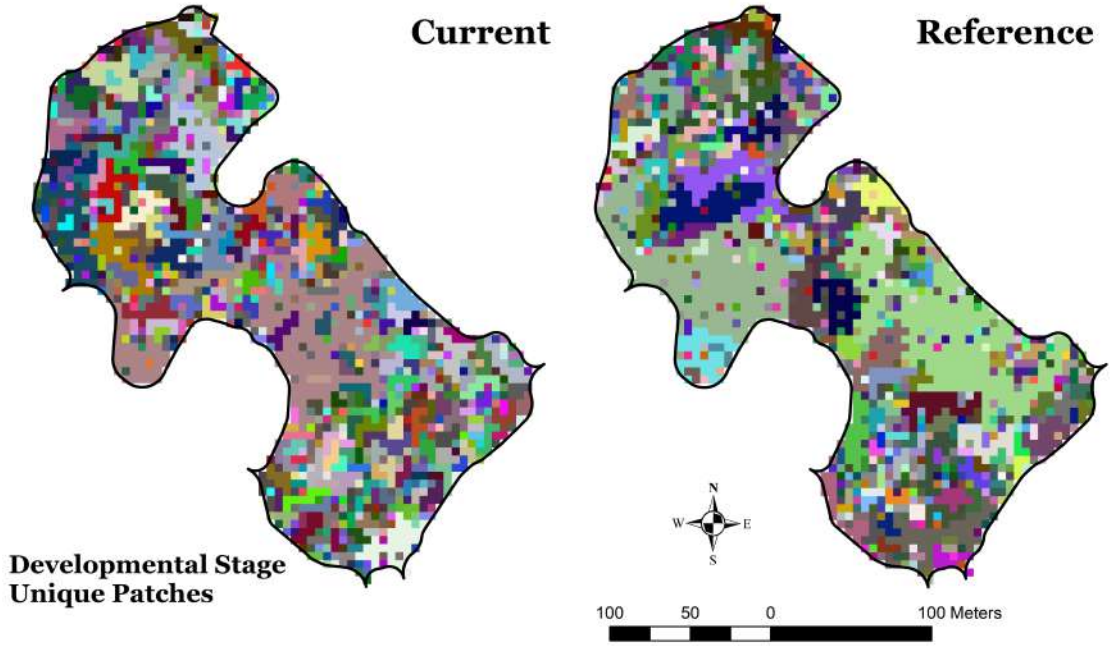

Figure 58: Focal Geophysical Unit (GPU) depicting unique patches of forest based on developmental stage at the 5 m cell level for the current GPU condition and a sample reference condition under historical dynamic equilibrium conditions.

Metric 6: Percent Large Trees

We measure departure in the percentage of cells in the Large tree size class ($\geq$ 30 in dbh) within the GPU, which is a measure of landscape *composition*. We chose this departure metric because of the importance of Large trees to wildlife and the important role this metric plays in the design of silvicultural treatments. GPUs with a departure index less than -1 have less area in the Large tree class than under HRV.

For example, the focal GPU depicted in **Figure 59** illustrates a GPU with a percent Large tree class that is currently well below the HRV for this GPU, as depicted by the reference condition under historical dynamic equilibrium conditions for the sample shown here. This results in a departure index of -4.41 and thus a corresponding departure score of 3.

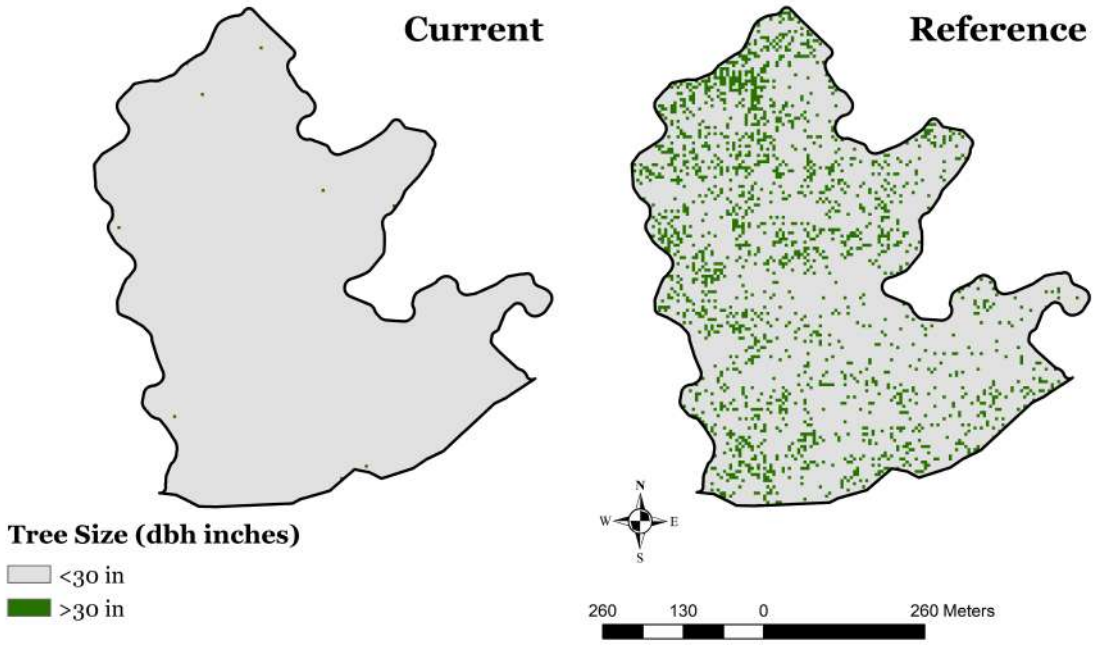

Figure 59: Focal Geophysical Unit (GPU) depicting forest in the Large tree size class (*geq* 30 in dbh) versus smaller trees at the 5 m cell level for the current GPU condition and a sample reference condition under historical dynamic equilibrium conditions.

Metric 7: Tree Size Class Diversity

We measure departure in the diversity of tree size classes within the GPU based on the Simpson's Diversity index, which is a measure of landscape *composition*. Here, Simpson's Diversity is defined as the probability that any two cells selected at random would be different tree size classes, given as follows:

$$SIDI_i = 1 - \sum P_j^2$$

where: P_j = proportion of forested cells in the j^{th} tree size class; and $SIDI_i$ = Simpson's Diversity index for the i^{th} cell. SIDI = 0 if the GPU contains a single tree size class and approaches 1 as the number of tree size classes increases and the proportional distribution of area among tree size classes becomes more equitable. We chose this metric to capture GPUs in which there is too little diversity in tree size class composition relative to HRV. The departure index for Simpson's Diversity is less than -1 if the current GPU has a diversity of tree size classes that is less than HRV.

For example, the focal GPU depicted in **Figure 60** illustrates a GPU with a relatively low Simpson's diversity index due to the preponderance of area in the intermediate tree size classes and a paucity of area in the very small and very large tree size classes. In contrast, the reference condition under historical dynamic equilibrium conditions for the sample shown here has a relatively even distribution of area among all six tree size classes. This results in a departure index of -3.83 and thus a corresponding departure score of 3.

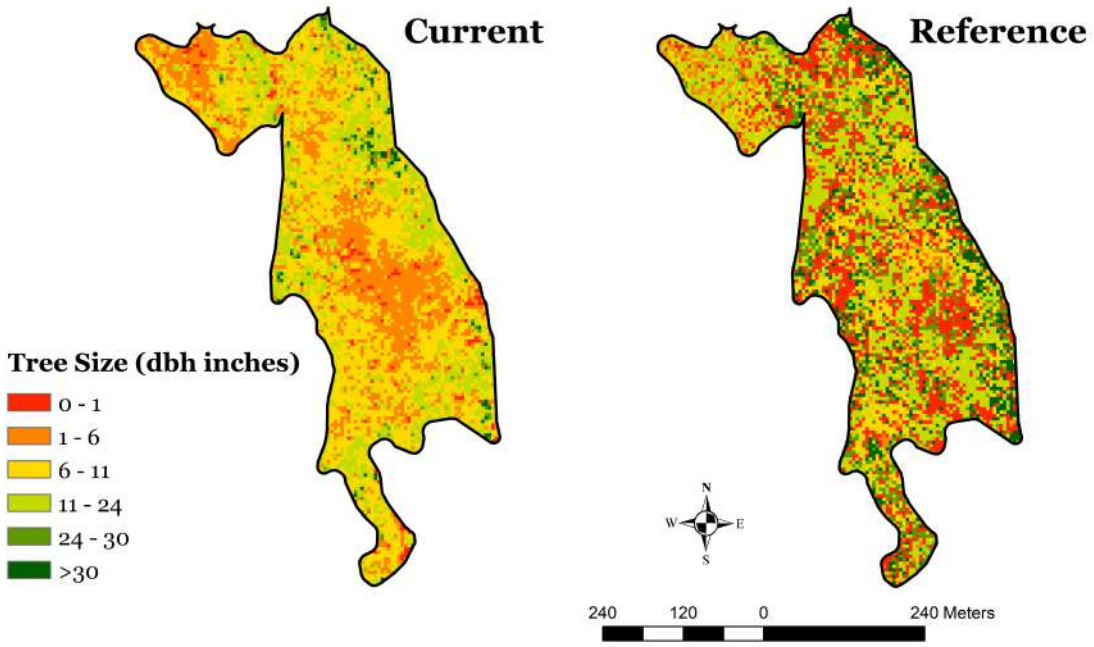

Figure 60: Focal Geophysical Unit (GPU) depicting tree size class at the 5 m cell level for the current GPU condition and a sample reference condition under historical dynamic equilibrium conditions.

Metric 8: Coefficient of Variation in Large Tree Patch Size

We measure departure in the CV in the size of all Large tree patches, including single cell patches, in which Large tree patches are defined by contiguous cells in the Large tree class ($\geq$ 30 in dbh) based on the 4-neighbor rule (i.e., orthogonal neighbors). CV is defined as the standard deviation divided by the mean times 100; here it is a measure of relative variability in Large tree patch size and thus serves as a measure of landscape *configuration*. We chose this metric to capture GPUs in which there is too little variability in the size of Large tree patches relative to HRV. The departure index is less than -1 if the current GPU has relatively invariant Large tree patch sizes compared to HRV.

For example, the focal GPU depicted in **Figure 61** illustrates a GPU currently with no variation in Large tree patch size, as all of the Large tree patches are 1 cell in size; hence a CV of zero. In contrast, the reference condition under historical dynamic equilibrium conditions for the sample shown here has a wide variety of Large tree patch sizes; hence, a relatively large CV. This results in a departure index of -7.09 and thus a corresponding departure score of 5.

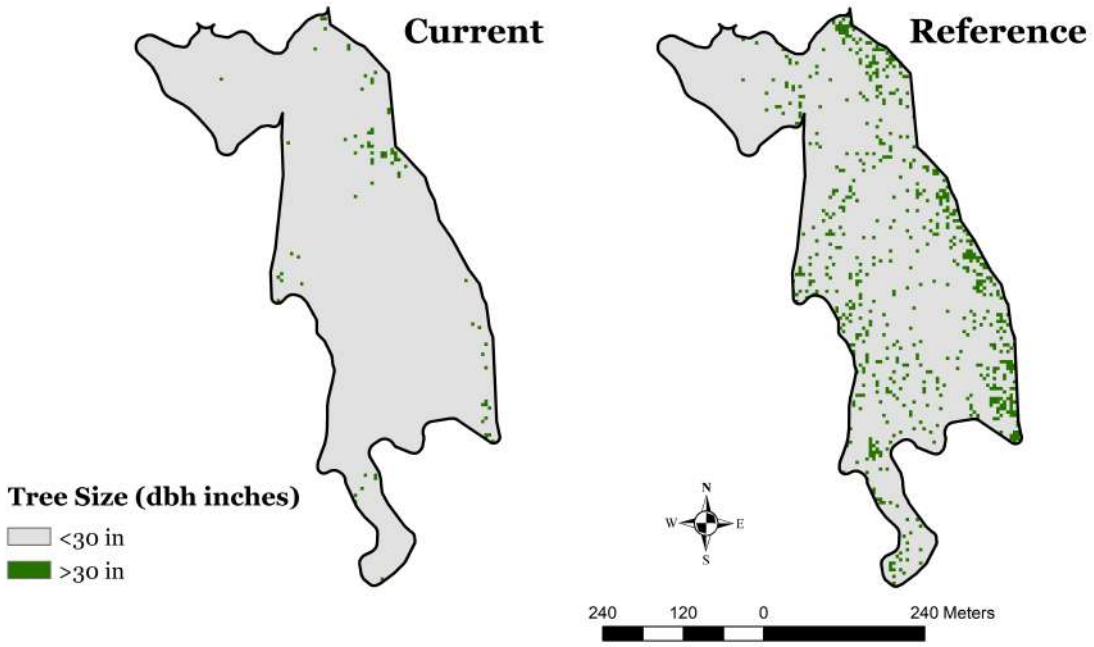

Figure 61: Focal Geophysical Unit (GPU) depicting the Large tree size class patches at the 5 m cell level for the current GPU condition and a sample reference condition under historical dynamic equilibrium conditions.

Metric 9: Coefficient of Variation in Tree Size Class Patch Size

We measure departure in the CV in the size of all tree size class patches, including single cell patches, in which patches are defined by contiguous cells in the same tree size class based on the 4-neighbor rule (i.e., orthogonal neighbors). CV is defined as the standard deviation divided by the mean times 100; here it is a measure of relative variability in tree size patch size and thus serves as a measure of landscape *configuration*. We chose this metric to capture GPUs in which there is too little heterogeneity in the size of tree size class patches relative to HRV. The departure index is less than -1 if the current GPU has relatively invariant tree size class patch sizes compared to HRV.

For example, the focal GPU depicted in **Figure 62** illustrates a GPU currently with a mean patch size of 46.25 m^2 and a standard deviation of 47 m^2, amounting to a CV of 101 %. In contrast, the reference condition under historical dynamic equilibrium conditions for the sample shown here has a mean patch size of 59.5 m^2 and a standard deviation of 119 m^2, amounting to a CV of 200 %. In this case, the current GPU and the sample reference GPU both have similar small mean patch sizes, reflecting a high degree of tree size class heterogeneity. However, the reference GPU has a much greater standard deviation in patch size than the current GPU, resulting in a greater CV. Thus, the reference GPU has much greater "relative" variation in patch size. This results in a departure index of -2.52 and thus a corresponding departure score of 3.

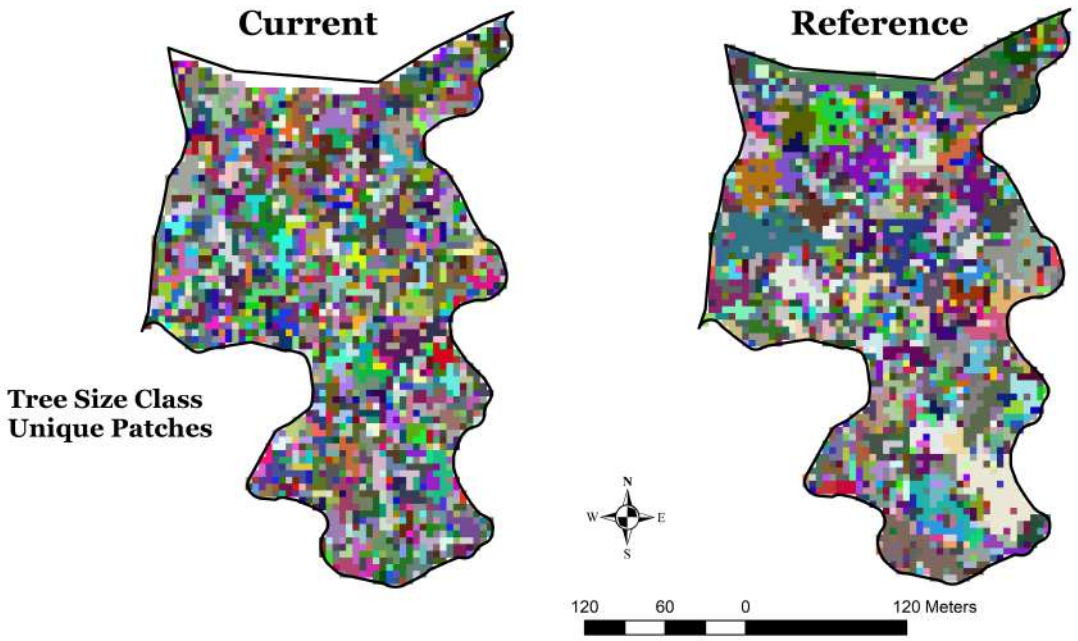

Figure 62: Focal Geophysical Unit (GPU) depicting tree size class patches at the 5 m cell level for the current GPU condition and a sample reference condition under historical dynamic equilibrium conditions.

Metric 10: Coefficient of Variation in Quadratic Mean Diameter

We measure departure in the CV in Site-level Quadratic Mean Diameter (QMD) of established trees within the GPU. Recall that a Site is defined as a 40-m radius window around each focal cell. Thus, QMD is computed for the Site associated with each focal cell, which produces a continuous surface of QMD values, from which the CV in QMD values is computed. CV is defined as the standard deviation divided by the mean times 100; here it is a measure of relative variability in Site-level QMD across the GPU and thus serves as a measure of landscape *configuration*. We chose this metric to capture GPUs in which there is too little spatial heterogeneity in the weighted average tree size (i.e., QMD) relative to HRV. The departure index is less than -1 if the current GPU has relatively homogeneous weighted average tree size compared to HRV.

For example, the focal GPU depicted in **Figure 63** illustrates a GPU currently with a mean QMD of 24.12 inches and a standard deviation of 1.64 inches, resulting in a CV of 7 %. In contrast, the reference condition under historical dynamic equilibrium conditions for the sample shown here has a mean QMD of 21.54 inches and a standard deviation of 6.4 inches, resulting in a CV of 30 %. Note that in this case the mean QMDs are fairly similar, but the standard deviations differ considerably; consequently, the standard deviation relative to the mean is much greater in the reference GPU, resulting in the greater CV. This GPU ended up with a departure index of -2.04 and thus a corresponding departure score of 3.

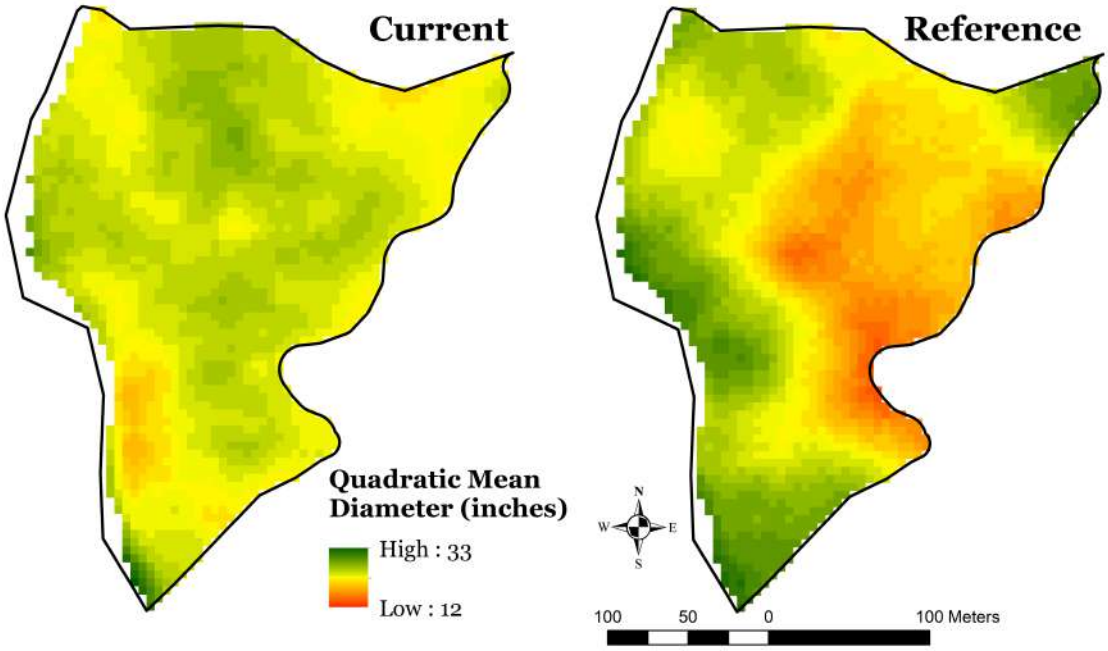

Figure 63: Focal Geophysical Unit (GPU) depicting unique patches of forest based on tree size class at the 5 m cell level for the current GPU condition and a sample reference condition under historical dynamic equilibrium conditions.

Metric 11: Coefficient of Variation in Percent Tree Cover

We measure departure in the CV in Site-level percent cover of established trees within the GPU. Recall that a Site is defined as a 40-m radius window around each focal cell. Thus, percent tree Cover computed for each Site produces a continuous surface of percent tree cover values, from which the CV in tree cover values is computed. CV is defined as the standard deviation divided by the mean times 100; here it is a measure of relative variability in Site-level percent tree cover across the GPU and thus serves as a measure of landscape *configuration*. We chose this metric to capture GPUs in which there is too little spatial heterogeneity in percent tree cover relative to HRV. The departure index is less than -1 if the current GPU has relatively homogeneous tree cover compared to HRV.

For example, the focal GPU depicted in **Figure 64** illustrates a GPU currently with a mean percent tree cover of 44.78 and a standard deviation of 8.06, resulting in a CV of 18 %. In contrast, the reference condition under historical dynamic equilibrium conditions for the sample shown here has a mean percent tree cover of 52.96 and a standard deviation of 24.36, resulting in a CV of 46 %. Note that in this case the mean percent tree cover is somewhat different between GPU conditions, but the sample reference condition has much greater relative variability about the mean as reflected in the greater CV. This GPU ended up with a departure index of -3.6 and thus a corresponding departure score of 3.

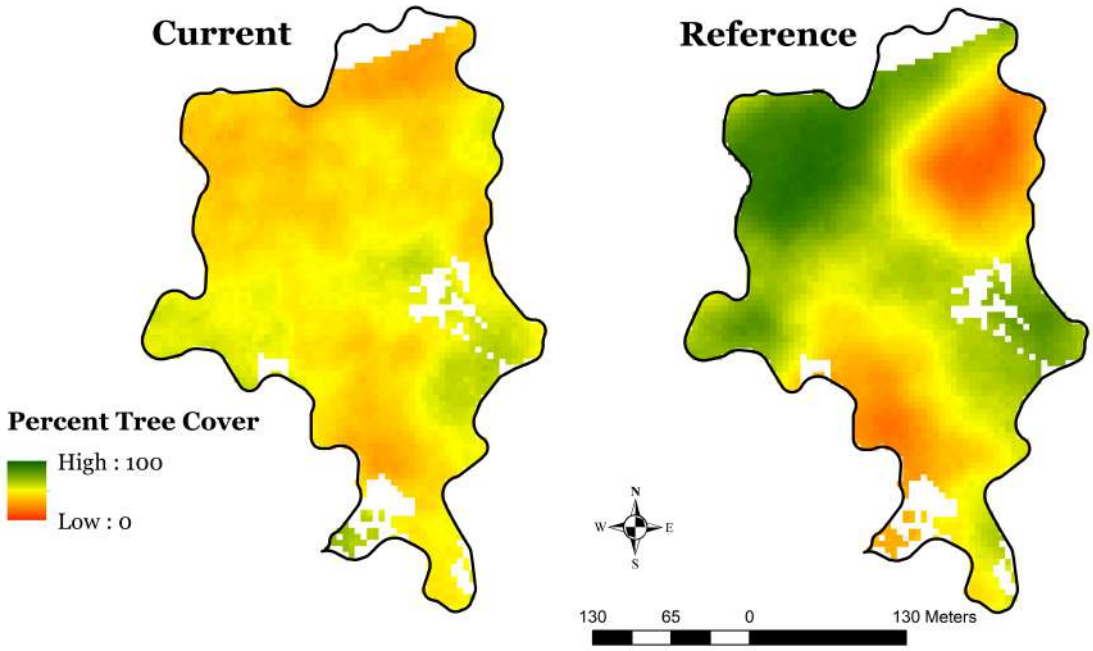

Figure 64: Focal Geophysical Unit (GPU) depicting percent tree cover at the 5 m cell level for the current GPU condition and a sample reference condition under historical dynamic equilibrium conditions.

Composite Departure Scores

We combine the 11 GPU-level departure scores above dealing with vegetation composition and configuration into two different composite departure scores. Note that we combine the departure "score", which is bounded 0 - 5 and is only positive, not the departure "index", which is unbounded and can be negative or positive depending on the metric. Both composite departure scores can be interpreted as a measure of overall GPU departure in vegetation composition and configuration, but with the following differences:

Negative Departure - In the first composite "negative" departure score, maximum departure occurs when GPUs have too little Open forest area, too few Large trees, too little diversity in forest developmental stages (i.e., tree heights) and tree size classes (i.e., dbh), too little variability in the size of patches based on forest developmental stage and tree size, and too little spatial variability in percent tree cover and weighted average tree size (i.e., QMD) relative to HRV. In other words, maximum departure occurs when the forest is too closed-canopy, depauperate in Large trees, and too homogeneous in vegetation composition and configuration. Note, this composite departure score focuses on GPUs that depart from HRV in one or more aspects of forest vegetation composition and configuration in the direction that is of most concern regarding ecological restoration of historical reference conditions. For example, we are most concerned with GPUs that currently have too little compositional diversity compared to HRV, and are generally not concerned with GPUs that currently have greater compositional diversity compared to HRV.

Absolute Departure - In the second composite "absolute" departure score, maximum departure occurs when GPUs have either too little or too much Open forest area, too few or too many Large trees, too little or too much diversity in forest developmental stages (i.e., tree heights) and tree size classes (i.e., dbh), too little or too much variability in the size of patches based on forest developmental stage and tree size, and too little or too much spatial variability in percent tree cover and weighted average tree size (i.e., QMD) relative to HRV. In other words, maximum departure occurs when the GPUs differ in both composition and configuration from their HRV in any direction, as measured by this suite of metrics.

We derive both of these composite departure scores as follows. The only difference between the composite negative and absolute departure scores is whether we use the absolute value of the component departure indices before compositing; otherwise, the calculations are the same. We assign equal weight to the four major vegetation attributes encompassed by the landscape metrics: 1) basal area, 2) tree cover, 3) tree developmental stage (i.e., height), and 4) tree size (i.e., dbh). Accordingly, we compute a weighted sum of the 11 component departure scores, in which each metric is scored on the range of 0 - 5 (see above), and divide the sum by the maximum score of 20 times 100, as follows:

$$CDS_i = \frac{\sum [b_i + c_i + 0.25d_i^1 + 0.25d_i^2 + 0.25d_i^3 + 0.25d_i^4 + 0.2s_i^1 + 0.2s_i^2 + 0.2s_i^3 + 0.2s_i^4 + 0.2s_i^5]}{20} 100$$

where: * b_i = basal area departure score for the i^{th} GPU; * c_i = CV in tree cover departure score for the i^{th} GPU; * $d^1{}_i$ = percent Open forest departure score for the i^{th} GPU; * $d^2{}_i$ = Simpson's diversity of developmental stages departure score for the i^{th} GPU; * $d^3{}_i$ = CV in Open patch size departure score for the i^{th} GPU; * $d^4{}_i$ = CV in developmental stage patch size departure score for the i^{th} GPU; * $s^1{}_i$ = percent Large tree departure score for the i^{th} GPU; * $s^2{}_i$ = Simpson's diversity of tree size classes departure score for the i^{th} GPU; * $s^3{}_i$ = CV in Large tree patch size departure score for the i^{th} GPU; * $s^4{}_i$ = CV in patch size based on tree size departure score for the i^{th} GPU; * $s^5{}_i$ = CV in Quadratic Mean Diameter departure score for the i^{th} GPU; * CDS_i = composite departure score for the i^{th} cell.

As weighted, the single metric based on basal area, the single metric based on percent tree cover, the combined equally-weighted 4 metrics based on developmental stage, and the combined equally-weighted 5 metrics based on tree size have equal weight in the summation. The weighted sum is then divided by the maximum possible score of 20 and multiplied by 100 to convert to a percentage of maximum. Thus, the final composite score can be interpreted as the percent of maximum possible departure. A composite departure score of 100 would occur only if the GPU receives a departure score of 5 for all 11 metrics.

As noted previously, the primary purpose of GPU-level departure is to identify local priorities for treatments. As such, the composite departure scores provide a first-tier filter for such purpose. As an example, the map of GPU negative departure scores for a small portion of one of the focal landscapes is depicted in **Figure 65**. The map illustrates strong local variation in GPU-level departure, with individual GPUs ranging in departure from near zero to 50 % of the theoretical maximum possible departure, and in so doing reveals logical priority locations for treatments aimed at restoring historical reference conditions - should that be the objective.

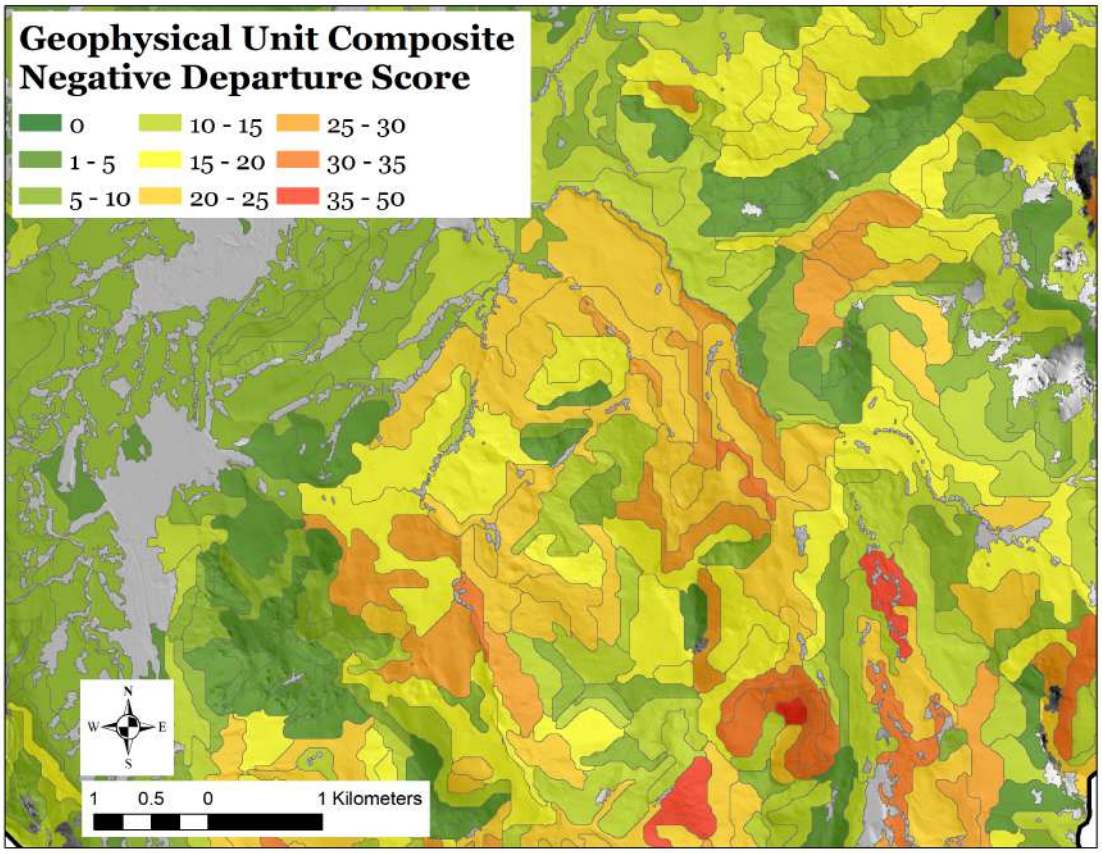

Figure 65: Composite Negative Departure Score for the Geophysical Units (GPUs) in a small portion of the Lake Tahoe Basin landscape. The composite departure score represents the weighted average of 11 component departure metrics (see text for details).

Management Applications

Like Site-level results, GPU-level results can aid unit and project-level planning and management. However, in contrast to Site-level results, which are best used to describe HRV and departure across the entire focal landscape as a whole, GPU-level results excel in quantifying HRV and departure at the local unit level. Recall that GPUs are assessed independently; i.e., each GPU has a unique current condition and HRV, and thus departure is determined separately for each GPU. As such, GPU-level HRV can provide a detailed, specific and quantitative basis for establishing desired conditions separately for each local unit, and GPU-level departure can provide a quantitative benchmark for determining the direction and magnitude of change needed to move the current unit towards historical reference conditions – should that be the goal. Of course, we acknowledge that current departure from historical reference conditions is only one consideration in establishing unit-level objectives and treatments and may be more useful in some parts of the landscape than others. It is not the purpose of our assessment to suggest where historical reference conditions should be used or whether they should be used at all.

Specific management applications of GPU-level results, as described below, should be interpreted with the following considerations in mind:

- First, it is important to recognize that GPUs do not have an explicitly-defined single spatial scale; i.e., units can vary in size and shape, and often markedly so, depending on the local terrain. Owing to these differences in scale, comparing landscape metrics among GPUs is fraught with challenges.

Thus, while the GPU is a useful concept and can serve as the basis for management within projects, it serves poorly for computing landscape metrics for comparative purposes, i.e., for comparing the HRV of one GPU to another. Consequently, we limit our analysis of HRV and current departure at this level by treating each GPU independently; i.e., we compare the current condition of each GPU to its own HRV in vegetation conditions. Thus, the measured HRV and current departure of a GPU is specific to that unit and independent of that measured for other units.

- Second, keep in mind that we chose the minimum and average scale of a GPU (given above) based on two major factors. First, we sought local units large enough to provide a reliable estimate of HRV and thus current departure so as to be able to identify local priorities for treatment. Second, we sought to create units roughly at the scale of real-world treatment units, but without biasing the HRV and current departure assessment by the many anthropogenic considerations that go into creating actual treatment units, such as ownership, operability, urban interface, etc.. Thus, while the range of scales of GPUs are representative of the range of scales of real-world treatment units, the delineations (i.e., shapes) of the GPUs do not necessarily reflect real-world potential treatment units.

- Third, it is important to recognize the distinction between GPUs delineated in forested areas and the conventional forest "stand". The latter is typically a spatial unit of forest defined and delineated based on similar forest vegetation composition and structure, geophysical setting and management history, specifically for the purpose of silviculture. Thus, a "stand" is distinctly a forest management unit and it is typically scaled and delineated for silvicultural purposes, whereas our GPUs are defined and delineated more broadly and based solely on geophysical criteria as a means of subdividing the landscape into meaningful smaller units for a wide variety of management applications, and for the purpose of generating unbiased estimates of HRV and current departure – roughly at the scale of treatment units within projects.

- Fourth, it is important to recognize that at the GPU level, the emphasis is on the *temporal* range of variability in landscape structure at the spatial extent of an individual GPU. The "temporal" variability stems from the fact that the variability is across time within a single GPU. Importantly, the measured HRV is specific to each GPU owing to the unique landscape context of each GPU. The HRV would likely differ somewhat if we were to define spatial units in some other manner or at a different scale.

- Fifth, it is important to distinguish between GPUs and BPCs. GPUs are defined based on geophysical variables without explicit consideration of current or historical vegetation, although we assume that GPUs affect vegetation patterns through the influence the geophysical setting has on succession and disturbance processes. However, the delineation of a GPU does not take into account the current local vegetation patterns or the simulated historical vegetation patterns. Moreover, GPUs are scaled to be roughly the same scale as potential treatment units, with a minimum size of ~ 4 ha (or 10 acres) and a mean of ~ 10 ha (or 50 acres). In contrast, BPCs are defined based on predicted site productivity (i.e. predicted cumulative tree biomass) under historical dynamic equilibrium conditions, as simulated) modeled from the same geophysical predictors. Thus, while GPUs aim to create local spatial units of relatively homogeneous geophysical conditions, BPCs aim to use geophysical variation at the cell level to predict site productivity for trees at the cell level. One is agnostic to vegetation per se, the other is not. GPUs represent local spatial units suitable for independent HRV and departure assessment, whereas BPCs are a landscape-wide classification of cells without any particular regard to creating local spatial units. Granted, BPCs can be depicted in their disjunct spatial units, which we call Biophysical Units (BPUs), but the individual BPUs are not used for any assessment.

- Lastly, it is important to understand the relationship between GPUs and "Stewardship Units" (STUs), which we define for the Stewardship Atlas dataset to inform initial project questions that drive management scope and direction. More specifically, STUs are a subdivision of the landscape based on current vegetation conditions, slope (operability), ladder fuel concentrations, and land ownership. Thus, whereas GPUs are based solely on geophysical criteria without regard to vegetation or explicit management objectives, STUs are typically smaller management units based on current vegetation characteristics and management criteria (such as operability). The HRV departure metrics

for GPUs are assigned to STUs based on zonal average statistics; i.e., the departure for each STU is derived as the average of the departure values for the GPUs it overlays. STUs are logical management units for applying vegetation treatments within projects and comprise the basic spatial unit of the Stewardship Atlas, which is populated with EcObject data, Pyrologix fire and fuels data, SilviaTerra generated tree lists, eDaRT and the GPU departure metrics from this study.

Subject to the considerations above, GPU-level results have the following specific management applications:

- GPU-level results can be used to identify local areas that depart from HRV, along with the nature and magnitude of that departure. Recall, the "negative" departure index identifies units in which the current condition of the unit has a value for the corresponding metric that is less than the HRV for the unit. The "absolute" departure index, on the other hand, identifies units in which the current condition of the unit simply differs from the HRV in either direction.

  Let's take, as an example, the Tree Size Class Diversity metric (metric #7 above), as mapped for the Bear River landscape **Figure 66**. The map reveals numerous concentrated local areas where the current tree size class diversity is much less than expected under HRV, especially along the lower South Fork of the Yuba River (which is contained within the Bear River landscape as we defined it for purposes of subdividing the Northern Sierra ecoregion into focal landscapes). These areas represent logical places to emphasize vegetation treatments that increase canopy height diversity; i.e., a more complex vertical structure.

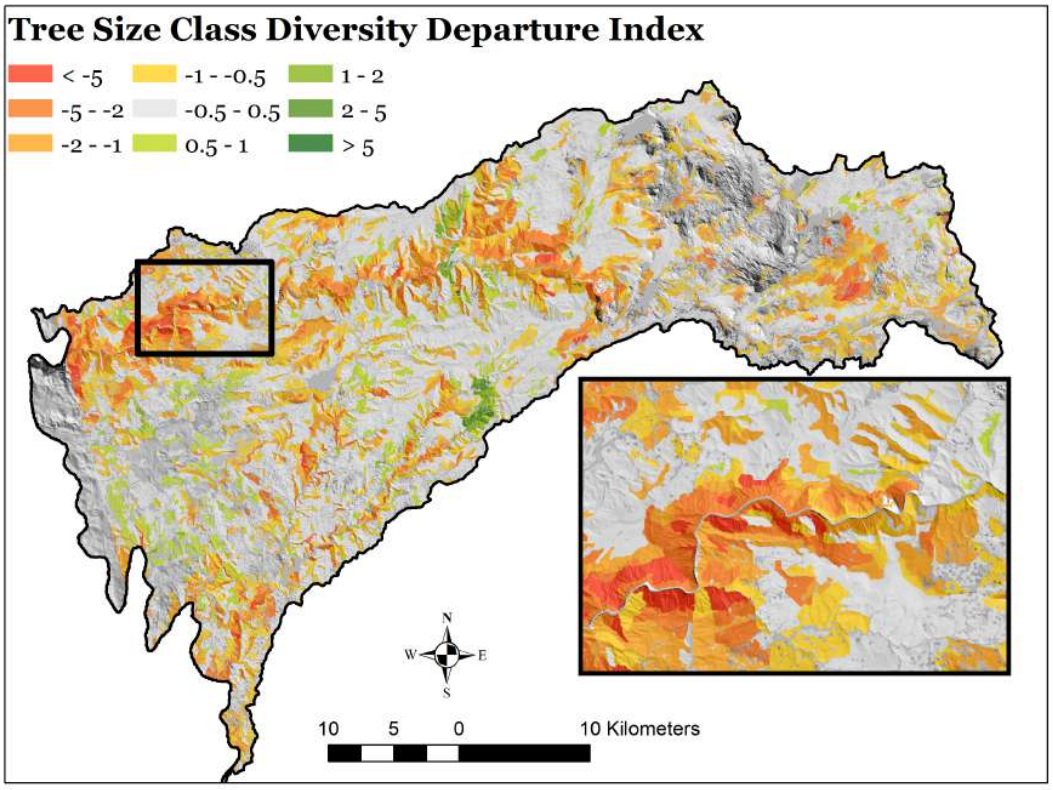

Figure 66: Departure Index for the Tree Size Class Diversity metric for the Geophysical Units (GPUs) in the Bear River landscape. The departure index represents the magnitude of deviation of the current GPU condition from its HRV. Negative values represent GPUs with less tree size diversity than expected under HRV (see text for details).

Of course, tree size diversity is but one vegetation attribute; some of the other vegetation metrics may suggest different priorities. The composite departure scores combine all 11 metrics to account for

many different aspects of vegetation composition and structure. The composite "negative" departure score identifies units in which the current condition exhibits negative departure for multiple metrics (**Figure 67**). In this case, while the lower South Fork of the Yuba River still stands out, the composite index refines the priorities and picks out the units that exhibit the most departure in multiple aspects of vegetation composition and structure. Given that management has limited capacity for applying treatments, these units might logically be the highest priorities for treatment.

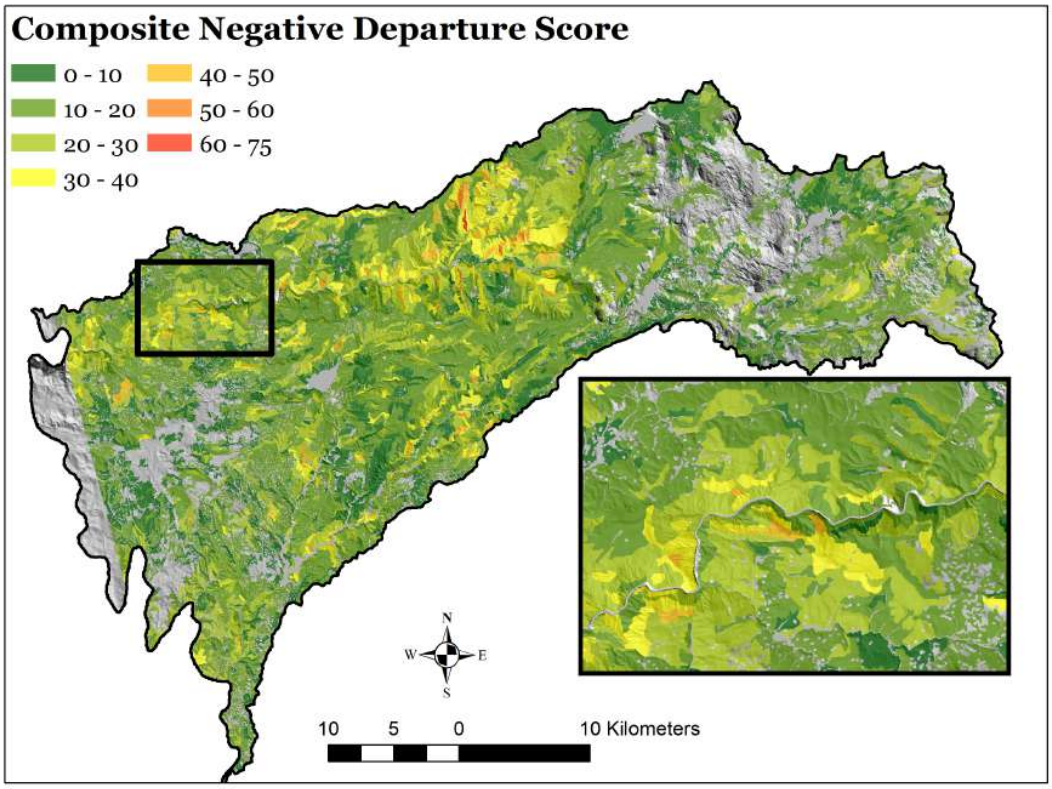

Figure 67: Composite Negative Departure Score for the Geophysical Units (GPUs) in the Bear River landscape. The composite departure score represents the weighted average of 11 component departure metrics (see text for details).

- As described previously, each GPU is attributed with descriptive labels for each of the 10 geophysical variables used to build the GPUs, plus classified aspect. These descriptive attributes can be used to query the data to create subsets of interest. In fact, given the 11 variables, each with 3 - 5 classes, there are 393,660 unique queries possible.

  Let's say, for example, we are interested in finding the most departed units in the Lower Montane elevation zone on gentle slopes (< 35 %) on southwesterly aspects to prioritize for treatments or, conversely, the least departed units in this setting to identify potential "reference" sites. **Figure 68** depicts the composite negative departure score for those GPUs with > 80 % of their area in this geophysical setting in the northern portion of the Lake Tahoe Basin landscape.

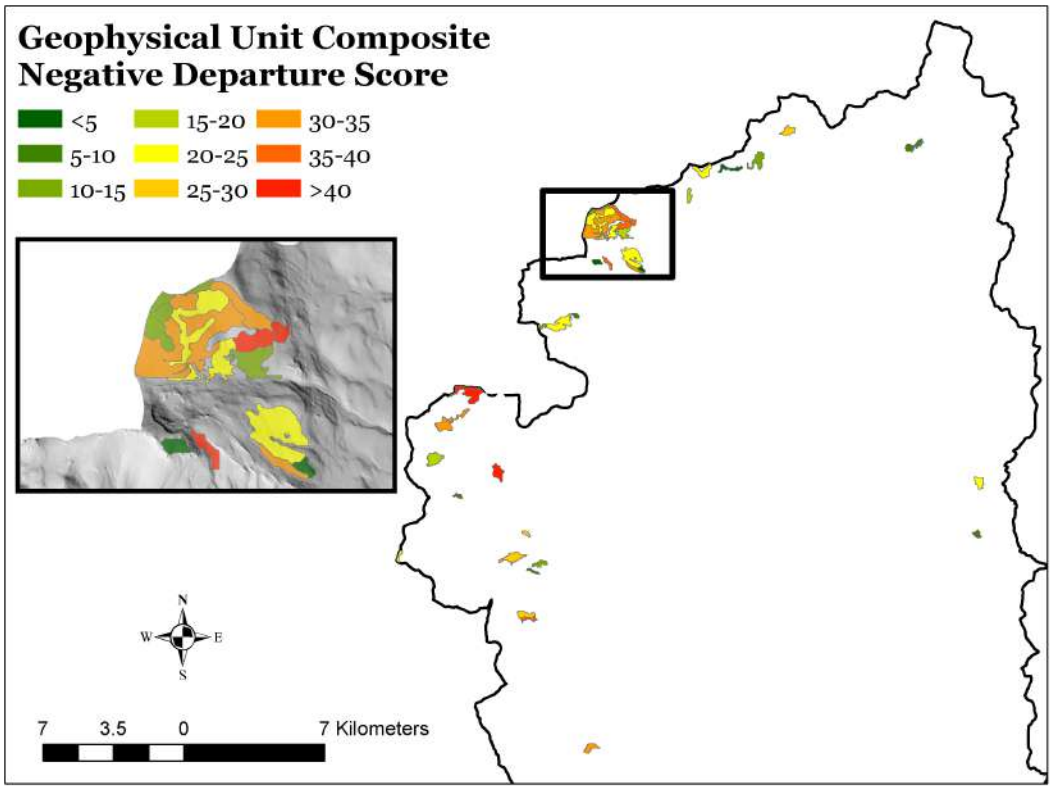

Figure 68: Composite Negative Departure Scores for Geophysical Units (GPUs) predominantly in the Lower Montane elevation zone on gentle slopes (<35 %) on southwestern aspects in the northern portion of the Lake Tahoe Basin landscape. The composite departure score represents the weighted average of 11 component departure metrics (see text for details).

- GPU results can provide loose qualitative and/or quantitative targets for desired vegetation conditions within each unit – should restoration of historical reference conditions be the objective. Importantly, the HRV for each GPU provides a range of reference conditions, not a single condition, providing a great deal of flexibility in designing treatments that meet multiple objectives.

  Let's take, as an example, the GPU highlighted with an asterisk in **Figure 69**. In this case, the composite "negative" departure is being driven by departure in Percent Open Forest (-2.63), CV in Percent Tree Cover (-2.01), CV in Tree QMD (-1,52), and CV in Developmental Stage Patch Sizes (-1.22) and Open Forest Patch Sizes (-1.07). Collectively, these indices result in a composite negative departure score of 41.5 %. Interestingly, in this unit the Percent Large Tree metric exhibits positive departure (1.25), indicating that the percentage of the unit covered by Large trees exceeds the HRV. Thus, we can conclude that the current stand has too little area in the Open developmental stage, and too little spatial heterogeneity in tree cover, developmental stage patches, and Open areas, but has an excess of Large trees. Treatment to move the stand towards its HRV – should that be the objective – would emphasize creating more openings of various patch sizes, thinning the overstory at variable densities, and maintaining small patches of trees in different developmental stages. Moreover, given the excess of Large trees, it could be deemed acceptable to remove some of the larger trees while achieving the other treatment objectives. A challenge in specifying a treatment prescription is determining how far to go or how much to do with regards to each of these vegetation conditions. The unit HRV and departure results provide some qualitative guidelines, such as those described above. However, they also can provide some loose quantitative guidelines. For example, the HRV for Percent Open Forest is 26 - 46 %, which equates to ~38 - 58 % canopy cover. The current Percent Open Forest is 9 %, which equates to 77 % canopy cover. Thus, the treatment could aim to reduce canopy cover by 20 - 30 %. In addition, the HRV for the CV in Open Forest Patch Sizes is ~

200 - 900 %, whereas the current condition is just under 200 %. Thus, removing patches of canopy to create openings could aim to create Open patches that vary several-fold in size.

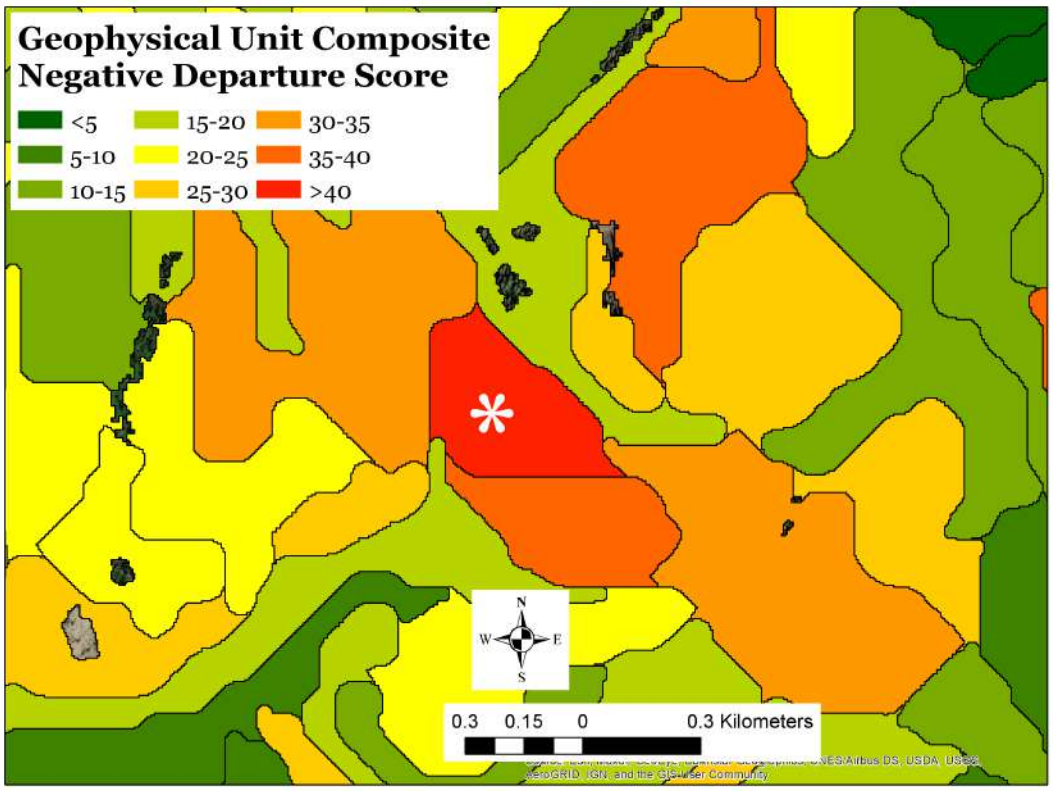

Figure 69: Composite Negative Departure Scores for Geophysical Units (GPUs) in a small portion of the Lake Tahoe Basin landscape, highlighting the central GPU. The composite departure score represents the weighted average of 11 component departure metrics (see text for details).

- GPU results can also provide a quantitative means of monitoring treatment effectiveness. Specifically, GPU departure indices provide detailed, specific and quantitative measures of current departure from HRV, and thus provide a benchmark for measuring where we are today. For example, the GPU in the previous example has a composite negative departure score of 41.5 %. Recomputing the departure indices after treatment, contingent on acquiring the necessary Lidar data, could be used to determine the magnitude and rate of change resulting from the treatment, and thus serve as the quantitative basis for monitoring unit-level changes pursuant to adaptive management.

- Lastly, GPU-level departure is being incorporated into a first-of-its-kind land management and planning tool called Land Tender (https://www.vibrantplanet.net/landtender) to help develop and prioritize forest health treatment projects. Land Tender uses delineated treatment units housed in a Stewardship Atlas to build optimized project areas based on a user's management goals; the tool is flexible enough to accommodate goals to avoid risk from disturbance (like wildfire) and/or improve forest health, and can also evaluate tradeoffs and co-benefits of treatments as they relate to anthropogenic assets, ecological resources, and/or strategic areas. The departure that is calculated at the GPU-level is distributed to the Stewardship Atlas unit (STU) level; STU-level departure is then used as a proxy for current ecological condition of forest-related ecological resources within each treatment unit to determine how treatments could affect their condition. This information gets combined with metrics related to avoided risk from disturbances, and is then used for prioritization within Land Tender.

Subbasin Level Departure

We quantify HRV and current departure at the spatial extent of a Subbasin-by-BPC partition; i.e., each Subbasin subdivided into BPCs and treated as a whole unit, primarily for the purpose of identifying and prioritizing broad areas within the focal landscape in most need of management attention should restoration of historical reference conditions be the goal. Note, as with the Site and GPU levels, we restrict our assessment of Subbasin-level HRV and departure to cells mapped as forest and where we have Lidar-derived vegetation attributes for the current landscape.

We use a parsimonious suite of landscape metrics (see below) that we deem meaningful for estimating departure at the Subbasin level and appropriate given the available data. However, we acknowledge that there may be other potentially meaningful metrics for this purpose - our chosen suite of metrics is not exhaustive. Specifically, we selected metrics that measure vegetation composition and configuration with respect to large forest openings, large trees (based on dbh) and the distribution of patch sizes based on developmental stages and tree size classes.

At the Subbasin level, our method for computing HRV and current departure differs depending on the landscape metric, which fall into two groups, as follows:

Landscape Composition Metrics - The first group includes two landscape composition metrics: 1) Percent Large Forest Openings; and 2) Percent Large Trees, as described in detail below. For these two metrics, the current condition of the Subbasin-by-BPC partition is given by the value of the metric computed for the partition in the current landscape, and the HRV of the partition is based on the variability in the metric under historical dynamic equilibrium conditions. To compute HRV, the Subbasin-by-BPC partition at each timestep of the simulation after model equilibration (N = 200 timesteps) is considered a single snapshot of what the Subbasin condition could have been like at any point in time under reference period conditions. Because of the enormous size of the data sets generated and the computational requirements, we evaluate snapshots of each Subbasin at 20-year (or 4 timestep) intervals after model equilibration for a total of 51 snapshots of each Subbasin. As before, we define HRV as the range in values between the 2.5^{th} and 97.5^{th} quantiles, which represents the 95 % range of variability in the metric under historical dynamic equilibrium conditions, analogous to a 95 % confidence interval.

To compute current departure for each of the landscape composition metrics, we compare the current condition value to the HRV distribution and derive a departure index and score for each Subbasin-by-BPC partition, as follows:

- First, we compute the value of the metric for the Subbasin-by-BPC partition in the current landscape.
- Next, we derive the HRV for the Subbasin-by-BPC partition by computing quantiles of the simulated distribution of values for the metric (based on the 11 snapshots). Here we are primarily interested in the values corresponding to the 2.5^{th} (Q2.5), 50^{th} (Q50) and 97.5^{th} (Q97.5) quantiles, as described next.
- Next, we derive a departure "index" for the Subbasin-by-BPC partition, as follows:

$$for\ (C_{ij} \geq Q50_{ij}) : DI_{ij} = \frac{C_{ij} - Q50_{ij}}{Q97.5_{ij} - Q50_{ij}}$$

$$for\ (C_{ij} < Q50_{ij}) : DI_{ij} = \frac{C_{ij} - Q50_{ij}}{Q50_{ij} - Q2.5_{ij}}$$

where: C_{ij} = current condition for the i^{th} Subbasin and j^{th} BPC; Q_{ij} = specified quantiles of the simulated distribution under historical dynamic equilibrium conditions for the i^{th} Subbasin and j^{th} BPC; and DI_{ij} is the departure index for the i^{th} Subbasin and j^{th} BPC. Thus, if the current condition is greater than the 50^{th} quantile of the HRV (i.e., the median of the HRV), the departure index will be positive. Conversely, if the current condition is less than the 50^{th} quantile of the HRV, the departure index will be negative. Moreover, if the current condition is equal to the 97.5^{th} quantile of

the HRV (i.e., the upper range of the HRV), the departure index will equal 1. Similarly, if the current condition is equal to the 2.5th quantile of the HRV (i.e., the lower range of the HRV), the departure index will equal -1. Accordingly, if the current condition is, say, twice the distance from the median HRV as the upper range of the HRV, the departure index will be 2, and so on. Thus, the departure index is unbounded on both sides and any values between -1 and 1 can be considered within the HRV, and values less than -1 or greater than 1 can be considered degrees of departure, with more negative numbers indicating greater negative departure and more positive numbers indicating greater positive departure. Note, this departure index is computed exactly the same as was previously described for the GPU-level departure index and illustrated in **Figure 55**. The only difference is that here the metric is computed for the Subbasin-by-BPC partition rather than the GPU.

- Lastly, we assign a departure "score" to the Subbasin-by-BPC partition as follows. First, we invert the departure index by multiplying by -1 so that positive values represent greater departure in the direction of interest (i.e., where the current landscape has less percent large forest openings and less percent large trees than the HRV), and setting all resulting negative values to zero. Thus, any partition in which the current landscape is deficient (relative to HRV) in large forest openings or large trees receives a positive departure score for the corresponding metric, and any partition in which the current landscape has an excess (relative to HRV) of large forest openings or large trees receives a zero departure score. Next, we assign a departure score to the partition by classifying the adjusted departure index, as follows:

$$if\ adjDI_i \geq 5,\ DS_i = 5$$

$$else\ DS_i = adjDS_i$$

where: adjDI$_i$ = adjusted departure index, as defined above, for the ith partition; and DS$_i$ = departure score for the ith partition. Thus, if the current condition is within the HRV or greater than the HRV (i.e., original departure index > 1), the departure score equals 0; otherwise, the current condition is less than the HRV and the original departure index will be less than -1 and the departure score will be 1 to 5 depending on the magnitude of negative departure. Note the difference between the departure "index" and departure "score". The departure index represents degrees of departure in either direction from the median HRV value and is unbounded, whereas the departure score is always positive and represents degrees of negative departure in this case and ranges 0 - 5. This negative departure scoring scheme reflects our principle concern for partitions in which the current condition has a value for the metric that is less than the HRV for that metric, which makes sense in the context of the specific landscape composition metrics described below. In addition, the departure score was created to standardize the departure indices across metrics (i.e., putting them all on a 0 - 5 scale) so as to be able to combine the landscape composition and configuration metrics into a composite departure score, as described below.

Landscape Configuration Metrics - The second group includes four landscape configuration metrics: 1) Large Forest Openings Patch Size Distribution; 2) Developmental Stage Patch Size Distribution; 3) Large Tree Patch Size Distribution; and 4) Tree Size Class Patch Size Distribution. Each of these metrics focuses on the distribution of patch sizes and differs only in the basis for defining patches. For each of these landscape metrics, the current condition of the Subbasin-by-BPC partition is given by the percentage of forest in patches of various sizes, as follows:

- 0 - 0.25 acres
- 0.25 - 0.5 acres
- 0.5 - 1 acres
- 1 - 3 acres
- 3 - 5 acres
- $>$ 5 acres

Thus, the current condition of the landscape is given as a distribution rather than a single value – the percent of forest in each patch size bin. The HRV of the Subbasin-by-BPC partition is based on the same

patch size distribution, but derived under historical dynamic equilibrium conditions. To compute HRV, the Subbasin-by-BPC partition at each timestep of the simulation after model equilibration (N = 200 timesteps) is considered a single snapshot of what the Subbasin condition could have been like at any point in time under reference period conditions. Because of the enormous size of the data sets being generated – each patch is a separate observation, resulting in millions of observations – and the computational requirements, we evaluate snapshots of each Subbasin at 20-year (or 4 timestep) intervals after model equilibration for a total of 51 snapshots of each Subbasin. We define HRV as the pooled patch size distribution across snapshots. Thus, we pool patches both across space within a single snapshot and across time over the 11 snapshots to create a single patch size distribution for the HRV. Note, here we chose not to construct a range in values for each bin size (e.g., by constructing a 95 % range of variability based on quantiles for each bin), as we deemed it unnecessary for our purpose and potentially confusing.

To compute current departure for each of the landscape configuration metrics, we compare the current patch size distribution to the HRV distribution and derive a departure index and score for each Subbasin-by-BPC partition, as follows:

- First, we compute the percent of the forest in the Subbasin-by-BPC partition in the current landscape in each of the six patch size bins given above.
- Next, we compute the percent of the forest in the Subbasin-by-BPC partition in each of the six patch size bins pooled across the 11 snapshots representing the historical reference period.
- Next, we derive a departure "index" for the Subbasin-by-BPC partition based on the Percentage Dissimilarity Index (also known as the Bray-Curtis or Sorensen Dissimilarity Index), as follows:

$$DI_{ij} = 100 * \left(\frac{\sum_{k=1}^{6} abs(H_{ijk} - C_{ijk})}{\sum_{k=1}^{6} (H_{ijk} + C_{ijk})} \right)$$

  where: C_{ijk} = current condition for the percent of forest in the i^{th} Subbasin and j^{th} BPC in the k^{th} patch size bin; H_{ijk} = historical reference period condition for the percent of forest in the i^{th} Subbasin and j^{th} BPC in the k^{th} patch size bin; k = patch size bin index {1:6}; abs = absolute value; and DI_{ij} = departure index for the i^{th} Subbasin and j^{th} BPC. Note, in the numerator, we are taking the absolute value of the difference between the current and HRV values in each patch size bin, and then summing across bins; thus, we are not distinguishing whether the current landscape has more or less than the HRV in any patch size bin, simply that it differs and by how much. In the denominator, we are summing the current and HRV values in each patch size bin, and then summing across bins. After multiplying by 100, the quotient of these two quantities represents the percentage of non-overlap between the two distributions. Equivalently, this index represents the compliment of the overlap between the two distributions. As such, if the current and HRV distributions are identical, the percentage dissimilarity (i.e., departure) will be zero, and if the two distributions do not overlap at all the percentage dissimilarity (or departure) will be 100 %. In other words, the departure index computed this way represents the percentage of maximum departure of the current landscape relative to the HRV, and it therefore has an intuitive interpretation.

  The departure index based on Percentage Dissimilarity in this application is best understood by example. **Figure 70** and **Figure 71** depict the CRV and HRV patch size distributions of large forest openings for two different Subbasin-by-BPC partitions in one of the focal landscapes. In **Figure 70** the CRV and HRV distributions are very similar, overlapping by 90 %, which results in a 10 % dissimilarity and departure index. In contrast, in **Figure 71** the CRV and HRV distributions are very dissimilar, overlapping by only 20 %, which results in an 80 % dissimilarity and departure index.

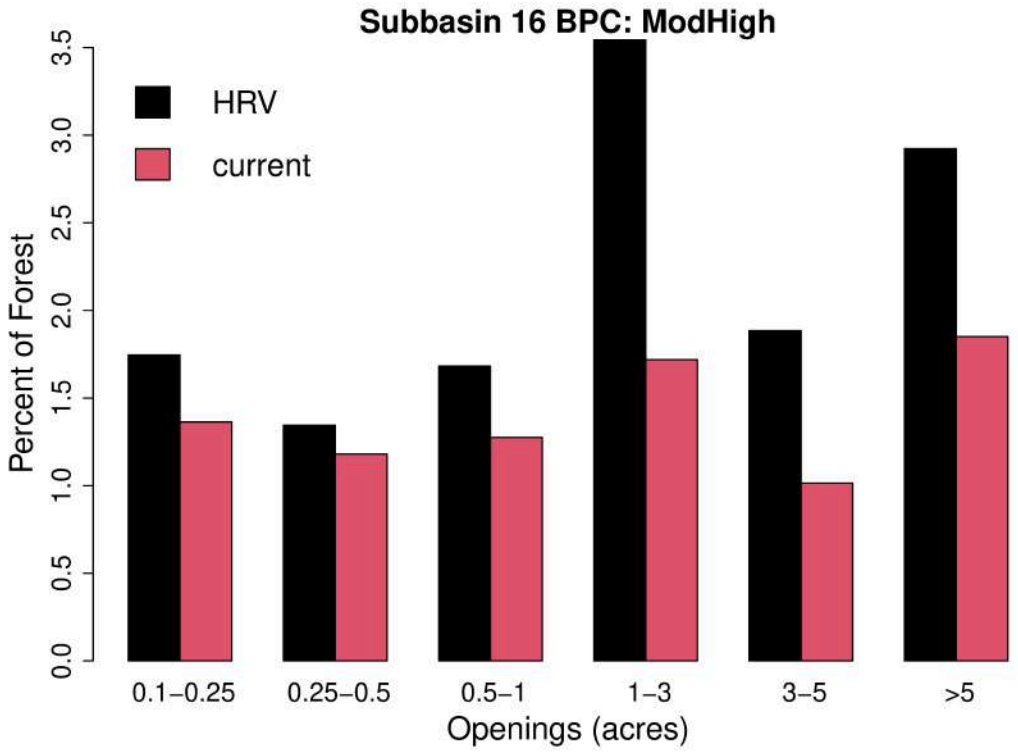

Figure 70: Patch size distributions of large forest openings under the current landscape (CRV) and historical reference period (HRV) conditions for one of the Subbasins and Biophysical Classes in one of the focal landscapes. The patch size distributions overlap by 90 %, resulting in a departure index of 10 %.

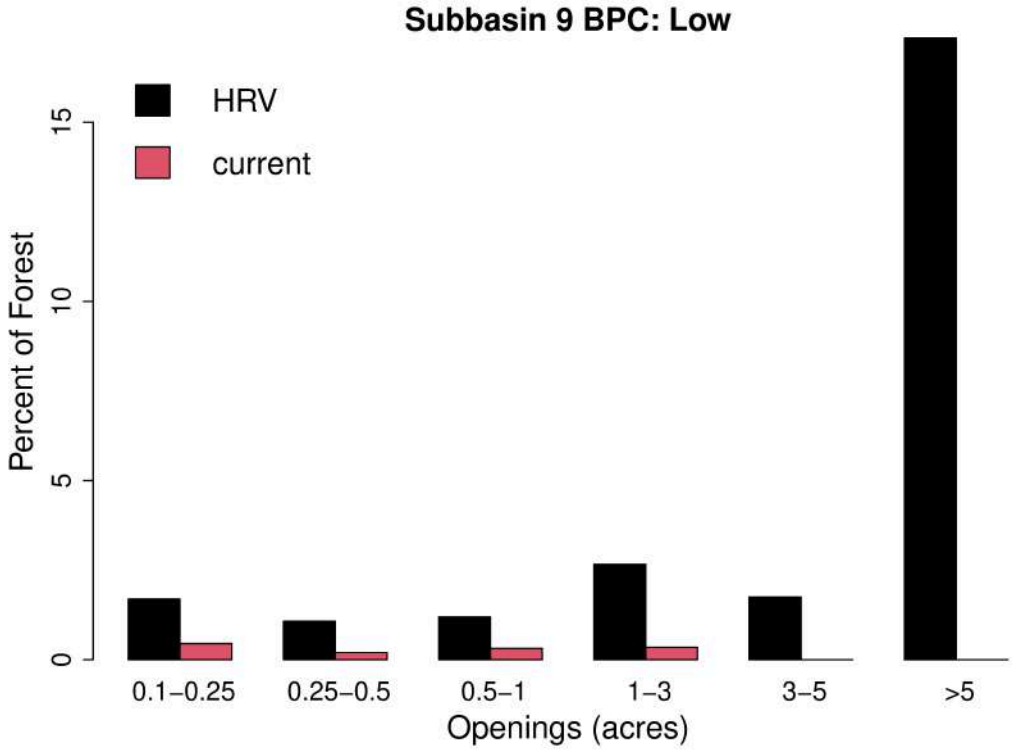

Figure 71: Patch size distributions of large forest openings under the current landscape (CRV) and historical reference period (HRV) conditions for one of the Subbasins and Biophysical Classes in one of the focal landscapes. The patch size distributions overlap by 20 %, resulting in a departure index of 80 %.

- Lastly, we assign a departure "score" to the Subbasin-by-BPC partition as follows:

$$if\ DI_i \geq 50,\ DS_i = 5$$

$$else\ DS_i = DS_i/10$$

where: DI_{ij} = departure index as defined above for the i^{th} Subbasin and j^{th} BPC; and DS_{ij} = departure score for the i^{th} Subbasin and j^{th} BPC. Thus, a 10 % departure index becomes a departure score of 1, a 20 % departure index becomes a departure score of 2, and so on, except that a departure index > 50 % is truncated to a departure score of 5. Thus, as with the departure index above, all departure scores are positive. As with the compositional metrics, the major difference between the departure index and the departure score is that the latter is transformed into a standard scale of 0 - 5 to allow for compositing the landscape composition and configuration metrics (see below).

Metric 1: Percent Large Forest Openings

We define large forest openings as contiguous forested cells in the Open developmental stage (i.e., no established trees to breast height) encompassing a minimum of 0.04 ha (0.1 acres). Contiguity is based on the 4-neighbor rule (i.e., orthogonal neighbors) that ensures a minimum width of 5 m for any opening. Our definition is not to be confused with how large forest openings have been defined in other applications (e.g., Jeronimo et al. 2019), and thus any comparison with other studies must be done with care. We define Percent Large Forest Openings as the percent of the forest within the Subbasin-by-BPC partition in large forest openings (as defined), and the departure index and score reflect whether or not the current landscape is deficient in large forest openings relative to HRV and, if so, the degree of deficiency. This metric is a measure of landscape *composition* as it reflects how much of the forest is in large openings but is agnostic as to the number, size and distribution of large forest openings. We chose this metric to identify Subbasins and BPCs in which there is too little area in large forest openings relative to HRV. The departure index is negative if the current landscape partition has less area in large forest openings than the median HRV condition and, conversely, positive if the current landscape partition has more area in large forest openings than the median HRV condition. The departure score, on the other hand, is positive if the current Subbasin-by-BPC partition has too little area in large forest openings compared to HRV, and otherwise is zero.

As an example, the Percent Large Forest Openings departure index for the Yuba River landscape is depicted in **Figure 72**. Note, the departure index (as opposed to the score) can vary from negative to positive values, depending on the direction of the departure. In this case, most Subbasin-by-BPC partitions exhibit negative departure values, indicating that the current landscape has less percentage area in large forest openings than expected under historical reference conditions, but only a few fall "outside" the HRV (i.e., < -1). Conversely, there are several partitions in the upper Yuba River watershed that exhibit positive departure; i.e., current landscape has a greater percentage area in large forest openings than expected under historical reference period conditions.

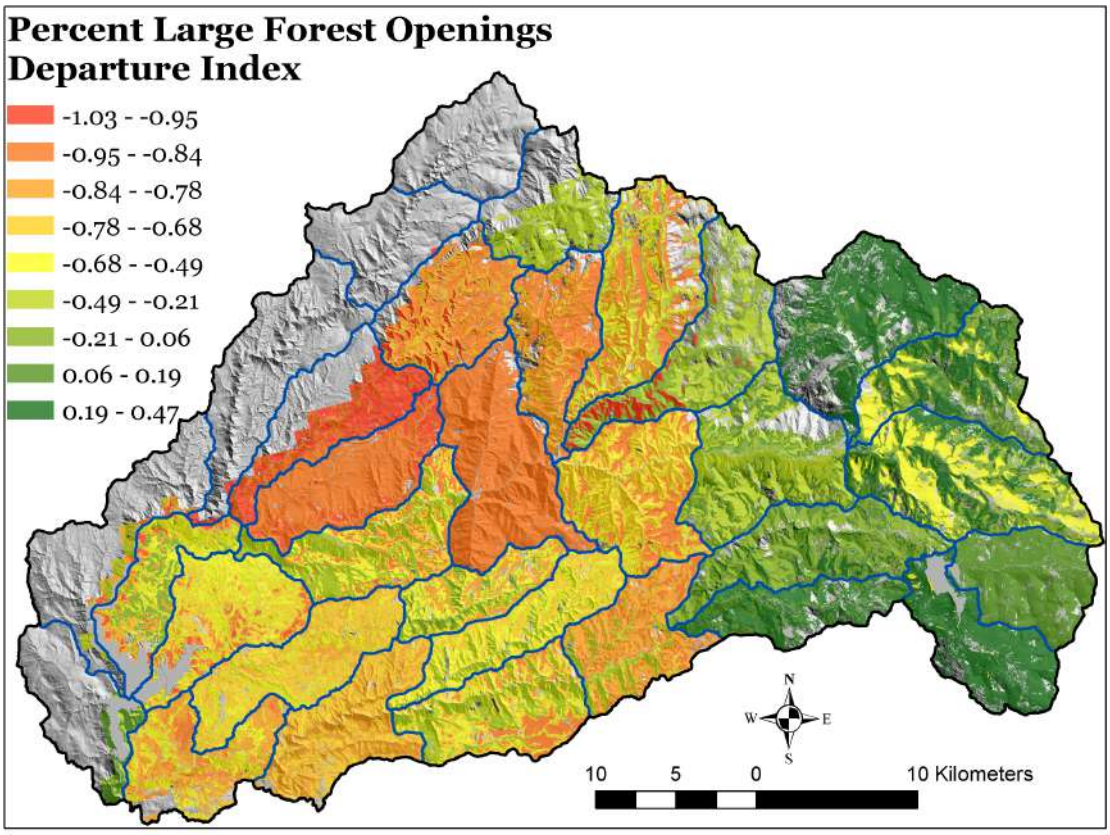

Figure 72: Percent Large Forest Openings departure index by Subbasin and Biophysical Class (BPC) for the Yuba River landscape. The departure index is negative if the percent of the Subbasin-by-BPC partition in large forest openings in the current landscape is less than the median value derived for the historical reference period. Note that in this case only a few partitions technically fall outside the negative departure range defined as < -1.

Metric 2: Large Forest Openings Patch Size Distribution

We define large forest openings as described above. Here, we quantify the size of individual large openings and determine the percent of forest within the Subbasin-by-BPC partition in large openings in each of several patch size classes or bins (see above), and compare the current and historical distributions. The departure index and score reflect whether or not the current landscape has a distribution of large forest opening patch sizes that differs from HRV and, if so, the degree of differences between the two distributions. This metric is a measure of landscape *configuration* as it reflects the number and size of large forest openings as opposed to just the total area in large forest openings. We chose this metric to identify Subbasins and BPCs in which the current landscape has too few or too many large forest openings in each of several patch size classes relative to HRV. An increasingly positive overall departure index (and score) warrants examining the comparative distributions to determine which patch size classes are under or over represented.

As an example, Large Forest Openings Patch Size Distribution departure index for the Yuba River landscape is depicted in **Figure 73**. Note, the departure index (as opposed to the score) is based on the percentage dissimilarity between the CRV and HRV distributions and thus is given on a percentage of maximum departure scale. In this case, Subbasin-by-BPC partitions vary in departure from ~ 0 - 100 %, and thus the majority of landscape partitions are rather severely departed with respect to the distribution of large forest opening patch sizes.

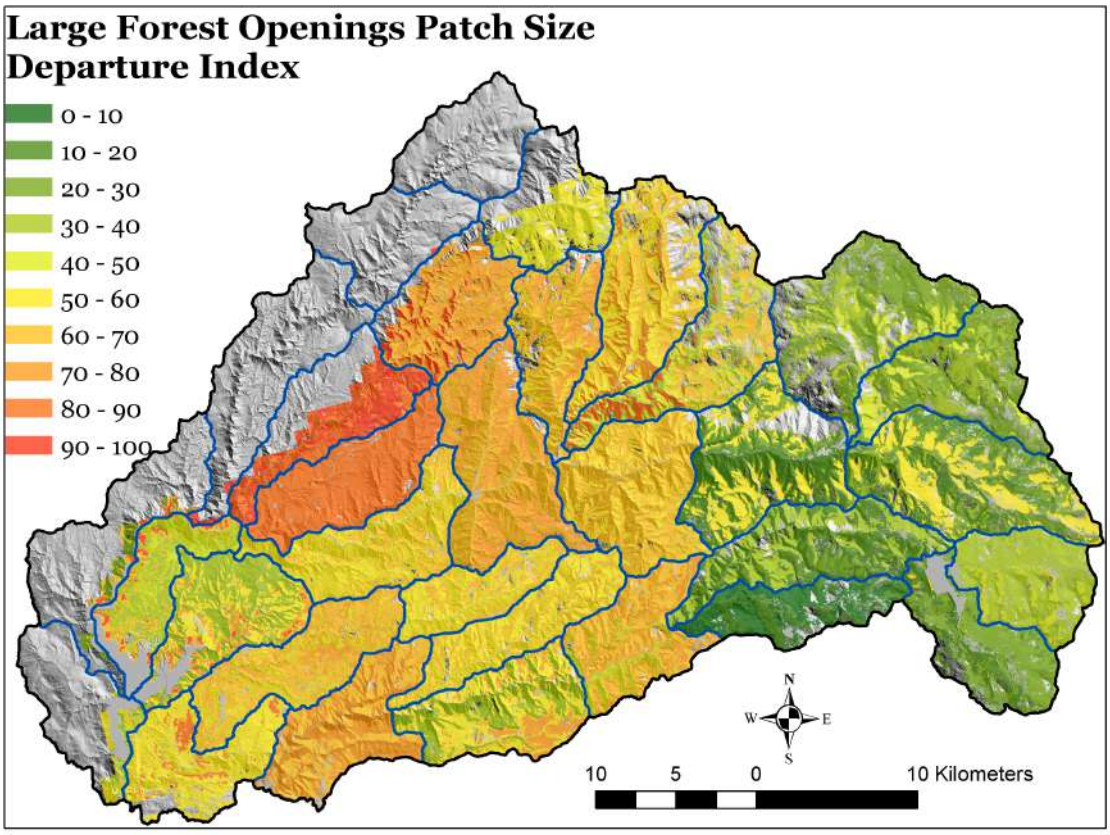

Figure 73: Large Forest Openings Patch Size departure index by Subbasin and Biophysical Class (BPC) for the Yuba River landscape. The departure index is given on percentage of maximum scale and reflects the percentage dissimilarity between the patch size distributions in the current landscape versus the historical reference period.

Metric 3: Developmental Stage Patch Size Distribution

We define developmental stages based on six tree height classes, ranging from Open (< 4.5 ft) to Tall Trees (> 125 ft), as described previously. Here, for each snapshot of the landscape we construct a patch mosaic comprised of developmental stages in which patches are defined using the 4-neighbor rule (i.e., orthogonal neighbors). For each snapshot, we quantify the size of each developmental stage patch and determine the percent of forest within the Subbasin-by-BPC partition in each of several patch size classes or bins (see above), and compare the current and historical distributions. The departure index and score reflect whether or not the current landscape has a distribution of developmental stage patch sizes that differs from HRV and, if so, the degree of differences in the two distributions. This metric is a measure of landscape *configuration* as it reflects the number and size of developmental stage patches as opposed to simply the total area in each developmental stage. As such, this metric is a measure of overall spatial heterogeneity of the forest in terms of developmental stages or tree height classes. We chose this metric to identify Subbasins and BPCs in which the current landscape has a forest that is too homogeneous in canopy height or too uniform in the canopy height patch mosaic relative to HRV. As before, an increasingly positive overall departure index (and score) warrants examining the comparative distributions to determine which patch size classes are under or over represented.

As an example, Developmental Stage Patch Size Distribution departure index for the Yuba River landscape is depicted in **Figure 74**. Note again that the departure index (as opposed to the score) is based on the percentage dissimilarity between the CRV and HRV distributions and thus is given on a percentage of

maximum departure scale. In this case, most Subbasin-by-BPC partitions exhibit relatively low to moderate departure ($< \sim 30$ %), although a few partitions approach 50 % departure.

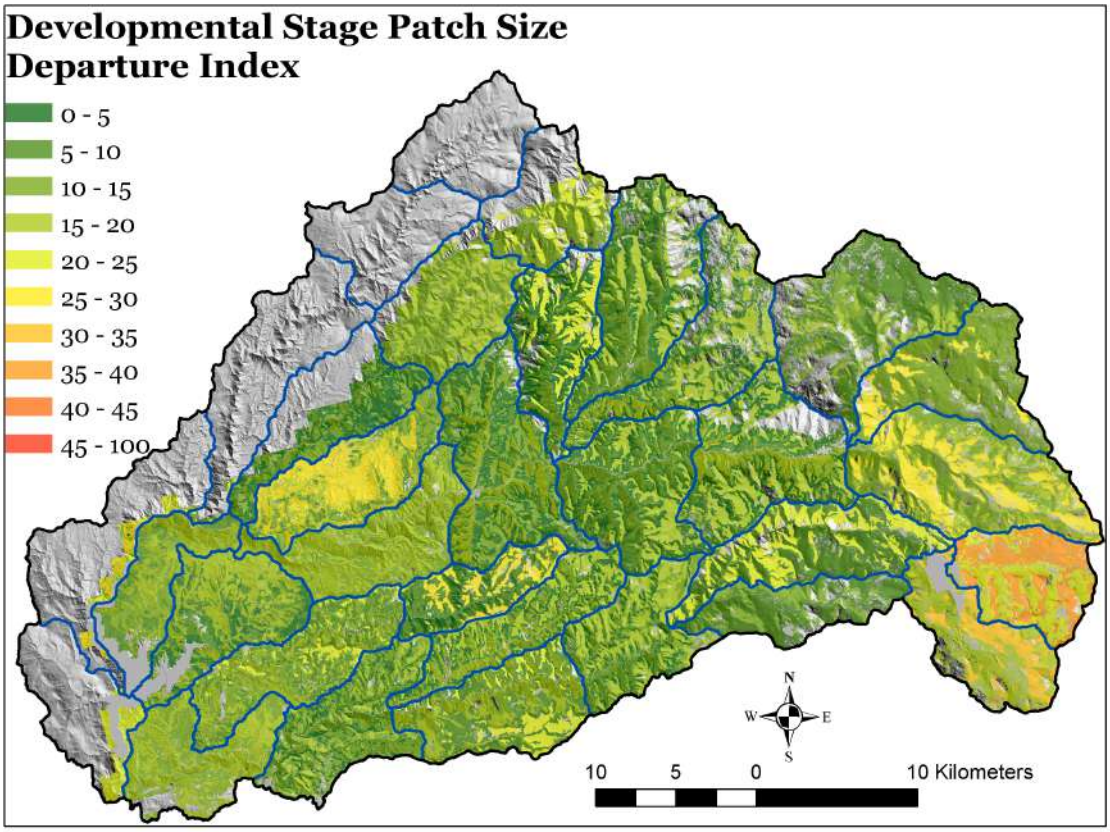

Figure 74: Developmental Stage Patch Size departure index by Subbasin and Biophysical Class (BPC) for the Yuba River landscape. The departure index is given on percentage of maximum scale and reflects the percentage dissimilarity between the patch size distributions in the current landscape versus the historical reference period.

Metric 4: Percent Large Trees

We define large trees as $>$ 30 inch dbh. Percent large trees is defined as the percent of the forest within the Subbasin-by-BPC partition in large trees, and the departure index and score reflect whether or not the current landscape is deficient in large trees relative to HRV and, if so, the degree of deficiency. This metric is a measure of landscape *composition* as it reflects how much of the forest is in large trees but is agnostic as to the spatial distribution of large trees. We chose this metric to identify Subbasins and BPCs in which there is too little area in large trees relative to HRV. The departure index is negative if the current landscape partition has less area in large trees than the median HRV condition and, conversely, positive if the current landscape partition has more area in large trees than the median HRV condition. The departure score, on the other hand, is positive if the current Subbasin-by-BPC partition has too little area in large trees compared to HRV, and otherwise is zero.

As an example, the Percent Large Trees departure index for the Yuba River landscape is depicted in **Figure 75**. Note, the departure index (as opposed to the score) can vary from negative to positive values, depending on the direction of the departure. In this case, all but a few of the Subbasin-by-BPC partitions exhibit negative departure values "outside" the HRV. Indeed, for most of the partitions the current

landscape has several-fold less area in large trees than expected under historical reference period conditions. Only a few of the partitions exhibit positive departure.

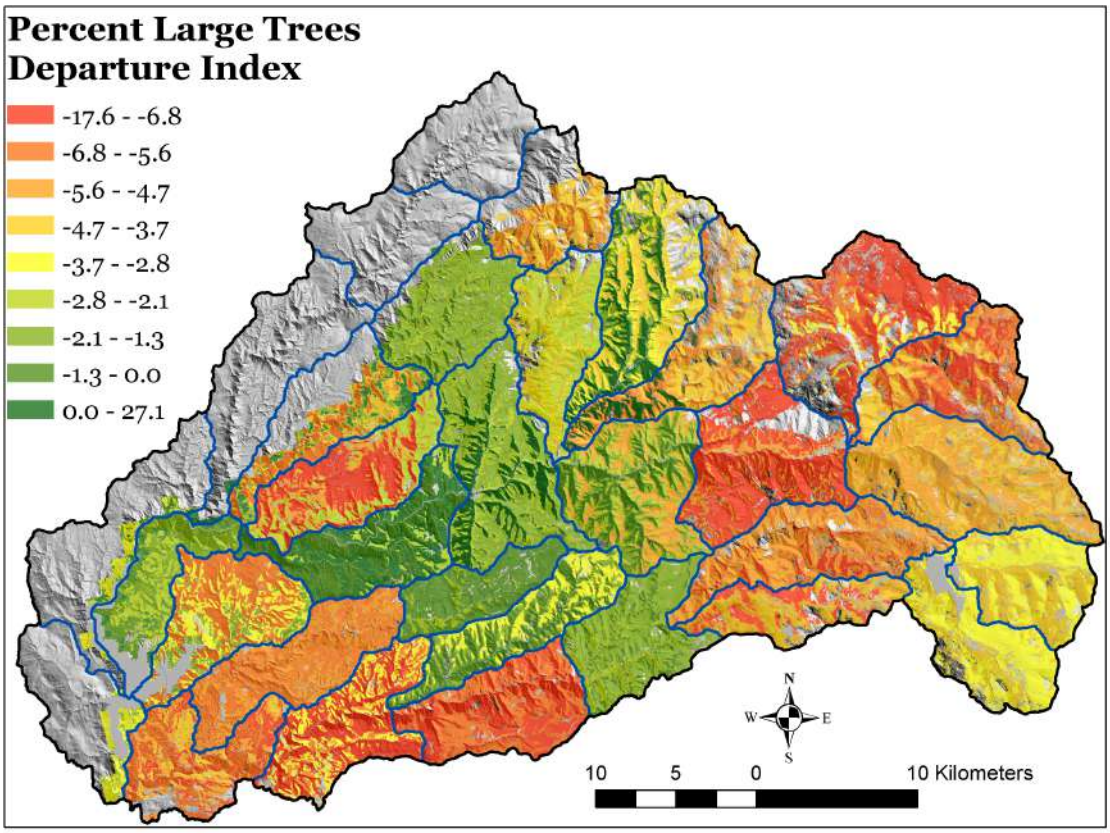

Figure 75: Percent Large Trees departure index by Subbasin and Biophysical Class (BPC) for the Yuba River landscape. The departure index is negative if the percent of the Subbasin-by-BPC partition in large trees in the current landscape is less than the median value derived for the historical reference period.

Metric 5: Large Tree Patch Size Distribution

We define large trees as described above. Here, we quantify the size of individual patches of large trees and determine the percent of forest within the Subbasin-by-BPC partition in large tree patches in each of several patch size classes or bins (see above), and compare the current and historical distributions. The departure index and score reflect whether or not the current landscape has a distribution of large tree patch sizes that differs from HRV and, if so, the degree of differences in the two distributions. This metric is a measure of landscape *configuration* as it reflects the number and size of large tree patches as opposed to just the total area in large trees. We chose this metric to identify Subbasins and BPCs in which the current landscape has too few or too many large tree patches in each of several patch size classes relative to HRV. As before, an increasingly positive overall departure index (and score) warrants examining the comparative distributions to determine which patch size classes are under or over represented.

As an example, Large Tree Patch Size Distribution departure index for the Yuba River landscape is depicted in **Figure 76**. Note again that the departure index (as opposed to the score) is based on the percentage dissimilarity between the CRV and HRV distributions and thus is given on a percentage of maximum departure scale. In this case, Subbasin-by-BPC partitions vary widely in departure from near 0 to 100 %.

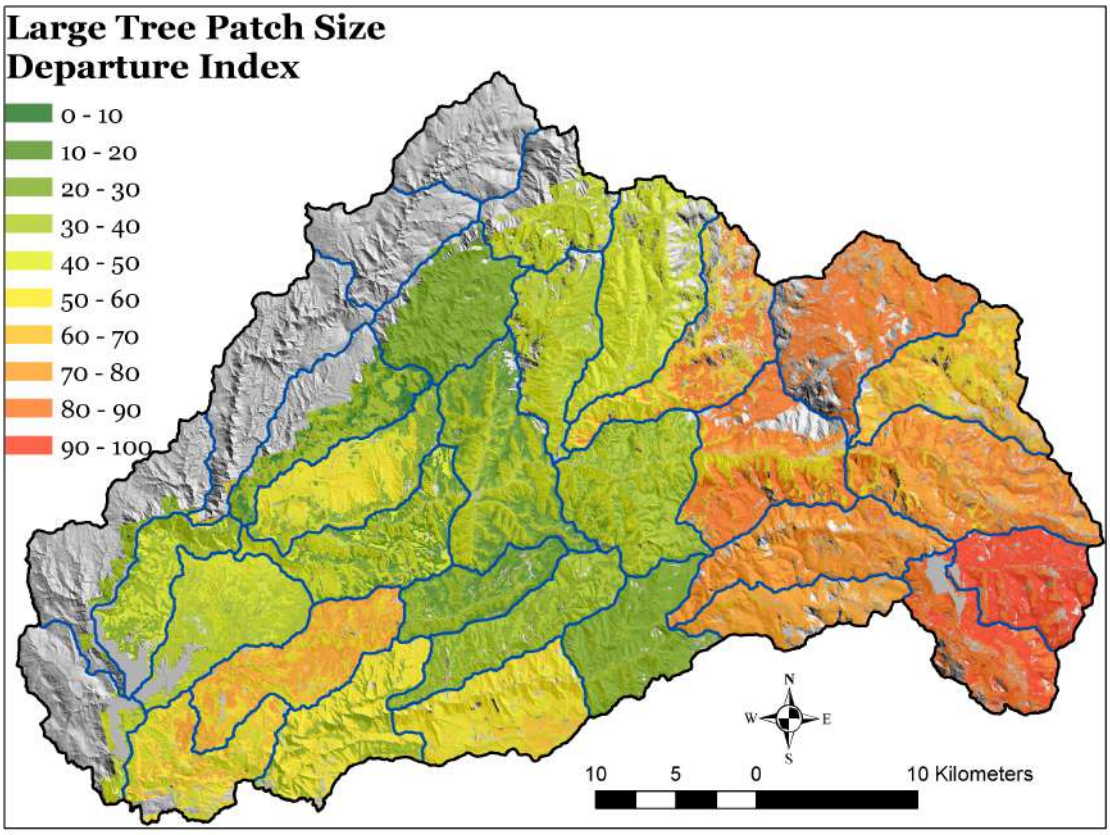

Figure 76: Large Tree Patch Size departure index by Subbasin and Biophysical Class (BPC) for the Yuba River landscape. The departure index is given on percentage of maximum scale and reflects the percentage dissimilarity between the patch size distributions in the current landscape versus the historical reference period.

Metric 6: Tree Size Class Patch Size Distribution

We define tree size class based on six tree diameter classes, ranging from Open (< 1 in dbh) to large Trees (> 30 in dbh), as described previously. Here, for each snapshot of the landscape, we construct a patch mosaic comprised of tree size classes in which patches are defined using the 4-neighbor rule (i.e., orthogonal neighbors). For each snapshot, we quantify the size of each tree size class patch and determine the percent of forest within the Subbasin-by-BPC partition in each of several patch size classes or bins (see above), and compare the current and historical distributions. The departure index and score reflect whether or not the current landscape has a distribution of tree size class patch sizes that differs from HRV and, if so, the degree of differences in the two distributions. This metric is a measure of landscape *configuration* as it reflects the number and size of tree size class patches as opposed to simply the total area in each tree size class. As such, this metric is a measure of overall spatial heterogeneity of the forest in terms of tree size (or diameter) classes. We chose this metric to identify Subbasins and BPCs in which the current landscape has a forest that is too homogeneous in tree size or too uniform in the tree size patch mosaic relative to HRV. As before, an increasingly positive overall departure index (and score) warrants examining the comparative distributions to determine which patch size classes are under or over represented.

As an example, the Tree Size Class Patch Size Distribution departure index for the Yuba River landscape is depicted in **Figure 77**. Note again that the departure index (as opposed to the score) is based on the percentage dissimilarity between the CRV and HRV distributions and thus is given on a percentage of maximum departure scale. In this case, all but one of the Subbasin-by-BPC partitions exhibit relatively low to moderate departure (< 30 %).

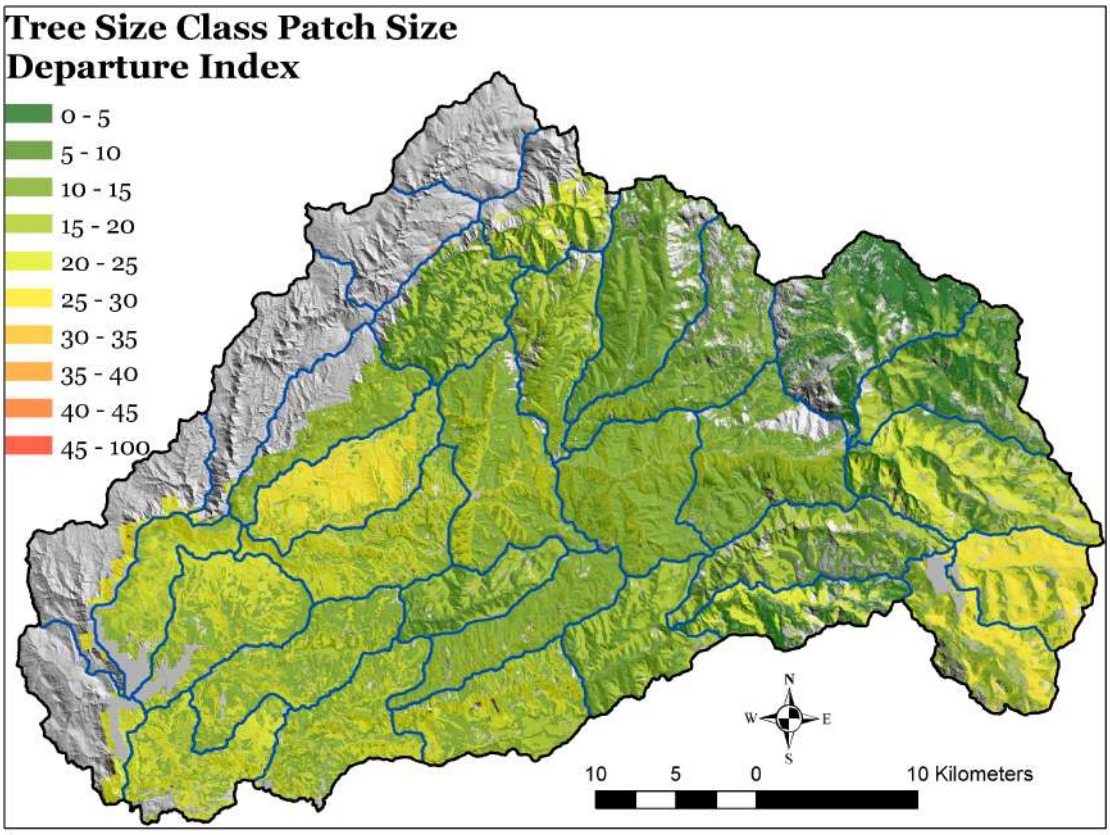

Figure 77: Tree Size Patch Size departure index by Subbasin and Biophysical Class (BPC) for the Yuba River landscape. The departure index is given on percentage of maximum scale and reflects the percentage dissimilarity between the patch size distributions in the current landscape versus the historical reference period.

Composite Departure Score

We combine the 6 Subbasin-level departure metrics above dealing with vegetation composition and configuration into a single composite departure score. This composite departure score can be interpreted as a measure of overall departure in vegetation composition and configuration within the Subbasin-by-BPC partition. Maximum departure occurs when the forest has too little area in large forest openings and/or large trees, and/or a vegetation patch mosaic configuration defined on the basis of either developmental stages (or tree height classes) or tree size classes (or tree diameter classes) that differs from the corresponding patch mosaic configuration under historical dynamic equilibrium conditions (i.e., too little or too much spatial variability). Note, this composite departure score, as with the individual component scores, focuses on Subbasins and BPCs that depart from HRV in one or more aspects of forest vegetation composition and configuration.

We derive the composite departure score by taking the simple average of the six component scores, since they all have a common 0 - 5 standard scale, as follows:

$$CDS_{ij} = \frac{\sum [D1_{ij} + D2_{ij} + D3_{ij} + D4_{ij} + D5_{ij} + D6_{ij}]}{30} * 100$$

where: $D1_{ij}$ = percent large forest openings departure score for the i^{th} Subbasin and j^{th} BPC; $D2_{ij}$ = large forest opening patch size distribution departure score for the i^{th} Subbasin and j^{th} BPC; $D3_{ij}$ =

developmental stage patch size distribution departure score for the i^{th} Subbasin and j^{th} BPC; $D4_{ij}$ = percent large trees departure score for the i^{th} Subbasin and j^{th} BPC; $D5_{ij}$ = large tree patch size distribution departure score for the i^{th} Subbasin and j^{th} BPC; $D6_{ij}$ = tree size class patch size distribution departure score for the i^{th} Subbasin and j^{th} BPC; CDS_{ij} = composite departure score for the i^{th} Subbasin and j^{th} BPC. Thus, final composite score can be interpreted as the percent of maximum possible departure. A composite departure score of 100 would occur only if the landscape partition receives a departure score of 5 for all 6 metrics.

As an example, the composite departure score for the Yuba River landscape is depicted in **Figure 78**. In this case, the departure scores range from 31 - 72 %; hence, from mild to strong overall departure. No partitions exhibited extreme departure when considering the composite of the six metrics. The greatest departure is in the North Cherokee Creek-North Yuba River Subbasin on the High productivity sites.

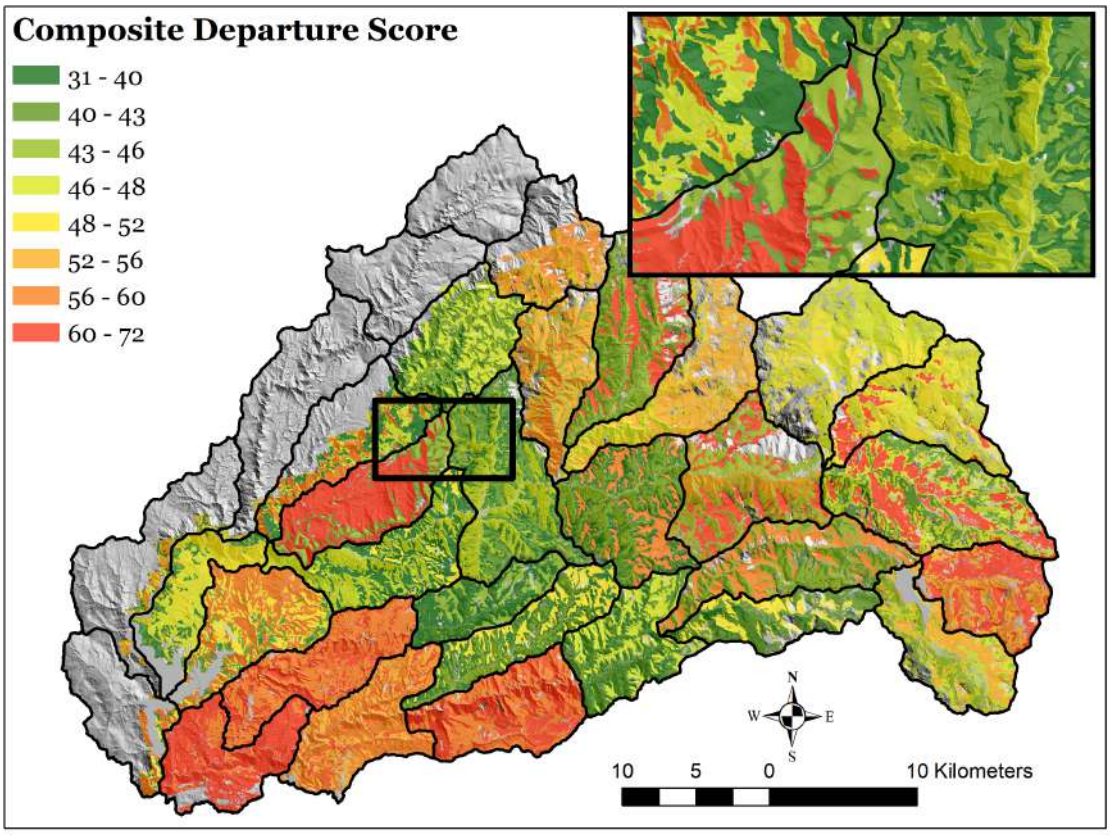

Figure 78: Composite Departure Score for the Subbasin-by-Biophysical Class (BPCs) partitions for the Yuba River landscape. The composite departure score represents the simple average of 6 component departure metrics (see text for details).

Management Applications

Subbasin-level results can provide a quantitative basis for determining which Subbasins and BPCs are in the greatest need of attention and the direction and magnitude of change needed to move the landscape towards historical reference conditions – should that be the goal. Of course, we acknowledge that current departure from historical reference conditions is only one consideration in defining project areas and establishing project-level objectives and may be more useful in some parts of the landscape than others. Again, it is not the purpose of our assessment to suggest where historical reference conditions should be used or whether they should be used at all.

Recall that Site-level results provide a perspective on HRV and departure at the scale of the entire focal landscape, albeit by evaluating conditions across plot-like Sites, and GPU-level results provide a local perspective on HRV and departure for areas large enough to consider the results as reliable and yet small enough to reflect spatial units akin to potential treatment units. Subbasin results, on the other hand, provide a perspective on HRV and departure at an intermediate scale - that of small landscapes embedded within the larger focal landscape.

Specific management applications of Subbasin-level results, as described below, should be interpreted with the following considerations in mind:

- It is important to remember that Subbasins are defined at the HUC12 level and mostly range between 10,000 - 20,000 acres, which roughly corresponds to the scale of many projects on federal lands. In most cases, HUC 12 Subbasins are large enough to represent the dynamic landscape changes driven by disturbance and succession processes under historical dynamic equilibrium conditions. At the same time, Subbasins, as defined, are small enough to reflect local variations in landscape features that affect disturbance and succession processes that result in idiosyncratic vegetation patterns.
- It is important to understand that here the emphasis is on the range of variability in landscape structure at the spatial extent of the entire *Subbasin* - albeit by BPC partition. The measured HRV and current departure is specific to each Subbasin-by-BPC partition. Owing to the idiosyncrasies of landscapes, the measured HRV and current departure for each Subbasin is expected to differ from that of any other Subbasin of the same extent because all landscapes are unique. In addition, the measured HRV and current departure of each Subbasin is specific to that extent, as the range of variability in landscape metrics would likely differ for larger or smaller extents.
- It is also important to understand that *Subbasin-level* variation is likely to be considerably less than *GPU-level* or *Site-level* variation, for the simple reason that large areas have the capacity to absorb small changes, either because changes to relatively small areas don't affect enough area to be consequential or because changes in one direction are compensated for by changes in the opposite direction in other parts of the landscape. In other words, larger landscape have the capacity to buffer relative small-scale changes. Importantly, the larger the landscape the greater the capacity to absorb small-scale changes. Thus, in general, the larger the landscape the less temporal variability, up to a point. At some point, increasing the extent of the landscape will not reduce the temporal variability because different drivers of landscape change are encountered (e.g., different climate regime). This scale dependency in landscape-level variability means that the results presented here are specific to the Subbasin and its extent.
- Lastly, it is important to recognize that here our focus is on current departure as a means of identifying individual Subbasins and BPCs that deviate most from historical conditions to help prioritize Subbasins for restoration treatment – should that be the goal. However, we acknowledge that current departure from historical reference conditions is only one consideration in establishing Subbasin-level objectives and treatments and may be more useful in some parts of the landscape than others. It is not the purpose of our assessment to suggest where historical reference conditions should be used to inform Subbasin-level objectives and treatments or whether they should be used at all.

Subject to the considerations above, Subbasin-level results have the following specific management applications:

- The composite departure score can serve as a first stage in identifying and prioritizing Subbasins and BPCs for treatment - should restoration of historical reference conditions be the goal. Specifically, Subbasin departure can point to broad areas within the focal landscape that exhibit the greatest departure from HRV, and the departure of individual BPC partitions within the Subbasin can point to the parts of the Subbasin that depart the most. This information along with the GPU-level results can serve as the initial focus for a management project aimed at restoring HRV

Let's take the example presented earlier for the Yuba River landscape (**Figure 78**). In this case, the composite departure score points to the North Cherokee Creek-North Yuba River Subbasin as having the most overall departure within this landscape. Thus, this area would serve as a logical focus for one or more management projects aimed at restoring historical reference conditions - should that be a desired goal for this area. In addition, further scrutiny of the results reveals that the High productivity sites (BPC = 4) exhibit the greatest departure in this Subbasin. Thus, treatment of a limited area within this Subbasin could prioritize these higher productivity Sites.

- While the composite departure score can point to areas within the focal landscape that exhibit the most departure overall, specific objectives and treatments for each area can be informed by decomposing the composite score into the component metrics to determine which aspects of the forest vegetation composition and/or configuration are departed and to what degree.

  Let's continue with the example above and decompose the composite departure score for High productivity Sites in the North Cherokee Creek-North Yuba River Subbasin on the High productivity Sites:

  - The current percent of forest in large openings is 0.38 % and the HRV is 0.03 - 16.28 % with a median of ~ 2.35 %, resulting in a departure index of -0.85. This indicates that the current condition is just barely "inside" the lower end of the range. The restoration objective would be to increase the percent of forest in large openings by a minimum of 2 %, but possibly as much as 16 %, depending on other objectives.
  - The CRV and average HRV distribution of large forest opening patch sizes is depicted in **Figure 79**. The average HRV distribution includes ~ 2 % of the forest in openings 0.1 - 1 acre, ~ 1 % in openings 1 - 3 acres, and ~ 1 % in openings > 3 acres. Note, the sum of these percentages is greater than the median reported above because the distribution of patch sizes is skewed towards the larger patch size. The restoration objective would be to create openings concordant with the distribution above, noting the skew towards the larger openings.

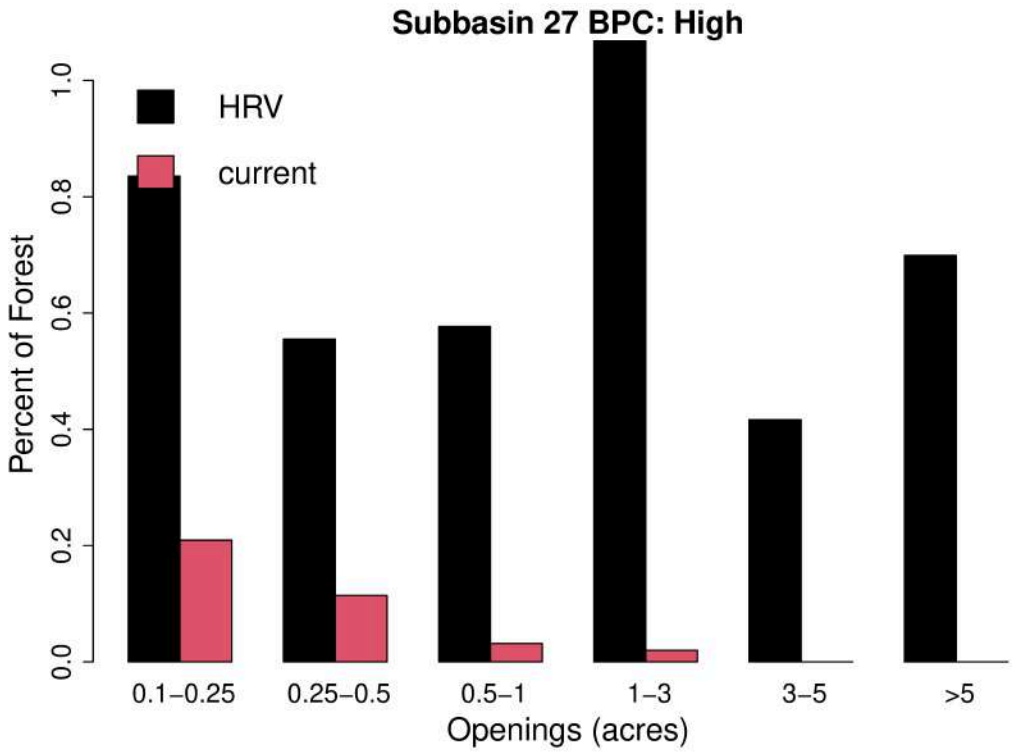

Figure 79: Current Range of Variability (CRV) and Historical Range of Variability (HRV) in the distribution of Large Forest Opening Patch Sizes for Subbasin 27 (North Cherokee Creek-North Yuba

River Subbasin) and High productivity Biophsical Class (BPC) sites in the Yuba River landscape. The HRV distribution represents the average across time under historical dynamic equilibrium conditions.

– The CRV and average HRV distribution of developmental stage patch sizes is depicted in **Figure 80**. The CRV distribution has a preponderance of very small (< 0.25 acres) and very large (> 5 acres) patches, possibly reflecting a relatively homogenous canopy of medium height with numerous small variations in height produced by individuals and clumps of shorter and taller treees. The average HRV distribion, in contrast, is comprised of predominantly small patches < 0.25 acres, but with patches of all sizes well represented. Thus, the average HRV condition is a relatively fine-scale mosaic of canopy heights with occasional larger patches of trees in the same developmental stage. The restoration objective would be to increase the patchiness or horizontal heterogeneity of the canopy, with a strong emphasis on creating small patches of trees in different developmental stages.

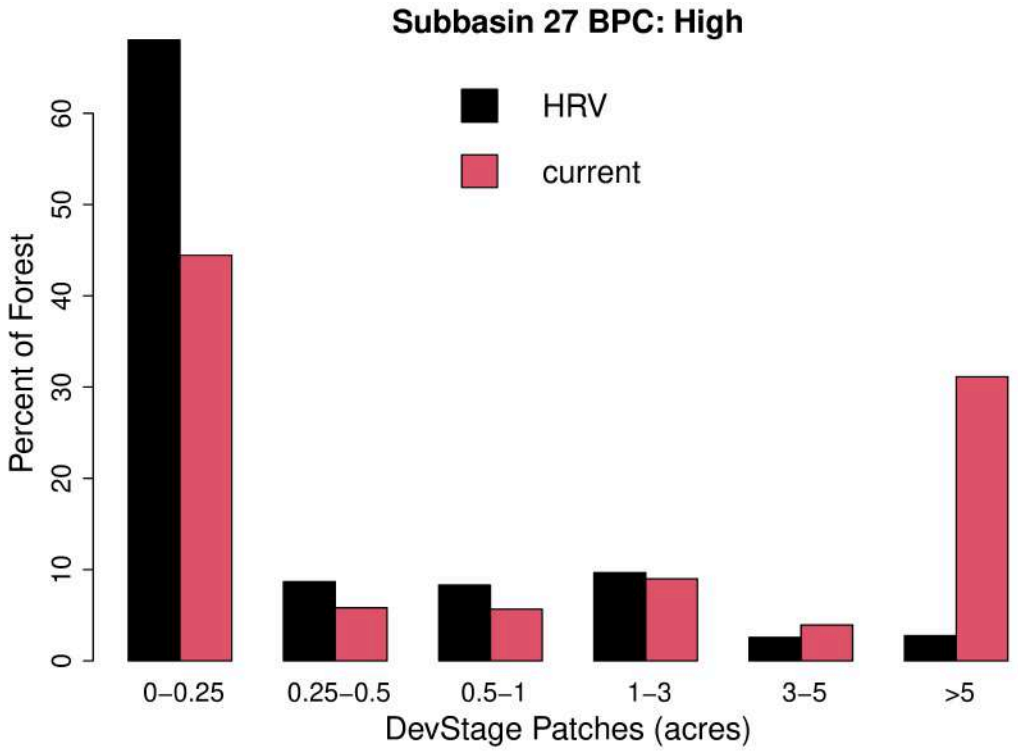

Figure 80: Current Range of Variability (CRV) and Historical Range of Variability (HRV) in the distribution of Developmental Stage Patch Sizes for Subbasin 27 (North Cherokee Creek-North Yuba River Subbasin) and High productivity Biophsical Class (BPC) sites in the Yuba River landscape. The HRV distribution represents the average across time under historical dynamic equilibrium conditions.

– The current percent of forest in Large Trees is ~ 8 % and the HRV is ~ 20 - 24 % with a median of ~ 23 %, resulting in a departure index of -6.83. This indicates that the current condition is well "outside" the lower end of the range. The restoration objective would be to increase the percent of forest in Large Trees by 12 - 16 %, which may be difficult to achieve in the short term, but Large Tree retention, thinning from below to facilitate diameter growth on the residual trees, and selective removal of small diameter trees to create the large openings (leaving a higher percentage of residual trees in the largest diameter class) all would help to achieve this objective.

– The CRV and average HRV distribution of Large Tree patch sizes is depicted in **Figure 81**. The average HRV distribution includes ~ 16 % of the forest in Large Tree patches < 0.25 acres, and the remaining ~ 6 % in larger patches ranging up to 5 acres or more. The restoration objective would be to emphasize small patches of Large Trees throughout, but take advantage of opportunities to create larger patches where they exist.

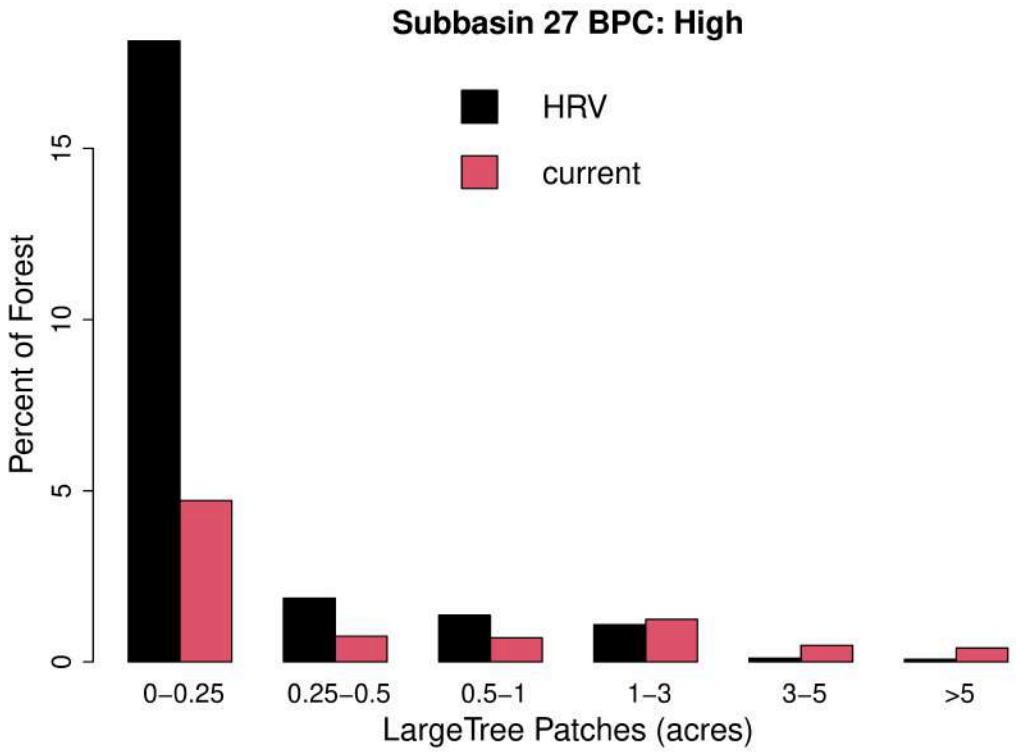

Figure 81: Current Range of Variability (CRV) and Historical Range of Variability (HRV) in the distribution of Large Tree Patch Sizes for Subbasin 27 (North Cherokee Creek-North Yuba River Subbasin) and High productivity Biophsical Class (BPC) sites in the Yuba River landscape. The HRV distribution represents the average across time under historical dynamic equilibrium conditions.

– The CRV and average HRV distribution of Tree Size Class patch sizes is depicted in **Figure 82** and is very similar to the distribution of Developmental Stage patch sizes described above. As suggested above, the restoration objective would be to increase the patchiness or horizontal heterogeneity of the forest canopy, with a strong emphasis on creating small patches of trees in different size classes.

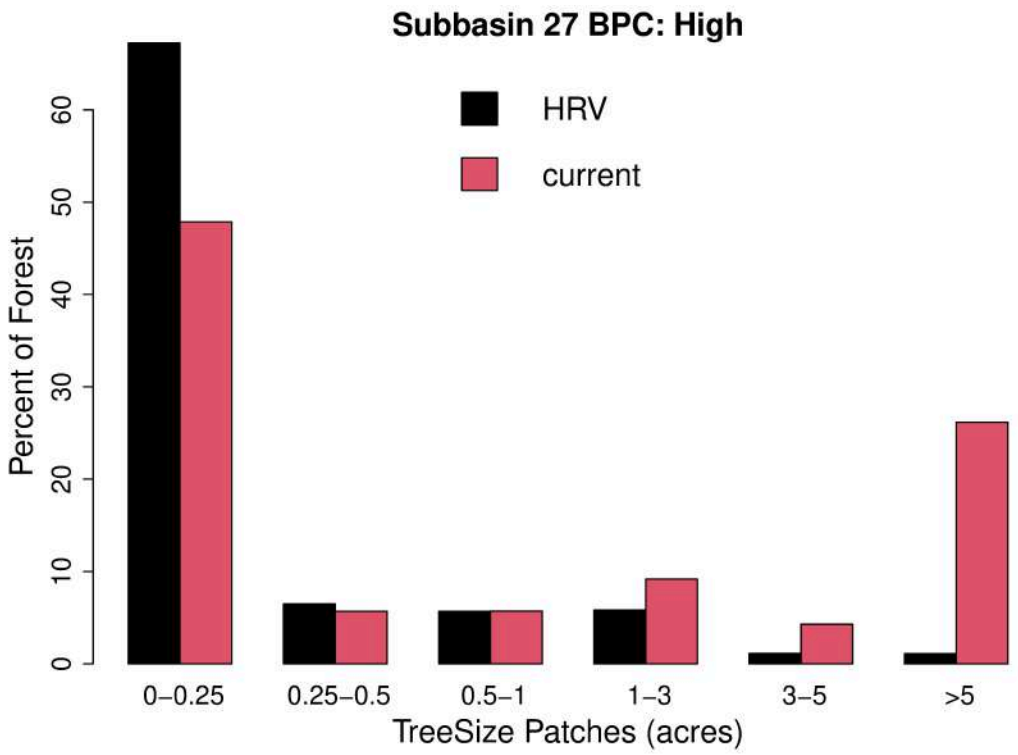

Figure 82: Current Range of Variability (CRV) and Historical Range of Variability (HRV) in the distribution of Tree Size Patch Sizes for Subbasin 27 (North Cherokee Creek-North Yuba River Subbasin) and High productivity Biophsical Class (BPC) sites in the Yuba River landscape. The HRV distribution represents the average across time under historical dynamic equilibrium conditions.

BIBLIOGRAPHY

Abella SR, Denton CW. 2009. Spatial variation in reference conditions: historical tree density and pattern on a Pinus ponderosa landscape. Can. J. For. Res. 39:2391–2403.

Agee JK. 1993. Fire ecology of Pacific Northwest forests. Washington, DC: Island Press.

Agee JK. 2007. Fire Severity. In: FireWords: Fire Science Glossary [electronic]. U.S. Department of Agriculture, Forest Service, Rocky Mountain Research Station, Fire Sciences Laboratory (Producer).

Alexander EB, Coleman RG, Keeler-Wolfe T, Harrison SP. 2006. Serpentine geoecology of western North America: geology, soils, and vegetation. Oxford University Press.

Anderson MK, Morrato MJ. 1996. Native American Land-Use Practices and Ecological Impacts. In Sierra Nevada Ecosystem Project: Final report to Congress, Volumer II, Pp. 187-206.

Baker W. 2014. Historical forest structure and fire in Sierran mixed-conifer forests reconstructed from General Land Offce survey data. Ecosphere, 5(7):1-70.

Beaty RM, Taylor AH. 2007. Fire disturbance and forest structure in old-growth mixed conifer forests in the northern Sierra Nevada, California. Journal of Vegetation Science, 18(6):879. Bormann FH, Likens GE 1979. Pattern and process in a forested ecosystem: disturbance, development and the steady state based on the Hubbard Brook ecosystem study. Springer-Verlag, New York.

Breiman L. 2001. Random Forests, Machine Learning 45:5-32.

Buse L, Perera A. 2002. Emulating natural forest landscape disturbances: concepts and applications. Technical report, Ontario Forest Research Institute. Chew JD, Stalling C, Moeller K. 2004. Integrating Knowledge for Simulation Vegetation Change at Landscape Scales. Western Journal of Applied Forestry 19(2): 102-108.

Christensen N L, Bartuska AM, Brown JH, Carpenter S, Antonio CD, Francis R, Franklin JF, Macmahon JA, Noss RF, Parsons J, Peterson CH, Turner MG, Woodmansee RG, Url S. 1996. The Report of the Ecological Society of America Committee on the Scientific Basis for Ecosystem Management.

Collins BM, Kelly M, van Wagtendonk JW, Stephens SL. 2007. Spatial patterns of large natural fires in Sierra Nevada wilderness areas. Landscape Ecology 22: 545-557.

Collins BM, Stephens SL. 2007. Managing natural wildfires in Sierra Nevada wilderness areas. Frontiers in Ecology and the Environment 5: 523–527.

Collins BM, Stephens SL. 2010. Stand-replacing patches within a 'mixed severity' re regime: Quantitative characterization using recent fires in a long-established natural fire area. Landscape Ecology, 25(6):927-939.

Cook ER. 2004. North American Summer PDSI Reconstructions. Cushman SA, Wasserman TN, McGarigal K. 2011. Modeling Landscape Fire and Wildlife Habitat. In The Landscape Ecology of Fire, D McKenzie, C Miller, and DA Falk, eds., Pp. 223-248. New York, New York, USA, Springer Science+Business Media.

Cook ER, Seager R, Heim RR, Vose RS, Herweijer C, and Woodhouse C. 2010. Megadroughts in North America: Placing IPCC projections of hydroclimatic change in a long-term paleoclimate context. Journal of Quaternary Science, 25(1), 48-61. doi: 10.1002/jqs.1303

Cushman SA, Wasserman TN, and McGarigal K. 2011. Modeling Landscape Fire and Wildlife Habitat. In The Landscape Ecology of Fire, D McKenzie, C Miller, and DA Falk, eds., Pp. 223-248. New York, New York, USA, Springer Science+Business Media.

Dellasala D, Bond M, Hanson C, Hutto R, Odion D. 2014. Complex Early Seral Forests of the Sierra Nevada: What are They and How Can They Be Managed for Ecological Integrity? Natural Areas Journal 34:310-324.

DeSiervo MH, Jules E, Safford HD. 2015. Disturbance response across a productivity gradient: postfire vegetation in serpentine and non-serpentine forests. Ecosphere 6: Article 60.

Dolph KL. 1987. Site index curves for young-growth California white fir on the western slopes of the Sierra Nevada. USDA Forest Service Research Paper PSW-185, 9 pp.

Dolph KL. 1991. Polymorphic site index curves for red fir in California and southern Oregon. USDA Forest Service Research Paper PSW-206, 18 pp.

Dunning D. 1942. A site classification for the mixed-conifer selection forests of the Sierra Nevada. USDA Forest Service Forest Research Notes No. 28, 21 pp.

Dunning D, and Reineke LH. 1933. Preliminary yield tables for second-growth stands in the California pine region. USDA Forest Service Technical Bulletin No. 354, 24 pp.

Estes B. 2013a. Historic Range of Variability for Aspen in the Sierra Nevada and South Cascades. Technical report, USDA Forest Service, Pacific Southwest Region, Vallejo, CA.

Estes B. 2013b. Historic Range of Variability for Chaparral in the Sierra Nevada and Southern Cascades. Technical report, USDA Forest Service, Pacific Southwest Region, Vallejo, CA. Fule PZ, Swetnam TW, Brown PM, Falk DA, Peterson DL, Allen CD, Aplet GH, Battaglia MA, Binkley D, Farris C, Keane RE, Margolis EQ, Grissino-Mayer H, Miller C, Sieg CH, Skinner CN, Stephens SL, Taylor AH. 2014. Unsupported inferences of high-severity fire in historical dry forests of the western United States: response to Williams and Baker. Global Ecology and Biogeography, 23:825-830.

Guo D. 2008. Regionalization with Dynamically Constrained Agglomerative Clustering and Partitioning (REDCAP). International Journal of Geographical Information Science 22 (7):801–23.

Gross S, Coppoletta M. 2013. Historic Range of Variability for Meadows in the Sierra Nevada and South Cascades. Technical report, USDA Forest Service, Pacific Southwest Region, Vallejo, CA.

Gustafson EJ. 2013. When relationships estimated in the past cannot be used to predict the future: using mechanistic models to predict landscape ecological dynamics in a changing world. Landscape Ecology 28: 1429-1437.

Gustafson EJ., Sturtevant BR, Shvidenko AS, Scheller RM. 2010. Using landscape disturbance and succession models to support forest management. In: Li, Chao; Lafortezza, Raffaele; Chen, Jiquan. Landscape Ecology in Forest Management and Conservation, Challenges and Solutions for Global Change. Dordrecht, The Netherlands; Springer: 99-118. Chapter 5.

He HS, Mladenoff DJ. 1999. Spatially Explicit and Stochastic Simulation of Forest-Landscape Fire Disturbance and Succession. Ecology 80(1):81-99.

Hessburg PF, Agee JK, Franklin JF. 2005. Dry forests and wildland fires of the inland Northwest USA: contrasting the landscape ecology of the pre-settlement and modern eras. Forest Ecology and Management, 211:117-139.

Jeronimo SMA, Kane VR, Churchill DJ, Lutz JA, North MP, Asner GP, and Franklin JF. 2019. Forest structure and pattern vary by climate and landform across active-fire landscapes in the montane Sierra Nevada. Forest Ecology and Management 437:70–86.

Kane VR, Lutz JA, Roberts SL, Smith DF, Mcgaughey RJ, Povak NA, Brooks ML. 2013. Forest Ecology and Management Landscape-scale effects of fire severity on mixed-conifer and red fir forest structure in Yosemite National Park. 287:17-31.

Keane RE. 2012. Creating Historical Range of Variation (HRV) Time Series Using Landscape Modeling: Overview and Issues. In Historical Environmental Variation in Conservation and Natural Resource Management, JA Wiens, GD Hayward, HD Safford, and CMGiffen, eds., chapter 8, Pp. 113-127. John Wiley & Sons, Ltd.

Keane RE, Cary GJ, Davies ID, Flannigan MD, Gardner RH, Lavorel S, Lenihan JM, Li C, Rupp TS. 2004. A classification of landscape fire succession models: spatial simulations of fire and vegetation dynamics. Ecological Modelling 179(1):3-27.

Keane RE, Hessburg PF, Landres PB, Swanson FJ. 2009. The use of historical range and variability (HRV) in landscape management. Forest Ecology and Management 258:1025-1037.

Kelly AE, and Goulden ML. 2016. A montane Mediterranean climate supports year-round photosynthesis and high forest biomass. Tree Physiology 36:459-468.

Knapp EE. 2015. Long-term dead wood changes in a Sierra Nevada mixed conifer forest: Habitat and fire hazard implications. Forest Ecology and Management 339: 87-95.

Knapp EE, Skinner CN, North MP, Estes BL. 2013. Long-term overstory and understory change following logging and fire exclusion in a Sierra Nevada mixed-conifer forest. Forest Ecology and Management, 310:903-914.

Landfire. 2007. LANDFIRE Project, U.S. Department of Agriculture, Forest Service; U.S. Department of the Interior. http://www.landfire.gov/national_veg_models_op2.php.

Landres PB, Morgan P, Swanson FJ. 1999. Overview of the use of natural variability concepts in managing ecological systems. Ecological Applications, 9(4):1179-1188.

Littell JS, Peterson DL, Millar CI, O'Halloran KA. 2012. U.S. National Forests adapt to climate change through Science-Management partnerships. Climatic Change, 110(1-2):269-296.

Long JN, and Shaw JD. 2012. A density management diagram for even-aged Sierra Nevada mixed-conifer stands. Western Journal of Applied Forestry 27:187-195.

Mallek C, Safford H, Viers J, Miller J. 2013. Modern departures in fire severity and area vary by forest type, Sierra Nevada and southern Cascades, California, USA. Ecosphere, 4(December):153.

McGarigal K, Mallek M, Estes B, Tierney M, Walsh T, Thane T, Safford H, and Cushman SA. 2018. Modeling historical range of variability and alternative management scenarios in the Yuba River watershed, Tahoe National Forest, California. Gen. Tech. Rep. RMRS-GTR-385. Fort Collins, CO: U.S. Department of Agriculture, Forest Service, Rocky Mountain Research Stations. 346 p.

McGarigal K, Romme WH. 2005a. Historic Range of Variability in Landscape Structure and Wildlife Habitat: San Juan National Forest. Unpubl. technical report, University of Massachustts.

McGarigal K, Romme WH. 2005b. Historic Range of Variability in Landscape Structure and Wildlife Habitat: Uncompahgre Plateau Landscape. Unpubl. technical report, University of Massachusetts.

McGarigal K, Romme WH. 2012. Modeling Historical Range of Variability at a Range of Scales: An Example Application. In Historical Environmental Variation in Conservation and Natural Resource Management, JA Wiens, GD Hayward, HD Safford, and CM Giffen, eds., chapter 9, Pp. 128-145. John Wiley & Sons, Ltd.

McGarigal K, Cushman SA, Ene E. 2012. FRAGSTATS v4: Spatial Pattern Analysis Program for Categorical and Continuous Maps. Computer software program produced by the authors at the University of Massachusetts, Amherst. Available at the following web site: www.umass.edu/landeco/research/fragstats/fragstats.html

McKelvey KS, Johnston JD. 1992. Historical perspectives on forests of the Sierra Nevada and the Transverse Ranges of southern California: forest conditions at the turn of the century. In: Verner J, McKelvey KS, Noon BR, Gutierrez JR, Gould Jr GI, Beck TW, eds. The California Spotted Owl: A Technical Assessment of its Current Status. General Technical Report PSW-GTR-133. Albany, CA: USDA Forest Service, Pacific Southwest Research Station: 225-246.

McKelvey KS, Skinner CN, Chang C, Eman DC, Husari SJ, Parsons DJ, van Wagtendonk JW, Weatherspoon CP. 1996. Sierra Nevada Ecosystem Project: Final report to Congress, vol. II, Assessments and scientific basis for management options. Davis: University of California, Centers for Water and Wildland Resources. 8 pp.

Merriam K. 2013. Natural Range of Variation in Hardwood Vegetation In the Sierra Nevada, California Over the Holocene Epoch. Technical report, USDA Forest Service, Pacific Southwest Region, Vallejo, CA.

Meyer MD. 2013a. Natural Range of Variation of Red Fir Forests in the Bioregional Assessment Area. Technical report, USDA Forest Service, Pacific Southwest Region, Vallejo, CA.

Meyer MD. 2013b. Natural Range of Variation of Subalpine Forests in the Bioregional Assessment Area. Technical report, USDA Forest Service, Pacific Southwest Region, Vallejo, CA.

Meyer CB, Knight DH, Dillon GK. 2008. Use of the Historic Range of Variability to Evaluate Ecosystem Sustainability. Forum on Public Policy: A Journal of the Oxford Round Table, (Summer).

Millar CI, Woolfenden WB. 1999. Sierra Nevada forests: where did they come from? Where are they going? What does it mean? . Pages 206-236 in Transactions of the North American Wildlife and Natural Resources Conference, San Francisco, California, USA.

Miller C, Urban DL. 1999. A model of surface fire, climate and forest pattern in the Sierra Nevada, California. Ecological Modelling, 114(2-3):113-135.

Miller JD, Knapp EE, Key CH, Skinner CN, Isbell CJ, Creasy RM, Sherlock JW. 2009. Calibration and validation of the relative differenced Normalized Burn Ratio (RdNBR) to three measures of fire severity in the Sierra Nevada and Klamath Mountains, California, USA. Remote Sensing of Environment, 113(3):645-656.

Miller JD, Safford HD, Crimmins M, Thode AE. 2009. Quantiative evidence for increasing forest fire severity in the Sierra Nevada and southern Cascade Mountains, California and Nevada, USA. Ecosystems 12: 16-32.

Miller JD, and Thode AE. 2007. Quantifying burn severity in a heterogeneous landscape with a relative version of the delta Normalized Burn Ratio (dNBR). Remote Sensing of Environment 109:66-80.

Minnich RA. 2007. Climate, paleoclimate, and paleovegetation. In Terrestrial vegetation of California, 3rd edition, M Barbour, T Keeler-Wolf, and AA Schoenherr, eds., Pp. 43-70. University of California Press.

Mladenoff DJ, Baker WL. 1999. Development of forest and landscape modeling approaches. In Spatial modeling of forest landscape change: approaches and applications, DJ Mladenoff and WL Baker, eds., Pp. 1-13. Cambridge: Cambirdge University Press.

Nekola JC, White PS. 1999. The distance decay of similarity in biogeography and ecology. Journal of Biogeography 26:867–878.

North M (ed). 2012. Managing Sierra Nevada forests. Gen. Tech. Rep. PSW-GTR-237. Albany, CA: U.S. Department of Agriculture, Forest Service, Pacific Southwest Research Station. 184 p.

North M, Stine P, O'Hara K, Zielinski W, Stephens S. 2009. An ecosystem management strategy for Sierran mixed-conifer forests. Gen. Tech. Rep. PSW-GTR-220. Albany, CA: U.S. Department of Agriculture, Forest Service, Pacific Southwest Research Station. 49 p.

O'Geen AT, Dahlgren RA, Sanchez-Mata D. 2007. California soils and examples of ultramafic vegetation. In Terrestrial Vegetation of California, MG Barbour, T Keeler-Wolf, and AA Schoenherr, eds., Pp. 71-106. Berkeley and Los Angeles, USA: University of California Press.

Perera AH, Schnekenburger F, Baldwin D, Boychuk D, Yemshanov D,Weaver KLJ, Buse AH. compilers. 2003. BFOLDS - A spatially explicit stochastic model to simulate boreal forest landscape dynamics. Pages 189 -191 in Meeting emerging ecological, ecomomic, and social challenges in the Great Lakes region: Popular summaries. Ontario Ministry of Natural Resources. Ontario forest Research Institute, Sault Ste. Marie, Ontario. Forestry Research Information Paper No. 155.

Pickett STA, Thompson JN. 1978. Patch dynamics and the design of nature reserves. Biological Conservation 13:27-37.

Pierce KB, Lookingbill T, Urban D. 2005. A simple method for estimating potential relative radiation (PRR) for landscape-scale vegetation analysis. Landscape Ecology 20:137-147.

Potter DA. 1998. Forested Communities of the Upper Montane in the Central and Southern Sierra Nevada. Technical report.

PRISM Climate Group. 2014. Oregon State University, http://prism.oregonstate.edu, created 4 Feb 2014.

Remmert H. 1991. The mosaic-cycle concept of ecosystems — an overview. Pages 1-21 In Remmert H, ed., Ecological Studies, Volume 85, Springer-Verlag.

Rodman KC,Sánchez Meador AJ, Moore MM, Huffman DW. 2017. Reference conditions are influenced by the physical template and vary by forest type: A synthesis of Pinus ponderosa-dominated sites in the southwestern United States. Forest Ecology and Management 404:316-329.

Romme WH, Floyd M, Hanna D, Redders J. 2000. Using natural disturbance regimes to mitigate forest fragmentation in the central Rocky Mountains. Pages 377-400 In Knight R, Smith F, Buskirk S, Romme WH, and Baker WL, eds., Forest fragmentation in the southern Rocky Mountains, University Press of Colorado, Boulder, CO, USA.

Romme WH, Wiens JA, Safford HD. 2012. Setting the stage: theoretical and conceptual background of historical range of variation. Pages 3-18 In J. A. Wiens, G. Hayward, H. D. Safford, and C.M. Giffen, eds., Historical environmental variation in conservation and natural resource management, John Wiley and Sons, New York, NY.

Safford HD, Stevens JT. 2017. Natural Range of Variation (NRV) for yellow pine and mixed conifer forests in the Sierra Nevada, southern Cascades, and Modoc and Inyo National Forests, California, USA. General Technical Report PSW-GTR-256, USDA Forest Service, Pacific Southwest Research Station, Albany, CA.

Safford HD, Stevens JT, Merriam K, Meyer MD, Latimer AM. 2012. Fuel treatment effectiveness in California yellow pine and mixed conifer forests. Forest Ecology and Management 274: 17-28.

Safford HD, Van de Water K. 2014. Using fire return interval departure (FRID) analysis to map spatial and temporal changes in fire frequency on national forest lands in California. Research Paper PSW-RP-266, USDA Forest Service, Pacific Southwest Research Station, Albany, CA.

Safford HD, and Van de Water K. 2014. Using fire return interval departure (FRID) analysis to map spatial and temporal changes in fire frequency on national forest lands in California. Research Paper PSW-RP-266, USDA Forest Service, Pacific Southwest Research Station, Albany, CA.

Safford HD, Viers JH, Harrison SP. 2005. Serpentine endemism in the California flora: a database of serpentine affinity. Madroño 52: 222-257.

Sánchez Meador AJ, Moore MM, Bakker JD, Parysow PF. 2009. 108 years of change in spatial pattern following selective harvest of a Pinus ponderosa stand in northern Arizona, USA. Journal of Vegetation Science 20:79-90.

Sessions J, Johnson KN, Sapsis D, Bahro B, Gabriel JT. 1997. Methodology for simulating forest growth, fire effects, timber harvest, and watershed disturbance under different management regimes. Sierra Nevada Ecosystem Project, Final Report to Congress, Addendum, II:115-174.

Shive KL, Preisler HK, Welch KR, Safford HD, Butz RJ, O'Hara KL, and Stephens SL. 2018. From the stand scale to the landscape scale: predicting the spatial patterns of forest regeneration after disturbance. Ecological Applications 28:1626-1639.

Sierra Nevada Framework Project. 2001. Sierra Nevada Forest Plan Amendment: Final Environmental Impact Statement, USDS Forest Service, Pacific Southwest Region, January 2001, Chapter 3, figure 3.1a.

SNEP. 1996a. Fire and fuels. In Sierra Nevada Ecosystem Project: Final report to Congress, vol. I, Assessment Summaries and Management Strategies, DC Erman and SS Team, eds., Pp. 61-72. Davis, CA: University of California, Centers for Water and Wildland Resources.

SNEP. 1996b. Summary of the Sierra Nevada Ecosystem Project Report. In Sierra Nevada Ecosystem Project: Final report to Congress, vol. I, Assessment Summaries and Management Strategies, number 39. Davis, CA: [publisher unknown].

Sprugel DJ. 1991. Disturbance, Equilibrium, and Environmental Variability: What is 'Natural' Vegetation in a Changing Environment? Biological Conservation 58:1-18.

Stephens SL, Lydersen JM, Collins BM, Fry DL, Meyer MD. 2015. Historical and current landscape-scale ponderosa pine and mixed conifer forest structure in the Southern Sierra Nevada. Ecosphere, 6(May):1-63.

Storer TI, Usinger RL. 1963. Sierra Nevada natural history. Berkeley and Los Angeles, USA: University of California Press.

Swanson ME, Studevant NM, Campbell JL, Donato DC. 2014. Biological associates of early-seral pre-forest in the Pacific Northwest. Forest Ecol. Manage. http://dx.doi.org/10.1016/j.foreco.2014.03.046

Swetnam TW, Allen CD, Betancourt JL. 1999. Applied Historical Ecology : Using the Past to Manage for the Future. Ecological Applications, 9(4):1189-1206.

Taylor AH, Skinner CN. 2003. Spatial patterns and controls on historical fire regimes and forest structure in the Klamath Mountains. Ecological Applications, 13(3):704-719.

USDA Forest Service. 1990. Land and Resource Management Plan for the Tahoe National Forest EIS. Technical report, Forest Service, Pacific Southwest Region.

USDA Forest Service. 1999. Pendola Fire Restoration Project, Tahoe National Forest, Yuba County, CA. Federal Register, 64(244):71406-71407.

USDA Forest Service. 2004. Final Supplemental Environmental Impact Statement, Volume 1. Sierra Nevada Forest Plan Amendment, 1(R5-MB-046).

USDA Forest Service. 2012. Managing Sierra Nevada Forests. Technical report, U.S. Department of Agriculture, Forest Service, Pacific Southwest Research Station, Albany, CA. USDA.

USDA Forest Service. 2014. More About the Forest. Tahoe National Forest. https://www.fs.usda.gov/detail/tahoe/about-forest/?cid=STELPRDB5194539.

Van de Water KM, Safford HD. 2011. A Summary of Fire Frequency Estimates for California Vegetation. Fire Ecology, 7(3):26-58.

Van Wagtendonk JW, Fites-Kaufmann JA. 2006. Sierra Nevada Bioregion. In Fire in California's Ecosystems, NG Sugihara, JW Van Wagtendonk, KE Shaffer, JA Fites-Kaufmann, and AE Thode, eds., Pp. 264-294. Berkeley, CA: University of California Press.

Zhang Z, Mann ME, Cook ER. 2004. Alternative methods of proxy-based climate field reconstruction: application to summer drought over the conterminous United States back to AD 1700 from tree-ring data. The Holocene 14: 502-516.

GLOSSARY of TERMS and ACRONYMS

Biophysical Class (BPC) - Categorical classification of predicted cumulative tree biomass under historical dynamic equilibrium conditions based on biophysical site variables; classified into four equal-area classes from low to high site productivity; created for the purpose of summarizing and reporting the historical range of variability and current departure in a suite of landscape metrics. [geospatial data layer]

Biophysical Unit (BPU) - Polygons (units) delineated on the basis of the Biophysical Class layer (see above). BPUs are the spatial units derived by aggregating raster cells of the same BPC into clusters and vectorizing so as to produce a polygon shapefile; created for the purpose of displaying results given by BPC. [geospatial data layer]

Cell-level - Spatial extent of an individual cell; 5 m on a side for this application.

CRV - Current range of variability.

Developmental stage - Successional stage of vegetation development based on modeled canopy height at the cell level; classified into six classes for forest and three classes for shrublands; ecological attribute for which a suite of landscape metrics are computed. [geospatial data layer]

EcObjects - Vegetation dataset derived from segmentation of Lidar-derived tree approximate objects and a 1-m canopy height model; source of cover type assigned to each cell. [geospatial data layer]

Geophysical Unit (GPU) - Spatial Unit of varying spatial extent delineated based on relative similarity in a suite of 10 geophysical attributes; level of HRV departure analysis.

EVeg - California vegetation dataset derived primarily from Landsat imagery at the 30 m spatial resolution; source of cover type assigned to each cell in the landscape buffer (i.e., cells without EcObjects coverage surrounding the core area of interest). [geospatial data layer]

FMR - Fire mortality rate; the probability that a burning cell will exhibit a high-mortality effect (i.e., complete canopy mortality), implemented at the cell level within individual fire events but summarized (e.g., averaged) for the landscape, cover type or some other designated subdivision of the landscape for some designated period of time.

FRI - Fire return interval; the average number of years between fires at a specific location (i.e. point-specific), or summarized (e.g., averaged) for the landscape, cover type or some other designated subdivision of the landscape for some designated period of time.

FRP - Fire rotation period; the number of years to cumulatively burn an area equal in size to the landscape, cover type or some other designated subdivision of the landscape for some designated period of time; aspatial measure of the point-specific mean fire return interval.

Forest regeneration - Probability of tree establishment after high-mortality disturbance; determines how quickly cells re-establish tree cover after canopy-replacing disturbance and thus how long cells remain in the Open developmental stage without tree cover; component of forest succession in the landscape disturbance and succession model.

HRV - Historical range of variability.

Landscape-level - Spatial extent of a designated landscape containing a spatially heterogeneous mosaic of one or more attributes of interest, such as a Subbasin; level at which many landscape metrics quantifying historical range of variability and current departure are computed.

Large forest opening - Contiguous forested cells in the Open developmental stage (i.e., no established trees to breast height) encompassing a minimum of 0.04 ha (0.1 acres) and 5 m minimum width; ecological feature for which a suite of landscape metrics are computed; not to be confused with how large forest openings have been defined in other applications (e.g., Jeronimo et al. 2019).

LDSM - Landscape disturbance-succession mode; class of stochastic simulation model used in this application.

LDSim - Landscape disturbance-succession simulator; LDSM developed for this project.

Patch - Spatial extent of an aggregation of cells of the same class based on some attribute (e.g., developmental stage), in which the adjacency can be based either on a 4-neighbor (i.e., orthogonal neighbor) rule such that only like-classed cells sharing a full side are considered part of the same patch, or on an 8-neighbor rule such that like-classed cells touching either on a side or on the diagonal are considered part of the same patch.

Persistence/ Vegetative Persistence - Likelihood of persisting in either an early- or late-seral condition, proxied by the observed mean fire return interval of high-mortality wildfires at the cell level. [geospatial data layer]

Site-level - Spatial extent of a 40-m radius neighborhood around each focal cell; level at which many landscape metrics quantifying historical range of variability and current departure are computed.

Spatial extent - Area of land encompassed at different levels of organization in modeled output (e.g., Cell, Patch, Site, Biophysical Unit, Geophysical Unit, Stewardship Unit, Subbasin, Landscape).

Spatial grain - Area of finest spatial resolution in modeled output; equivalent to a single 5 m cell in this application.

Stewardship Unit (STU) - Unit of varying spatial extent delineated either due to relatively homogeneous ecological attributes or for management purposes based on logistical considerations such as operability and ownership.

Succession - Establishment, gradual growth and/or development, and eventual senescence of vegetation over time; key dynamic, multi-step, and stochastic process in the landscape disturbance and succession model.

Temporal extent - Duration of time over which landscape dynamics are observed; set to the ~ 300-year historical reference period, circa 1550 - 1850.

Temporal grain - Finest temporal resolution (i.e., single timestep) in the landscape disturbance and succession model; set to 5 years in this application.

TNF - Tahoe National Forest.

Vegetation state - Discrete states of vegetation composition and structure that a single cell could exist in during the simulation. [geospatial data layer]

APPENDICES

The appendices to this GTR are organized as follows:

- Appendix A - Geospatial data layers
- Appendix B - Yuba River landscape
- Appendix C - Truckee River landscape
- Appendix D - Lake Tahoe Basin landscape
- Appendix E - Bear River landscape
- Appendix F - American River North landscape
- Appendix G - American River South landscape

Appendix A provides a detailed description of the geospatial data layers we developed for the region or, in some cases just the focal landscape, to support the Historical Range of Variability and current departure Assessment, and is illustrated with maps for the Yuba River landscape. Appendices B - G include detailed results for each of the focal landscapes assessed within the Northern Sierra ecoregion, including those within the TCSI area of interest. Each of these appendices depends on the background and methods presented in this GTR and is thus tiered to this parent document. However, each of these appendices is published as a separate document for organizational purposes. In addition, each of these appendices is accompanied by a suite of datasets, including geospatial data layers associated with the spatial inputs to LDSim and the HRV and current departure results.

These appendices, including all associated datasets, as well as any additional future appendices associated with this GTR (e.g., other focal landscapes within the Northern Sierra ecoregion) can be found at the following site:

https://drive.google.com/drive/folders/13RNruEJ5pdfy1h5GGXovvxtMGRVVBT7-?usp=sharing

APPENDIX A

This appendix provides a detailed description of the geospatial data layers we developed for the region or, in some cases just the focal landscape, to support the Historical Range of Variability and current departure Assessment. Here we illustrate each layer for the Yuba River landscape as an example. All final layers are represented as 5-meter rasters (in a geotiff data format) with the following spatial reference system:

- *Projected Coordinate System: California Albers (EPSG=3310)*
  - false_easting: 0.0
  - false_northing: -4000000.0
  - central_meridian: -120.0
  - standard_parallel_1: 34.0
  - standard_parallel_2: 40.5
  - latitude_of_origin: 0.0
  - Linear Unit: Meter
- *Geographic Coordinate System: GCS_GRS 1980(IUGG, 1980)*
  - Datum: NAD83
  - Prime Meridian: Greenwich
  - Angular Unit: Degree

Age

The Age layer represented vegetation age (years) and was a primary geospatial layer input to LDSim (**Figure A.1**). Age was treated as a dynamic variable in the model, meaning that it potentially changed with each timestep. For non-seral cover types, Age was treated as constant and given a null value (9998). For shrubland cover types, Age represented the number of years since the last high-mortality disturbance. For forested cover types, Age represented the number of years since establishment of trees to breast height (i.e., breast height age) and was an important input to the vegetation succession model, affecting the probability of tree establishment following a high-mortality disturbance and vegetation growth following establishment. Age was also an important input to the wildfire disturbance model, affecting susceptibility to wildfire and severity via coarse fuel loads and tree resistance to wildfire intensity.

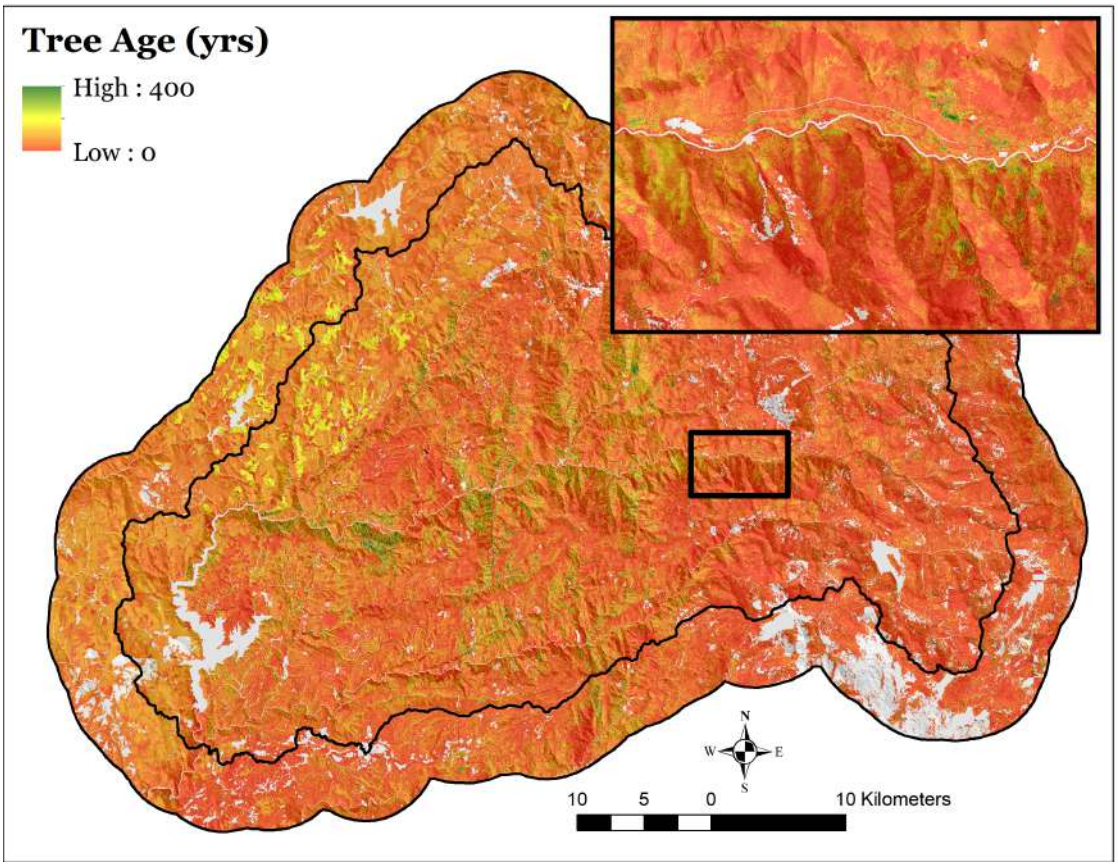

Figure A.1: Map of the Age layer (breast height age; units = years) for the Yuba River landscape (displayed with hillshading).

The initial Age layer was developed from two primary sources:

1. Lidar: Lidar canopy height 1 m raster data was obtained from the Tahoe National Forest with a nominal date of June 2014. We used the Lidar data exclusively within the focal landscape core and where it existed in the buffer for cells classified as forest. Specifically, we resampled the 1 m height data to 5 m (based on the "near" resampling algorithm that assigns to each 5m cell the value of the nearest underlying 1 m cell) and truncated the maximum height to 230 ft.

   Shrublands: The shrubland cover types included: Shrubland, Big Sagebrush, Black and Low Sagebrush, Curl-leaf Mountain Mahogany and Chaparral, although only Big Sagebrush and Chaparral occurred in the Yuba River landscape. Canopy height for shrublands was classified into Age as follows:

- Height < 1.5 ft -> Age = 0
- Height 1.5 - 6 ft -> Age = 50
- Height > 6 ft -> Age = 100

Non-mafic forest: The non-mafic forest cover types included: Forest, Oak Woodland, Yellow Pine, Yellow Pine_Aspen, Oak-Conifer Forest and Woodland, Oak-Conifer Forest and Woodland_Aspen, Mixed Evergreen, Mixed Evergreen_Aspen, Sierra Mixed Conifer, Sierra Mixed Conifer_Aspen, Lodgepole Pine,Lodgepole Pine_Aspen, Subalpine Conifer, and Subalpine Conifer_Aspen. Next, we used canopy height and our custom Site Index variable (see below) to predict total tree Age based on growth equations that we developed using FIA data (see main text for details). Briefly, we subtracted 7 years from total tree age to estimate breast height age on non-mafic sites and 10 years on ultramafic sites to account for lower site productivity (Dunning and Reineke 1933, Dunning 1942), which served as Age in our model. We recognized that many other local factors such as tree species and tree spacing affect real-world tree height growth, and thus using Canopy Height and Site Index provided only a crude approximation of true tree age, but we deemed this sufficient for the purposes of this modeling exercise. We fit a Monomolecular function to the FIA plot tree data, but substituted our custom Site Index variable for the conventional site index. The final growth equation to predict Height from total Age and Site Index was given in the main text and depicted in **Figure 27**. To predict breast height Age from Height and Site Index, we simply transformed the growth equation as follows:

$$A_{it} = \frac{log(1 - \frac{H_{it}}{b_0 + b_2 S_i})}{-b_1} - 7$$

where: b_0 - b_2 were estimated parameters; H_{it} = Height of the i^{th} cell in the t^{th} timestep; S_i = Site Index of the i^{th} cell; and A_{it} = breast height Age of the i^{th} cell in the t^{th} timestep. Note the subtraction of 7 years to adjust from total tree age to breast height Age. In addition, we set the maximum predicted Age to 400 years.

Ultramafic forest: The ultramafic forest cover types included: Yellow Pine_Ultramafic, Oak-Conifer Forest and Woodland_Ultramafic, Mixed Evergreen_Ultramafic, Sierra Mixed Conifer_Ultramafic, Lodgepole Pine_Ultramafic, Red Fir_Ultramafic, and Subalpine Conifer_Ultramafic. The final growth equation for ultramafic forest was based on the non-mafic forest growth equation above but with height reduced by 15 % for any given total Age and Site Index (based on an analysis of FIA data). To predict breast height Age from Height, we simply transformed the growth equation as follows:

$$A_{it} = \frac{log(1 - \frac{H_{it}}{0.85(b_0 + b_2 S_i)})}{-b_1} - 10$$

Note the subtraction of 10 years to adjust from total tree age to breast height Age. Again, we set the maximum predicted Age to 400 years.

All other cover types: All other cover types included: Urban, Powerline, Agriculture, Water, Wetland, Desert Riparian, Foothill Riparian, Montane Riparian, Barren, Herbaceous, Grassland, and Meadow. We assigned No Age (= 9998) to cells in these cover types within the extent of the Lidar data, reflecting the fact that we chose to treat these cover types as static in LDSim.

2. Eveg: The California Eveg (Existing Vegetation) data was obtained from the USDA Forest Service FSGeodata Clearinghouse (https://data.fs.usda.gov/geodata/edw/datasets.php) with a nominal date of March 22 - Jan 18, 2018 (depending on the CalVeg Zone). We used the Eveg data to derive Age only for cells in the landscape buffer for which Lidar data were not available.

   Shrublands: We assigned Age to shrubland cells based on the Shrub Cover-From-Above attribute (SHRUB_CFA), as follows:

   - SHRUB_CFA = '05' -> Age 5
   - SHRUB_CFA = '15' -> Age 20
   - SHRUB_CFA = '25' -> Age 30
   - SHRUB_CFA = '35' -> Age 40

- SHRUB_CFA = ‘45’ -> Age 50
- SHRUB_CFA = ‘55’ -> Age 60
- SHRUB_CFA = ‘65’ -> Age 80
- SHRUB_CFA = ‘75’ -> Age 100
- SHRUB_CFA = ‘85’ -> Age 125
- SHRUB_CFA = ‘95’ -> Age 150

We recognized that the relationship between Age and Shrub Cover-From-Above was imperfect, but we deemed this sufficient for the purposes of this modeling exercise, especially given our emphasis on forested communities.

Forests: We assigned Age to all forest cells, including both non-mafic and ultramafic types, based on the TREE_DBH attribute, as follows:

- TREE_DBH = ‘00’ -> Age 0
- TREE_DBH = ‘02’ -> Age 15
- TREE_DBH = ‘07’ -> Age 30
- TREE_DBH = ‘15’ -> Age 60
- TREE_DBH = ‘25’ -> Age 100
- TREE_DBH = ‘40’ -> Age 200

Again, we recognized that the relationship between Age and Tree DBH was imperfect, but we deemed this sufficient for the purposes of this modeling exercise, especially given that we applied this heuristic only to the landscape buffer where Lidar data were not available.

All other cover types: We assigned No Age (= 9998) to cells in all other cover types as noted previously.

Aspect

The Aspect layer represented slope aspect class (**Figure A.2**). Aspect was treated as a static variable in the model, meaning that it remained constant throughout the simulation. Aspect served as an input to other layers as well as a direct input to LDSim. Specifically, Aspect was used in the derivation of the Heat Load Index, which was used as an input to the Mesic and Energy Index layers and the composite Site Index layer (see below), which were used in the vegetation succession model to affect vegetation establishment and growth following a high-mortality disturbance. Aspect and the Heat Load Index were also used directly in the wildfire disturbance model to affect the risk of wildfire.

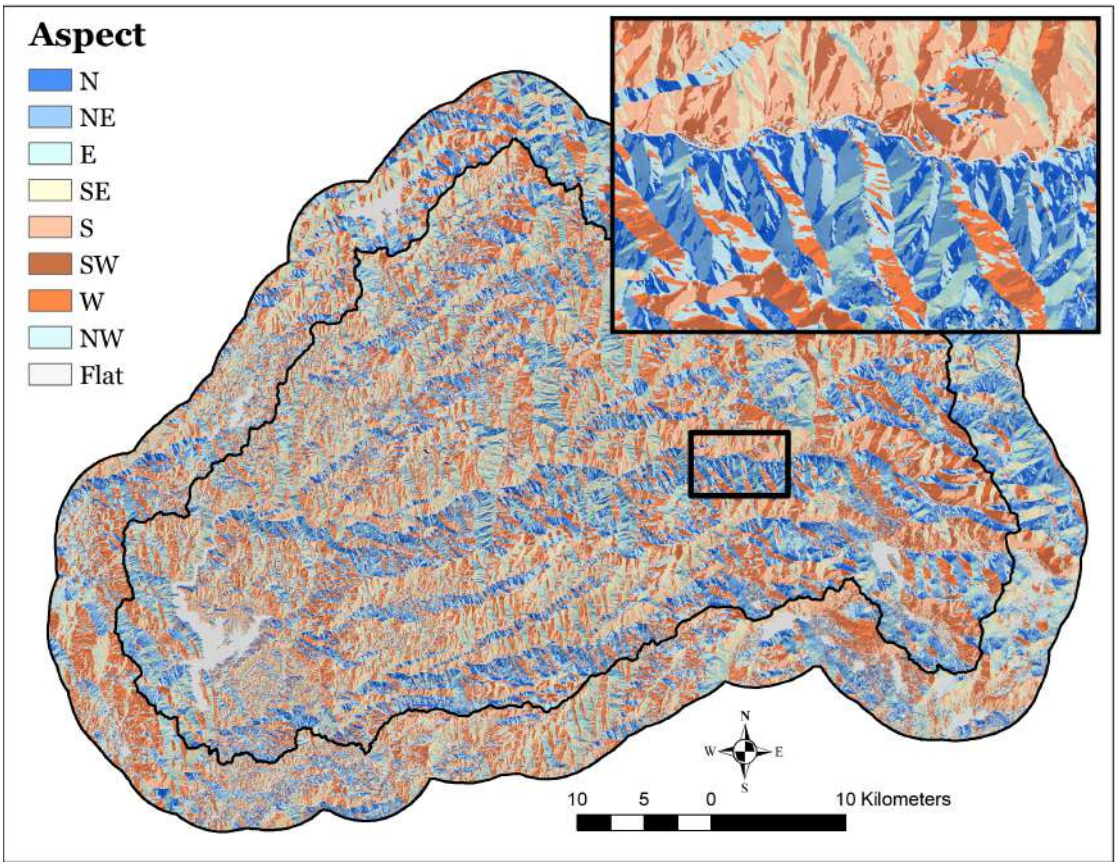

Figure A.2: Map of the classified Aspect layer for the Yuba River landscape (displayed with hillshading).

The initial Aspect layer (degrees) was derived from the Elevation raster (see below) using the terrain() function in the R Terra package. We subsequently classified the resulting layer into nine bins (eight 45 degree bins plus flat), as follows:

- 1: 337.5 - 22.4 degrees -> North (N)
- 2: 22.5 - 67.4 degrees -> Northeast (NE)
- 3: 67.5 - 112.4 degrees -> East (E)
- 4: 112.5 - 157.4 degrees -> Southeast (SE)
- 5: 157.5 - 202.4 degrees -> South (S)
- 6: 202.5 - 247.4 degrees -> Southwest (SW)
- 7: 247.5 - 282.4 degrees -> West (W)
- 8: 282.5 - 337.4 degrees -> Northwest (NW)
- 9: flat

We smoothed the classified raster based on the mode within a 25x25 m (5x5 cell) window using the focal() function in the Terra package, resolving ties to the lowest class and ensuring that flat areas, water and wetlands retained a class of 9.

Lastly, we also created a linear transformation of Aspect using a cosine transformation oriented along a NE - SW axis such that 0 was due SW and 100 was due NE. This linear aspect was used in the derivation of the Tau Index layer (described elsewhere).

Available Water Storage

The Available Water Storage (AWS) layer represented the potential soil water storage (ml) to a depth of 150 cm (**Figure A.3**). AWS was treated as a static variable, meaning that it remained constant throughout the simulation. AWS served as an input to the derivation of other layers and not as a direct input to LDSim. Specifically, AWS was an input to the Mesic Index layer, which was used in the vegetation succession model to affect vegetation establishment and growth following a high-mortality disturbance, as described in detail in the main text.

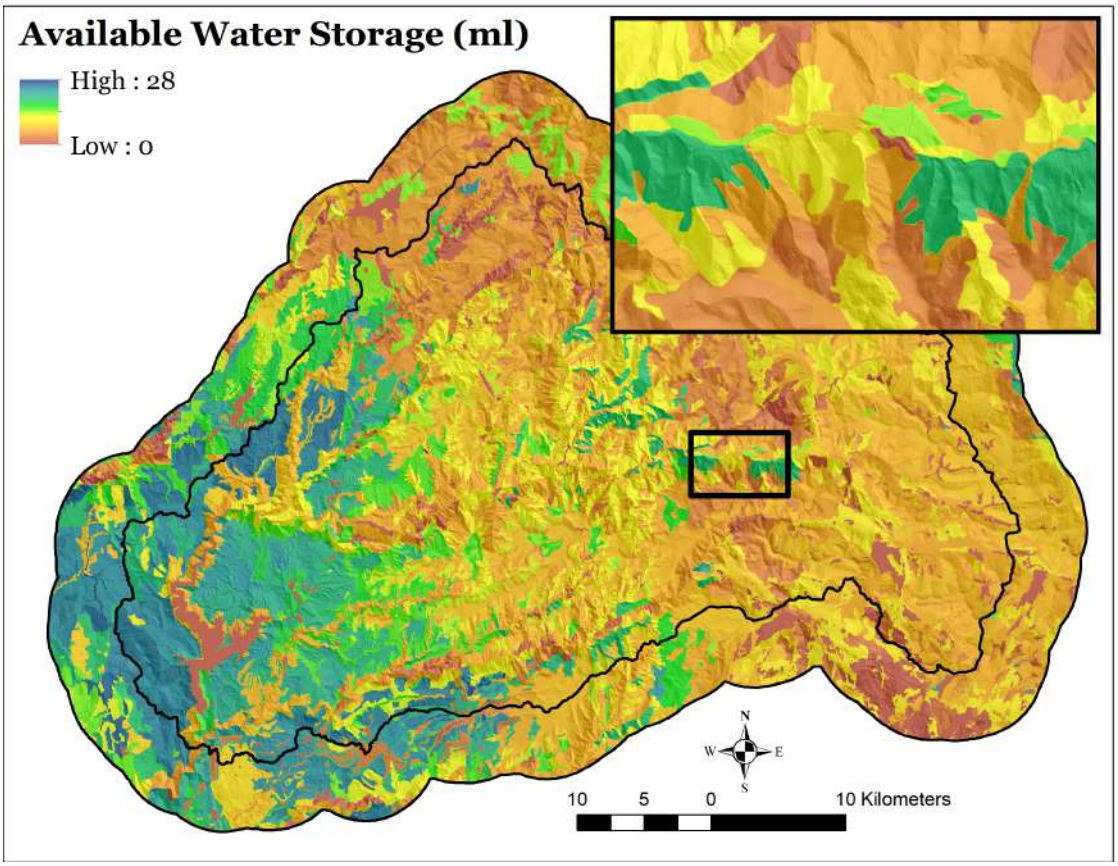

Figure A.3: Map of the Available Water Storage (AWS) to 150 cm layer (units = ml) for the Yuba River landscape (displayed with hillshading).

The AWS layer was derived from USGS NRCS gSSURGO soil data, downloaded from the NRCS Geospatial data gateway (https://gdg.sc.egov.usda.gov/), with a nominal date of January 18, 2019. We used ArcMap to extract the MasterunitRaster_10m layer from the gSSURGO geodatabase, clipped to our landscape extent, then joined the aws0150 attribute, and then exported the raster. Lastly, we processed the final raster in R to reproject and resample to our landscape 5 m reference raster.

Biophysical Classes

The Biophysical Class (BPC) layer represented biophysical setting classes derived for the purpose of summarizing and describing (i.e., packaging) the HRV results (**Figure A.4**).

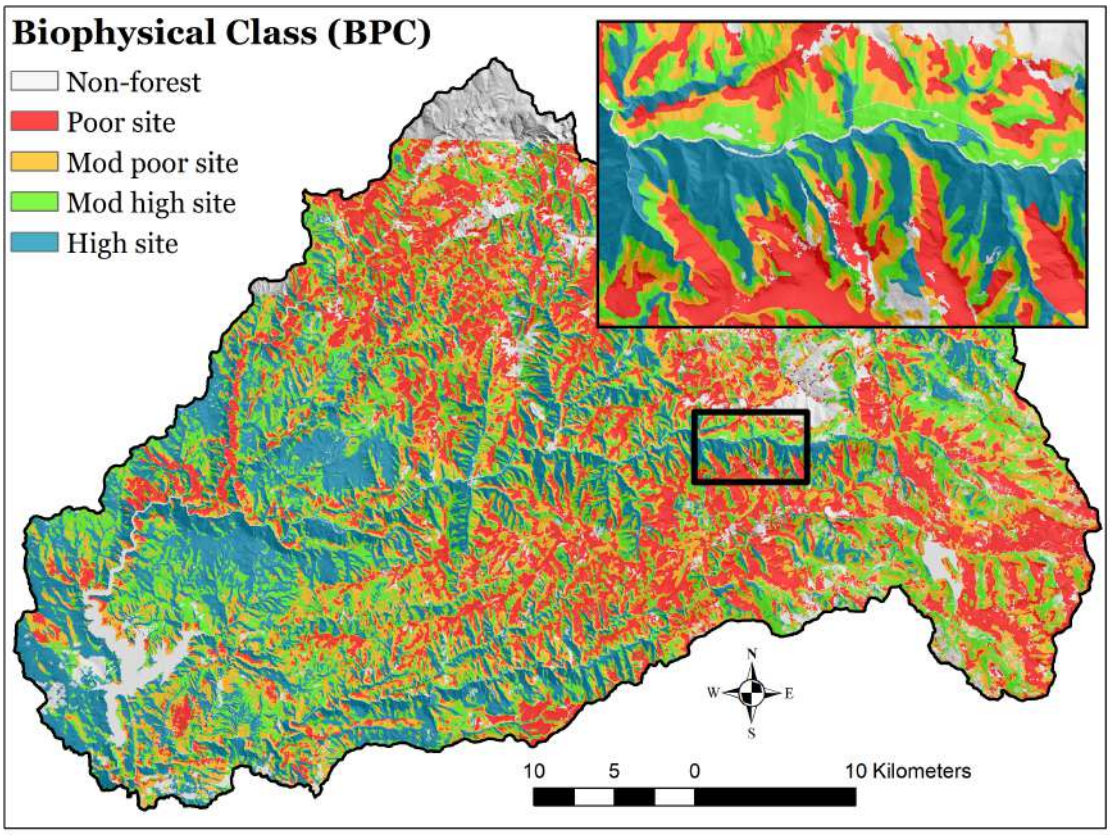

Figure A.4: Map of the Biophysical Classes (BPCs) for the Yuba River landscape (displayed with hillshading).

The BPC layer was created after the simulation was complete as described in detail in the main text and briefly as follows:

- First, we derived a proxy for cumulative tree biomass production under dynamic equilibrium conditions (i.e., HRV) at the cell level for all forested cells by summing tree Height (ft) values every 20 years between simulation years 500 - 1,500.
- Next, to reduce the "noise" in the data owing to pixelation, we applied a 25x25 m focal mean smoothing of the cumulative tree biomass layer. Thus, each 5 m cell value was replaced with the mean of the cell values within a 5x5 cell window centered on the focal cell.
- Next, we randomly sampled one million cells and extracted the values of Biomass and the following 10 biophysical variables:
  - Precipitation
  - Water balance deficit
  - Available soil water
  - Topographic wetness index
  - Heat load index

  - Growing degree days
  - Topographic position index
  - Solar radiation index
  - Slope
  - Elevation

- Next, we used a Random Forest analytical framework (Breiman 2001) to predict Biomass from the biophysical site variables. Random Forest is a non-parametric machine learning technique that allows for non-linear and heterogeneous responses (e.g., biomass may respond differently to precipitation as elevation increases) and thus can account for complex interactions among the predictors.

- Lastly, we classified predicted Biomass into 4 equal-area classes based on quartiles of the data, plus a zero class for all non-forest cells. The final BPC layer included 4 classes ranging from the least productive to most productive sites; i.e., supporting on average low to high cumulative tree Biomass under historical dynamic equilibrium conditions (as simulated), plus an "unknown" class representing non-forest areas (as mapped), with each class encompassing ~ 20 % of the landscape.

- Postscript, although we used the final BPC layer described above to summarize and describe the range of variation in landscape metrics, we also derived another BPC layer for management purposes by simplifying the BPC raster into more practical Biophysical Units (BPUs), represented as polygons, as follows:

  - Removed water bodies (Lakes and streams)
  - Dissolved all BPC patches < 10 acres into neighboring patches (i.e., minimum mapping unit = 10 acres)
  - Simplified BPC patches further by dissolving narrow "arms" or appendages < 22.86 m (75 ft) wide into neighboring patches.
  - Deleted all "island" patches < 5 acres, which left a handful of meaningful patches between 5 and 10 acres.
  - Converted the final raster layer to a vector (i.e., polygon) shapefile.

Buffer

The Buffer layer represented the categorical distinction between the landscape "core" and "buffer" and was a primary geospatial layer input to LDSim (**Figure A.5**). The Buffer layer was treated as a static layer, meaning that it remained constant throughout the simulation. The Buffer layer served to distinguish the simulation landscape (core plus buffer) from the target landscape (core). The purpose of the buffer was to minimize boundary effects by allowing contagious disturbance events (i.e., wildfires) to spread onto and off of the target landscape (i.e., the core).

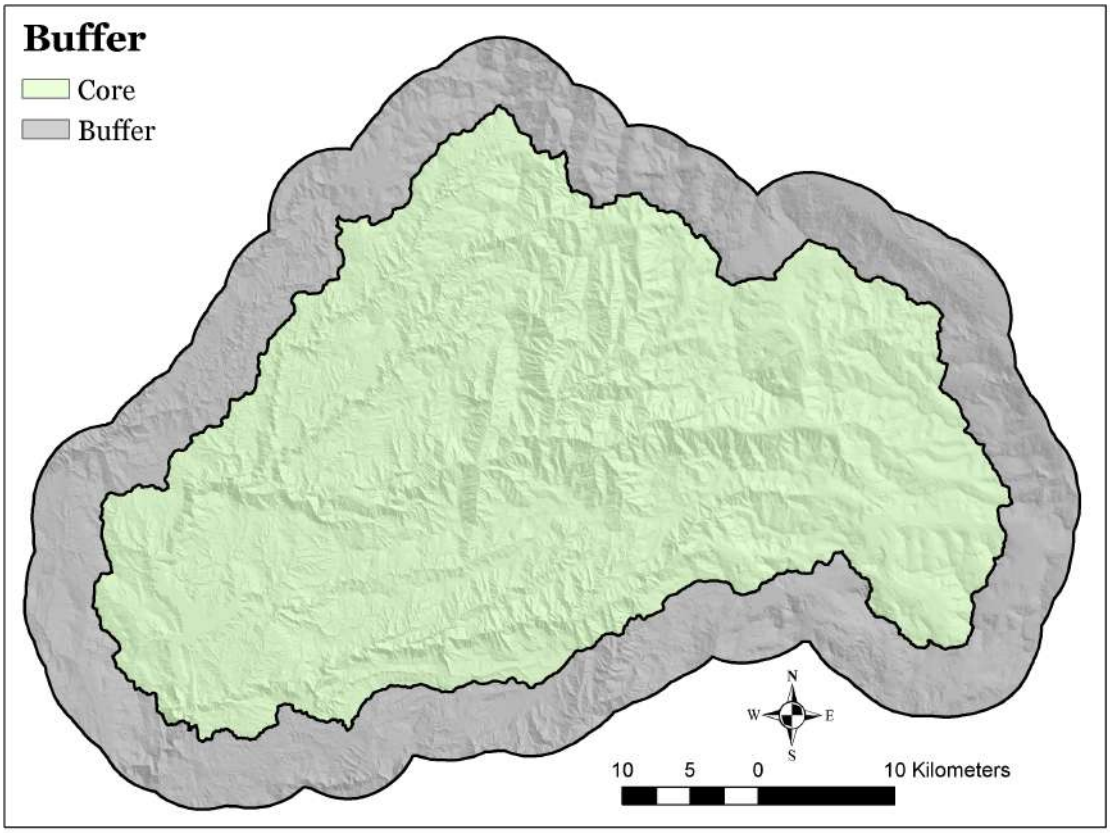

Figure A.5: Map of the Core and Buffer zones for the Yuba River landscape (displayed with hillshading). The Core represents the target landscape and the extent for which all historical range of variability statistics were computed. The Buffer represents a 5 km buffer around the Core and was included in the simulated landscape to minimize boundary effects on the computed statistics.

For this application, the core was determined by the extent of the Lidar-based EcObjects data within the Yuba River watershed and the buffer was derived by creating a 5 km buffer around the core. The final simulation landscape was the core plus the buffer, although all simulation results were computed and reported for the core only.

The Buffer layer was classified as follows:

- 1: core
- 2: buffer

Cover

The Cover layer represented the cover type (categorical) and was a primary geospatial layer input to LDSim (**Figure A.6**). Cover was treated as a static variable, meaning that it remained constant throughout the simulation. Cover served as a primary organizational layer in the model, affecting most aspects of succession and disturbance. Cover type was interpreted to be a relatively stable biophysical setting that supports a characteristic vegetation community under a natural disturbance regime. Hence, Cover was treated as a categorical variable with a relatively discrete set of cover types that were assumed to be relatively stable over time, at least under the historical reference period.

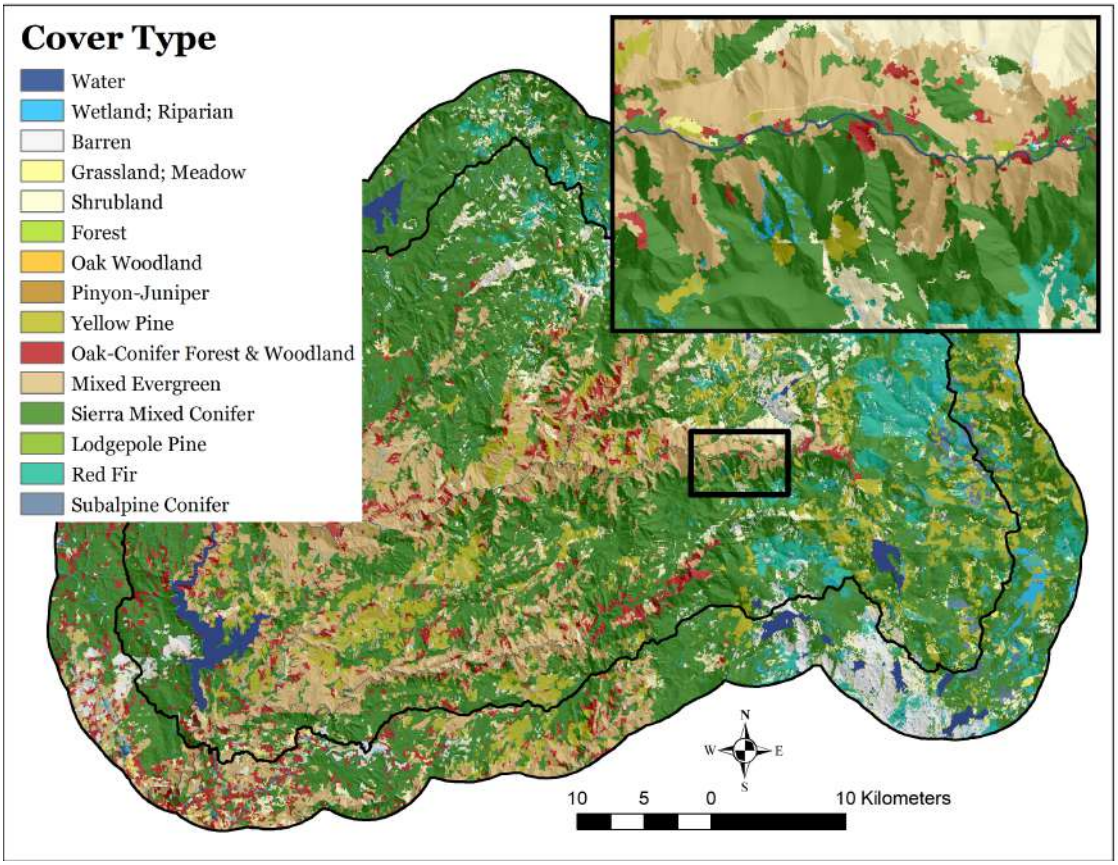

Figure A.6: Map of the Cover layer for the Yuba River landscape (displayed with hillshading). Note, some of the cover types have been aggregated to facilitate the display and shorten the legend

We developed a system of land cover classification building on the work of McGarigal et al. (2018), which was based on LandFire (2007) biophysical settings and the presettlement fire regimes of Van de Water and Safford (2011), cross-walked to the Forest Service corporate spatial data based on the Northern Sierra CALVEG classification using the Forest Service Region 5 existing vegetation layer (EVeg). We also considered information from the updated A Guide to Wildlife Habitats of California (Mayer and Laudenslayer 1988), popularly known as the "Wildlife Habitat Relationship" cover types. Our classification included 41 cover types, although many of these were variants of the major types based on the inclusion of Aspen in the stands or the occurrence on ultramafic soils. The full classification included both potential natural vegetation types (i.e., the expected vegetation community in the presence of natural disturbance regimes, such as Sierran Mixed Conifer) and current anthropogenic cover types (Urban, Powerline, and Agriculture). However, the anthropogenic cover types were omitted from the historical cover layer (Hcover) that we used in the HRV simulation, as discussed below, and retained in the existing cover layer (Ecover) that we used solely for post-processing the current departure results.

The full cover type classification was as follows:

ID	Cover type	Abbreviation
1	Urban	URB
2	Powerline	POW
3	Agriculture	AGR
10	Water	WAT
11	Wetland	WET
12	Desert Riparian	DRIP
13	Foothill Riparian	FRIP
14	Montane Riparian	MRIP
20	Barren	BAR
30	Herbaceous	HERB
31	Grassland	GRASS
32	Meadow	MED
40	Shrubland	SHRUB
41	Big Sagebrush	SAGE
42	Black and Low Sagebrush	LSG
43	Curl-leaf Mountain Mahogany	CMM
44	Chaparral	MCP
50	Forest	FOREST
51	Oak Woodland	OAK
52	Pinyon-Juniper	PJ
53	Yellow Pine	YPN
54	Yellow Pine_Aspen	YPN_A
55	Yellow Pine_Ultramafic	YPN_U
56	Oak-Conifer Forest and Woodland	OCFW
57	Oak-Conifer Forest and Woodland_Aspen	OCFW_A
58	Oak-Conifer Forest and Woodland_Ultramafic	OCFW_U
59	Mixed Evergreen	MEG
60	Mixed Evergreen_Aspen	MEG_A
61	Mixed Evergreen_Ultramafic	MEG_U
62	Sierra Mixed Conifer	SMC
63	Sierra Mixed Conifer_Aspen	SMC_A
64	Sierra Mixed Conifer_Ultramafic	SMC_U
65	Lodgepole Pine	LPN
66	Lodgepole Pine_Aspen	LPN_A
67	Lodgepole Pine_Ultramafic	LPN_U
68	Red Fir	RFR
69	Red Fir_Aspen	RFR_A
70	Red Fir_Ultramafic	RFR_U
71	Subalpine Conifer	SCN
72	Subalpine Conifer_Aspen	SCN_A
73	Subalpine Conifer_Ultramafic	SCN_U

The historical and existing cover layers were developed from the following primary sources:

1. EcObjects: The EcObjects vector data was obtained from the Tahoe National Forest with a nominal date of June 2014. We used this data exclusively where it existed. With the modifications noted

below, a set of heuristic rules (S.Conway) were applied to assign one of the cover types to each Ecobject polygon.

2. Eveg: The California Eveg (Existing Vegetation) vector data was obtained from the USDA Forest Service FSGeodata Clearinghouse (https://data.fs.usda.gov/geodata/edw/datasets.php) with a nominal date of March 22 - Jan 18, 2018 (depending on the CalVeg Zone). We used this data only where EcObjects data were not available.

3. Industrial timberland: Vector data obtained from S. Conway depicting industrial forest ownership polygons. We used the industrial timberland data to reclassify areas classified as existing grassland or shrubland to a forest cover type based on a nearest neighbor rule, under the assumption that although the existing vegetation is in a grassland or shrubland state that it is highly likely to be seral to forest on industrial timberlands, at least in the vast majority of cases.

4. Potential natural vegetation: Vector data obtained from a variety of sources, including an historical vegetation layer obtained from the TNF and a terrestrial ecosystem unit layer obtained from B. Estes for the Lake Tahoe Basin. We used the potential natural vegetation (PNV) data from these sources to reclassify areas classified as existing grassland or shrubland to a forest cover type based on a nearest neighbor rule, under the assumption that although the existing vegetation is in a grassland or shrubland state that it is highly likely to be seral to forest on areas mapped as PNV forest, at least in the vast majority of cases.

5. Ultramafic soils: Vector data obtained from the California Geological Survey (https://pubs.usgs.gov/of/2005/1305/#CA) depicting near-surface lithology. We used this data to identify areas with ultramafic soils (ORIG_LABEL == 'um'), as described below.

6. Buildings: Vector data obtained from Microsoft (https://github.com/microsoft/USBuildingFootprints) depicting the outline of all identified building structures. We used this data to supplement the Eveg data to derive the Urban cover class in the existing cover layer, as described below.

To derive the historical cover layer (Hcover) for use in the landscape simulation, we processed the source data as follows:

- First, we reclassified the Eveg layer to our cover types, based on the Eveg CWHR_TYPE attribute, as follows:

CWHR type	**Abbreviation**	**Cover type**
Urban	URB	Urban
Pasture	PAS	Agriculture
Cropland	CRP	Agriculture
Dryland Grain Crops	DGR	Agriculture
Deciduous Orchard	DOR	Agriculture
Evergreen Orchard	EOR	Agriculture
Irrigated Grain Crops	IGR	Agriculture
Irrigated Row and Field Crops	IRF	Agriculture
Irrigated Hayfield	IRH	Agriculture
Orchard - Vineyard	OVN	Agriculture
Rice	RIC	Agriculture
Vineyard	VIN	Agriculture
Estuarine	EST	Water
Lacustrine	LAC	Water
Marine	MAR	Water

(continued)

CWHR type	Abbreviation	Cover type
Riverine	RIV	Water
Fresh Emergent Wetland	FEW	Wetland
Saline Emergent Wetland	SEW	Wetland
Desert Riparian	DRI	Desert Riparian
Valley Foothill Riparian	VRI	Foothill Riparian
Montane Riparian	MRI	Montane Riparian
Barren	BAR	Barren
Annual Grass	AGS	Grassland
Perennial Grass	PGS	Grassland
Wet Meadow	WTM	Meadow
Alpine Dwarf-Shrub	ADS	Shrubland
Alkali Desert Scrub	ASC	Shrubland
Bitterbrush	BBR	Shrubland
Chamise-Redshank Chaparral	CRC	Shrubland
Coastal Scrub	CSC	Shrubland
Desert Scrub	DSC	Shrubland
Desert Succulent Shrub	DSS	Shrubland
Desert Wash	DSW	Shrubland
Sagebrush	SGB	Big Sagebrush
Low Sage	LSG	Curl-leaf Mountain Mahogany
Mixed Chaparral	MCH	Chaparral
Montane Chaparral	MCP	Chaparral
Closed-Cone Pine-Cypress	CPC	Forest
Eucalyptus	EUC	Forest
Joshua Tree	JST	Forest
Palm Oasis	POS	Forest
Redwood	RDW	Forest
Blue Oak Woodland	BOW	Oak Woodland
Coastal Oak Woodland	COW	Oak Woodland
Valley Oak Woodland	VOW	Oak Woodland
Juniper	JUN	Pinyon-Juniper
Pinyon-Juniper	PJN	Pinyon-Juniper
Eastside Pine	EPN	Yellow Pine
Jeffrey Pine	JPN	Yellow Pine
Ponderosa Pine	PPN	Yellow Pine
Blue Oak-Foothill Pine	BOP	Oak-Conifer Forest and Woodland
Montane Hardwood-Conifer	MHC	Oak-Conifer Forest and Woodland
Douglas Fir	DFR	Mixed Evergreen
Montane Hardwood	MHW	Mixed Evergreen
Klamath Mixed Conifer	KMC	Sierra Mixed Conifer
Sierran Mixed Conifer	SMC	Sierra Mixed Conifer
White fir	WFR	Sierra Mixed Conifer
Lodgepole Pine	LPN	Lodgepole Pine
Red fir	RFR	Red Fir
Subalpine Conifer	SCN	Subalpine Conifer
Aspen	ASP	Aspen

- Second, we combined the EcObjects and Eveg layers, giving precedence to the EcObjects layer so that Eveg was used only where EcObjects was missing, and rasterized the layer to align with the focal landscape reference raster.
- Third, we replaced cells classified as developed (Urban, Powerline and Agriculture) with the nearest neighboring cover type (except Water) to reflect the likely pre-settlement cover type.
- Fourth, we replaced cells classified as Aspen with the nearest neighboring forest type, under the assumption that all cells classified as existing Aspen are likely to be seral to one of the conifer forest types (i.e., there is no "stable" Aspen), resulting in one of several different mixed conifer-aspen types.
- Fifth, we replaced cells classified as grassland or shrubland on either industrial timberland or cells classified as having forest PNV with the nearest neighboring forest type. Note, many of the areas classified as grassland or shrubland in their existing vegetation state were previously forested and are currently in a grassland or shrubland state because of past wildfires and anthropogenic disturbances (e.g., timber harvest, mining), although some of these areas are likely sites that support persistent grasslands or shrublands with few to no trees. We sought to distinguish the former from the latter. We made the assumption that all cells classified as existing grassland or shrubland located on industrial timberland or PNV forest are likely to be seral to one of the forest types, at least in the vast majority of cases.
- Sixth, we reclassified cells classified as forest on ultramafic soils (based on the CA lithology layer) to the corresponding ultramafic forest cover type.
- Seventh, we smoothed patches of barren, grassland, shrubland and forest with a 3x3 focal majority; i.e., replacing the focal cell with the majority class within the 3x3 cell neighborhood, given precedence to the least vegetated class in the case of ties.
- Eighth, we dissolved small patches of barren, grass, shrub and forest < 160 cells (0.4 ha, 1 acre), replacing cells with the nearest neighbor. Thus, the minimum resulting patch size for all cover types except Water, Wetland and Riparian was 1 acre.
- Ninth, we overlaid medium and large streams and modeled potential beaver wetlands and reclassified these cells as Water and Wetland, respectively. Note, we developed a custom model to predict the potential for flooding of streamside cells by beaver under the assumption of a saturated beaver population at carrying capacity during the historical reference period. For each stream centerline cell with an estimated stream gradient of < 10 % (computed based on the stream reach of the focal cell up to a maximum of 100 m upstream and downstream) and a flow accumulation of $< 155{,}000{,}000$ m^2, we built a virtual beaver dam of 2 m in height and then used a custom algorithm to flood all cells above that cell in the flow grid that were < 2 m elevation above and within 300 m flow distance of the focal cell. After iteratively applying the algorithm to every focal cell that met these criteria, we treated any cell that was virtually flooded above a minimum threshold value as a Wetland cell.
- Lastly, we dissolved small patches of wetland < 4 cells created by the process of overlaying rivers and beaver wetlands.

To derive the existing cover layer (Ecover) for use in post-processing the current departure metrics, we processed the data as follows:

- First, we started with the historical cover layer (Hcover) derived above.
- Second, we buffered all buildings from the Microsoft layer (see above) by 30 m and then reclassified all underlying forest cells in the Hcover layer as Urban. Note, we only reclassified forest cells as Urban to reflect "urban forest".

- Third, we dissolved small patches < 480 cells (1.2 ha, 3 acres) contained within urban (i.e., embedded) and reclassified forest cells in these nonurban islands to Urban. Note, this was to reflect our assumption that these urban forest islands were effectively urban forest and thus not likely to be treated as conventional forest lands.
- Lastly, we dissolved small patches of Urban < 0.25 ha (30-m radius circle) and eliminated appendages < 30 m wide to simply the final representation of Urban.

Developmental Stage

The Developmental Stage layer represented the successional stage of vegetation development (categorical) and was a major component of the Vegetation State layer (see below) that served as a primary geospatial layer input to LDSim (**Figure A.7**). Developmental Stage was treated as a dynamic variable in the model, meaning that it potentially changed with each timestep. Developmental Stage was primarily used in the classification of vegetation states for the purpose of characterizing and quantifying landscape structure.

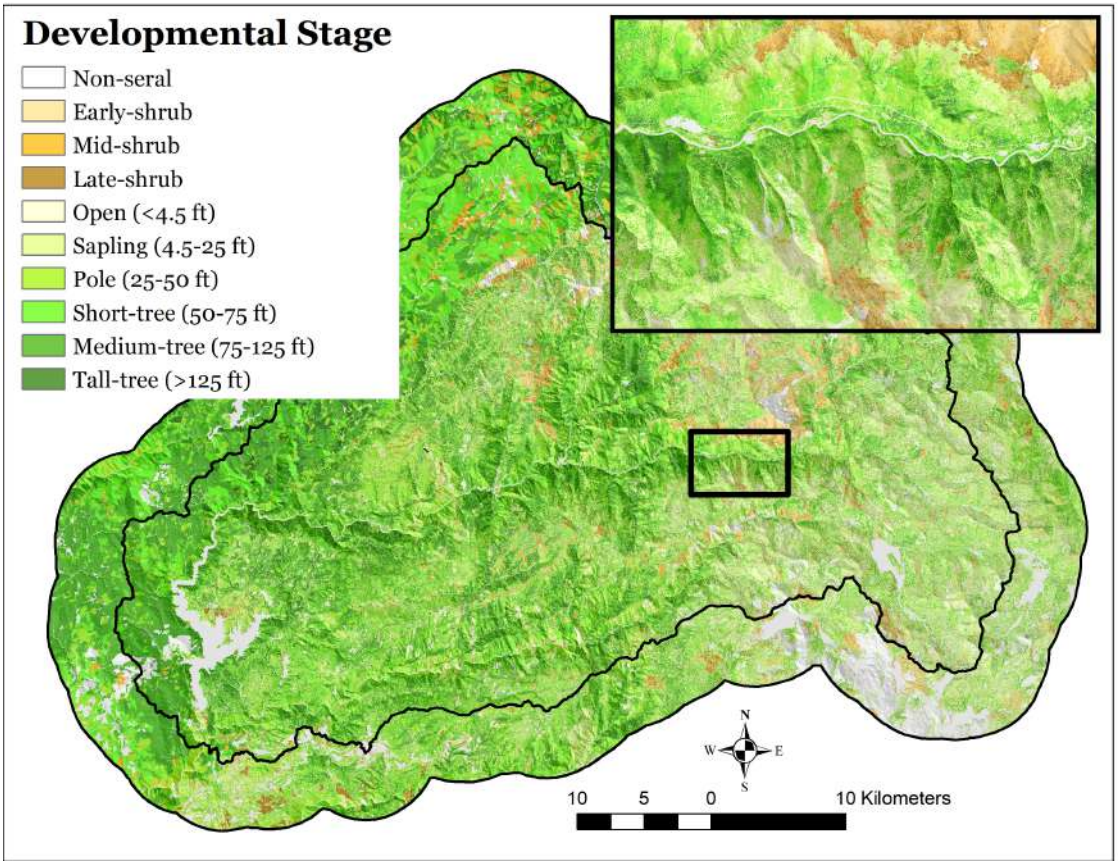

Figure A.7: Map of the Developmental Stage layer for the Yuba River landscape (displayed with hillshading).

The Developmental Stage layer was developed from two primary sources:

1. Lidar: The Lidar-derived canopy height layer (see Age above) was used exclusively within the landscape core and where the data were available in the landscape buffer, as follows:

   Shrublands: The shrubland cover types included: Shrubland, Big Sagebrush, Black and Low Sagebrush, Curl-leaf Mountain Mahogany and Chaparral, although only Big Sagebrush and Chaparral occurred in the Yuba River landscape. Canopy height for shrublands was classified into Developmental Stages as follows:

   - Height $<$ 3 ft -> Developmental Stage 1 (Early shrub)
   - Height 3 - 6 ft -> Developmental Stage 2 (Mid shrub)
   - Height $\geq$ 6 ft -> Developmental Stage 3 (Late shrub)

   Forests: The forest cover types included all forest types, including both non-mafic and ultramafic types. Canopy height for forested areas was classified into Developmental Stages as follows:

- Height < 4.5 ft -> Developmental Stage 4 (Open)
- Height 4.5 - 24 ft -> Developmental Stage 5 (Sapling)
- Height 25 - 49 ft -> Developmental Stage 6 (Pole)
- Height 50 - 74 ft -> Developmental Stage 7 (Short-tree)
- Height 75 124 ft -> Developmental Stage 8 (Medium-tree)
- Height ≥ 125 ft -> Developmental Stage 9 (Mature)

All other cover types: All other cover types included: Urban, Powerline, Agriculture, Water, Wetland, Desert Riparian, Foothill Riparian, Montane Riparian, Barren, Herbaceous, Grassland, and Meadow. We assigned a non-seral Developmental Stage (= 0) to cells in these cover types, reflecting the fact that we chose to treat these cover types as static in LDSim.

2. Eveg: The Eveg data was used only within the landscape buffer where Lidar data were not available, as follows:

   Shrublands: The initial Developmental Stage for shrublands was also derived from the Age and Site Index layers. However, we treated shrublands as having only three Developmental Stages: Early-shrub, Mid-shrub and Late-shrub. We assigned cells to a stage based on a transition probability given by the following Logistic function. Cells with a probability of < 0.5 of transitioning to the Mid-shrub stage were assigned to the Early-shrub stage; otherwise, cells with Age > 100 were assigned to the Late-shrub stage, and all remaining cells were assigned to the Mid-shrub stage:

$$P_{it} = \frac{e^{(b_0+b_1 A_{it}+b_2 S_i)}}{1+e^{(b_0+b_1 A_{it}+b_2 S_i)}}$$

   where: b_0 - b_{-2} were user-specified Logistic parameters that could vary among shrubland cover types; A_{it} = Age of the i^{th} cell in the t^{th} timestep; S_i = Site Index of the i^{th} cell; and P_{it} = probability of Developmental Stage transition of the i^{th} cell in the t^{th} timestep.

   The transition from Early- to Mid-shrub stage for the Big Sagebrush cover type was as depicted in **Figure 17**. The transition from Mid to Late Developmental Stage for the Chaparral cover type was as depicted in **Figure 18**.

   Forests: The initial Developmental Stage for forests was derived from the Age and Site Index layers. We used Age and our custom Site Index variable (see below) to predict tree Height based on the growth equation described in the main text, with the adjustment noted above for ultramafic forest types (i.e., 15 % reduction in height for any given age and site index). Predicted tree height was then classified into Developmental Stages as given above:

   All other cover types: We assigned a non-seral Developmental Stage (= 0) to cells in all other cover types as noted previously.

Elevation

The Elevation layer represented elevation (m) and was a primary geospatial layer input to LDSim (**Figure A.8**). Elevation was treated as a static variable in the model, meaning that it remained constant throughout the simulation. Elevation served as an input to the derivation of several other layers as well as a direct input to LDSim. Specifically, Elevation was used to derive several terrain indices, including Slope, Aspect, Topographic Wetness Index, Topographic Position Index, Heat Load Index, and Solar Radiation Index that were directly or indirectly inputs to the Mesic, Energy and Site Index layers, which were used in the vegetation succession model to affect vegetation establishment and growth following a high-mortality disturbance, as described in detail in the main text. Elevation was also used directly in the wildfire disturbance model to affect the spread of wildfires related to the rate of spread uphill versus downhill during an individual disturbance event. Lastly, Elevation was used to determine stream gradient which was an input to the model of potential beaver impounded wetlands which was incorporated into the Cover layer.

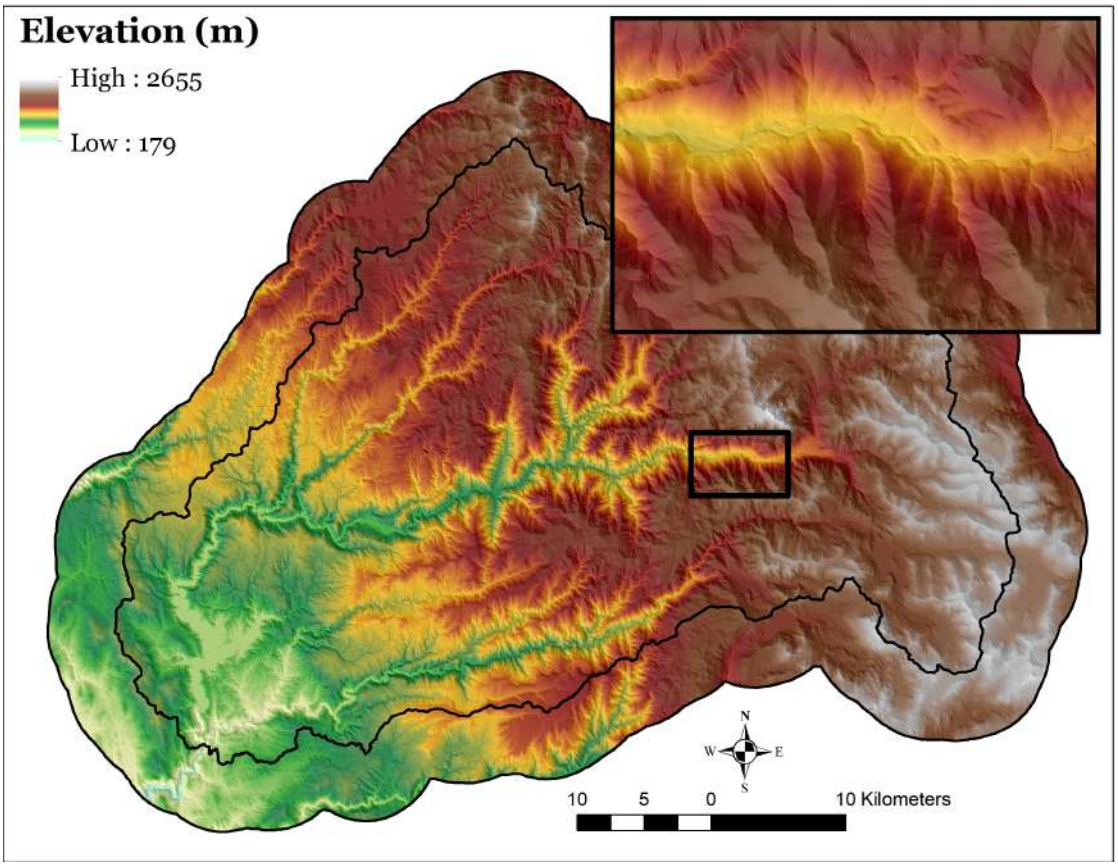

Figure A.8: Map of the Elevation layer (units = m) for the Yuba River landscape (displayed with hillshading).

The Elevation layer was derived from two primary sources:

1. Lidar: The Lidar 1 m raster data was obtained from the Tahoe National Forest with a nominal date of June 2014. We used the Lidar data exclusively within the landscape core and where the data existed within the buffer. We resampled the original 1 m raster to our reference 5 m raster for use in LDSim.
2. National Elevation Data (NED): The USGS Digital Elevation Model (DEM) 1/3 arc (~ 10 m) data was obtained from the National Geospatial Program (https://viewer.nationalmap.gov/basic/). We used the NED primarily to derive the terrain indices as discussed below, which we deemed were more

meaningfully derived from the coarser 10 m resolution data than from the finer resolution data available for the landscape core from EcObjects, and for the landscape buffer. We derived a smoothed version of the 10 m NED for use in deriving the terrain indices (Topographic Wetness Index, Topographic Position Index, and Heat Load Index) based on a subjective evaluation of the terrain indices derived from the raw versus smoothed 10 m NED. Specifically, we used the R gauss2dsmooth() function in the smoothie package with a lambda (bandwidth or standard deviation of 3 cells, 15 m) to derive the smoothed 10 m raster. We processed the final raster in R to reproject and resample to our landscape 5 m reference raster.

Energy Index

The Energy Index layer represented an unitless index of site productivity based on heat and light energy inputs (**Figure A.9**). The Energy Index was treated as a static variable, meaning that it remained constant throughout the simulation. The Energy Index served as an input to the derivation of the Site Index layer and not as a direct input to LDSim. Specifically, the Energy Index was combined with the Mesic Index to create the composite Site Index layer (see below), which was used in the vegetation succession model to affect vegetation growth following tree establishment, as described in detail in the main text.

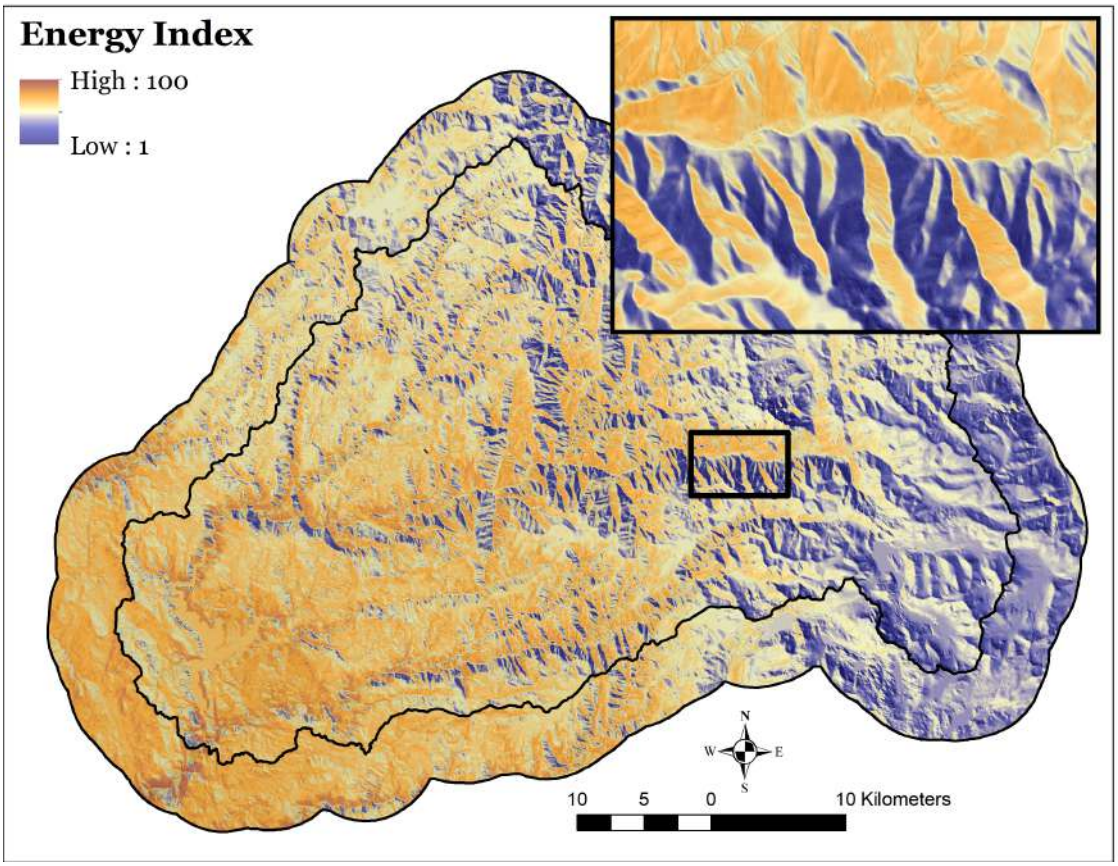

Figure A.9: Map of the unitless Energy Index layer for the Yuba River landscape (displayed with hillshading).

The Energy Index layer was derived from the following layers: Growing Degree Days, Heat Load Index and Solar Radiation Index (described elsewhere), as follows:

- First, we rescaled each of the component layers using z-scores (i.e., subtracting the regional mean and dividing by the regional standard deviation) and truncated at $\pm$ 3 standard deviation units. Each of the resulting layers had a mean of 0 and a standard deviation of 1. Note, this put each layer on the standard deviation unit scale and trimmed any outliers that occurred beyond 3 standard deviation units from the mean. To achieve consistency in the results when applied to other landscapes within the Northern Sierra ecoregion, we developed each of the component layers for the entire Northern Sierra ecoregion, computed the mean and standard deviation for each layer, and used these as the benchmarks for the standardization (**Table A.1**).

Table A.1: Benchmarks (mean and standard deviation) derived from the Northern Sierra ecoregion used to rescale several geophysical layers as described in the text.

Layer	Mean	Standard.Deviation
Precipitation	1269.24	469.01
Topographic Wetness Index	9.44	2.22
Heat Load Index	0.80	0.15
Water Balance Deficit	695.02	96.16
Available Water Storage	9.21	6.36
Topographic Position Index	0.05	20.58
Growing Degree Days	3548.20	1057.63
Solar Radiation Index	125352.43	9801.89
Energy Index	61.35	14.34
Mesic Index	43.02	9.18
Site Index	49.72	14.59

- Second, each of the component layers was range rescaled 0 - 100. This had the sole effect of maintaining the shape of the distribution but stretching the scale from -3 to 3 in z-scores to 0 to 100. This was done solely for the purpose of allowing the data format of the stored layer to be an unsigned integer and thus have a smaller file size.
- Third, we computed the average value across the three layers and stored this as the "raw" Energy Index layer.
- Lastly, we rescaled the raw Energy Index using z-scores based on benchmarks derived from the Northern Sierra ecoregion (**Table A.1**) and range-rescaled the result as described above. The final index had a theoretical range of 0 - 100. We processed the final raster in R to project and resample to our landscape 5 m reference raster.

Geophysical Units

The Geophysical Units (GPUs) layer represents local polygon units derived from geophysical variables for the purpose of summarizing and describing (i.e., packaging) the HRV results (**Figure A.10**).

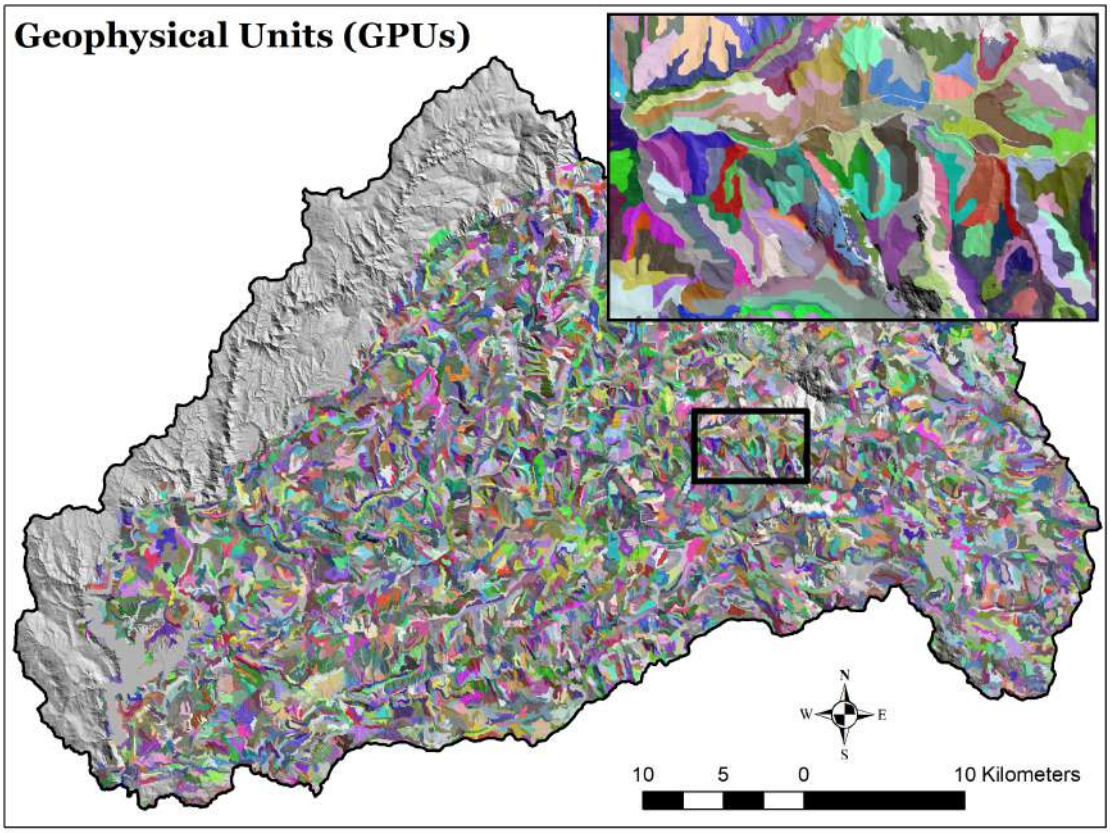

Figure A.10: Map of the Geophysical Units (GPUs) for the Yuba River landscape (displayed with hillshading).

The GPU layer was created prior to the simulation as described in detail in the main text and briefly as follows:

- First, we resample the following 10 geophysical layers (described elsewhere in this **Appendix A**) to a 40 m spatial resolution and extract the values of the variables for each cell:
  - Precipitation
  - Water balance deficit
  - Available water storage
  - Topographic wetness index
  - Heat load index
  - Growing degree days
  - Topographic position index
  - Solar radiation index
  - Elevation
  - Slope
- Next, we use a Spatially-Constrained Multivariate Clustering analytical framework to cluster cells into GPUs within each HUC12 Subbasin, constraining the algorithm to produce units with a minimum area of 4 hectares (~ 10 acres) and an average area of 20 hectares (~ 50 acres).

- Next, we apply a spatial filter to remove mapped non-forested areas based on our existing cover layer (ECover) and areas without Lidar coverage, and then apply a custom algorithm to dissolve residual GPUs < 4 ha (~ 10 acres) and eliminate residual appendages < 40 m in width.
- Next, we resample the final GPU layer to 5 m for consistency with other spatial layers.
- Lastly, we describe each GPU based on each of the 10 geophysical variables (plus Aspect) to assist in the interpretation of the GPUs and to facilitate queries of the GPU database. Specifically, we classify each of the geophysical variables into 3 - 5 classes, described in detail in the main text, as follows: Table A.2:

Variable	Method	Class	Value	Label
elevWest	literature	1	914	woodland-chaparral
elevWest	literature	2	2134	lower montane
elevWest	literature	3	2743	upper montane
elevWest	literature	4	9999	subalpine
elevEast	literature	1	2103	woodland-chaparral
elevEast	literature	2	2682	lower montane
elevEast	literature	3	3322	upper montane
elevEast	literature	4	9999	subalpine
slope	expert	1	35	gentle
slope	expert	2	65	steep
slope	expert	3	126	very steep
aspect	expert	1	1	northeast
aspect	expert	2	2	southeast
aspect	expert	3	3	southwest
aspect	expert	4	4	northwest
aspect	expert	9	9	flat
sri	quantiles	1	60	low
sri	quantiles	2	92	moderate
sri	quantiles	3	100	high
tpi	quantiles	1	38	valley-lower slope
tpi	quantiles	2	61	mid slope
tpi	quantiles	3	100	ridge-upper slope
twi	quantiles	1	39	wet
twi	quantiles	2	56	mesic
twi	quantiles	3	100	xeric
hli	quantiles	1	45	cool
hli	quantiles	2	78	moderate
hli	quantiles	3	100	warm
wbd	quantiles	1	36	low
wbd	quantiles	2	62	moderate
wbd	quantiles	3	100	high
aws	quantiles	1	14	low
aws	quantiles	2	49	moderate
aws	quantiles	3	100	high
precip	quantiles	1	27	low
precip	quantiles	2	62	moderate
precip	quantiles	3	100	high
gdd	quantiles	1	31	short
gdd	quantiles	2	69	moderate
gdd	quantiles	3	95	long

Growing Degree Days

The Growing Degree Days (GDD) layer represented an estimate of the average number of degree days above 0 degrees Celsius per year between 1981 - 2010 (**Figure A.11**). GDD was treated as a static variable, meaning that it remained constant throughout the simulation. GDD was an input to the derivation of the Energy Index (described elsewhere) and not as a direct input to LDSim. Specifically, GDD was one of two inputs to the Energy Index which was one of two components to the composite Site

Index layer (see below), which was used in the vegetation succession model to affect vegetation growth following tree establishment, as described in detail in the main text.

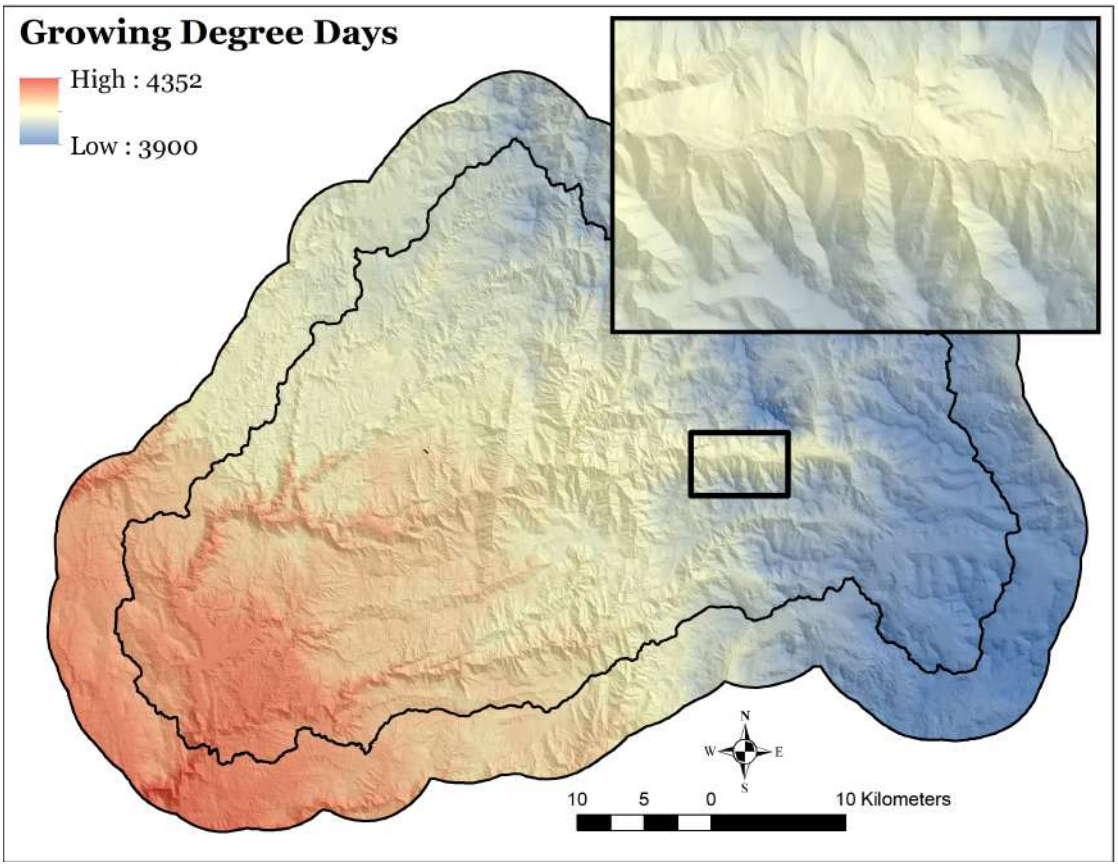

Figure A.11: Map of the Growing Degree Days layer (units = growing degree days) for the Yuba River landscape (displayed with hillshading).

The GDD layer was derived from the California Landscape Conservation Partnership Climate Commons 2014 California BCM (Basin Characterization Model) Downscaled Climate and Hydrology - 30-year Summaries for the period 1981 - 2010 at 270m resolution (http://climate.calcommons.org/dataset/2014-CA-BCM). We computed the 30-year average of the monthly maximum and minimum temperatures for each month of the year, multiplied the number of degrees Celsius above 0 by the number of days in the month, and summed the computed degree days across the 12 months of the year. The resulting GDD provided an estimate of the total heat energy input to a site over the course of a year. The use of a 0 degree Celsius threshold was based on Kelly and Goulden (2016) who documented significant photosynthetic activity (> 50 % of maximum) among conifers in Sierra Nevada forests when temperatures exceeded 0 degrees Celsius.

We rescaled GDD using z-scores based on benchmarks derived from the Northern Sierra ecoregion (**Table A.1**) and range-rescaled the result, as described above for the Energy Index. The final index had a theoretical range of 0 - 100. We processed the final raster in R to project and resample to our landscape 5 m reference raster.

Heat Load Index

The Heat Load Index (HLI) layer represented a unitless index of heat load based on potential direct incident solar radiation and was a primary geospatial layer input to LDSim (**Figure A.12**). HLI was treated as a static variable in the model, meaning that it remained constant throughout the simulation. HLI was an input to both the Energy and Mesic Indices which were components of the composite Site Index layer (see below), which was used in the vegetation succession model to affect vegetation growth following tree establishment, as described in detail in the main text. HLI was also used directly in the wildfire disturbance model to affect the susceptibility to wildfire.

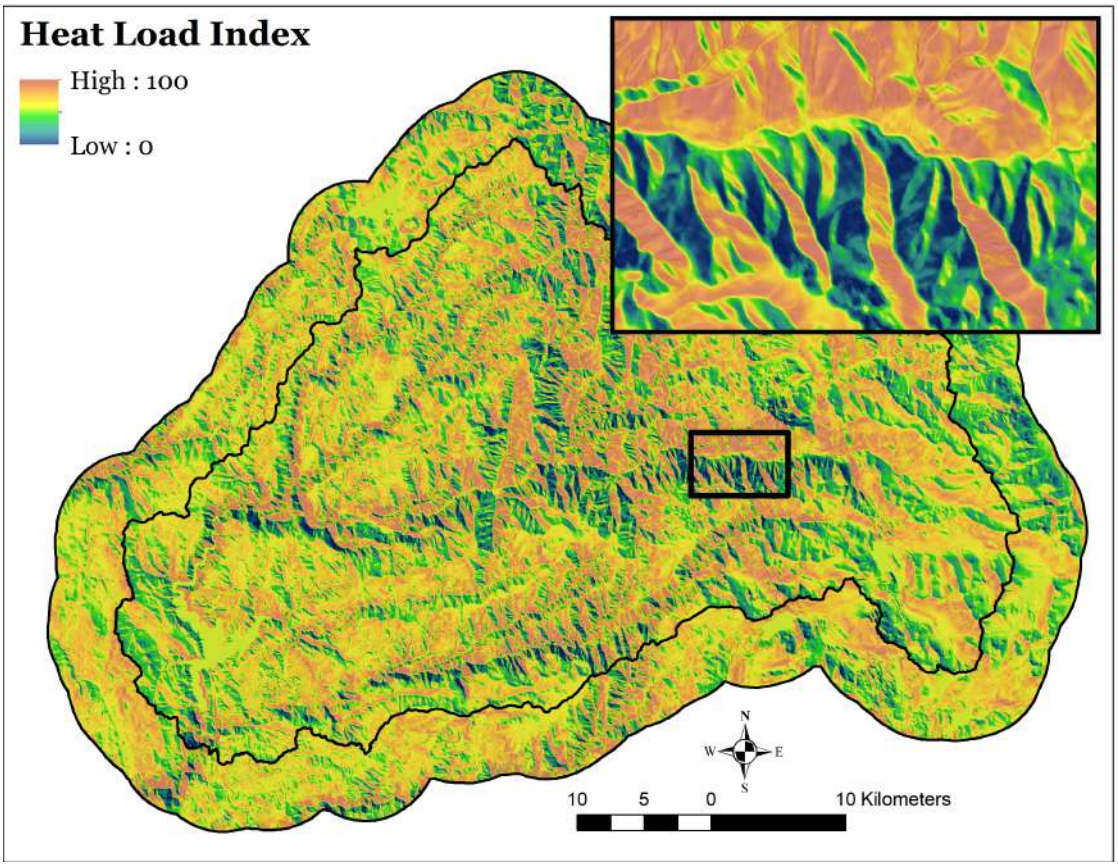

Figure A.12: Map of the unitless Heat Load Index (HLI)layer for the Yuba River landscape (displayed with hillshading).

The HLI layer was derived from the Slope and Aspect layers derived from the smoothed 10 m Elevation layer (descriptions elsewhere) and the latitude of the region based on equation 1 in McCune and Keon (2002), as implemented in the R hli() function in the spatialEco package. Note, as McCune and Keon state, "while potential direct incident radiation is symmetrical about the north - south axis, temperatures are not, because a slope with afternoon sun will have higher maximum temperatures than an equivalent slope with morning sun. A reasonable approximation to heat load (as implemented in HLI) is to make the scale symmetrical about the northeast - southwest line."

We rescaled HLI using z-scores based on benchmarks derived from the Northern Sierra ecoregion (**Table A.1**) and range-rescaled the result, as described above for the Energy Index. The final index had a theoretical range of 0 - 100. We processed the final raster in R to project and resample to our landscape 5 m reference raster.

Mesic Index

The Mesic Index layer represented an unitless index of site productivity based on moisture availability and was a primary geospatial layer input to LDSim (**Figure A.13**). Mesic Index was treated as a static variable in the model, meaning that it remained constant throughout the simulation. The Mesic Index was used directly in the vegetation succession model to affect vegetation establishment. The Mesic Index was also combined with the Energy Index to create the composite Site Index layer (see below), which was used in the vegetation succession model to affect vegetation growth following tree establishment, as described in detail in the main text.

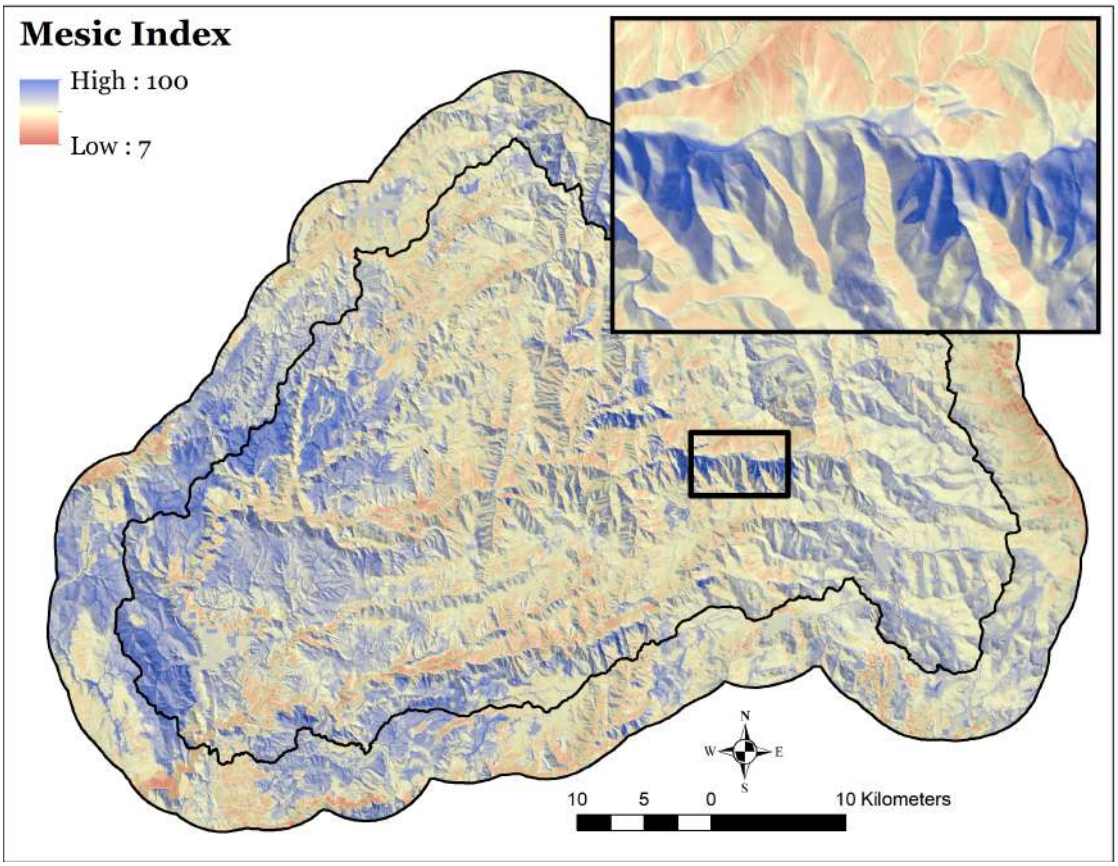

Figure A.13: Map of the unitless Mesic Index layer for the Yuba River landscape (displayed with hillshading).

The Mesic Index layer was derived from the following layers: Precipitation, Topographic Wetness Index, Heat Load Index, Water Balance Deficit, and Available Water Storage (see descriptions elsewhere), as follows:

- First, we rescaled each of the component layers using z-scores based on benchmarks derived from the Northern Sierra ecoregion (**Table A.1**) and range-rescaled the result, as described above for the Energy Index.
- Next, we computed the average value across the five layers, after taking the compliment of the Heat Load Index and Water Balance Deficit layers so that all all layers were scaled such that increasing values represented increasing wetness, and stored this as the "raw" Mesic Index layer.
- Lastly, we rescaled the raw Mesic Index using z-scores based on benchmarks derived from the Northern Sierra ecoregion (**Table A.1**) and range-rescaled the result, as described above for the

Energy Index. The final index had a theoretical range of 0 - 100. We processed the final raster in R to project and resample to our landscape 5 m reference raster.

Precipitation

The Precipitation layer represented an estimate of total annual precipitation (mm) for the period 1981 - 2010 (**Figure A.14**). Precipitation served as an input to the derivation of other layers and not as a direct input to LDSim. Specifically, Precipitation served as an input to the Mesic Index, which was used in the vegetation succession model to affect vegetation establishment following a high-mortality disturbance, and which was one of the components of the composite Site Index layer (see below), which was used in the vegetation succession model to affect vegetation growth following tree establishment, as described in detail in the main text.

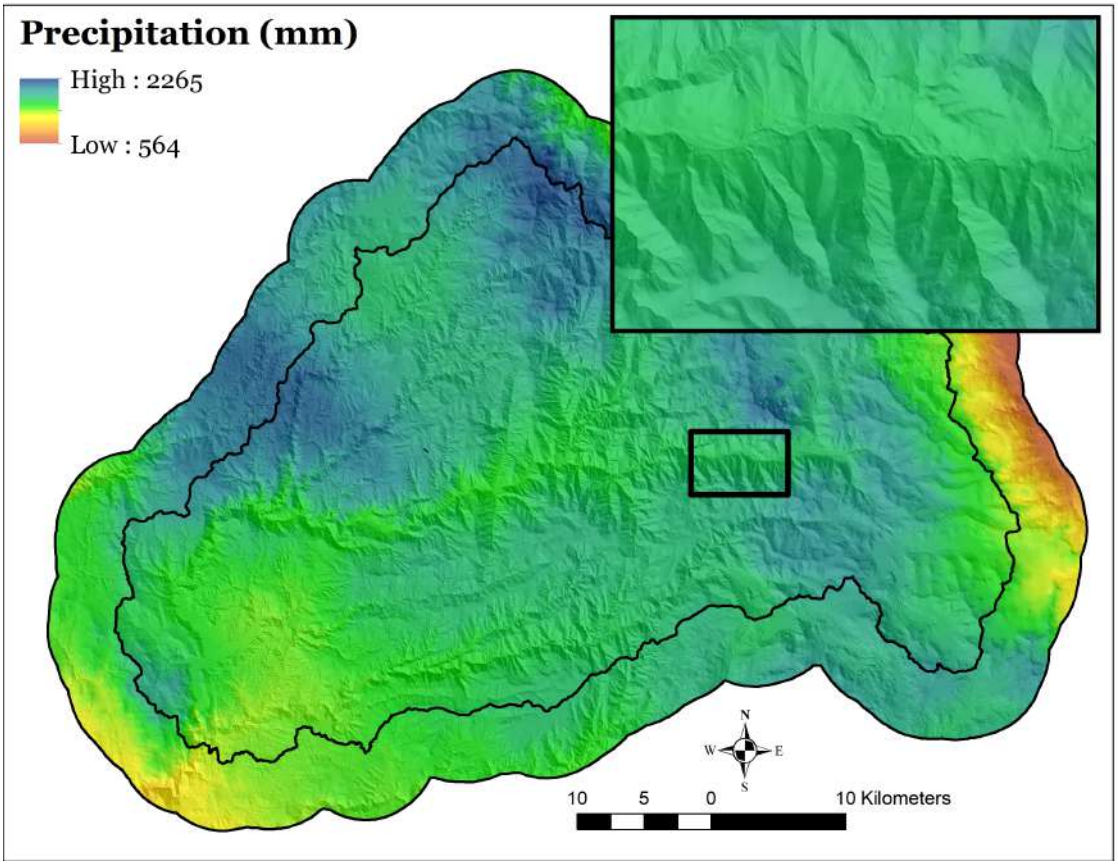

Figure A.14: Map of the Precipitation layer (units = mm) for the Yuba River landscape (displayed with hillshading).

The Precipitation layer was derived from the California Landscape Conservation Partnership Climate Commons 2014 California BCM (Basin Characterization Model) Downscaled Climate and Hydrology - 30-year Summaries for the period 1981 - 2010 at 270 m resolution (http://climate.calcommons.org/dataset/2014-CA-BCM).

We rescaled HLI using z-scores based on benchmarks derived from the Northern Sierra ecoregion (**Table A.1**) and range-rescaled the result, as described above for the Energy Index. The final index had a theoretical range of 0 - 100. We processed the final raster in R to project and resample to our landscape 5 m reference raster.

Site Index

The Site Index layer represented an unitless index of site productivity and was a primary geospatial layer input to LDSim (**Figure A.15**). Site Index was treated as a static variable in the model, meaning that it remained constant throughout the simulation. Site Index was used in the vegetation succession model to affect vegetation growth following tree establishment, as described in detail in the main text.

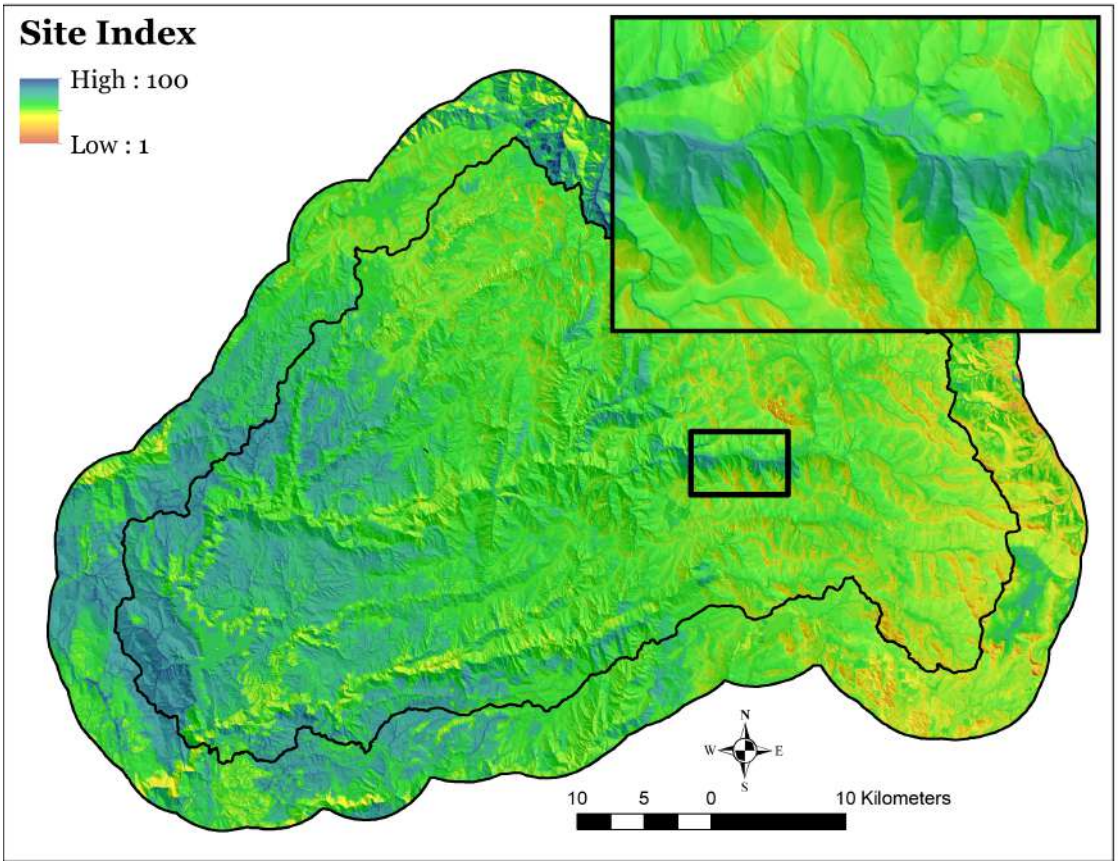

Figure A.15: Map of the unitless Site Index layer for the Yuba River landscape (displayed with hillshading).

The Site Index layer was derived as a weighted composite of the Mesic Index and Energy Index (described elsewhere), as described in detail in the main text. Briefly, we used FIA tree data to model tree height as a Monomolecular function of Age and Site Index (i.e.,site index curves), but such that the Site Index was derived as a weighted combination of the Mesic and Energy Indices. The relative weighting of the two indices varied with elevation according a Logistic function in which the parameters of the Logistic function were estimated while fitting the site index curves. In addition, the Logistic weighting function was fit separately for sites on the westside versus eastside of the Sierra crest owing to differences in the relative importance of moisture versus energy limitations on tree growth between westside and eastside forests.

As with the component Mesic and Energy Indices, we rescaled fitted raw Site Index using z-scores based on benchmarks derived from the Northern Sierra ecoregion (**Table A.1**) and range-rescaled the result, as described above for the Energy Index. The final index had a theoretical range of 0 - 100. The final index has a theoretical range of 0 - 100. We processed the final raster in R to project and resample to our landscape 5 m reference raster.

Slope

The Slope layer represented percent slope (**Figure A.16**). Slope was treated as a static variable, meaning that it remained constant throughout the simulation. Slope served as in input to the derivation of other layers and not as a direct input to LDSim. Specifically, Slope was in input to the Heat Load Index which was an input to both the Mesic and Energy Indices and thus the composite Site Index layer, which were used in the vegetation succession model to affect vegetation establishment and growth following a high-mortality disturbance. Slope indirectly affected other aspects of the model, such as the spread of wildfires, but in this regard slope was calculated "on the fly" via the Elevation layer (which was an input to LDSim).

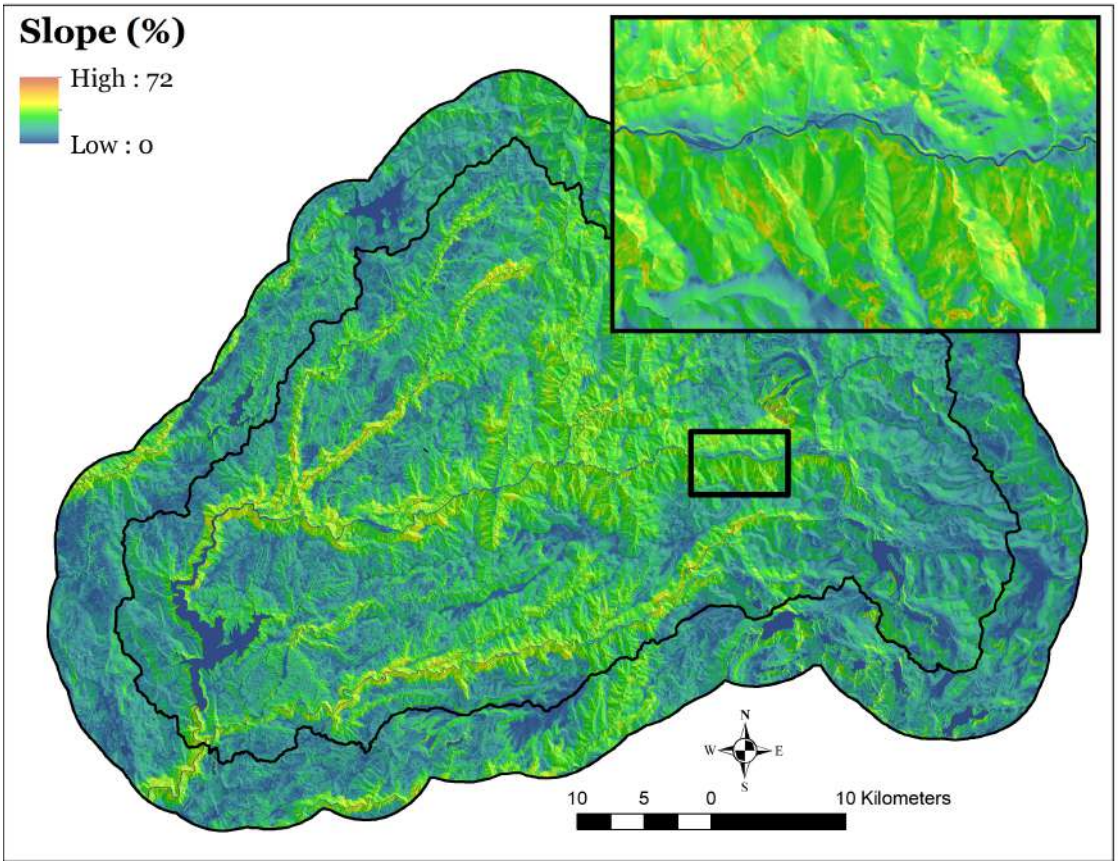

Figure A.16: Map of the Slope layer (units = percent) for the Yuba River landscape (displayed with hillshading).

The Slope layer (percent) was derived from the 10 m elevation layer using the terrain() function in the R Terra package. We truncated the maximum slope to 126 percent, then smoothed the surface using Gaussian kernel with a lambda (bandwidth or standard deviation of 3 cells, 15 m) using the focal() function in the Terra package, and finally resampled to our landscape 5 m reference raster.

Solar Radiation Index

The Solar Radiation Index (SRI) layer represented a unitless index of direct solar radiation (or insolation) based on the approach described by Pierce et al. (2005)(**Figure A.17**). SRI was treated as a static variable, meaning that it remained constant throughout the simulation. SRI served as an input to the derivation of other layers and not as a direct input to LDSim. Specifically, SRI was an input to the Energy Index and thus the Site Index layer, which was used in the vegetation succession model to affect vegetation establishment and growth following a high-mortality disturbance, as described in detail in the main text. SRI was also included as one of several geophysical predictors used to model cumulative tree biomass in the development of Biophysical classes (BPCs) and Biophysical Units (BPUs), as described elsewhere, and as one of several geophysical variables used to develop Geophysical Units (GPUs), as described elsewhere.

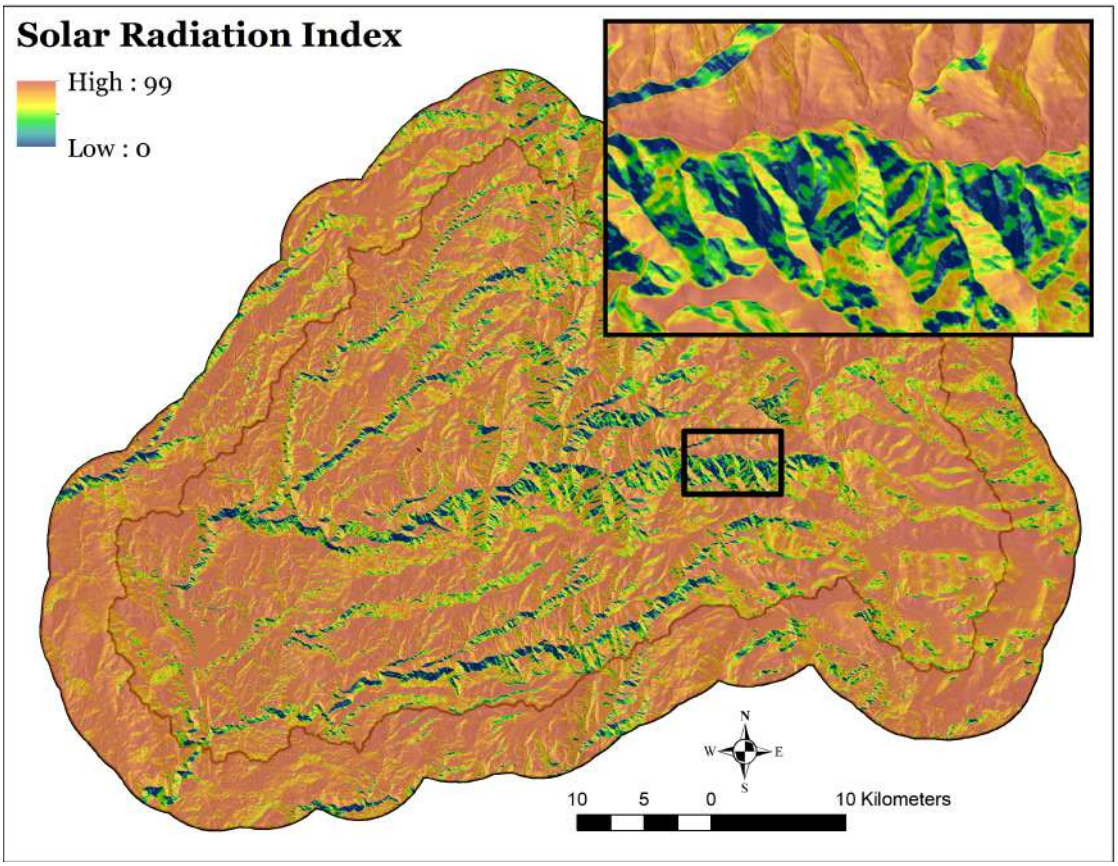

Figure A.17: Map of the unitless Solar Radiation Index layer for the Yuba River landscape (displayed with hillshading).

The SRI layer was derived from the smoothed 10 m Elevation layer (see above) using a custom R script as follows:

- First, we computed Slope and Aspect in radians from the smoothed 10 m Elevation layer.
- Next, we derived the mean latitude and longitude of the Northern Sierra ecoregion.
- Next, we selected the 15th of each month of the designated growing season: April 15 to September 15 for a total of 6 days.
- Next, we select 10 equally spaced times between sunrise and sunset for each of the days above, resulting in a total of 60 solar observations (6 days x 10 times).

- Next, we derived the solar period for each day, defined as the duration of sunlight between sunrise and sunset, using the getSunlightTimes function in the suncalc R package.
- Next, for each solar observation, we derived the vertical sun angle above the horizon and the sun azimuth (north = 0 degrees) using the getSunlightPosition function in the suncalc R package.
- Next, for each solar observation, we derived an index of direct solar radiation that accounts for latitude and longitude, sun angle and azimuth, and topographic shading using the shade function in the terra R package. We used the "normalize" option which sets radiation values to zero for values below zero and the results are multiplied by 255.
- Next, for each day, we summed the radiation values across times and multiplied the result bt the solar period. This weighted each of the 6 representative days by their solar periods so that June 15th would get weighted more than, say, April 15th.
- Next, we summed the weighted radiation values across days to produce the final SRI in its raw scale.

We rescaled SRI using z-scores based on benchmarks derived from the Northern Sierra ecoregion (**Table A.1**) and range-rescaled the result, as described above for the Energy Index. The final index had a theoretical range of 0 - 100. We processed the final raster in R to project and resample to our landscape 5 m reference raster.

Streams

The Streams layer represented rivers and streams categorically based on size and was a primary geospatial layer input to LDSim (**Figure A.18**). Streams was treated as a static variable in the model, meaning that it remained constant throughout the simulation. Streams was used as input to the Cover layer (see above) and in the wildfire disturbance model to affect the spread of fires.

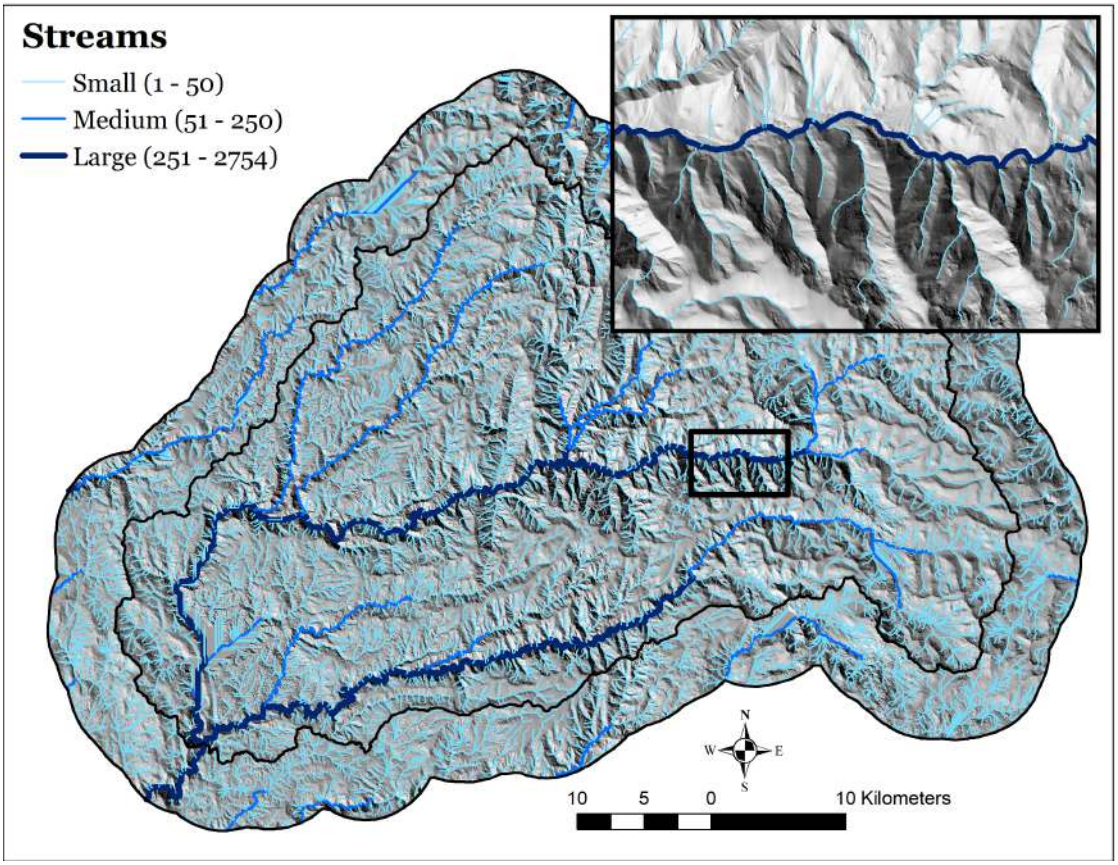

Figure A.18: Map of the Streams layer for the Yuba River landscape (displayed with hillshading). Note, the legend labels parenthetically indicate the range of stream orders assigned to each stream class

We initially derived streams from the USGS NHD High Resolution streams data downloaded from USGS National Geospatial Program: The National Map (http://prd-tnm.s3-website-us-west-2.amazonaws.com/?prefix=StagedProducts/Hydrography/NHD/State/HighResolution/GDB/NHD_H_California_State_GDB.zip), but ultimately decided to create streams from the elevation raster for consistency with the other elevation-derived layers (e.g., Topographic Wetness Index) and because they appeared to be more accurate than the NHD streams on average. The final Streams layer for the focal landscape was derived as follows:

- First, we filled sinks in the 1 m elevation raster using the Fill Sinks (Wang & Liu) tool in the Preprocessing toolbox in SAGA GIS.
- Next, we computed flow direction and flow accumulation based on filled DEM using the Flow Accumulation (Flow Tracing) tool in the Hydrology toolbox in SAGA GIS.
- Next, we derived vector stream channels based on the filled DEM and flow direction grids using the Channel Network tool in the Channels toolbox in SAGA GIS. We initiated channels with a flow

accumulation of 50,000 m^2 or greater and a minimum length of 100 m. This resulted in a shapefile with stream order (or link magnitude) as an attribute.

- Next, we classified streams into three size classes based on stream Order, as follows:
  - Order > 249 -> stream class 1 (Large)
  - Order 51 - 249 -> stream class 2 (Medium)
  - Order < 51 -> stream class 3 (Small)
- Next, we buffered streams based on stream class such that the buffer width was 0.5 m for small streams and increased progressively from 1 to 12.5 m for larger streams as stream Order increased. Note, buffer width refers to the distance imposed on each side of the stream, so the total width of the final buffered stream was equal to twice the buffer width (i.e., 1 m for small stream and 25 m for the largest river)
- Lastly, we rasterized the shapefile file based on stream class, ensuring alignment with our landscape 5 m reference raster.

Tau Index

The Tau Index layer represented a unitless index used to apply polymorphous site index curves and was a primary geospatial layer input to LDSim (**Figure A.19**). The Tau Index was treated as a static variable in the model, meaning that it remained constant throughout the simulation. The Tau Index corresponded to a set of parameters used to construct site index curves for each cell that affected tree height growth in the vegetation succession model, as described in detail in the main text. Briefly, the Tau Index was constructed as follows:

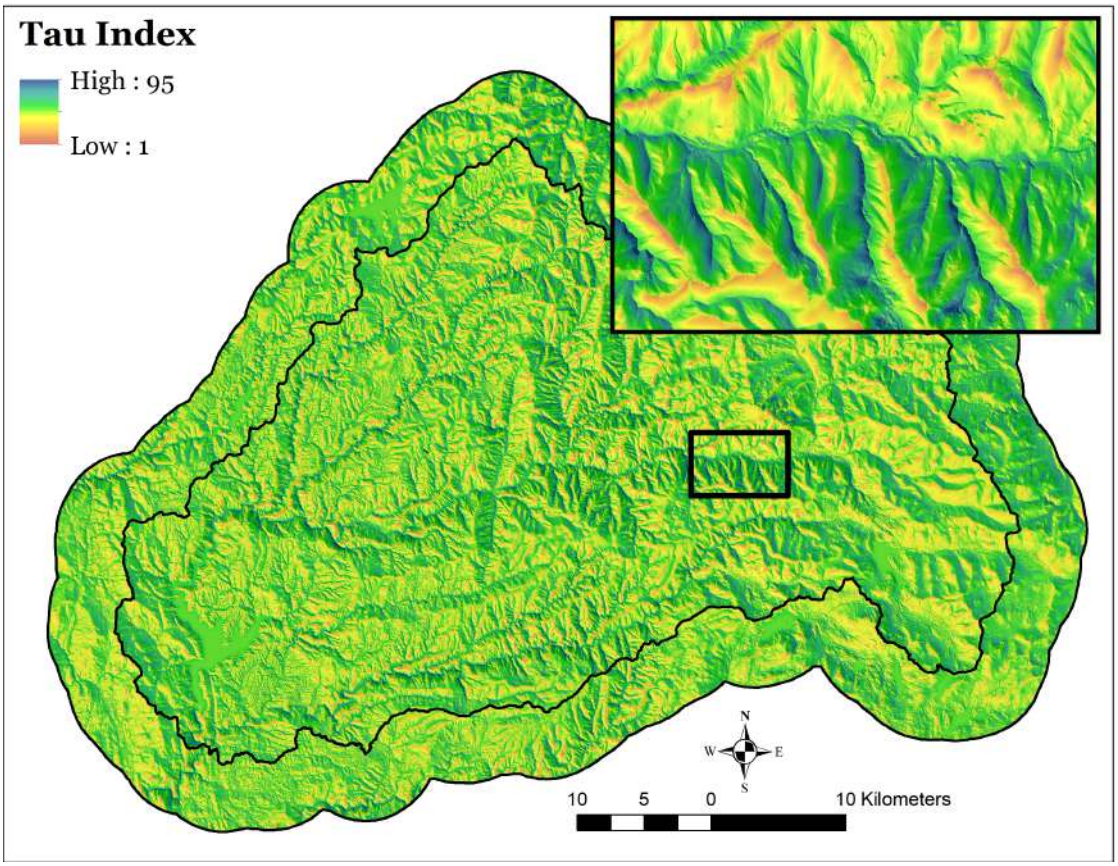

Figure A.19: Map of the unitless Tau Index layer for the Yuba River landscape (displayed with hillshading).

- First, using FIA tree data, we fit a model to predict tree height as a Monomolecular function of total tree age and site index (i.e., site index curves) using NLS in R. The fitted model predicted the expected or average tree height given total tree age and site index.
- Next, We fit a normal distribution to the residuals of the function above. Each residual represented the deviation of the observed tree height from the expected or average tree height given the tree's total age and site index. We rescaled the residuals to range 0 - 1 prior to fitting a normal distribution, and saved the estimated standard deviation to quantify the spread of observed tree heights (i.e., variation) around the expected or average value to be used below. In effect, the standard deviation provided a quantitative measure of the "noise" or uncertainty in the fitted site index curves.
- Next, we fit the same model above but with Nonlinear Quantile Regression (NLRQ) in R, for quantiles (termed Tau in NLRQ) ranging from 0.01 - 0.99 at intervals of 0.01. For example, a Tau of 0.01 fit the Monomolecular function to the observations representing the 1st quantile of the data; i.e., observations falling well below the expected or average value given total age and site index.

Conversely, a Tau of 0.99 fit the same function to the observations falling well above the expected or average value. Thus, Tau values ranging from 0.01 - 0.99 fit Monomolecular functions (i.e., site index curves) to the full range of the data. Each Tau value produced a unique set of estimates for the parameters of the Monomolecular function, and thus produced a site index curve that varied slightly in shape as the Tau value increased. The result was a set of polymorphic site index curves that captured the full range of the observed data.

- Lastly, we assigned a Tau value to each cell that determined site index curve applied to each cell for the duration of the simulation. The assigned Tau value determined whether each cell adopted a site index curve above or below the average for the cell's Site Index. For example, a cell assigned a Tau of 0.5 would realize the expected or average site index curve for that cell's Site Index, whereas a cell assigned a Tau of, say, 0.9 would realize a site index curve much higher than the expected or average for that cell's Site Index. For this purpose, we opted not to randomly assign a Tau value to each cell as this would not preserve the observed spatial autocorrelation in tree height growth. Instead, we surmised that the spatial autocorrelation in tree height growth was likely driven by the spatial autocorrelation in underlying physical site conditions (e.g., terrain). Exploratory analyses indicated that tree height growth was weakly related to topographic position and aspect. Consequently, we modeled Tau as a Logistic function of Topographic Position Index (TPI) and a linear transformation of Aspect along a NE - SW axis, and assigned equal weight to TPI and Aspect such that Tau decreased with increasing topographic position and increased towards northeasterly aspects. We transformed the resulting Tau distribution to match that of the residual distribution described above.

Topographic Position Index

The Topographic Position Index (TPI) layer represented a unitless index of topographic position based on the elevation surface and was a primary geospatial layer input to LDSim (**Figure A.20**). TPI was treated as a static variable in the model, meaning that it remained constant throughout the simulation. TPI was used in the wildfire disturbance model to affect the intensity and thus severity of wildfire.

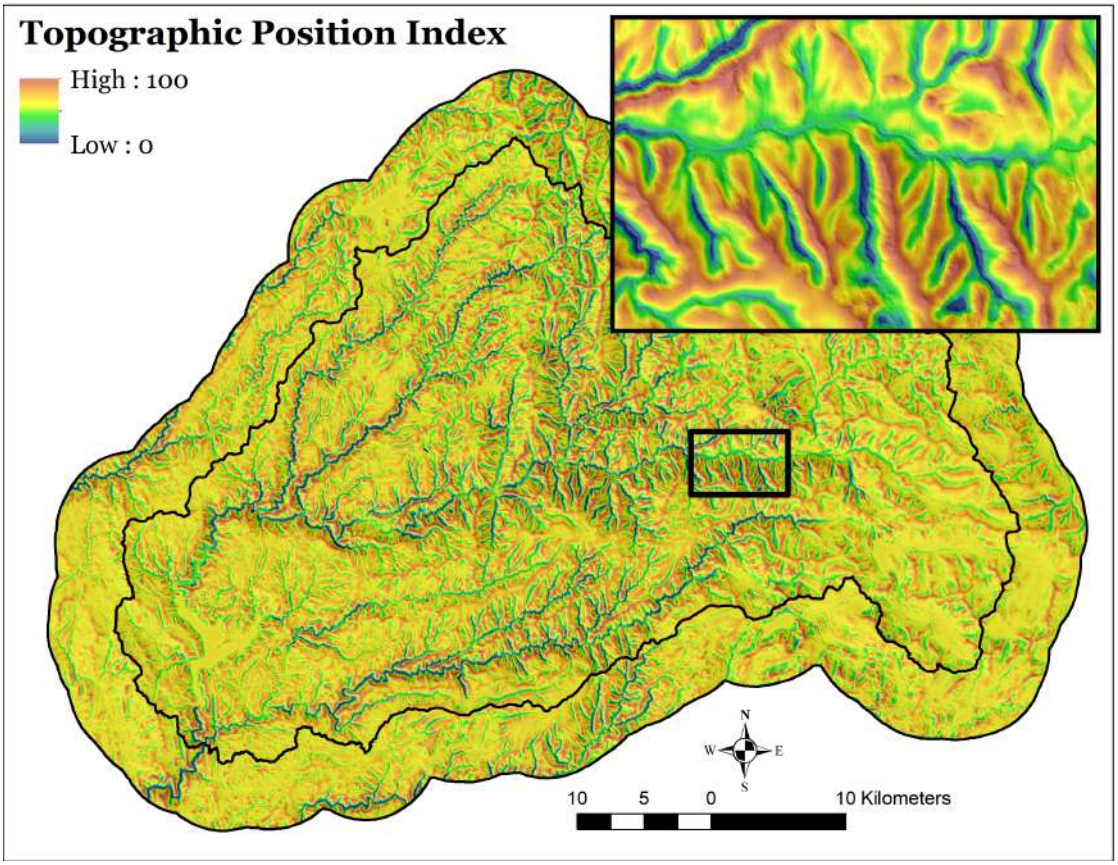

Figure A.20: Map of the unitless Topgraphic Position Index (TPI) layer for the Yuba River landscape (displayed with hillshading). Note, higher values are associated with upper slopes and ridges, and lower values are associated with lower slopes and valleys.

The TPI layer was derived from the smoothed 10 m Elevation layer (see above) using the R tpi() function in the spatialEco package. TPI is based on the mean deviation in elevation between the focal cell and the neighboring cells within a specified window. The optimal window size depends on the scale of the topography and the objective of the analysis. Here, we subjectively evaluated a wide range of window sizes and ultimately selected a size of 305 m (61 cells) as this appeared to capture the distinction between the major ridges and valleys the best.

We rescaled TPI using z-scores based on benchmarks derived from the Northern Sierra ecoregion (**Table A.1**) and range-rescaled the result, as described above for the Energy Index. The final index had a theoretical range of 0 - 100. We processed the final raster in R to project and resample to our landscape 5 m reference raster.

Topographic Wetness Index

The Topographic Wetness Index (TPI) layer represented a unitless index of topographic wetness based on the potential for water to accumulate resulting from the predicted quantity of water flowing to a site and the predicted rate of drainage from the site (i.e., water balance) (**Figure A.21**). TWI was treated as a static variable, meaning that it remained constant throughout the simulation. TWI served as an input to the derivation of other layers and not as a direct input to LDSim. Specifically, TWI was an input to the Mesic Index and Site Index layers, which were used in the vegetation succession model to affect vegetation establishment and growth following a high-mortality disturbance, as described in detail in the main text.

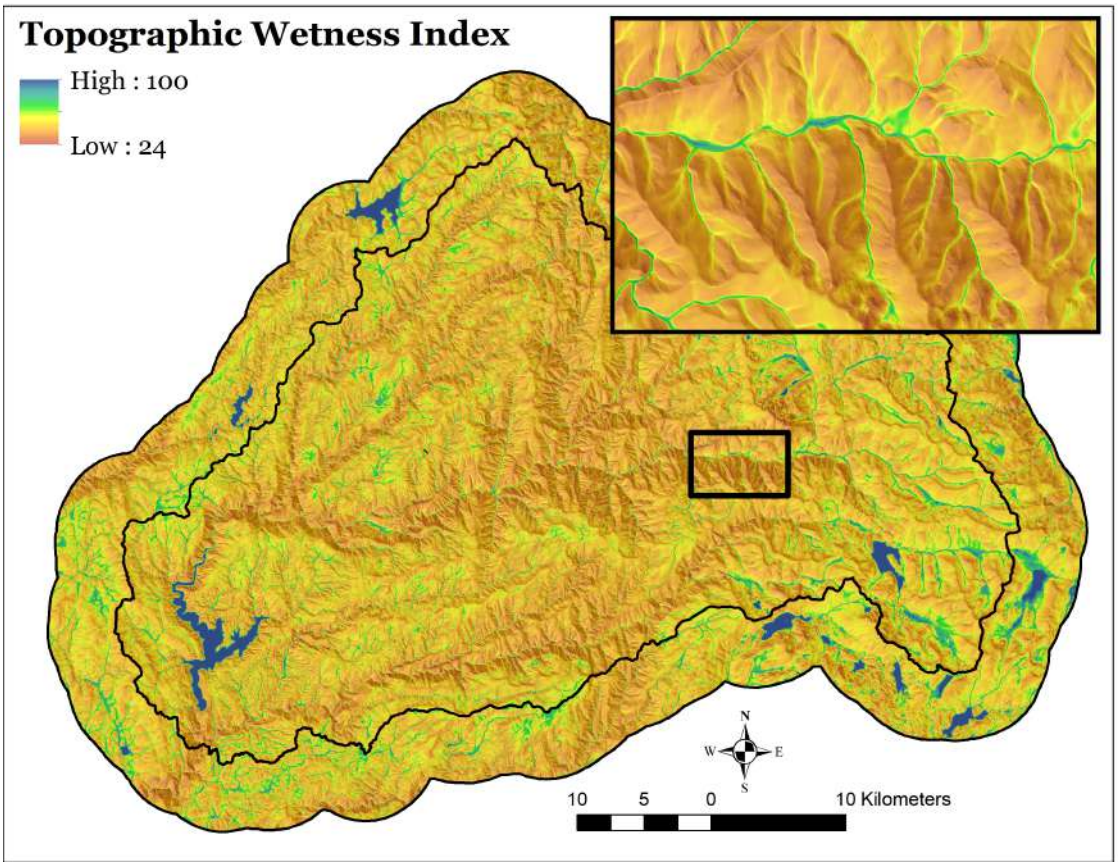

Figure A.21: Map of the unitless Topgraphic Wetness Index (TWI) layer for the Yuba River landscape (displayed with hillshading). Note, higher values are associated with wetter areas and lower values are associated with drier areas.

The TWI layer was derived from the 10 m precipitation and smoothed Elevation layers (see above) by computing the Sage Wetness Index (SWI) in the Hydrology toolbox in SAGA GIS. The Precipitation layer was used as weights in the calculation of SWI, such that each cell was weighted based on its Precipitation value in contributing to the watershed flow accumulation component of the index. The TWI layer effectively distinguished low-lying valley bottoms and floodplains (i.e., areas likely to collect water) from drier ridetops and steep slopes.

We rescaled TWI using z-scores based on benchmarks derived from the Northern Sierra ecoregion (**Table A.1**) and range-rescaled the result, as described above for the Energy Index. The final index had a theoretical range of 0 - 100. We processed the final raster in R to project and resample to our landscape 5 m reference raster.

Tree Cover and Tree Cover Class

The Tree Cover layer represented the density of neighboring cells with established trees and given as the percentage of cells in the neighborhood, as defined, with established trees to breast height (i.e., in the Sapling, Pole, Small Tree, Medium Tree or Tall Tree developmental stages) and was a major component of the Vegetation State layer (see below) that served as a primary geospatial layer input to LDSim (**Figure A.22**). Tree Cover was treated as a dynamic variable in the model, meaning that it potentially changed with each timestep. Tree Cover Class, as defined below, was primarily used in the classification of vegetation states for the purpose of characterizing and quantifying landscape structure.

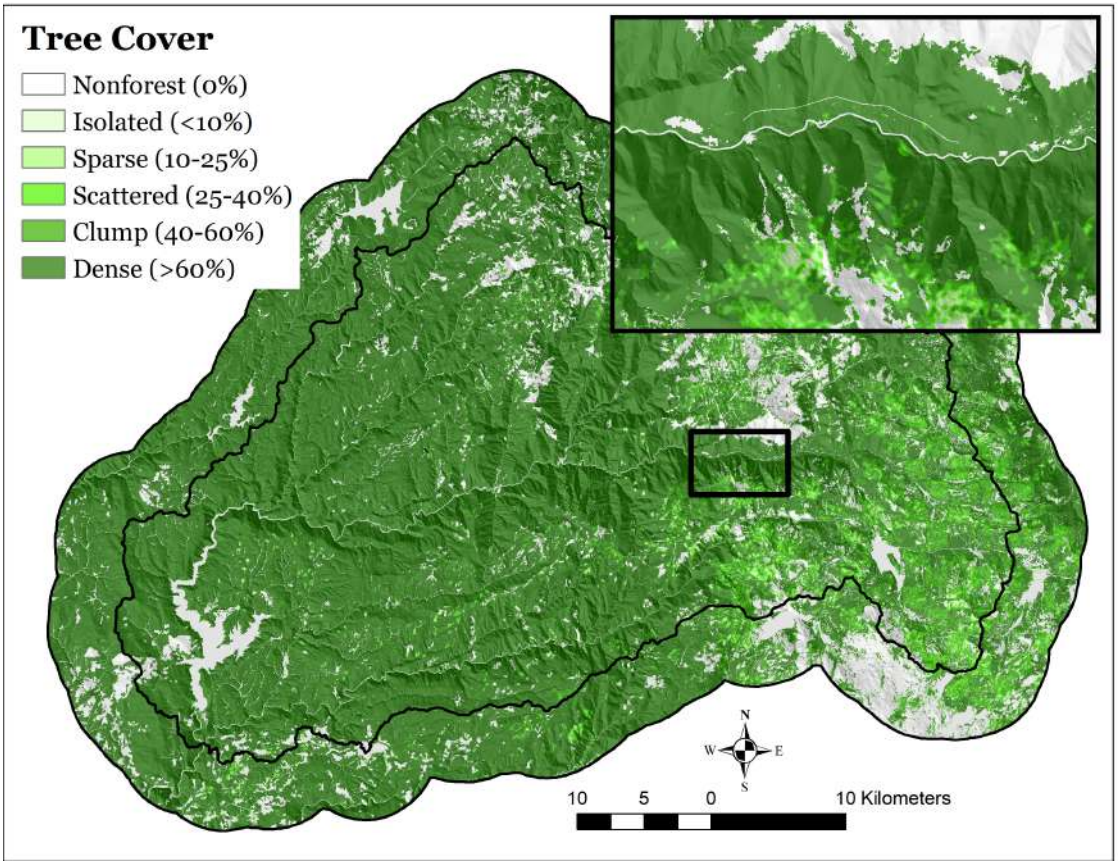

Figure A.22: Map of the Tree Cover Class layer for the Yuba River landscape (displayed with hillshading).

The Tree Cover layer was derived from the Developmental Stage and Cover layers. We computed Tree Cover only for cells classified as forest; all other cells were assigned the value zero. Tree Cover was calculated as follows:

- First, we constructed a uniform circular kernel with a radius of 40 m. The resulting kernel in its raster form gave equal weight to all cells within 40 m of the focal cell.
- Next, we computed the kernel density of valid cells (i.e., cells of forest cover based on the Cover layer with established trees based on the Developmental Stage layer) and divided it by the maximum potential density that would have been obtained if all the forested cells in the kernel had established trees. The resulting index represented the proportion of neighboring forested cells with established trees and was loosely interpreted as a biased estimate of percent canopy cover (although subsequent analyses revealed that this estimate of Tree Cover is on average 16 % greater than actual tree canopy cover).

- Lastly, we classified the kernel density index into tree size classes, applying the same thresholds for all forest cover types, plus a zero class for all non-forest cells, as follows:
  - Density < 0.1 -> Tree Cover class 1 (Isolated)
  - Density 0.1 - 0.24 -> Tree Cover class 2 (Sparse)
  - Density 0.25 - 0.39 -> Tree Cover class 3 (Scattered)
  - Density 0.4 - 0.59 -> Tree Cover class 4 (Clump)
  - Density ≥ 0.6 -> Tree Cover class 5 (Dense)

Tree Diameter

The Tree Diameter layer represented the estimated diameter (in) at breast height (DBH) of a cell with an established tree (**Figure A.23**). Tree Diameter was treated as a dynamic variable in the model, meaning that it potentially changed with each timestep. Tree Diameter was the input to the Tree Quadratic Mean Diameter layer (see below) which was created primarily for the purpose of characterizing and quantifying landscape structure.

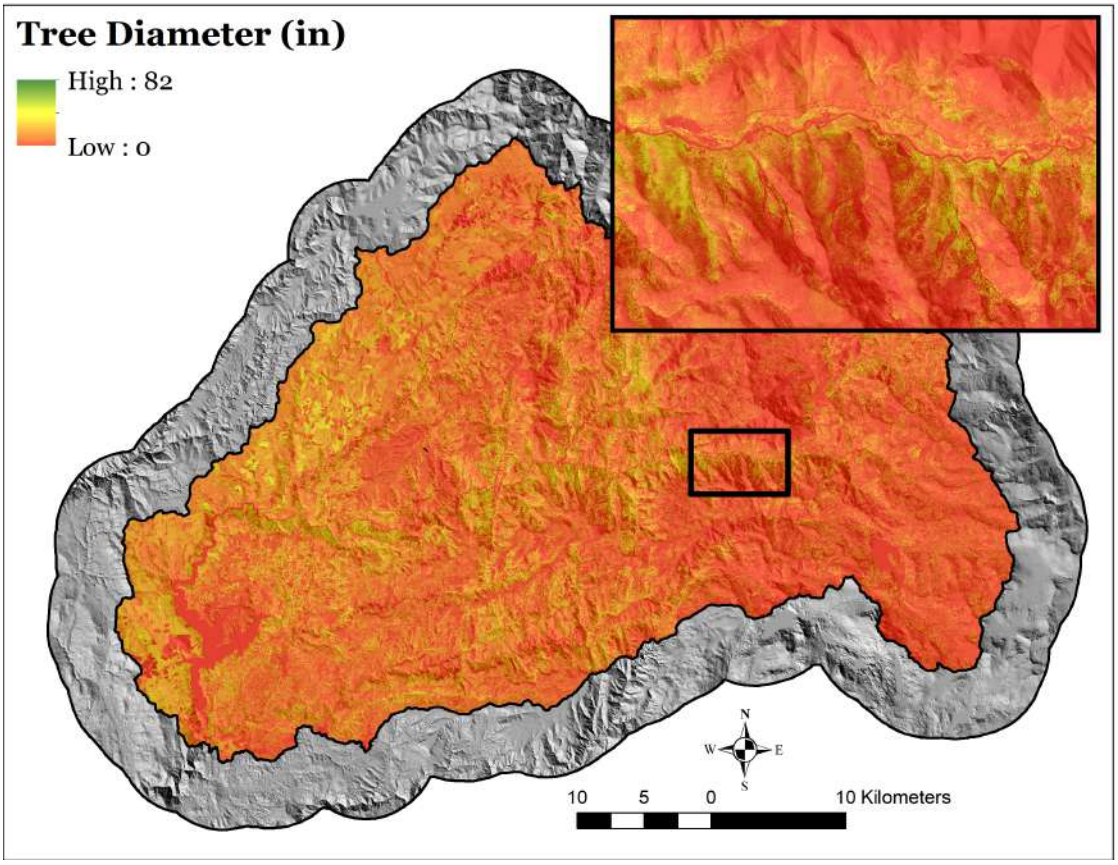

Figure A.23: Map of the Tree Diameter (in) layer for the Yuba River landscape (displayed with hillshading).

The Tree Diameter layer was derived from the Tree Height (see below) and Cover type layers. We computed Tree Diameter only for cells classified as forest with an established tree; all other cells were assigned the value zero. The creation of the Tree Diameter layer is described in detail in the main text, and thus only briefly summarized here.

- First, we used Forest Inventory and Analysis (FIA) data from the Northern Sierra ecoregion and Quantile Regression (QR) estimation to fit the following polynomial function for a range of quantiles (also referred to a Tau in QR) for each cover type. Specifically, we fit the following quadratic polynomial function to Tau values ranging from 0.01 - 0.99 at intervals of 0.01:

$$D_{it} = b_{0[k]}H_{it} + b_{1[k]}H_{it}^2$$

where: $b_{0[k]}$ and $b_{0[k]}$ were estimated slope parameters representing the rate at which tree diameter increased nonlinearly per unit increase in tree height for the k^{th} cover type; H_{it} = tree height (ft) the i^{th} cell in the t^{th} times step; and D_{it} = tree diameter (in) of the i^{th} cell in the t^{th} timestep.

- Next, we randomly assigned a Tau value to each cell to indicate whether that cell would realize a diameter growth curve above or below the average for the cell's cover type. For this purpose, we opted to randomly assign a Tau value to each cell because we reasoned that diameter growth was largely determined by the distance to neighboring trees at a very fine scale which we could not relate to any spatial variable we could account for. Thus, we simply assigned a random Tau value drawn from a normal distribution with a mean of 0.5 and a standard deviation equal to that observed in the normalized residuals from the fitted equation above (i.e., 0.16) to each cell, ensuring that the random Tau values fell within the range 0.01 - 0.99 corresponding to the range of Tau values fitted.
- Lastly, at each timestep we applied the fitted equation above corresponding to the cell's cover type and Tau to predict tree diameter.

Tree Height

The Tree Height layer represented the estimated height (ft) of a cell with an established tree (**Figure A.24**). Tree Height was treated as a dynamic variable in the model, meaning that it potentially changed with each timestep. Tree Height was the primary input to the Developmental Stage and Tree Diameter layers which were created primarily for the purpose of characterizing and quantifying landscape structure.

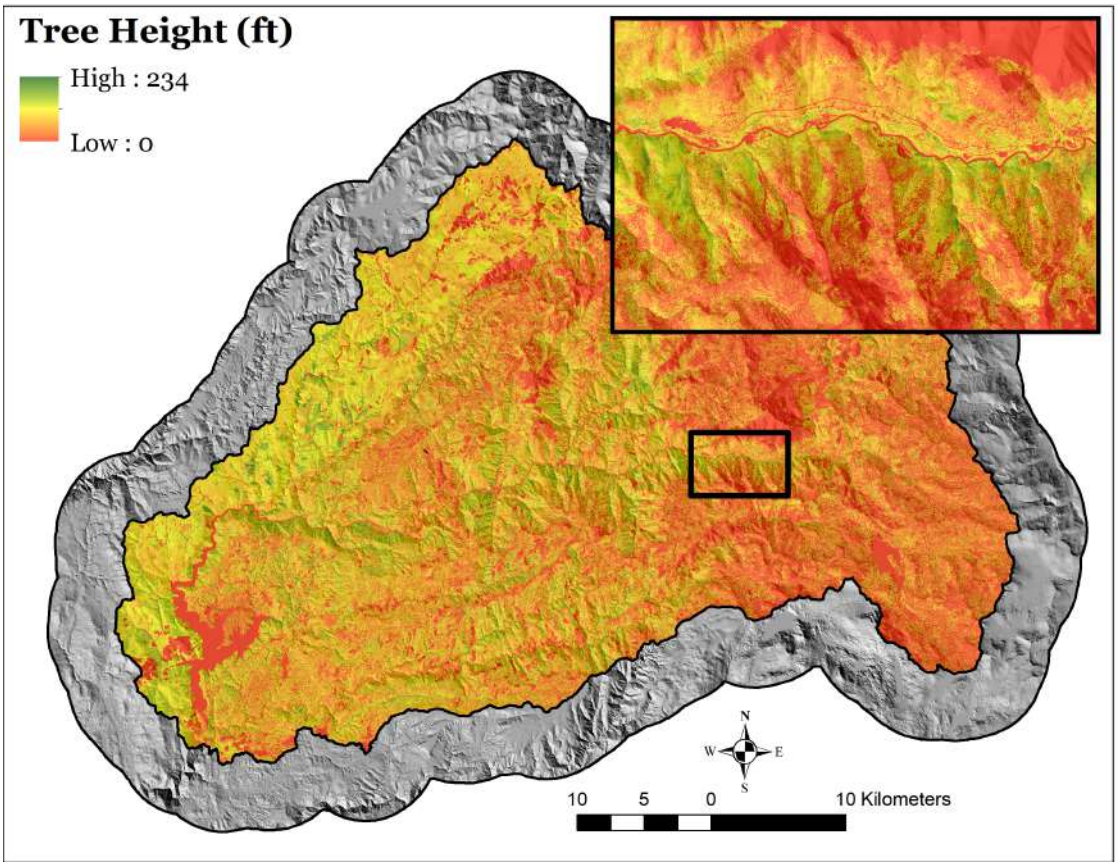

Figure A.24: Map of the Tree Height (ft) layer for the Yuba River landscape (displayed with hillshading).

The Tree Height layer was derived from the Age, Site Index and Cover type layers. We computed Tree Height only for cells classified as forest with an established tree; all other cells were assigned the value zero. The creation of the Tree Height layer is described in detail in the main text, and thus only briefly summarized here.

- First, we used Forest Inventory and Analysis (FIA) data from the Northern Sierra ecoregion and Non-Linear Quantile Regression (NLQR) estimation to fit the following Monomolecular function for a range of quantiles (also referred to a Tau in QR) for non-mafic forest cover types pooled. Specifically, we fit the following Monomolecular function to Tau values ranging from 0.01 - 0.99 at intervals of 0.01:

  $$H_{it} = (b_0 + b_3 SI_i)(1 - e^{-b_2 TA_{it}})$$

  where: b_0 - b_2 were estimated parameters; SI_i = site index of the i^{th} cell; TA_{it} = total tree age of the i^{th} cell in the t^{th} timestep; and H_{it} = predicted tree height (ft) of the i^{th} cell in the t^{th} timestep. Note, the site index variable in this equation was our custom Site Index variable (described previously).

  Each Tau value produced a unique set of estimates for the parameters of the Monomolecular function, and thus produced a site index curve that varied slightly in shape as the Tau value

increased. The result was a set of polymorphic site index curves that captured the full range of the observed height growth relationships. In addition, there were insufficient data to model height growth separately for ultramafic sites, and based on additional analyses chose to use the fitted model above but reduce height growth by 15 % for ultramafic sites.

- Next, we randomly assigned a Tau value to each cell to indicate whether that cell would realize a site index curve above or below the average for the cell's Site Index. For this purpose, we created an index layer that partially preserved the spatial autocorrelation in the Site Index layer. Thus, we simply assigned a random Tau value drawn from a normal distribution with a mean of 0.5 and a standard deviation equal to that observed in the normalized residuals from the fitted equation above (i.e., 0.12) to each cluster of cells with the same index value, ensuring that the random Tau values fell within the range 0.01 - 0.99 corresponding to the range of Tau values fitted.
- Lastly, at each timestep we applied the fitted equation above corresponding to the cell's cover type and Tau to predict tree height.

Tree Size (QMD) and Tree Size Class

The Tree Size layer represented the quadratic mean diameter (QMD) of established trees in the neighborhood of the focal cell (**Figure A.25**). Tree Size was treated as a dynamic variable in the model, meaning that it potentially changed with each timestep. Tree Size was created primarily for the purpose of characterizing and quantifying landscape structure.

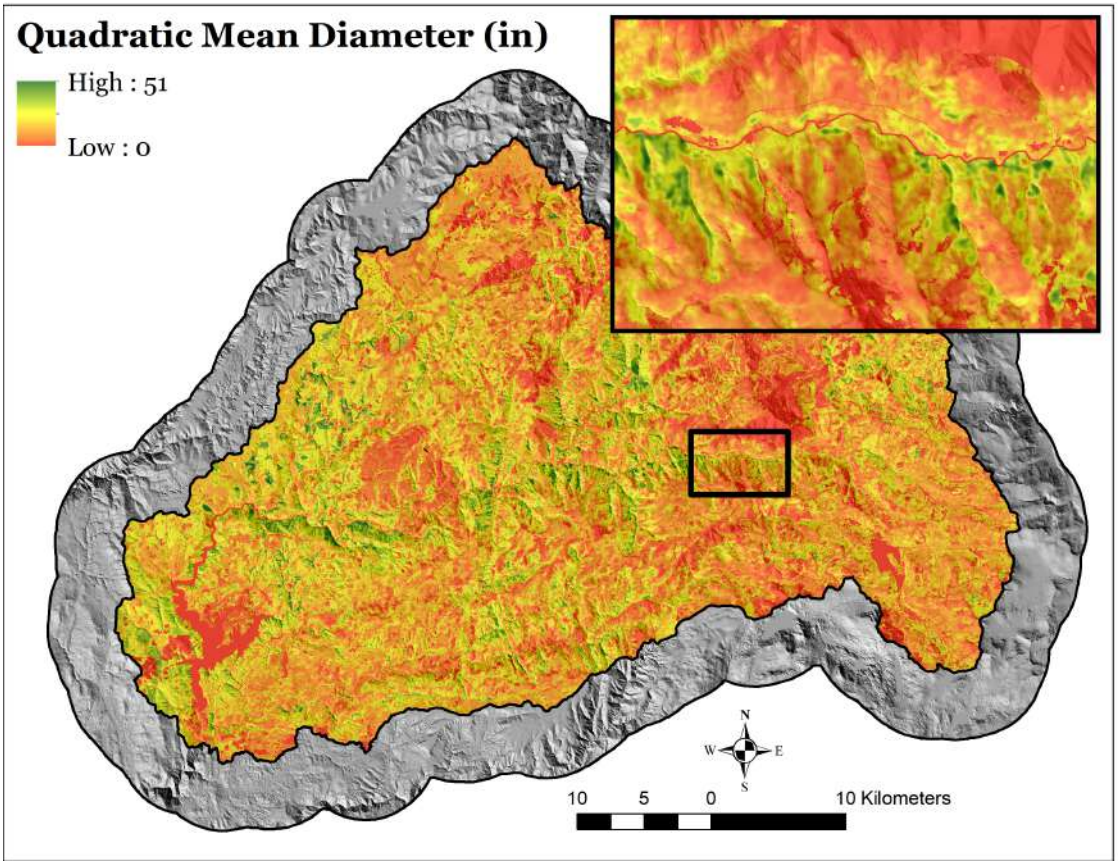

Figure A.25: Map of the Tree Size (Quadratic Mean Diameter, QMD) layer for the Yuba River landscape (displayed with hillshading).

The Tree Size layer was derived from the Tree Diameter layer. We computed Tree Size only for cells classified as forest; all other cells were assigned the value zero. Tree Size was calculated as follows:

- First, we constructed a uniform circular kernel with a radius of 40 m. The resulting kernel in its raster form gave equal weight to all cells within 40 m of the focal cell.
- Second, we computed QMD as follows:

$$Q_{it} = \sqrt{\frac{\sum d_{ijk}^2}{n_{it}}}$$

where: $d_{ijk}{}^2$ = diameter at breast height of the k^{th} cell with an established tree within the window of the i^{th} cell in the t^th timestep; n_{it} = number of cells with an established tree within the window of the i^{th} cell in the t^{th} timestep; and Q_{it} = QMD (in) of the i^{th} cell in the t^{th} timestep. Note, QMD was computed for all forested cells regardless of whether the focal cell had an established tree or not; thus, it was a measure of the neighborhood QMD centered on the forested focal cell. All non-forest cells were assigned a QMD of 0.

- Lastly, we classified QMD into tree size classes, applying the same thresholds for all forest cover types, plus a zero class for all non-forest cells and forested cells without established trees (i.e., developmental stage = 4), as follows:

  - QMD $\leq$ 1 in -> Tree Size class 1 (non-established trees or seedlings)
  - QMD 1.1 - 5.9 in -> Tree Size class 2 (Sapling)
  - QMD 6 - 10.9 in -> Tree Size class 3 (Pole)
  - QMD 11 - 23.9 in -> Tree Size class 4 (Small-tree)
  - QMD 24 - 29.9 in -> Tree Size class 5 (Medium-tree)
  - QMD $\geq$ 30 in -> Tree Size class 6 (Large-tree)

Vegetation State

The Vegetation State layer represented the discrete states of vegetation composition and structure that a cover type could exist in during the simulation and was a primary geospatial layer input to LDSim (**Figure A.26**). Vegetation State was treated as a dynamic variable in the model, meaning that it potentially changed with each timestep. Vegetation State was created primarily for the purpose of characterizing and quantifying landscape structure.

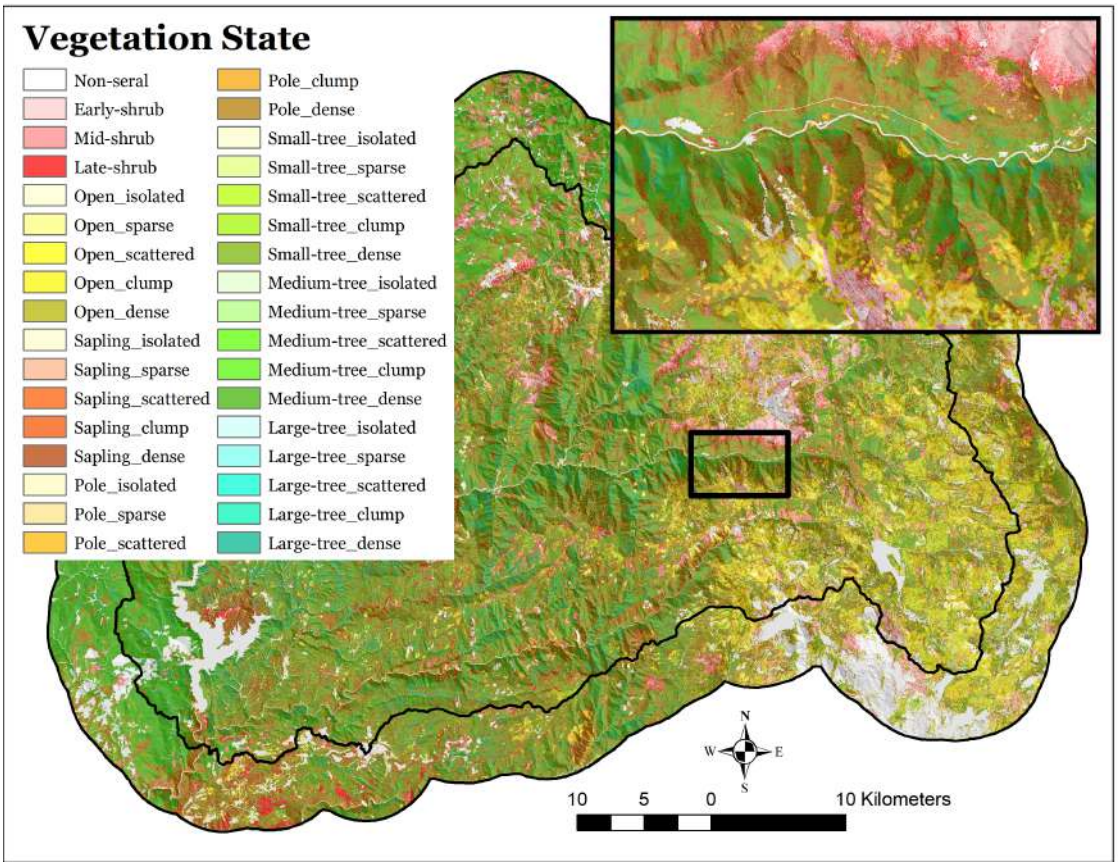

Figure A.26: Map of the Vegetation States layer for the Yuba River landscape (displayed with hillshading).

The Vegetation State for non-seral cover types remained constant (i.e., there was only a single state defined). The Vegetation State for seral cover types was derived from the combination of Developmental Stage and Tree Cover. However, since shrublands did not have varying Tree Cover classes, their final states were equivalent to their Developmental Stage (Early-shrub, Mid-shrub, and Late-shrub). The final set of Vegetation States were as follows:

Class	State	Abbreviation
0	Non-seral	NS
10	Early-shrub	EARLY_SHRUB
20	Mid-shrub	MID_SHRUB
30	Late-shrub	LATE_SHRUB
41	Open_isolated	OPEN_ISO
42	Open_sparse	OPEN_SPARSE
43	Open_scattered	OPEN_SCAT

(continued)

Class	State	Abbreviation
44	Open_clump	OPEN_CLUMP
45	Open_dense	OPEN_DENSE
51	Sapling_isolated	SAPLING_ISO
52	Sapling_sparse	SAPLING_SPARSE
53	Sapling_scattered	SAPLING_SCAT
54	Sapling_clump	SAPLING_CLUMP
55	Sapling_dense	SAPLING_DENSE
61	Pole_isolated	POLE_ISO
62	Pole_sparse	POLE_SPARSE
63	Pole_scattered	POLE_SCAT
64	Pole_clump	POLE_CLUMP
65	Pole_dense	POLE_DENSE
71	Short-tree_isolated	SHORT_ISO
72	Short-tree_sparse	SHORT_SPARSE
73	Short-tree_scattered	SHORT_SCAT
74	Short-tree_clump	SHORT_CLUMP
75	Short-tree_dense	SHORT_DENSE
81	Medium-tree_isolated	MEDIUM_ISO
82	Medium-tree_sparse	MEDIUM_SPARSE
83	Medium-tree_scattered	MEDIUM_SCAT
84	Medium-tree_clump	MEDIUM_CLUMP
85	Medium-tree_dense	MEDIUM_DENSE
91	Tall-tree_isolated	TALL_ISO
92	Tall-tree_sparse	TALL_SPARSE
93	Tall-tree_scattered	TALL_SCAT
94	Tall-tree_clump	TALL_CLUMP
95	Tall-tree_dense	TALL_DENSE

Vegetation State Age

The Vegetation State Age layer represented the number of years in the current Vegetation State and was a primary geospatial layer input to LDSim (**Figure A.27**). Vegetation State Age was treated as a dynamic variable in the model, meaning that it potentially changed with each timestep. As with Age, for non-seral cover types Vegetation State Age was treat as constant and given a null value (9998). For seral cover types Vegetation State Age represented the number of years in the current Developmental Stage. Note, we used Developmental Stage instead of Vegetation State here since Developmental Stage represented the primary successional gradient. The Tree Cover class that combined with Developmental Stage to form the Vegetation States was considered more of a secondary attribute created for the purpose of describing landscape structure. Vegetation State Age was an input to LDSim and tracked during the simulation, but in this particular application it was not used in any of the succession and wildfire disturbance models so it was essentially benign.

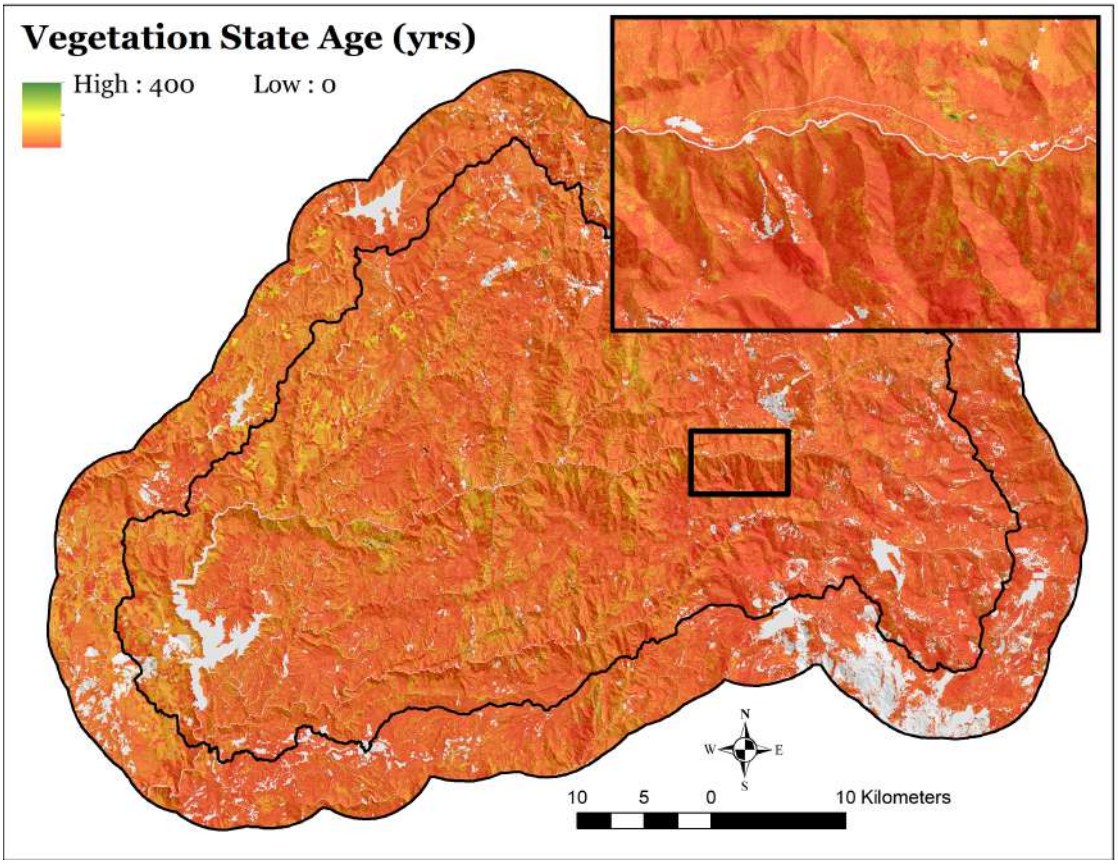

Figure A.27: Map of the Vegetation State Age layer (units = years) for the Yuba River landscape (displayed with hillshading).

Nevertheless, the initial Vegetation State Age layer was derived as follows:

Non-mafic forest: For the non-mafic forest cover types we derived Vegetation State Age by subtracting the current Age from the minimum Age for each Developmental Stage. We computed the minimum Age for each Developmental Stage by substituting the minimum canopy height in the vegetation growth equations that we developed to predict Age from vegetation height and Site Index, as follows:

$$A_{it} = \frac{log(1 - \frac{H_{it}}{b_0 + b_2 S_i})}{-b_1} - 7$$

- Developmental Stage 4 (Open):

$$V_{it} = 0$$

- Developmental Stage 5 (Sapling):

$$V_{it} = A_{it} - \frac{log(1 - \frac{4.5}{25.1311947 + 2.1416027 S_i})}{-0.0079204} - 7$$

- Developmental Stage 6 (Pole):

$$V_{it} = A_{it} - \frac{log(1 - \frac{25}{25.1311947 + 2.1416027 S_i})}{-0.0079204} - 7)$$

- Developmental Stage 7 (Short-tree):

$$V_{it} = A_{it} - \frac{log(1 - \frac{50}{25.1311947 + 2.1416027 S_i})}{-0.0079204} - 7)$$

- Developmental Stage 8 (Medium-tree):

$$V_{it} = A_{it} - \frac{log(1 - \frac{75}{25.1311947 + 2.1416027 S_i})}{-0.0079204} - 7)$$

- Developmental Stage 9 (Tall-tree):

$$V_{it} = A_{it} - \frac{log(1 - \frac{125}{25.1311947 + 2.1416027 S_i})}{-0.0079204} - 7)$$

where: b_0 - b_2 were estimated parameters; A_{it} = Age of the i^{th} cell in the t^{th} timestep; S_i = Site Index of the i^{th} cell; and V_{it} = Vegetation State Age of the i^{th} cell in the t^{th} timestep. Note the subtraction of 7 years to adjust from total tree age to breast height Age.

Ultramafic forest: For the ultramafic forest cover types we derived Vegetation State Age by subtracting the current Age from the minimum Age for each Developmental Stage. We computed the minimum Age for each Developmental Stage by substituting the minimum canopy Height in the vegetation growth equations that we developed to predict Age from vegetation Height and Site Index for the ultramafic forest cover types, which involved a 15 % reduction in Height for a given Age and Site Index, as follows:

- Developmental Stage 4 (Open):

$$V_{it} = 0$$

- Developmental Stage 5 (Sapling):

$$V_{it} = A_{it} - \frac{log(1 - \frac{4.5}{0.85(b_0 + b_2 S_i)})}{-b_1} - 10$$

- Developmental Stage 6 (Pole):

$$V_{it} = A_{it} - \frac{log(1 - \frac{25}{0.85(b_0 + b_2 S_i)})}{-b_1} - 10$$

- Developmental Stage 7 (Short-tree):

$$V_{it} = A_{it} - \frac{log(1 - \frac{50}{0.85(b_0 + b_2 S_i)})}{-b_1} - 10$$

- Developmental Stage 8 (Medium-tree):

$$V_{it} = A_{it} - \frac{log(1 - \frac{75}{0.85(b_0 + b_2 S_i)})}{-b_1} - 10$$

- Developmental Stage 9 (Tall-tree):

$$V_{it} = A_{it} - \frac{log(1 - \frac{125}{0.85(b_0 + b_2 S_i)})}{-b_1} - 10$$

Note the subtraction of 10 years to adjust from total tree age to breast height Age.

Shrublands: For the shrubland cover types we derived Vegetation State Age by subtracting the current Age from the minimum Age for each Developmental Stage, as follows:

- Developmental Stage 1 (Open):

$$V_{it} = A_{it}$$

- Developmental Stage 4 (Young):

$$V_{it} = A_{it} - 20$$

- Developmental Stage 5 (Mature):

$$V_{it} = A_{it} - 60$$

Water Balance Deficit

The Water Balance Deficit (WBD) layer represented the potential water balance deficit (mm) based on the difference between an estimate of Potential Evapotranspiration (PET) and an estimate of Actual Evapotranspiration (AET) (**Figure A.28**). WBD was treated as a static variable, meaning that it remained constant throughout the simulation. WBD served as in input to the derivation of other layers and not as a direct input to LDSim. Specifically, WBD was an input to the Mesic Index which was a component of the composite Site Index layer, which were used in the vegetation succession model to affect vegetation establishment and growth following a high-mortality disturbance, as described in detail in the main text.

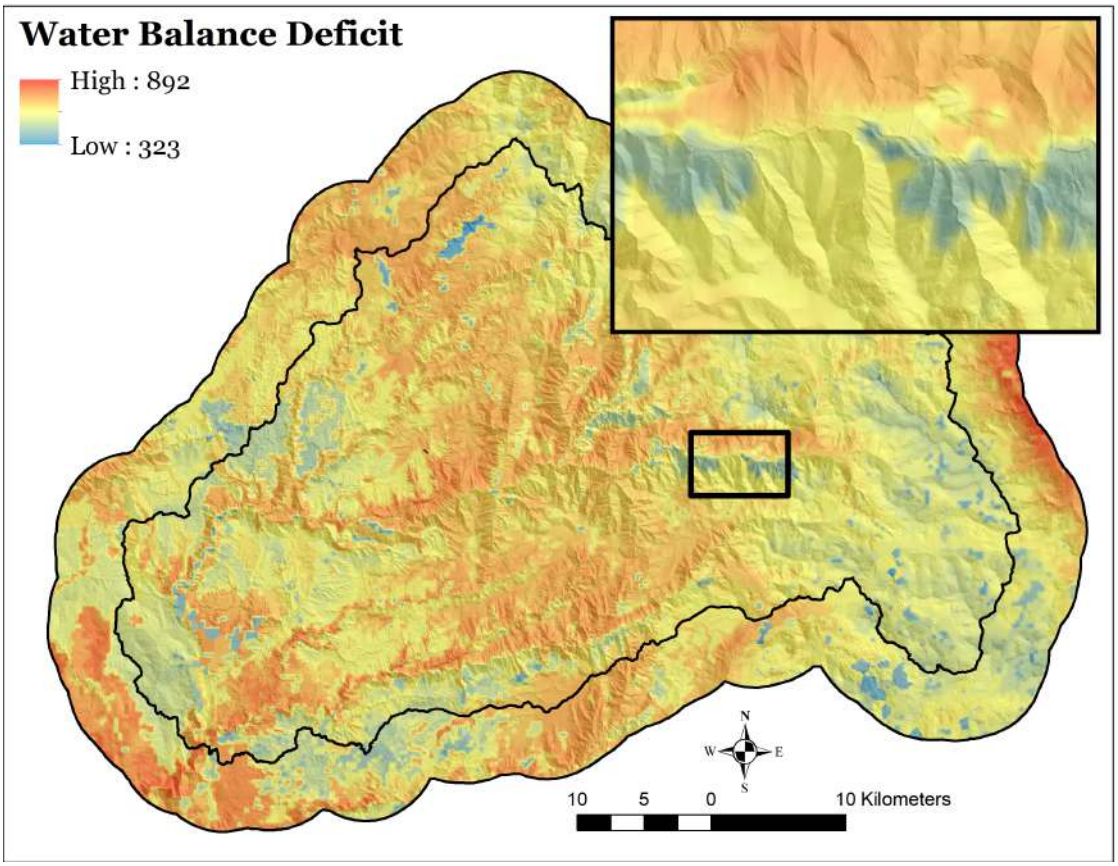

Figure A.28: Map of the Water Balance Deficit (WBD) layer (units = mm) for the Yuba River landscape (displayed with hillshading).

The WBD layer was derived from the California Landscape Conservation Partnership Climate Commons 2014 California BCM (Basin Characterization Model) Downscaled Climate and Hydrology - 30-year Summaries for the period 1981 - 2020 at 270m resolution (http://climate.calcommons.org/dataset/2014-CA-BCM).

We difference the PET and AET rasters in R to create the raw WBD layer. We rescaled WBD using z-scores based on benchmarks derived from the Northern Sierra ecoregion (**Table A.1**) and range-rescaled the result, as described above for the Energy Index. The final index had a theoretical range of 0 - 100. We processed the final raster in R to project and resample to our landscape 5 m reference raster.

Appendix B - Yuba River Landscape Historical Range of Variability and Current Landscape Departure

DRAFT Report

Kevin McGarigal Becky Estes Scott Conway Danielle Perrot
Marilyn Tierney Terri Walsh Christina Liang Laurie Perrot
Edward Smith

June, 2022

Authors

- Kevin McGarigal is a landscape ecologist with Vibrant Planet, proprietor of LandEco Consulting and retired professor of landscape ecology at the University of Massachusetts, Amherst. He received a B.S. in Forestry and Wildlife from Virginia Tech, an M.S. in Wildlife Science from Oregon State University, and a Ph.D. in Forest Science from Oregon State University.
- Becky Estes is the Central Sierra Province Ecologist (Tahoe, Eldorado, Stanislaus, and Lake Tahoe Basin Management Unit), Pacific Southwest Region, USDA Forest Service. She received a Ph.D. in Forestry from Auburn University and is a Certified Ecologist with the Ecological Society of America.
- Scott Conway is the chief resilience officer with Vibrant Planet and former forest ecologist with Pacific Southwest Region, USDA Forest Service Remote Sensing Lab and Truckee District Ranger, Tahoe National Forest, Pacific Southwest Region, USDA Forest Service. He received a B.S. in Natural Resources Management from Colorado State University.
- Danielle Perrot is an applied ecologist with Vibrant Planet. She received a B.S. in Environmental Science from University of California, Los Angeles and an M.A. in Geography with a Graduate Certificate in Hydrologic Sciences from University of Colorado, Boulder.
- Marilyn Tierney is retired District Biologist for the Yuba River Ranger District, Tahoe National Forest, Pacific Southwest Region, USDA Forest Service. She received a B.S. in Biology and an M.A. in Biology with an emphasis in Ecology and Systematics from San Francisco State University.
- Terri Walsh is retired silviculturist for the Tahoe National Forest, Pacific Southwest Region, USDA Forest Service. She is a certified silviculturist and studied Forestry at Cal Poly San Luis Obispo.
- Christina Liang is Forest Biologist for the Tahoe National Forest, Pacific Southwest Region, USDA Forest Service. She received a Ph.D. in Ecology from University of California, Davis.
- Laurie Perrot is Forest Environmental Coordinator for the Tahoe National Forest, Pacific Southwest Region, USDA Forest Service. She received a B.S. in forestry from the University of California, Berkeley.
- Edward Smith is Senior Forest Ecologist and Fire Manager for The Nature Conservancy in California. He received a B.A. in Biology from the University of California, San Diego and a M.S. in Forestry from Northern Arizona University.

Preface

This document[1] is an appendix to the Northern Sierra Historical Range of Variability and Current Landscape Departure General Technical Report (GTR) and includes detailed results for the Yuba River landscape. Importantly, the background and detailed methods behind these results are presented in the GTR and not repeated here, and thus it behooves the reader to review the GTR before interpreting these results. In addition, here we present details pertaining the Landscape Disturbance-Succession Model parameterization and calibration specific to this focal landscape; all other model parameterization and calibration generalized to the Northern Sierra ecoregion is presented in the GTR. Lastly, here we present results specific to this focal landscape, but with minimal interpretation or discussion of these results or their application to management, as this was all done in the GTR. The GTR describes how to interpret the results for any of the focal landscapes and how they can be applied to management; here, we simply provide the raw results specific to this focal landscape.

Note, all datasets associated with the results for this focal landscape can be made available. Please contact Becky Estes, becky.estes@usda.gov for access.

---

[1] In accordance with Federal law and U.S. Department of Agriculture policy, this institution is prohibited from discriminating on the basis of race, color, national origin, sex, age, or disability. (Not all prohibited bases apply to all programs.) To file a complaint of discrimination, write USDA, Director, Office of Civil Rights, Room 326-W, Whitten Building, 1400 Independence Avenue, SW, Washington, DC 20250-9410 or call (202) 720-5964 (voice and TDD). USDA is an equal opportunity provider and employer.

FOCAL LANDSCAPE

The Yuba River landscape, as we defined it, is comprised of the middle and north forks of the Yuba River watershed, a HUC8 level watershed located on the western slopes of the Sierra Nevada Mountains in the north Sierra ecoregion (**Figure 1**). The Yuba River landscape encompasses 181,549 ha and otherwise reflects the description of the north Sierra ecoregion presented in the general technical report.

Figure 1: The Yuba River landscape, including the middle and north forks of the Yuba River, defined for the purpose of simulating wildfire disturbance and vegetation succession.

MODEL PARAMETERIZATION

In this section, we present only model parameters specific to this focal landscape; all north Sierra-wide parameters are discussed in the GTR. In addition, here we do not discuss in detail the methods and use of the model parameters in LDSim, as this was already done in the GTR. Please refer to the GTR for a full understanding of how the model parameters were used in LDSim.

Wildfire Climate

Climate conditions affecting wildfire disturbance during each timestep of the simulation were governed by a single global parameter, the Wildfire Climate Index based on the Palmer Modified Drought Severity Index (PMDI), in which a single coefficient was assigned to each timestep of the simulation. The final Wildfire Climate Index trajectory represented a vector of coefficients, one for each timestep, as shown in **Figure 2**.

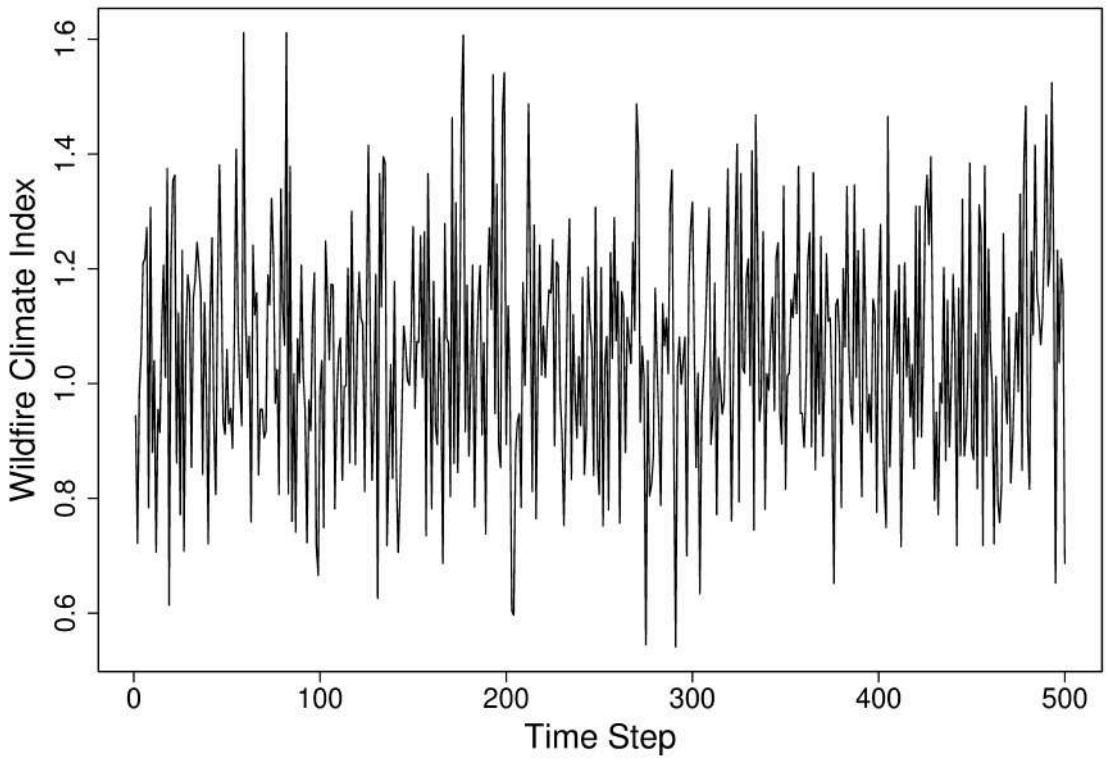

Figure 2: Wildfire Climate Index trajectory for the Yuba River landscape corresponding to 500 5-year timesteps in the simulation. The Climate Index was based on the inverted and rescaled 5-year averaged, inverse-distance weighted mean Palmer Modified Drought Severity Index (PMDI) for the sample point locations within the north Sierra ecoregion relative to the focal landscape (Yuba River watershed in this case). Note, here we inverted PMDI so that positive values represented drier conditions and negative values represented wetter conditions, and we also rescaled the index to have a standard deviation of 0.2 (see text for details).

Wildfire Susceptibility

Wildfire susceptibility for any given cell in each timestep was modeled as a complex function of fuels and climate, separately for each cover type, as described in the GTR. The final Wildfire Susceptibility Index on the probability scale (0-1) was used in the wildfire initiation and spread functions such that a value of 0 would prevent wildfires from initiating in or spreading into the cell, and as the value increased to 1 the probability of initiating a wildfire would increase as would the probability of a wildfire spreading to the focal cell from an adjacent burning cell, all other things being equal.

Briefly, we varied the beta coefficients of the wildfire susceptibility function for each cover type to reflect differences in reported historical mean fire return intervals among cover types - shifting the response curves left or right - as a means of calibrating the model to achieve target mean fire return intervals for each cover type (see Model Calibration). The calibrated wildfire susceptibility functions for each cover type are included in **Appendix B1**.

Wildfire Initiation

The number and spatial distribution of wildfire initiations in any given timestep was governed by: 1) a global wildfire initiation rate parameter that controlled the number of initiation attempts per unit area and

remained constant over time; 2) the current climate conditions, as represented by the Wildfire Climate Index, that varied over time but not space; and 3) the susceptibility to wildfire, as represented by the Wildfire Susceptibility Index, that varied over both space and time. We treated the global wildfire initiation rate as a calibration parameter - shifting it up or down to increase or decrease the overall amount of realized wildfire over time - and ultimately settled on a rate of 400 attempted initiations per 100,000 ha/year. Note, this parameter affected the attempted number of wildfire initiations, not the realized number of wildfires, which was considerably less due to the vegetation and climate conditions that affected whether an attempt (i.e., lightning strike) materialized into an actual wildfire. The realized number of wildfire initiations for the Yuba River landscape is shown in **Figure 3**.

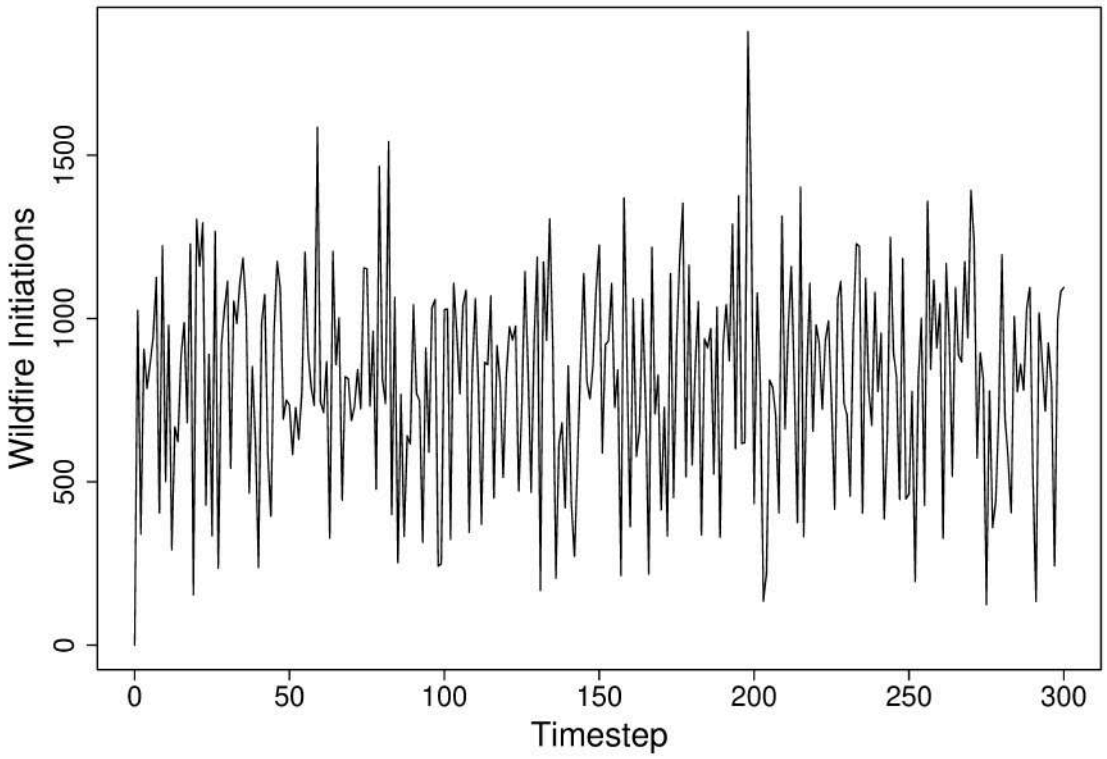

Figure 3: Realized simulated number of wildfire initiations per 5-year timestep for the Yuba River landscape.

Wildfire Mortality

Following the termination of a wildfire event the probability of high versus low mortality of the overstory vegetation in each 5 m cell that burned was determined by two major factors combined in a complex function as described in the general technical report: 1) fire intensity, which was a function of the fuel loads in the neighborhood of the focal cell (proxied by the age of the vegetation and time since the last fire), the topographic position of the focal cell, and the climate conditions of the current timestep; and 2) the resistance of the focal cell, which was a function of the age of the vegetation in the focal cell.

Briefly, we varied the beta coefficients of the resistance component of the complex function for each cover type to reflect differences in reported historical mean fire return intervals and high mortality rates among cover types - increasing or decreasing the rate of exponential decline in high mortality with increasing vegetation ages as a function of fire intensity - as a means of calibrating the model to achieve target high mortality rates for each cover type (see Model Calibration). The calibrated wildfire mortality functions for each cover type are included in **Appendix B2**.

Succession Climate

Climate conditions affecting vegetation succession during each timestep of the simulation were governed by a single global parameter, the Succession Climate Index based on the Palmer Modified Drought Severity Index (PMDI), in which a single coefficient was assigned to each timestep of the simulation. The final Succession Climate Index trajectory represented a vector of coefficients, one for each timestep, and is shown in **Figure 4**.

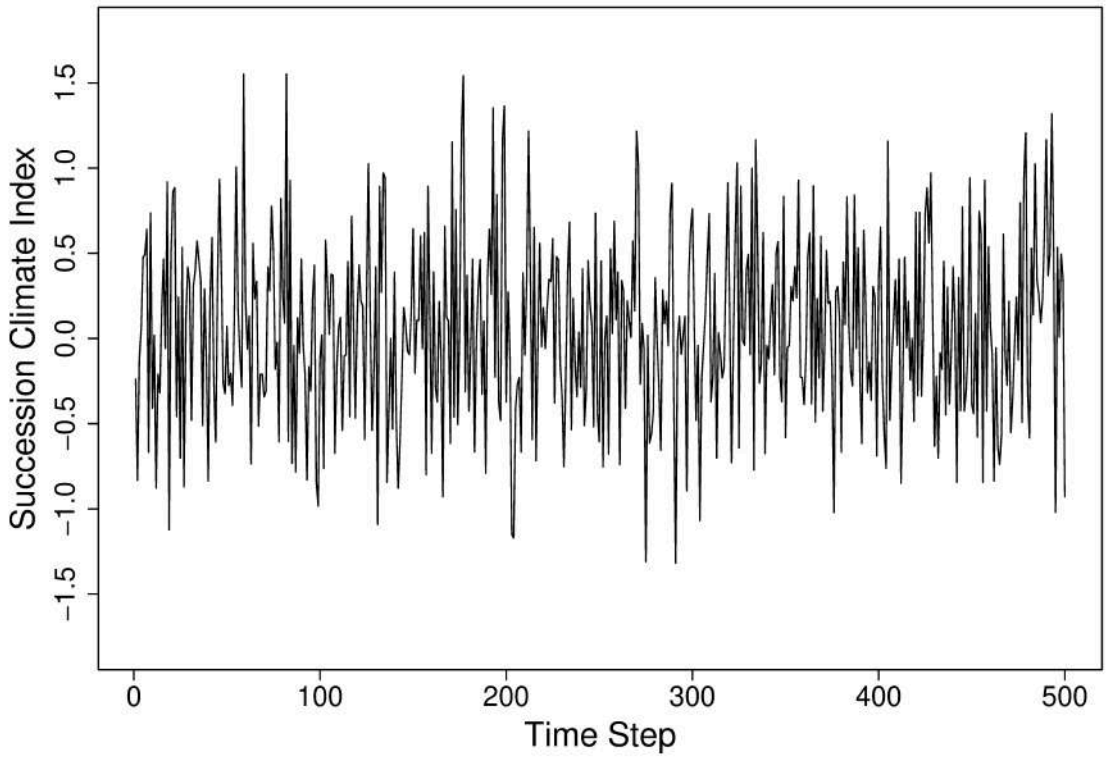

Figure 4: Succession Climate Index trajectory for the Yuba River landscape corresponding to 500 5-year timesteps in the simulation. The Climate Index was based on the inverted 5-year averaged, inverse-distance weighted mean Palmer Modified Drought Severity Index (PMDI) for the sample point locations within the north Sierra ecoregion relative to the focal landscape (Yuba River watershed in this case). Note, here we inverted PMDI so that positive values represented drier conditions and negative values represented wetter conditions (see text for details).

MODEL CALIBRATION

Although LDSim is a process-oriented model with individual parameters sourced either from data, literature, or expert opinion, the model outcomes reflect the complex spatio-temporal interactions of the various stochastic disturbance and succession processes. Consequently, it is necessary to calibrate the model by tuning (i.e., adjusting up or down) one or more of the model parameters to produce selected outcomes that are consistent with the data, literature and expert opinion. Importantly, in this context, we considered the parameters associated with the disturbance process to be "independent" variables and the

vegetation conditions (e.g., seral stage distribution, spatial patterns of vegetation states, etc.) to be "dependent" outcomes. Therefore, we calibrated select disturbance parameters (i.e., independent variables) to achieve the targeted disturbance regime without any attention to the vegetation response, which we treated as the dependent outcome of the disturbance regime. Importantly, we did not tune disturbance regime parameters to achieve desired vegetation outcomes. To calibrate the model, we focused on the following five disturbance regime attributes that we considered emergent properties of the disturbance regime, as discussed in detail in the GTR.

Fire Rotation Period

Fire Rotation Period (FRP) is the number of years required to burn a cumulative area equal to the extent under consideration. FRP combines fire frequency and fire size into a single integrated measure of how much fire is actually applied to a unit of ground. FRP is equivalent to the "point-specific" or "population" mean Fire Return Interval (FRI); i.e., the average number of years between fires to a single point on the ground (or cell), and is roughly equivalent to the oft reported "grand mean" FRI computed from a large sample of point-specific intervals (e.g., from a set of fire-scarred trees).

Briefly, we tuned the global wildfire initiation rate parameter, which controlled the number of wildfire initiation attempts per unit area within each timestep and remained constant over time (see Wildfire Initiation above), and two of the wildfire susceptibility coefficients (b_0 and b_1) for each cover type, which affected the susceptibility of fire initiation and spread in each cover type (see Wildfire Susceptibility above), and measured calibration success based on agreement with the pre-specified target FRP for each cover type. We set our calibration goal as within 10% of the target FRP for forested cover types with extents > 1,000 ha. We met our calibration target for all the forest cover types with > 1,000 ha, as shown in **Table 1**.

Table 1: Target and simulated Fire Rotation Periods (FRP) for the Yuba River landscape.

Cover type	**Area (ha)**	**Target FRP**	**Simulated FRP**	**%Deviation**
Sierra Mixed Conifer	88536	26	26	0
Mixed Evergreen	29963	45	45	0
Yellow Pine	17551	20	20	0
Red Fir	9671	50	51	2
Oak-Conifer Forest and Woodland	8675	21	21	0
Chaparral	7853	55	49	-11
Sierra Mixed Conifer_Ultramafic	3160	60	58	-3
Montane Riparian	2095	53	57	8
Mixed Evergreen_Ultramafic	1620	120	122	2
Subalpine Conifer	907	296	242	-18
Yellow Pine_Ultramafic	786	40	40	0
Lodgepole Pine	780	52	53	2
Grassland	674	60	68	13
Oak-Conifer Forest and Woodland_Ultramafic	217	42	41	-2
Total	172621	30	30	0

Fire Mortality Rate

Fire mortality rate (FMR) is the percentage of burned cells that exhibit a high-mortality response (i.e., complete overstory mortality). For the purpose of model calibration, we considered the FMR only for cells in the "short", "medium" and "tall" tree developmental stages (i.e., "mature" trees) since this was the basis for specifying the target values.

Briefly, we tuned two of the wildfire mortality coefficients (b_5 and b_6) for each cover type, which affected the probability of high mortality fire as a function of age and fire intensity in each cover type (see Wildfire Mortality above), and measured calibration success based on conformity to pre-specified fire mortality targets for each cover type. We set our calibration goal as within 10% of the targets for forested cover types with > 1,000 ha in the focal landscapes. We closely met our calibration targets for 5 of the 7 forested cover types with > 1,000 ha, and came acceptably close for the remaining 2 cover types (note, even though the percent difference was rather large, the absolute difference was relatively minor), as shown in **Table 2**.

Table 2: Target and simulated Fire Mortality Rates (FMR) for the Yuba River landscape.

Cover type	**Area (ha)**	**Target FMR**	**Simulated FMR**	**%Deviation**
Sierra Mixed Conifer	88536	7	7.34	5
Mixed Evergreen	29963	7	6.75	-4
Yellow Pine	17551	5	5.94	19
Red Fir	9671	10	11.14	11
Oak-Conifer Forest and Woodland	8675	5	5.08	2
Sierra Mixed Conifer_Ultramafic	3160	7	7.55	8
Mixed Evergreen_Ultramafic	1620	7	7.22	3
Subalpine Conifer	907	10	10.08	1
Yellow Pine_Ultramafic	786	5	5.34	7
Lodgepole Pine	780	24	25.02	4
Oak-Conifer Forest and Woodland_Ultramafic	217	5	5.20	4

Fire Size Distribution

Fire size distribution (FSD) is the percentage of realized fire sizes across bins of increasing fire size. We opted not to tune the parameters affecting the fire size distribution as these were empirically based. Instead, we treated the realized fire size distribution as an emergent outcome of the model and measured calibration success based on agreement with the pre-specified fire distribution derived from the post-settlement period of 1908 - 1979 from which we had an empirical record. We set our calibration goal as a subjective evaluation of the realized fire size distribution compared to the target fire size distribution. We met our calibration target reasonably well, as depicted in **Figure 5**.

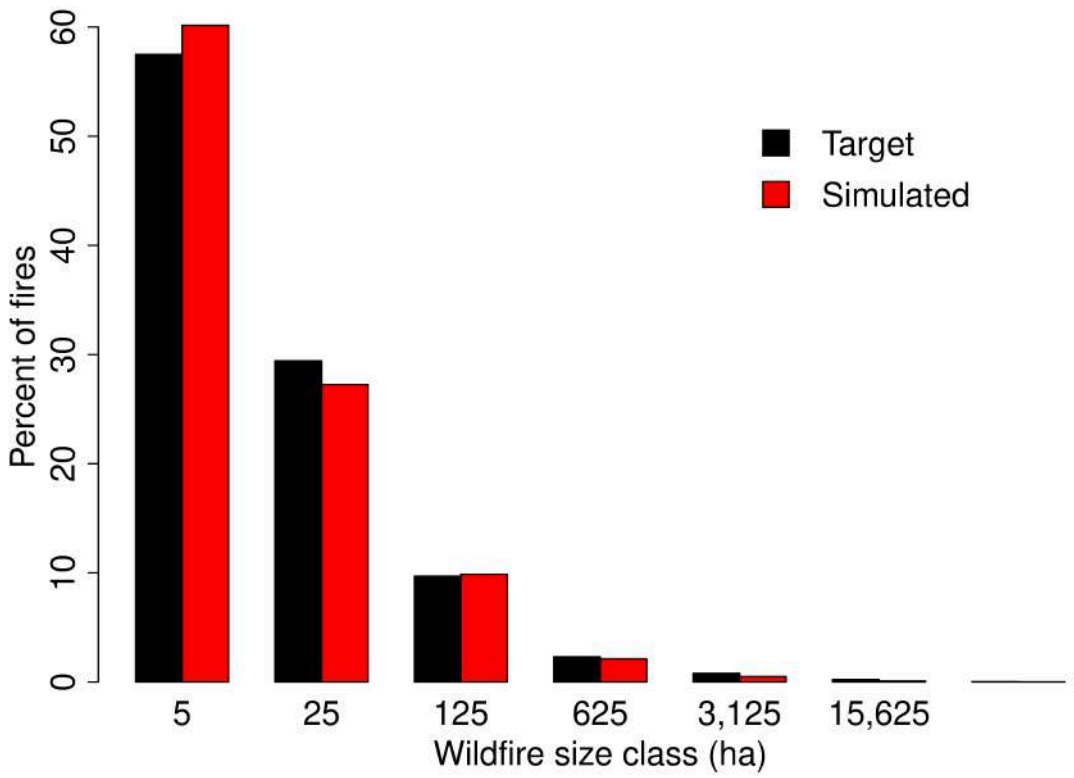

Figure 5: Target and simulated wildfire size distribution for the Yuba River landscape.

Variability in Total Area Burned

Variability in total area burned over time is a measure of the temporal variability in the wildfire disturbance regime. We opted not to tune the primary parameter affecting the temporal variability in total area burned - the Wildfire Climate Index - as it was empirically based. Instead, we treated the variability in total area burned as an emergent outcome of the model and measured calibration success based on agreement with the observed variability in total area burned for the post-settlement period of 1908 - 1979 from which we had an empirical record. We set our calibration goal as within 10% of the target coefficient of variation (CV) in total area burned per timestep (CV = 91.8%, see GTR). We met our calibration target for the Yuba River landscape, as depicted in **Figure 6**.

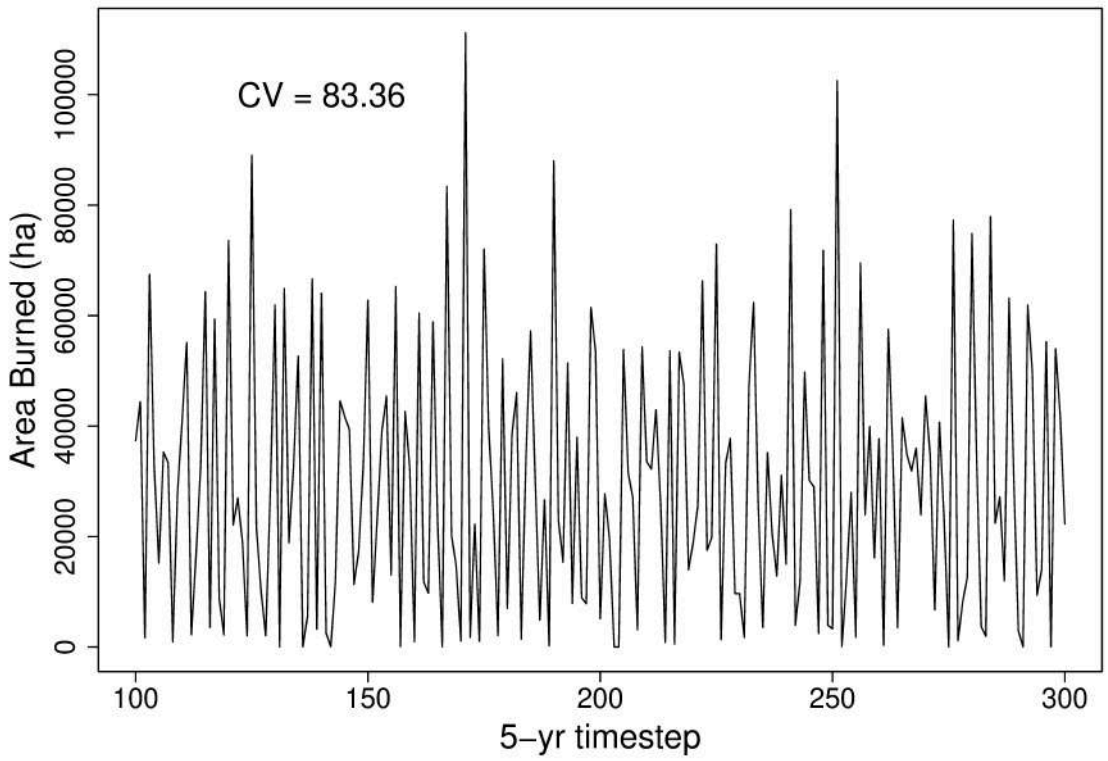

Figure 6: Total simulated area burned per 5 years in the Yuba River landscape representing the historical reference period of 1550-1850 and the computed Coefficient of Variation (CV).

Relationship Between Total Area Burned and Climate

The relationship between total area burned and climate is a measure of the degree to which the simulated total area burned is affected by variability in the specified Wildfire Climate Index. We opted not to tune the Wildfire Climate Index, in particular, or any parameter associated with the wildfire disturbance process with regards to this calibration metric. Instead, we treated the observed relationship between total area burned and the climate index as an emergent outcome of the model and measured calibration success based on agreement with the strength of the relationship for the post-settlement period of 1908 - 1979 from which we had an empirical record. We set our calibration goal as within 10% of the target coefficient of determination (R2) in the fit of a linear regression to the target data (R2 = 0.25, see GTR). In general, we failed to meet this calibration target closely for the Yuba River landscape, instead simulating a stronger relationship between total area burned and climate than we observed during the post-settlement period and simulating a distinctly non-linear relationship compared with observed post-settlement observations, as depicted in **Figure 7**.

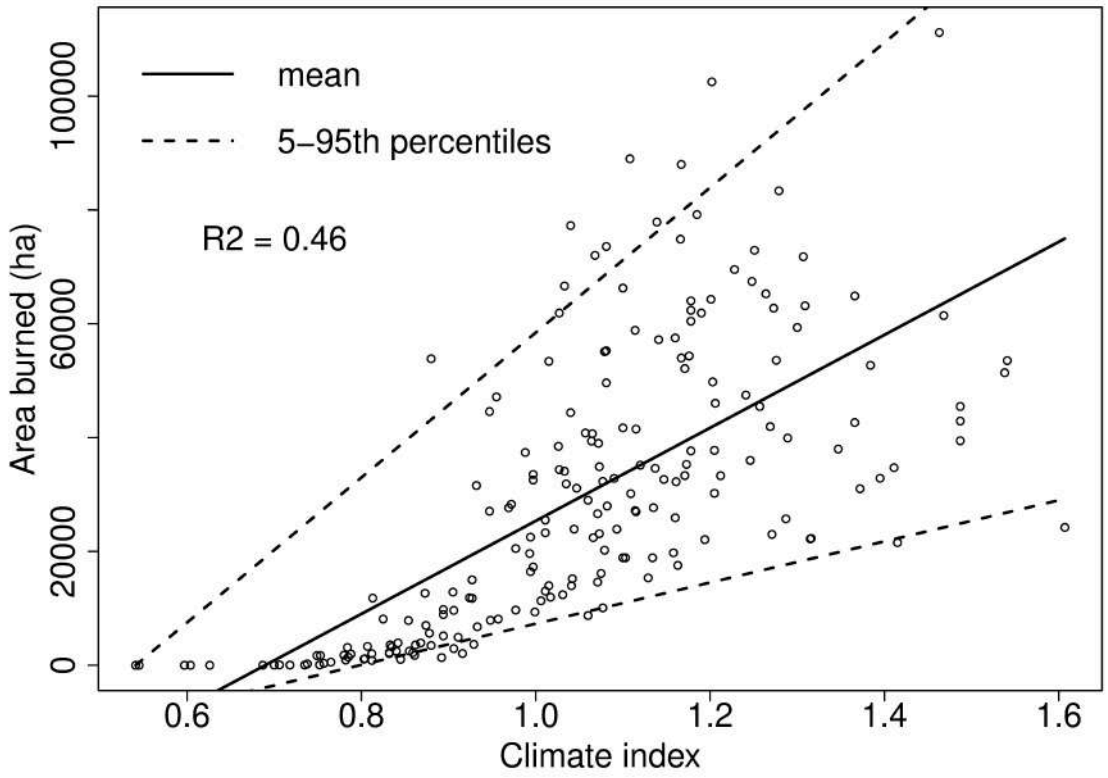

Figure 7: Scatterplot of the modified wildfire Climate Index based on the modified Palmer Drought Severity Index (see text for details) and the log of simulated total area burned per 5 years in the Yuba River landscape representing the historical reference period of 1550-1850, and the fitted linear regression for the mean and 5-95th quantiles (see text for details) along with the Coefficient of Determination (R2) of the fit.

HISTORICAL RANGE OF VARIABILITY and CURRENT DEPARTURE

Biophysical Classes and Units

To summarize HRV and current departure in landscape structure at the Site and Subbasin levels, we subdivided the landscape into a set of Biophysical Classes (BPCs), as described in detail in the GTR. Briefly, we indexed site productivity based on the cumulative tree biomass generated over the course of the simulation, after model equilibration, and then modeled tree biomass as a function of 10 geophysical variables using a Random Forest analytical framework, and lastly classified predicted Biomass into 4 equal-area classes based on quartiles of the data, plus a zero class for all non-forest cells. The final BPC layer included 4 classes ranging from the least productive to most productive sites, plus a non-forest class, as depicted in **Figure 8**.

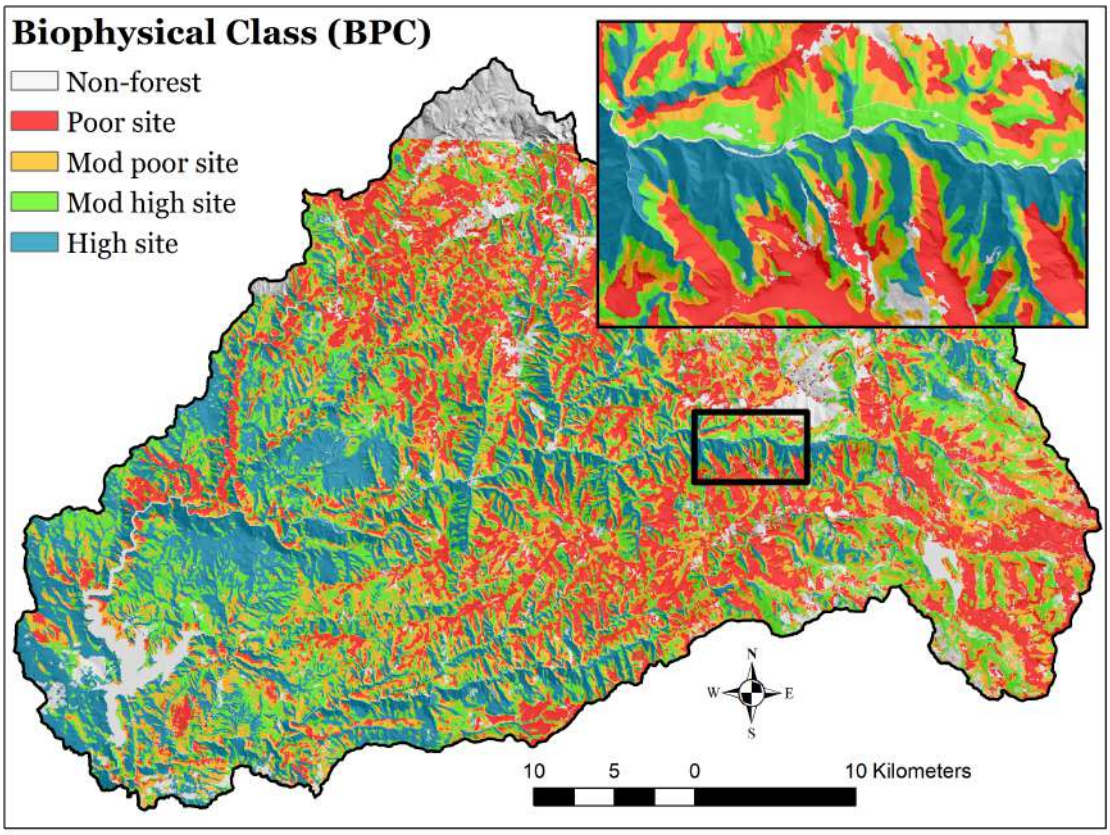

Figure 8: Biophysical Classes (BPCs) based on quartiles of predicted Biomass derived from a Random Forest model to predict Biomass (i.e., simulated cumulative tree height) from 10 biophysical variables. The Random Forest model explained ~70% of the variation in Biomass under simulated historical dynamic equilibrium conditions in the Yuba River landscape.

The final BPCs were distinguishable on the basis of the 10 geophysical variables and cover type, although there was considerable overlap among BPCs in each of the variables, as described below for a select set of the variables.

- *Cover Type* - The distribution of each cover type among BPCs (as a percentage of the cover type), ordered roughly from low to high elevation distributions, is given in **Table 3**. Most forest types were well distributed among BPCs, suggesting that cover type was generally not a good discriminator of BPCs. However, there were some notable exceptions. For example, Lodgepole Pine and Red Fir were extremely rare on Low productivity sites and Subalpine Conifer was essentially absent from High productivity sites; whereas, Yellow Pine was disproportionately found on Low and Moderately Low productivity sites. Mixed Evergreen increased in relative abundance as site productivity increased, whereas Sierra Mixed Conifer showed a weak opposite trend.

  Table 3: Percentage of each cover type in each Biophysical Class (BPC) for the Yuba River landscape.

Cover type	Area (ha)	Low	ModLow	ModHigh	High
Yellow Pine	17402	38.92	29.31	19.05	12.72
Yellow Pine_Ultramafic	781	20.04	30.72	28.09	21.15
Oak-Conifer Forest and Woodland	8548	24.06	22.07	22.14	31.73
Oak-Conifer Forest and Woodland_Ultramafic	216	8.81	21.21	28.44	41.54
Mixed Evergreen	29860	11.62	21.58	25.30	41.50
Mixed Evergreen_Ultramafic	1613	9.22	27.78	25.91	37.09
Sierra Mixed Conifer	86013	30.25	26.06	23.43	20.26
Sierra Mixed Conifer_Ultramafic	2784	10.80	23.36	25.06	40.77
Lodgepole Pine	775	7.27	24.69	50.36	17.69
Red Fir	9442	8.21	22.53	42.72	26.54
Subalpine Conifer	907	20.84	45.55	33.18	0.43

- *Mesic Index* - The distribution of the Mesic Index for each BPC (given as quantiles of the index) is given in **Table 4**. As expected, the Mesic Index distribution increased as the site productivity class increased from Low to High, but with considerable overlap in distributions between adjacent BPC classes. Despite the strong overlap, the BPC classes represented a gradient in expected site moisture, with the Low site class representing the driest sites and the High site class representing the wettest sites.

  Table 4: Distribution of the Mesic Index in each Biophysical Class (BPC), given as quantiles for the Yuba River landscape.

BPC	2.5%	25%	50%	75%	97.5%
Low	32	42	48	54	67
ModLow	32	48	56	63	78
ModHigh	39	56	63	70	85
High	50	65	73	81	96

- *Topographic Position* - The distribution of the Topographic Position Index for each BPC (given as quantiles of the index) is given in **Table 5**. As expected, the Topographic Position Index distribution decreased as the site productivity class increased from Low to High, but with considerable overlap in distributions between adjacent BPC classes. The High site productivity class showed the strongest gradient in TPI, with a strong prevalence for lower topographic positions. Despite the strong overlap, the BPC classes represented a clear gradient in topographic position, with the Low site class found more commonly on the upper slopes and ridgetops and the High site class found more commonly on the lower slopes and valley bottoms.

  Table 5: Distribution of the Topographic Position Index each each Biophysical Class (BPC), given as quantiles for the Yuba River landscape.

BPC	2.5%	25%	50%	75%	97.5%
Low	23	47	58	70	96
ModLow	10	39	50	61	86
ModHigh	6	37	47	58	82
High	0	30	44	55	78

- *Aspect* - The distribution of aspect classes among BPCs (as a percentage of the BPC) is given in **Table 6**. Not surprisingly, each BPC class was distributed across all aspect classes, but still exhibited a pronounced orientation, with the Low site class disproportionately occupying southwesterly aspects and the High site class disproportionately occupying northeasterly aspects.

  Table 6: Percentage of each Biophysical Class (BPC) in each aspect class for the Yuba River landscape.

Aspect	N	NE	E	SE	S	SW	W	NW	Flat
Low	2.66	0.91	1.26	9.39	19.12	25.94	20.30	18.93	1.48
ModLow	8.39	5.04	6.05	14.81	14.64	17.18	12.31	19.29	2.29
ModHigh	10.53	11.99	13.91	16.10	10.05	11.51	7.84	15.58	2.48
High	16.71	22.64	22.66	12.08	4.03	4.23	3.29	12.57	1.79

Fire Return Interval and Departure

Mean point-specific Fire Return Interval (FRI) represents the average number of years between fire events at the 5 m cell level. We interpreted the observed mean FRI after model equilibration (N = 200 timesteps) at the cell level as a single integrated (albeit not comprehensive) summary of the historical wildfire disturbance regime. The historical mean FRI varied from < 15 years to > 300 years across the landscape, with evident influences of both cover type and terrain (**Figure 9**).

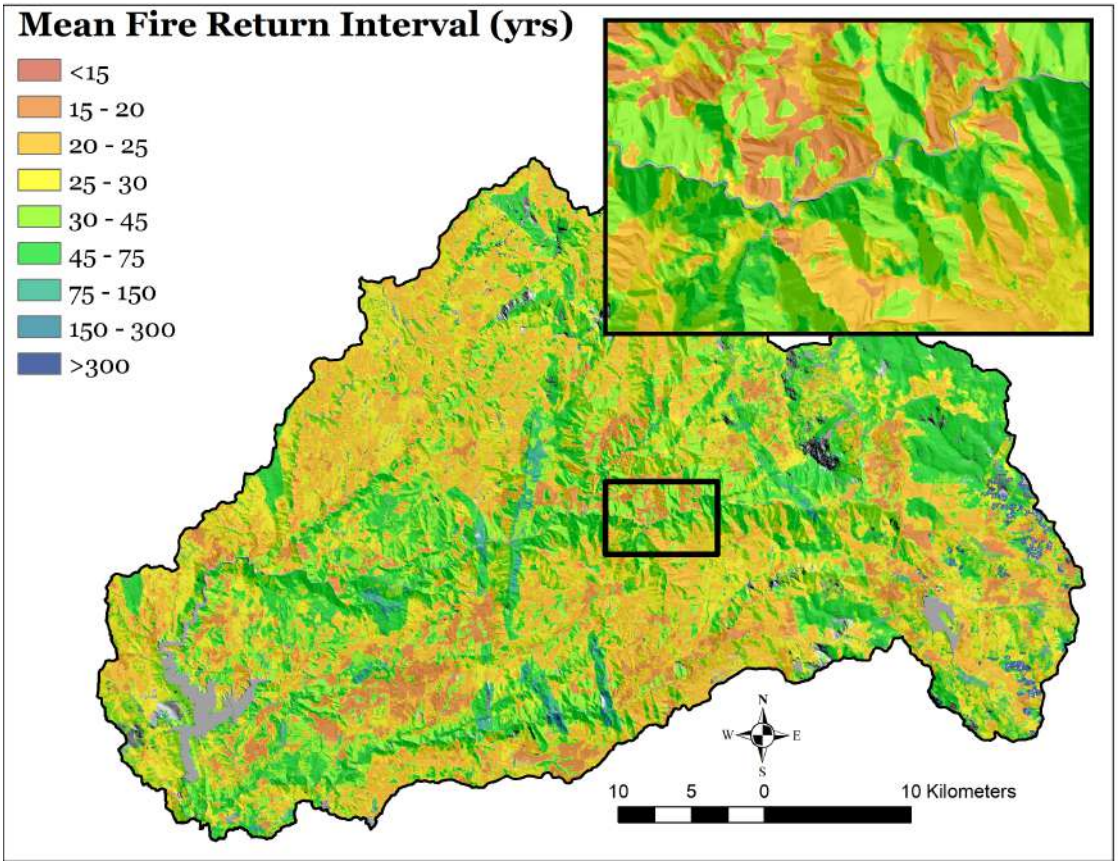

Figure 9: Simulated Fire Return Interval (FRI) (yrs) at the 5 m cell level for the Yuba River landscape.

In addition, the historical mean FRI varied among BPCs as expected (**Table 7**). Specifically, the median FRI increased steadily from 23 to 35 years with increasing site productivity; i.e., from Low to High BPC. Low productivity sites that occurred disproportionately on upper slopes and ridgetops and southwesterly aspects were warmer and drier and thus more susceptible to wildfire, despite having less fuel build-up over time. Conversely, High productivity sites that occurred disproportionately on lower slopes and valley bottoms and on northeasterly aspects were cooler and wetter and thus less susceptible to wildfire, despite having more fuel build-up over time. The relatively short median FRIs across all sites indicates that historically wildfires typically occurred frequently enough to keep surface and ladder fuel loads low enough to reduce the occurrence of high-severity wildfire.

Table 7: Range of variability (given as quantiles) in the mean fire return interval (FRI) by Biophysical Class (BPC) for the Yuba River landscape.

BPC	HRV2.5%	HRV25%	HRV50%	HRV75%	HRV97.5%
Low	16	21	23	26	52
ModLow	17	23	26	38	97
ModHigh	18	25	30	44	107
High	20	28	35	50	99

These results also indicate that the HRV in mean FRI varied several-fold across sites within each BPC. For example, on High productivity sites FRI varied roughly five-fold between 20-99 years across sites. The wide range of variation in FRI within BPCs indicates that wildfire risk varied markedly across sites even within a single BPC and, consequently, that FRI is only loosely correlated with predicted cumulative tree biomass. For example, sites classified as having high long-term productivity under historical dynamic equilibrium conditions could have FRIs as short as 20 years (or shorter for the extremes) or as long as 99 years (or longer for the extremes) depending on local topographic and vegetative conditions and chance. This is visually evident in the map of mean FRI for the High site BPC (**Figure 10**).

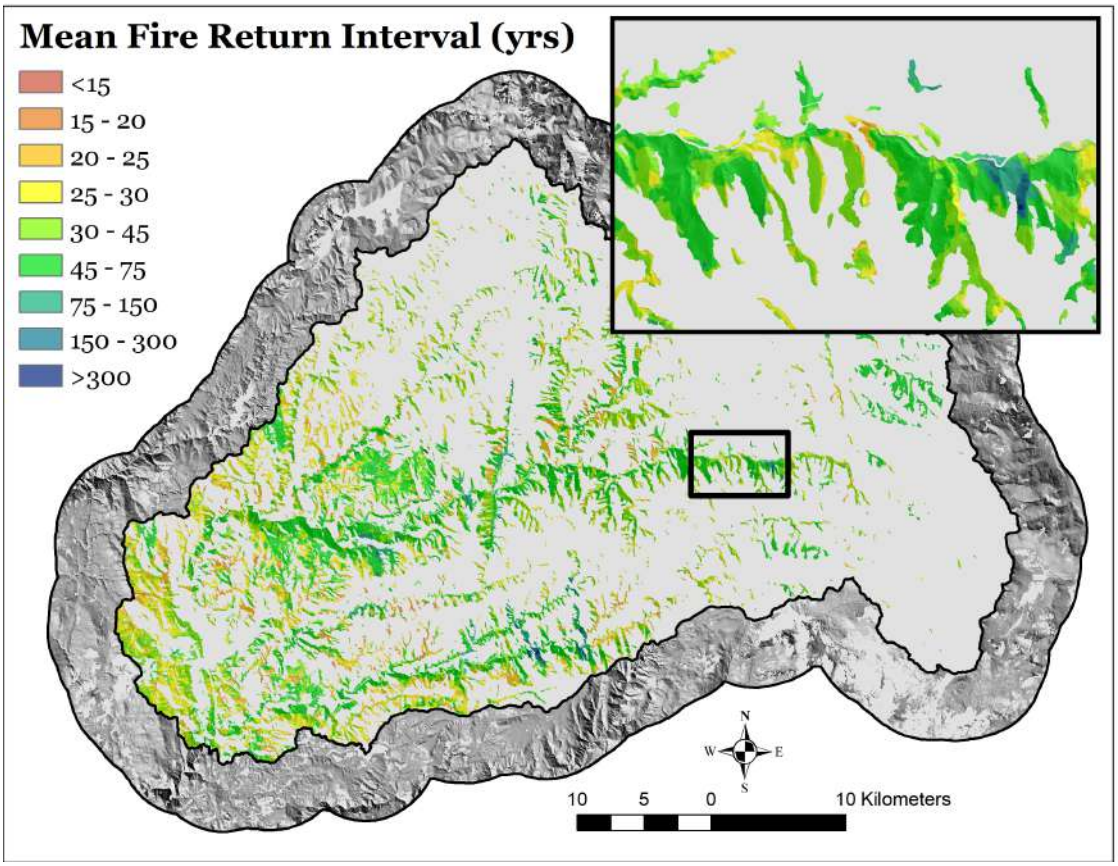

Figure 10: Simulated Fire Return Interval (FRI) (yrs) at the 5 m cell level on High productivity sites (Biophysical Class = 4) in the Yuba River landscape.

Fire Return Interval Departure (FRID) represents the percentage deviation of the contemporary (post-settlement) mean point-specific FRI from the mean point-specific FRI under historical (i.e., pre-settlement) dynamic equilibrium conditions. Briefly, FRID measures the degree, in percent, to which contemporary fires (i.e., since 1909) are burning at frequencies similar to the frequencies that occurred prior to significant Euro-American settlement, as simulated (**Figure 11**). Positive departure indicates that the contemporary fire frequency is less than the historical fire frequency. Not surprisingly most of the landscape is severely departed with respect to fire frequency.

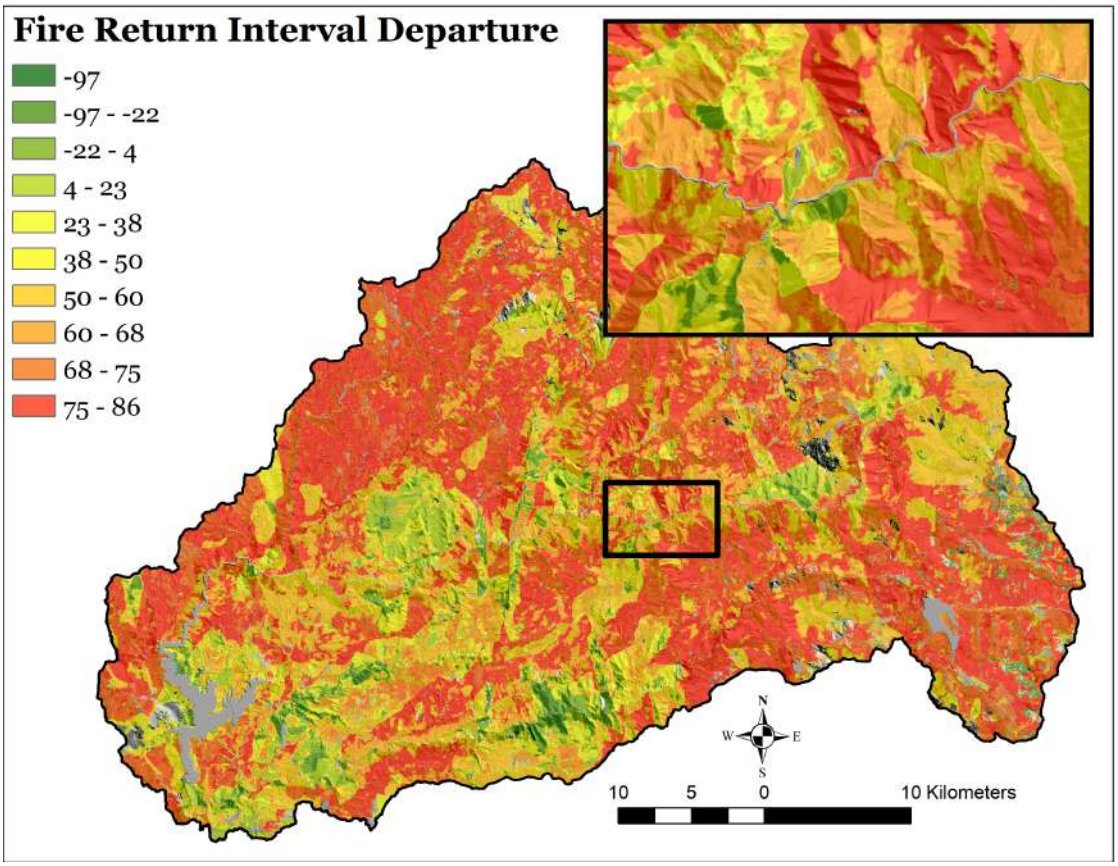

Figure 11: Fire Return Interval Departure (FRID) at the 5 m cell level in the Yuba River landscape, representing the percent to which contemporary fires (i.e., since 1909) are burning at frequencies similar to the frequencies that occurred prior to significant Euro-American settlement, as simulated. Positive values represent a contemporary FRI > the pre-settlement FRI and, conversely, negative values represent a contemporary FRI < the pre-settlement FRI.

In addition to the cell-level map of FRID, we also summarized the mean FRID for each GPU to include in the Stewardship Atlas as a means of prioritizing GPUs for treatment with fire (**Figure 12**).

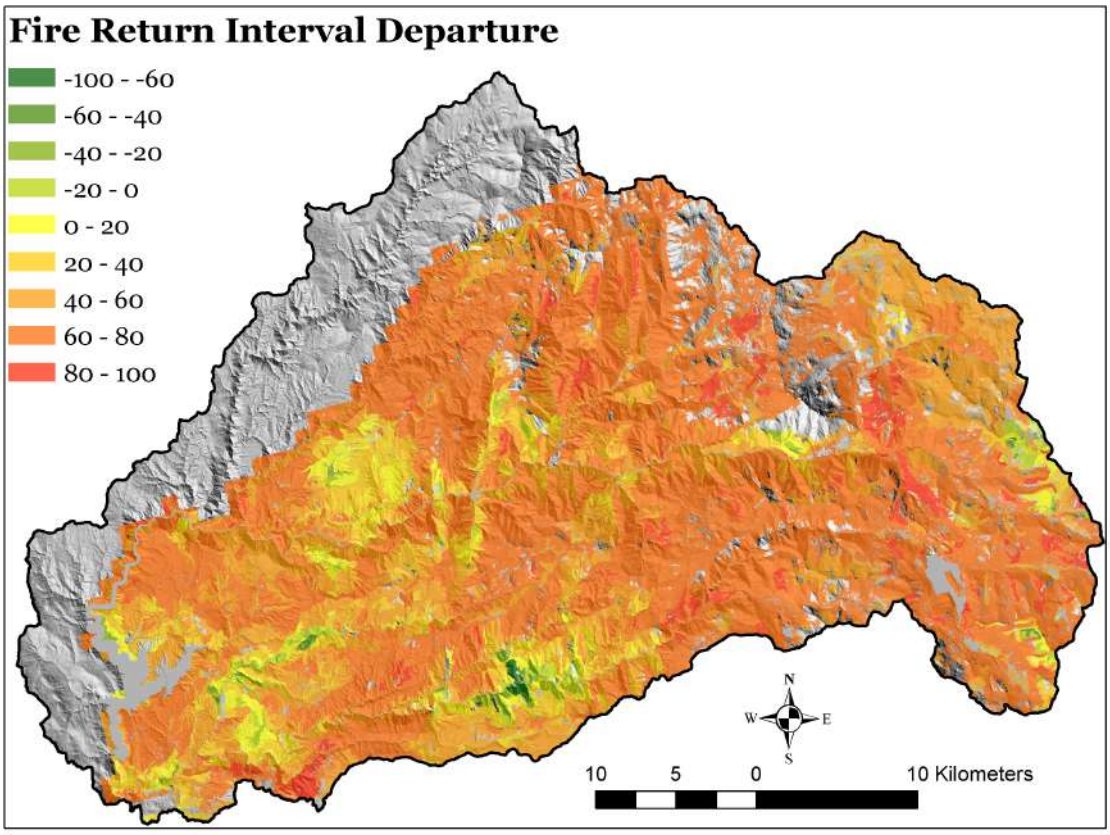

Figure 12: Geophysical Unit-level Fire Return Interval Departure (FRID) for the Yuba River landscape, representing the average 5 m cell value in the percent to which contemporary fires (i.e., since 1909) are burning at frequencies similar to the frequencies that occurred prior to significant Euro-American settlement, as simulated.

Vegtation Persistence

We defined vegetation persistence as the likelihood of persisting in either an early- or late-seral condition at the 5 m cell level. We interpreted the observed mean FRI of high-mortality wildfires after model equilibration (N = 200 timesteps) at the cell level as a proxy for vegetation persistence, under the assumption that locations with shorter high-mortality FRIs would likely persist longer in early-seral stages and, conversely, locations with longer high-mortality FRIs would likely persist longer in late-seral stages.

Figure 13 depicts several areas with relatively long high-mortality FRIs (dark blue areas in the map) and these are sites that have a high likelihood of supporting late-seral vegetation under a natural disturbance regime. Conversely, the map depicts several areas with relatively short high-mortality FRIs (yellow and orange areas in the map) and these are sites that have a high likelihood of supporting early-seral vegetation much of the time under a natural disturbance regime. Accordingly, management objectives for these areas could be designed to capitalize on these focal areas. For example, establishing treatment objectives to maintain and enhance late-seral conditions for old forest associated species in areas with a lower likelihood of high-mortality wildfire (i.e., longer FRI) would be logical.

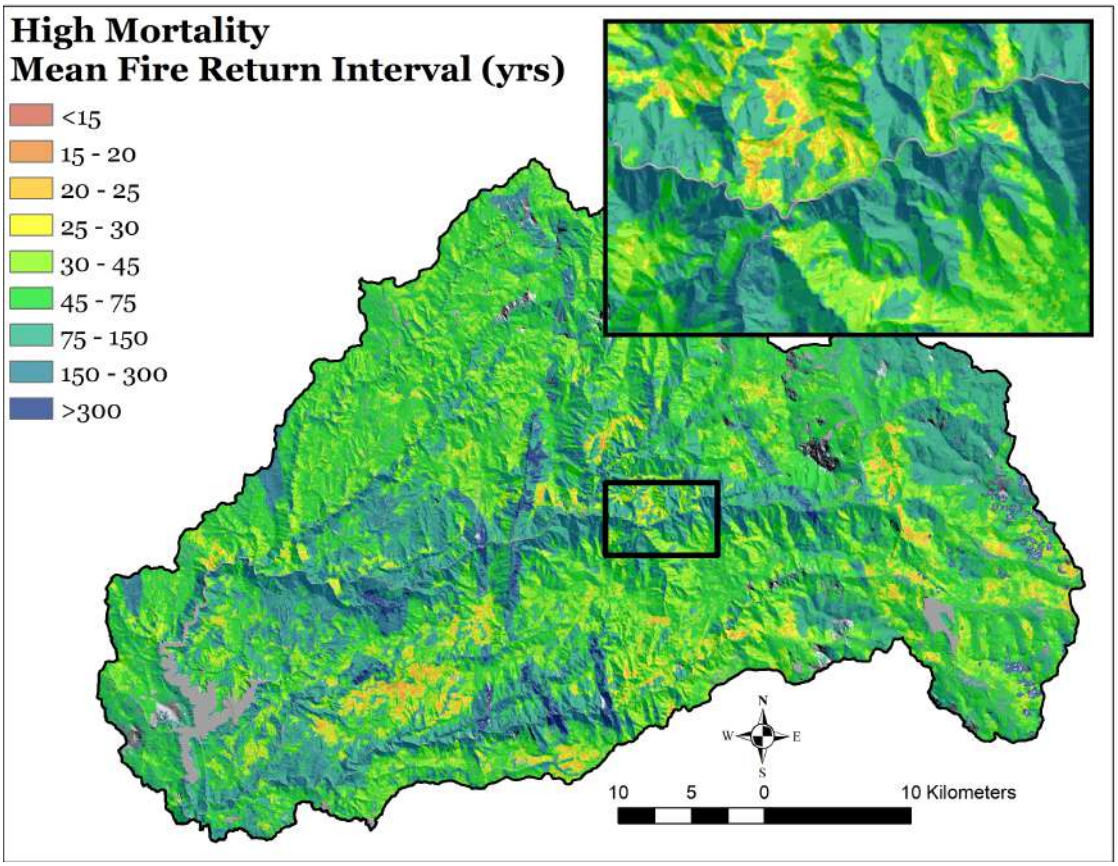

Figure 13: Simulated high-mortality Fire Return Interval (FRI) (yrs) at the 5 m cell level in the Yuba River landscape.

Site-level HRV and Departure

The results presented in this section address landscape metrics quantified at the "Site" level. Recall from the GTR that we defined a Site as a 40-m radius window around each focal cell. Here, each Site falls within a single BPC based on the location of the focal cell and has a single value computed for each landscape metric for each point in time (i.e., snapshot). HRV represents the variation in the landscape metric across Sites and over time under historical dynamic equilibrium conditions. Further recall that the current landscape also has a range of values across Sites (CRV), rather than a single value. Thus, a comparison of the HRV and CRV distributions depicts the degree to which CRV deviates from HRV (i.e., current departure). It is important to remember that Site-level departure reflects the deviation between the CRV across Sites within the focal landscape and the HRV across Sites and over time within the focal landscape. Thus, departure for a Site is not based on a comparison of the current Site condition to its own HRV (as is the case with GPU and Subbasin departure, see below); rather it is the distribution of current Site conditions across the entire landscape compared to the historical distribution across Sites that forms the basis for Site-level departure.

Recall from the GTR that we used a parsimonious suite of landscape metrics that we deemed meaningful for estimating departure at the Site-level across the focal landscape and appropriate given the available data, and computed departure as described in the GTR (and not repeated here), including the following metrics:

Metric 1: Developmental Stage

Developmental stage at the Site level was based on discrete stages of canopy height development. We quantified the composition of forest developmental stages at the Site level based on the percentage of the forested portion of the Site in each developmental stage. The HRV and CRV in Developmental Stage composition by BPC at the Site level is given in **Table 8** and depicted in **Figure 14**.

Table 8: Range of variability (given as quantiles) in each developmental stage class across sites (40-m radius window centered on each focal cell) by Biophysical Class (BPC) for the current range of variability (CRV) and the historical range of variability (HRV) for the Yuba River landscape.

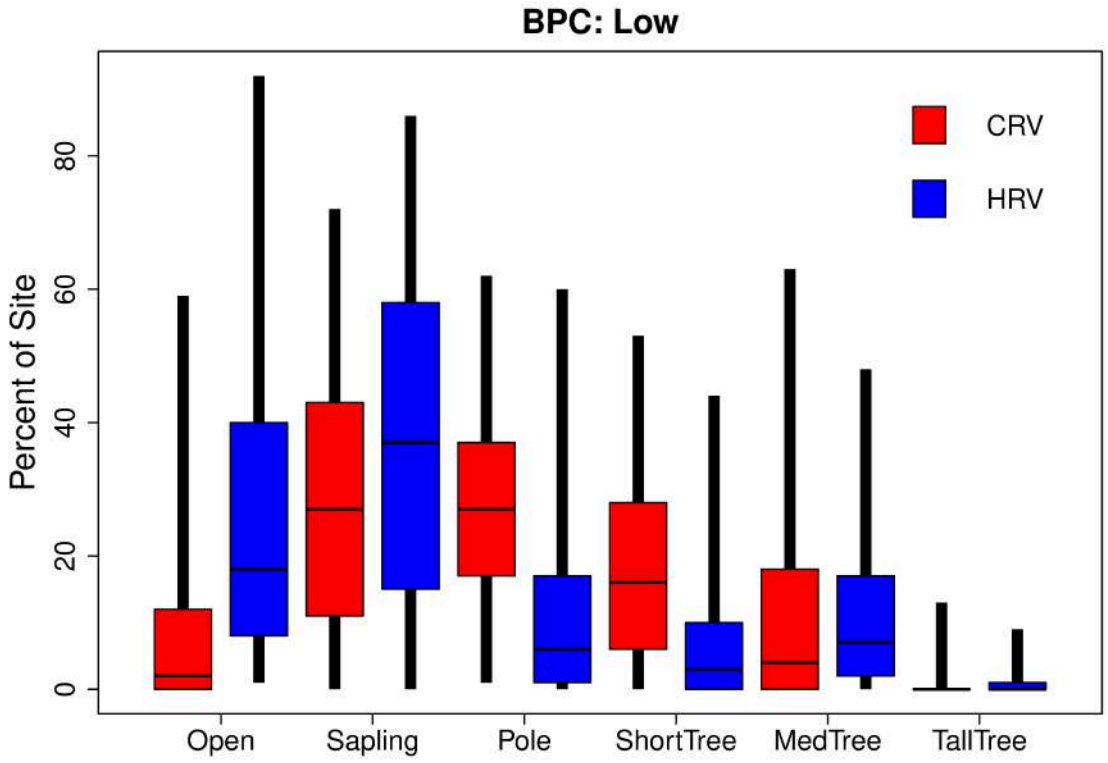

BPC	Class	Scenario	HRV 2.5%	HRV 25%	HRV 50%	HRV 75%	HRV 97.5%
Low	Open	CRV	0	0	2	12	59
Low	Open	HRV	1	8	18	40	92
Low	Sapling	CRV	0	11	27	43	72
Low	Sapling	HRV	0	15	37	58	86
Low	Pole	CRV	1	17	27	37	62
Low	Pole	HRV	0	1	6	17	60
Low	ShortTree	CRV	0	6	16	28	53
Low	ShortTree	HRV	0	0	3	10	44
Low	MedTree	CRV	0	0	4	18	63
Low	MedTree	HRV	0	2	7	17	48
Low	TallTree	CRV	0	0	0	0	13
Low	TallTree	HRV	0	0	0	1	9
ModLow	Open	CRV	0	0	1	10	54
ModLow	Open	HRV	1	6	12	28	81
ModLow	Sapling	CRV	0	6	23	41	71
ModLow	Sapling	HRV	0	12	29	49	80
ModLow	Pole	CRV	1	15	25	35	63
ModLow	Pole	HRV	0	3	9	21	59
ModLow	ShortTree	CRV	0	7	18	29	56
ModLow	ShortTree	HRV	0	1	5	14	46
ModLow	MedTree	CRV	0	0	7	26	66
ModLow	MedTree	HRV	0	6	14	26	54
ModLow	TallTree	CRV	0	0	0	0	23
ModLow	TallTree	HRV	0	0	1	4	17
ModHigh	Open	CRV	0	0	0	7	47
ModHigh	Open	HRV	1	5	9	21	72
ModHigh	Sapling	CRV	0	4	18	38	71
ModHigh	Sapling	HRV	0	8	22	41	74
ModHigh	Pole	CRV	1	13	24	34	63
ModHigh	Pole	HRV	0	4	11	23	59
ModHigh	ShortTree	CRV	0	9	19	29	56
ModHigh	ShortTree	HRV	0	2	7	15	45
ModHigh	MedTree	CRV	0	1	11	32	68
ModHigh	MedTree	HRV	1	9	19	31	59
ModHigh	TallTree	CRV	0	0	0	2	34
ModHigh	TallTree	HRV	0	1	3	9	26
High	Open	CRV	0	0	0	1	33
High	Open	HRV	1	4	8	16	61
High	Sapling	CRV	0	1	7	24	66
High	Sapling	HRV	0	2	14	30	66
High	Pole	CRV	0	9	19	32	69
High	Pole	HRV	0	4	11	23	57
High	ShortTree	CRV	0	11	20	30	57
High	ShortTree	HRV	0	3	7	15	42
High	MedTree	CRV	0	6	25	44	73
High	MedTree	HRV	1	11	21	33	59
High	TallTree	CRV	0	0	1	9	48
High	TallTree	HRV	0	6	13	22	46

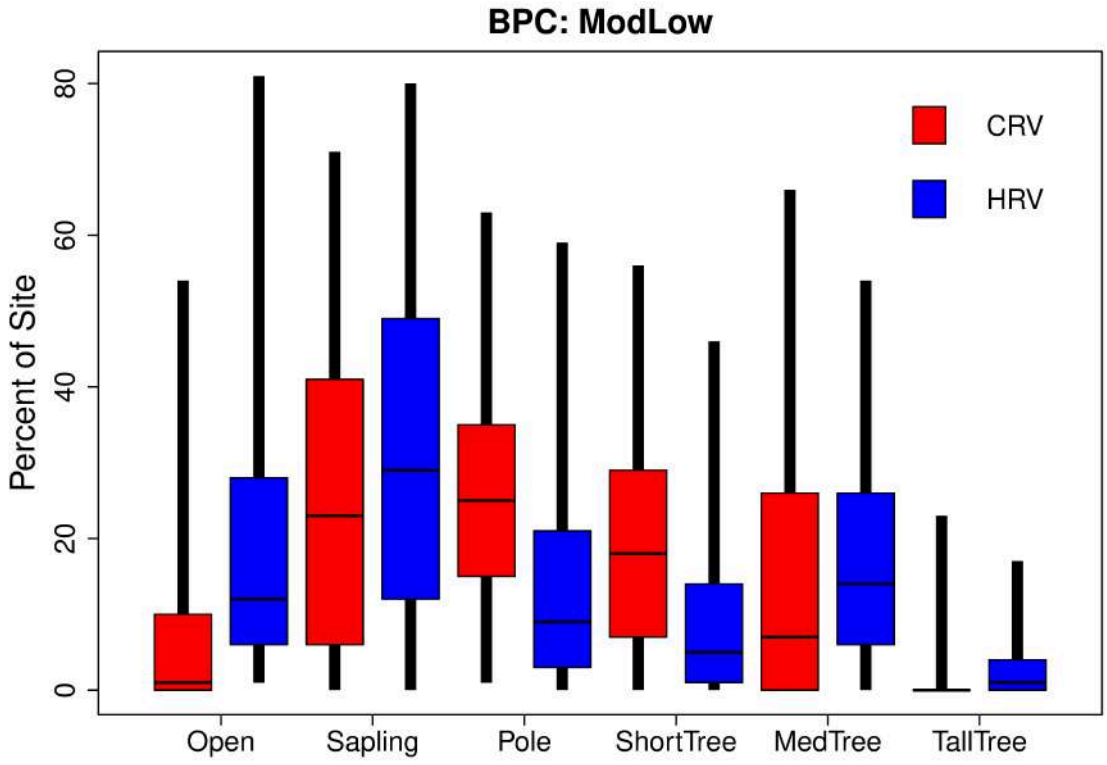
BPC: ModLow
Percent of Site
0
20
40
60
80
CRV
HRV
Open
Sapling
Pole
ShortTree
MedTree
TallTree

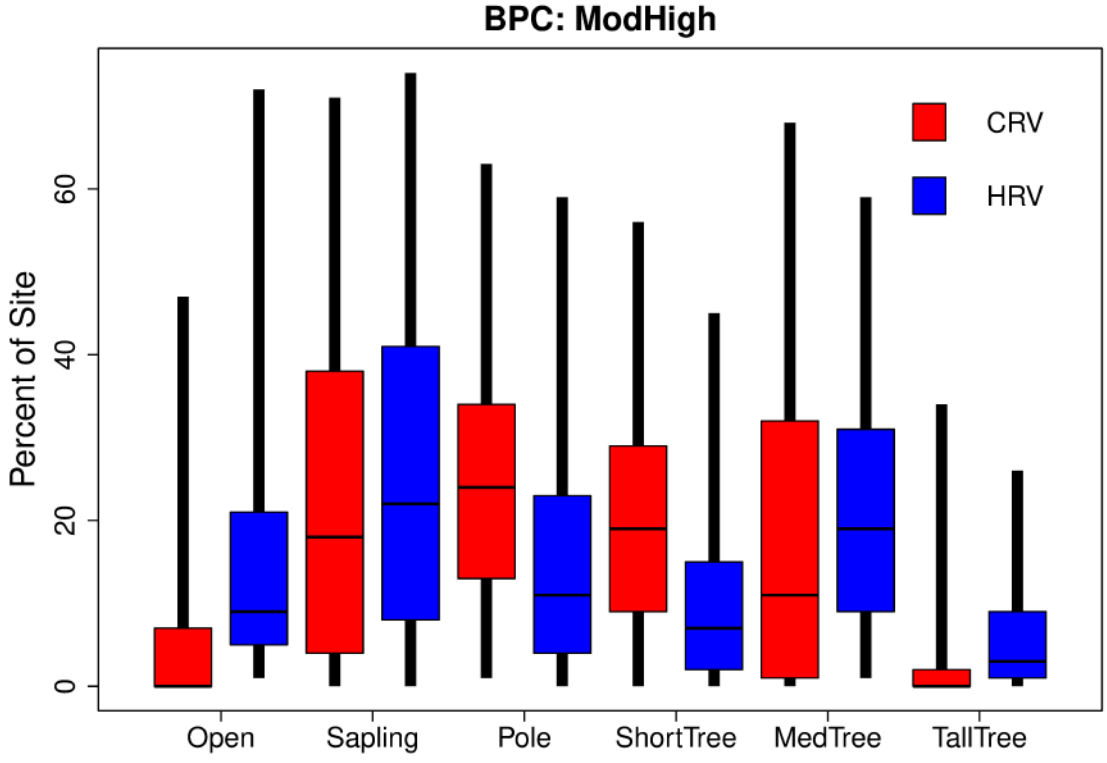
BPC: ModHigh
Percent of Site
0
20
40
60
CRV
HRV
Open
Sapling
Pole
ShortTree
MedTree
TallTree

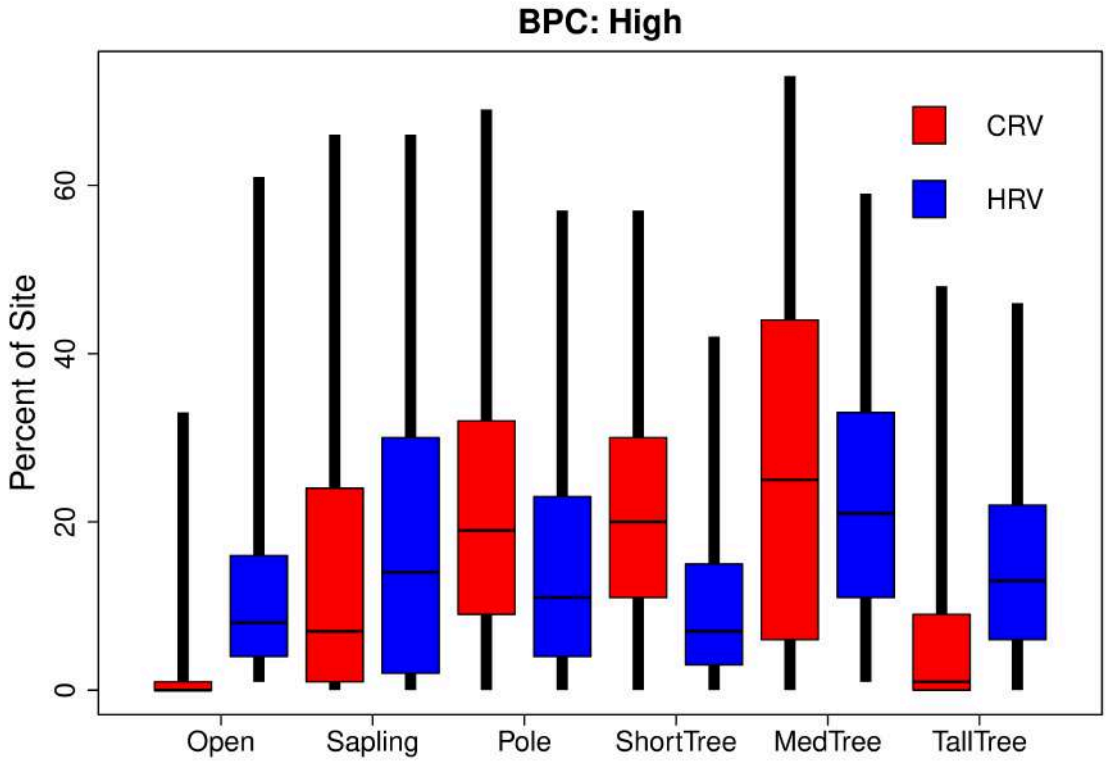

Figure 14: Historical Range of Variability (HRV) and Current range of variabiilty (CRV) among Sites (i.e., 40-m radius window) in the percent of forest in each developmental stage within the Low, Moderately Low, Moderately High and High site productivity Biophysical Classes (BPCs) in the Yuba River landscape. Box = 25-50 percentiles; whiskers = 2.5-97.5 percentiles

Recall that current departure in the Site-level metrics provides a basis for prioritizing management at the unit level. For example, given the results above, to reduce the current departure in developmental stage composition on High productivity Sites, management could prioritize treatments that produce units with a greater percentage of Open areas intermixed with Tall trees to shift the overall developmental stage distribution across the landscape to be more aligned with the HRV distribution. The same priorities could be given to Low productivity Sites, although here the emphasis would be predominantly on increasing the proportion of Sites with a greater proportion of Open areas. Of course, aside from controlling the percentage in Open, there is only limited ability to actively manage developmental stage succession (i.e., height growth). Indeed, much of the succession required to shift the current distribution towards the later stages of development simply requires time (e.g., to allow trees in the Pole and Short Tree stages to grow into the Medium and Tall Tree stages). However, managing surface and ladder fuels to inhibit high severity wildfire and retaining current taller trees may be an effective strategy to gradually shift the CRV towards better alignment with HRV with respect to the later developmental stages.

Metric 2: Tree Size (QMD)

Tree Size at the Site level was based on the Quadratic Mean Diameter (QMD) of established trees within a 40-m radius of the focal cell. Recall that QMD was based on only the cells with established trees in the window. Thus, if there was a single cell with an established tree in the window, then QMD was based on that single tree and equaled the tree's diameter at breast height (DBH). Accordingly, QMD can be quite high even in relatively open areas if the few neighborhood trees are large in diameter. The HRV and CRV in Tree Size composition at the Site level by BPC is given in **Table 9** and depicted in **Figure 15**.

BPC	Scenario	HRV 2.5%	HRV 25%	HRV 50%	HRV 75%	HRV 97.5%
Low	CRV	2	5	7	10	19
Low	HRV	3	8	12	15	23
ModLow	CRV	2	6	9	13	23
ModLow	HRV	6	11	15	18	25
ModHigh	CRV	3	7	11	16	27
ModHigh	HRV	8	14	18	21	28
High	CRV	4	11	17	23	35
High	HRV	11	18	22	26	34

Table 9: Range of variability (given as quantiles) in tree size (quadratic mean diameter) across Sites (40-m radius window centered on each focal cell) by Biophysical Class (BPC) for the current range of variability (CRV) and the historical range of variability (HRV) for the Yuba River landscape.

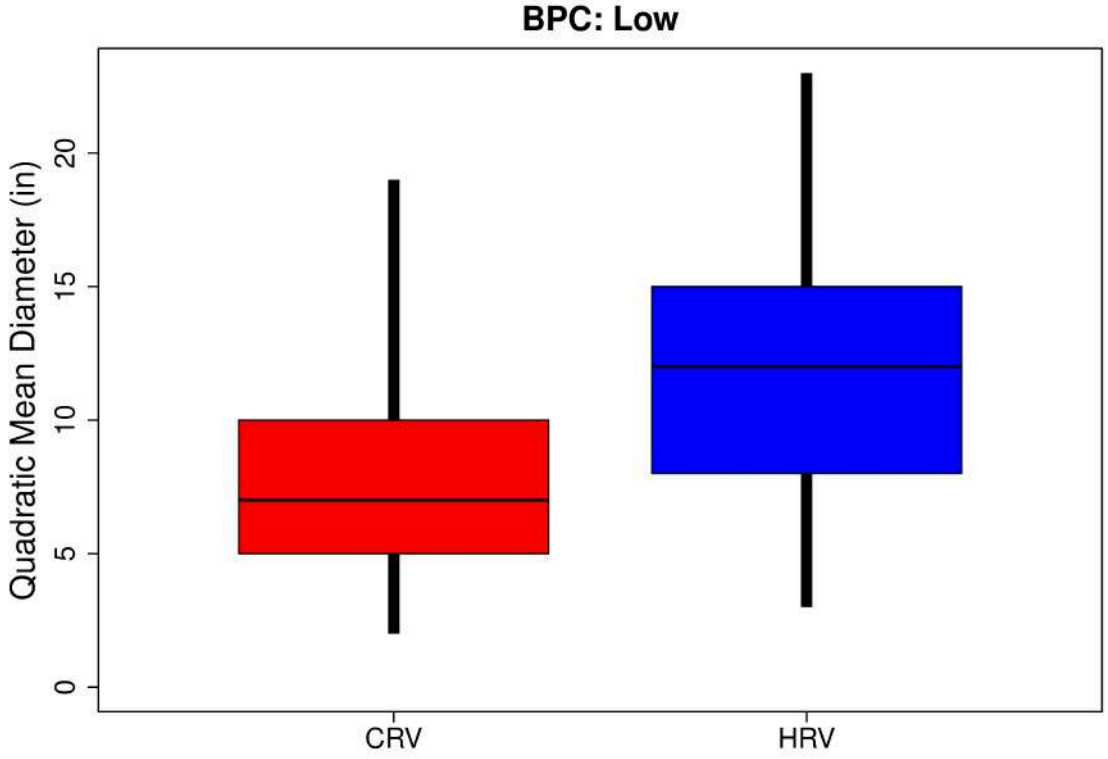

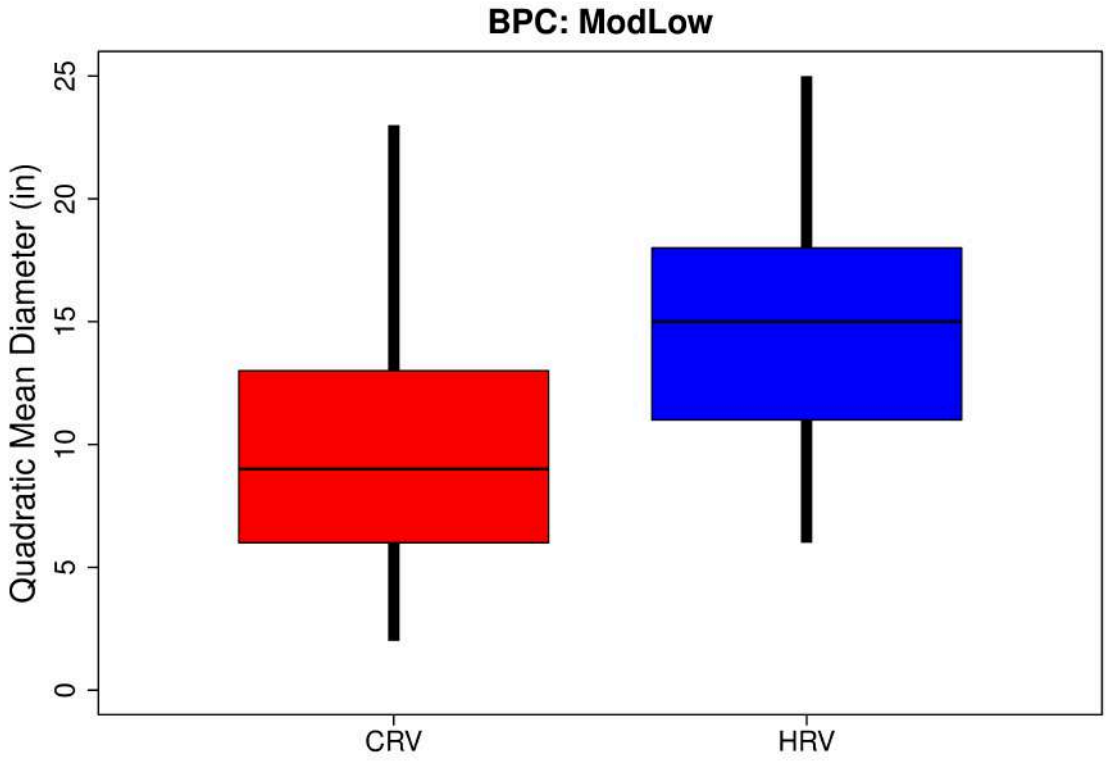
BPC: ModLow
Quadratic Mean Diameter (in)
0
5
10
15
20
25
CRV
HRV

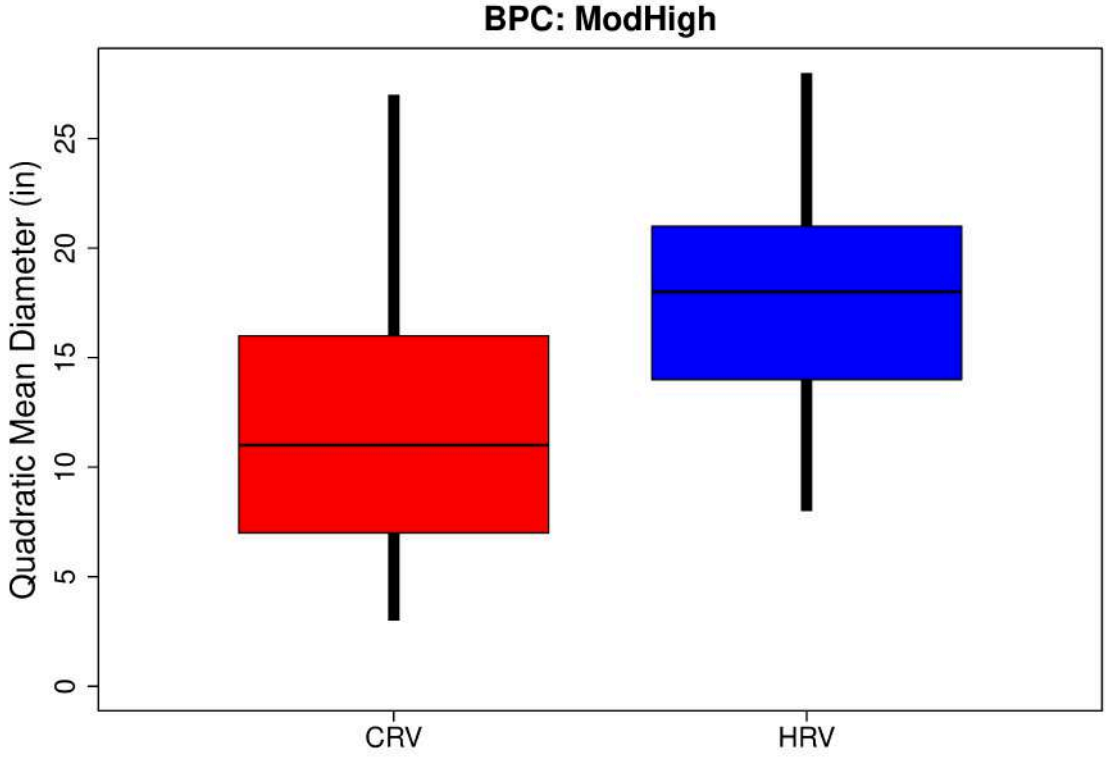
BPC: ModHigh
Quadratic Mean Diameter (in)
0
5
10
15
20
25
CRV
HRV

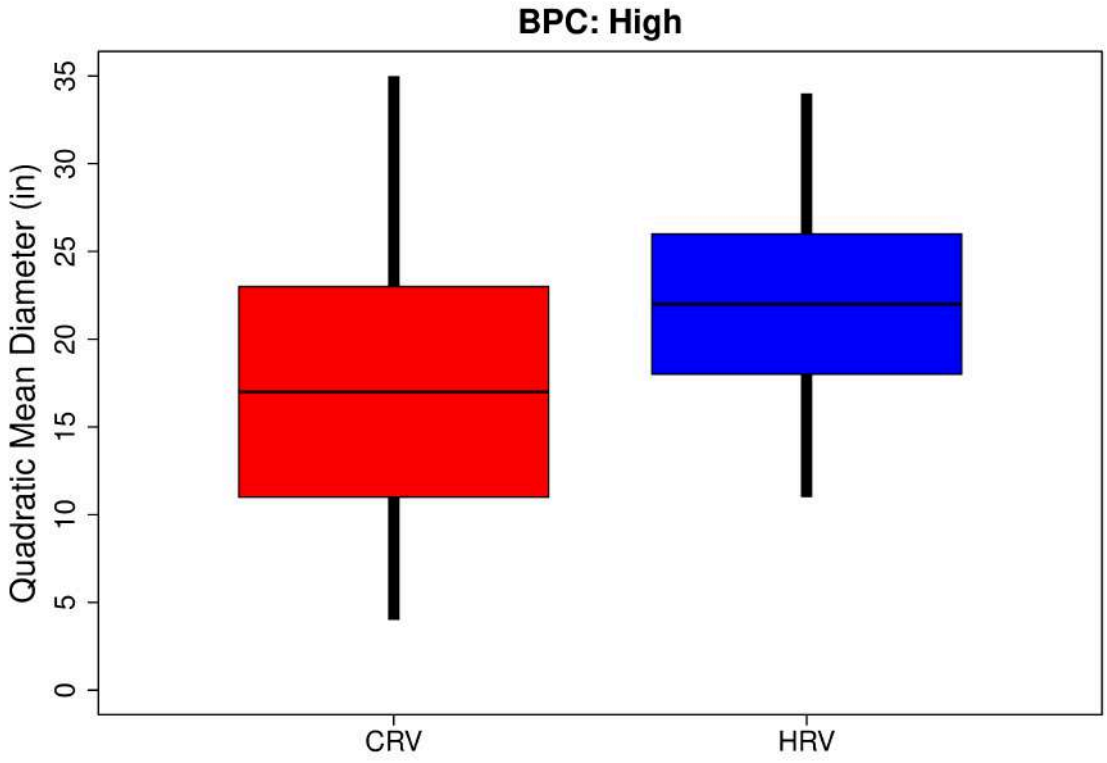

Figure 15: Historical Range of Variability (HRV) and Current range of variabiilty (CRV) among Sites (i.e., 40-m radius window) in the Quadratic Mean Diameter (QMD) of established trees to breast height within the Low, Moderately Low, Moderately High and High site productivity Biophysical Classes (BPCs) in the Yuba River landscape. Box = 25-50 percentiles; whiskers = 2.5-97.5 percentiles

Metric 3: Tree Cover

Tree Cover at the Site level was based on the percentage of 5-m cells with established trees to breast height within a 40-m radius of the focal cell. Recall that even a cell in the Open developmental stage (i.e., forest cell without an established tree to breast height) has a percent tree cover > 0 % so long as there was a single established tree within 40 m of the focal cell. In addition, recall that Tree Cover, as computed here, represents the percentage of cells within 40 m containing one or more established trees to breast height, not actual tree canopy cover, and as such is biased high by an average of 16% over actual tree canopy cover (i.e., actual tree canopy cover will be less than reported here by an average of 16%). The HRV and CRV in Tree Cover composition at the Site level by BPC is given in **Table 10** and depicted in **Figure 16**.

Table 10: Range of variability (given as quantiles) in percent tree cover across Sites (40-m radius window centered on each focal cell) by Biophysical Class (BPC) for the current range of variability (CRV) and the historical range of variability (HRV) for the Yuba River landscape.

BPC	Scenario	HRV 2.5%	HRV 25%	HRV 50%	HRV 75%	HRV 97.5%
Low	CRV	40	87	97	100	100
Low	HRV	7	59	81	91	98
ModLow	CRV	45	89	98	100	100
ModLow	HRV	18	71	87	93	98
ModHigh	CRV	52	92	99	100	100
ModHigh	HRV	27	78	90	94	98
High	CRV	66	98	100	100	100
High	HRV	38	83	91	95	98

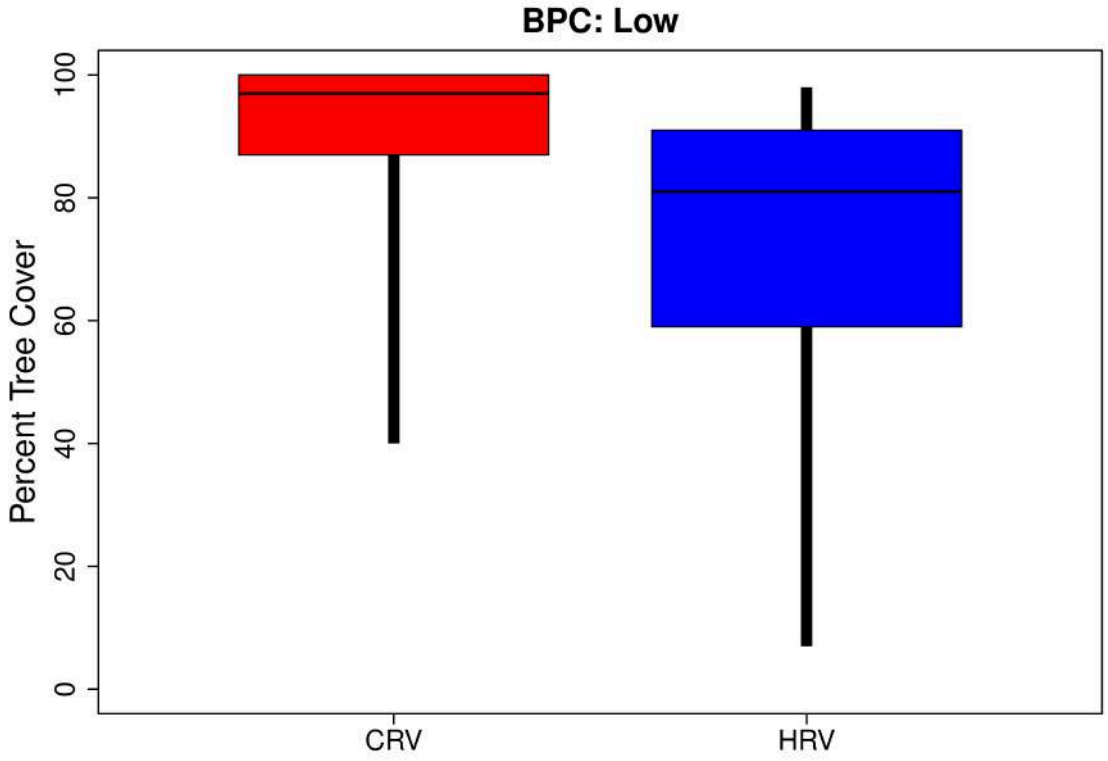

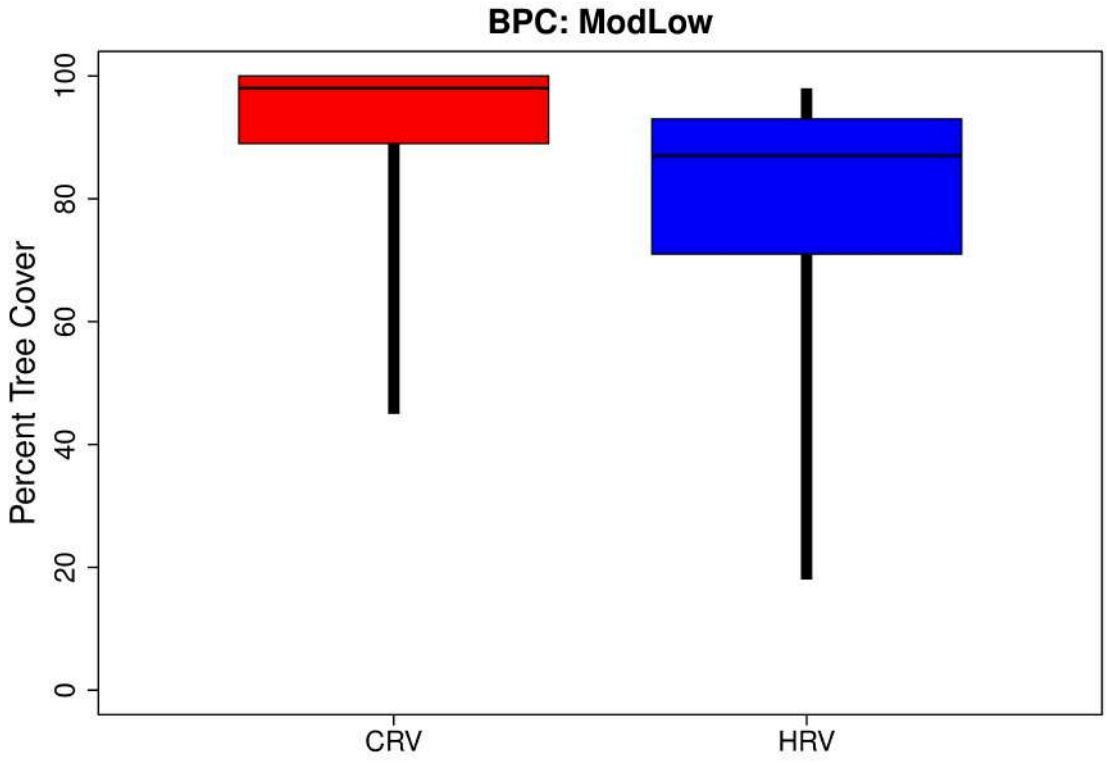
BPC: ModLow
Percent Tree Cover
0
20
40
60
80
100
CRV
HRV

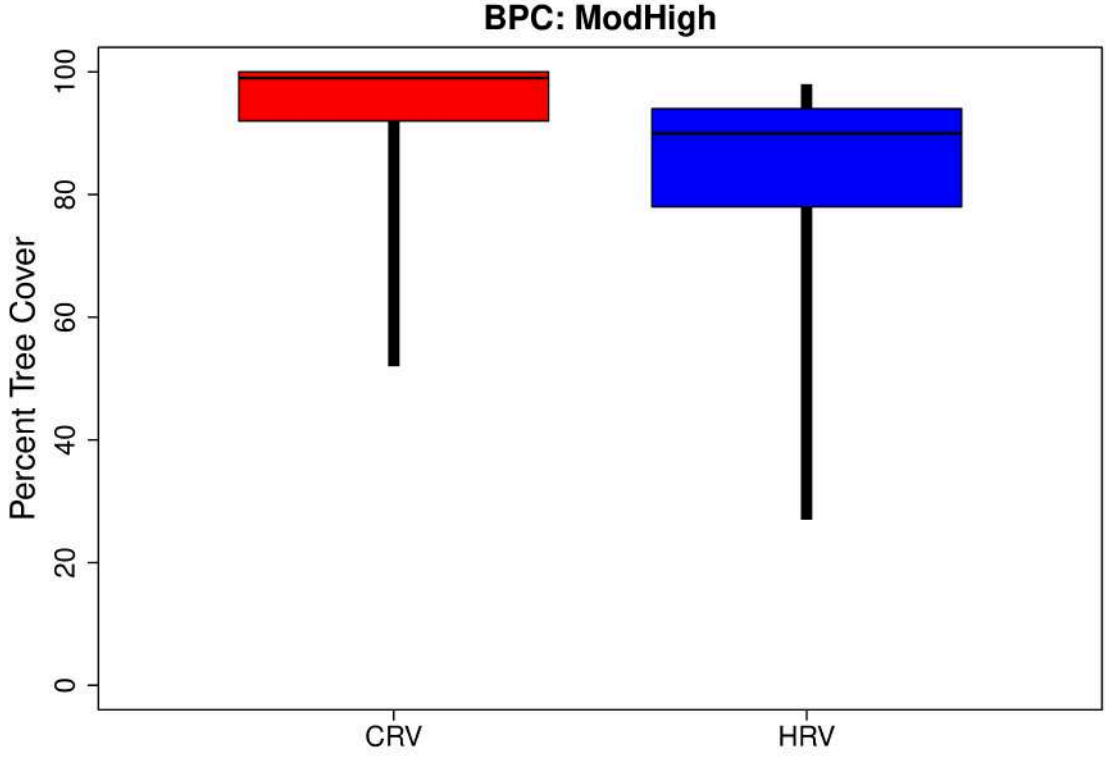
BPC: ModHigh
Percent Tree Cover
0
20
40
60
80
100
CRV
HRV

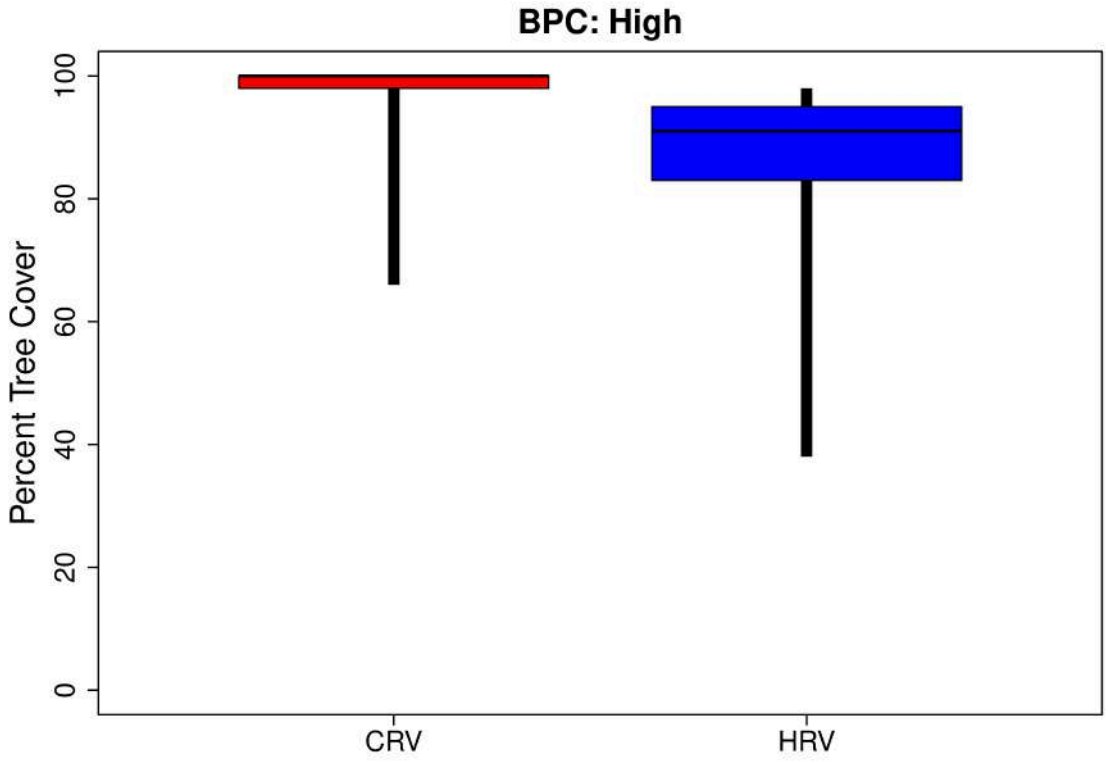

Figure 16: Historical Range of Variability (HRV) and Current range of variabiilty (CRV) among Sites (i.e., 40-m radius window) in the percent Tree Cover of established trees to breast height within the Low, Moderately Low, Moderately High and High site productivity Biophysical Classes (BPCs) in the Yuba River landscape. Box = 25-50 percentiles; whiskers = 2.5-97.5 percentiles

Geophysical Unit Level Departure

The results presented in this section address current departure in landscape metrics quantified at the spatial extent of a single Geophysical Unit (GPU). The Yuba River landscape was divided into 6,815 separate GPUs, which collectively encompass the area mapped as forest in the Existing Cover layer (Ecover) and within existing Lidar at the time of this analysis. Recall from the GTR that we defined GPUs based on similarity in a suite of 10 geophysical attributes and that they were defined only for the forested portion of the landscape and only where we had Lidar coverage. In addition, recall that each GPU was assessed independently; i.e., that we compared the current condition of each GPU to its own HRV in vegetation conditions. Thus, current departure of a GPU was specific to that GPU and independent of that measured for other GPUs. Lastly, recall that we used a large but parsimonious suite of landscape metrics that we deemed meaningful for estimating departure at the GPU level and appropriate given the available data, and computed departure as described in the GTR (and not repeated here), including the following:

Metric 1: Basal Area Departure

Departure in basal area of trees within the GPU was based on a metric derived by the TCSI project and adapted here for our purposes (**Figure 17**). GPUs with an increasingly positive departure have a current basal area that is greater than expected under HRV.

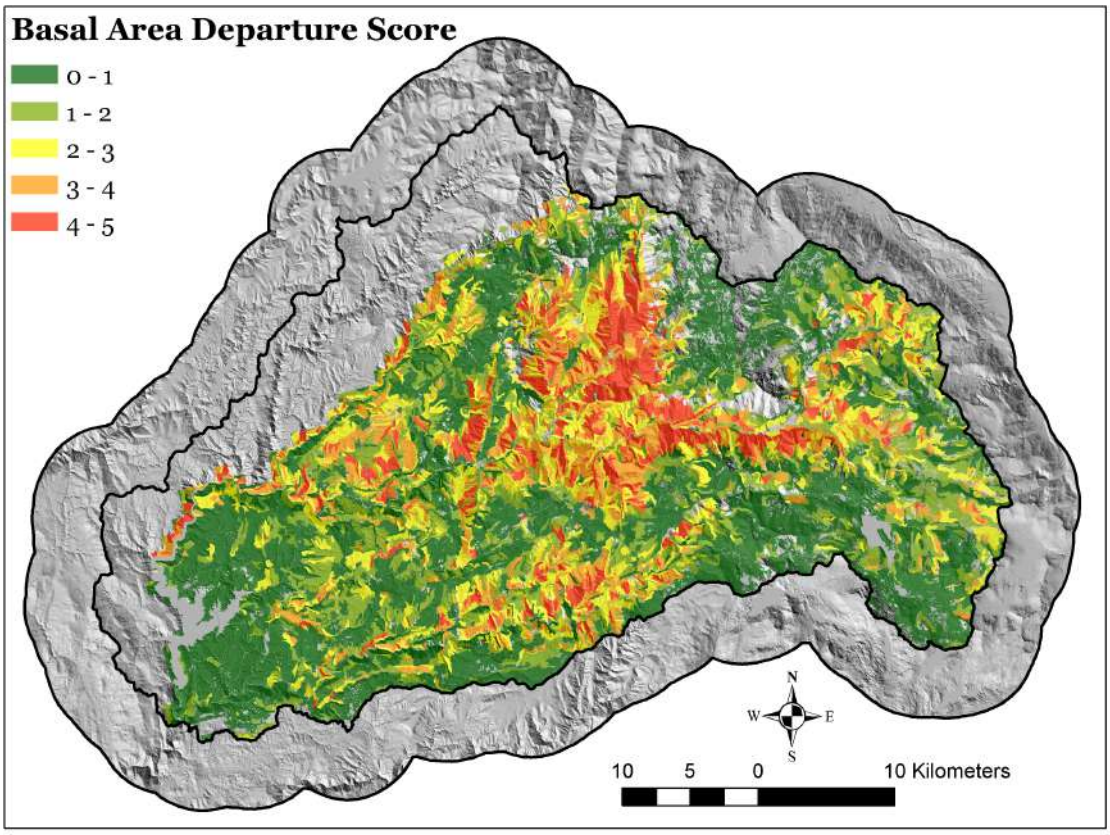

Figure 17: Geophysical Unit (GPU)-level basal area departure score for the Yuba River landscape. The departure score (0-5) represents the deviation of the current GPU condition from its historical range of variability (HRV), as estimated from a suite of contemporary reference sites. Values increase with increasing degrees of departure.

Metric 2: Percent Open Forest

We measured departure in the percent of forested cells within the GPU in the Open developmental stage (**Figure 18**). GPUs with a departure index less than -1 have less area in the Open developmental stage than under HRV.

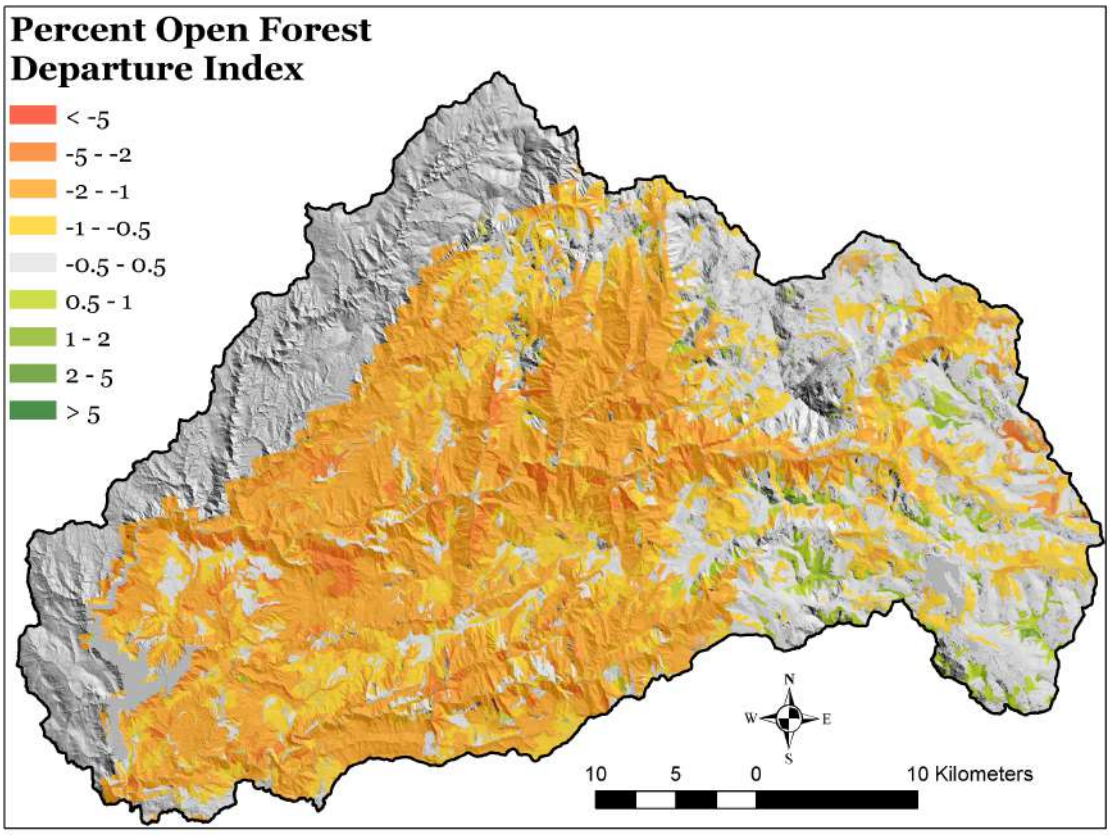

Figure 18: Geophysical Unit (GPU)-level departure index (unbounded) for the percentage of the forest within the GPU in the Open developmental stage for the Yuba River landscape. The departure Index represents the deviation of the current GPU condition from its historical range of variability (HRV), as simulated. Values < -1 represent a current condition that is less than the HRV for the GPU, and increasingly negative values represent increasing degrees of negative departure.

Metric 3: Developmental Stage Diversity

We measured departure in the diversity of forest developmental stages within the GPU based on the Simpson's Diversity index (**Figure 19**). Here, Simpson's Diversity is defined as the probability that any two cells selected at random would be different developmental stages. The departure index for Simpson's Diversity is less than -1 if the current GPU has a diversity of developmental stages that is less than HRV.

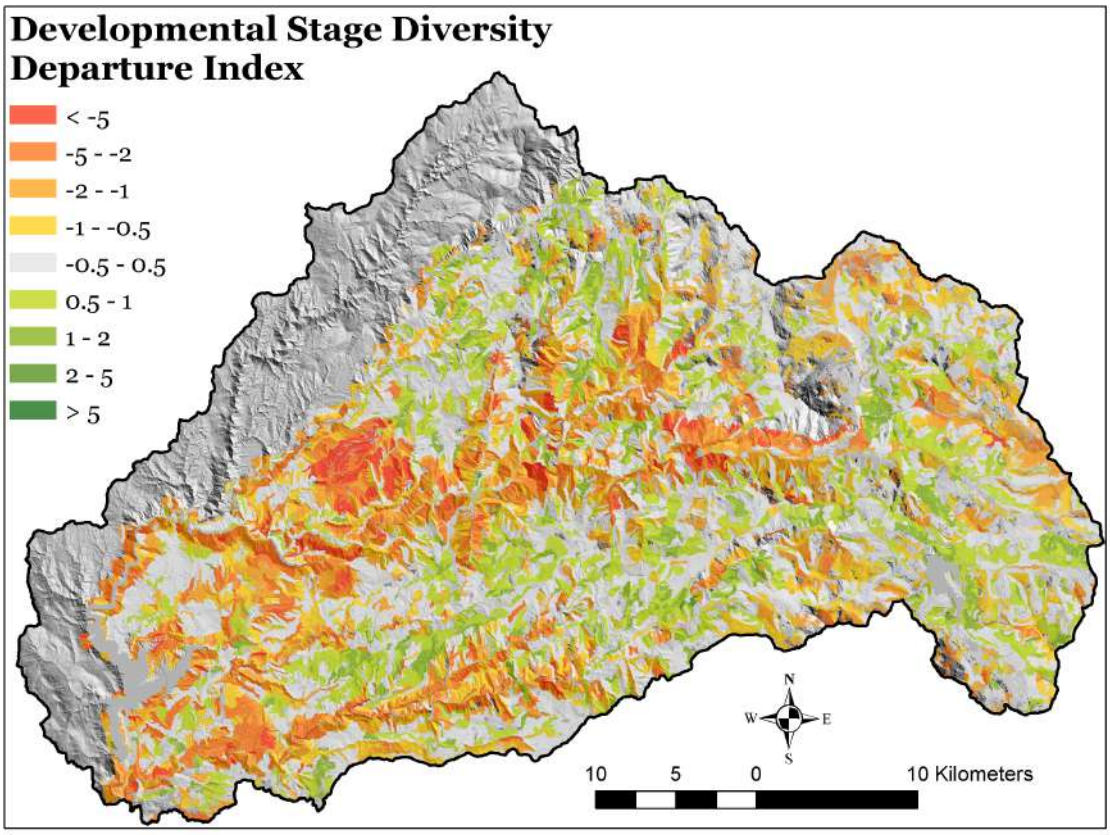

Figure 19: Geophysical Unit (GPU)-level departure index (unbounded) for the Simpson Diversity of developmental stages within the GPU for the Yuba River landscape. The departure Index represents the deviation of the current GPU condition from its historical range of variability (HRV), as simulated. Values < -1 represent a current condition that is less than the HRV for the GPU, and increasingly negative values represent increasing degrees of negative departure.

Metric 4: Coefficient of Variation in Open Patch Size

We measured departure in the Coefficient of Variation (CV) in the size of all Open forest patches, including single cell patches, in which forest openings are defined by contiguous cells in the Open developmental stage based on the 4-neighbor rule (i.e., orthogonal neighbors)(**Figure 20**). The departure index is less than -1 if the current GPU has relatively invariant Open patch sizes compared to HRV.

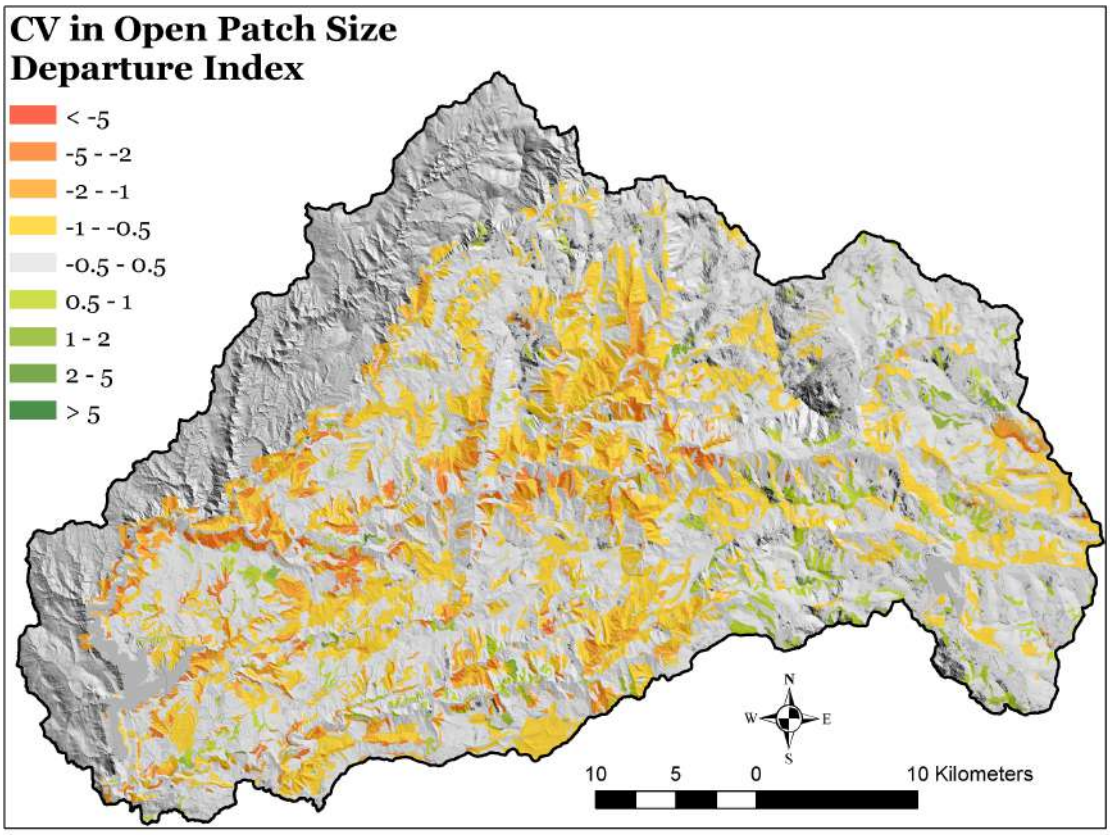

Figure 20: Geophysical Unit (GPU)-level departure index (unbounded) for the Coefficient of Variation (CV) in the size of patches in the Open developmental stage within the GPU for the Yuba River landscape. The departure Index represents the deviation of the current GPU condition from its historical range of variability (HRV), as simulated. Values < -1 represent a current condition that is less than the HRV for the GPU, and increasingly negative values represent increasing degrees of negative departure.

Metric 5: Coefficient of Variation in Developmental Stage Patch Size

We measured departure in the CV in the size of all forest developmental stage patches, including single cell patches, in which patches are defined by contiguous cells in the same developmental stage based on the 4-neighbor rule (**Figure 21**). The departure index is less than -1 if the current GPU has relatively invariant developmental stage patch sizes compared to HRV.

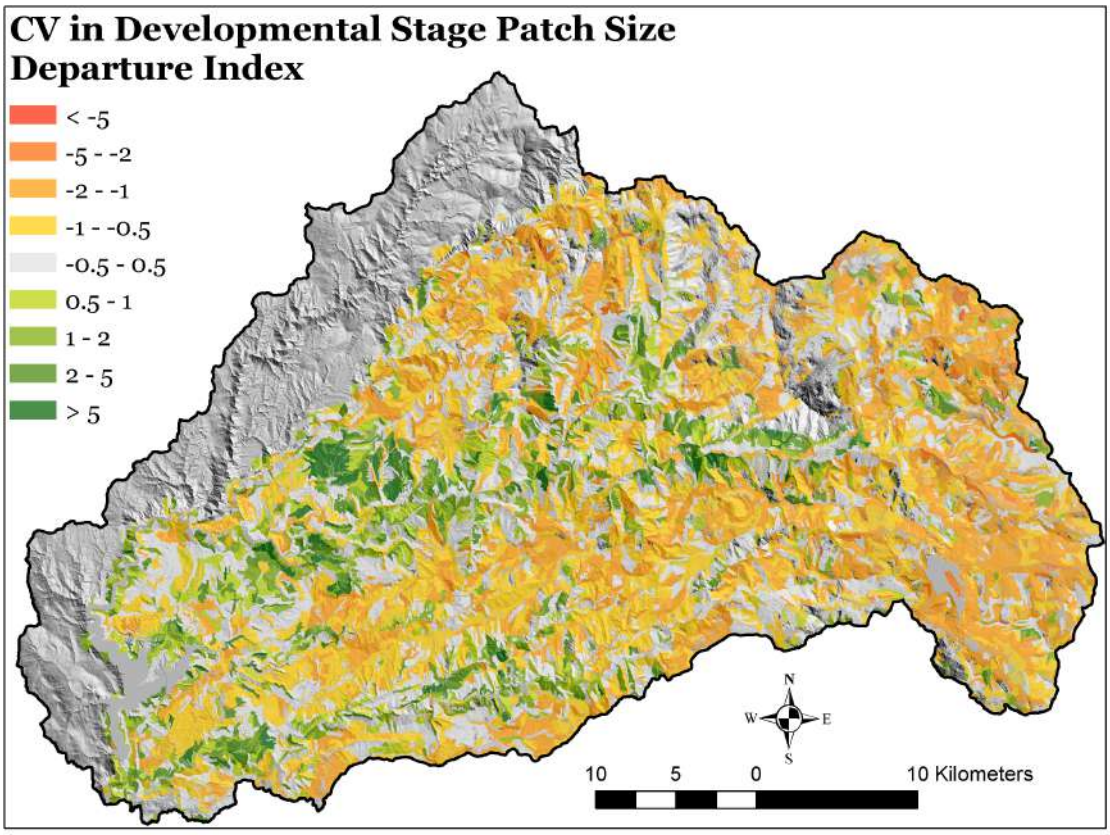

Figure 21: Geophysical Unit (GPU)-level departure index (unbounded) for the Coefficient of Variation (CV) in the size of patches based on developmental stages within the GPU for the Yuba River landscape. The departure Index represents the deviation of the current GPU condition from its historical range of variability (HRV), as simulated. Values < -1 represent a current condition that is less than the HRV for the GPU, and increasingly negative values represent increasing degrees of negative departure.

Metric 6: Percent Large Trees

We measured departure in the percent of forested cells within the GPU in the Large tree size class ($\geq$ 30 in dbh)(**Figure 22**). GPUs with a departure index less than -1 have less area in the Large tree class than under HRV.

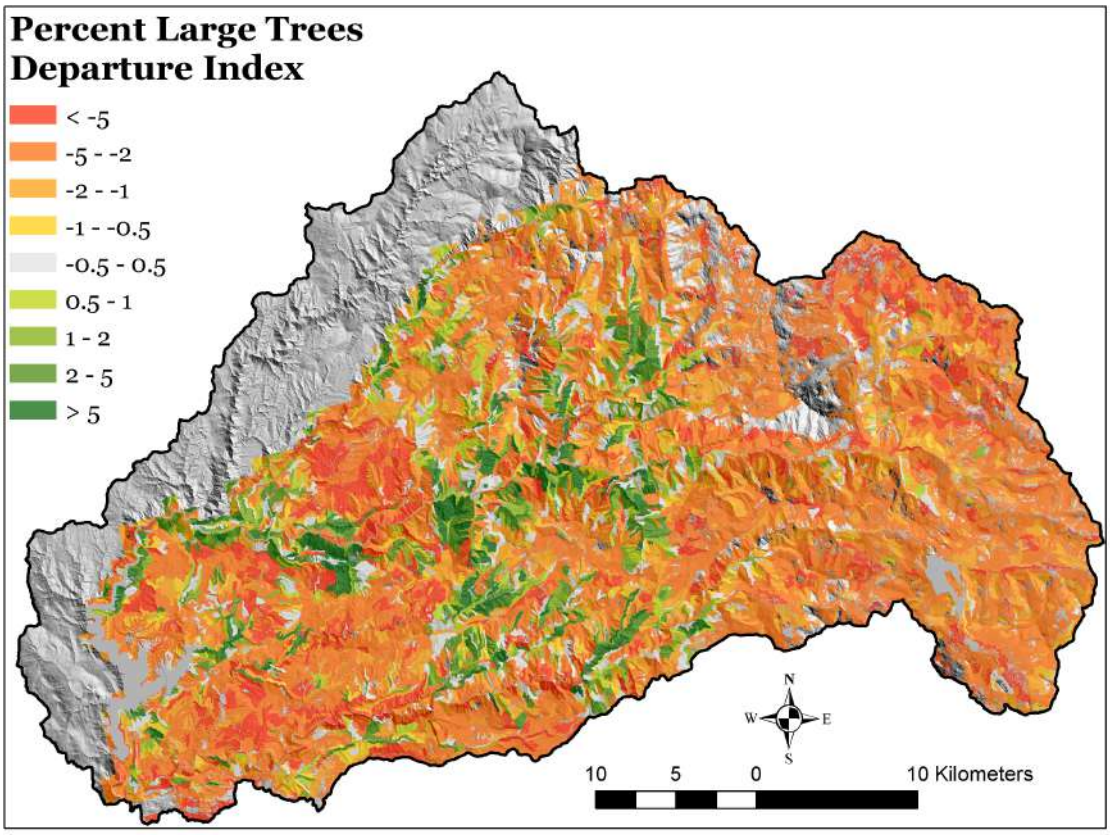

Figure 22: Geophysical Unit (GPU)-level departure index (unbounded) for the percentage of the forest in the Large tree size class (*geq* 30 in dbh) within the GPU for the Yuba River landscape. The departure Index represents the deviation of the current GPU condition from its historical range of variability (HRV), as simulated. Values < -1 represent a current condition that is less than the HRV for the GPU, and increasingly negative values represent increasing degrees of negative departure.

Metric 7: Tree Size Class Diversity

We measured departure in the diversity of tree size classes within the forested portion of the GPU based on the Simpson's Diversity index (**Figure 23**). Here, Simpson's Diversity is defined as the probability that any two cells selected at random would be from different tree size classes. The departure index for Simpson's Diversity is less than -1 if the current GPU has a diversity of tree size classes that is less than HRV.

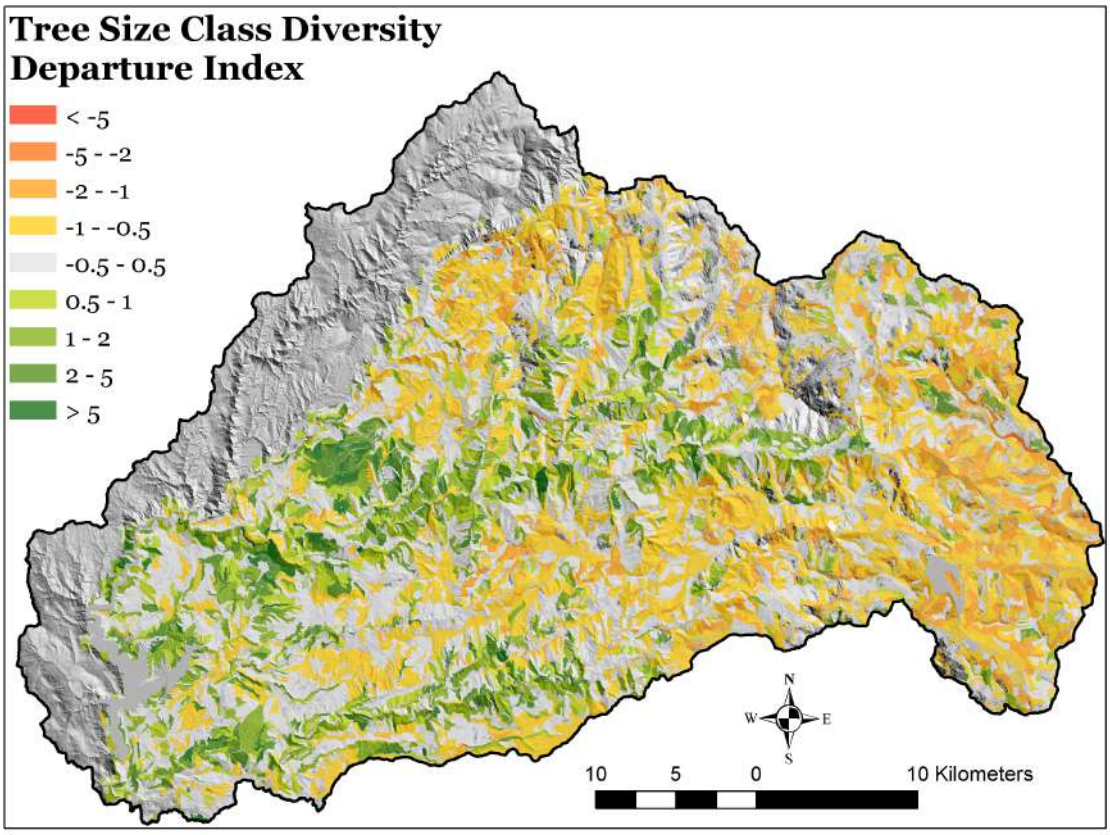

Figure 23: Geophysical Unit (GPU)-level departure index (unbounded) for the Simpson Diversity of tree size clases within the GPU for the Yuba River landscape. The departure Index represents the deviation of the current GPU condition from its historical range of variability (HRV), as simulated. Values < -1 represent a current condition that is less than the HRV for the GPU, and increasingly negative values represent increasing degrees of negative departure.

Metric 8: Coefficient of Variation in Large Tree Patch Size

We measured departure in the CV in the size of all Large tree patches, including single cell patches, in which Large tree patches were defined by contiguous cells in the Large tree class ($\geq$ 30 in dbh) based on the 4-neighbor rule (**Figure 24**). The departure index is less than -1 if the current GPU has relatively invariant Large tree patch sizes compared to HRV.

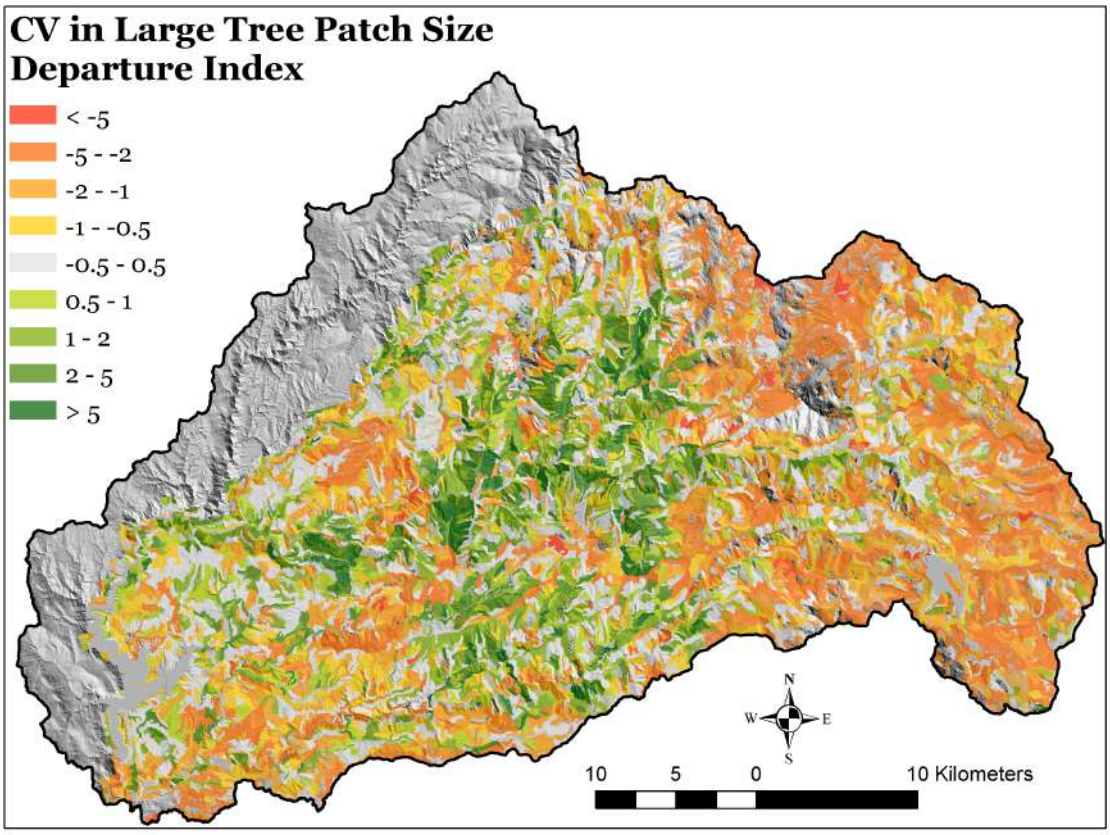

Figure 24: Geophysical Unit (GPU)-level departure index (unbounded) for the Coefficient of Variation (CV) in the size of patches in the Large tree size class (*geq* 30 in dbh) within the GPU for the Yuba River landscape. The departure Index represents the deviation of the current GPU condition from its historical range of variability (HRV), as simulated. Values < -1 represent a current condition that is less than the HRV for the GPU, and increasingly negative values represent increasing degrees of negative departure.

Metric 9: Coefficient of Variation in Tree Size Class Patch Size

We measured departure in the CV in the size of all tree size class patches, including single cell patches, in which patches were defined by contiguous cells in the same tree size class based on the 4-neighbor rule (**Figure 25**). The departure index is less than -1 if the current GPU has relatively invariant tree size class patch sizes compared to HRV.

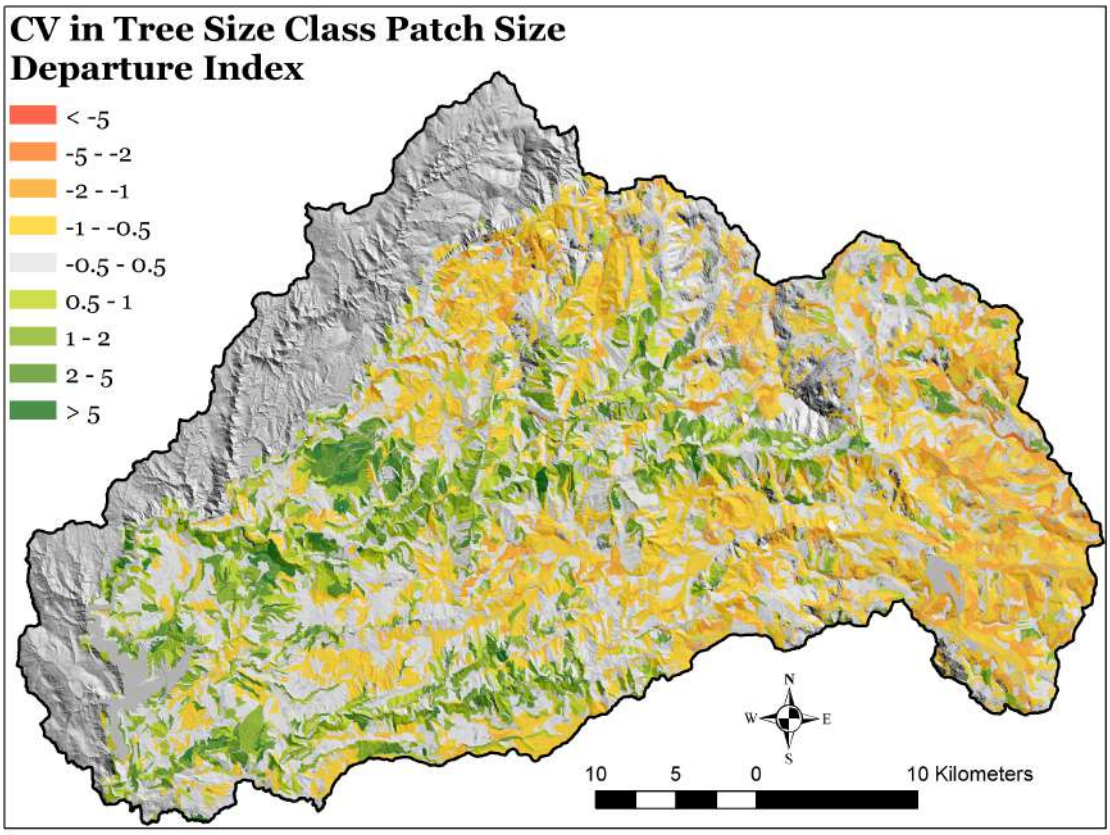

Figure 25: Geophysical Unit (GPU)-level departure index (unbounded) for the Coefficient of Variation (CV) in the size of patches based on tree size classes within the GPU for the Yuba River landscape. The departure Index represents the deviation of the current GPU condition from its historical range of variability (HRV), as simulated. Values < -1 represent a current condition that is less than the HRV for the GPU, and increasingly negative values represent increasing degrees of negative departure.

Metric 10: Coefficient of Variation in Quadratic Mean Diameter

We measured departure in the CV in site-level Quadratic Mean Diameter (QMD) of established trees within the GPU (**Figure 26**). Recall that a site was defined as a 40-m radius window around each focal cell. Thus, QMD was computed for the site associated with each focal cell, which produced a continuous surface of QMD values, from which the CV in QMD values within the GPU was computed. The departure index is less than -1 if the current GPU has relatively homogeneous QMD compared to HRV.

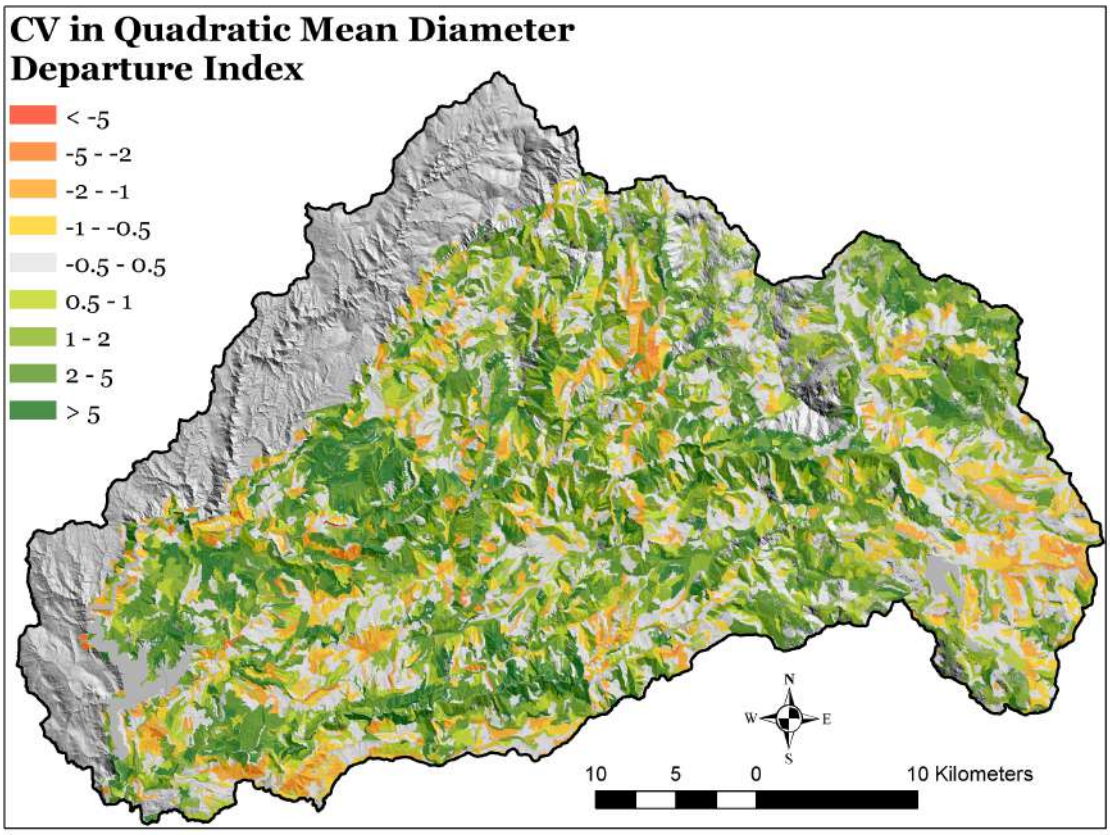

Figure 26: Geophysical Unit (GPU)-level departure index (unbounded) for the Coefficient of Variation (CV) in Site-level (i.e., 40 m radius window around each focal cell) Quadratic Mean Diameter (QMD, in inches) within the GPU for the Yuba River landscape. The departure Index represents the deviation of the current GPU condition from its historical range of variability (HRV), as simulated. Values < -1 represent a current condition that is less than the HRV for the GPU, and increasingly negative values represent increasing degrees of negative departure.

Metric 11: Coefficient of Variation in Percent Tree Cover

We measured departure in the CV in site-level percent cover of established trees within the GPU (**Figure 27**). Again, recall that a site was defined as a 40-m radius window around each focal cell. Thus, percent tree Cover was computed for the site associated with each focal cell, which produced a continuous surface of percent tree cover values, from which the CV in tree cover within the GPU was computed. The departure index is less than -1 if the current GPU has relatively homogeneous tree cover compared to HRV.

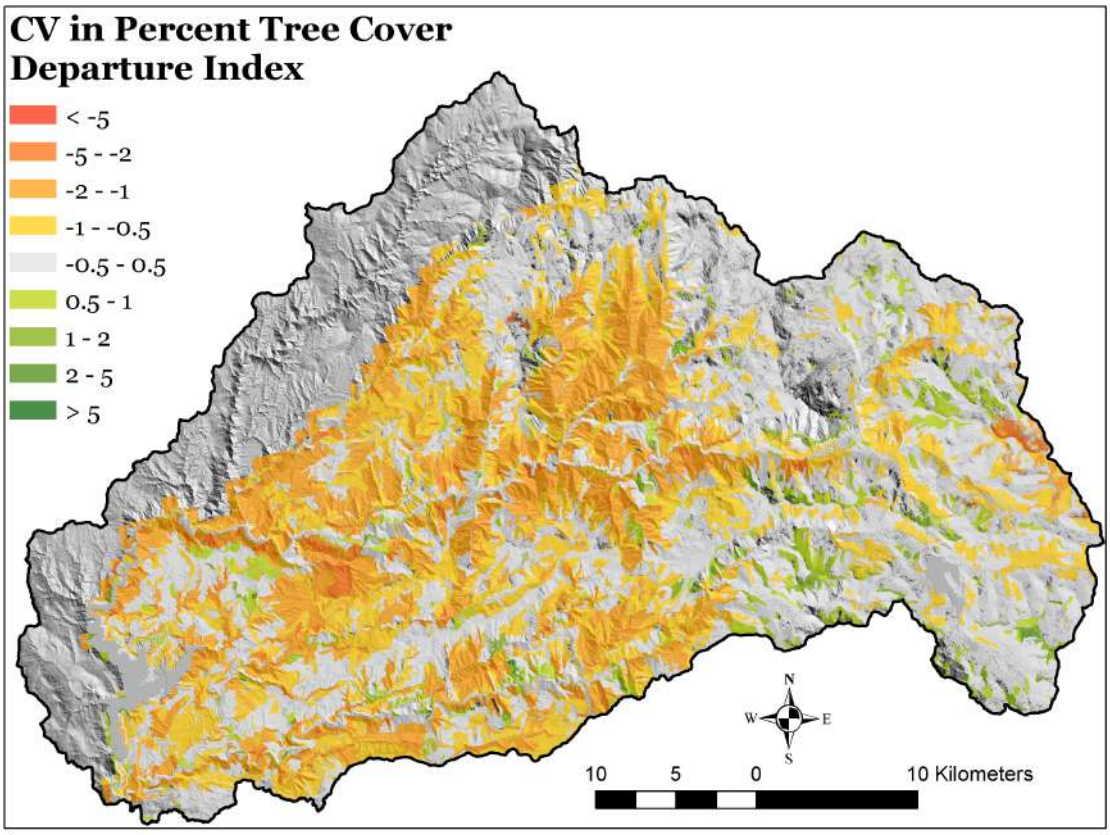

Figure 27: Geophysical Unit (GPU)-level departure index (unbounded) for the Coefficient of Variation (CV) in Site-level (i.e., 40 m radius window around each focal cell) percent tree cover within the GPU for the Yuba River landscape. Note, percent tree cover as measured is on average 16 % greater than percent canopy cover. The departure Index represents the deviation of the current GPU condition from its historical range of variability (HRV), as simulated. Values < -1 represent a current condition that is less than the HRV for the GPU, and increasingly negative values represent increasing degrees of negative departure.

Composite Departure Index

We combined the 11 GPU-level departure indices above into two composite departure scores: 1) composite "negative" departure, and 2) composite "absolute" departure (see GTR for details). Both of these composite scores can be interpreted as a measure of overall GPU departure in vegetation composition and configuration. Increasing departure scores (given as a percent of maximum) indicate increasing degrees of departure.

Negative Departure - Maximum "negative" departure occurs when a GPU has too little Open forest area, too few Large trees, too little diversity in forest developmental stages (i.e., tree heights) and tree size classes (i.e., dbh), too little variability in the size of patches based on forest developmental stage and tree size, and too little spatial variability in percent tree cover and weighted average tree size (i.e., QMD) relative to its HRV. In other words, maximum negative departure occurs when the forest is too closed-canopy, depauperate in Large trees, and too homogeneous in vegetation composition and configuration.

The composite negative departure score is depicted in **Figure 28**. This score can be interpreted as the percent of maximum deviation in negative departure. Thus, a value of 0 represents no departure in any of the component metrics and a value of 100 represents maximum negative departure in each of the component metrics. GPUs with relatively high scores are the logical ones to prioritize for restoration

treatment - should that be the goal. Importantly, this composite departure score can serve as a first stage in identifying and prioritizing GPUs for treatment, but specific objectives and treatments for each GPU requires decomposing the composite score into the component metrics to determine which aspects of the forest vegetation composition and/or configuration are most departed.

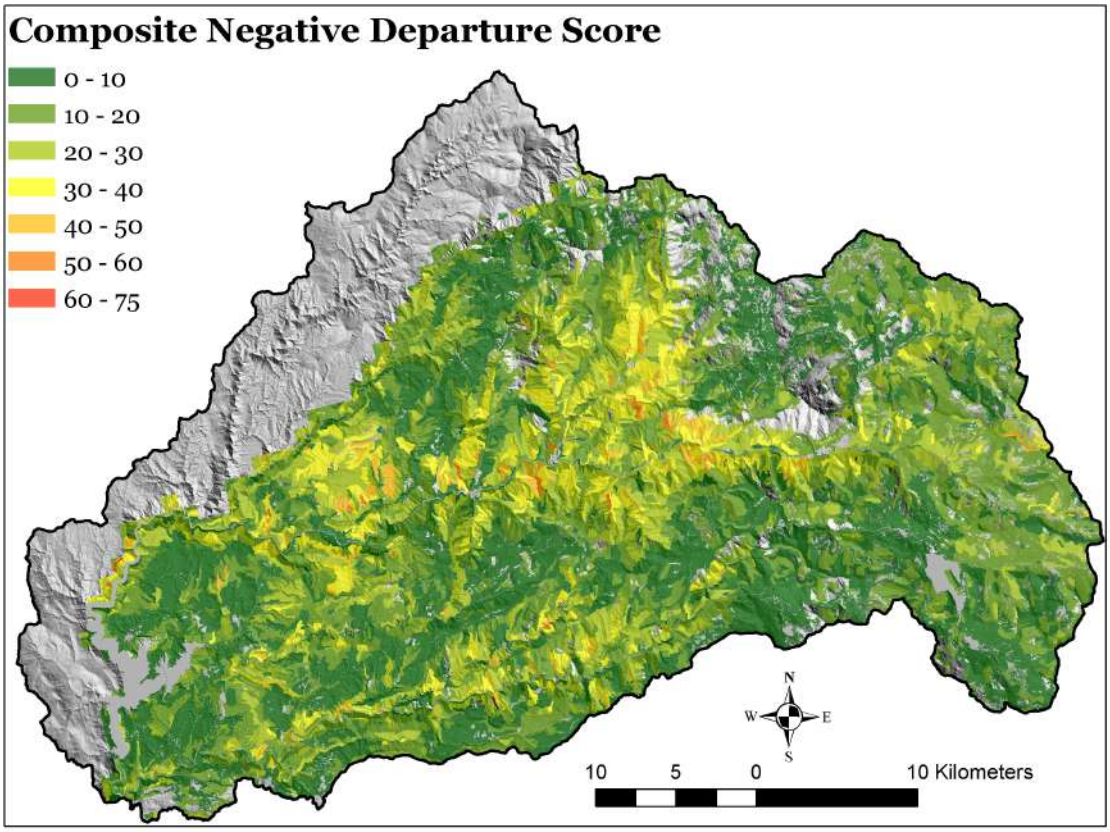

Figure 28: Geophysical Unit (GPU)-level composite negative departure score composed of a weighted combination of 11 individual departure metrics within the GPU for the Yuba River landscape. The score represents the percentage of maximum departure of the current GPU condition from its historical range of variability (HRV), as simulated. Larger values indicate increasing degrees of departure.

Absolute Departure - Maximum "absolute" departure occurs when a GPU has either too little or too much Open forest area, too few or too many Large trees, too little or too much diversity in forest developmental stages (i.e., tree heights) and tree size classes (i.e., dbh), too little or too much variability in the size of patches based on forest developmental stage and tree size, and too little or too much spatial variability in percent tree cover and weighted average tree size (i.e., QMD) relative to HRV. In other words, maximum departure occurs when the GPU differs in any way in both composition and configuration from its HRV, as measured by this suite of metrics.

Subbasin Level Departure

The results presented in this section represent landscape metrics quantified at the Subbasin-by-BPC level; i.e., each Subbasin subdivided into BPCs treated as a whole unit (a.k.a. "zones"). The Yuba River landscape was divided into 32 distinct Subbasins (**Figure 29**), each of which was partitioned into the BPCs for a total of 122 Subbasin-by-BPC partitions or zones. Recall from the GTR that each partition was assessed independently to create a departure index; i.e., that we compared the current condition of each partition to its own HRV in vegetation conditions. In addition, recall that the final departure score

reflected negative departure in the percent of the partition in large openings and large trees (i.e., in which the current landscape contains less area in large openings and large trees than expected under HRV), but was bidirectional with respect to the landscape configuration metrics; i.e., it reflected the magnitude of the absolute differences between the current and historical landscape conditions, regardless of whether the current condition was greater or less than the historical condition. In other words, any differences between current and historical vegetation conditions with respect to landscape configuration registered as departure. Lastly, recall that we used a parsimonious suite of landscape metrics (see below) that we deemed meaningful for estimating departure at the Subbasin level and appropriate given the available data, and computed departure as described in the GTR (and not repeated here), including the following metrics:

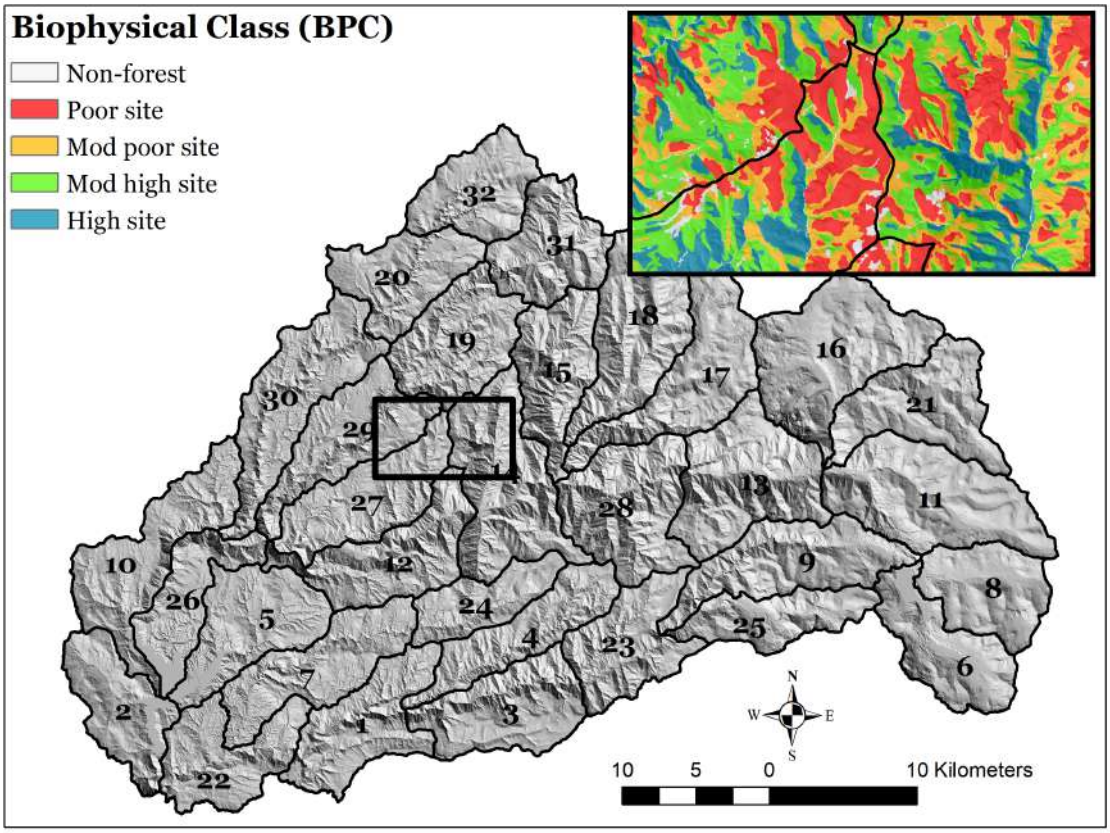

Figure 29: The Yuba River landscape HUC12 Subbasins, as modified, defined for the purpose of summarizing Historical Range of Variability (HRV) and current departure.

Metric 1: Percent Large Forest Openings

We defined large forest openings as contiguous forested cells in the Open developmental stage (i.e., no established trees to breast height) encompassing a minimum of 0.04 ha (0.1 acres). Contiguity was based on the 4-neighbor rule (i.e., orthogonal neighbors) that ensured a minimum width of 5 m for any opening. We defined Percent Large Forest Openings as the percent of the forest within the Subbasin-by-BPC partition in large forest openings (as defined), and the departure index reflected whether or not the current landscape was deficient in large forest openings relative to HRV and, if so, the degree of deficiency.

The Percent Large Forest Openings departure index is depicted in **Figure 30**. Note, the departure index was assigned to each Subbasin-by-BPC partition; consequently, there were 75 distinct values assigned. Thus, to better assess departure by Subbasin and BPC, one needs to examine the attribute table for the departure layer.

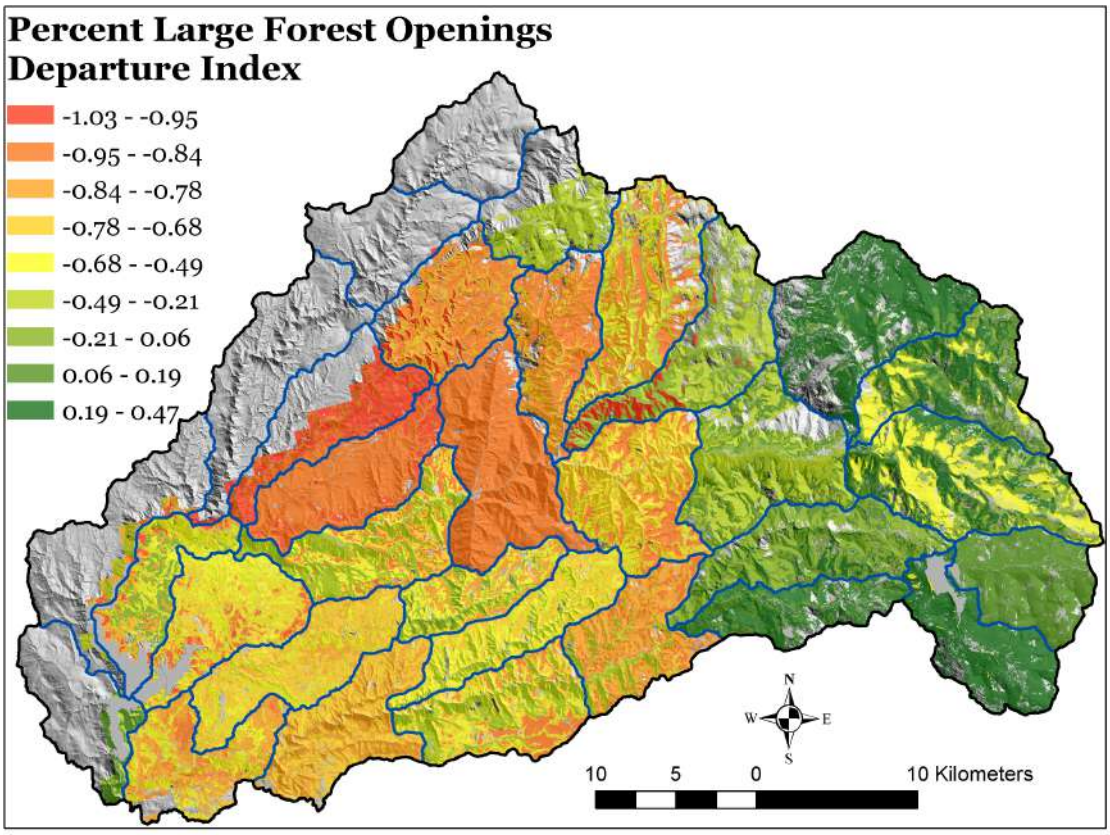

Figure 30: Subbasin-by-BPC level departure index for large forest openings (> 0.04 ha or 0.1 acres and > 5 m mininum width) for the Yuba River landscape. The departure index represents the deviation of the current Subbasin and biophysical class (BPC) condition from its historical reference period condition, as simulated. Departure indices < -1 represent a current landscape with less total area in large forest openings than during the historical reference period, as simulated, and increasing negative values represent increasing degrees of departure.

As discussed in the GTR, the Percent Large Forest Openings Departure Index can be miss-interpreted if not understood well. As the previous figure depicts, the distribution of index values would suggest that most of the subbasin-by-BPC partitions are within the HRV given that most of the partitions have values between -1 - 1. Recall, index values within this range reflect a current landscape condition that is within the 2.5% and 97.5% HRV. This would seem to indicate that most of the partitions are within HRV. While this might technically be correct, the reality is that most of the partitions are close to the lower limit of HRV and have index values close to -1. Consequently, the distribution of index values is heavily skewed towards values on the lower limit of HRV, suggesting that the landscape as a whole is, on average, deficient in large forest openings. A alternative and more useful way to assess current departure in this metric is to compare the distribution of values representing the percentage of the partition in large forest openings between the HRV and CRV, as shown **Figure 31**.

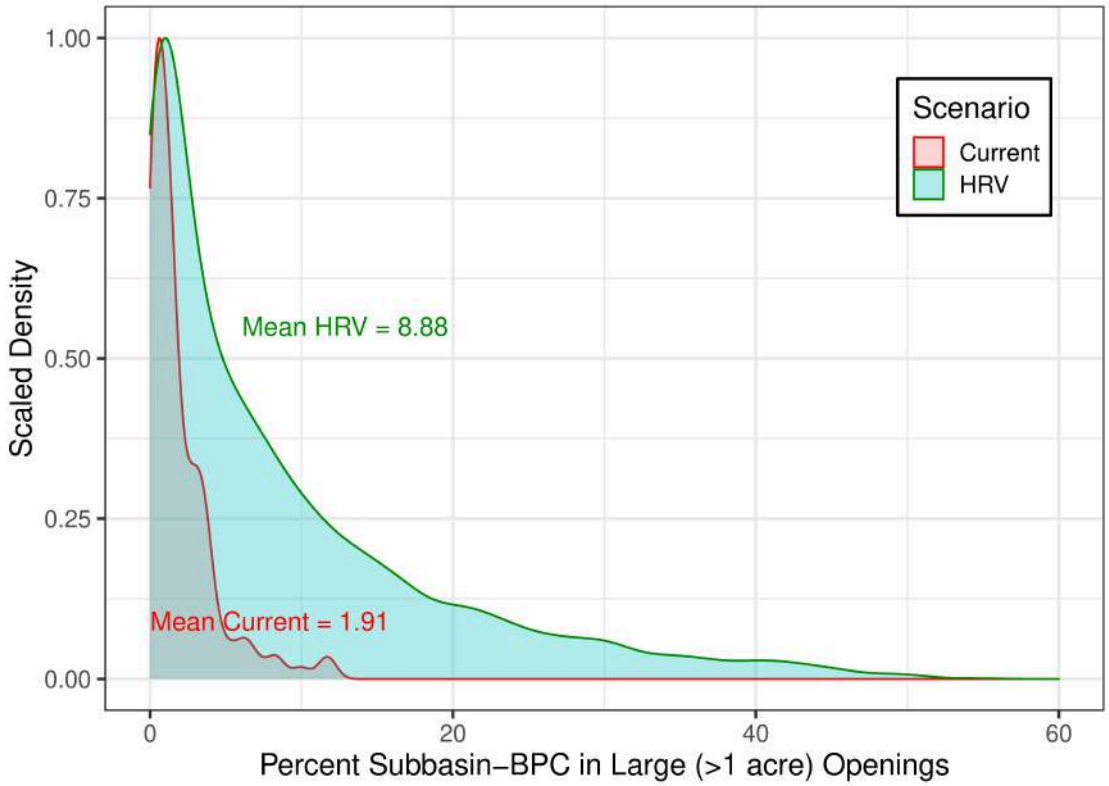

Figure 31: Current and historical distribution of Percent Large Forest Openings across the Subbasin-by-Biophysical Class (BPC) landscape partitions for the Yuba River landscape. The comparative distributions reveal that even though the departure index for most of the partitions technically may fall with the historical range of variation (see previous figure), the overall distributions in the raw metric values differ markedly and reflect departure for the landscape as a whole

Metric 2: Large Forest Openings Patch Size Distribution

We defined large forest openings as described above. Here, we quantified the size of individual openings and determined the percent of forest within the Subbasin-by-BPC partition in large openings in each of several patch size classes or bins (see GTR). The departure index reflects whether or not the current landscape has a distribution of large forest opening patch sizes that differed from HRV and, if so, the degree of differences in the two distributions.

The Large Forest Openings Patch Size Distribution departure index is depicted in **Figure 32**. As before, the departure index was assigned to each Subbasin-by-BPC partition; consequently, there were 75 distinct values assigned. Thus, to better assess departure by Subbasin and BPC, one needs to examine the attribute table for the departure layer.

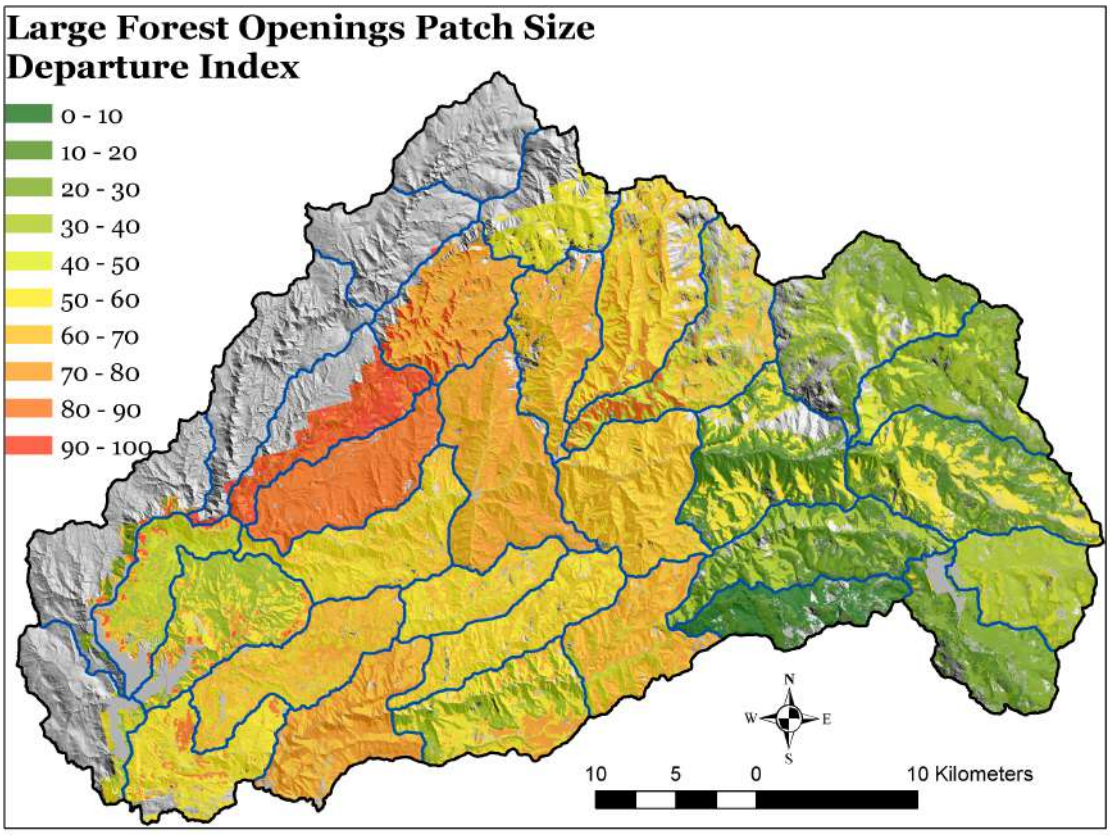

Figure 32: Subbasin-by-BPC level departure index for large forest openings (> 0.04 ha or 0.1 acres and > 5 m mininum width) patch size distribution for the Yuba River landscape. The departure index represents the deviation of the current Subbasin and biophysical class (BPC) condition from its historical reference period condition, as simulated. Departure indices > 0 represent a current landscape with a distribution of developmental stage patch sizes that differs in some way from the historical reference period distribution, as simulated, and increasing values represent increasing degrees of departure.

To further evaluate departure in this patch size distribution metric, it is necessary to examine the CRV and HRV patch size distributions for the selected Subbasin-by-BPC partition, for example as depicted in **Figure 33**.

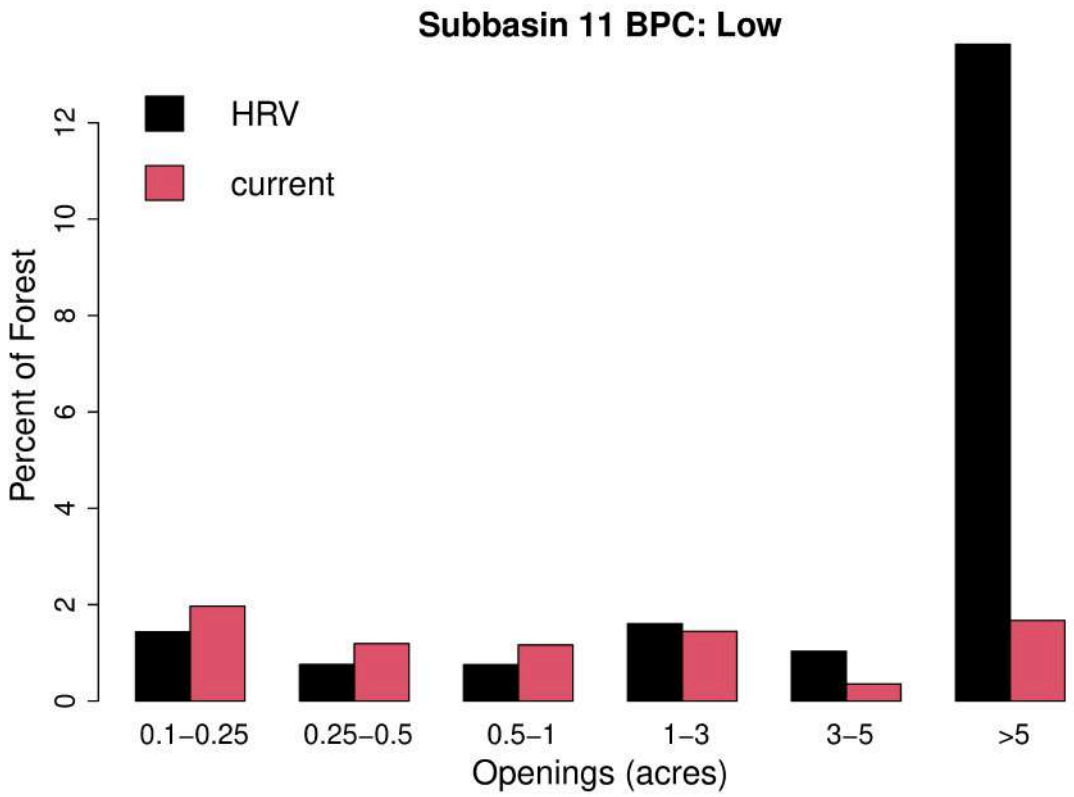

Figure 33: Barplot of the distribution of large forest openings (> 0.04 ha or 0.1 acres and > 5 m mininum width) patch sizes for the current landscape and the historical reference period (HRV) for Subbasin 11 and the Low productivity Biophysical Class (BPC = 1) for the Yuba River landscape. Each bar represents the percent of forest within the Subbasin and Biophysical Class (BPC) in large forest openings of a particular patch size. The departure index represents the percentage dissimilarity between the CRV and HRV distributions. Departure indices > 0 represent a current landscape with a distribution of large forest opening patch sizes that differs in some way from the historical reference period distribution, as simulated, and increasing values represent increasing degrees of departure.

Metric 3: Developmental Stage Patch Size Distribution

We defined developmental stages based on six tree height classes, ranging from Open (< 4.5 ft) to Tall Trees (> 125 ft), as described in the GTR. Here, for each snapshot of the landscape we constructed a patch mosaic comprised of developmental stages in which patches were defined using the 4-neighbor rule. For each snapshot, we quantified the size of each developmental stage patch and determined the percent of forest within the Subbasin-by-BPC partition in each of several patch size classes or bins. The departure index reflects whether or not the current landscape has a distribution of developmental stage patch sizes that differs from HRV and, if so, the degree of differences in the two distributions.

The Developmental Stage Patch Size Distribution departure index is depicted in **Figure 34**. As before, the departure index was assigned to each Subbasin-by-BPC partition; consequently, there were 75 distinct values assigned. Thus, to better assess departure by Subbasin and BPC, one needs to examine the attribute table for the departure layer.

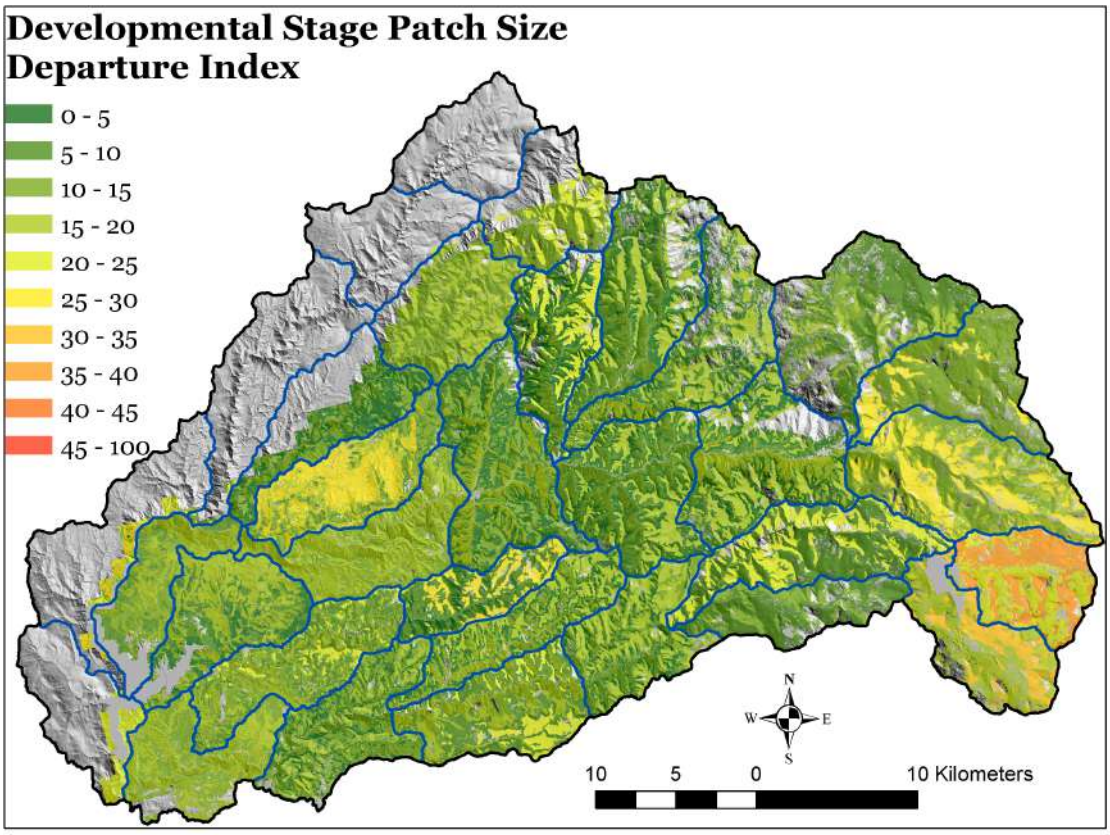

Figure 34: Subbasin-by-BPC level departure index for the developmental stage patch size distribution for the Yuba River landscape. Developmental stages were based on tree height classes and patches were based on the 4-neighbor adjacency rule. The departure index represents the deviation of the current Subbasin and biophysical class (BPC) condition from its historical reference period condition, as simulated. Departure indices > 0 represent a current landscape with a distribution of developmental stage patch sizes that differs in some way from the historical reference period distribution, as simulated, and increasing values represent increasing degrees of departure.

To further evaluate departure in this patch size distribution metric, it is necessary to examine the CRV and HRV patch size distributions for the selected Subbasin-by-BPC partition, for example as depicted in **Figure 35**.

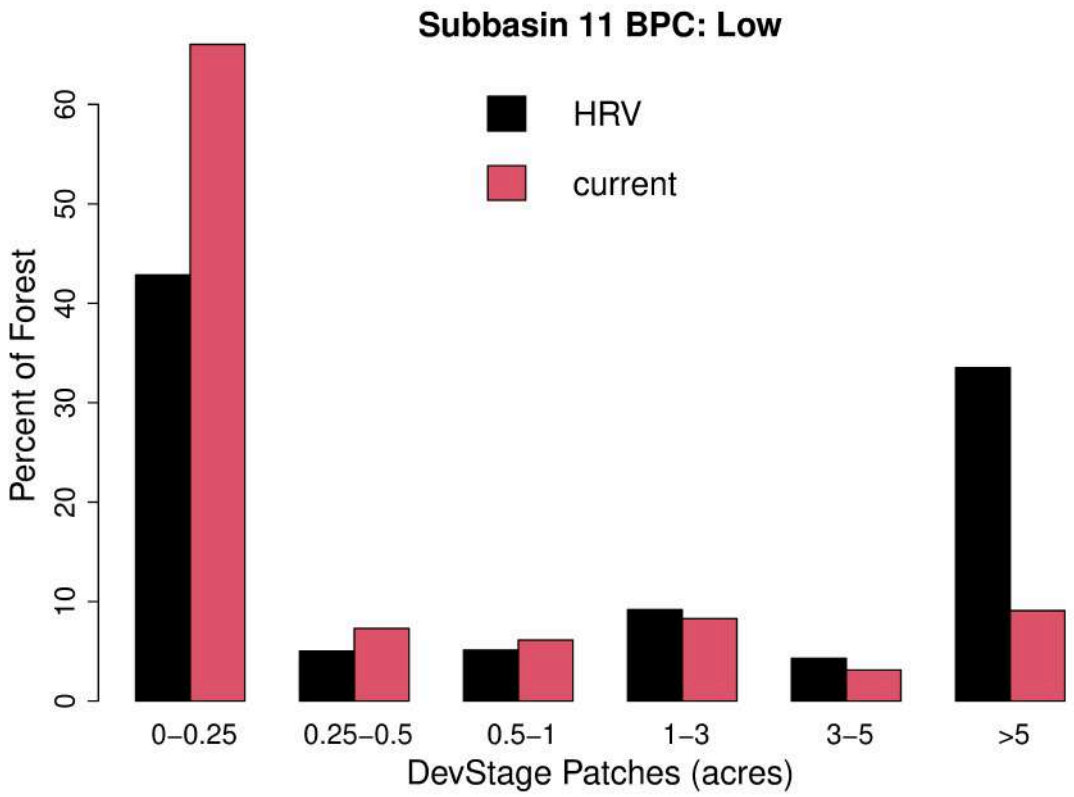

Figure 35: Barplot of the distribution of developmental stage patch sizes for the current landscape and the historical reference period (HRV) for Subbasin 11 and the Low productivity Biophysical Class (BPC = 1) for the Yuba River landscape. Developmental stages were based on tree height classes and patches were based on the 4-neighbor adjacency rule. Each bar represents the percent of forest within the Subbasin and BPC in developmental stage patches of a particular size. The departure index represents the sum of the deviations between the current and HRV bars. Departure indices > 0 represent a current landscape with a distribution of developmental stage patch sizes that differs in some way from the historical reference period distribution, as simulated, and increasing values represent increasing degrees of departure.

Metric 4: Percent Large Trees

We defined large trees as $>$ 30 inch dbh. Percent Large Trees is defined as the percent of the forest within the Subbasin-by-BPC partition in large trees, as defined, and the departure index reflects whether or not the current landscape is deficient in large trees relative to HRV and, if so, the degree of deficiency. The departure index is negative if the current landscape has too little area in large trees compared to HRV.

The Percent Large Trees departure index is depicted in **Figure 36**. As before, the departure index was assigned to each Subbasin-by-BPC partition; consequently, there were 75 distinct values assigned. Thus, to better assess departure by Subbasin and BPC, one needs to examine the attribute table for the departure layer.

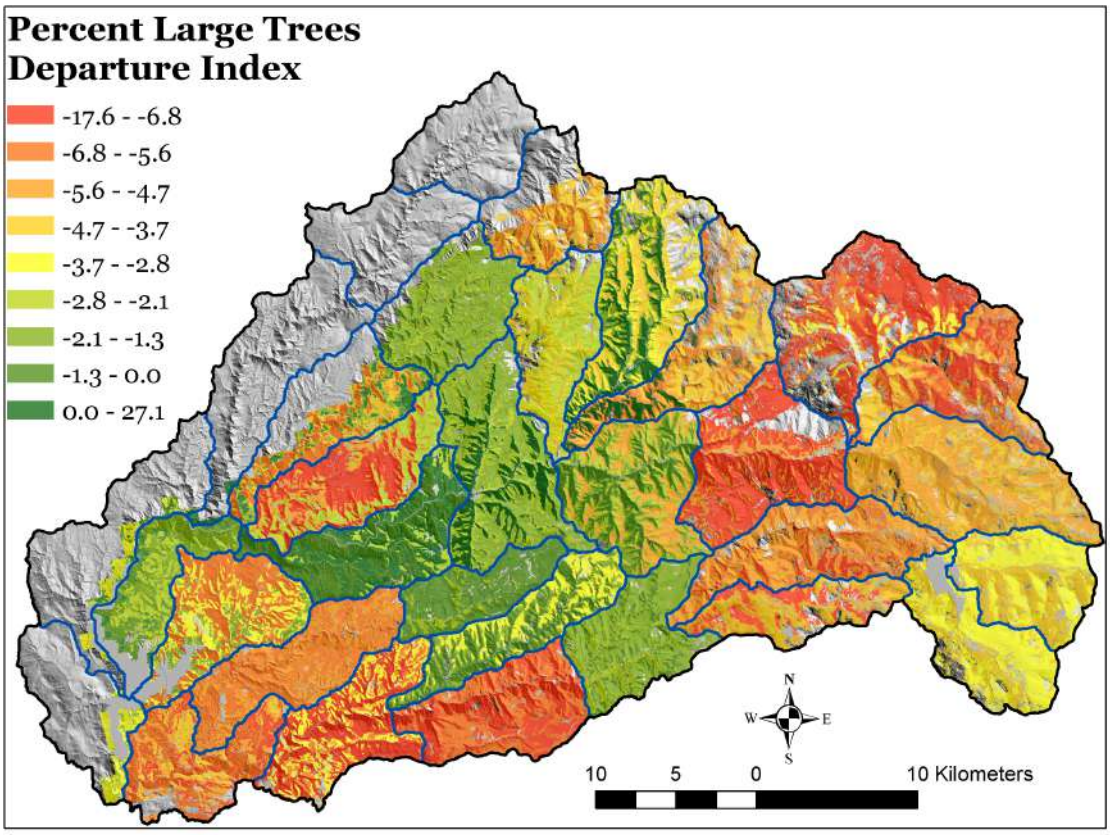

Figure 36: Subbasin-by-BPC level departure index for large trees (> 30 inch dbh) for the Yuba River landscape. The departure index represents the deviation of the current Subbasin and biophysical class (BPC) condition from its historical reference period condition, as simulated. Departure indices < -1 represent a current landscape with less total area in large trees than during the historical reference period, as simulated, and increasing negative values represent increasing degrees of departure.

Metric 5: Large Tree Patch Size Distribution

We defined large trees as described above. Here, we quantified the size of individual patches of large trees and determined the percent of forest within the Subbasin-by-BPC partition in large tree patches in each of several patch size classes or bins (see above), and compared the current and historical distributions. The departure index reflects whether or not the current landscape has a distribution of large tree patch sizes that differs from HRV and, if so, the degree of differences in the two distributions.

The Large Tree Patch Size Distribution departure index is depicted in **Figure 37**. As before, the departure index was assigned to each Subbasin-by-BPC partition; consequently, there were 75 distinct values assigned. Thus, to better assess departure by Subbasin and BPC, one needs to examine the attribute table for the departure layer.

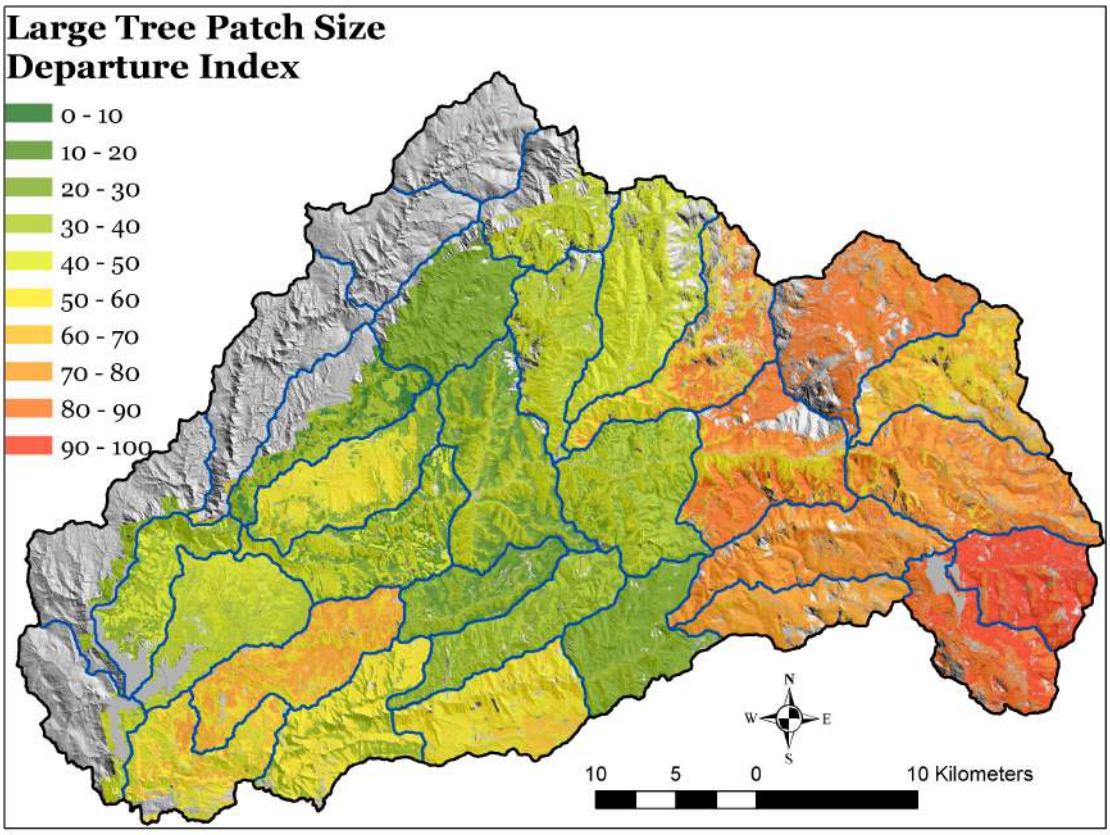

Figure 37: Subbasin-by-BPC level departure index for large tree (> 30 inch dbh) patch size distribution for the Yuba River landscape. The departure index represents the deviation of the current Subbasin and biophysical class (BPC) condition from its historical reference period condition, as simulated. Departure indices > 0 represent a current landscape with a distribution of large tree patch sizes that differs in some way from the historical reference period distribution, as simulated, and increasing values represent increasing degrees of departure.

To further evaluate departure in this patch size distribution metric, it is necessary to examine the CRV and HRV patch size distributions for the selected Subbasin-by-BPC partition, for example as depicted in **Figure 38**.

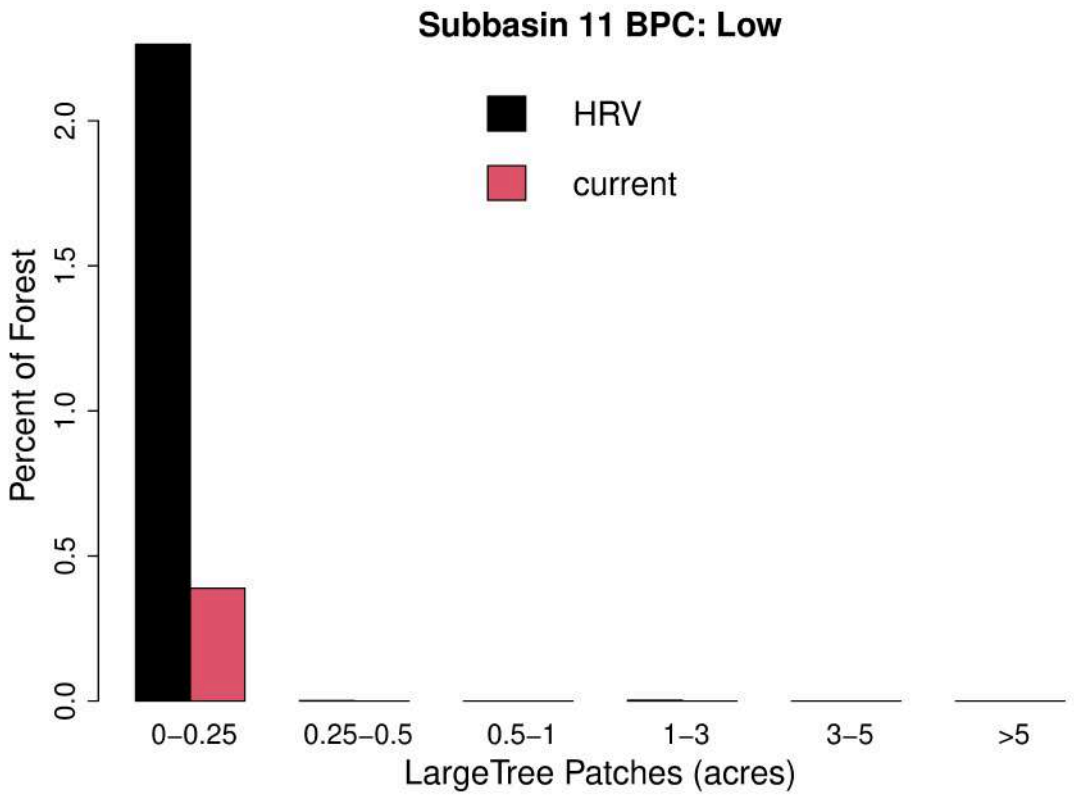

Figure 38: Barplot of the distribution of large tree (> 30 inch dbh) patch sizes for the current landscape and the historical reference period (HRV) for Subbasin 11 and the Low productivity Biophysical Class (BPC = 4) for the Yuba River landscape. See previous barplot caption for details on interpretation.

Metric 6: Tree Size Class Patch Size Distribution

We defined tree size class based on six tree diameter classes, ranging from Open (< 1 in dbh) to large Trees (> 30 in dbh), as described previously. Here, for each snapshot of the landscape we constructed a patch mosaic comprised of tree size classes in which patches were defined using the 4-neighbor rule. For each snapshot, we quantified the size of each tree size class patch and determined the percent of forest within the Subbasin-by-BPC partition in each of several patch size classes or bins. The departure index reflects whether or not the current landscape has a distribution of tree size class patch sizes that differs from HRV and, if so, the degree of differences in the two distributions.

The Tree Size Class Patch Size Distribution departure index is depicted in **Figure 39**. As before, the departure index was assigned to each Subbasin-by-BPC partition; consequently, there were 75 distinct values assigned. Thus, to better assess departure by Subbasin and BPC, one needs to examine the attribute table for the departure layer.

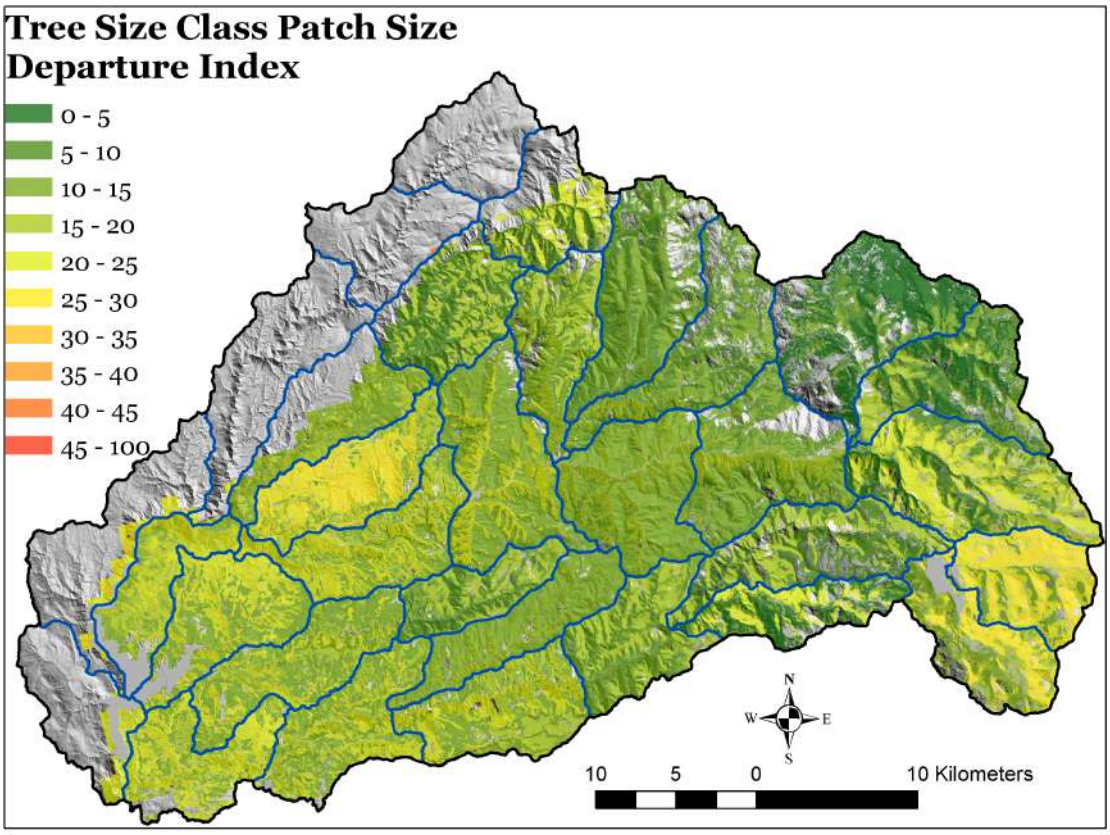

Figure 39: Subbasin-by-BPC level departure index for tree size class (based on dbh) patch size distribution for the Yuba River landscape. The departure index represents the deviation of the current Subbasin and biophysical class (BPC) condition from its historical reference period condition, as simulated. Departure indices > 0 represent a current landscape with a distribution of tree size patch sizes that differs in some way from the historical reference period distribution, as simulated, and increasing values represent increasing degrees of departure.

To further evaluate departure in this patch size distribution metric, it is necessary to examine the CRV and HRV patch size distributions for the selected Subbasin-by-BPC partition, for example as depicted in **Figure 40**.

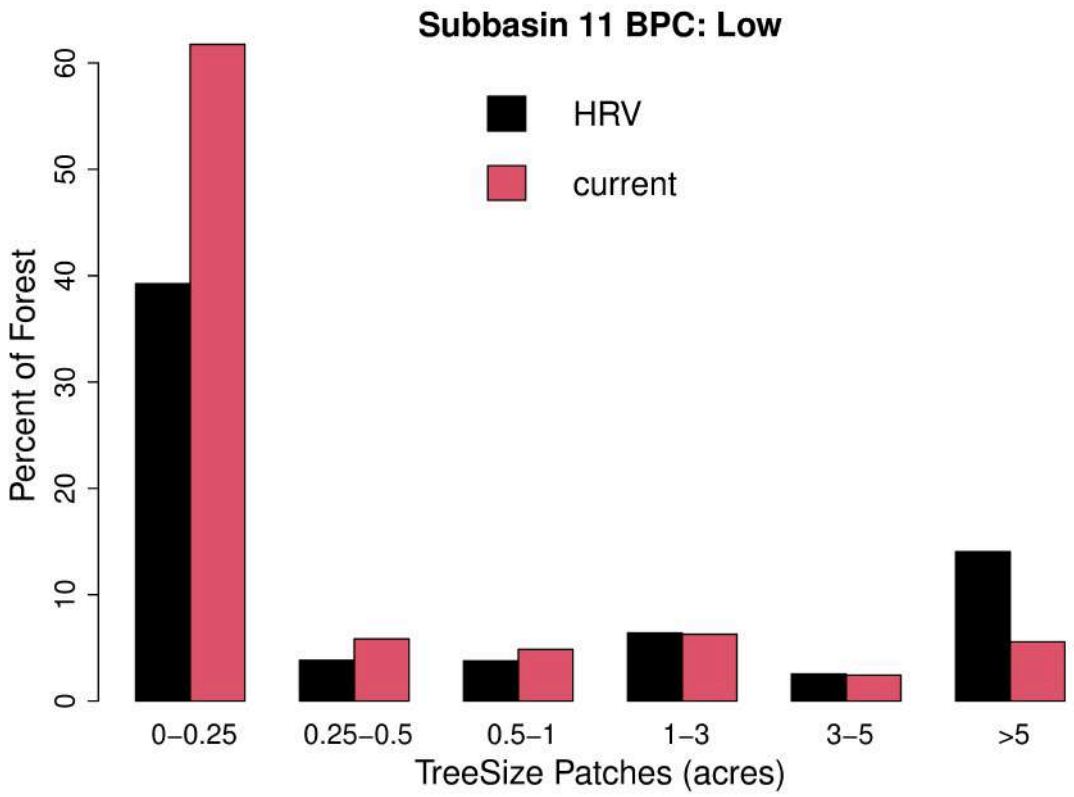

Figure 40: Barplot of the distribution of tree size class (based on dbh) patch sizes for the current landscape and the historical reference period (HRV) for Subbasin 11 and the Low productivity Biophysical Class (BPC = 4) for the Yuba River landscape. See previous barplot caption for details on interpretation.

Composite Departure Score

We combined the 6 Subbasin-level departure metrics above into a single composite departure score, which can be interpreted as a measure of overall departure in vegetation composition and configuration within the Subbasin-by-BPC partition. Maximum departure occurs when the forest has too little area in large forest openings and/or large trees, and/or too homogeneous or uniform a vegetation patch mosaic (i.e., too little spatial variability) defined on the basis of either developmental stages (or tree height classes) or tree size classes (or tree diameter classes).

The composite departure score is depicted in **Figure 41**. Not surprisingly, the Subbasins and BPCs vary somewhat in their overall departure from HRV, and these differences provide a basis for prioritizing project locations with this landscape.

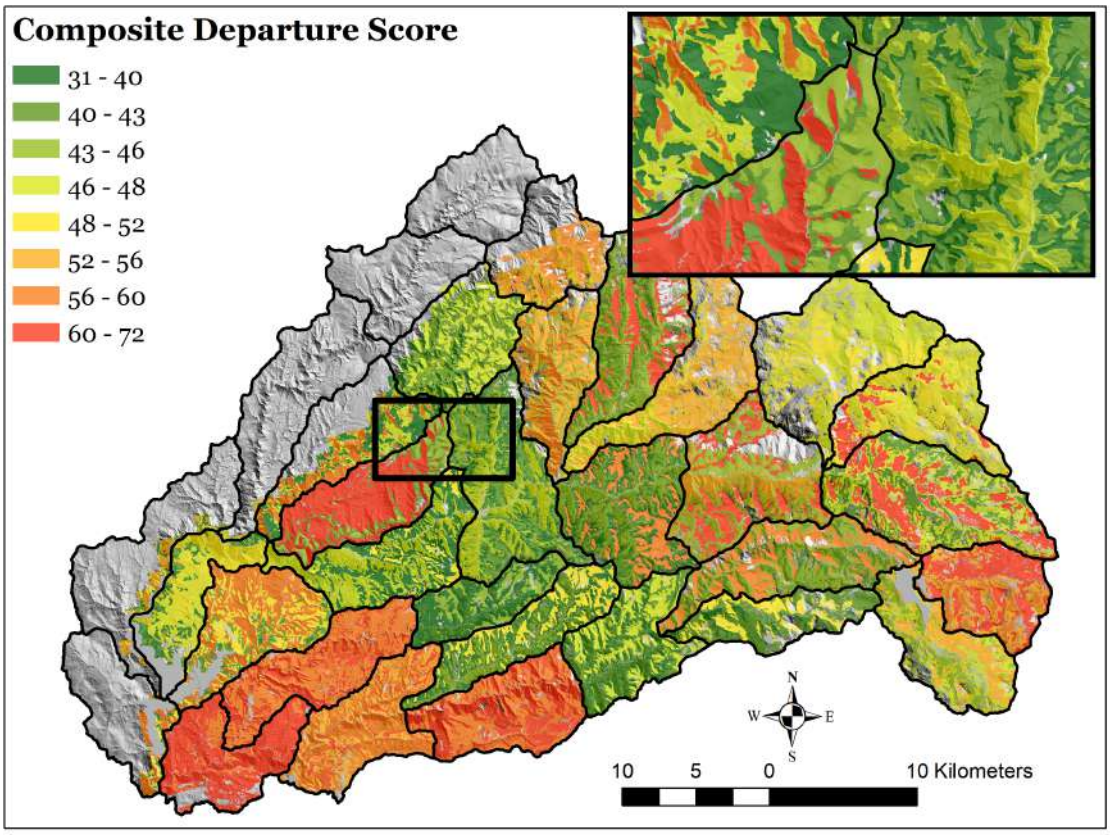

Figure 41: Subbasin-by-BPC level composite departure index derived from the average of the six component metrics for the Yuba River landscape. The composite departure index represents the percentage of maximum departure of the current GPU condition from its historical range of variability (HRV), as simulated. Larger values indicate increasing degrees of departure.

APPENDIX B1 - Wildfire Susceptibility

As described in the GTR, wildfire susceptibility was modeled as a Logistic function of fuels and climate for most cover types. The fuels component was modeled as a Logistic function of the number of years since the last fire (fuelAge) and the Heat Load Index (hli). The climate component was modeled as a Logistic function of the Wildfire Climate Index which was based on the inverted and rescaled 5-year mean Palmer Modified Drought Index. The fuels and climate components were combined with a geometric mean to produce the final Wildfire Susceptibility Index. The final function included 5 beta coefficients (b_0 - b_4). We used expert opinion to specify the beta coefficients for each cover type. We varied the b_0 and b_1 coefficients among cover types to reflect differences in reported historical mean fire return intervals among cover types - shifting the response curves left or right so that the inflection point (Wildfire Susceptibility Index = 0.5) roughly equaled the target mean return interval - and held the Heat Load Index coefficient (b_2) and Climate coefficients (b_3 and b_4) the same across all cover types to reflect the global affect of topography and climate on wildfire susceptibility.

The figures below depict the final wildfire susceptibility response functions for each cover type in alphabetical order (noting that some cover types did not have response functions, as noted in the text). The response functions depict the wildfire Susceptibility Index as a Logistic function of the number of years since the last fire (Years since fire). The dashed, solid and dotted lines depict the response functions for the minimum, mean and maximum Heat Load Index (hli), and the red, black and green sets of lines depict the response functions for the minimum, mean and maximum Wildfire Climate Index. The values of the Logistic parameters (b_0 - b_4) for the cover type are shown as well.

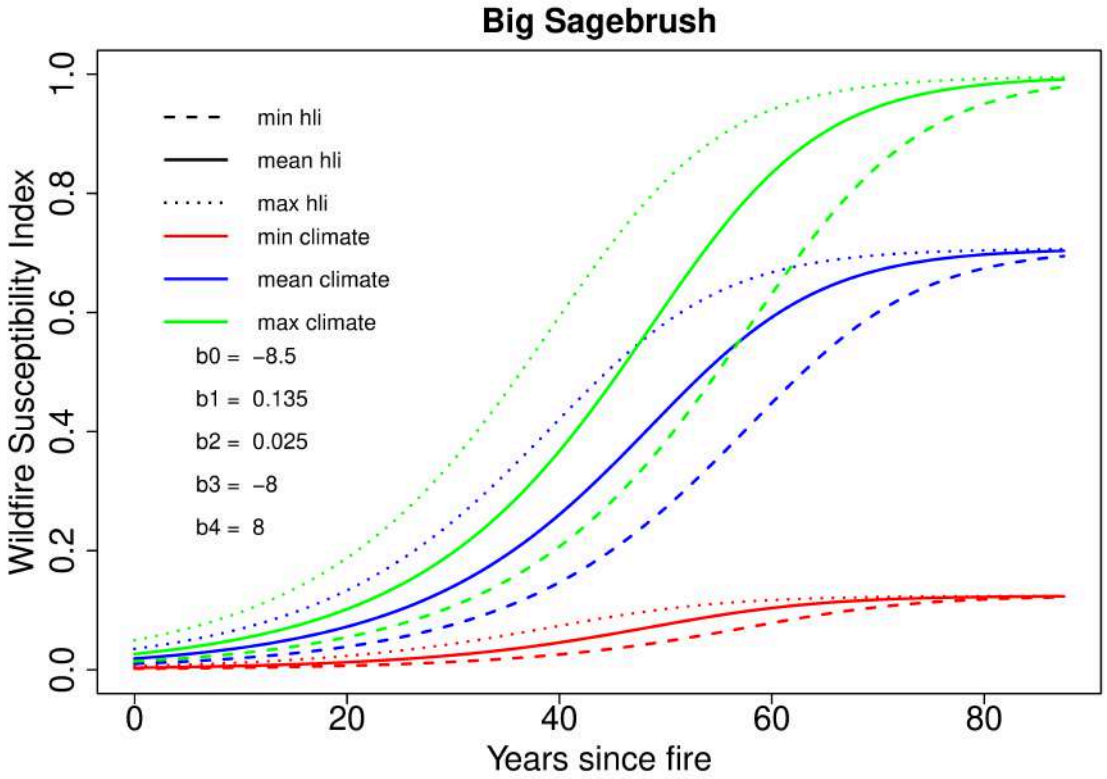

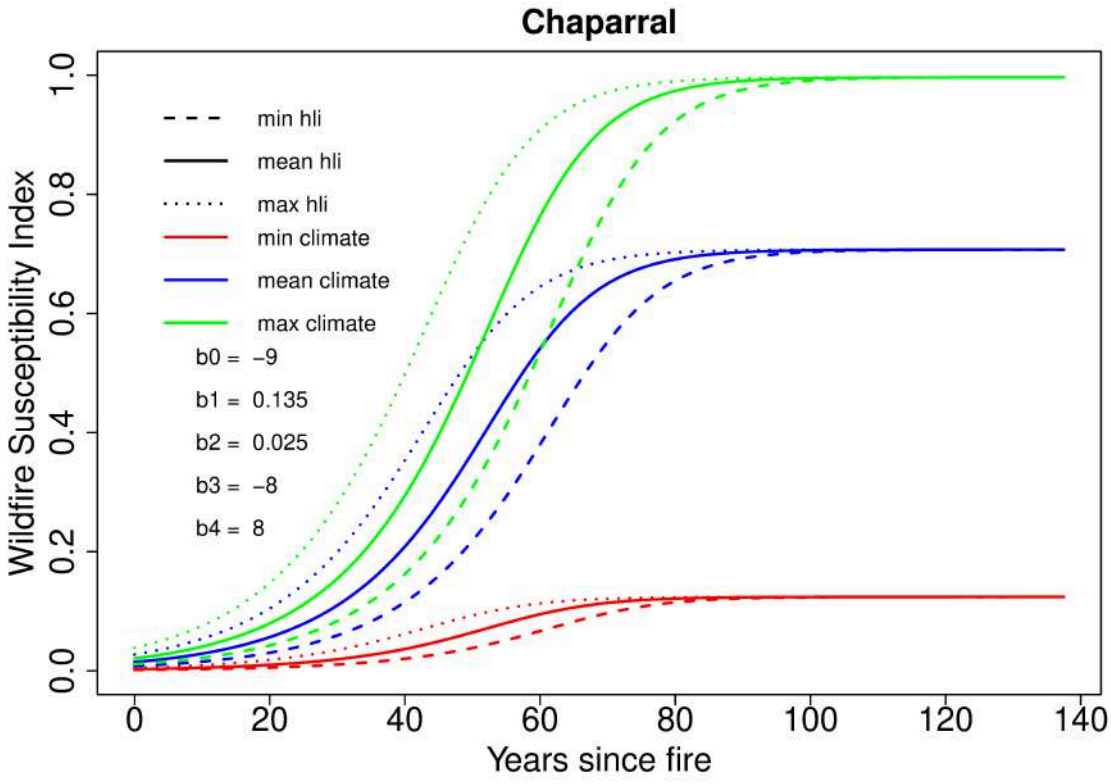
Chaparral
Wildfire Susceptibility Index
Years since fire
min hli
mean hli
max hli
min climate
mean climate
max climate
b0 = −9
b1 = 0.135
b2 = 0.025
b3 = −8
b4 = 8
0.0
0.2
0.4
0.6
0.8
1.0
0
20
40
60
80
100
120
140

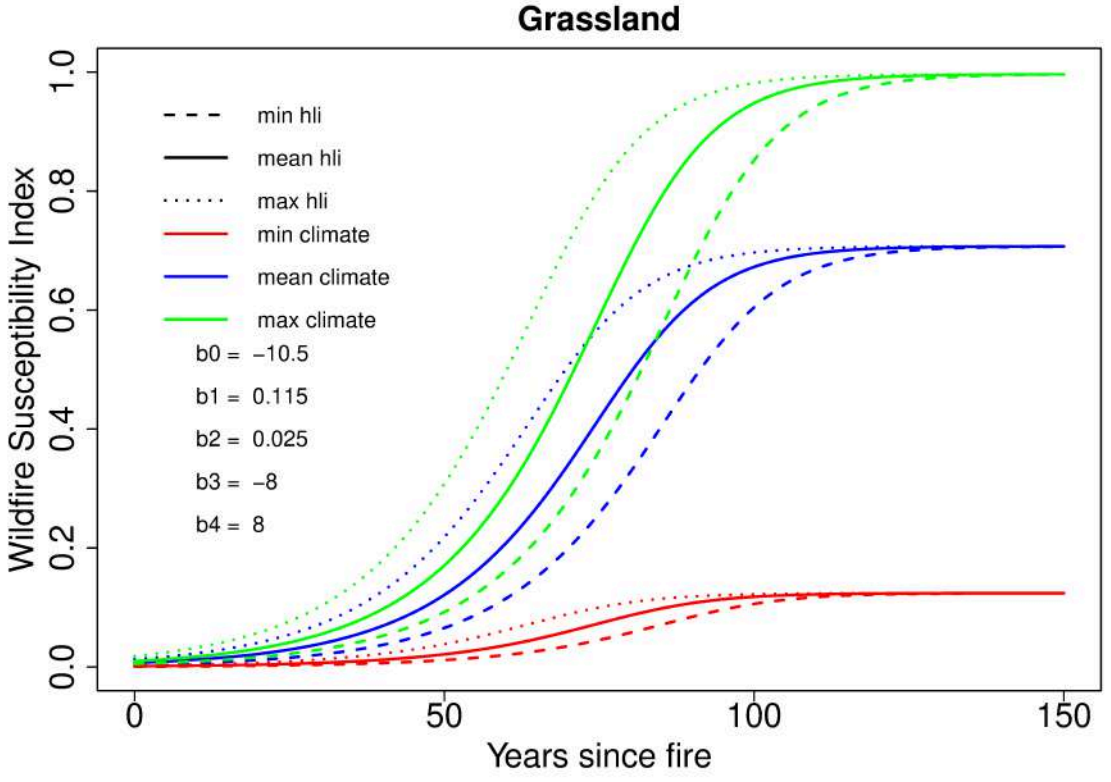
Grassland
Wildfire Susceptibility Index
Years since fire
min hli
mean hli
max hli
min climate
mean climate
max climate
b0 = −10.5
b1 = 0.115
b2 = 0.025
b3 = −8
b4 = 8
0.0
0.2
0.4
0.6
0.8
1.0
0
50
100
150

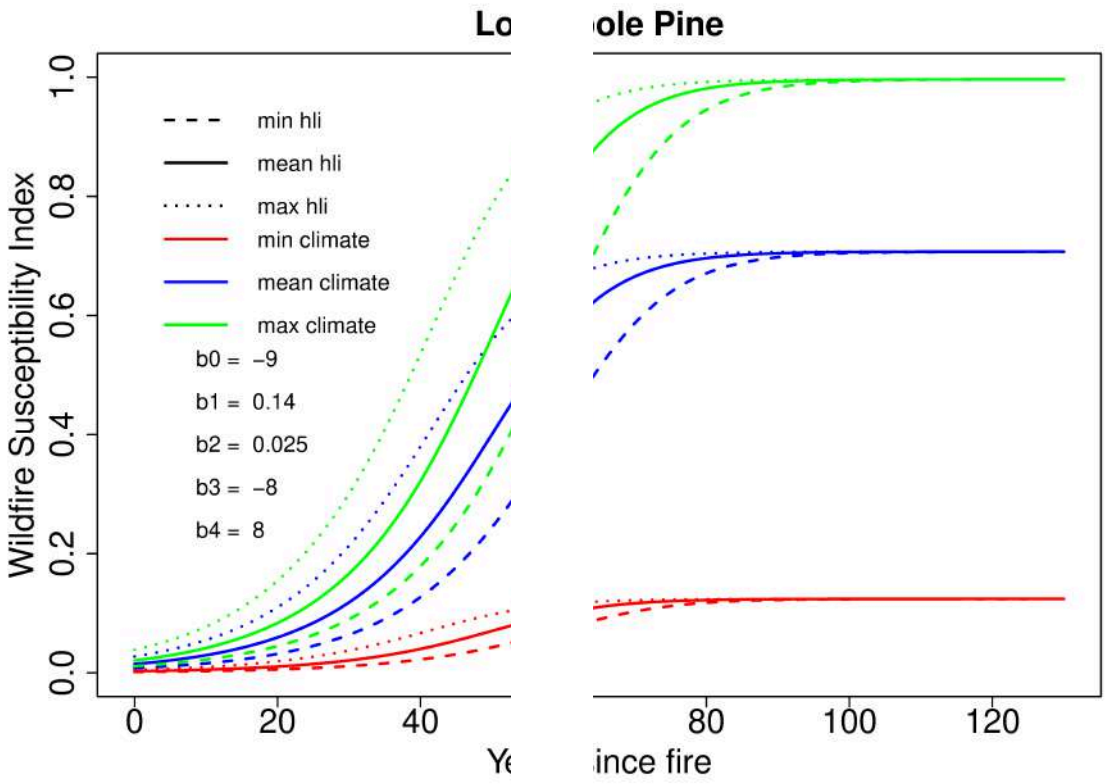
Lo
ole Pine
Wildfire Susceptibility Index
0.0
0.2
0.4
0.6
0.8
1.0
min hli
mean hli
max hli
min climate
mean climate
max climate
b0 = −9
b1 = 0.14
b2 = 0.025
b3 = −8
b4 = 8
0
20
40
80
100
120
Ye
ince fire

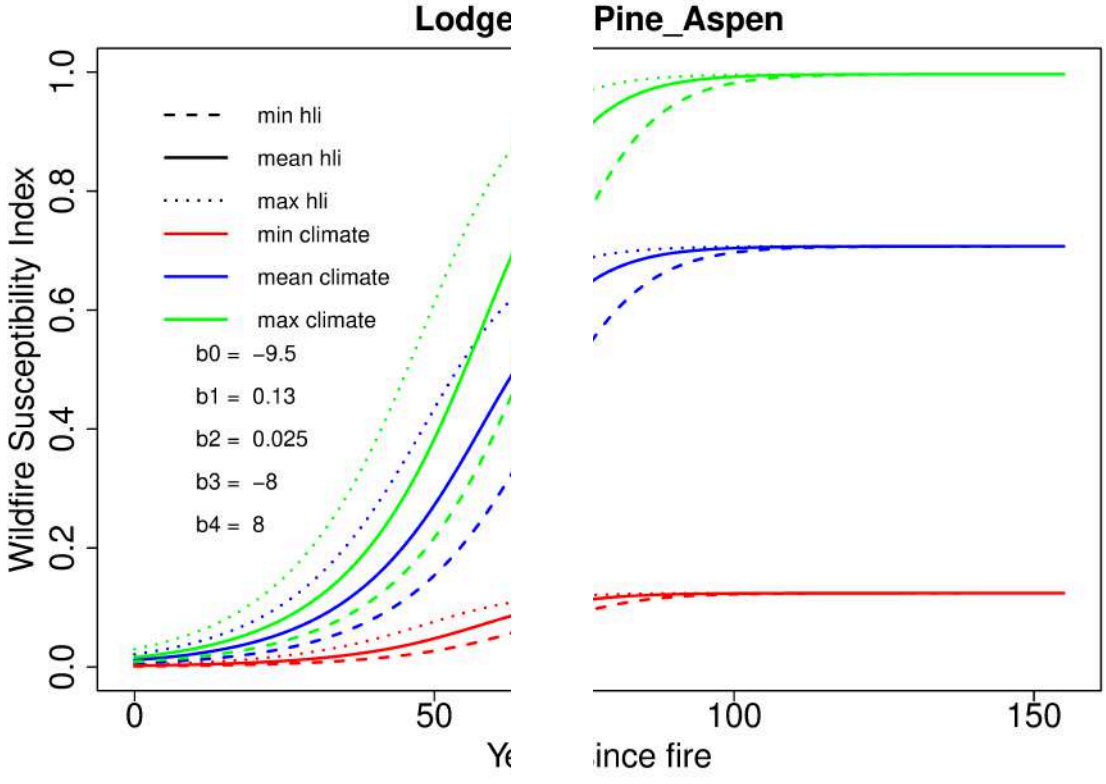
Lodge
Pine_Aspen
Wildfire Susceptibility Index
0.0
0.2
0.4
0.6
0.8
1.0
min hli
mean hli
max hli
min climate
mean climate
max climate
b0 = −9.5
b1 = 0.13
b2 = 0.025
b3 = −8
b4 = 8
0
50
100
150
Ye
ince fire

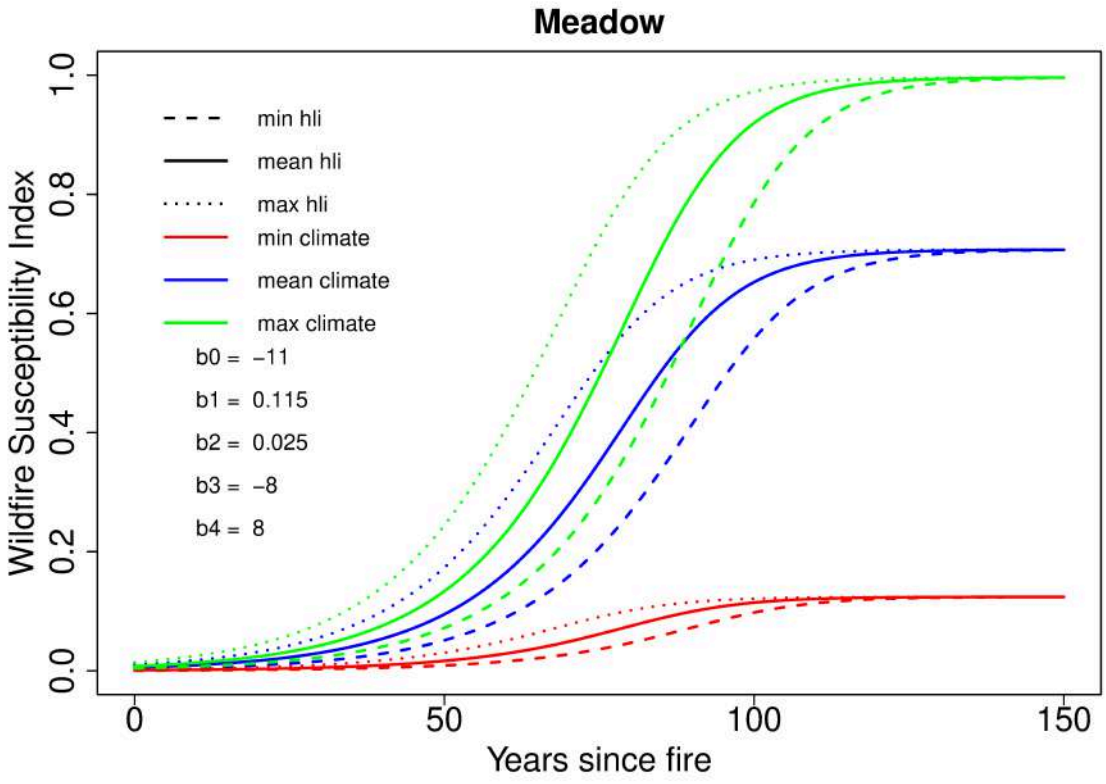
Meadow
Wildfire Susceptibility Index
0.0
0.2
0.4
0.6
0.8
1.0
min hli
mean hli
max hli
min climate
mean climate
max climate
b0 = −11
b1 = 0.115
b2 = 0.025
b3 = −8
b4 = 8
0
50
100
150
Years since fire

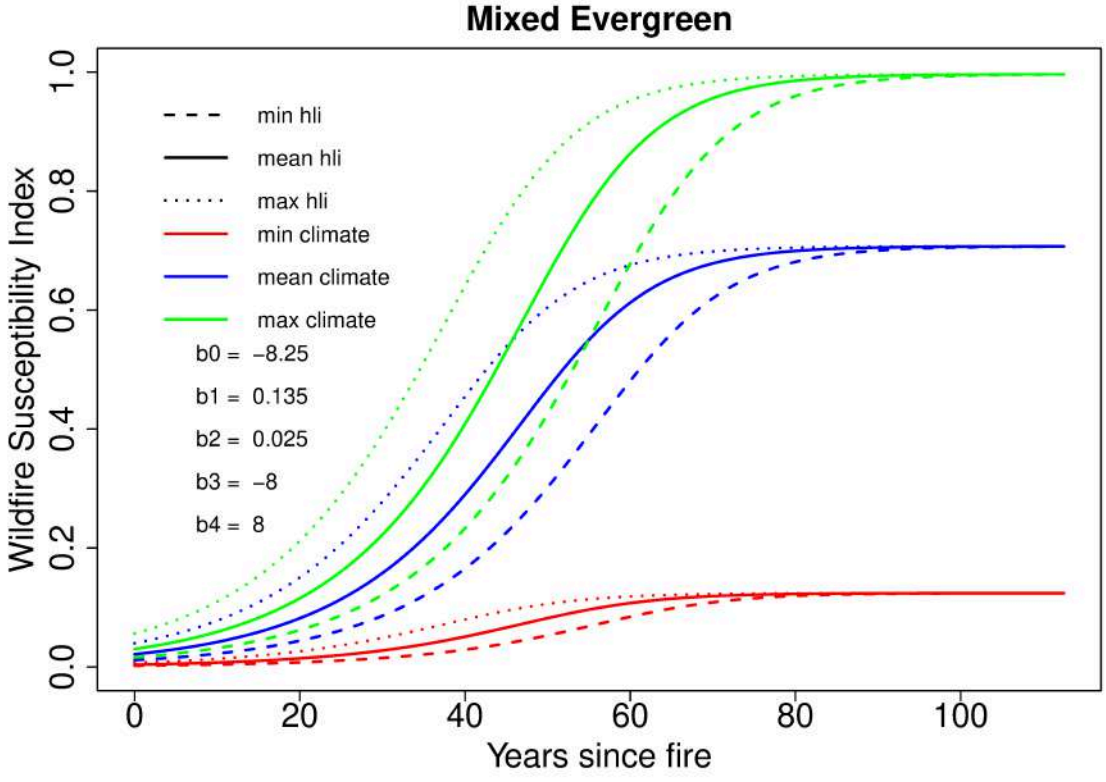
Mixed Evergreen
Wildfire Susceptibility Index
0.0
0.2
0.4
0.6
0.8
1.0
min hli
mean hli
max hli
min climate
mean climate
max climate
b0 = −8.25
b1 = 0.135
b2 = 0.025
b3 = −8
b4 = 8
0
20
40
60
80
100
Years since fire

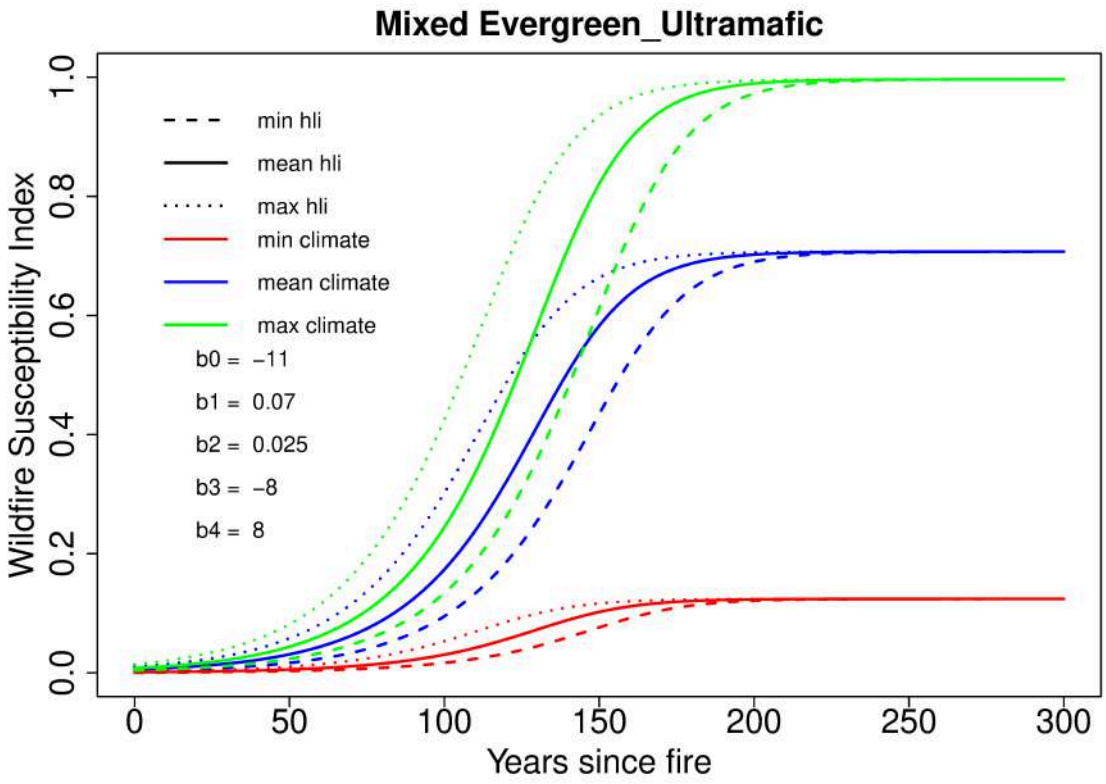
Mixed Evergreen_Ultramafic
Wildfire Susceptibility Index
Years since fire
min hli
mean hli
max hli
min climate
mean climate
max climate
b0 = −11
b1 = 0.07
b2 = 0.025
b3 = −8
b4 = 8
0.0
0.2
0.4
0.6
0.8
1.0
0
50
100
150
200
250
300

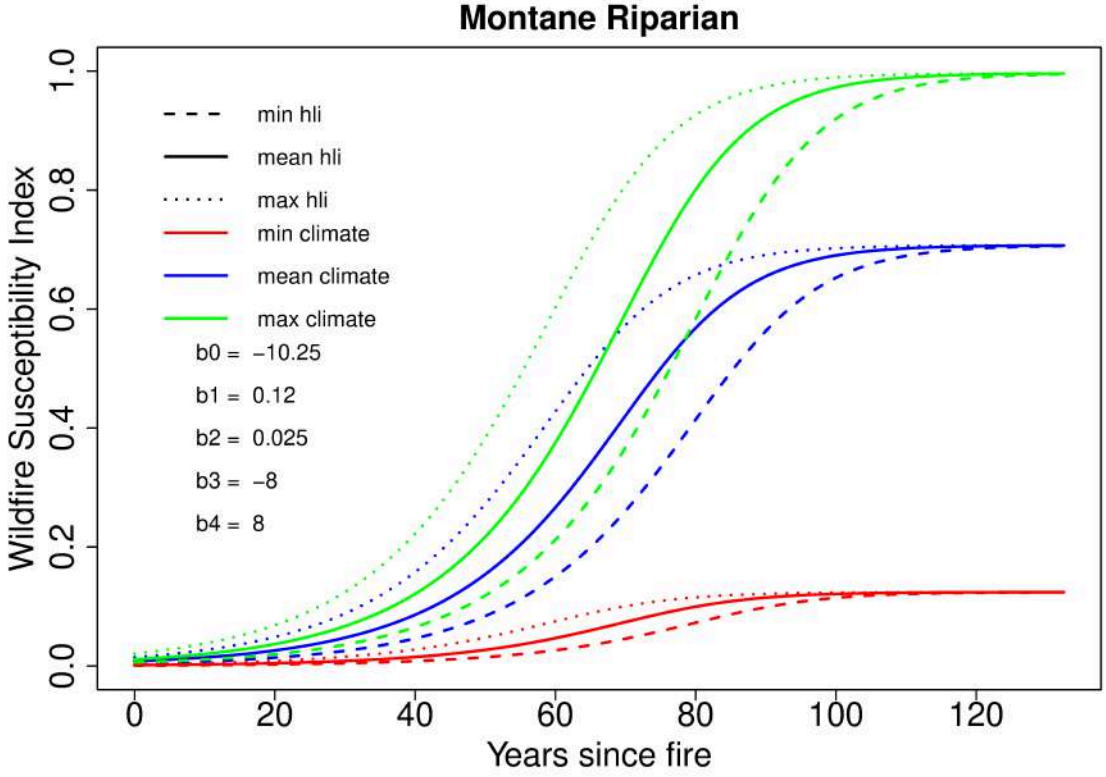
Montane Riparian
Wildfire Susceptibility Index
Years since fire
min hli
mean hli
max hli
min climate
mean climate
max climate
b0 = −10.25
b1 = 0.12
b2 = 0.025
b3 = −8
b4 = 8
0.0
0.2
0.4
0.6
0.8
1.0
0
20
40
60
80
100
120

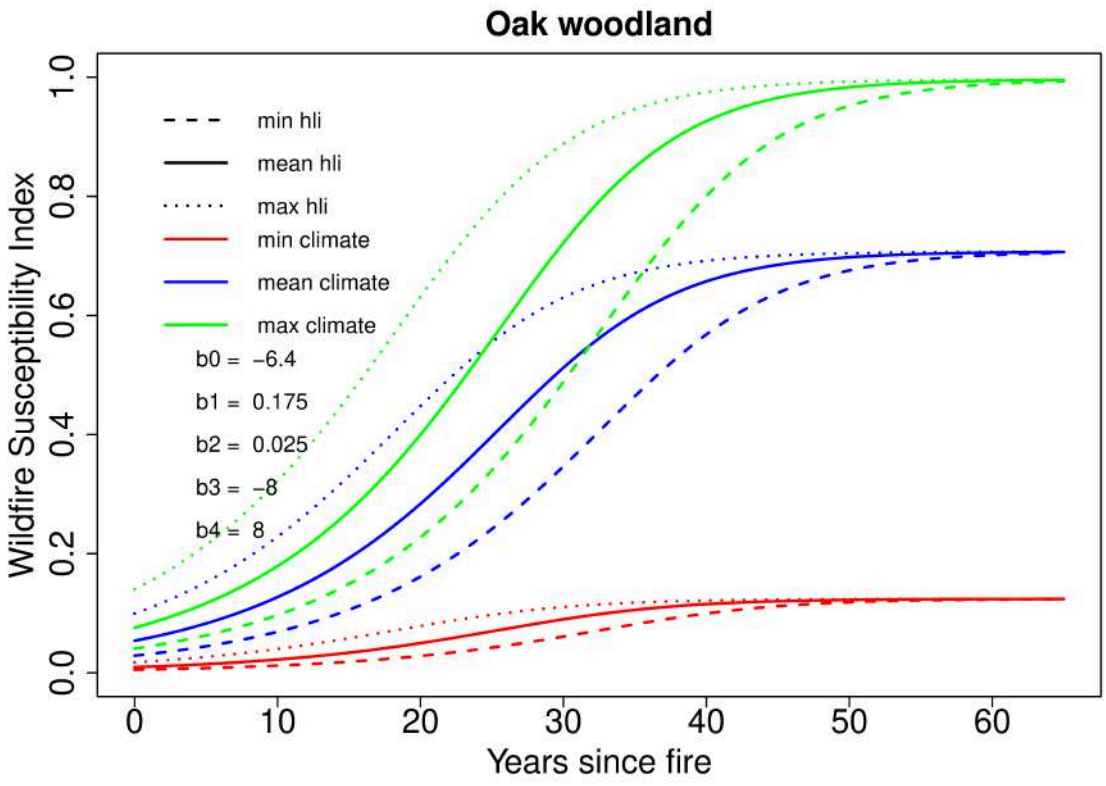
Oak woodland
Wildfire Susceptibility Index
Years since fire
min hli
mean hli
max hli
min climate
mean climate
max climate
b0 = −6.4
b1 = 0.175
b2 = 0.025
b3 = −8
b4 = 8
0.0
0.2
0.4
0.6
0.8
1.0
0
10
20
30
40
50
60

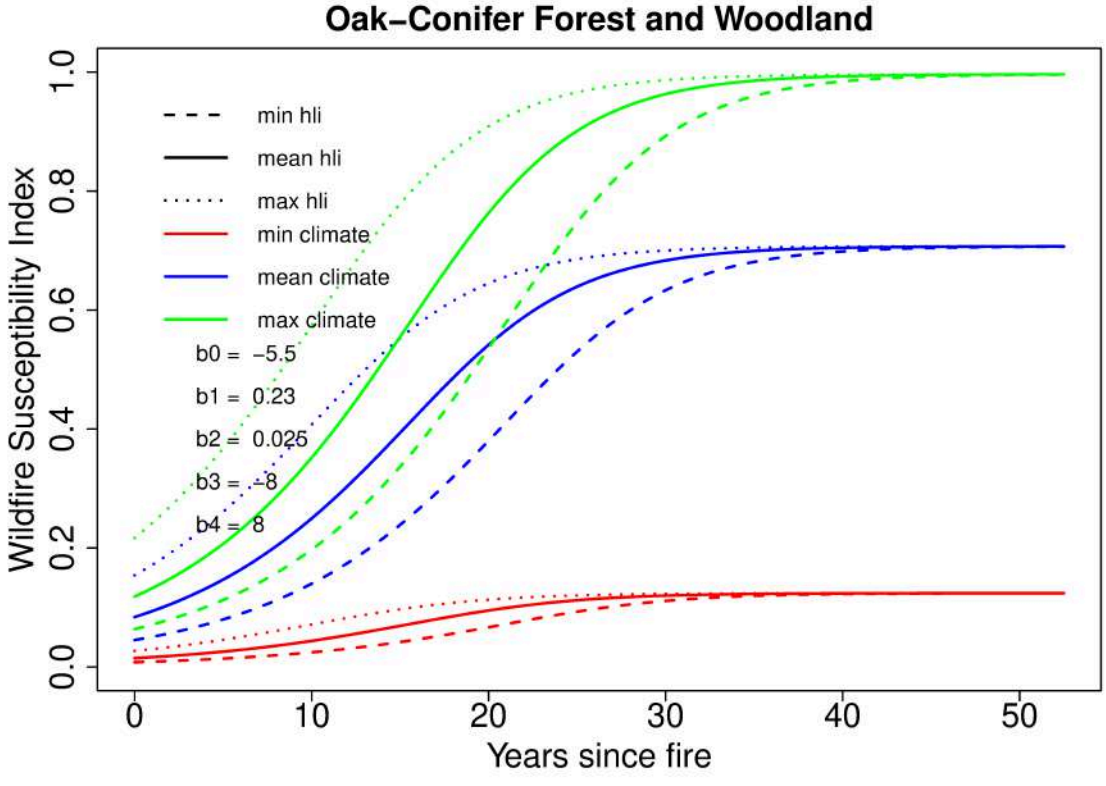
Oak−Conifer Forest and Woodland
Wildfire Susceptibility Index
Years since fire
min hli
mean hli
max hli
min climate
mean climate
max climate
b0 = −5.5
b1 = 0.23
b2 = 0.026
b3 = −8
b4 = 8
0.0
0.2
0.4
0.6
0.8
1.0
0
10
20
30
40
50

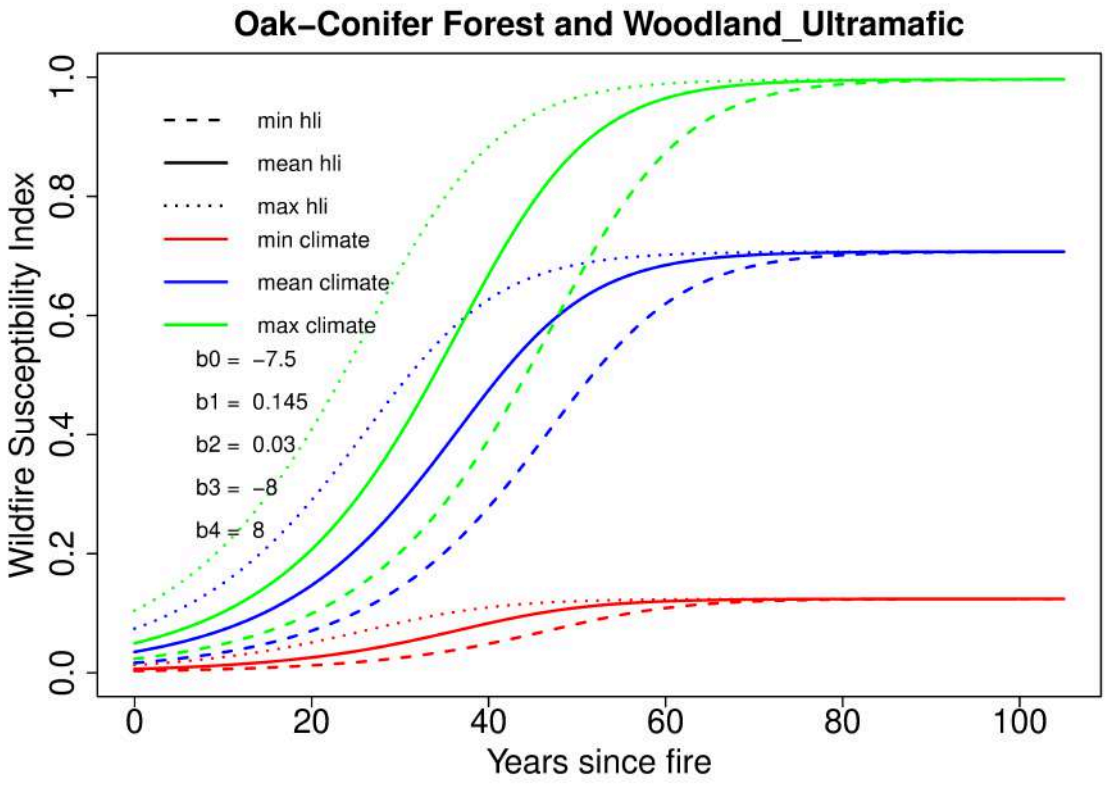
Oak–Conifer Forest and Woodland_Ultramafic
Wildfire Susceptibility Index
0.0
0.2
0.4
0.6
0.8
1.0
min hli
mean hli
max hli
min climate
mean climate
max climate
b0 = −7.5
b1 = 0.145
b2 = 0.03
b3 = −8
b4 = 8
0
20
40
60
80
100
Years since fire

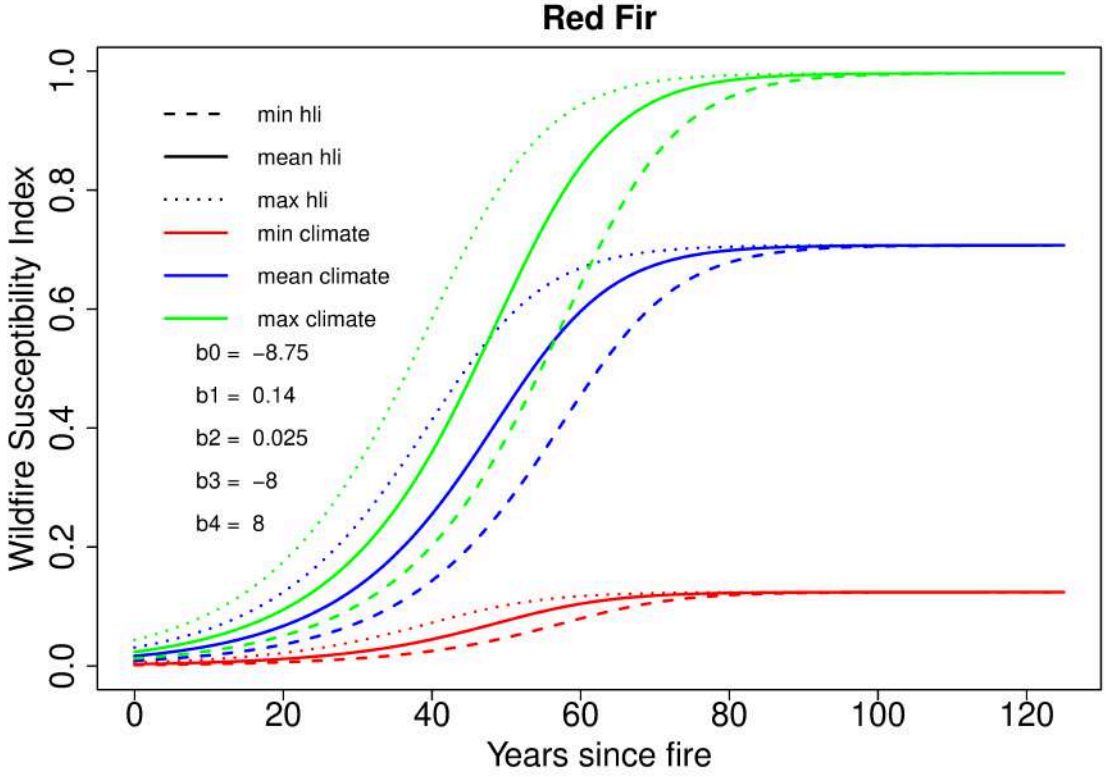
Red Fir
Wildfire Susceptibility Index
0.0
0.2
0.4
0.6
0.8
1.0
min hli
mean hli
max hli
min climate
mean climate
max climate
b0 = −8.75
b1 = 0.14
b2 = 0.025
b3 = −8
b4 = 8
0
20
40
60
80
100
120
Years since fire

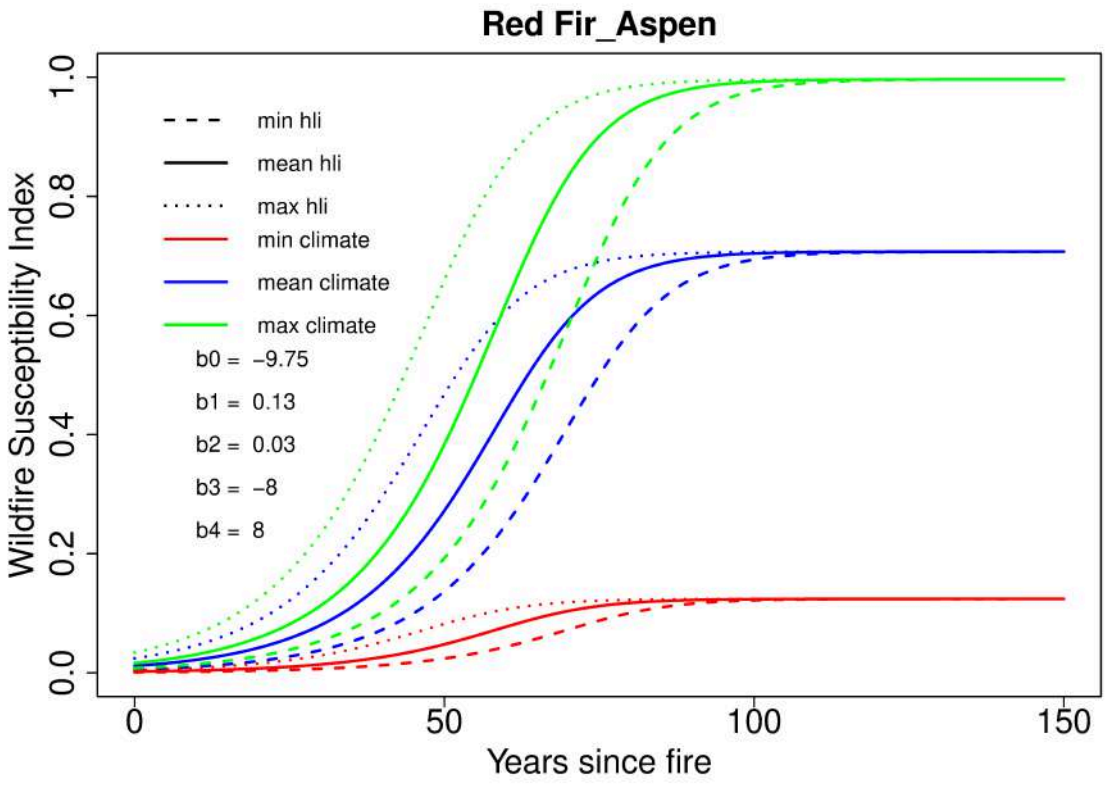
Red Fir_Aspen
Wildfire Susceptibility Index
0.0
0.2
0.4
0.6
0.8
1.0
min hli
mean hli
max hli
min climate
mean climate
max climate
b0 = −9.75
b1 = 0.13
b2 = 0.03
b3 = −8
b4 = 8
0
50
100
150
Years since fire

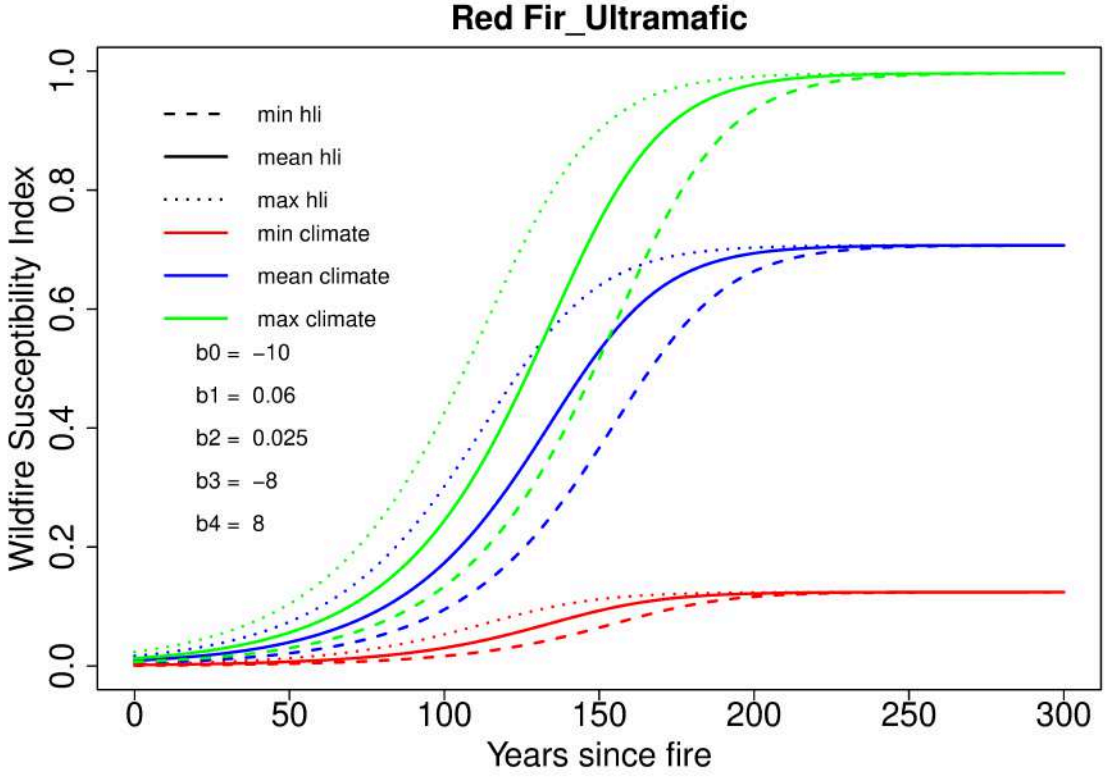
Red Fir_Ultramafic
Wildfire Susceptibility Index
0.0
0.2
0.4
0.6
0.8
1.0
min hli
mean hli
max hli
min climate
mean climate
max climate
b0 = −10
b1 = 0.06
b2 = 0.025
b3 = −8
b4 = 8
0
50
100
150
200
250
300
Years since fire

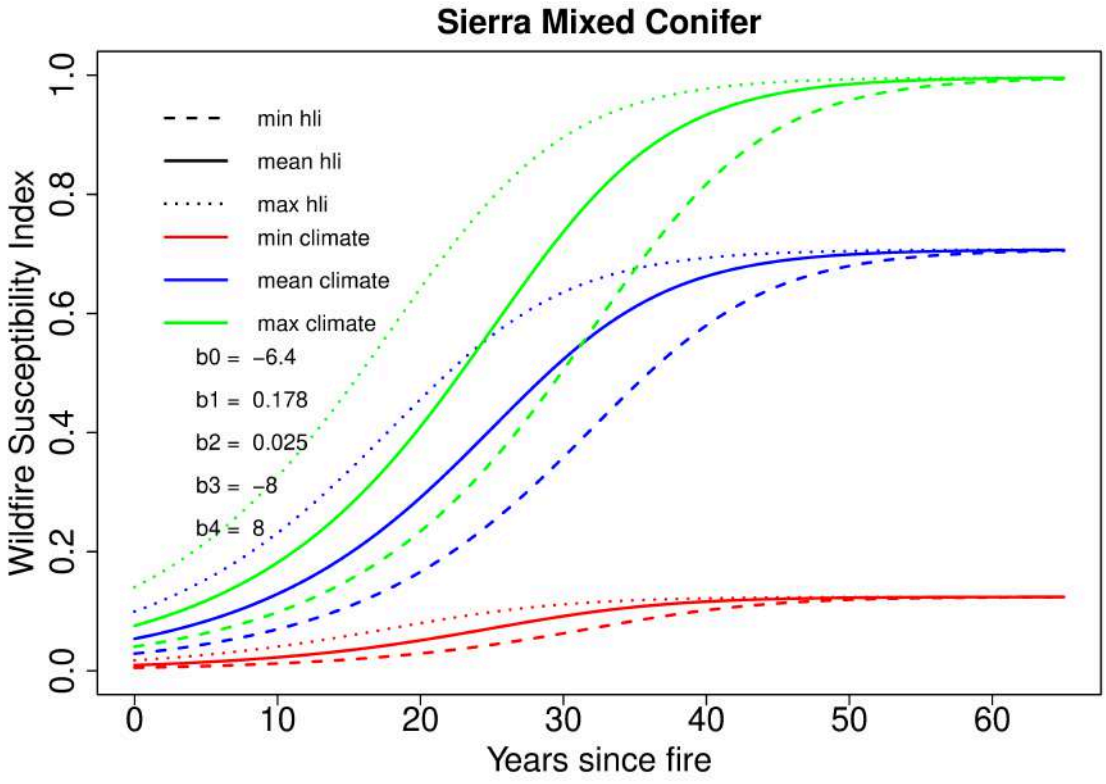
Sierra Mixed Conifer
Wildfire Susceptibility Index
Years since fire
min hli
mean hli
max hli
min climate
mean climate
max climate
b0 = −6.4
b1 = 0.178
b2 = 0.025
b3 = −8
b4 = 8
0.0
0.2
0.4
0.6
0.8
1.0
0
10
20
30
40
50
60

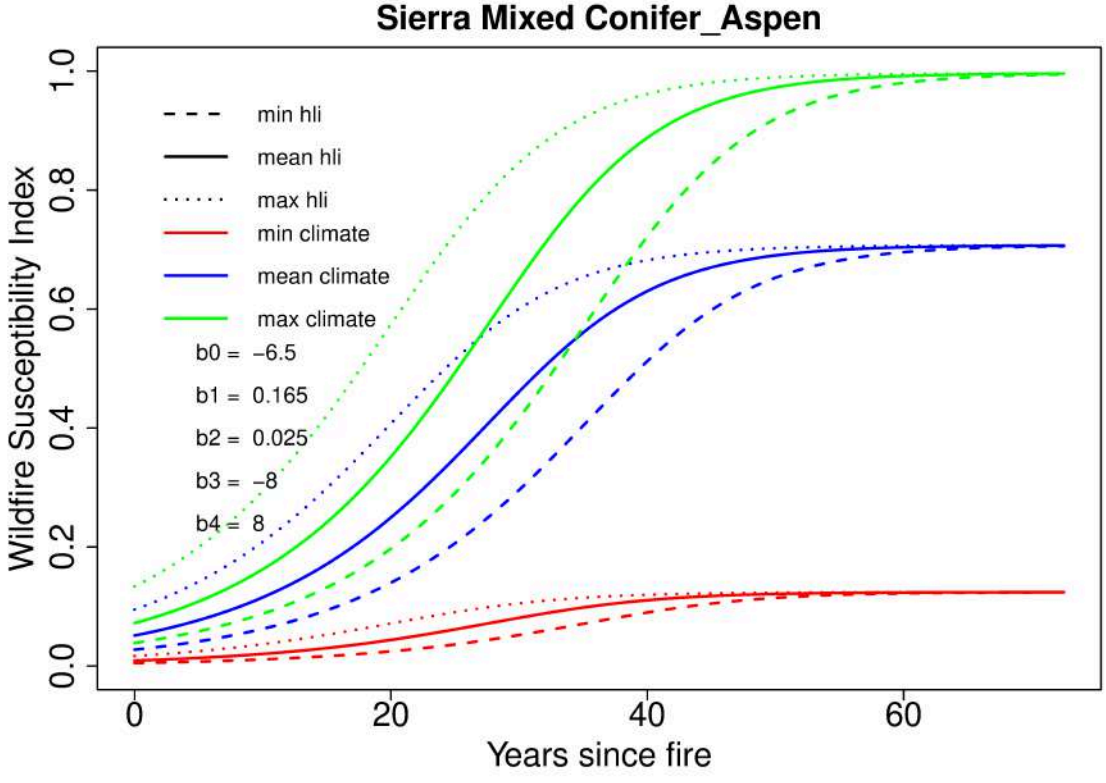
Sierra Mixed Conifer_Aspen
Wildfire Susceptibility Index
Years since fire
min hli
mean hli
max hli
min climate
mean climate
max climate
b0 = −6.5
b1 = 0.165
b2 = 0.025
b3 = −8
b4 = 8
0.0
0.2
0.4
0.6
0.8
1.0
0
20
40
60

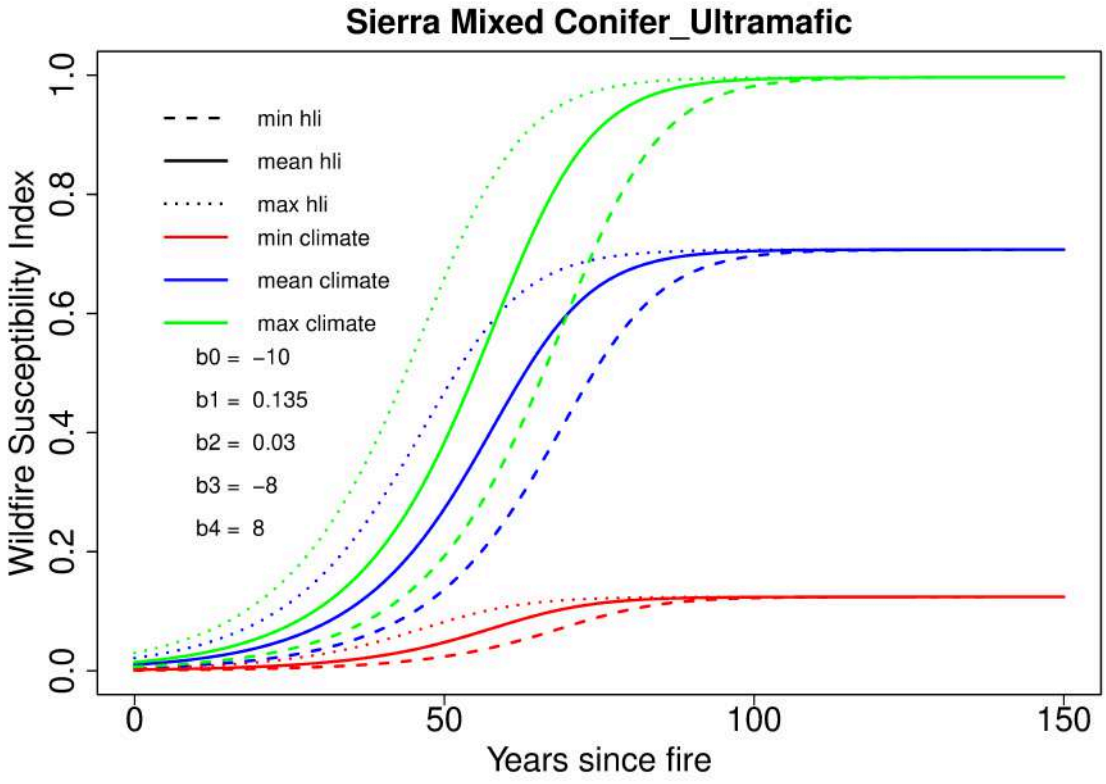
Sierra Mixed Conifer_Ultramafic
min hli
mean hli
max hli
min climate
mean climate
max climate
b0 = −10
b1 = 0.135
b2 = 0.03
b3 = −8
b4 = 8
Wildfire Susceptibility Index
0.0
0.2
0.4
0.6
0.8
1.0
0
50
100
150
Years since fire

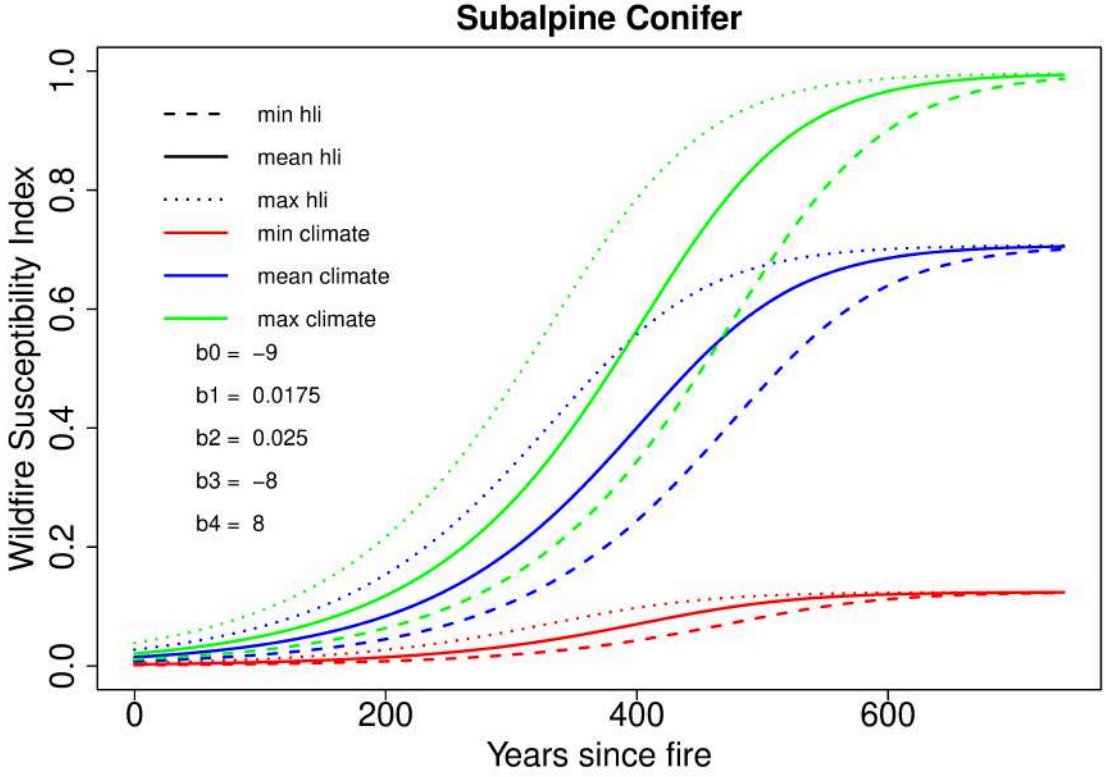
Subalpine Conifer
min hli
mean hli
max hli
min climate
mean climate
max climate
b0 = −9
b1 = 0.0175
b2 = 0.025
b3 = −8
b4 = 8
Wildfire Susceptibility Index
0.0
0.2
0.4
0.6
0.8
1.0
0
200
400
600
Years since fire

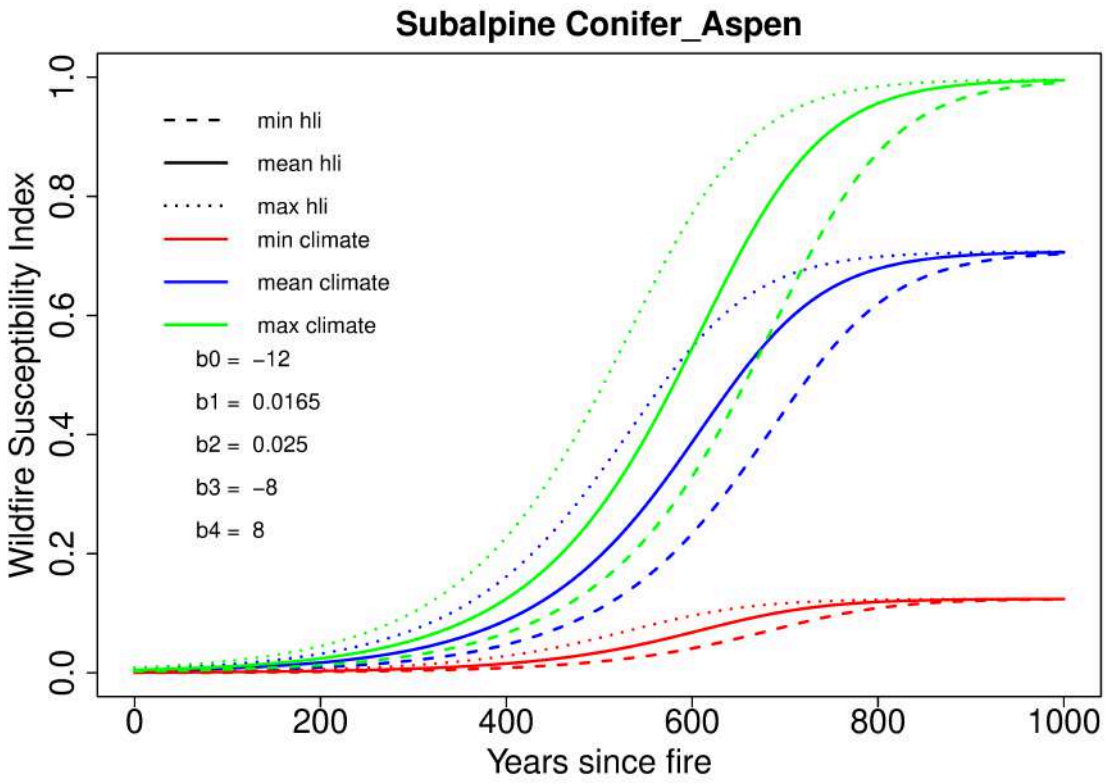
Subalpine Conifer_Aspen
Wildfire Susceptibility Index
0.0
0.2
0.4
0.6
0.8
1.0
min hli
mean hli
max hli
min climate
mean climate
max climate
b0 = −12
b1 = 0.0165
b2 = 0.025
b3 = −8
b4 = 8
0
200
400
600
800
1000
Years since fire

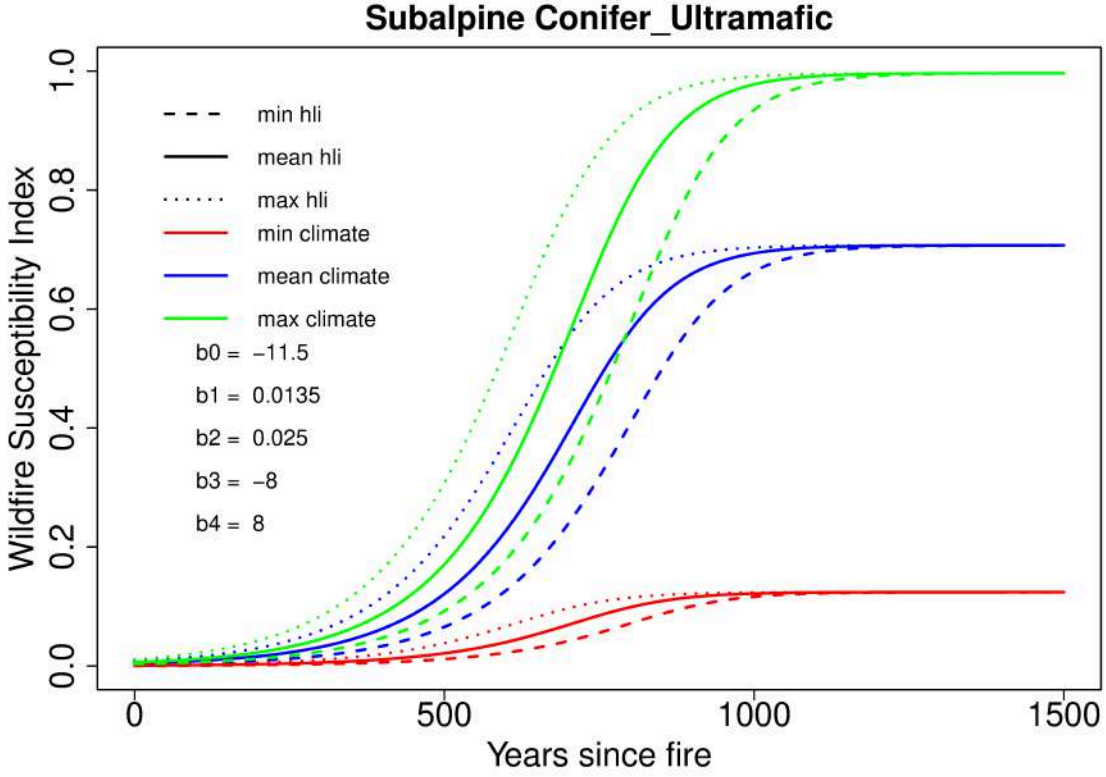
Subalpine Conifer_Ultramafic
Wildfire Susceptibility Index
0.0
0.2
0.4
0.6
0.8
1.0
min hli
mean hli
max hli
min climate
mean climate
max climate
b0 = −11.5
b1 = 0.0135
b2 = 0.025
b3 = −8
b4 = 8
0
500
1000
1500
Years since fire

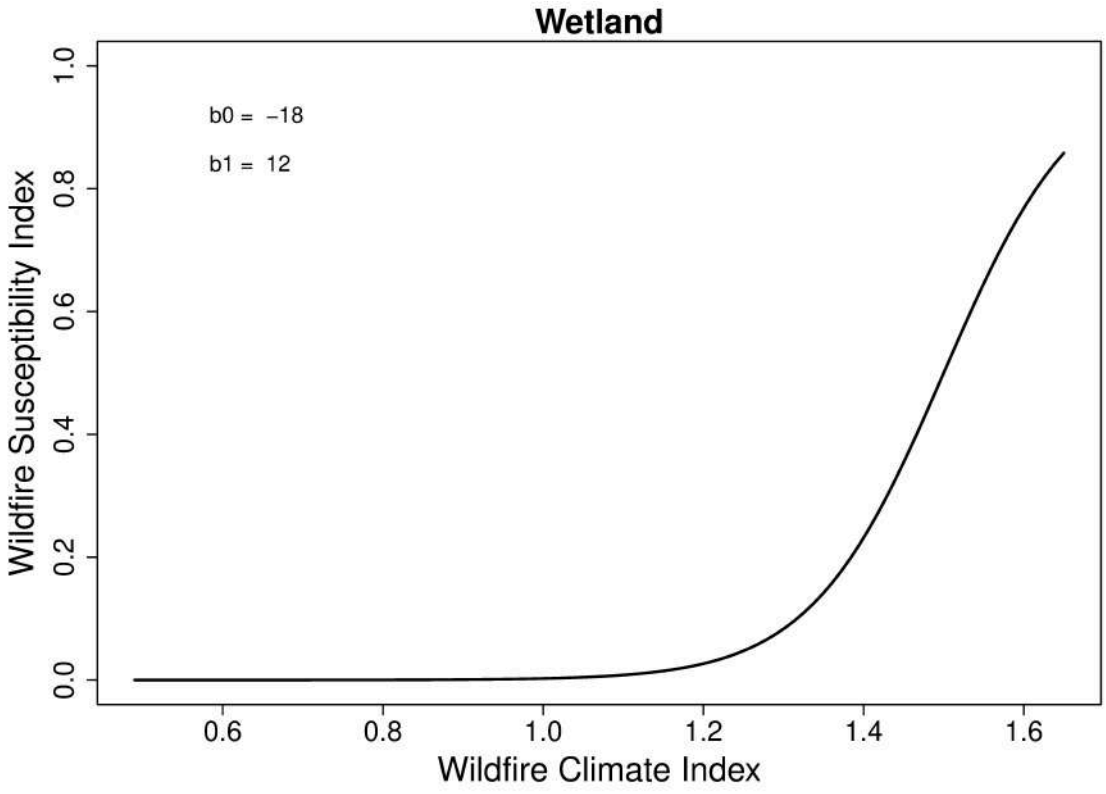
Wetland
b0 = −18
b1 = 12
Wildfire Susceptibility Index
0.0
0.2
0.4
0.6
0.8
1.0
0.6
0.8
1.0
1.2
1.4
1.6
Wildfire Climate Index

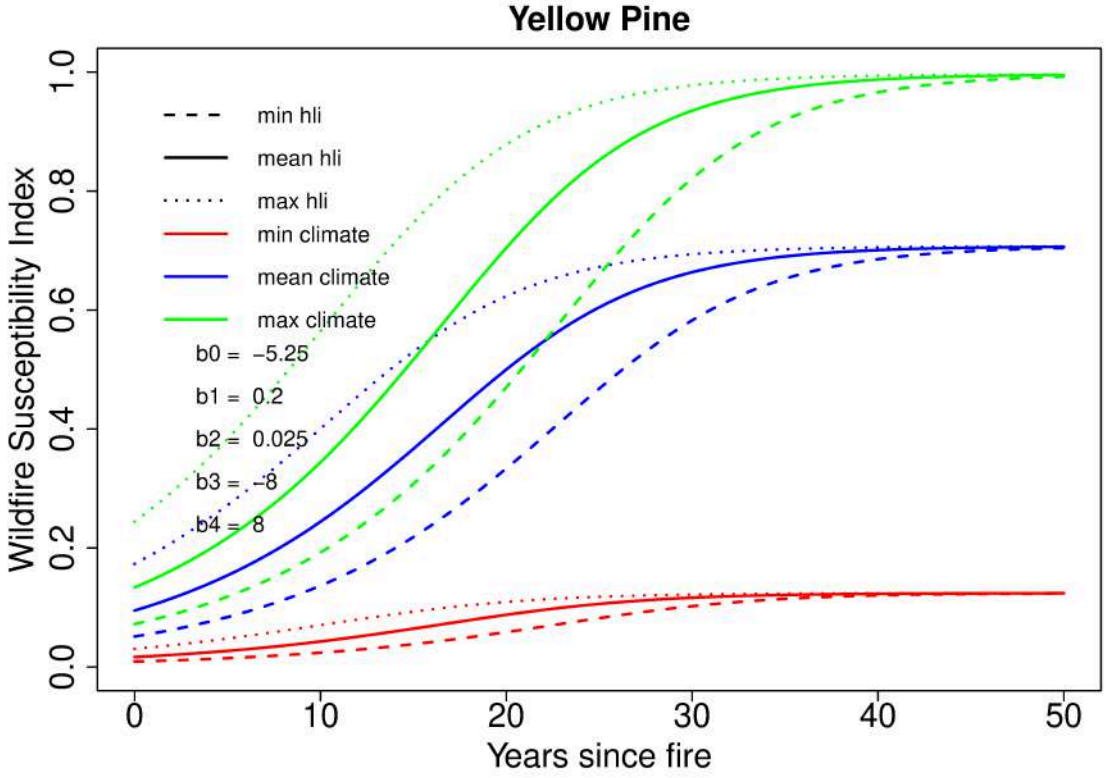
Yellow Pine
min hli
mean hli
max hli
min climate
mean climate
max climate
b0 = −5.25
b1 = 0.2
b2 = 0.025
b3 = −8
b4 = 8
Wildfire Susceptibility Index
0.0
0.2
0.4
0.6
0.8
1.0
0
10
20
30
40
50
Years since fire

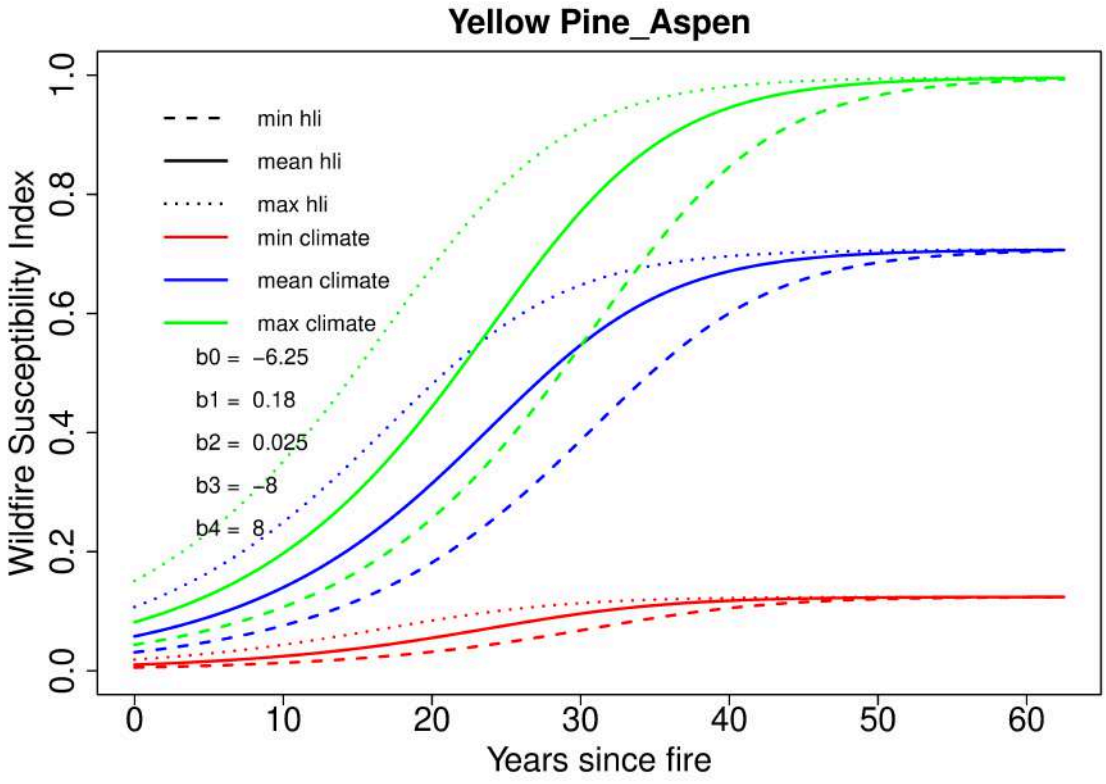
Yellow Pine_Aspen
Wildfire Susceptibility Index
0.0
0.2
0.4
0.6
0.8
1.0
min hli
mean hli
max hli
min climate
mean climate
max climate
b0 = −6.25
b1 = 0.18
b2 = 0.025
b3 = −8
b4 = 8
0
10
20
30
40
50
60
Years since fire

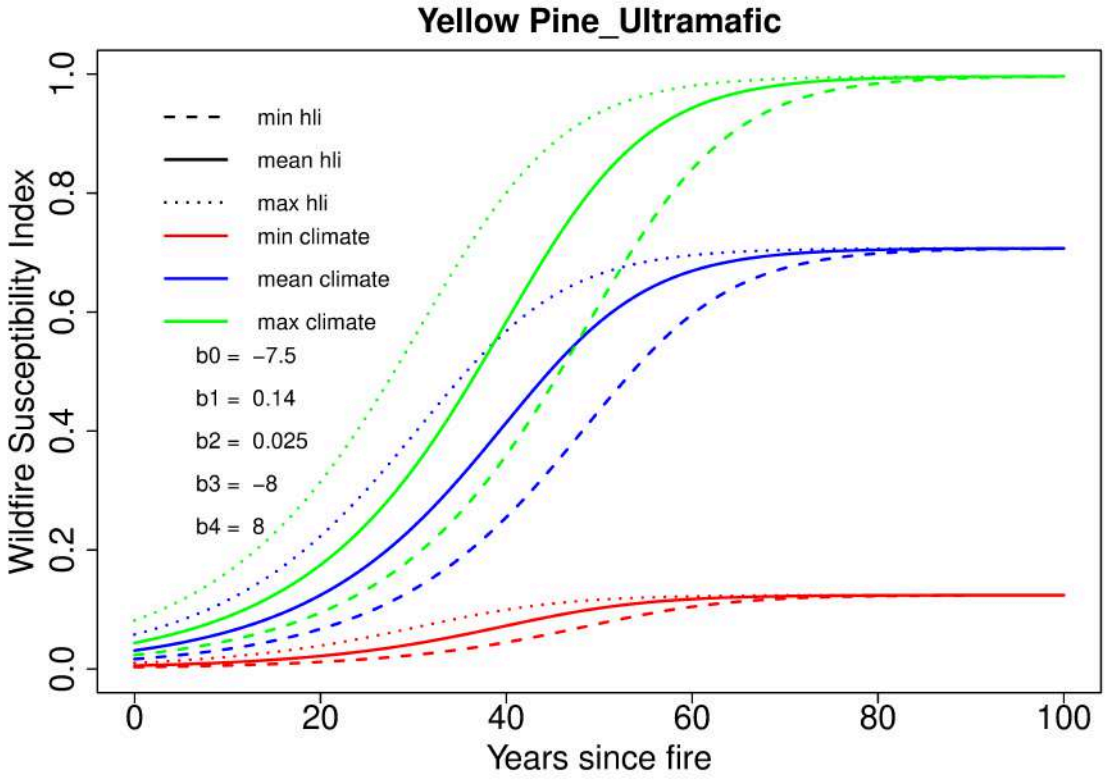
Yellow Pine_Ultramafic
Wildfire Susceptibility Index
0.0
0.2
0.4
0.6
0.8
1.0
min hli
mean hli
max hli
min climate
mean climate
max climate
b0 = −7.5
b1 = 0.14
b2 = 0.025
b3 = −8
b4 = 8
0
20
40
60
80
100
Years since fire

APPENDIX B2 - Wildfire Mortality

As described in the GTR, wildfire mortality (i.e., the probability of high mortality or death of the overstory vegetation in each 5 m cell that burned) was determined by a complex function involving two major factors: 1) fire intensity, which was a Logistic function of the fuel loads in the neighborhood of the focal cell (proxied by the age of the vegetation and time since the last fire), the topographic position of the focal cell, and the climate conditions in the current time step; and 2) the resistance of the focal cell, which was a negative exponential function of the age of the vegetation in the focal cell in which the rate of exponential decline with age decreased with increasing fire intensity (see main text for details). The complex wildfire mortality function included 6 user-specified beta coefficients. As described in the main text, b_0 - b_4 were held constant across all cover types. We varied b_5 and b_6 among cover types to reflect differences in reported historical mean fire return intervals and high mortality rates among cover types. Specifically, we varied these two beta coefficients during model calibration to either increase or decrease the rate of exponential decline in high mortality with increasing vegetation age as a function of fire intensity to achieve the target percentage of high mortality rate in each cover type.

The figures below depict the final wildfire mortality response functions for each cover type in alphabetical order. Cover types not shown either were not eligible to burn (e.g., water, barren) or were always assigned a high mortality response after burning (e.g., grassland, meadow). The response functions depict the probability of high mortality wildfire as a negative exponential function of vegetation Age (yrs) and fire intensity (as indexed). The dashed, solid and dotted lines depict the response functions for the minimum, mean and maximum Fire Intensity Index. Universally, the probability of high mortality decreased with increasing vegetation Age, but the rate of exponential decline decreased (i.e.,shallower slope) with increasing fire intensity, such that for any given Age the probability of high mortality increased with increasing fire intensity.

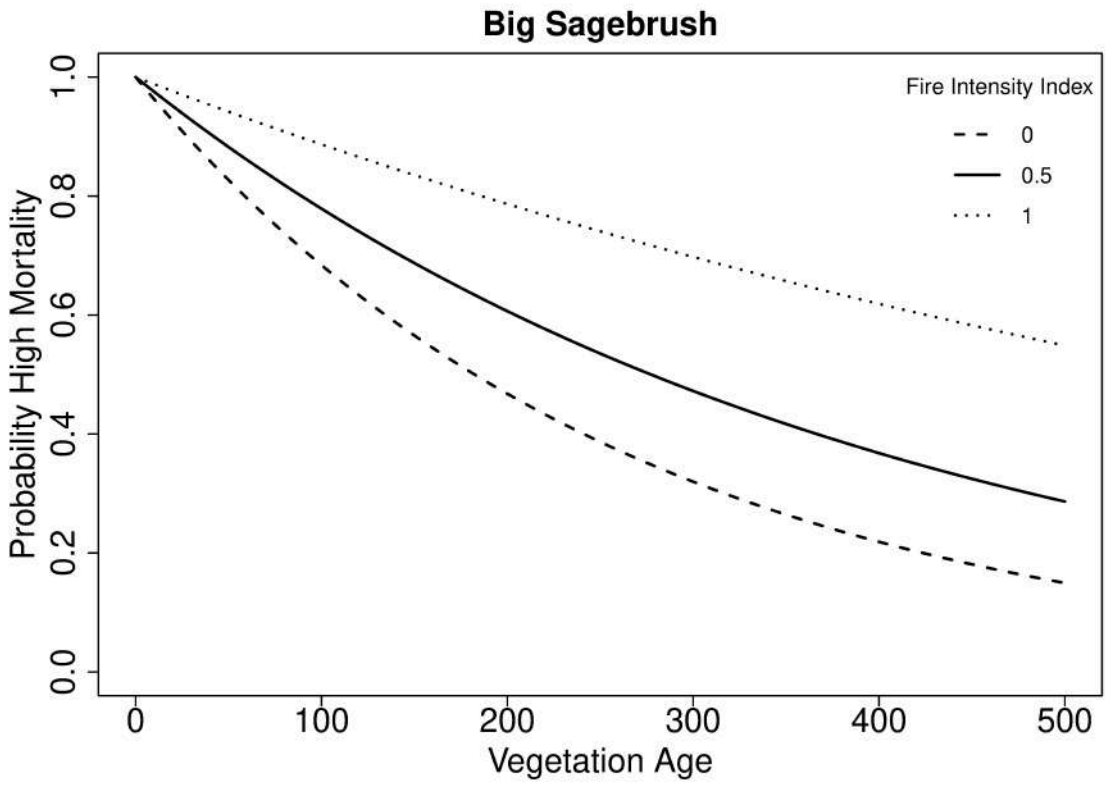

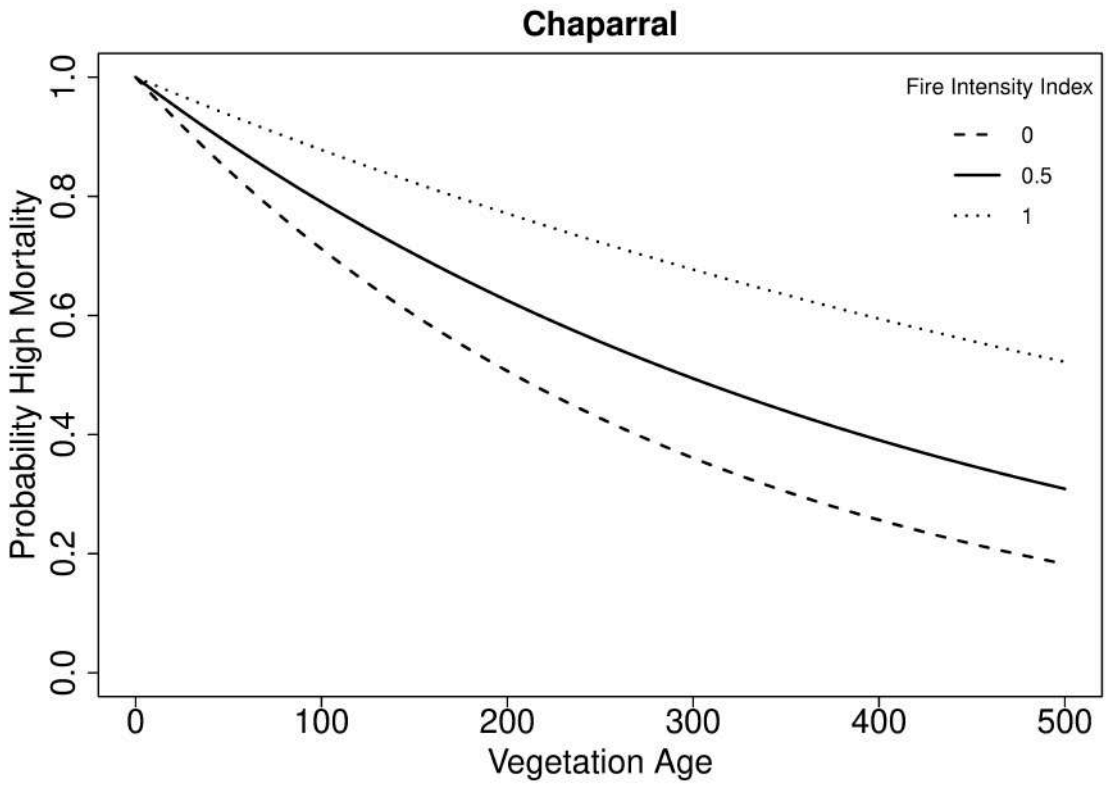
Chaparral
Fire Intensity Index
0
0.5
1
Probability High Mortality
0.0
0.2
0.4
0.6
0.8
1.0
0
100
200
300
400
500
Vegetation Age

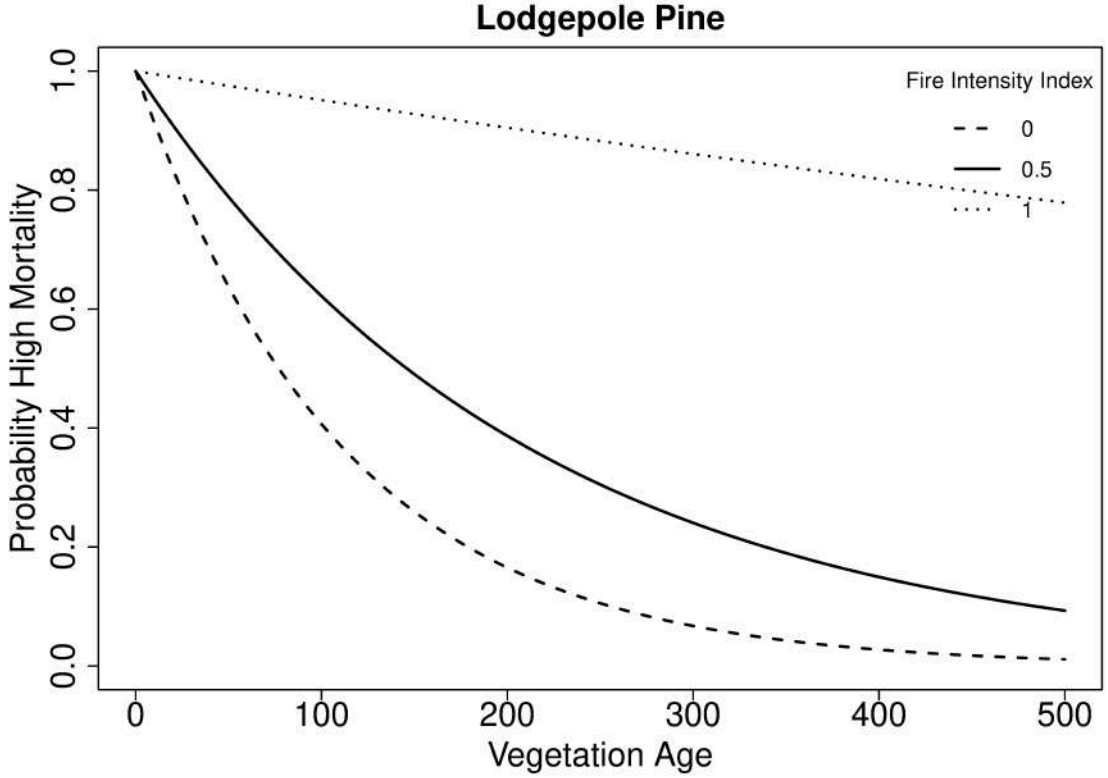
Lodgepole Pine
Fire Intensity Index
0
0.5
1
Probability High Mortality
0.0
0.2
0.4
0.6
0.8
1.0
0
100
200
300
400
500
Vegetation Age

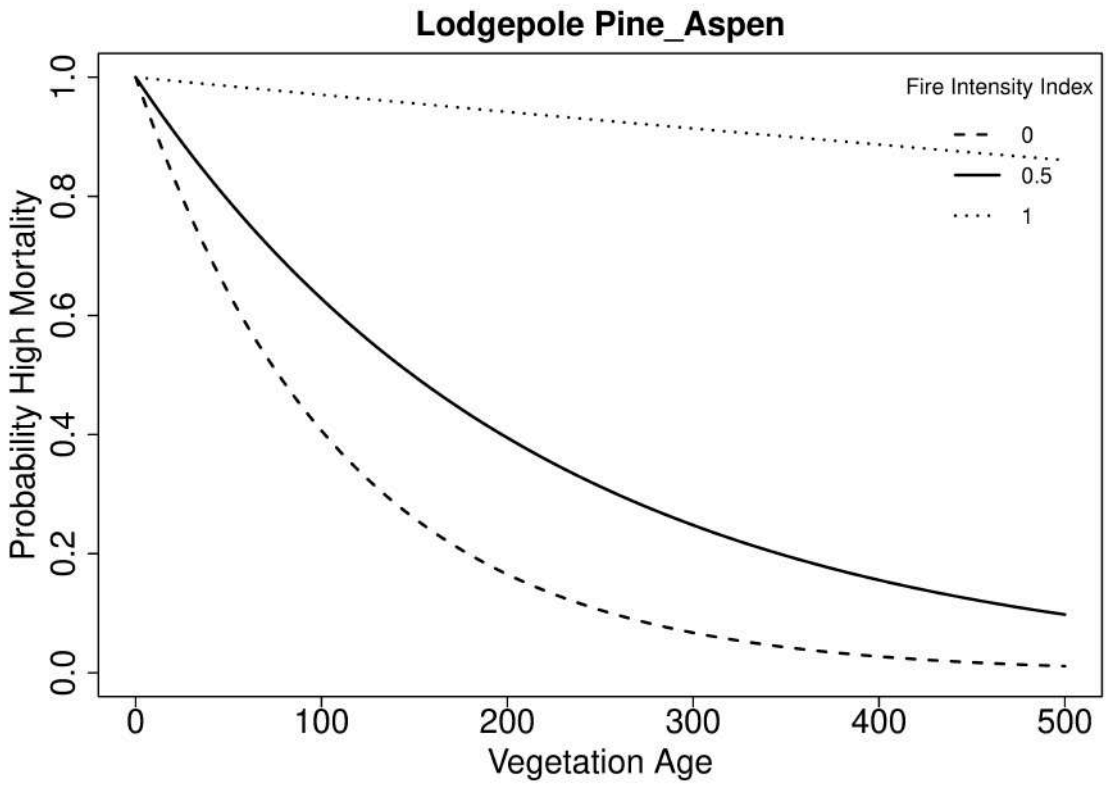
Lodgepole Pine_Aspen
Fire Intensity Index
0
0.5
1
Probability High Mortality
0.0
0.2
0.4
0.6
0.8
1.0
0
100
200
300
400
500
Vegetation Age

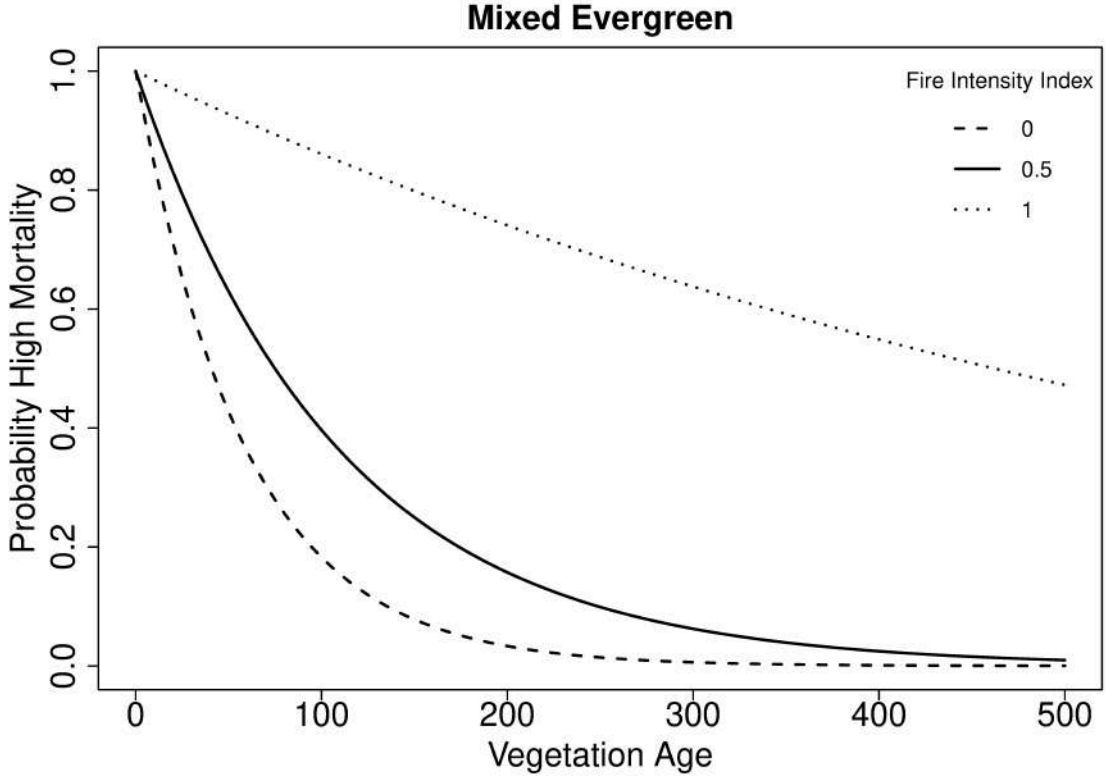
Mixed Evergreen
Fire Intensity Index
0
0.5
1
Probability High Mortality
0.0
0.2
0.4
0.6
0.8
1.0
0
100
200
300
400
500
Vegetation Age

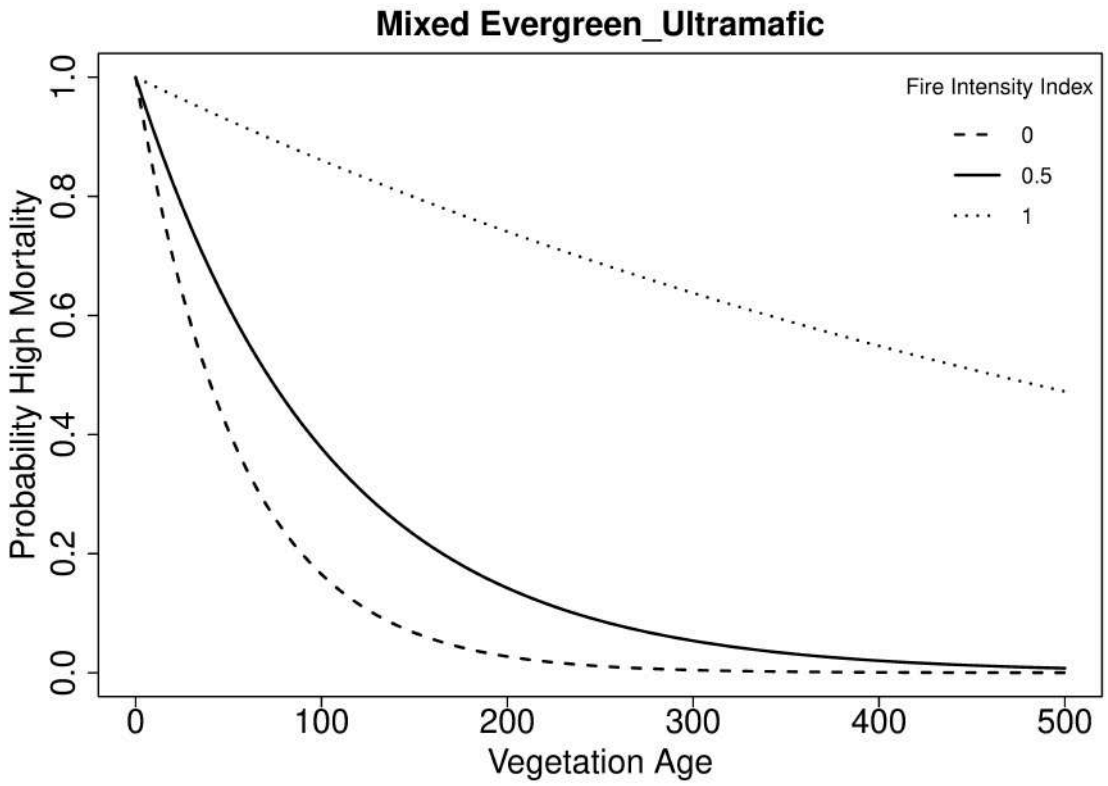
Mixed Evergreen_Ultramafic
Fire Intensity Index
0
0.5
1
Probability High Mortality
0.0
0.2
0.4
0.6
0.8
1.0
0
100
200
300
400
500
Vegetation Age

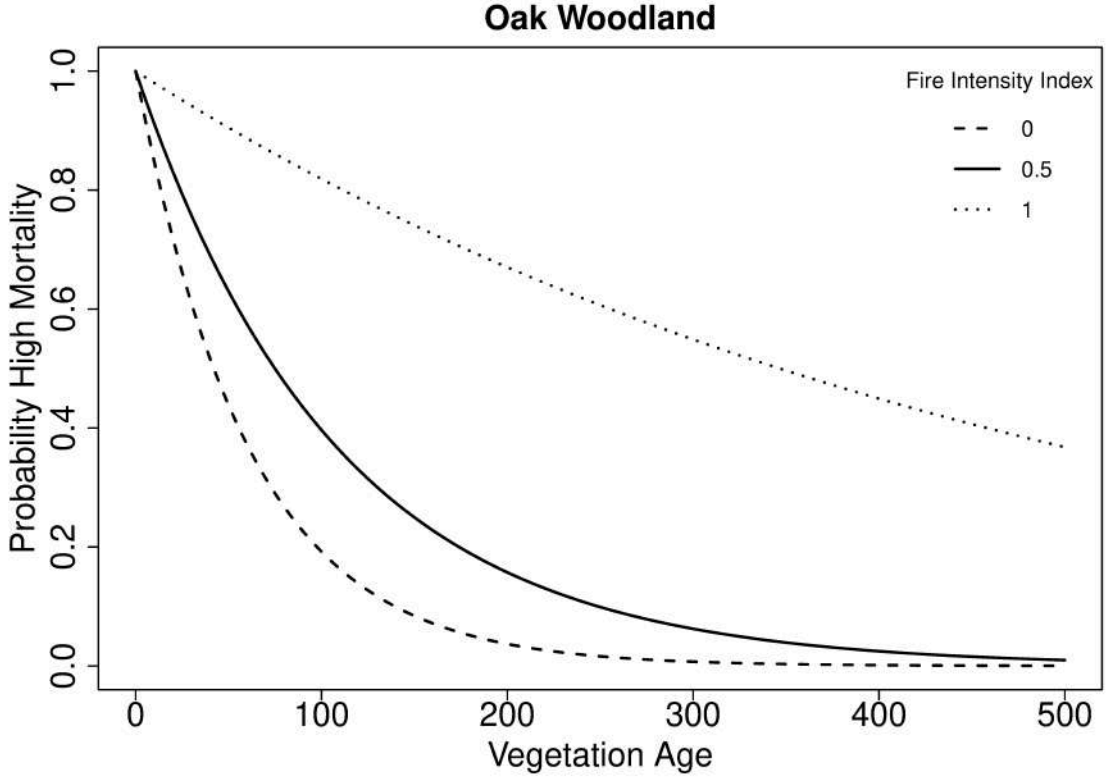
Oak Woodland
Fire Intensity Index
0
0.5
1
Probability High Mortality
0.0
0.2
0.4
0.6
0.8
1.0
0
100
200
300
400
500
Vegetation Age

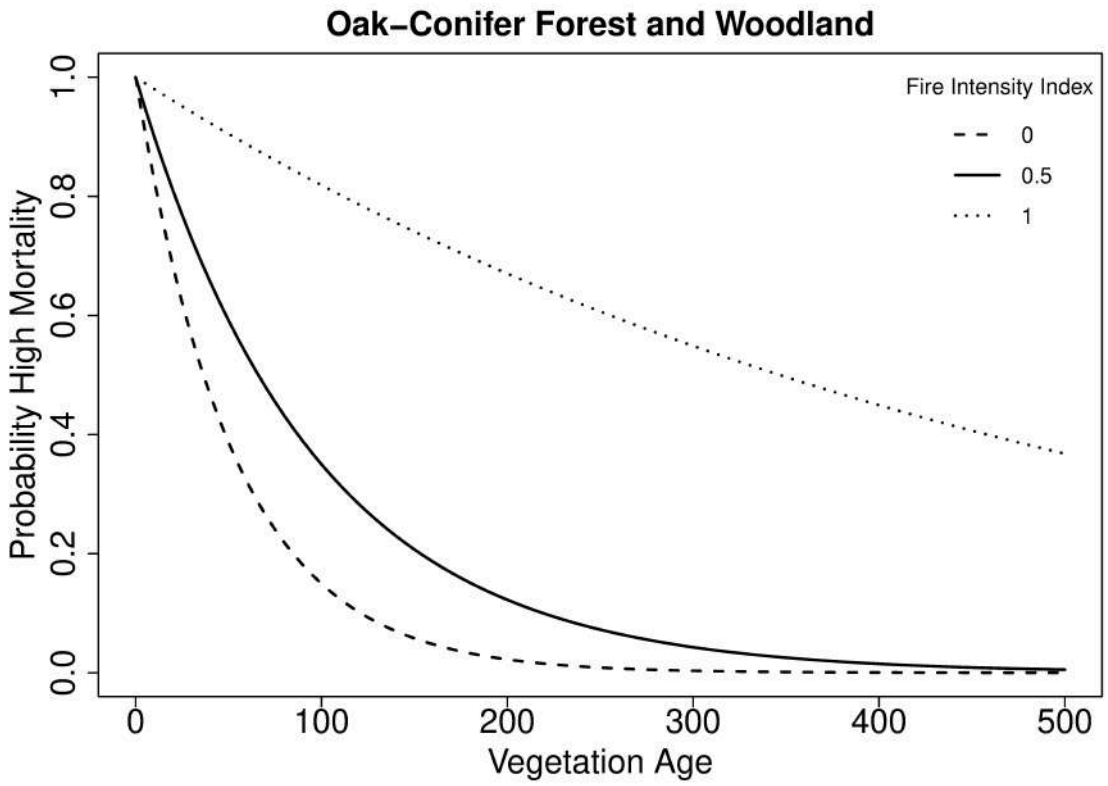
Oak–Conifer Forest and Woodland
Fire Intensity Index
0
0.5
1
Probability High Mortality
0.0
0.2
0.4
0.6
0.8
1.0
0
100
200
300
400
500
Vegetation Age

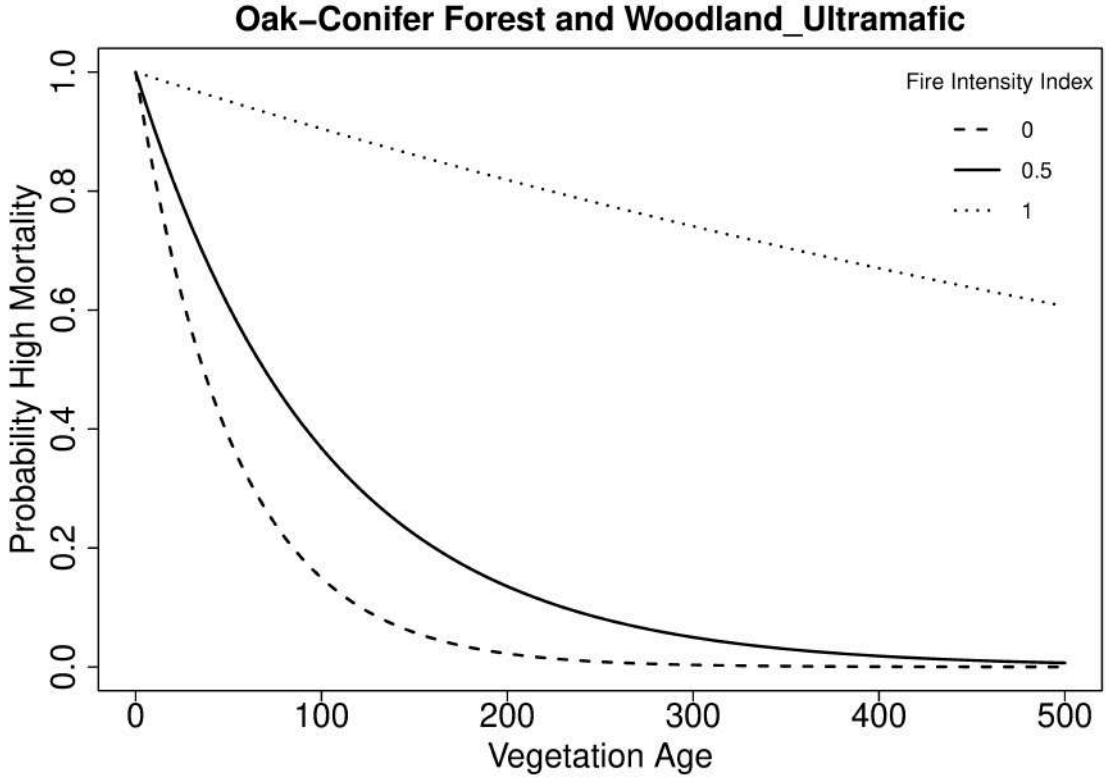
Oak–Conifer Forest and Woodland_Ultramafic
Fire Intensity Index
0
0.5
1
Probability High Mortality
0.0
0.2
0.4
0.6
0.8
1.0
0
100
200
300
400
500
Vegetation Age

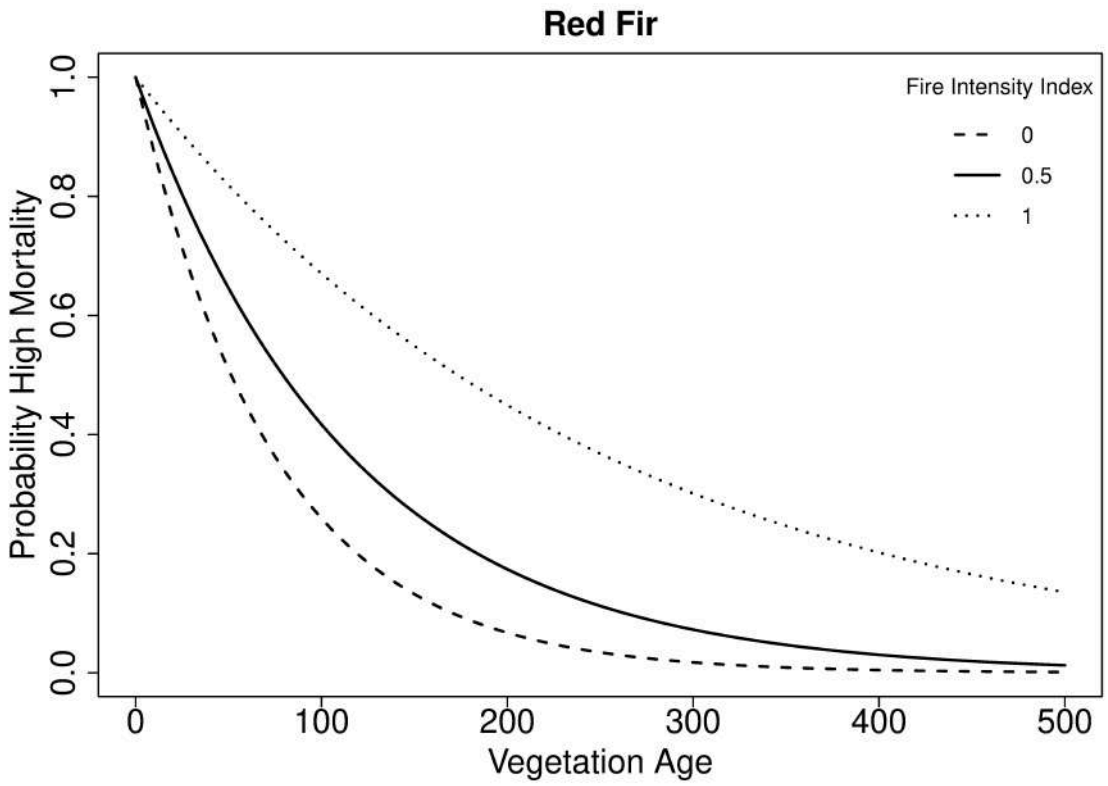
Red Fir
Fire Intensity Index
0
0.5
1
Probability High Mortality
0.0
0.2
0.4
0.6
0.8
1.0
0
100
200
300
400
500
Vegetation Age

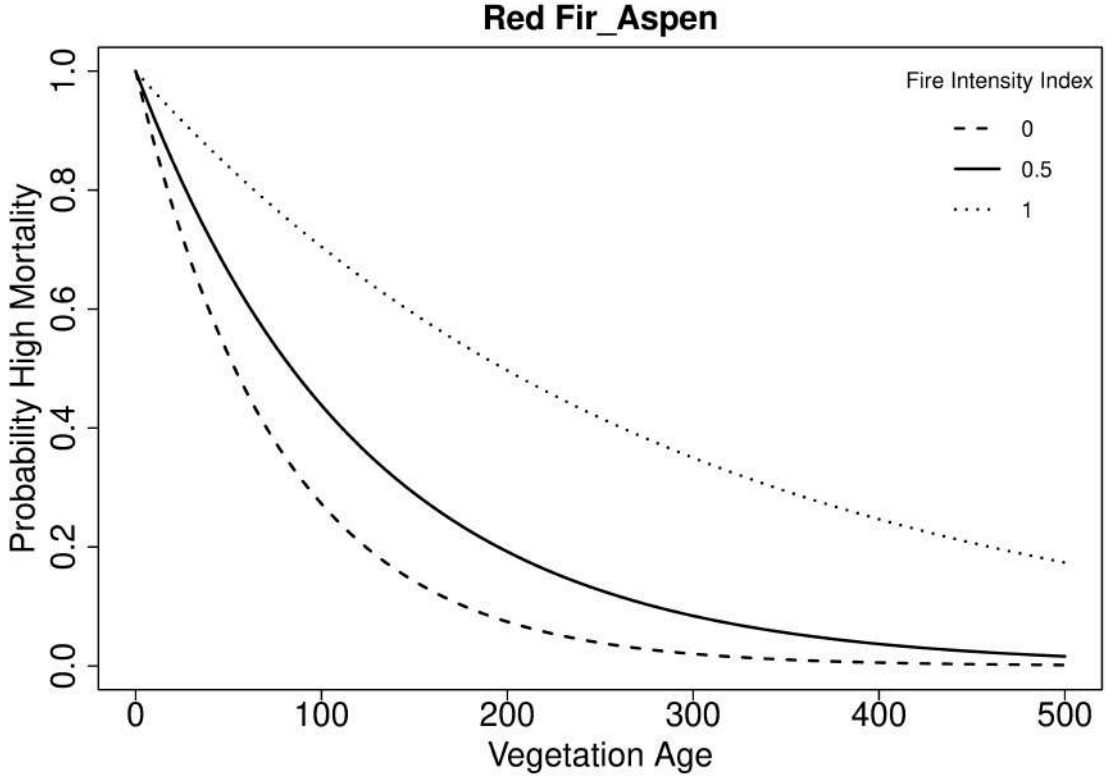
Red Fir_Aspen
Fire Intensity Index
0
0.5
1
Probability High Mortality
0.0
0.2
0.4
0.6
0.8
1.0
0
100
200
300
400
500
Vegetation Age

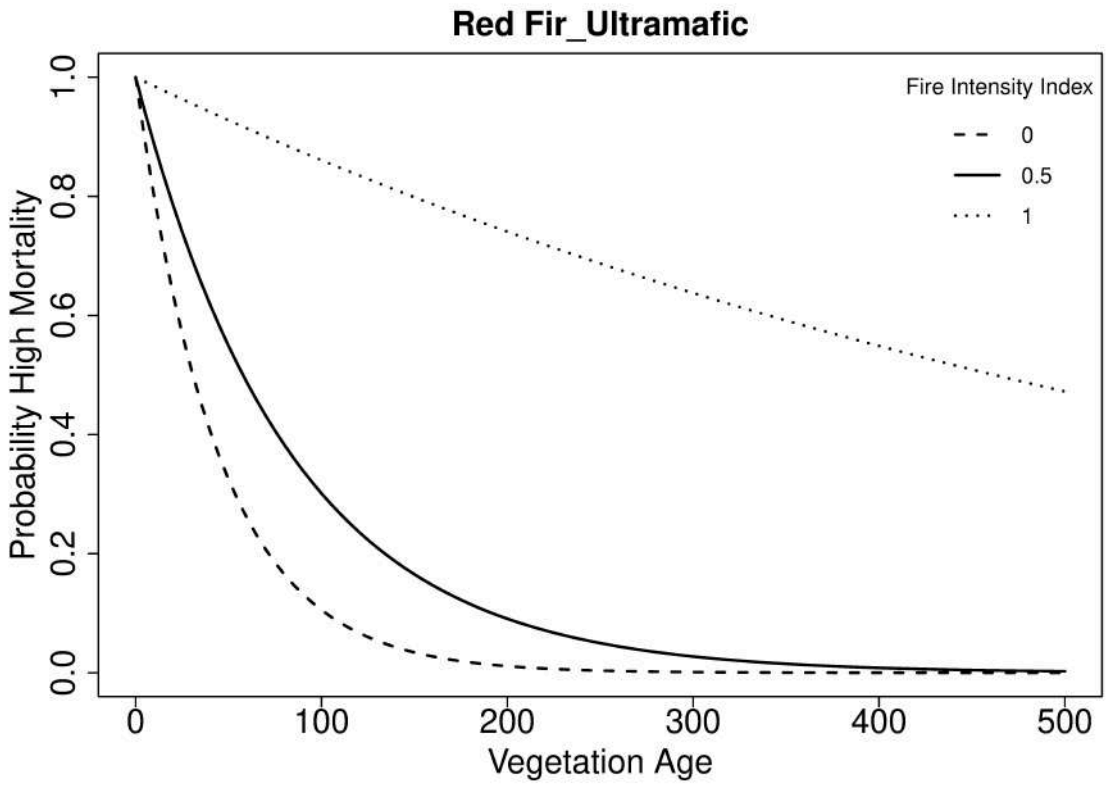
Red Fir_Ultramafic
Fire Intensity Index
0
0.5
1
Probability High Mortality
0.0
0.2
0.4
0.6
0.8
1.0
0
100
200
300
400
500
Vegetation Age

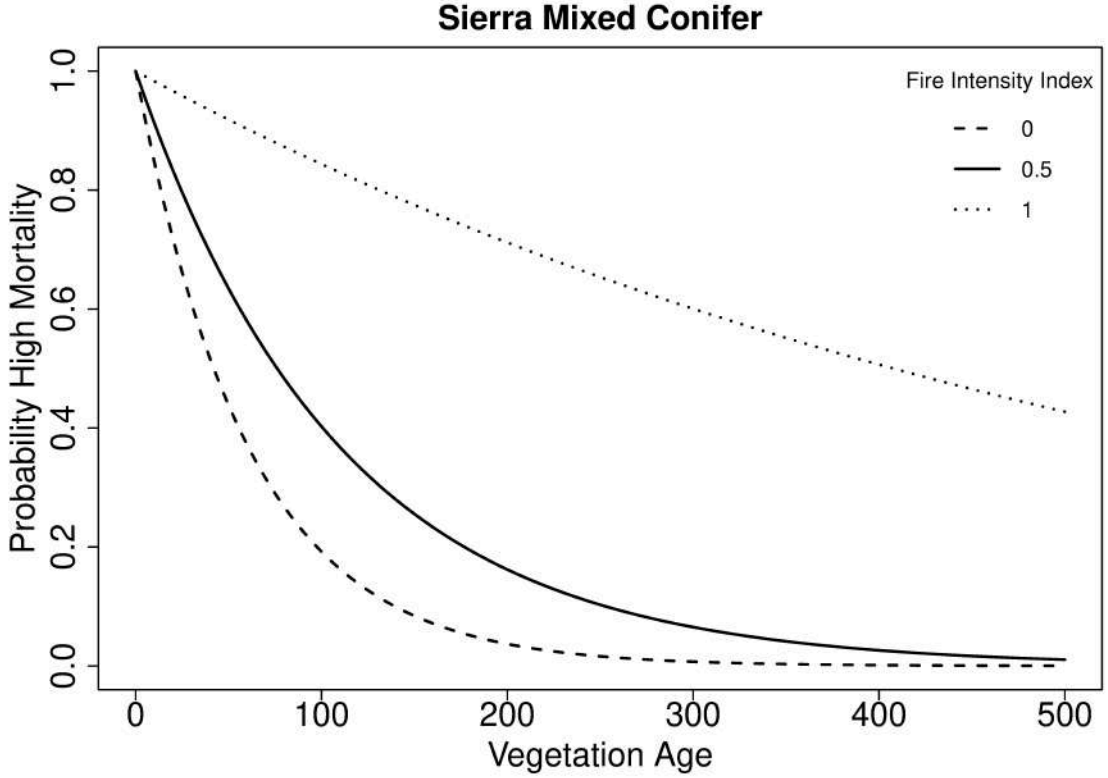
Sierra Mixed Conifer
Fire Intensity Index
0
0.5
1
Probability High Mortality
0.0
0.2
0.4
0.6
0.8
1.0
0
100
200
300
400
500
Vegetation Age

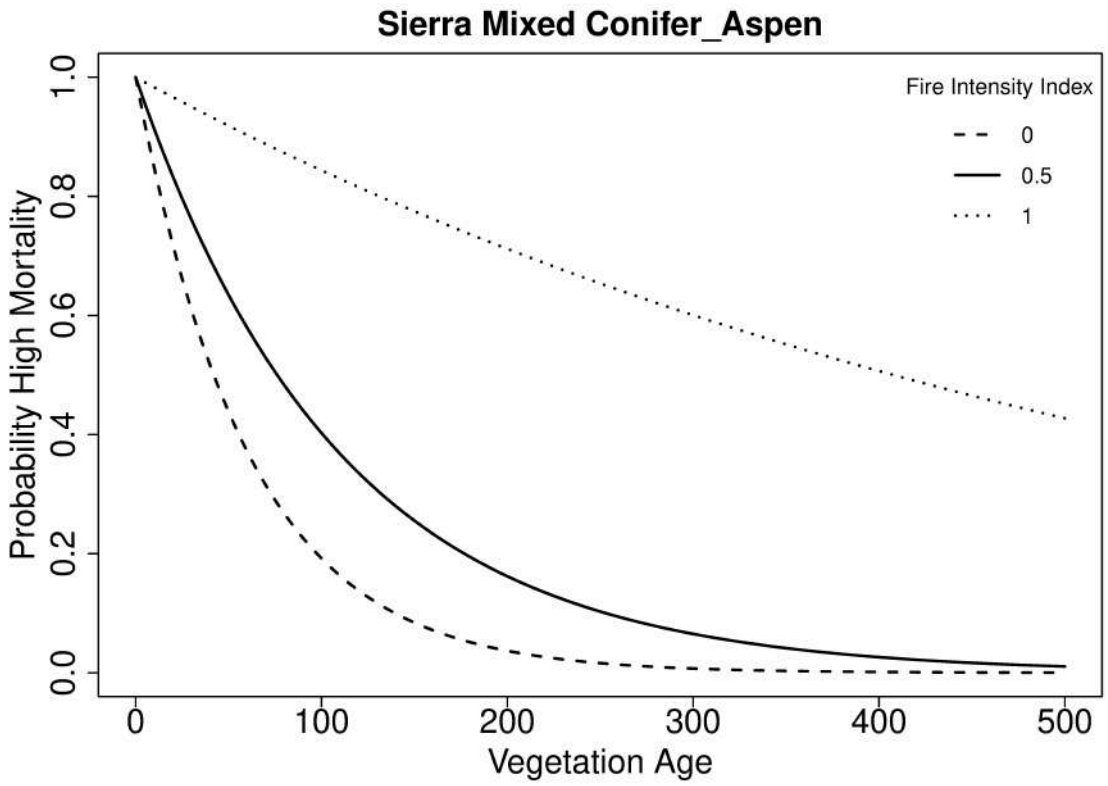
Sierra Mixed Conifer_Aspen
Fire Intensity Index
0
0.5
1
Probability High Mortality
0.0
0.2
0.4
0.6
0.8
1.0
0
100
200
300
400
500
Vegetation Age

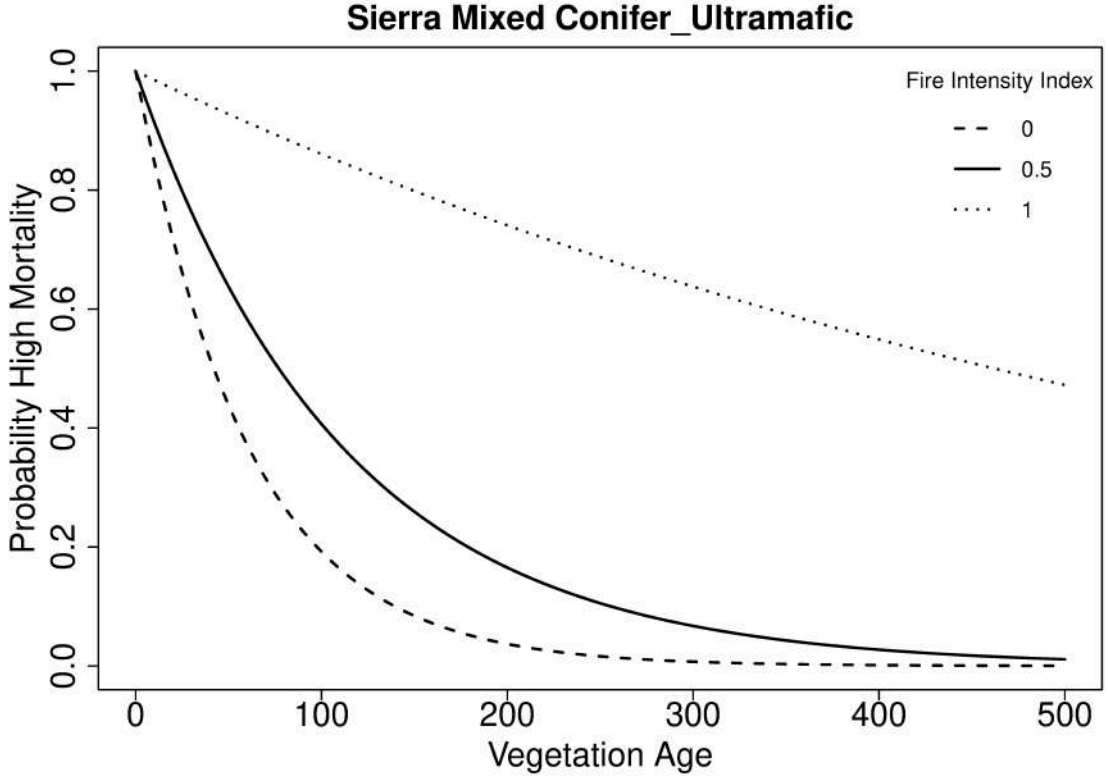
Sierra Mixed Conifer_Ultramafic
Fire Intensity Index
0
0.5
1
Probability High Mortality
0.0
0.2
0.4
0.6
0.8
1.0
0
100
200
300
400
500
Vegetation Age

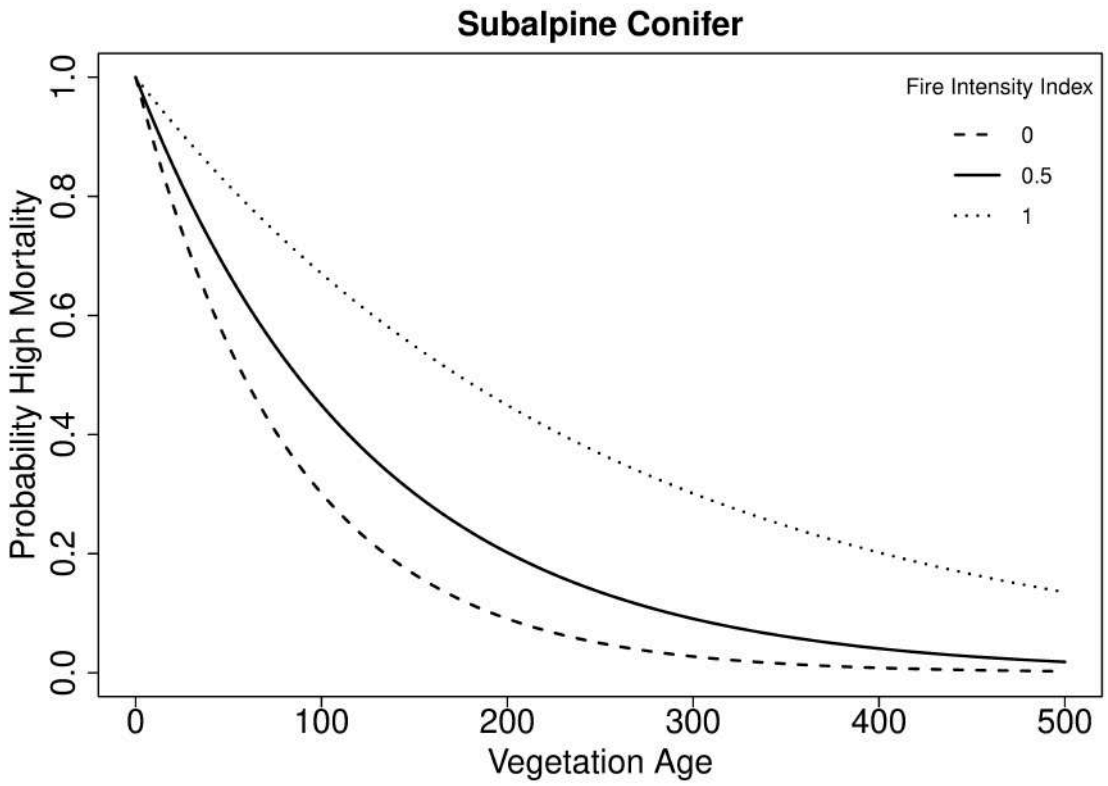
Subalpine Conifer
Fire Intensity Index
0
0.5
1
Probability High Mortality
0.0
0.2
0.4
0.6
0.8
1.0
0
100
200
300
400
500
Vegetation Age

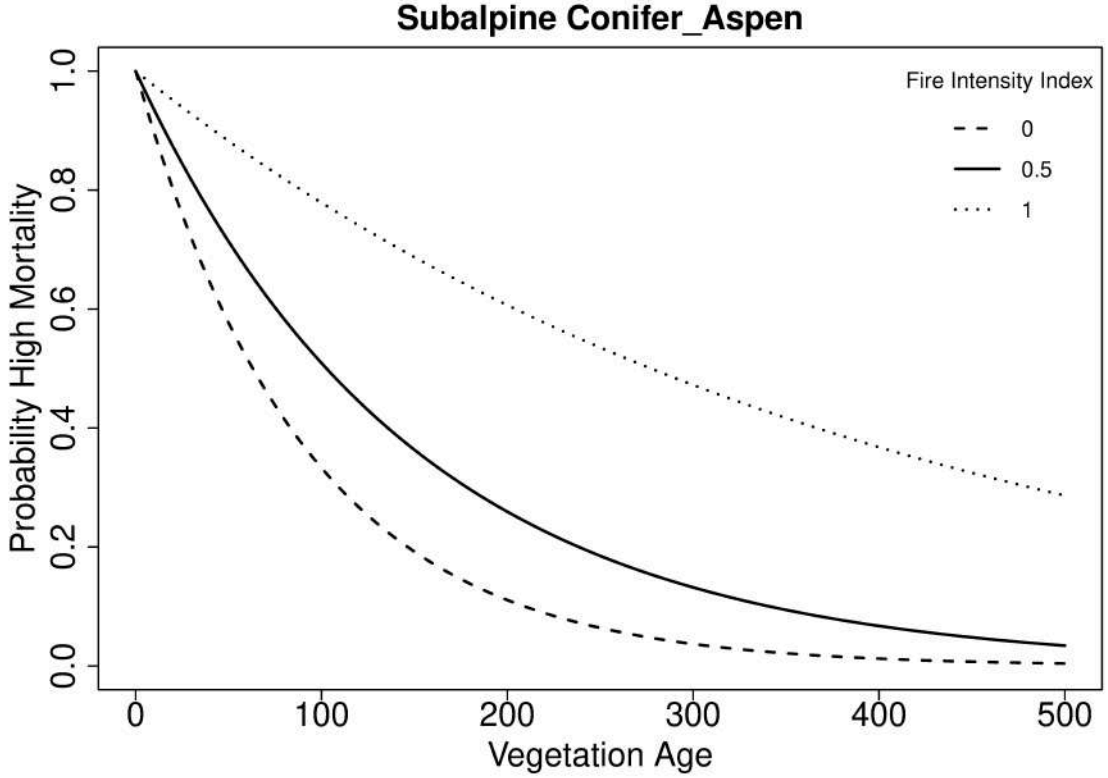
Subalpine Conifer_Aspen
Fire Intensity Index
0
0.5
1
Probability High Mortality
0.0
0.2
0.4
0.6
0.8
1.0
0
100
200
300
400
500
Vegetation Age

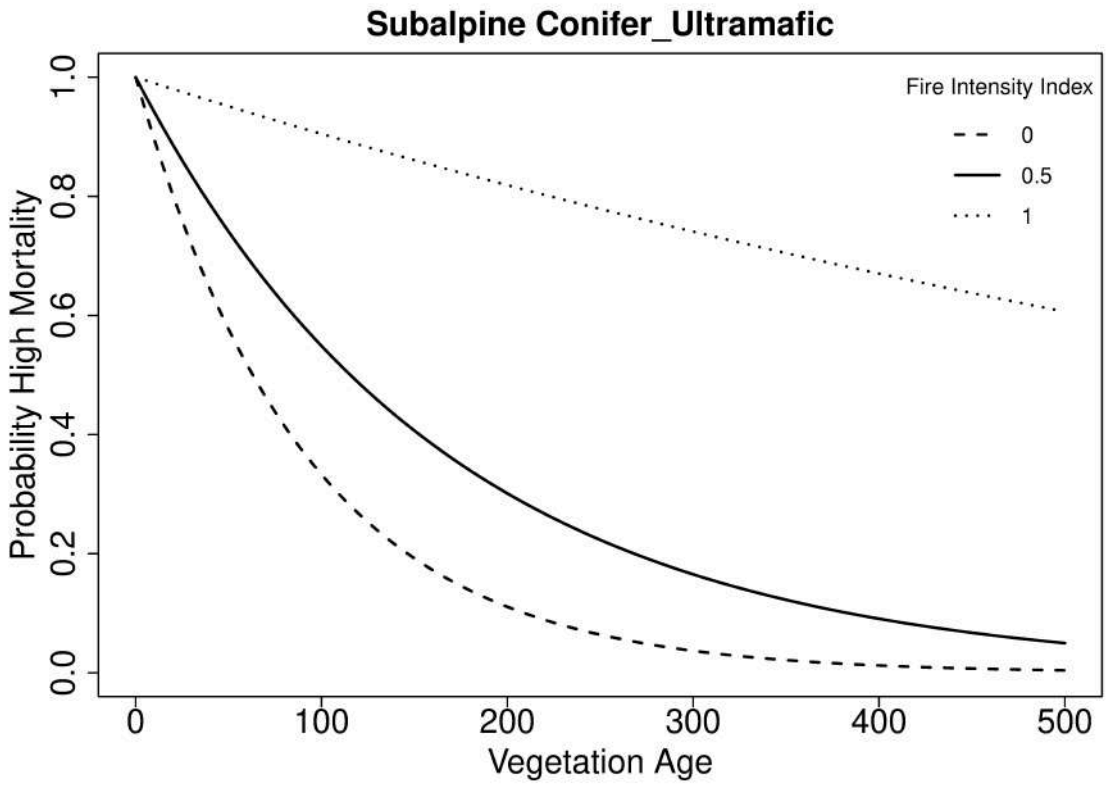
Subalpine Conifer_Ultramafic
Fire Intensity Index
0
0.5
1
Probability High Mortality
0.0
0.2
0.4
0.6
0.8
1.0
0
100
200
300
400
500
Vegetation Age

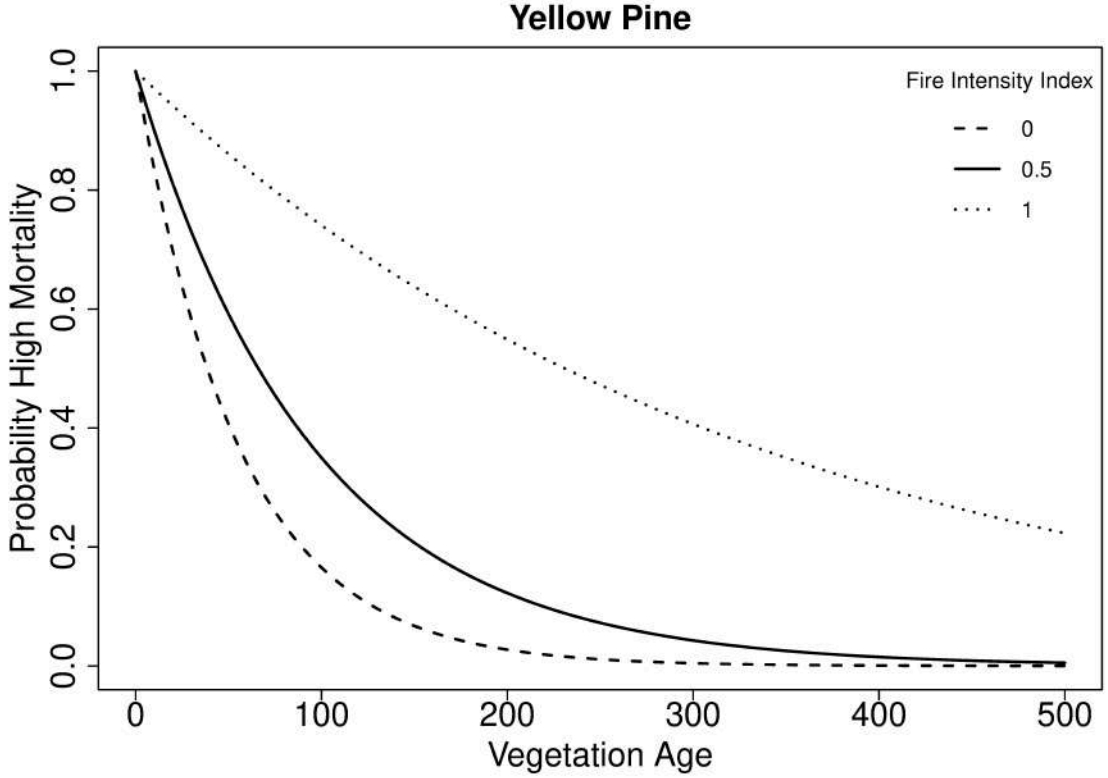
Yellow Pine
Fire Intensity Index
0
0.5
1
Probability High Mortality
0.0
0.2
0.4
0.6
0.8
1.0
0
100
200
300
400
500
Vegetation Age

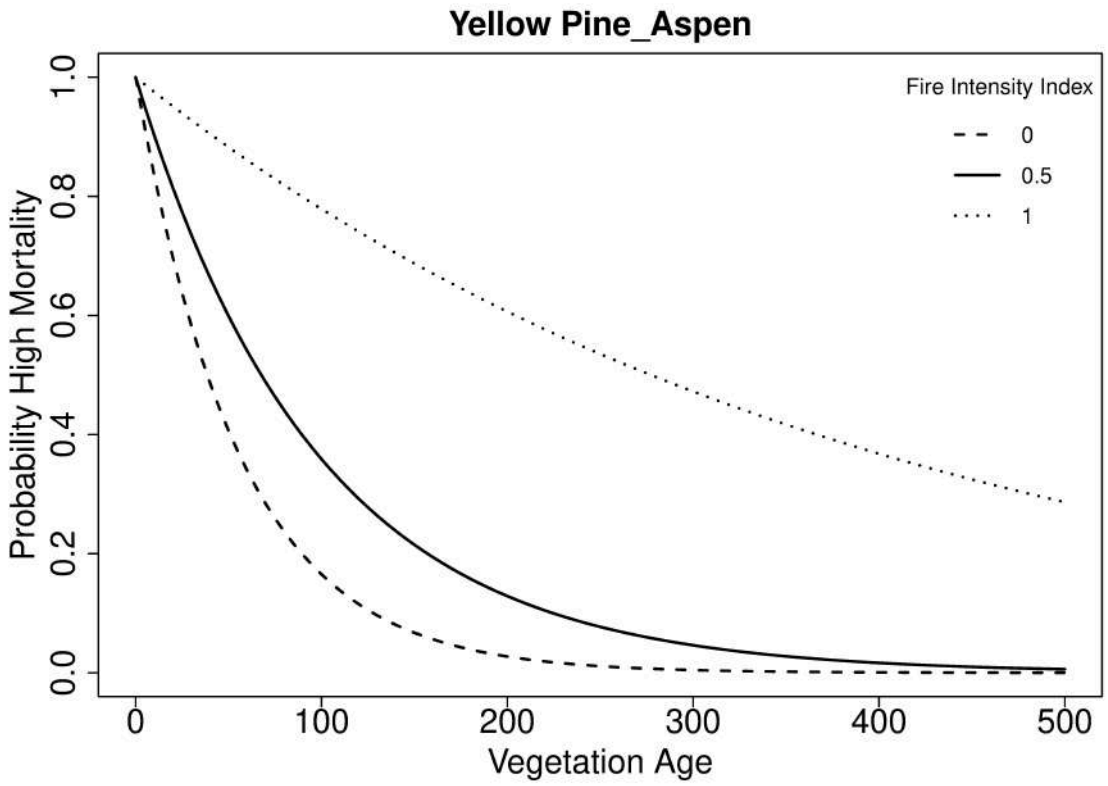
Yellow Pine_Aspen
Fire Intensity Index
0
0.5
1
Probability High Mortality
0.0
0.2
0.4
0.6
0.8
1.0
0
100
200
300
400
500
Vegetation Age

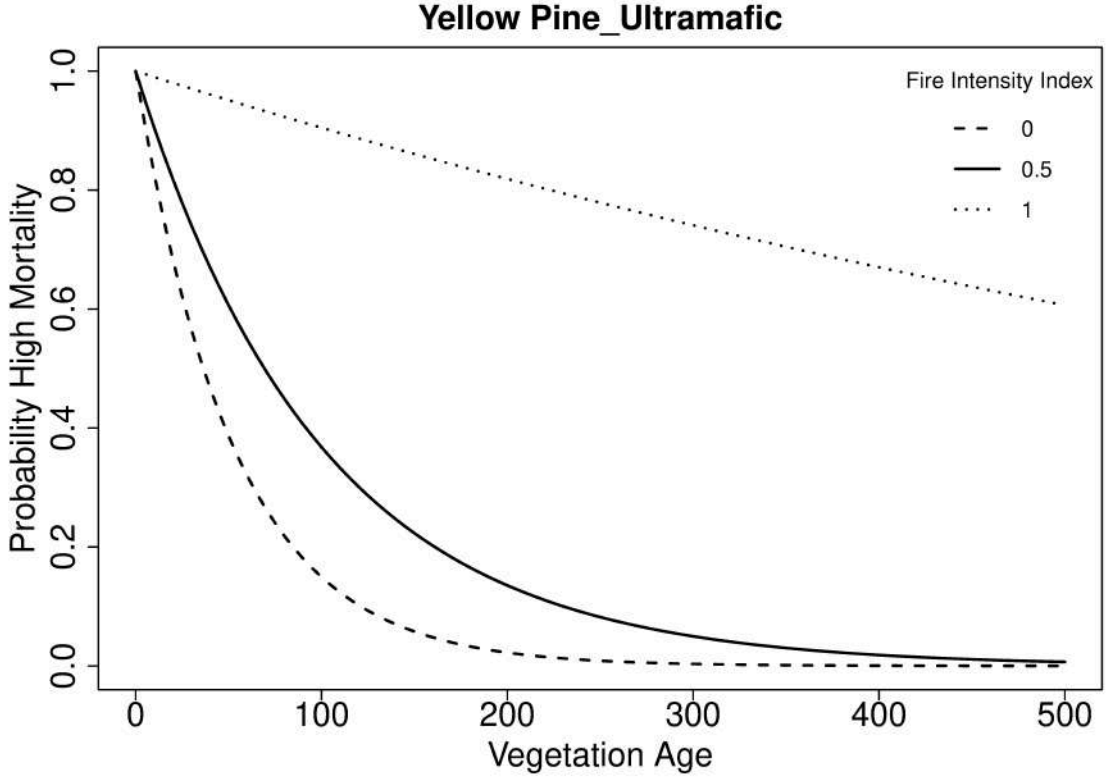
Yellow Pine_Ultramafic
Fire Intensity Index
0
0.5
1
Probability High Mortality
0.0
0.2
0.4
0.6
0.8
1.0
0
100
200
300
400
500
Vegetation Age

Appendix C - Truckee River Landscape Historical Range of Variability and Current Landscape Departure

DRAFT Report

Kevin McGarigal Becky Estes Scott Conway Danielle Perrot
Marilyn Tierney Terri Walsh Christina Liang Laurie Perrot
Edward Smith

February, 2022

Authors

- Kevin McGarigal is a landscape ecologist with Vibrant Planet, proprietor of LandEco Consulting and retired professor of landscape ecology at the University of Massachusetts, Amherst. He received a B.S. in Forestry and Wildlife from Virginia Tech, an M.S. in Wildlife Science from Oregon State University, and a Ph.D. in Forest Science from Oregon State University.
- Becky Estes is the Central Sierra Province Ecologist (Tahoe, Eldorado, Stanislaus, and Lake Tahoe Basin Management Unit), Pacific Southwest Region, USDA Forest Service. She received a Ph.D. in Forestry from Auburn University and is a Certified Ecologist with the Ecological Society of America.
- Scott Conway is the chief resilience officer with Vibrant Planet and former forest ecologist with Pacific Southwest Region, USDA Forest Service Remote Sensing Lab and Truckee District Ranger, Tahoe National Forest, Pacific Southwest Region, USDA Forest Service. He received a B.S. in Natural Resources Management from Colorado State University.
- Danielle Perrot is an applied ecologist with Vibrant Planet. She received a B.S. in Environmental Science from University of California, Los Angeles and an M.A. in Geography with a Graduate Certificate in Hydrologic Sciences from University of Colorado, Boulder.
- Marilyn Tierney is retired District Biologist for the Truckee River Ranger District, Tahoe National Forest, Pacific Southwest Region, USDA Forest Service. She received a B.S. in Biology and an M.A. in Biology with an emphasis in Ecology and Systematics from San Francisco State University.
- Terri Walsh is retired silviculturist for the Tahoe National Forest, Pacific Southwest Region, USDA Forest Service. She is a certified silviculturist and studied Forestry at Cal Poly San Luis Obispo.
- Christina Liang is Forest Biologist for the Tahoe National Forest, Pacific Southwest Region, USDA Forest Service. She received a Ph.D. in Ecology from University of California, Davis.
- Laurie Perrot is Forest Environmental Coordinator for the Tahoe National Forest, Pacific Southwest Region, USDA Forest Service. She received a B.S. in forestry from the University of California, Berkeley.
- Edward Smith is Senior Forest Ecologist and Fire Manager for The Nature Conservancy in California. He received a B.A. in Biology from the University of California, San Diego and a M.S. in Forestry from Northern Arizona University.

Preface

This document[1] is an appendix to the Northern Sierra Historical Range of Variability and Current Landscape Departure General Technical Report (GTR) and includes detailed results for the Truckee River landscape. Importantly, the background and detailed methods behind these results are presented in the GTR and not repeated here, and thus it behooves the reader to review the GTR before interpreting these results. In addition, here we present details pertaining the Landscape Disturbance-Succession Model parameterization and calibration specific to this focal landscape; all other model parameterization and calibration generalized to the Northern Sierra ecoregion is presented in the GTR. Lastly, here we present results specific to this focal landscape, but with minimal interpretation or discussion of these results or their application to management, as this was all done in the GTR. The GTR describes how to interpret the results for any of the focal landscapes and how they can be applied to management; here, we simply provide the raw results specific to this focal landscape.

Note, all datasets associated with the results for this focal landscape can be made available. Please contact Becky Estes, becky.estes@usda.gov for access.

---

[1] In accordance with Federal law and U.S. Department of Agriculture policy, this institution is prohibited from discriminating on the basis of race, color, national origin, sex, age, or disability. (Not all prohibited bases apply to all programs.) To file a complaint of discrimination, write USDA, Director, Office of Civil Rights, Room 326-W, Whitten Building, 1400 Independence Avenue, SW, Washington, DC 20250-9410 or call (202) 720-5964 (voice and TDD). USDA is an equal opportunity provider and employer.

FOCAL LANDSCAPE

The Truckee River landscape, as we defined it, is comprised of the upper portion of the Truckee River watershed, a HUC8 level watershed located on the eastern slopes of the Sierra Nevada Mountains in the north Sierra ecoregion (**Figure 1**). The Truckee River landscape encompasses 126,717 ha and otherwise reflects the description of the north Sierra ecoregion presented in the general technical report.

Figure 1: The Truckee River landscape, including the middle and north forks of the Truckee River, defined for the purpose of simulating wildfire disturbance and vegetation succession.

MODEL PARAMETERIZATION

In this section, we present only model parameters specific to this focal landscape; all north Sierra-wide parameters are discussed in the GTR. In addition, here we do not discuss in detail the methods and use of the model parameters in LDSim, as this was already done in the GTR. Please refer to the GTR for a full understanding of how the model parameters were used in LDSim.

Wildfire Climate

Climate conditions affecting wildfire disturbance during each timestep of the simulation were governed by a single global parameter, the Wildfire Climate Index based on the Palmer Modified Drought Severity Index (PMDI), in which a single coefficient was assigned to each timestep of the simulation. The final Wildfire Climate Index trajectory represented a vector of coefficients, one for each timestep, as shown in **Figure 2**.

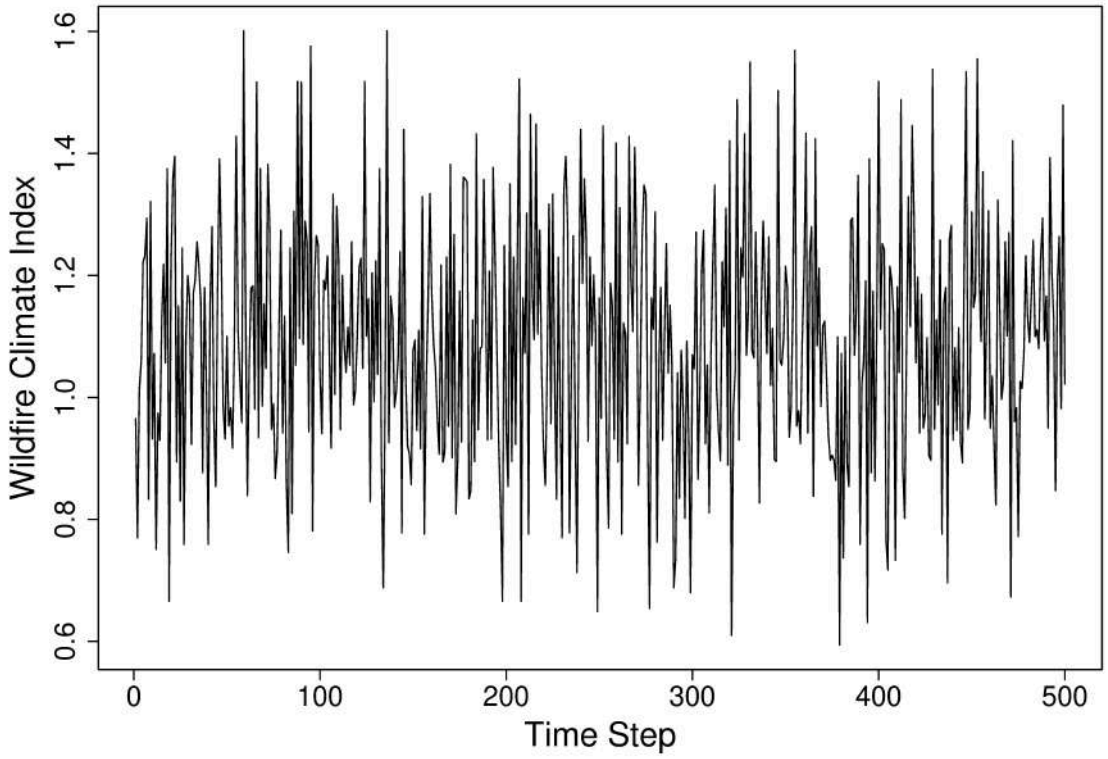

Figure 2: Wildfire Climate Index trajectory for the Truckee River landscape corresponding to 500 5-year timesteps in the simulation. The Climate Index was based on the inverted and rescaled 5-year averaged, inverse-distance weighted mean Palmer Modified Drought Severity Index (PMDI) for the sample point locations within the north Sierra ecoregion relative to the focal landscape (Truckee River watershed in this case). Note, here we inverted PMDI so that positive values represented drier conditions and negative values represented wetter conditions, and we also rescaled the index to have a standard deviation of 0.2 (see text for details).

Wildfire Susceptibility

Wildfire susceptibility for any given cell in each timestep was modeled as a complex function of fuels and climate, separately for each cover type, as described in the GTR. The final Wildfire Susceptibility Index on the probability scale (0-1) was used in the wildfire initiation and spread functions such that a value of 0 would prevent wildfires from initiating in or spreading into the cell, and as the value increased to 1 the probability of initiating a wildfire would increase as would the probability of a wildfire spreading to the focal cell from an adjacent burning cell, all other things being equal.

Briefly, we varied the beta coefficients of the wildfire susceptibility function for each cover type to reflect differences in reported historical mean fire return intervals among cover types - shifting the response curves left or right - as a means of calibrating the model to achieve target mean fire return intervals for each cover type (see Model Calibration). The calibrated wildfire susceptibility functions for each cover type are included in **Appendix C1**.

Wildfire Initiation

The number and spatial distribution of wildfire initiations in any given timestep was governed by: 1) a global wildfire initiation rate parameter that controlled the number of initiation attempts per unit area and

remained constant over time; 2) the current climate conditions, as represented by the Wildfire Climate Index, that varied over time but not space; and 3) the susceptibility to wildfire, as represented by the Wildfire Susceptibility Index, that varied over both space and time. We treated the global wildfire initiation rate as a calibration parameter - shifting it up or down to increase or decrease the overall amount of realized wildfire over time - and ultimately settled on a rate of 400 attempted initiations per 100,000 ha/year. Note, this parameter affected the attempted number of wildfire initiations, not the realized number of wildfires, which was considerably less due to the vegetation and climate conditions that affected whether an attempt (i.e., lightning strike) materialized into an actual wildfire. The realized number of wildfire initiations for the Truckee River landscape is shown in **Figure 3**.

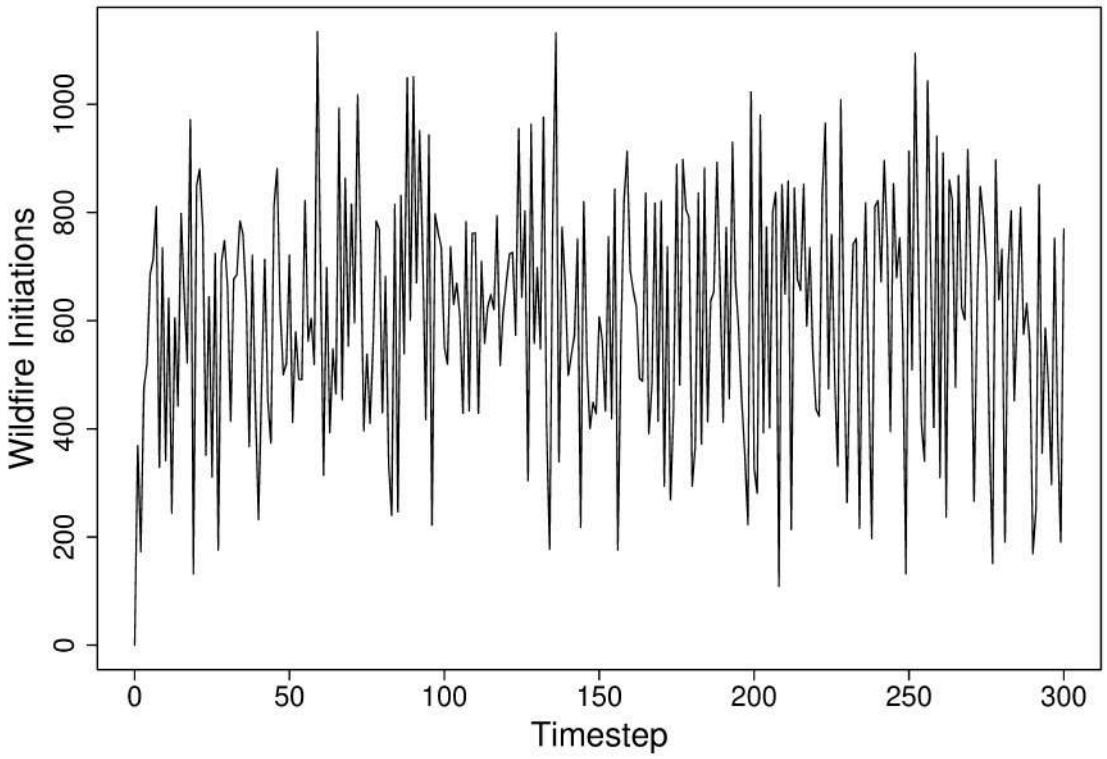

Figure 3: Realized simulated number of wildfire initiations per 5-year timestep for the Truckee River landscape.

Wildfire Mortality

Following the termination of a wildfire event the probability of high versus low mortality of the overstory vegetation in each 5 m cell that burned was determined by two major factors combined in a complex function as described in the general technical report: 1) fire intensity, which was a function of the fuel loads in the neighborhood of the focal cell (proxied by the age of the vegetation and time since the last fire), the topographic position of the focal cell, and the climate conditions of the current timestep; and 2) the resistance of the focal cell, which was a function of the age of the vegetation in the focal cell.

Briefly, we varied the beta coefficients of the resistance component of the complex function for each cover type to reflect differences in reported historical mean fire return intervals and high mortality rates among cover types - increasing or decreasing the rate of exponential decline in high mortality with increasing vegetation ages as a function of fire intensity - as a means of calibrating the model to achieve target high mortality rates for each cover type (see Model Calibration). The calibrated wildfire mortality functions for each cover type are included in **Appendix C2**.

Succession Climate

Climate conditions affecting vegetation succession during each timestep of the simulation were governed by a single global parameter, the Succession Climate Index based on the Palmer Modified Drought Severity Index (PMDI), in which a single coefficient was assigned to each timestep of the simulation. The final Succession Climate Index trajectory represented a vector of coefficients, one for each timestep, and is shown in **Figure 4**.

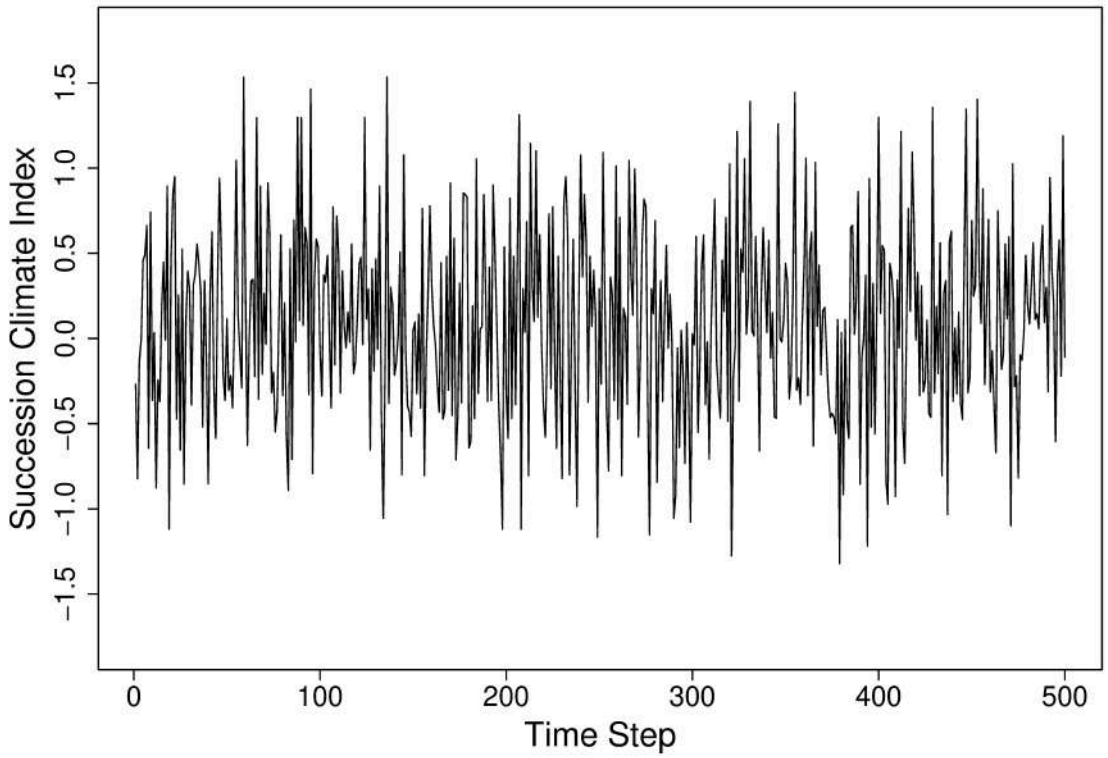

Figure 4: Succession Climate Index trajectory for the Truckee River landscape corresponding to 500 5-year timesteps in the simulation. The Climate Index was based on the inverted 5-year averaged, inverse-distance weighted mean Palmer Modified Drought Severity Index (PMDI) for the sample point locations within the north Sierra ecoregion relative to the focal landscape (Truckee River watershed in this case). Note, here we inverted PMDI so that positive values represented drier conditions and negative values represented wetter conditions (see text for details).

MODEL CALIBRATION

Although LDSim is a process-oriented model with individual parameters sourced either from data, literature, or expert opinion, the model outcomes reflect the complex spatio-temporal interactions of the various stochastic disturbance and succession processes. Consequently, it is necessary to calibrate the model by tuning (i.e., adjusting up or down) one or more of the model parameters to produce selected outcomes that are consistent with the data, literature and expert opinion. Importantly, in this context, we considered the parameters associated with the disturbance process to be "independent" variables and the

vegetation conditions (e.g., seral stage distribution, spatial patterns of vegetation states, etc.) to be "dependent" outcomes. Therefore, we calibrated select disturbance parameters (i.e., independent variables) to achieve the targeted disturbance regime without any attention to the vegetation response, which we treated as the dependent outcome of the disturbance regime. Importantly, we did not tune disturbance regime parameters to achieve desired vegetation outcomes. To calibrate the model, we focused on the following five disturbance regime attributes that we considered emergent properties of the disturbance regime, as discussed in detail in the GTR.

Fire Rotation Period

Fire Rotation Period (FRP) is the number of years required to burn a cumulative area equal to the extent under consideration. FRP combines fire frequency and fire size into a single integrated measure of how much fire is actually applied to a unit of ground. FRP is equivalent to the "point-specific" or "population" mean Fire Return Interval (FRI); i.e., the average number of years between fires to a single point on the ground (or cell), and is roughly equivalent to the oft reported "grand mean" FRI computed from a large sample of point-specific intervals (e.g., from a set of fire-scarred trees).

Briefly, we tuned the global wildfire initiation rate parameter, which controlled the number of wildfire initiation attempts per unit area within each timestep and remained constant over time (see Wildfire Initiation above), and two of the wildfire susceptibility coefficients (b_0 and b_1) for each cover type, which affected the susceptibility of fire initiation and spread in each cover type (see Wildfire Susceptibility above), and measured calibration success based on agreement with the pre-specified target FRP for each cover type. We set our calibration goal as within 10% of the target FRP for forested cover types with extents > 1,000 ha. We met our calibration target for all the forest cover types with > 1,000 ha, as shown in **Table 1**.

Table 1: Target and simulated Fire Rotation Periods (FRP) for the Truckee River landscape.

Cover type	**Area (ha)**	**Target FRP**	**Simulated FRP**	**%Deviation**
Yellow Pine	37129	20	19	-5
Sierra Mixed Conifer	30766	26	26	0
Chaparral	13278	55	50	-9
Shrubland	8289	55	49	-11
Montane Riparian	4798	53	48	-9
Red Fir	4668	50	49	-2
Lodgepole Pine	4463	52	53	2
Subalpine Conifer	4428	296	309	4
Big Sagebrush	3680	35	42	20
Grassland	2481	60	58	-3
Meadow	309	60	60	0
Curl-leaf Mountain Mahogany	294	76	75	-1
Sierra Mixed Conifer_Aspen	284	29	29	0
Oak-Conifer Forest and Woodland	250	21	23	10
Total	115507	30	28	-7

Fire Mortality Rate

Fire mortality rate (FMR) is the percentage of burned cells that exhibit a high-mortality response (i.e., complete overstory mortality). For the purpose of model calibration, we considered the FMR only for cells in the "short", "medium" and "tall" tree developmental stages (i.e., "mature" trees) since this was the basis for specifying the target values.

Briefly, we tuned two of the wildfire mortality coefficients (b_5 and b_6) for each cover type, which affected the probability of high mortality fire as a function of age and fire intensity in each cover type (see Wildfire Mortality above), and measured calibration success based on conformity to pre-specified fire mortality targets for each cover type. We set our calibration goal as within 10% of the targets for forested cover types with > 1,000 ha in the focal landscapes. We met our calibration target for 1 of the 5 of the forested cover types with > 1,000 ha, and came acceptably close for the remaining 4 cover types (note, even though the percent difference was rather large, the absolute difference was relatively minor), as shown in **Table 2**.

Table 2: Target and simulated Fire Mortality Rates (FMR) for the Truckee River landscape.

Cover type	**Area (ha)**	**Target FMR**	**Simulated FMR**	**%Deviation**
Yellow Pine	37129	5	5.66	13
Sierra Mixed Conifer	30766	7	7.53	8
Red Fir	4668	10	11.13	11
Lodgepole Pine	4463	24	21.11	-12
Subalpine Conifer	4428	10	12.03	20
Oak-Conifer Forest and Woodland	250	5	5.54	11

Fire Size Distribution

Fire size distribution (FSD) is the percentage of realized fire sizes across bins of increasing fire size. We opted not to tune the parameters affecting the fire size distribution as these were empirically based. Instead, we treated the realized fire size distribution as an emergent outcome of the model and measured calibration success based on agreement with the pre-specified fire distribution derived from the post-settlement period of 1908 - 1979 from which we had an empirical record. We set our calibration goal as a subjective evaluation of the realized fire size distribution compared to the target fire size distribution. We met our calibration target reasonably well, as depicted in **Figure 5**.

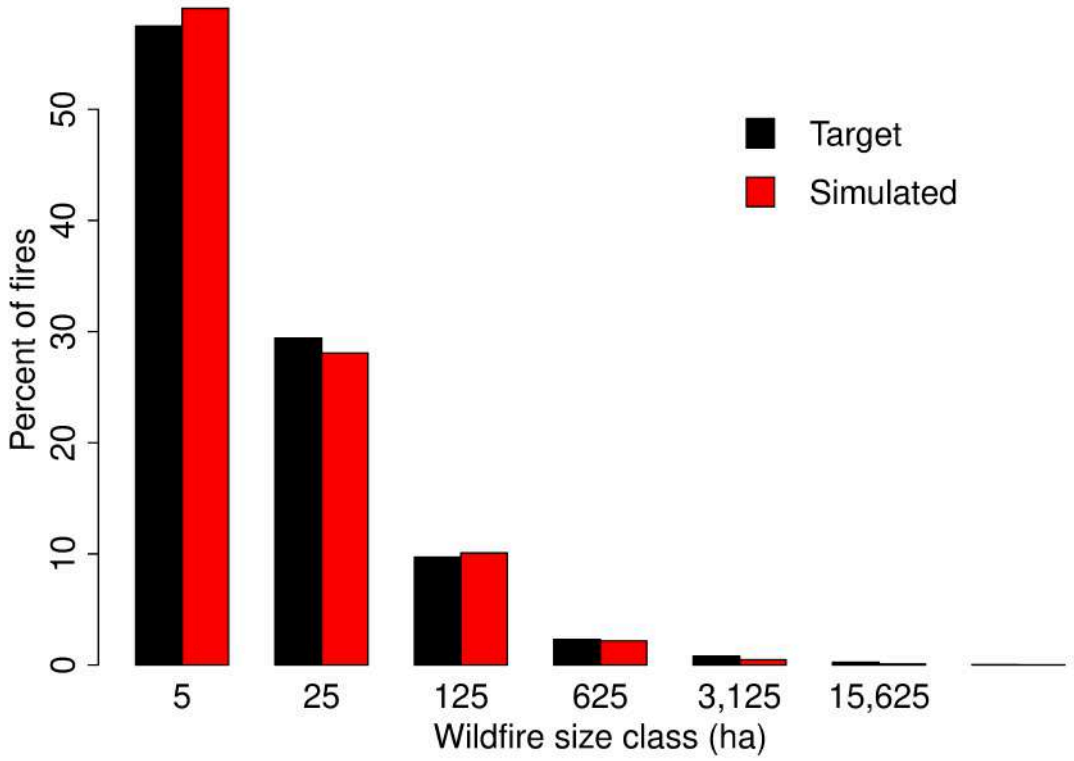

Figure 5: Target and simulated wildfire size distribution for the Truckee River landscape.

Variability in Total Area Burned

Variability in total area burned over time is a measure of the temporal variability in the wildfire disturbance regime. We opted not to tune the primary parameter affecting the temporal variability in total area burned - the Wildfire Climate Index - as it was empirically based. Instead, we treated the variability in total area burned as an emergent outcome of the model and measured calibration success based on agreement with the observed variability in total area burned for the post-settlement period of 1908 - 1979 from which we had an empirical record. We set our calibration goal as within 10% of the target coefficient of variation (CV) in total area burned per timestep (CV = 91.8%, see GTR). We fell just shy of meeting our calibration target for the Truckee River landscape, as depicted in **Figure 6**.

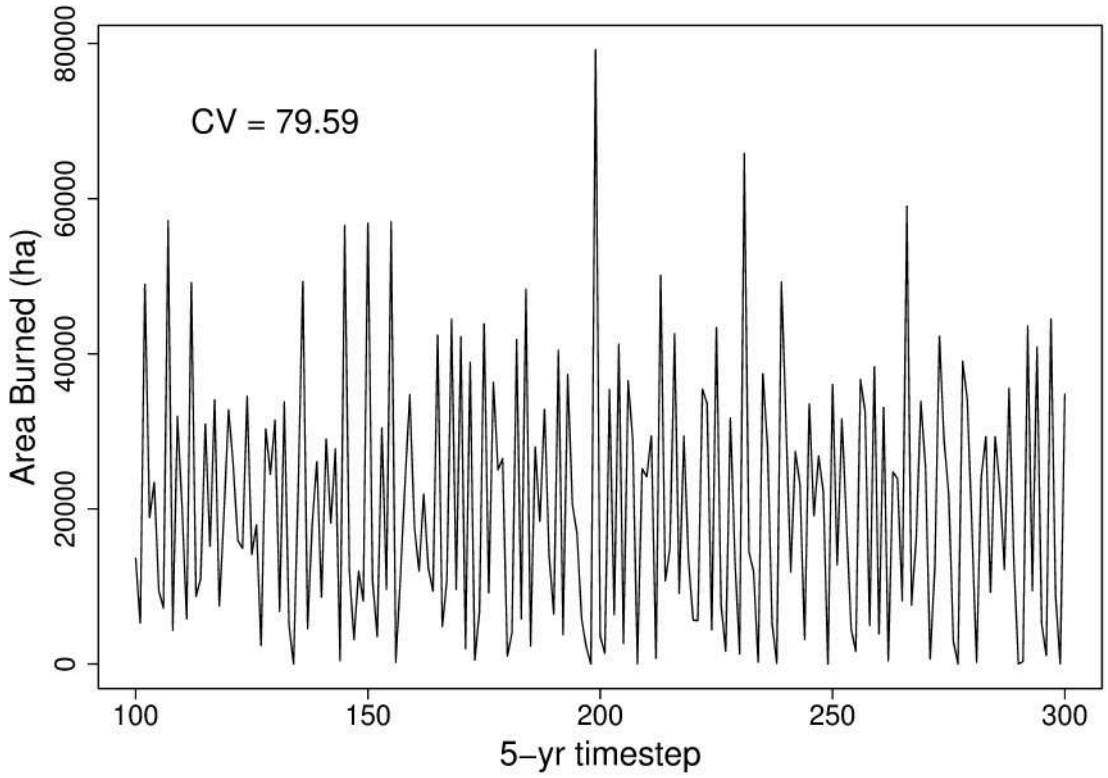

Figure 6: Total simulated area burned per 5 years in the Truckee River landscape representing the historical reference period of 1550-1850 and the computed Coefficient of Variation (CV).

Relationship Between Total Area Burned and Climate

The relationship between total area burned and climate is a measure of the degree to which the simulated total area burned is affected by variability in the specified Wildfire Climate Index. We opted not to tune the Wildfire Climate Index, in particular, or any parameter associated with the wildfire disturbance process with regards to this calibration metric. Instead, we treated the observed relationship between total area burned and the climate index as an emergent outcome of the model and measured calibration success based on agreement with the strength of the relationship for the post-settlement period of 1908 - 1979 from which we had an empirical record. We set our calibration goal as within 10% of the target coefficient of determination (R2) in the fit of a linear regression to the target data (R2 = 0.25, see GTR). In general, we failed to meet this calibration target closely for the Truckee River landscape, instead simulating a stronger relationship between total area burned and climate than we observed during the post-settlement period and simulating a distinctly non-linear relationship compared with observed post-settlement observations, as depicted in **Figure 7**.

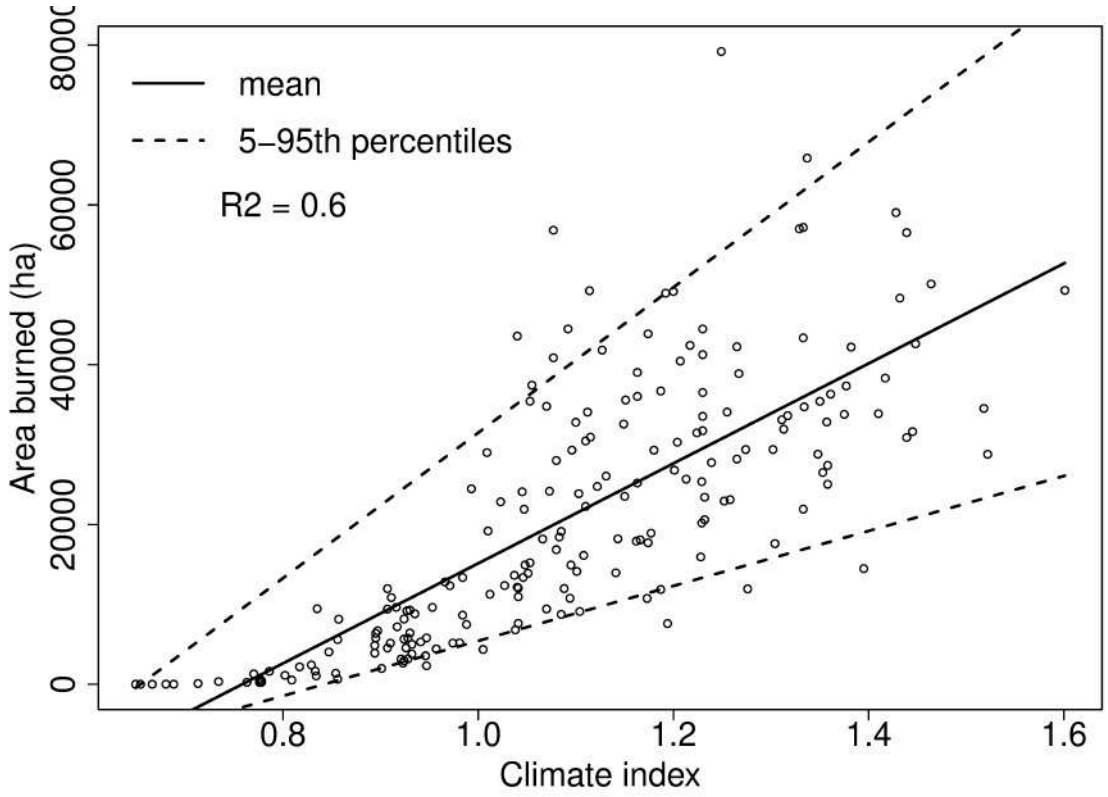

Figure 7: Scatterplot of the modified wildfire Climate Index based on the modified Palmer Drought Severity Index (see text for details) and the log of simulated total area burned per 5 years in the Truckee River landscape representing the historical reference period of 1550-1850, and the fitted linear regression for the mean and 5-95th quantiles (see text for details) along with the Coefficient of Determination (R2) of the fit.

HISTORICAL RANGE OF VARIABILITY and CURRENT DEPARTURE

Biophysical Classes and Units

To summarize HRV and current departure in landscape structure at the Site and Subbasin levels, we subdivided the landscape into a set of Biophysical Classes (BPCs), as described in detail in the GTR. Briefly, we indexed site productivity based on the cumulative tree biomass generated over the course of the simulation, after model equilibration, and then modeled tree biomass as a function of 10 geophysical variables using a Random Forest analytical framework, and lastly classified predicted Biomass into 4 equal-area classes based on quartiles of the data, plus a zero class for all non-forest cells. The final BPC layer included 4 classes ranging from the least productive to most productive sites, plus a non-forest class, as depicted in **Figure 8**.

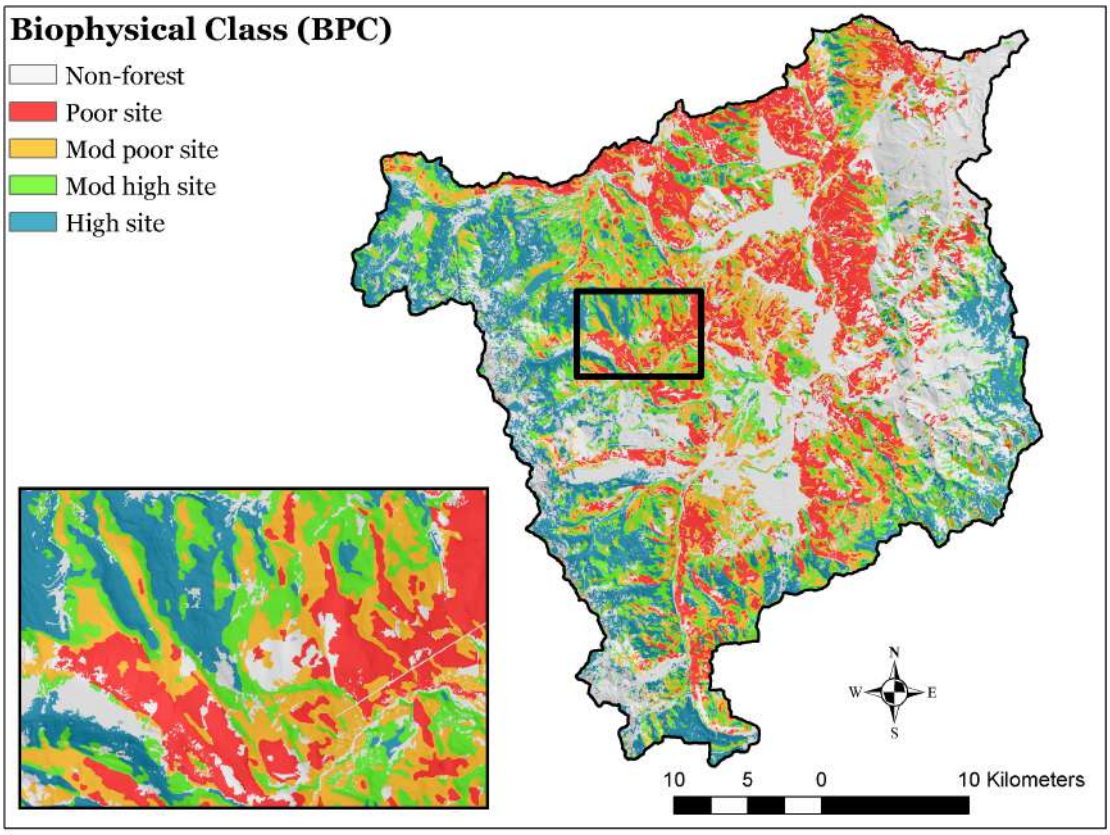

Figure 8: Biophysical Classes (BPCs) based on quartiles of predicted Biomass derived from a Random Forest model to predict Biomass (i.e., simulated cumulative tree height) from 10 biophysical variables. The Random Forest model explained ~70% of the variation in Biomass under simulated historical dynamic equilibrium conditions in the Truckee River landscape.

The final BPCs were distinguishable on the basis of the 10 geophysical variables and cover type, although there was considerable overlap among BPCs in each of the variables, as described below for a select set of the variables.

- *Cover Type* - The distribution of each cover type among BPCs (as a percentage of the cover type), ordered roughly from low to high elevation distributions, is given in **Table 3**. Most forest types were distributed across all BPCs, although most cover types exhibited a distinctly non-uniform distribution. For example, Oak-Conifer Forest and Woodland, Sierra Mixed Conifer_Aspen, Lodgepole Pine, Lodgepole Pine_Aspen, Red Fir, and Subalpine Conifer were all extremely rare on Low and moderately Low productivity sites. Yellow Pine was the only cover type disproportionately found on Low and Moderately Low productivity sites.

  Table 3: Percentage of each cover type in each Biophysical Class (BPC) for the Truckee River landscape.

Cover type	Area (ha)	Low	ModLow	ModHigh	High
Yellow Pine	35184	46.51	32.74	17.03	3.71
Oak-Conifer Forest and Woodland	232	8.66	14.65	39.85	36.83
Sierra Mixed Conifer	29345	12.28	22.96	32.85	31.90
Sierra Mixed Conifer_Aspen	283	1.07	14.47	47.85	36.61
Lodgepole Pine	4144	1.77	8.35	23.11	66.77
Lodgepole Pine_Aspen	111	0.00	0.00	8.65	91.35
Red Fir	4648	0.74	6.08	26.42	66.76
Subalpine Conifer	4379	1.38	6.08	26.13	66.41

- *Mesic Index* - The distribution of the Mesic Index for each BPC (given as quantiles of the index) is given in **Table 4**. As expected, the Mesic Index distribution increased as the site productivity class increased from Low to High, but with considerable overlap in distributions between adjacent BPC classes. There was no overlap between Low and High productivity sites. Despite the strong overlap, the BPC classes represented a gradient in expected site moisture, with the Low site class representing the driest sites and the High site class representing the wettest sites.

  Table 4: Distribution of the Mesic Index in each Biophysical Class (BPC), given as quantiles for the Truckee River landscape.

BPC	2.5%	25%	50%	75%	97.5%
Low	15	28	34	38	47
ModLow	26	37	42	46	57
ModHigh	31	43	48	53	68
High	41	51	56	63	74

- *Topographic Position* - The distribution of the Topographic Position Index for each BPC (given as quantiles of the index) is given in **Table 5**. Topographic Position Index exhibted a weak inverse relationship with site productivity, i.e., topographic position decreased with increasing site productivity. The High site productivity class showed the strongest gradient in TPI, with a prevalence for lower topographic positions. Table 5: Distribution of the Topographic Position Index each each Biophysical Class (BPC), given as quantiles for the Truckee River landscape.

BPC	2.5%	25%	50%	75%	97.5%
Low	29	44	50	57	75
ModLow	27	44	49	55	77
ModHigh	25	43	49	57	83
High	19	38	45	52	72

- *Aspect* - The distribution of aspect classes among BPCs (as a percentage of the BPC) is given in **Table 6**. Not surprisingly, each BPC class was distributed across all aspect classes, but still exhibited a pronounced orientation, with the Low site class disproportionately occupying southwesterly aspects and the High site class disproportionately occupying northeasterly aspects.

  Table 6: Percentage of each Biophysical Class (BPC) in each aspect class for the Truckee River landscape.

Aspect	N	NE	E	SE	S	SW	W	NW	Flat
Low	1.04	0.73	1.84	14.16	19.27	25.72	17.80	14.79	4.66
ModLow	8.38	8.38	12.95	16.71	8.05	8.50	6.73	20.87	9.42
ModHigh	16.02	18.33	13.31	10.71	3.96	4.90	5.86	18.93	7.98
High	18.53	26.24	15.45	7.17	2.18	3.89	5.53	14.24	6.78

Fire Return Interval and Departure

Mean point-specific Fire Return Interval (FRI) represents the average number of years between fire events at the 5 m cell level. We interpreted the observed mean FRI after model equilibration (N = 200 timesteps) at the cell level as a single integrated (albeit not comprehensive) summary of the historical wildfire disturbance regime. The historical mean FRI varied from < 15 years to > 300 years across the landscape, with evident influences of both cover type and terrain (**Figure 9**).

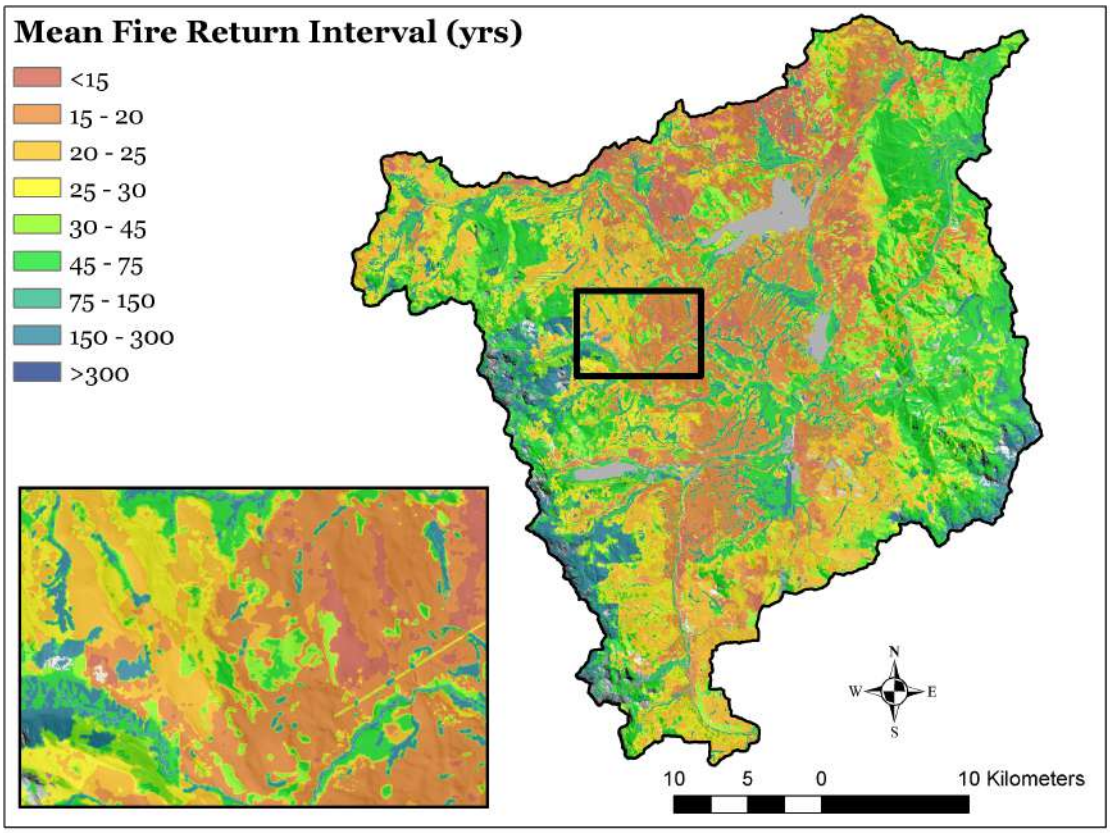

Figure 9: Simulated Fire Return Interval (FRI) (yrs) at the 5 m cell level for the Truckee River landscape.

In addition, the historical mean FRI varied among BPCs as expected (**Table 7**). Specifically, the median FRI increased steadily from 17 to 37 years with increasing site productivity; i.e., from Low to High BPC. Low productivity sites that occurred disproportionately on upper slopes and ridgetops and southwesterly aspects were warmer and drier and thus more susceptible to wildfire, despite having less fuel build-up over time. Conversely, High productivity sites that occurred disproportionately on lower slopes and valley bottoms and on northeasterly aspects were cooler and wetter and thus less susceptible to wildfire, despite having more fuel build-up over time. The relatively short median FRIs across all sites indicates that historically wildfires typically occurred frequently enough to keep surface and ladder fuel loads low enough to reduce the occurrence of high-severity wildfire.

Table 7: Range of variability (given as quantiles) in the mean fire return interval (FRI) by Biophysical Class (BPC) for the Truckee River landscape.

BPC	HRV2.5%	HRV25%	HRV50%	HRV75%	HRV97.5%
Low	14	16	17	21	44
ModLow	15	18	21	25	122
ModHigh	17	23	26	35	292
High	21	27	37	54	300

These results also indicate that the HRV in mean FRI varied several-fold across sites within each BPC. For example, on High productivity sites FRI varied more than 10-fold between 21-300 years across sites. The wide range of variation in FRI within BPCs indicates that wildfire risk varied markedly across sites even within a single BPC and, consequently, that FRI is only loosely correlated with predicted cumulative tree biomass. For example, sites classified as having high long-term productivity under historical dynamic equilibrium conditions could have FRIs as short as 21 years (or shorter for the extremes) or as long as 300 years (or longer for the extremes) depending on local topographic and vegetative conditions and chance. This is visually evident in the map of mean FRI for the High site BPC (**Figure 10**).

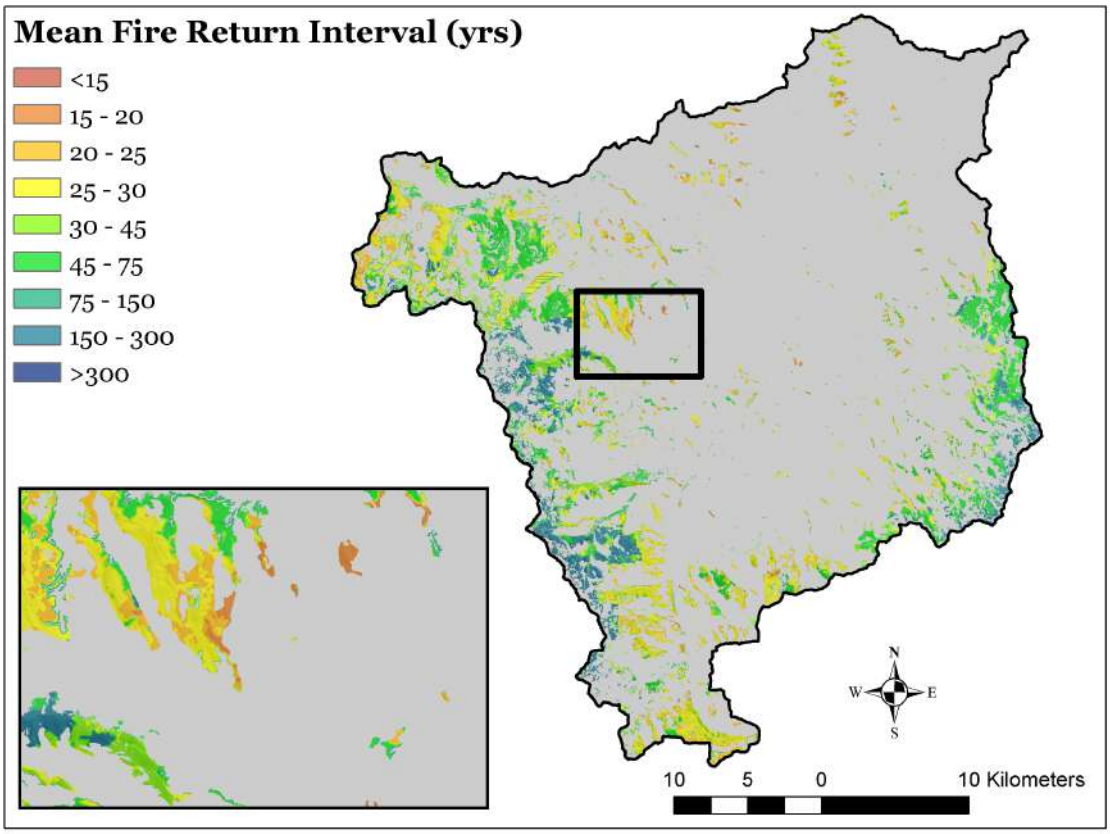

Figure 10: Simulated Fire Return Interval (FRI) (yrs) at the 5 m cell level on High productivity sites (Biophysical Class = 4) in the Truckee River landscape.

Fire Return Interval Departure (FRID) represents the percentage deviation of the contemporary (post-settlement) mean point-specific FRI from the mean point-specific FRI under historical (i.e., pre-settlement) dynamic equilibrium conditions. Briefly, FRID measures the degree, in percent, to which contemporary fires (i.e., since 1909) are burning at frequencies similar to the frequencies that occurred prior to significant Euro-American settlement, as simulated (**Figure 11**). Positive departure indicates that

the contemporary fire frequency is less than the historical fire frequency. Not surprisingly most of the landscape is severely departed with respect to fire frequency.

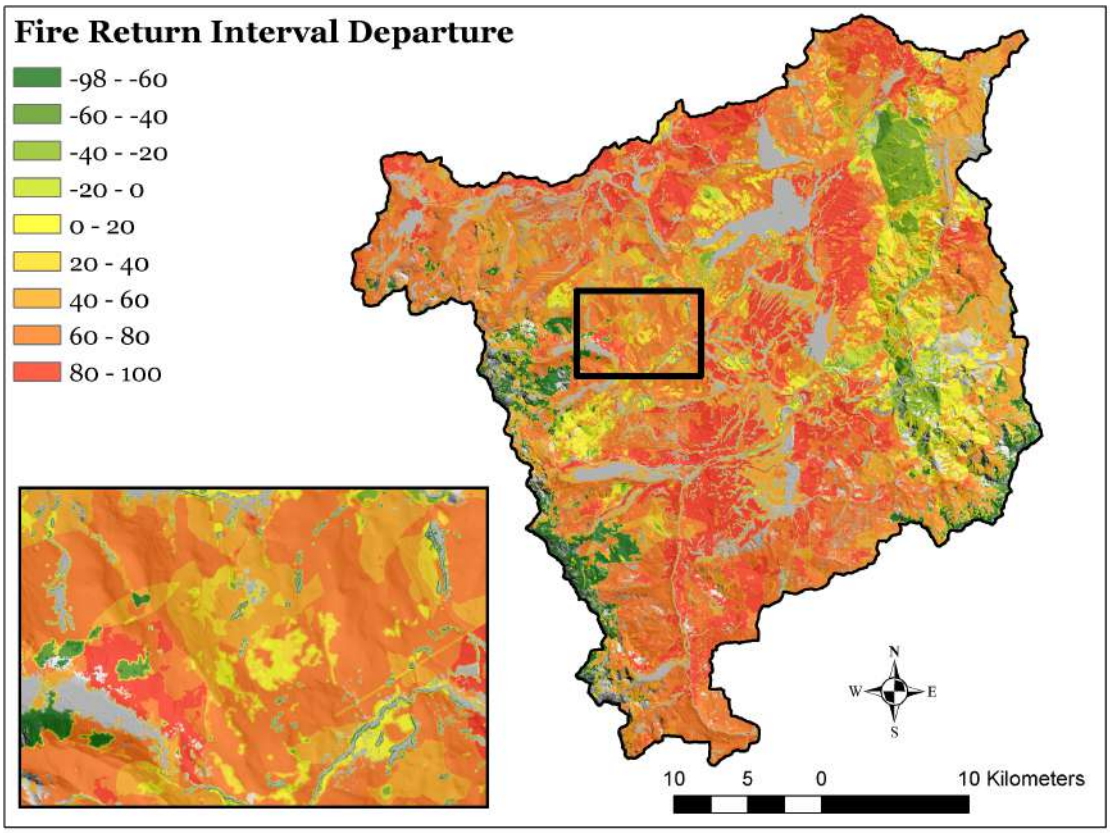

Figure 11: Fire Return Interval Departure (FRID) at the 5 m cell level in the Truckee River landscape, representing the percent to which contemporary fires (i.e., since 1909) are burning at frequencies similar to the frequencies that occurred prior to significant Euro-American settlement, as simulated. Positive values represent a contemporary FRI > the pre-settlement FRI and, conversely, negative values represent a contemporary FRI < the pre-settlement FRI.

In addition to the cell-level map of FRID, we also summarized the mean FRID for each GPU to include in the Stewardship Atlas as a means of prioritizing GPUs for treatment with fire (**Figure 12**).

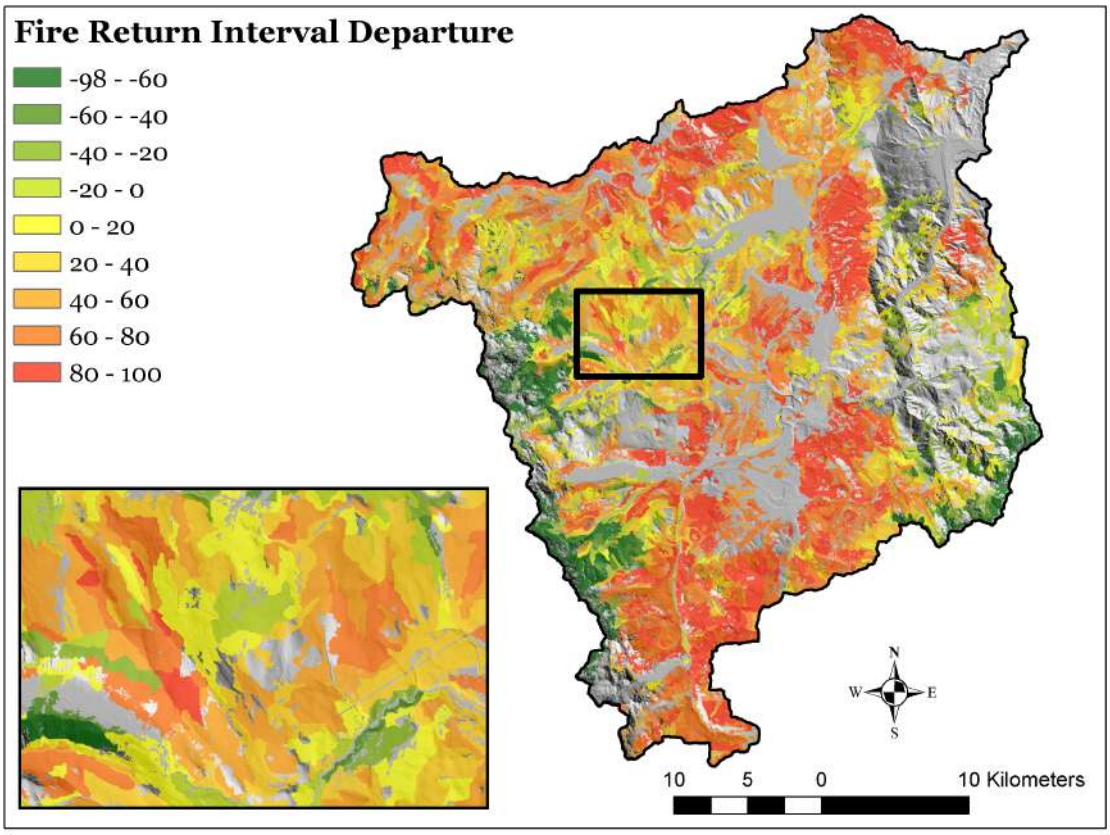

Figure 12: Geophysical Unit-level Fire Return Interval Departure (FRID) for the Truckee River landscape, representing the average 5 m cell value in the percent to which contemporary fires (i.e., since 1909) are burning at frequencies similar to the frequencies that occurred prior to significant Euro-American settlement, as simulated.

Vegtation Persistence

We defined vegetation persistence as the likelihood of persisting in either an early- or late-seral condition at the 5 m cell level. We interpreted the observed mean FRI of high-mortality wildfires after model equilibration (N = 200 timesteps) at the cell level as a proxy for vegetation persistence, under the assumption that locations with shorter high-mortality FRIs would likely persist longer in early-seral stages and, conversely, locations with longer high-mortality FRIs would likely persist longer in late-seral stages.

Figure 13 depicts several areas with relatively long high-mortality FRIs (dark blue areas in the map) and these are sites that have a high likelihood of supporting late-seral vegetation under a natural disturbance regime. Conversely, the map depicts several areas with relatively short high-mortality FRIs (yellow and orange areas in the map) and these are sites that have a high likelihood of supporting early-seral vegetation much of the time under a natural disturbance regime. Accordingly, management objectives for these areas could be designed to capitalize on these focal areas. For example, establishing treatment objectives to maintain and enhance late-seral conditions for old forest associated species in areas with a lower likelihood of high-mortality wildfire (i.e., longer FRI) would be logical.

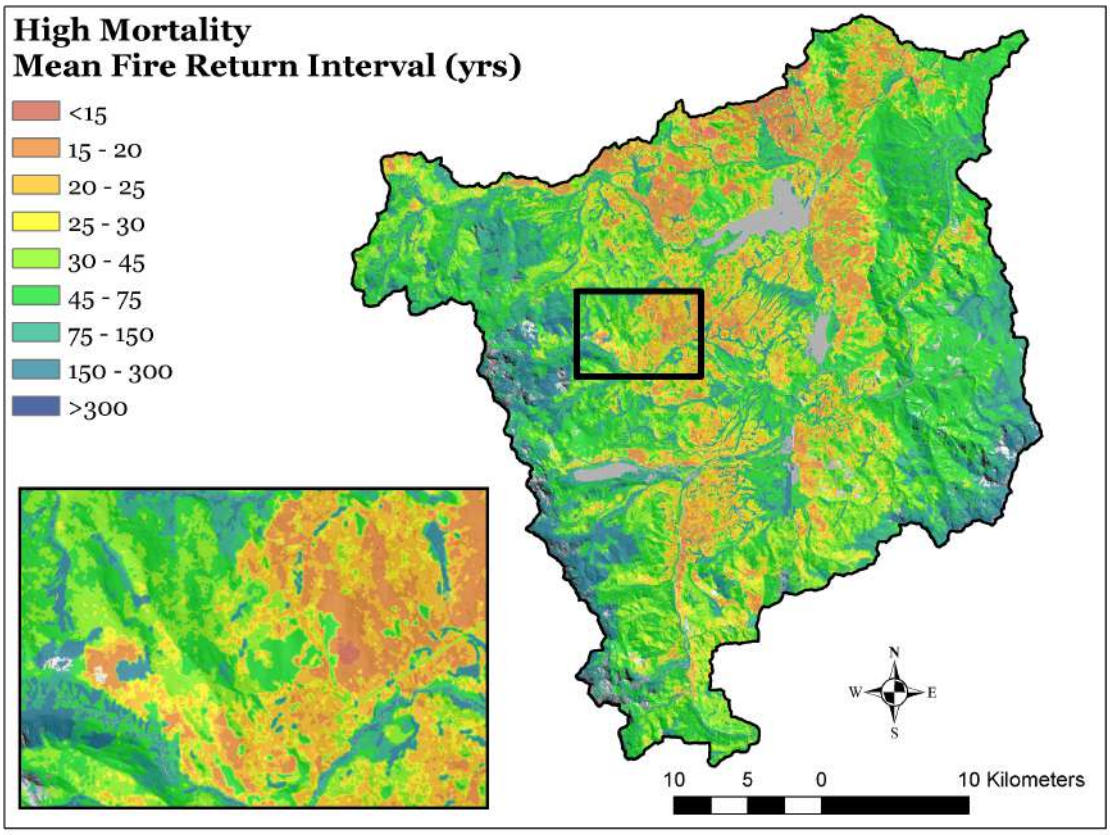

Figure 13: Simulated high-mortality Fire Return Interval (FRI) (yrs) at the 5 m cell level in the Truckee River landscape.

Site-level HRV and Departure

The results presented in this section address landscape metrics quantified at the "Site" level. Recall from the GTR that we defined a Site as a 40-m radius window around each focal cell. Here, each Site falls within a single BPC based on the location of the focal cell and has a single value computed for each landscape metric for each point in time (i.e., snapshot). HRV represents the variation in the landscape metric across Sites and over time under historical dynamic equilibrium conditions. Further recall that the current landscape also has a range of values across Sites (CRV), rather than a single value. Thus, a comparison of the HRV and CRV distributions depicts the degree to which CRV deviates from HRV (i.e., current departure). It is important to remember that Site-level departure reflects the deviation between the CRV across Sites within the focal landscape and the HRV across Sites and over time within the focal landscape. Thus, departure for a Site is not based on a comparison of the current Site condition to its own HRV (as is the case with GPU and Subbasin departure, see below); rather it is the distribution of current Site conditions across the entire landscape compared to the historical distribution across Sites that forms the basis for Site-level departure.

Recall from the GTR that we used a parsimonious suite of landscape metrics that we deemed meaningful for estimating departure at the Site-level across the focal landscape and appropriate given the available data, and computed departure as described in the GTR (and not repeated here), including the following metrics:

Metric 1: Developmental Stage

Developmental stage at the Site level was based on discrete stages of canopy height development. We quantified the composition of forest developmental stages at the Site level based on the percentage of the forested portion of the Site in each developmental stage. The HRV and CRV in Developmental Stage composition by BPC at the Site level is given in **Table 8** and depicted in **Figure 14**.

Table 8: Range of variability (given as quantiles) in each developmental stage class across sites (40-m radius window centered on each focal cell) by Biophysical Class (BPC) for the current range of variability (CRV) and the historical range of variability (HRV) for the Truckee River landscape.

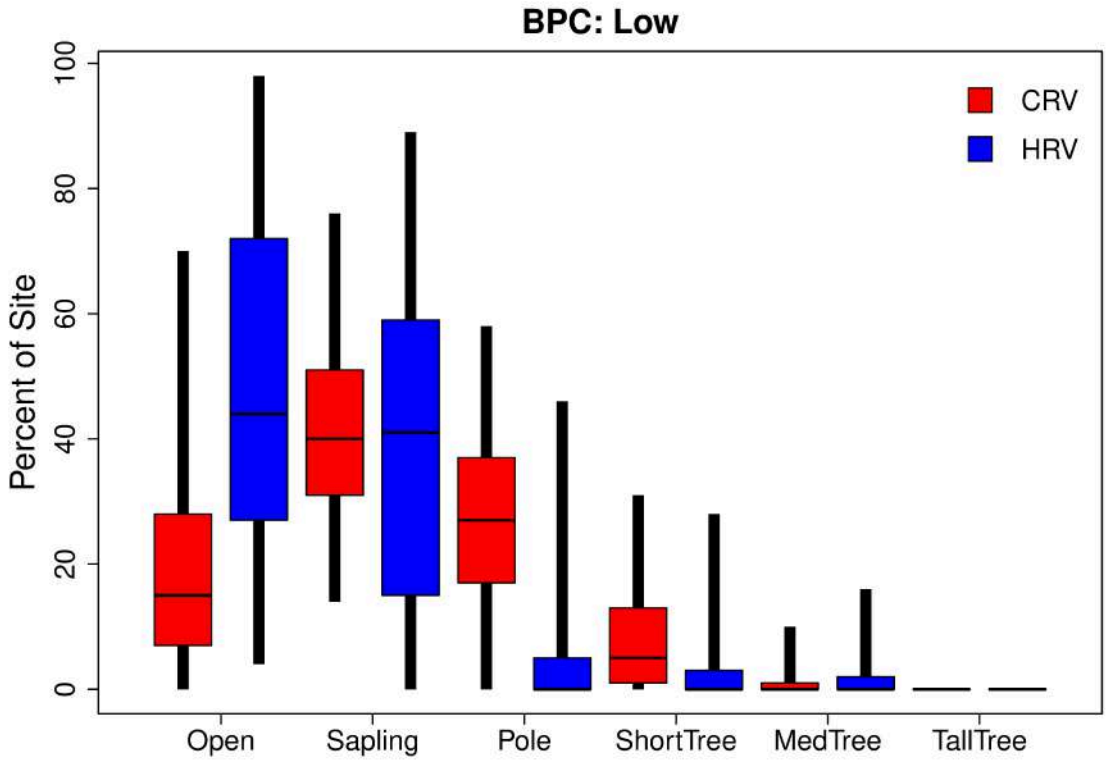

BPC	Class	Scenario	HRV 2.5%	HRV 25%	HRV 50%	HRV 75%	HRV 97.5%
Low	Open	CRV	0	7	15	28	70
Low	Open	HRV	4	27	44	72	98
Low	Sapling	CRV	14	31	40	51	76
Low	Sapling	HRV	0	15	41	59	89
Low	Pole	CRV	0	17	27	37	58
Low	Pole	HRV	0	0	0	5	46
Low	ShortTree	CRV	0	1	5	13	31
Low	ShortTree	HRV	0	0	0	3	28
Low	MedTree	CRV	0	0	0	1	10
Low	MedTree	HRV	0	0	0	2	16
Low	TallTree	CRV	0	0	0	0	0
Low	TallTree	HRV	0	0	0	0	0
ModLow	Open	CRV	0	5	13	27	78
ModLow	Open	HRV	2	17	31	55	93
ModLow	Sapling	CRV	9	28	37	47	73
ModLow	Sapling	HRV	0	17	38	56	82
ModLow	Pole	CRV	1	18	28	38	58
ModLow	Pole	HRV	0	1	4	13	57
ModLow	ShortTree	CRV	0	2	8	16	34
ModLow	ShortTree	HRV	0	0	2	7	38
ModLow	MedTree	CRV	0	0	0	2	14
ModLow	MedTree	HRV	0	1	4	9	36
ModLow	TallTree	CRV	0	0	0	0	0
ModLow	TallTree	HRV	0	0	0	0	2
ModHigh	Open	CRV	0	4	11	24	88
ModHigh	Open	HRV	2	11	21	41	85
ModHigh	Sapling	CRV	6	28	37	47	74
ModHigh	Sapling	HRV	0	13	32	50	76
ModHigh	Pole	CRV	0	19	29	38	58
ModHigh	Pole	HRV	0	2	7	19	61
ModHigh	ShortTree	CRV	0	2	8	17	35
ModHigh	ShortTree	HRV	0	1	4	11	46
ModHigh	MedTree	CRV	0	0	0	3	16
ModHigh	MedTree	HRV	0	4	9	19	49
ModHigh	TallTree	CRV	0	0	0	0	0
ModHigh	TallTree	HRV	0	0	0	1	10
High	Open	CRV	0	3	8	20	76
High	Open	HRV	1	7	14	31	74
High	Sapling	CRV	8	27	37	47	74
High	Sapling	HRV	0	5	20	39	70
High	Pole	CRV	0	20	29	37	57
High	Pole	HRV	0	3	9	22	61
High	ShortTree	CRV	0	4	11	19	36
High	ShortTree	HRV	0	2	6	14	49
High	MedTree	CRV	0	0	1	5	24
High	MedTree	HRV	1	8	17	30	60
High	TallTree	CRV	0	0	0	0	0
High	TallTree	HRV	0	0	2	8	31

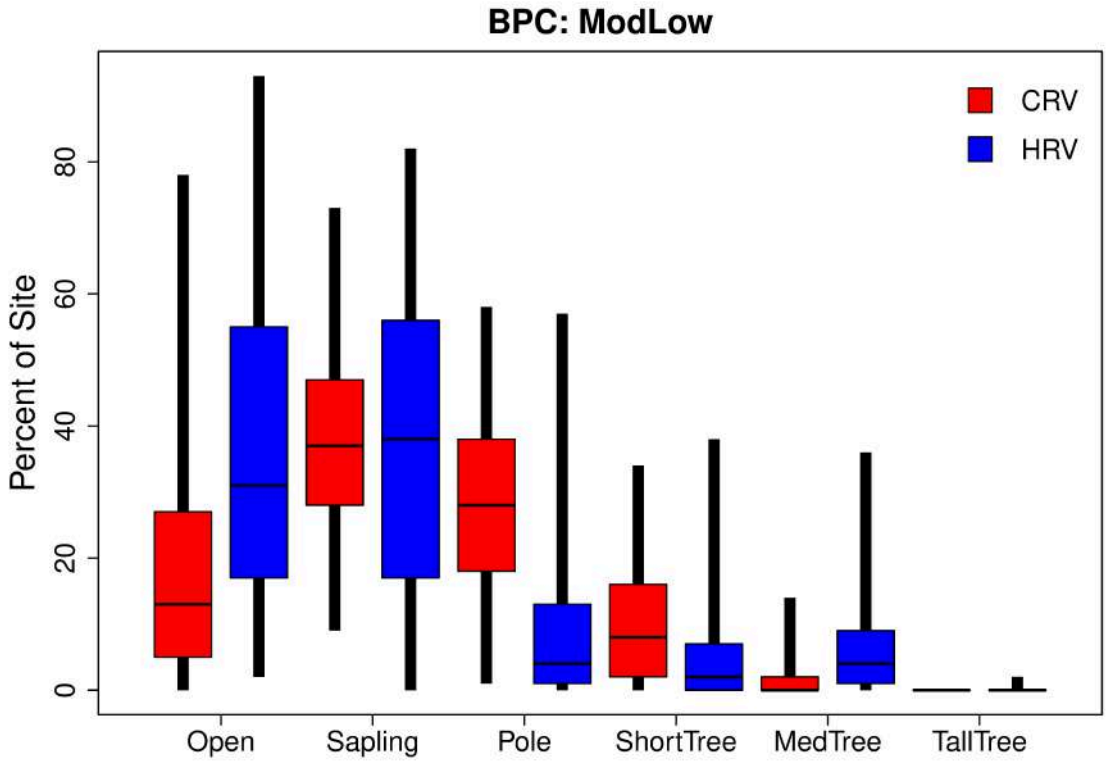
BPC: ModLow
CRV
HRV
Percent of Site
0
20
40
60
80
Open
Sapling
Pole
ShortTree
MedTree
TallTree

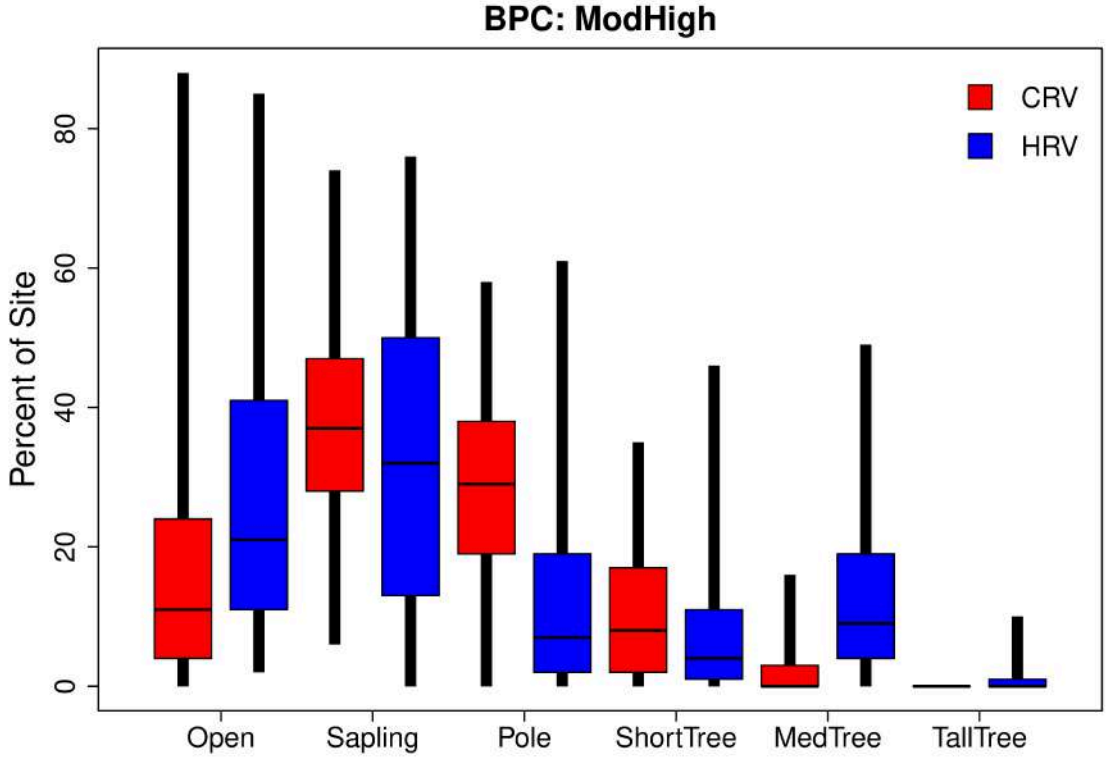
BPC: ModHigh
CRV
HRV
Percent of Site
0
20
40
60
80
Open
Sapling
Pole
ShortTree
MedTree
TallTree

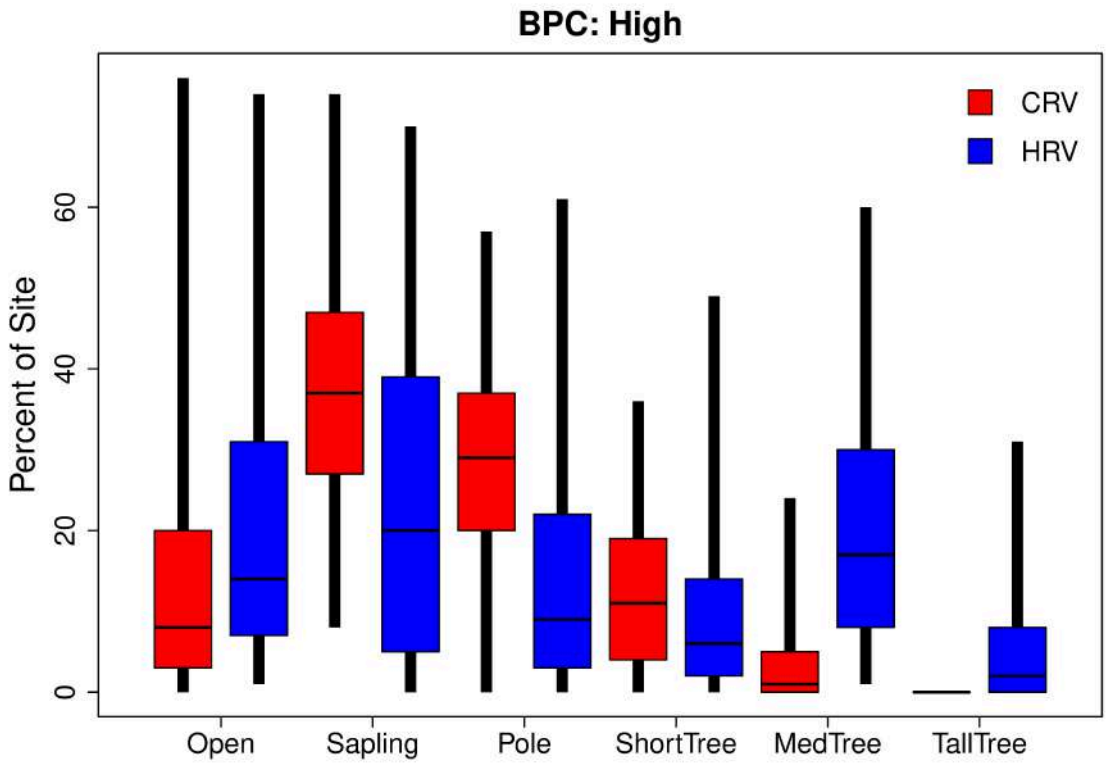

Figure 14: Historical Range of Variability (HRV) and Current range of variabiilty (CRV) among Sites (i.e., 40-m radius window) in the percent of forest in each developmental stage within the Low, Moderately Low, Moderately High and High site productivity Biophysical Classes (BPCs) in the Truckee River landscape. Box = 25-50 percentiles; whiskers = 2.5-97.5 percentiles

Recall that current departure in the Site-level metrics provides a basis for prioritizing management at the unit level. For example, given the results above, to reduce the current departure in developmental stage composition on High productivity Sites, management could prioritize treatments that produce units with a greater percentage of Open areas intermixed with Tall trees to shift the overall developmental stage distribution across the landscape to be more aligned with the HRV distribution. The same priorities could be given to Low productivity Sites, although here the emphasis would be predominantly on increasing the proportion of Sites with a greater proportion of Open areas. Of course, aside from controlling the percentage in Open, there is only limited ability to actively manage developmental stage succession (i.e., height growth). Indeed, much of the succession required to shift the current distribution towards the later stages of development simply requires time (e.g., to allow trees in the Pole and Short Tree stages to grow into the Medium and Tall Tree stages). However, managing surface and ladder fuels to inhibit high severity wildfire and retaining current taller trees may be an effective strategy to gradually shift the CRV towards better alignment with HRV with respect to the later developmental stages.

Metric 2: Tree Size (QMD)

Tree Size at the Site level was based on the Quadratic Mean Diameter (QMD) of established trees within a 40-m radius of the focal cell. Recall that QMD was based on only the cells with established trees in the window. Thus, if there was a single cell with an established tree in the window, then QMD was based on that single tree and equaled the tree's diameter at breast height (DBH). Accordingly, QMD can be quite high even in relatively open areas if the few neighborhood trees are large in diameter. The HRV and CRV in Tree Size composition at the Site level by BPC is given in **Table 9** and depicted in **Figure 15**.

BPC	Scenario	HRV 2.5%	HRV 25%	HRV 50%	HRV 75%	HRV 97.5%
Low	CRV	1	3	5	6	9
Low	HRV	1	3	5	9	18
ModLow	CRV	2	4	6	8	11
ModLow	HRV	3	7	9	13	21
ModHigh	CRV	1	5	7	8	12
ModHigh	HRV	5	10	13	16	24
High	CRV	2	6	8	10	16
High	HRV	8	14	18	22	32

Table 9: Range of variability (given as quantiles) in tree size (quadratic mean diameter) across Sites (40-m radius window centered on each focal cell) by Biophysical Class (BPC) for the current range of variability (CRV) and the historical range of variability (HRV) for the Truckee River landscape.

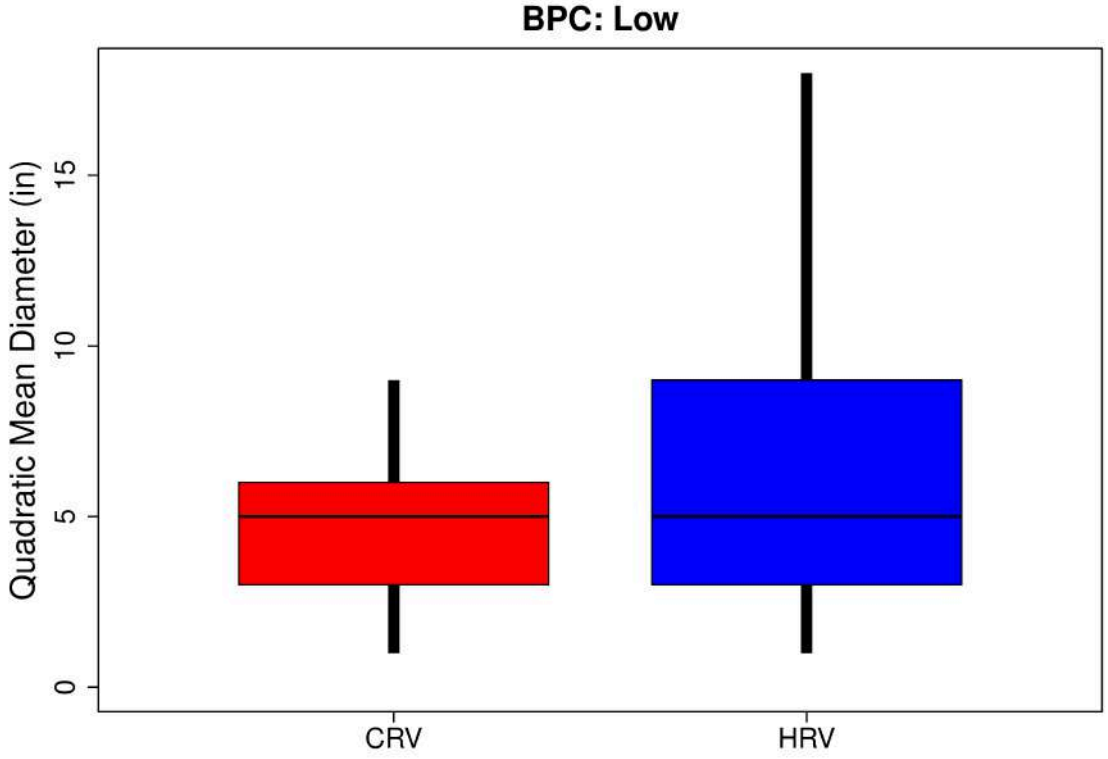

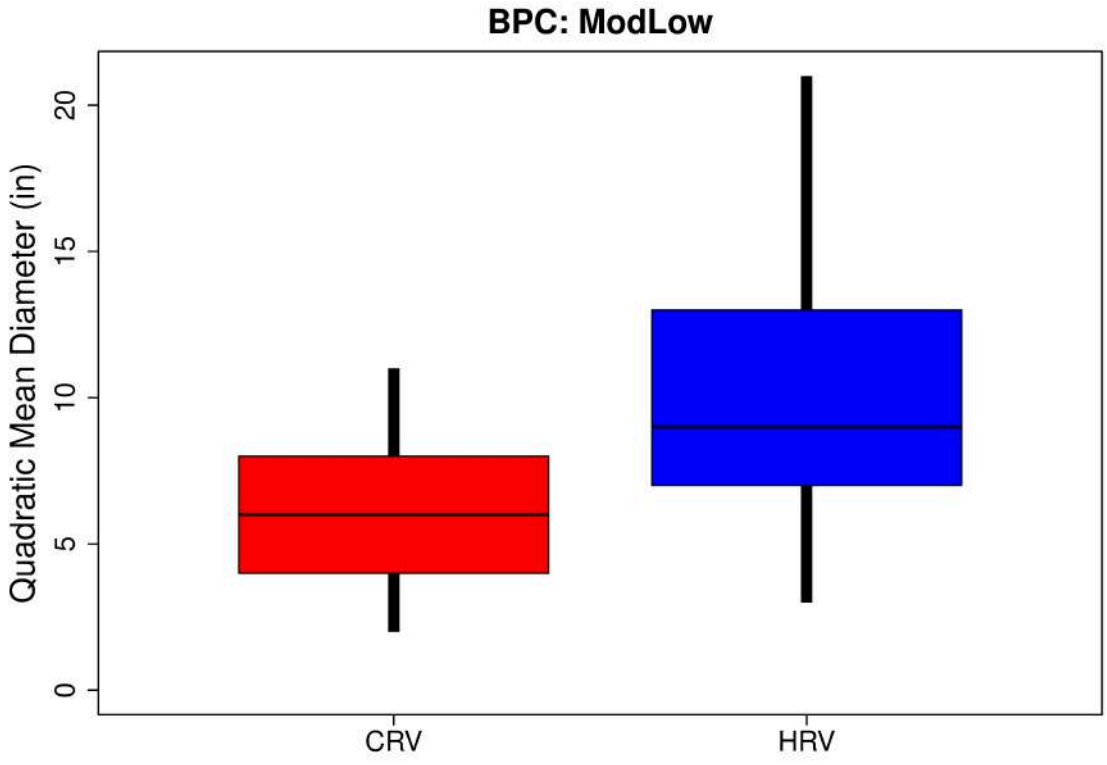
BPC: ModLow
Quadratic Mean Diameter (in)
0
5
10
15
20
CRV
HRV

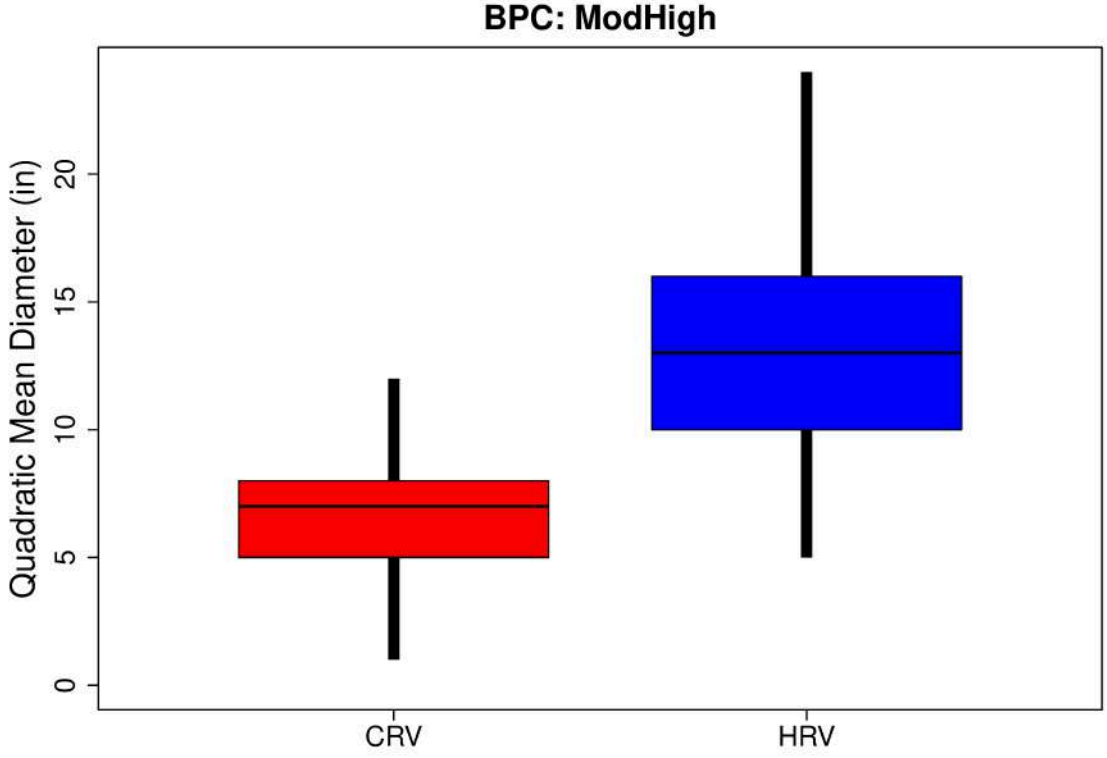
BPC: ModHigh
Quadratic Mean Diameter (in)
0
5
10
15
20
CRV
HRV

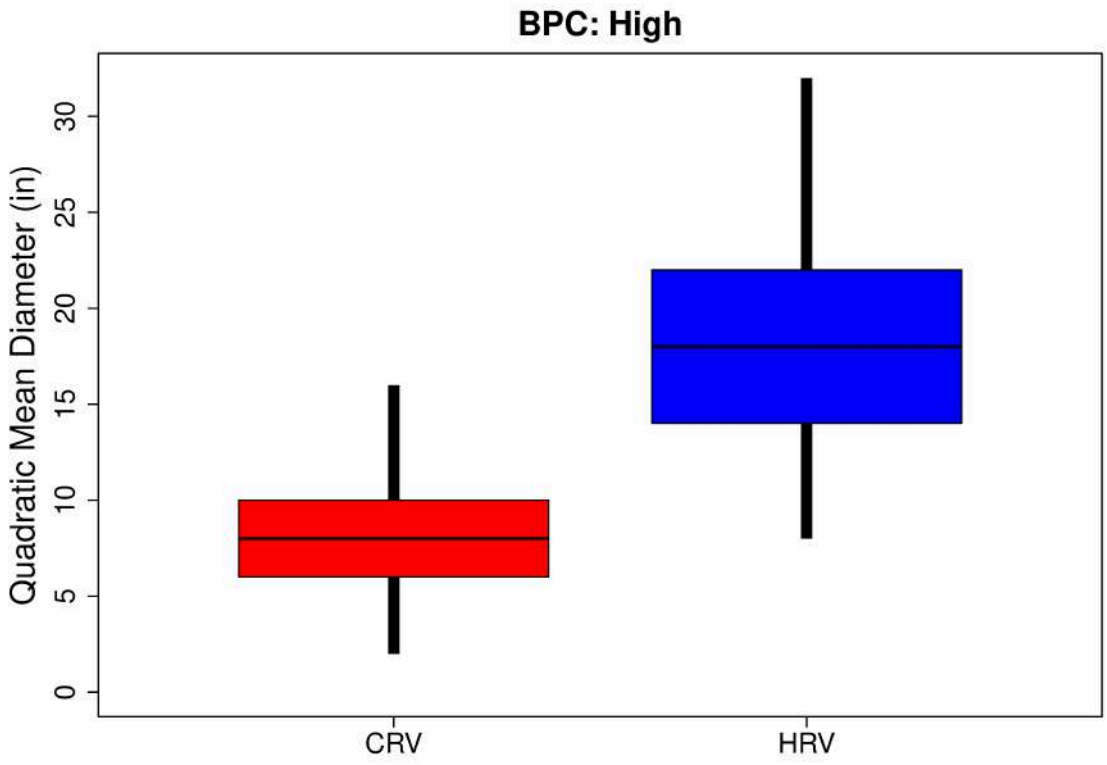

Figure 15: Historical Range of Variability (HRV) and Current range of variabiilty (CRV) among Sites (i.e., 40-m radius window) in the Quadratic Mean Diameter (QMD) of established trees to breast height within the Low, Moderately Low, Moderately High and High site productivity Biophysical Classes (BPCs) in the Truckee River landscape. Box = 25-50 percentiles; whiskers = 2.5-97.5 percentiles

Metric 3: Tree Cover

Tree Cover at the Site level was based on the percentage of 5-m cells with established trees to breast height within a 40-m radius of the focal cell. Recall that even a cell in the Open developmental stage (i.e., forest cell without an established tree to breast height) has a percent tree cover > 0 % so long as there was a single established tree within 40 m of the focal cell. In addition, recall that Tree Cover, as computed here, represents the percentage of cells within 40 m containing one or more established trees to breast height, not actual tree canopy cover, and as such is biased high by an average of 16% over actual tree canopy cover (i.e., actual tree canopy cover will be less than reported here by an average of 16%). The HRV and CRV in Tree Cover composition at the Site level by BPC is given in **Table 10** and depicted in **Figure 16**.

Table 10: Range of variability (given as quantiles) in percent tree cover across Sites (40-m radius window centered on each focal cell) by Biophysical Class (BPC) for the current range of variability (CRV) and the historical range of variability (HRV) for the Truckee River landscape.

BPC	Scenario	HRV 2.5%	HRV 25%	HRV 50%	HRV 75%	HRV 97.5%
Low	CRV	29	71	84	92	99
Low	HRV	1	27	55	72	95
ModLow	CRV	21	72	86	94	100
ModLow	HRV	6	44	68	82	97
ModHigh	CRV	11	75	88	95	100
ModHigh	HRV	14	58	78	88	97
High	CRV	23	79	91	96	100
High	HRV	25	68	85	92	98

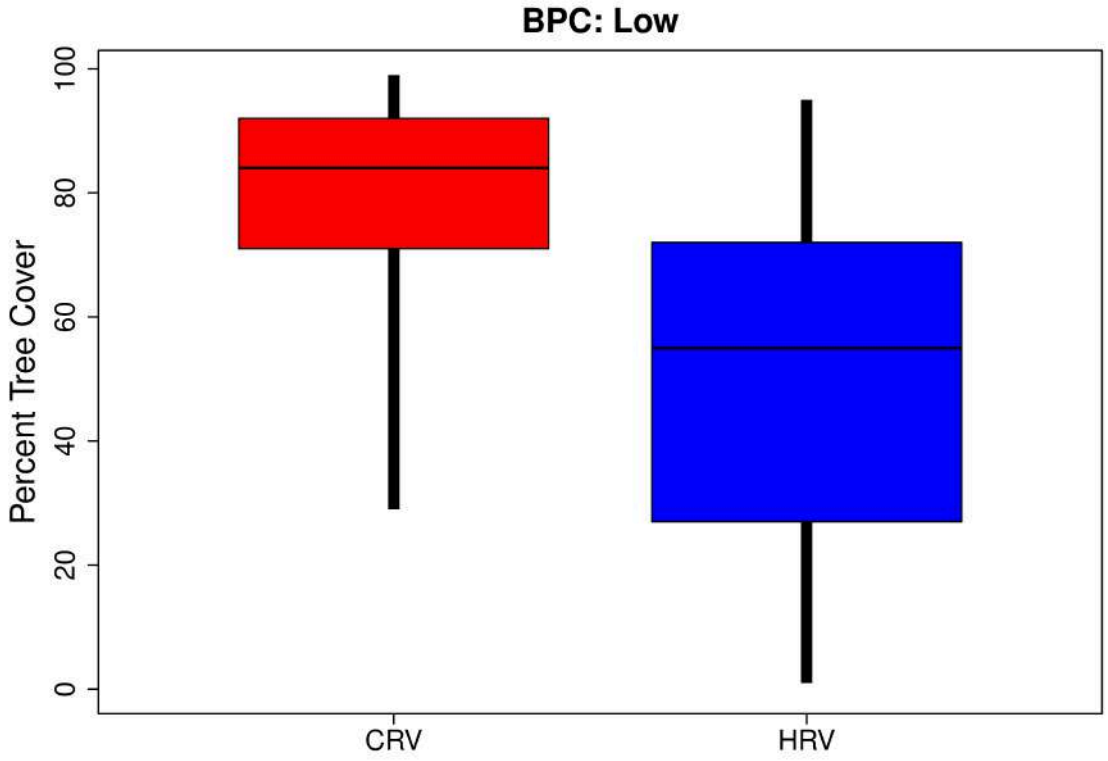

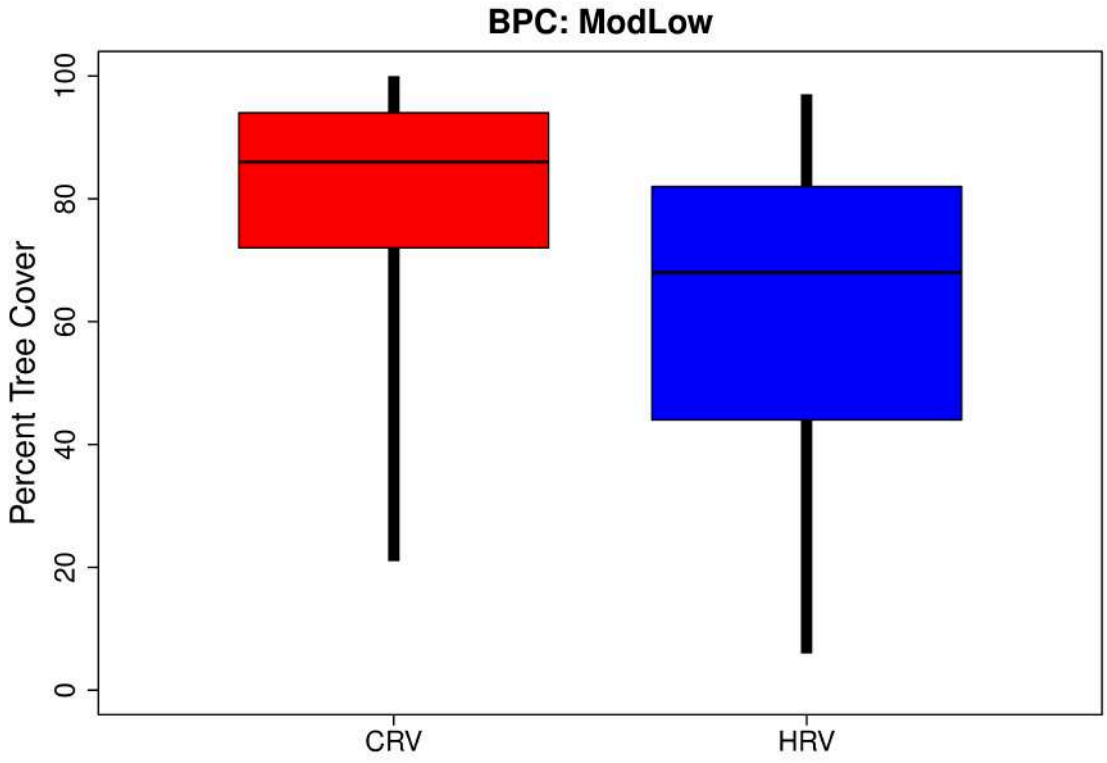

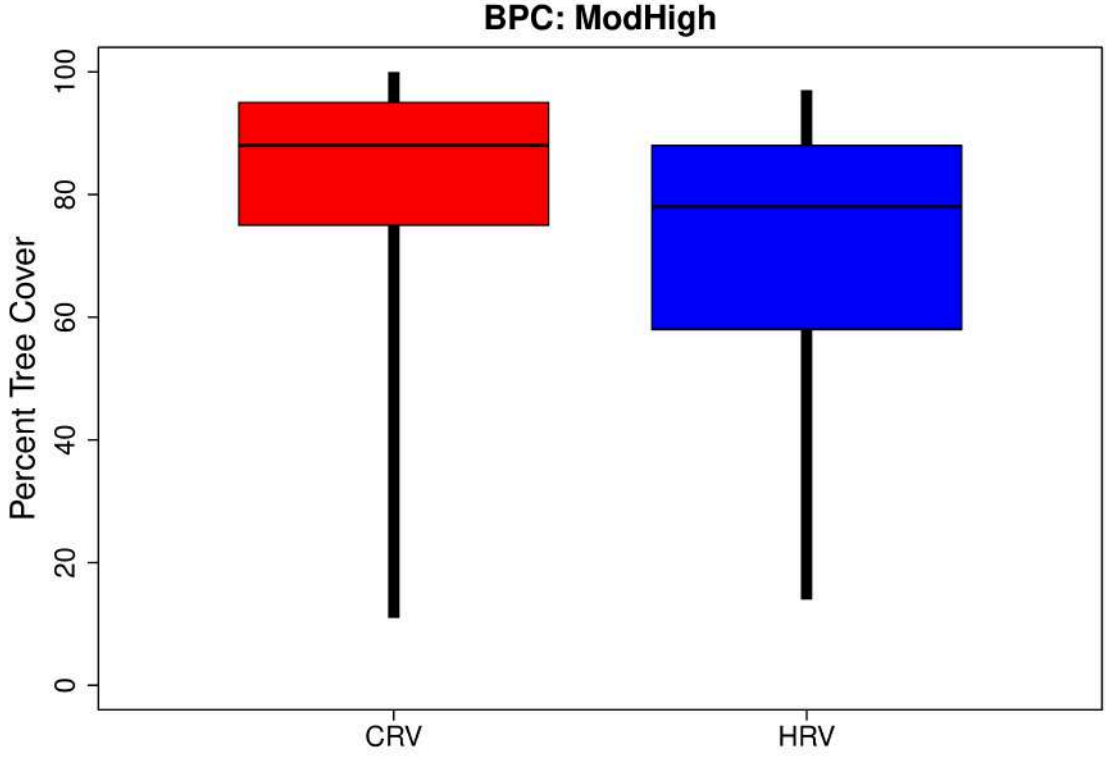

Type text here

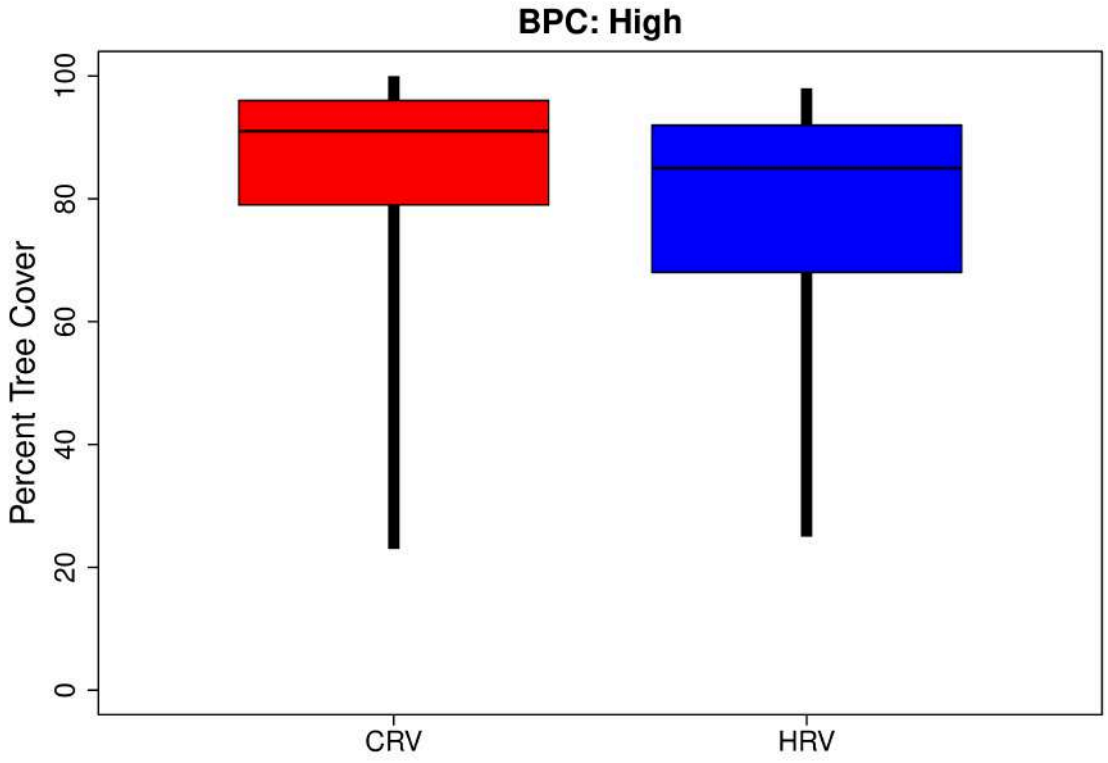

Figure 16: Historical Range of Variability (HRV) and Current range of variabiilty (CRV) among Sites (i.e., 40-m radius window) in the percent Tree Cover of established trees to breast height within the Low, Moderately Low, Moderately High and High site productivity Biophysical Classes (BPCs) in the Truckee River landscape. Box = 25-50 percentiles; whiskers = 2.5-97.5 percentiles

Geophysical Unit Level Departure

The results presented in this section address current departure in landscape metrics quantified at the spatial extent of a single Geophysical Unit (GPU). The Truckee River landscape was divided into 6,815 separate GPUs, which collectively encompass the area mapped as forest in the Existing Cover layer (Ecover) and within existing Lidar at the time of this analysis. Recall from the GTR that we defined GPUs based on similarity in a suite of 10 geophysical attributes and that they were defined only for the forested portion of the landscape and only where we had Lidar coverage. In addition, recall that each GPU was assessed independently; i.e., that we compared the current condition of each GPU to its own HRV in vegetation conditions. Thus, current departure of a GPU was specific to that GPU and independent of that measured for other GPUs. Lastly, recall that we used a large but parsimonious suite of landscape metrics that we deemed meaningful for estimating departure at the GPU level and appropriate given the available data, and computed departure as described in the GTR (and not repeated here), including the following:

Metric 1: Basal Area Departure

Departure in basal area of trees within the GPU was based on a metric derived by the TCSI project and adapted here for our purposes (**Figure 17**). GPUs with an increasingly positive departure have a current basal area that is greater than expected under HRV.

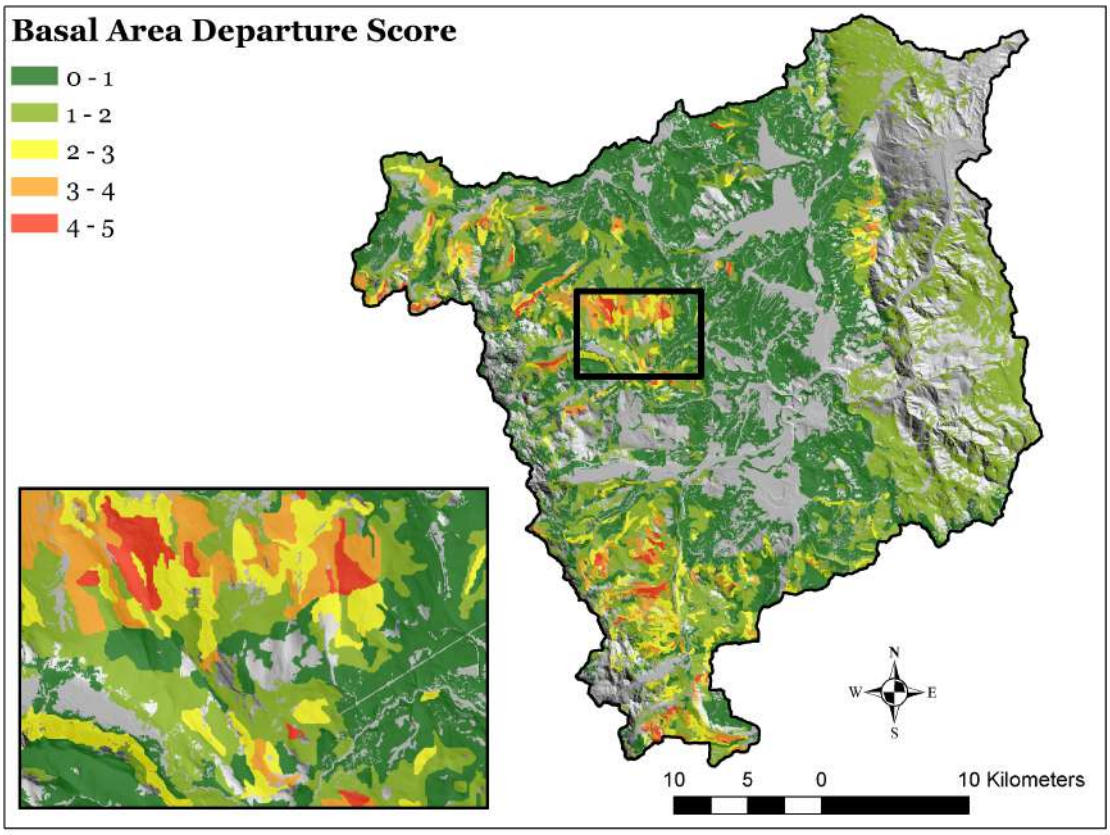

Figure 17: Geophysical Unit (GPU)-level basal area departure score for the Truckee River landscape. The departure score (0-5) represents the deviation of the current GPU condition from its historical range of variability (HRV), as estimated from a suite of contemporary reference sites. Values increase with increasing degrees of departure.

Metric 2: Percent Open Forest

We measured departure in the percent of forested cells within the GPU in the Open developmental stage (**Figure 18**). GPUs with a departure index less than -1 have less area in the Open developmental stage than under HRV.

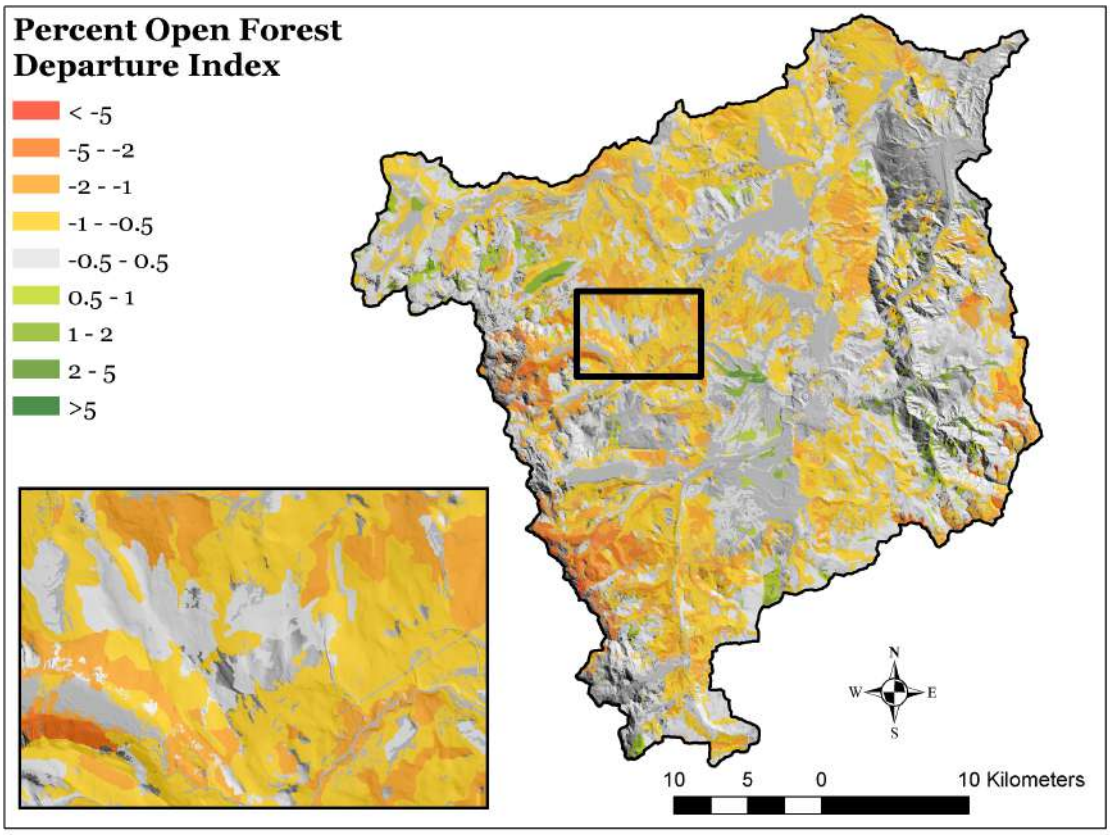

Figure 18: Geophysical Unit (GPU)-level departure index (unbounded) for the percentage of the forest within the GPU in the Open developmental stage for the Truckee River landscape. The departure Index represents the deviation of the current GPU condition from its historical range of variability (HRV), as simulated. Values < -1 represent a current condition that is less than the HRV for the GPU, and increasingly negative values represent increasing degrees of negative departure.

Metric 3: Developmental Stage Diversity

We measured departure in the diversity of forest developmental stages within the GPU based on the Simpson's Diversity index (**Figure 19**). Here, Simpson's Diversity is defined as the probability that any two cells selected at random would be different developmental stages. The departure index for Simpson's Diversity is less than -1 if the current GPU has a diversity of developmental stages that is less than HRV.

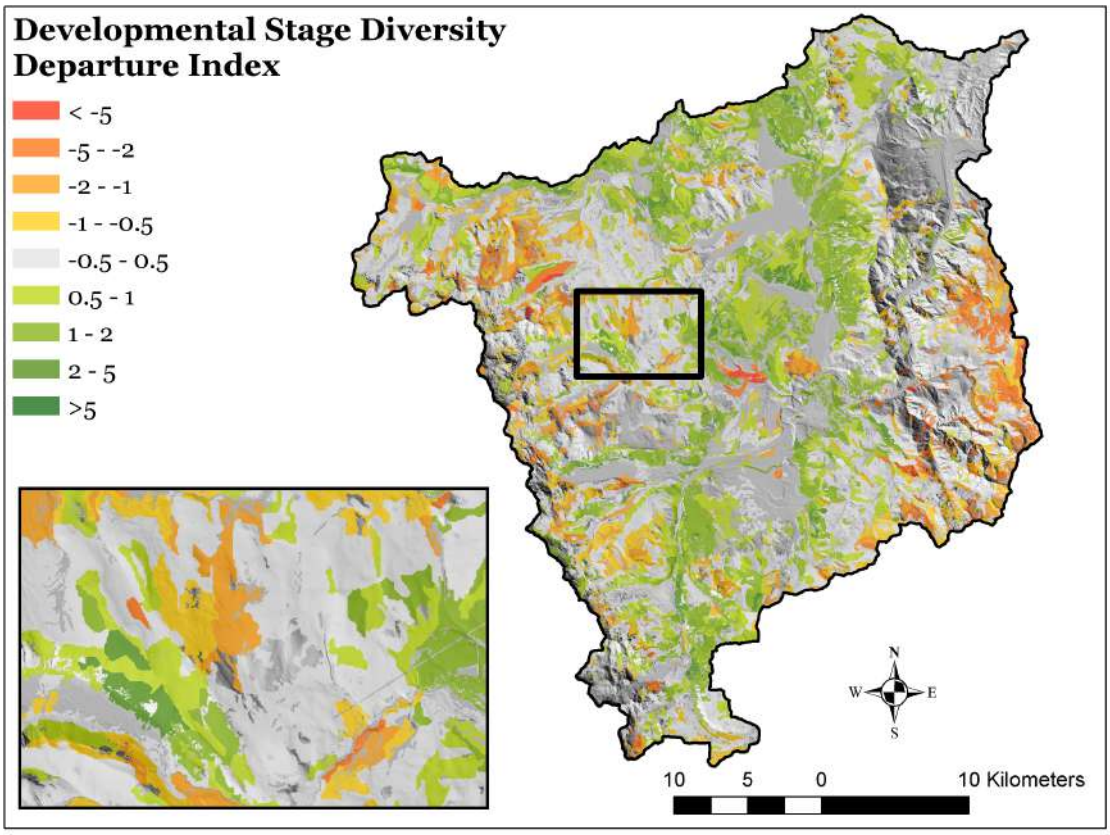

Figure 19: Geophysical Unit (GPU)-level departure index (unbounded) for the Simpson Diversity of developmental stages within the GPU for the Truckee River landscape. The departure Index represents the deviation of the current GPU condition from its historical range of variability (HRV), as simulated. Values < -1 represent a current condition that is less than the HRV for the GPU, and increasingly negative values represent increasing degrees of negative departure.

Metric 4: Coefficient of Variation in Open Patch Size

We measured departure in the Coefficient of Variation (CV) in the size of all Open forest patches, including single cell patches, in which forest openings are defined by contiguous cells in the Open developmental stage based on the 4-neighbor rule (i.e., orthogonal neighbors)(**Figure 20**). The departure index is less than -1 if the current GPU has relatively invariant Open patch sizes compared to HRV.

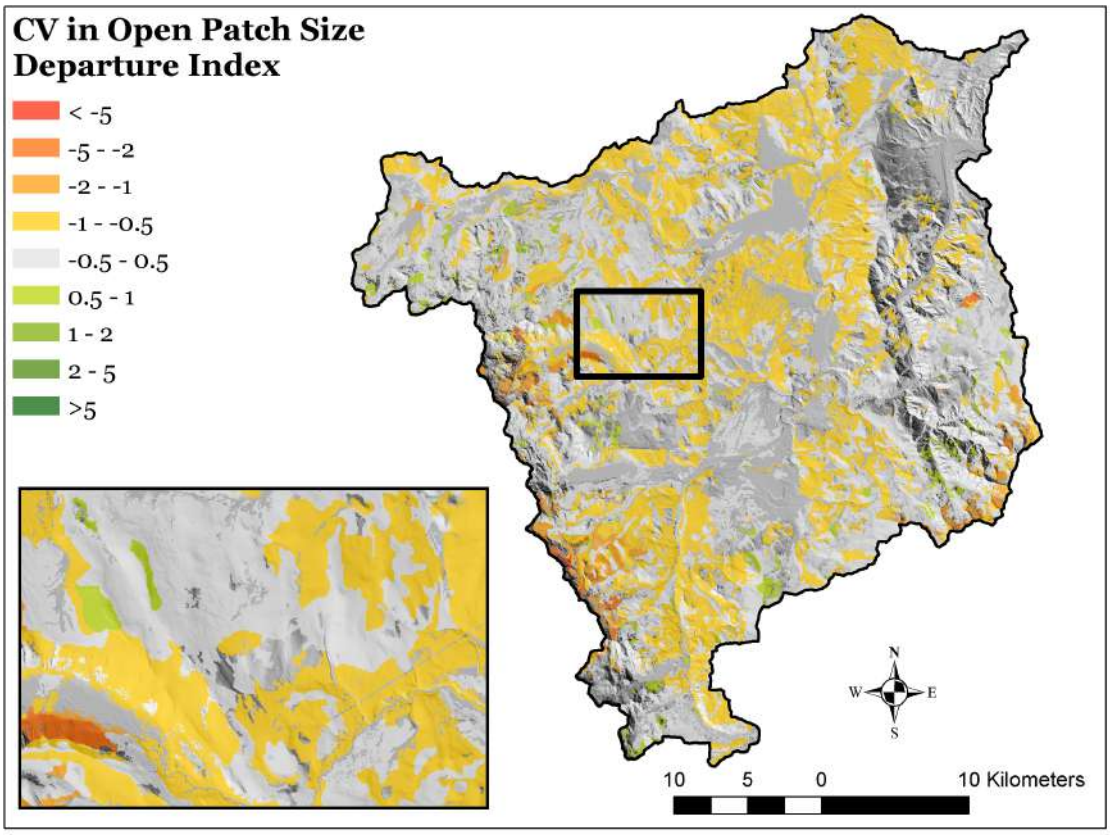

Figure 20: Geophysical Unit (GPU)-level departure index (unbounded) for the Coefficient of Variation (CV) in the size of patches in the Open developmental stage within the GPU for the Truckee River landscape. The departure Index represents the deviation of the current GPU condition from its historical range of variability (HRV), as simulated. Values < -1 represent a current condition that is less than the HRV for the GPU, and increasingly negative values represent increasing degrees of negative departure.

Metric 5: Coefficient of Variation in Developmental Stage Patch Size

We measured departure in the CV in the size of all forest developmental stage patches, including single cell patches, in which patches are defined by contiguous cells in the same developmental stage based on the 4-neighbor rule (**Figure 21**). The departure index is less than -1 if the current GPU has relatively invariant developmental stage patch sizes compared to HRV.

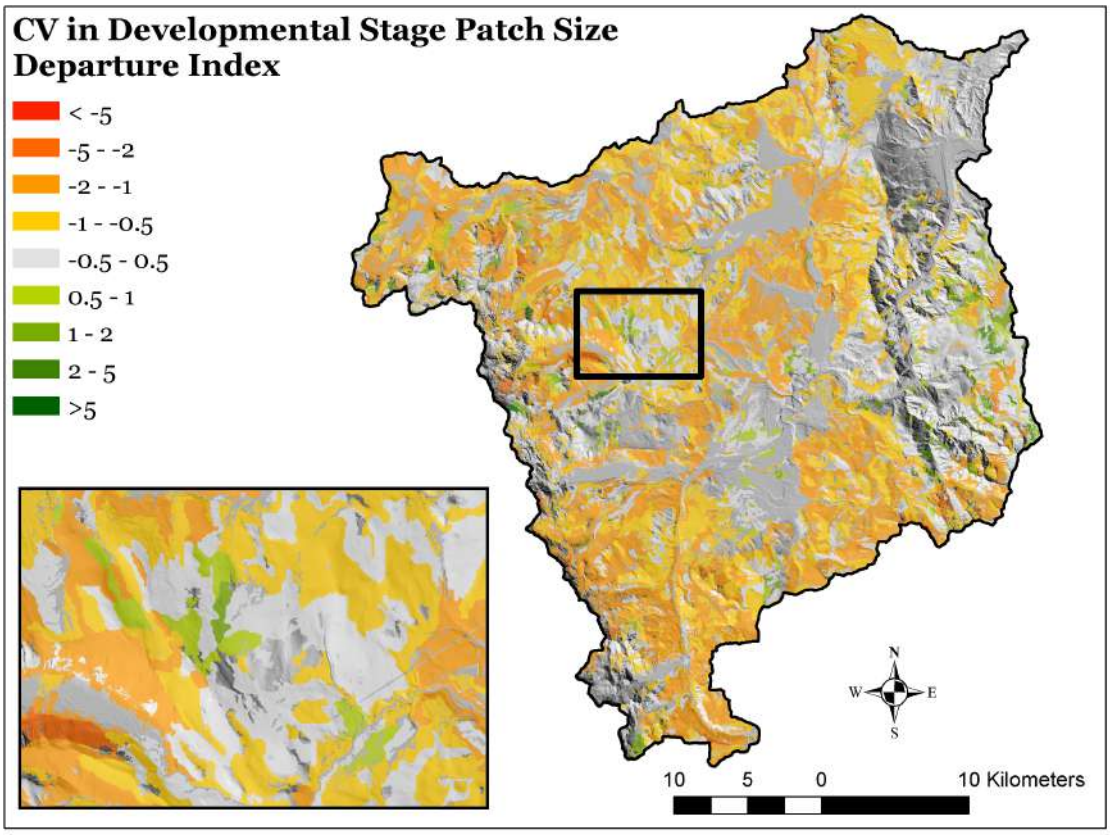

Figure 21: Geophysical Unit (GPU)-level departure index (unbounded) for the Coefficient of Variation (CV) in the size of patches based on developmental stages within the GPU for the Truckee River landscape. The departure Index represents the deviation of the current GPU condition from its historical range of variability (HRV), as simulated. Values < -1 represent a current condition that is less than the HRV for the GPU, and increasingly negative values represent increasing degrees of negative departure.

Metric 6: Percent Large Trees

We measured departure in the percent of forested cells within the GPU in the Large tree size class ($\geq$ 30 in dbh)(**Figure 22**). GPUs with a departure index less than -1 have less area in the Large tree class than under HRV.

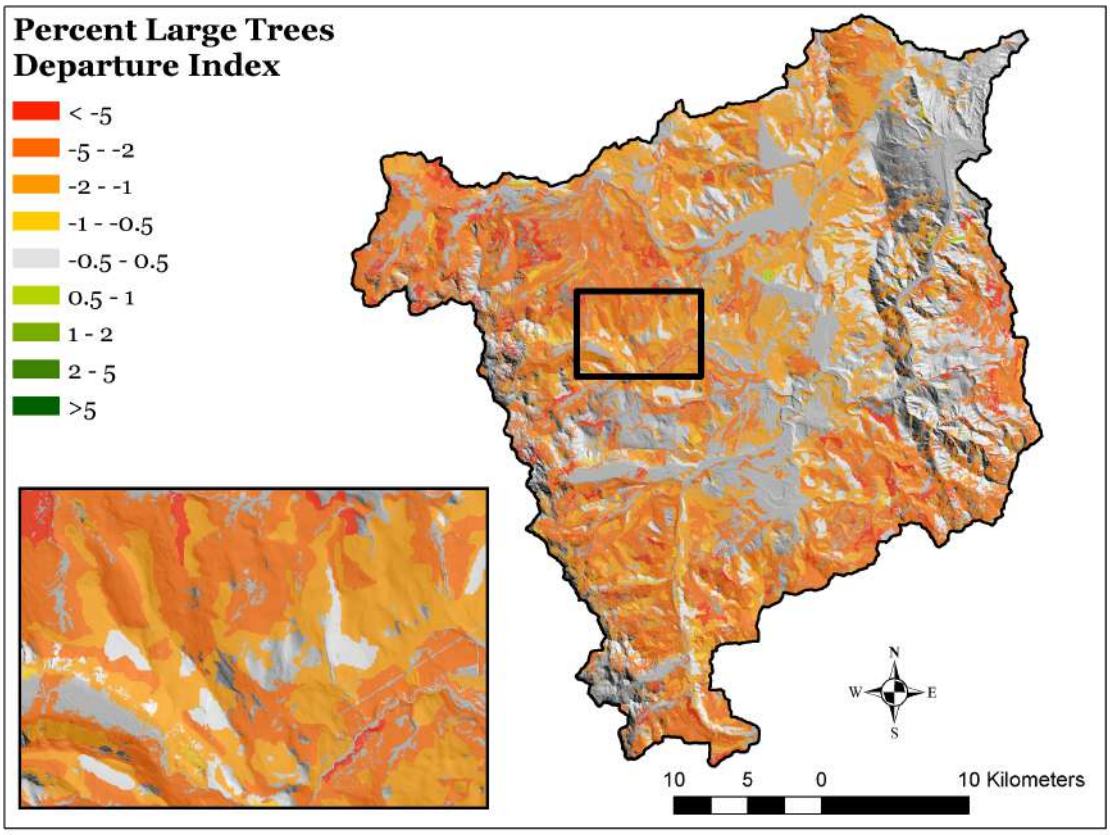

Figure 22: Geophysical Unit (GPU)-level departure index (unbounded) for the percentage of the forest in the Large tree size class (*geq* 30 in dbh) within the GPU for the Truckee River landscape. The departure Index represents the deviation of the current GPU condition from its historical range of variability (HRV), as simulated. Values < -1 represent a current condition that is less than the HRV for the GPU, and increasingly negative values represent increasing degrees of negative departure.

Metric 7: Tree Size Class Diversity

We measured departure in the diversity of tree size classes within the forested portion of the GPU based on the Simpson's Diversity index (**Figure 23**). Here, Simpson's Diversity is defined as the probability that any two cells selected at random would be from different tree size classes. The departure index for Simpson's Diversity is less than -1 if the current GPU has a diversity of tree size classes that is less than HRV.

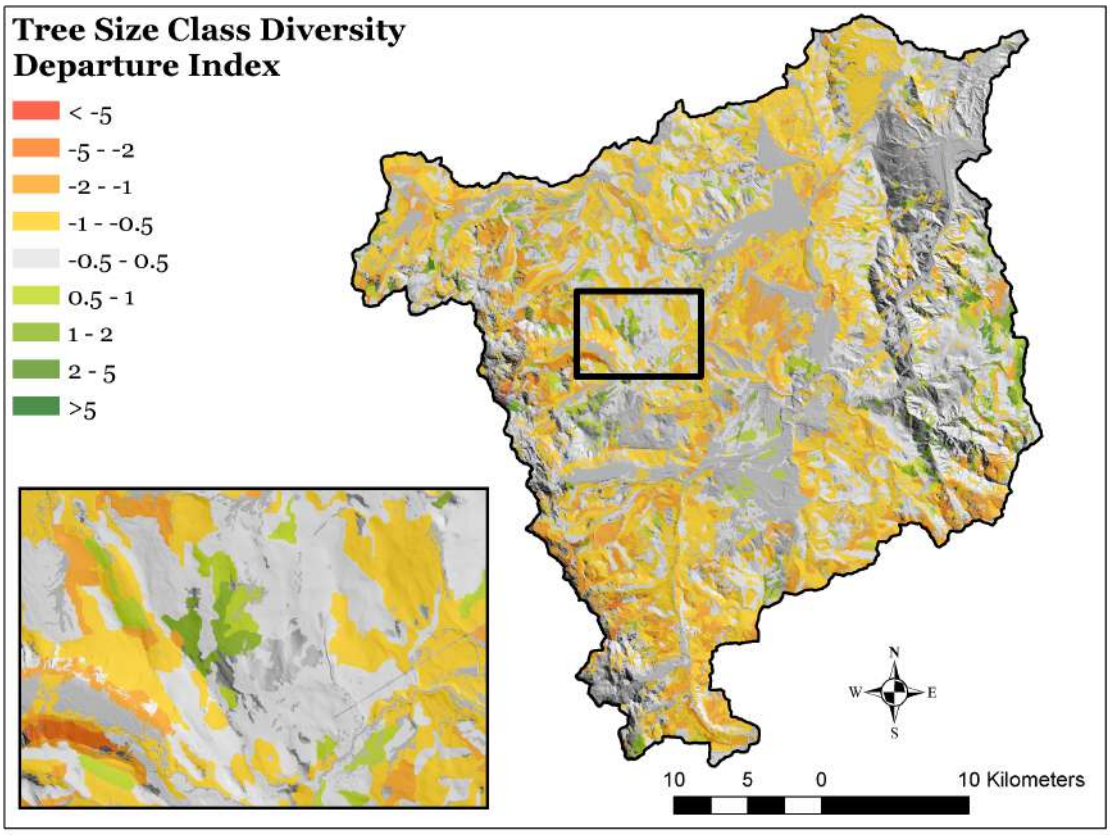

Figure 23: Geophysical Unit (GPU)-level departure index (unbounded) for the Simpson Diversity of tree size clases within the GPU for the Truckee River landscape. The departure Index represents the deviation of the current GPU condition from its historical range of variability (HRV), as simulated. Values < -1 represent a current condition that is less than the HRV for the GPU, and increasingly negative values represent increasing degrees of negative departure.

Metric 8: Coefficient of Variation in Large Tree Patch Size

We measured departure in the CV in the size of all Large tree patches, including single cell patches, in which Large tree patches were defined by contiguous cells in the Large tree class ($\geq$ 30 in dbh) based on the 4-neighbor rule (**Figure 24**). The departure index is less than -1 if the current GPU has relatively invariant Large tree patch sizes compared to HRV.

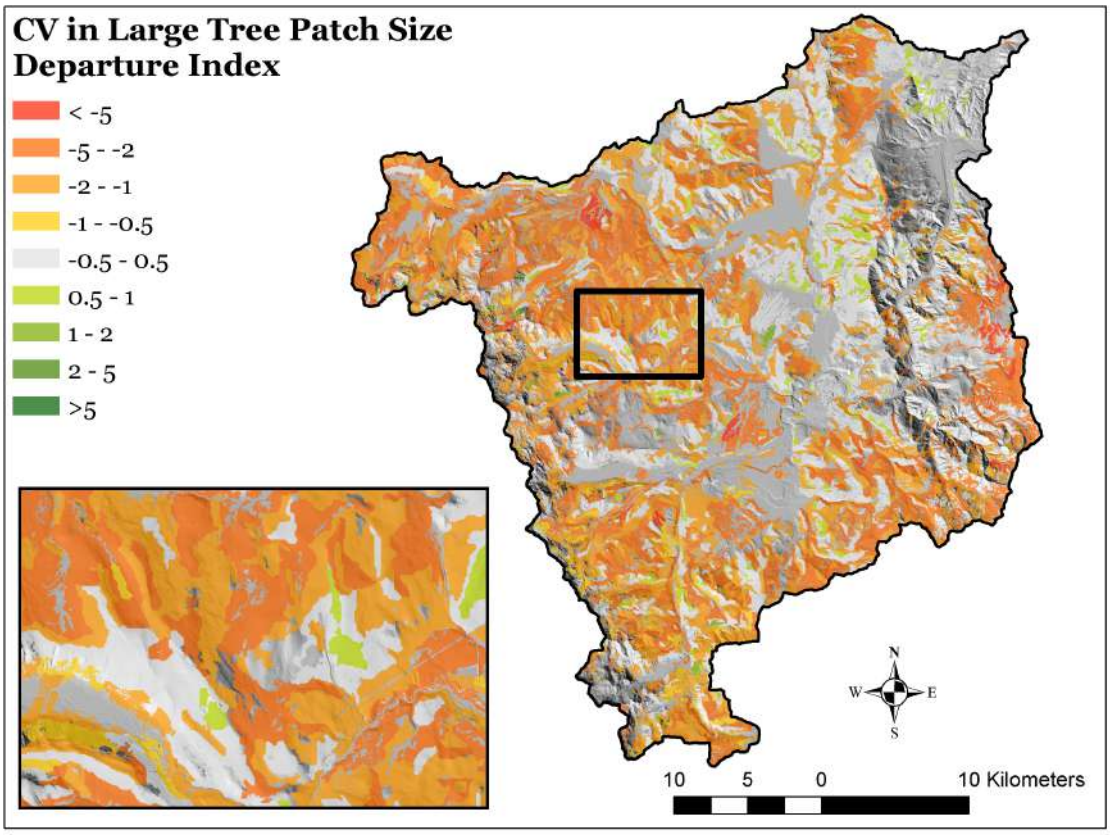

Figure 24: Geophysical Unit (GPU)-level departure index (unbounded) for the Coefficient of Variation (CV) in the size of patches in the Large tree size class (*geq* 30 in dbh) within the GPU for the Truckee River landscape. The departure Index represents the deviation of the current GPU condition from its historical range of variability (HRV), as simulated. Values < -1 represent a current condition that is less than the HRV for the GPU, and increasingly negative values represent increasing degrees of negative departure.

Metric 9: Coefficient of Variation in Tree Size Class Patch Size

We measured departure in the CV in the size of all tree size class patches, including single cell patches, in which patches were defined by contiguous cells in the same tree size class based on the 4-neighbor rule (**Figure 25**). The departure index is less than -1 if the current GPU has relatively invariant tree size class patch sizes compared to HRV.

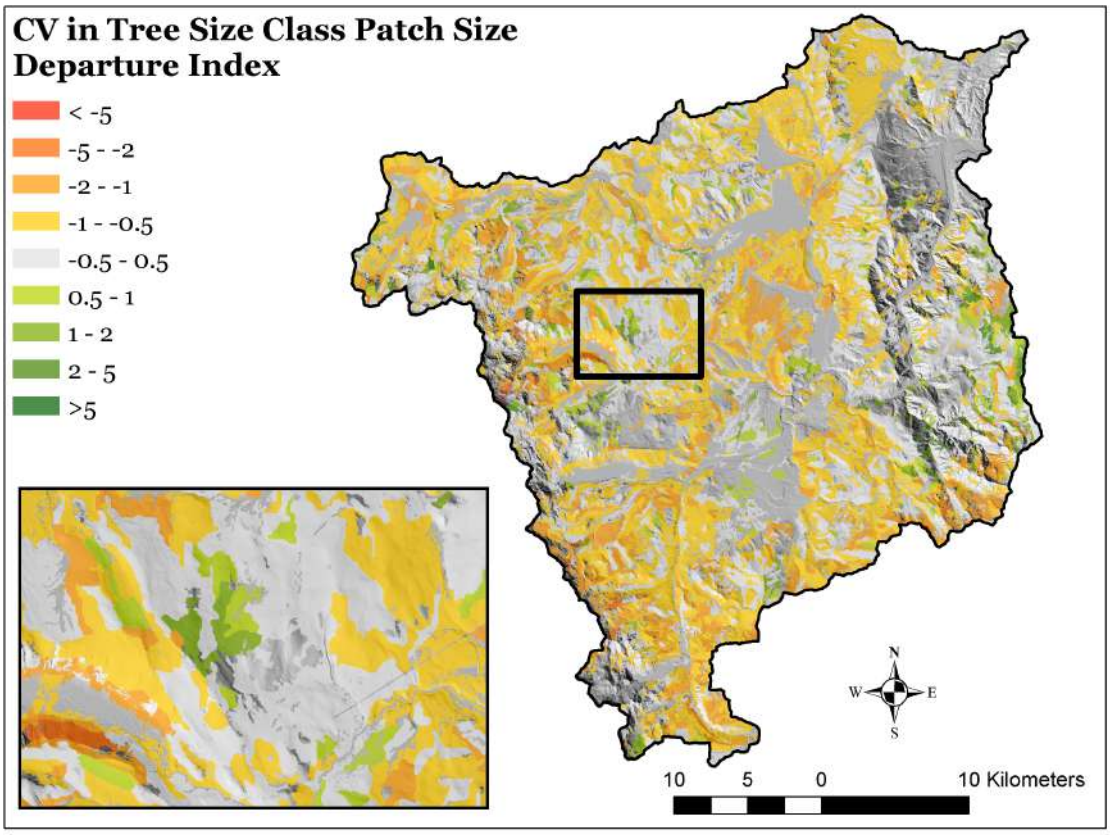

Figure 25: Geophysical Unit (GPU)-level departure index (unbounded) for the Coefficient of Variation (CV) in the size of patches based on tree size classes within the GPU for the Truckee River landscape. The departure Index represents the deviation of the current GPU condition from its historical range of variability (HRV), as simulated. Values < -1 represent a current condition that is less than the HRV for the GPU, and increasingly negative values represent increasing degrees of negative departure.

Metric 10: Coefficient of Variation in Quadratic Mean Diameter

We measured departure in the CV in site-level Quadratic Mean Diameter (QMD) of established trees within the GPU (**Figure 26**). Recall that a site was defined as a 40-m radius window around each focal cell. Thus, QMD was computed for the site associated with each focal cell, which produced a continuous surface of QMD values, from which the CV in QMD values within the GPU was computed. The departure index is less than -1 if the current GPU has relatively homogeneous QMD compared to HRV.

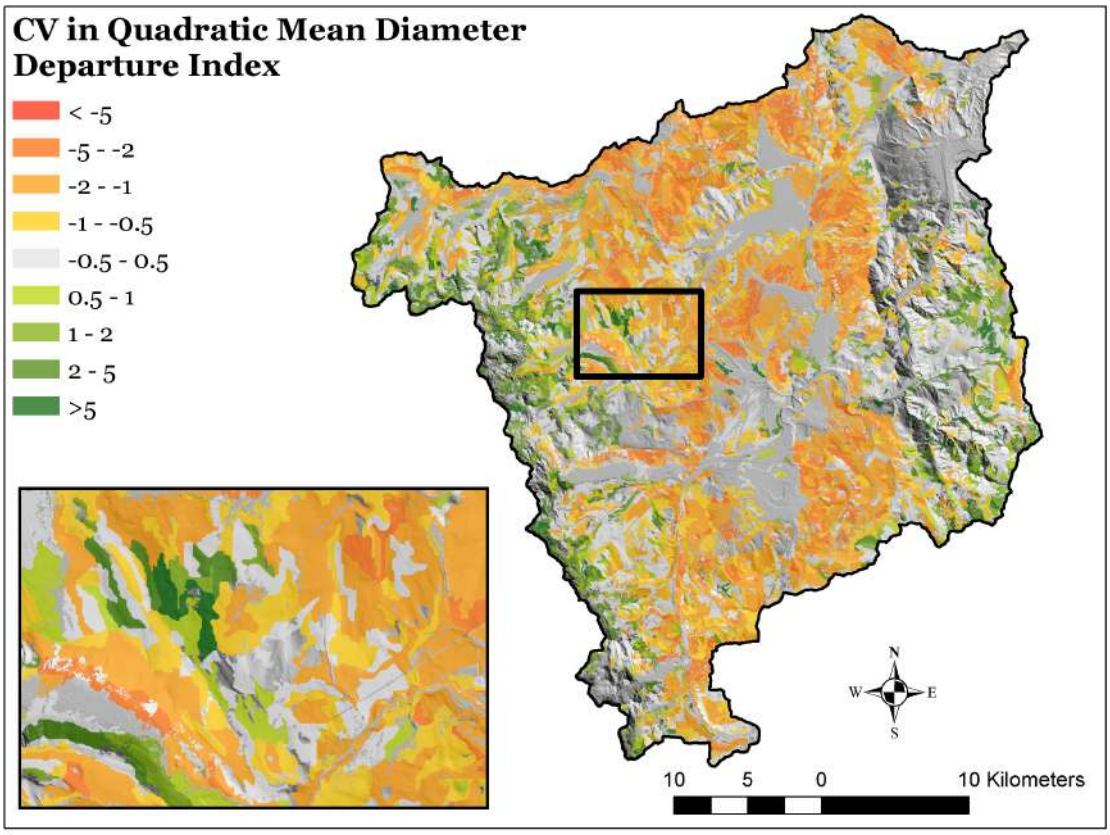

Figure 26: Geophysical Unit (GPU)-level departure index (unbounded) for the Coefficient of Variation (CV) in Site-level (i.e., 40 m radius window around each focal cell) Quadratic Mean Diameter (QMD, in inches) within the GPU for the Truckee River landscape. The departure Index represents the deviation of the current GPU condition from its historical range of variability (HRV), as simulated. Values < -1 represent a current condition that is less than the HRV for the GPU, and increasingly negative values represent increasing degrees of negative departure.

Metric 11: Coefficient of Variation in Percent Tree Cover

We measured departure in the CV in site-level percent cover of established trees within the GPU (**Figure 27**). Again, recall that a site was defined as a 40-m radius window around each focal cell. Thus, percent tree Cover was computed for the site associated with each focal cell, which produced a continuous surface of percent tree cover values, from which the CV in tree cover within the GPU was computed. The departure index is less than -1 if the current GPU has relatively homogeneous tree cover compared to HRV.

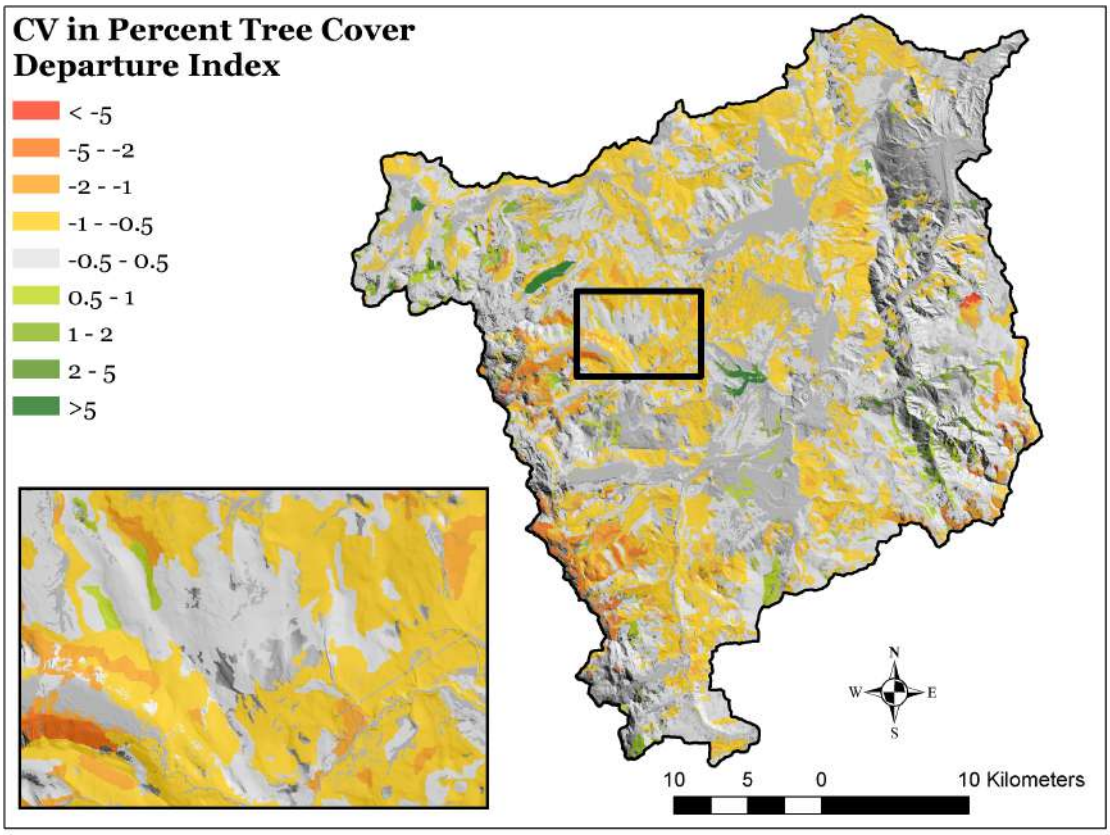

Figure 27: Geophysical Unit (GPU)-level departure index (unbounded) for the Coefficient of Variation (CV) in Site-level (i.e., 40 m radius window around each focal cell) percent tree cover within the GPU for the Truckee River landscape. Note, percent tree cover as measured is on average 16 % greater than percent canopy cover. The departure Index represents the deviation of the current GPU condition from its historical range of variability (HRV), as simulated. Values < -1 represent a current condition that is less than the HRV for the GPU, and increasingly negative values represent increasing degrees of negative departure.

Composite Departure Index

We combined the 11 GPU-level departure indices above into two composite departure scores: 1) composite "negative" departure, and 2) composite "absolute" departure (see GTR for details). Both of these composite scores can be interpreted as a measure of overall GPU departure in vegetation composition and configuration. Increasing departure scores (given as a percent of maximum) indicate increasing degrees of departure.

Negative Departure - Maximum "negative" departure occurs when a GPU has too little Open forest area, too few Large trees, too little diversity in forest developmental stages (i.e., tree heights) and tree size classes (i.e., dbh), too little variability in the size of patches based on forest developmental stage and tree size, and too little spatial variability in percent tree cover and weighted average tree size (i.e., QMD) relative to its HRV. In other words, maximum negative departure occurs when the forest is too closed-canopy, depauperate in Large trees, and too homogeneous in vegetation composition and configuration.

The composite negative departure score is depicted in **Figure 28**. This score can be interpreted as the percent of maximum deviation in negative departure. Thus, a value of 0 represents no departure in any of the component metrics and a value of 100 represents maximum negative departure in each of the component metrics. GPUs with relatively high scores are the logical ones to prioritize for restoration

treatment - should that be the goal. Importantly, this composite departure score can serve as a first stage in identifying and prioritizing GPUs for treatment, but specific objectives and treatments for each GPU requires decomposing the composite score into the component metrics to determine which aspects of the forest vegetation composition and/or configuration are most departed.

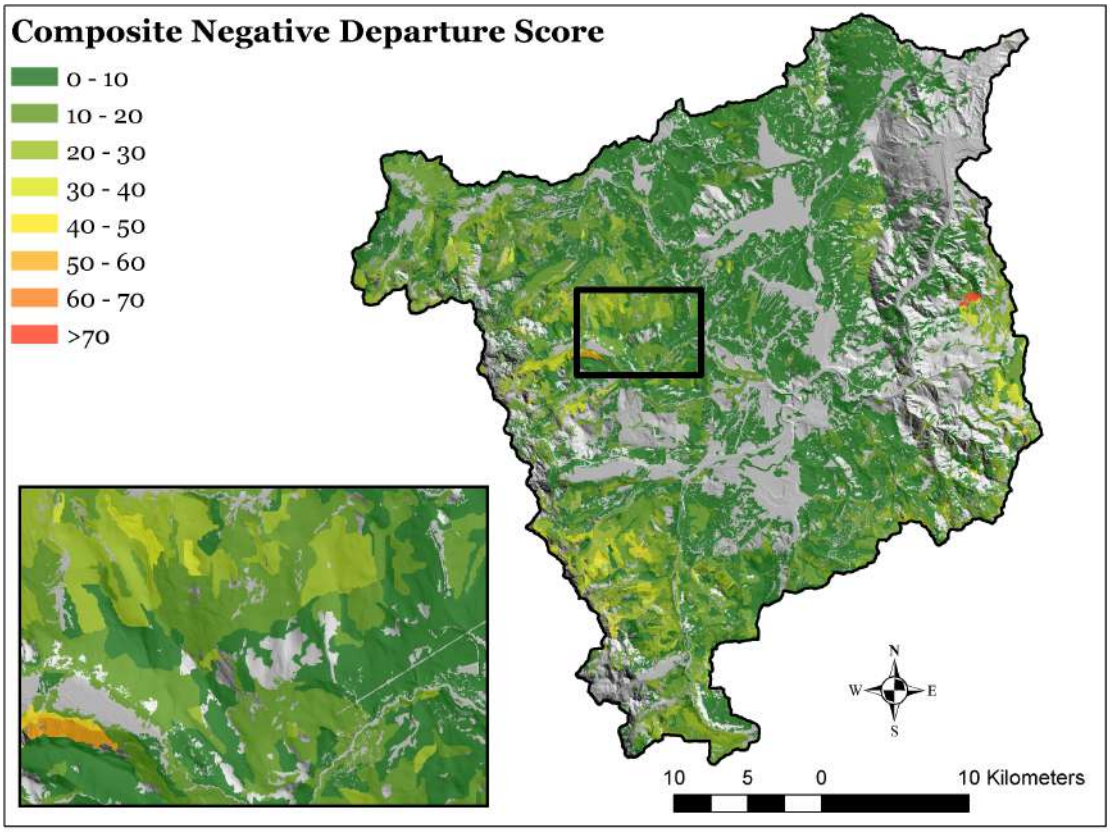

Figure 28: Geophysical Unit (GPU)-level composite negative departure score composed of a weighted combination of 11 individual departure metrics within the GPU for the Truckee River landscape. The score represents the percentage of maximum departure of the current GPU condition from its historical range of variability (HRV), as simulated. Larger values indicate increasing degrees of departure.

Absolute Departure - Maximum "absolute" departure occurs when a GPU has either too little or too much Open forest area, too few or too many Large trees, too little or too much diversity in forest developmental stages (i.e., tree heights) and tree size classes (i.e., dbh), too little or too much variability in the size of patches based on forest developmental stage and tree size, and too little or too much spatial variability in percent tree cover and weighted average tree size (i.e., QMD) relative to HRV. In other words, maximum departure occurs when the GPU differs in any way in both composition and configuration from its HRV, as measured by this suite of metrics.

Subbasin Level Departure

The results presented in this section represent landscape metrics quantified at the Subbasin-by-BPC level; i.e., each Subbasin subdivided into BPCs treated as a whole unit (a.k.a. "zones"). The Truckee River landscape was divided into 20 distinct Subbasins (**Figure 29**), each of which was partitioned into the BPCs for a total of 80 Subbasin-by-BPC partitions or zones. Recall from the GTR that each partition was assessed independently to create a departure index; i.e., that we compared the current condition of each partition to its own HRV in vegetation conditions. In addition, recall that the final departure score

reflected negative departure in the percent of the partition in large openings and large trees (i.e., in which the current landscape contains less area in large openings and large trees than expected under HRV), but was bidirectional with respect to the landscape configuration metrics; i.e., it reflected the magnitude of the absolute differences between the current and historical landscape conditions, regardless of whether the current condition was greater or less than the historical condition. In other words, any differences between current and historical vegetation conditions with respect to landscape configuration registered as departure. Lastly, recall that we used a parsimonious suite of landscape metrics (see below) that we deemed meaningful for estimating departure at the Subbasin level and appropriate given the available data, and computed departure as described in the GTR (and not repeated here), including the following metrics:

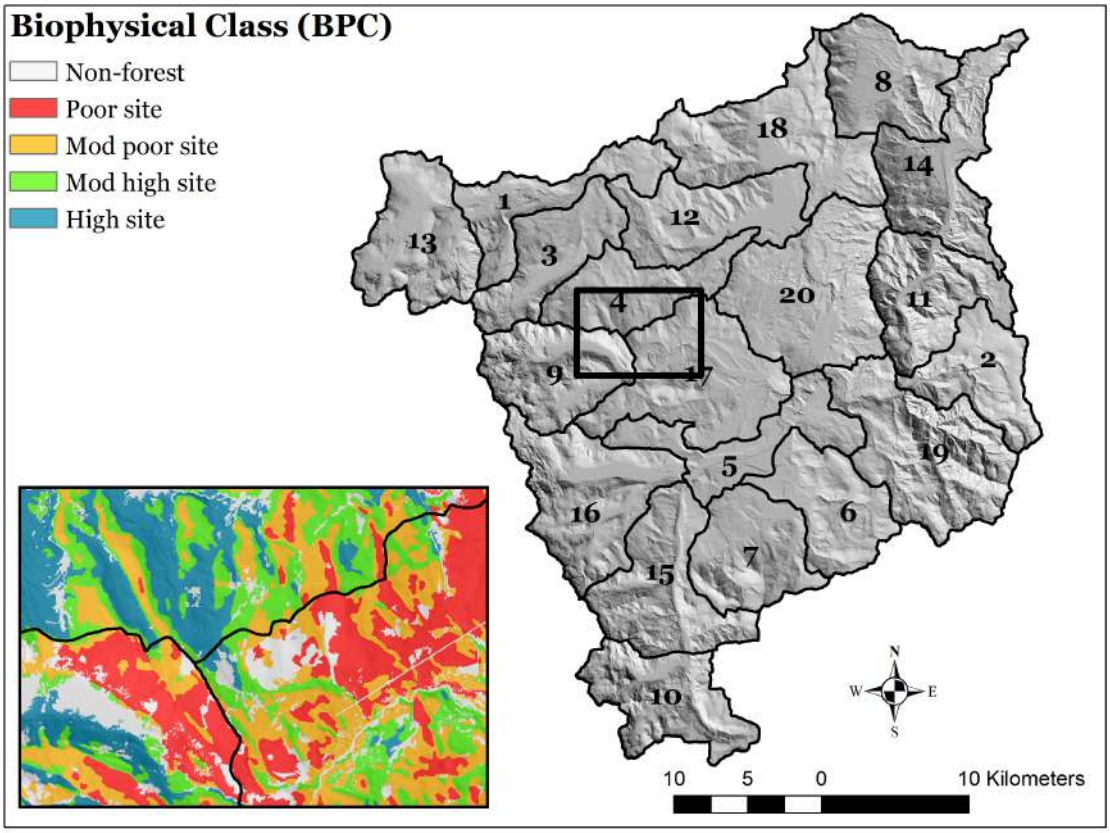

Figure 29: The Truckee River landscape HUC12 Subbasins, as modified, defined for the purpose of summarizing Historical Range of Variability (HRV) and current departure.

Metric 1: Percent Large Forest Openings

We defined large forest openings as contiguous forested cells in the Open developmental stage (i.e., no established trees to breast height) encompassing a minimum of 0.04 ha (0.1 acres). Contiguity was based on the 4-neighbor rule (i.e., orthogonal neighbors) that ensured a minimum width of 5 m for any opening. We defined Percent Large Forest Openings as the percent of the forest within the Subbasin-by-BPC partition in large forest openings (as defined), and the departure index reflected whether or not the current landscape was deficient in large forest openings relative to HRV and, if so, the degree of deficiency.

The Percent Large Forest Openings departure index is depicted in **Figure 30**. Note, the departure index was assigned to each Subbasin-by-BPC partition; consequently, there were 80 distinct values assigned. Thus, to better assess departure by Subbasin and BPC, one needs to examine the attribute table for the departure layer.

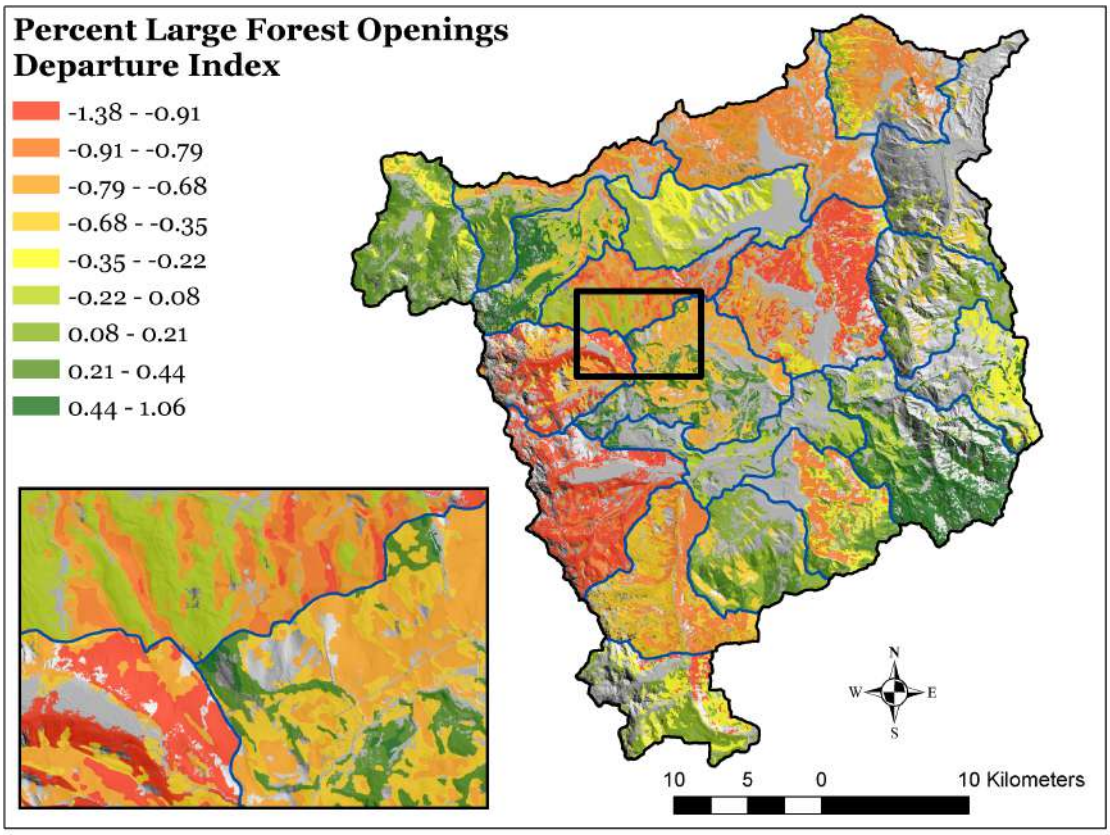

Figure 30: Subbasin-by-BPC level departure index for large forest openings (> 0.04 ha or 0.1 acres and > 5 m mininum width) for the Truckee River landscape. The departure index represents the deviation of the current Subbasin and biophysical class (BPC) condition from its historical reference period condition, as simulated. Departure indices < -1 represent a current landscape with less total area in large forest openings than during the historical reference period, as simulated, and increasing negative values represent increasing degrees of departure.

As discussed in the GTR, the Percent Large Forest Openings Departure Index can be miss-interpreted if not understood well. As the previous figure depicts, the distribution of index values would suggest that most of the subbasin-by-BPC partitions are within the HRV given that most of the partitions have values between -1 - 1. Recall, index values within this range reflect a current landscape condition that is within the 2.5% and 97.5% HRV. This would seem to indicate that most of the partitions are within HRV. While this might technically be correct, the reality is that most of the partitions are close to the lower limit of HRV and have index values close to -1. Consequently, the distribution of index values is heavily skewed towards values on the lower limit of HRV, suggesting that the landscape as a whole is, on average, deficient in large forest openings. A alternative and more useful way to assess current departure in this metric is to compare the distribution of values representing the percentage of the partition in large forest openings between the HRV and CRV, as shown **Figure 31**.

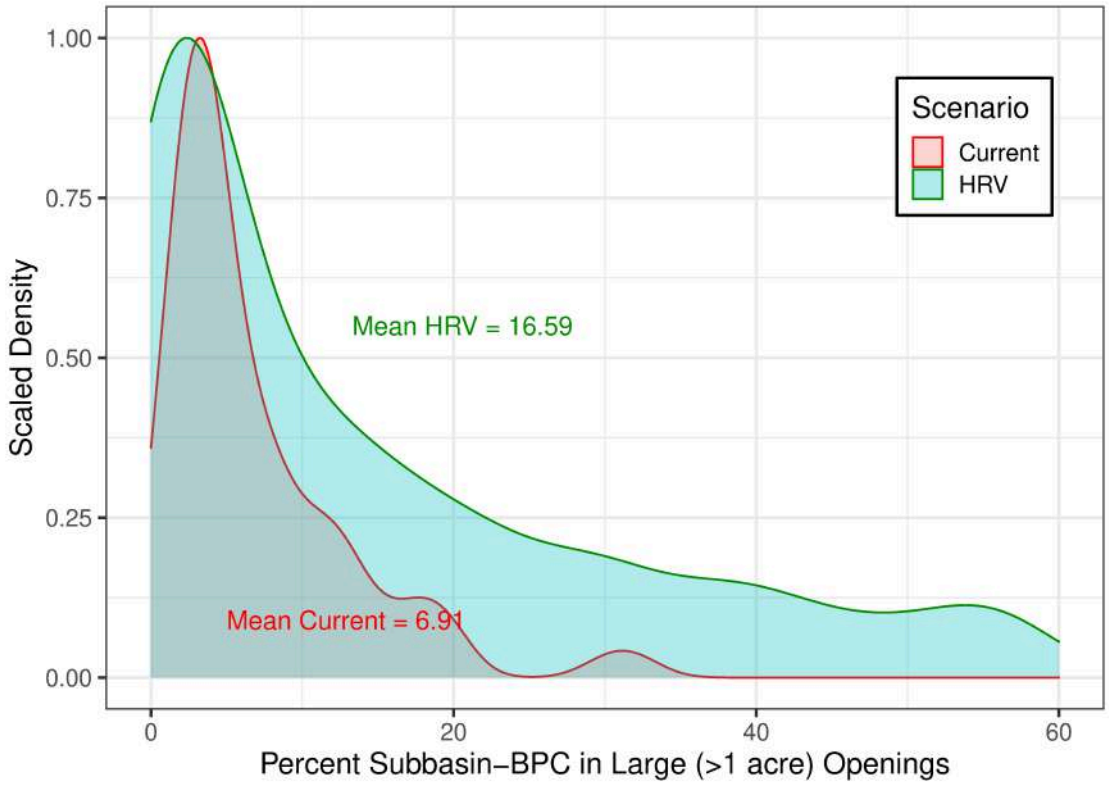

Figure 31: Current and historical distribution of Percent Large Forest Openings across the Subbasin-by-Biophysical Class (BPC) landscape partitions for the Truckee River landscape. The comparative distributions reveal that even though the departure index for most of the partitions technically may fall with the historical range of variation (see previous figure), the overall distributions in the raw metric values differ markedly and reflect departure for the landscape as a whole

Metric 2: Large Forest Openings Patch Size Distribution

We defined large forest openings as described above. Here, we quantified the size of individual openings and determined the percent of forest within the Subbasin-by-BPC partition in large openings in each of several patch size classes or bins (see GTR). The departure index reflects whether or not the current landscape has a distribution of large forest opening patch sizes that differed from HRV and, if so, the degree of differences in the two distributions.

The Large Forest Openings Patch Size Distribution departure index is depicted in **Figure 32**. As before, the departure index was assigned to each Subbasin-by-BPC partition; consequently, there were 80 distinct values assigned. Thus, to better assess departure by Subbasin and BPC, one needs to examine the attribute table for the departure layer.

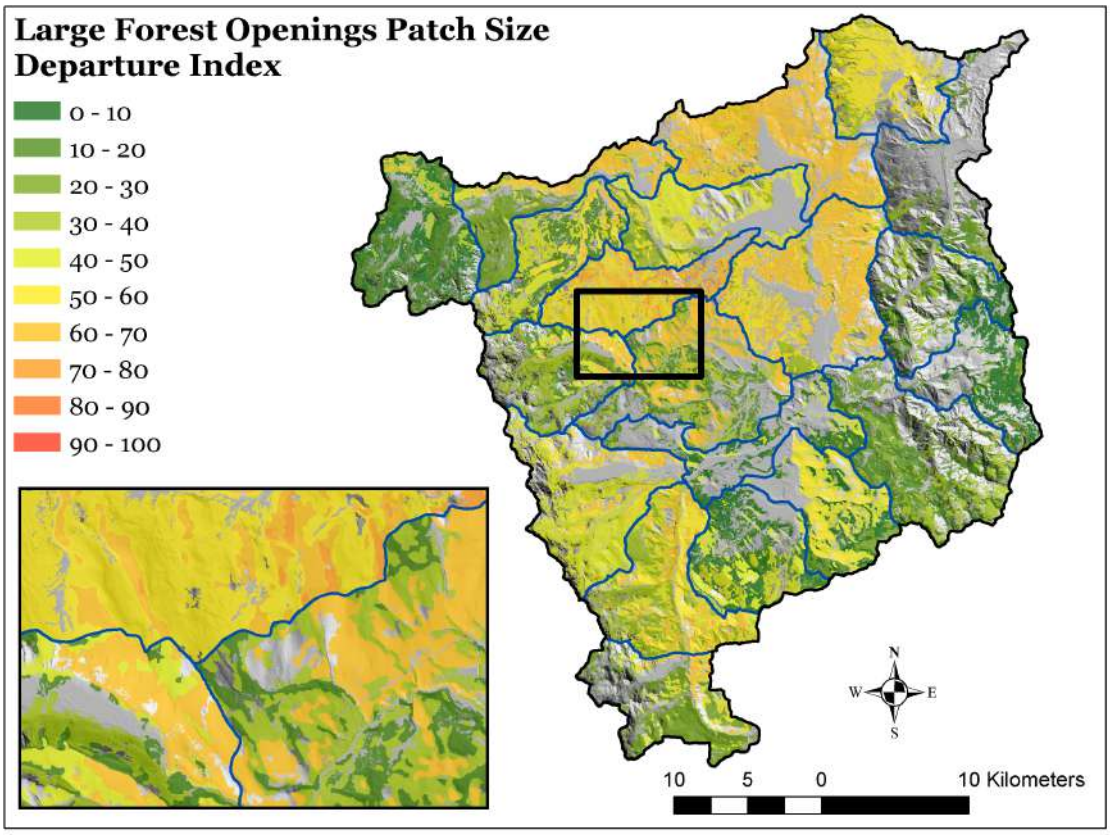

Figure 32: Subbasin-by-BPC level departure index for large forest openings (> 0.04 ha or 0.1 acres and > 5 m mininum width) patch size distribution for the Truckee River landscape. The departure index represents the deviation of the current Subbasin and biophysical class (BPC) condition from its historical reference period condition, as simulated. Departure indices > 0 represent a current landscape with a distribution of developmental stage patch sizes that differs in some way from the historical reference period distribution, as simulated, and increasing values represent increasing degrees of departure.

To further evaluate departure in this patch size distribution metric, it is necessary to examine the CRV and HRV patch size distributions for the selected Subbasin-by-BPC partition, for example as depicted in **Figure 33**.

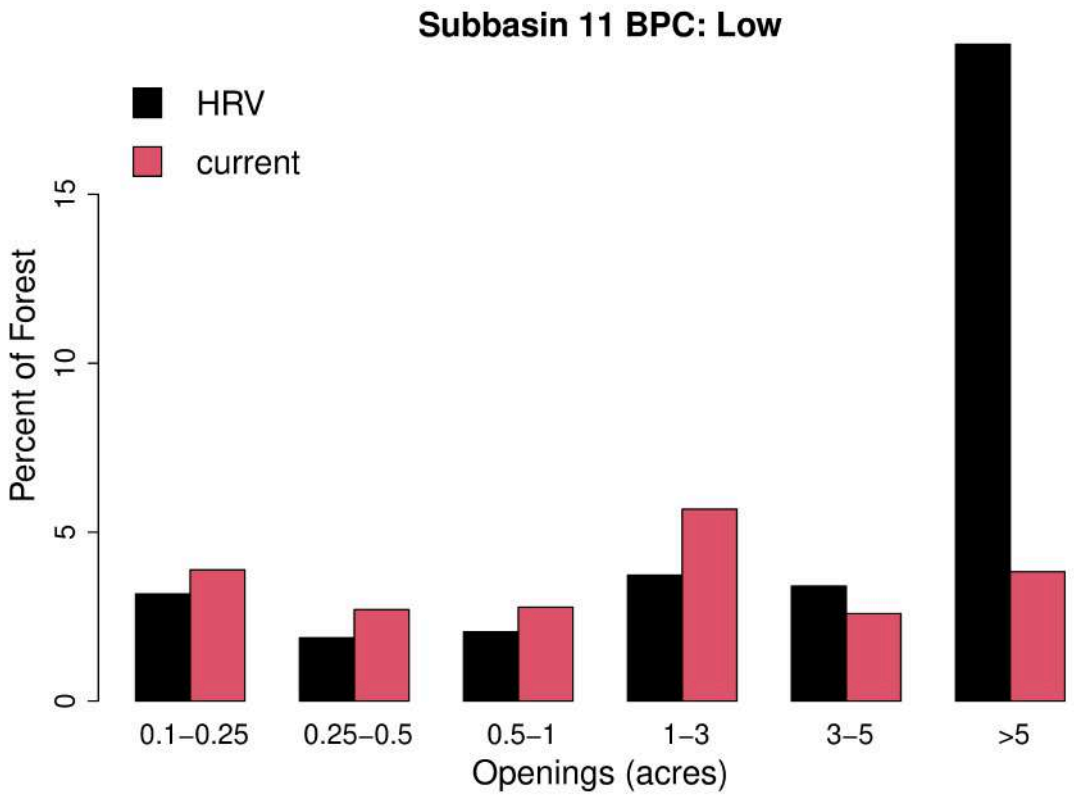

Figure 33: Barplot of the distribution of large forest openings (> 0.04 ha or 0.1 acres and > 5 m mininum width) patch sizes for the current landscape and the historical reference period (HRV) for Subbasin 11 and the Low productivity Biophysical Class (BPC = 1) for the Truckee River landscape. Each bar represents the percent of forest within the Subbasin and Biophysical Class (BPC) in large forest openings of a particular patch size. The departure index represents the percentage dissimilarity between the CRV and HRV distributions. Departure indices > 0 represent a current landscape with a distribution of large forest opening patch sizes that differs in some way from the historical reference period distribution, as simulated, and increasing values represent increasing degrees of departure.

Metric 3: Developmental Stage Patch Size Distribution

We defined developmental stages based on six tree height classes, ranging from Open (< 4.5 ft) to Tall Trees (> 125 ft), as described in the GTR. Here, for each snapshot of the landscape we constructed a patch mosaic comprised of developmental stages in which patches were defined using the 4-neighbor rule. For each snapshot, we quantified the size of each developmental stage patch and determined the percent of forest within the Subbasin-by-BPC partition in each of several patch size classes or bins. The departure index reflects whether or not the current landscape has a distribution of developmental stage patch sizes that differs from HRV and, if so, the degree of differences in the two distributions.

The Developmental Stage Patch Size Distribution departure index is depicted in **Figure 34**. As before, the departure index was assigned to each Subbasin-by-BPC partition; consequently, there were 80 distinct values assigned. Thus, to better assess departure by Subbasin and BPC, one needs to examine the attribute table for the departure layer.

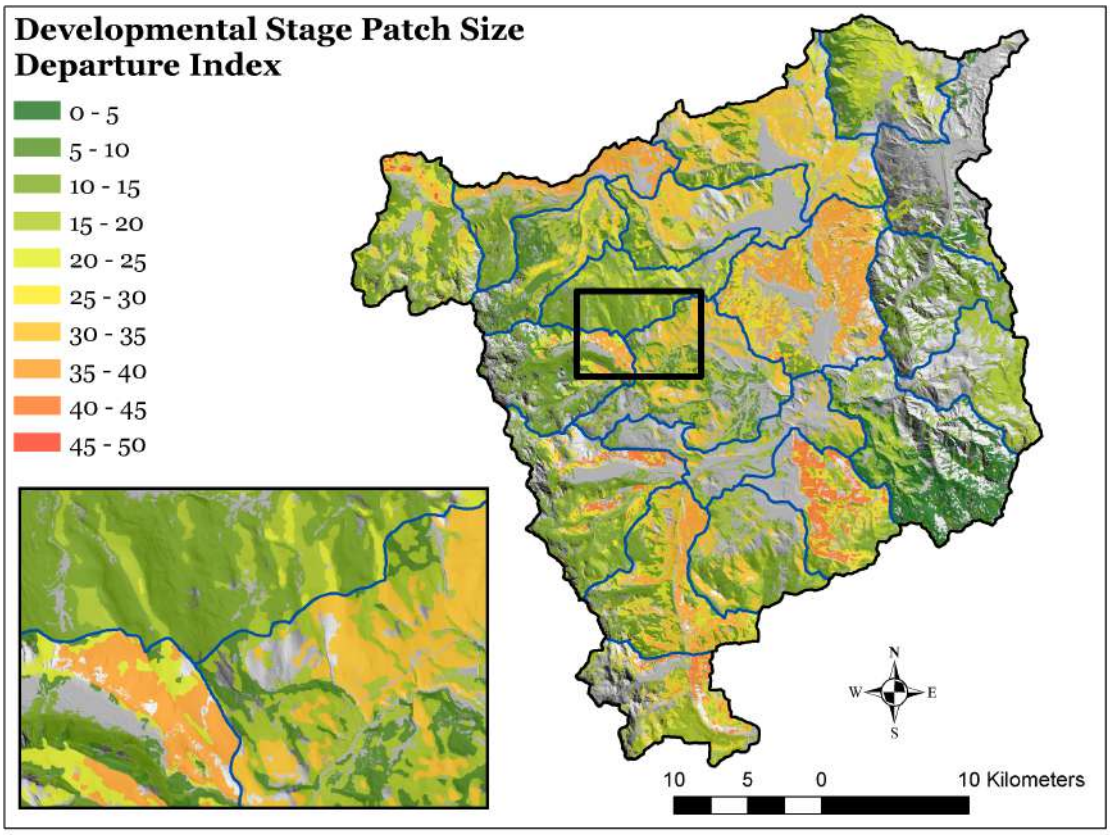

Figure 34: Subbasin-by-BPC level departure index for the developmental stage patch size distribution for the Truckee River landscape. Developmental stages were based on tree height classes and patches were based on the 4-neighbor adjacency rule. The departure index represents the deviation of the current Subbasin and biophysical class (BPC) condition from its historical reference period condition, as simulated. Departure indices > 0 represent a current landscape with a distribution of developmental stage patch sizes that differs in some way from the historical reference period distribution, as simulated, and increasing values represent increasing degrees of departure.

To further evaluate departure in this patch size distribution metric, it is necessary to examine the CRV and HRV patch size distributions for the selected Subbasin-by-BPC partition, for example as depicted in **Figure 35**.

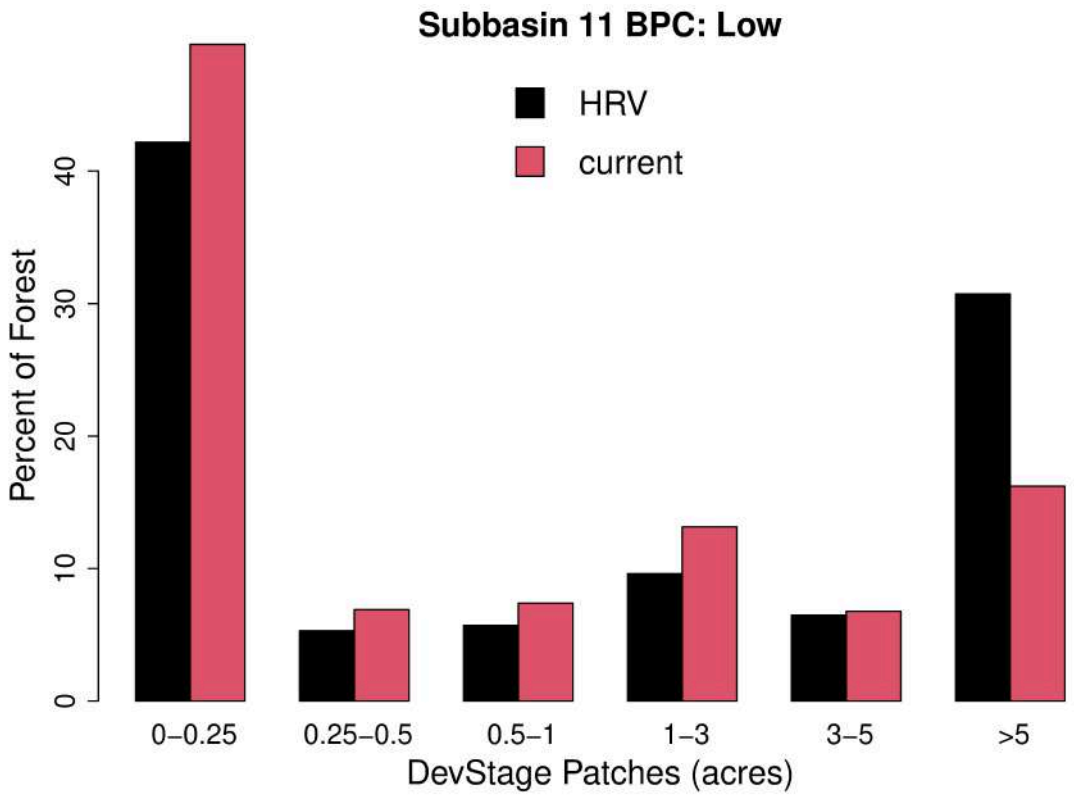

Figure 35: Barplot of the distribution of developmental stage patch sizes for the current landscape and the historical reference period (HRV) for Subbasin 11 and the Low productivity Biophysical Class (BPC = 1) for the Truckee River landscape. Developmental stages were based on tree height classes and patches were based on the 4-neighbor adjacency rule. Each bar represents the percent of forest within the Subbasin and BPC in developmental stage patches of a particular size. The departure index represents the sum of the deviations between the current and HRV bars. Departure indices > 0 represent a current landscape with a distribution of developmental stage patch sizes that differs in some way from the historical reference period distribution, as simulated, and increasing values represent increasing degrees of departure.

Metric 4: Percent Large Trees

We defined large trees as $>$ 30 inch dbh. Percent Large Trees is defined as the percent of the forest within the Subbasin-by-BPC partition in large trees, as defined, and the departure index reflects whether or not the current landscape is deficient in large trees relative to HRV and, if so, the degree of deficiency. The departure index is negative if the current landscape has too little area in large trees compared to HRV.

The Percent Large Trees departure index is depicted in **Figure 36**. As before, the departure index was assigned to each Subbasin-by-BPC partition; consequently, there were 80 distinct values assigned. Thus, to better assess departure by Subbasin and BPC, one needs to examine the attribute table for the departure layer.

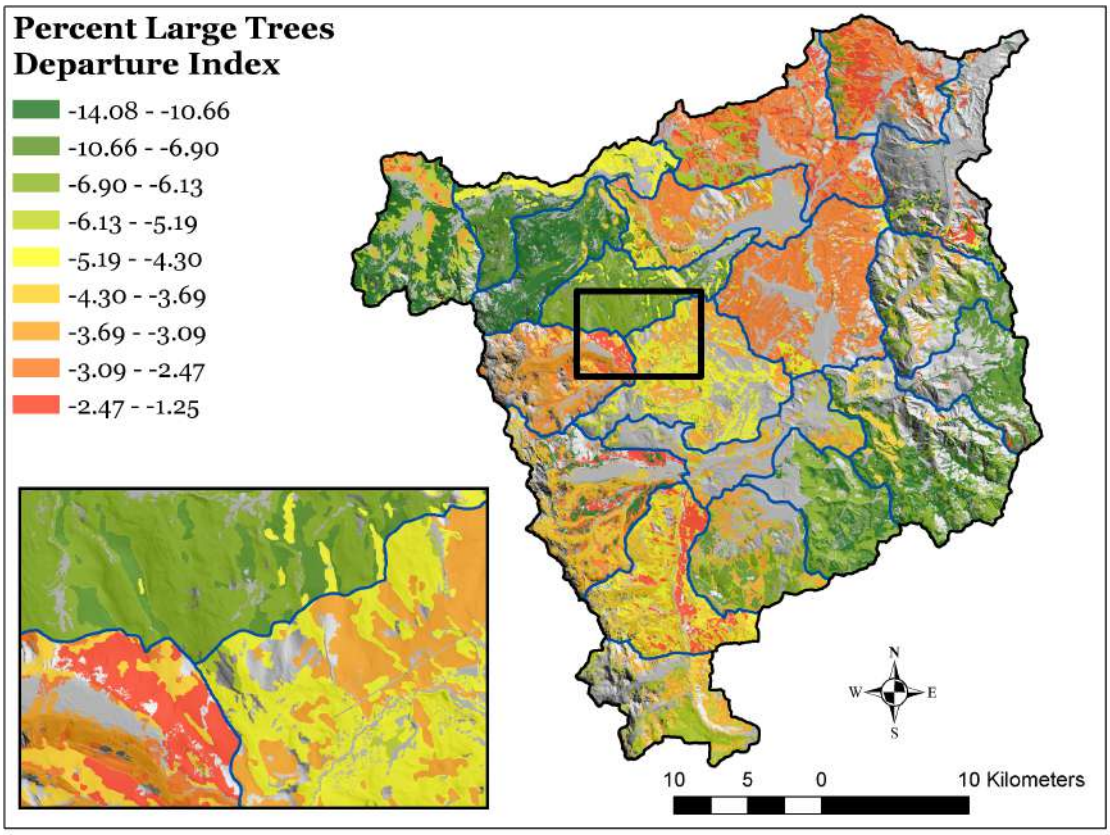

Figure 36: Subbasin-by-BPC level departure index for large trees (> 30 inch dbh) for the Truckee River landscape. The departure index represents the deviation of the current Subbasin and biophysical class (BPC) condition from its historical reference period condition, as simulated. Departure indices < -1 represent a current landscape with less total area in large trees than during the historical reference period, as simulated, and increasing negative values represent increasing degrees of departure.

Metric 5: Large Tree Patch Size Distribution

We defined large trees as described above. Here, we quantified the size of individual patches of large trees and determined the percent of forest within the Subbasin-by-BPC partition in large tree patches in each of several patch size classes or bins (see above), and compared the current and historical distributions. The departure index reflects whether or not the current landscape has a distribution of large tree patch sizes that differs from HRV and, if so, the degree of differences in the two distributions.

The Large Tree Patch Size Distribution departure index is depicted in **Figure 37**. As before, the departure index was assigned to each Subbasin-by-BPC partition; consequently, there were 80 distinct values assigned. Thus, to better assess departure by Subbasin and BPC, one needs to examine the attribute table for the departure layer.

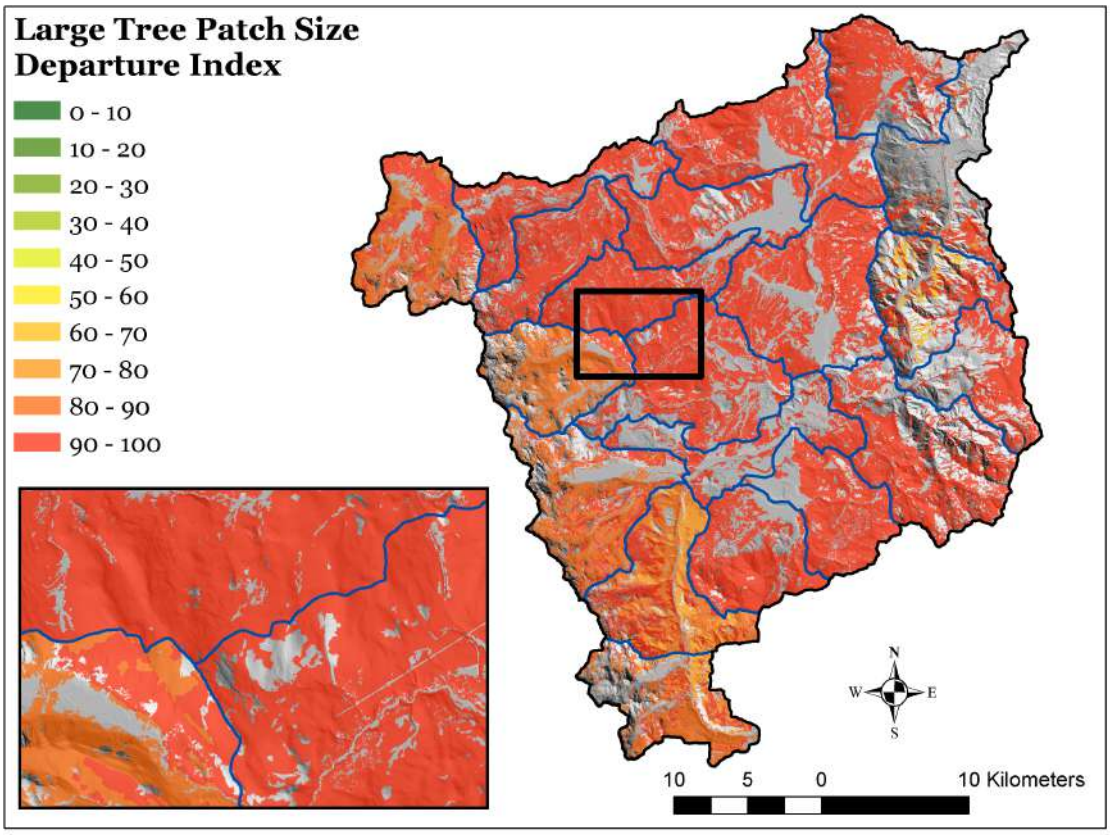

Figure 37: Subbasin-by-BPC level departure index for large tree (> 30 inch dbh) patch size distribution for the Truckee River landscape. The departure index represents the deviation of the current Subbasin and biophysical class (BPC) condition from its historical reference period condition, as simulated. Departure indices > 0 represent a current landscape with a distribution of large tree patch sizes that differs in some way from the historical reference period distribution, as simulated, and increasing values represent increasing degrees of departure.

To further evaluate departure in this patch size distribution metric, it is necessary to examine the CRV and HRV patch size distributions for the selected Subbasin-by-BPC partition, for example as depicted in **Figure 38**.

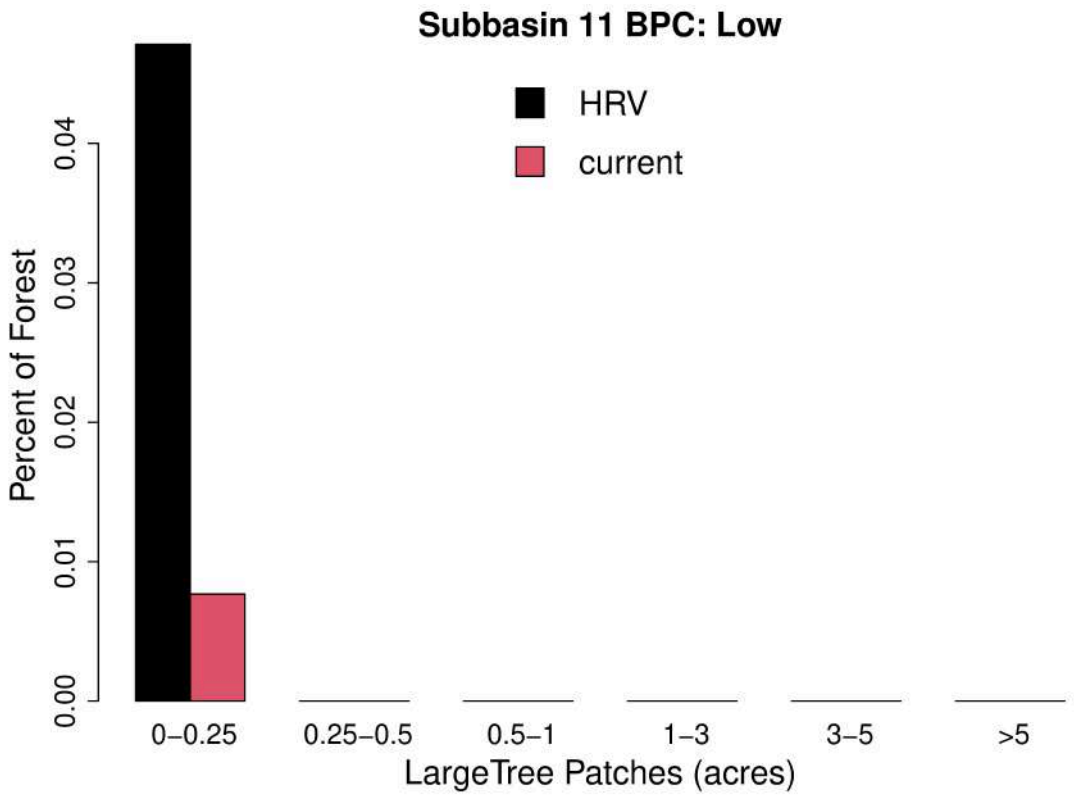

Figure 38: Barplot of the distribution of large tree (> 30 inch dbh) patch sizes for the current landscape and the historical reference period (HRV) for Subbasin 11 and the Low productivity Biophysical Class (BPC = 4) for the Truckee River landscape. See previous barplot caption for details on interpretation.

Metric 6: Tree Size Class Patch Size Distribution

We defined tree size class based on six tree diameter classes, ranging from Open (< 1 in dbh) to large Trees (> 30 in dbh), as described previously. Here, for each snapshot of the landscape we constructed a patch mosaic comprised of tree size classes in which patches were defined using the 4-neighbor rule. For each snapshot, we quantified the size of each tree size class patch and determined the percent of forest within the Subbasin-by-BPC partition in each of several patch size classes or bins. The departure index reflects whether or not the current landscape has a distribution of tree size class patch sizes that differs from HRV and, if so, the degree of differences in the two distributions.

The Tree Size Class Patch Size Distribution departure index is depicted in **Figure 39**. As before, the departure index was assigned to each Subbasin-by-BPC partition; consequently, there were 80 distinct values assigned. Thus, to better assess departure by Subbasin and BPC, one needs to examine the attribute table for the departure layer.

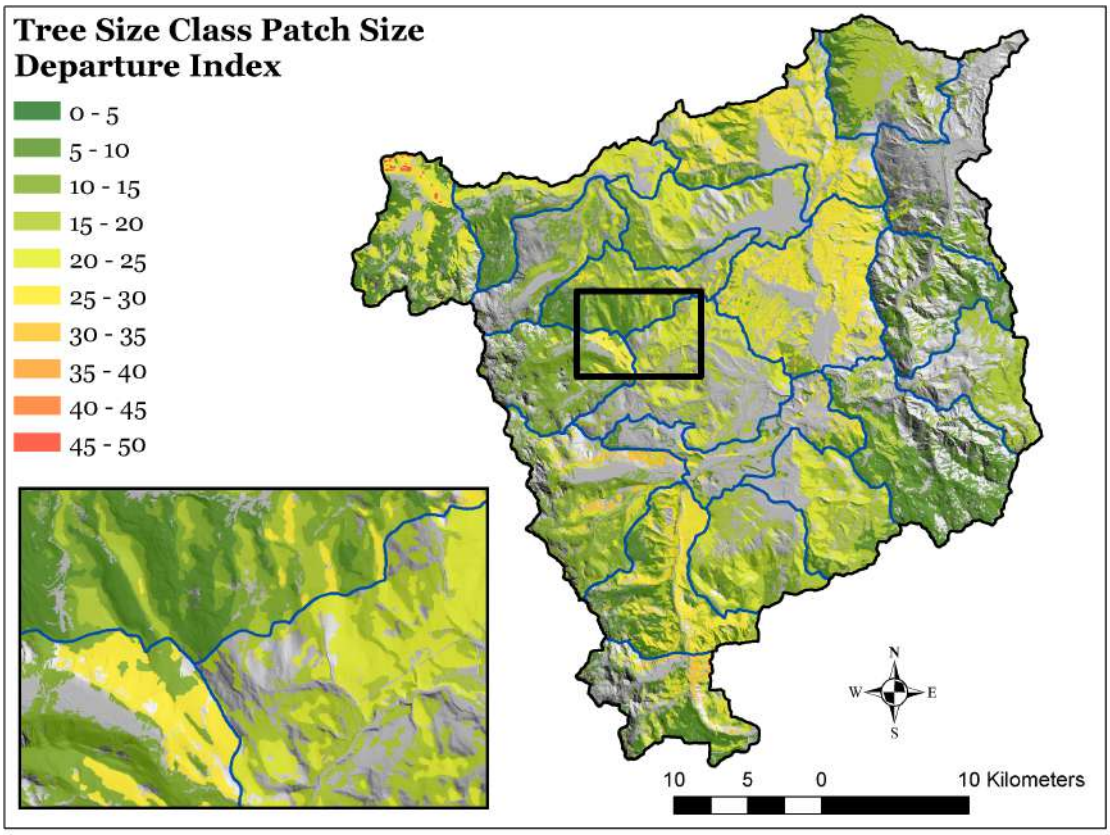

Figure 39: Subbasin-by-BPC level departure index for tree size class (based on dbh) patch size distribution for the Truckee River landscape. The departure index represents the deviation of the current Subbasin and biophysical class (BPC) condition from its historical reference period condition, as simulated. Departure indices > 0 represent a current landscape with a distribution of tree size patch sizes that differs in some way from the historical reference period distribution, as simulated, and increasing values represent increasing degrees of departure.

To further evaluate departure in this patch size distribution metric, it is necessary to examine the CRV and HRV patch size distributions for the selected Subbasin-by-BPC partition, for example as depicted in **Figure 40**.

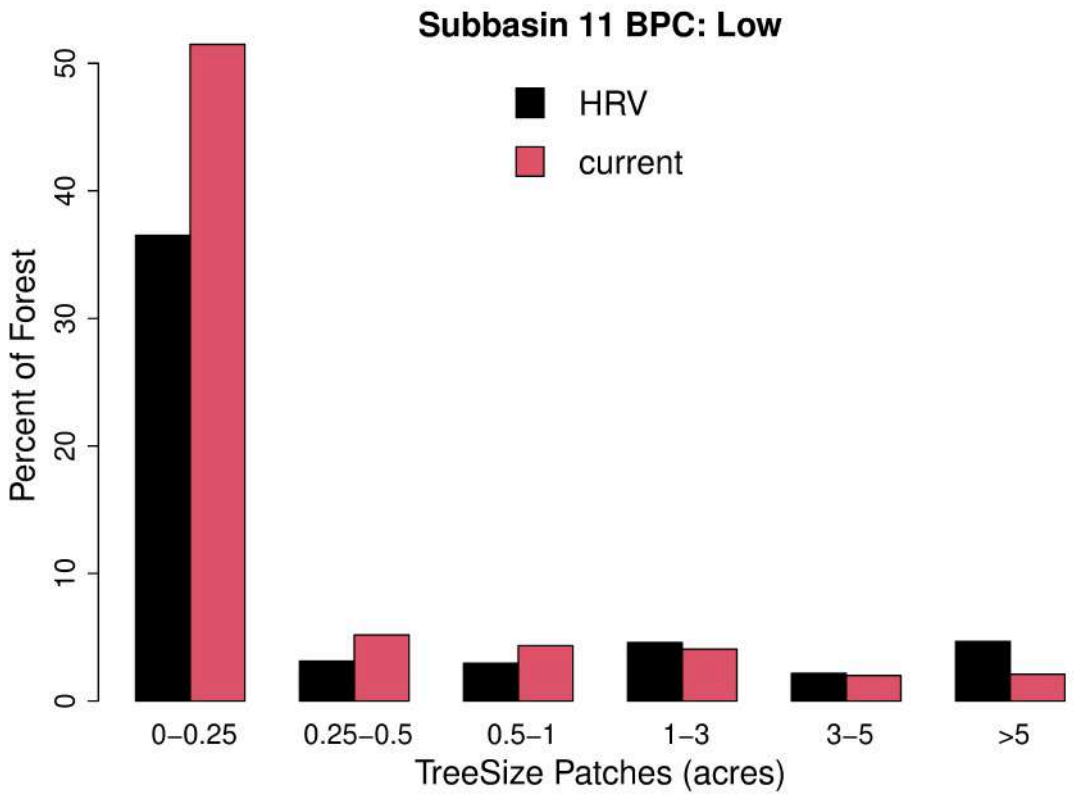

Figure 40: Barplot of the distribution of tree size class (based on dbh) patch sizes for the current landscape and the historical reference period (HRV) for Subbasin 11 and the Low productivity Biophysical Class (BPC = 4) for the Truckee River landscape. See previous barplot caption for details on interpretation.

Composite Departure Score

We combined the 6 Subbasin-level departure metrics above into a single composite departure score, which can be interpreted as a measure of overall departure in vegetation composition and configuration within the Subbasin-by-BPC partition. Maximum departure occurs when the forest has too little area in large forest openings and/or large trees, and/or too homogeneous or uniform a vegetation patch mosaic (i.e., too little spatial variability) defined on the basis of either developmental stages (or tree height classes) or tree size classes (or tree diameter classes).

The composite departure score is depicted in **Figure 41**. Not surprisingly, the Subbasins and BPCs vary somewhat in their overall departure from HRV, and these differences provide a basis for prioritizing project locations with this landscape.

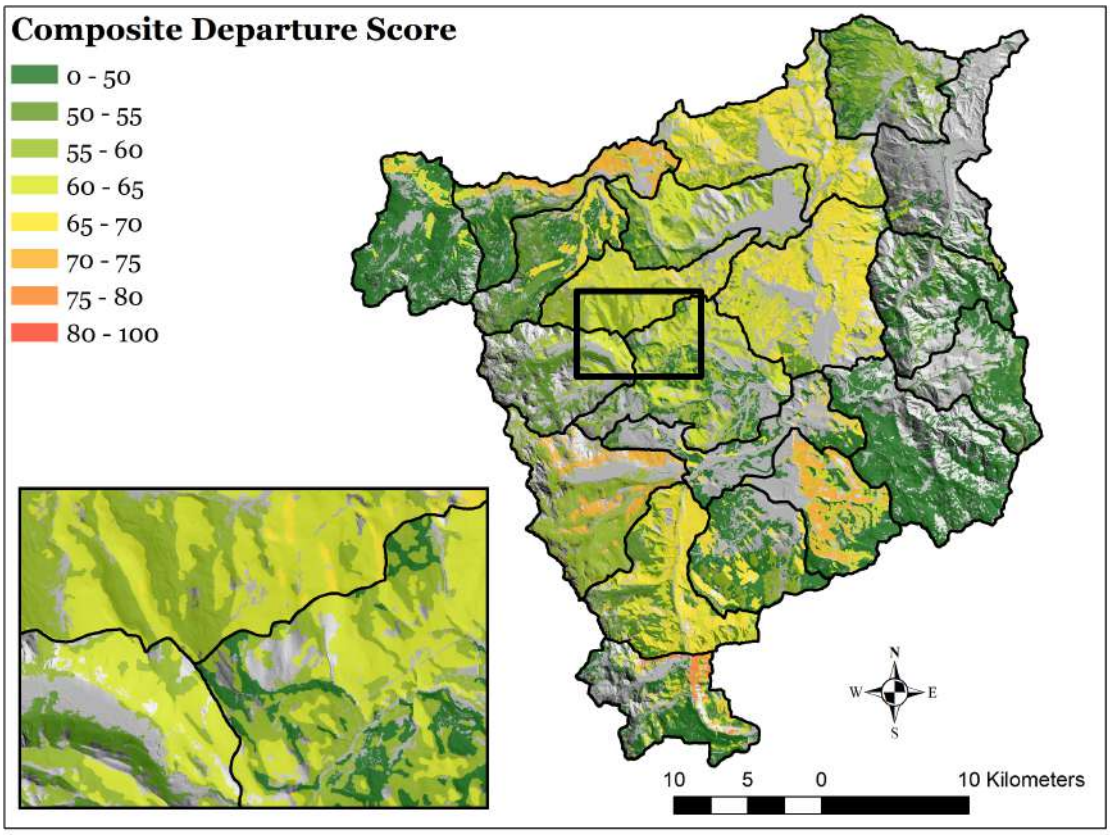

Figure 41: Subbasin-by-BPC level composite departure index derived from the average of the six component metrics for the Truckee River landscape. The composite departure index represents the percentage of maximum departure of the current GPU condition from its historical range of variability (HRV), as simulated. Larger values indicate increasing degrees of departure.

APPENDIX C1 - Wildfire Susceptibility

As described in the GTR, wildfire susceptibility was modeled as a Logistic function of fuels and climate for most cover types. The fuels component was modeled as a Logistic function of the number of years since the last fire (fuelAge) and the Heat Load Index (hli). The climate component was modeled as a Logistic function of the Wildfire Climate Index which was based on the inverted and rescaled 5-year mean Palmer Modified Drought Index. The fuels and climate components were combined with a geometric mean to produce the final Wildfire Susceptibility Index. The final function included 5 beta coefficients (b_0 - b_4). We used expert opinion to specify the beta coefficients for each cover type. We varied the b_0 and b_1 coefficients among cover types to reflect differences in reported historical mean fire return intervals among cover types - shifting the response curves left or right so that the inflection point (Wildfire Susceptibility Index = 0.5) roughly equaled the target mean return interval - and held the Heat Load Index coefficient (b_2) and Climate coefficients (b_3 and b_4) the same across all cover types to reflect the global affect of topography and climate on wildfire susceptibility.

The figures below depict the final wildfire susceptibility response functions for each cover type in alphabetical order (noting that some cover types did not have response functions, as noted in the text). The response functions depict the wildfire Susceptibility Index as a Logistic function of the number of years since the last fire (Years since fire). The dashed, solid and dotted lines depict the response functions for the minimum, mean and maximum Heat Load Index (hli), and the red, black and green sets of lines depict the response functions for the minimum, mean and maximum Wildfire Climate Index. The values of the Logistic parameters (b_0 - b_4) for the cover type are shown as well.

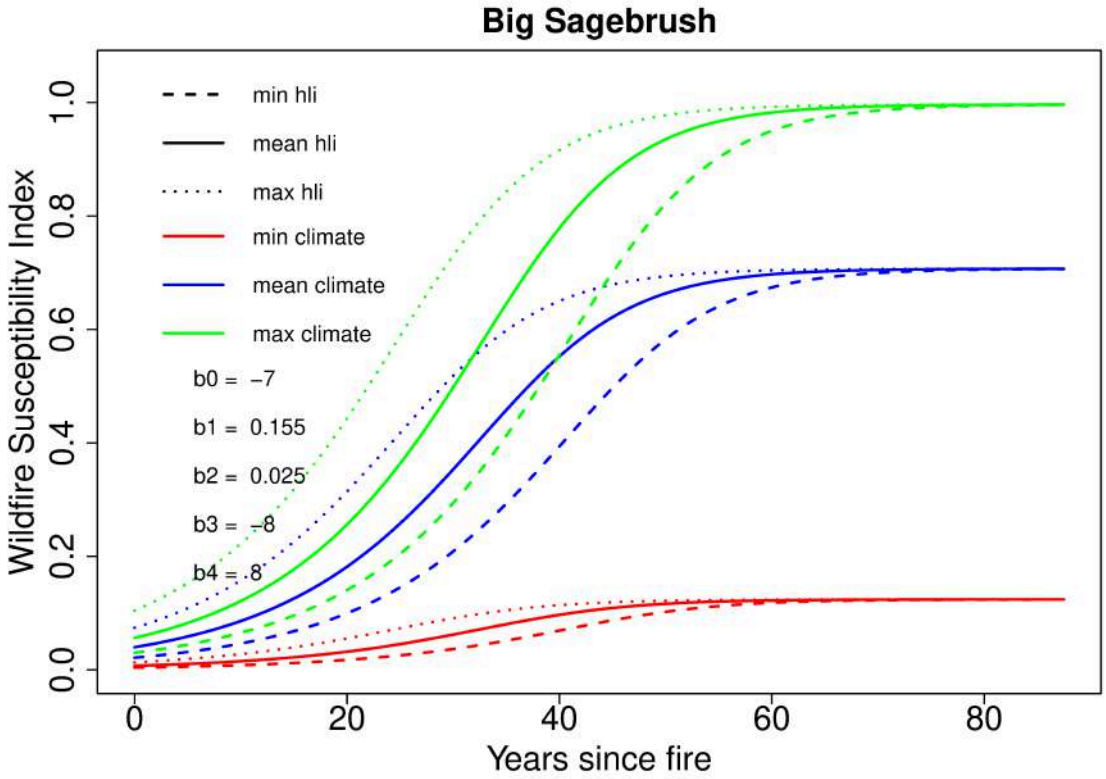

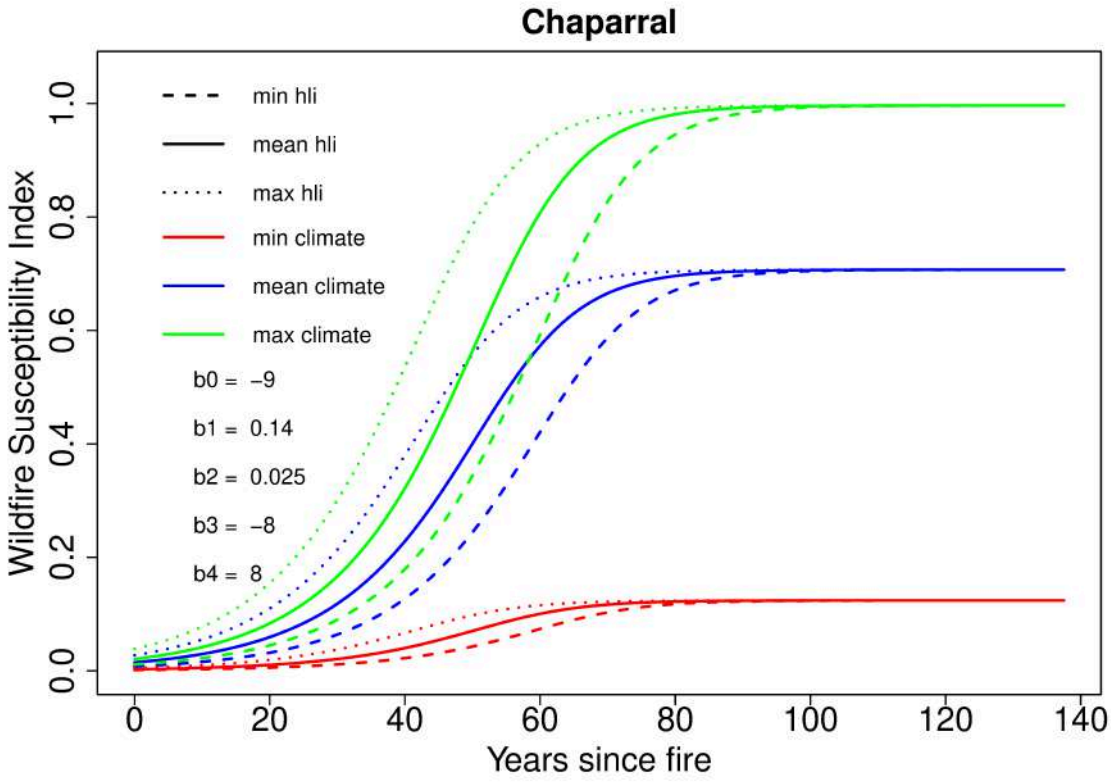
Chaparral
min hli
mean hli
max hli
min climate
mean climate
max climate
b0 = −9
b1 = 0.14
b2 = 0.025
b3 = −8
b4 = 8
Wildfire Susceptibility Index
0.0
0.2
0.4
0.6
0.8
1.0
0
20
40
60
80
100
120
140
Years since fire

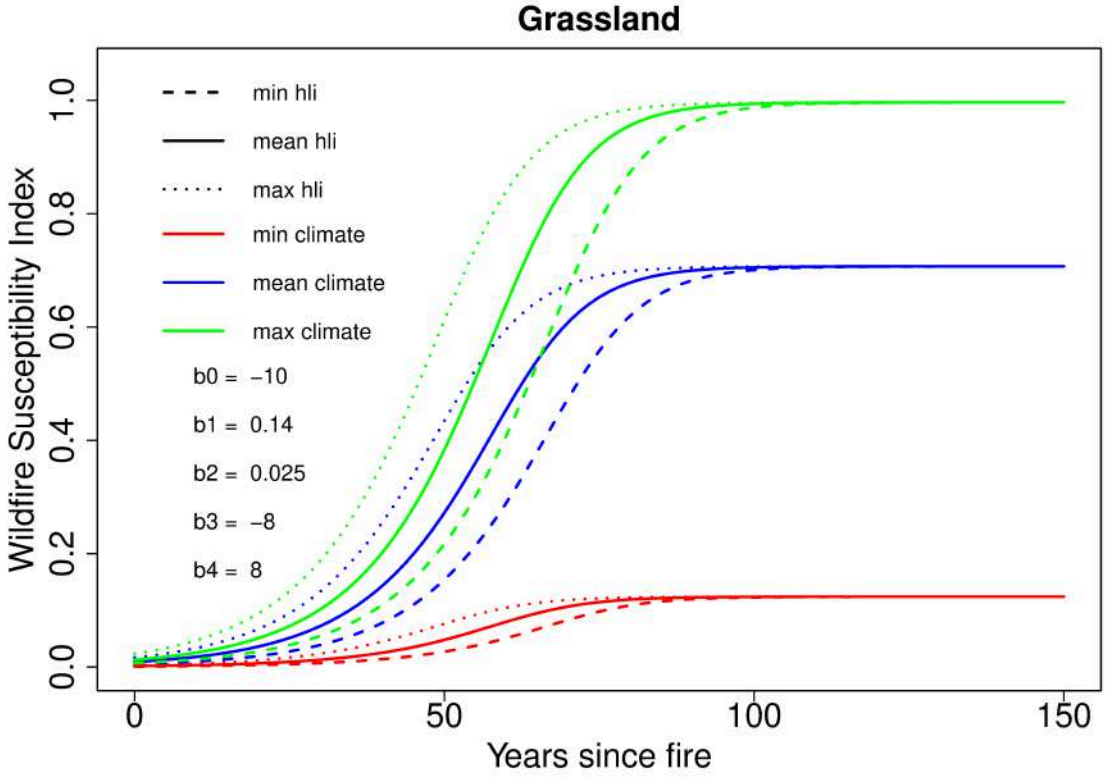
Grassland
min hli
mean hli
max hli
min climate
mean climate
max climate
b0 = −10
b1 = 0.14
b2 = 0.025
b3 = −8
b4 = 8
Wildfire Susceptibility Index
0.0
0.2
0.4
0.6
0.8
1.0
0
50
100
150
Years since fire

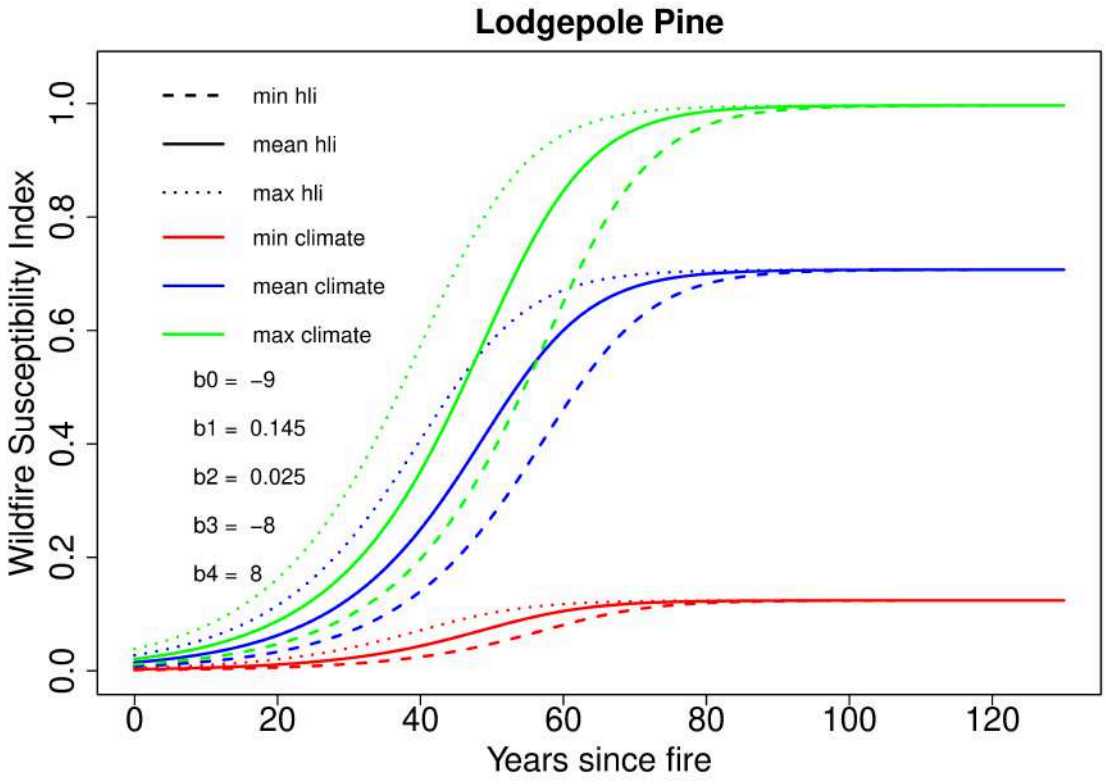
Lodgepole Pine
min hli
mean hli
max hli
min climate
mean climate
max climate
b0 = −9
b1 = 0.145
b2 = 0.025
b3 = −8
b4 = 8
Wildfire Susceptibility Index
0.0
0.2
0.4
0.6
0.8
1.0
0
20
40
60
80
100
120
Years since fire

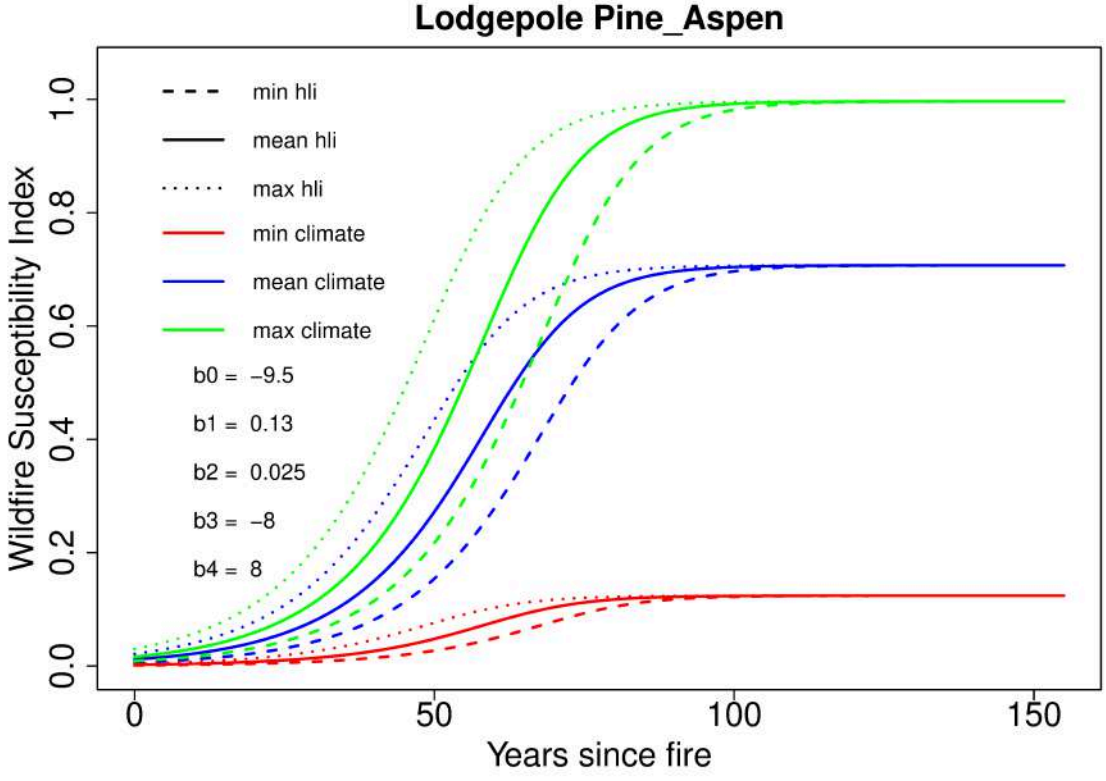
Lodgepole Pine_Aspen
min hli
mean hli
max hli
min climate
mean climate
max climate
b0 = −9.5
b1 = 0.13
b2 = 0.025
b3 = −8
b4 = 8
Wildfire Susceptibility Index
0.0
0.2
0.4
0.6
0.8
1.0
0
50
100
150
Years since fire

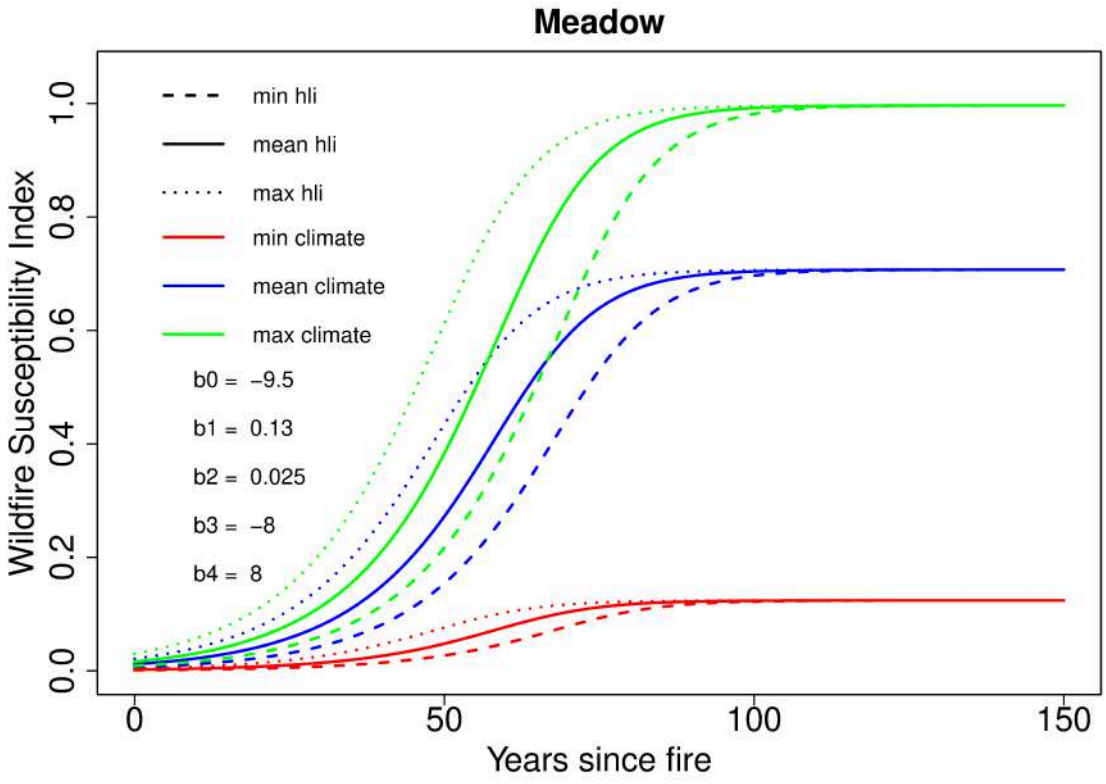
Meadow
min hli
mean hli
max hli
min climate
mean climate
max climate
b0 = −9.5
b1 = 0.13
b2 = 0.025
b3 = −8
b4 = 8
Wildfire Susceptibility Index
0.0
0.2
0.4
0.6
0.8
1.0
0
50
100
150
Years since fire

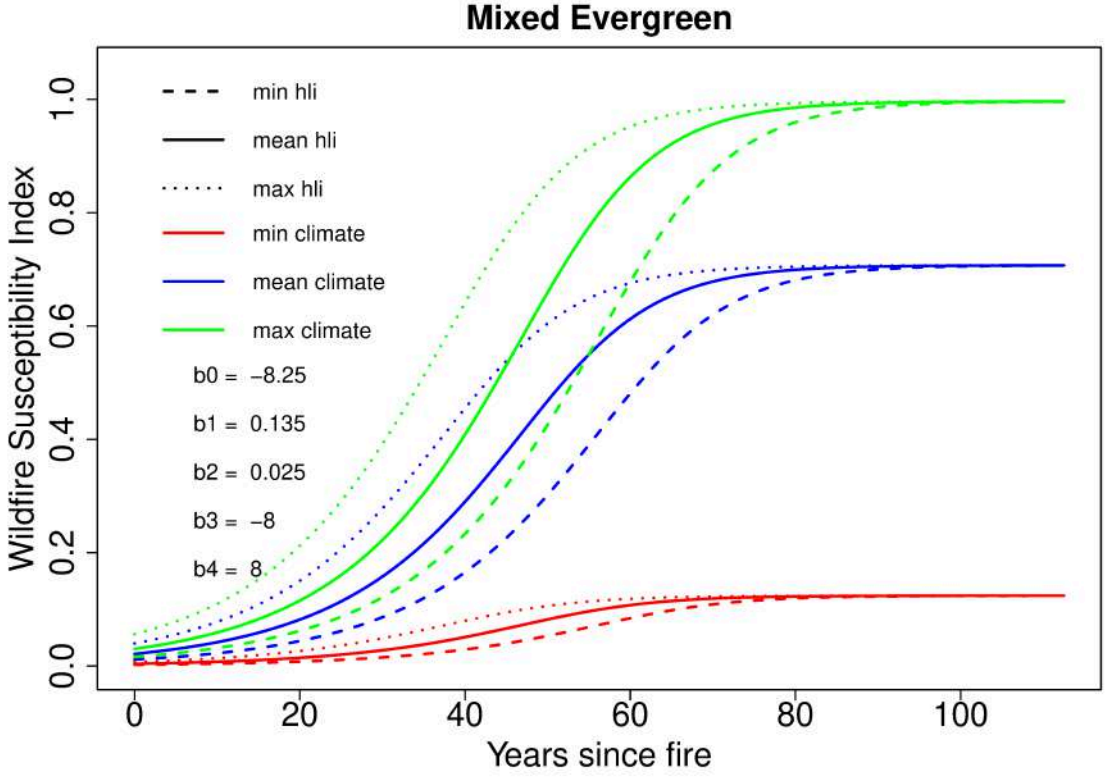
Mixed Evergreen
min hli
mean hli
max hli
min climate
mean climate
max climate
b0 = −8.25
b1 = 0.135
b2 = 0.025
b3 = −8
b4 = 8
Wildfire Susceptibility Index
0.0
0.2
0.4
0.6
0.8
1.0
0
20
40
60
80
100
Years since fire

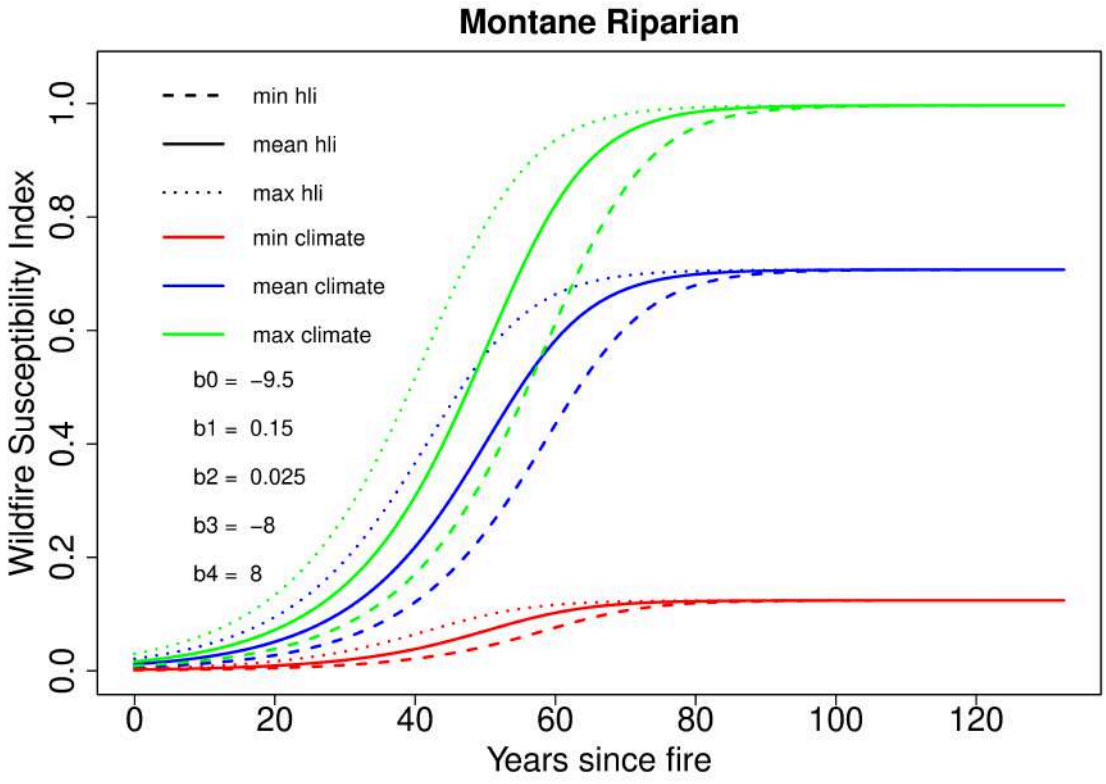
Montane Riparian
min hli
mean hli
max hli
min climate
mean climate
max climate
b0 = −9.5
b1 = 0.15
b2 = 0.025
b3 = −8
b4 = 8
Wildfire Susceptibility Index
0.0
0.2
0.4
0.6
0.8
1.0
0
20
40
60
80
100
120
Years since fire

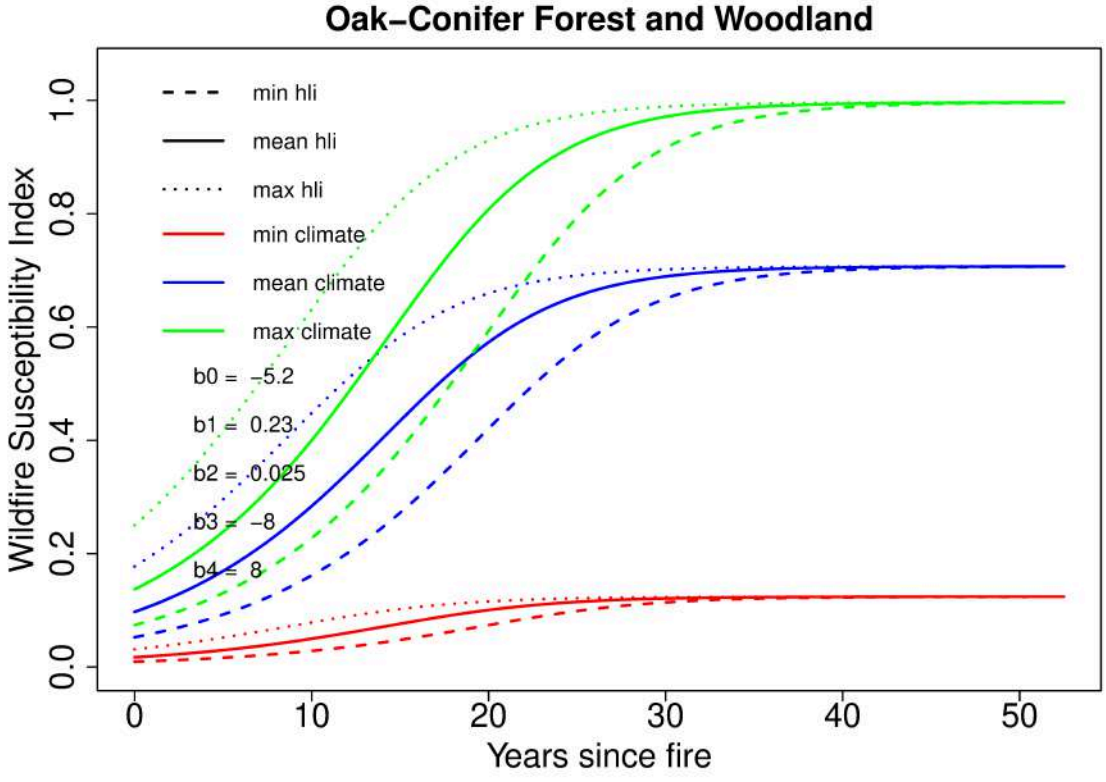
Oak−Conifer Forest and Woodland
min hli
mean hli
max hli
min climate
mean climate
max climate
b0 = −5.2
b1 = 0.23
b2 = 0.025
b3 = −8
b4 = 8
Wildfire Susceptibility Index
0.0
0.2
0.4
0.6
0.8
1.0
0
10
20
30
40
50
Years since fire

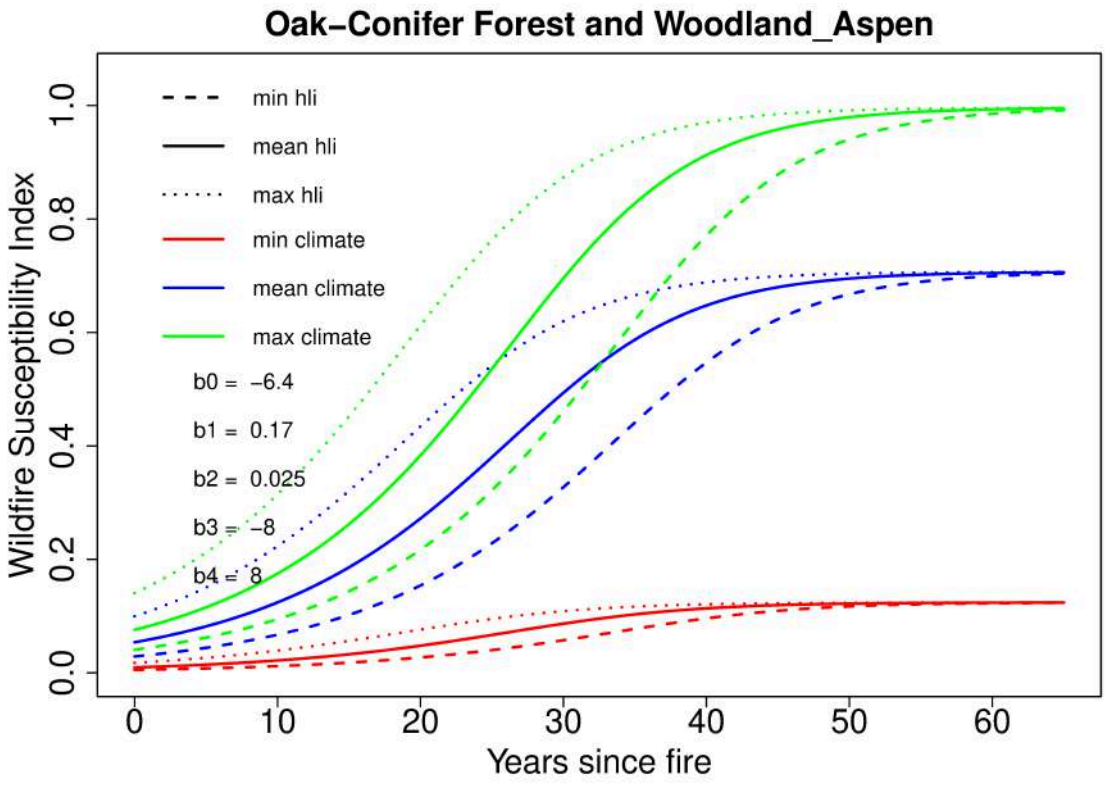
Oak–Conifer Forest and Woodland_Aspen
min hli
mean hli
max hli
min climate
mean climate
max climate
b0 = −6.4
b1 = 0.17
b2 = 0.025
b3 = −8
b4 = 8
Wildfire Susceptibility Index
0.0
0.2
0.4
0.6
0.8
1.0
0
10
20
30
40
50
60
Years since fire

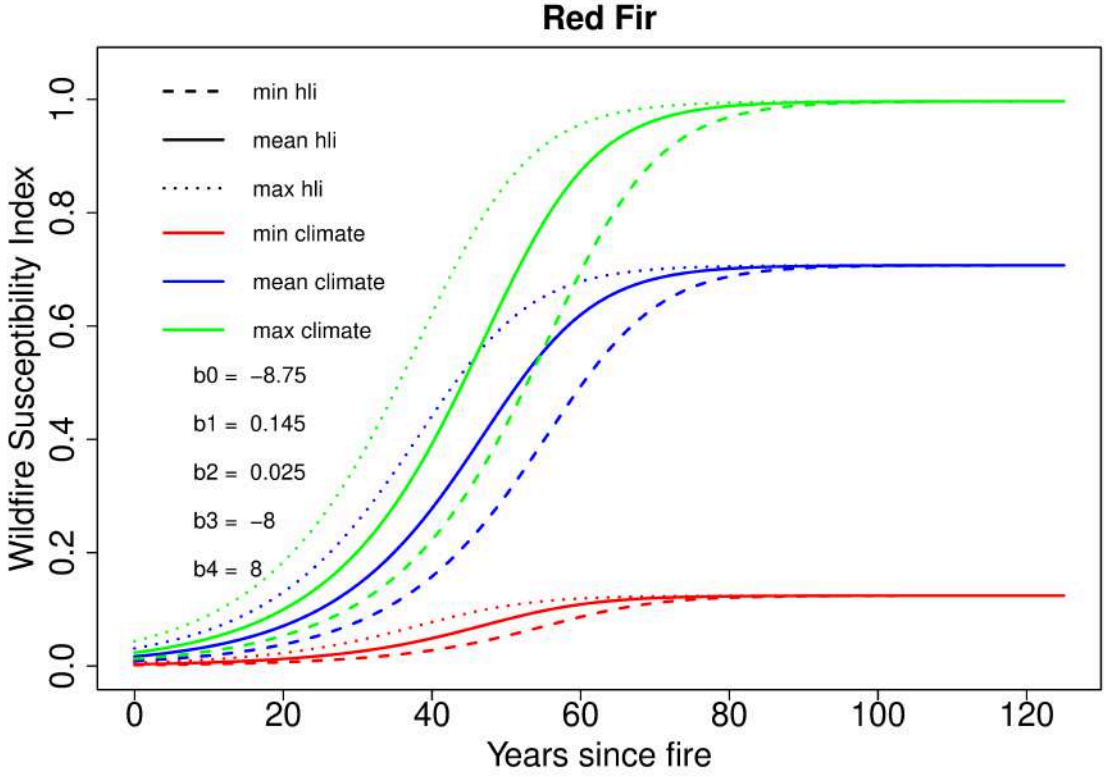
Red Fir
min hli
mean hli
max hli
min climate
mean climate
max climate
b0 = −8.75
b1 = 0.145
b2 = 0.025
b3 = −8
b4 = 8
Wildfire Susceptibility Index
0.0
0.2
0.4
0.6
0.8
1.0
0
20
40
60
80
100
120
Years since fire

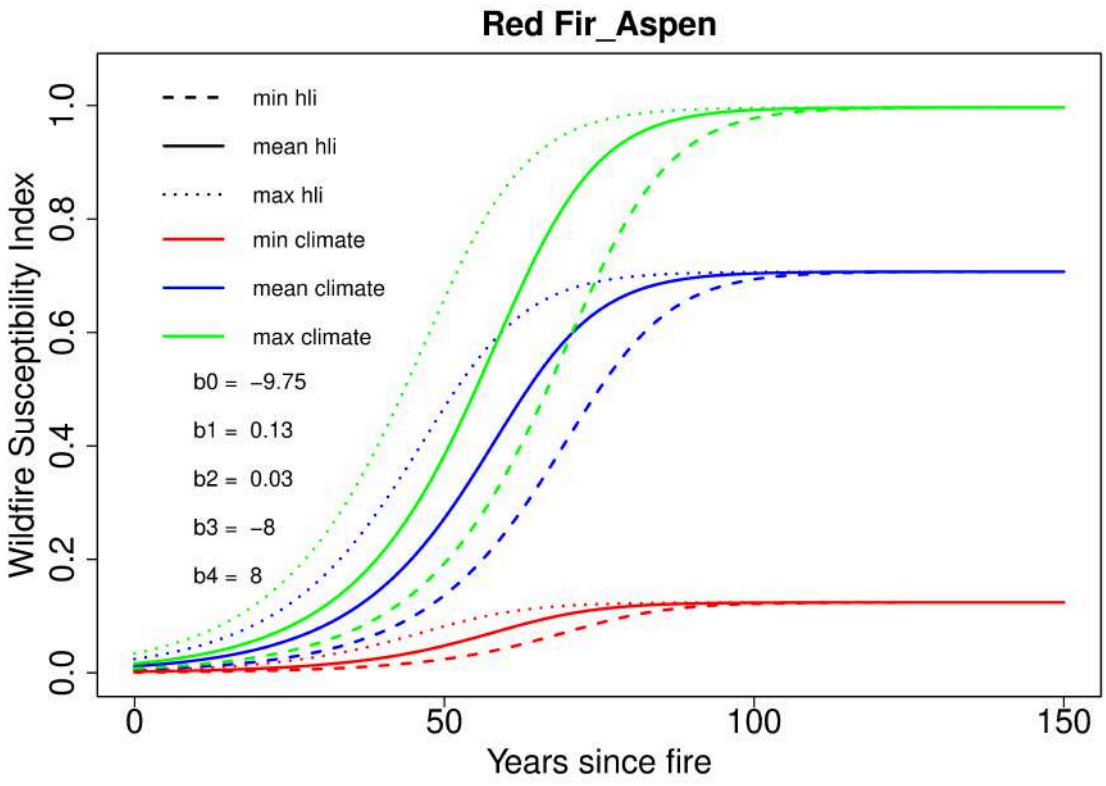
Red Fir_Aspen
min hli
mean hli
max hli
min climate
mean climate
max climate
b0 = −9.75
b1 = 0.13
b2 = 0.03
b3 = −8
b4 = 8
Wildfire Susceptibility Index
0.0
0.2
0.4
0.6
0.8
1.0
0
50
100
150
Years since fire

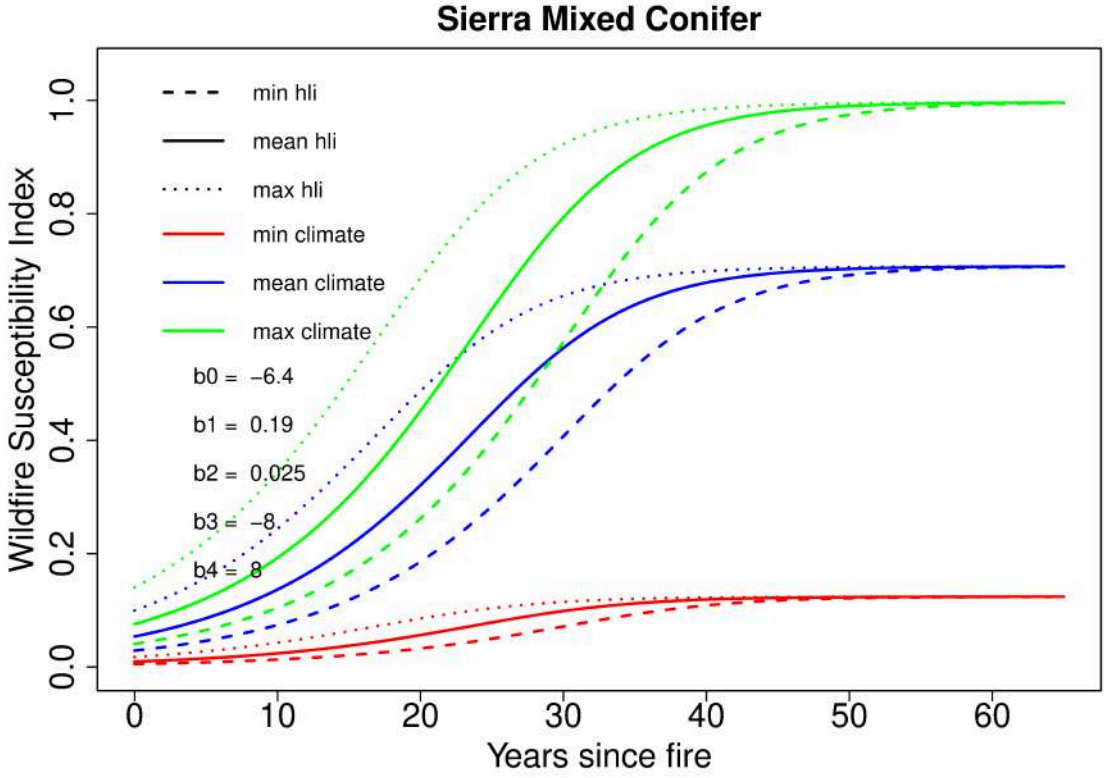
Sierra Mixed Conifer
min hli
mean hli
max hli
min climate
mean climate
max climate
b0 = −6.4
b1 = 0.19
b2 = 0.025
b3 = −8
b4 = 8
Wildfire Susceptibility Index
0.0
0.2
0.4
0.6
0.8
1.0
0
10
20
30
40
50
60
Years since fire

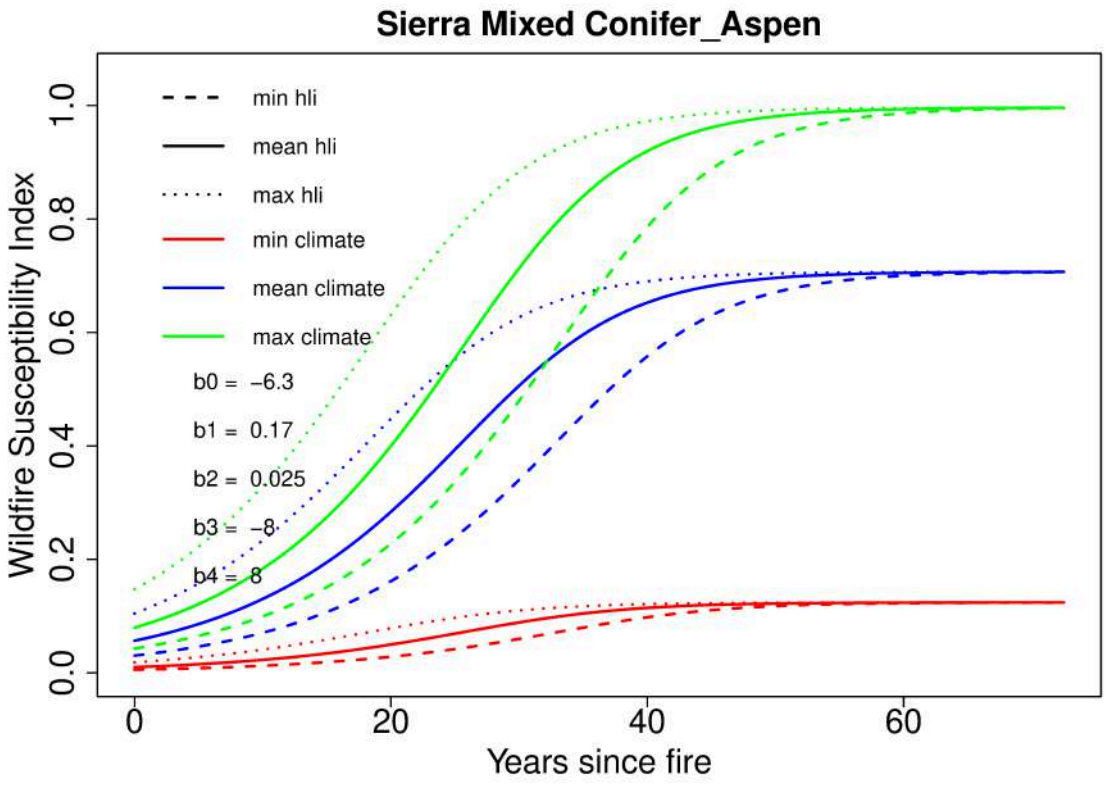
Sierra Mixed Conifer_Aspen
min hli
mean hli
max hli
min climate
mean climate
max climate
b0 = −6.3
b1 = 0.17
b2 = 0.025
b3 = −8
b4 = 8
Wildfire Susceptibility Index
0.0
0.2
0.4
0.6
0.8
1.0
0
20
40
60
Years since fire

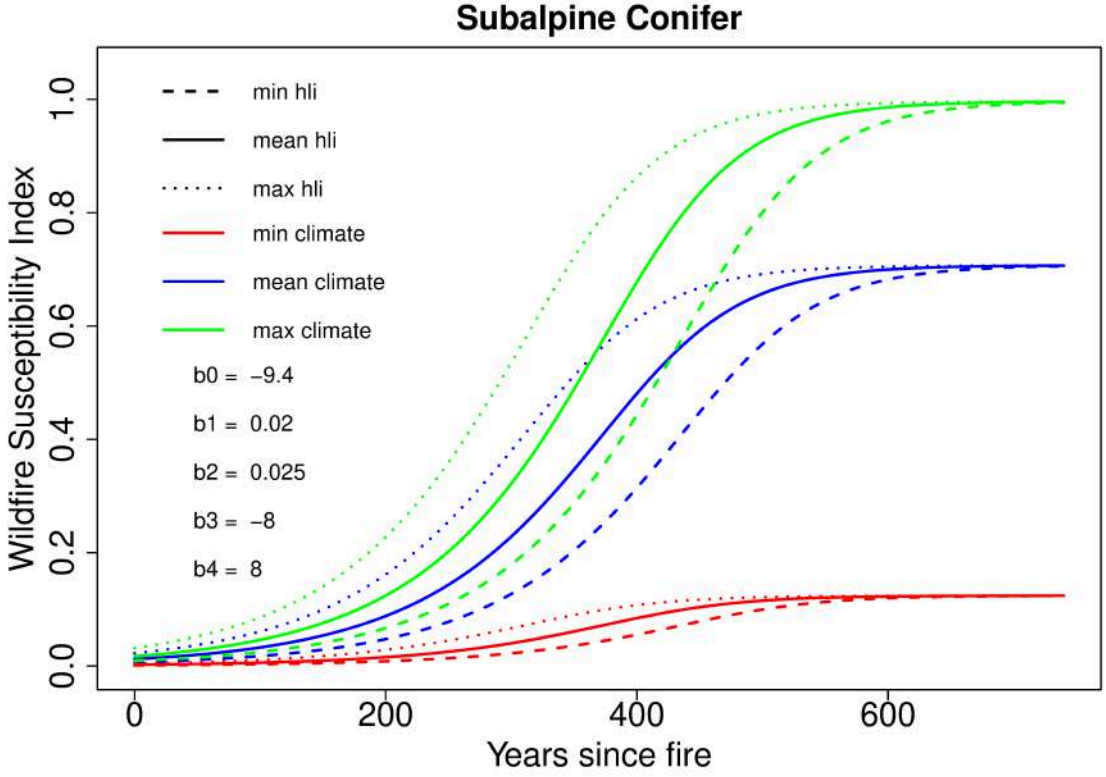
Subalpine Conifer
min hli
mean hli
max hli
min climate
mean climate
max climate
b0 = −9.4
b1 = 0.02
b2 = 0.025
b3 = −8
b4 = 8
Wildfire Susceptibility Index
0.0
0.2
0.4
0.6
0.8
1.0
0
200
400
600
Years since fire

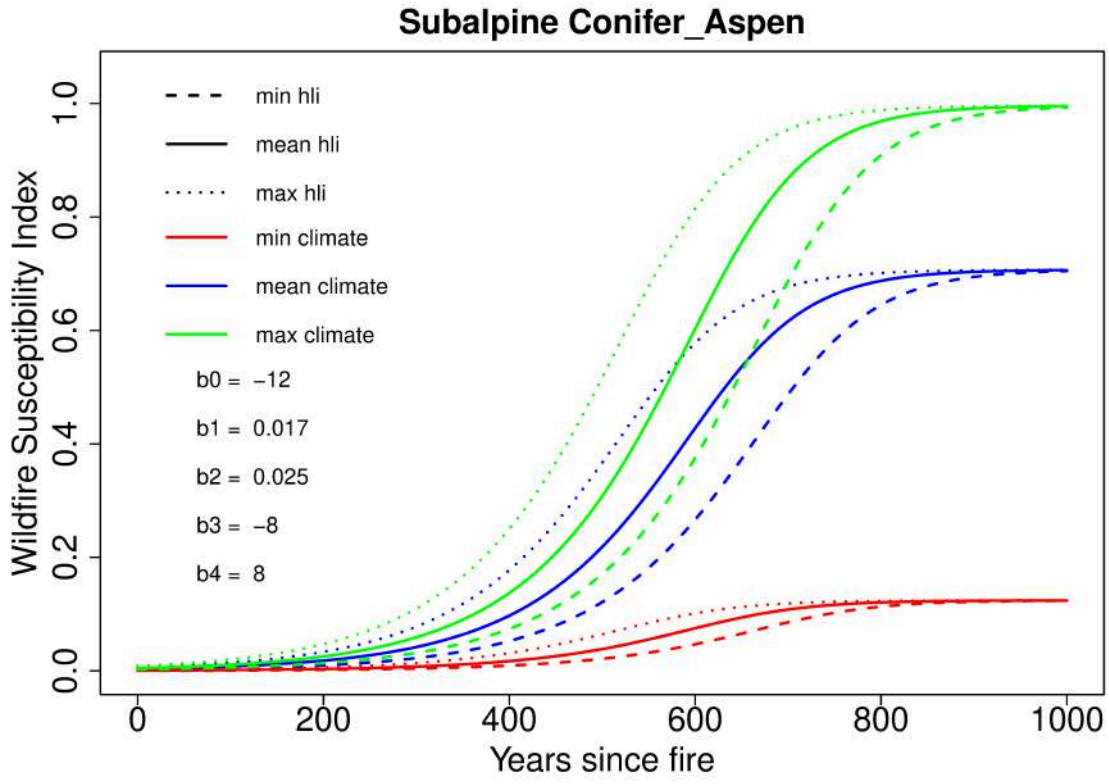
Subalpine Conifer_Aspen
min hli
mean hli
max hli
min climate
mean climate
max climate
b0 = −12
b1 = 0.017
b2 = 0.025
b3 = −8
b4 = 8
Wildfire Susceptibility Index
0.0
0.2
0.4
0.6
0.8
1.0
0
200
400
600
800
1000
Years since fire

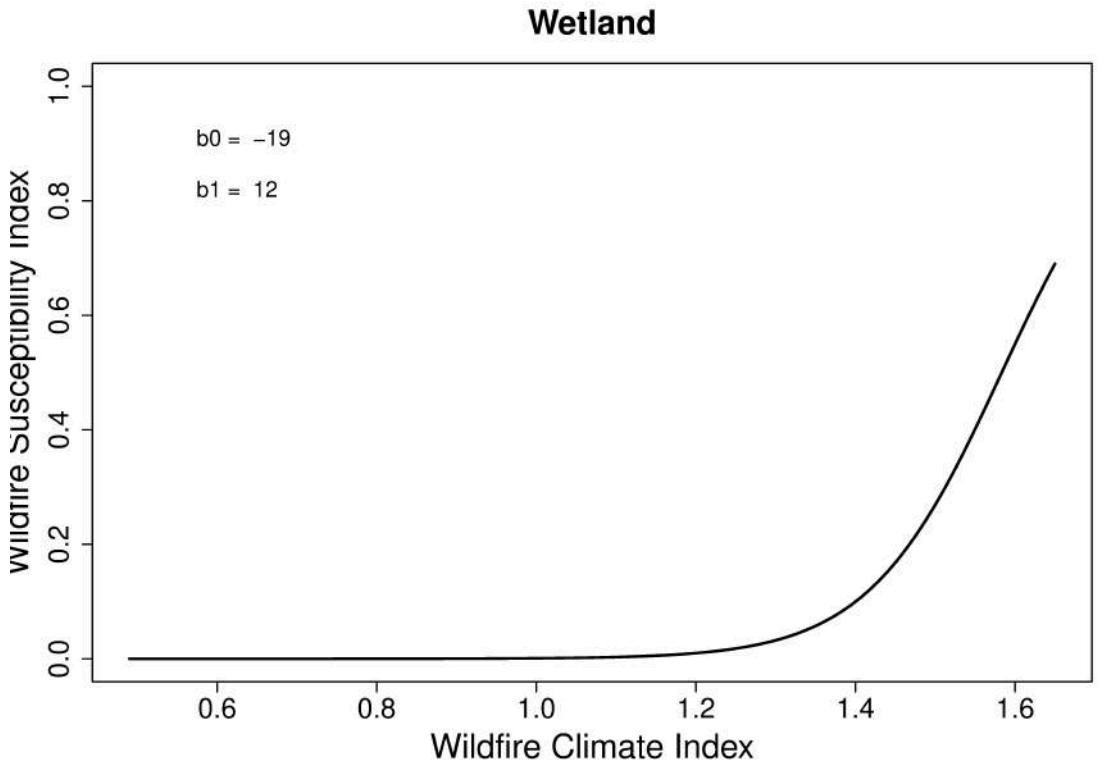
Wetland
b0 = −19
b1 = 12
Wildfire Susceptibility Index
0.0
0.2
0.4
0.6
0.8
1.0
0.6
0.8
1.0
1.2
1.4
1.6
Wildfire Climate Index

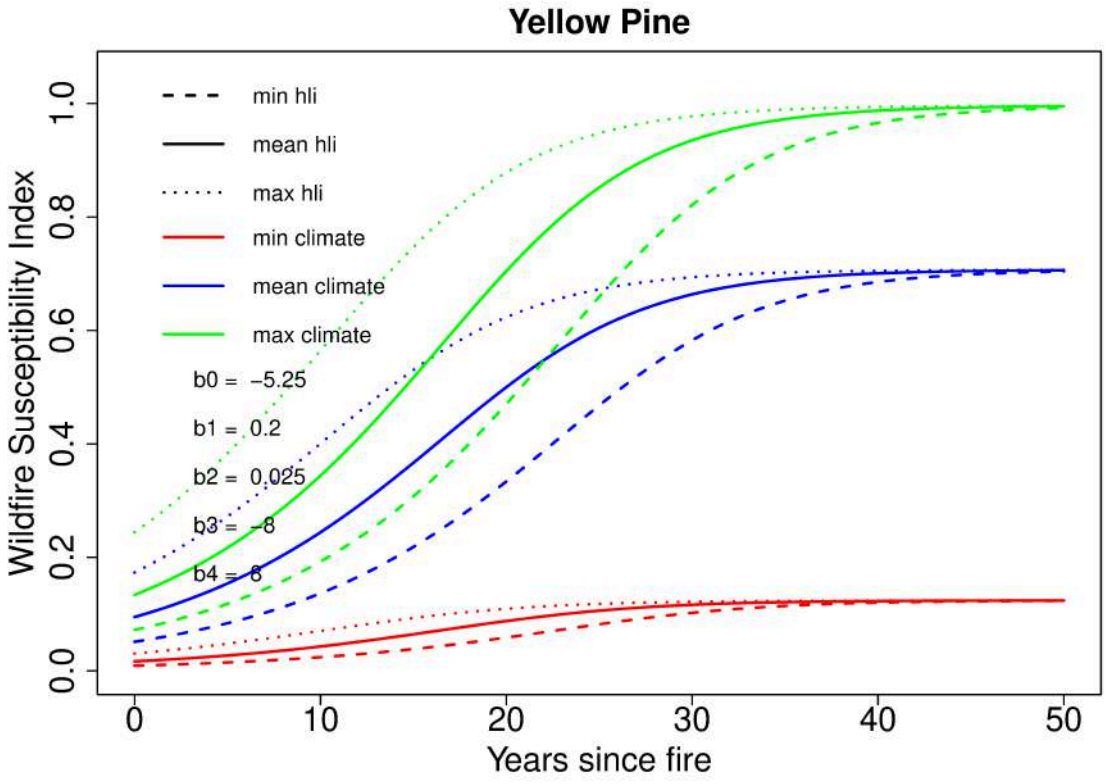
Yellow Pine
min hli
mean hli
max hli
min climate
mean climate
max climate
b0 = −5.25
b1 = 0.2
b2 = 0.025
b3 = −8
b4 = 8
Wildfire Susceptibility Index
0.0
0.2
0.4
0.6
0.8
1.0
0
10
20
30
40
50
Years since fire

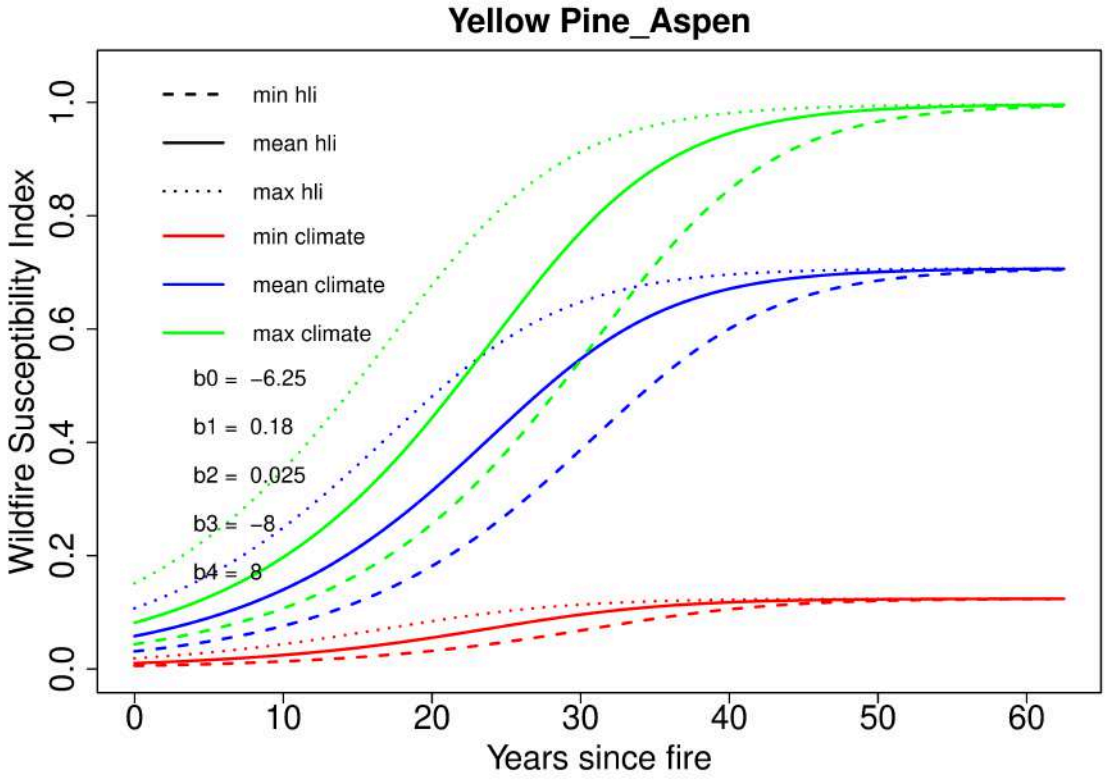
Yellow Pine_Aspen
min hli
mean hli
max hli
min climate
mean climate
max climate
b0 = −6.25
b1 = 0.18
b2 = 0.025
b3 = −8
b4 = 8
Wildfire Susceptibility Index
0.0
0.2
0.4
0.6
0.8
1.0
0
10
20
30
40
50
60
Years since fire

APPENDIX C2 - Wildfire Mortality

As described in the GTR, wildfire mortality (i.e., the probability of high mortality or death of the overstory vegetation in each 5 m cell that burned) was determined by a complex function involving two major factors: 1) fire intensity, which was a Logistic function of the fuel loads in the neighborhood of the focal cell (proxied by the age of the vegetation and time since the last fire), the topographic position of the focal cell, and the climate conditions in the current time step; and 2) the resistance of the focal cell, which was a negative exponential function of the age of the vegetation in the focal cell in which the rate of exponential decline with age decreased with increasing fire intensity (see main text for details). The complex wildfire mortality function included 6 user-specified beta coefficients. As described in the main text, b_0 - b_4 were held constant across all cover types. We varied b_5 and b_6 among cover types to reflect differences in reported historical mean fire return intervals and high mortality rates among cover types. Specifically, we varied these two beta coefficients during model calibration to either increase or decrease the rate of exponential decline in high mortality with increasing vegetation age as a function of fire intensity to achieve the target percentage of high mortality rate in each cover type.

The figures below depict the final wildfire mortality response functions for each cover type in alphabetical order. Cover types not shown either were not eligible to burn (e.g., water, barren) or were always assigned a high mortality response after burning (e.g., grassland, meadow). The response functions depict the probability of high mortality wildfire as a negative exponential function of vegetation Age (yrs) and fire intensity (as indexed). The dashed, solid and dotted lines depict the response functions for the minimum, mean and maximum Fire Intensity Index. Universally, the probability of high mortality decreased with increasing vegetation Age, but the rate of exponential decline decreased (i.e.,shallower slope) with increasing fire intensity, such that for any given Age the probability of high mortality increased with increasing fire intensity.

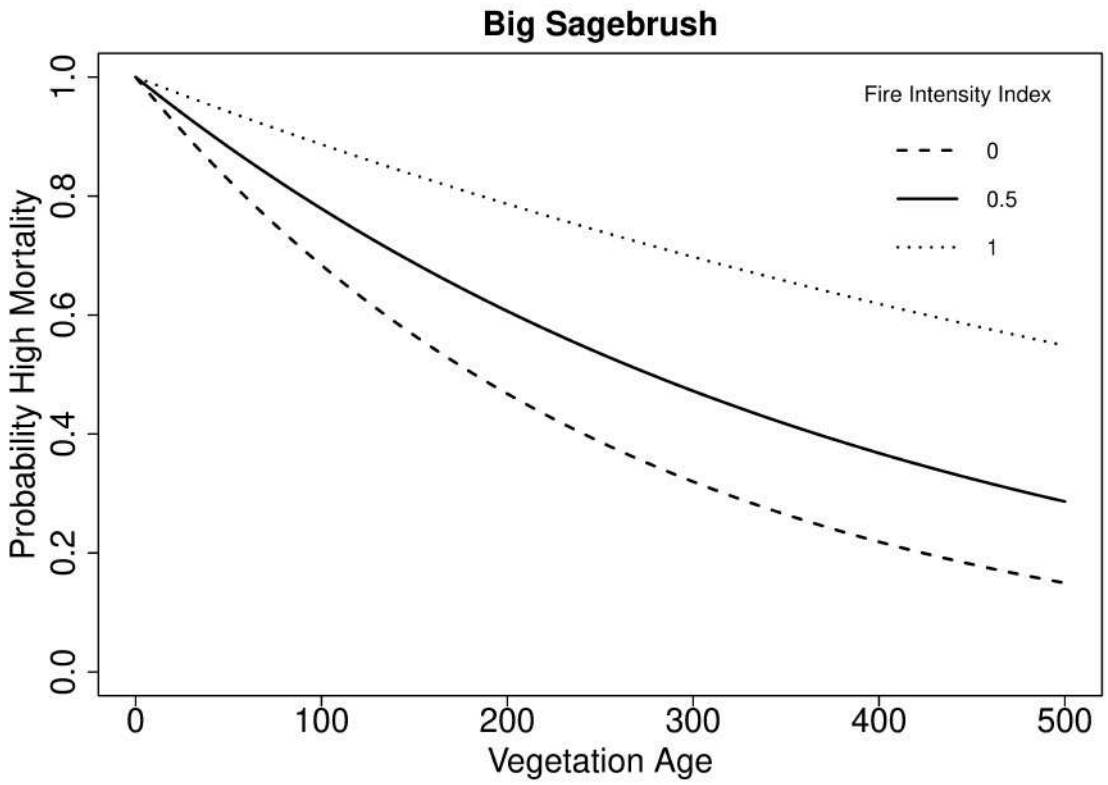

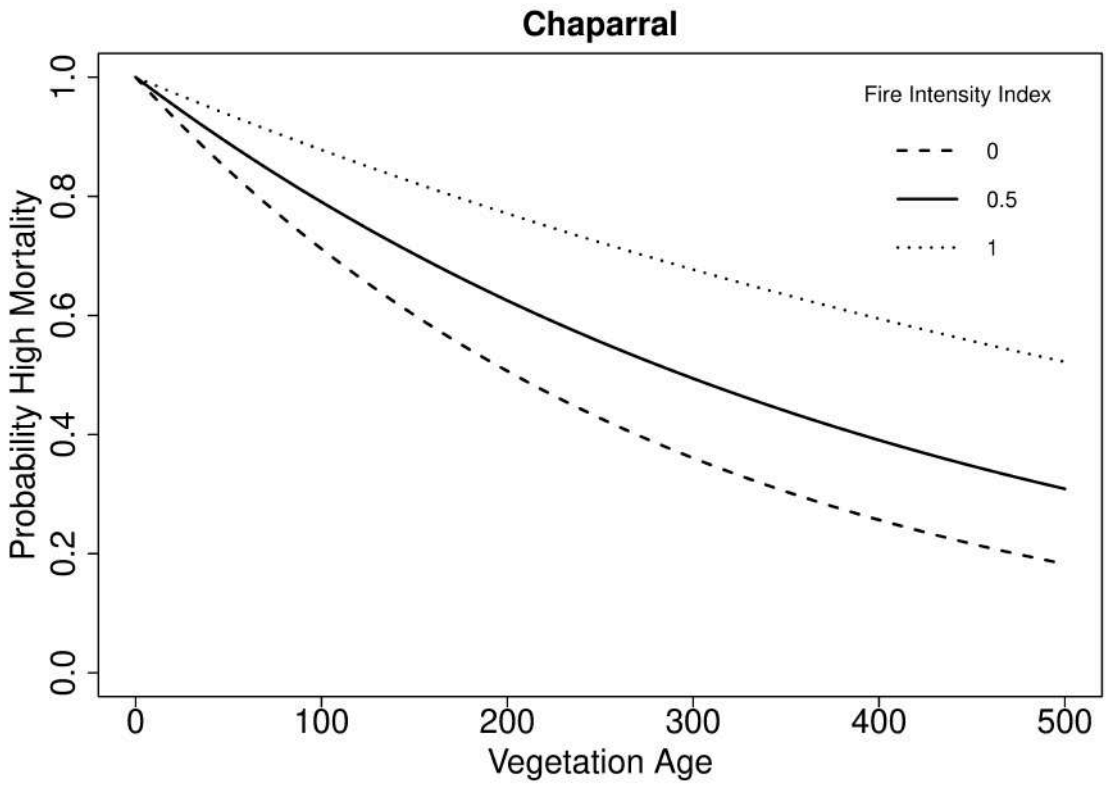
Chaparral
Fire Intensity Index
0
0.5
1
Probability High Mortality
0.0
0.2
0.4
0.6
0.8
1.0
0
100
200
300
400
500
Vegetation Age

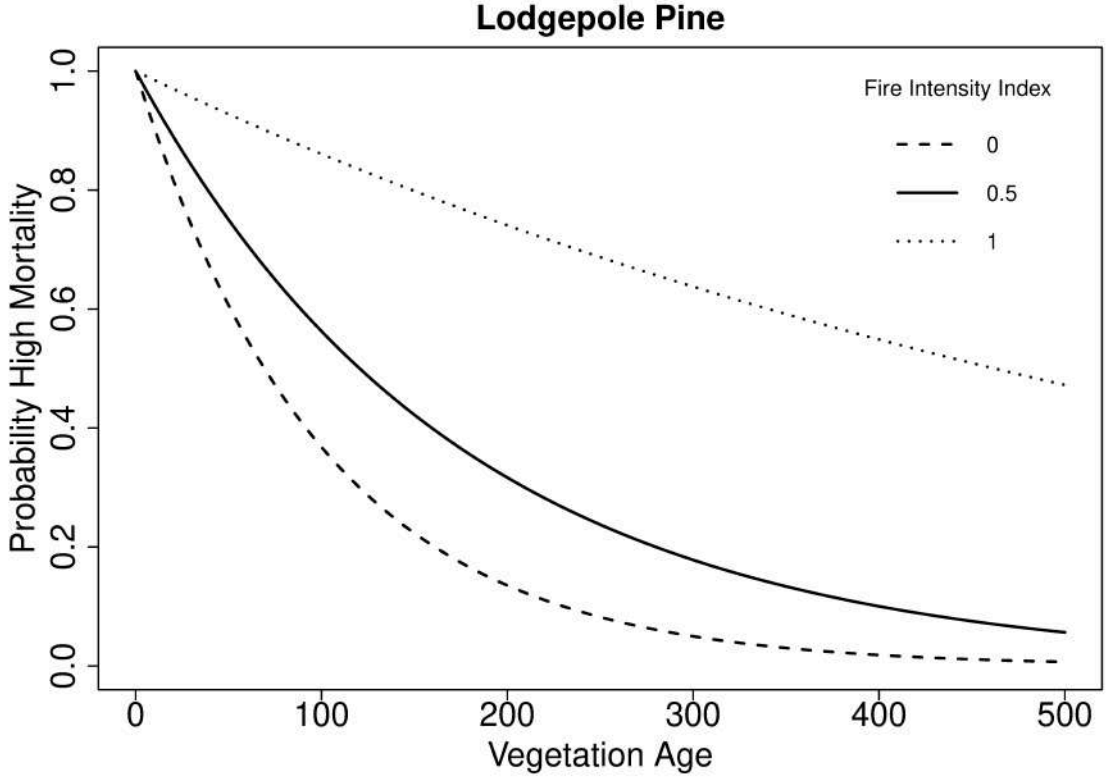
Lodgepole Pine
Fire Intensity Index
0
0.5
1
Probability High Mortality
0.0
0.2
0.4
0.6
0.8
1.0
0
100
200
300
400
500
Vegetation Age

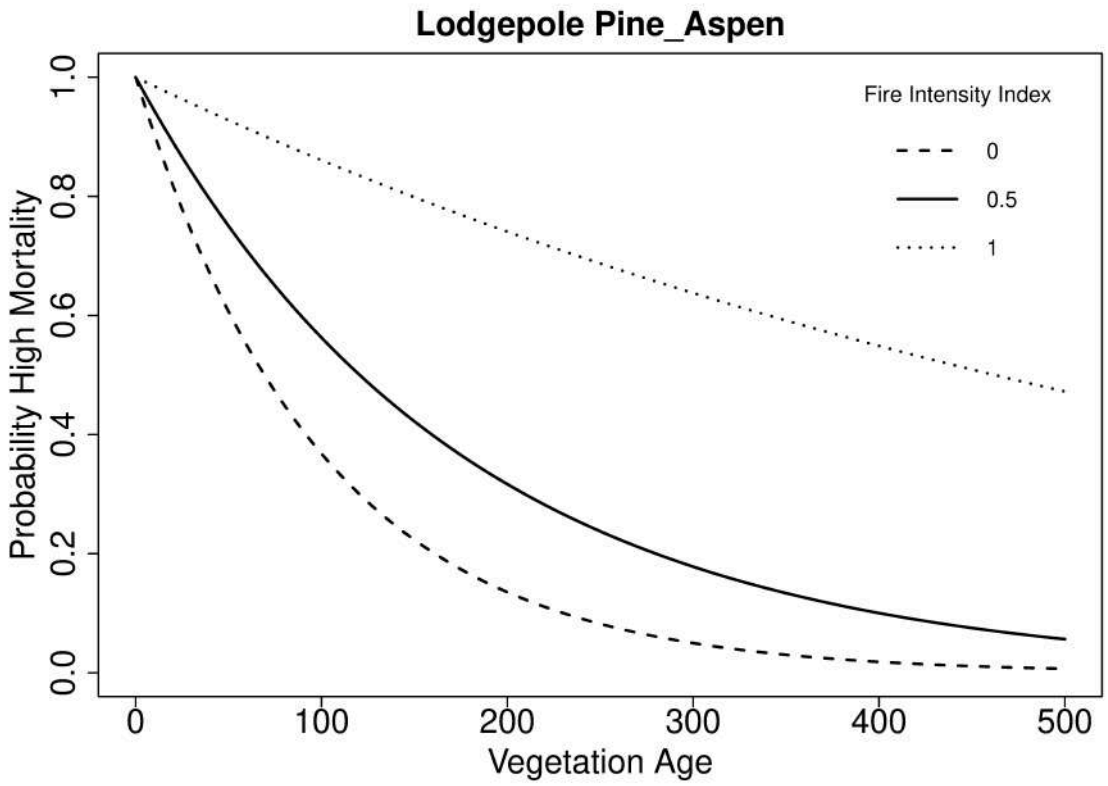
Lodgepole Pine_Aspen
Fire Intensity Index
0
0.5
1
Probability High Mortality
0.0
0.2
0.4
0.6
0.8
1.0
0
100
200
300
400
500
Vegetation Age

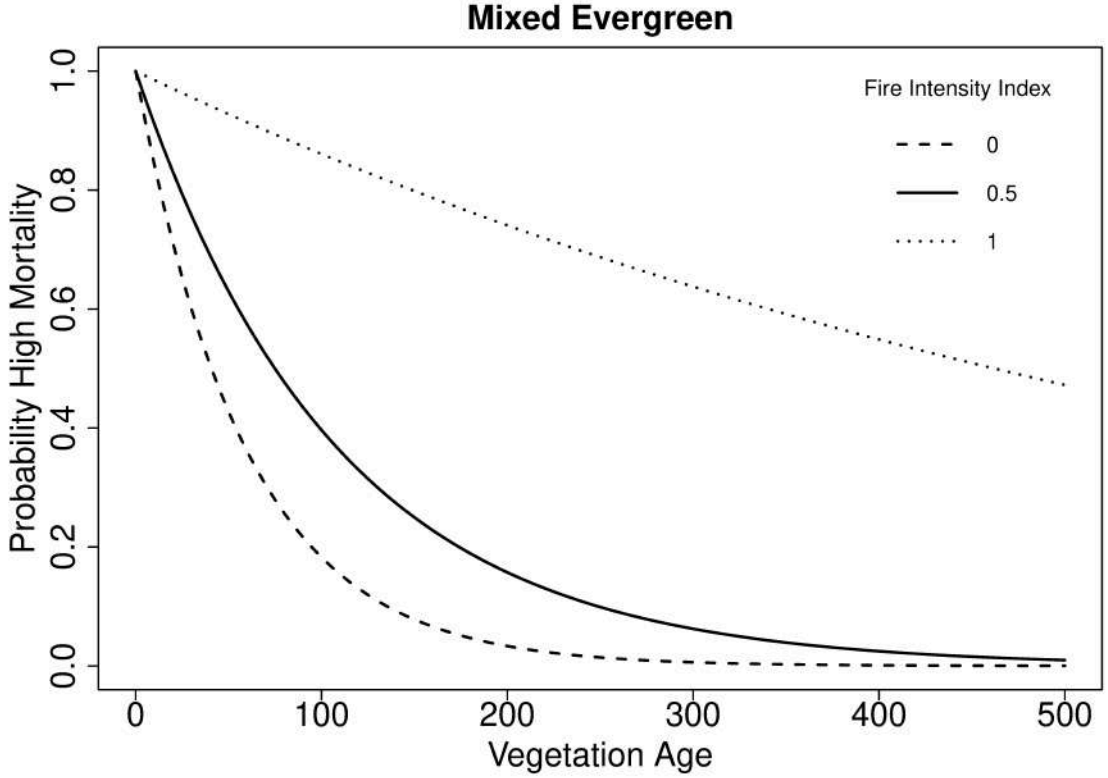
Mixed Evergreen
Fire Intensity Index
0
0.5
1
Probability High Mortality
0.0
0.2
0.4
0.6
0.8
1.0
0
100
200
300
400
500
Vegetation Age

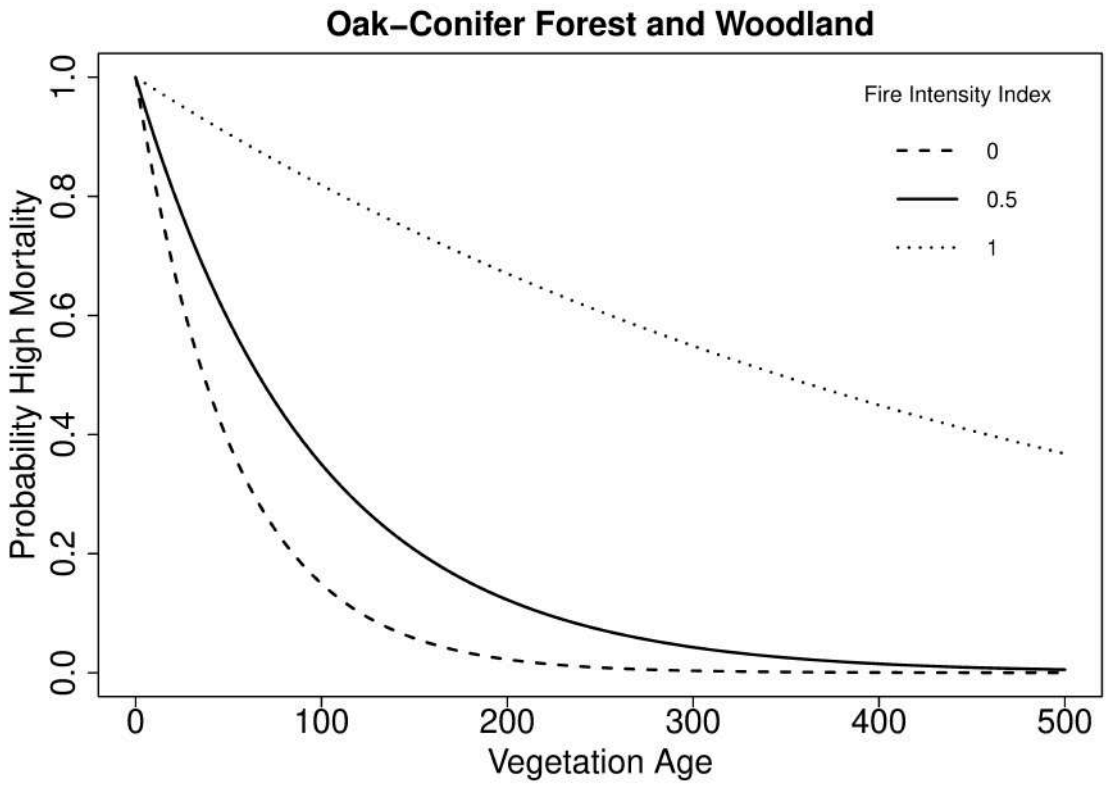
Oak–Conifer Forest and Woodland
Fire Intensity Index
0
0.5
1
Probability High Mortality
0.0
0.2
0.4
0.6
0.8
1.0
0
100
200
300
400
500
Vegetation Age

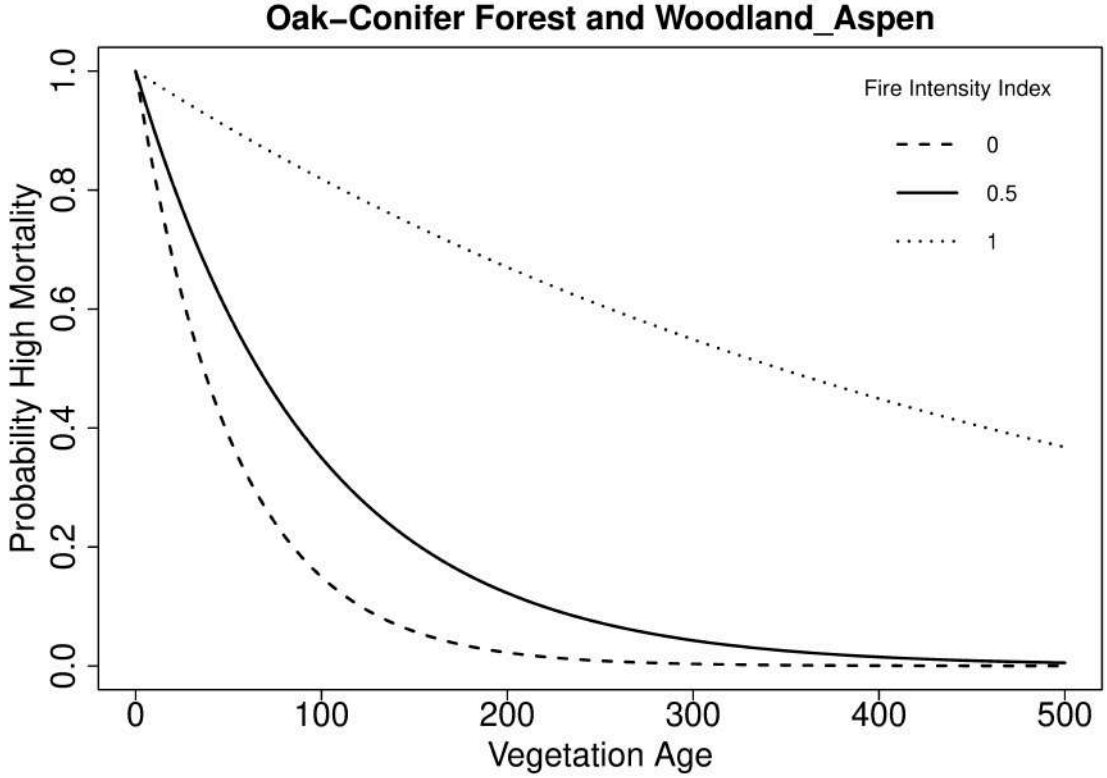
Oak–Conifer Forest and Woodland_Aspen
Fire Intensity Index
0
0.5
1
Probability High Mortality
0.0
0.2
0.4
0.6
0.8
1.0
0
100
200
300
400
500
Vegetation Age

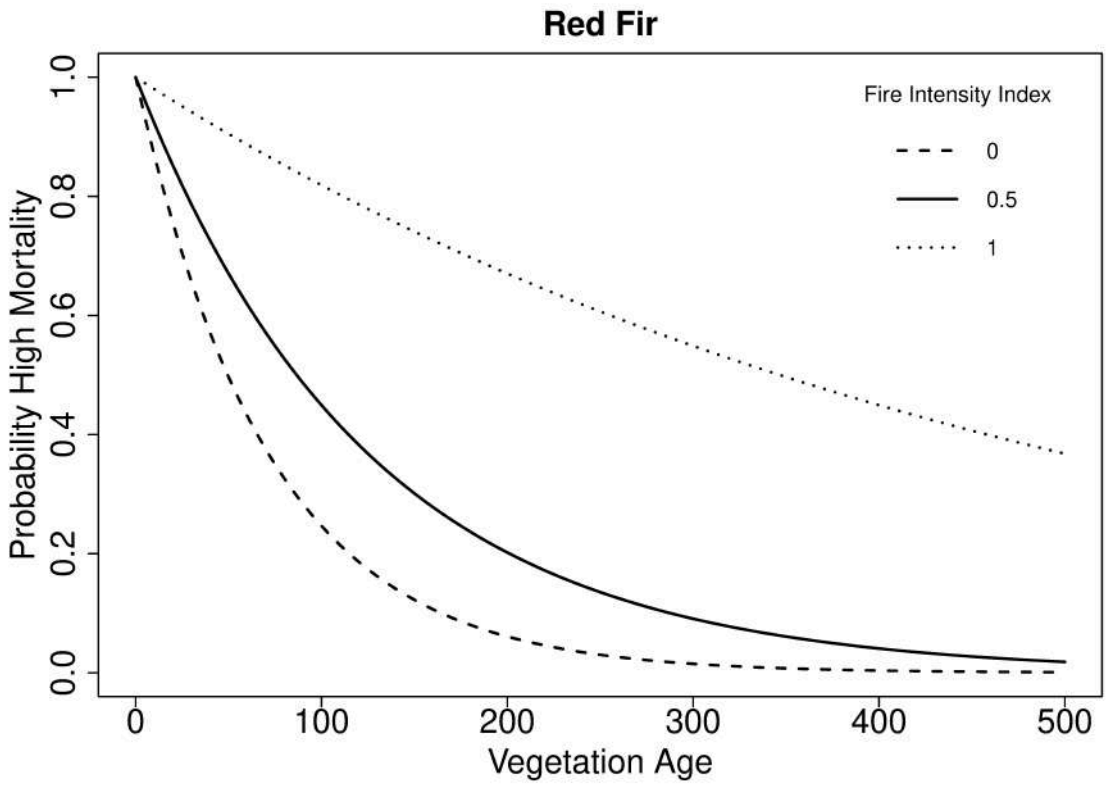
Red Fir
Fire Intensity Index
0
0.5
1
Probability High Mortality
0.0
0.2
0.4
0.6
0.8
1.0
0
100
200
300
400
500
Vegetation Age

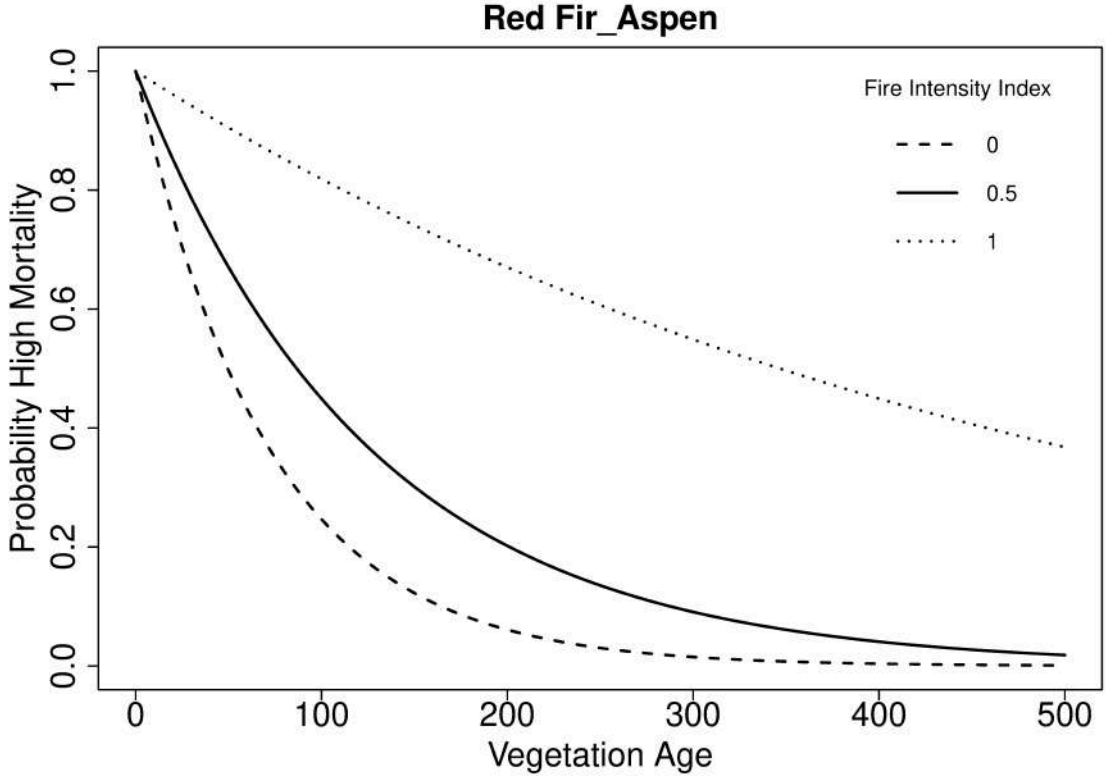
Red Fir_Aspen
Fire Intensity Index
0
0.5
1
Probability High Mortality
0.0
0.2
0.4
0.6
0.8
1.0
0
100
200
300
400
500
Vegetation Age

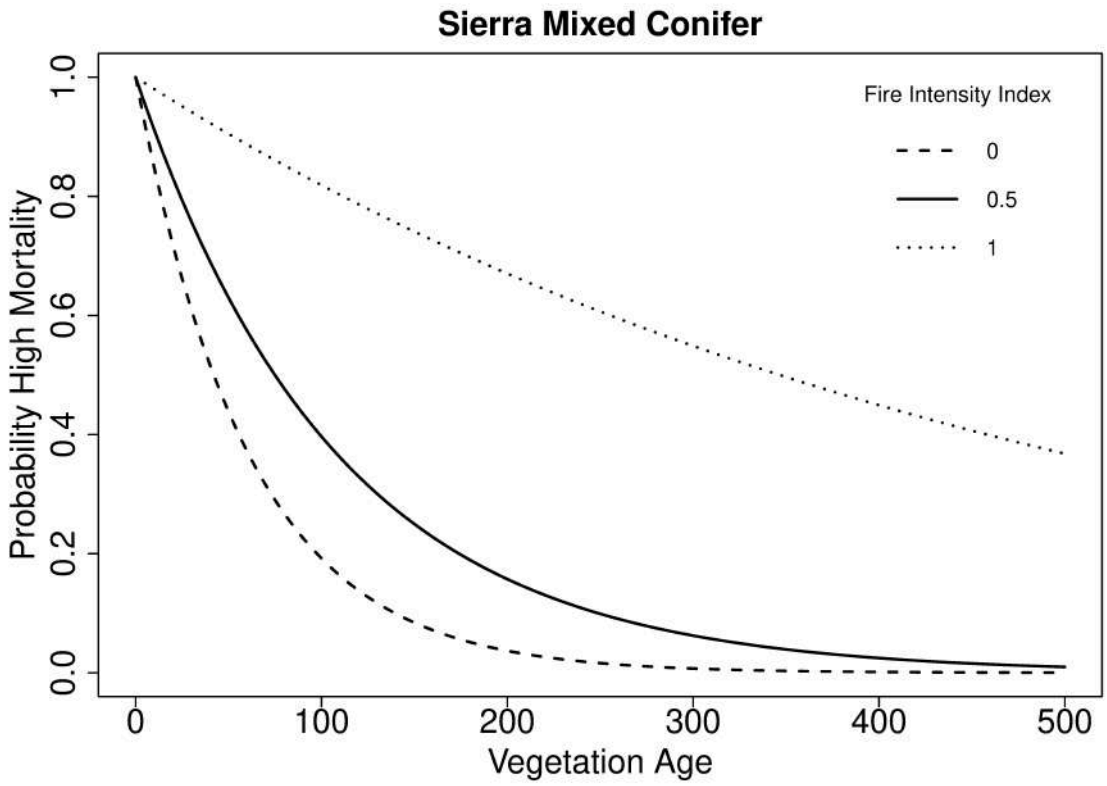
Sierra Mixed Conifer
Fire Intensity Index
0
0.5
1
Probability High Mortality
0.0
0.2
0.4
0.6
0.8
1.0
0
100
200
300
400
500
Vegetation Age

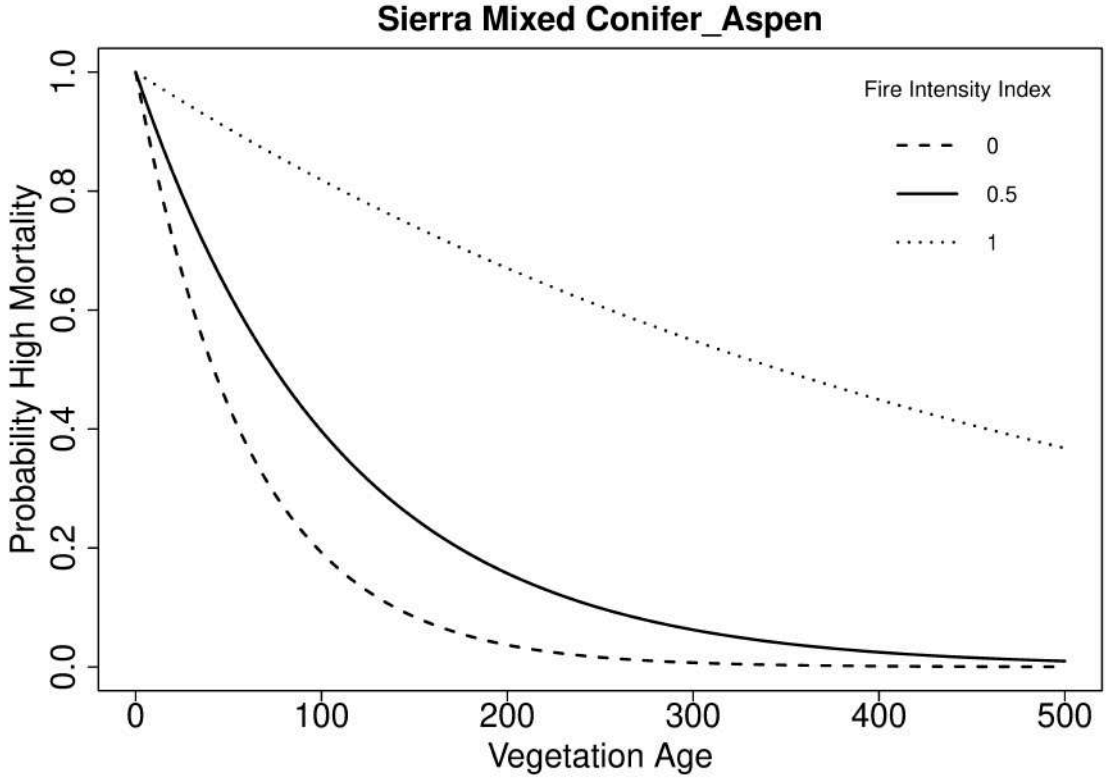
Sierra Mixed Conifer_Aspen
Fire Intensity Index
0
0.5
1
Probability High Mortality
0.0
0.2
0.4
0.6
0.8
1.0
0
100
200
300
400
500
Vegetation Age

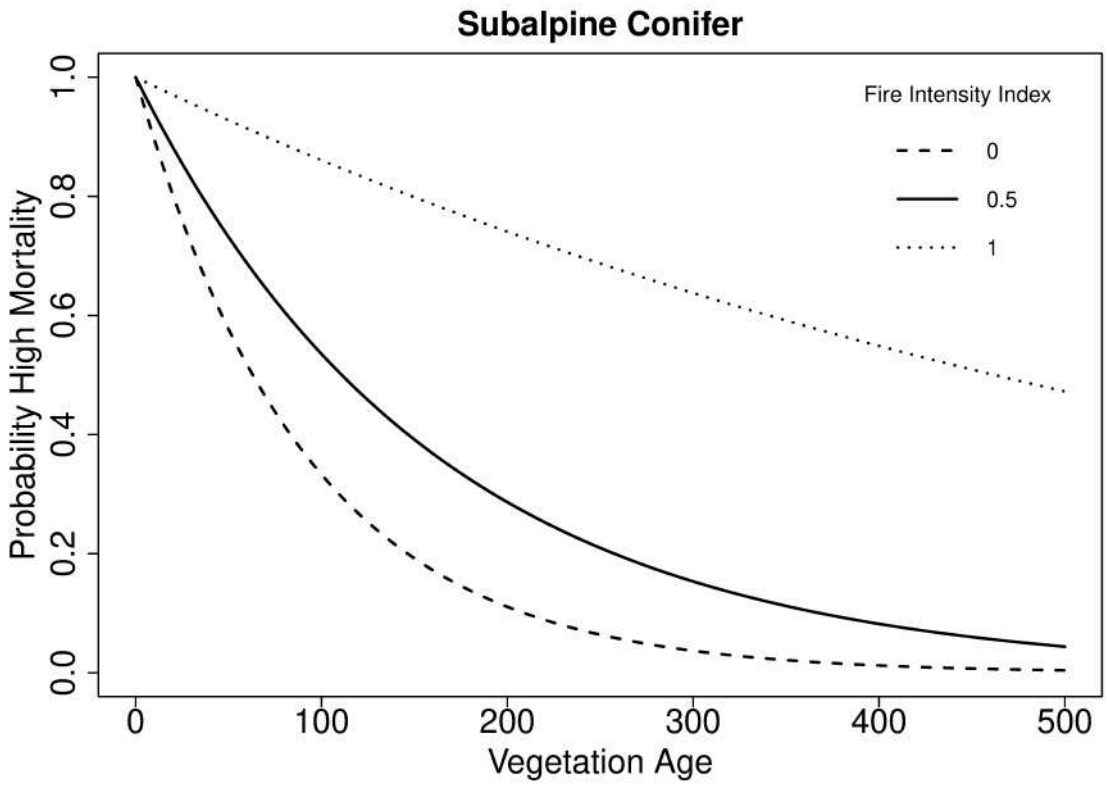
Subalpine Conifer
Fire Intensity Index
0
0.5
1
Probability High Mortality
0.0
0.2
0.4
0.6
0.8
1.0
0
100
200
300
400
500
Vegetation Age

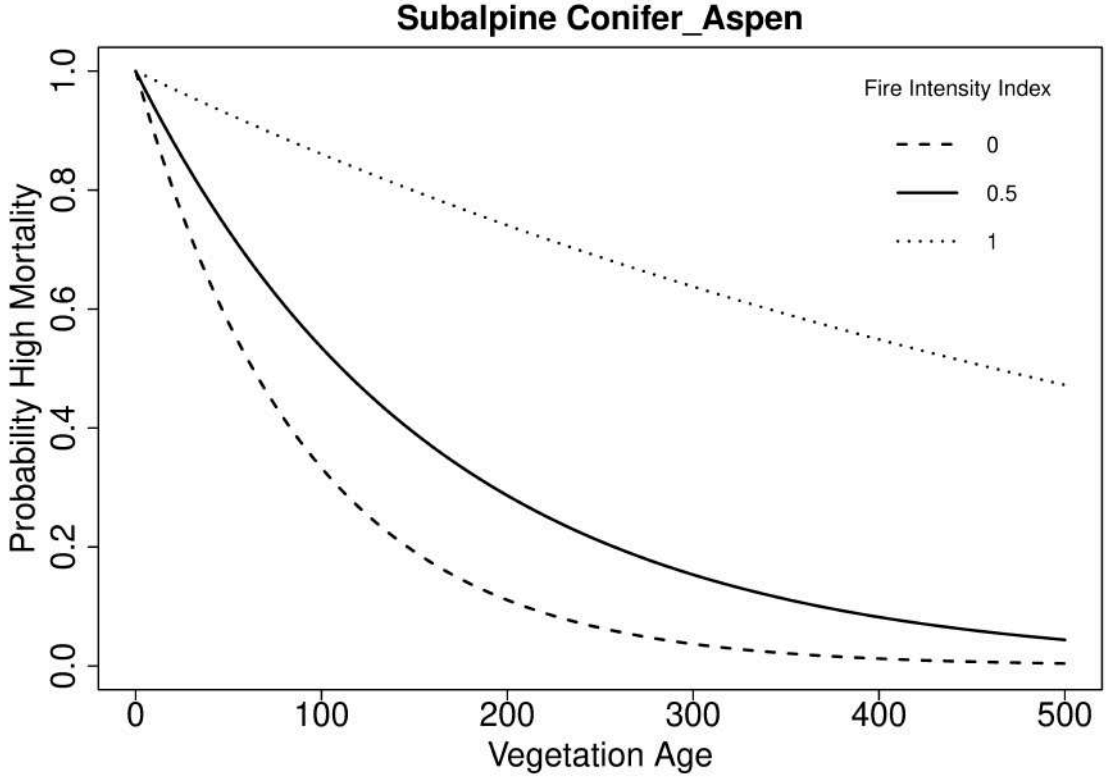
Subalpine Conifer_Aspen
Fire Intensity Index
0
0.5
1
Probability High Mortality
0.0
0.2
0.4
0.6
0.8
1.0
0
100
200
300
400
500
Vegetation Age

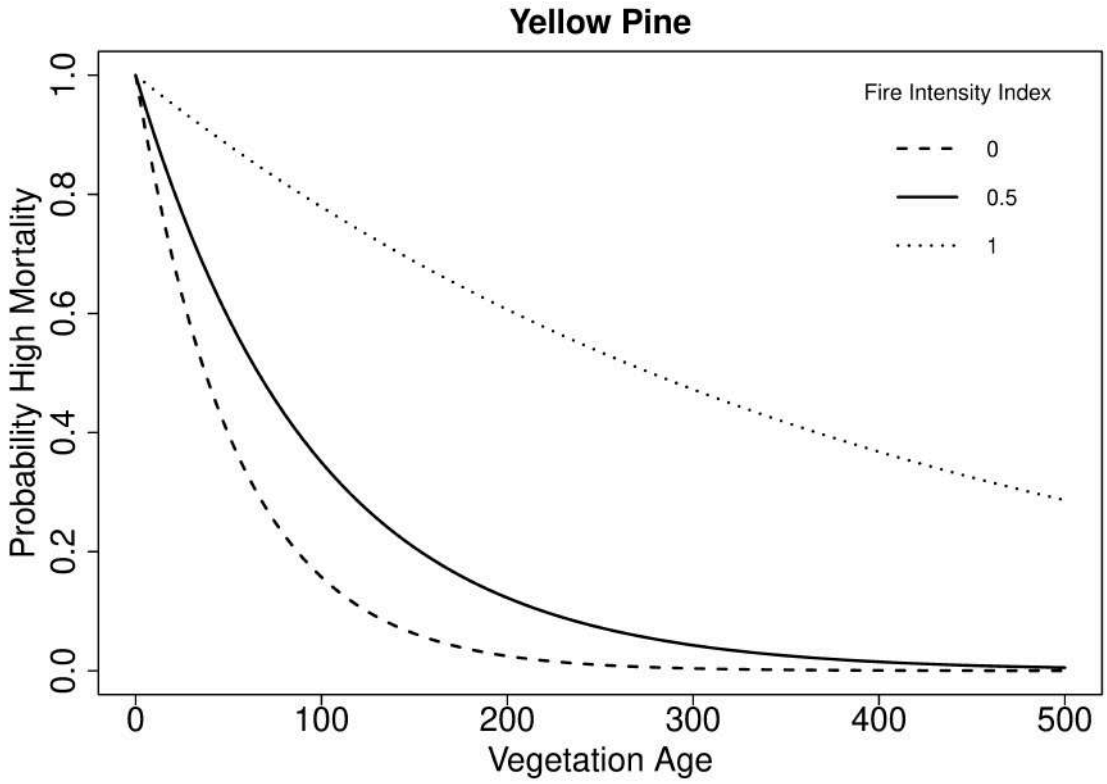
Yellow Pine
Fire Intensity Index
0
0.5
1
Probability High Mortality
0.0
0.2
0.4
0.6
0.8
1.0
0
100
200
300
400
500
Vegetation Age

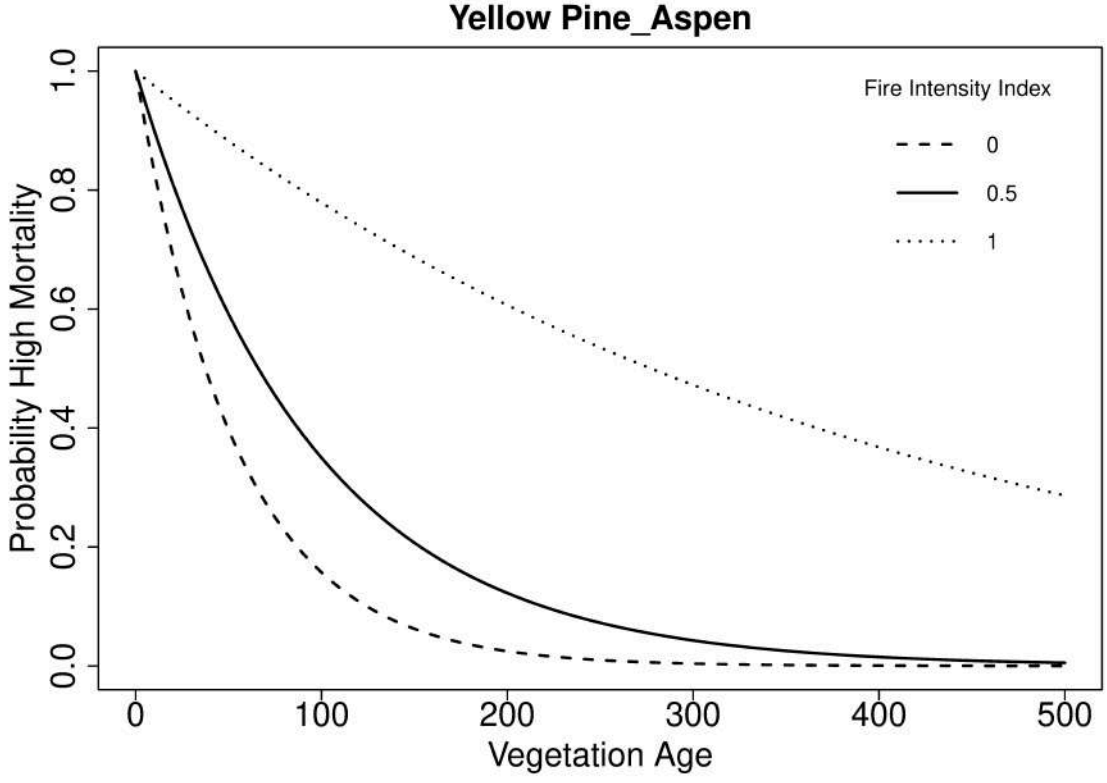
Yellow Pine_Aspen
Fire Intensity Index
0
0.5
1
Probability High Mortality
0.0
0.2
0.4
0.6
0.8
1.0
0
100
200
300
400
500
Vegetation Age

Appendix D - Lake Tahoe Basin Landscape Historical Range of Variability and Current Landscape Departure

DRAFT Report

Kevin McGarigal Becky Estes Scott Conway Danielle Perrot
Marilyn Tierney Terri Walsh Christina Liang Laurie Perrot
Edward Smith

June, 2022

Authors

- Kevin McGarigal is a landscape ecologist with Vibrant Planet, proprietor of LandEco Consulting and retired professor of landscape ecology at the University of Massachusetts, Amherst. He received a B.S. in Forestry and Wildlife from Virginia Tech, an M.S. in Wildlife Science from Oregon State University, and a Ph.D. in Forest Science from Oregon State University.
- Becky Estes is the Central Sierra Province Ecologist (Tahoe, Eldorado, Stanislaus, and Lake Tahoe Basin Management Unit), Pacific Southwest Region, USDA Forest Service. She received a Ph.D. in Forestry from Auburn University and is a Certified Ecologist with the Ecological Society of America.
- Scott Conway is the chief resilience officer with Vibrant Planet and former forest ecologist with Pacific Southwest Region, USDA Forest Service Remote Sensing Lab and Truckee District Ranger, Tahoe National Forest, Pacific Southwest Region, USDA Forest Service. He received a B.S. in Natural Resources Management from Colorado State University.
- Danielle Perrot is an applied ecologist with Vibrant Planet. She received a B.S. in Environmental Science from University of California, Los Angeles and an M.A. in Geography with a Graduate Certificate in Hydrologic Sciences from University of Colorado, Boulder.
- Marilyn Tierney is retired District Biologist for the Lake Tahoe Basin Ranger District, Tahoe National Forest, Pacific Southwest Region, USDA Forest Service. She received a B.S. in Biology and an M.A. in Biology with an emphasis in Ecology and Systematics from San Francisco State University.
- Terri Walsh is retired silviculturist for the Tahoe National Forest, Pacific Southwest Region, USDA Forest Service. She is a certified silviculturist and studied Forestry at Cal Poly San Luis Obispo.
- Christina Liang is Forest Biologist for the Tahoe National Forest, Pacific Southwest Region, USDA Forest Service. She received a Ph.D. in Ecology from University of California, Davis.
- Laurie Perrot is Forest Environmental Coordinator for the Tahoe National Forest, Pacific Southwest Region, USDA Forest Service. She received a B.S. in forestry from the University of California, Berkeley.
- Edward Smith is Senior Forest Ecologist and Fire Manager for The Nature Conservancy in California. He received a B.A. in Biology from the University of California, San Diego and a M.S. in Forestry from Northern Arizona University.

Preface

This document[1] is an appendix to the Northern Sierra Historical Range of Variability and Current Landscape Departure General Technical Report (GTR) and includes detailed results for the Lake Tahoe Basin landscape. Importantly, the background and detailed methods behind these results are presented in the GTR and not repeated here, and thus it behooves the reader to review the GTR before interpreting these results. In addition, here we present details pertaining the Landscape Disturbance-Succession Model parameterization and calibration specific to this focal landscape; all other model parameterization and calibration generalized to the Northern Sierra ecoregion is presented in the GTR. Lastly, here we present results specific to this focal landscape, but with minimal interpretation or discussion of these results or their application to management, as this was all done in the GTR. The GTR describes how to interpret the results for any of the focal landscapes and how they can be applied to management; here, we simply provide the raw results specific to this focal landscape.

Note, all datasets associated with the results for this focal landscape can be made available. Please contact Becky Estes, becky.estes@usda.gov for access.

---

[1] In accordance with Federal law and U.S. Department of Agriculture policy, this institution is prohibited from discriminating on the basis of race, color, national origin, sex, age, or disability. (Not all prohibited bases apply to all programs.) To file a complaint of discrimination, write USDA, Director, Office of Civil Rights, Room 326-W, Whitten Building, 1400 Independence Avenue, SW, Washington, DC 20250-9410 or call (202) 720-5964 (voice and TDD). USDA is an equal opportunity provider and employer.

FOCAL LANDSCAPE

The Lake Tahoe Basin landscape, as we defined it, is comprised of the Lake Tahoe Basin watershed, a HUC8 level watershed located on the eastern slopes of the Sierra Nevada Mountains in the north Sierra ecoregion (**Figure 1**). The Lake Tahoe Basin landscape encompasses 131,270 ha (although Lake Tahoe itself encompasses ~ 51,000 ha of the total landscape extent) and otherwise reflects the description of the north Sierra ecoregion presented in the general technical report.

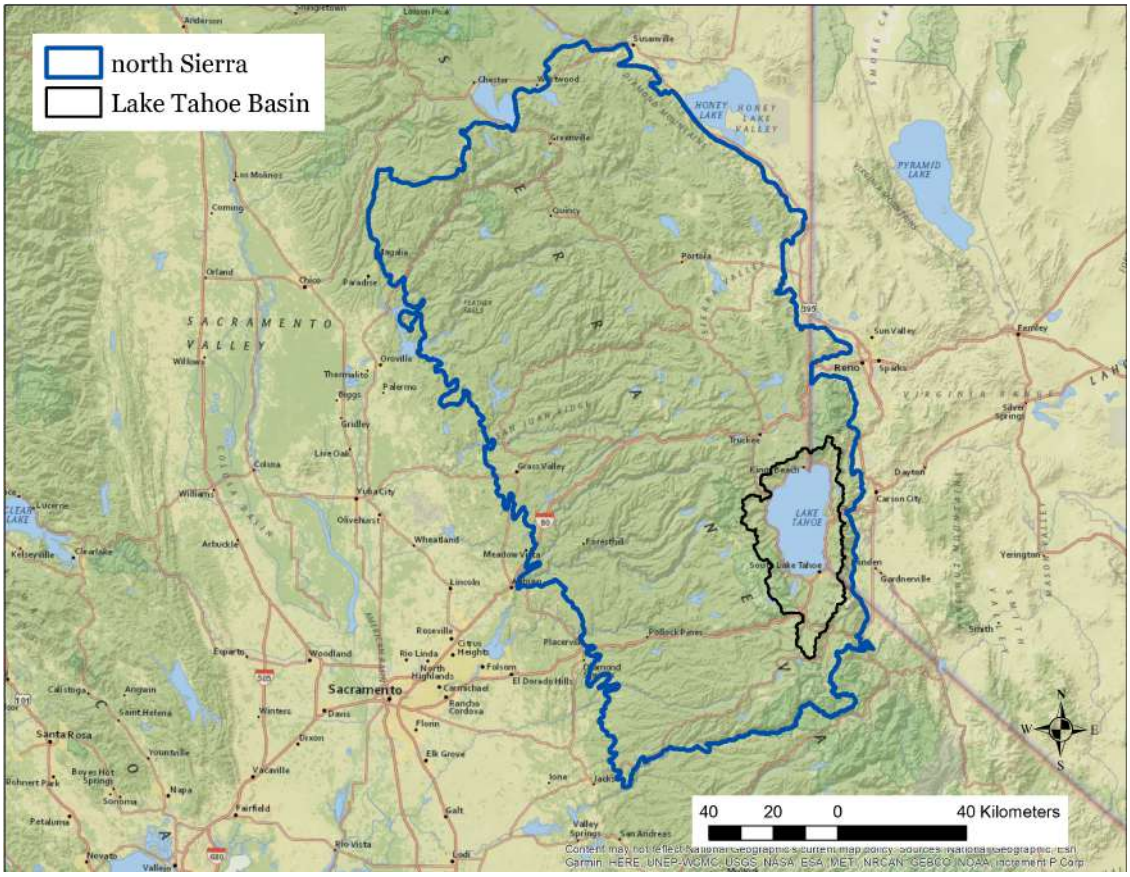

Figure 1: The Lake Tahoe Basin landscape, including the middle and north forks of the Lake Tahoe Basin, defined for the purpose of simulating wildfire disturbance and vegetation succession.

MODEL PARAMETERIZATION

In this section, we present only model parameters specific to this focal landscape; all north Sierra-wide parameters are discussed in the GTR. In addition, here we do not discuss in detail the methods and use of the model parameters in LDSim, as this was already done in the GTR. Please refer to the GTR for a full understanding of how the model parameters were used in LDSim.

Wildfire Climate

Climate conditions affecting wildfire disturbance during each timestep of the simulation were governed by a single global parameter, the Wildfire Climate Index based on the Palmer Modified Drought Severity Index

(PMDI), in which a single coefficient was assigned to each timestep of the simulation. The final Wildfire Climate Index trajectory represented a vector of coefficients, one for each timestep, as shown in **Figure 2**.

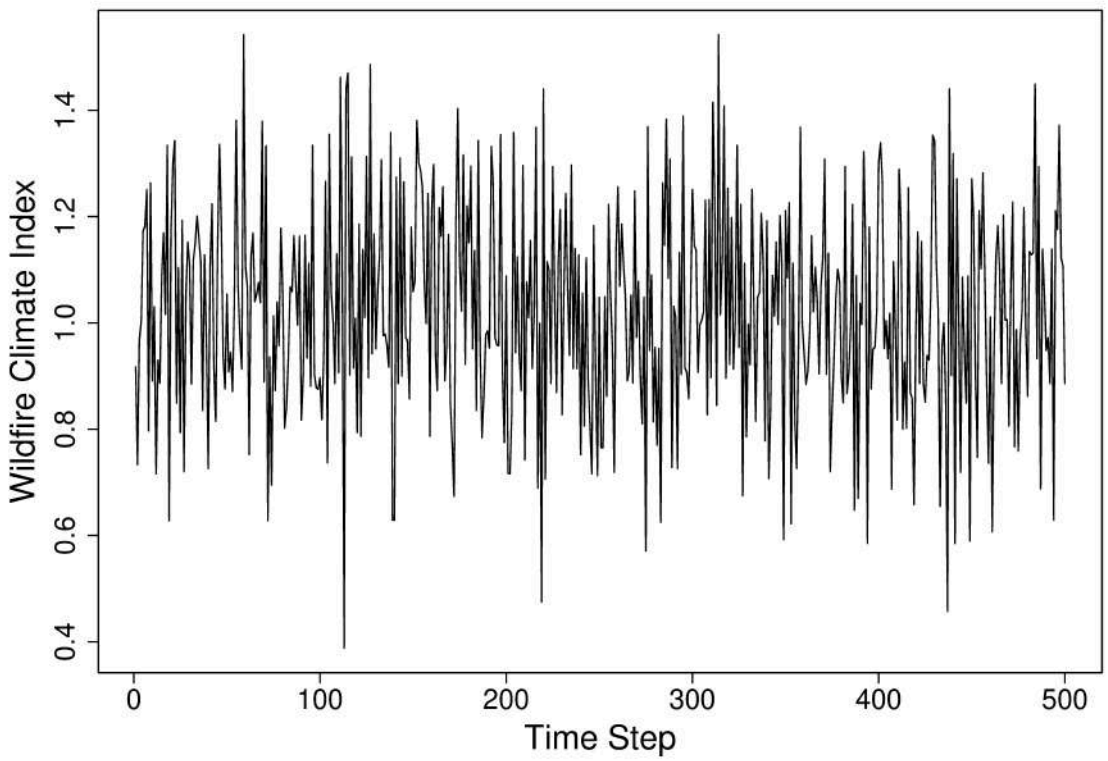

Figure 2: Wildfire Climate Index trajectory for the Lake Tahoe Basin landscape corresponding to 500 5-year timesteps in the simulation. The Climate Index was based on the inverted and rescaled 5-year averaged, inverse-distance weighted mean Palmer Modified Drought Severity Index (PMDI) for the sample point locations within the north Sierra ecoregion relative to the focal landscape (Lake Tahoe Basin watershed in this case). Note, here we inverted PMDI so that positive values represented drier conditions and negative values represented wetter conditions, and we also rescaled the index to have a standard deviation of 0.2 (see text for details).

Wildfire Susceptibility

Wildfire susceptibility for any given cell in each timestep was modeled as a complex function of fuels and climate, separately for each cover type, as described in the GTR. The final Wildfire Susceptibility Index on the probability scale (0-1) was used in the wildfire initiation and spread functions such that a value of 0 would prevent wildfires from initiating in or spreading into the cell, and as the value increased to 1 the probability of initiating a wildfire would increase as would the probability of a wildfire spreading to the focal cell from an adjacent burning cell, all other things being equal.

Briefly, we varied the beta coefficients of the wildfire susceptibility function for each cover type to reflect differences in reported historical mean fire return intervals among cover types - shifting the response curves left or right - as a means of calibrating the model to achieve target mean fire return intervals for each cover type (see Model Calibration). The calibrated wildfire susceptibility functions for each cover type are included in **Appendix D1**.

Wildfire Initiation

The number and spatial distribution of wildfire initiations in any given timestep was governed by: 1) a global wildfire initiation rate parameter that controlled the number of initiation attempts per unit area and remained constant over time; 2) the current climate conditions, as represented by the Wildfire Climate Index, that varied over time but not space; and 3) the susceptibility to wildfire, as represented by the Wildfire Susceptibility Index, that varied over both space and time. We treated the global wildfire initiation rate as a calibration parameter - shifting it up or down to increase or decrease the overall amount of realized wildfire over time - and ultimately settled on a rate of 400 attempted initiations per 100,000 ha/year. Note, this parameter affected the attempted number of wildfire initiations, not the realized number of wildfires, which was considerably less due to the vegetation and climate conditions that affected whether an attempt (i.e., lightning strike) materialized into an actual wildfire. The realized number of wildfire initiations for the Lake Tahoe Basin landscape is shown in **Figure 3**.

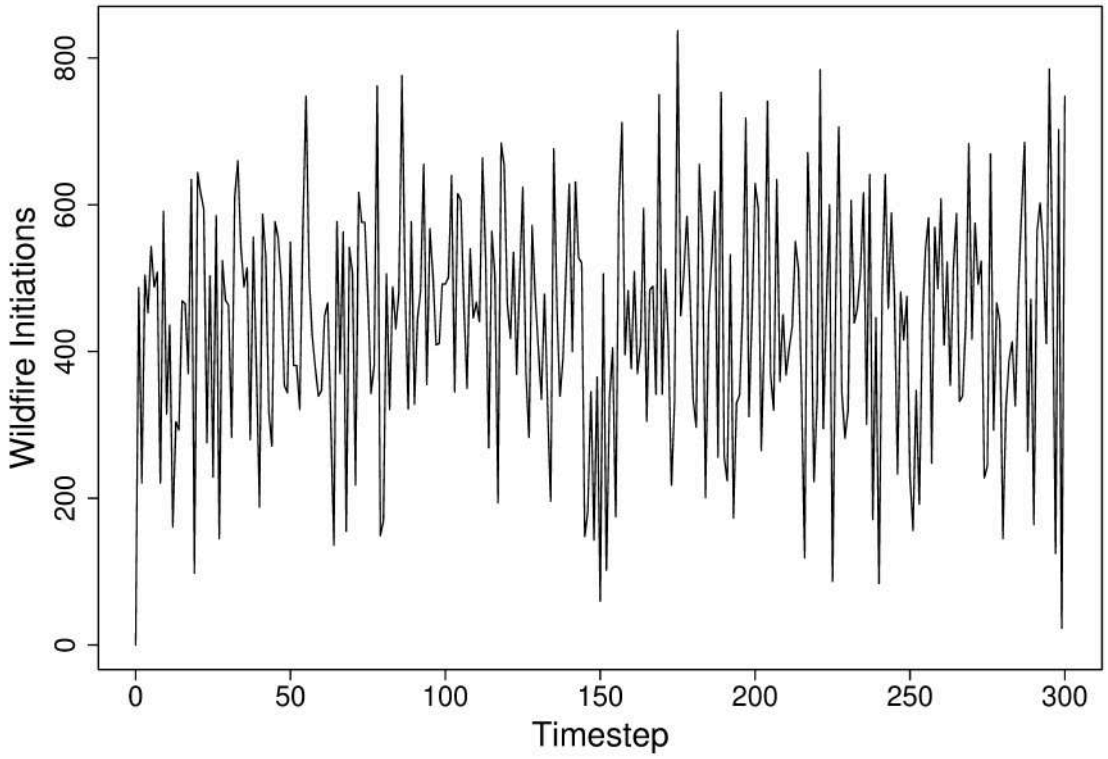

Figure 3: Realized simulated number of wildfire initiations per 5-year timestep for the Lake Tahoe Basin landscape.

Wildfire Mortality

Following the termination of a wildfire event the probability of high versus low mortality of the overstory vegetation in each 5 m cell that burned was determined by two major factors combined in a complex function as described in the general technical report: 1) fire intensity, which was a function of the fuel loads in the neighborhood of the focal cell (proxied by the age of the vegetation and time since the last fire), the topographic position of the focal cell, and the climate conditions of the current timestep; and 2) the resistance of the focal cell, which was a function of the age of the vegetation in the focal cell.

Briefly, we varied the beta coefficients of the resistance component of the complex function for each cover type to reflect differences in reported historical mean fire return intervals and high mortality rates among cover types - increasing or decreasing the rate of exponential decline in high mortality with increasing vegetation ages as a function of fire intensity - as a means of calibrating the model to achieve target high mortality rates for each cover type (see Model Calibration). The calibrated wildfire mortality functions for each cover type are included in **Appendix D2**.

Succession Climate

Climate conditions affecting vegetation succession during each timestep of the simulation were governed by a single global parameter, the Succession Climate Index based on the Palmer Modified Drought Severity Index (PMDI), in which a single coefficient was assigned to each timestep of the simulation. The final Succession Climate Index trajectory represented a vector of coefficients, one for each timestep, and is shown in **Figure 4**.

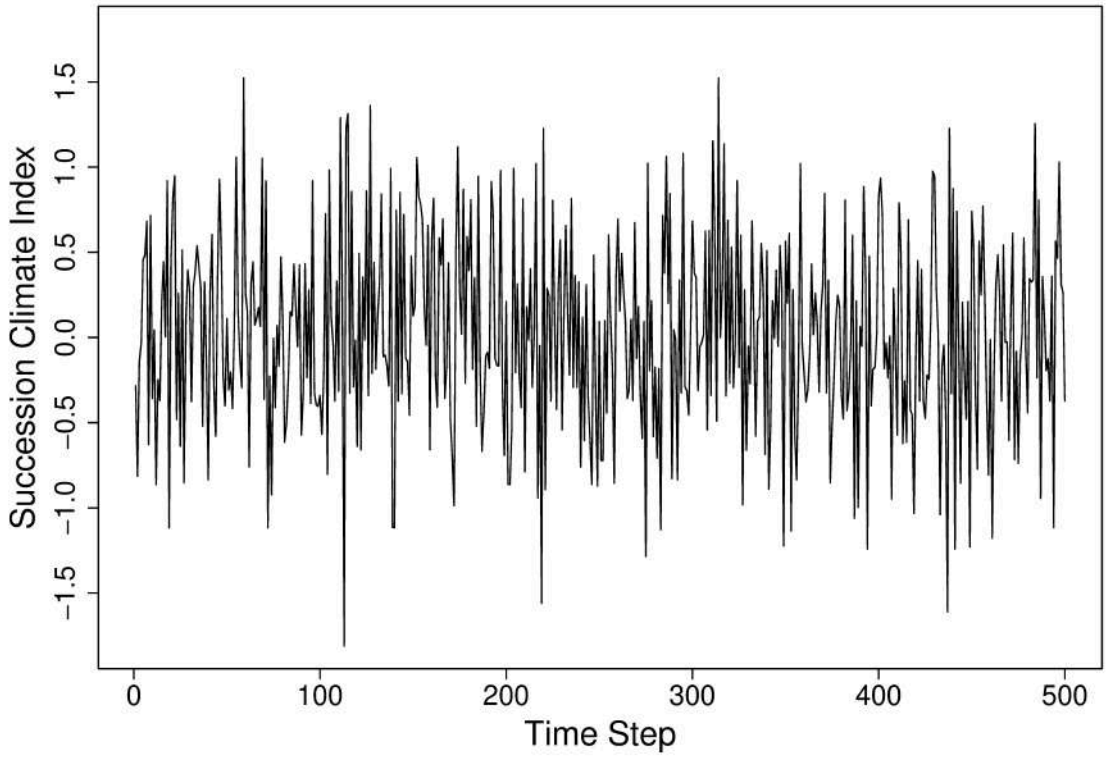

Figure 4: Succession Climate Index trajectory for the Lake Tahoe Basin landscape corresponding to 500 5-year timesteps in the simulation. The Climate Index was based on the inverted 5-year averaged, inverse-distance weighted mean Palmer Modified Drought Severity Index (PMDI) for the sample point locations within the north Sierra ecoregion relative to the focal landscape (Lake Tahoe Basin watershed in this case). Note, here we inverted PMDI so that positive values represented drier conditions and negative values represented wetter conditions (see text for details).

MODEL CALIBRATION

Although LDSim is a process-oriented model with individual parameters sourced either from data, literature, or expert opinion, the model outcomes reflect the complex spatio-temporal interactions of the various stochastic disturbance and succession processes. Consequently, it is necessary to calibrate the model by tuning (i.e., adjusting up or down) one or more of the model parameters to produce selected outcomes that are consistent with the data, literature and expert opinion. Importantly, in this context, we considered the parameters associated with the disturbance process to be "independent" variables and the vegetation conditions (e.g., seral stage distribution, spatial patterns of vegetation states, etc.) to be "dependent" outcomes. Therefore, we calibrated select disturbance parameters (i.e., independent variables) to achieve the targeted disturbance regime without any attention to the vegetation response, which we treated as the dependent outcome of the disturbance regime. Importantly, we did not tune disturbance regime parameters to achieve desired vegetation outcomes. To calibrate the model, we focused on the following five disturbance regime attributes that we considered emergent properties of the disturbance regime, as discussed in detail in the GTR.

Fire Rotation Period

Fire Rotation Period (FRP) is the number of years required to burn a cumulative area equal to the extent under consideration. FRP combines fire frequency and fire size into a single integrated measure of how much fire is actually applied to a unit of ground. FRP is equivalent to the "point-specific" or "population" mean Fire Return Interval (FRI); i.e., the average number of years between fires to a single point on the ground (or cell), and is roughly equivalent to the oft reported "grand mean" FRI computed from a large sample of point-specific intervals (e.g., from a set of fire-scarred trees).

Briefly, we tuned the global wildfire initiation rate parameter, which controlled the number of wildfire initiation attempts per unit area within each timestep and remained constant over time (see Wildfire Initiation above), and two of the wildfire susceptibility coefficients (b_0 and b_1) for each cover type, which affected the susceptibility of fire initiation and spread in each cover type (see Wildfire Susceptibility above), and measured calibration success based on agreement with the pre-specified target FRP for each cover type. We set our calibration goal as within 10% of the target FRP for forested cover types with extents > 1,000 ha. We met our calibration target for all the forest cover types with > 1,000 ha, as shown in **Table 1**.

Table 1: Target and simulated Fire Rotation Periods (FRP) for the Lake Tahoe Basin landscape.

Cover type	**Area (ha)**	**Target FRP**	**Simulated FRP**	**%Deviation**
Sierra Mixed Conifer	28340	26	25	-4
Yellow Pine	16108	20	18	-10
Red Fir	11720	50	50	0
Subalpine Conifer	6764	296	297	0
Lodgepole Pine	4824	52	52	0
Chaparral	2188	55	56	2
Grassland	681	60	61	2
Meadow	594	60	63	5
Montane Riparian	589	53	52	-2
Shrubland	333	55	57	4
Big Sagebrush	280	35	46	31
Total	73080	30	29	-3

Fire Mortality Rate

Fire mortality rate (FMR) is the percentage of burned cells that exhibit a high-mortality response (i.e., complete overstory mortality). For the purpose of model calibration, we considered the FMR only for cells in the "short", "medium" and "tall" tree developmental stages (i.e., "mature" trees) since this was the basis for specifying the target values.

Briefly, we tuned two of the wildfire mortality coefficients (b_5 and b_6) for each cover type, which affected the probability of high mortality fire as a function of age and fire intensity in each cover type (see Wildfire Mortality above), and measured calibration success based on conformity to pre-specified fire mortality targets for each cover type. We set our calibration goal as within 10% of the targets for forested cover types with > 1,000 ha in the focal landscapes. We met our calibration targets for 3 of the 5 forested cover types with > 1,000 ha, and came acceptably close for the remaining 2 cover types (note, even though the percent difference was rather large, the absolute difference was relatively minor), as shown in **Table 2**.

Table 2: Target and simulated Fire Mortality Rates (FMR) for the Lake Tahoe Basin landscape.

Cover type	**Area (ha)**	**Target FMR**	**Simulated FMR**	**%Deviation**
Sierra Mixed Conifer	28340	7	7.51	7
Yellow Pine	16108	5	5.78	16
Red Fir	11720	10	11.06	11
Subalpine Conifer	6764	10	10.92	9
Lodgepole Pine	4824	24	24.73	3

Fire Size Distribution

Fire size distribution (FSD) is the percentage of realized fire sizes across bins of increasing fire size. We opted not to tune the parameters affecting the fire size distribution as these were empirically based. Instead, we treated the realized fire size distribution as an emergent outcome of the model and measured calibration success based on agreement with the pre-specified fire distribution derived from the post-settlement period of 1908 - 1979 from which we had an empirical record. We set our calibration goal as a subjective evaluation of the realized fire size distribution compared to the target fire size distribution. We met our calibration target reasonably well, as depicted in **Figure 5**.

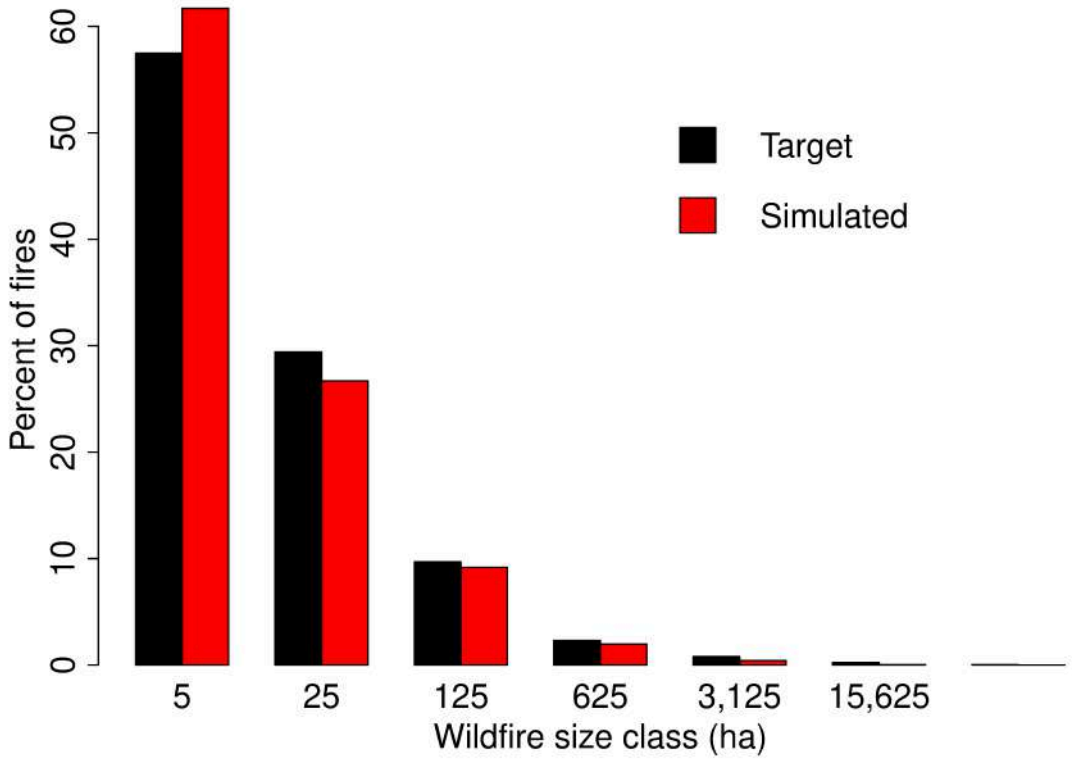

Figure 5: Target and simulated wildfire size distribution for the Lake Tahoe Basin landscape.

Variability in Total Area Burned

Variability in total area burned over time is a measure of the temporal variability in the wildfire disturbance regime. We opted not to tune the primary parameter affecting the temporal variability in total area burned - the Wildfire Climate Index - as it was empirically based. Instead, we treated the variability in total area burned as an emergent outcome of the model and measured calibration success based on agreement with the observed variability in total area burned for the post-settlement period of 1908 - 1979 from which we had an empirical record. We set our calibration goal as within 10% of the target coefficient of variation (CV) in total area burned per timestep (CV = 91.8%, see GTR). We fell just short of our calibration target for the Lake Tahoe Basin landscape, as depicted in **Figure 6**.

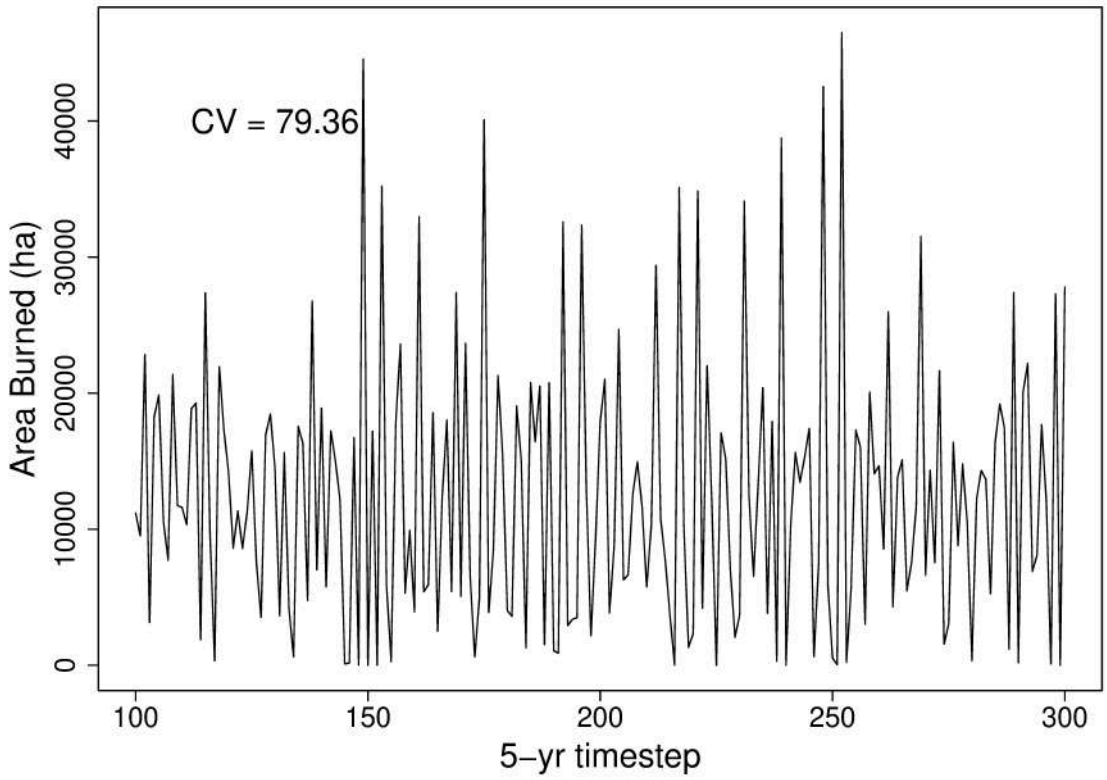

Figure 6: Total simulated area burned per 5 years in the Lake Tahoe Basin landscape representing the historical reference period of 1550-1850 and the computed Coefficient of Variation (CV).

Relationship Between Total Area Burned and Climate

The relationship between total area burned and climate is a measure of the degree to which the simulated total area burned is affected by variability in the specified Wildfire Climate Index. We opted not to tune the Wildfire Climate Index, in particular, or any parameter associated with the wildfire disturbance process with regards to this calibration metric. Instead, we treated the observed relationship between total area burned and the climate index as an emergent outcome of the model and measured calibration success based on agreement with the strength of the relationship for the post-settlement period of 1908 - 1979 from which we had an empirical record. We set our calibration goal as within 10% of the target coefficient of determination (R2) in the fit of a linear regression to the target data (R2 = 0.25, see GTR). In general, we failed to meet this calibration target closely for the Lake Tahoe Basin landscape, instead simulating a stronger relationship between total area burned and climate than we observed during the post-settlement period and simulating a distinctly non-linear relationship compared with observed post-settlement observations, as depicted in **Figure 7**.

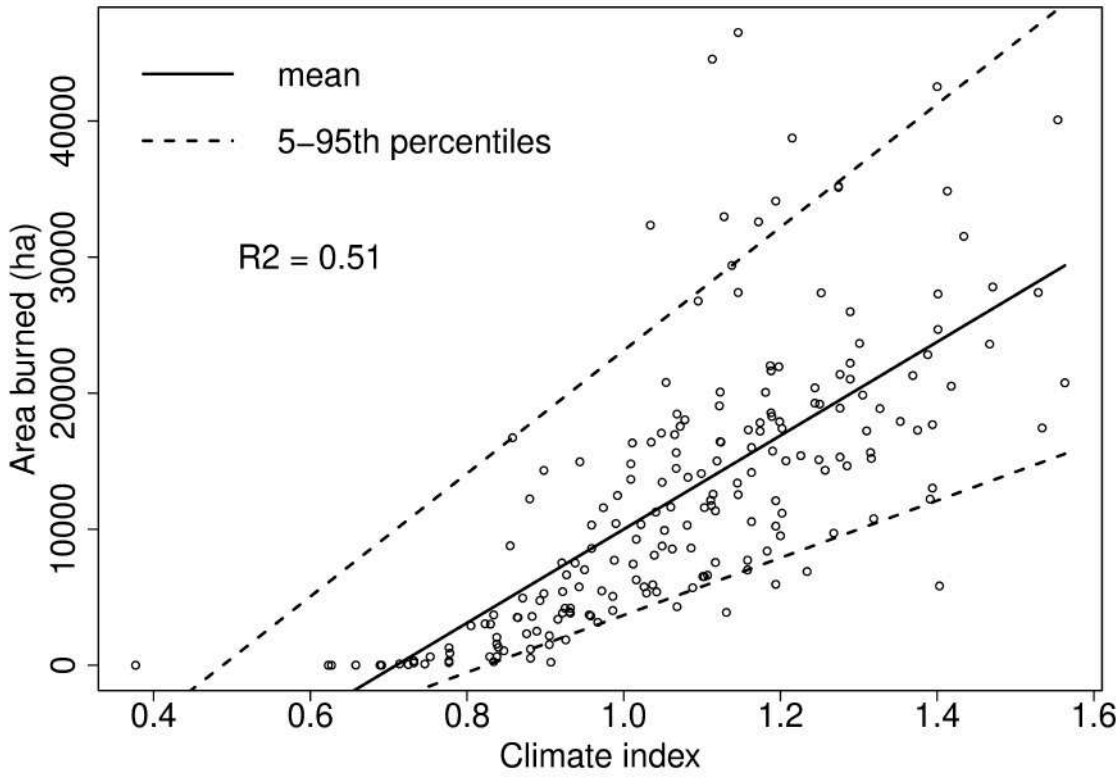

Figure 7: Scatterplot of the modified wildfire Climate Index based on the modified Palmer Drought Severity Index (see text for details) and the log of simulated total area burned per 5 years in the Lake Tahoe Basin landscape representing the historical reference period of 1550-1850, and the fitted linear regression for the mean and 5-95th quantiles (see text for details) along with the Coefficient of Determination (R2) of the fit.

HISTORICAL RANGE OF VARIABILITY and CURRENT DEPARTURE

Biophysical Classes and Units

To summarize HRV and current departure in landscape structure at the Site and Subbasin levels, we subdivided the landscape into a set of Biophysical Classes (BPCs), as described in detail in the GTR. Briefly, we indexed site productivity based on the cumulative tree biomass generated over the course of the simulation, after model equilibration, and then modeled tree biomass as a function of 10 geophysical variables using a Random Forest analytical framework, and lastly classified predicted Biomass into 4 equal-area classes based on quartiles of the data, plus a zero class for all non-forest cells. The final BPC layer included 4 classes ranging from the least productive to most productive sites, plus a non-forest class, as depicted in **Figure 8**.

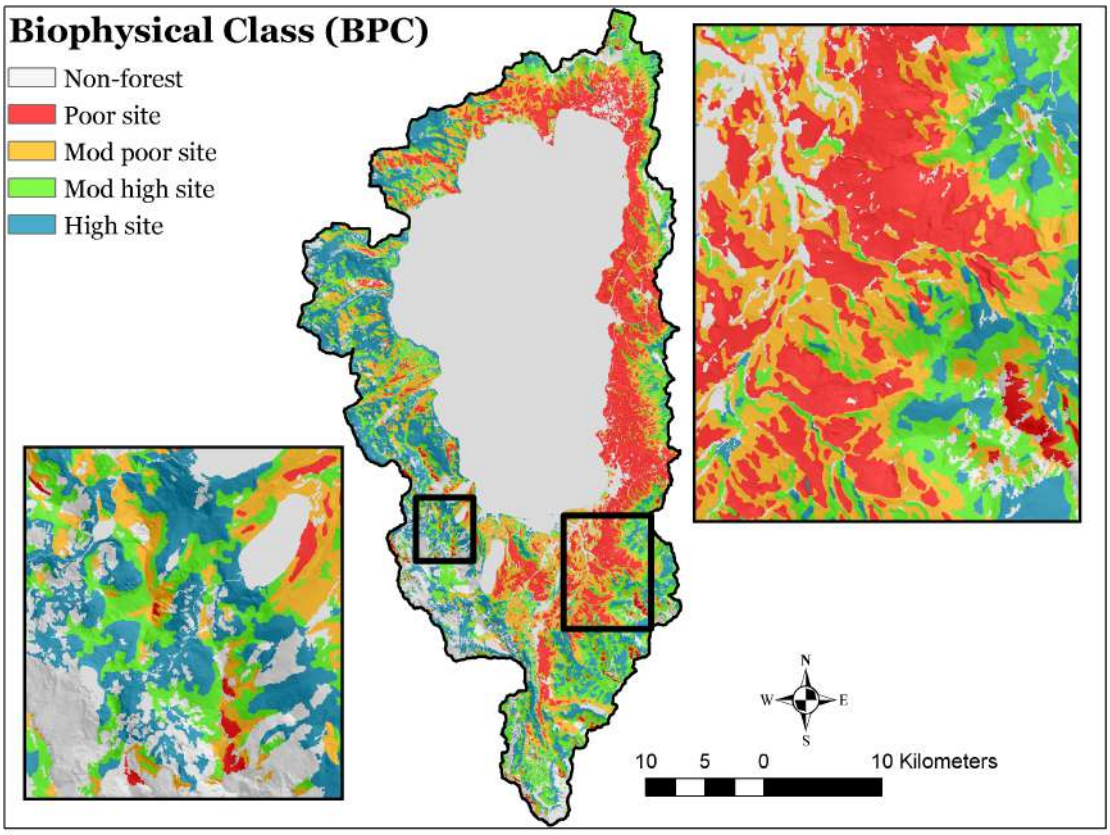

Figure 8: Biophysical Classes (BPCs) based on quartiles of predicted Biomass derived from a Random Forest model to predict Biomass (i.e., simulated cumulative tree height) from 10 biophysical variables. The Random Forest model explained ~70% of the variation in Biomass under simulated historical dynamic equilibrium conditions in the Lake Tahoe Basin landscape.

The final BPCs were distinguishable on the basis of the 10 geophysical variables and cover type, although there was considerable overlap among BPCs in each of the variables, as described below for a select set of the variables.

- *Cover Type* - The distribution of each cover type among BPCs (as a percentage of the cover type), ordered roughly from low to high elevation distributions, is given in **Table 3**. Most forest types were well distributed among BPCs, suggesting that cover type was generally not a good discriminator of BPCs. However, there were some notable exceptions. For example, Lodgepole Pine, Red Fir, and Subalpine Conifer were extremely rare on Low productivity sites; whereas, Yellow Pine was disproportionately found on Low and Moderately Low productivity sites and almost absent from High productivity sites. Sierra Mixed Conifer, the most abundant forest cover type, was relatively evenly distributed across all productivity classes.

  Table 3: Percentage of each cover type in each Biophysical Class (BPC) for the Lake Tahoe Basin landscape.

Cover type	Area (ha)	Low	ModLow	ModHigh	High
Yellow Pine	14768	59.39	25.69	9.37	5.55
Sierra Mixed Conifer	28141	24.54	33.95	18.40	23.11
Sierra Mixed Conifer_Aspen	186	7.15	47.02	26.30	19.53
Lodgepole Pine	4782	2.28	18.54	49.99	29.19
Red Fir	11689	0.71	11.49	36.47	51.33
Subalpine Conifer	6741	6.95	14.19	52.25	26.61

- *Mesic Index* - The distribution of the Mesic Index for each BPC (given as quantiles of the index) is given in **Table 4**. As expected, the Mesic Index distribution increased as the site productivity class increased from Low to High, but with considerable overlap in distributions between adjacent BPC classes. Despite the strong overlap, the BPC classes represented a gradient in expected site moisture, with the Low site class representing the driest sites and the High site class representing the wettest sites.

  Table 4: Distribution of the Mesic Index in each Biophysical Class (BPC), given as quantiles for the Lake Tahoe Basin landscape.

BPC	2.5%	25%	50%	75%	97.5%
Low	10	21	28	36	56
ModLow	22	36	43	50	67
ModHigh	21	39	46	55	70
High	26	48	56	64	80

- *Topographic Position* - The distribution of the Topographic Position Index for each BPC (given as quantiles of the index) is given in **Table 5**. Surprisingly, the Topographic Position Index distribution did not show a strong relationship with site productivity, the exception being that the High productivity class was found disproportionately on lower topographic positions.

  Table 5: Distribution of the Topographic Position Index each each Biophysical Class (BPC), given as quantiles for the Lake Tahoe Basin landscape.

BPC	2.5%	25%	50%	75%	97.5%
Low	24	42	49	58	84
ModLow	24	42	49	58	92
ModHigh	26	43	51	61	86
High	17	36	44	50	67

- *Aspect* - The distribution of aspect classes among BPCs (as a percentage of the BPC) is given in **Table 6**. Not surprisingly, each BPC class was distributed across all aspect classes, but still exhibited a pronounced orientation, with the Low site class disproportionately occupying southwesterly and westerly aspects and the High site class disproportionately occupying northeasterly aspects.

  Table 6: Percentage of each Biophysical Class (BPC) in each aspect class for the Lake Tahoe Basin landscape.

Fire Return Interval and Departure

Mean point-specific Fire Return Interval (FRI) represents the average number of years between fire events at the 5 m cell level. We interpreted the observed mean FRI after model equilibration (N = 200 timesteps)

Aspect	N	NE	E	SE	S	SW	W	NW	Flat
Low	2.63	2.62	2.39	11.16	16.44	20.16	20.33	20.06	4.21
ModLow	8.28	7.12	8.39	18.72	11.49	10.45	7.50	17.63	10.42
ModHigh	10.54	10.15	12.31	13.96	7.44	11.01	8.97	17.95	7.68
High	15.70	21.36	17.95	8.40	4.27	3.83	6.57	14.91	7.02

at the cell level as a single integrated (albeit not comprehensive) summary of the historical wildfire disturbance regime. The historical mean FRI varied from < 15 years to > 300 years across the landscape, with evident influences of both cover type and terrain (**Figure 9**).

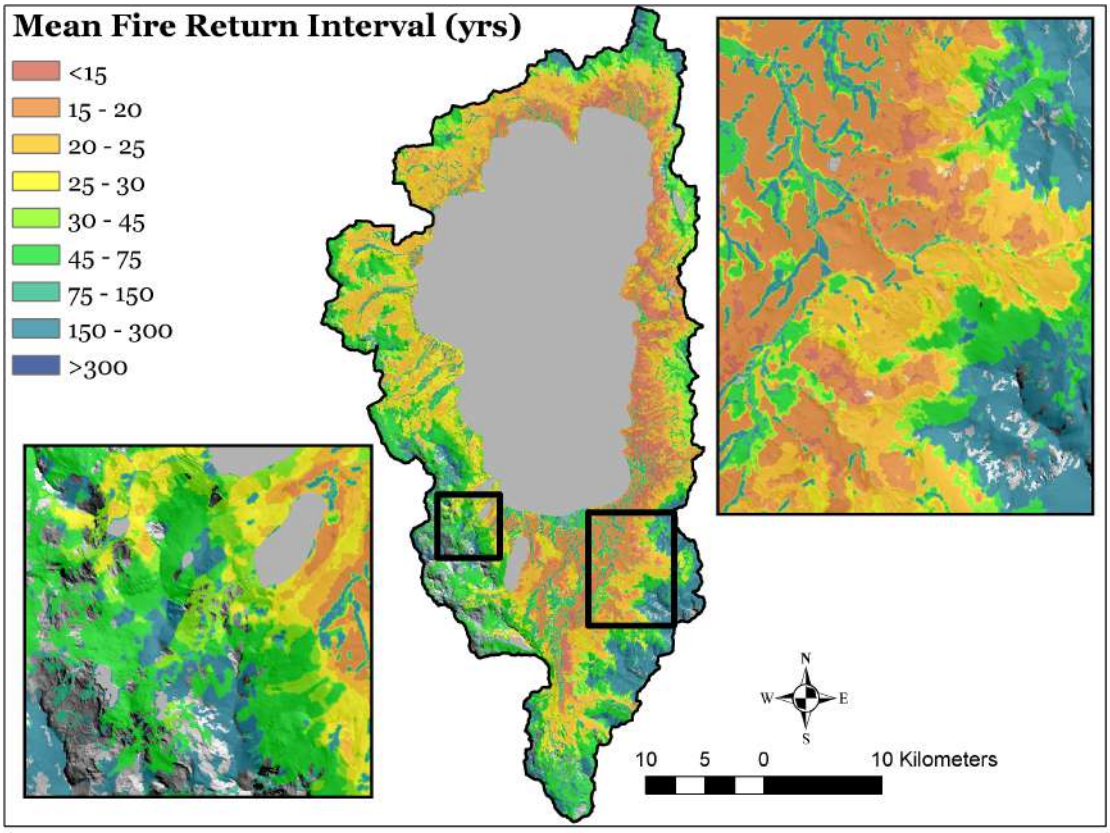

Figure 9: Simulated Fire Return Interval (FRI) (yrs) at the 5 m cell level for the Lake Tahoe Basin landscape.

In addition, the historical mean FRI varied among BPCs as expected (**Table 7**). Specifically, the median FRI increased steadily from 18 to 46 years with increasing site productivity; i.e., from Low to High BPC. Higher productivity sites that occurred disproportionately on lower slopes and valley bottoms and on northeasterly aspects were cooler and wetter and thus less susceptible to wildfire, despite having more fuel build-up over time. The relatively short median FRIs across all sites indicates that historically wildfires typically occurred frequently enough to keep surface and ladder fuel loads low enough to reduce the occurrence of high-severity wildfire.

Table 7: Range of variability (given as quantiles) in the mean fire return interval (FRI) by Biophysical Class (BPC) for the Lake Tahoe Basin landscape.

These results also indicate that the HRV in mean FRI varied several-fold across sites within each BPC. For example, on High productivity sites FRI varied more than ten-fold between 23-290 years across sites. The

BPC	HRV2.5%	HRV25%	HRV50%	HRV75%	HRV97.5%
Low	13	16	18	21	284
ModLow	17	21	24	34	299
ModHigh	19	26	46	72	299
High	23	28	46	56	290

wide range of variation in FRI within BPCs indicates that wildfire risk varied markedly across sites even within a single BPC and, consequently, that FRI is only loosely correlated with predicted cumulative tree biomass. For example, sites classified as having high long-term productivity under historical dynamic equilibrium conditions could have FRIs as short as 23 years (or shorter for the extremes) or as long as 290 years (or longer for the extremes) depending on local topographic and vegetative conditions and chance. This is visually evident in the map of mean FRI for the High site BPC (**Figure 10**).

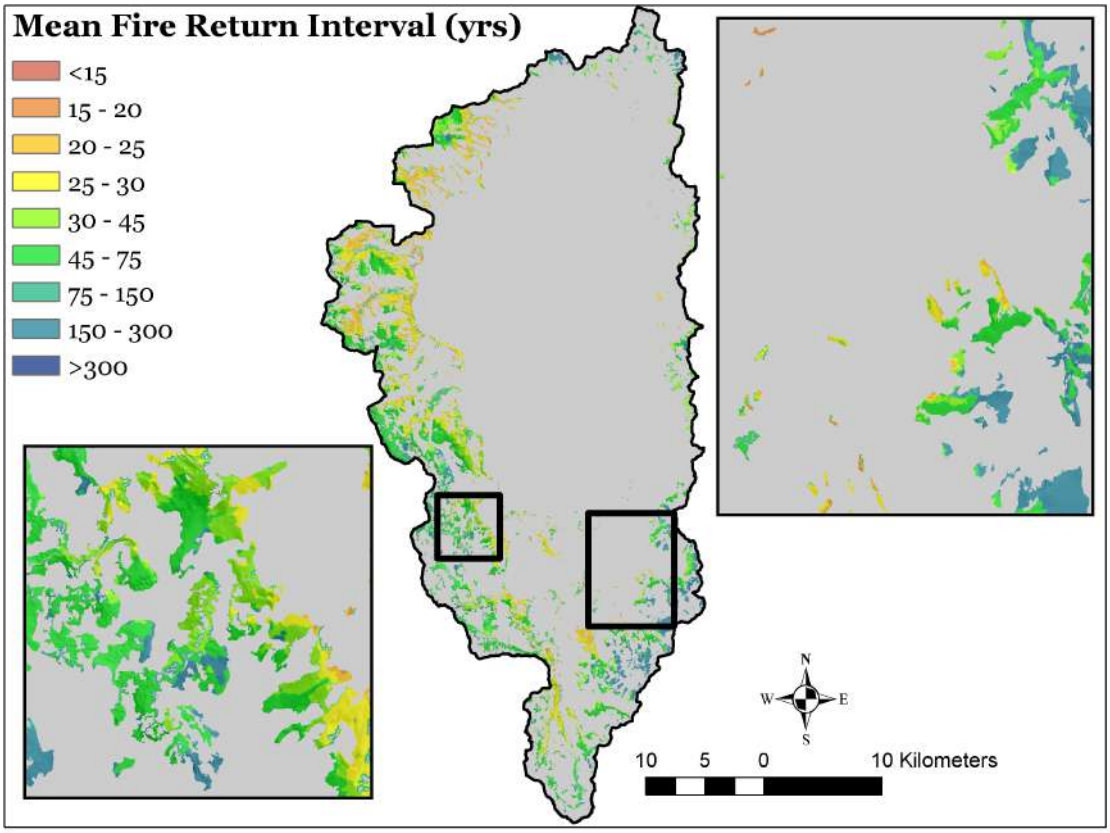

Figure 10: Simulated Fire Return Interval (FRI) (yrs) at the 5 m cell level on High productivity sites (Biophysical Class = 4) in the Lake Tahoe Basin landscape.

Fire Return Interval Departure (FRID) represents the percentage deviation of the contemporary (post-settlement) mean point-specific FRI from the mean point-specific FRI under historical (i.e., pre-settlement) dynamic equilibrium conditions. Briefly, FRID measures the degree, in percent, to which contemporary fires (i.e., since 1909) are burning at frequencies similar to the frequencies that occurred prior to significant Euro-American settlement, as simulated (**Figure 11**). Positive departure indicates that the contemporary fire frequency is less than the historical fire frequency. Not surprisingly most of the landscape is severely departed with respect to fire frequency.

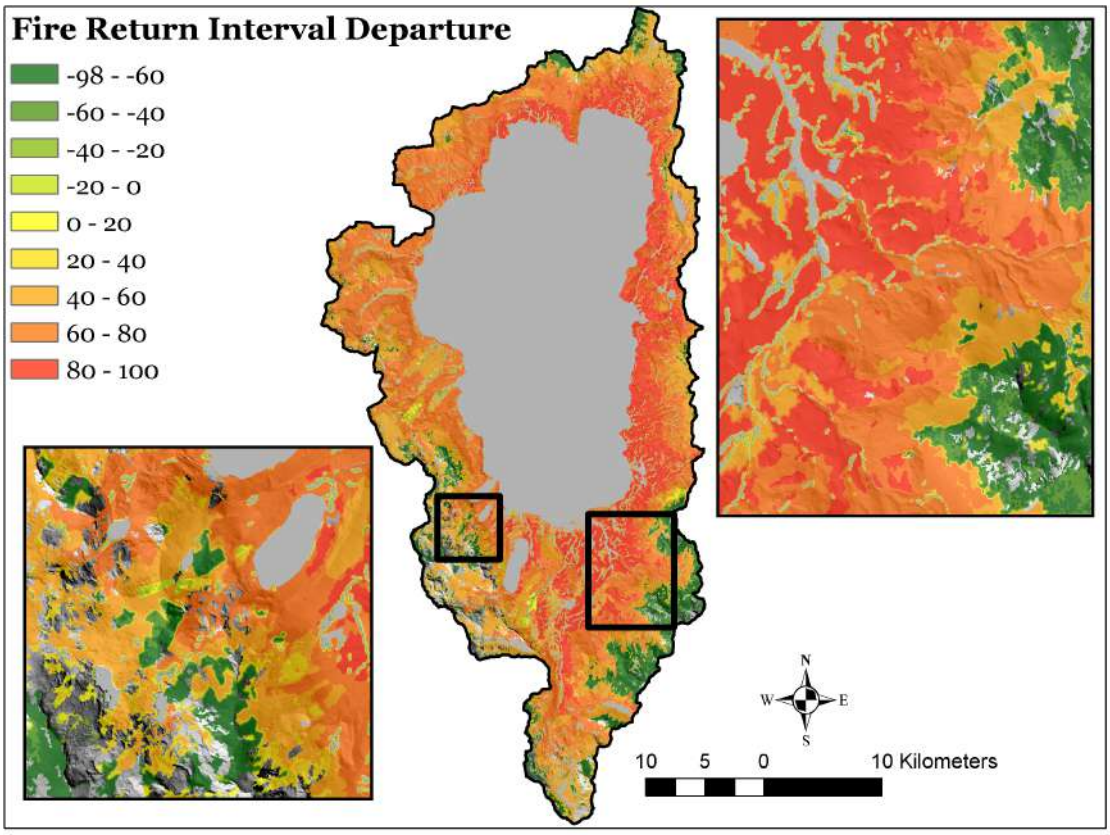

Figure 11: Fire Return Interval Departure (FRID) at the 5 m cell level in the Lake Tahoe Basin landscape, representing the percent to which contemporary fires (i.e., since 1909) are burning at frequencies similar to the frequencies that occurred prior to significant Euro-American settlement, as simulated. Positive values represent a contemporary FRI > the pre-settlement FRI and, conversely, negative values represent a contemporary FRI < the pre-settlement FRI.

In addition to the cell-level map of FRID, we also summarized the mean FRID for each GPU to include in the Stewardship Atlas as a means of prioritizing GPUs for treatment with fire (**Figure 12**).

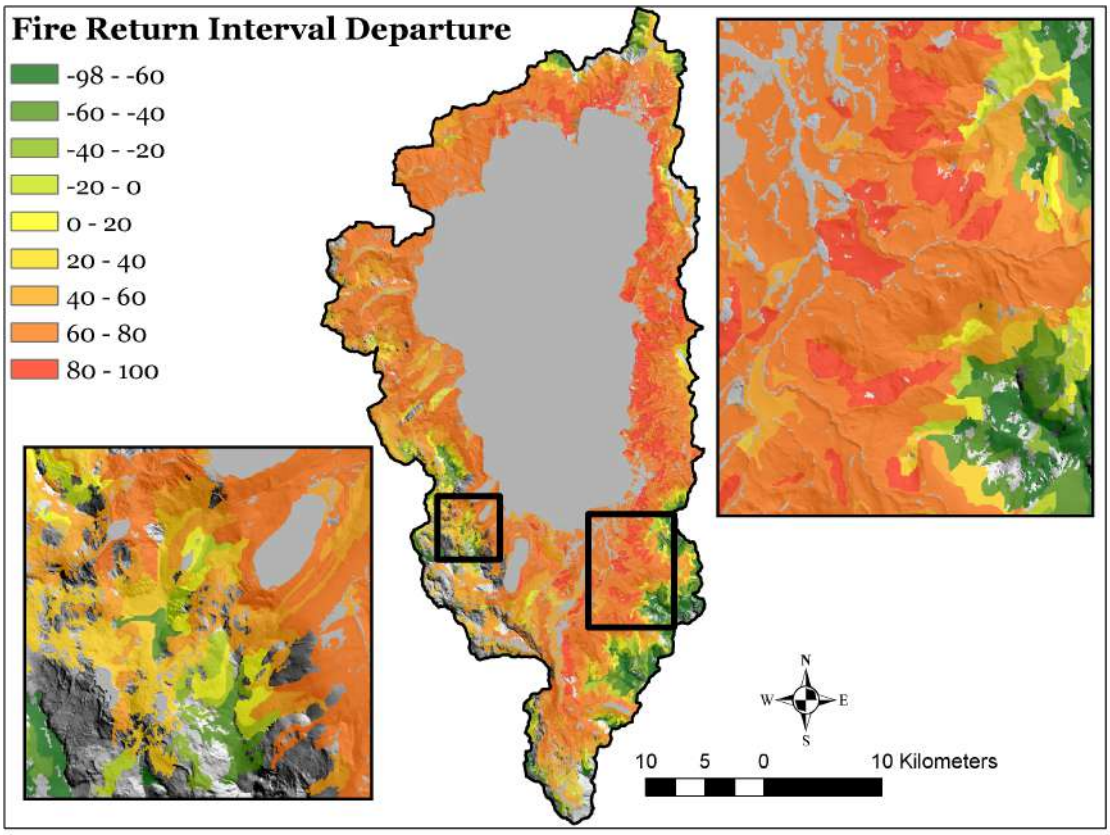

Figure 12: Geophysical Unit-level Fire Return Interval Departure (FRID) for the Lake Tahoe Basin landscape, representing the average 5 m cell value in the percent to which contemporary fires (i.e., since 1909) are burning at frequencies similar to the frequencies that occurred prior to significant Euro-American settlement, as simulated. Positive values represent a contemporary FRI > the pre-settlement FRI and, conversely, negative values represent a contemporary FRI < the pre-settlement FRI.

Vegtation Persistence

We defined vegetation persistence as the likelihood of persisting in either an early- or late-seral condition at the 5 m cell level. We interpreted the observed mean FRI of high-mortality wildfires after model equilibration (N = 200 timesteps) at the cell level as a proxy for vegetation persistence, under the assumption that locations with shorter high-mortality FRIs would likely persist longer in early-seral stages and, conversely, locations with longer high-mortality FRIs would likely persist longer in late-seral stages.

Figure 13 depicts several areas with relatively long high-mortality FRIs (dark blue areas in the map) and these are sites that have a high likelihood of supporting late-seral vegetation under a natural disturbance regime. Conversely, the map depicts several areas with relatively short high-mortality FRIs (yellow and orange areas in the map) and these are sites that have a high likelihood of supporting early-seral vegetation much of the time under a natural disturbance regime. Accordingly, management objectives for these areas could be designed to capitalize on these focal areas. For example, establishing treatment objectives to maintain and enhance late-seral conditions for old forest associated species in areas with a lower likelihood of high-mortality wildfire (i.e., longer FRI) would be logical.

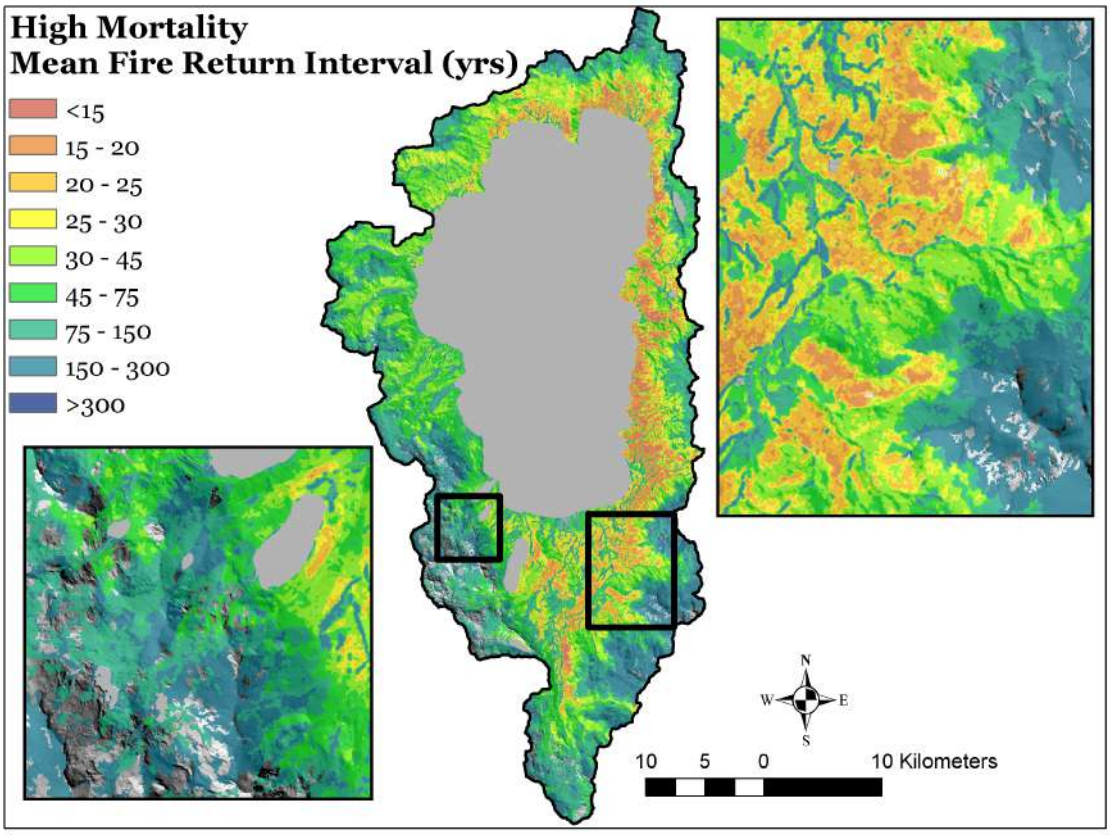

Figure 13: Simulated high-mortality Fire Return Interval (FRI) (yrs) at the 5 m cell level in the Lake Tahoe Basin landscape.

Site-level HRV and Departure

The results presented in this section address landscape metrics quantified at the "Site" level. Recall from the GTR that we defined a Site as a 40-m radius window around each focal cell. Here, each Site falls within a single BPC based on the location of the focal cell and has a single value computed for each landscape metric for each point in time (i.e., snapshot). HRV represents the variation in the landscape metric across Sites and over time under historical dynamic equilibrium conditions. Further recall that the current landscape also has a range of values across Sites (CRV), rather than a single value. Thus, a comparison of the HRV and CRV distributions depicts the degree to which CRV deviates from HRV (i.e., current departure). It is important to remember that Site-level departure reflects the deviation between the CRV across Sites within the focal landscape and the HRV across Sites and over time within the focal landscape. Thus, departure for a Site is not based on a comparison of the current Site condition to its own HRV (as is the case with GPU and Subbasin departure, see below); rather it is the distribution of current Site conditions across the entire landscape compared to the historical distribution across Sites that forms the basis for Site-level departure.

Recall from the GTR that we used a parsimonious suite of landscape metrics that we deemed meaningful for estimating departure at the Site-level across the focal landscape and appropriate given the available data, and computed departure as described in the GTR (and not repeated here), including the following metrics:

Metric 1: Developmental Stage

Developmental stage at the Site level was based on discrete stages of canopy height development. We quantified the composition of forest developmental stages at the Site level based on the percentage of the forested portion of the Site in each developmental stage. The HRV and CRV in Developmental Stage composition by BPC at the Site level is given in **Table 8** and depicted in **Figure 14**.

Table 8: Range of variability (given as quantiles) in each developmental stage class across sites (40-m radius window centered on each focal cell) by Biophysical Class (BPC) for the current range of variability (CRV) and the historical range of variability (HRV) for the Lake Tahoe Basin landscape.

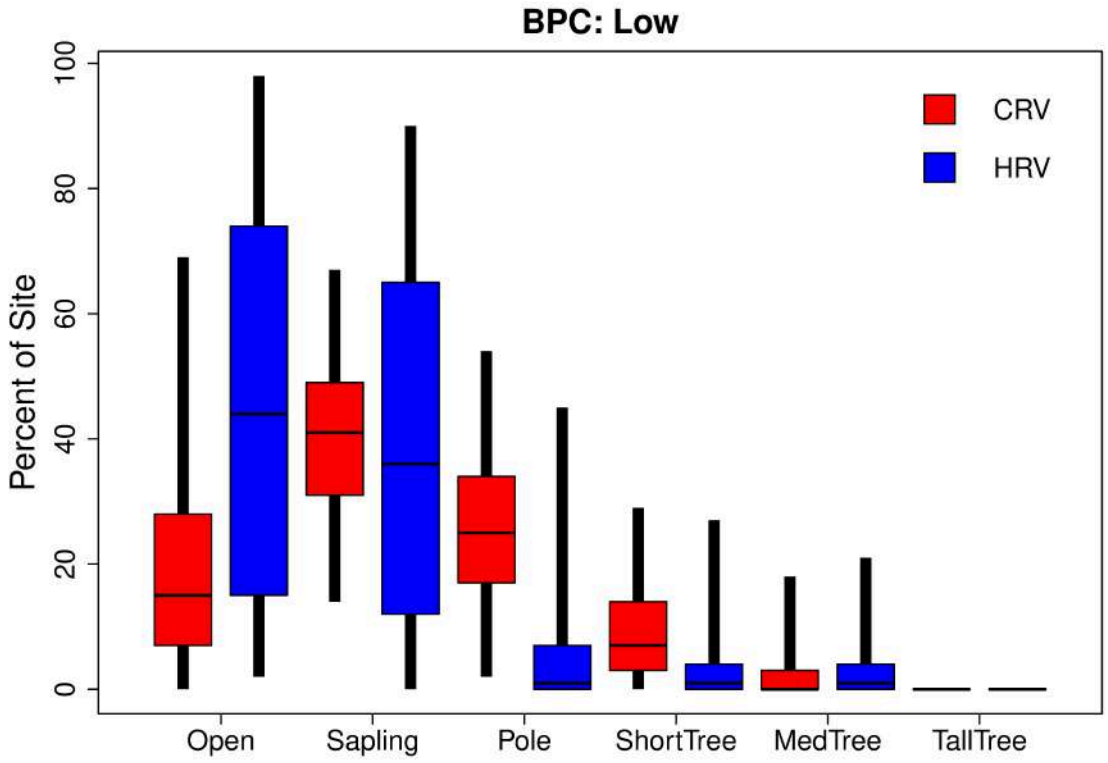

BPC	Class	Scenario	HRV 2.5%	HRV 25%	HRV 50%	HRV 75%	HRV 97.5%
Low	Open	CRV	0	7	15	28	69
Low	Open	HRV	2	15	44	74	98
Low	Sapling	CRV	14	31	41	49	67
Low	Sapling	HRV	0	12	36	65	90
Low	Pole	CRV	2	17	25	34	54
Low	Pole	HRV	0	0	1	7	45
Low	ShortTree	CRV	0	3	7	14	29
Low	ShortTree	HRV	0	0	1	4	27
Low	MedTree	CRV	0	0	0	3	18
Low	MedTree	HRV	0	0	1	4	21
Low	TallTree	CRV	0	0	0	0	0
Low	TallTree	HRV	0	0	0	0	0
ModLow	Open	CRV	0	6	15	29	76
ModLow	Open	HRV	1	7	21	48	88
ModLow	Sapling	CRV	11	29	39	48	69
ModLow	Sapling	HRV	0	15	34	57	86
ModLow	Pole	CRV	0	16	25	34	53
ModLow	Pole	HRV	0	2	7	18	60
ModLow	ShortTree	CRV	0	3	8	15	33
ModLow	ShortTree	HRV	0	1	4	11	45
ModLow	MedTree	CRV	0	0	1	4	20
ModLow	MedTree	HRV	0	2	6	14	41
ModLow	TallTree	CRV	0	0	0	0	0
ModLow	TallTree	HRV	0	0	0	0	7
ModHigh	Open	CRV	0	7	17	34	81
ModHigh	Open	HRV	1	6	16	36	74
ModHigh	Sapling	CRV	10	30	39	48	72
ModHigh	Sapling	HRV	0	7	24	44	78
ModHigh	Pole	CRV	0	13	24	32	51
ModHigh	Pole	HRV	0	3	10	23	62
ModHigh	ShortTree	CRV	0	1	7	15	32
ModHigh	ShortTree	HRV	0	2	8	19	55
ModHigh	MedTree	CRV	0	0	0	3	18
ModHigh	MedTree	HRV	0	6	13	23	51
ModHigh	TallTree	CRV	0	0	0	0	0
ModHigh	TallTree	HRV	0	0	0	0	11
High	Open	CRV	0	4	12	28	78
High	Open	HRV	0	4	10	26	67
High	Sapling	CRV	9	27	36	46	67
High	Sapling	HRV	0	5	19	37	73
High	Pole	CRV	0	16	25	34	51
High	Pole	HRV	0	4	11	24	61
High	ShortTree	CRV	0	4	11	19	35
High	ShortTree	HRV	0	3	8	18	52
High	MedTree	CRV	0	0	1	6	27
High	MedTree	HRV	1	10	20	32	60
High	TallTree	CRV	0	0	0	0	1
High	TallTree	HRV	0	0	0	6	32

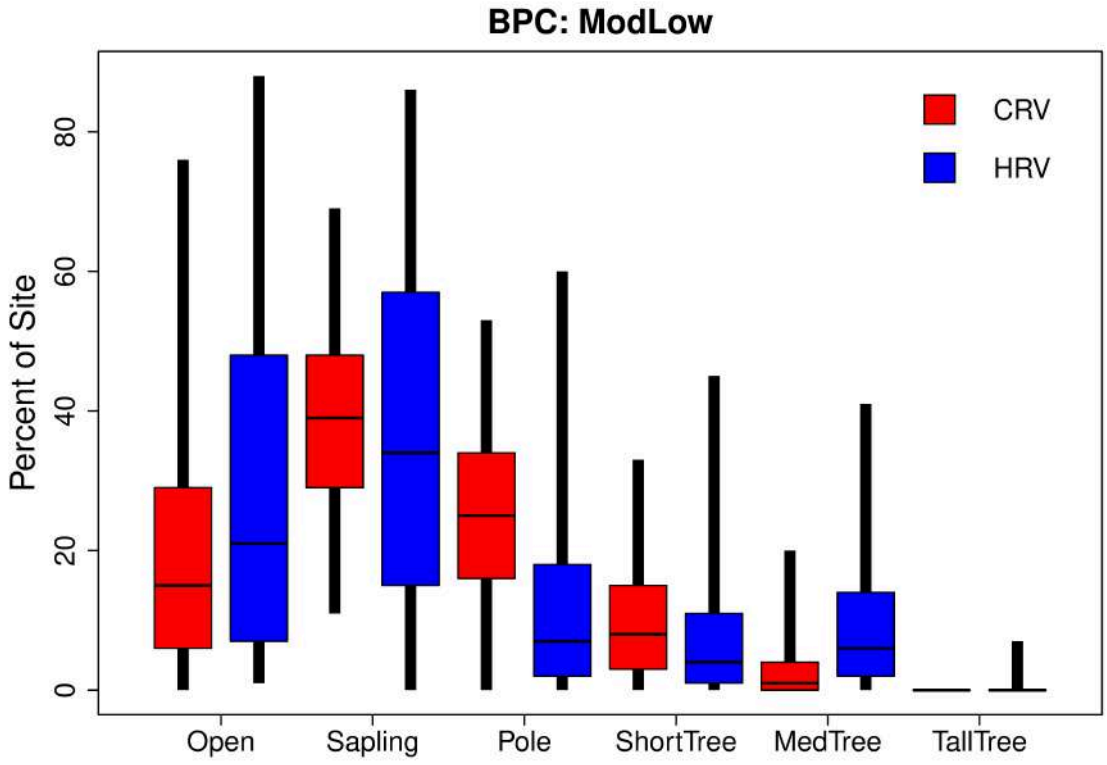
BPC: ModLow
Percent of Site
0
20
40
60
80
CRV
HRV
Open
Sapling
Pole
ShortTree
MedTree
TallTree

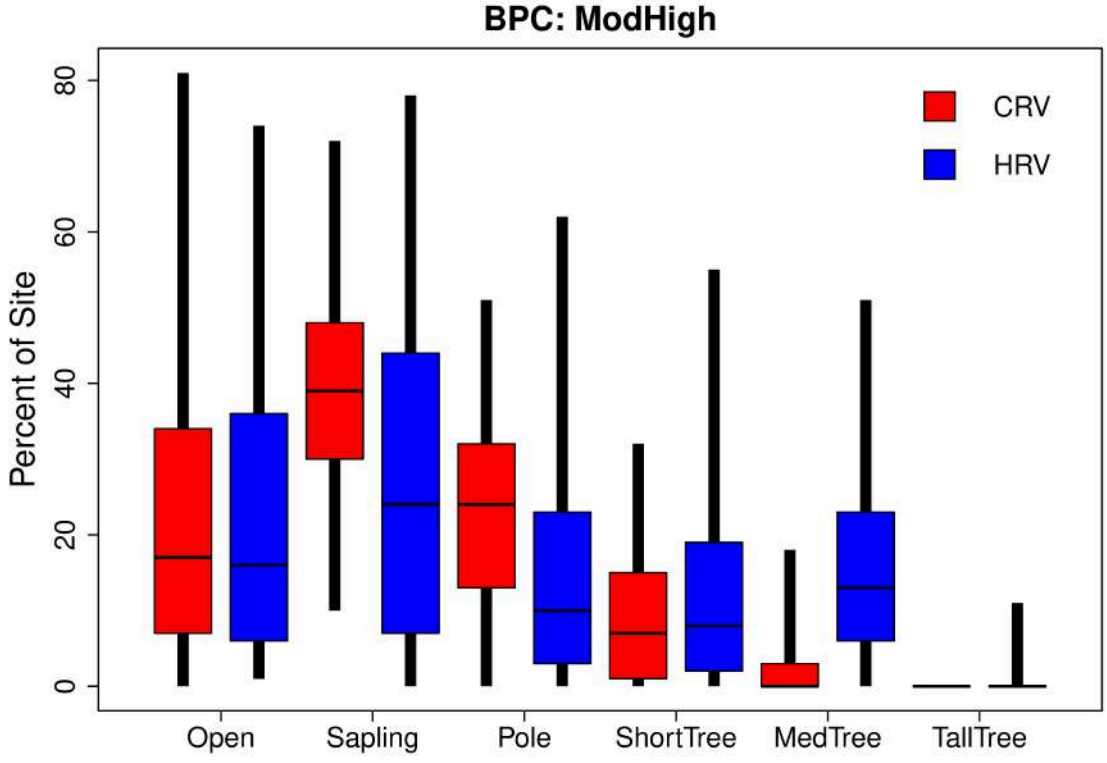
BPC: ModHigh
Percent of Site
0
20
40
60
80
CRV
HRV
Open
Sapling
Pole
ShortTree
MedTree
TallTree

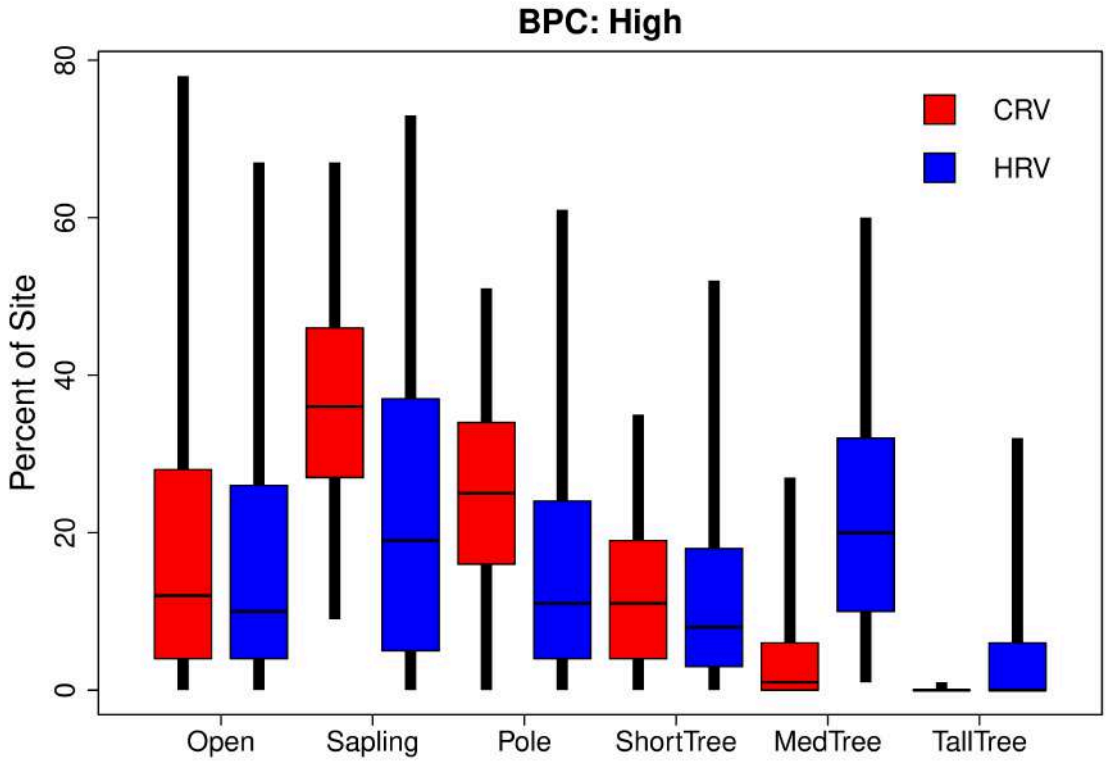

Figure 14: Historical Range of Variability (HRV) and Current range of variabiilty (CRV) among Sites (i.e., 40-m radius window) in the percent of forest in each developmental stage within the Low, Moderately Low, Moderately High and High site productivity Biophysical Classes (BPCs) in the Lake Tahoe Basin landscape. Box = 25-50 percentiles; whiskers = 2.5-97.5 percentiles

Recall that current departure in the Site-level metrics provides a basis for prioritizing management at the unit level. For example, given the results above, to reduce the current departure in developmental stage composition on High productivity Sites, management could prioritize treatments that produce units with a greater percentage of Open areas intermixed with Tall trees to shift the overall developmental stage distribution across the landscape to be more aligned with the HRV distribution. The same priorities could be given to Low productivity Sites, although here the emphasis would be predominantly on increasing the proportion of Sites with a greater proportion of Open areas. Of course, aside from controlling the percentage in Open, there is only limited ability to actively manage developmental stage succession (i.e., height growth). Indeed, much of the succession required to shift the current distribution towards the later stages of development simply requires time (e.g., to allow trees in the Pole and Short Tree stages to grow into the Medium and Tall Tree stages). However, managing surface and ladder fuels to inhibit high severity wildfire and retaining current taller trees may be an effective strategy to gradually shift the CRV towards better alignment with HRV with respect to the later developmental stages.

Metric 2: Tree Size (QMD)

Tree Size at the Site level was based on the Quadratic Mean Diameter (QMD) of established trees within a 40-m radius of the focal cell. Recall that QMD was based on only the cells with established trees in the window. Thus, if there was a single cell with an established tree in the window, then QMD was based on that single tree and equaled the tree's diameter at breast height (DBH). Accordingly, QMD can be quite high even in relatively open areas if the few neighborhood trees are large in diameter. The HRV and CRV in Tree Size composition at the Site level by BPC is given in **Table 9** and depicted in **Figure 15**.

BPC	Scenario	HRV 2.5%	HRV 25%	HRV 50%	HRV 75%	HRV 97.5%
Low	CRV	2	4	6	8	12
Low	HRV	1	4	7	10	18
ModLow	CRV	1	5	6	9	13
ModLow	HRV	4	8	11	15	22
ModHigh	CRV	1	5	7	9	14
ModHigh	HRV	7	12	15	18	25
High	CRV	2	6	9	11	18
High	HRV	9	15	18	21	29

Table 9: Range of variability (given as quantiles) in tree size (quadratic mean diameter) across Sites (40-m radius window centered on each focal cell) by Biophysical Class (BPC) for the current range of variability (CRV) and the historical range of variability (HRV) for the Lake Tahoe Basin landscape.

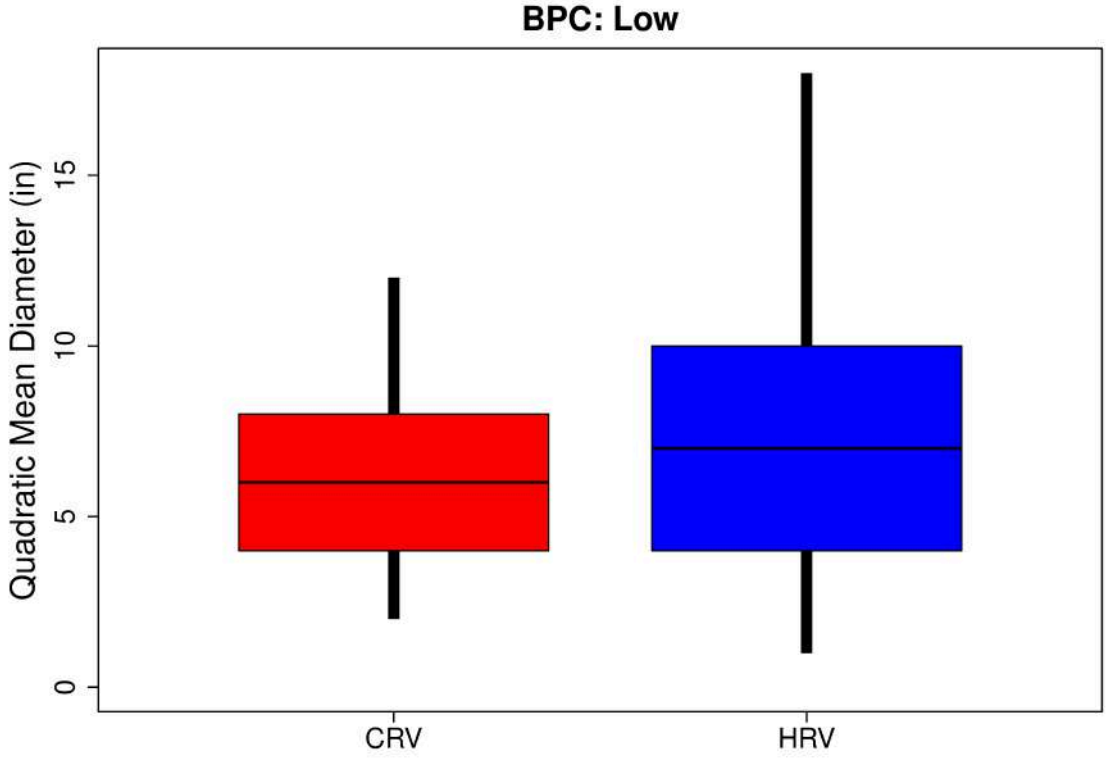

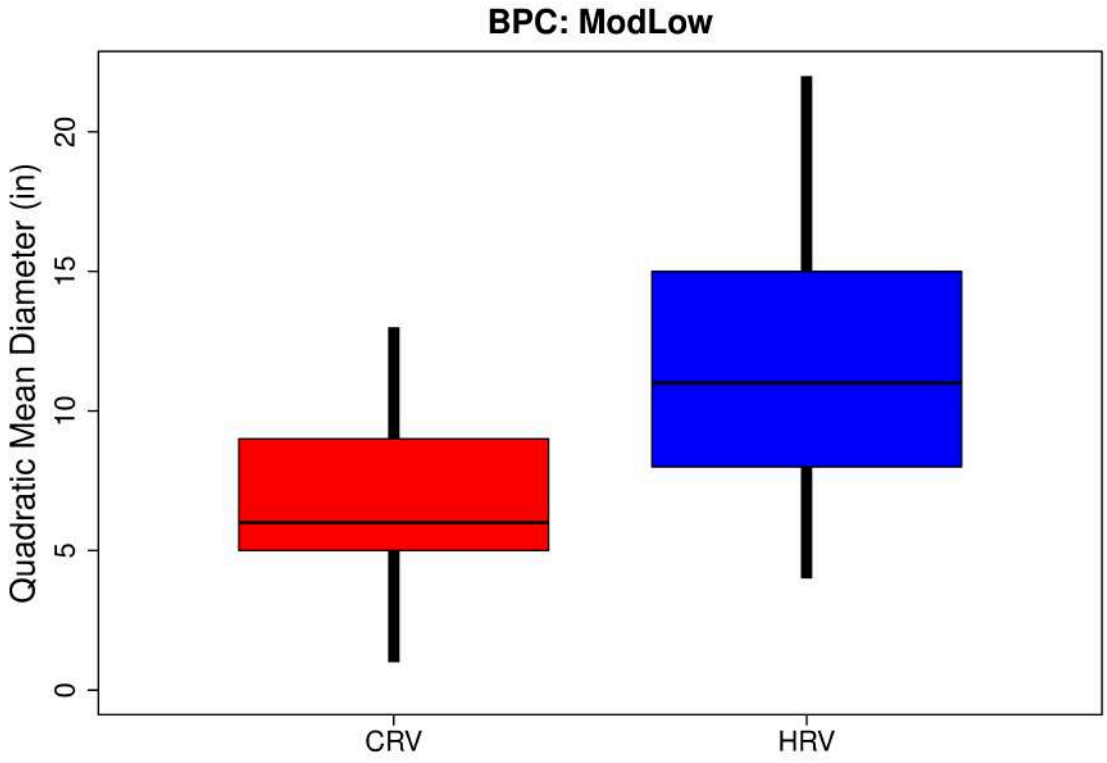
BPC: ModLow
Quadratic Mean Diameter (in)
0
5
10
15
20
CRV
HRV

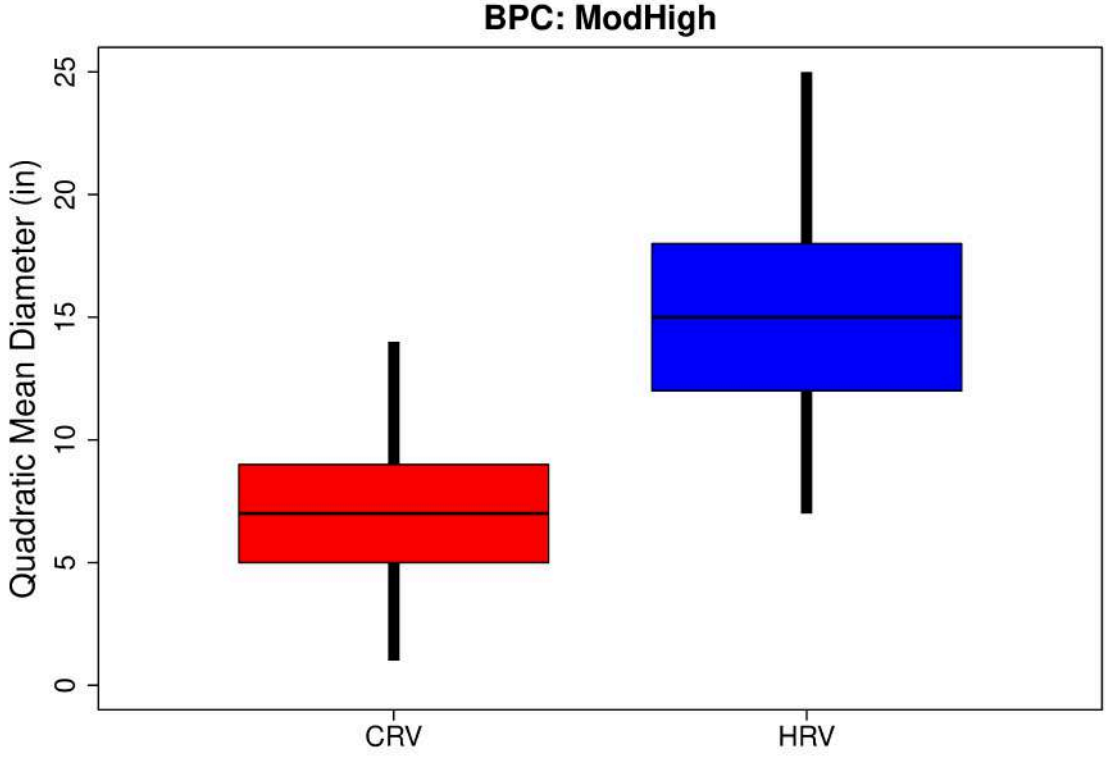
BPC: ModHigh
Quadratic Mean Diameter (in)
0
5
10
15
20
25
CRV
HRV

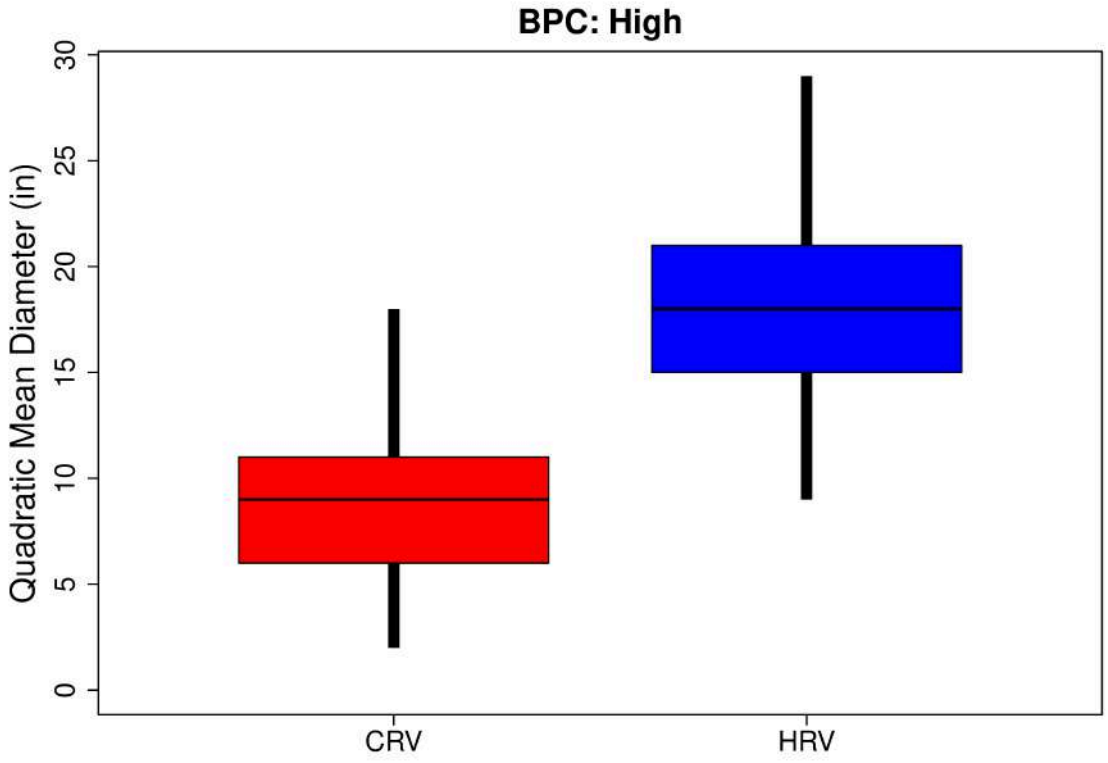

Figure 15: Historical Range of Variability (HRV) and Current range of variabiilty (CRV) among Sites (i.e., 40-m radius window) in the Quadratic Mean Diameter (QMD) of established trees to breast height within the Low, Moderately Low, Moderately High and High site productivity Biophysical Classes (BPCs) in the Lake Tahoe Basin landscape. Box = 25-50 percentiles; whiskers = 2.5-97.5 percentiles

Metric 3: Tree Cover

Tree Cover at the Site level was based on the percentage of 5-m cells with established trees to breast height within a 40-m radius of the focal cell. Recall that even a cell in the Open developmental stage (i.e., forest cell without an established tree to breast height) has a percent tree cover > 0 % so long as there was a single established tree within 40 m of the focal cell. In addition, recall that Tree Cover, as computed here, represents the percentage of cells within 40 m containing one or more established trees to breast height, not actual tree canopy cover, and as such is biased high by an average of 16% over actual tree canopy cover (i.e., actual tree canopy cover will be less than reported here by an average of 16%). The HRV and CRV in Tree Cover composition at the Site level by BPC is given in **Table 10** and depicted in **Figure 16**.

Table 10: Range of variability (given as quantiles) in percent tree cover across Sites (40-m radius window centered on each focal cell) by Biophysical Class (BPC) for the current range of variability (CRV) and the historical range of variability (HRV) for the Lake Tahoe Basin landscape.

BPC	Scenario	HRV 2.5%	HRV 25%	HRV 50%	HRV 75%	HRV 97.5%
Low	CRV	30	71	84	92	99
Low	HRV	1	25	55	84	97
ModLow	CRV	23	70	84	93	100
ModLow	HRV	11	51	78	92	98
ModHigh	CRV	18	65	82	92	100
ModHigh	HRV	25	63	83	93	98
High	CRV	21	71	87	95	100
High	HRV	32	73	89	95	99

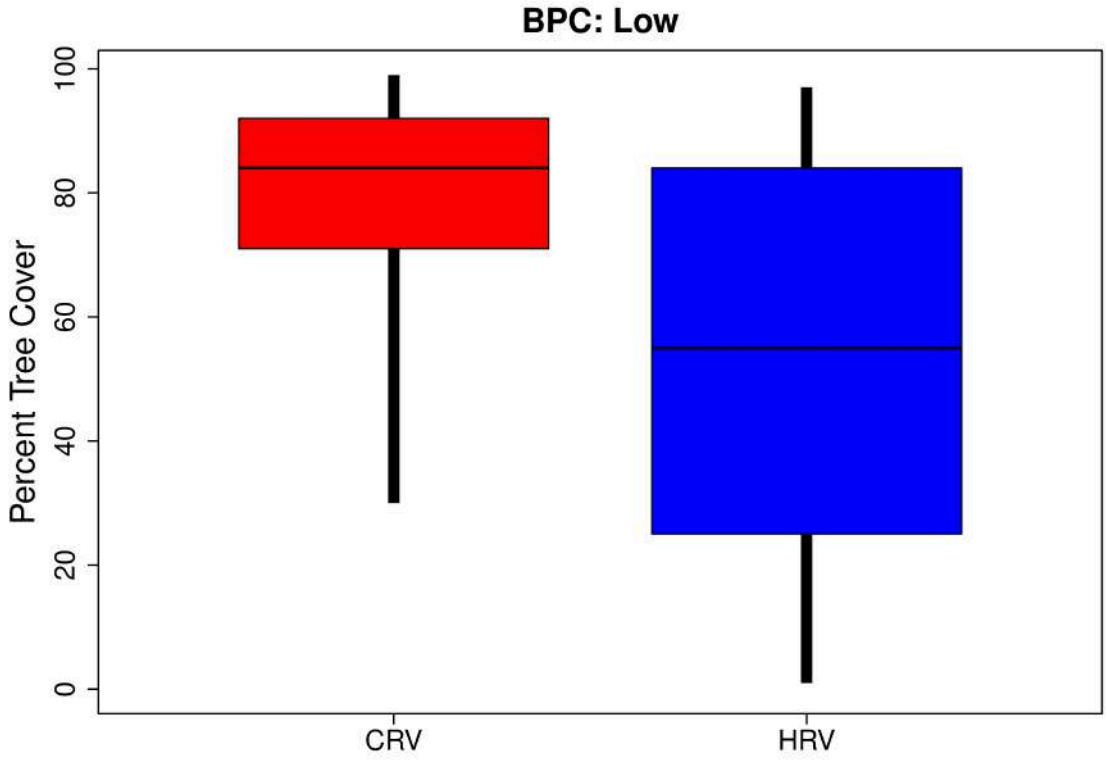

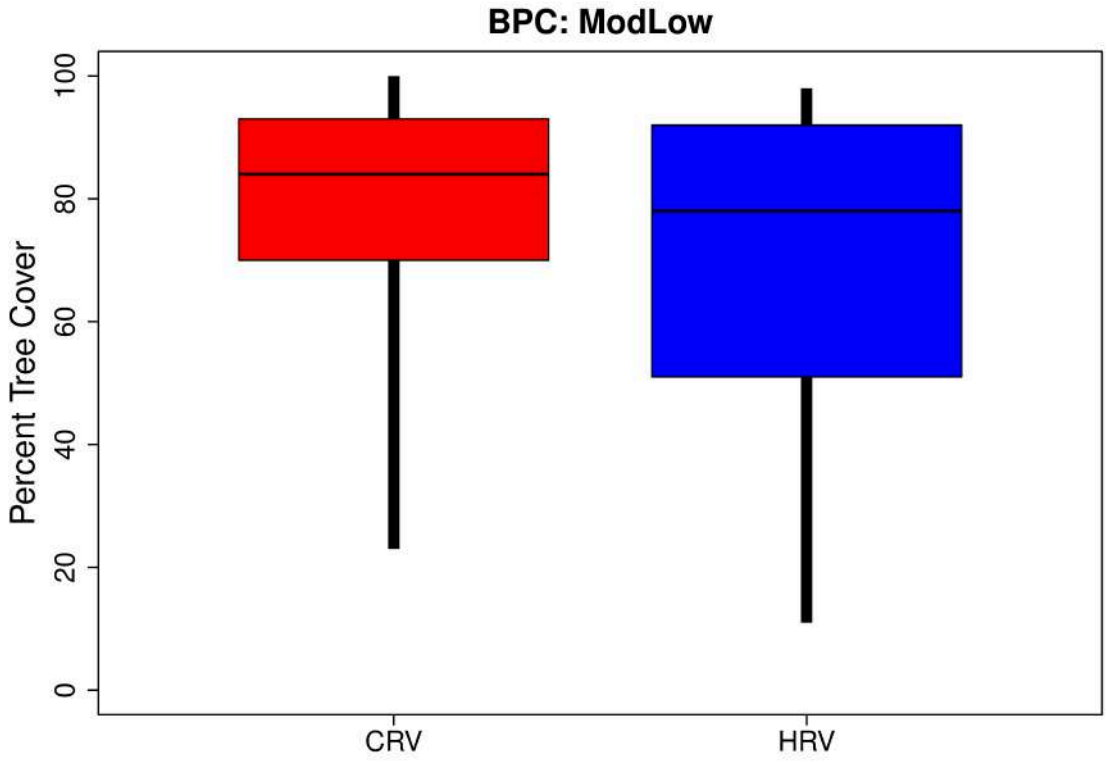
BPC: ModLow
Percent Tree Cover
0
20
40
60
80
100
CRV
HRV

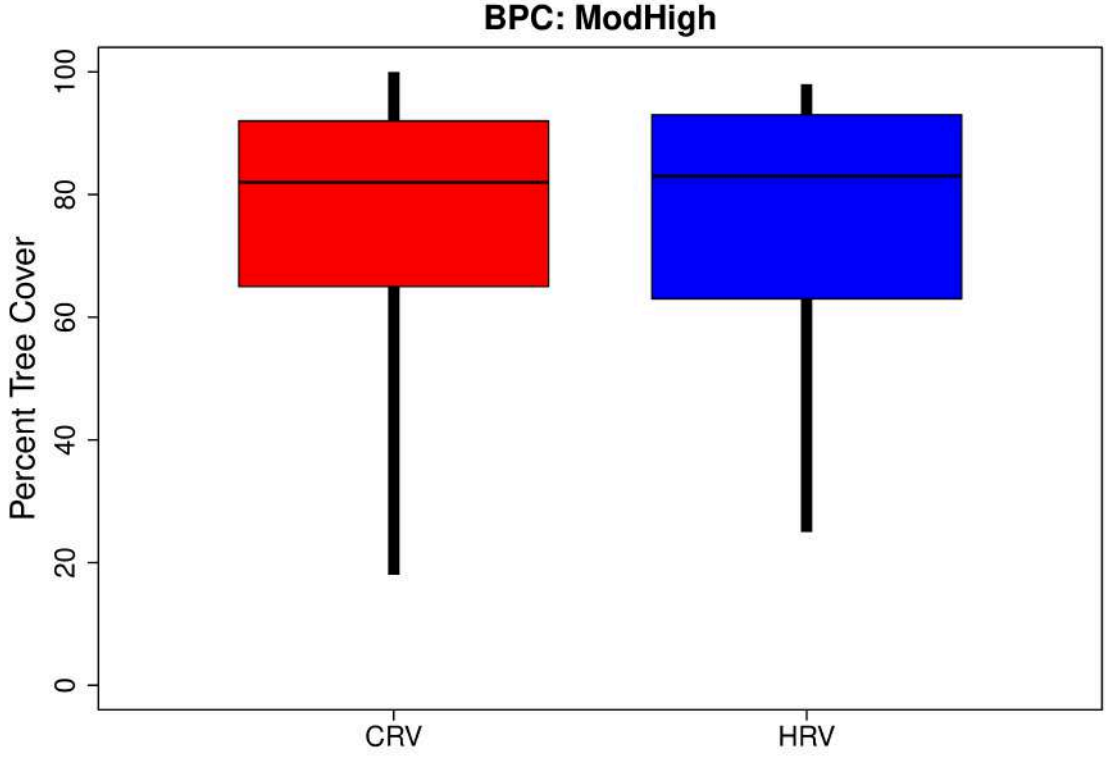
BPC: ModHigh
Percent Tree Cover
0
20
40
60
80
100
CRV
HRV

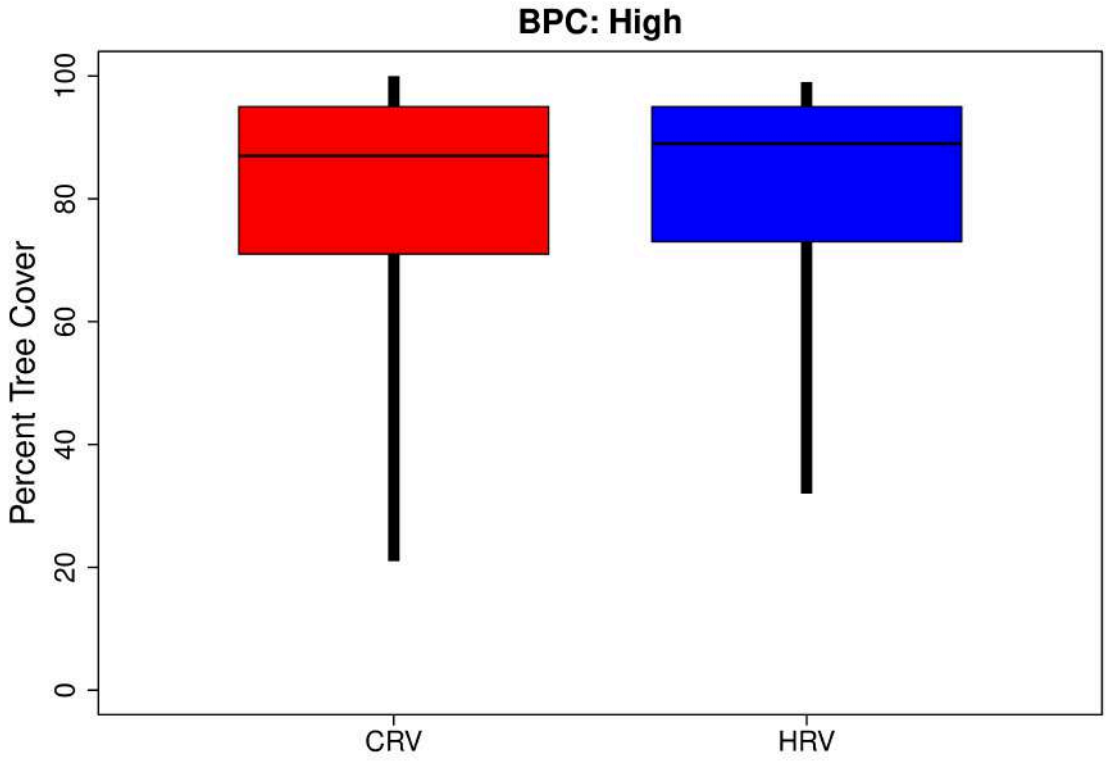

Figure 16: Historical Range of Variability (HRV) and Current range of variabiilty (CRV) among Sites (i.e., 40-m radius window) in the percent Tree Cover of established trees to breast height within the Low, Moderately Low, Moderately High and High site productivity Biophysical Classes (BPCs) in the Lake Tahoe Basin landscape. Box = 25-50 percentiles; whiskers = 2.5-97.5 percentiles

Geophysical Unit Level Departure

The results presented in this section address current departure in landscape metrics quantified at the spatial extent of a single Geophysical Unit (GPU). The Lake Tahoe Basin landscape was divided into 6,815 separate GPUs, which collectively encompass the area mapped as forest in the Existing Cover layer (Ecover) and within existing Lidar at the time of this analysis. Recall from the GTR that we defined GPUs based on similarity in a suite of 10 geophysical attributes and that they were defined only for the forested portion of the landscape and only where we had Lidar coverage. In addition, recall that each GPU was assessed independently; i.e., that we compared the current condition of each GPU to its own HRV in vegetation conditions. Thus, current departure of a GPU was specific to that GPU and independent of that measured for other GPUs. Lastly, recall that we used a large but parsimonious suite of landscape metrics that we deemed meaningful for estimating departure at the GPU level and appropriate given the available data, and computed departure as described in the GTR (and not repeated here), including the following:

Metric 1: Basal Area Departure

Departure in basal area of trees within the GPU was based on a metric derived by the TCSI project and adapted here for our purposes (**Figure 17**). GPUs with an increasingly positive departure have a current basal area that is greater than expected under HRV.

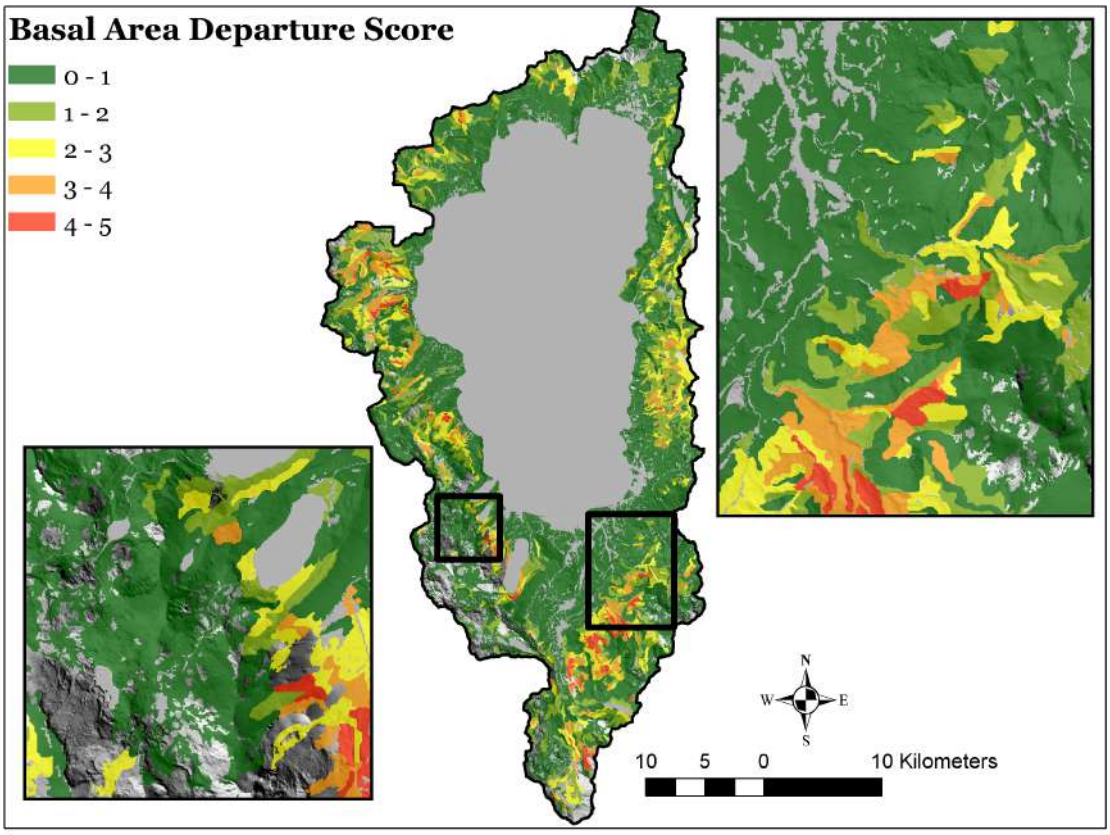

Figure 17: Geophysical Unit (GPU)-level basal area departure score for the Lake Tahoe Basin landscape. The departure score (0-5) represents the deviation of the current GPU condition from its historical range of variability (HRV), as estimated from a suite of contemporary reference sites. Values increase with increasing degrees of departure.

Metric 2: Percent Open Forest

We measured departure in the percent of forested cells within the GPU in the Open developmental stage (**Figure 18**). GPUs with a departure index less than -1 have less area in the Open developmental stage than under HRV.

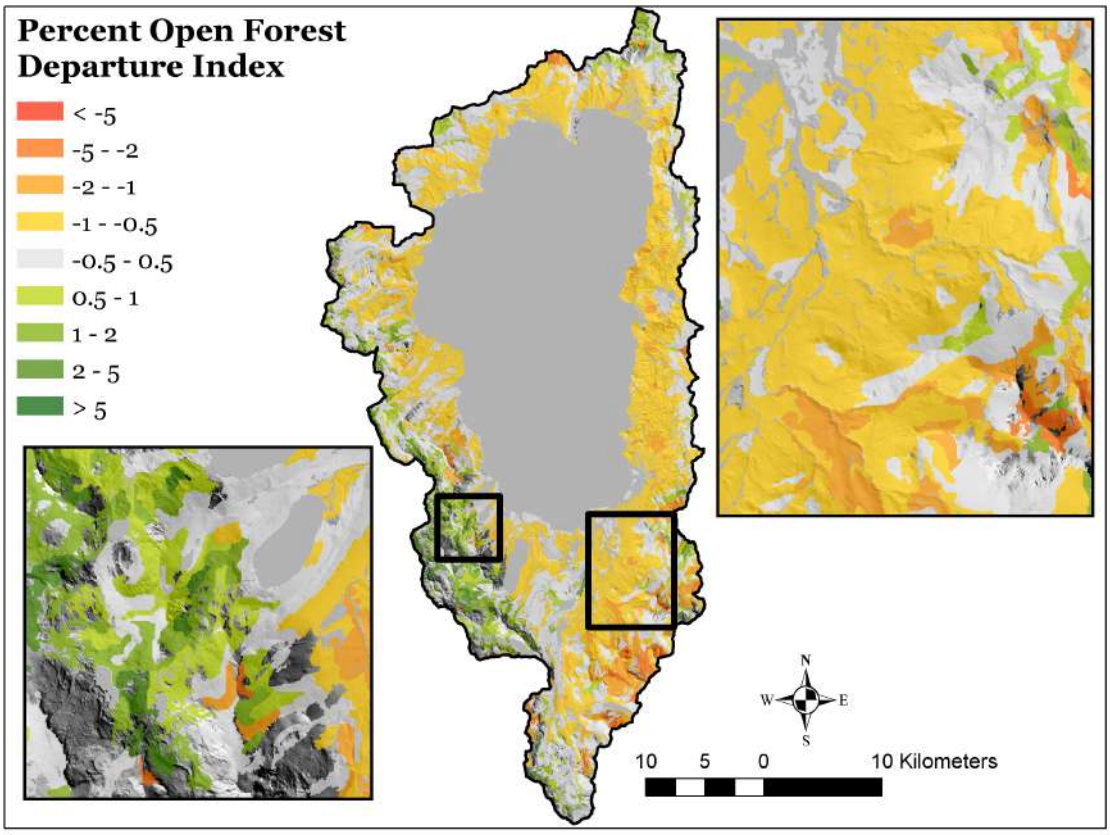

Figure 18: Geophysical Unit (GPU)-level departure index (unbounded) for the percentage of the forest within the GPU in the Open developmental stage for the Lake Tahoe Basin landscape. The departure Index represents the deviation of the current GPU condition from its historical range of variability (HRV), as simulated. Values < -1 represent a current condition that is less than the HRV for the GPU, and increasingly negative values represent increasing degrees of negative departure.

Metric 3: Developmental Stage Diversity

We measured departure in the diversity of forest developmental stages within the GPU based on the Simpson's Diversity index (**Figure 19**). Here, Simpson's Diversity is defined as the probability that any two cells selected at random would be different developmental stages. The departure index for Simpson's Diversity is less than -1 if the current GPU has a diversity of developmental stages that is less than HRV.

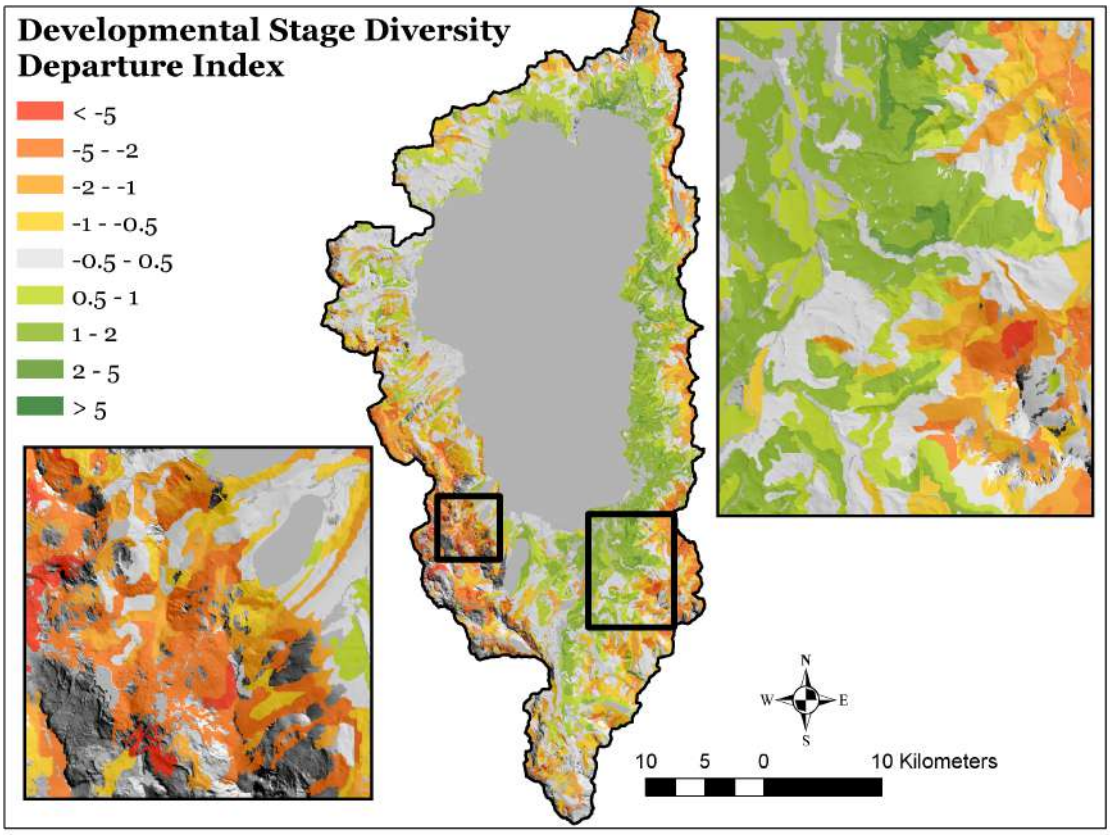

Figure 19: Geophysical Unit (GPU)-level departure index (unbounded) for the Simpson Diversity of developmental stages within the GPU for the Lake Tahoe Basin landscape. The departure Index represents the deviation of the current GPU condition from its historical range of variability (HRV), as simulated. Values < -1 represent a current condition that is less than the HRV for the GPU, and increasingly negative values represent increasing degrees of negative departure.

Metric 4: Coefficient of Variation in Open Patch Size

We measured departure in the Coefficient of Variation (CV) in the size of all Open forest patches, including single cell patches, in which forest openings are defined by contiguous cells in the Open developmental stage based on the 4-neighbor rule (i.e., orthogonal neighbors)(**Figure 20**). The departure index is less than -1 if the current GPU has relatively invariant Open patch sizes compared to HRV.

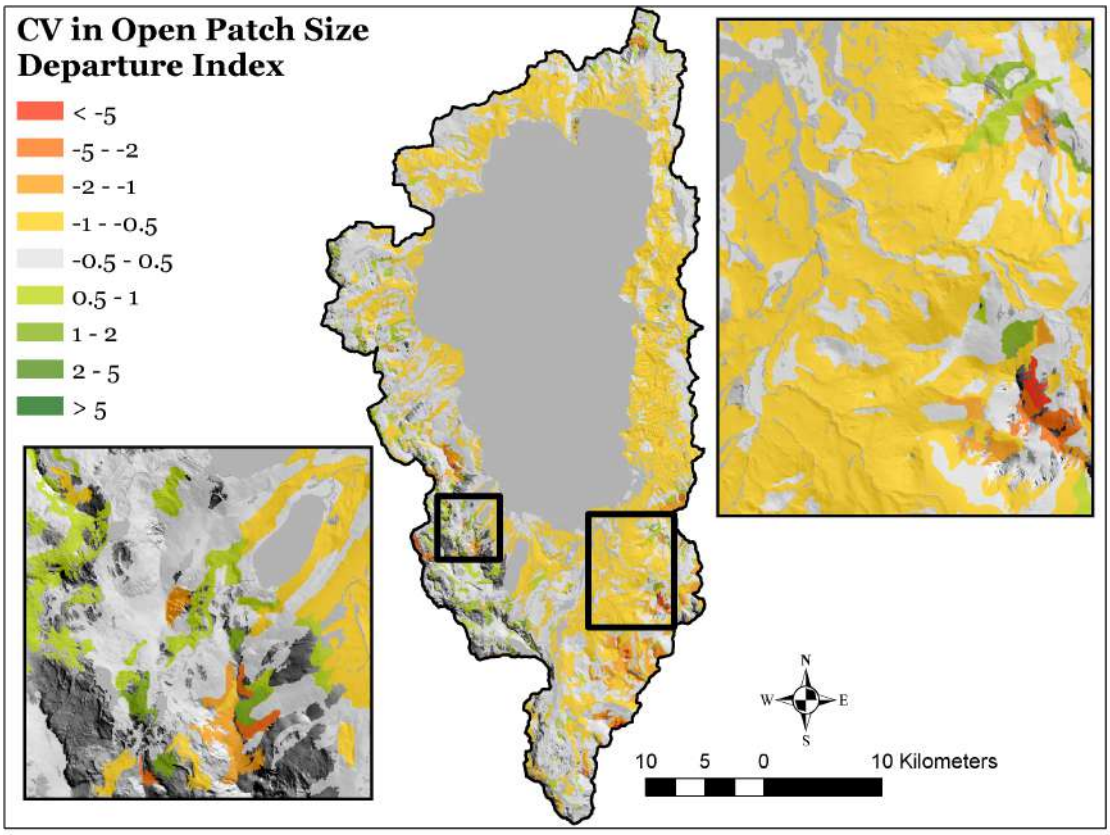

Figure 20: Geophysical Unit (GPU)-level departure index (unbounded) for the Coefficient of Variation (CV) in the size of patches in the Open developmental stage within the GPU for the Lake Tahoe Basin landscape. The departure Index represents the deviation of the current GPU condition from its historical range of variability (HRV), as simulated. Values < -1 represent a current condition that is less than the HRV for the GPU, and increasingly negative values represent increasing degrees of negative departure.

Metric 5: Coefficient of Variation in Developmental Stage Patch Size

We measured departure in the CV in the size of all forest developmental stage patches, including single cell patches, in which patches are defined by contiguous cells in the same developmental stage based on the 4-neighbor rule (**Figure 21**). The departure index is less than -1 if the current GPU has relatively invariant developmental stage patch sizes compared to HRV.

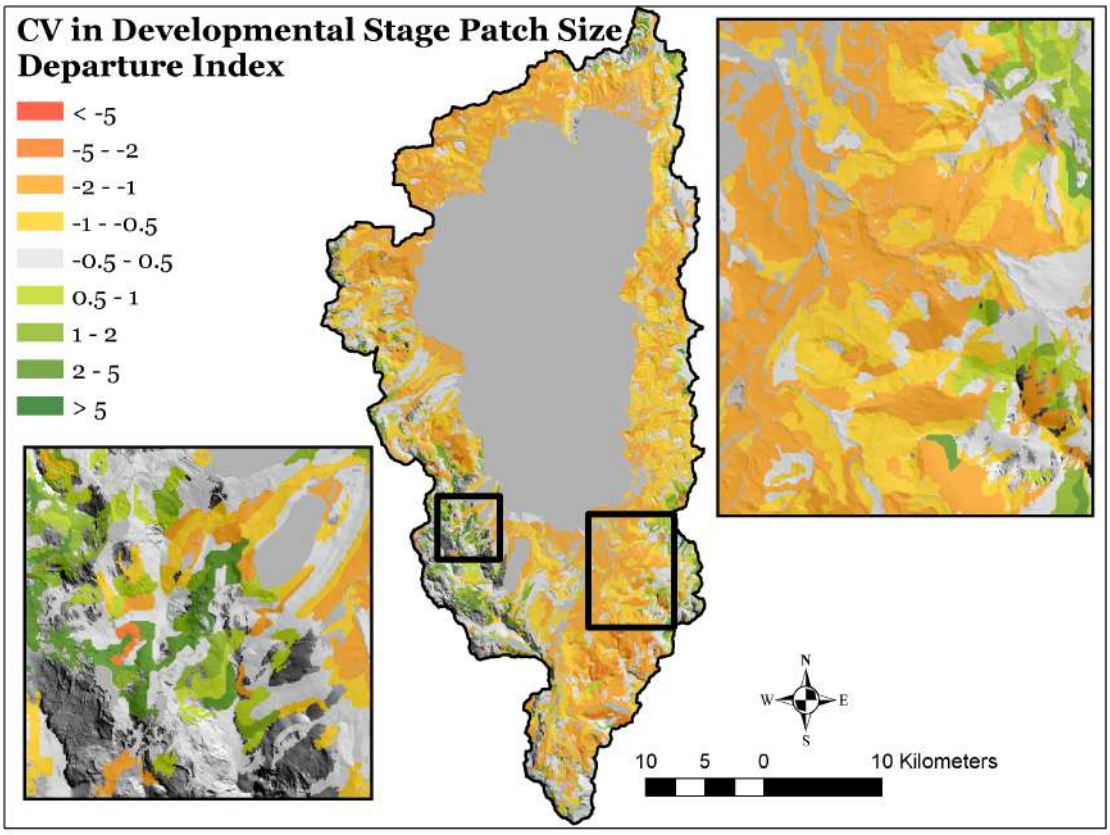

Figure 21: Geophysical Unit (GPU)-level departure index (unbounded) for the Coefficient of Variation (CV) in the size of patches based on developmental stages within the GPU for the Lake Tahoe Basin landscape. The departure Index represents the deviation of the current GPU condition from its historical range of variability (HRV), as simulated. Values < -1 represent a current condition that is less than the HRV for the GPU, and increasingly negative values represent increasing degrees of negative departure.

Metric 6: Percent Large Trees

We measured departure in the percent of forested cells within the GPU in the Large tree size class ($\geq$ 30 in dbh)(**Figure 22**). GPUs with a departure index less than -1 have less area in the Large tree class than under HRV.

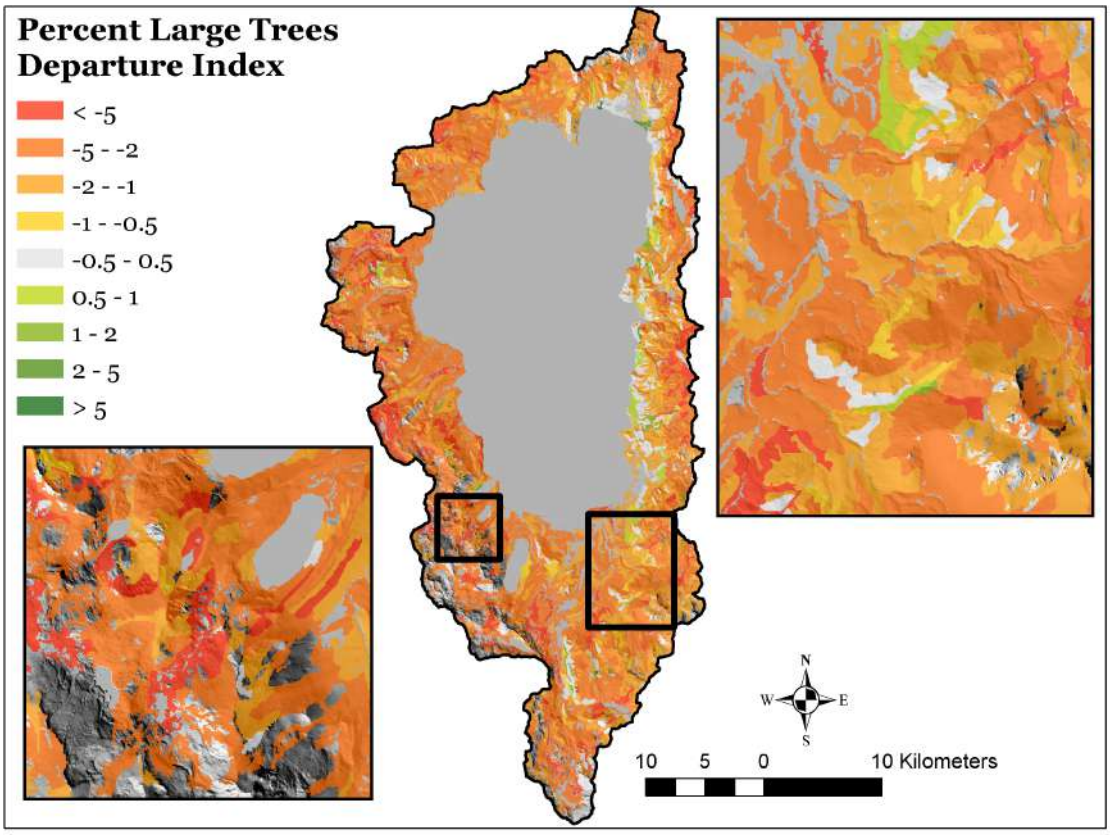

Figure 22: Geophysical Unit (GPU)-level departure index (unbounded) for the percentage of the forest in the Large tree size class (*geq* 30 in dbh) within the GPU for the Lake Tahoe Basin landscape. The departure Index represents the deviation of the current GPU condition from its historical range of variability (HRV), as simulated. Values < -1 represent a current condition that is less than the HRV for the GPU, and increasingly negative values represent increasing degrees of negative departure.

Metric 7: Tree Size Class Diversity

We measured departure in the diversity of tree size classes within the forested portion of the GPU based on the Simpson's Diversity index (**Figure 23**). Here, Simpson's Diversity is defined as the probability that any two cells selected at random would be from different tree size classes. The departure index for Simpson's Diversity is less than -1 if the current GPU has a diversity of tree size classes that is less than HRV.

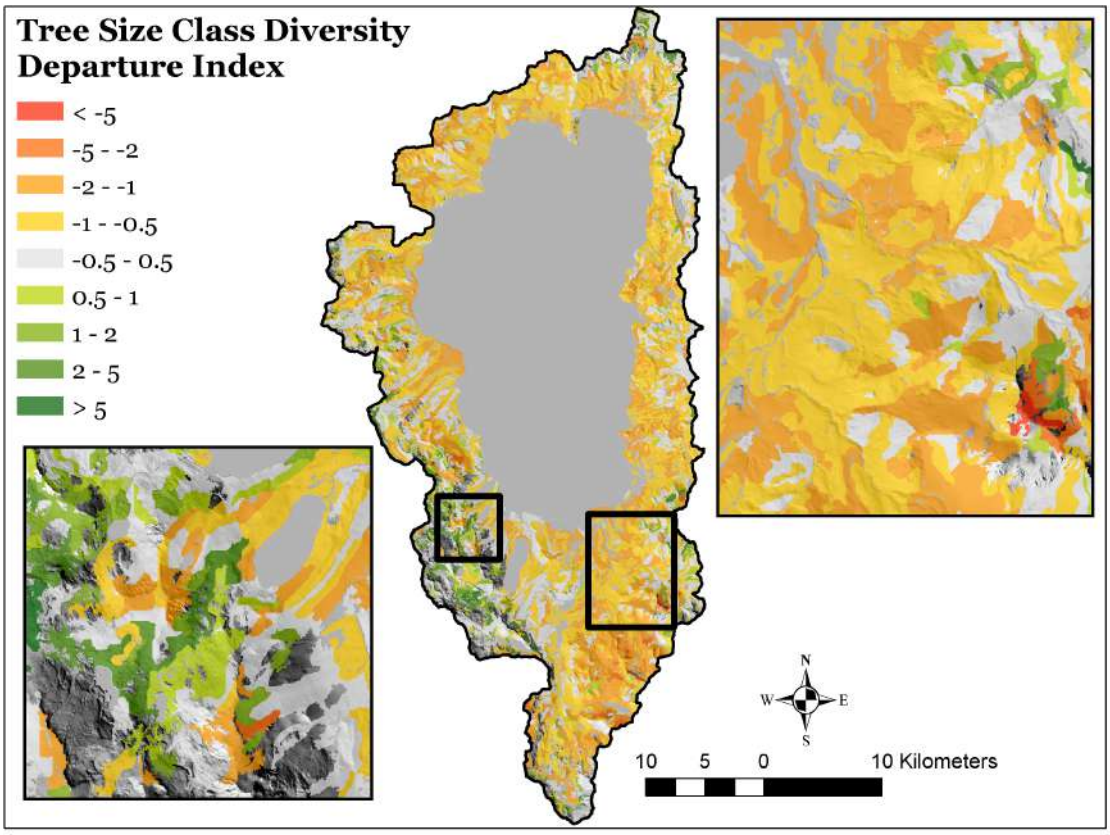

Figure 23: Geophysical Unit (GPU)-level departure index (unbounded) for the Simpson Diversity of tree size clases within the GPU for the Lake Tahoe Basin landscape. The departure Index represents the deviation of the current GPU condition from its historical range of variability (HRV), as simulated. Values < -1 represent a current condition that is less than the HRV for the GPU, and increasingly negative values represent increasing degrees of negative departure.

Metric 8: Coefficient of Variation in Large Tree Patch Size

We measured departure in the CV in the size of all Large tree patches, including single cell patches, in which Large tree patches were defined by contiguous cells in the Large tree class ($\geq$ 30 in dbh) based on the 4-neighbor rule (**Figure 24**). The departure index is less than -1 if the current GPU has relatively invariant Large tree patch sizes compared to HRV.

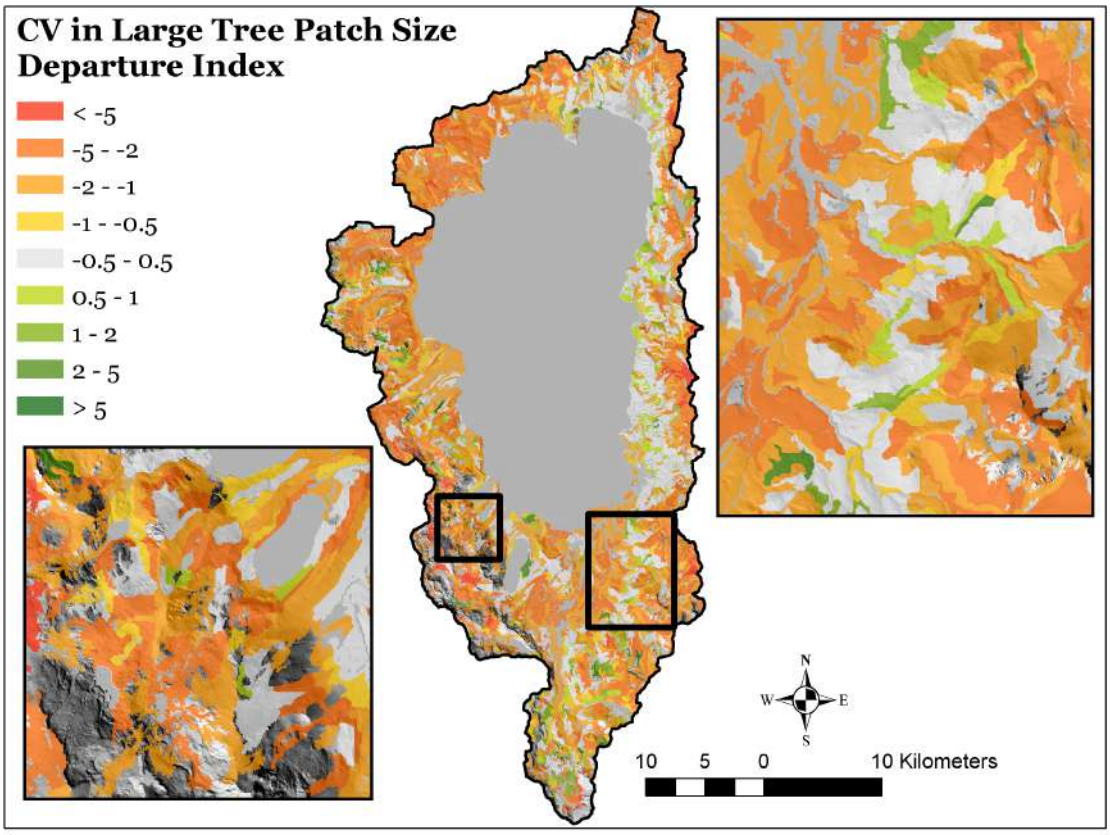

Figure 24: Geophysical Unit (GPU)-level departure index (unbounded) for the Coefficient of Variation (CV) in the size of patches in the Large tree size class (*geq* 30 in dbh) within the GPU for the Lake Tahoe Basin landscape. The departure Index represents the deviation of the current GPU condition from its historical range of variability (HRV), as simulated. Values < -1 represent a current condition that is less than the HRV for the GPU, and increasingly negative values represent increasing degrees of negative departure.

Metric 9: Coefficient of Variation in Tree Size Class Patch Size

We measured departure in the CV in the size of all tree size class patches, including single cell patches, in which patches were defined by contiguous cells in the same tree size class based on the 4-neighbor rule (**Figure 25**). The departure index is less than -1 if the current GPU has relatively invariant tree size class patch sizes compared to HRV.

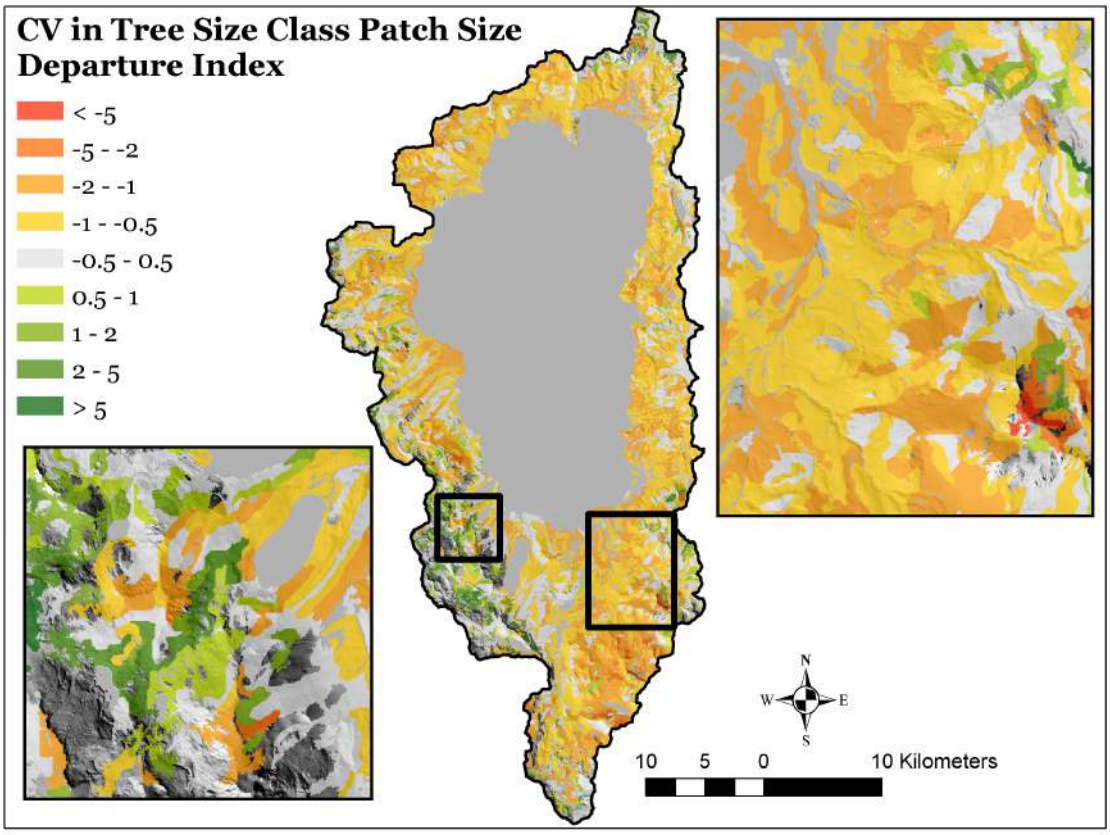

Figure 25: Geophysical Unit (GPU)-level departure index (unbounded) for the Coefficient of Variation (CV) in the size of patches based on tree size classes within the GPU for the Lake Tahoe Basin landscape. The departure Index represents the deviation of the current GPU condition from its historical range of variability (HRV), as simulated. Values < -1 represent a current condition that is less than the HRV for the GPU, and increasingly negative values represent increasing degrees of negative departure.

Metric 10: Coefficient of Variation in Quadratic Mean Diameter

We measured departure in the CV in site-level Quadratic Mean Diameter (QMD) of established trees within the GPU (**Figure 26**). Recall that a site was defined as a 40-m radius window around each focal cell. Thus, QMD was computed for the site associated with each focal cell, which produced a continuous surface of QMD values, from which the CV in QMD values within the GPU was computed. The departure index is less than -1 if the current GPU has relatively homogeneous QMD compared to HRV.

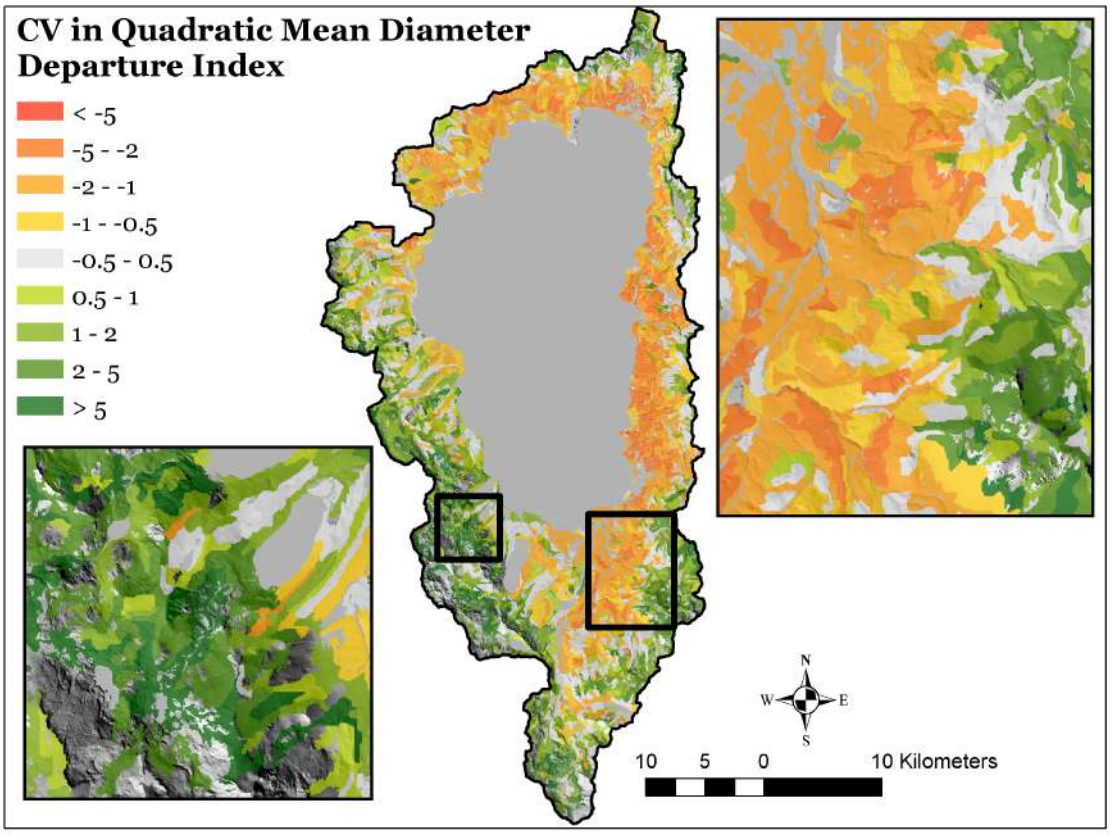

Figure 26: Geophysical Unit (GPU)-level departure index (unbounded) for the Coefficient of Variation (CV) in Site-level (i.e., 40 m radius window around each focal cell) Quadratic Mean Diameter (QMD, in inches) within the GPU for the Lake Tahoe Basin landscape. The departure Index represents the deviation of the current GPU condition from its historical range of variability (HRV), as simulated. Values < -1 represent a current condition that is less than the HRV for the GPU, and increasingly negative values represent increasing degrees of negative departure.

Metric 11: Coefficient of Variation in Percent Tree Cover

We measured departure in the CV in site-level percent cover of established trees within the GPU (**Figure 27**). Again, recall that a site was defined as a 40-m radius window around each focal cell. Thus, percent tree Cover was computed for the site associated with each focal cell, which produced a continuous surface of percent tree cover values, from which the CV in tree cover within the GPU was computed. The departure index is less than -1 if the current GPU has relatively homogeneous tree cover compared to HRV.

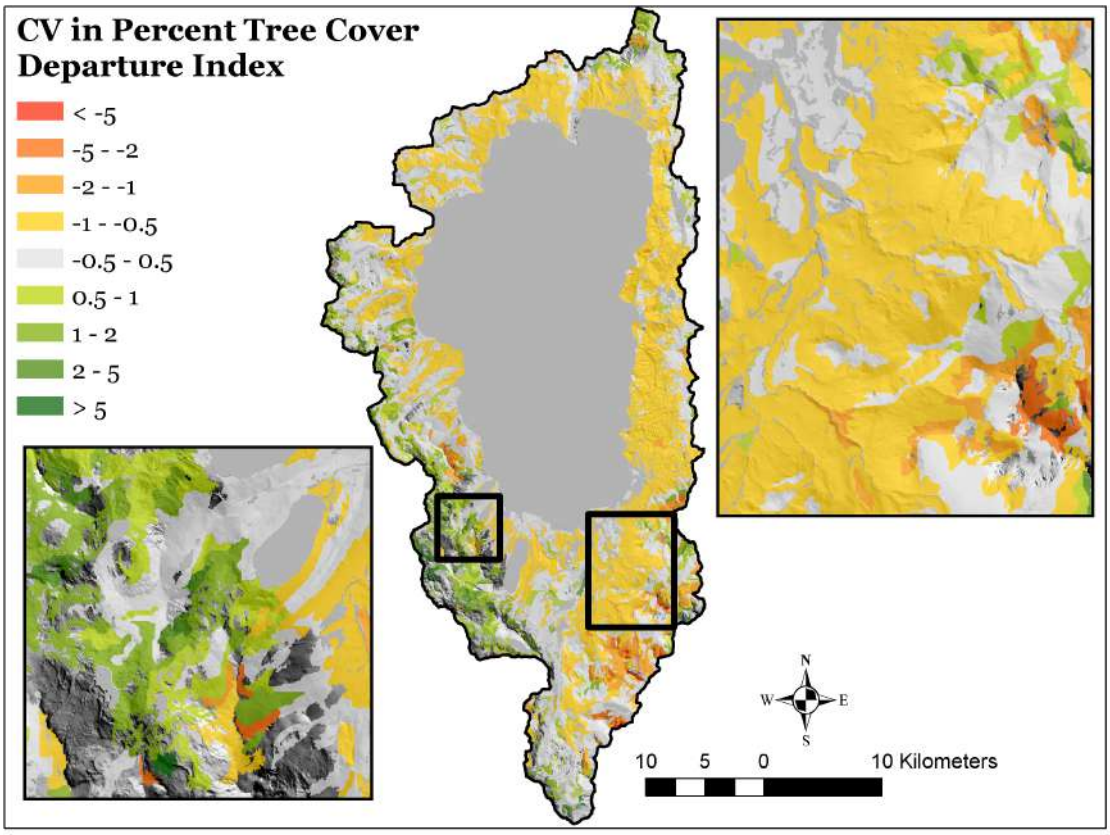

Figure 27: Geophysical Unit (GPU)-level departure index (unbounded) for the Coefficient of Variation (CV) in Site-level (i.e., 40 m radius window around each focal cell) percent tree cover within the GPU for the Lake Tahoe Basin landscape. Note, percent tree cover as measured is on average 16 % greater than percent canopy cover. The departure Index represents the deviation of the current GPU condition from its historical range of variability (HRV), as simulated. Values < -1 represent a current condition that is less than the HRV for the GPU, and increasingly negative values represent increasing degrees of negative departure.

Composite Departure Index

We combined the 11 GPU-level departure indices above into two composite departure scores: 1) composite "negative" departure, and 2) composite "absolute" departure (see GTR for details). Both of these composite scores can be interpreted as a measure of overall GPU departure in vegetation composition and configuration. Increasing departure scores (given as a percent of maximum) indicate increasing degrees of departure.

Negative Departure - Maximum "negative" departure occurs when a GPU has too little Open forest area, too few Large trees, too little diversity in forest developmental stages (i.e., tree heights) and tree size classes (i.e., dbh), too little variability in the size of patches based on forest developmental stage and tree size, and too little spatial variability in percent tree cover and weighted average tree size (i.e., QMD) relative to its HRV. In other words, maximum negative departure occurs when the forest is too closed-canopy, depauperate in Large trees, and too homogeneous in vegetation composition and configuration.

The composite negative departure score is depicted in **Figure 28**. This score can be interpreted as the percent of maximum deviation in negative departure. Thus, a value of 0 represents no departure in any of the component metrics and a value of 100 represents maximum negative departure in each of the component metrics. GPUs with relatively high scores are the logical ones to prioritize for restoration

treatment - should that be the goal. Importantly, this composite departure score can serve as a first stage in identifying and prioritizing GPUs for treatment, but specific objectives and treatments for each GPU requires decomposing the composite score into the component metrics to determine which aspects of the forest vegetation composition and/or configuration are most departed.

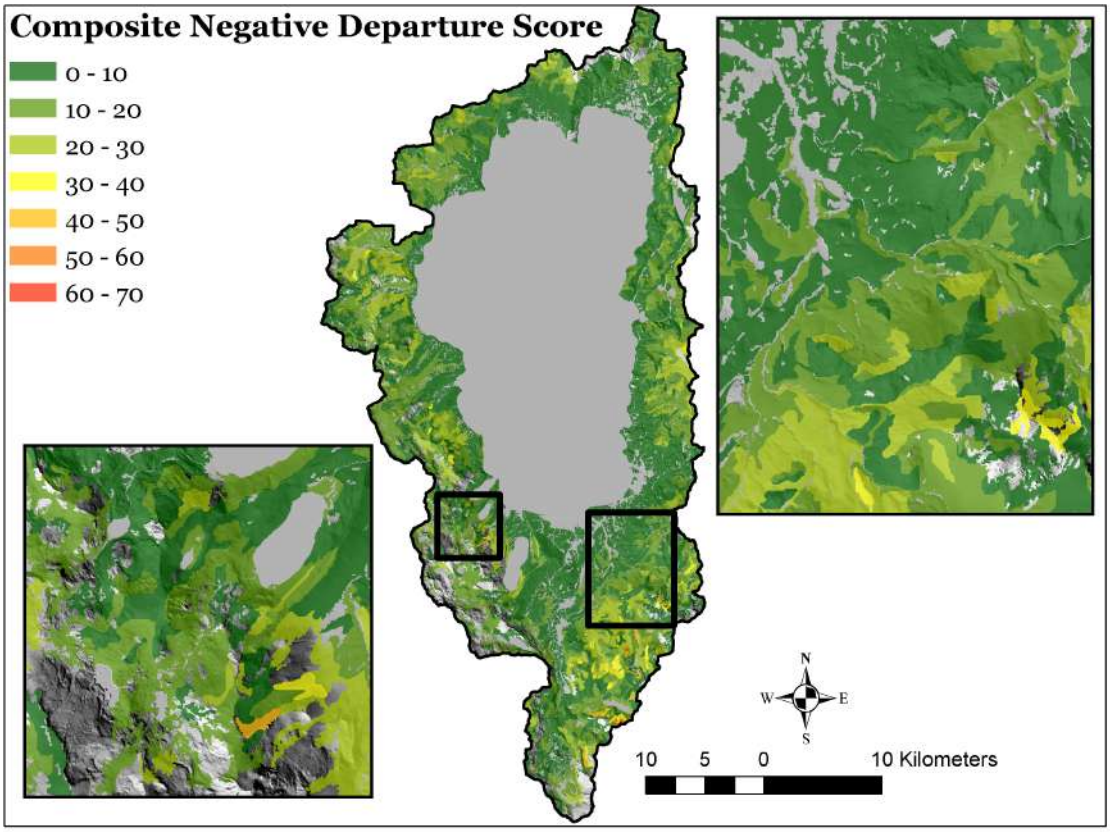

Figure 28: Geophysical Unit (GPU)-level composite negative departure score composed of a weighted combination of 11 individual departure metrics within the GPU for the Lake Tahoe Basin landscape. The score represents the percentage of maximum departure of the current GPU condition from its historical range of variability (HRV), as simulated. Larger values indicate increasing degrees of departure.

Absolute Departure - Maximum "absolute" departure occurs when a GPU has either too little or too much Open forest area, too few or too many Large trees, too little or too much diversity in forest developmental stages (i.e., tree heights) and tree size classes (i.e., dbh), too little or too much variability in the size of patches based on forest developmental stage and tree size, and too little or too much spatial variability in percent tree cover and weighted average tree size (i.e., QMD) relative to HRV. In other words, maximum departure occurs when the GPU differs in any way in both composition and configuration from its HRV, as measured by this suite of metrics.

Subbasin Level Departure

The results presented in this section represent landscape metrics quantified at the Subbasin-by-BPC level; i.e., each Subbasin subdivided into BPCs treated as a whole unit (a.k.a. "zones"). The Lake Tahoe Basin landscape was divided into 12 distinct Subbasins (**Figure 29**), each of which was partitioned into the BPCs for a total of 48 Subbasin-by-BPC partitions or zones. Recall from the GTR that each partition was assessed independently to create a departure index; i.e., that we compared the current condition of each partition to its own HRV in vegetation conditions. In addition, recall that the final departure score

reflected negative departure in the percent of the partition in large openings and large trees (i.e., in which the current landscape contains less area in large openings and large trees than expected under HRV), but was bidirectional with respect to the landscape configuration metrics; i.e., it reflected the magnitude of the absolute differences between the current and historical landscape conditions, regardless of whether the current condition was greater or less than the historical condition. In other words, any differences between current and historical vegetation conditions with respect to landscape configuration registered as departure. Lastly, recall that we used a parsimonious suite of landscape metrics (see below) that we deemed meaningful for estimating departure at the Subbasin level and appropriate given the available data, and computed departure as described in the GTR (and not repeated here), including the following metrics:

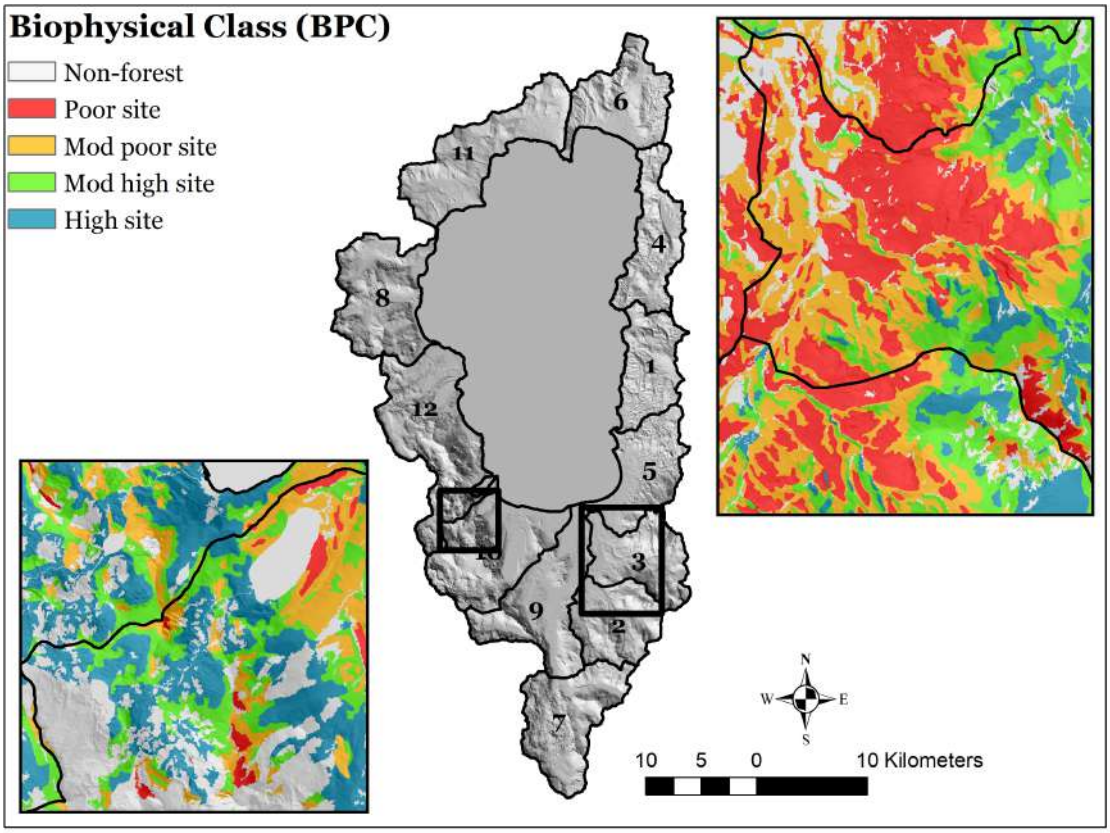

Figure 29: The Lake Tahoe Basin landscape HUC12 Subbasins, as modified, defined for the purpose of summarizing Historical Range of Variability (HRV) and current departure.

Metric 1: Percent Large Forest Openings

We defined large forest openings as contiguous forested cells in the Open developmental stage (i.e., no established trees to breast height) encompassing a minimum of 0.04 ha (0.1 acres). Contiguity was based on the 4-neighbor rule (i.e., orthogonal neighbors) that ensured a minimum width of 5 m for any opening. We defined Percent Large Forest Openings as the percent of the forest within the Subbasin-by-BPC partition in large forest openings (as defined), and the departure index reflected whether or not the current landscape was deficient in large forest openings relative to HRV and, if so, the degree of deficiency.

The Percent Large Forest Openings departure index is depicted in **Figure 30**. Note, the departure index was assigned to each Subbasin-by-BPC partition; consequently, there were 48 distinct values assigned. Thus, to better assess departure by Subbasin and BPC, one needs to examine the attribute table for the departure layer.

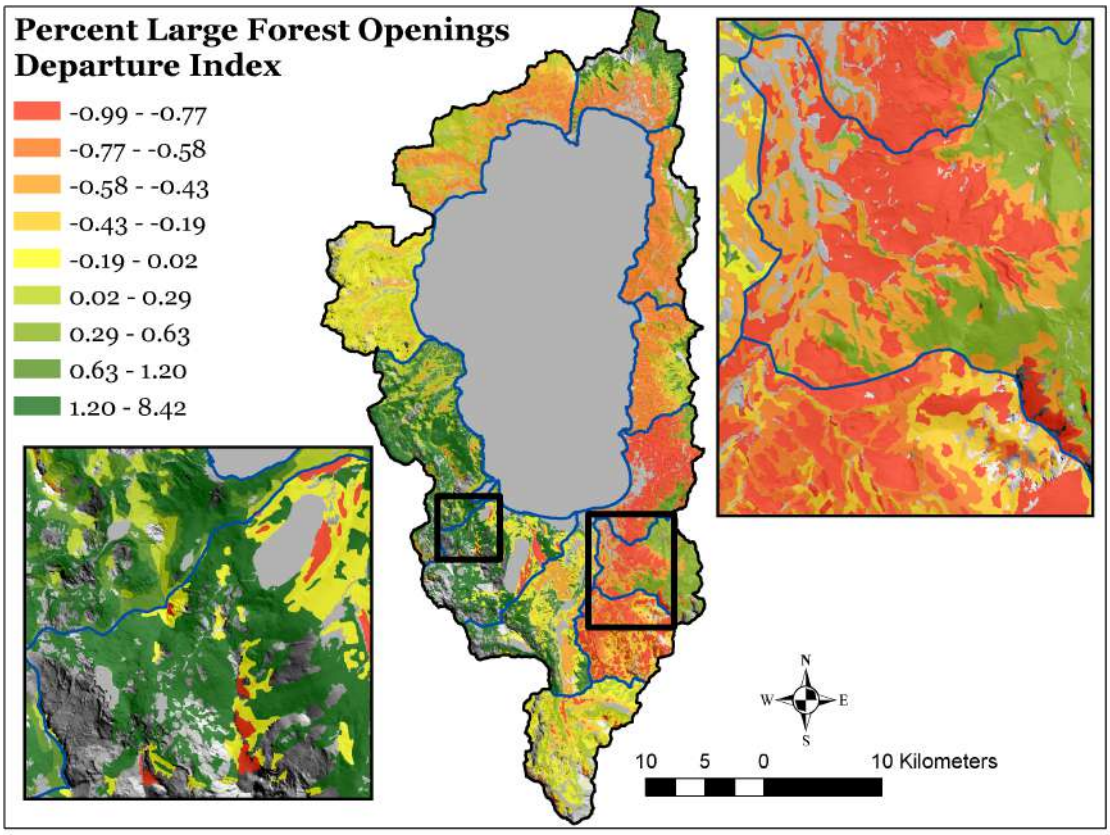

Figure 30: Subbasin-by-BPC level departure index for large forest openings (> 0.04 ha or 0.1 acres and > 5 m mininum width) for the Lake Tahoe Basin landscape. The departure index represents the deviation of the current Subbasin and biophysical class (BPC) condition from its historical reference period condition, as simulated. Departure indices < -1 represent a current landscape with less total area in large forest openings than during the historical reference period, as simulated, and increasing negative values represent increasing degrees of departure.

As discussed in the GTR, the Percent Large Forest Openings Departure Index can be miss-interpreted if not understood well. As the previous figure depicts, the distribution of index values would suggest that most of the subbasin-by-BPC partitions are within the HRV given that most of the partitions have values between -1 - 1. Recall, index values within this range reflect a current landscape condition that is within the 2.5% and 97.5% HRV. This would seem to indicate that most of the partitions are within HRV. While this might technically be correct, the reality is that most of the partitions are close to the lower limit of HRV and have index values close to -1. Consequently, the distribution of index values is heavily skewed towards values on the lower limit of HRV, suggesting that the landscape as a whole is, on average, deficient in large forest openings. A alternative and more useful way to assess current departure in this metric is to compare the distribution of values representing the percentage of the partition in large forest openings between the HRV and CRV, as shown **Figure 31**.

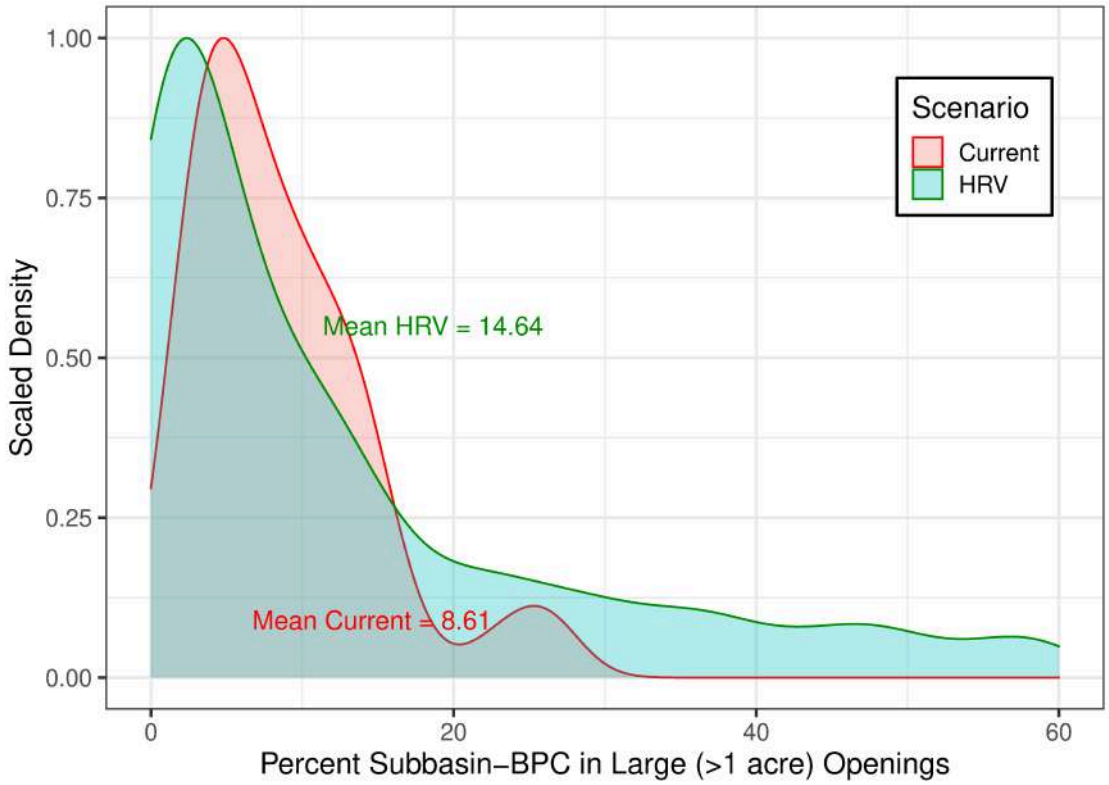

Figure 31: Current and historical distribution of Percent Large Forest Openings across the Subbasin-by-Biophysical Class (BPC) landscape partitions for the Lake Tahoe Basin landscape. The comparative distributions reveal that even though the departure index for most of the partitions technically may fall with the historical range of variation (see previous figure), the overall distributions in the raw metric values differ markedly and reflect departure for the landscape as a whole

Metric 2: Large Forest Openings Patch Size Distribution

We defined large forest openings as described above. Here, we quantified the size of individual openings and determined the percent of forest within the Subbasin-by-BPC partition in large openings in each of several patch size classes or bins (see GTR). The departure index reflects whether or not the current landscape has a distribution of large forest opening patch sizes that differed from HRV and, if so, the degree of differences in the two distributions.

The Large Forest Openings Patch Size Distribution departure index is depicted in **Figure 32**. As before, the departure index was assigned to each Subbasin-by-BPC partition; consequently, there were 48 distinct values assigned. Thus, to better assess departure by Subbasin and BPC, one needs to examine the attribute table for the departure layer.

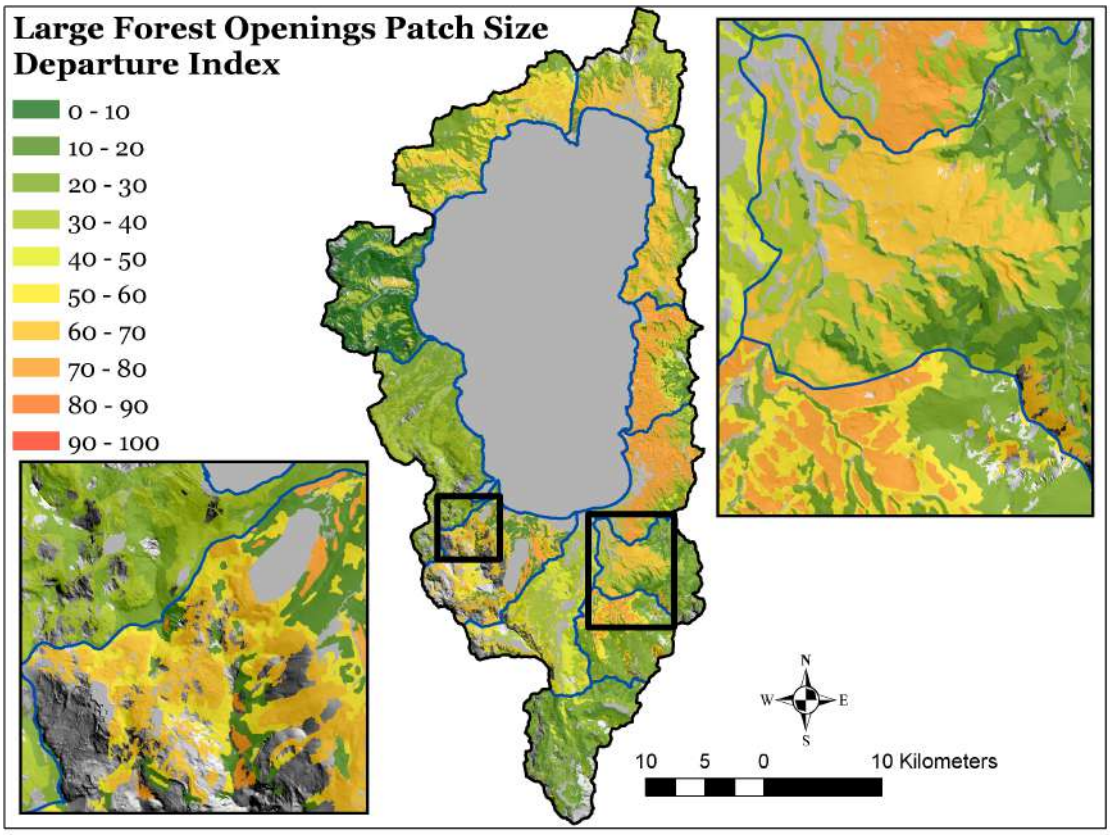

Figure 32: Subbasin-by-BPC level departure index for large forest openings (> 0.04 ha or 0.1 acres and > 5 m mininum width) patch size distribution for the Lake Tahoe Basin landscape. The departure index represents the deviation of the current Subbasin and biophysical class (BPC) condition from its historical reference period condition, as simulated. Departure indices > 0 represent a current landscape with a distribution of developmental stage patch sizes that differs in some way from the historical reference period distribution, as simulated, and increasing values represent increasing degrees of departure.

To further evaluate departure in this patch size distribution metric, it is necessary to examine the CRV and HRV patch size distributions for the selected Subbasin-by-BPC partition, for example as depicted in **Figure 33**.

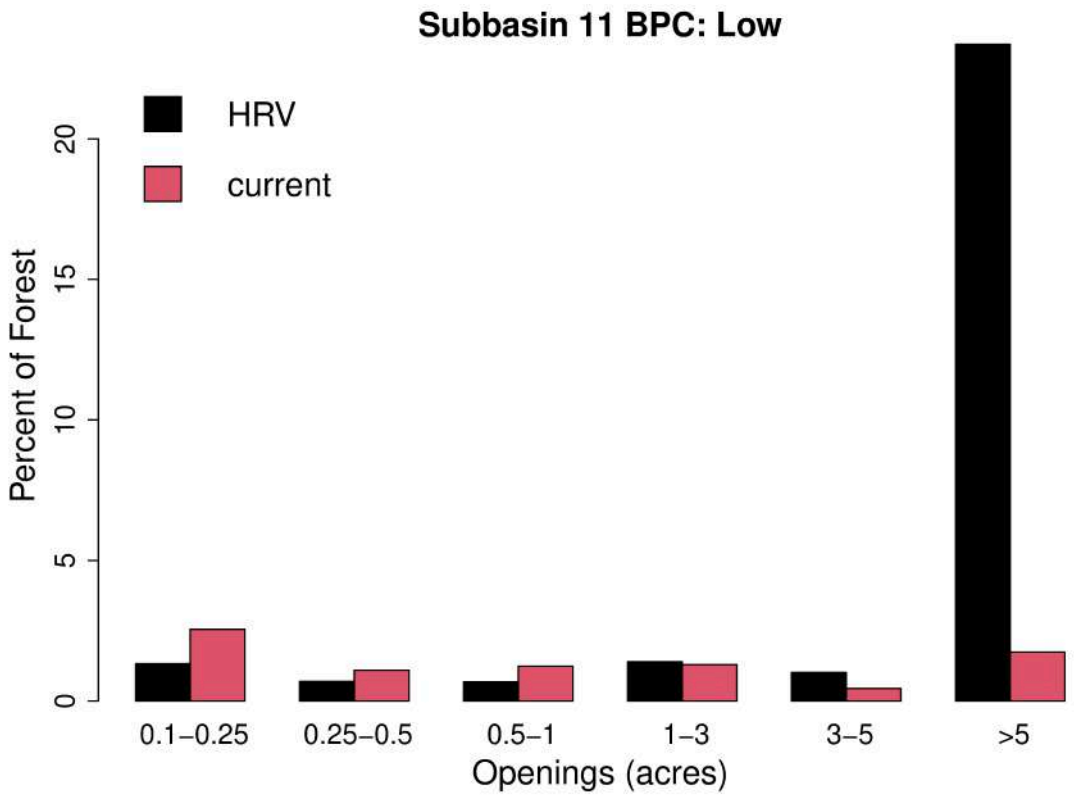

Figure 33: Barplot of the distribution of large forest openings (> 0.04 ha or 0.1 acres and > 5 m mininum width) patch sizes for the current landscape and the historical reference period (HRV) for Subbasin 11 and the Low productivity Biophysical Class (BPC = 1) for the Lake Tahoe Basin landscape. Each bar represents the percent of forest within the Subbasin and Biophysical Class (BPC) in large forest openings of a particular patch size. The departure index represents the percentage dissimilarity between the CRV and HRV distributions. Departure indices > 0 represent a current landscape with a distribution of large forest opening patch sizes that differs in some way from the historical reference period distribution, as simulated, and increasing values represent increasing degrees of departure.

Metric 3: Developmental Stage Patch Size Distribution

We defined developmental stages based on six tree height classes, ranging from Open (< 4.5 ft) to Tall Trees (> 125 ft), as described in the GTR. Here, for each snapshot of the landscape we constructed a patch mosaic comprised of developmental stages in which patches were defined using the 4-neighbor rule. For each snapshot, we quantified the size of each developmental stage patch and determined the percent of forest within the Subbasin-by-BPC partition in each of several patch size classes or bins. The departure index reflects whether or not the current landscape has a distribution of developmental stage patch sizes that differs from HRV and, if so, the degree of differences in the two distributions.

The Developmental Stage Patch Size Distribution departure index is depicted in **Figure 34**. As before, the departure index was assigned to each Subbasin-by-BPC partition; consequently, there were 48 distinct values assigned. Thus, to better assess departure by Subbasin and BPC, one needs to examine the attribute table for the departure layer.

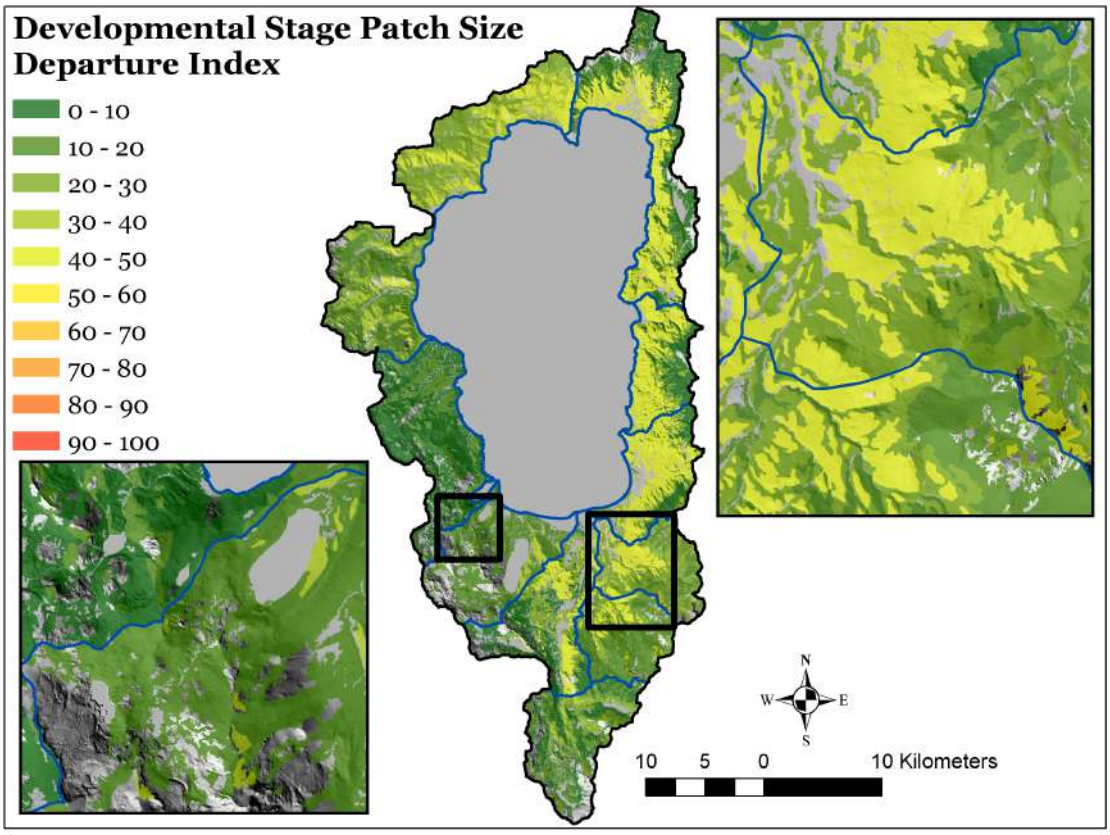

Figure 34: Subbasin-by-BPC level departure index for the developmental stage patch size distribution for the Lake Tahoe Basin landscape. Developmental stages were based on tree height classes and patches were based on the 4-neighbor adjacency rule. The departure index represents the deviation of the current Subbasin and biophysical class (BPC) condition from its historical reference period condition, as simulated. Departure indices > 0 represent a current landscape with a distribution of developmental stage patch sizes that differs in some way from the historical reference period distribution, as simulated, and increasing values represent increasing degrees of departure.

To further evaluate departure in this patch size distribution metric, it is necessary to examine the CRV and HRV patch size distributions for the selected Subbasin-by-BPC partition, for example as depicted in **Figure 35**.

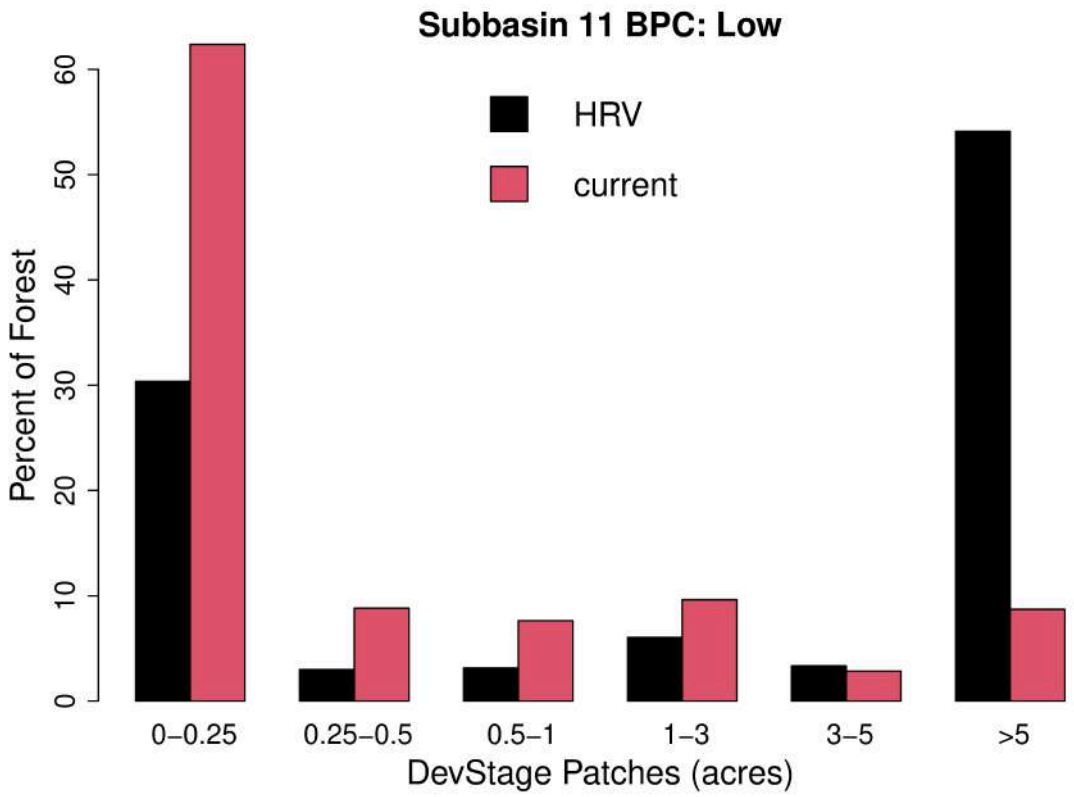

Figure 35: Barplot of the distribution of developmental stage patch sizes for the current landscape and the historical reference period (HRV) for Subbasin 11 and the Low productivity Biophysical Class (BPC = 1) for the Lake Tahoe Basin landscape. Developmental stages were based on tree height classes and patches were based on the 4-neighbor adjacency rule. Each bar represents the percent of forest within the Subbasin and BPC in developmental stage patches of a particular size. The departure index represents the sum of the deviations between the current and HRV bars. Departure indices > 0 represent a current landscape with a distribution of developmental stage patch sizes that differs in some way from the historical reference period distribution, as simulated, and increasing values represent increasing degrees of departure.

Metric 4: Percent Large Trees

We defined large trees as > 30 inch dbh. Percent Large Trees is defined as the percent of the forest within the Subbasin-by-BPC partition in large trees, as defined, and the departure index reflects whether or not the current landscape is deficient in large trees relative to HRV and, if so, the degree of deficiency. The departure index is negative if the current landscape has too little area in large trees compared to HRV.

The Percent Large Trees departure index is depicted in **Figure 36**. As before, the departure index was assigned to each Subbasin-by-BPC partition; consequently, there were 48 distinct values assigned. Thus, to better assess departure by Subbasin and BPC, one needs to examine the attribute table for the departure layer.

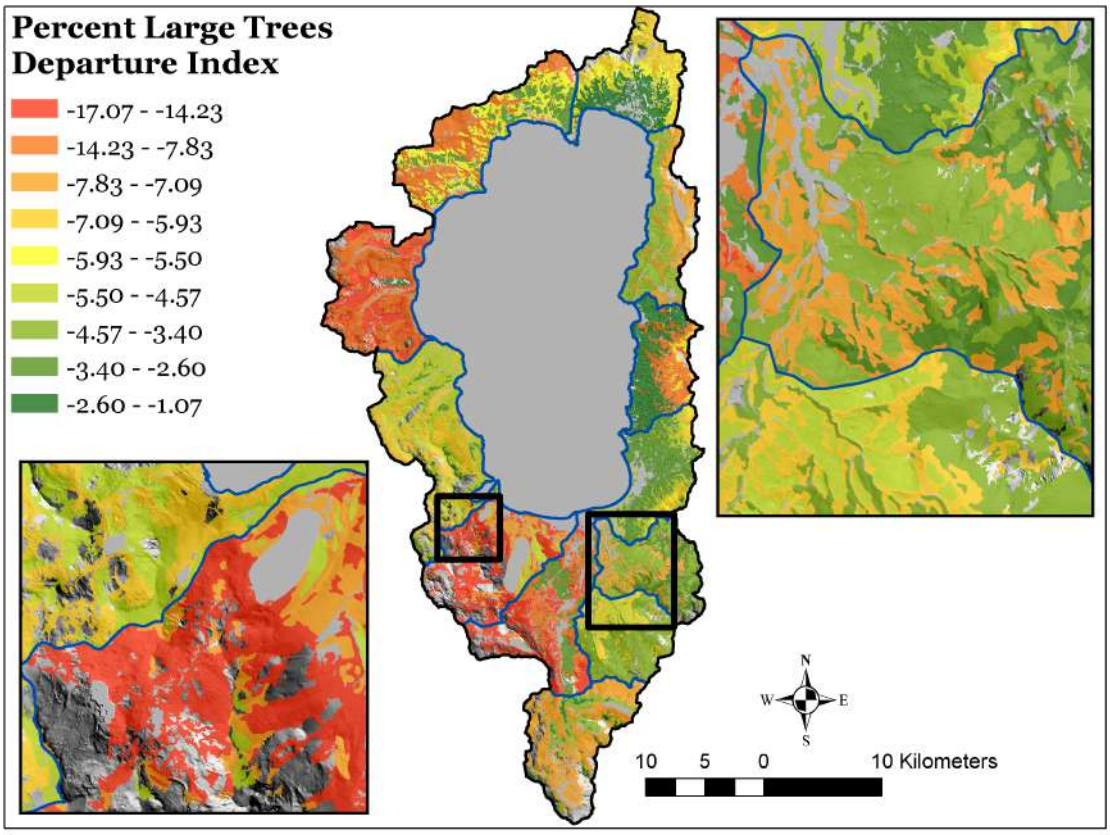

Figure 36: Subbasin-by-BPC level departure index for large trees (> 30 inch dbh) for the Lake Tahoe Basin landscape. The departure index represents the deviation of the current Subbasin and biophysical class (BPC) condition from its historical reference period condition, as simulated. Departure indices < -1 represent a current landscape with less total area in large trees than during the historical reference period, as simulated, and increasing negative values represent increasing degrees of departure.

Metric 5: Large Tree Patch Size Distribution

We defined large trees as described above. Here, we quantified the size of individual patches of large trees and determined the percent of forest within the Subbasin-by-BPC partition in large tree patches in each of several patch size classes or bins (see above), and compared the current and historical distributions. The departure index reflects whether or not the current landscape has a distribution of large tree patch sizes that differs from HRV and, if so, the degree of differences in the two distributions.

The Large Tree Patch Size Distribution departure index is depicted in **Figure 37**. As before, the departure index was assigned to each Subbasin-by-BPC partition; consequently, there were 48 distinct values assigned. Thus, to better assess departure by Subbasin and BPC, one needs to examine the attribute table for the departure layer.

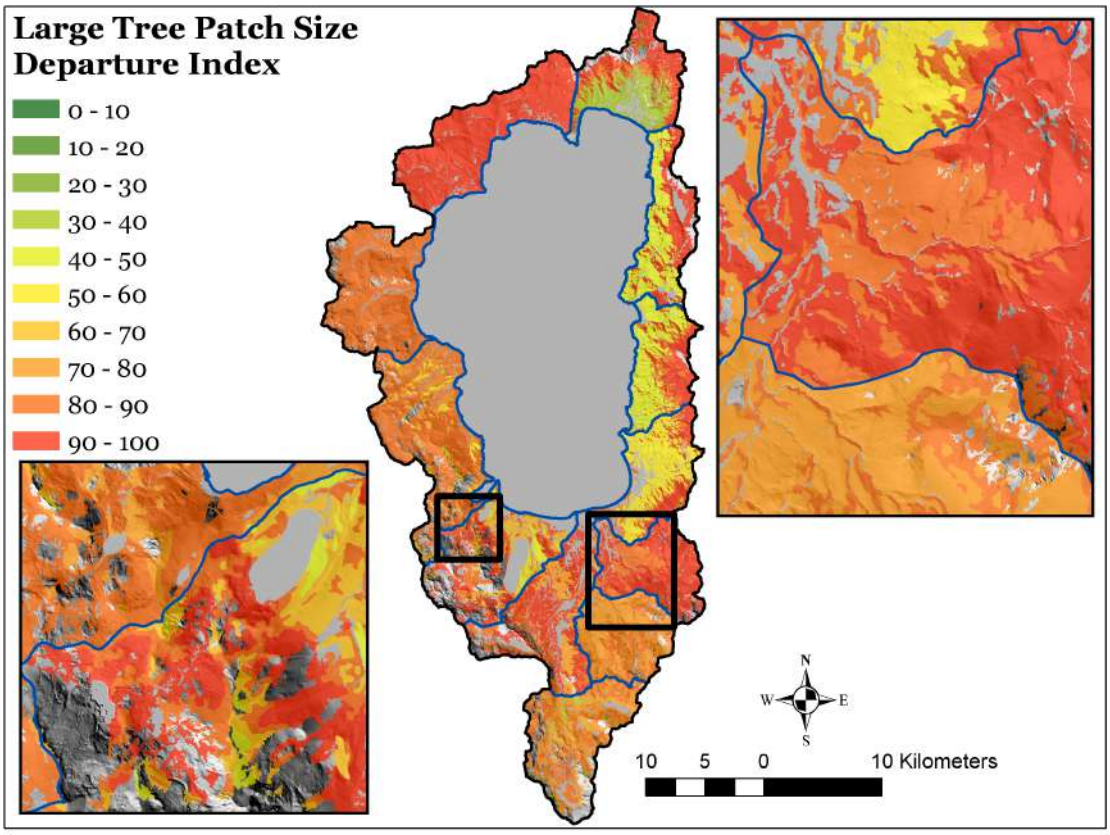

Figure 37: Subbasin-by-BPC level departure index for large tree (> 30 inch dbh) patch size distribution for the Lake Tahoe Basin landscape. The departure index represents the deviation of the current Subbasin and biophysical class (BPC) condition from its historical reference period condition, as simulated. Departure indices > 0 represent a current landscape with a distribution of large tree patch sizes that differs in some way from the historical reference period distribution, as simulated, and increasing values represent increasing degrees of departure.

To further evaluate departure in this patch size distribution metric, it is necessary to examine the CRV and HRV patch size distributions for the selected Subbasin-by-BPC partition, for example as depicted in **Figure 38**.

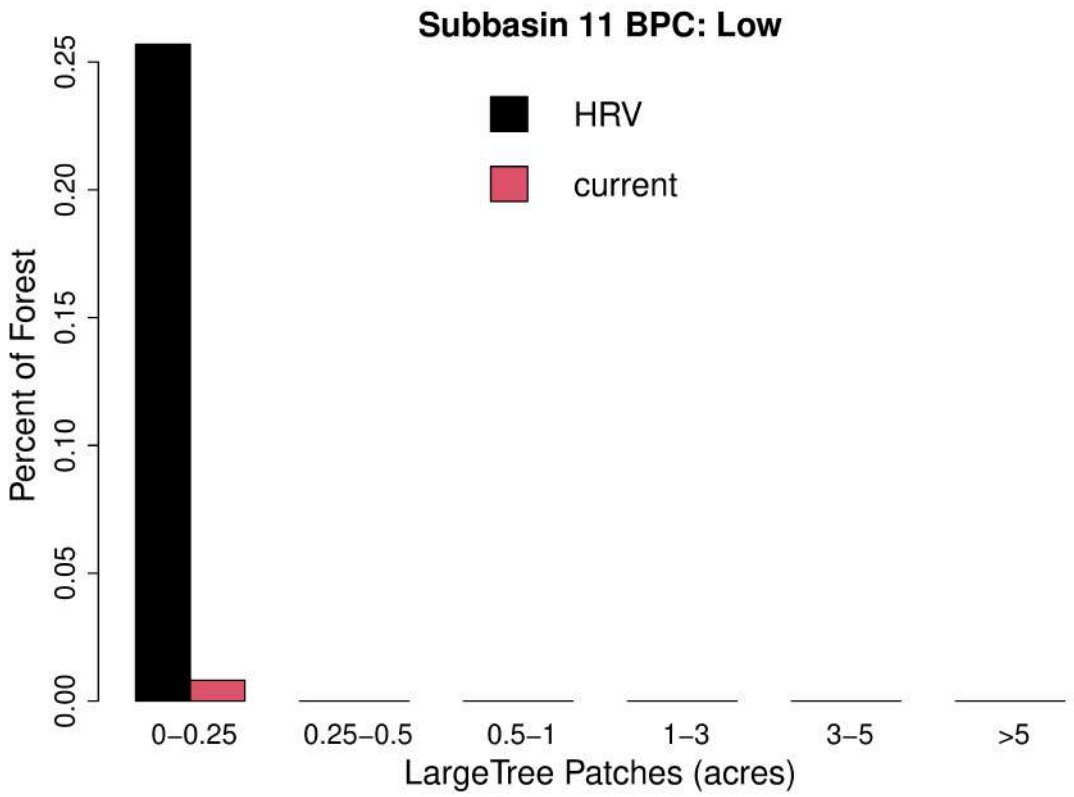

Figure 38: Barplot of the distribution of large tree (> 30 inch dbh) patch sizes for the current landscape and the historical reference period (HRV) for Subbasin 11 and the Low productivity Biophysical Class (BPC = 4) for the Lake Tahoe Basin landscape. See previous barplot caption for details on interpretation.

Metric 6: Tree Size Class Patch Size Distribution

We defined tree size class based on six tree diameter classes, ranging from Open (< 1 in dbh) to large Trees (> 30 in dbh), as described previously. Here, for each snapshot of the landscape we constructed a patch mosaic comprised of tree size classes in which patches were defined using the 4-neighbor rule. For each snapshot, we quantified the size of each tree size class patch and determined the percent of forest within the Subbasin-by-BPC partition in each of several patch size classes or bins. The departure index reflects whether or not the current landscape has a distribution of tree size class patch sizes that differs from HRV and, if so, the degree of differences in the two distributions.

The Tree Size Class Patch Size Distribution departure index is depicted in **Figure 39**. As before, the departure index was assigned to each Subbasin-by-BPC partition; consequently, there were 48 distinct values assigned. Thus, to better assess departure by Subbasin and BPC, one needs to examine the attribute table for the departure layer.

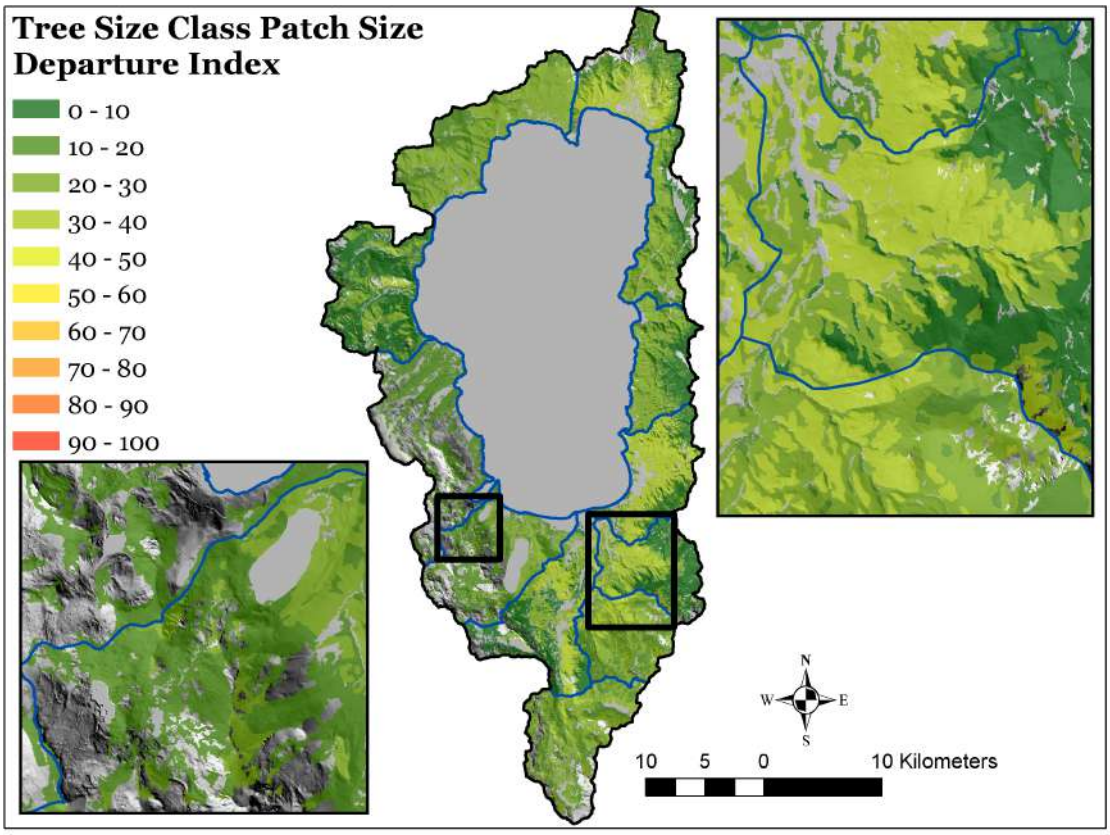

Figure 39: Subbasin-by-BPC level departure index for tree size class (based on dbh) patch size distribution for the Lake Tahoe Basin landscape. The departure index represents the deviation of the current Subbasin and biophysical class (BPC) condition from its historical reference period condition, as simulated. Departure indices > 0 represent a current landscape with a distribution of tree size patch sizes that differs in some way from the historical reference period distribution, as simulated, and increasing values represent increasing degrees of departure.

To further evaluate departure in this patch size distribution metric, it is necessary to examine the CRV and HRV patch size distributions for the selected Subbasin-by-BPC partition, for example as depicted in **Figure 40**.

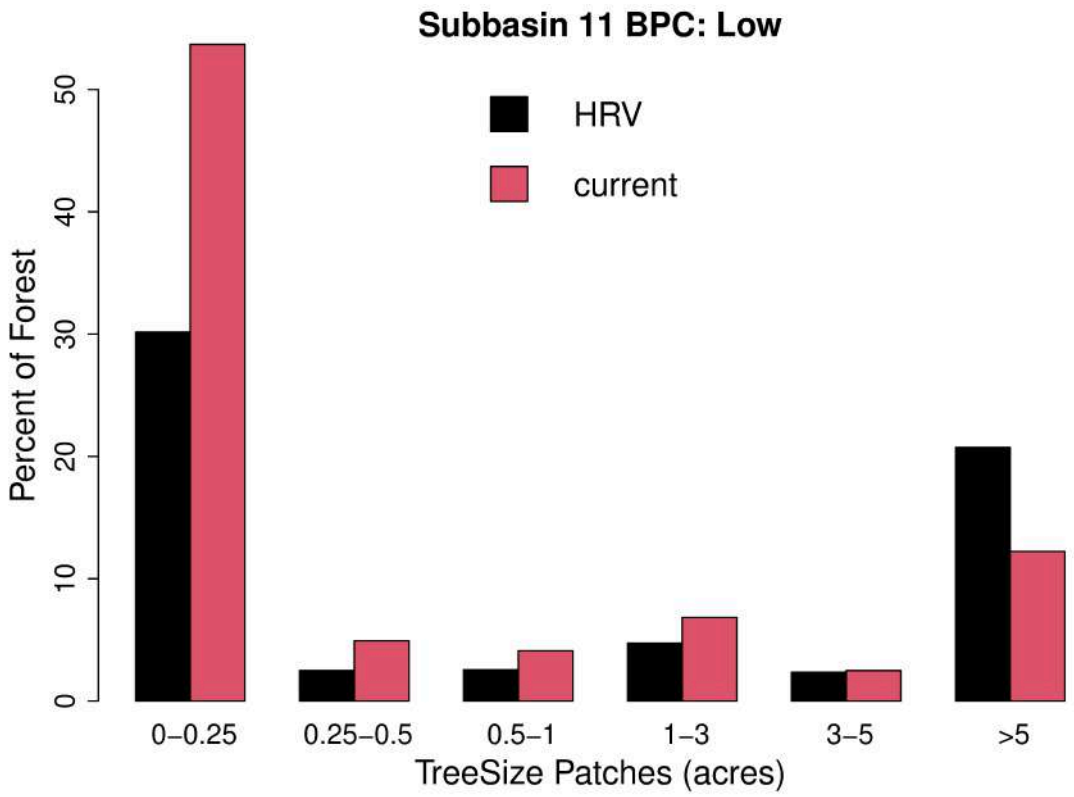

Figure 40: Barplot of the distribution of tree size class (based on dbh) patch sizes for the current landscape and the historical reference period (HRV) for Subbasin 11 and the Low productivity Biophysical Class (BPC = 4) for the Lake Tahoe Basin landscape. See previous barplot caption for details on interpretation.

Composite Departure Score

We combined the 6 Subbasin-level departure metrics above into a single composite departure score, which can be interpreted as a measure of overall departure in vegetation composition and configuration within the Subbasin-by-BPC partition. Maximum departure occurs when the forest has too little area in large forest openings and/or large trees, and/or too homogeneous or uniform a vegetation patch mosaic (i.e., too little spatial variability) defined on the basis of either developmental stages (or tree height classes) or tree size classes (or tree diameter classes).

The composite departure score is depicted in **Figure 41**. Not surprisingly, the Subbasins and BPCs vary somewhat in their overall departure from HRV, and these differences provide a basis for prioritizing project locations with this landscape.

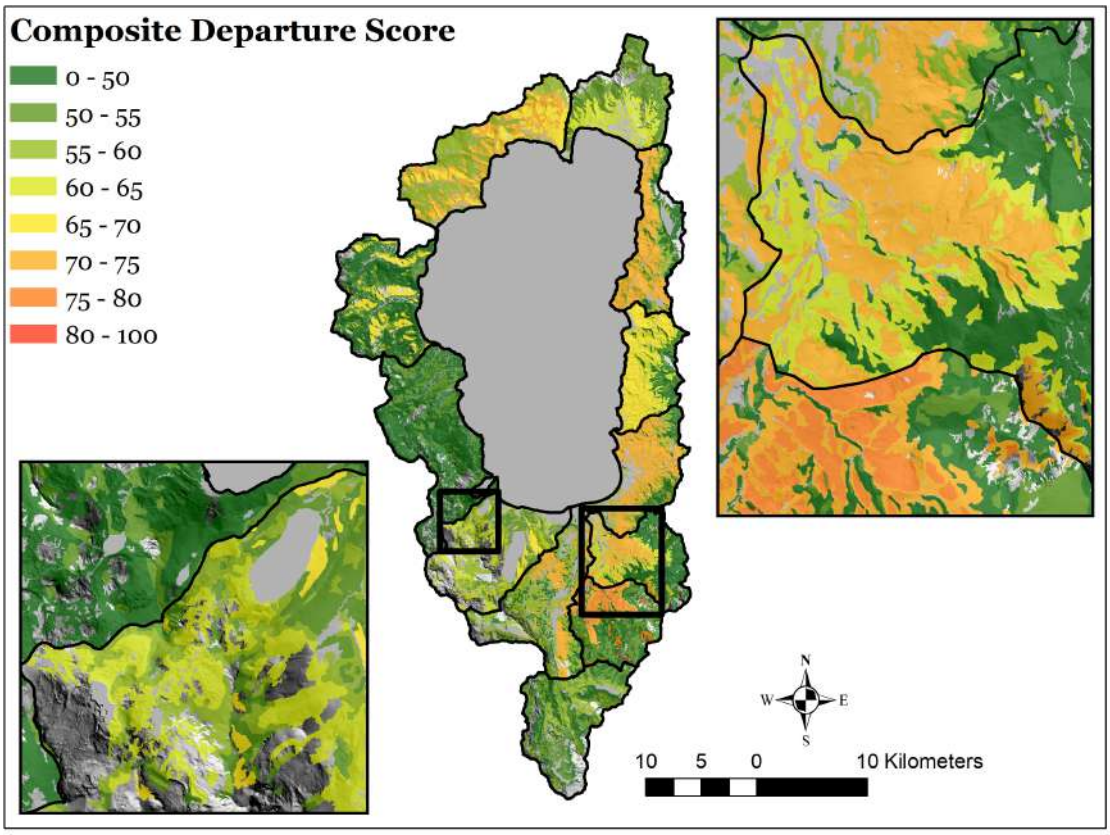

Figure 41: Subbasin-by-BPC level composite departure index derived from the average of the six component metrics for the Lake Tahoe Basin landscape. The composite departure index represents the percentage of maximum departure of the current GPU condition from its historical range of variability (HRV), as simulated. Larger values indicate increasing degrees of departure.

APPENDIX D1 - Wildfire Susceptibility

As described in the GTR, wildfire susceptibility was modeled as a Logistic function of fuels and climate for most cover types. The fuels component was modeled as a Logistic function of the number of years since the last fire (fuelAge) and the Heat Load Index (hli). The climate component was modeled as a Logistic function of the Wildfire Climate Index which was based on the inverted and rescaled 5-year mean Palmer Modified Drought Index. The fuels and climate components were combined with a geometric mean to produce the final Wildfire Susceptibility Index. The final function included 5 beta coefficients (b_0 - b_4). We used expert opinion to specify the beta coefficients for each cover type. We varied the b_0 and b_1 coefficients among cover types to reflect differences in reported historical mean fire return intervals among cover types - shifting the response curves left or right so that the inflection point (Wildfire Susceptibility Index = 0.5) roughly equaled the target mean return interval - and held the Heat Load Index coefficient (b_2) and Climate coefficients (b_3 and b_4) the same across all cover types to reflect the global affect of topography and climate on wildfire susceptibility.

The figures below depict the final wildfire susceptibility response functions for each cover type in alphabetical order (noting that some cover types did not have response functions, as noted in the text). The response functions depict the wildfire Susceptibility Index as a Logistic function of the number of years since the last fire (Years since fire). The dashed, solid and dotted lines depict the response functions for the minimum, mean and maximum Heat Load Index (hli), and the red, black and green sets of lines depict the response functions for the minimum, mean and maximum Wildfire Climate Index. The values of the Logistic parameters (b_0 - b_4) for the cover type are shown as well.

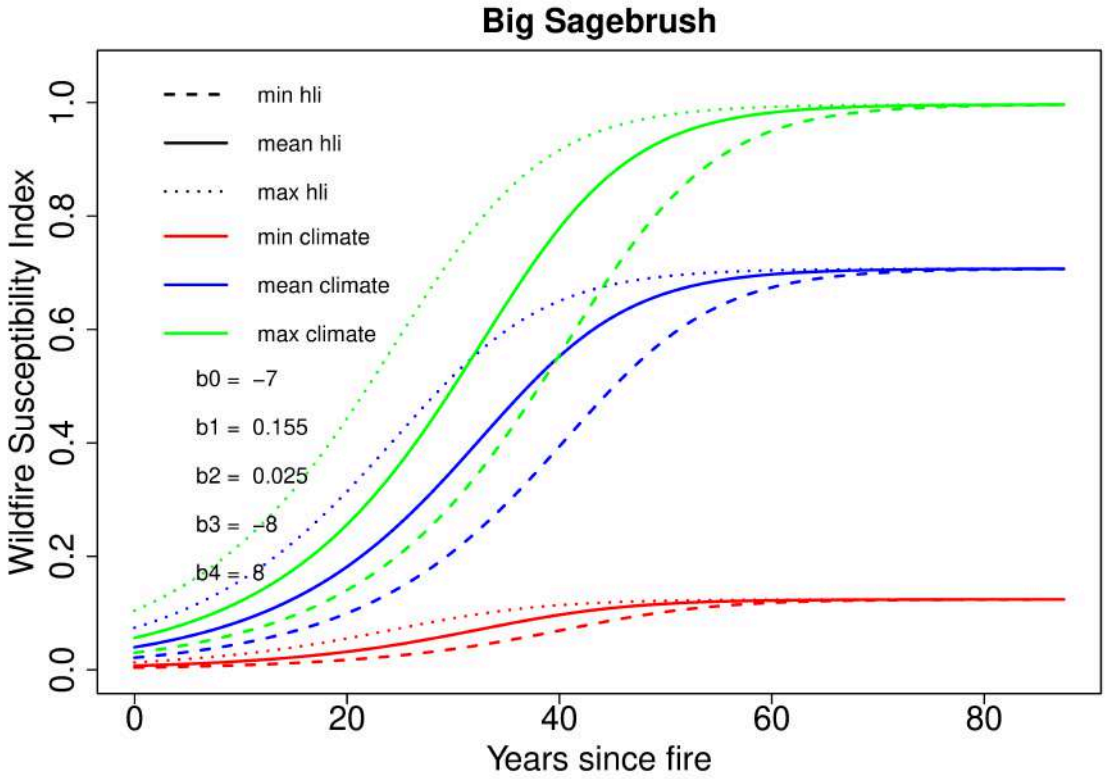

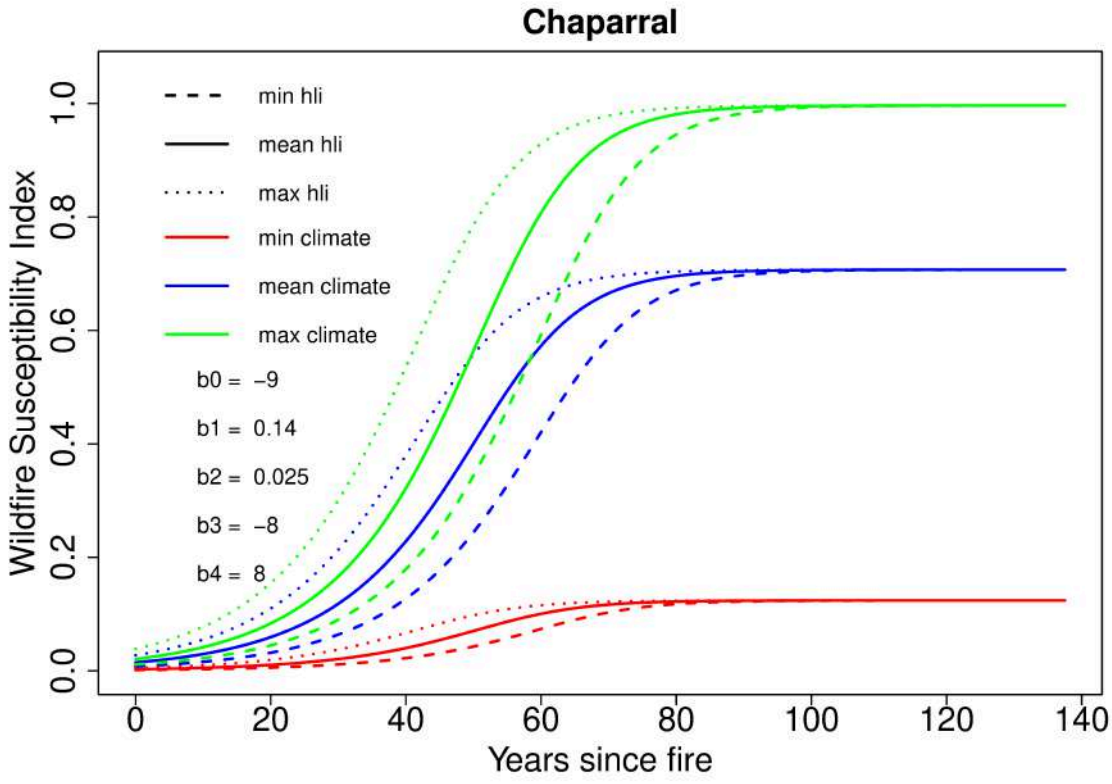
Chaparral
min hli
mean hli
max hli
min climate
mean climate
max climate
b0 = −9
b1 = 0.14
b2 = 0.025
b3 = −8
b4 = 8
Wildfire Susceptibility Index
0.0
0.2
0.4
0.6
0.8
1.0
0
20
40
60
80
100
120
140
Years since fire

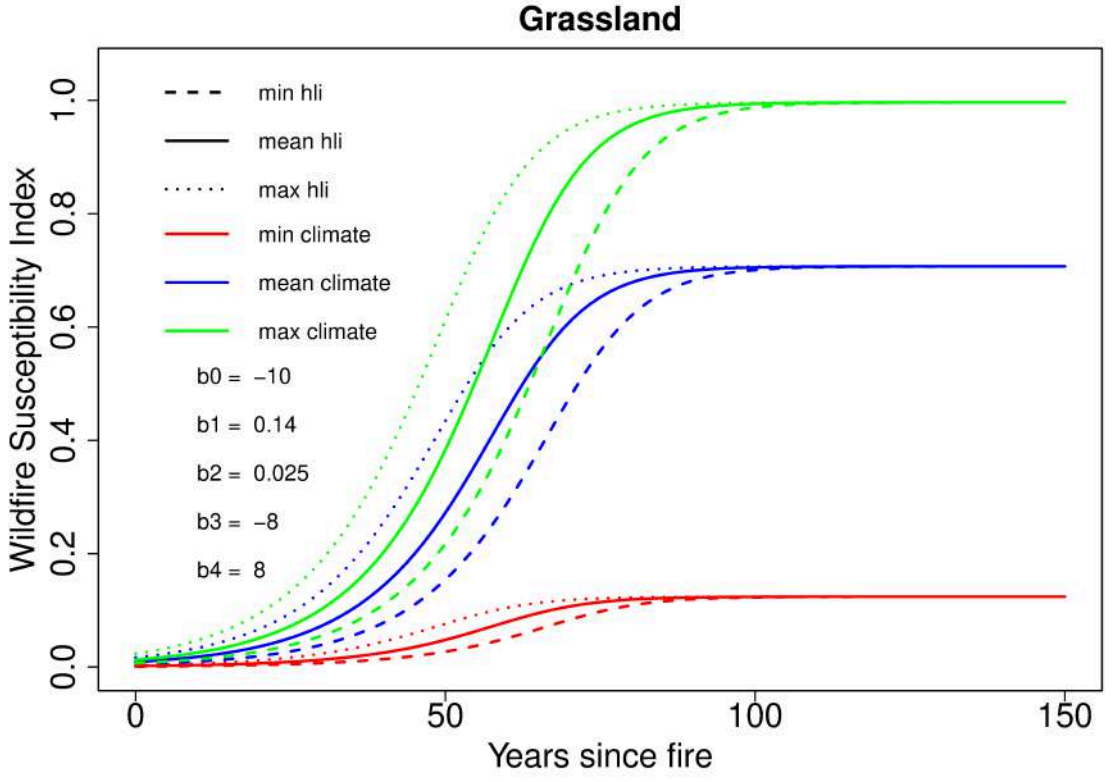
Grassland
min hli
mean hli
max hli
min climate
mean climate
max climate
b0 = −10
b1 = 0.14
b2 = 0.025
b3 = −8
b4 = 8
Wildfire Susceptibility Index
0.0
0.2
0.4
0.6
0.8
1.0
0
50
100
150
Years since fire

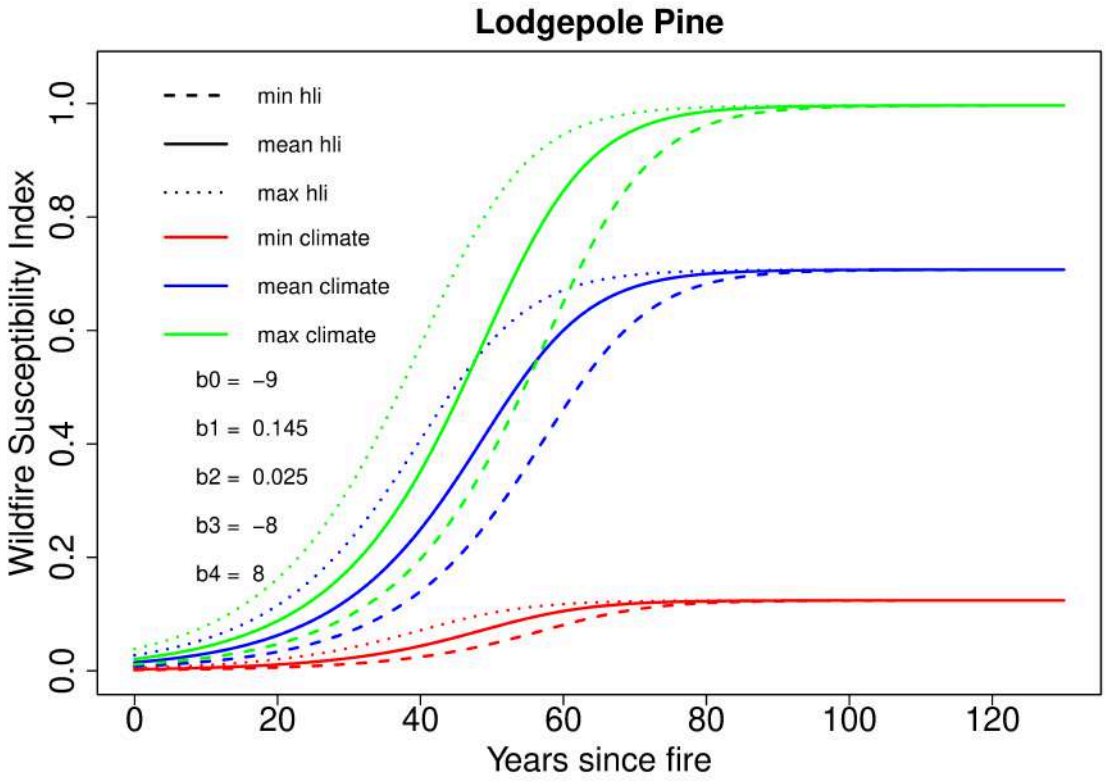
Lodgepole Pine
min hli
mean hli
max hli
min climate
mean climate
max climate
b0 = −9
b1 = 0.145
b2 = 0.025
b3 = −8
b4 = 8
Wildfire Susceptibility Index
0.0
0.2
0.4
0.6
0.8
1.0
0
20
40
60
80
100
120
Years since fire

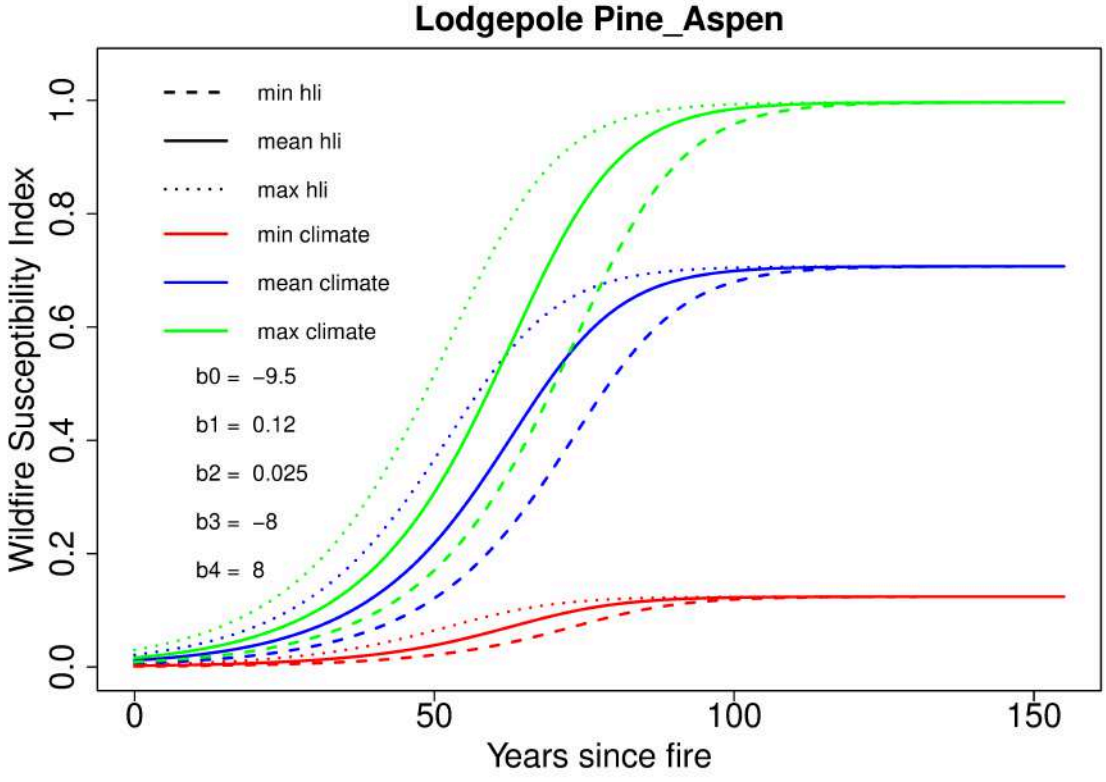
Lodgepole Pine_Aspen
min hli
mean hli
max hli
min climate
mean climate
max climate
b0 = −9.5
b1 = 0.12
b2 = 0.025
b3 = −8
b4 = 8
Wildfire Susceptibility Index
0.0
0.2
0.4
0.6
0.8
1.0
0
50
100
150
Years since fire

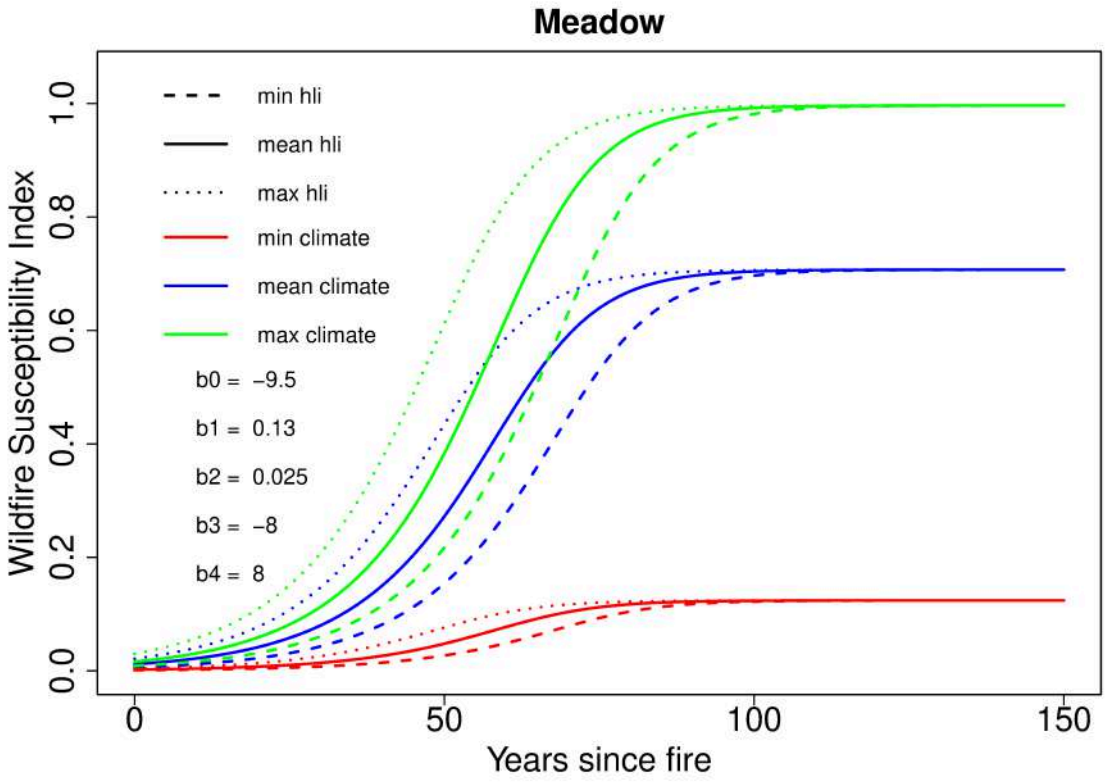
Meadow
min hli
mean hli
max hli
min climate
mean climate
max climate
b0 = −9.5
b1 = 0.13
b2 = 0.025
b3 = −8
b4 = 8
Wildfire Susceptibility Index
0.0
0.2
0.4
0.6
0.8
1.0
0
50
100
150
Years since fire

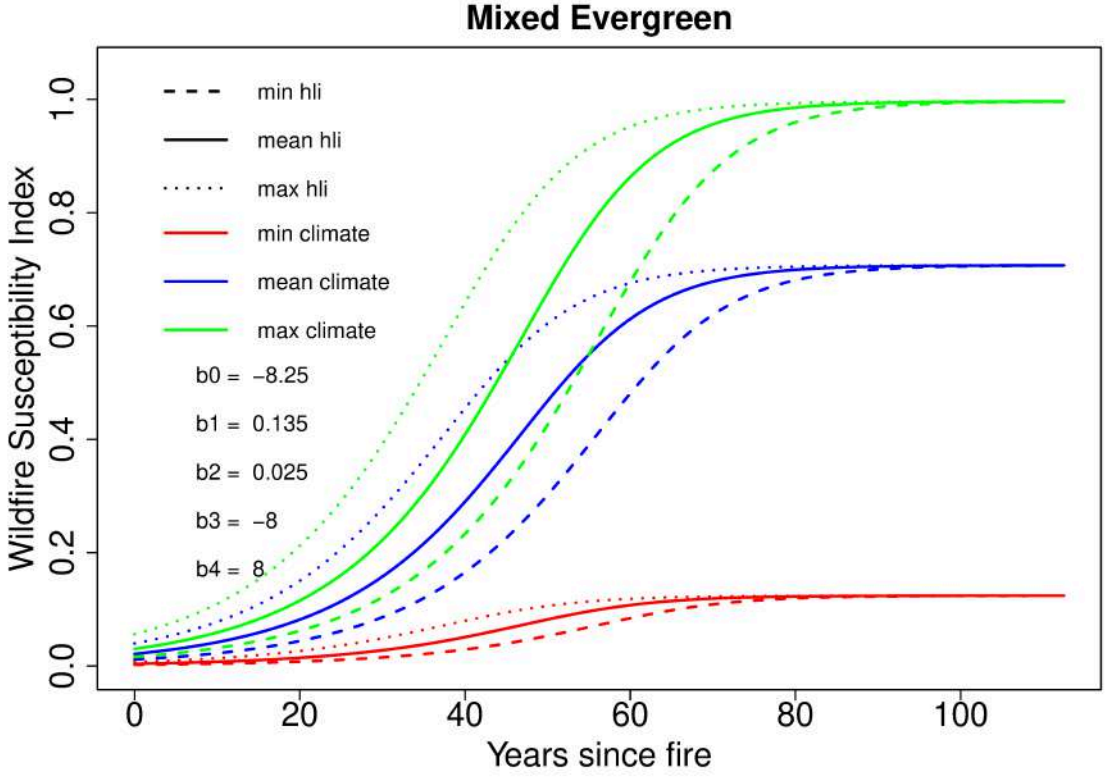
Mixed Evergreen
min hli
mean hli
max hli
min climate
mean climate
max climate
b0 = −8.25
b1 = 0.135
b2 = 0.025
b3 = −8
b4 = 8
Wildfire Susceptibility Index
0.0
0.2
0.4
0.6
0.8
1.0
0
20
40
60
80
100
Years since fire

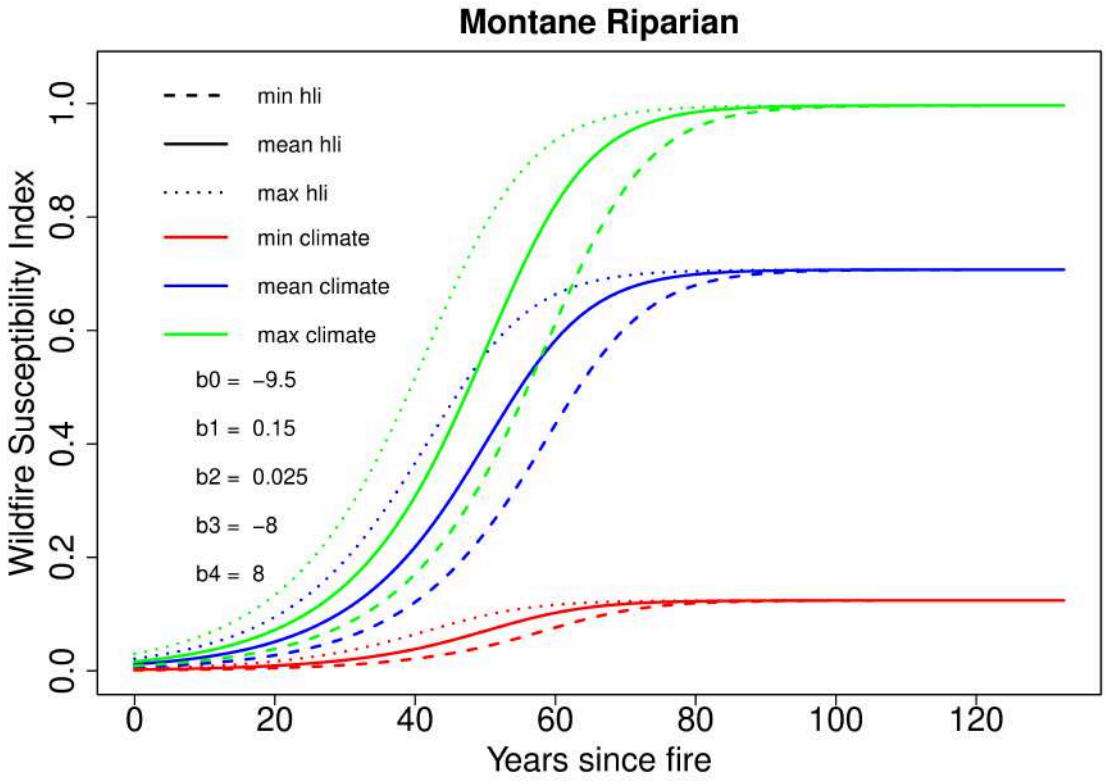
Montane Riparian
min hli
mean hli
max hli
min climate
mean climate
max climate
b0 = −9.5
b1 = 0.15
b2 = 0.025
b3 = −8
b4 = 8
Wildfire Susceptibility Index
0.0
0.2
0.4
0.6
0.8
1.0
0
20
40
60
80
100
120
Years since fire

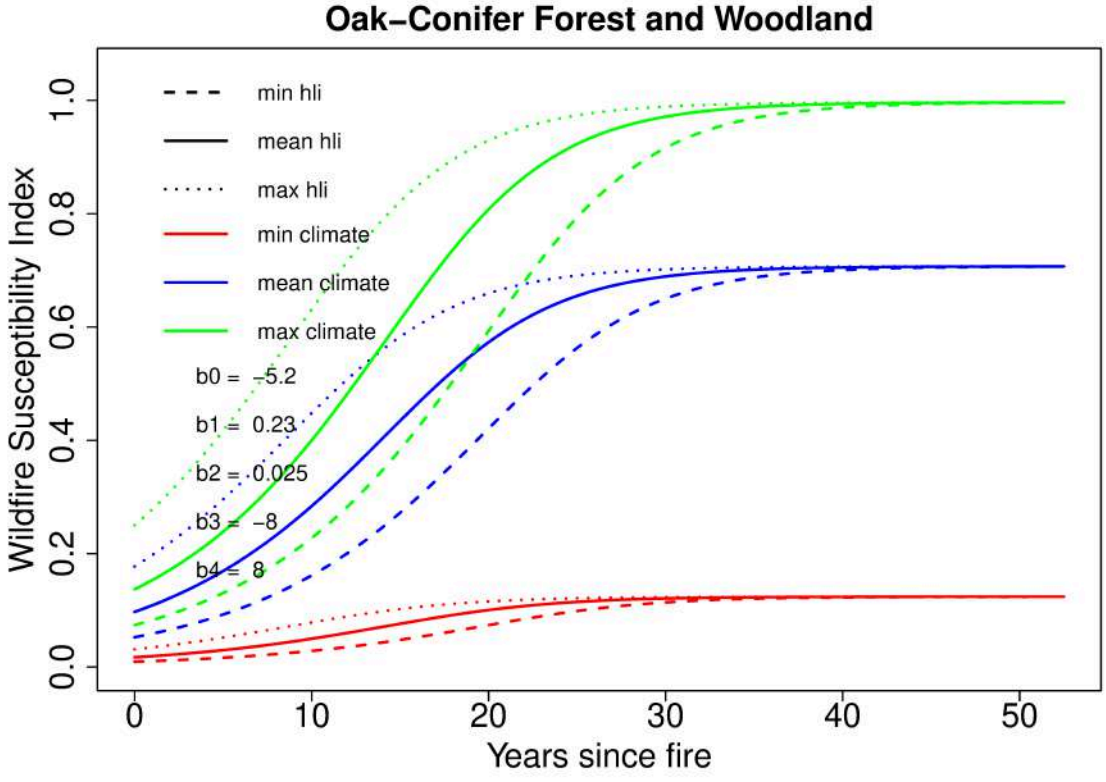
Oak−Conifer Forest and Woodland
min hli
mean hli
max hli
min climate
mean climate
max climate
b0 = −5.2
b1 = 0.23
b2 = 0.025
b3 = −8
b4 = 8
Wildfire Susceptibility Index
0.0
0.2
0.4
0.6
0.8
1.0
0
10
20
30
40
50
Years since fire

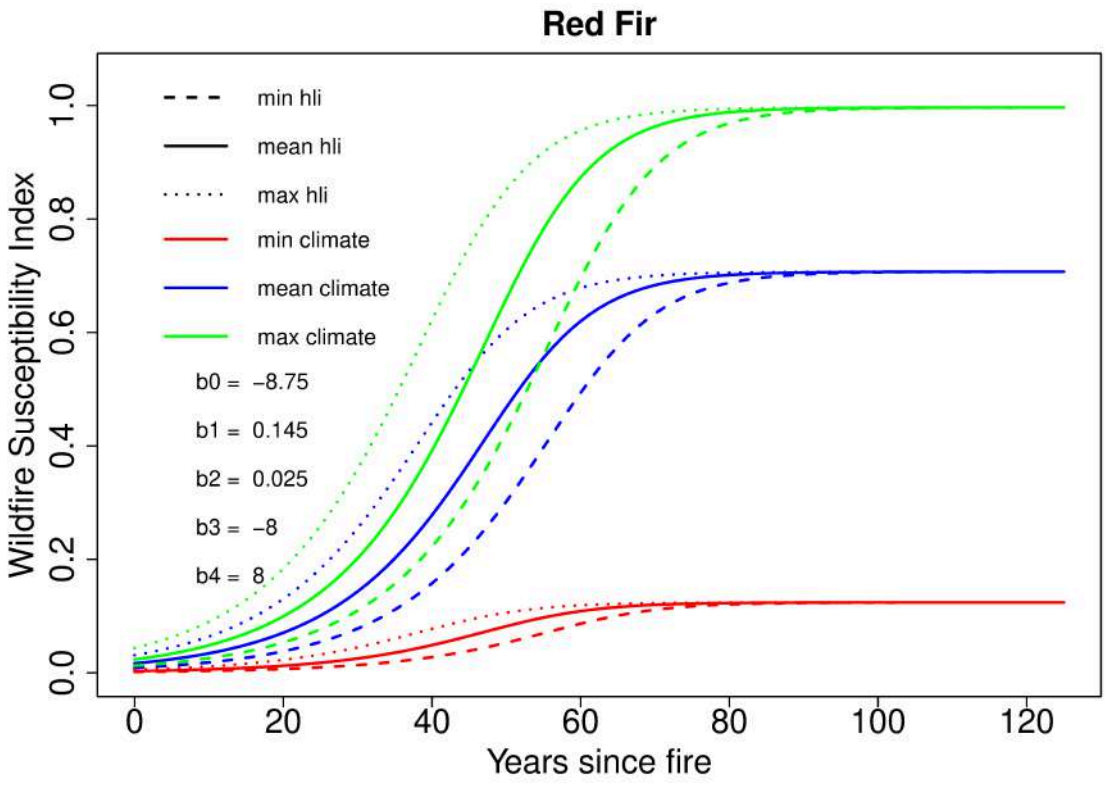
Red Fir
min hli
mean hli
max hli
min climate
mean climate
max climate
b0 = −8.75
b1 = 0.145
b2 = 0.025
b3 = −8
b4 = 8
Wildfire Susceptibility Index
0.0
0.2
0.4
0.6
0.8
1.0
0
20
40
60
80
100
120
Years since fire

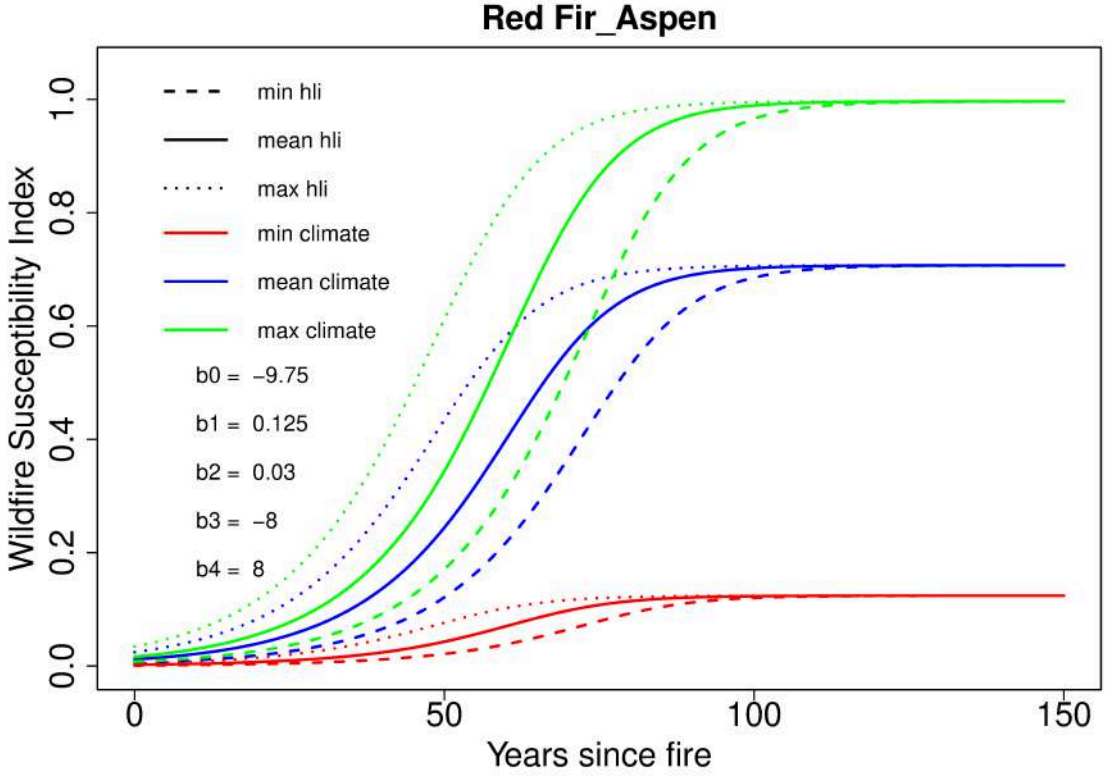
Red Fir_Aspen
min hli
mean hli
max hli
min climate
mean climate
max climate
b0 = −9.75
b1 = 0.125
b2 = 0.03
b3 = −8
b4 = 8
Wildfire Susceptibility Index
0.0
0.2
0.4
0.6
0.8
1.0
0
50
100
150
Years since fire

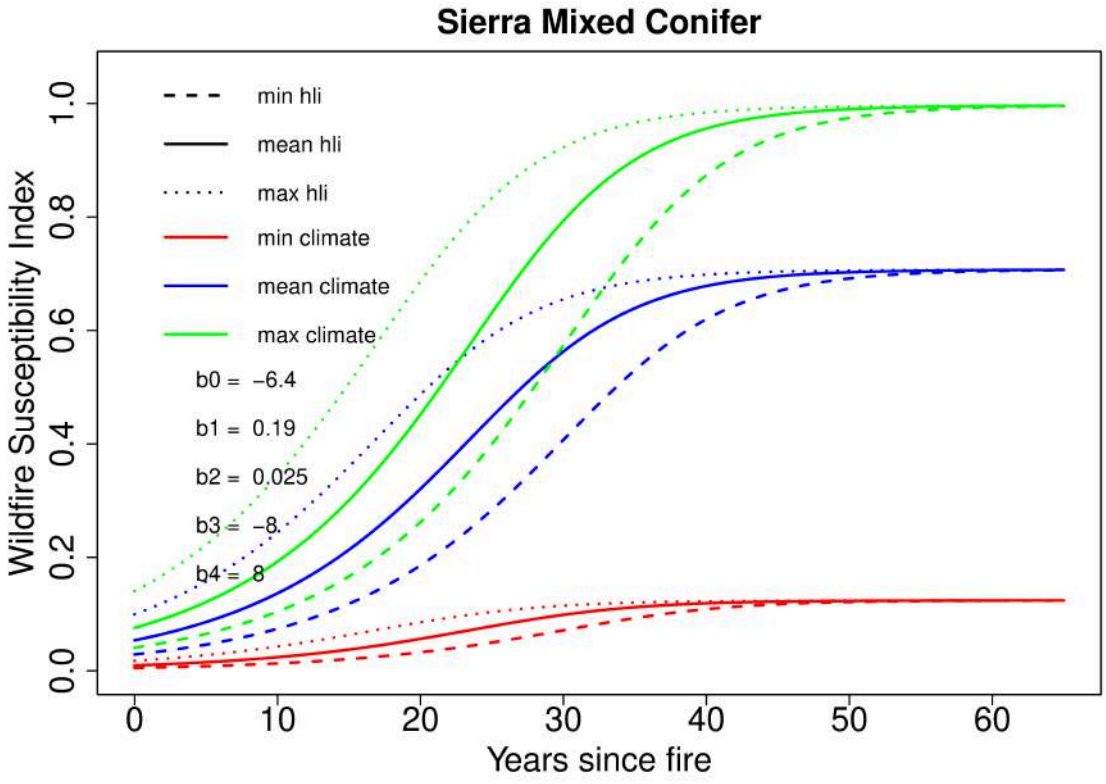
Sierra Mixed Conifer
min hli
mean hli
max hli
min climate
mean climate
max climate
b0 = −6.4
b1 = 0.19
b2 = 0.025
b3 = −8
b4 = 8
Wildfire Susceptibility Index
0.0
0.2
0.4
0.6
0.8
1.0
0
10
20
30
40
50
60
Years since fire

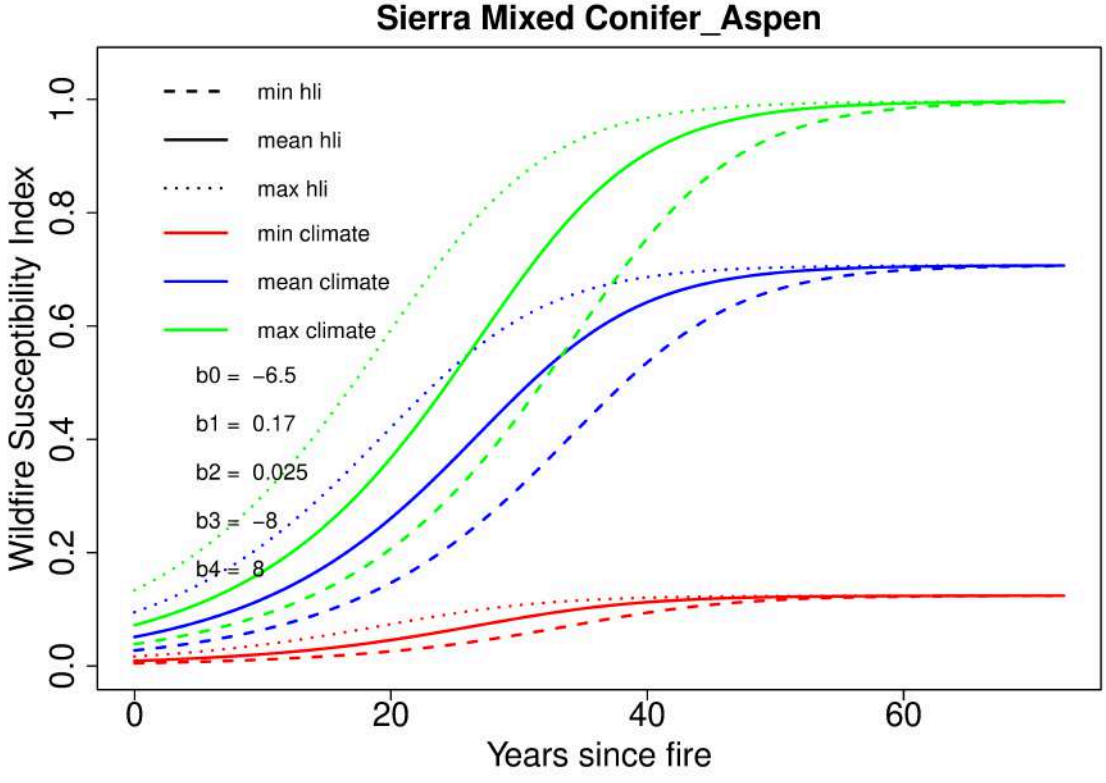
Sierra Mixed Conifer_Aspen
min hli
mean hli
max hli
min climate
mean climate
max climate
b0 = −6.5
b1 = 0.17
b2 = 0.025
b3 = −8
b4 = 8
Wildfire Susceptibility Index
0.0
0.2
0.4
0.6
0.8
1.0
0
20
40
60
Years since fire

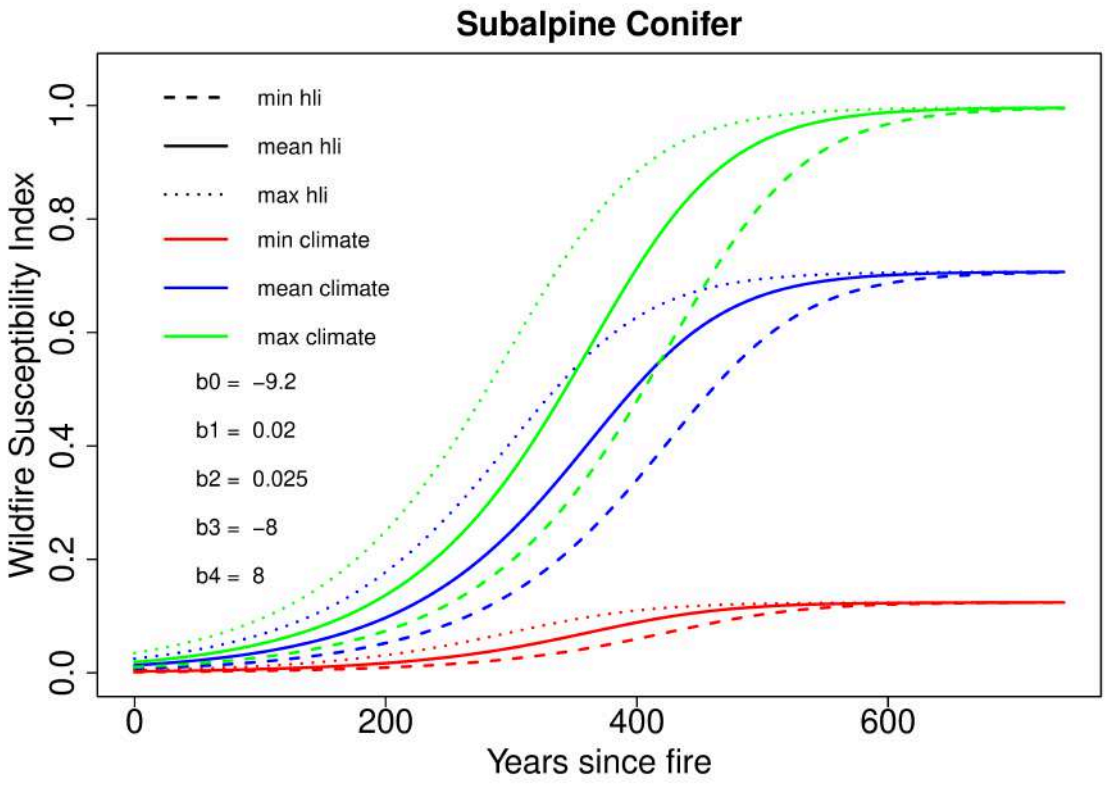
Subalpine Conifer
min hli
mean hli
max hli
min climate
mean climate
max climate
b0 = −9.2
b1 = 0.02
b2 = 0.025
b3 = −8
b4 = 8
Wildfire Susceptibility Index
0.0
0.2
0.4
0.6
0.8
1.0
0
200
400
600
Years since fire

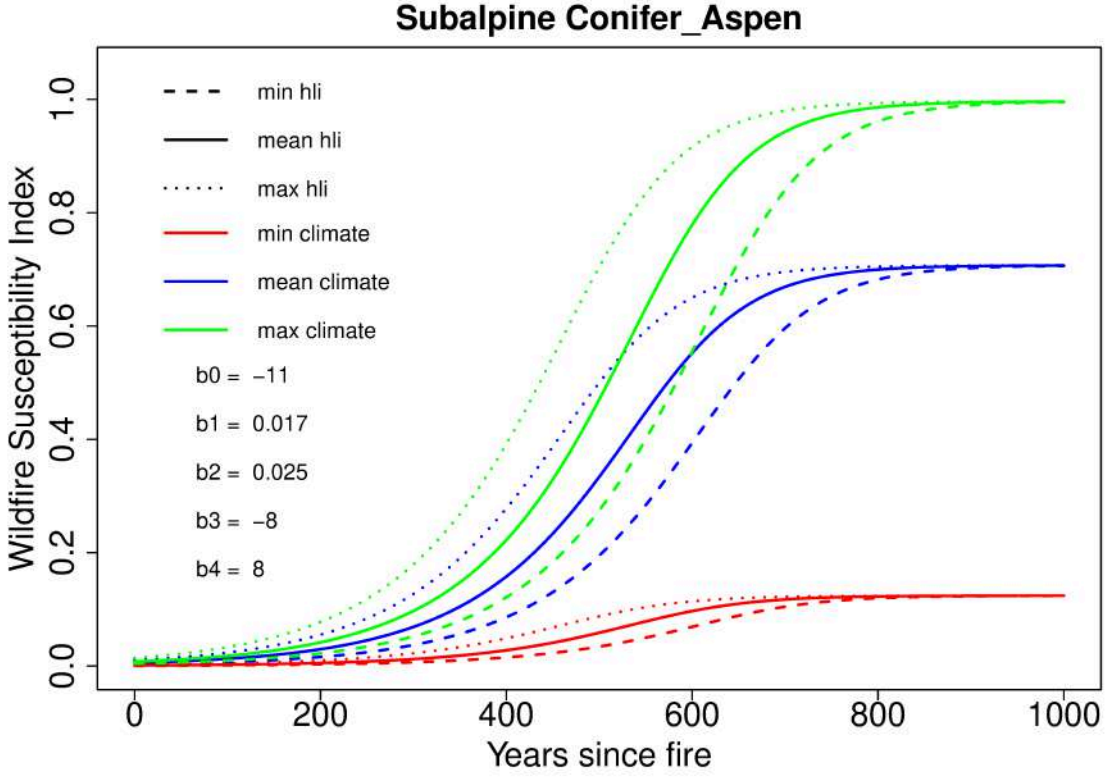
Subalpine Conifer_Aspen
min hli
mean hli
max hli
min climate
mean climate
max climate
b0 = −11
b1 = 0.017
b2 = 0.025
b3 = −8
b4 = 8
Wildfire Susceptibility Index
0.0
0.2
0.4
0.6
0.8
1.0
0
200
400
600
800
1000
Years since fire

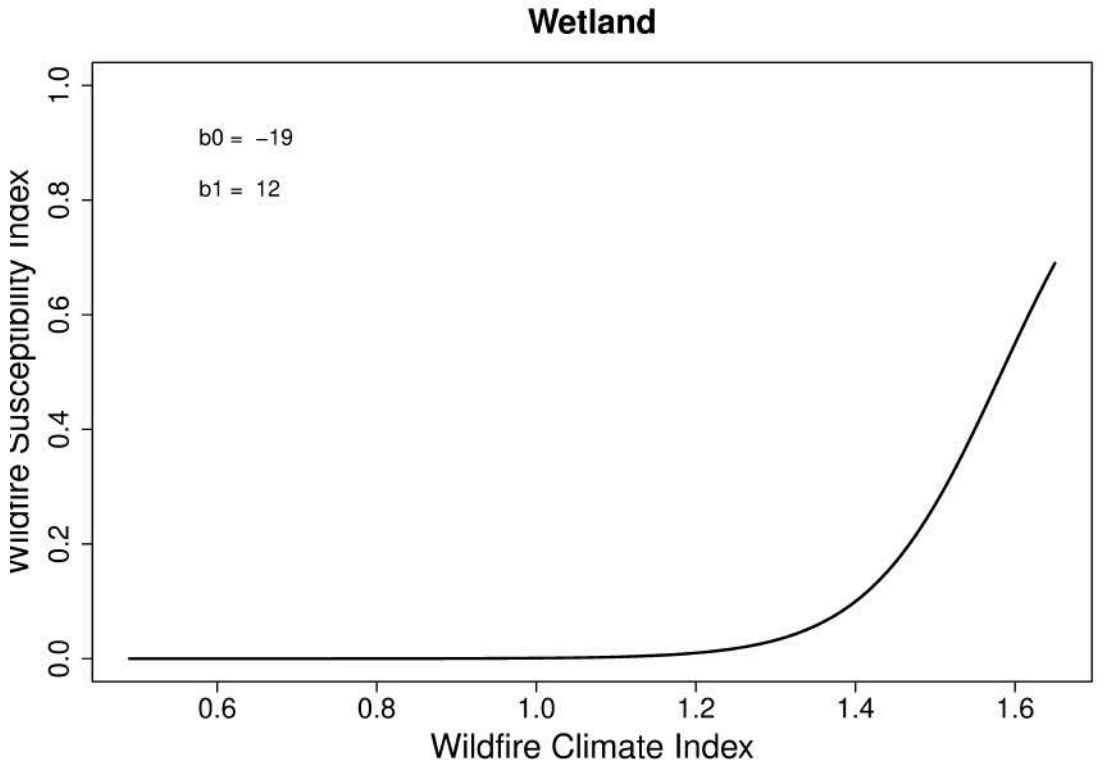
Wetland
b0 = −19
b1 = 12
Wildfire Susceptibility Index
0.0
0.2
0.4
0.6
0.8
1.0
0.6
0.8
1.0
1.2
1.4
1.6
Wildfire Climate Index

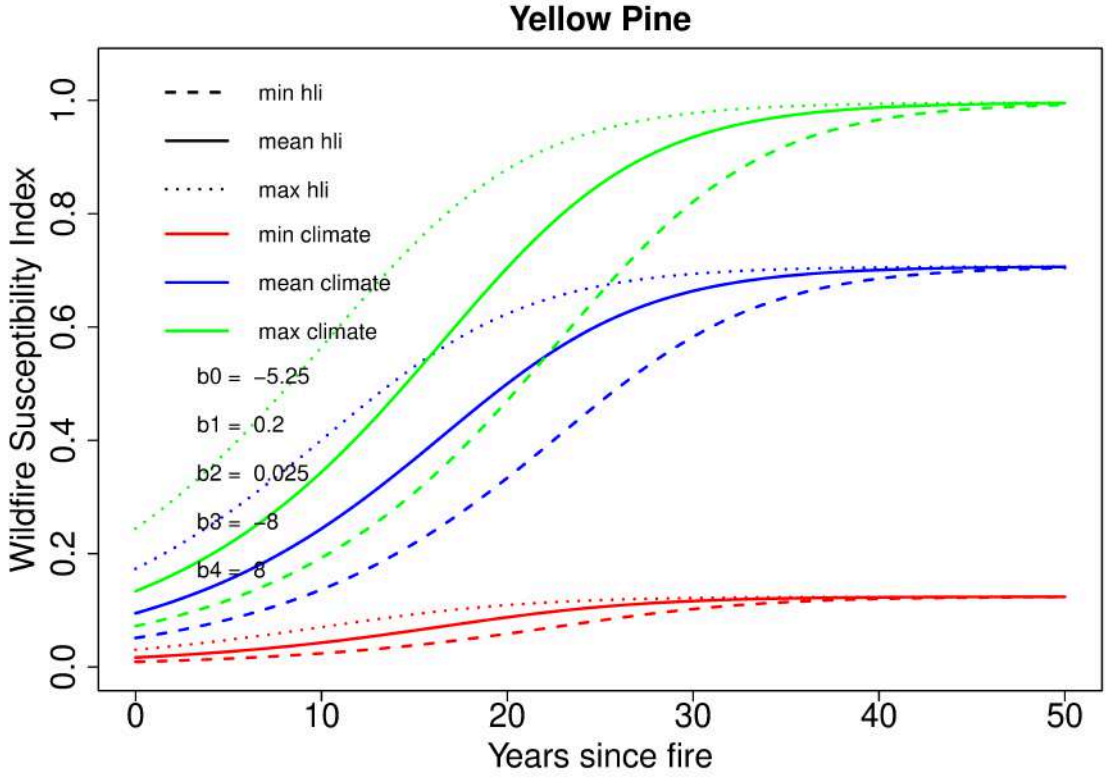
Yellow Pine
min hli
mean hli
max hli
min climate
mean climate
max climate
b0 = −5.25
b1 = 0.2
b2 = 0.025
b3 = −8
b4 = 8
Wildfire Susceptibility Index
0.0
0.2
0.4
0.6
0.8
1.0
0
10
20
30
40
50
Years since fire

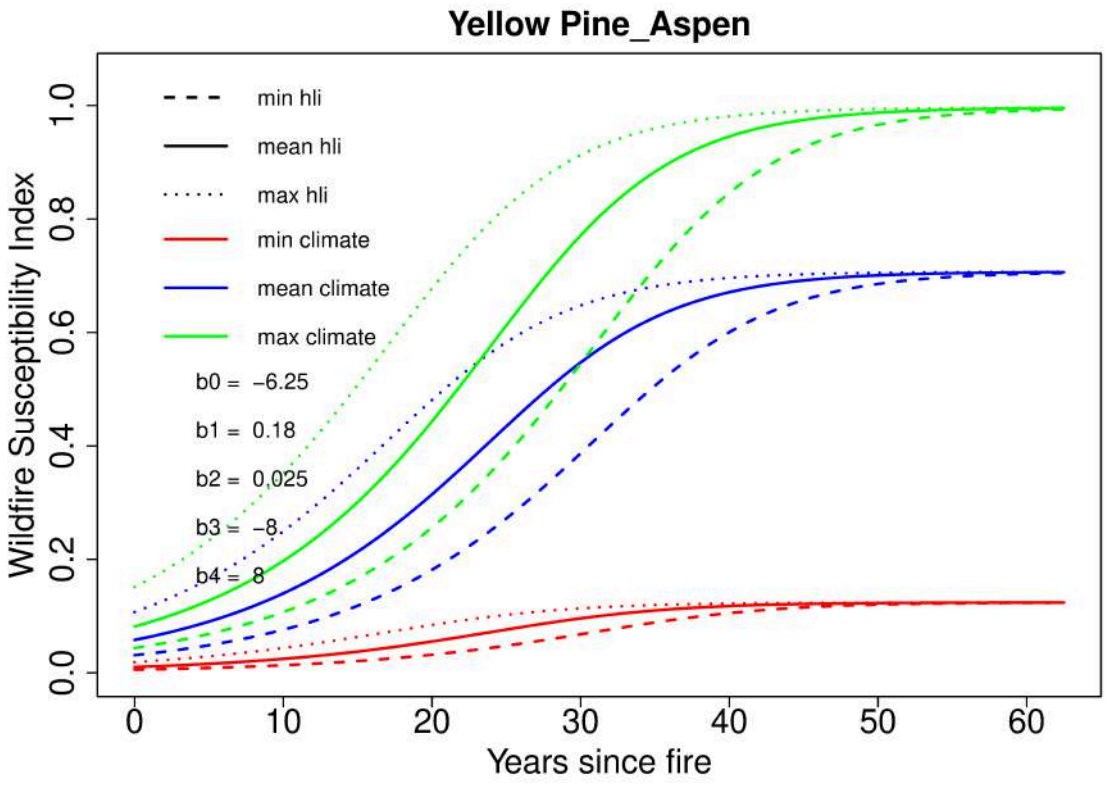
Yellow Pine_Aspen
min hli
mean hli
max hli
min climate
mean climate
max climate
b0 = −6.25
b1 = 0.18
b2 = 0.025
b3 = −8
b4 = 8
Wildfire Susceptibility Index
0.0
0.2
0.4
0.6
0.8
1.0
0
10
20
30
40
50
60
Years since fire

APPENDIX D2 - Wildfire Mortality

As described in the GTR, wildfire mortality (i.e., the probability of high mortality or death of the overstory vegetation in each 5 m cell that burned) was determined by a complex function involving two major factors: 1) fire intensity, which was a Logistic function of the fuel loads in the neighborhood of the focal cell (proxied by the age of the vegetation and time since the last fire), the topographic position of the focal cell, and the climate conditions in the current time step; and 2) the resistance of the focal cell, which was a negative exponential function of the age of the vegetation in the focal cell in which the rate of exponential decline with age decreased with increasing fire intensity (see main text for details). The complex wildfire mortality function included 6 user-specified beta coefficients. As described in the main text, b_0 - b_4 were held constant across all cover types. We varied b_5 and b_6 among cover types to reflect differences in reported historical mean fire return intervals and high mortality rates among cover types. Specifically, we varied these two beta coefficients during model calibration to either increase or decrease the rate of exponential decline in high mortality with increasing vegetation age as a function of fire intensity to achieve the target percentage of high mortality rate in each cover type.

The figures below depict the final wildfire mortality response functions for each cover type in alphabetical order. Cover types not shown either were not eligible to burn (e.g., water, barren) or were always assigned a high mortality response after burning (e.g., grassland, meadow). The response functions depict the probability of high mortality wildfire as a negative exponential function of vegetation Age (yrs) and fire intensity (as indexed). The dashed, solid and dotted lines depict the response functions for the minimum, mean and maximum Fire Intensity Index. Universally, the probability of high mortality decreased with increasing vegetation Age, but the rate of exponential decline decreased (i.e.,shallower slope) with increasing fire intensity, such that for any given Age the probability of high mortality increased with increasing fire intensity.

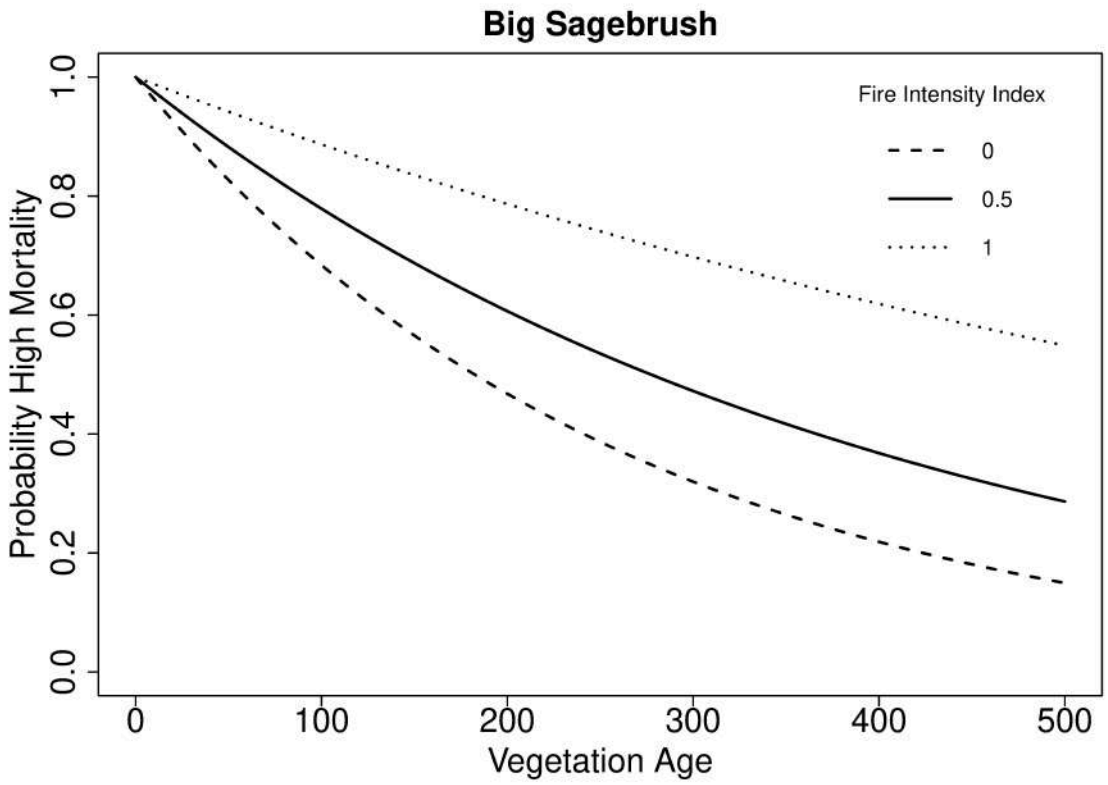

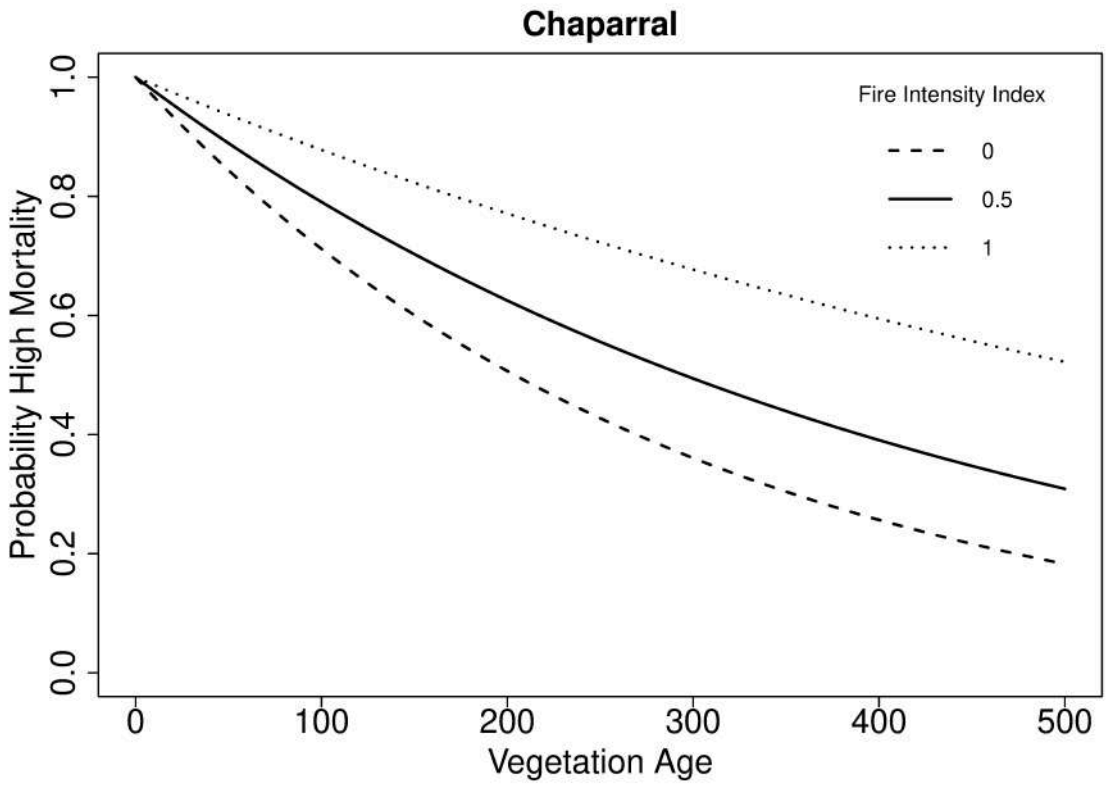
Chaparral
Fire Intensity Index
0
0.5
1
Probability High Mortality
0.0
0.2
0.4
0.6
0.8
1.0
0
100
200
300
400
500
Vegetation Age

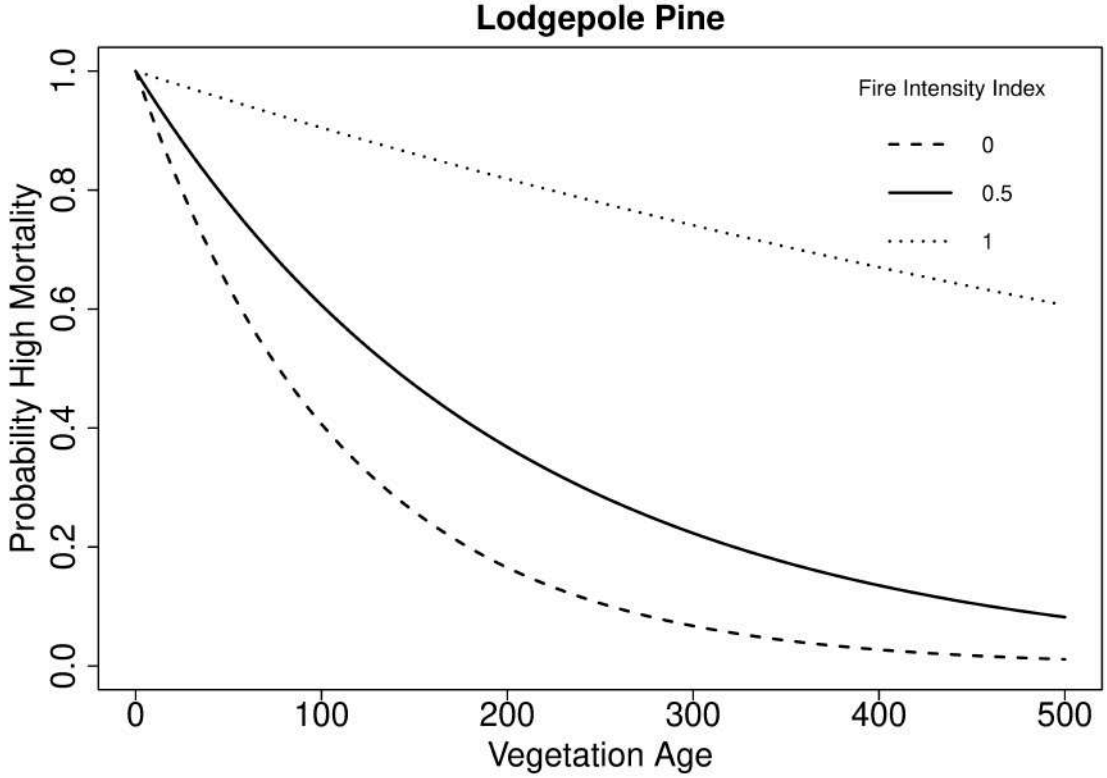
Lodgepole Pine
Fire Intensity Index
0
0.5
1
Probability High Mortality
0.0
0.2
0.4
0.6
0.8
1.0
0
100
200
300
400
500
Vegetation Age

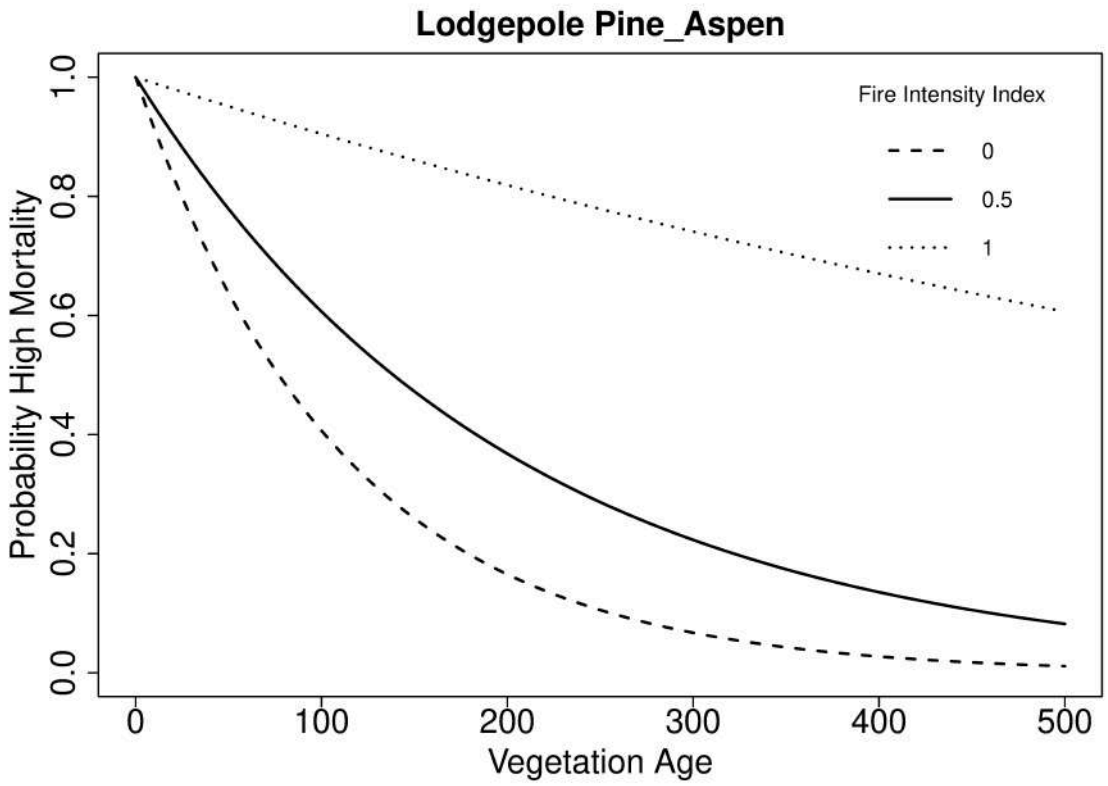
Lodgepole Pine_Aspen
Fire Intensity Index
0
0.5
1
Probability High Mortality
0.0
0.2
0.4
0.6
0.8
1.0
0
100
200
300
400
500
Vegetation Age

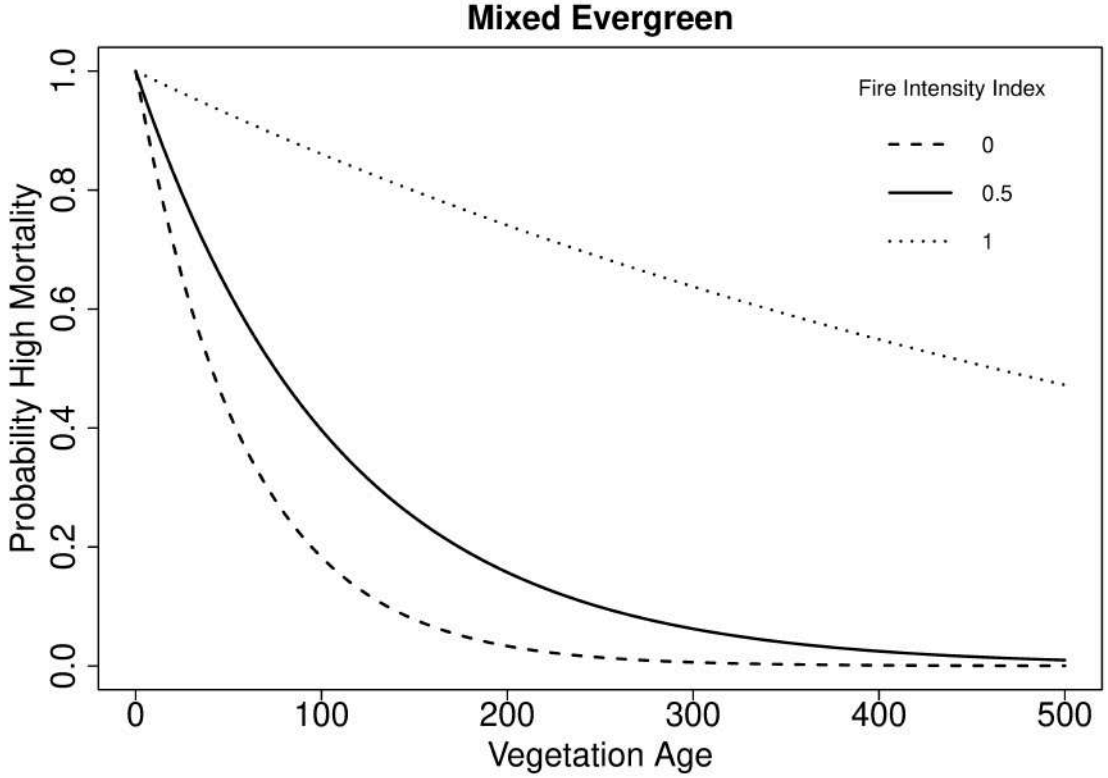
Mixed Evergreen
Fire Intensity Index
0
0.5
1
Probability High Mortality
0.0
0.2
0.4
0.6
0.8
1.0
0
100
200
300
400
500
Vegetation Age

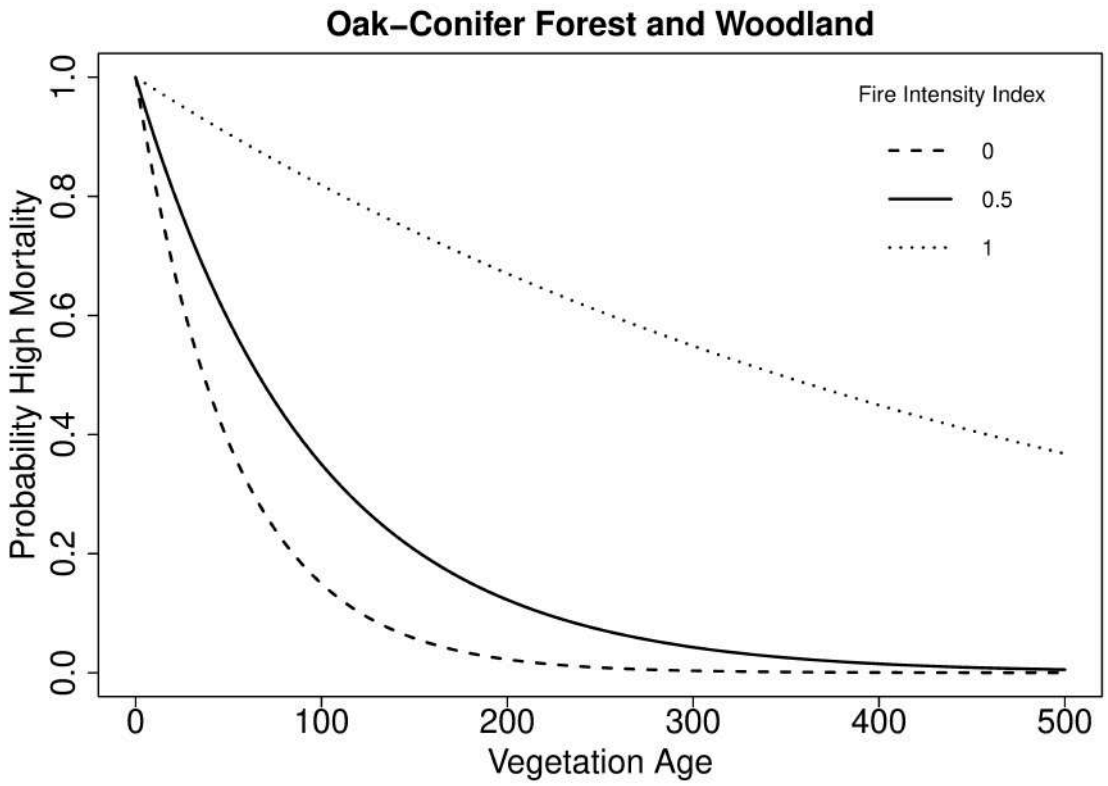
Oak–Conifer Forest and Woodland
Fire Intensity Index
0
0.5
1
Probability High Mortality
0.0
0.2
0.4
0.6
0.8
1.0
0
100
200
300
400
500
Vegetation Age

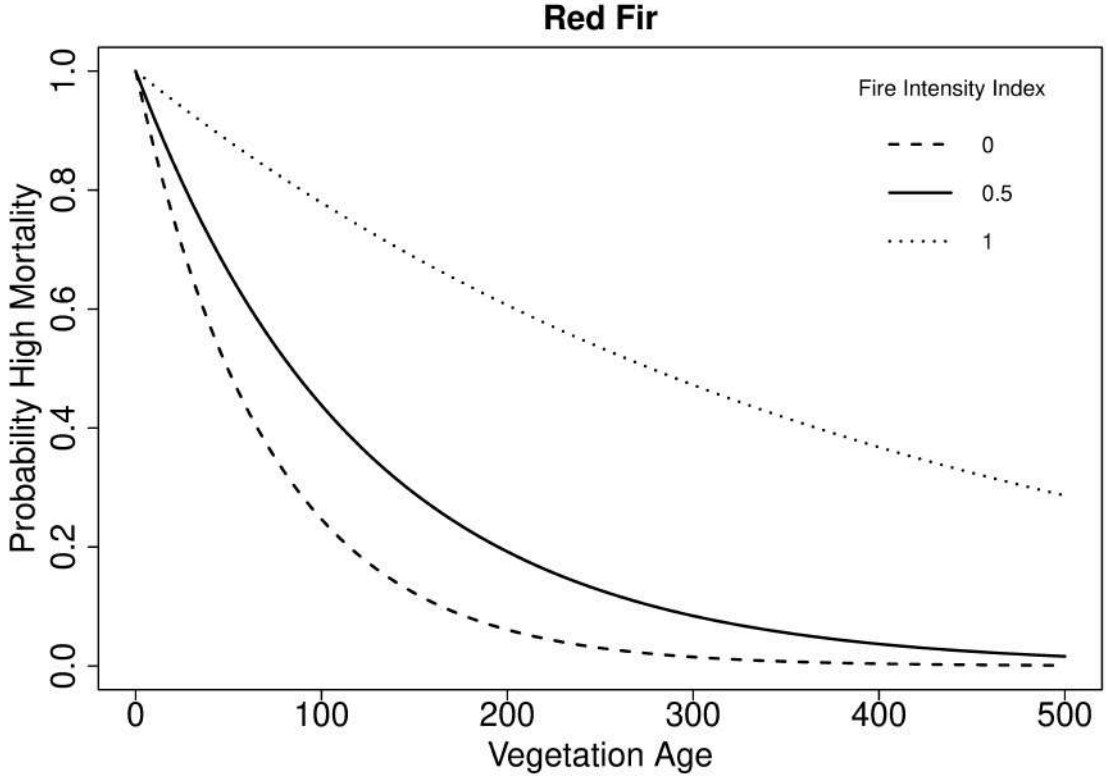
Red Fir
Fire Intensity Index
0
0.5
1
Probability High Mortality
0.0
0.2
0.4
0.6
0.8
1.0
0
100
200
300
400
500
Vegetation Age

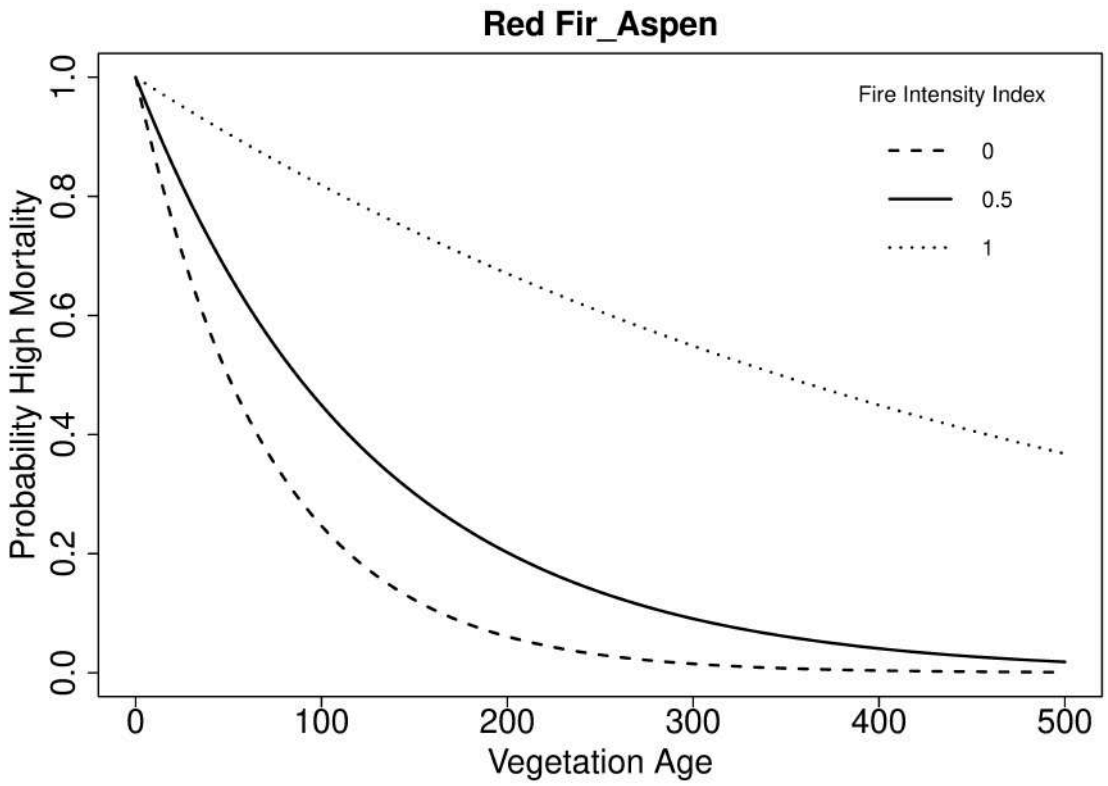
Red Fir_Aspen
Fire Intensity Index
0
0.5
1
Probability High Mortality
0.0
0.2
0.4
0.6
0.8
1.0
0
100
200
300
400
500
Vegetation Age

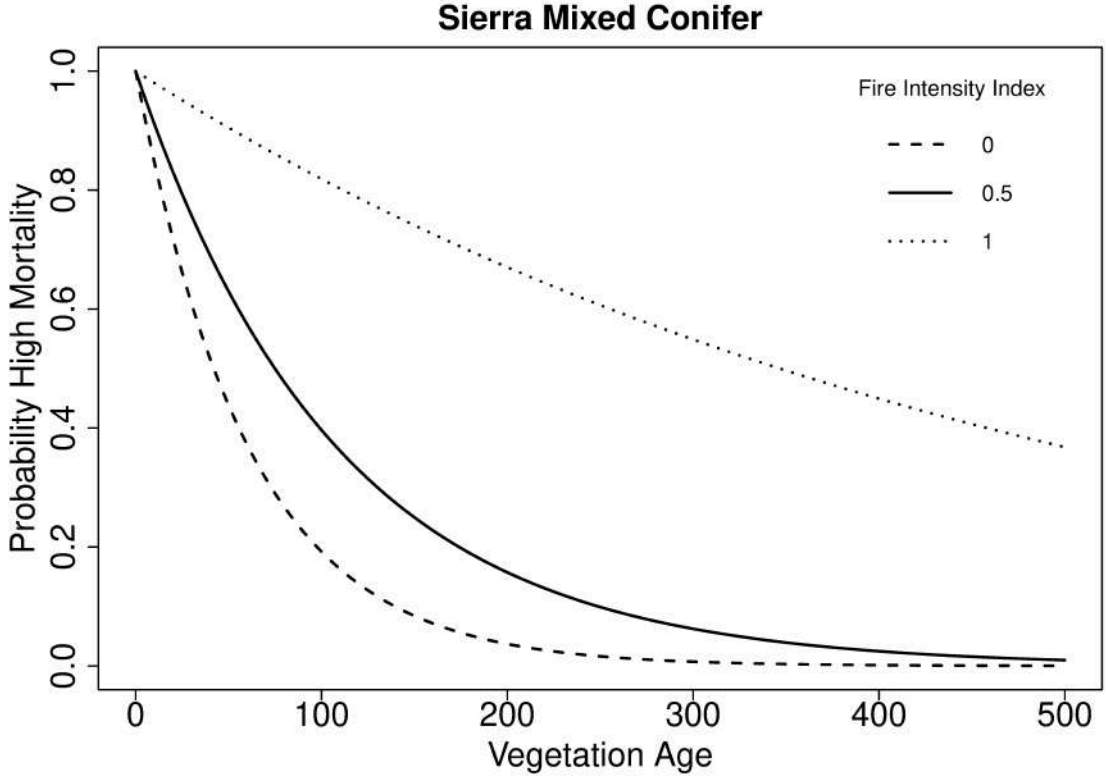
Sierra Mixed Conifer
Fire Intensity Index
0
0.5
1
Probability High Mortality
0.0
0.2
0.4
0.6
0.8
1.0
0
100
200
300
400
500
Vegetation Age

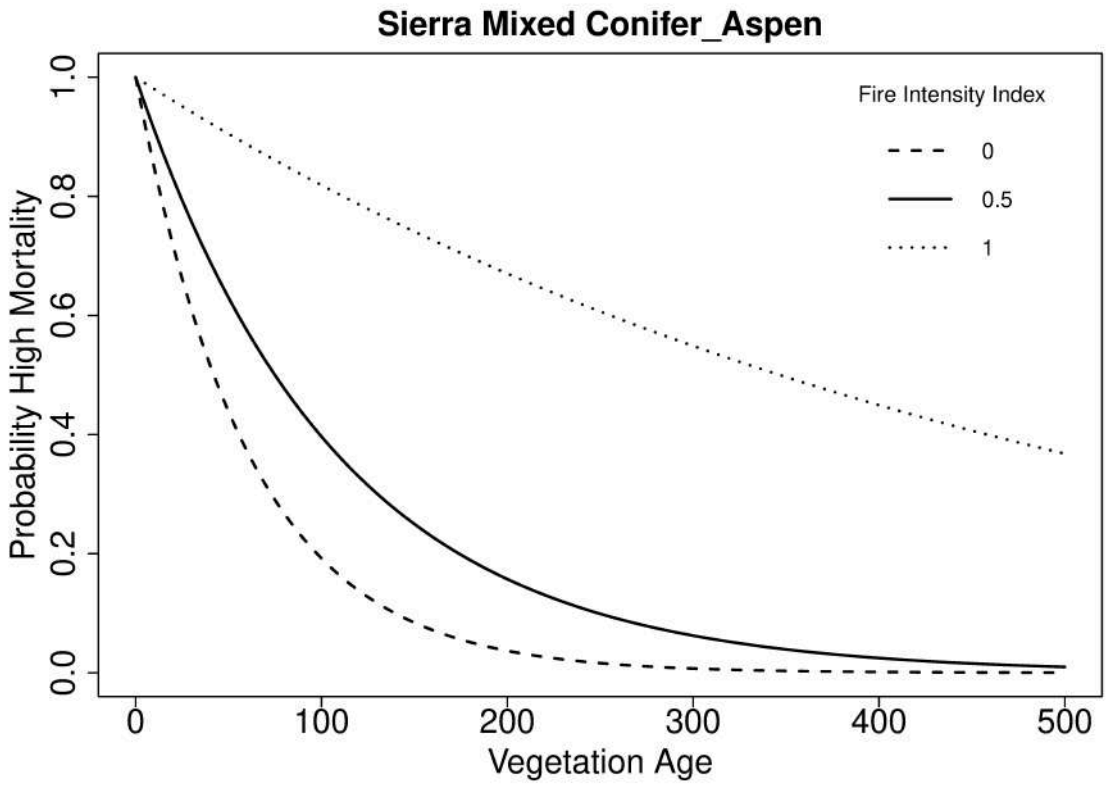
Sierra Mixed Conifer_Aspen
Fire Intensity Index
0
0.5
1
Probability High Mortality
0.0
0.2
0.4
0.6
0.8
1.0
0
100
200
300
400
500
Vegetation Age

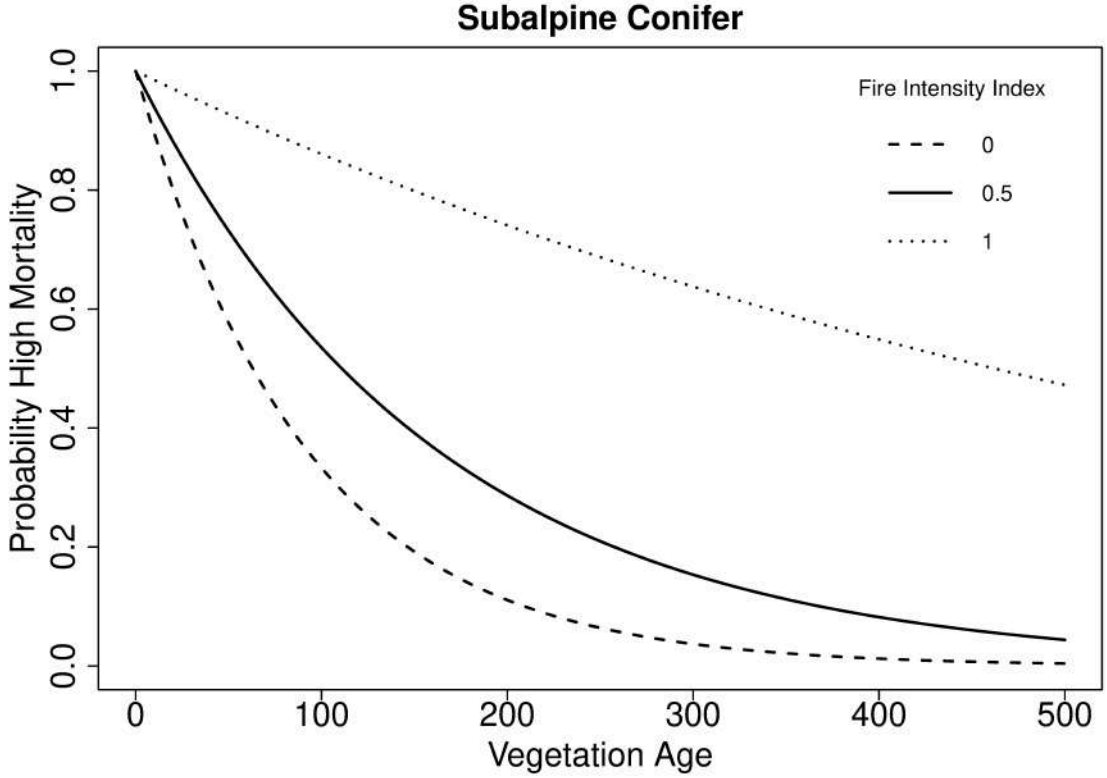
Subalpine Conifer
Fire Intensity Index
0
0.5
1
Probability High Mortality
0.0
0.2
0.4
0.6
0.8
1.0
0
100
200
300
400
500
Vegetation Age

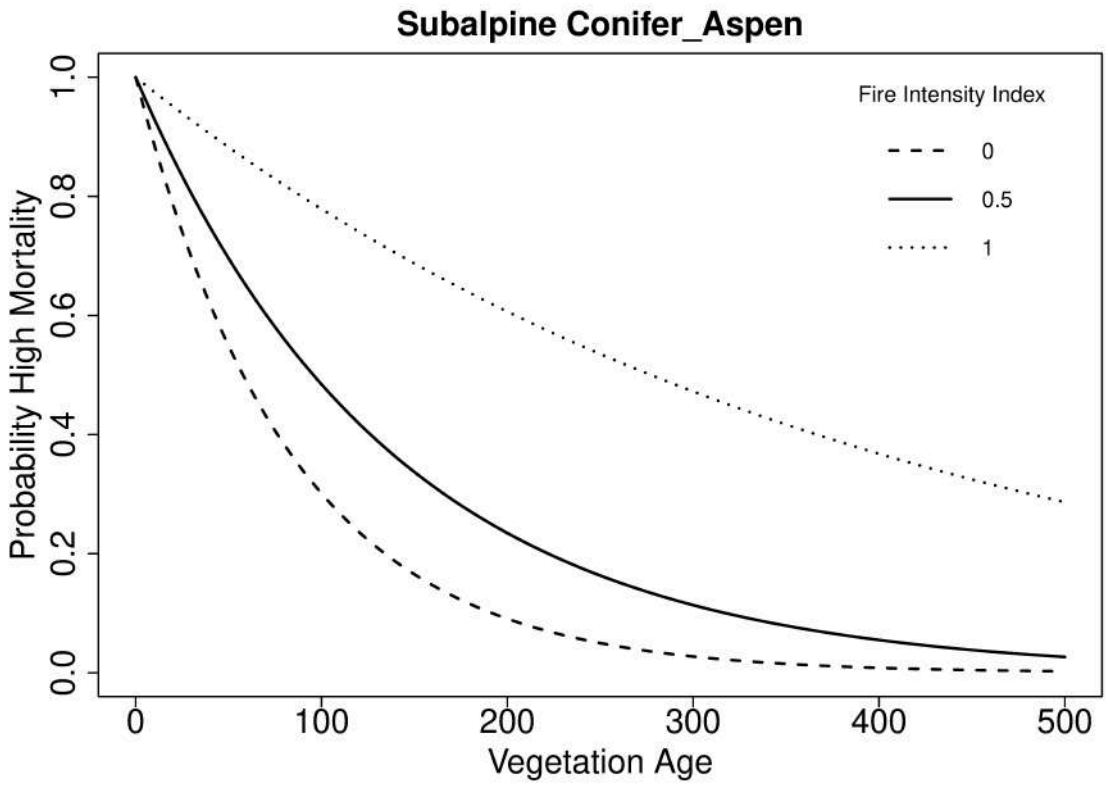
Subalpine Conifer_Aspen
Fire Intensity Index
0
0.5
1
Probability High Mortality
0.0
0.2
0.4
0.6
0.8
1.0
0
100
200
300
400
500
Vegetation Age

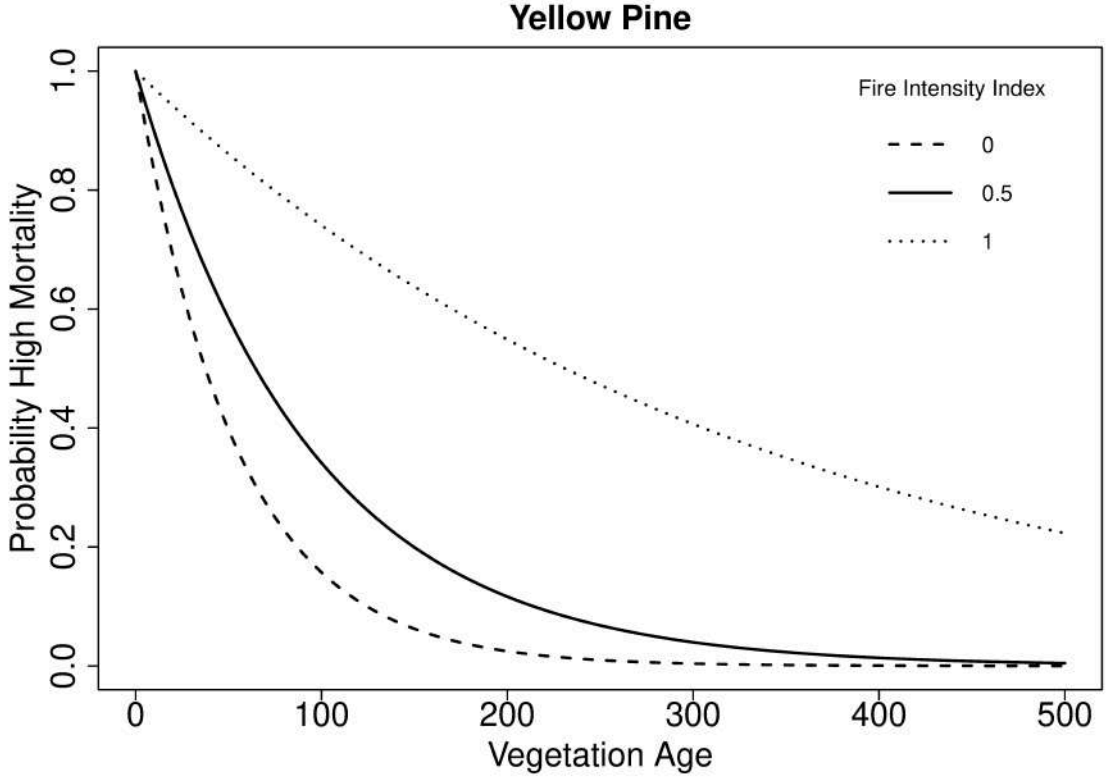
Yellow Pine
Fire Intensity Index
0
0.5
1
Probability High Mortality
0.0
0.2
0.4
0.6
0.8
1.0
0
100
200
300
400
500
Vegetation Age

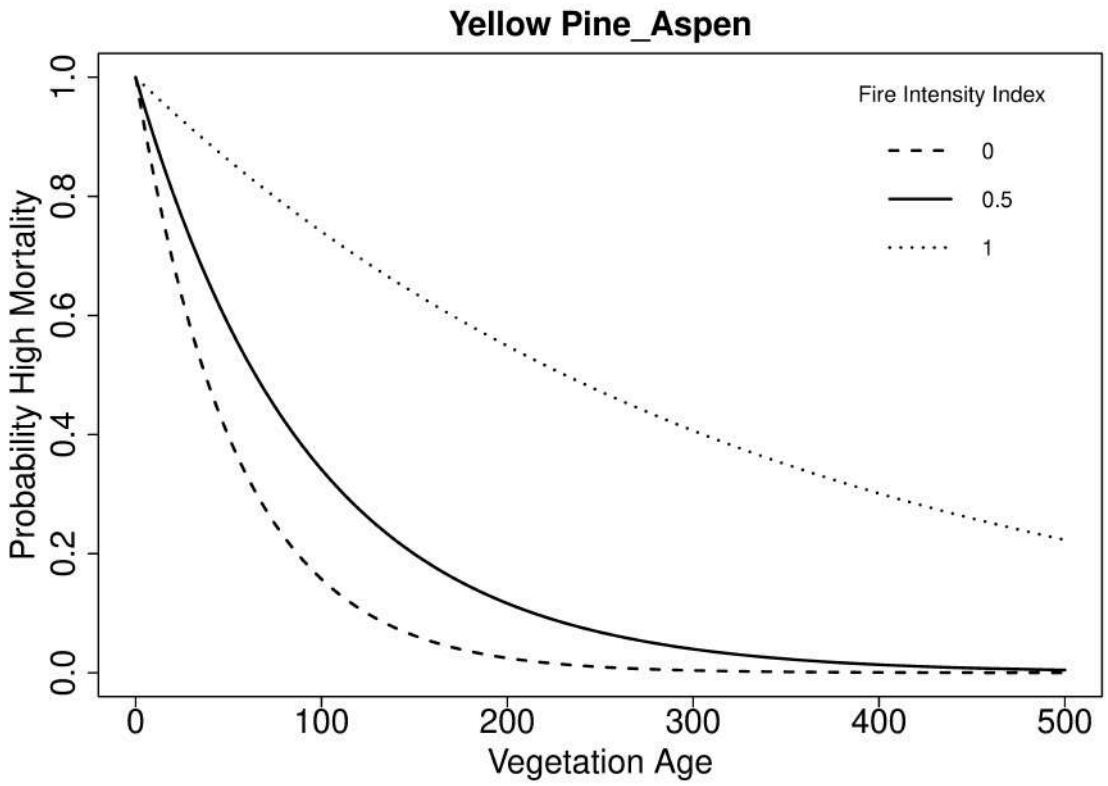
Yellow Pine_Aspen
Fire Intensity Index
0
0.5
1
Probability High Mortality
0.0
0.2
0.4
0.6
0.8
1.0
0
100
200
300
400
500
Vegetation Age

Appendix E - Bear River Landscape Historical Range of Variability and Current Landscape Departure

DRAFT Report

Kevin McGarigal Becky Estes Scott Conway Danielle Perrot
Marilyn Tierney Terri Walsh Christina Liang Laurie Perrot
Edward Smith

February, 2022

Authors

- Kevin McGarigal is a landscape ecologist with Vibrant Planet, proprietor of LandEco Consulting and retired professor of landscape ecology at the University of Massachusetts, Amherst. He received a B.S. in Forestry and Wildlife from Virginia Tech, an M.S. in Wildlife Science from Oregon State University, and a Ph.D. in Forest Science from Oregon State University.
- Becky Estes is the Central Sierra Province Ecologist (Tahoe, Eldorado, Stanislaus, and Lake Tahoe Basin Management Unit), Pacific Southwest Region, USDA Forest Service. She received a Ph.D. in Forestry from Auburn University and is a Certified Ecologist with the Ecological Society of America.
- Scott Conway is the chief resilience officer with Vibrant Planet and former forest ecologist with Pacific Southwest Region, USDA Forest Service Remote Sensing Lab and Truckee District Ranger, Tahoe National Forest, Pacific Southwest Region, USDA Forest Service. He received a B.S. in Natural Resources Management from Colorado State University.
- Danielle Perrot is an applied ecologist with Vibrant Planet. She received a B.S. in Environmental Science from University of California, Los Angeles and an M.A. in Geography from University of Colorado, Boulder.
- Marilyn Tierney is retired District Biologist for the Bear River Ranger District, Tahoe National Forest, Pacific Southwest Region, USDA Forest Service. She received a B.S. in Biology and an M.A. in Biology with an emphasis in Ecology and Systematics from San Francisco State University.
- Terri Walsh is silviculturist for the Tahoe National Forest, Pacific Southwest Region, USDA Forest Service. She is a certified silviculturist and studied Forestry at Cal Poly San Luis Obispo.
- Christina Liang is Forest Biologist for the Tahoe National Forest, Pacific Southwest Region, USDA Forest Service. She received a Ph.D. in Ecology from University of California, Davis.
- Laurie Perrot is Forest Environmental Coordinator for the Tahoe National Forest, Pacific Southwest Region, USDA Forest Service. She received a B.S. in forestry from the University of California, Berkeley.
- Edward Smith is Senior Forest Ecologist and Fire Manager for The Nature Conservancy in California. He received a BA in Biology from the University of California, San Diego and a MS in Forestry from Northern Arizona University.

Preface

This document[1] is an appendix to the Northern Sierra Historical Range of Variability and Current Landscape Departure General Technical Report (GTR) and includes detailed results for the Bear River landscape. Importantly, the background and detailed methods behind these results are presented in the GTR and not repeated here, and thus it behooves the reader to review the GTR before interpreting these results. In addition, here we present details pertaining the Landscape Disturbance-Succession Model parameterization and calibration specific to this focal landscape; all other model parameterization and calibration generalized to the Northern Sierra ecoregion is presented in the GTR. Lastly, here we present results specific to this focal landscape, but with minimal interpretation or discussion of these results or their application to management, as this was all done in the GTR. The GTR describes how to interpret the results for any of the focal landscapes and how they can be applied to management; here, we simply provide the raw results specific to this focal landscape.

Note, all datasets associated with the results for this focal landscape can be made available. Please contact Becky Estes, becky.estes@usda.gov for access.

---

[1] In accordance with Federal law and U.S. Department of Agriculture policy, this institution is prohibited from discriminating on the basis of race, color, national origin, sex, age, or disability. (Not all prohibited bases apply to all programs.) To file a complaint of discrimination, write USDA, Director, Office of Civil Rights, Room 326-W, Whitten Building, 1400 Independence Avenue, SW, Washington, DC 20250-9410 or call (202) 720-5964 (voice and TDD). USDA is an equal opportunity provider and employer.

FOCAL LANDSCAPE

The Bear River landscape, as we defined it, is comprised of the HUC8-level Upper Bear River watershed and the HUC10-level Upper and Lower South Fork of the Yuba River and Deer Creek watersheds, and is located on the western slopes of the Sierra Nevada Mountains in the north Sierra ecoregion (**Figure 1**). The Bear River landscape encompasses 149,191 ha and otherwise reflects the description of the north Sierra ecoregion presented in the GTR.

Figure 1: The Bear River landscape, including the middle and north forks of the Bear River, defined for the purpose of simulating wildfire disturbance and vegetation succession.

MODEL PARAMETERIZATION

In this section, we present only model parameters specific to this focal landscape; all north Sierra-wide parameters are discussed in the GTR. In addition, here we do not discuss in detail the methods and use of the model parameters in LDSim, as this was already done in the GTR. Please refer to the GTR for a full understanding of how the model parameters were used in LDSim.

Wildfire Climate

Climate conditions affecting wildfire disturbance during each timestep of the simulation were governed by a single global parameter, the Wildfire Climate Index based on the Palmer Modified Drought Severity Index

(PMDI), in which a single coefficient was assigned to each timestep of the simulation. The final Wildfire Climate Index trajectory represented a vector of coefficients, one for each timestep, as shown in **Figure 2**.

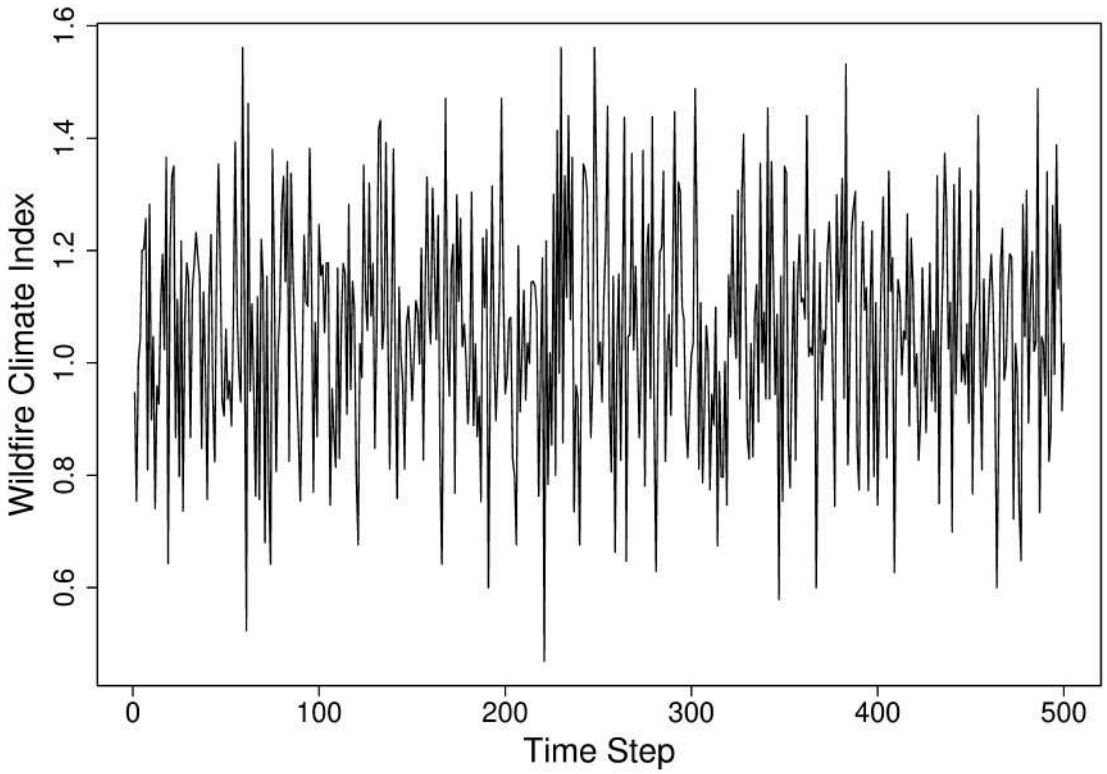

Figure 2: Wildfire Climate Index trajectory for the Bear River landscape corresponding to 500 5-year timesteps in the simulation. The Climate Index was based on the inverted and rescaled 5-year averaged, inverse-distance weighted mean Palmer Modified Drought Severity Index (PMDI) for the sample point locations within the north Sierra ecoregion relative to the focal landscape (Bear River watershed in this case). Note, here we inverted PMDI so that positive values represented drier conditions and negative values represented wetter conditions, and we also rescaled the index to have a standard deviation of 0.2 (see text for details).

Wildfire Susceptibility

Wildfire susceptibility for any given cell in each timestep was modeled as a complex function of fuels and climate, separately for each cover type, as described in the GTR. The final Wildfire Susceptibility Index on the probability scale (0-1) was used in the wildfire initiation and spread functions such that a value of 0 would prevent wildfires from initiating in or spreading into the cell, and as the value increased to 1 the probability of initiating a wildfire would increase as would the probability of a wildfire spreading to the focal cell from an adjacent burning cell, all other things being equal.

Briefly, we varied the beta coefficients of the wildfire susceptibility function for each cover type to reflect differences in reported historical mean fire return intervals among cover types - shifting the response curves left or right - as a means of calibrating the model to achieve target mean fire return intervals for each cover type (see Model Calibration). The calibrated wildfire susceptibility functions for each cover type are included in **Appendix E1**.

Wildfire Initiation

The number and spatial distribution of wildfire initiations in any given timestep was governed by: 1) a global wildfire initiation rate parameter that controlled the number of initiation attempts per unit area and remained constant over time; 2) the current climate conditions, as represented by the Wildfire Climate Index, that varied over time but not space; and 3) the susceptibility to wildfire, as represented by the Wildfire Susceptibility Index, that varied over both space and time. We treated the global wildfire initiation rate as a calibration parameter - shifting it up or down to increase or decrease the overall amount of realized wildfire over time - and ultimately settled on a rate of 400 attempted initiations per 100,000 ha/year. Note, this parameter affected the attempted number of wildfire initiations, not the realized number of wildfires, which was considerably less due to the vegetation and climate conditions that affected whether an attempt (i.e., lightning strike) materialized into an actual wildfire. The realized number of wildfire initiations for the Bear River landscape is shown in **Figure 3**.

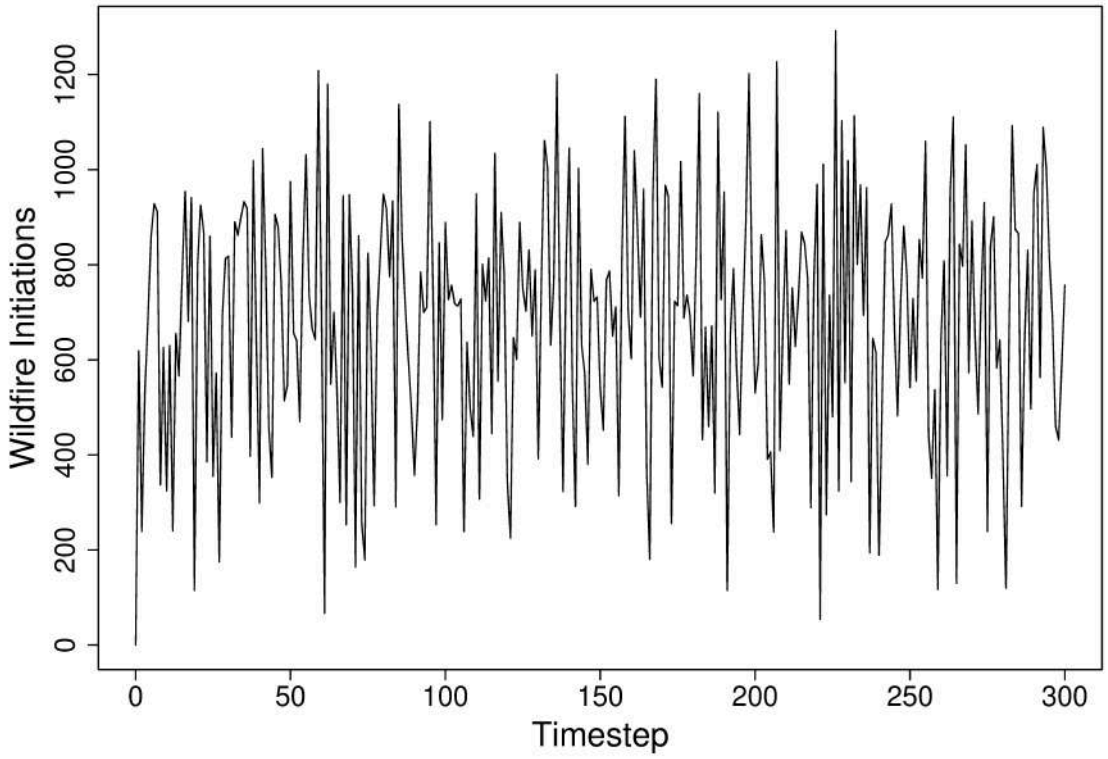

Figure 3: Realized simulated number of wildfire initiations per 5-year timestep for the Bear River landscape.

Wildfire Mortality

Following the termination of a wildfire event the probability of high versus low mortality of the overstory vegetation in each 5 m cell that burned was determined by two major factors combined in a complex function, as described in the GTR: 1) fire intensity, which was a function of the fuel loads in the neighborhood of the focal cell (proxied by the age of the vegetation and time since the last fire), the topographic position of the focal cell, and the climate conditions of the current timestep; and 2) the resistance of the focal cell, which was a function of the age of the vegetation in the focal cell.

Briefly, we varied the beta coefficients of the resistance component of the complex function for each cover type to reflect differences in reported historical mean fire return intervals and high mortality rates among cover types - increasing or decreasing the rate of exponential decline in high mortality with increasing vegetation ages as a function of fire intensity - as a means of calibrating the model to achieve target high mortality rates for each cover type (see Model Calibration). The calibrated wildfire mortality functions for each cover type are included in **Appendix E2**.

Succession Climate

Climate conditions affecting vegetation succession during each timestep of the simulation were governed by a single global parameter, the Succession Climate Index based on the Palmer Modified Drought Severity Index (PMDI), in which a single coefficient was assigned to each timestep of the simulation. The final Succession Climate Index trajectory represented a vector of coefficients, one for each timestep, and is shown in **Figure 4**.

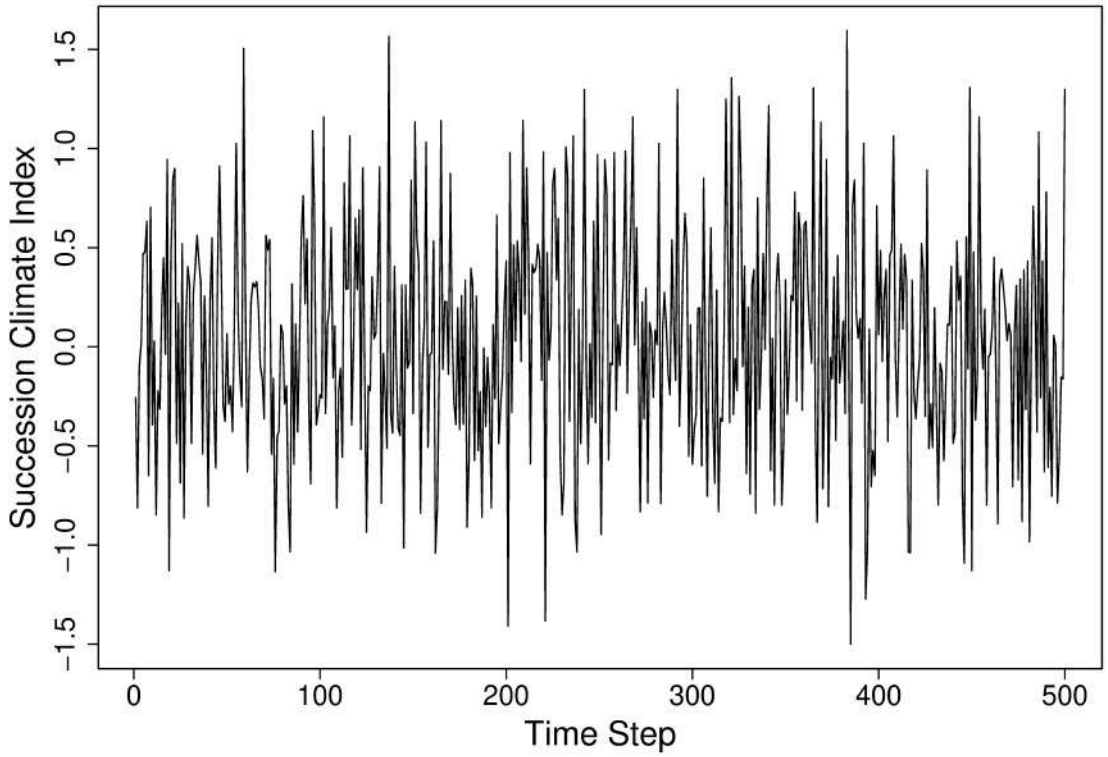

Figure 4: Succession Climate Index trajectory for the Bear River landscape corresponding to 500 5-year timesteps in the simulation. The Climate Index was based on the inverted 5-year averaged, inverse-distance weighted mean Palmer Modified Drought Severity Index (PMDI) for the sample point locations within the north Sierra ecoregion relative to the focal landscape (Bear River watershed in this case). Note, here we inverted PMDI so that positive values represented drier conditions and negative values represented wetter conditions (see text for details).

MODEL CALIBRATION

Although LDSim is a process-oriented model with individual parameters sourced either from data, literature, or expert opinion, the model outcomes reflect the complex spatio-temporal interactions of the various stochastic disturbance and succession processes. Consequently, it is necessary to calibrate the model by tuning (i.e., adjusting up or down) one or more of the model parameters to produce selected outcomes that are consistent with the data, literature and expert opinion. Importantly, in this context, we considered the parameters associated with the disturbance process to be "independent" variables and the vegetation conditions (e.g., seral stage distribution, spatial patterns of vegetation states, etc.) to be "dependent" outcomes. Therefore, we calibrated select disturbance parameters (i.e., independent variables) to achieve the targeted disturbance regime without any attention to the vegetation response, which we treated as the dependent outcome of the disturbance regime. Importantly, we did not tune disturbance regime parameters to achieve desired vegetation outcomes. To calibrate the model, we focused on the following five disturbance regime attributes that we considered emergent properties of the disturbance regime, as discussed in detail in the GTR.

Fire Rotation Period

Fire Rotation Period (FRP) is the number of years required to burn a cumulative area equal to the extent under consideration. FRP combines fire frequency and fire size into a single integrated measure of how much fire is actually applied to a unit of ground. FRP is equivalent to the "point-specific" or "population" mean Fire Return Interval (FRI); i.e., the average number of years between fires to a single point on the ground (or cell), and is roughly equivalent to the oft reported "grand mean" FRI computed from a large sample of point-specific intervals (e.g., from a set of fire-scarred trees).

Briefly, we tuned the global wildfire initiation rate parameter, which controlled the number of wildfire initiation attempts per unit area within each timestep and remained constant over time (see Wildfire Initiation above), and two of the wildfire susceptibility coefficients (b_0 and b_1) for each cover type, which affected the susceptibility of fire initiation and spread in each cover type (see Wildfire Susceptibility above), and measured calibration success based on agreement with the pre-specified target FRP for each cover type. We set our calibration goal as within 10% of the target FRP for forested cover types with extents > 1,000 ha. We closely met our calibration target for 6 of the 7 forest cover types with > 1,000 ha, and came acceptably close for the remaining cover type, as shown in **Table 1**.

Table 1: Target and simulated Fire Rotation Periods (FRP) for the Bear River landscape.

Cover type	**Area (ha)**	**Target FRP**	**Simulated FRP**	**%Deviation**
Sierra Mixed Conifer	52688	26	27	4
Mixed Evergreen	21427	45	44	-2
Yellow Pine	20368	20	19	-5
Oak-Conifer Forest and Woodland	16863	21	20	-5
Red Fir	6120	50	54	8
Lodgepole Pine	2561	52	59	13
Sierra Mixed Conifer_Ultramafic	1100	60	61	2
Yellow Pine_Ultramafic	706	40	41	2
Oak Woodland	652	26	27	4
Oak-Conifer Forest and Woodland_Ultramafic	552	42	39	-7
Subalpine Conifer	520	296	305	3
Mixed Evergreen_Ultramafic	518	120	122	2
Total	129839	30	27	-10

Fire Mortality Rate

Fire mortality rate (FMR) is the percentage of burned cells that exhibit a high-mortality response (i.e., complete overstory mortality). For the purpose of model calibration, we considered the FMR only for cells in the "short", "medium" and "tall" tree developmental stages (i.e., "mature" trees) since this was the basis for specifying the target values.

Briefly, we tuned two of the wildfire mortality coefficients (b_5 and b_6) for each cover type, which affected the probability of high mortality fire as a function of age and fire intensity in each cover type (see Wildfire Mortality above), and measured calibration success based on conformity to pre-specified fire mortality targets for each cover type. We set our calibration goal as within 10% of the targets for forested cover types with > 1,000 ha in the focal landscapes. We closely met our calibration targets for 6 of the 7 for the forested cover types with > 1,000 ha, and came acceptably close for the remaining cover type (note, even though the percent difference was rather large, the absolute difference was relatively minor), as shown in **Table 2**.

Table 2: Target and simulated Fire Mortality Rates (FMR) for the Bear River landscape.

Cover type	**Area (ha)**	**Target FMR**	**Simulated FMR**	**%Deviation**
Sierra Mixed Conifer	52688	7	7.37	5
Mixed Evergreen	21427	7	6.80	-3
Yellow Pine	20368	5	5.77	15
Oak-Conifer Forest and Woodland	16863	5	5.02	0
Red Fir	6120	10	10.58	6
Lodgepole Pine	2561	24	24.64	3
Sierra Mixed Conifer_Ultramafic	1100	7	7.28	4
Yellow Pine_Ultramafic	706	5	4.96	-1
Oak Woodland	652	6	7.30	22
Oak-Conifer Forest and Woodland_Ultramafic	552	5	5.07	1
Subalpine Conifer	520	10	12.92	29
Mixed Evergreen_Ultramafic	518	7	6.83	-2

Fire Size Distribution

Fire size distribution (FSD) is the percentage of realized fire sizes across bins of increasing fire size. We opted not to tune the parameters affecting the fire size distribution as these were empirically based. Instead, we treated the realized fire size distribution as an emergent outcome of the model and measured calibration success based on agreement with the pre-specified fire distribution derived from the post-settlement period of 1908 - 1979 from which we had an empirical record. We set our calibration goal as a subjective evaluation of the realized fire size distribution compared to the target fire size distribution. We met our calibration target reasonably well, as depicted in **Figure 5**.

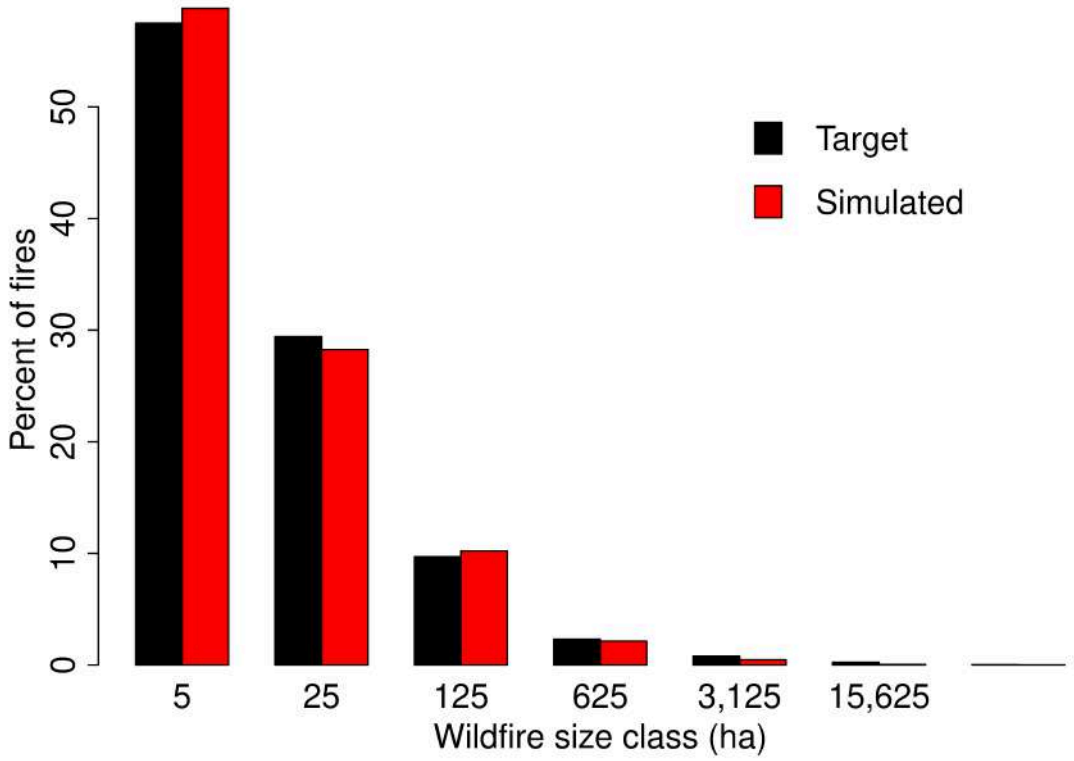

Figure 5: Target and simulated wildfire size distribution for the Bear River landscape.

Variability in Total Area Burned

Variability in total area burned over time is a measure of the temporal variability in the wildfire disturbance regime. We opted not to tune the primary parameter affecting the temporal variability in total area burned - the Wildfire Climate Index - as it was empirically based. Instead, we treated the variability in total area burned as an emergent outcome of the model and measured calibration success based on agreement with the observed variability in total area burned for the post-settlement period of 1908 - 1979 from which we had an empirical record. We set our calibration goal as within 10% of the target coefficient of variation (CV) in total area burned per timestep (CV = 91.8%, see GTR). We just barely met our calibration target, as depicted in **Figure 6**.

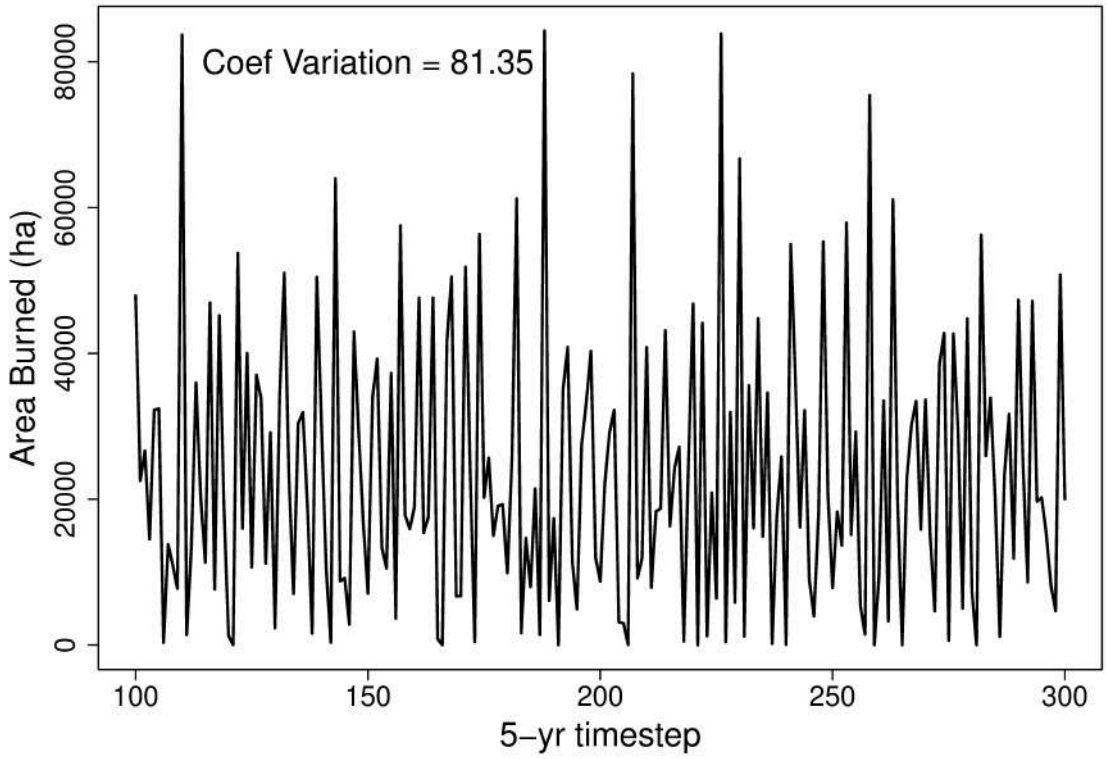

Figure 6: Total simulated area burned per 5 years in the Bear River landscape representing the historical reference period of 1550-1850 and the computed Coefficient of Variation (CV).

Relationship Between Total Area Burned and Climate

The relationship between total area burned and climate is a measure of the degree to which the simulated total area burned is affected by variability in the specified Wildfire Climate Index. We opted not to tune the Wildfire Climate Index, in particular, or any parameter associated with the wildfire disturbance process with regards to this calibration metric. Instead, we treated the observed relationship between total area burned and the climate index as an emergent outcome of the model and measured calibration success based on agreement with the strength of the relationship for the post-settlement period of 1908 - 1979 from which we had an empirical record. We set our calibration goal as within 10% of the target coefficient of determination (R2) in the fit of a linear regression to the target data (R2 = 0.25, see GTR). We did not met this calibration target very well, as we simulated a more closely fitting relationship between total area burned and the climate index and a relationship that was distinctly more non-linear compared to observed post-settlement observations, as depicted in **Figure 7**.

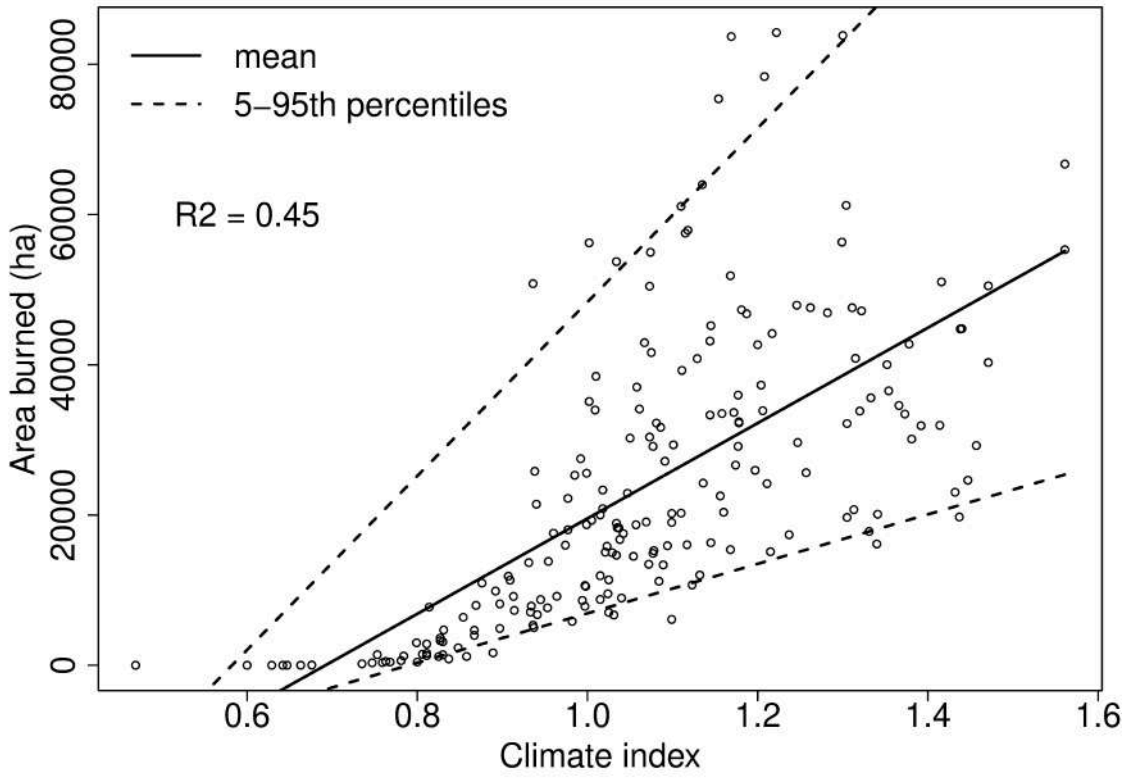

Figure 7: Scatterplot of the modified wildfire Climate Index based on the modified Palmer Drought Severity Index (see text for details) and the log of simulated total area burned per 5 years in the Bear River landscape representing the historical reference period of 1550-1850, and the fitted linear regression for the mean and 5-95th quantiles (see text for details) along with the Coefficient of Determination (R2) of the fit.

HISTORICAL RANGE OF VARIABILITY and CURRENT DEPARTURE

Biophysical Classes and Units

To summarize HRV and current departure in landscape structure at the Site and subbasin levels, we subdivided the landscape into a set of Biophysical Classes (BPCs), as described in detail in the GTR. Briefly, we indexed site productivity based on the cumulative tree biomass generated over the course of the simulation, after model equilibration, and then modeled tree biomass as a function of 10 geophysical variables using a Random Forest analytical framework, and lastly classified predicted Biomass into 4 equal-area classes based on quartiles of the data, plus a zero class for all non-forest cells. The final BPC layer included 4 classes ranging from the least productive to most productive sites, plus a non-forest class, as depicted in **Figure 8**.

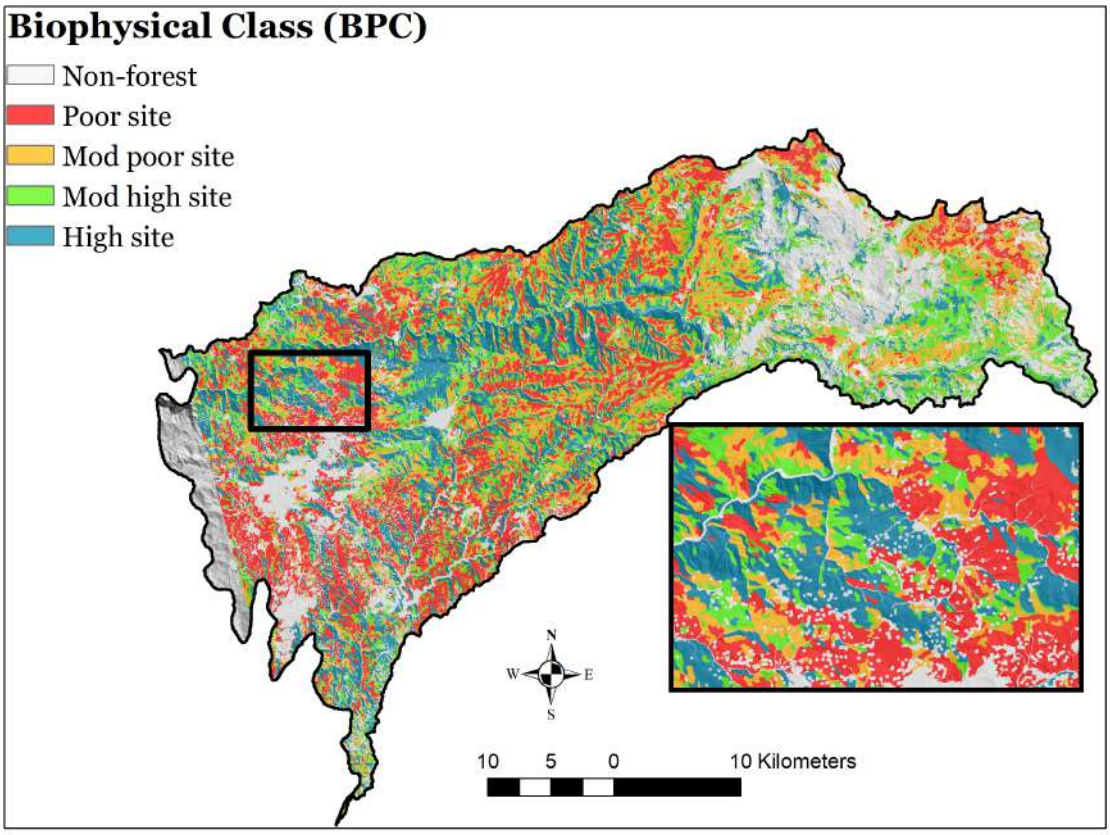

Figure 8: Biophysical Classes (BPCs) based on quartiles of predicted Biomass derived from a Random Forest model to predict Biomass (i.e., simulated cumulative tree height) from 10 biophysical variables. The Random Forest model explained ~70% of the variation in Biomass under simulated historical dynamic equilibrium conditions in the Bear River landscape.

The final BPCs were distinguishable on the basis of the 10 geophysical variables and cover type, although there was considerable overlap among BPCs in each of the variables, as described below for a select set of the variables.

- *Cover Type* - The distribution of each cover type among BPCs (as a percentage of the cover type), ordered roughly from low to high elevation distributions, is given in **Table 3**. Most forest types were well distributed among BPCs, suggesting that cover type was generally not a good discriminator of BPCs. However, there were some notable exceptions. For example, Lodgepole Pine and Red Fir were essentially absent from Low productivity sites and Subalpine Conifer from High productivity sites; whereas, Yellow Pine was disproportionately found on Low productivity sites. Oak-Conifer Forest and Woodland decreased in relative abundance as site productivity increased, whereas Mixed Evergreen showed the opposite trend. The most abundant cover type, Sierra Mixed Conifer, was equally distributed across site productivity classes.

  Table 3: Percentage of each cover type in each Biophysical Class (BPC) for the Bear River landscape.

Cover type	Area (ha)	Low	ModLow	ModHigh	High
Oak Woodland	543	15.80	23.16	30.16	30.89
Yellow Pine	16750	49.19	21.97	13.89	14.95
Yellow Pine_Ultramafic	592	53.87	22.91	14.65	8.58
Oak-Conifer Forest and Woodland	14737	35.72	23.05	17.92	23.30
Oak-Conifer Forest and Woodland_Ultramafic	456	45.77	19.67	18.74	15.82
Mixed Evergreen	19964	13.19	19.30	24.94	42.57
Mixed Evergreen_Ultramafic	505	33.26	28.34	24.11	14.29
Sierra Mixed Conifer	50597	23.16	29.66	24.81	22.37
Sierra Mixed Conifer_Ultramafic	1056	22.90	27.64	25.93	23.53
Lodgepole Pine	2310	1.12	20.60	58.16	20.12
Red Fir	5909	1.69	13.41	49.87	35.03
Subalpine Conifer	515	24.24	57.06	16.88	1.81

- *Mesic Index* - The distribution of the Mesic Index for each BPC (given as quantiles of the index) is given in **Table 4**. As expected, the Mesic Index distribution increased as the site productivity class increased from Low to High, but with considerable overlap in distributions between adjacent BPC classes. Despite the strong overlap, the BPC classes represented a gradient in expected site moisture, with the Low site class representing the driest sites and the High site class representing the wettest sites.

  Table 4: Distribution of the Mesic Index in each Biophysical Class (BPC), given as quantiles for the Bear River landscape.

BPC	2.5%	25%	50%	75%	97.5%
Low	30	43	51	60	79
ModLow	32	49	57	66	81
ModHigh	33	54	61	68	84
High	40	60	68	78	91

- *Topographic Position* - The distribution of the Topographic Position Index for each BPC (given as quantiles of the index) is given in **Table 5**. As expected, the Topographic Position Index distribution decreased as the site productivity class increased from Low to High, but with considerable overlap in distributions between adjacent BPC classes. The High site productivity class showed the strongest gradient in TPI, with a strong prevalence for lower topographic positions. Despite the strong overlap, the BPC classes represented a clear gradient in topographic position, with the Low site class found more commonly on the upper slopes and ridgetops and the High site class found more commonly on the lower slopes and valley bottoms.

  Table 5: Distribution of the Topographic Position Index each each Biophysical Class (BPC), given as quantiles for the Bear River landscape.

- *Aspect* - The distribution of aspect classes among BPCs (as a percentage of the BPC) is given in **Table 6**. Not surprisingly, each BPC class was distributed across all aspect classes, but still exhibited a pronounced orientation, with the Low site class disproportionately occupying southwesterly aspects and the High site class disproportionately occupying northeasterly aspects.

  Table 6: Percentage of each Biophysical Class (BPC) in each aspect class for the Bear River landscape.

BPC	2.5%	25%	50%	75%	97.5%
Low	30	46	54	63	87
ModLow	23	42	50	58	79
ModHigh	18	40	48	56	77
High	3	34	44	53	74

Aspect	N	NE	E	SE	S	SW	W	NW	Flat
Low	1.97	1.10	2.11	12.17	18.53	26.64	18.43	15.46	3.59
ModLow	4.69	2.88	5.08	16.33	16.55	17.38	12.04	20.73	4.34
ModHigh	11.51	7.92	9.34	15.77	11.20	11.04	7.52	20.68	5.03
High	20.64	22.81	17.20	10.93	4.06	3.83	2.97	14.52	3.03

Fire Return Interval and Departure

Mean point-specific Fire Return Interval (FRI) represents the average number of years between fire events at the 5 m cell level. We interpreted the observed mean FRI after model equilibration (N = 200 timesteps) at the cell level as a single integrated (albeit not comprehensive) summary of the historical wildfire disturbance regime. The historical mean FRI varied from < 15 years to > 300 years across the landscape, with evident influences of both cover type and terrain (**Figure 9**).

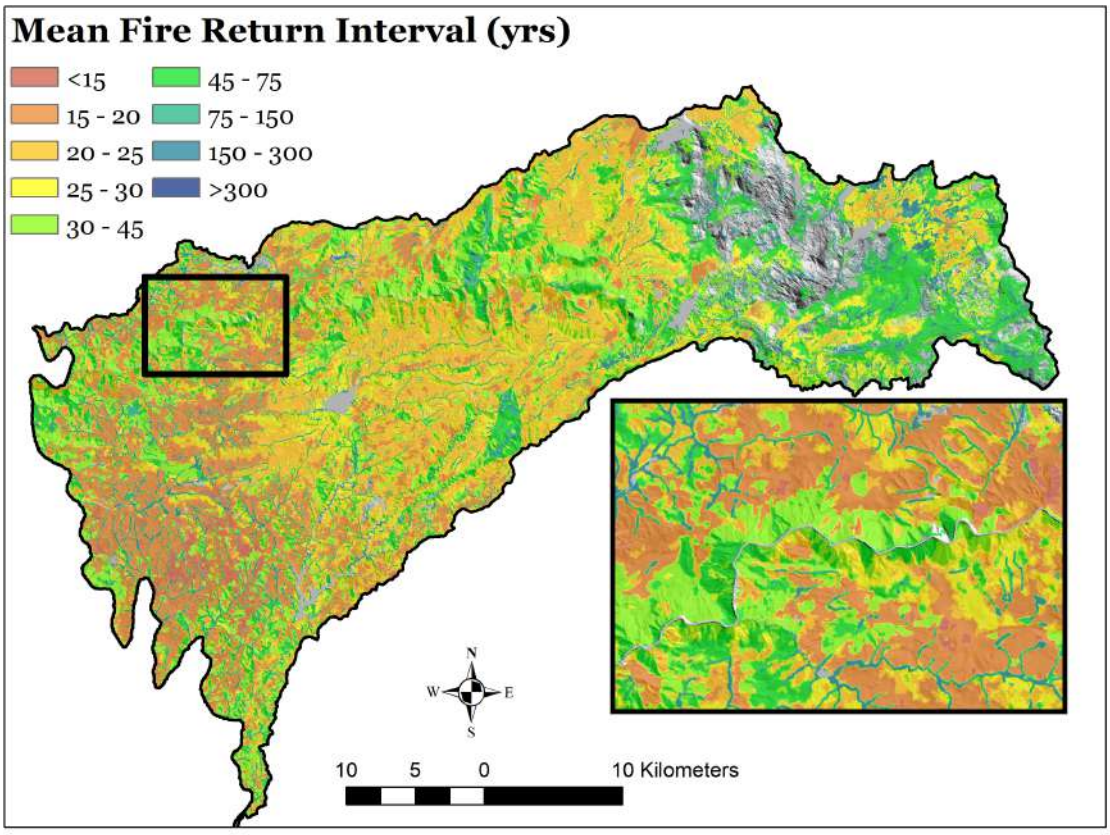

Figure 9: Simulated Fire Return Interval (FRI) (yrs) at the 5 m cell level for the Bear River landscape.

In addition, the historical mean FRI varied among BPCs as expected (**Table 7**). Specifically, the median FRI increased steadily from 22 to 33 years with increasing site productivity; i.e., from Low to High BPC.

Low productivity sites that occurred disproportionately on upper slopes and ridgetops and southwesterly aspects were warmer and drier and thus more susceptible to wildfire, despite having less fuel build-up over time. Conversely, High productivity sites that occurred disproportionately on lower slopes and valley bottoms and on northeasterly aspects were cooler and wetter and thus less susceptible to wildfire, despite having more fuel build-up over time. The relatively short median FRIs across all sites indicates that historically wildfires typically occurred frequently enough to keep surface and ladder fuel loads low enough to reduce the occurrence of high-severity wildfire.

Table 7: Range of variability (given as quantiles) in the mean fire return interval (FRI) by Biophysical Class (BPC) for the Bear River landscape.

BPC	HRV2.5%	HRV25%	HRV50%	HRV75%	HRV97.5%
Low	15	18	22	26	87
ModLow	16	22	25	38	121
ModHigh	17	25	30	46	130
High	19	26	33	49	113

These results also indicate that the HRV in mean FRI varied several-fold across sites within each BPC. For example, on High productivity sites FRI varied roughly five-fold between 19-113 years across sites. The wide range of variation in FRI within BPCs indicates that wildfire risk varied markedly across sites even within a single BPC and, consequently, that FRI is only loosely correlated with predicted cumulative tree biomass. For example, sites classified as having high long-term productivity under historical dynamic equilibrium conditions could have FRIs as short as 19 years (or shorter for the extremes) or as long as 113 years (or longer for the extremes) depending on local topographic and vegetative conditions and chance. This is visually evident in the map of mean FRI for the High site BPC (**Figure 10**).

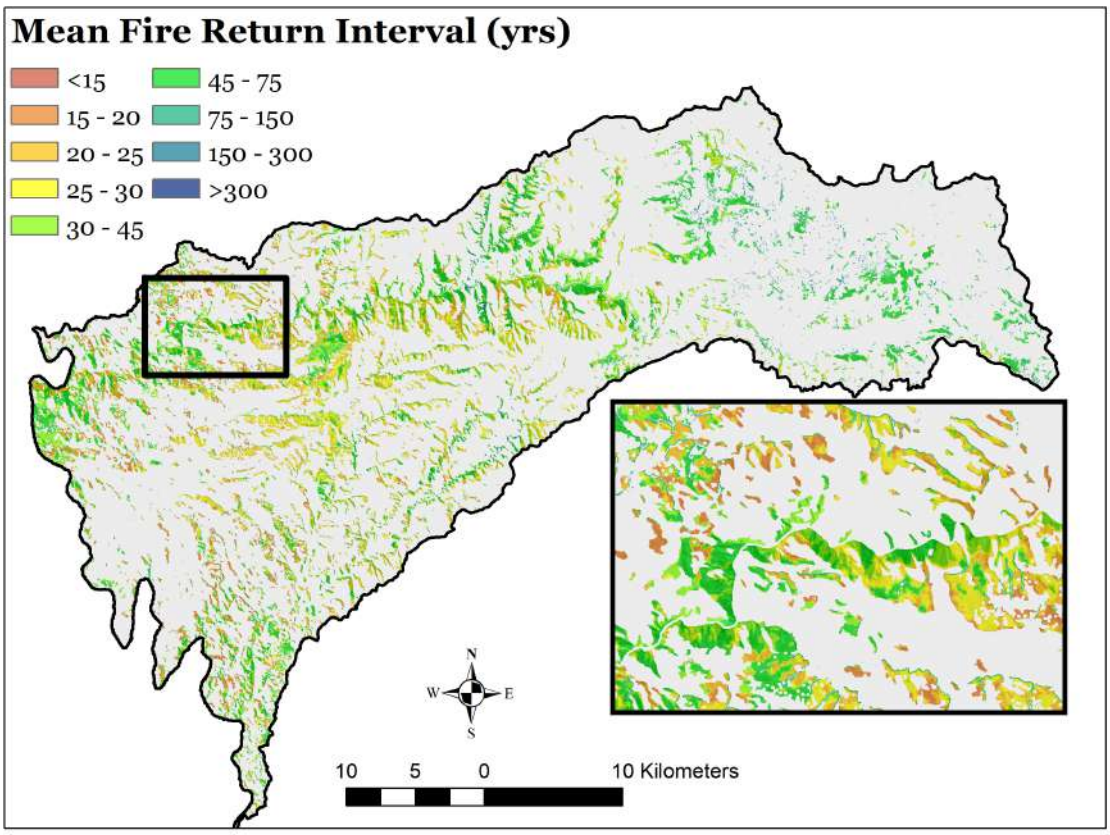

Figure 10: Simulated Fire Return Interval (FRI) (yrs) at the 5 m cell level on High productivity sites (Biophysical Class = 4) in the Bear River landscape.

Fire Return Interval Departure (FRID) represents the percentage deviation of the contemporary (post-settlement) mean point-specific FRI from the mean point-specific FRI under historical (i.e., pre-settlement) dynamic equilibrium conditions. Briefly, FRID measures the degree, in percent, to which contemporary fires (i.e., since 1909) are burning at frequencies similar to the frequencies that occurred prior to significant Euro-American settlement, as simulated (**Figure 11**). Positive departure indicates that the contemporary fire frequency is less than the historical fire frequency.

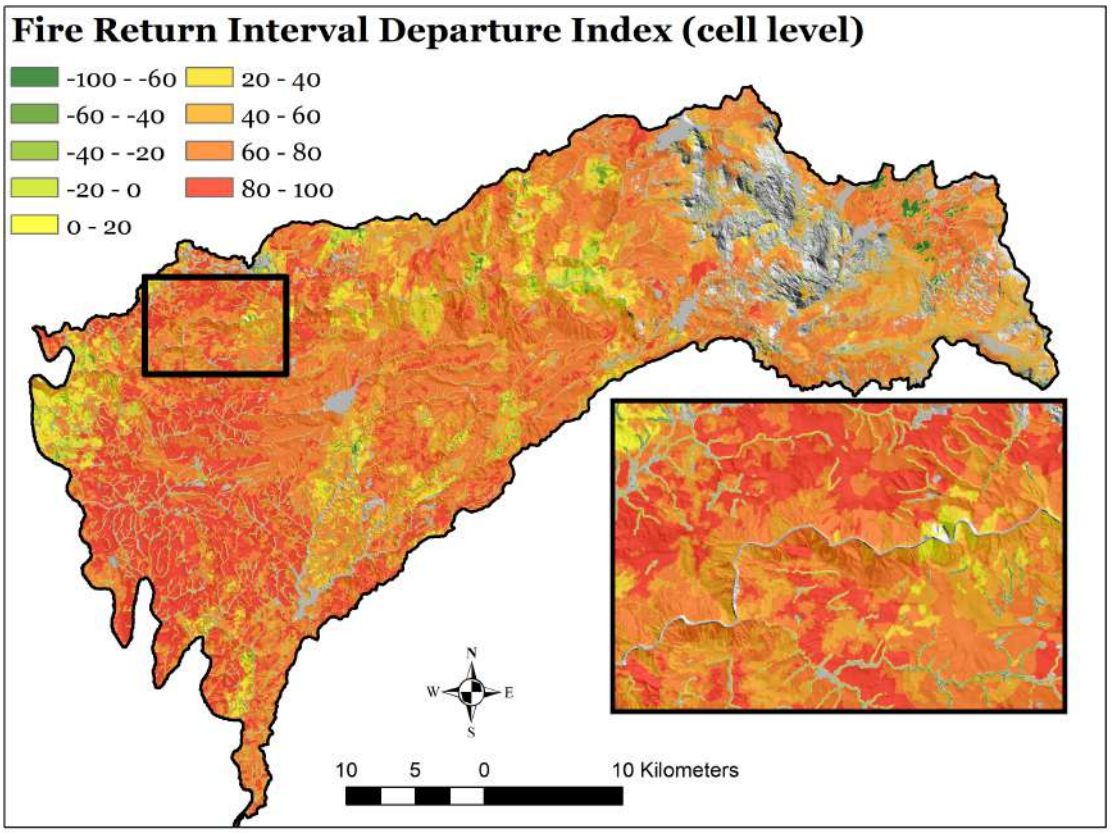

Figure 11: Fire Return Interval Departure (FRID) at the 5 m cell level in the Bear River landscape, representing the percent to which contemporary fires (i.e., since 1909) are burning at frequencies similar to the frequencies that occurred prior to significant Euro-American settlement, as simulated.

In addition to the cell-level map of FRID, we also summarized the mean FRID for each GPU to include in the Stewardship Atlas as a means of prioritizing units for treatment with fire (**Figure 12**).

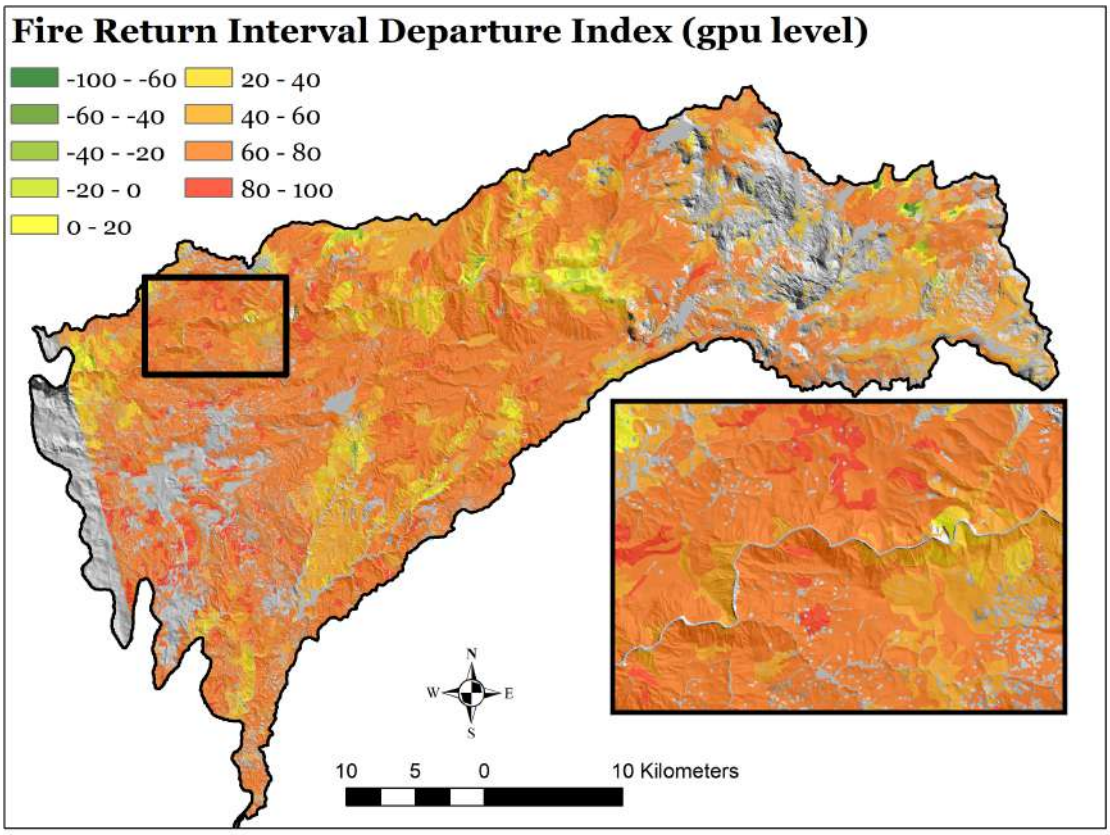

Figure 12: Geophysical Unit-level Fire Return Interval Departure (FRID) for the Bear River landscape, representing the average 5 m cell value in the percent to which contemporary fires (i.e., since 1909) are burning at frequencies similar to the frequencies that occurred prior to significant Euro-American settlement, as simulated.

Vegtation Persistence

We defined vegetation persistence as the likelihood of persisting in either an early- or late-seral condition at the 5 m cell level. We interpreted the observed mean FRI of high-mortality wildfires after model equilibration (N = 200 timesteps) at the cell level as a proxy for vegetation persistence, under the assumption that locations with shorter high-mortality FRIs would likely persist longer in early-seral stages and, conversely, locations with longer high-mortality FRIs would likely persist longer in late-seral stages.

Figure 13 depicts several areas with relatively long high-mortality FRIs (dark blue areas in the map) and these are sites that have a high likelihood of supporting late-seral vegetation under a natural disturbance regime. Conversely, the map depicts several areas with relatively short high-mortality FRIs (yellow and orange areas in the map) and these are sites that have a high likelihood of supporting early-seral vegetation much of the time under a natural disturbance regime. Accordingly, management objectives for these areas could be designed to capitalize on these focal areas. For example, establishing treatment objectives to maintain and enhance late-seral conditions for old forest associated species in areas with a lower likelihood of high-mortality wildfire (i.e., longer FRI) would be logical.

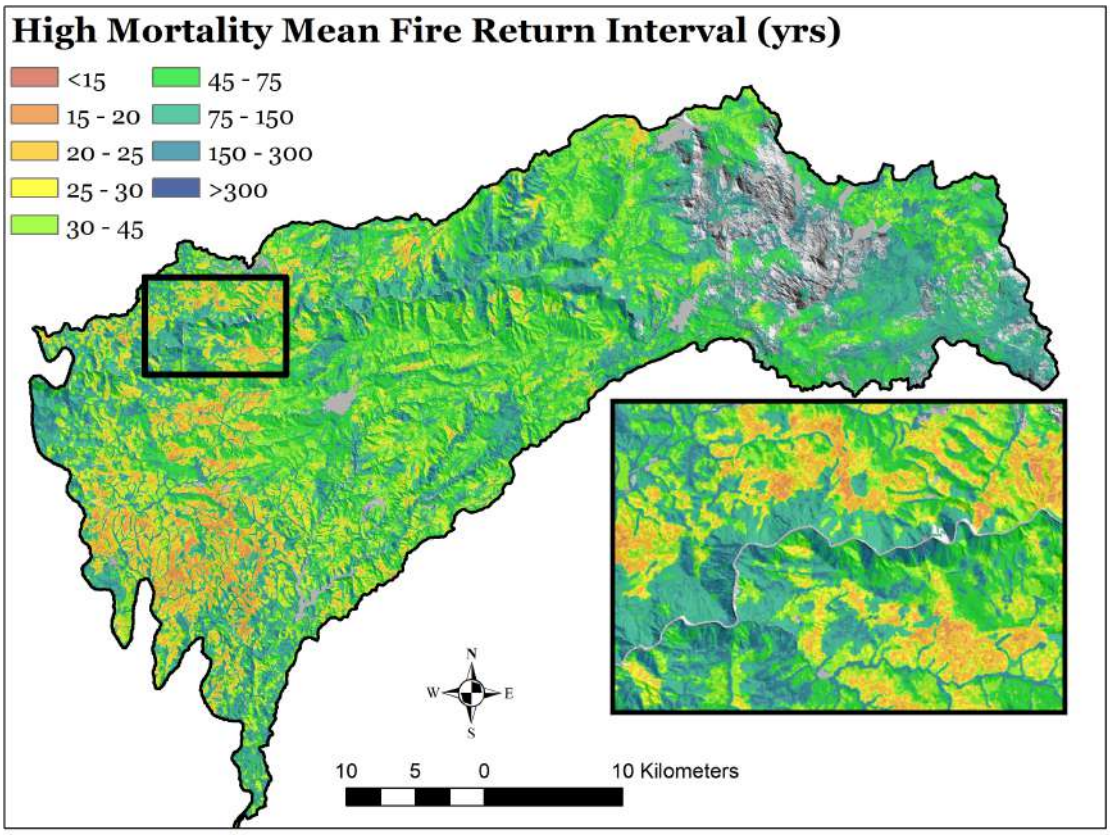

Figure 13: Simulated high-mortality Fire Return Interval (FRI) (yrs) at the 5 m cell level in the Bear River landscape.

Site Level HRV and Departure

The results presented in this section address landscape metrics quantified at the "Site" level. Recall from the GTR that we defined a Site as a 40-m radius window around each focal cell. Here, each Site falls within a single BPC based on the location of the focal cell and has a single value computed for each landscape metric for each point in time (i.e., snapshot). HRV represents the variation in the landscape metric across Sites and over time under historical dynamic equilibrium conditions. Further recall that the current landscape also has a range of values across Sites (CRV), rather than a single value. Thus, a comparison of the HRV and CRV distributions depicts the degree to which CRV deviates from HRV (i.e., current departure). It is important to remember that Site-level departure reflects the deviation between the CRV across Sites within the focal landscape and the HRV across Sites and over time within the focal landscape. Thus, departure for a Site is not based on a comparison of the current Site condition to its own HRV (as is the case with GPU and subbasin departure, see below); rather it is the distribution of current Site conditions across the entire landscape compared to the historical distribution across Sites that forms the basis for Site-level departure.

Recall from the GTR that we used a parsimonious suite of landscape metrics that we deemed meaningful for estimating departure at the Site-level across the focal landscape and appropriate given the available data, and computed departure as described in the GTR (and not repeated here), including the following metrics:

Developmental Stage

Developmental stage at the Site level was based on discrete stages of canopy height development. We quantified the composition of forest developmental stages at the Site level based on the percentage of the forested portion of the Site in each developmental stage. The HRV and CRV in Developmental Stage composition by BPC at the Site level is given in **Table 8** and depicted in **Figure 14**.

Table 8: Range of variability (given as quantiles) in each developmental stage class across sites (40-m radius window centered on each focal cell) by Biophysical Class (BPC) for the current range of variability (CRV) and the historical range of variability (HRV) for the Bear River landscape.

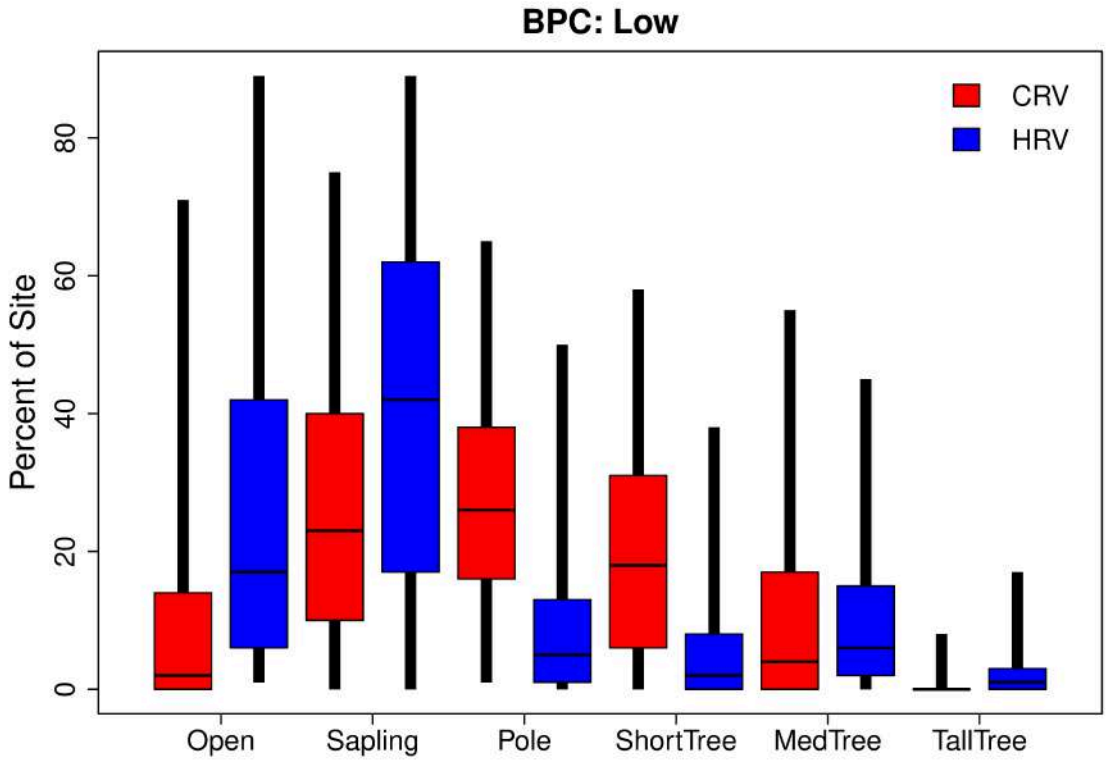

BPC	Class	Scenario	HRV 2.5%	HRV 25%	HRV 50%	HRV 75%	HRV 97.5%
Low	Open	CRV	0	0	2	14	71
Low	Open	HRV	1	6	17	42	89
Low	Sapling	CRV	0	10	23	40	75
Low	Sapling	HRV	0	17	42	62	89
Low	Pole	CRV	1	16	26	38	65
Low	Pole	HRV	0	1	5	13	50
Low	ShortTree	CRV	0	6	18	31	58
Low	ShortTree	HRV	0	0	2	8	38
Low	MedTree	CRV	0	0	4	17	55
Low	MedTree	HRV	0	2	6	15	45
Low	TallTree	CRV	0	0	0	0	8
Low	TallTree	HRV	0	0	1	3	17
ModLow	Open	CRV	0	0	3	15	69
ModLow	Open	HRV	1	5	12	31	81
ModLow	Sapling	CRV	0	10	24	40	72
ModLow	Sapling	HRV	0	13	34	53	83
ModLow	Pole	CRV	1	15	25	36	64
ModLow	Pole	HRV	0	2	8	18	54
ModLow	ShortTree	CRV	0	6	17	29	56
ModLow	ShortTree	HRV	0	1	4	11	42
ModLow	MedTree	CRV	0	0	4	19	57
ModLow	MedTree	HRV	0	4	11	22	52
ModLow	TallTree	CRV	0	0	0	0	13
ModLow	TallTree	HRV	0	0	2	7	24
ModHigh	Open	CRV	0	0	3	14	66
ModHigh	Open	HRV	1	4	9	23	73
ModHigh	Sapling	CRV	0	9	24	40	71
ModHigh	Sapling	HRV	0	10	26	46	77
ModHigh	Pole	CRV	2	16	25	36	64
ModHigh	Pole	HRV	0	4	10	21	56
ModHigh	ShortTree	CRV	0	7	17	29	57
ModHigh	ShortTree	HRV	0	2	6	13	43
ModHigh	MedTree	CRV	0	0	5	20	59
ModHigh	MedTree	HRV	0	7	16	27	56
ModHigh	TallTree	CRV	0	0	0	0	15
ModHigh	TallTree	HRV	0	1	4	10	31
High	Open	CRV	0	0	0	7	53
High	Open	HRV	1	4	8	17	66
High	Sapling	CRV	0	3	13	31	68
High	Sapling	HRV	0	5	18	37	72
High	Pole	CRV	1	13	23	35	68
High	Pole	HRV	0	4	11	24	58
High	ShortTree	CRV	0	11	21	34	64
High	ShortTree	HRV	0	2	6	13	41
High	MedTree	CRV	0	1	12	35	70
High	MedTree	HRV	0	7	16	28	57
High	TallTree	CRV	0	0	0	1	26
High	TallTree	HRV	0	5	12	22	46

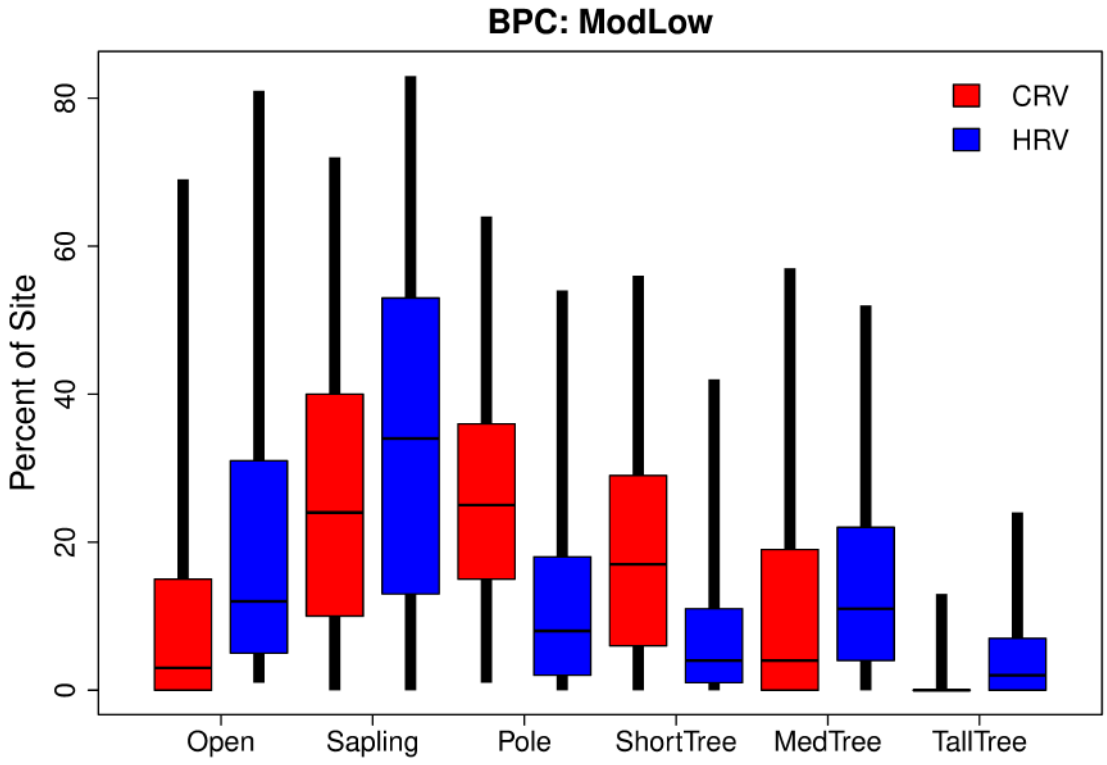
BPC: ModLow
CRV
HRV
Percent of Site
0
20
40
60
80
Open
Sapling
Pole
ShortTree
MedTree
TallTree

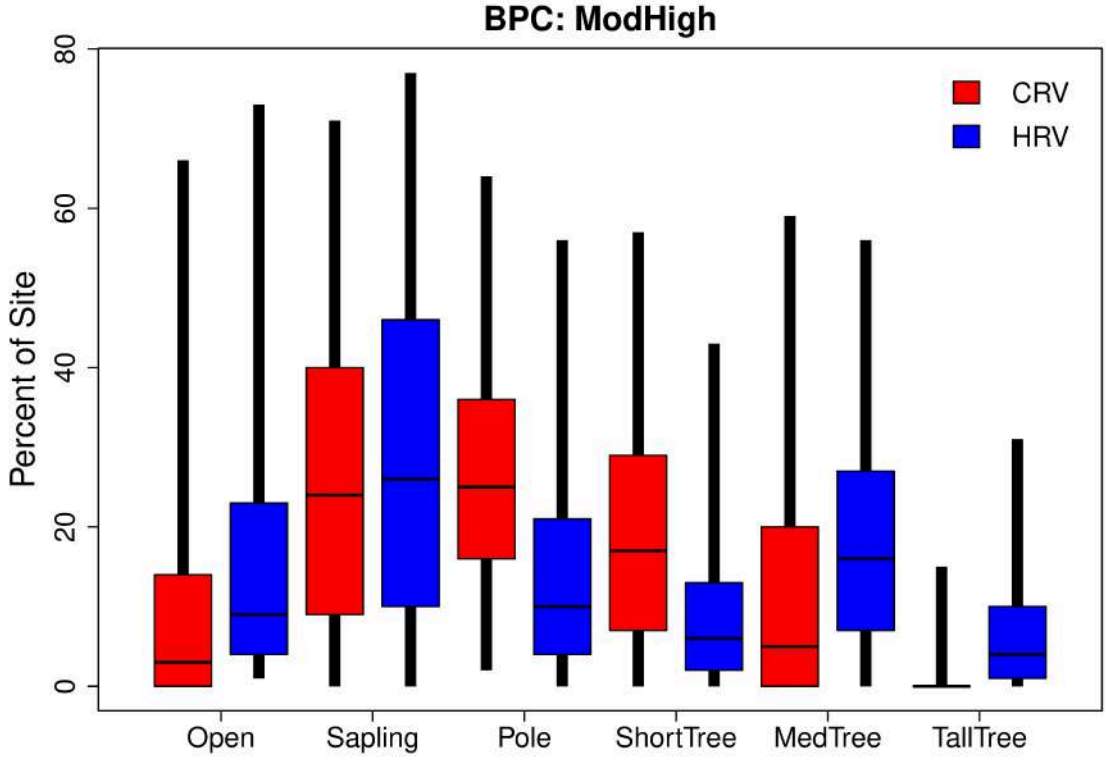
BPC: ModHigh
CRV
HRV
Percent of Site
0
20
40
60
80
Open
Sapling
Pole
ShortTree
MedTree
TallTree

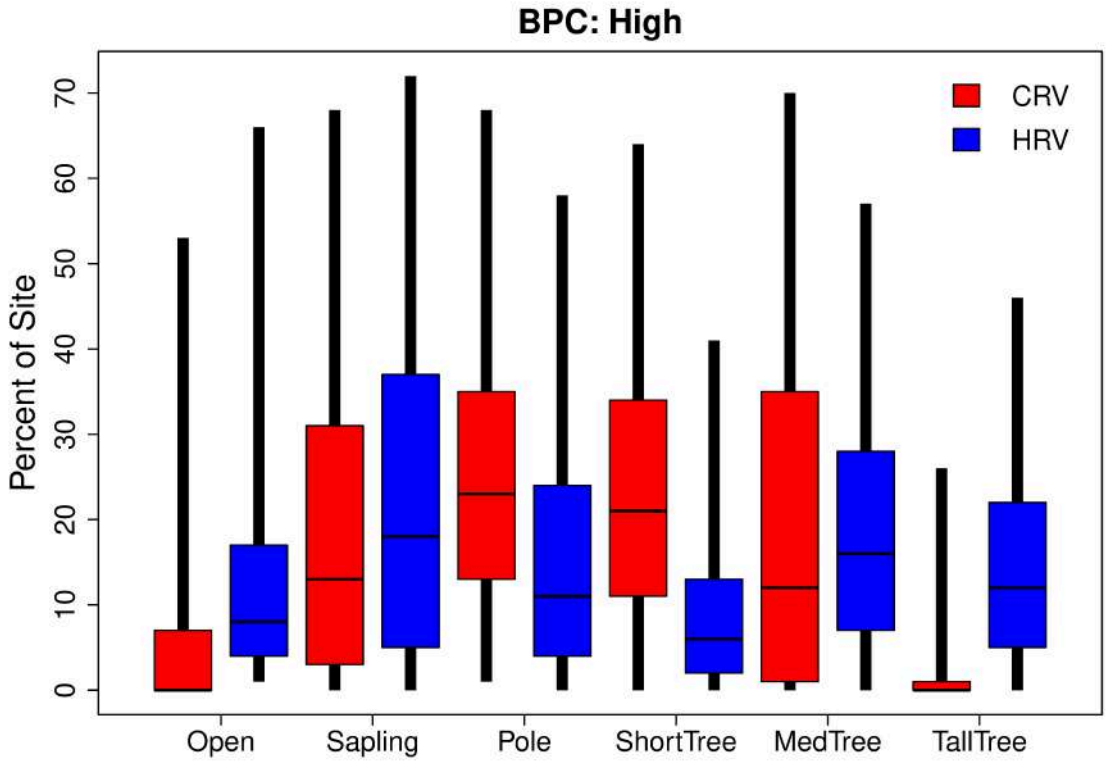

Figure 14: Historical Range of Variability (HRV) and Current range of variabiilty (CRV) among Sites (i.e., 40-m radius window) in the percent of forest in each developmental stage within the Low, Moderately Low, Moderately High and High site productivity Biophysical Classes (BPCs) in the Bear River landscape. Box = 25-50 percentiles; whiskers = 2.5-97.5 percentiles

Recall that current departure in the Site-level metrics provides a basis for prioritizing management at the unit level. For example, given the results above, to reduce the current departure in developmental stage composition on High productivity Sites, management could prioritize treatments that produce units with a greater percentage of Open areas intermixed with Tall trees to shift the overall developmental stage distribution across the landscape to be more aligned with the HRV distribution. The same priorities could be given to Low productivity Sites, although here the emphasis would be predominantly on increasing the proportion of Sites with a greater proportion of Open areas. Of course, aside from controlling the percentage in Open, there is only limited ability to actively manage developmental stage succession (i.e., height growth). Indeed, much of the succession required to shift the current distribution towards the later stages of development simply requires time (e.g., to allow trees in the Pole and Short Tree stages to grow into the Medium and Tall Tree stages). However, managing surface and ladder fuels to inhibit high severity wildfire and retaining current taller trees may be an effective strategy to gradually shift the CRV towards better alignment with HRV with respect to the later developmental stages.

Tree Size (QMD)

Tree Size at the Site level was based on the Quadratic Mean Diameter (QMD) of established trees within a 40-m radius of the focal cell. Recall that QMD was based on only the cells with established trees in the window. Thus, if there was a single cell with an established tree in the window, then QMD was based on that single tree and equaled the tree's diameter at breast height (DBH). Accordingly, QMD can be quite high even in relatively open areas if the few neighborhood trees are large in diameter. The HRV and CRV in Tree Size composition at the Site level by BPC is given in **Table 9** and depicted in **Figure 15**.

BPC	Scenario	HRV 2.5%	HRV 25%	HRV 50%	HRV 75%	HRV 97.5%
Low	CRV	2	5	8	11	18
Low	HRV	3	8	12	16	25
ModLow	CRV	2	6	8	12	21
ModLow	HRV	6	12	15	19	27
ModHigh	CRV	2	6	9	13	23
ModHigh	HRV	8	14	18	21	28
High	CRV	3	9	13	18	30
High	HRV	10	17	21	25	33

Table 9: Range of variability (given as quantiles) in tree size (quadratic mean diameter) across Sites (40-m radius window centered on each focal cell) by Biophysical Class (BPC) for the current range of variability (CRV) and the historical range of variability (HRV) for the Bear River landscape.

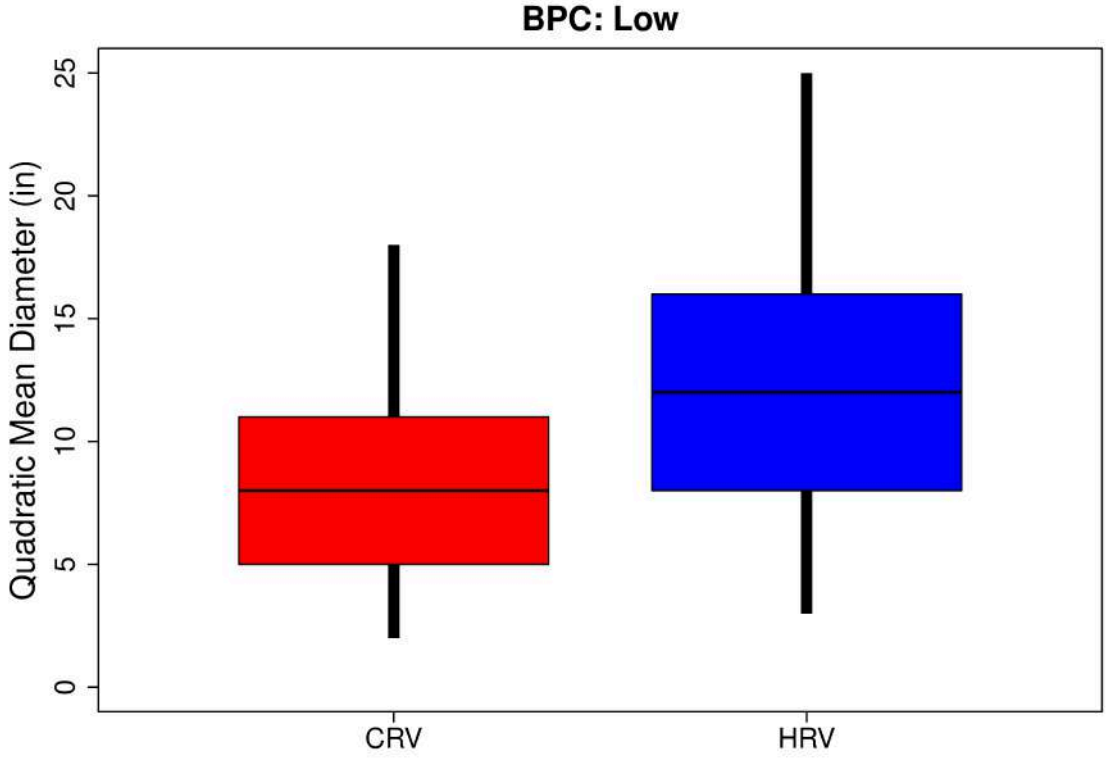

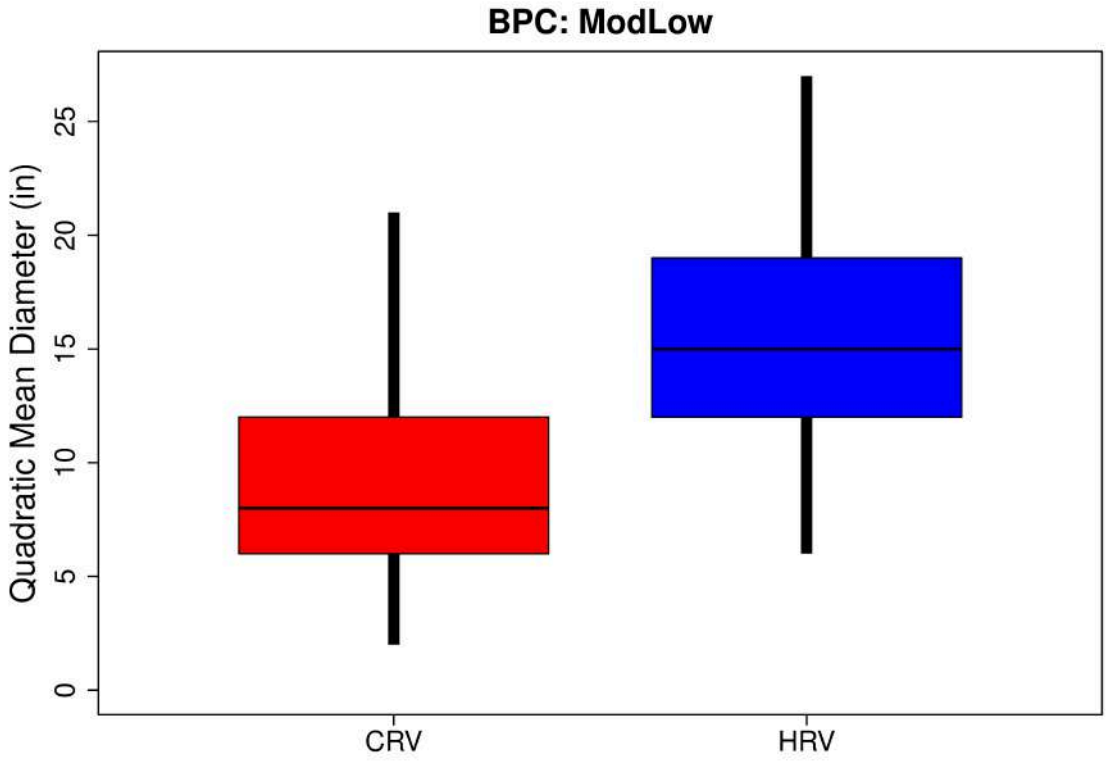
BPC: ModLow
Quadratic Mean Diameter (in)
0
5
10
15
20
25
CRV
HRV

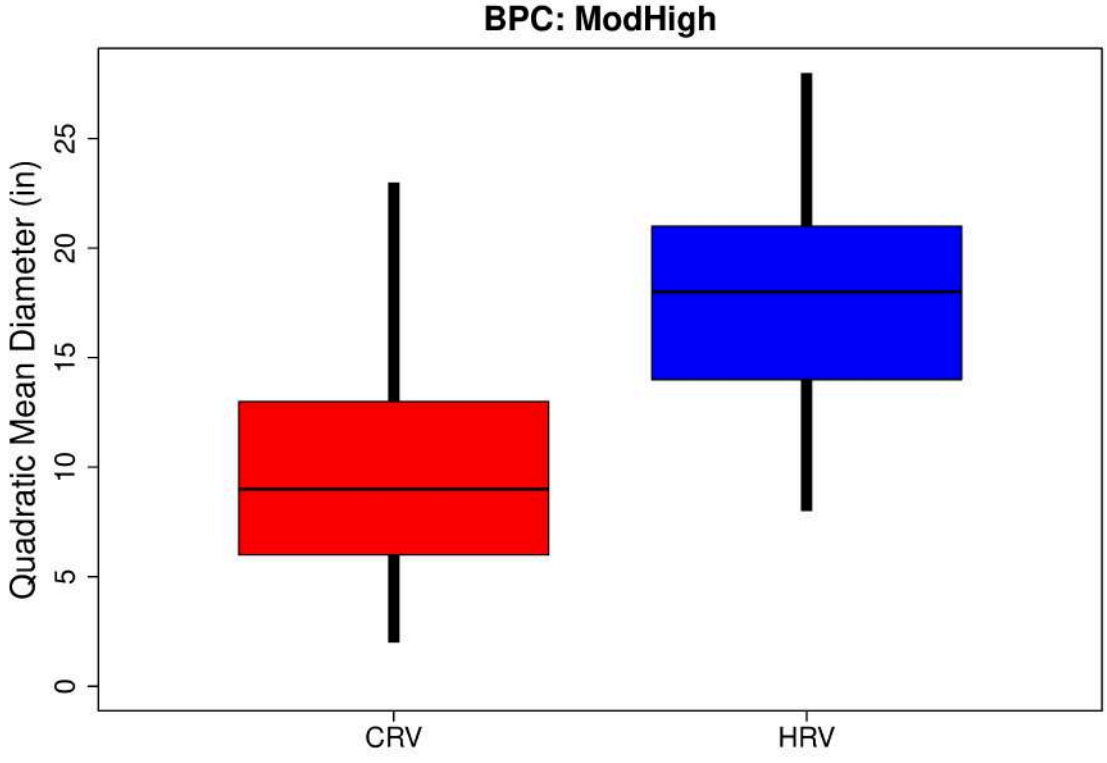
BPC: ModHigh
Quadratic Mean Diameter (in)
0
5
10
15
20
25
CRV
HRV

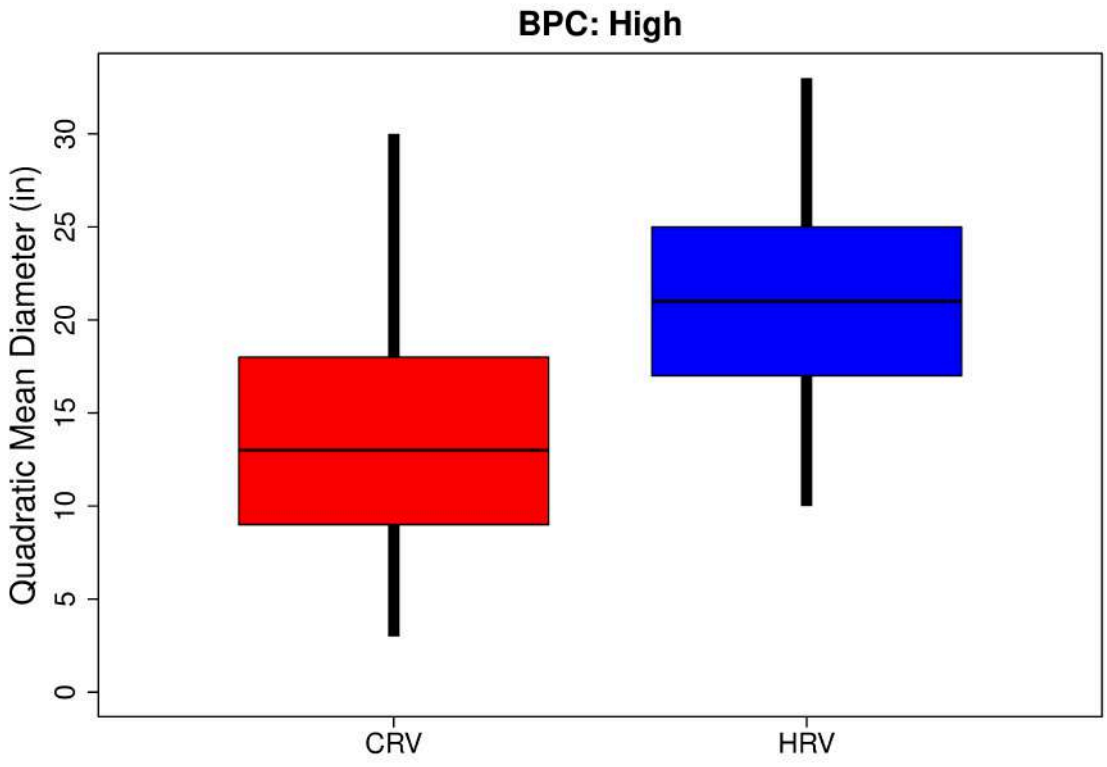

Figure 15: Historical Range of Variability (HRV) and Current range of variabiilty (CRV) among Sites (i.e., 40-m radius window) in the Quadratic Mean Diameter (QMD) of established trees to breast height within the Low, Moderately Low, Moderately High and High site productivity Biophysical Classes (BPCs) in the Bear River landscape. Box = 25-50 percentiles; whiskers = 2.5-97.5 percentiles

Tree Cover

Tree Cover at the Site level was based on the percentage of 5-m cells with established trees to breast height within a 40-m radius of the focal cell. Recall that even a cell in the Open developmental stage (i.e., forest cell without an established tree to breast height) has a percent tree cover > 0 % so long as there was a single established tree within 40 m of the focal cell. In addition, recall that Tree Cover, as computed here, represents the percentage of cells within 40 m containing one or more established trees to breast height, not actual tree canopy cover, and as such is biased high by an average of 16% over actual tree canopy cover (i.e., actual tree canopy cover will be less than reported here by an average of 16%). The HRV and CRV in Tree Cover composition at the Site level by BPC is given in **Table 10** and depicted in **Figure 16**.

Table 10: Range of variability (given as quantiles) in percent tree cover across Sites (40-m radius window centered on each focal cell) by Biophysical Class (BPC) for the current range of variability (CRV) and the historical range of variability (HRV) for the Bear River landscape.

BPC	Scenario	HRV 2.5%	HRV 25%	HRV 50%	HRV 75%	HRV 97.5%
Low	CRV	28	85	97	100	100
Low	HRV	10	57	82	93	98
ModLow	CRV	30	84	96	100	100
ModLow	HRV	18	68	87	94	98
ModHigh	CRV	33	85	96	100	100
ModHigh	HRV	26	76	90	95	98
High	CRV	46	92	99	100	100
High	HRV	33	82	91	95	98

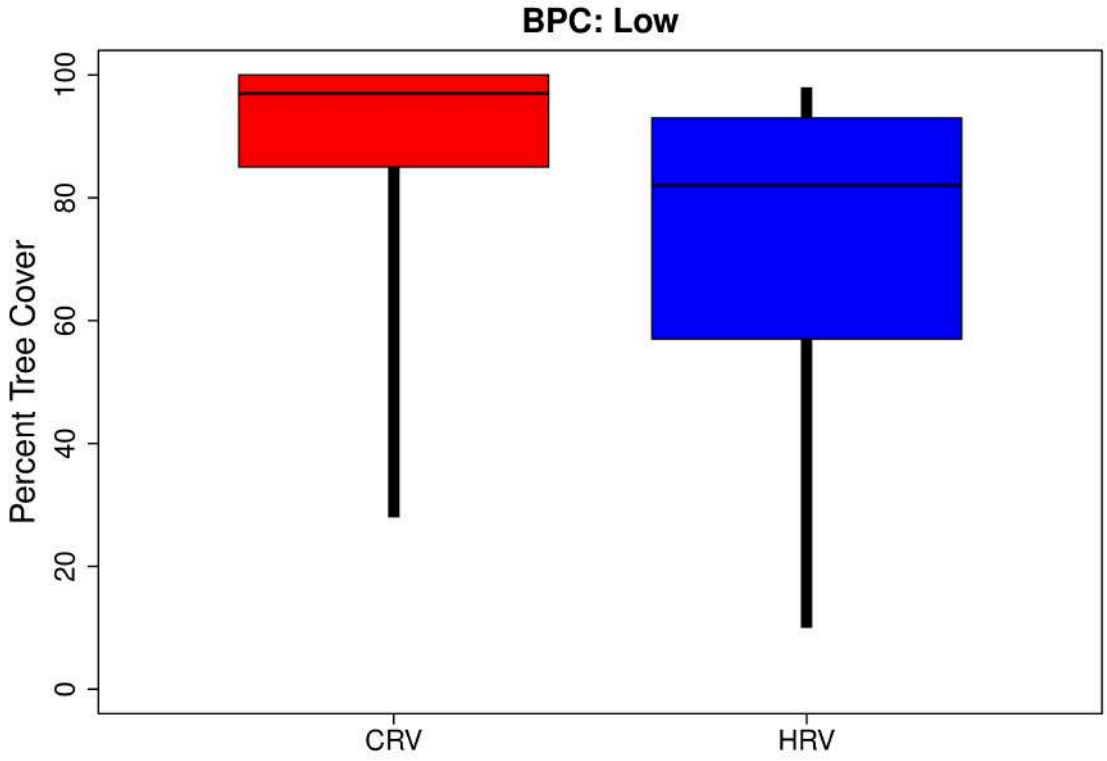

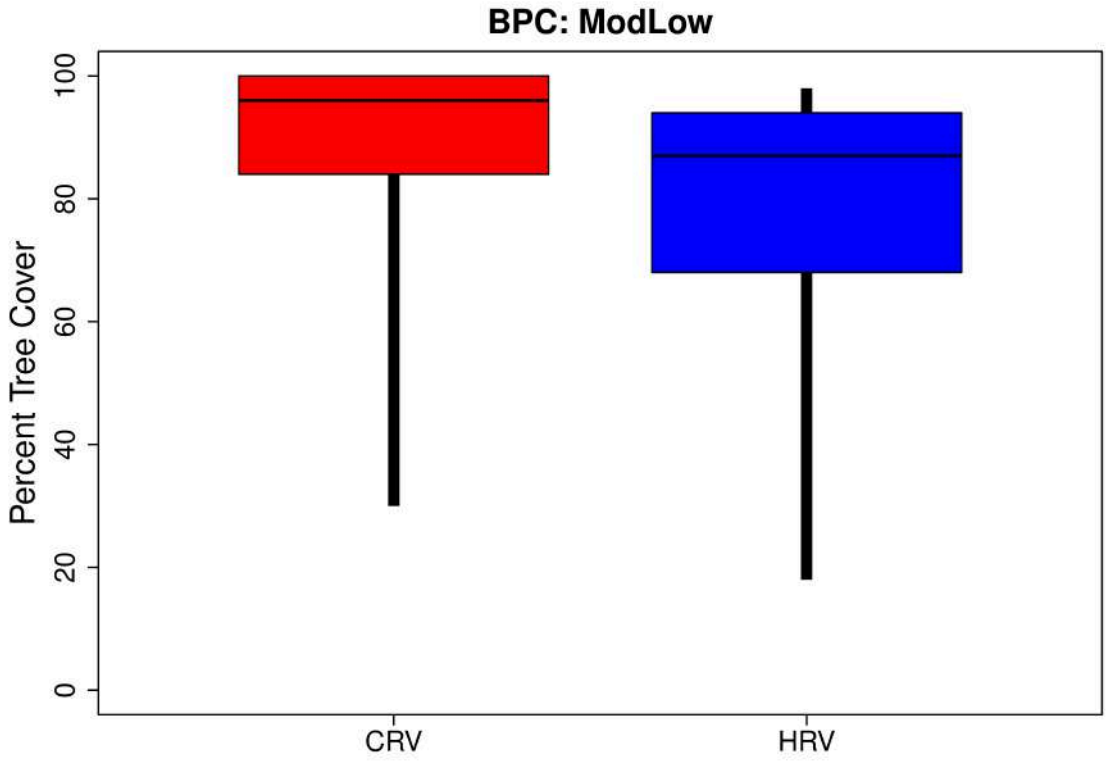
BPC: ModLow
Percent Tree Cover
0
20
40
60
80
100
CRV
HRV

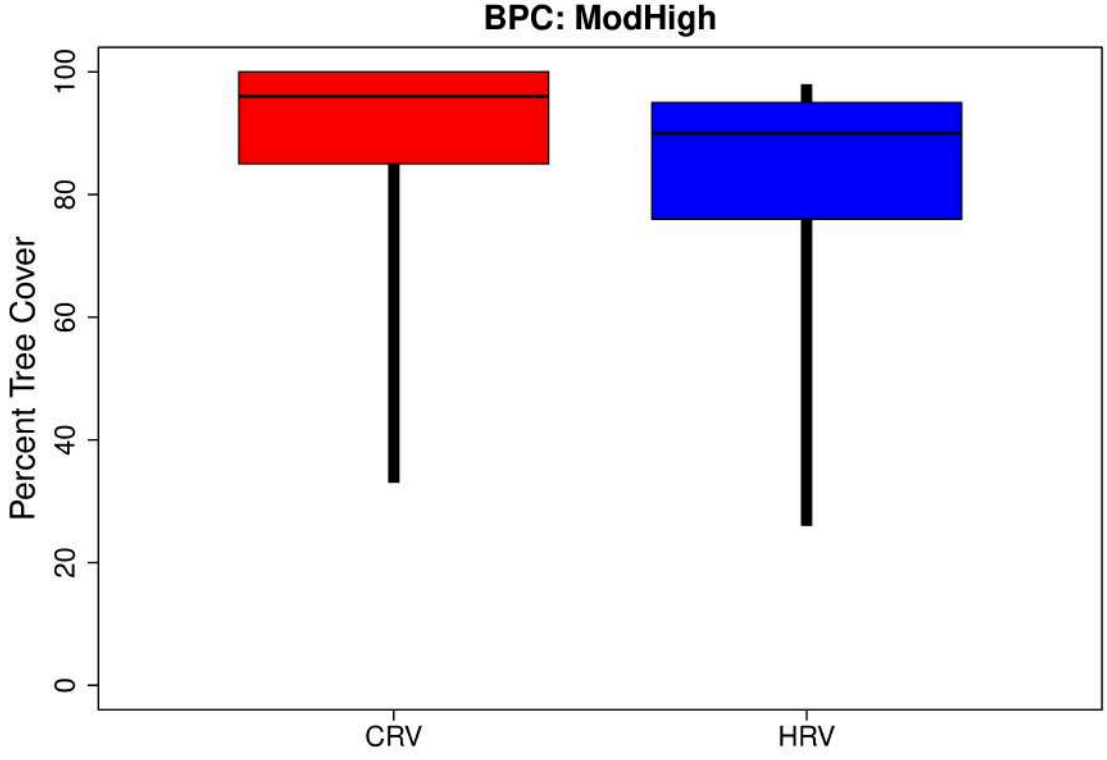
BPC: ModHigh
Percent Tree Cover
0
20
40
60
80
100
CRV
HRV

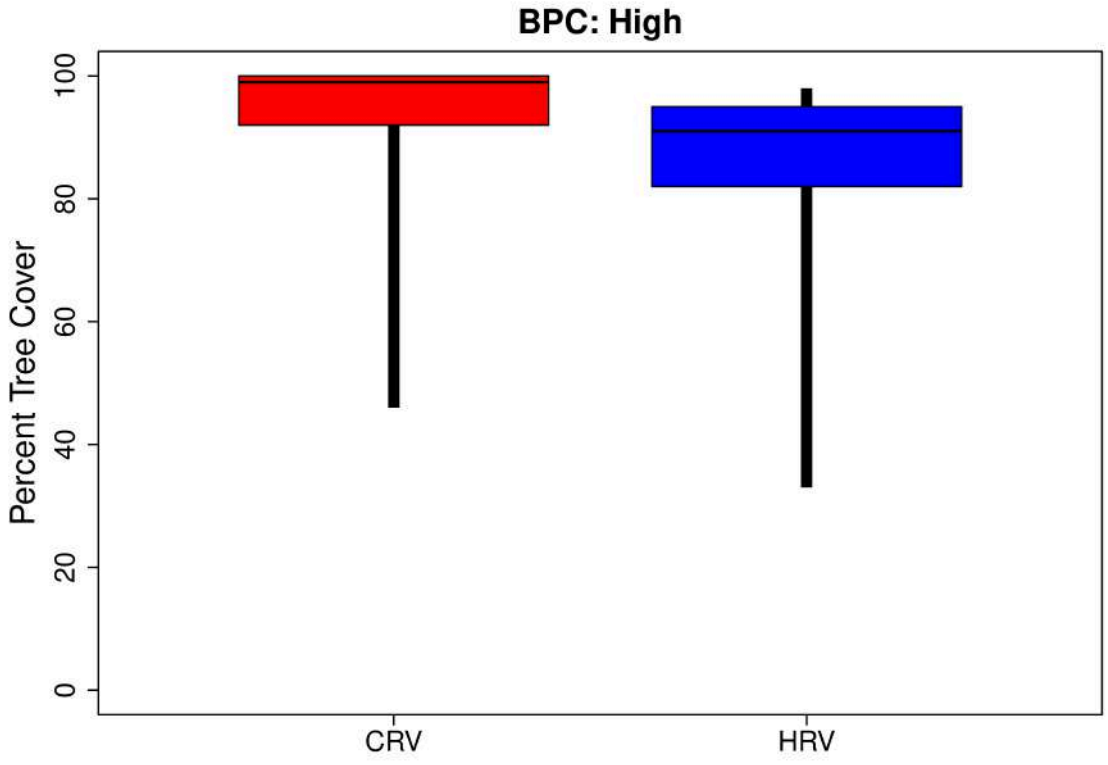

Figure 16: Historical Range of Variability (HRV) and Current range of variabiilty (CRV) among Sites (i.e., 40-m radius window) in the percent Tree Cover of established trees to breast height within the Low, Moderately Low, Moderately High and High site productivity Biophysical Classes (BPCs) in the Bear River landscape. Box = 25-50 percentiles; whiskers = 2.5-97.5 percentiles

Geophysical Unit Level Departure

The results presented in this section address current departure in landscape metrics quantified at the spatial extent of a single Geophysical Unit (GPU). The Bear River landscape was divided into 5,383 separate GPUs, which collectively encompass the area mapped as forest in the Existing Cover layer (Ecover) and within existing Lidar at the time of this analysis. Recall from the GTR that we defined GPUs based on similarity in a suite of 10 geophysical attributes and that they were defined only for the forested portion of the landscape and only where we had Lidar coverage. In addition, recall that each GPU was assessed independently; i.e., that we compared the current condition of each GPU to its own HRV in vegetation conditions. Thus, current departure of a GPU was specific to that GPU and independent of that measured for other GPUs. Lastly, recall that we used a large but parsimonious suite of landscape metrics that we deemed meaningful for estimating departure at the GPU level and appropriate given the available data, and computed departure as described in the GTR (and not repeated here), including the following:

Metric 1: Basal Area Departure

Departure in basal area of trees within the GPU was based on a metric derived by the TCSI project and adapted here for our purposes (**Figure 17**). GPUs with an increasingly positive departure have a current basal area that is greater than expected under HRV.

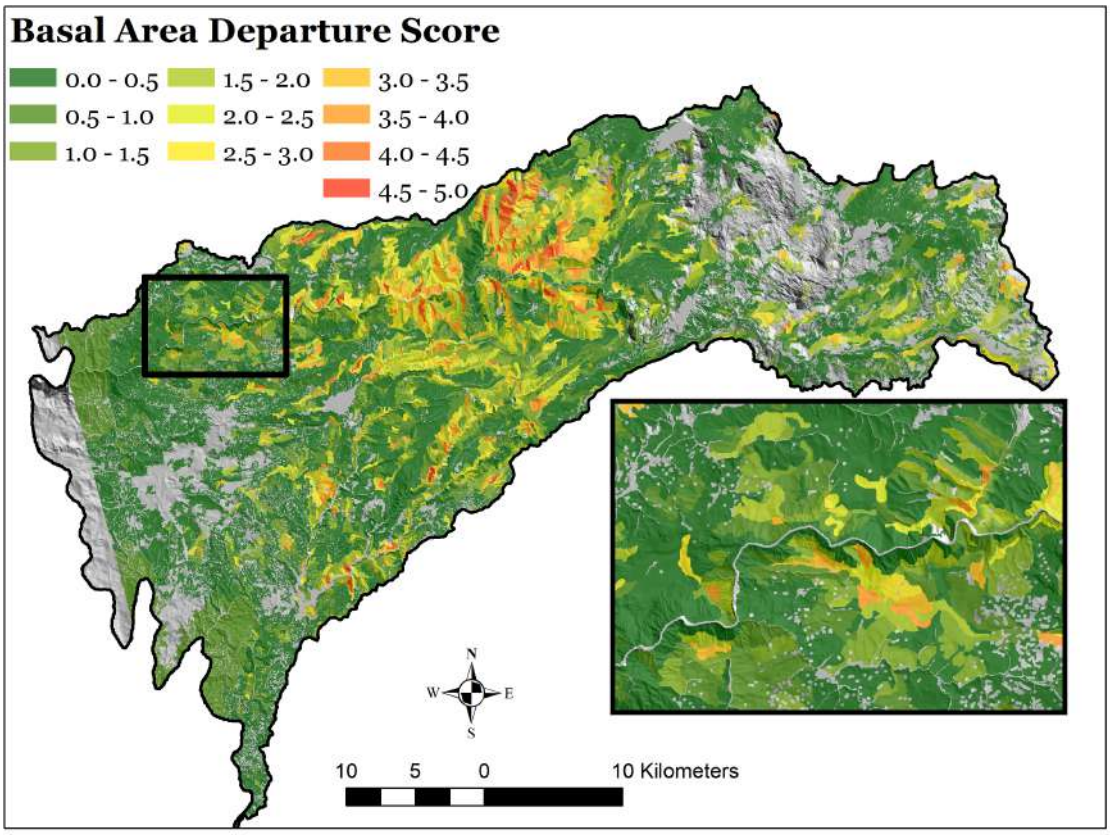

Figure 17: Geophysical Unit (GPU)-level basal area departure score for the Bear River landscape. The departure score (0-5) represents the deviation of the current GPU condition from its historical range of variability (HRV), as estimated from a suite of contemporary reference sites. Values increase with increasing degrees of departure.

Metric 2: Percent Open Forest

We measured departure in the percent of forested cells within the GPU in the Open developmental stage (**Figure 18**). GPUs with a departure index less than -1 have less area in the Open developmental stage than under HRV.

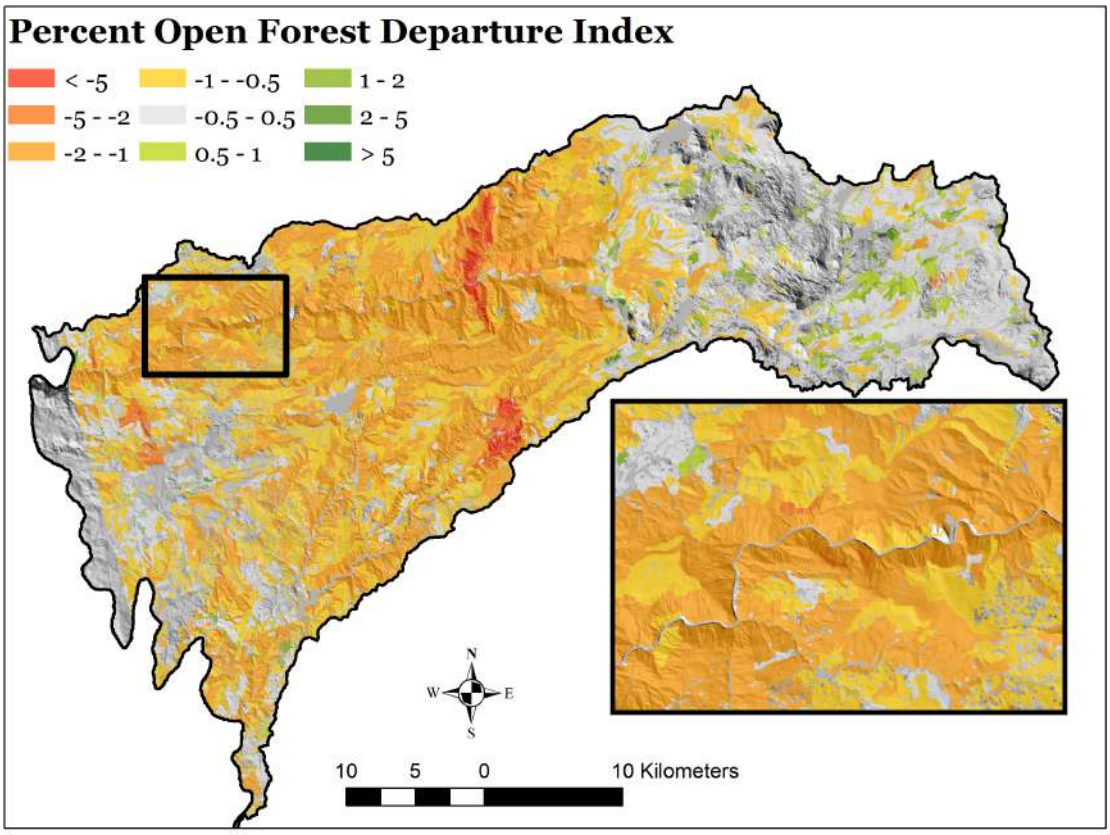

Figure 18: Geophysical Unit (GPU)-level departure index (unbounded) for the percentage of the forest within the GPU in the Open developmental stage for the Bear River landscape. The departure Index represents the deviation of the current GPU condition from its historical range of variability (HRV), as simulated. Values < -1 represent a current condition that is less than the HRV for the GPU, and increasingly negative values represent increasing degrees of negative departure.

Metric 3: Developmental Stage Diversity

We measured departure in the diversity of forest developmental stages within the GPU based on the Simpson's Diversity index (**Figure 19**). Here, Simpson's Diversity is defined as the probability that any two cells selected at random would be different developmental stages. The departure index for Simpson's Diversity is less than -1 if the current GPU has a diversity of developmental stages that is less than HRV.

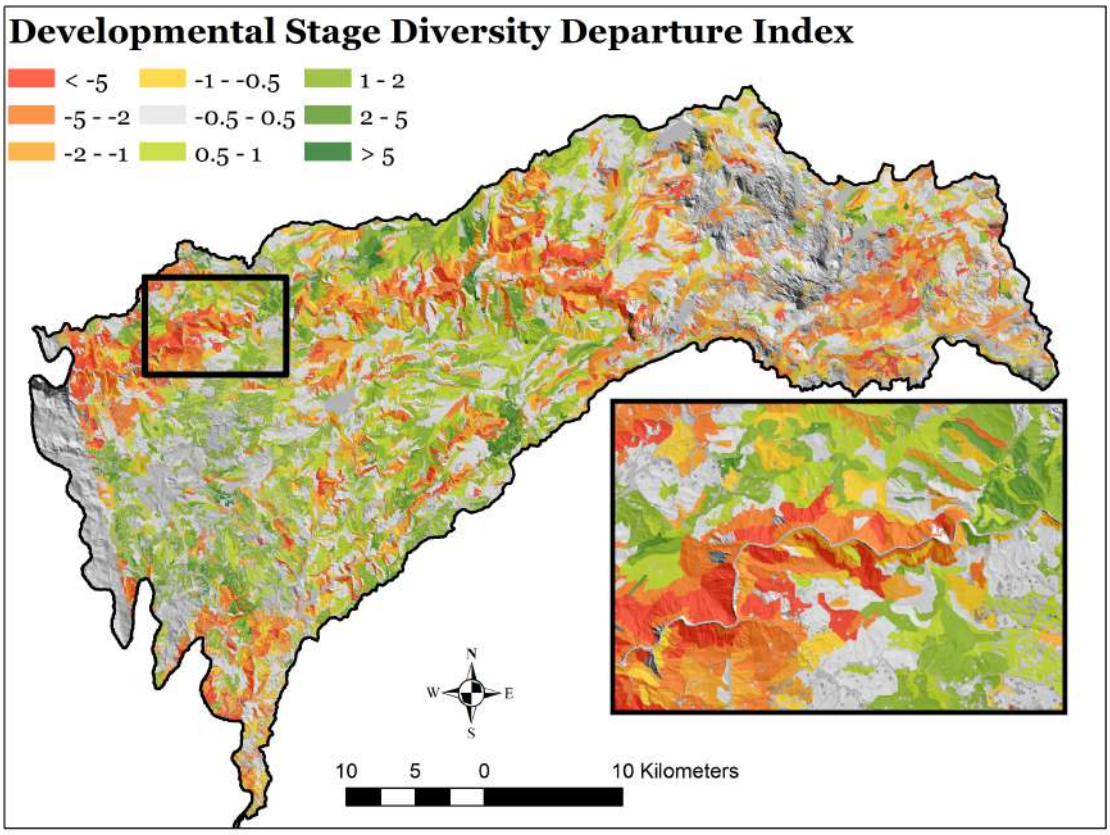

Figure 19: Geophysical Unit (GPU)-level departure index (unbounded) for the Simpson Diversity of developmental stages within the GPU for the Bear River landscape. The departure Index represents the deviation of the current GPU condition from its historical range of variability (HRV), as simulated. Values < -1 represent a current condition that is less than the HRV for the GPU, and increasingly negative values represent increasing degrees of negative departure.

Metric 4: Coefficient of Variation in Open Patch Size

We measured departure in the Coe icient of Variation (CV) in the size of all Open forest patches, including single cell patches, in which forest openings are defined by contiguous cells in the Open developmental stage based on the 4-neighbor rule (i.e., orthogonal neighbors)(**Figure 20**). The departure index is less than -1 if the current GPU has relatively invariant Open patch sizes compared to HRV.

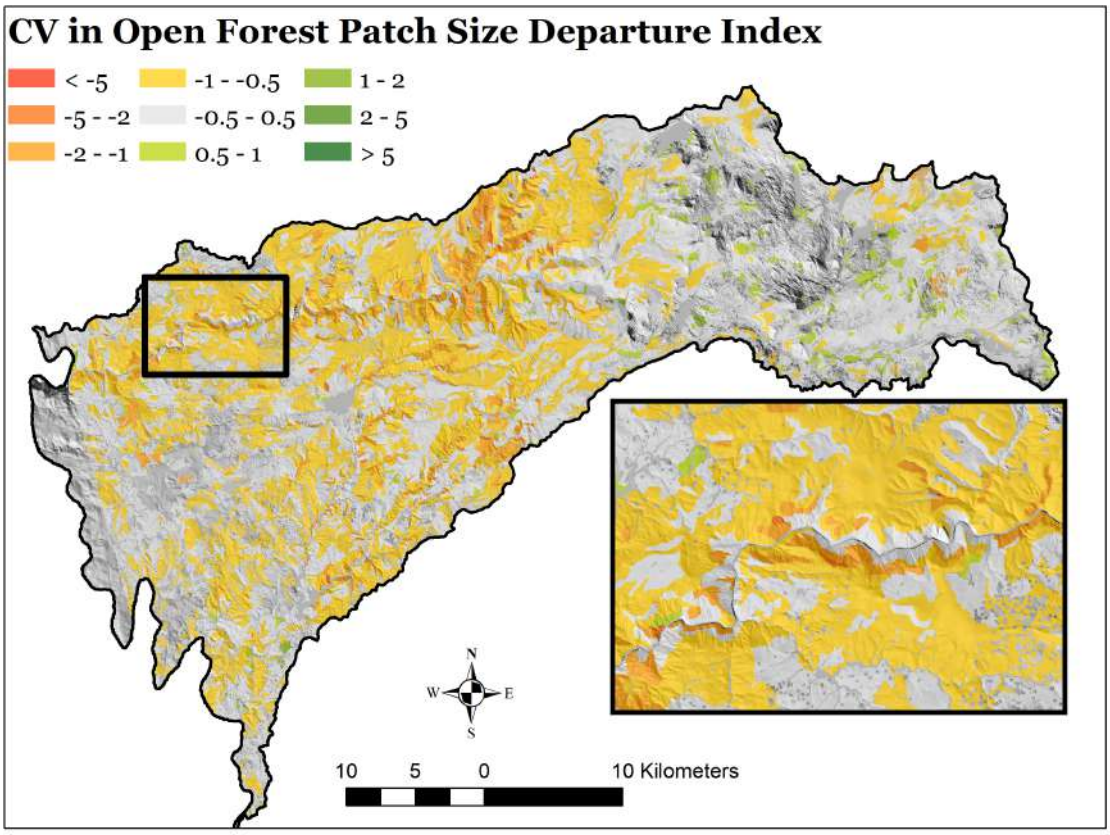

Figure 20: Geophysical Unit (GPU)-level departure index (unbounded) for the Coefficient of Variation (CV) in the size of patches in the Open developmental stage within the GPU for the Bear River landscape. The departure Index represents the deviation of the current GPU condition from its historical range of variability (HRV), as simulated. Values < -1 represent a current condition that is less than the HRV for the GPU, and increasingly negative values represent increasing degrees of negative departure.

Metric 5: Coefficient of Variation in Developmental Stage Patch Size

We measured departure in the CV in the size of all forest developmental stage patches, including single cell patches, in which patches are defined by contiguous cells in the same developmental stage based on the 4-neighbor rule (**Figure 21**). The departure index is less than -1 if the current GPU has relatively invariant developmental stage patch sizes compared to HRV.

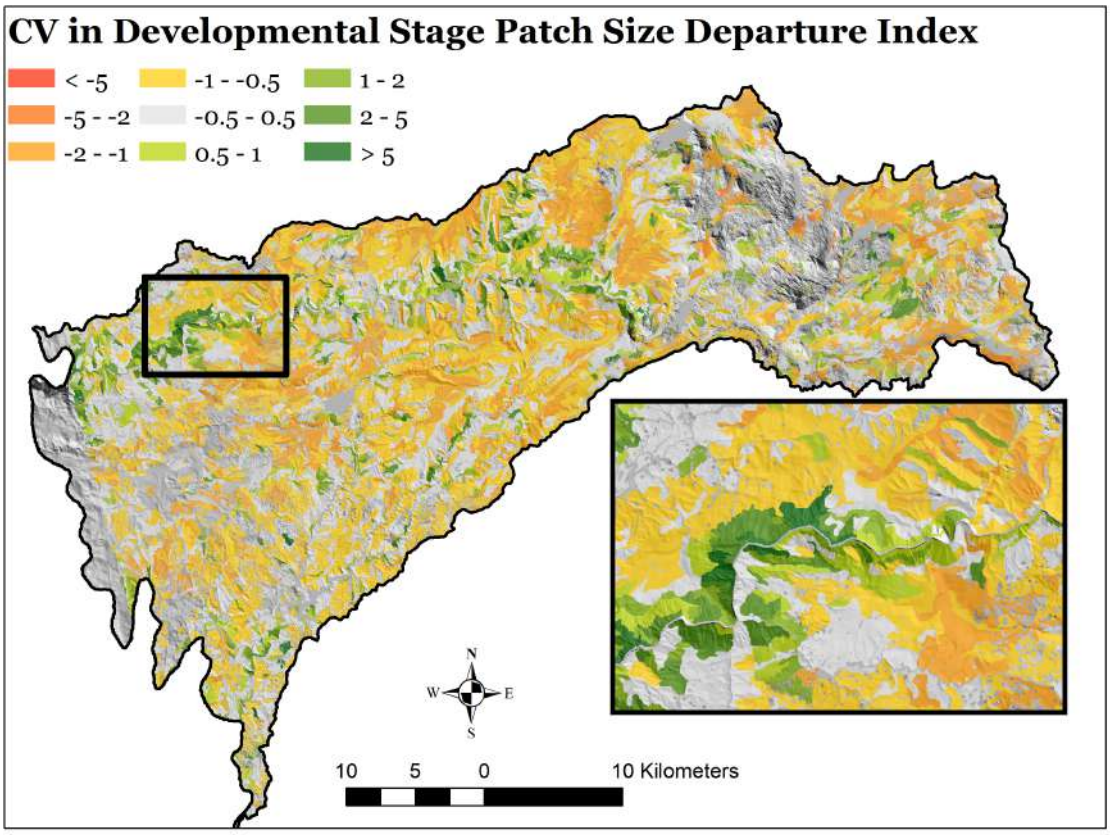

Figure 21: Geophysical Unit (GPU)-level departure index (unbounded) for the Coefficient of Variation (CV) in the size of patches based on developmental stages within the GPU for the Bear River landscape. The departure Index represents the deviation of the current GPU condition from its historical range of variability (HRV), as simulated. Values < -1 represent a current condition that is less than the HRV for the GPU, and increasingly negative values represent increasing degrees of negative departure.

Metric 6: Percent Large Trees

We measured departure in the percent of forested cells within the GPU in the Large tree size class (≥30 in dbh)(**Figure 22**). GPUs with a departure index less than -1 have less area in the Large tree class than under HRV.

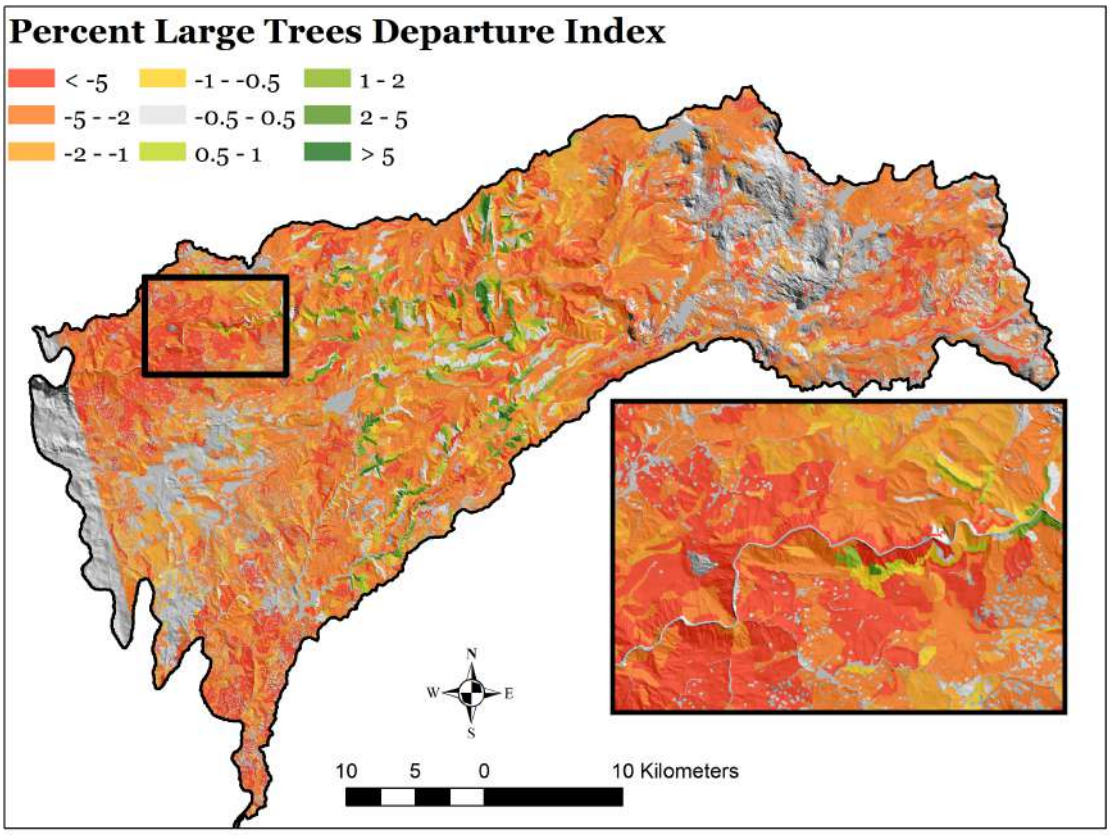

Figure 22: Geophysical Unit (GPU)-level departure index (unbounded) for the percentage of the forest in the Large tree size class (30 in dbh) within the GPU for the Bear River landscape. The departure Index represents the deviation of the current GPU condition from its historical range of variability (HRV), as simulated. Values < -1 represent a current condition that is less than the HRV for the GPU, and increasingly negative values represent increasing degrees of negative departure.

Metric 7: Tree Size Class Diversity

We measured departure in the diversity of tree size classes within the forested portion of the GPU based on the Simpson's Diversity index (**Figure 23**). Here, Simpson's Diversity is defined as the probability that any two cells selected at random would be from different tree size classes. The departure index for Simpson's Diversity is less than -1 if the current GPU has a diversity of tree size classes that is less than HRV.

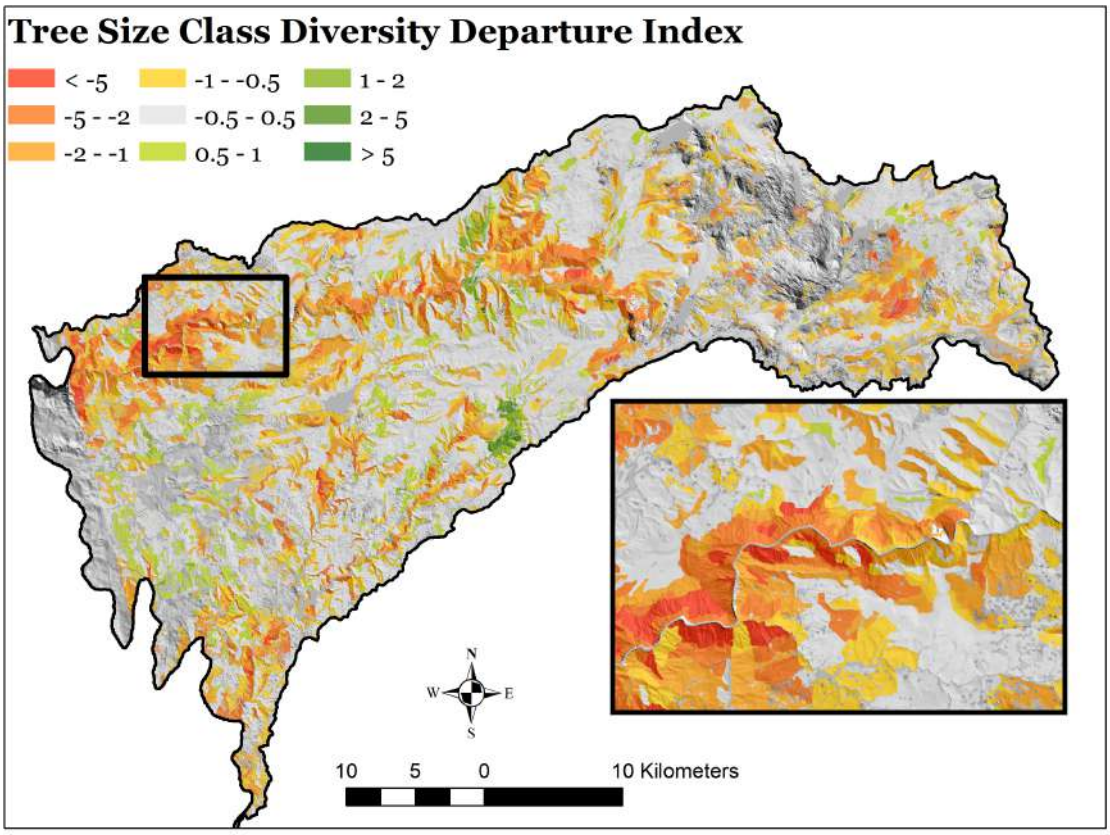

Figure 23: Geophysical Unit (GPU)-level departure index (unbounded) for the Simpson Diversity of tree size classes within the GPU for the Bear River landscape. The departure Index represents the deviation of the current GPU condition from its historical range of variability (HRV), as simulated. Values < -1 represent a current condition that is less than the HRV for the GPU, and increasingly negative values represent increasing degrees of negative departure.

Metric 8: Coefficient of Variation in Large Tree Patch Size

We measured departure in the CV in the size of all Large tree patches, including single cell patches, in which Large tree patches were defined by contiguous cells in the Large tree class (≥30 in dbh) based on the 4-neighbor rule (**Figure 24**). The departure index is less than -1 if the current GPU has relatively invariant Large tree patch sizes compared to HRV.

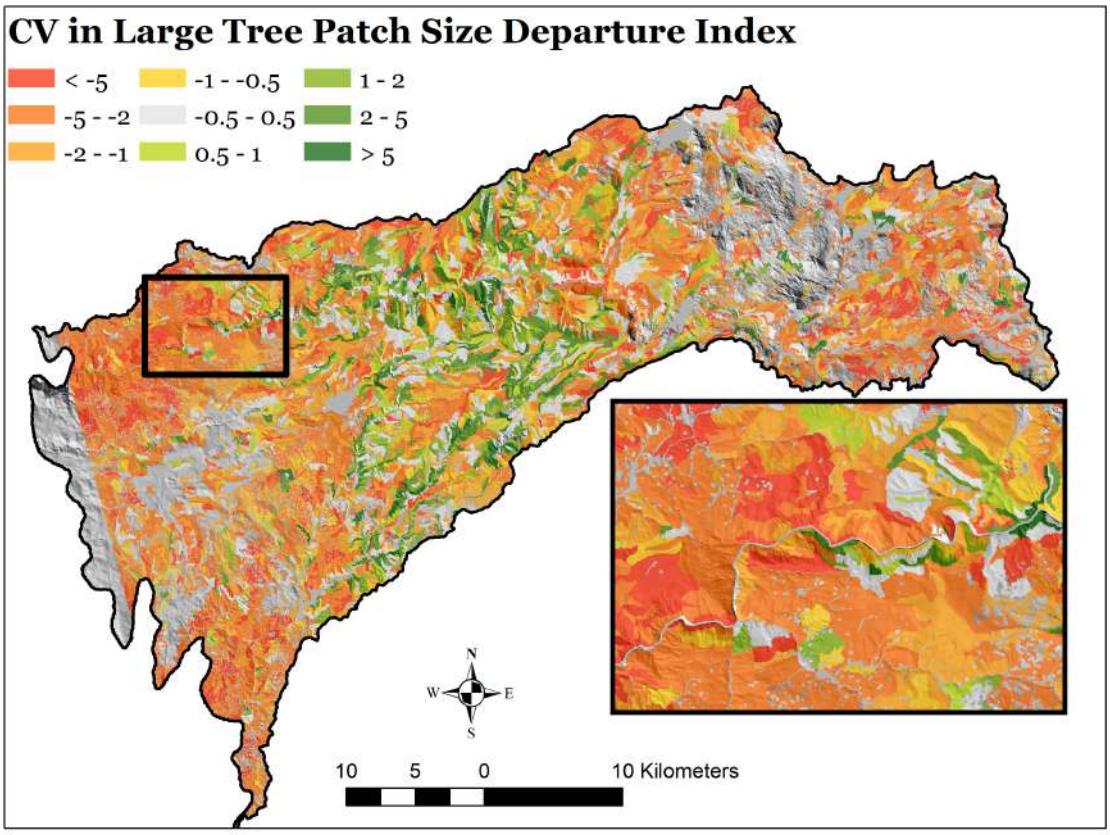

Figure 24: Geophysical Unit (GPU)-level departure index (unbounded) for the Coefficient of Variation (CV) in the size of patches in the Large tree size class (30 in dbh) within the GPU for the Bear River landscape. The departure Index represents the deviation of the current GPU condition from its historical range of variability (HRV), as simulated. Values < -1 represent a current condition that is less than the HRV for the GPU, and increasingly negative values represent increasing degrees of negative departure.

Metric 9: Coefficient of Variation in Tree Size Class Patch Size

We measured departure in the CV in the size of all tree size class patches, including single cell patches, in which patches were defined by contiguous cells in the same tree size class based on the 4-neighbor rule (**Figure 25**). The departure index is less than -1 if the current GPU has relatively invariant tree size class patch sizes compared to HRV.

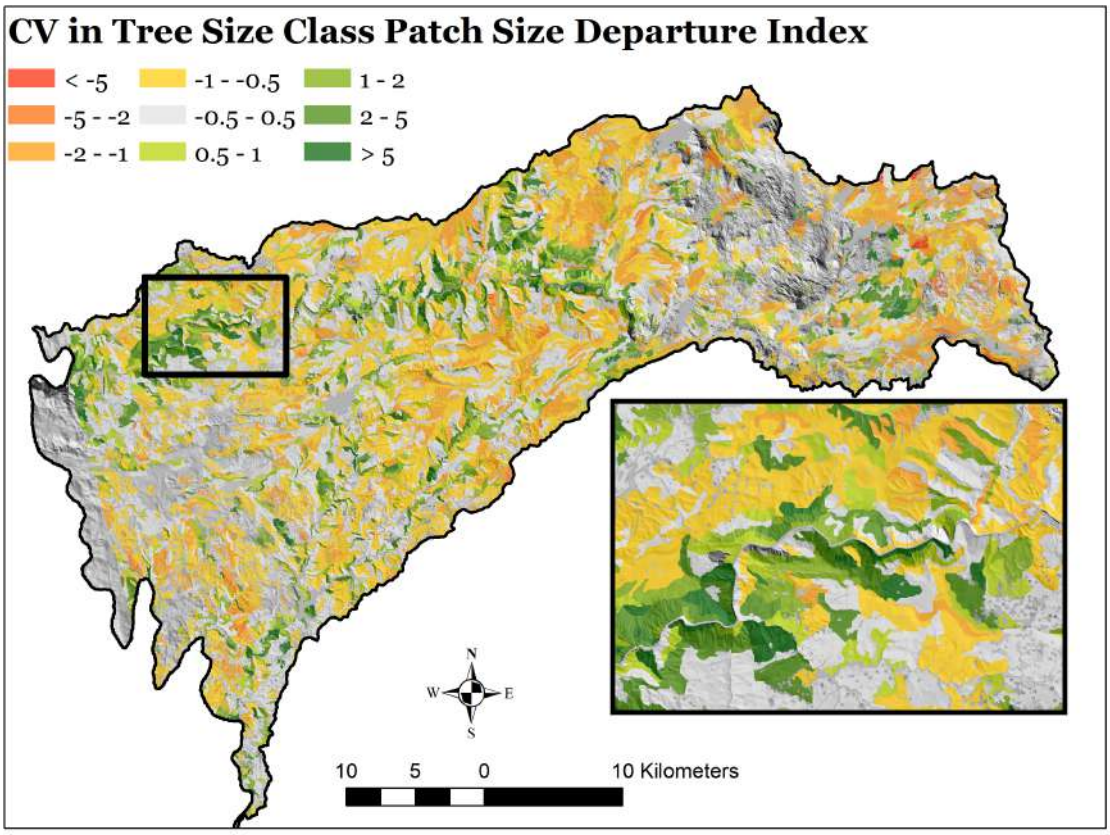

Figure 25: Geophysical Unit (GPU)-level departure index (unbounded) for the Coefficient of Variation (CV) in the size of patches based on tree size classes within the GPU for the Bear River landscape. The departure Index represents the deviation of the current GPU condition from its historical range of variability (HRV), as simulated. Values < -1 represent a current condition that is less than the HRV for the GPU, and increasingly negative values represent increasing degrees of negative departure.

Metric 10: Coefficient of Variation in Quadratic Mean Diameter

We measured departure in the CV in site-level Quadratic Mean Diameter (QMD) of established trees within the GPU (**Figure 26**). Recall that a site was defined as a 40-m radius window around each focal cell. Thus, QMD was computed for the site associated with each focal cell, which produced a continuous surface of QMD values, from which the CV in QMD values within the GPU was computed. The departure index is less than -1 if the current GPU has relatively homogeneous QMD compared to HRV.

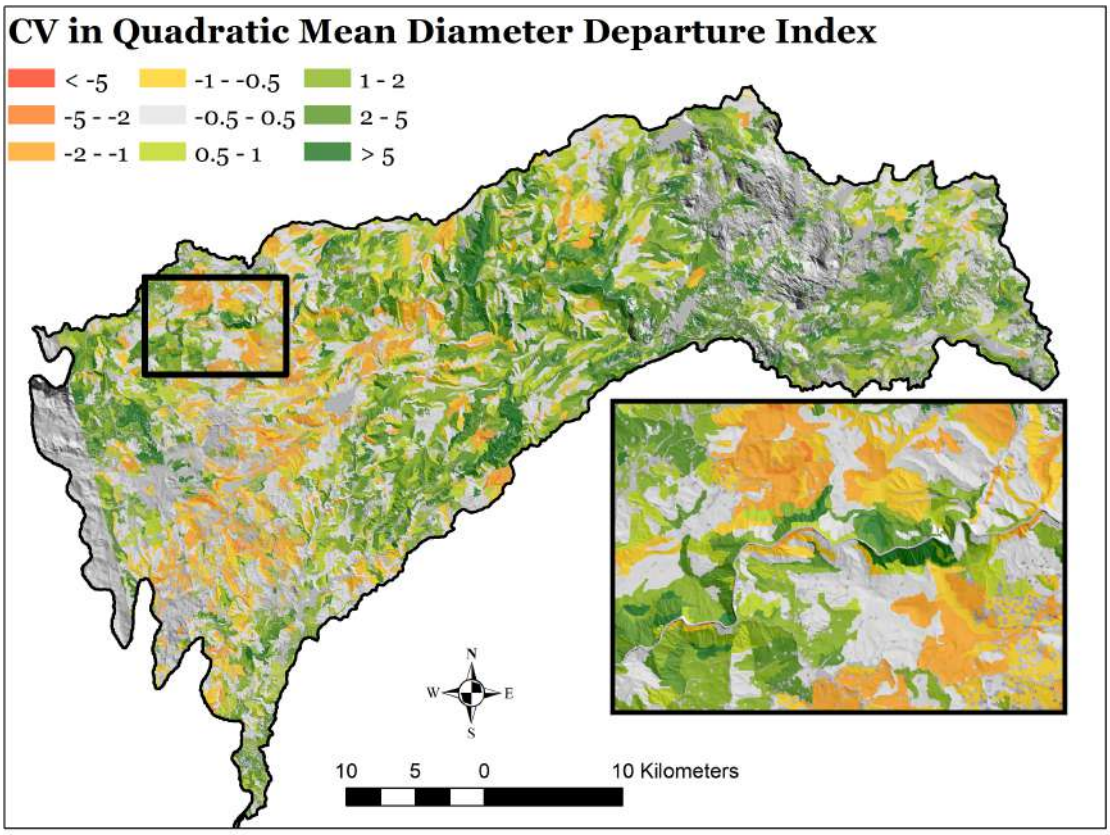

Figure 26: Geophysical Unit (GPU)-level departure index (unbounded) for the Coefficient of Variation (CV) in Site-level (i.e., 40 m radius window around each focal cell) Quadratic Mean Diameter (QMD, in inches) within the GPU for the Bear River landscape. The departure Index represents the deviation of the current GPU condition from its historical range of variability (HRV), as simulated. Values < -1 represent a current condition that is less than the HRV for the GPU, and increasingly negative values represent increasing degrees of negative departure.

Metric 11: Coefficient of Variation in Percent Tree Cover

We measured departure in the CV in site-level percent cover of established trees within the GPU (**Figure 27**). Again, recall that a site was defined as a 40-m radius window around each focal cell. Thus, percent tree Cover was computed for the site associated with each focal cell, which produced a continuous surface of percent tree cover values, from which the CV in tree cover within the GPU was computed. The departure index is less than -1 if the current GPU has relatively homogeneous tree cover compared to HRV.

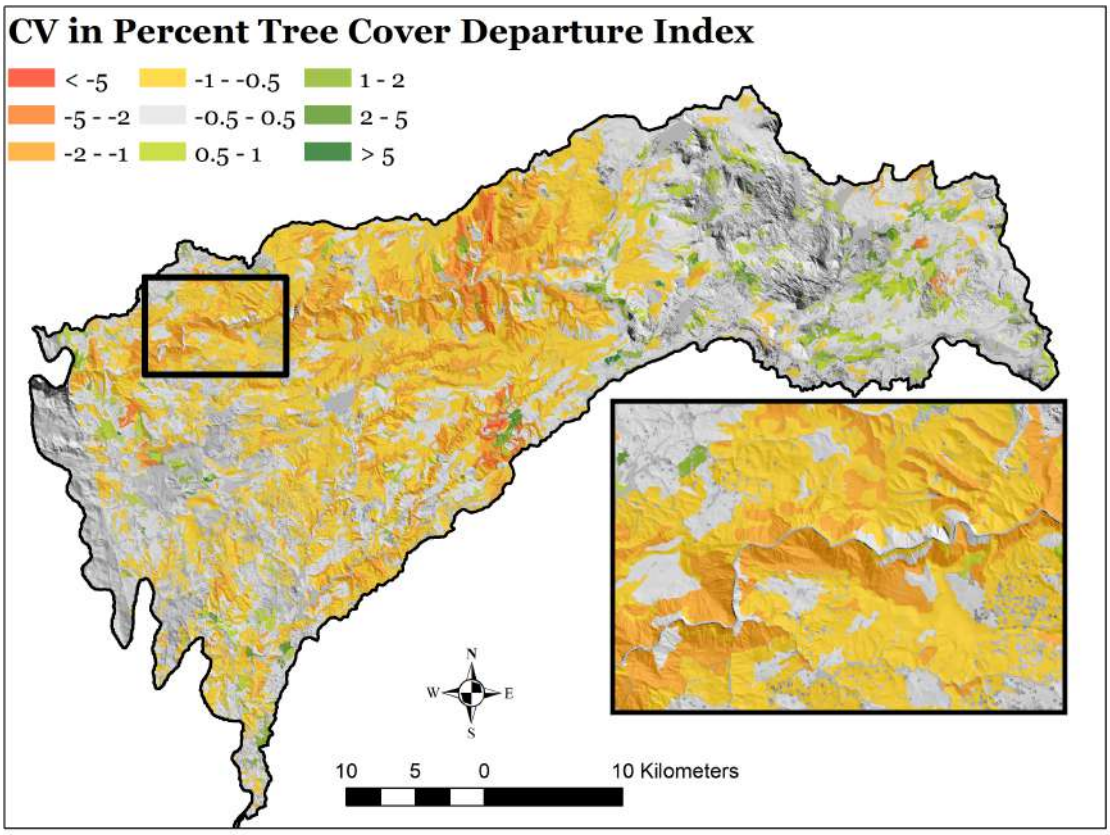

Figure 27: Geophysical Unit (GPU)-level departure index (unbounded) for the Coefficient of Variation (CV) in Site-level (i.e., 40 m radius window around each focal cell) percent tree cover within the GPU for the Bear River landscape. Note, percent tree cover as measured is on average 16 % greater than percent canopy cover. The departure Index represents the deviation of the current GPU condition from its historical range of variability (HRV), as simulated. Values < -1 represent a current condition that is less than the HRV for the GPU, and increasingly negative values represent increasing degrees of negative departure.

Composite Departure Index

We combined the 11 GPU-level departure indices above into two composite departure scores: 1) composite "negative" departure, and 2) composite "absolute" departure (see GTR for details). Both of these composite scores can be interpreted as a measure of overall GPU departure in vegetation composition and configuration. Increasing departure scores (given as a percent of maximum) indicate increasing degrees of departure.

Negative Departure - Maximum "negative" departure occurs when a GPU has too little Open forest area, too few Large trees, too little diversity in forest developmental stages (i.e., tree heights) and tree size classes (i.e., dbh), too little variability in the size of patches based on forest developmental stage and tree size, and too little spatial variability in percent tree cover and weighted average tree size (i.e., QMD) relative to its HRV. In other words, maximum negative departure occurs when the forest is too closed-canopy, depauperate in Large trees, and too homogeneous in vegetation composition and configuration.

The composite negative departure score is depicted in **Figure 28**. This score can be interpreted as the percent of maximum deviation in negative departure. Thus, a value of 0 represents no departure in any of the component metrics and a value of 100 represents maximum negative departure in each of the component metrics. GPUs with relatively high scores are the logical ones to prioritize for restoration treatment - should that be the goal. Importantly, this composite departure score can serve as a first stage in identifying and prioritizing GPUs for treatment, but specific objectives and treatments for each GPU requires decomposing the composite score into the component metrics to determine which aspects of the forest vegetation composition and/or configuration are most departed.

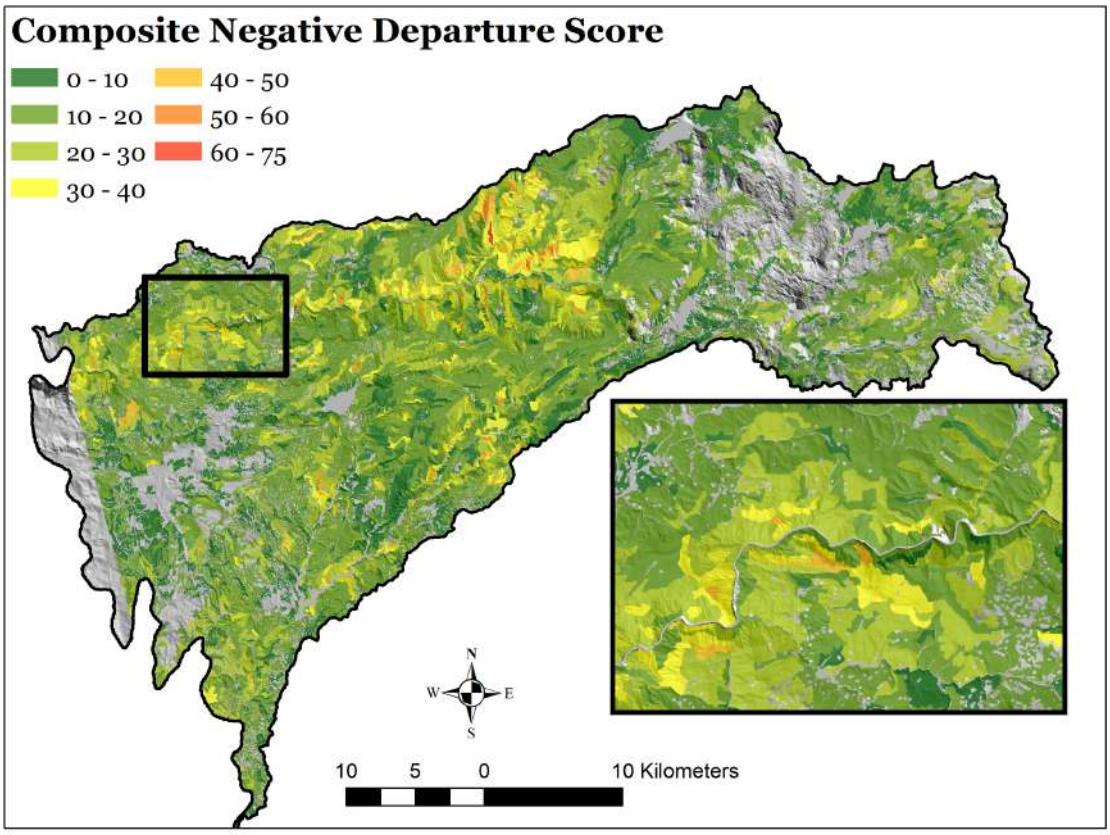

Figure 28: Geophysical Unit (GPU)-level composite negative departure score composed of a weighted combination of 11 individual departure metrics within the GPU for the Bear River landscape. The score represents the percentage of maximum departure of the current GPU condition from its historical range of variability (HRV), as simulated. Larger values indicate increasing degrees of departure.

Absolute Departure - Maximum "absolute" departure occurs when a GPU has either too little or too much Open forest area, too few or too many Large trees, too little or too much diversity in forest developmental stages (i.e., tree heights) and tree size classes (i.e., dbh), too little or too much variability in the size of patches based on forest developmental stage and tree size, and too little or too much spatial variability in percent tree cover and weighted average tree size (i.e., QMD) relative to HRV. In other words, maximum departure occurs when the GPU differs in any way in both composition and configuration from its HRV, as measured by this suite of metrics.

Subbasin Level Departure

The results presented in this section represent landscape metrics quantified at the subbasin-by-BPC level; i.e., each subbasin subdivided into BPCs treated as a whole unit (a.k.a. "zones"). The Bear River landscape was divided into 19 distinct subbasins (**Figure 29**), each of which was partitioned into the four forested BPCs for a total of 75 subbasin-by-BPC partitions or zones. Recall from the GTR that each partition was assessed independently to create a departure index; i.e., that we compared the current condition of each partition to its own HRV in vegetation conditions. In addition, recall that the final departure score reflected negative departure in the percent of the partition in large openings and large trees (i.e., in which the current landscape contains less area in large openings and large trees than expected under HRV), but was bidirectional with respect to the landscape configuration metrics; i.e., it reflected the magnitude of the absolute differences between the current and historical landscape conditions, regardless of whether the current condition was greater or less than the historical condition. In other words, any

differences between current and historical vegetation conditions with respect to landscape configuration registered as departure. Lastly, recall that we used a parsimonious suite of landscape metrics (see below) that we deemed meaningful for estimating departure at the subbasin level and appropriate given the available data, and computed departure as described in the GTR (and not repeated here), including the following metrics:

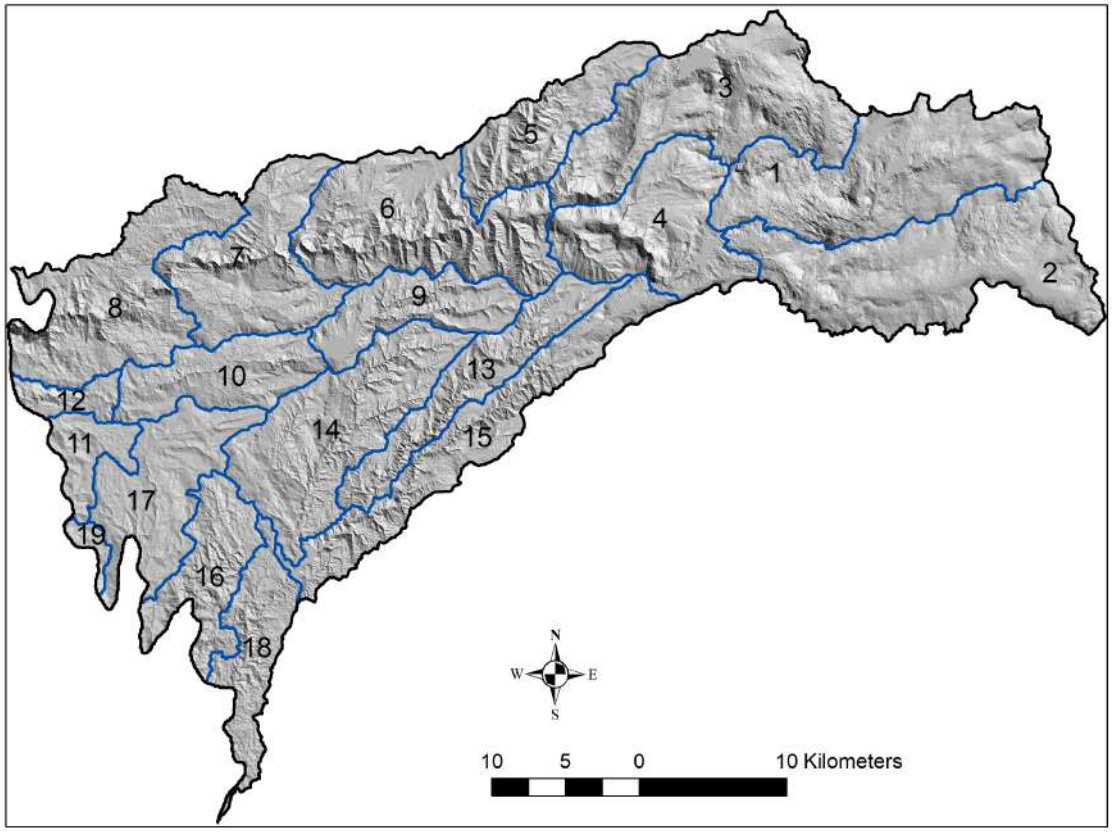

Figure 29: The Bear River landscape HUC12 subbasins, as modified, defined for the purpose of summarizing Historical Range of Variability (HRV) and current departure.

Metric 1: Percent Large Forest Openings

We defined large forest openings as contiguous forested cells in the Open developmental stage (i.e., no established trees to breast height) encompassing a minimum of 0.04 ha (0.1 acres). Contiguity was based on the 4-neighbor rule (i.e., orthogonal neighbors) that ensured a minimum width of 5 m for any opening. We defined Percent Large Forest Openings as the percent of the forest within the subbasin-by-BPC partition in large forest openings (as defined), and the departure index reflected whether or not the current landscape was deficient in large forest openings relative to HRV and, if so, the degree of deficiency.

The Percent Large Forest Openings departure index is depicted in **Figure 30**. Note, the departure index was assigned to each subbasin-by-BPC partition; consequently, there were 75 distinct values assigned. Thus, to better assess departure by subbasin and BPC, one needs to examine the attribute table for the departure layer.

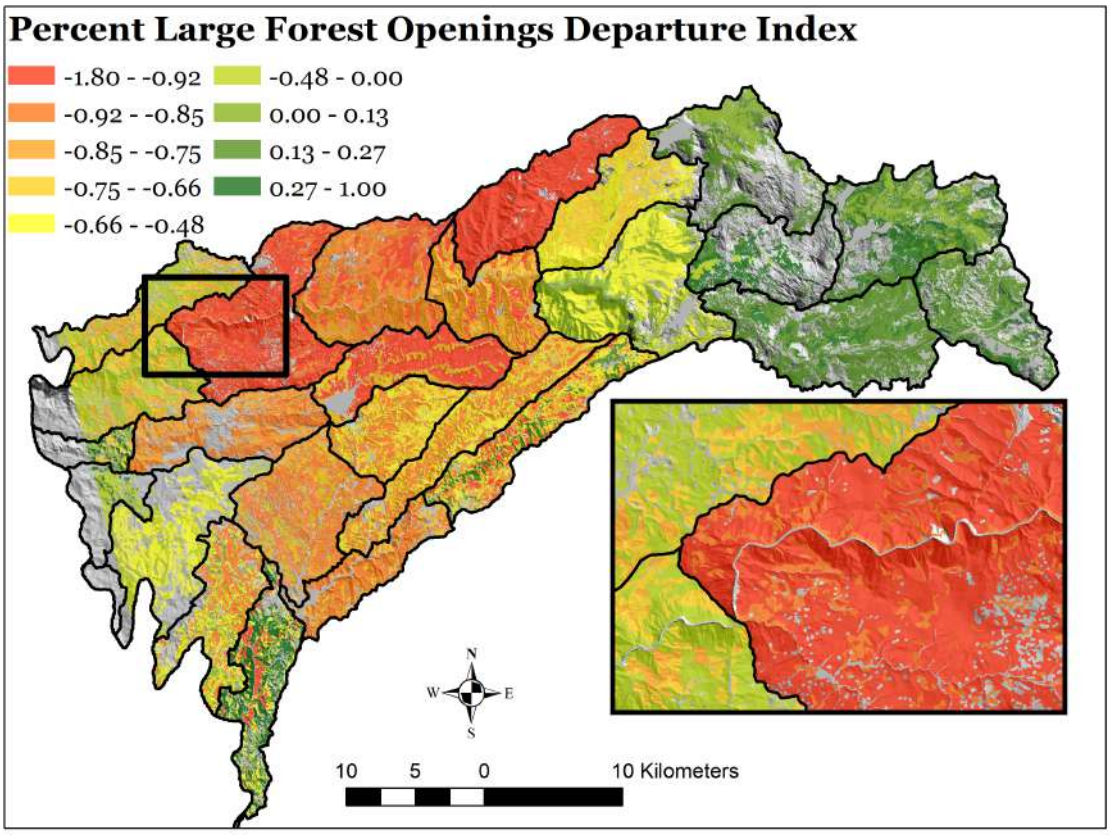

Figure 30: Subbasin-by-BPC level departure index for large forest openings (> 0.04 ha or 0.1 acres and > 5 m mininum width) for the Bear River landscape. The departure index represents the deviation of the current subbasin and biophsyical class (BPC) condition from its historical reference period condition, as simulated. Departure indices < -1 represent a current landscape with less total area in large forest openings than during the historical reference period, as simulated, and increasing negative values represent increasing degrees of departure.

As discussed in the GTR, the Percent Large Forest Openings Departure Index can be miss-interpreted if not understood well. As the previous figure depicts, the distribution of index values would suggest that most of the subbasin-by-BPC partitions are within the HRV given that most of the partitions have values between -1 - 1. Recall, index values within this range reflect a current landscape condition that is within the 2.5% and 97.5% HRV. This would seem to indicate that most of the partitions are within HRV. While this might technically be correct, the reality is that most of the partitions are close to the lower limit of HRV and have index values close to -1. Consequently, the distribution of index values is heavily skewed towards values on the lower limit of HRV, suggesting that the landscape as a whole is, on average, deficient in large forest openings. A alternative and more useful way to assess current departure in this metric is to compare the distribution of values representing the percentage of the partition in large forest openings between the HRV and CRV, as shown **Figure 31**.

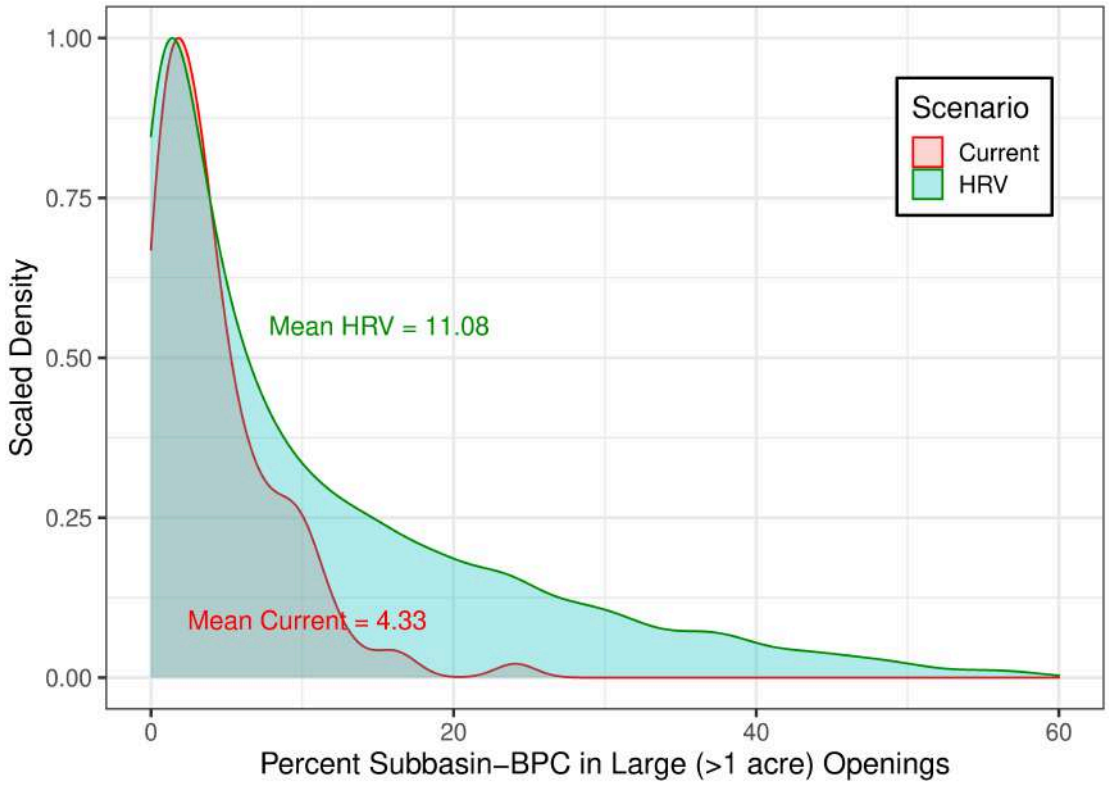

Figure 31: Current and historical distribution of Percent Large Forest Openings across the Subbasin-by-Biophysical Class (BPC) landscape partitions for the Bear River landscape. The comparative distributions reveal that even though the departure index for most of the partitions technically may fall with the historical range of variation (see previous figure), the overall distributions in the raw metric values differ markedly and reflect departure for the landscape as a whole

Metric 2: Large Forest Openings Patch Size Distribution

We defined large forest openings as described above. Here, we quantified the size of individual openings and determined the percent of forest within the subbasin-by-BPC partition in large openings in each of several patch size classes or bins (see GTR). The departure index reflects whether or not the current landscape has a distribution of large forest opening patch sizes that differed from HRV and, if so, the degree of differences in the two distributions.

The Large Forest Openings Patch Size Distribution departure index is depicted in **Figure 32**. As before, the departure index was assigned to each subbasin-by-BPC partition; consequently, there were 75 distinct values assigned. Thus, to better assess departure by subbasin and BPC, one needs to examine the attribute table for the departure layer.

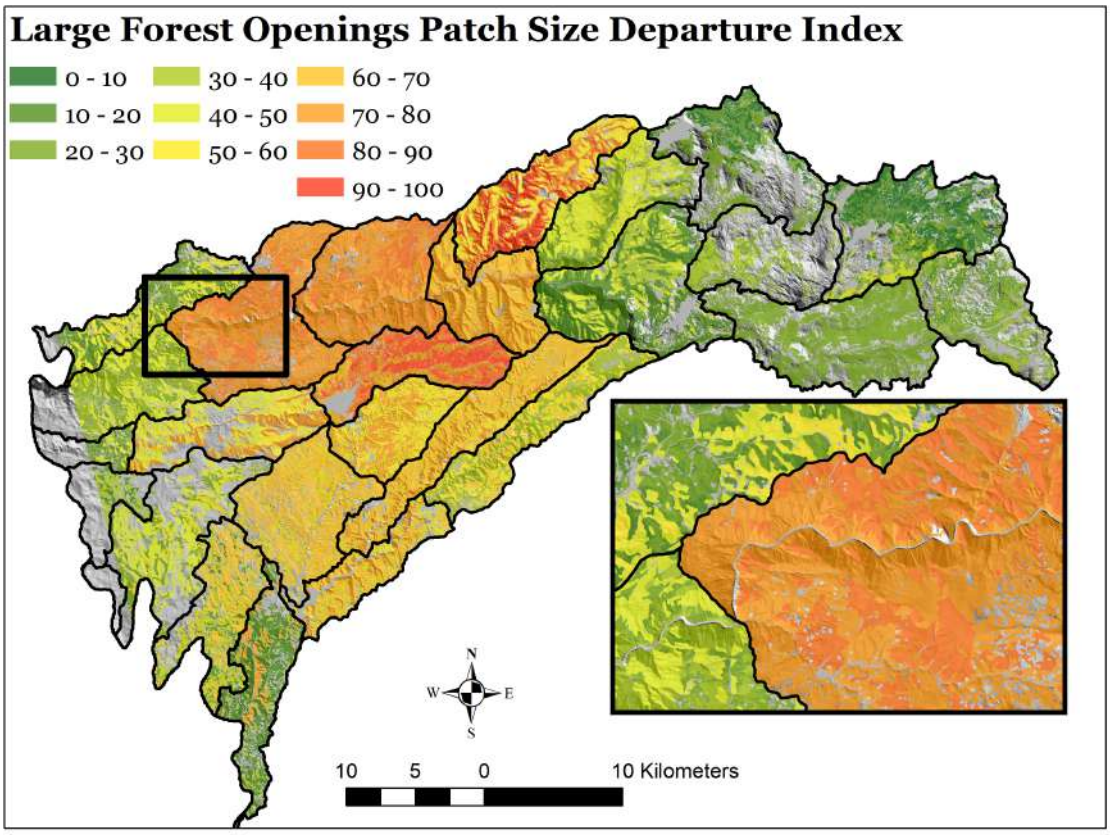

Figure 32: Subbasin-by-BPC level departure index for large forest openings ($>$ 0.04 ha or 0.1 acres and $>$ 5 m mininum width) patch size distribution for the Bear River landscape. The departure index represents the deviation of the current subbasin and biophsyical class (BPC) condition from its historical reference period condition, as simulated. Departure indices $>$ 0 represent a current landscape with a distribution of large forest opening patch sizes that differs in some way from the historical reference period distribution, as simulated, and increasing values represent increasing degrees of departure.

To further evaluate departure in this patch size distribution metric, it is necessary to examine the CRV and HRV patch size distributions for the selected subbasin-by-BPC partition, for example as depicted in **Figure 33**.

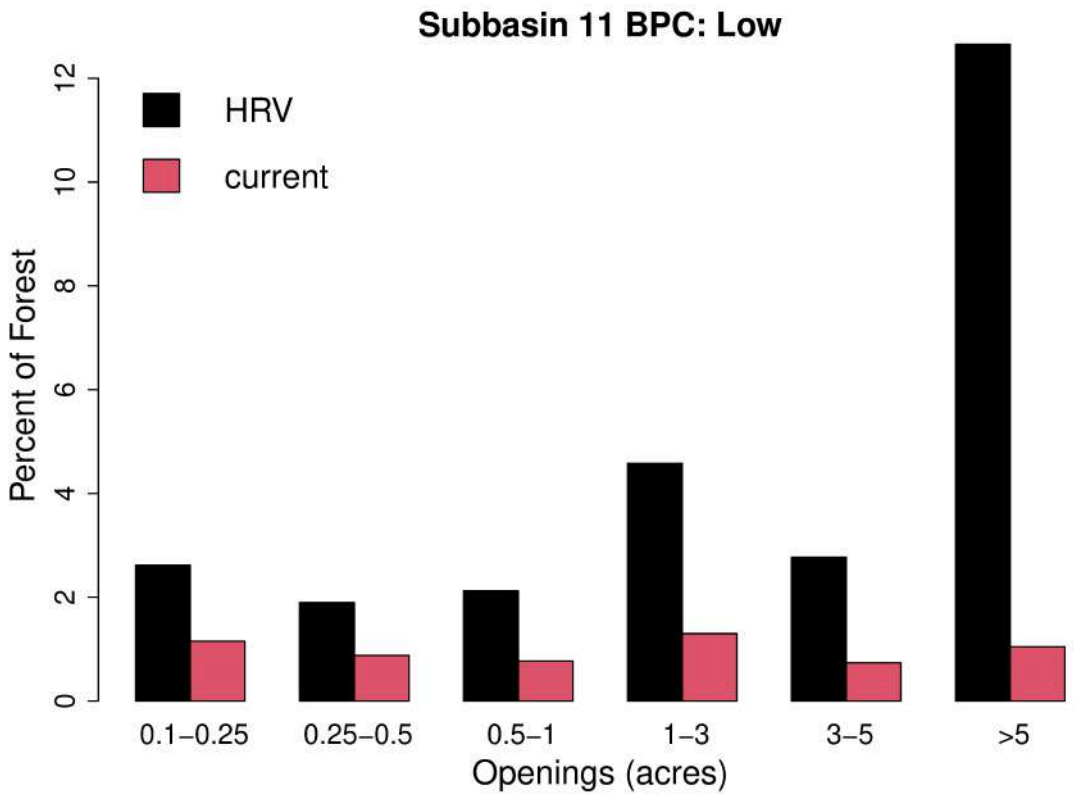

Figure 33: Barplot of the distribution of large forest openings (> 0.04 ha or 0.1 acres and > 5 m mininum width) patch sizes for the current landscape and the historical reference period (HRV) for subbasin 11 and the Low productivity Biophysical Class (BPC = 1) for the Bear River landscape. Each bar represents the percent of forest within the subbasin and Biophysical Class (BPC) in large forest openings of a particular patch size. The departure index represents the percentage dissimilarity between the CRV and HRV distributions. Departure indices > 0 represent a current landscape with a distribution of large forest opening patch sizes that differs in some way from the historical reference period distribution, as simulated, and increasing values represent increasing degrees of departure.

Metric 3: Developmental Stage Patch Size Distribution

We defined developmental stages based on six tree height classes, ranging from Open (< 4.5 ft) to Tall Trees (> 125 ft), as described in the GTR. Here, for each snapshot of the landscape we constructed a patch mosaic comprised of developmental stages in which patches were defined using the 4-neighbor rule. For each snapshot, we quantified the size of each developmental stage patch and determined the percent of forest within the subbasin-by-BPC partition in each of several patch size classes or bins. The departure index reflects whether or not the current landscape has a distribution of developmental stage patch sizes that differs from HRV and, if so, the degree of differences in the two distributions.

The Developmental Stage Patch Size Distribution departure index is depicted in **Figure 34**. As before, the departure index was assigned to each subbasin-by-BPC partition; consequently, there were 75 distinct values assigned. Thus, to better assess departure by subbasin and BPC, one needs to examine the attribute table for the departure layer.

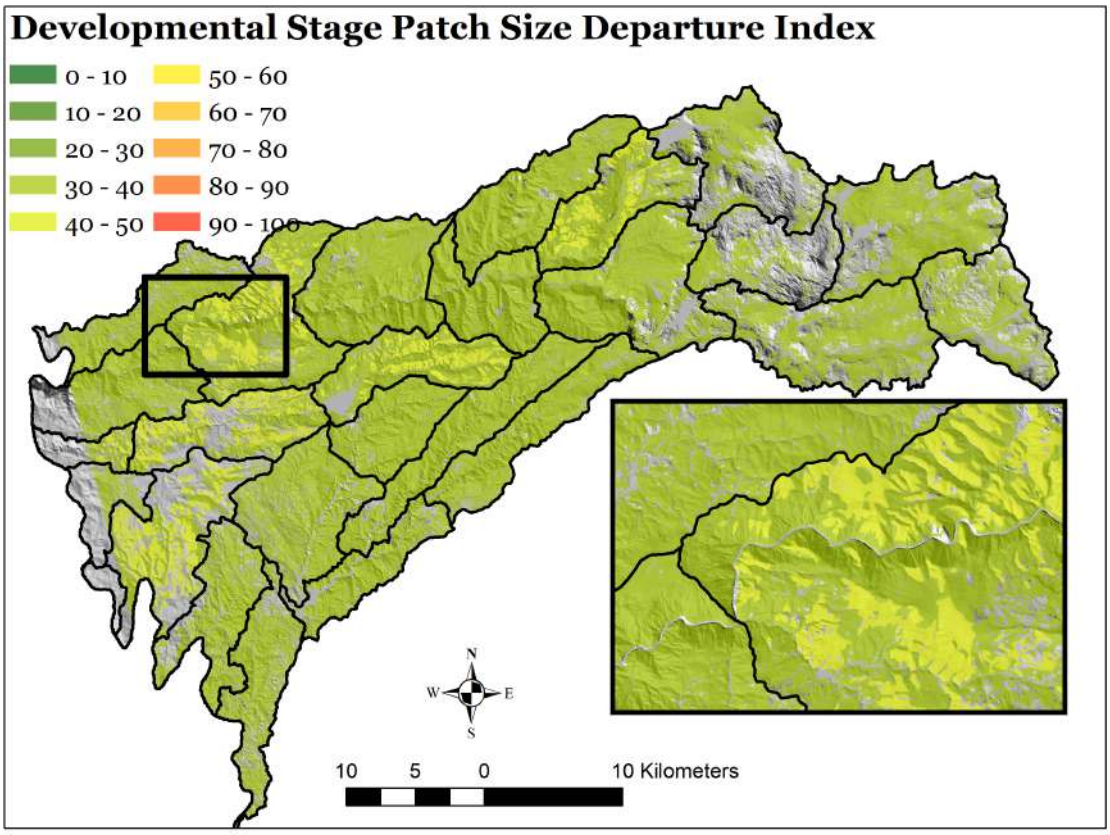

Figure 34: Subbasin-by-BPC level departure index for the developmental stage patch size distribution for the Bear River landscape. Developmental stages were based on tree height classes and patches were based on the 4-neighbor adjacency rule. The departure index represents the deviation of the current subbasin and biophsyical class (BPC) condition from its historical reference period condition, as simulated. Departure indices > 0 represent a current landscape with a distribution of developmental stage patch sizes that differs in some way from the historical reference period distribution, as simulated, and increasing values represent increasing degrees of departure.

To further evaluate departure in this patch size distribution metric, it is necessary to examine the CRV and HRV patch size distributions for the selected subbasin-by-BPC partition, for example as depicted in **Figure 35**.

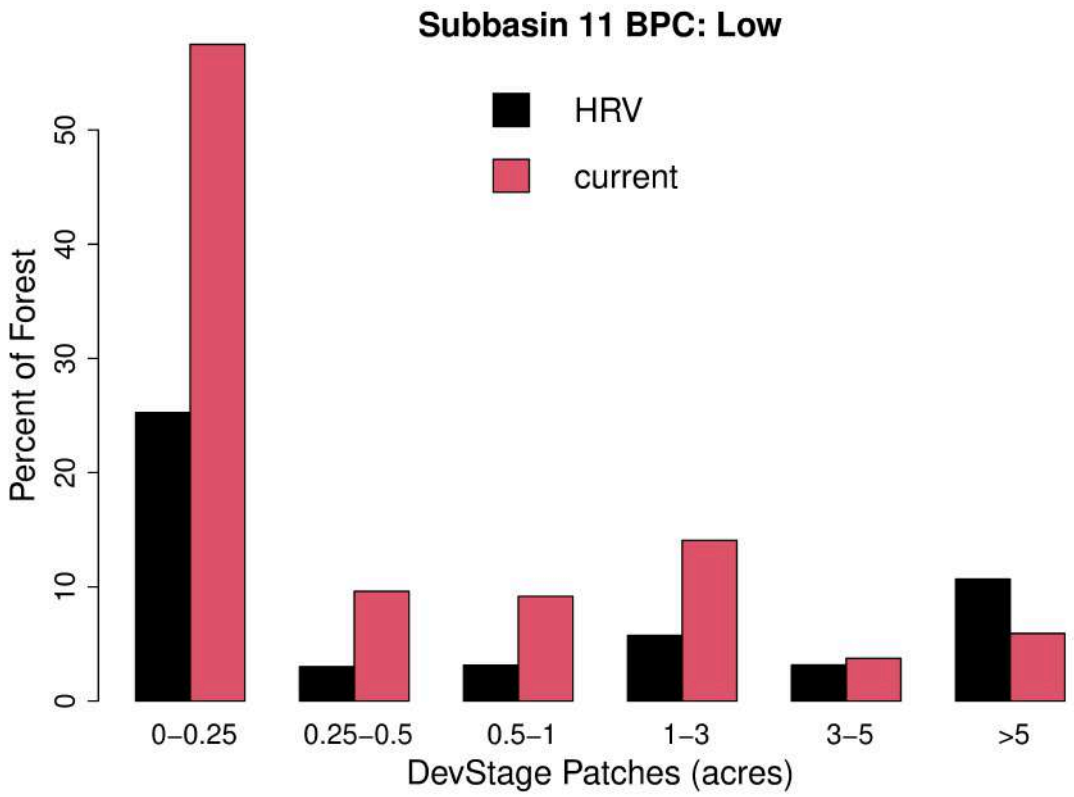

Figure 35: Barplot of the distribution of developmental stage patch sizes for the current landscape and the historical reference period (HRV) for subbasin 11 and the Low productivity Biophysical Class (BPC = 1) for the Bear River landscape. Developmental stages were based on tree height classes and patches were based on the 4-neighbor adjacency rule. Each bar represents the percent of forest within the subbasin and BPC in developmental stage patches of a particular size. The departure index represents the sum of the deviations between the current and HRV bars. Departure indices > 0 represent a current landscape with a distribution of developmental stage patch sizes that differs in some way from the historical reference period distribution, as simulated, and increasing values represent increasing degrees of departure.

Metric 4: Percent Large Trees

We defined large trees as > 30 inch dbh. Percent Large Trees is defined as the percent of the forest within the subbasin-by-BPC partition in large trees, as defined, and the departure index reflects whether or not the current landscape is deficient in large trees relative to HRV and, if so, the degree of deficiency. The departure index is negative if the current landscape has too little area in large trees compared to HRV.

The Percent Large Trees departure index is depicted in **Figure 36**. As before, the departure index was assigned to each subbasin-by-BPC partition; consequently, there were 75 distinct values assigned. Thus, to better assess departure by subbasin and BPC, one needs to examine the attribute table for the departure layer.

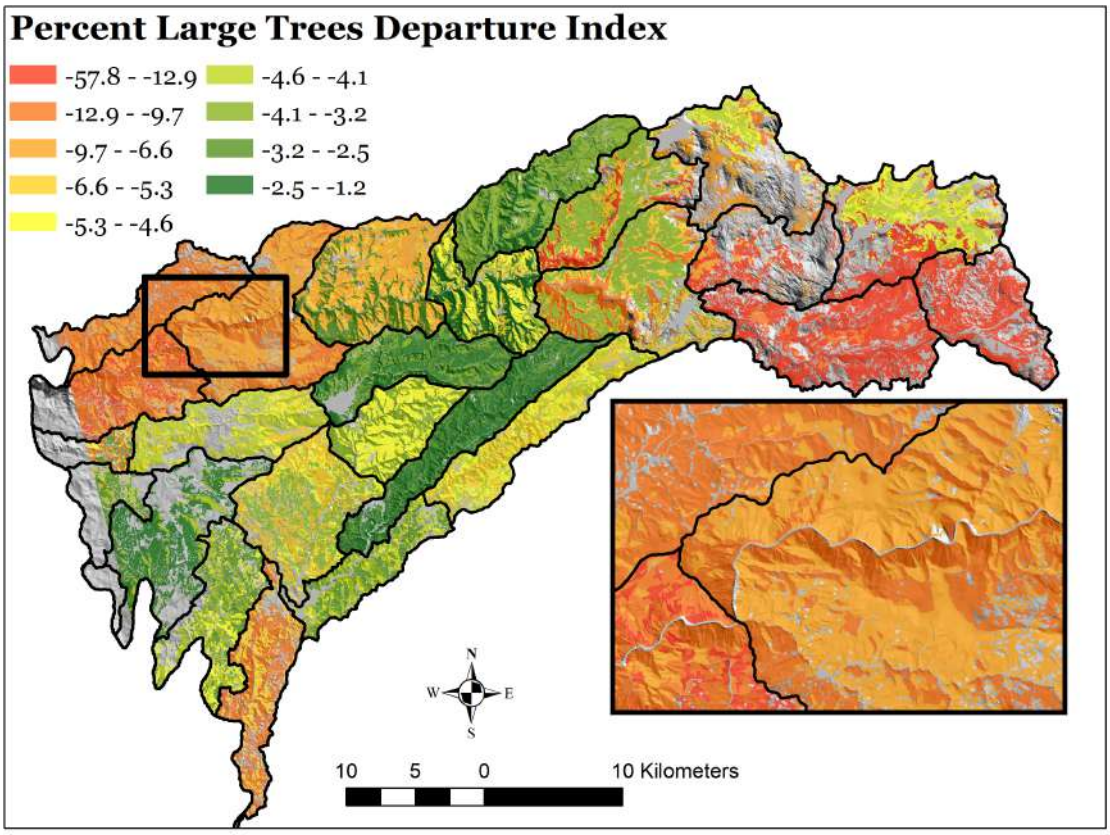

Figure 36: Subbasin-by-BPC level departure index for large trees (> 30 inch dbh) for the Bear River landscape. The departure index represents the deviation of the current subbasin and biophsyical class (BPC) condition from its historical reference period condition, as simulated. Departure indices < -1 represent a current landscape with less total area in large trees than during the historical reference period, as simulated, and increasing negative values represent increasing degrees of departure.

Metric 5: Large Tree Patch Size Distribution

We defined large trees as described above. Here, we quantified the size of individual patches of large trees and determined the percent of forest within the subbasin-by-BPC partition in large tree patches in each of several patch size classes or bins (see above), and compared the current and historical distributions. The departure index reflects whether or not the current landscape has a distribution of large tree patch sizes that differs from HRV and, if so, the degree of differences in the two distributions.

The Large Tree Patch Size Distribution departure index is depicted in **Figure 37**. As before, the departure index was assigned to each subbasin-by-BPC partition; consequently, there were 75 distinct values assigned. Thus, to better assess departure by subbasin and BPC, one needs to examine the attribute table for the departure layer.

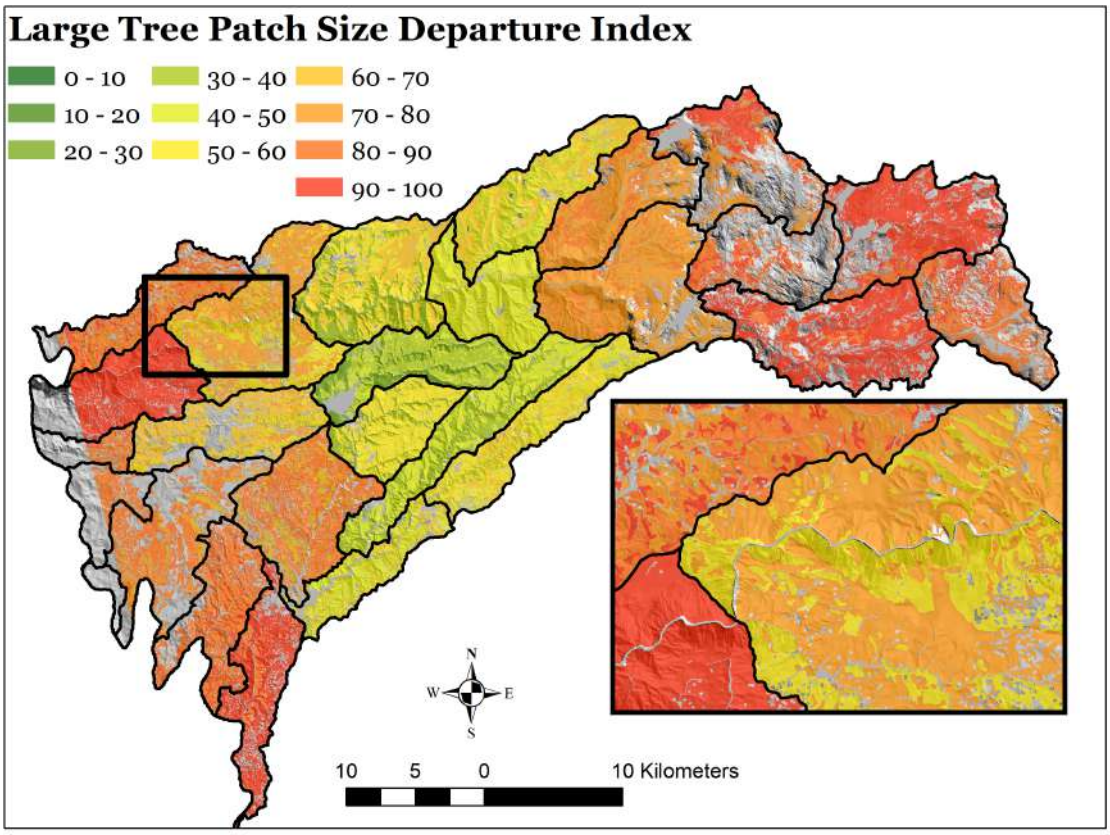

Figure 37: Subbasin-by-BPC level departure index for large tree (> 30 inch dbh) patch size distribution for the Bear River landscape. The departure index represents the deviation of the current subbasin and biophsyical class (BPC) condition from its historical reference period condition, as simulated. Departure indices > 0 represent a current landscape with a distribution of large tree patch sizes that differs in some way from the historical reference period distribution, as simulated, and increasing values represent increasing degrees of departure.

To further evaluate departure in this patch size distribution metric, it is necessary to examine the CRV and HRV patch size distributions for the selected subbasin-by-BPC partition, for example as depicted in **Figure 38**.

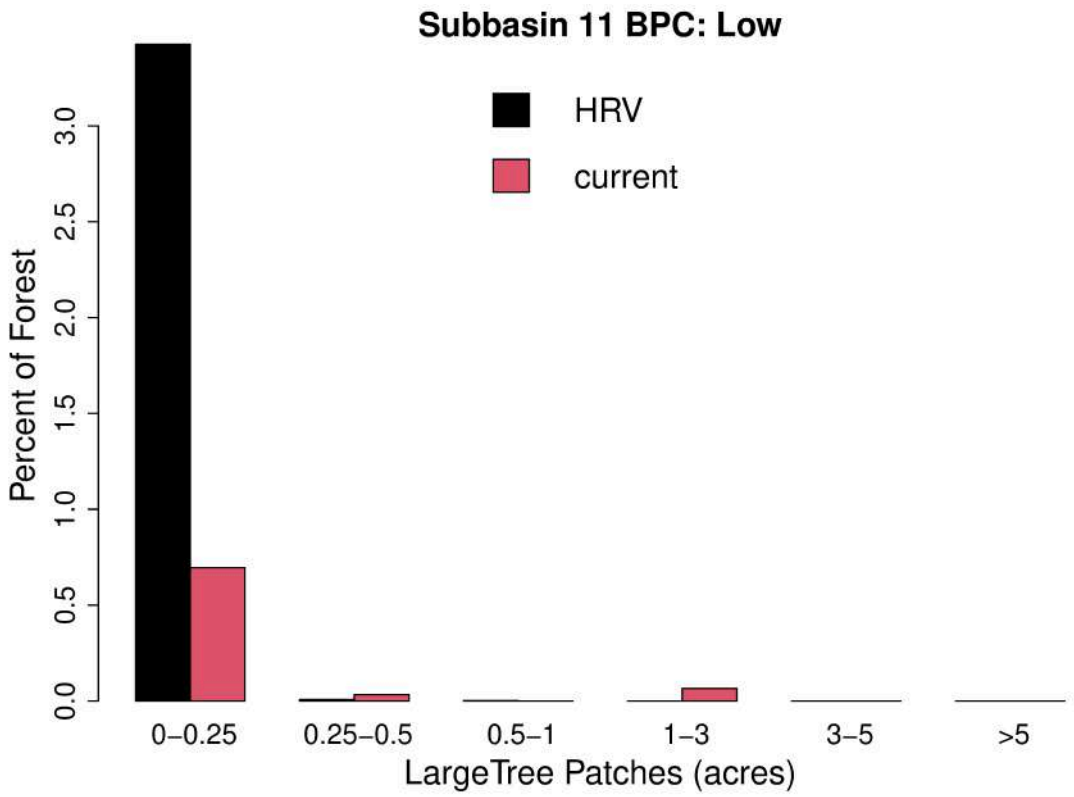

Figure 38: Barplot of the distribution of large tree (> 30 inch dbh) patch sizes for the current landscape and the historical reference period (HRV) for subbasin 11 and the Low productivity Biophysical Class (BPC = 4) for the Bear River landscape. See previous barplot caption for details on interpretation.

Metric 6: Tree Size Class Patch Size Distribution

We defined tree size class based on six tree diameter classes, ranging from Open (< 1 in dbh) to large Trees (> 30 in dbh), as described previously. Here, for each snapshot of the landscape we constructed a patch mosaic comprised of tree size classes in which patches were defined using the 4-neighbor rule. For each snapshot, we quantified the size of each tree size class patch and determined the percent of forest within the subbasin-by-BPC partition in each of several patch size classes or bins. The departure index reflects whether or not the current landscape has a distribution of tree size class patch sizes that differs from HRV and, if so, the degree of differences in the two distributions.

The Tree Size Class Patch Size Distribution departure index is depicted in **Figure 39**. As before, the departure index was assigned to each subbasin-by-BPC partition; consequently, there were 75 distinct values assigned. Thus, to better assess departure by subbasin and BPC, one needs to examine the attribute table for the departure layer.

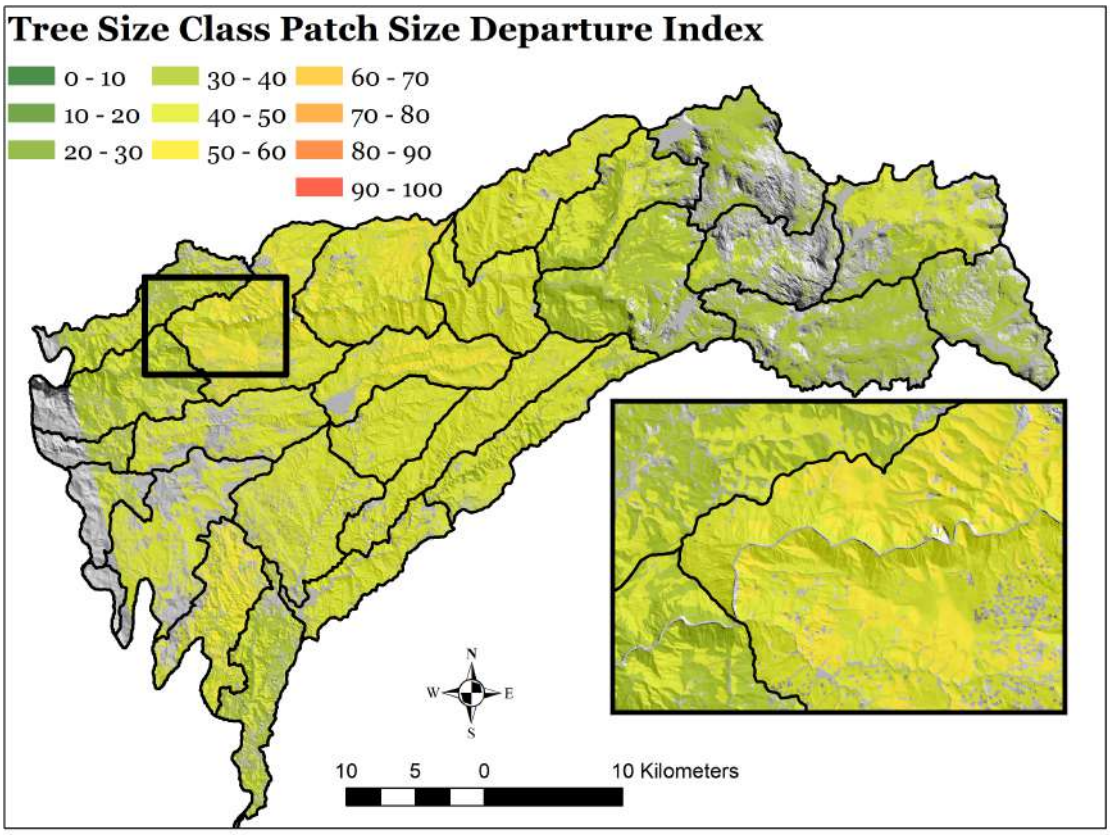

Figure 39: Subbasin-by-BPC level departure index for tree size class (based on dbh) patch size distribution for the Bear River landscape. The departure index represents the deviation of the current subbasin and biophsyical class (BPC) condition from its historical reference period condition, as simulated. Departure indices > 0 represent a current landscape with a distribution of tree size patch sizes that differs in some way from the historical reference period distribution, as simulated, and increasing values represent increasing degrees of departure.

To further evaluate departure in this patch size distribution metric, it is necessary to examine the CRV and HRV patch size distributions for the selected subbasin-by-BPC partition, for example as depicted in **Figure 40**.

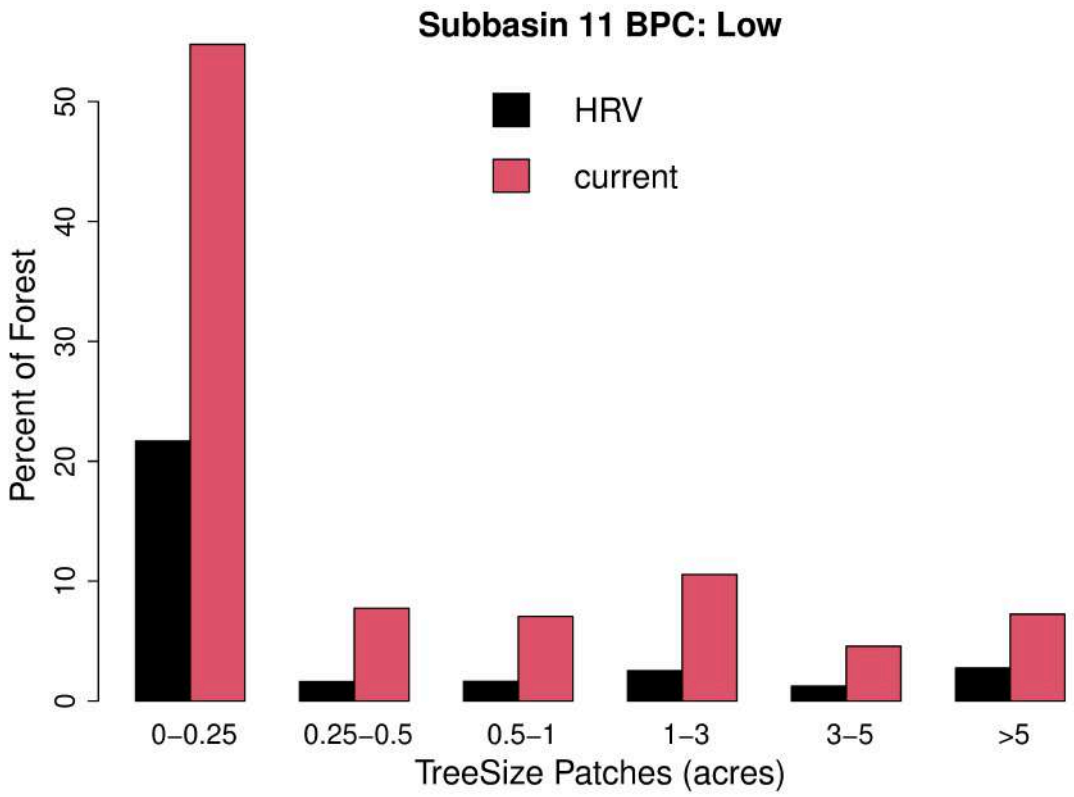

Figure 40: Barplot of the distribution of tree size class (based on dbh) patch sizes for the current landscape and the historical reference period (HRV) for subbasin 11 and the Low productivity Biophysical Class (BPC = 4) for the Bear River landscape. See previous barplot caption for details on interpretation.

Composite Departure Score

We combined the 6 subbasin-level departure metrics above into a single composite departure score, which can be interpreted as a measure of overall departure in vegetation composition and configuration within the subbasin-by-BPC partition. Maximum departure occurs when the forest has too little area in large forest openings and/or large trees, and/or too homogeneous or uniform a vegetation patch mosaic (i.e., too little spatial variability) defined on the basis of either developmental stages (or tree height classes) or tree size classes (or tree diameter classes).

The composite departure score is depicted in **Figure 41**. Not surprisingly, the subbasins and BPCs vary somewhat in their overall departure from HRV, and these differences provide a basis for prioritizing project locations with this landscape.

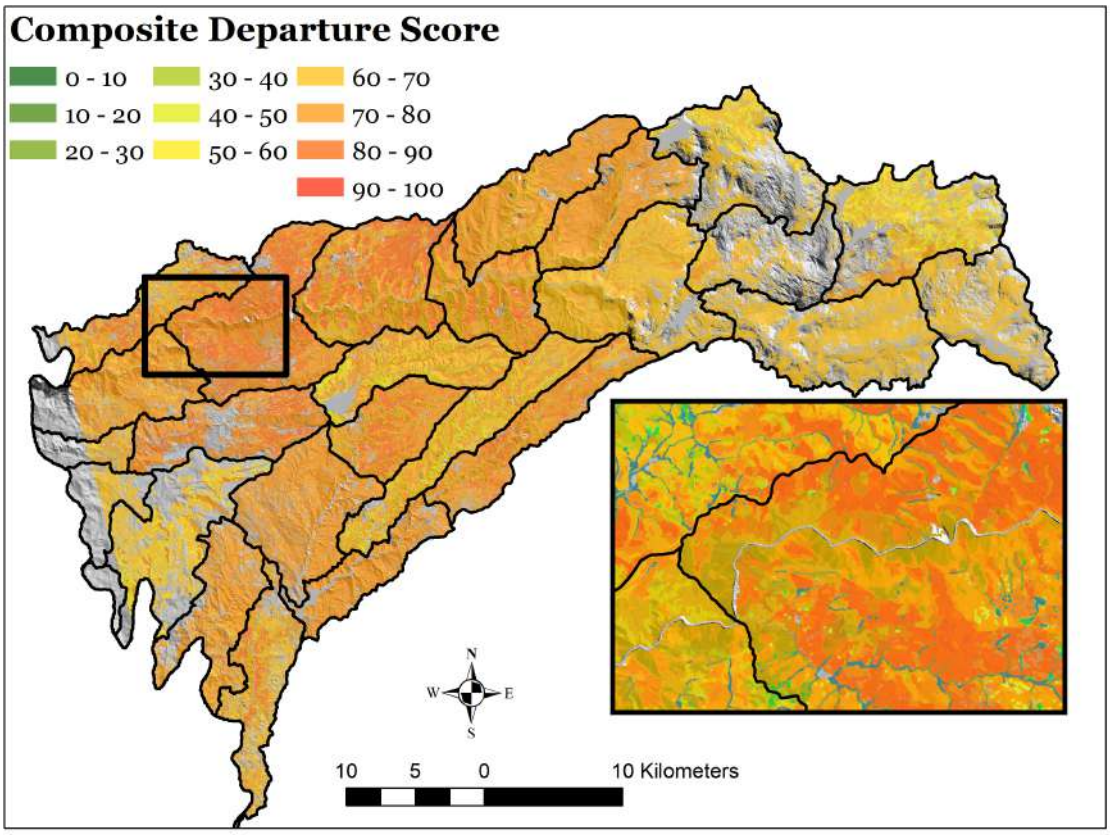

Figure 41: Subbasin-by-BPC level composite departure index derived from the average of the six component metrics for the Bear River landscape. The composite departure index represents the percentage of maximum departure of the current GPU condition from its historical range of variability (HRV), as simulated. Larger values indicate increasing degrees of departure.

APPENDIX E1 - Wildfire Susceptibility

As described in the text, wildfire susceptibility was modeled as a Logistic function of fuels and climate for most cover types. The fuels component was modeled as a Logistic function of the number of years since the last fire (fuelAge) and the Heat Load Index (hli). The climate component was modeled as a Logistic function of the Wildfire Climate Index which was based on the inverted and rescaled 5-year mean Palmer Modified Drought Index. The fuels and climate components were combined with a geometric mean to produce the final Wildfire Susceptibility Index. The final function included 5 beta coefficients (b_0 - b_4). We used expert opinion to specify the beta coefficients for each cover type. We varied the b_0 and b_1 coefficients among cover types to reflect differences in reported historical mean fire return intervals among cover types - shifting the response curves left or right so that the inflection point (Wildfire Susceptibility Index = 0.5) roughly equaled the target mean return interval - and held the Heat Load Index coefficient (b_2) and Climate coefficients (b_3 and b_4) the same across all cover types to reflect the global affect of topography and climate on wildfire susceptibility.

The figures below depict the final wildfire susceptibility response functions for each cover type in alphabetical order (noting that some cover types did not have response functions as noted in the text). The response functions depict the wildfire Susceptibility Index as a Logistic function of the number of years since the last fire (Years since fire). The dashed, solid and dotted lines depict the response functions for the minimum, mean and maximum Heat Load Index (hli), and the red, black and green sets of lines depict the response functions for the minimum, mean and maximum Wildfire Climate Index. The values of the Logistic parameters (b_0 - b_4) for the cover type are shown as well.

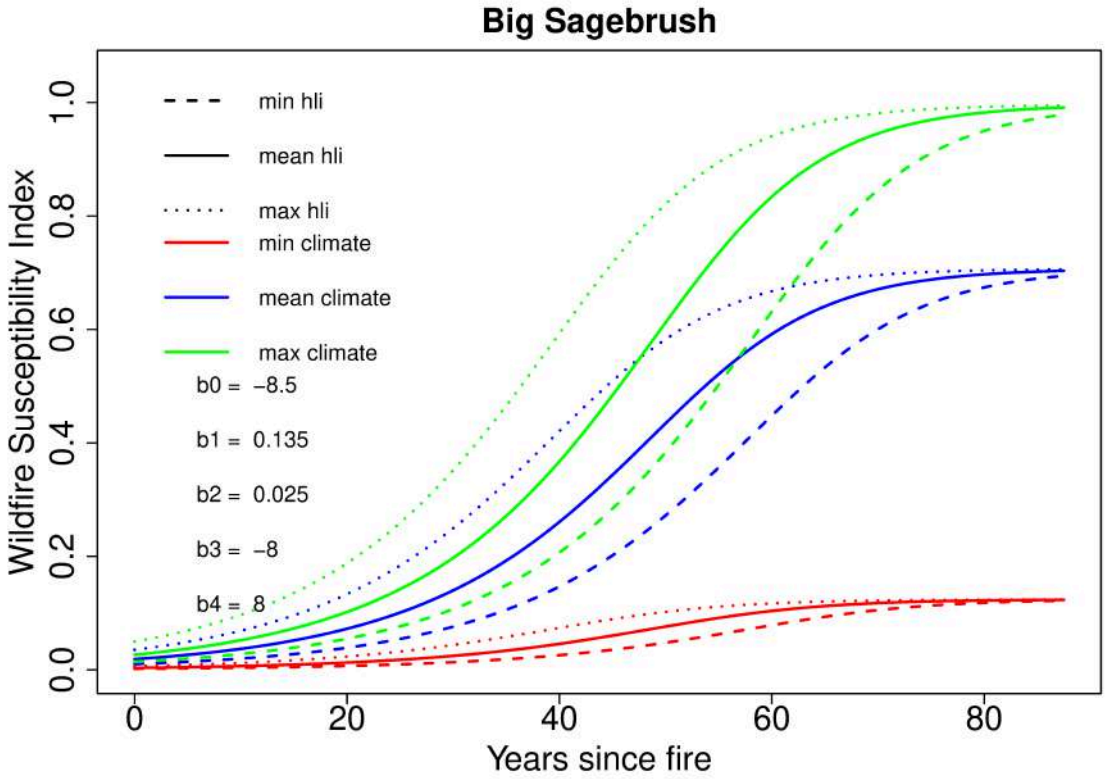

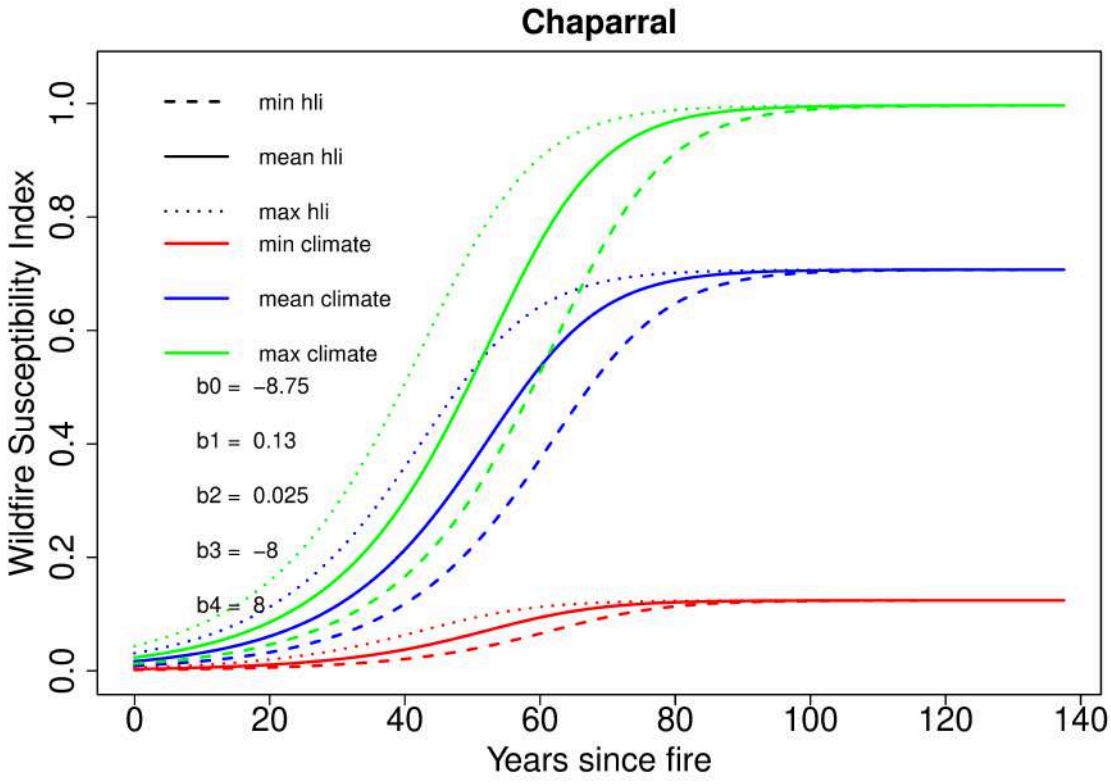
Chaparral
min hli
mean hli
max hli
min climate
mean climate
max climate
b0 = −8.75
b1 = 0.13
b2 = 0.025
b3 = −8
b4 = 8
Wildfire Susceptibility Index
0.0
0.2
0.4
0.6
0.8
1.0
0
20
40
60
80
100
120
140
Years since fire

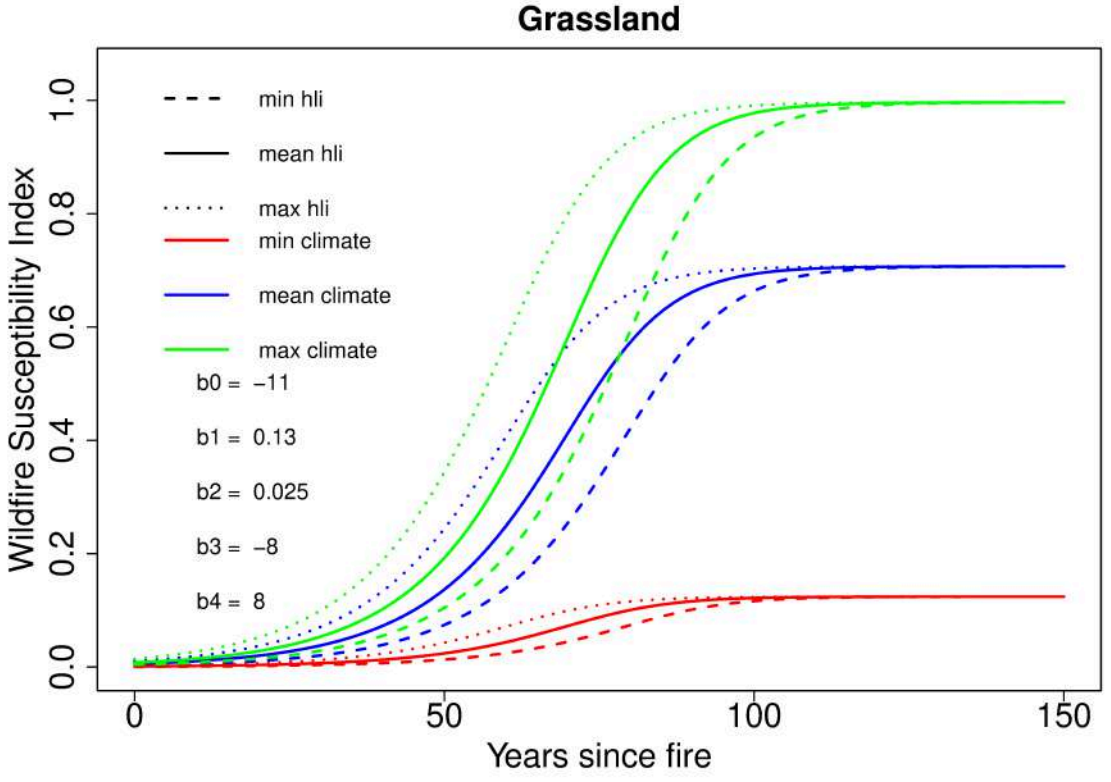
Grassland
min hli
mean hli
max hli
min climate
mean climate
max climate
b0 = −11
b1 = 0.13
b2 = 0.025
b3 = −8
b4 = 8
Wildfire Susceptibility Index
0.0
0.2
0.4
0.6
0.8
1.0
0
50
100
150
Years since fire

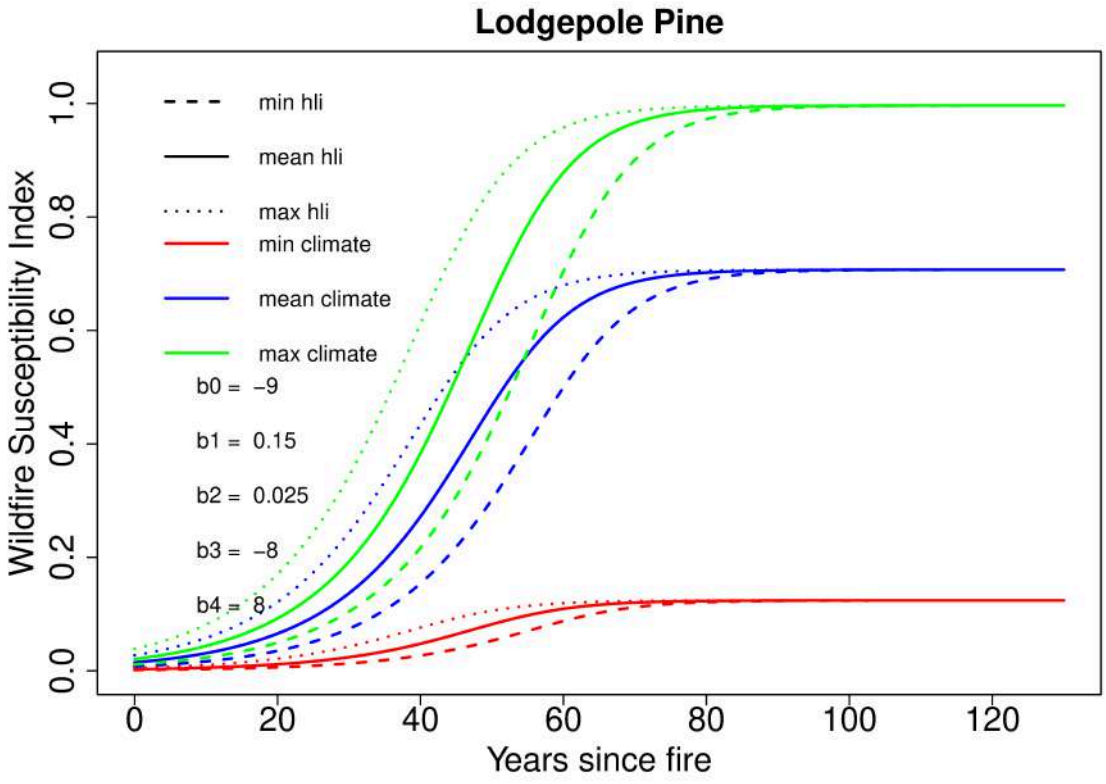
Lodgepole Pine
min hli
mean hli
max hli
min climate
mean climate
max climate
b0 = −9
b1 = 0.15
b2 = 0.025
b3 = −8
b4 = 8
Wildfire Susceptibility Index
0.0
0.2
0.4
0.6
0.8
1.0
0
20
40
60
80
100
120
Years since fire

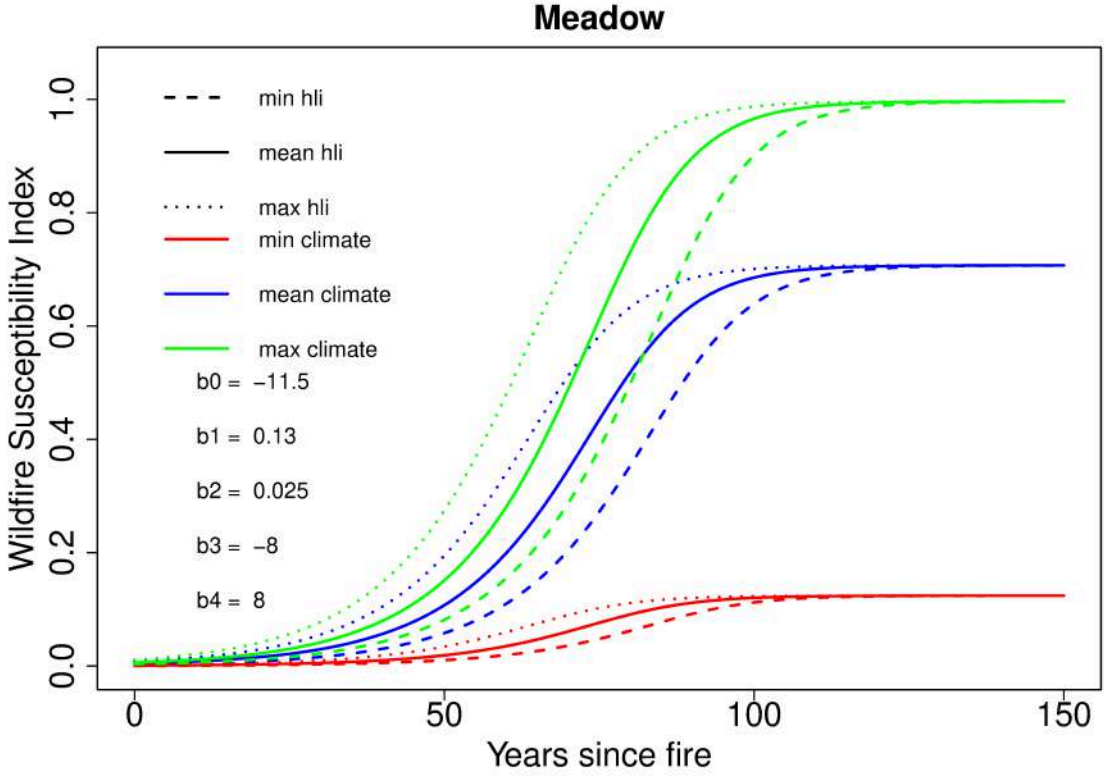
Meadow
min hli
mean hli
max hli
min climate
mean climate
max climate
b0 = −11.5
b1 = 0.13
b2 = 0.025
b3 = −8
b4 = 8
Wildfire Susceptibility Index
0.0
0.2
0.4
0.6
0.8
1.0
0
50
100
150
Years since fire

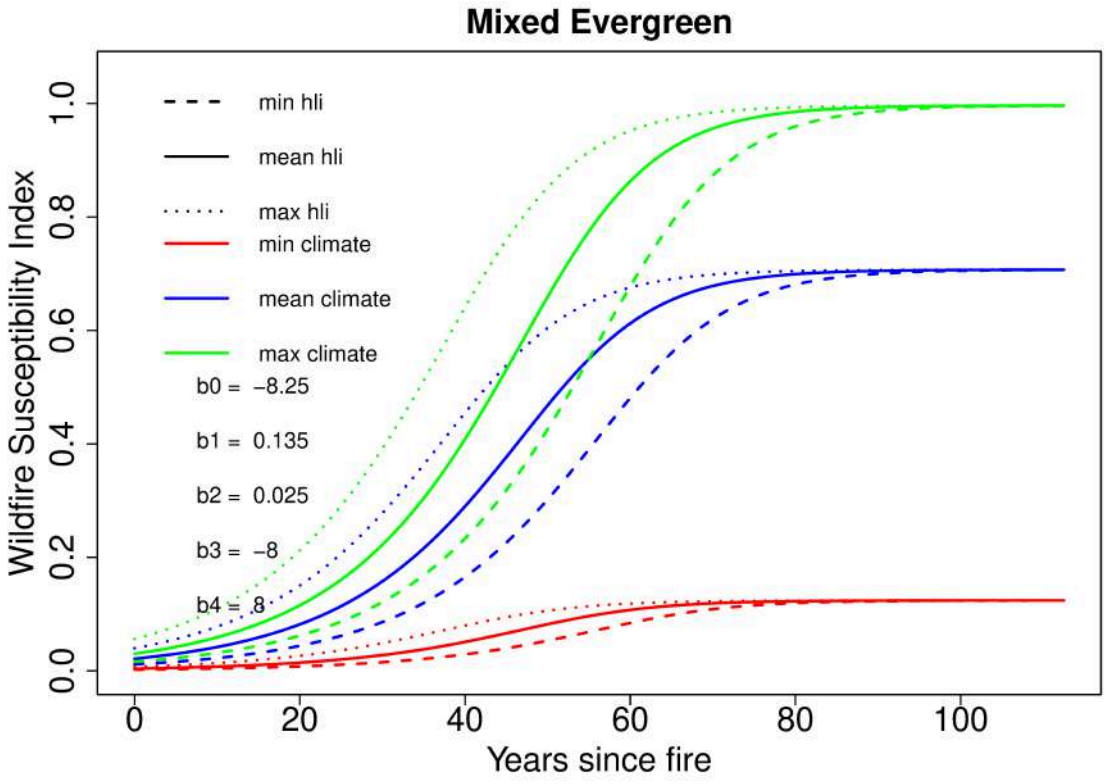
Mixed Evergreen
min hli
mean hli
max hli
min climate
mean climate
max climate
b0 = −8.25
b1 = 0.135
b2 = 0.025
b3 = −8
b4 = .8
Wildfire Susceptibility Index
0.0
0.2
0.4
0.6
0.8
1.0
0
20
40
60
80
100
Years since fire

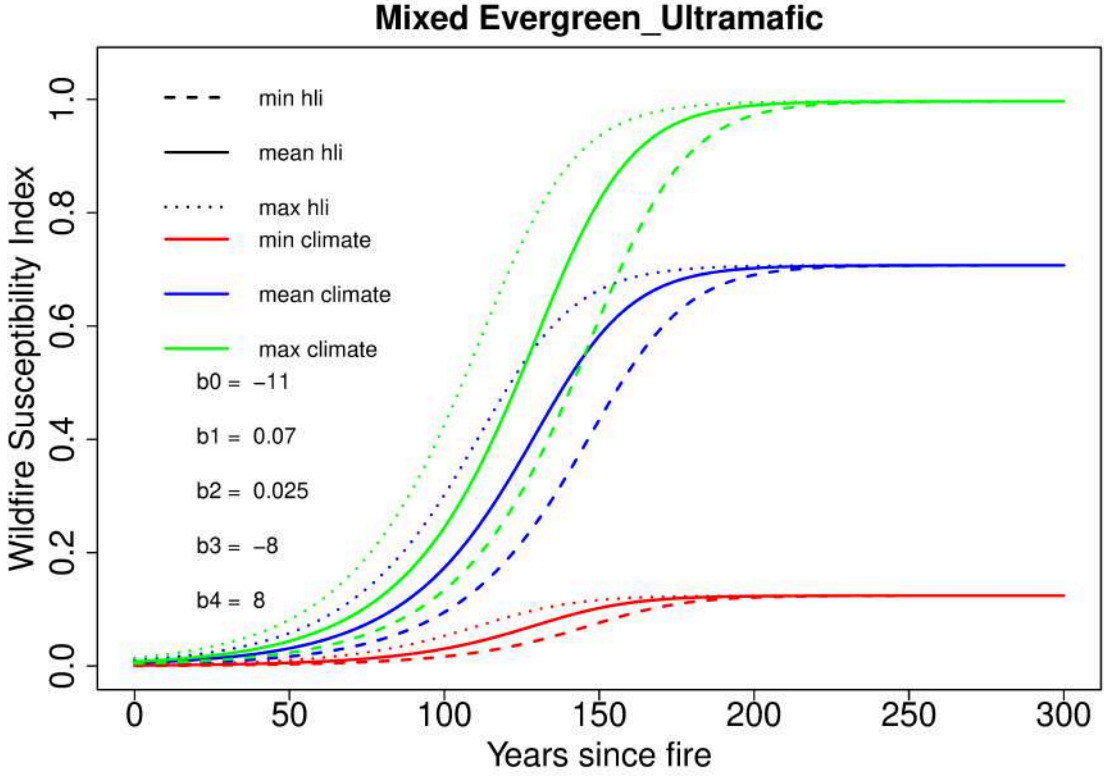
Mixed Evergreen_Ultramafic
min hli
mean hli
max hli
min climate
mean climate
max climate
b0 = −11
b1 = 0.07
b2 = 0.025
b3 = −8
b4 = 8
Wildfire Susceptibility Index
0.0
0.2
0.4
0.6
0.8
1.0
0
50
100
150
200
250
300
Years since fire

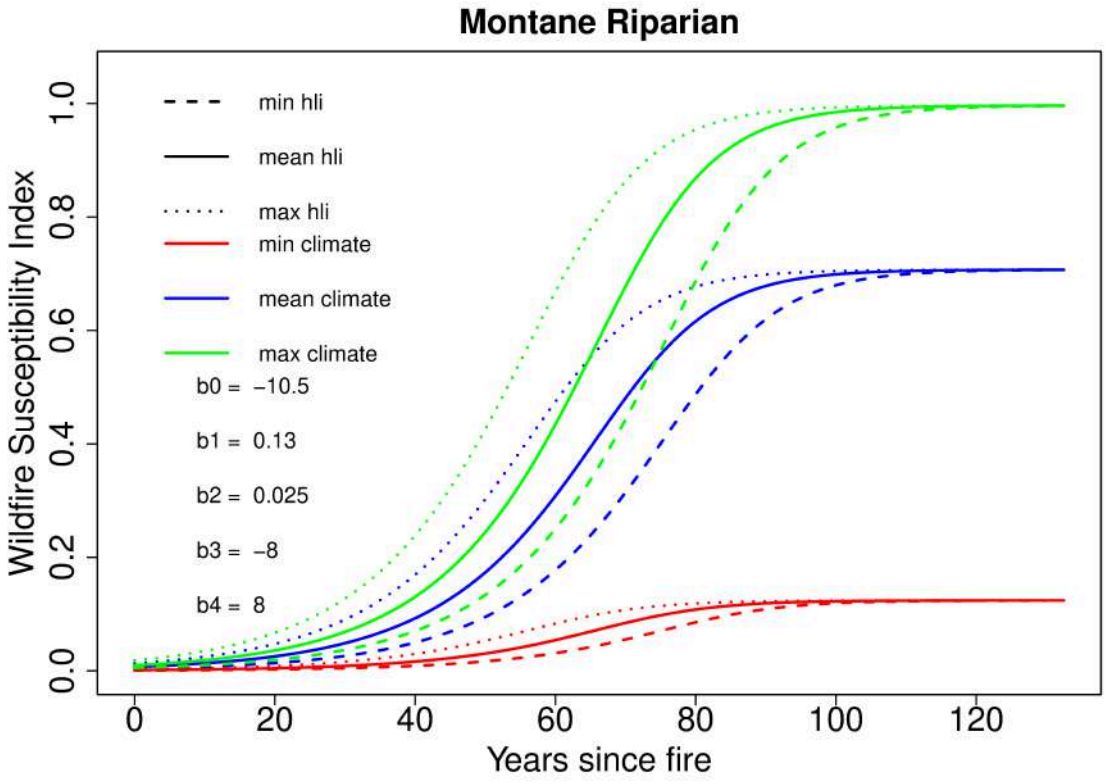
Montane Riparian
min hli
mean hli
max hli
min climate
mean climate
max climate
b0 = −10.5
b1 = 0.13
b2 = 0.025
b3 = −8
b4 = 8
Wildfire Susceptibility Index
0.0
0.2
0.4
0.6
0.8
1.0
0
20
40
60
80
100
120
Years since fire

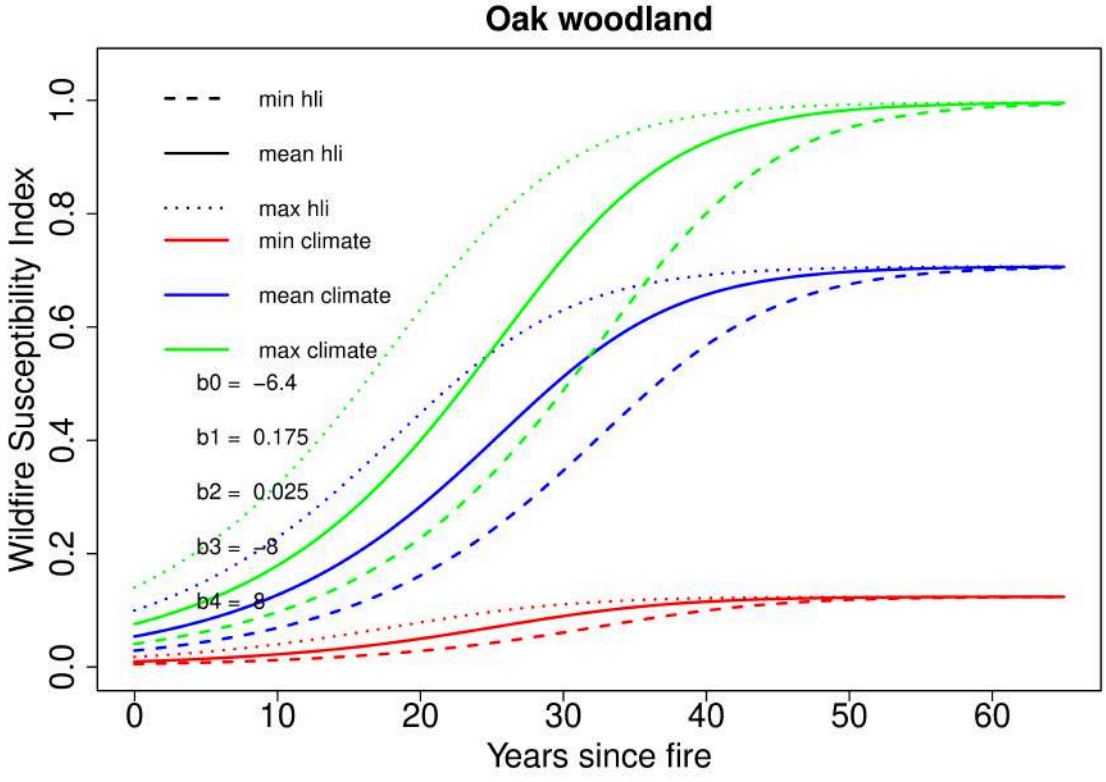
Oak woodland
min hli
mean hli
max hli
min climate
mean climate
max climate
b0 = −6.4
b1 = 0.175
b2 = 0.025
b3 = −8
b4 = 8
Wildfire Susceptibility Index
0.0
0.2
0.4
0.6
0.8
1.0
0
10
20
30
40
50
60
Years since fire

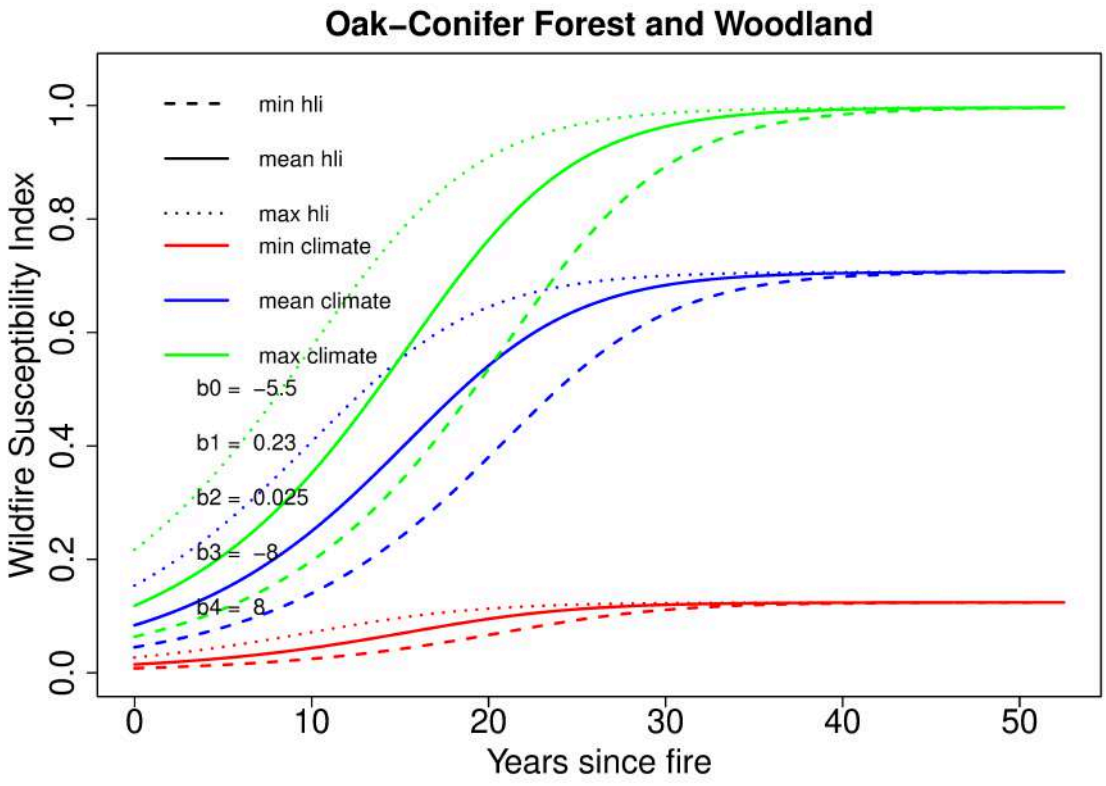
Oak–Conifer Forest and Woodland
min hli
mean hli
max hli
min climate
mean climate
max climate
b0 = −5.5
b1 = 0.23
b2 = 0.025
b3 = −8
b4 = 8
Wildfire Susceptibility Index
0.0
0.2
0.4
0.6
0.8
1.0
0
10
20
30
40
50
Years since fire

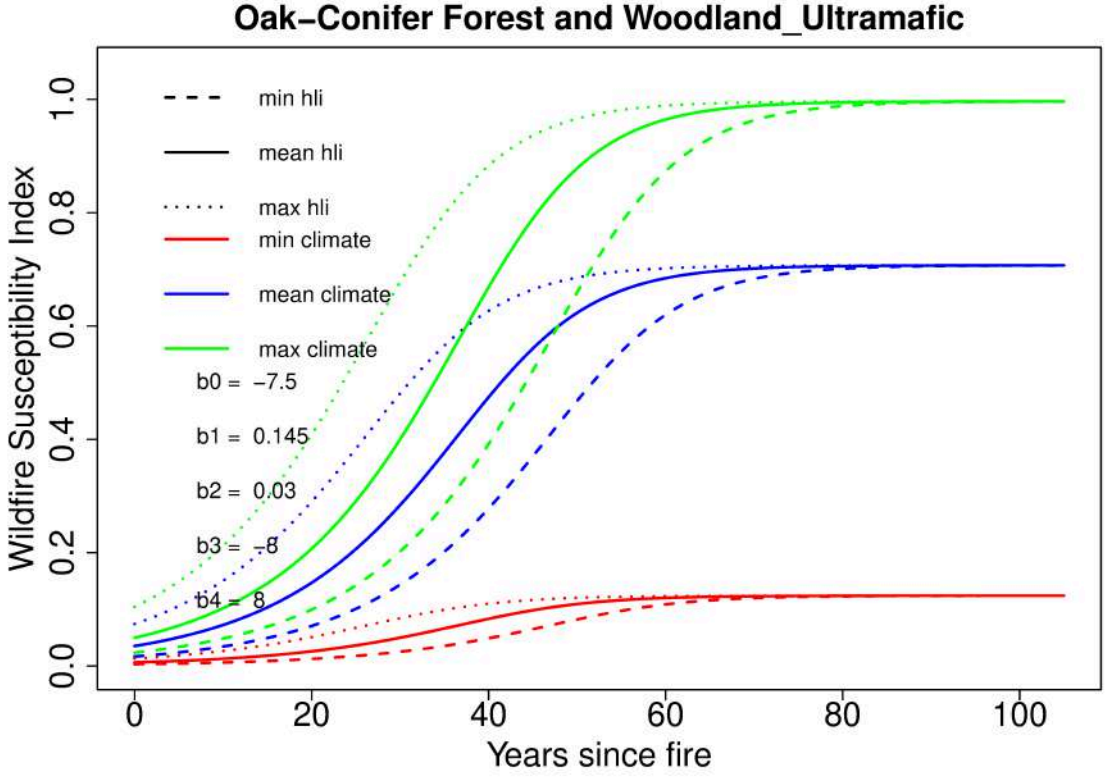
Oak–Conifer Forest and Woodland_Ultramafic
min hli
mean hli
max hli
min climate
mean climate
max climate
b0 = −7.5
b1 = 0.145
b2 = 0.03
b3 = −8
b4 = 8
Wildfire Susceptibility Index
0.0
0.2
0.4
0.6
0.8
1.0
0
20
40
60
80
100
Years since fire

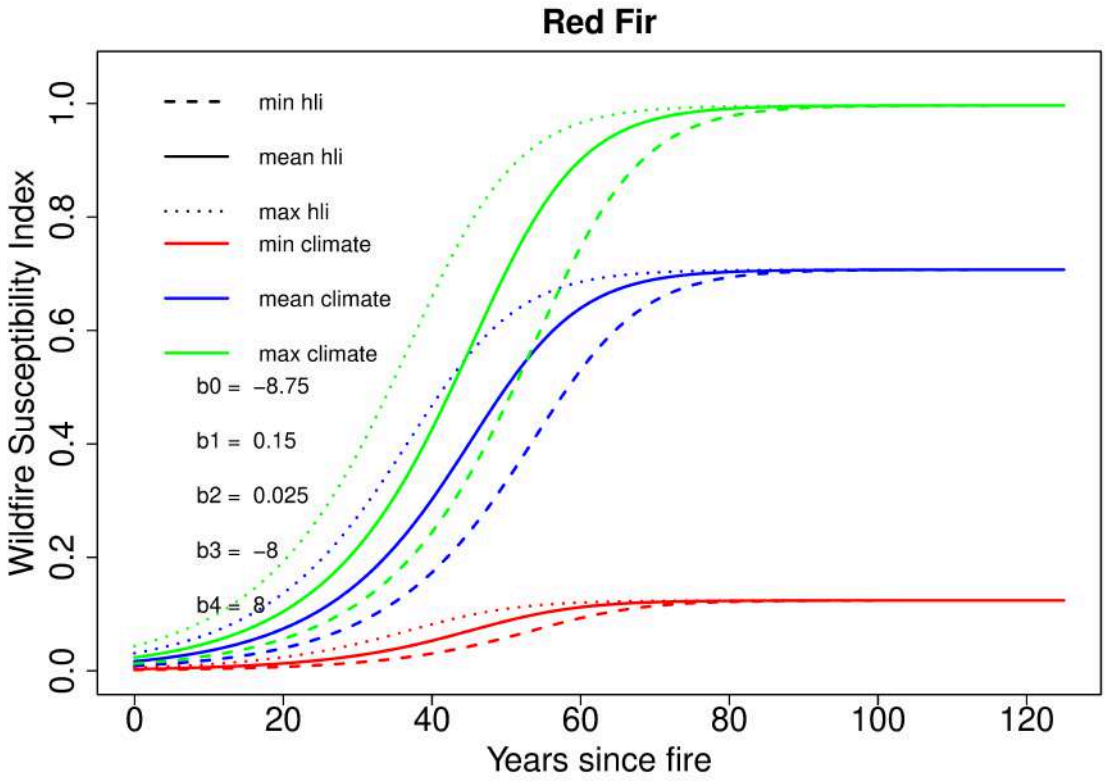
Red Fir
min hli
mean hli
max hli
min climate
mean climate
max climate
b0 = −8.75
b1 = 0.15
b2 = 0.025
b3 = −8
b4 = 8
Wildfire Susceptibility Index
0.0
0.2
0.4
0.6
0.8
1.0
0
20
40
60
80
100
120
Years since fire

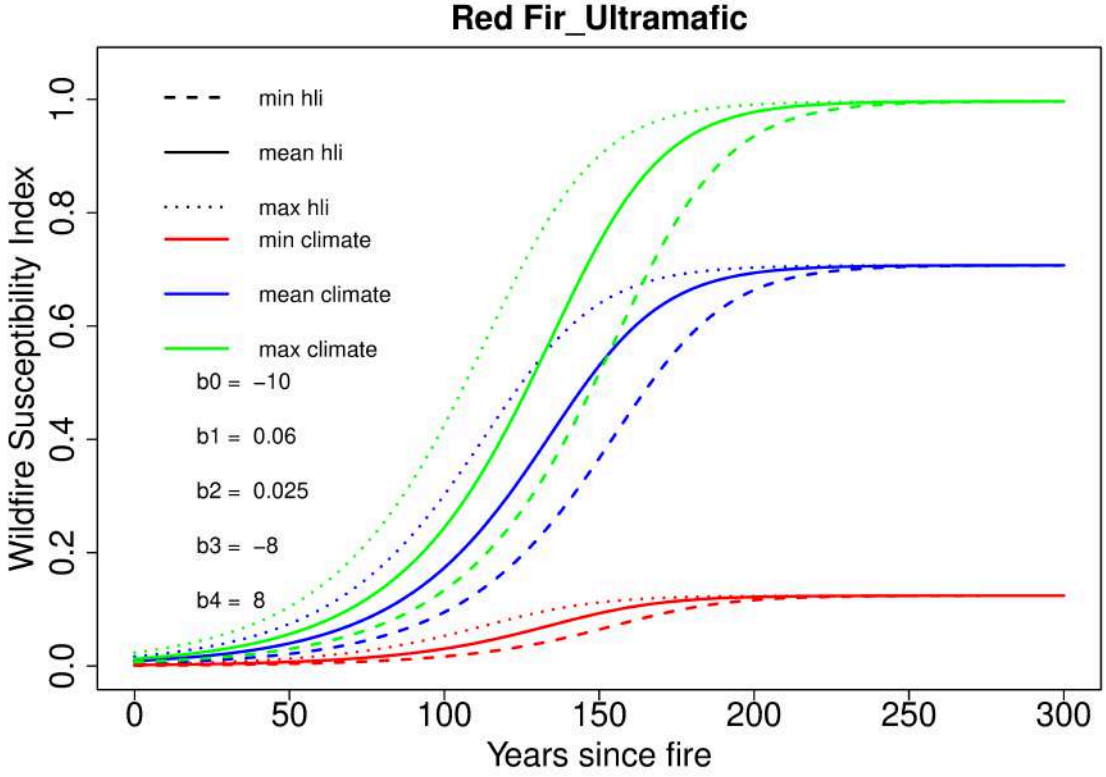
Red Fir_Ultramafic
min hli
mean hli
max hli
min climate
mean climate
max climate
b0 = −10
b1 = 0.06
b2 = 0.025
b3 = −8
b4 = 8
Wildfire Susceptibility Index
0.0
0.2
0.4
0.6
0.8
1.0
0
50
100
150
200
250
300
Years since fire

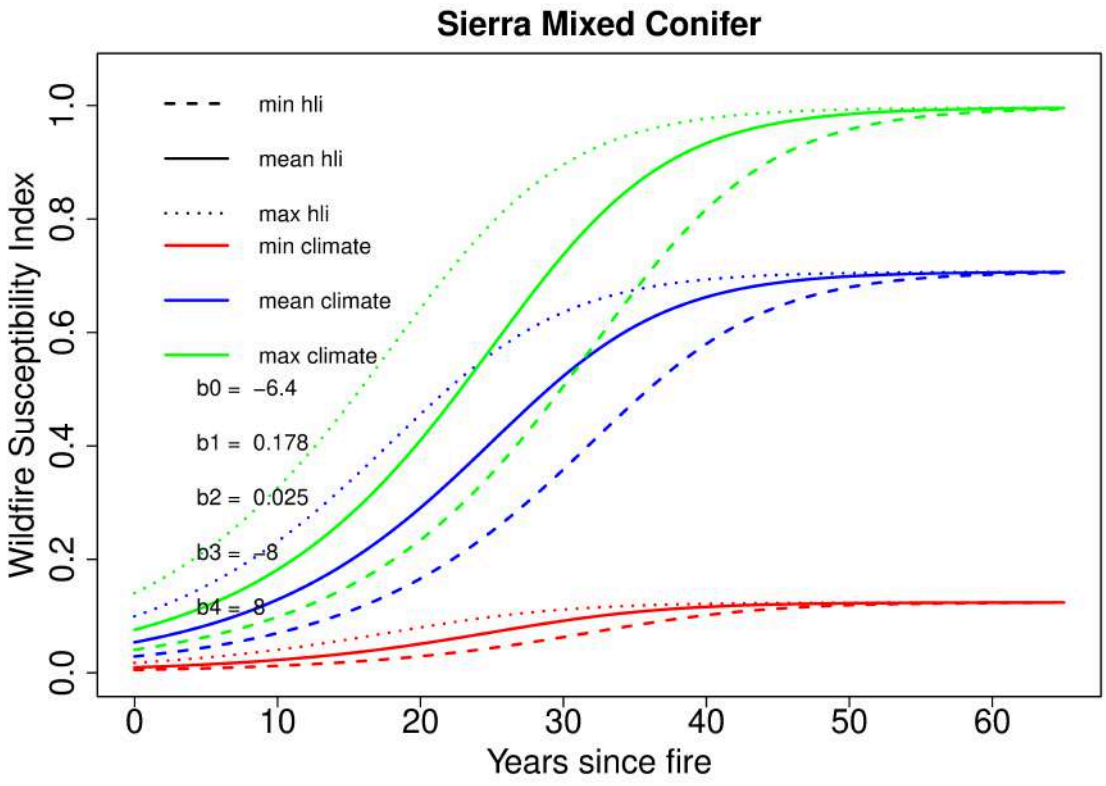
Sierra Mixed Conifer
min hli
mean hli
max hli
min climate
mean climate
max climate
b0 = −6.4
b1 = 0.178
b2 = 0.025
b3 = −8
b4 = 8
Wildfire Susceptibility Index
0.0
0.2
0.4
0.6
0.8
1.0
0
10
20
30
40
50
60
Years since fire

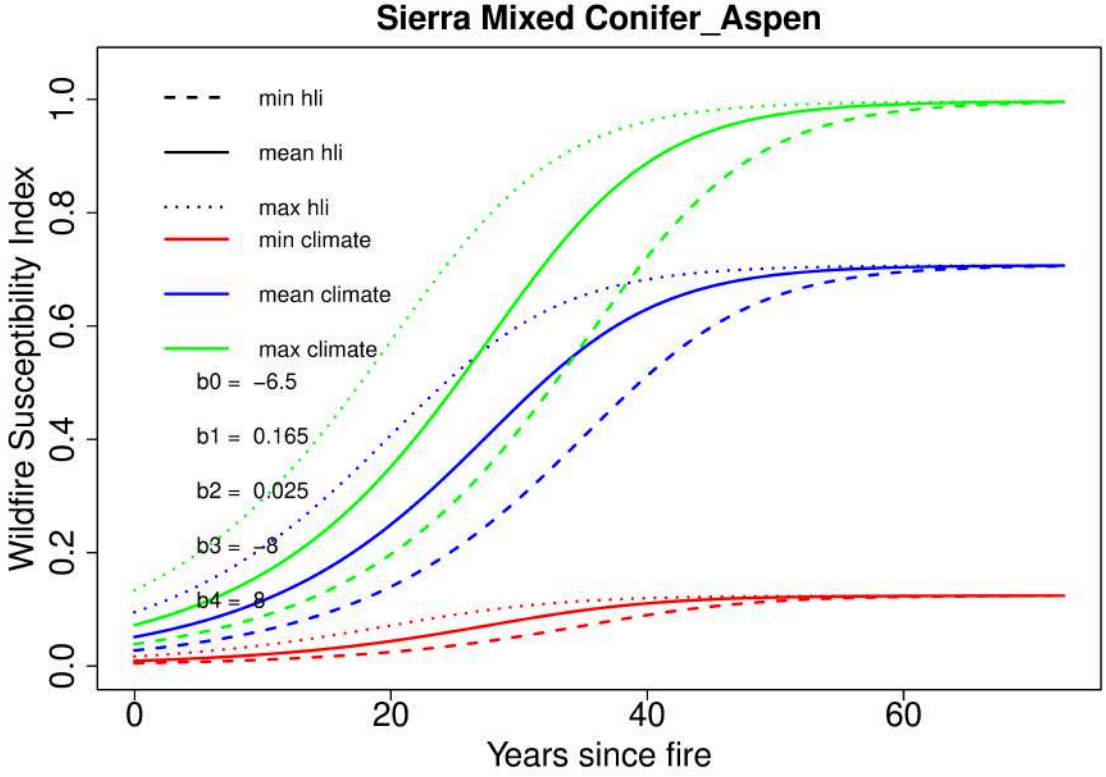
Sierra Mixed Conifer_Aspen
min hli
mean hli
max hli
min climate
mean climate
max climate
b0 = −6.5
b1 = 0.165
b2 = 0.025
b3 = −8
b4 = 8
Wildfire Susceptibility Index
0.0
0.2
0.4
0.6
0.8
1.0
0
20
40
60
Years since fire

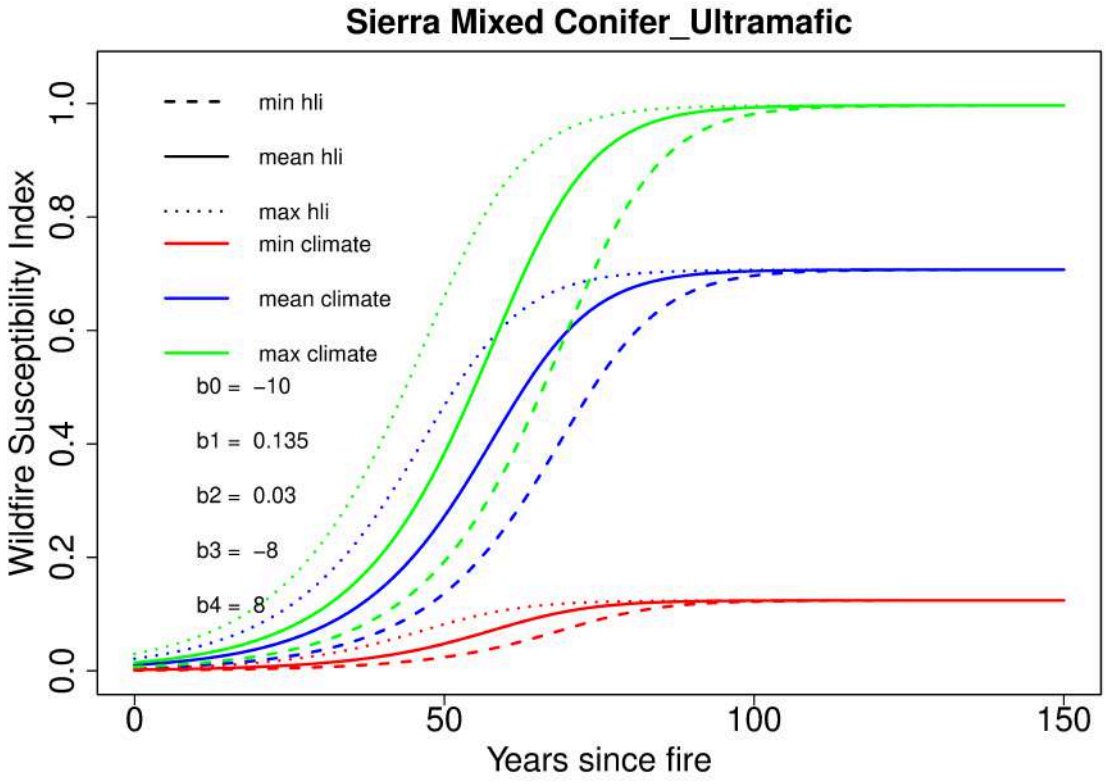
Sierra Mixed Conifer_Ultramafic
min hli
mean hli
max hli
min climate
mean climate
max climate
b0 = −10
b1 = 0.135
b2 = 0.03
b3 = −8
b4 = 8
Wildfire Susceptibility Index
0.0
0.2
0.4
0.6
0.8
1.0
0
50
100
150
Years since fire

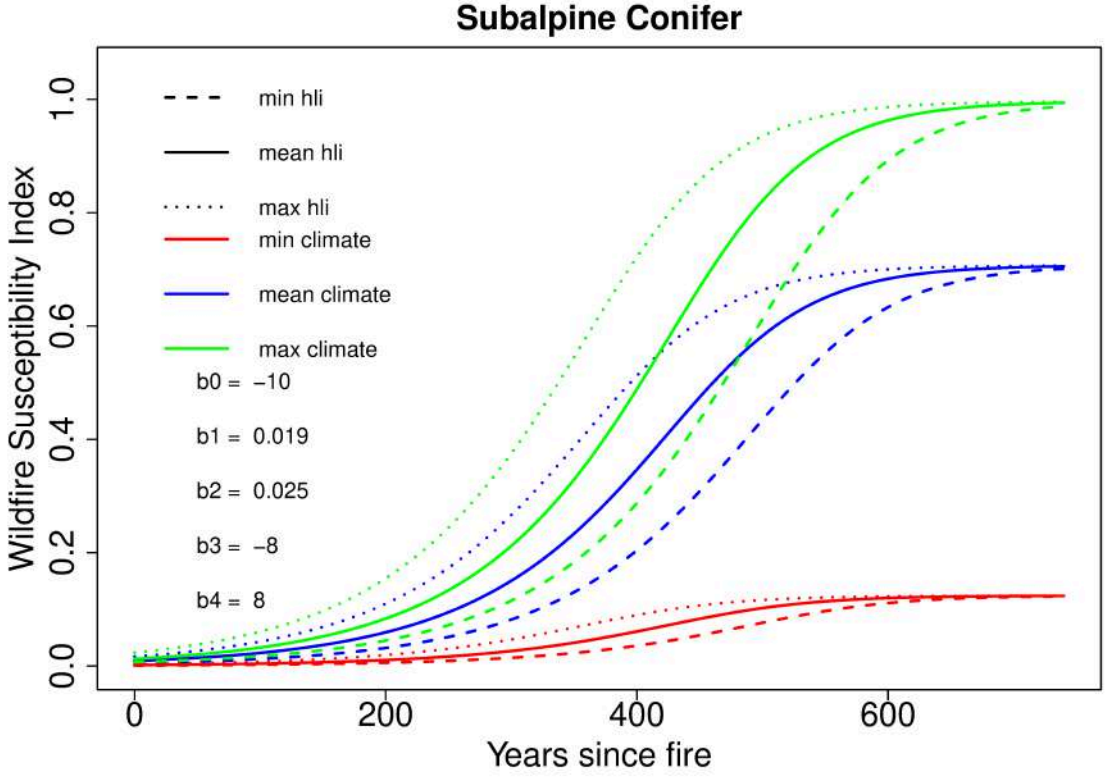
Subalpine Conifer
min hli
mean hli
max hli
min climate
mean climate
max climate
b0 = −10
b1 = 0.019
b2 = 0.025
b3 = −8
b4 = 8
Wildfire Susceptibility Index
0.0
0.2
0.4
0.6
0.8
1.0
0
200
400
600
Years since fire

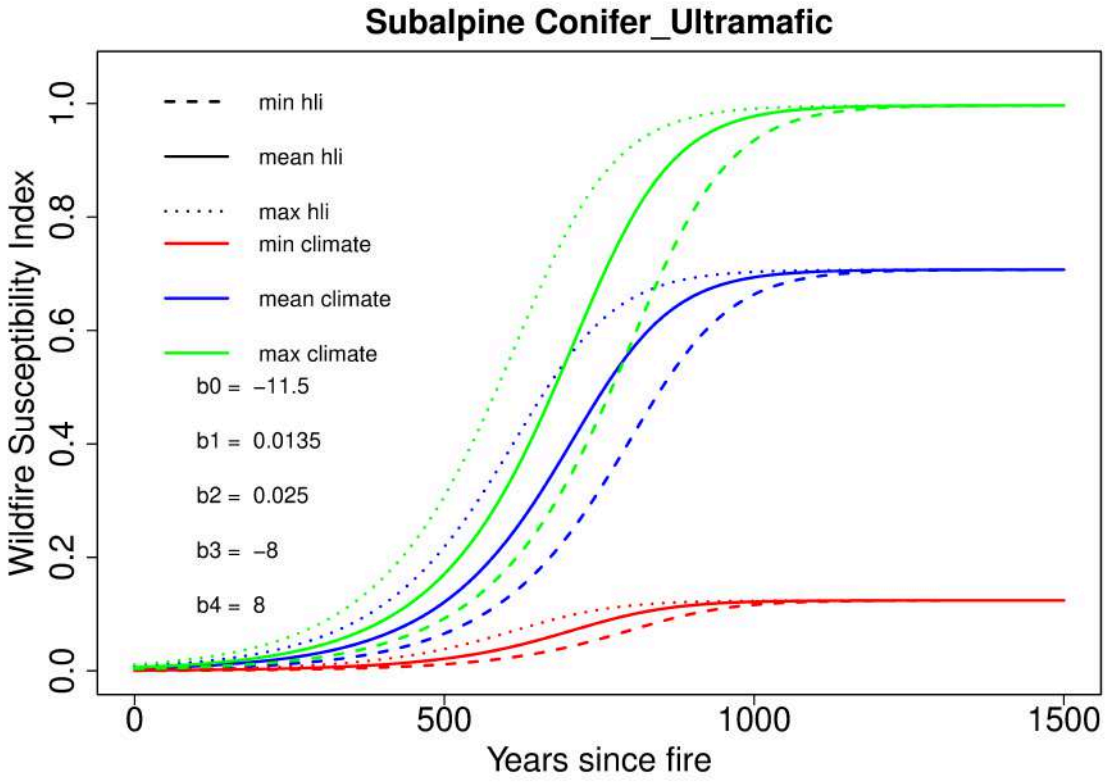
Subalpine Conifer_Ultramafic
min hli
mean hli
max hli
min climate
mean climate
max climate
b0 = −11.5
b1 = 0.0135
b2 = 0.025
b3 = −8
b4 = 8
Wildfire Susceptibility Index
0.0
0.2
0.4
0.6
0.8
1.0
0
500
1000
1500
Years since fire

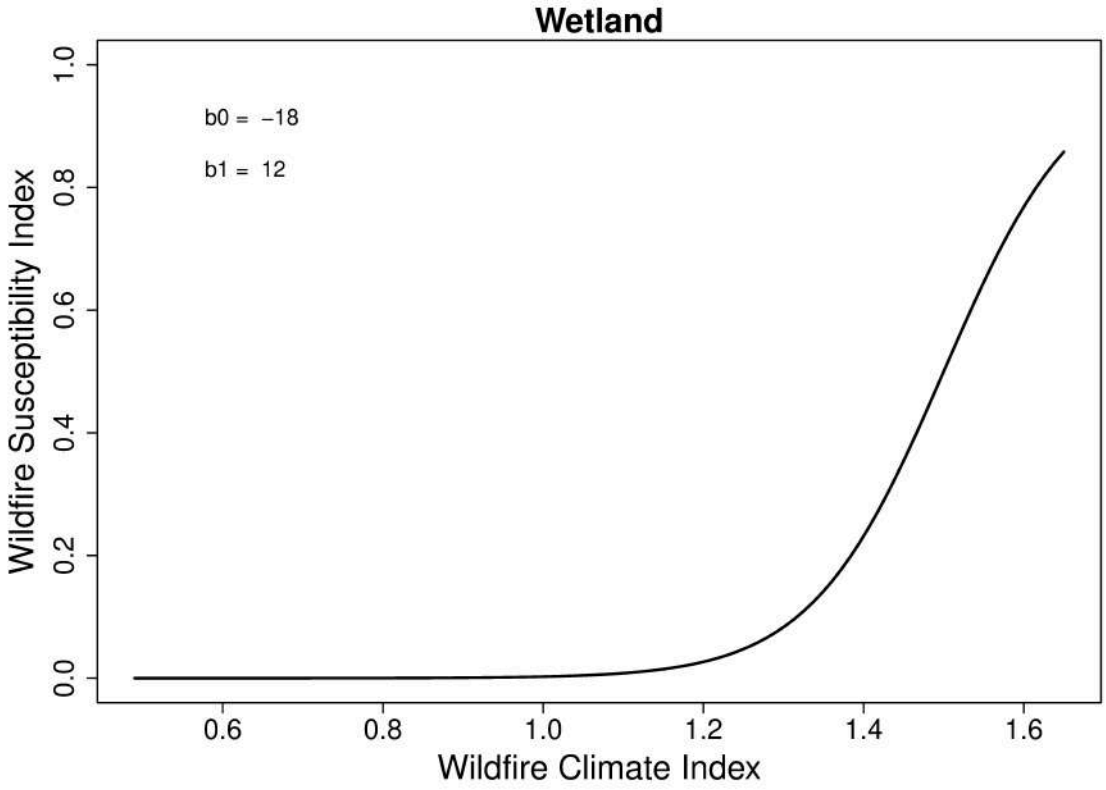
Wetland
b0 = −18
b1 = 12
Wildfire Susceptibility Index
0.0
0.2
0.4
0.6
0.8
1.0
0.6
0.8
1.0
1.2
1.4
1.6
Wildfire Climate Index

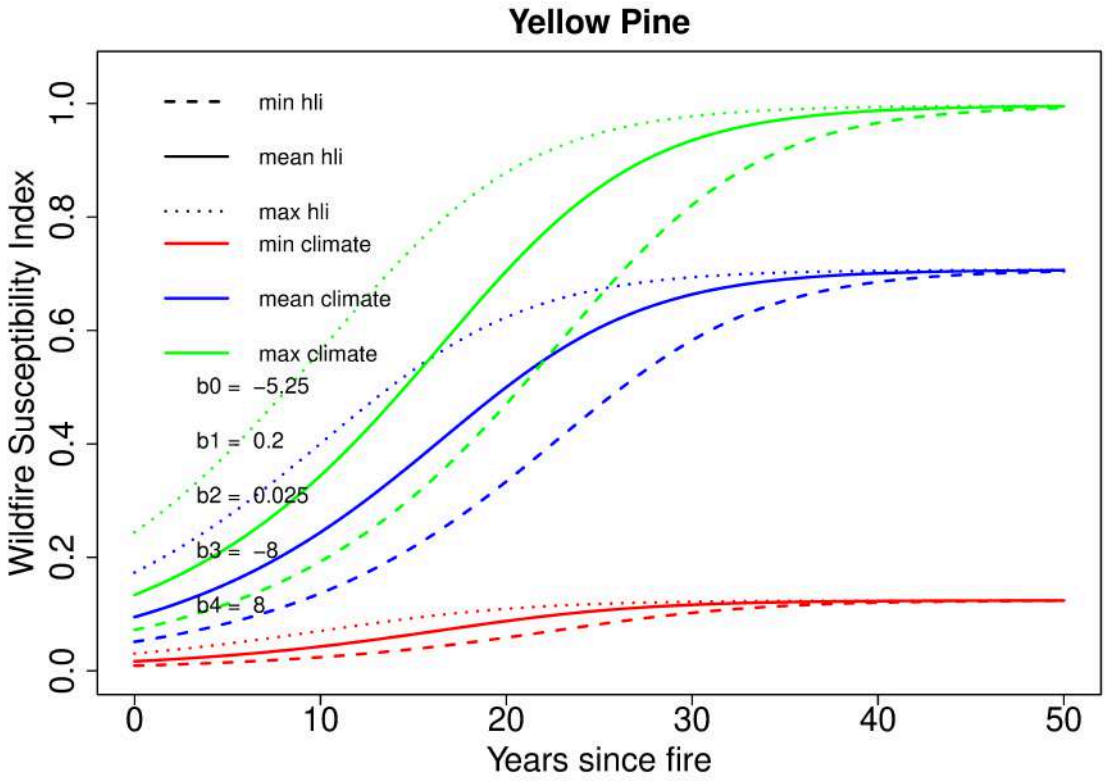
Yellow Pine
min hli
mean hli
max hli
min climate
mean climate
max climate
b0 = −5.25
b1 = 0.2
b2 = 0.025
b3 = −8
b4 = 8
Wildfire Susceptibility Index
0.0
0.2
0.4
0.6
0.8
1.0
0
10
20
30
40
50
Years since fire

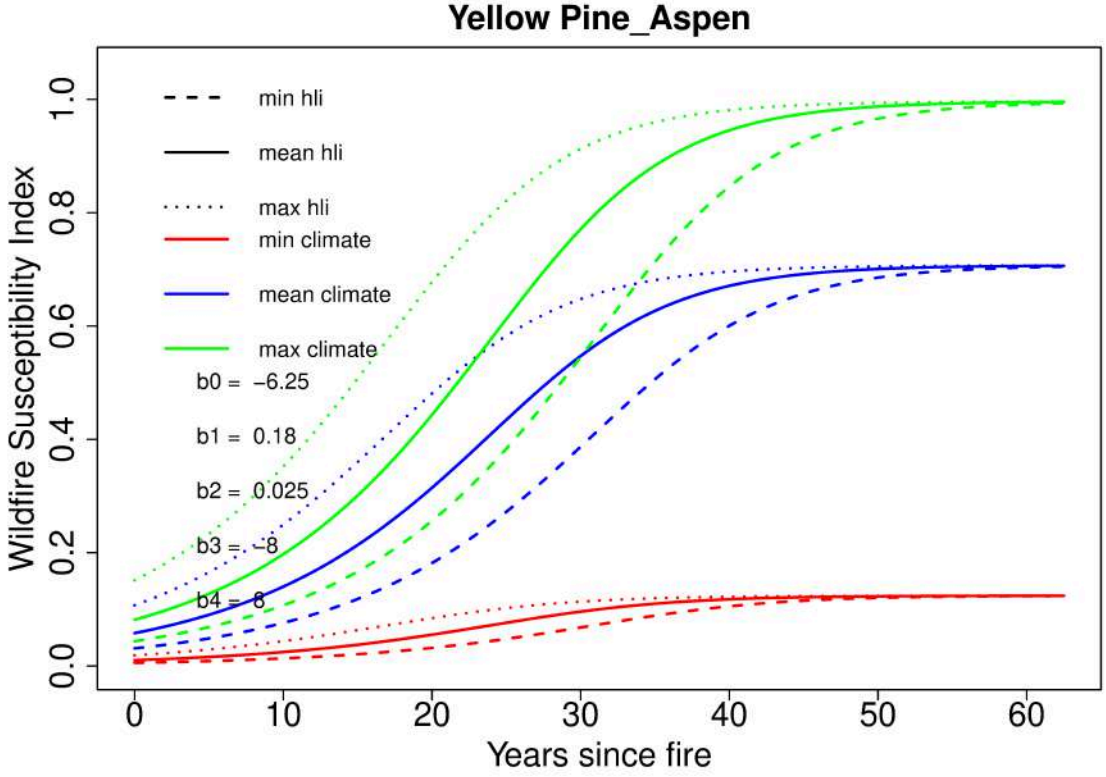
Yellow Pine_Aspen
min hli
mean hli
max hli
min climate
mean climate
max climate
b0 = −6.25
b1 = 0.18
b2 = 0.025
b3 = −8
b4 = 8
Wildfire Susceptibility Index
0.0
0.2
0.4
0.6
0.8
1.0
0
10
20
30
40
50
60
Years since fire

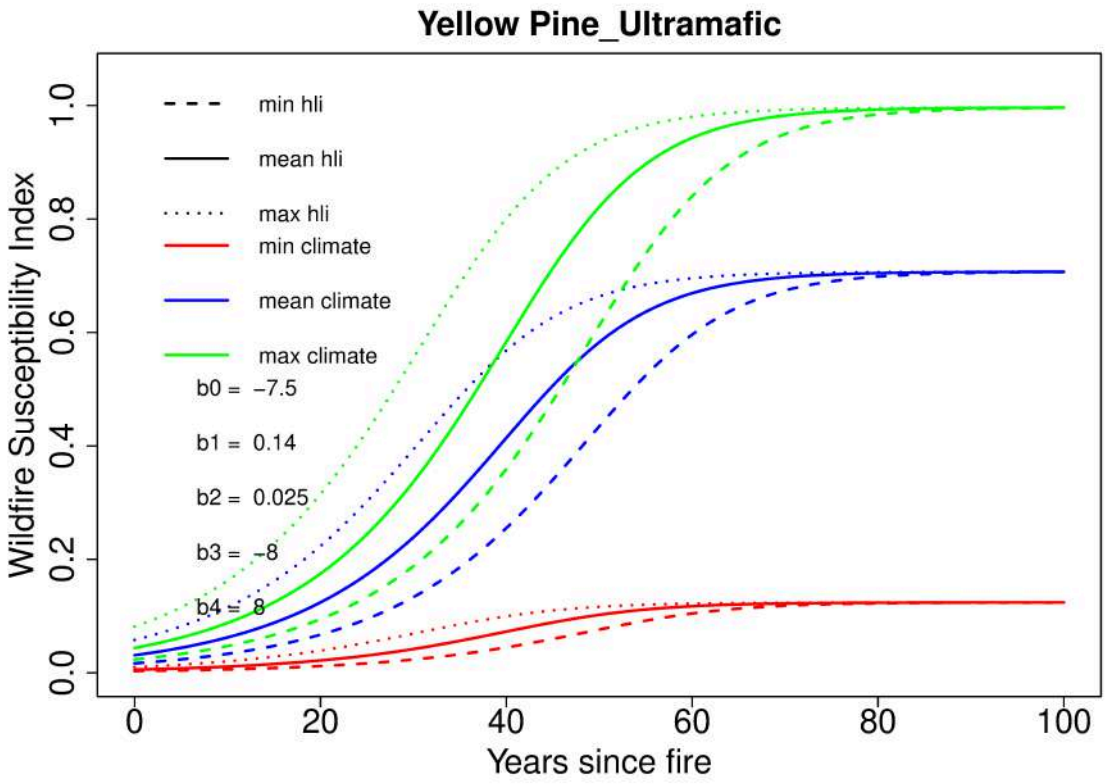
Yellow Pine_Ultramafic
min hli
mean hli
max hli
min climate
mean climate
max climate
b0 = −7.5
b1 = 0.14
b2 = 0.025
b3 = −8
b4 = 8
Wildfire Susceptibility Index
0.0
0.2
0.4
0.6
0.8
1.0
0
20
40
60
80
100
Years since fire

APPENDIX E2 - Wildfire Mortality

As described in the GTR, wildfire mortality (i.e., the probability of high mortality or death of the overstory vegetation in each 5 m cell that burned) was determined by a complex function involving two major factors: 1) fire intensity, which was a Logistic function of the fuel loads in the neighborhood of the focal cell (proxied by the age of the vegetation and time since the last fire), the topographic position of the focal cell, and the climate conditions in the current time step; and 2) the resistance of the focal cell, which was a negative exponential function of the age of the vegetation in the focal cell in which the rate of exponential decline with age decreased with increasing fire intensity (see main text for details). The complex wildfire mortality function included 6 user-specified beta coefficients. As described in the main text, b_0 - b_4 were held constant across all cover types. We varied b_5 and b_6 among cover types to reflect differences in reported historical mean fire return intervals and high mortality rates among cover types. Specifically, we varied these two beta coefficients during model calibration to either increase or decrease the rate of exponential decline in high mortality with increasing vegetation age as a function of fire intensity to achieve the target percentage of high mortality rate in each cover type.

The figures below depict the final wildfire mortality response functions for each cover type in alphabetical order. Cover types not shown either were not eligible to burn (e.g., water, barren) or were always assigned a high mortality response after burning (e.g., grassland, meadow). The response functions depict the probability of high mortality wildfire as a negative exponential function of vegetation Age (yrs) and fire intensity (as indexed). The dashed, solid and dotted lines depict the response functions for the minimum, mean and maximum Fire Intensity Index. Universally, the probability of high mortality decreased with increasing vegetation Age, but the rate of exponential decline decreased (i.e.,shallower slope) with increasing fire intensity, such that for any given Age the probability of high mortality increased with increasing fire intensity.

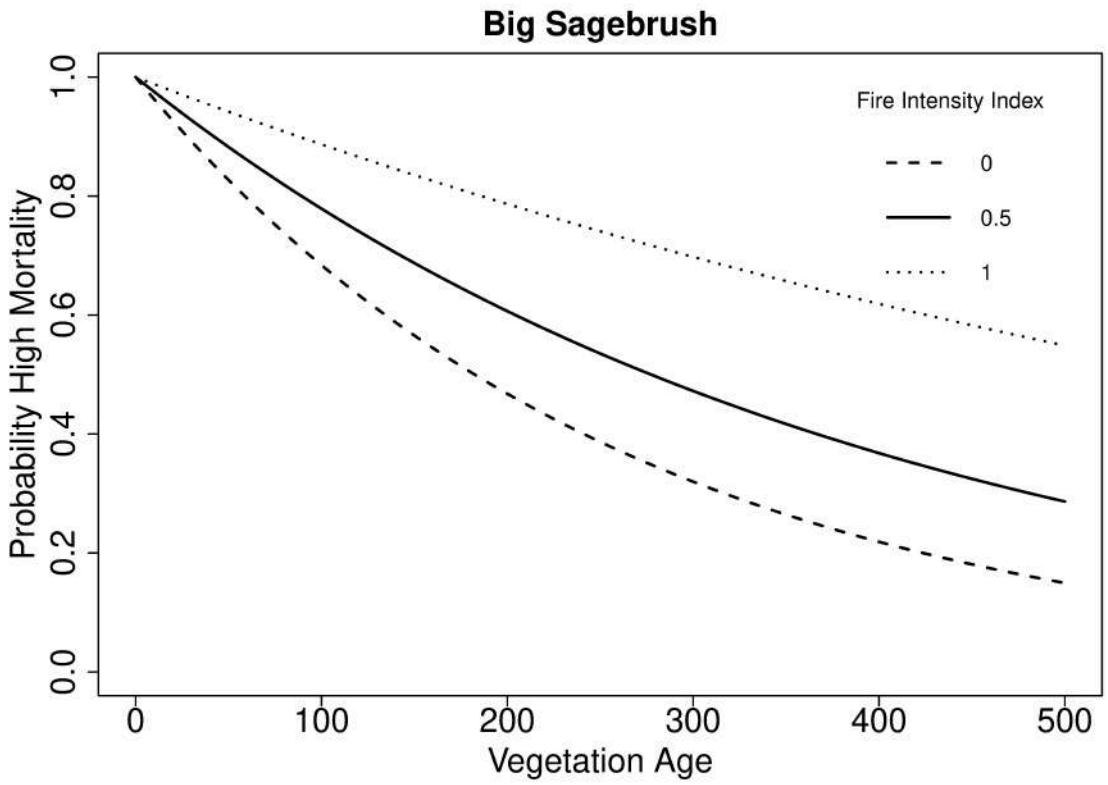

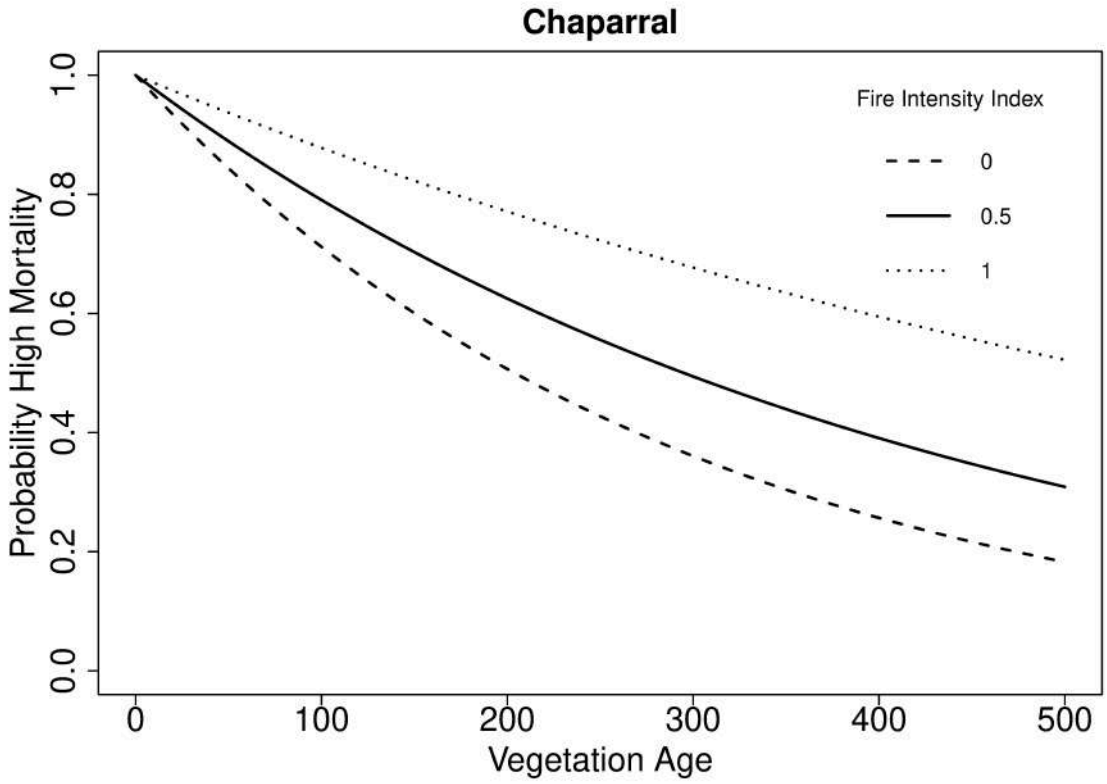
Chaparral
Probability High Mortality
0.0
0.2
0.4
0.6
0.8
1.0
0
100
200
300
400
500
Vegetation Age
Fire Intensity Index
0
0.5
1

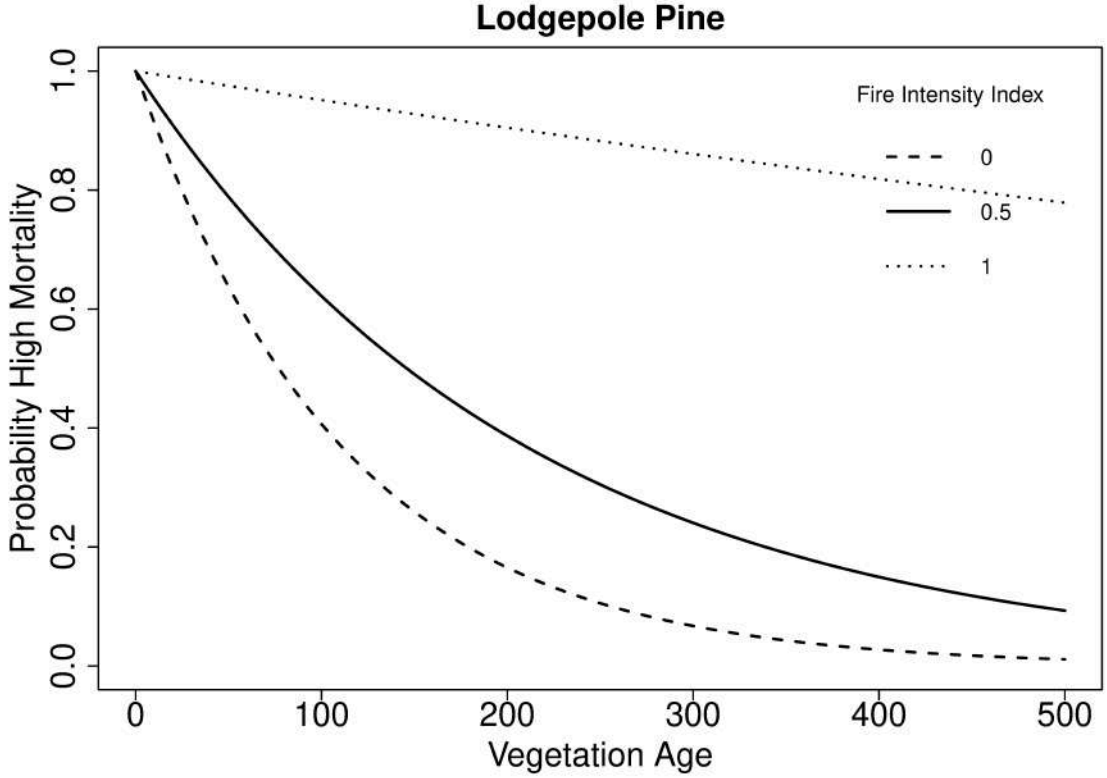
Lodgepole Pine
Probability High Mortality
0.0
0.2
0.4
0.6
0.8
1.0
0
100
200
300
400
500
Vegetation Age
Fire Intensity Index
0
0.5
1

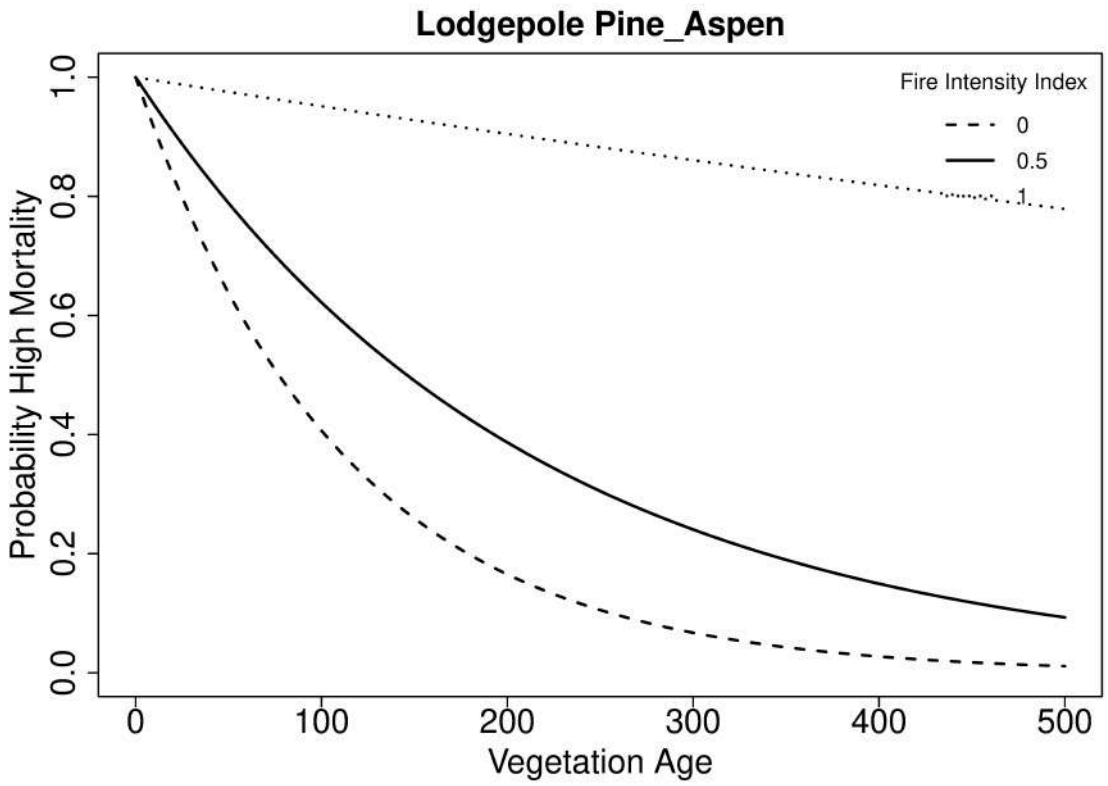
Lodgepole Pine_Aspen
Fire Intensity Index
0
0.5
1
Probability High Mortality
0.0
0.2
0.4
0.6
0.8
1.0
0
100
200
300
400
500
Vegetation Age

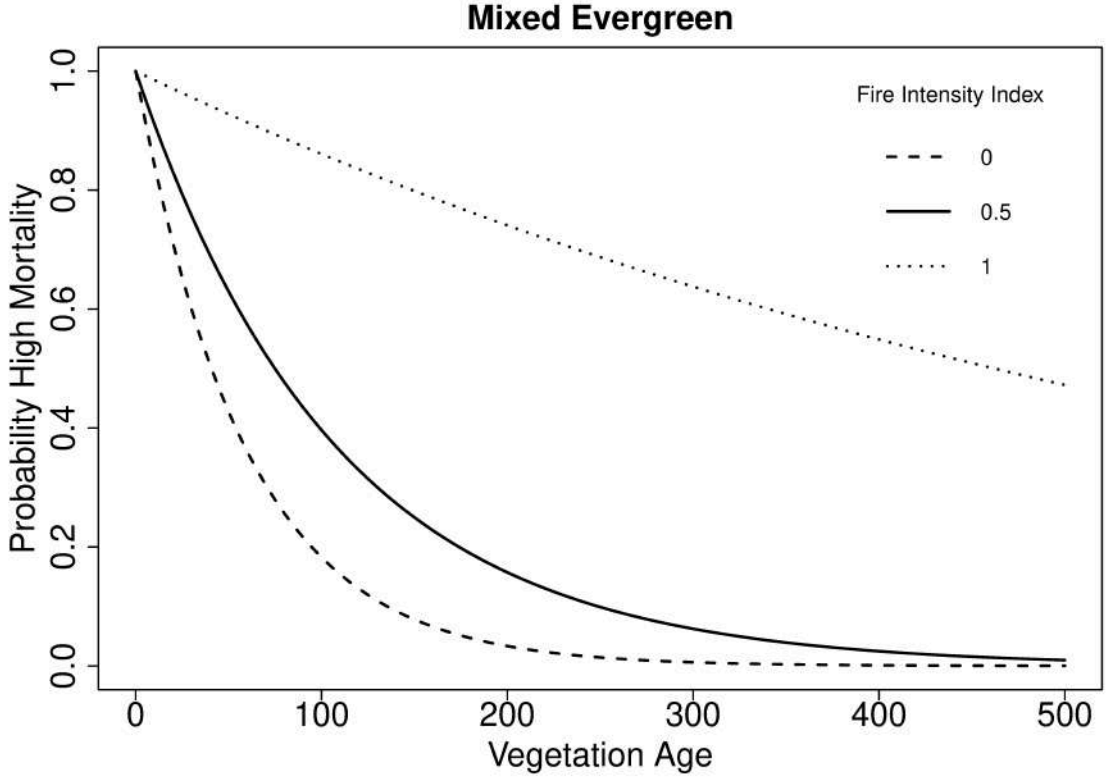
Mixed Evergreen
Fire Intensity Index
0
0.5
1
Probability High Mortality
0.0
0.2
0.4
0.6
0.8
1.0
0
100
200
300
400
500
Vegetation Age

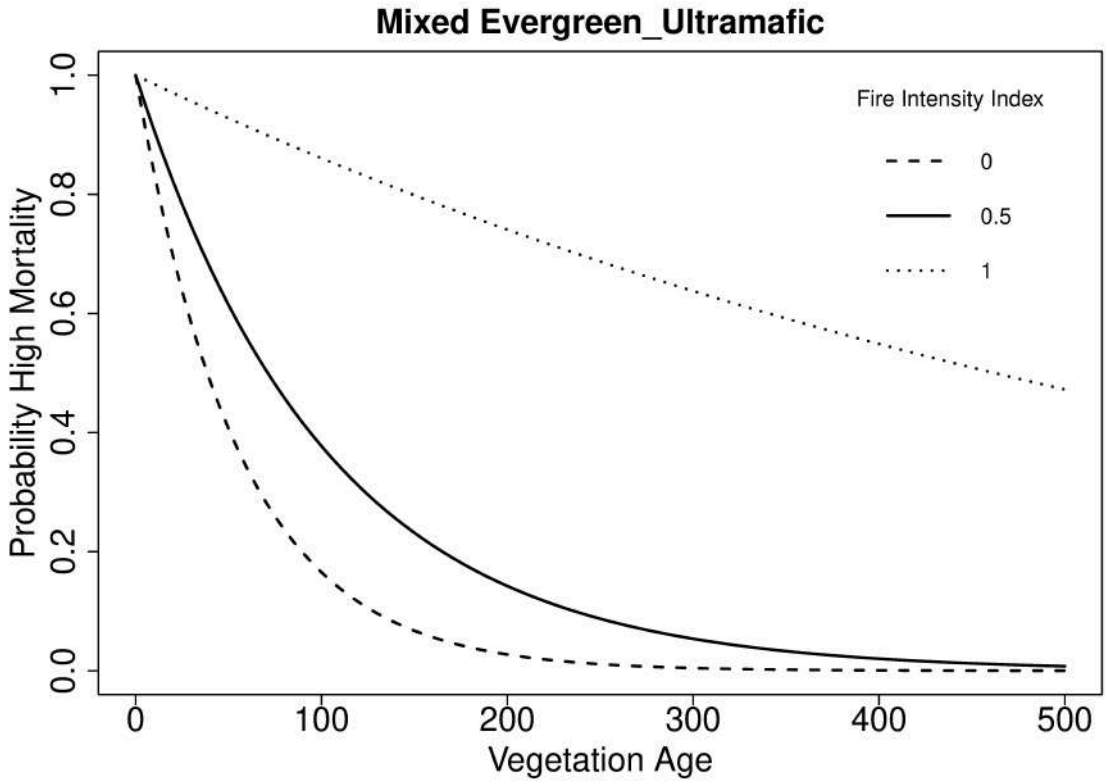
Mixed Evergreen_Ultramafic
Fire Intensity Index
0
0.5
1
Probability High Mortality
0.0
0.2
0.4
0.6
0.8
1.0
0
100
200
300
400
500
Vegetation Age

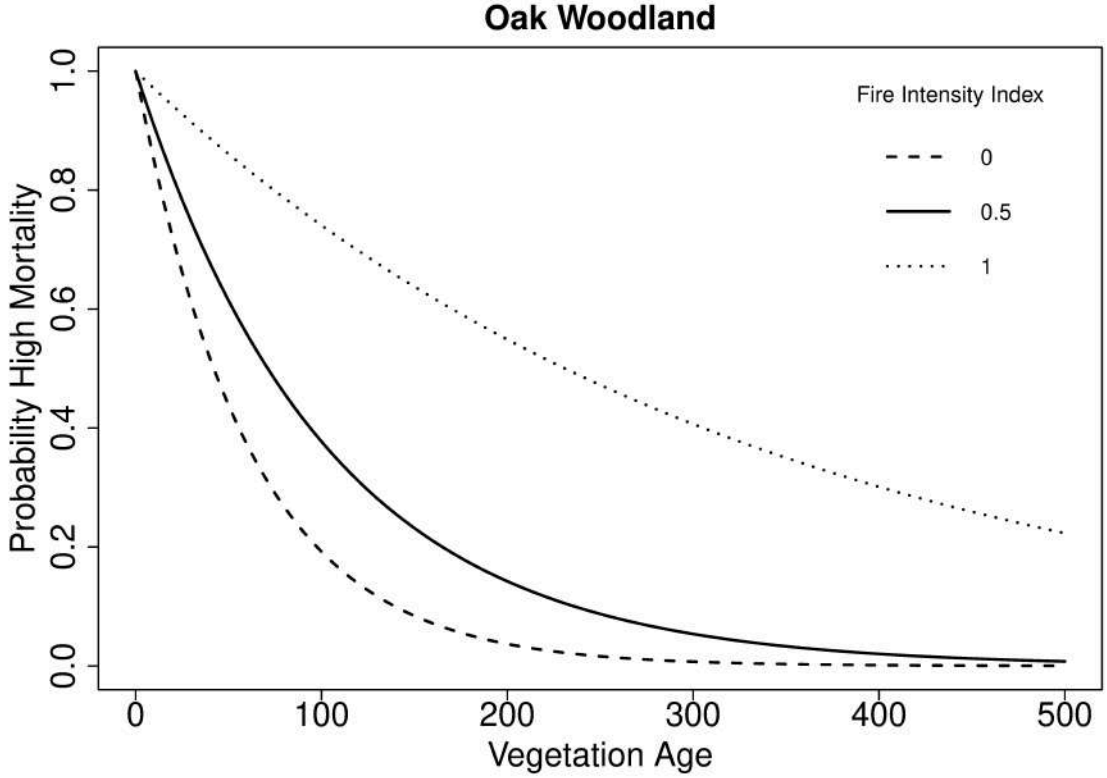
Oak Woodland
Fire Intensity Index
0
0.5
1
Probability High Mortality
0.0
0.2
0.4
0.6
0.8
1.0
0
100
200
300
400
500
Vegetation Age

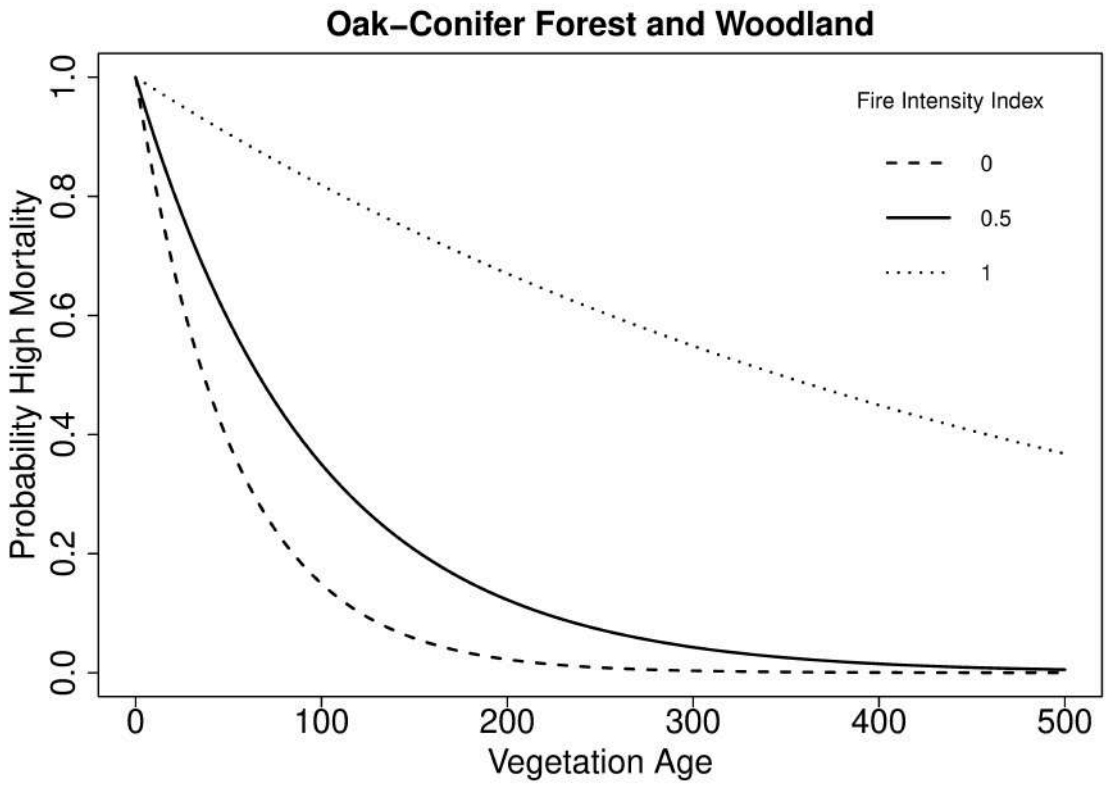
Oak–Conifer Forest and Woodland
Fire Intensity Index
0
0.5
1
Probability High Mortality
0.0
0.2
0.4
0.6
0.8
1.0
0
100
200
300
400
500
Vegetation Age

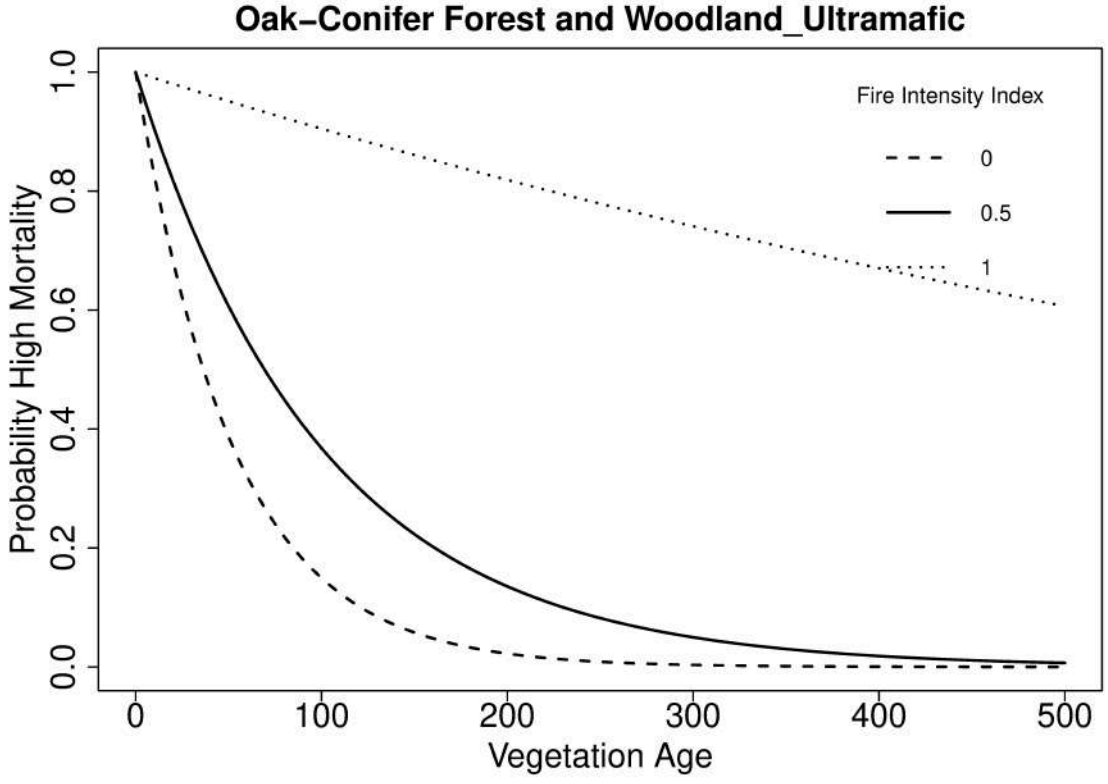
Oak–Conifer Forest and Woodland_Ultramafic
Fire Intensity Index
0
0.5
1
Probability High Mortality
0.0
0.2
0.4
0.6
0.8
1.0
0
100
200
300
400
500
Vegetation Age

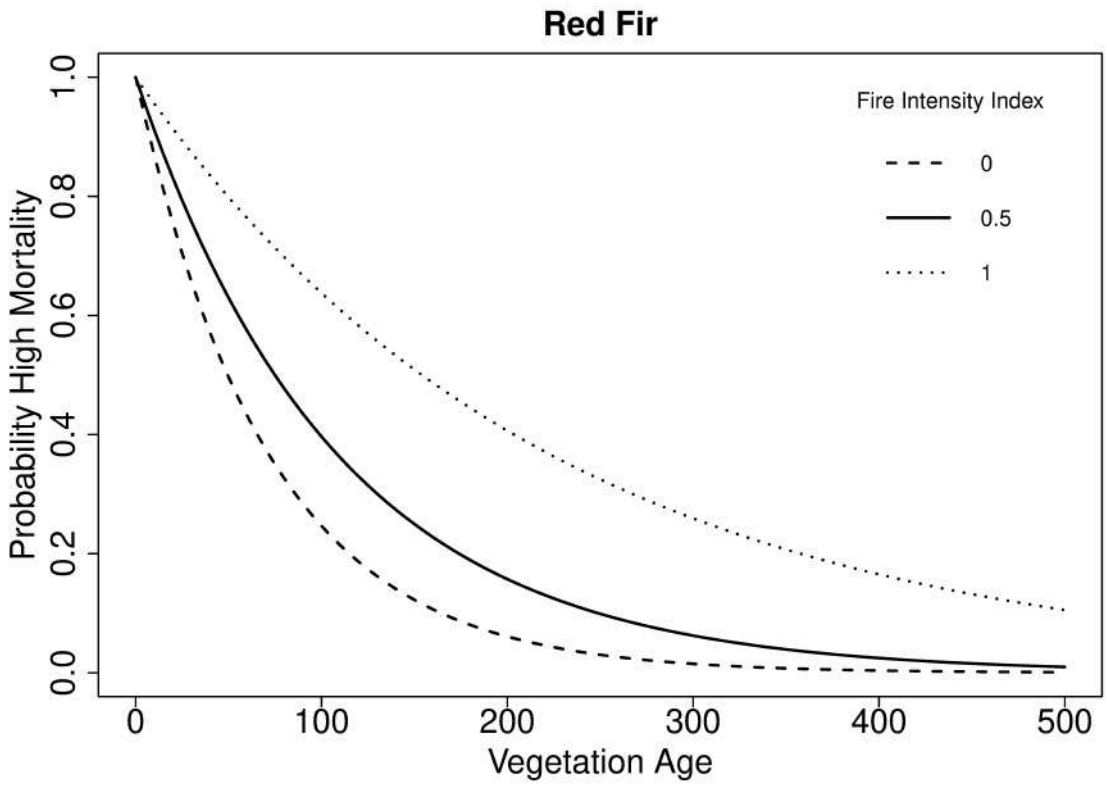
Red Fir
Fire Intensity Index
0
0.5
1
Probability High Mortality
0.0
0.2
0.4
0.6
0.8
1.0
0
100
200
300
400
500
Vegetation Age

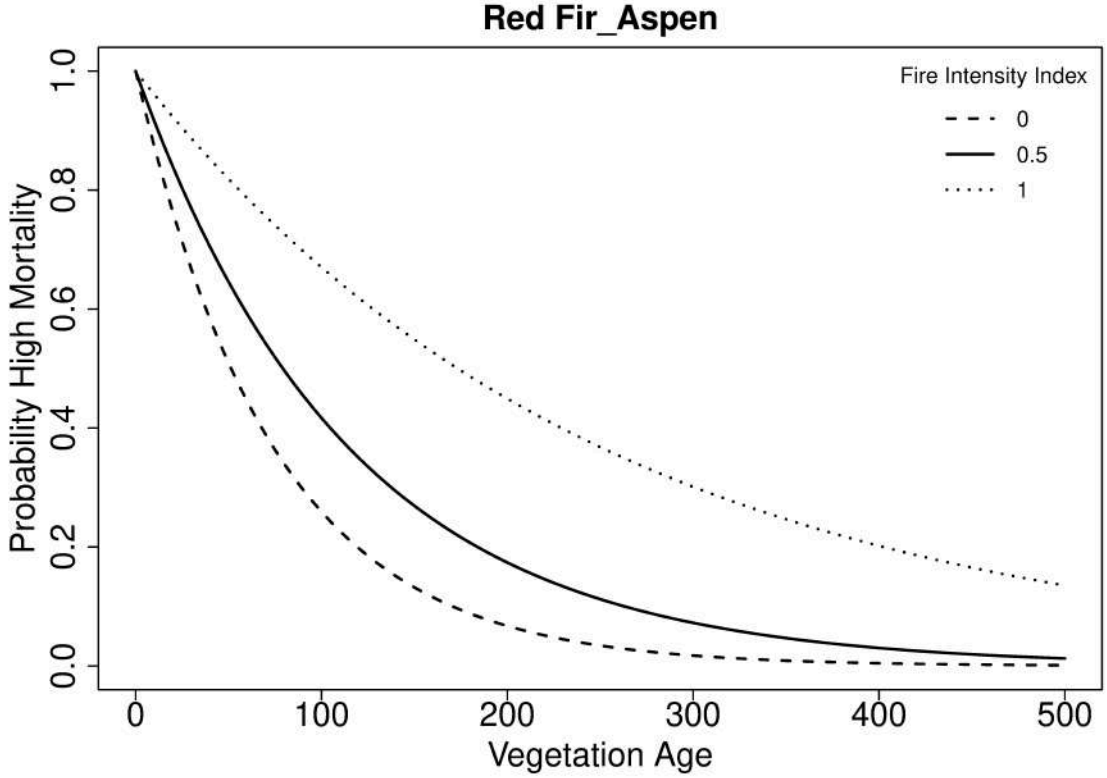
Red Fir_Aspen
Fire Intensity Index
0
0.5
1
Probability High Mortality
0.0
0.2
0.4
0.6
0.8
1.0
0
100
200
300
400
500
Vegetation Age

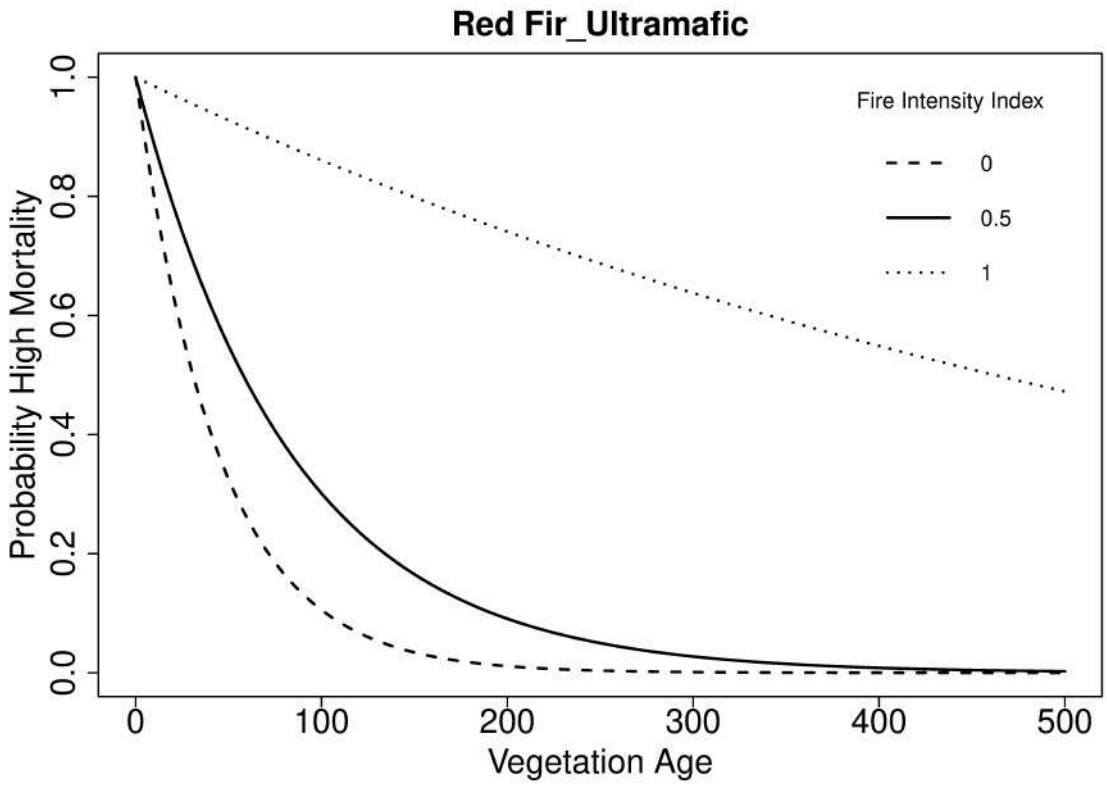
Red Fir_Ultramafic
Fire Intensity Index
0
0.5
1
Probability High Mortality
0.0
0.2
0.4
0.6
0.8
1.0
0
100
200
300
400
500
Vegetation Age

Sierra Mixed Conifer
Fire Intensity Index
0
0.5
1
Probability High Mortality
0.0
0.2
0.4
0.6
0.8
1.0
0
100
200
300
400
500
Vegetation Age

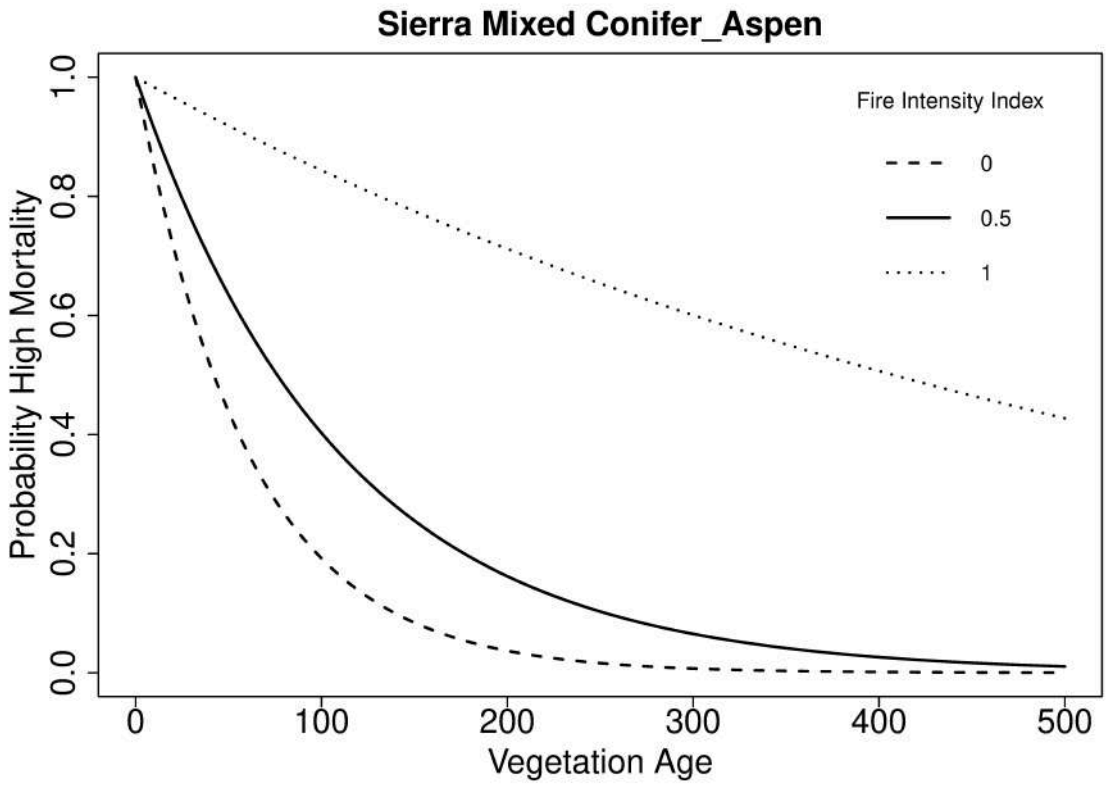
Sierra Mixed Conifer_Aspen
Fire Intensity Index
0
0.5
1
Probability High Mortality
0.0
0.2
0.4
0.6
0.8
1.0
0
100
200
300
400
500
Vegetation Age

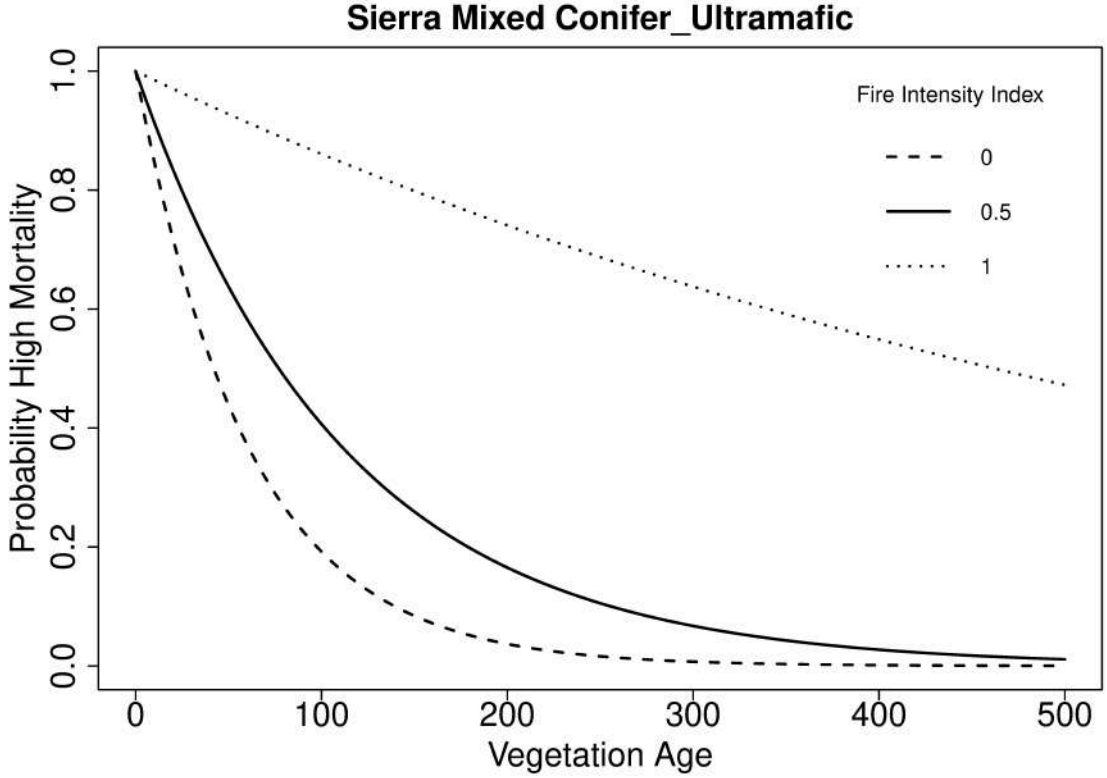
Sierra Mixed Conifer_Ultramafic
Fire Intensity Index
0
0.5
1
Probability High Mortality
0.0
0.2
0.4
0.6
0.8
1.0
0
100
200
300
400
500
Vegetation Age

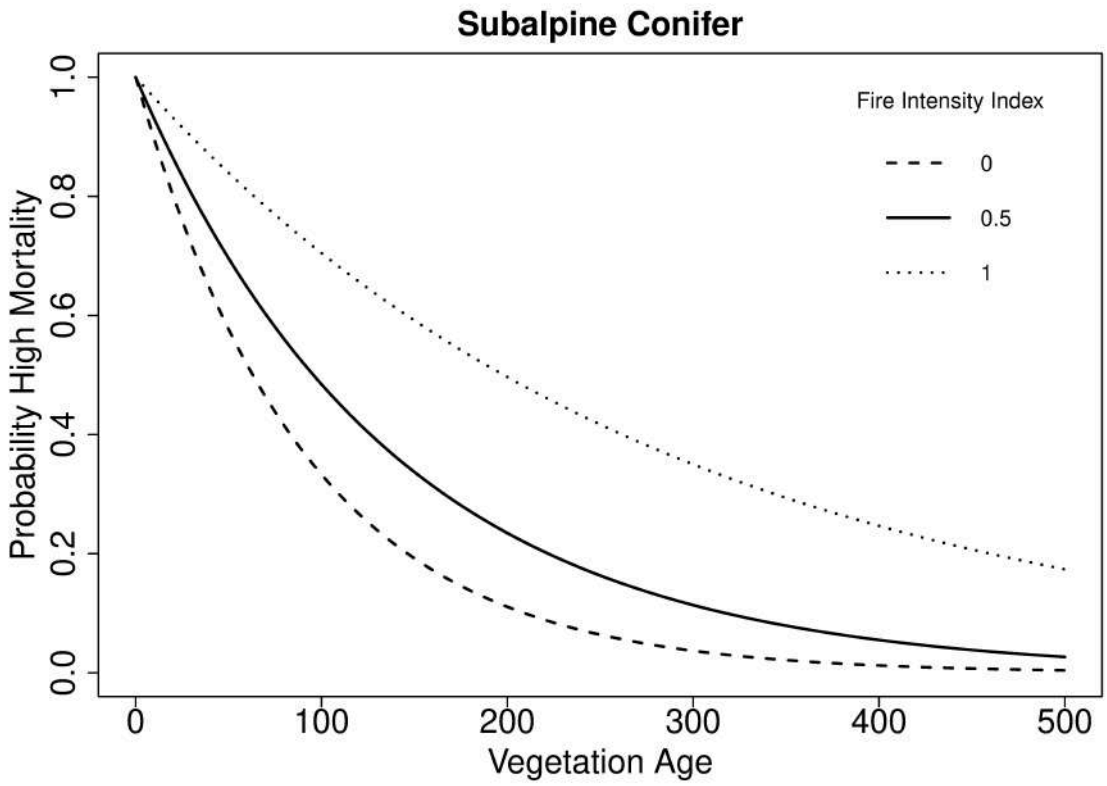
Subalpine Conifer
Probability High Mortality
0.0
0.2
0.4
0.6
0.8
1.0
0
100
200
300
400
500
Vegetation Age
Fire Intensity Index
0
0.5
1

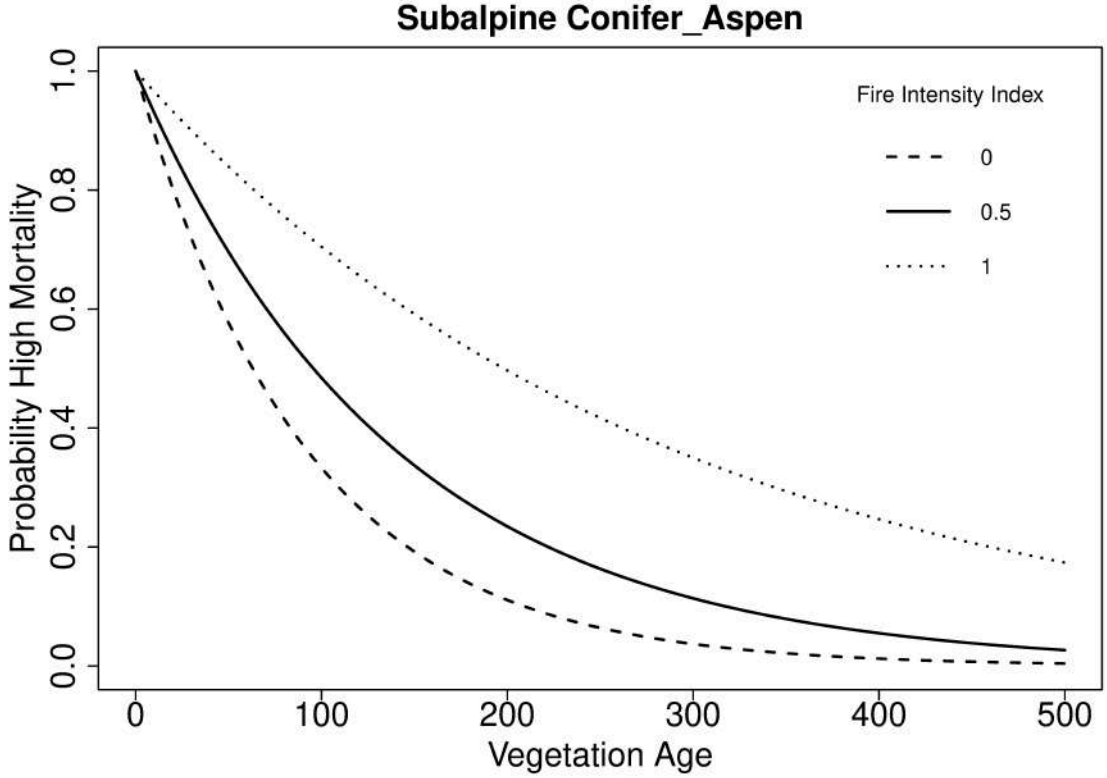
Subalpine Conifer_Aspen
Probability High Mortality
0.0
0.2
0.4
0.6
0.8
1.0
0
100
200
300
400
500
Vegetation Age
Fire Intensity Index
0
0.5
1

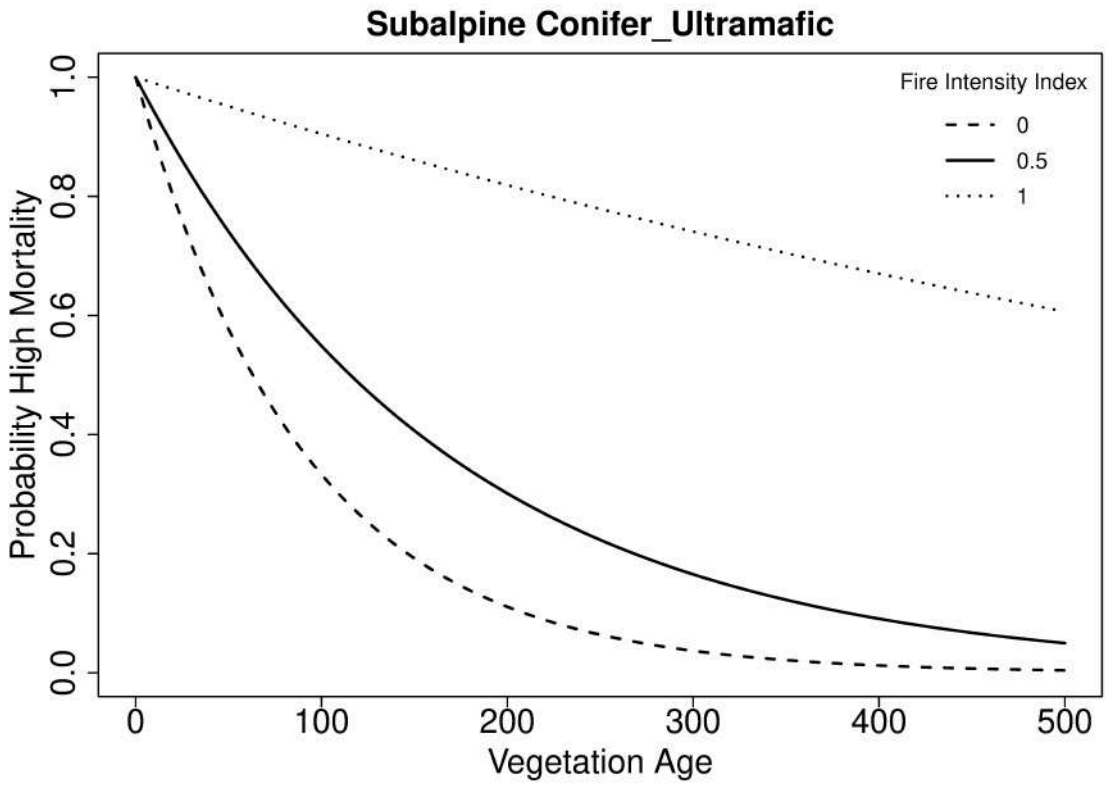
Subalpine Conifer_Ultramafic
Fire Intensity Index
0
0.5
1
Probability High Mortality
0.0
0.2
0.4
0.6
0.8
1.0
0
100
200
300
400
500
Vegetation Age

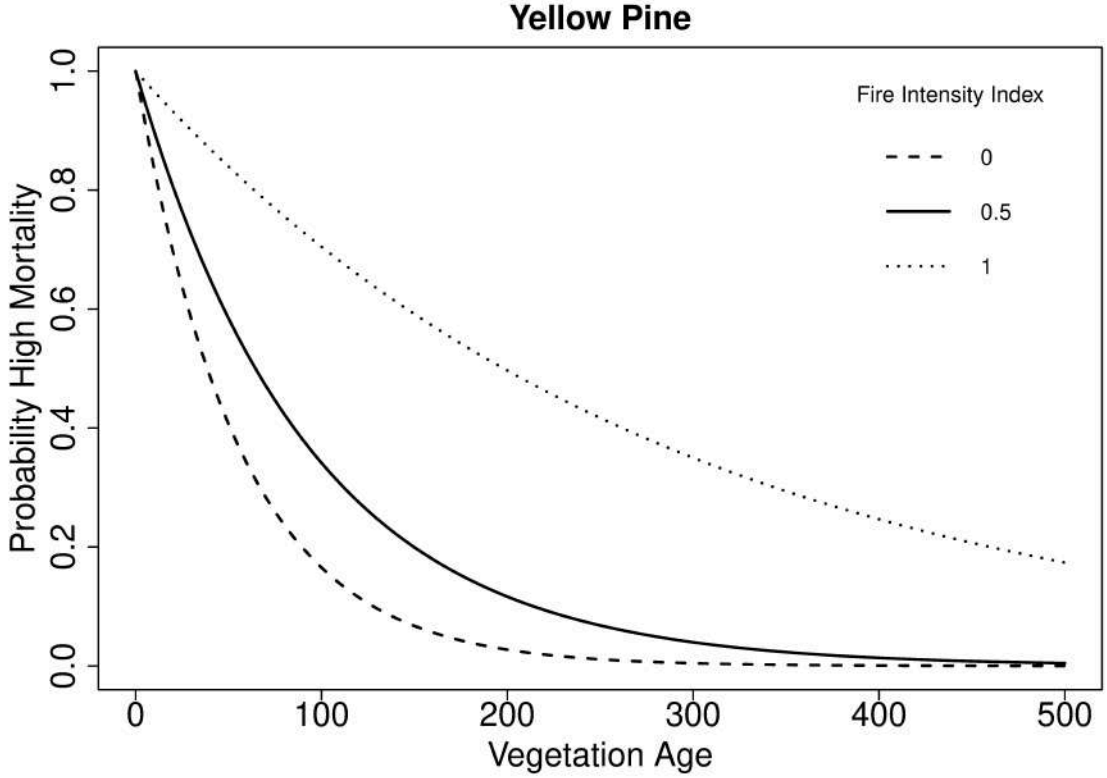
Yellow Pine
Fire Intensity Index
0
0.5
1
Probability High Mortality
0.0
0.2
0.4
0.6
0.8
1.0
0
100
200
300
400
500
Vegetation Age

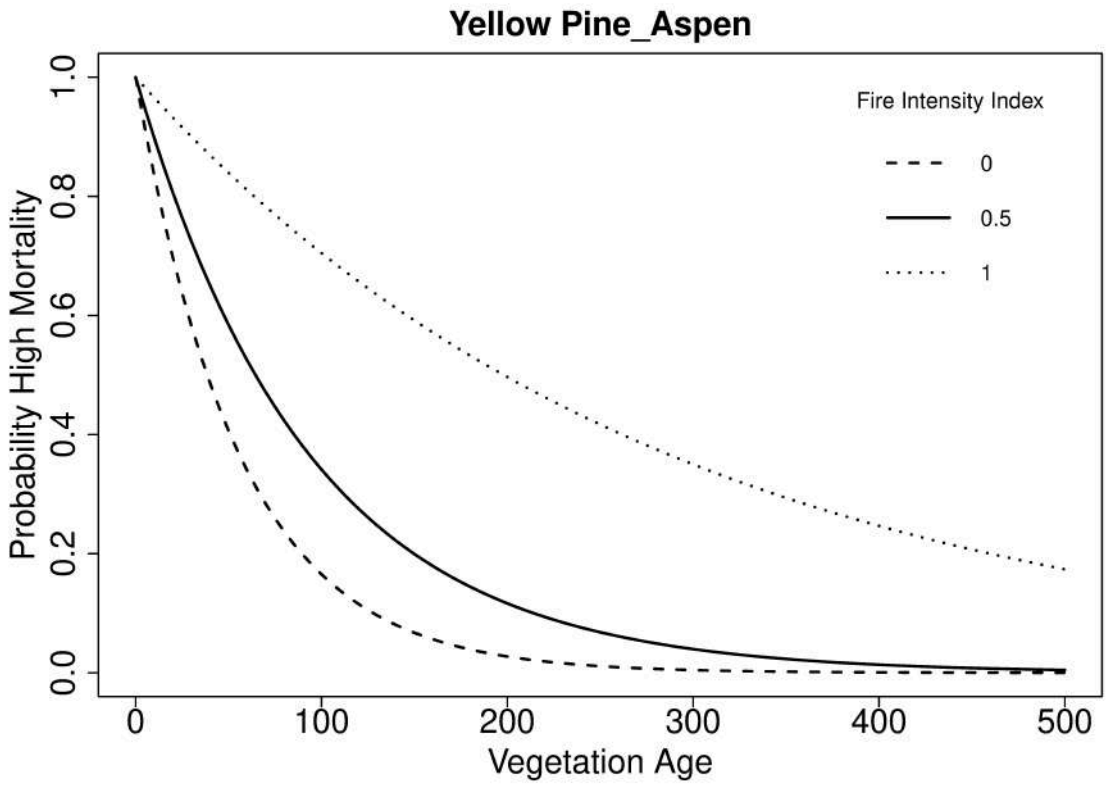
Yellow Pine_Aspen
Fire Intensity Index
0
0.5
1
Probability High Mortality
0.0
0.2
0.4
0.6
0.8
1.0
0
100
200
300
400
500
Vegetation Age

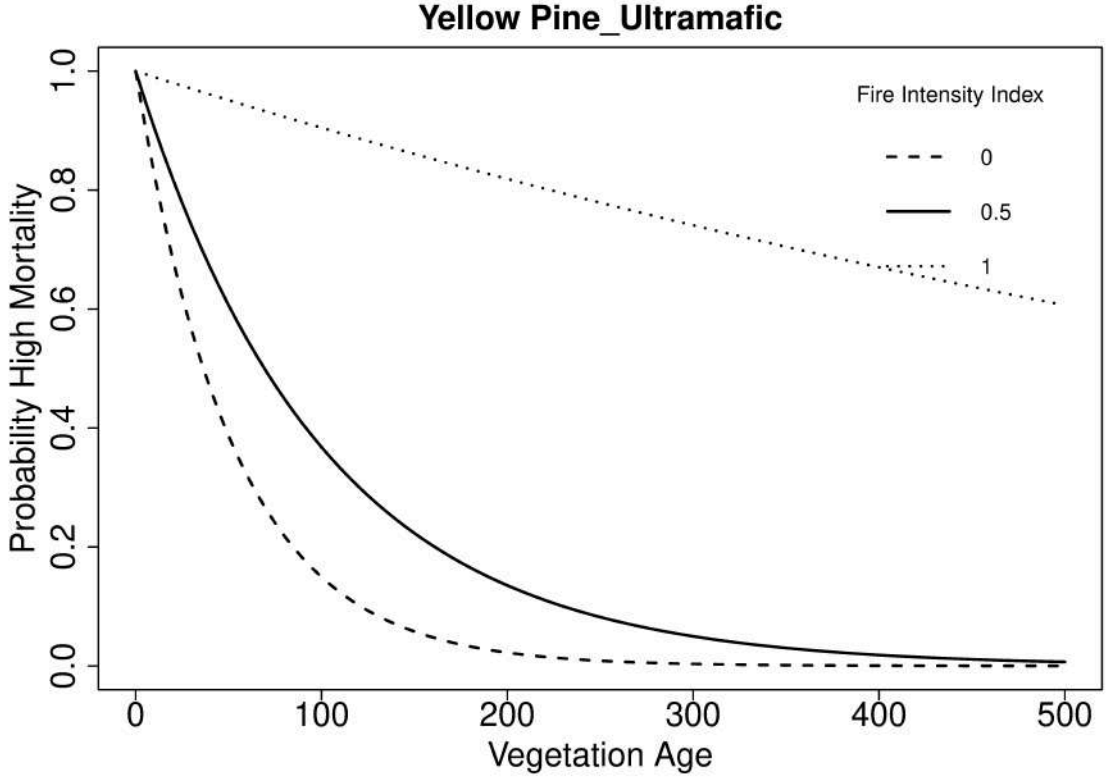
Yellow Pine_Ultramafic
Fire Intensity Index
0
0.5
1
Probability High Mortality
0.0
0.2
0.4
0.6
0.8
1.0
0
100
200
300
400
500
Vegetation Age

Appendix F - American North Fork River Landscape Historical Range of Variability and Current Landscape Departure

DRAFT Report

Kevin McGarigal Becky Estes Scott Conway Danielle Perrot
Marilyn Tierney Terri Walsh Christina Liang Laurie Perrot
Edward Smith

June, 2022

Authors

- Kevin McGarigal is a landscape ecologist with Vibrant Planet, proprietor of LandEco Consulting and retired professor of landscape ecology at the University of Massachusetts, Amherst. He received a B.S. in Forestry and Wildlife from Virginia Tech, an M.S. in Wildlife Science from Oregon State University, and a Ph.D. in Forest Science from Oregon State University.
- Becky Estes is the Central Sierra Province Ecologist (Tahoe, Eldorado, Stanislaus, and Lake Tahoe Basin Management Unit), Pacific Southwest Region, USDA Forest Service. She received a Ph.D. in Forestry from Auburn University and is a Certified Ecologist with the Ecological Society of America.
- Scott Conway is the chief resilience officer with Vibrant Planet and former forest ecologist with Pacific Southwest Region, USDA Forest Service Remote Sensing Lab and Truckee District Ranger, Tahoe National Forest, Pacific Southwest Region, USDA Forest Service. He received a B.S. in Natural Resources Management from Colorado State University.
- Danielle Perrot is an applied ecologist with Vibrant Planet. She received a B.S. in Environmental Science from University of California, Los Angeles and an M.A. in Geography from University of Colorado, Boulder.
- Marilyn Tierney is retired District Biologist for the American North Fork River Ranger District, Tahoe National Forest, Pacific Southwest Region, USDA Forest Service. She received a B.S. in Biology and an M.A. in Biology with an emphasis in Ecology and Systematics from San Francisco State University.
- Terri Walsh is silviculturist for the Tahoe National Forest, Pacific Southwest Region, USDA Forest Service. She is a certified silviculturist and studied Forestry at Cal Poly San Luis Obispo.
- Christina Liang is Forest Biologist for the Tahoe National Forest, Pacific Southwest Region, USDA Forest Service. She received a Ph.D. in Ecology from University of California, Davis.
- Laurie Perrot is Forest Environmental Coordinator for the Tahoe National Forest, Pacific Southwest Region, USDA Forest Service. She received a B.S. in forestry from the University of California, Berkeley.
- Edward Smith is Senior Forest Ecologist and Fire Manager for The Nature Conservancy in California. He received a BA in Biology from the University of California, San Diego and a MS in Forestry from Northern Arizona University.

Preface

This document[1] is an appendix to the Northern Sierra Historical Range of Variability and Current Landscape Departure General Technical Report (GTR) and includes detailed results for the American North Fork River landscape. Importantly, the background and detailed methods behind these results are presented in the GTR and not repeated here, and thus it behooves the reader to review the GTR before interpreting these results. In addition, here we present details pertaining the Landscape Disturbance-Succession Model parameterization and calibration specific to this focal landscape; all other model parameterization and calibration generalized to the Northern Sierra ecoregion is presented in the GTR. Lastly, here we present results specific to this focal landscape, but with minimal interpretation or discussion of these results or their application to management, as this was all done in the GTR. The GTR describes how to interpret the results for any of the focal landscapes and how they can be applied to management; here, we simply provide the raw results specific to this focal landscape.

Note, all datasets associated with the results for this focal landscape can be made available. Please contact Becky Estes, becky.estes@usda.gov for access.

---

[1] In accordance with Federal law and U.S. Department of Agriculture policy, this institution is prohibited from discriminating on the basis of race, color, national origin, sex, age, or disability. (Not all prohibited bases apply to all programs.) To file a complaint of discrimination, write USDA, Director, Office of Civil Rights, Room 326-W, Whitten Building, 1400 Independence Avenue, SW, Washington, DC 20250-9410 or call (202) 720-5964 (voice and TDD). USDA is an equal opportunity provider and employer.

FOCAL LANDSCAPE

The American North Fork River landscape, as we defined it, is comprised of the HUC8-level Upper American North Fork River watershed and is located on the western slopes of the Sierra Nevada Mountains in the north Sierra ecoregion (**Figure 1**). The American North Fork River landscape encompasses 249,269 ha and otherwise reflects the description of the north Sierra ecoregion presented in the GTR.

Figure 1: The American North Fork River landscape, including the middle and north forks of the American North Fork River, defined for the purpose of simulating wildfire disturbance and vegetation succession.

MODEL PARAMETERIZATION

In this section, we present only model parameters specific to this focal landscape; all north Sierra-wide parameters are discussed in the GTR. In addition, here we do not discuss in detail the methods and use of the model parameters in LDSim, as this was already done in the GTR. Please refer to the GTR for a full understanding of how the model parameters were used in LDSim.

Wildfire Climate

Climate conditions affecting wildfire disturbance during each timestep of the simulation were governed by a single global parameter, the Wildfire Climate Index based on the Palmer Modified Drought Severity Index (PMDI), in which a single coefficient was assigned to each timestep of the simulation. The final Wildfire Climate Index trajectory represented a vector of coefficients, one for each timestep, as shown in **Figure 2**.

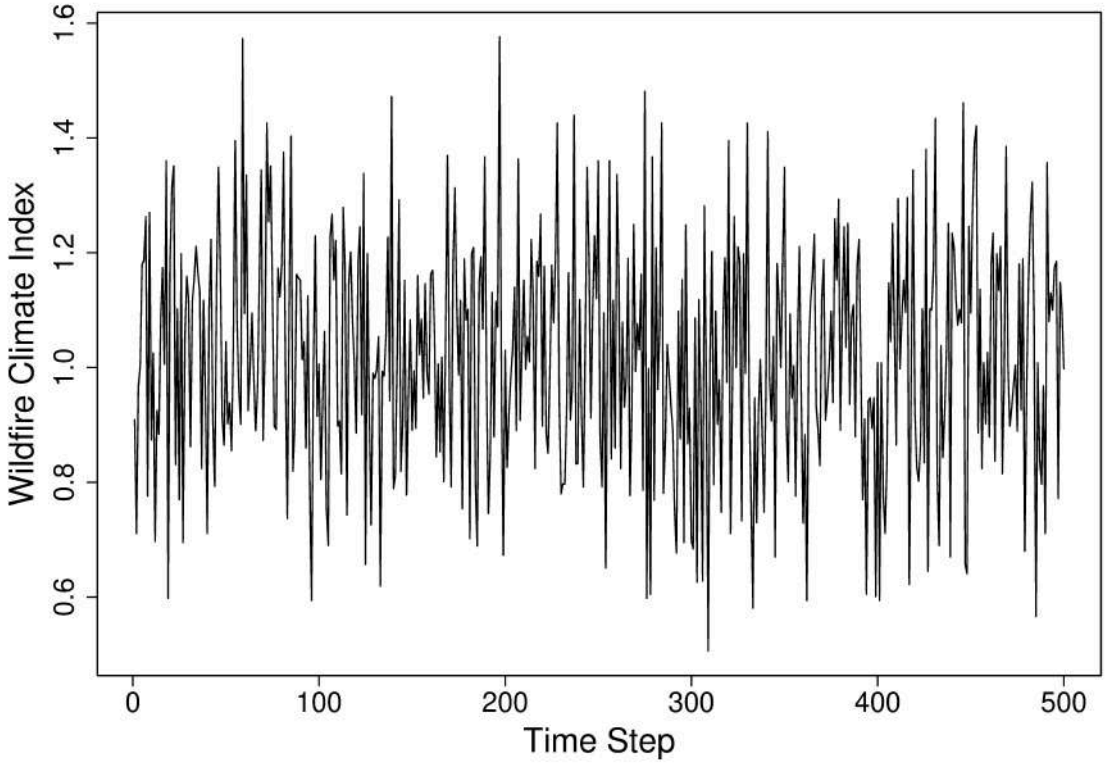

Figure 2: Wildfire Climate Index trajectory for the American North Fork River landscape corresponding to 500 5-year timesteps in the simulation. The Climate Index was based on the inverted and rescaled 5-year averaged, inverse-distance weighted mean Palmer Modified Drought Severity Index (PMDI) for the sample point locations within the north Sierra ecoregion relative to the focal landscape (American North Fork River watershed in this case). Note, here we inverted PMDI so that positive values represented drier conditions and negative values represented wetter conditions, and we also rescaled the index to have a standard deviation of 0.2 (see text for details).

Wildfire Susceptibility

Wildfire susceptibility for any given cell in each timestep was modeled as a complex function of fuels and climate, separately for each cover type, as described in the GTR. The final Wildfire Susceptibility Index on the probability scale (0-1) was used in the wildfire initiation and spread functions such that a value of 0 would prevent wildfires from initiating in or spreading into the cell, and as the value increased to 1 the probability of initiating a wildfire would increase as would the probability of a wildfire spreading to the focal cell from an adjacent burning cell, all other things being equal.

Briefly, we varied the beta coefficients of the wildfire susceptibility function for each cover type to reflect differences in reported historical mean fire return intervals among cover types - shifting the response curves left or right - as a means of calibrating the model to achieve target mean fire return intervals for each cover type (see Model Calibration). The calibrated wildfire susceptibility functions for each cover type are included in **Appendix E1**.

Wildfire Initiation

The number and spatial distribution of wildfire initiations in any given timestep was governed by: 1) a global wildfire initiation rate parameter that controlled the number of initiation attempts per unit area and

remained constant over time; 2) the current climate conditions, as represented by the Wildfire Climate Index, that varied over time but not space; and 3) the susceptibility to wildfire, as represented by the Wildfire Susceptibility Index, that varied over both space and time. We treated the global wildfire initiation rate as a calibration parameter - shifting it up or down to increase or decrease the overall amount of realized wildfire over time - and ultimately settled on a rate of 400 attempted initiations per 100,000 ha/year. Note, this parameter affected the attempted number of wildfire initiations, not the realized number of wildfires, which was considerably less due to the vegetation and climate conditions that affected whether an attempt (i.e., lightning strike) materialized into an actual wildfire. The realized number of wildfire initiations for the American North Fork River landscape is shown in **Figure 3**.

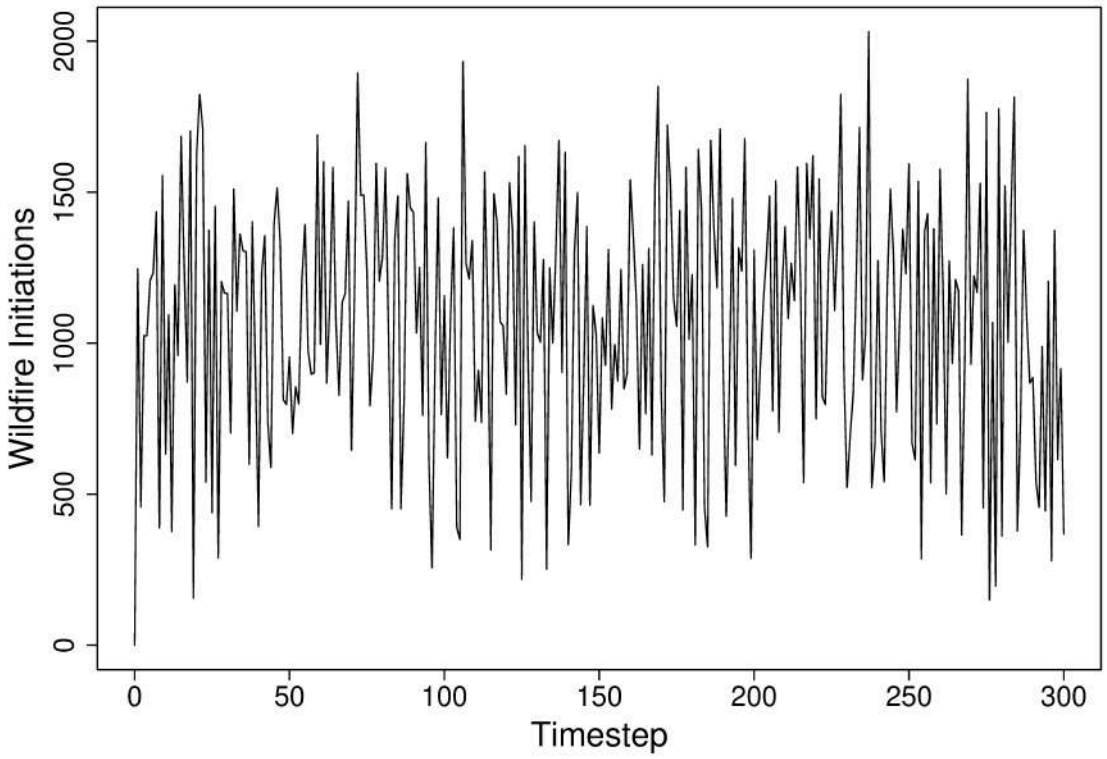

Figure 3: Realized simulated number of wildfire initiations per 5-year timestep for the American North Fork River landscape.

Wildfire Mortality

Following the termination of a wildfire event the probability of high versus low mortality of the overstory vegetation in each 5 m cell that burned was determined by two major factors combined in a complex function, as described in the GTR: 1) fire intensity, which was a function of the fuel loads in the neighborhood of the focal cell (proxied by the age of the vegetation and time since the last fire), the topographic position of the focal cell, and the climate conditions of the current timestep; and 2) the resistance of the focal cell, which was a function of the age of the vegetation in the focal cell.

Briefly, we varied the beta coefficients of the resistance component of the complex function for each cover type to reflect differences in reported historical mean fire return intervals and high mortality rates among cover types - increasing or decreasing the rate of exponential decline in high mortality with increasing vegetation ages as a function of fire intensity - as a means of calibrating the model to achieve target high mortality rates for each cover type (see Model Calibration). The calibrated wildfire mortality functions for each cover type are included in **Appendix E2**.

Succession Climate

Climate conditions affecting vegetation succession during each timestep of the simulation were governed by a single global parameter, the Succession Climate Index based on the Palmer Modified Drought Severity Index (PMDI), in which a single coefficient was assigned to each timestep of the simulation. The final Succession Climate Index trajectory represented a vector of coefficients, one for each timestep, and is shown in **Figure 4**.

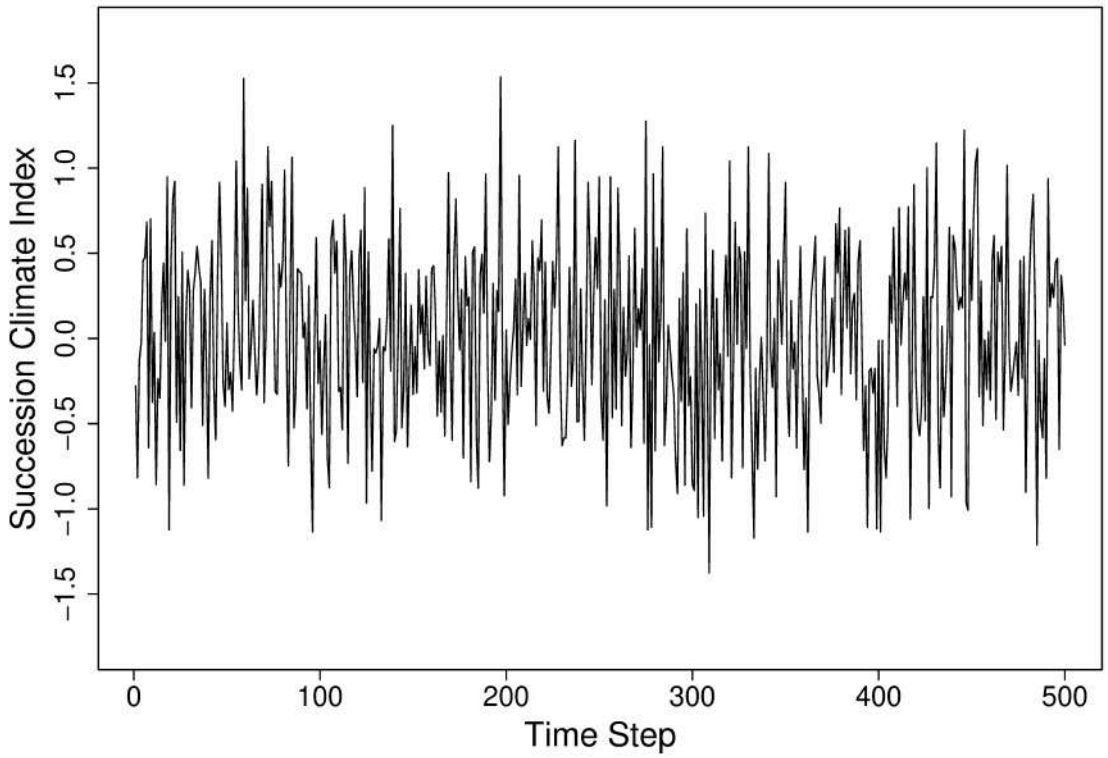

Figure 4: Succession Climate Index trajectory for the American North Fork River landscape corresponding to 500 5-year timesteps in the simulation. The Climate Index was based on the inverted 5-year averaged, inverse-distance weighted mean Palmer Modified Drought Severity Index (PMDI) for the sample point locations within the north Sierra ecoregion relative to the focal landscape (American North Fork River watershed in this case). Note, here we inverted PMDI so that positive values represented drier conditions and negative values represented wetter conditions (see text for details).

MODEL CALIBRATION

Although LDSim is a process-oriented model with individual parameters sourced either from data, literature, or expert opinion, the model outcomes reflect the complex spatio-temporal interactions of the various stochastic disturbance and succession processes. Consequently, it is necessary to calibrate the model by tuning (i.e., adjusting up or down) one or more of the model parameters to produce selected outcomes that are consistent with the data, literature and expert opinion. Importantly, in this context, we considered the parameters associated with the disturbance process to be "independent" variables and the

vegetation conditions (e.g., seral stage distribution, spatial patterns of vegetation states, etc.) to be "dependent" outcomes. Therefore, we calibrated select disturbance parameters (i.e., independent variables) to achieve the targeted disturbance regime without any attention to the vegetation response, which we treated as the dependent outcome of the disturbance regime. Importantly, we did not tune disturbance regime parameters to achieve desired vegetation outcomes. To calibrate the model, we focused on the following five disturbance regime attributes that we considered emergent properties of the disturbance regime, as discussed in detail in the GTR.

Fire Rotation Period

Fire Rotation Period (FRP) is the number of years required to burn a cumulative area equal to the extent under consideration. FRP combines fire frequency and fire size into a single integrated measure of how much fire is actually applied to a unit of ground. FRP is equivalent to the "point-specific" or "population" mean Fire Return Interval (FRI); i.e., the average number of years between fires to a single point on the ground (or cell), and is roughly equivalent to the oft reported "grand mean" FRI computed from a large sample of point-specific intervals (e.g., from a set of fire-scarred trees).

Briefly, we tuned the global wildfire initiation rate parameter, which controlled the number of wildfire initiation attempts per unit area within each timestep and remained constant over time (see Wildfire Initiation above), and two of the wildfire susceptibility coefficients (b_0 and b_1) for each cover type, which affected the susceptibility of fire initiation and spread in each cover type (see Wildfire Susceptibility above), and measured calibration success based on agreement with the pre-specified target FRP for each cover type. We set our calibration goal as within 10% of the target FRP for forested cover types with extents > 1,000 ha. We closely met our calibration target for all forest cover types with > 1,000 ha, and came acceptably close for the remaining cover type, as shown in **Table 1**.

Table 1: Target and simulated Fire Rotation Periods (FRP) for the American North Fork River landscape.

Cover type	**Area (ha)**	**Target FRP**	**Simulated FRP**	**%Deviation**
Sierra Mixed Conifer	99469	26	27	4
Mixed Evergreen	43052	45	46	2
Oak-Conifer Forest and Woodland	19864	21	22	5
Yellow Pine	19000	20	21	5
Red Fir	18868	50	52	4
Sierra Mixed Conifer_Ultramafic	2155	60	61	2
Mixed Evergreen_Ultramafic	1102	120	125	4
Yellow Pine_Ultramafic	969	40	42	5
Lodgepole Pine	434	52	56	8
Oak-Conifer Forest and Woodland_Ultramafic	429	42	43	2
Subalpine Conifer	259	296	361	22
Oak Woodland	257	26	29	12
Total	226589	30	31	3

Fire Mortality Rate

Fire mortality rate (FMR) is the percentage of burned cells that exhibit a high-mortality response (i.e., complete overstory mortality). For the purpose of model calibration, we considered the FMR only for cells in the "short", "medium" and "tall" tree developmental stages (i.e., "mature" trees) since this was the basis for specifying the target values.

Briefly, we tuned two of the wildfire mortality coefficients (b_5 and b_6) for each cover type, which affected the probability of high mortality fire as a function of age and fire intensity in each cover type (see Wildfire

Mortality above), and measured calibration success based on conformity to pre-specified fire mortality targets for each cover type. We set our calibration goal as within 10% of the targets for forested cover types with > 1,000 ha in the focal landscapes. We closely met our calibration targets for 6 of the 7 for the forested cover types with > 1,000 ha, and came acceptably close for the remaining cover type (note, even though the percent difference was rather large, the absolute difference was relatively minor), as shown in **Table 2**.

Table 2: Target and simulated Fire Mortality Rates (FMR) for the American North Fork River landscape.

Cover type	**Area (ha)**	**Target FMR**	**Simulated FMR**	**%Deviation**
Sierra Mixed Conifer	99469	7	7.45	6
Mixed Evergreen	43052	7	8.00	14
Oak-Conifer Forest and Woodland	19864	5	5.23	5
Yellow Pine	19000	5	5.07	1
Red Fir	18868	10	9.01	-10
Sierra Mixed Conifer_Ultramafic	2155	7	7.18	3
Mixed Evergreen_Ultramafic	1102	7	6.94	-1
Yellow Pine_Ultramafic	969	5	5.83	17
Lodgepole Pine	434	24	24.49	2
Oak-Conifer Forest and Woodland_Ultramafic	429	5	5.17	3
Subalpine Conifer	259	10	8.71	-13
Oak Woodland	257	6	7.43	24

Fire Size Distribution

Fire size distribution (FSD) is the percentage of realized fire sizes across bins of increasing fire size. We opted not to tune the parameters affecting the fire size distribution as these were empirically based. Instead, we treated the realized fire size distribution as an emergent outcome of the model and measured calibration success based on agreement with the pre-specified fire distribution derived from the post-settlement period of 1908 - 1979 from which we had an empirical record. We set our calibration goal as a subjective evaluation of the realized fire size distribution compared to the target fire size distribution. We met our calibration target reasonably well, as depicted in **Figure 5**.

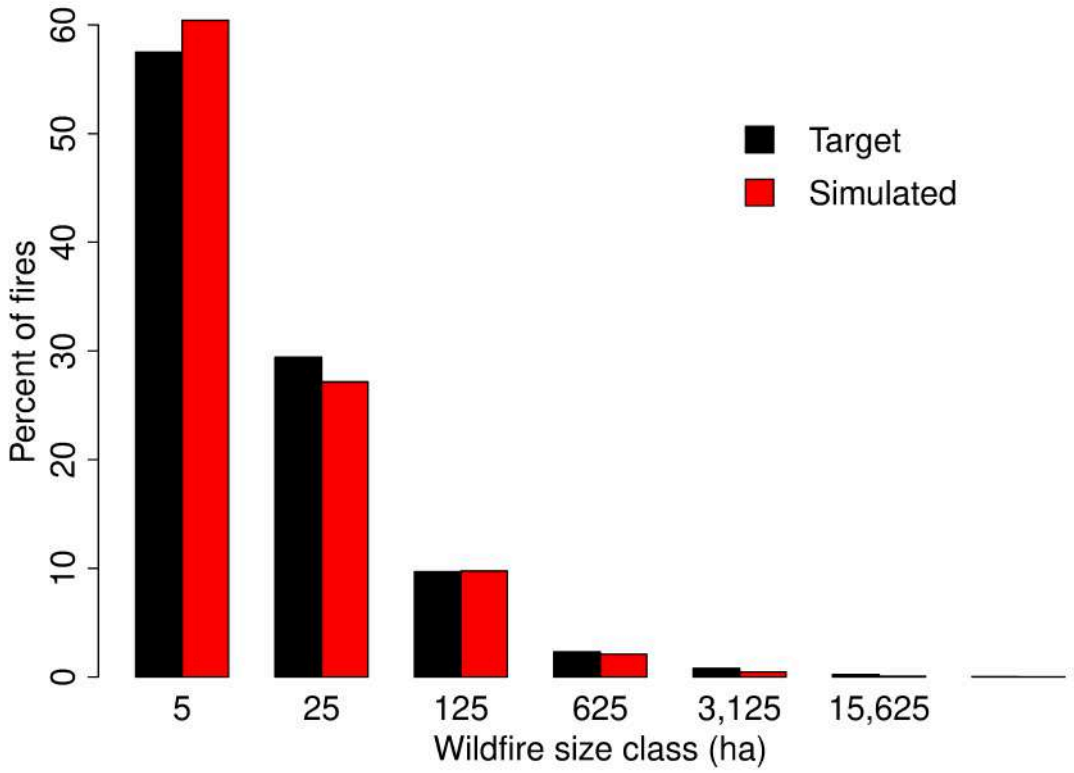

Figure 5: Target and simulated wildfire size distribution for the American North Fork River landscape.

Variability in Total Area Burned

Variability in total area burned over time is a measure of the temporal variability in the wildfire disturbance regime. We opted not to tune the primary parameter affecting the temporal variability in total area burned - the Wildfire Climate Index - as it was empirically based. Instead, we treated the variability in total area burned as an emergent outcome of the model and measured calibration success based on agreement with the observed variability in total area burned for the post-settlement period of 1908 - 1979 from which we had an empirical record. We set our calibration goal as within 10% of the target coefficient of variation (CV) in total area burned per timestep (CV = 91.8%, see GTR). We closely met our calibration target, as depicted in **Figure 6**.

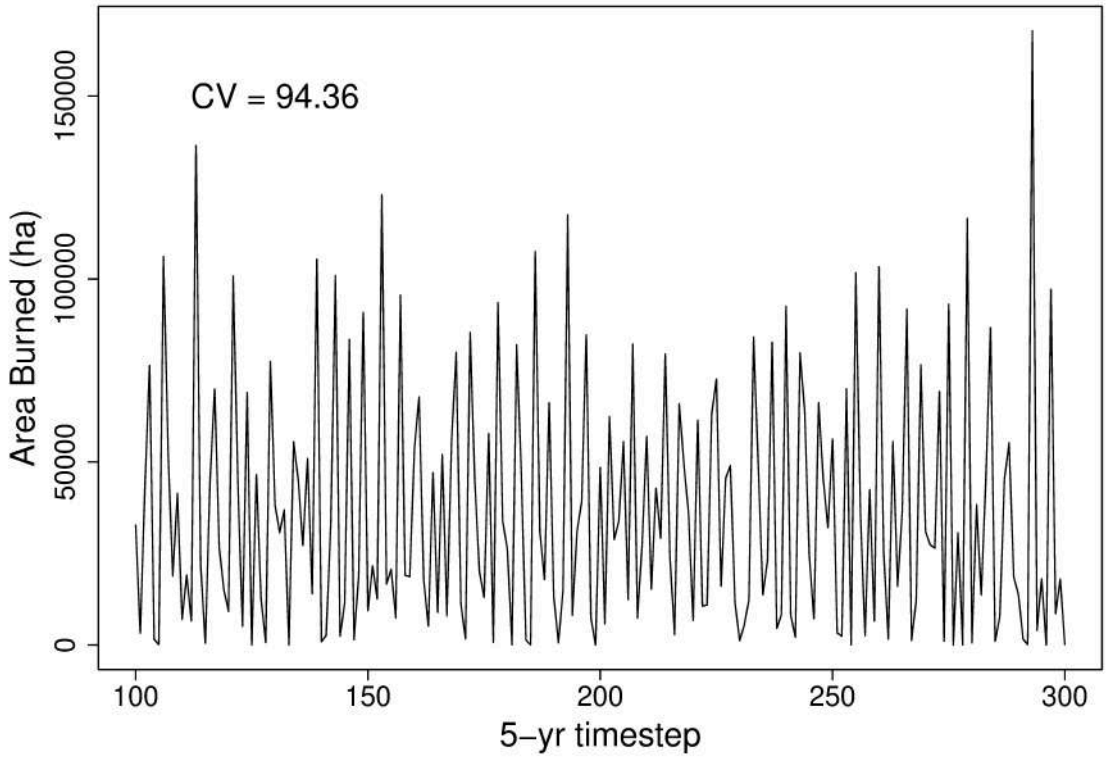

Figure 6: Total simulated area burned per 5 years in the American North Fork River landscape representing the historical reference period of 1550-1850 and the computed Coefficient of Variation (CV).

Relationship Between Total Area Burned and Climate

The relationship between total area burned and climate is a measure of the degree to which the simulated total area burned is affected by variability in the specified Wildfire Climate Index. We opted not to tune the Wildfire Climate Index, in particular, or any parameter associated with the wildfire disturbance process with regards to this calibration metric. Instead, we treated the observed relationship between total area burned and the climate index as an emergent outcome of the model and measured calibration success based on agreement with the strength of the relationship for the post-settlement period of 1908 - 1979 from which we had an empirical record. We set our calibration goal as within 10% of the target coefficient of determination (R2) in the fit of a linear regression to the target data (R2 = 0.25, see GTR). We did not met this calibration target very well, as we simulated a more closely fitting relationship between total area burned and the climate index and a relationship that was distinctly more non-linear compared to observed post-settlement observations, as depicted in **Figure 7**.

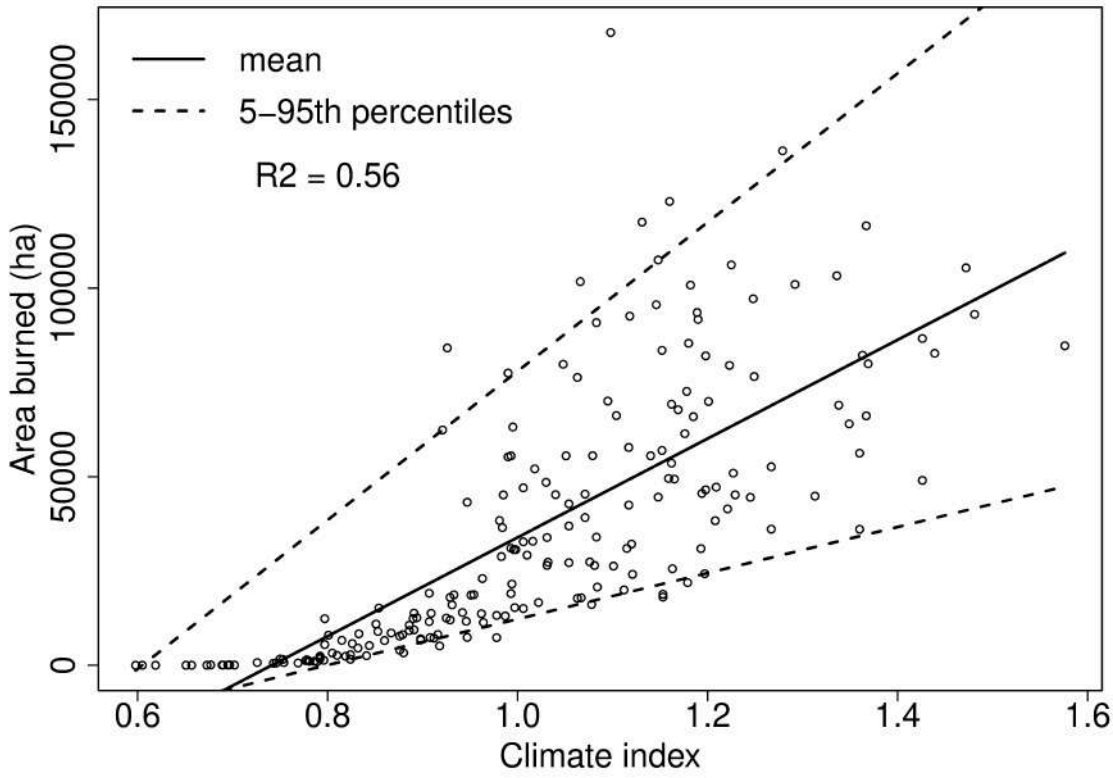

Figure 7: Scatterplot of the modified wildfire Climate Index based on the modified Palmer Drought Severity Index (see text for details) and the log of simulated total area burned per 5 years in the American North Fork River landscape representing the historical reference period of 1550-1850, and the fitted linear regression for the mean and 5-95th quantiles (see text for details) along with the Coefficient of Determination (R2) of the fit.

HISTORICAL RANGE OF VARIABILITY and CURRENT DEPARTURE

Biophysical Classes and Units

To summarize HRV and current departure in landscape structure at the Site and subbasin levels, we subdivided the landscape into a set of Biophysical Classes (BPCs), as described in detail in the GTR. Briefly, we indexed site productivity based on the cumulative tree biomass generated over the course of the simulation, after model equilibration, and then modeled tree biomass as a function of 10 geophysical variables using a Random Forest analytical framework, and lastly classified predicted Biomass into 4 equal-area classes based on quartiles of the data, plus a zero class for all non-forest cells. The final BPC layer included 4 classes ranging from the least productive to most productive sites, plus a non-forest class, as depicted in **Figure 8**.

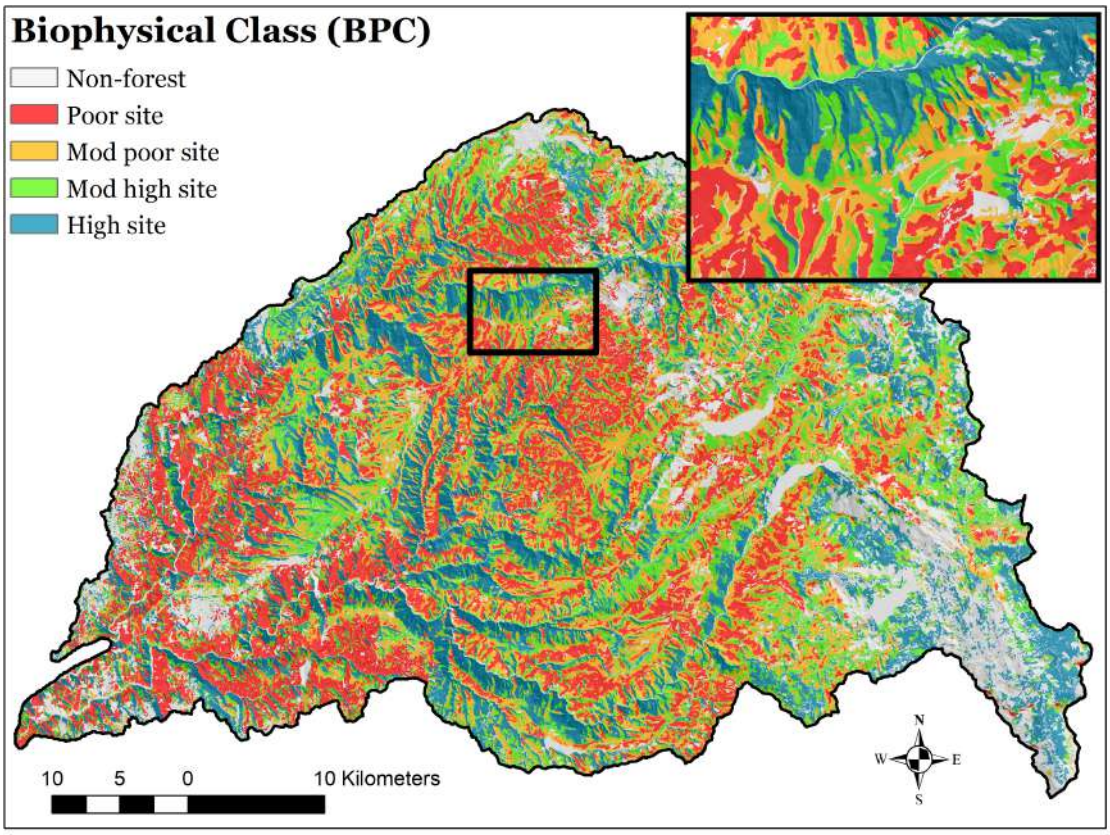

Figure 8: Biophysical Classes (BPCs) based on quartiles of predicted Biomass derived from a Random Forest model to predict Biomass (i.e., simulated cumulative tree height) from 10 biophysical variables. The Random Forest model explained ~70% of the variation in Biomass under simulated historical dynamic equilibrium conditions in the American North Fork River landscape.

The final BPCs were distinguishable on the basis of the 10 geophysical variables and cover type, although there was considerable overlap among BPCs in each of the variables, as described below for a select set of the variables.

- *Cover Type* - The distribution of each cover type among BPCs (as a percentage of the cover type), ordered roughly from low to high elevation distributions, is given in **Table 3**. Most forest types were well distributed among BPCs, suggesting that cover type was generally not a good discriminator of BPCs. However, there were some notable exceptions. For example, Lodgepole Pine and Red Fir were essentially absent from Low productivity sites; whereas, Yellow Pine was disproportionately found on lower productivity sites as were all of the ultra-mafic cover types. The most abundant cover type, Sierra Mixed Conifer, was equally distributed across site productivity classes.

  Table 3: Percentage of each cover type in each Biophysical Class (BPC) for the American North Fork River landscape.

Cover type	Area (ha)	Low	ModLow	ModHigh	High
Forest	296	50.48	13.27	12.59	23.65
Oak Woodland	208	48.15	16.49	18.38	16.98
Yellow Pine	18534	37.45	30.76	20.77	11.02
Yellow Pine_Ultramafic	963	53.52	25.52	14.31	6.65
Oak-Conifer Forest and Woodland	19050	34.80	20.10	19.69	25.41
Oak-Conifer Forest and Woodland_Ultramafic	423	47.09	18.80	12.30	21.81
Mixed Evergreen	41938	26.21	21.79	21.10	30.91
Mixed Evergreen_Ultramafic	1093	44.83	17.67	14.31	23.18
Sierra Mixed Conifer	98641	25.84	28.31	26.00	19.84
Sierra Mixed Conifer_Ultramafic	2139	33.73	26.93	22.20	17.14
Lodgepole Pine	420	3.44	10.86	51.03	34.66
Red Fir	18764	3.27	13.30	31.95	51.47
Subalpine Conifer	252	26.68	20.34	25.90	27.08

- *Mesic Index* - The distribution of the Mesic Index for each BPC (given as quantiles of the index) is given in **Table 4**. As expected, the Mesic Index distribution increased as the site productivity class increased from Low to High, but with considerable overlap in distributions between adjacent BPC classes. Despite the strong overlap, the BPC classes represented a gradient in expected site moisture, with the Low site class representing the driest sites and the High site class representing the wettest sites.

  Table 4: Distribution of the Mesic Index in each Biophysical Class (BPC), given as quantiles for the American North Fork River landscape.

BPC	2.5%	25%	50%	75%	97.5%
Low	17	32	41	48	62
ModLow	28	45	51	58	73
ModHigh	34	50	57	64	77
High	41	56	64	72	86

- *Topographic Position* - The distribution of the Topographic Position Index for each BPC (given as quantiles of the index) is given in **Table 5**. As expected, the Topographic Position Index distribution decreased as the site productivity class increased from Low to High, but with considerable overlap in distributions between adjacent BPC classes. The High site productivity class showed the strongest gradient in TPI, with a strong prevalence for lower topographic positions. Despite the strong overlap, the BPC classes represented a clear gradient in topographic position, with the Low site class found more commonly on the upper slopes and ridgetops and the High site class found more commonly on the lower slopes and valley bottoms.

  Table 5: Distribution of the Topographic Position Index each each Biophysical Class (BPC), given as quantiles for the American North Fork River landscape.

- *Aspect* - The distribution of aspect classes among BPCs (as a percentage of the BPC) is given in **Table 6**. Not surprisingly, each BPC class was distributed across all aspect classes, but still exhibited a pronounced orientation, with the Low site class disproportionately occupying southwesterly aspects and the High site class disproportionately occupying northeasterly aspects.

BPC	2.5%	25%	50%	75%	97.5%
Low	14	46	57	68	98
ModLow	15	41	50	59	83
ModHigh	7	39	48	58	83
High	0	31	43	53	80

Table 6: Percentage of each Biophysical Class (BPC) in each aspect class for the American North Fork River landscape.

Aspect	N	NE	E	SE	S	SW	W	NW	Flat
Low	2.63	0.97	1.82	9.93	19.24	23.73	19.01	20.64	2.03
ModLow	6.83	2.23	3.55	15.22	15.96	16.68	11.54	23.62	4.36
ModHigh	13.45	8.39	10.99	18.05	9.12	9.38	6.56	19.14	4.92
High	17.96	23.09	21.15	11.21	3.42	4.35	3.46	12.13	3.22

Fire Return Interval and Departure

Mean point-specific Fire Return Interval (FRI) represents the average number of years between fire events at the 5 m cell level. We interpreted the observed mean FRI after model equilibration (N = 200 timesteps) at the cell level as a single integrated (albeit not comprehensive) summary of the historical wildfire disturbance regime. The historical mean FRI varied from < 15 years to > 300 years across the landscape, with evident influences of both cover type and terrain (**Figure 9**).

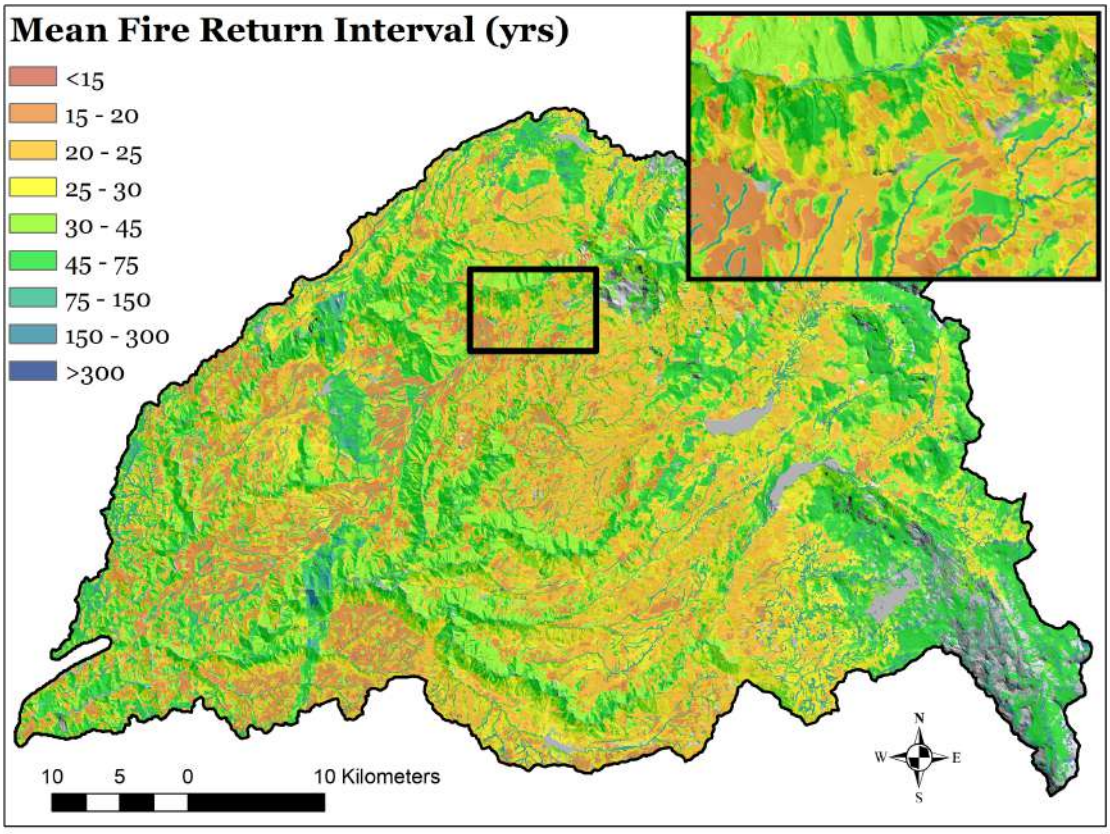

Figure 9: Simulated Fire Return Interval (FRI) (yrs) at the 5 m cell level for the American North Fork River landscape.

In addition, the historical mean FRI varied among BPCs as expected (**Table 7**). Specifically, the median FRI increased steadily from 24 to 42 years with increasing site productivity; i.e., from Low to High BPC. Low productivity sites that occurred disproportionately on upper slopes and ridgetops and southwesterly aspects were warmer and drier and thus more susceptible to wildfire, despite having less fuel build-up over time. Conversely, High productivity sites that occurred disproportionately on lower slopes and valley bottoms and on northeasterly aspects were cooler and wetter and thus less susceptible to wildfire, despite having more fuel build-up over time. The relatively short median FRIs across all sites indicates that historically wildfires typically occurred frequently enough to keep surface and ladder fuel loads low enough to reduce the occurrence of high-severity wildfire.

Table 7: Range of variability (given as quantiles) in the mean fire return interval (FRI) by Biophysical Class (BPC) for the American North Fork River landscape.

BPC	HRV2.5%	HRV25%	HRV50%	HRV75%	HRV97.5%
Low	17	22	24	36	64
ModLow	18	24	26	40	87
ModHigh	19	26	30	46	114
High	21	29	42	53	122

These results also indicate that the HRV in mean FRI varied several-fold across sites within each BPC. For example, on High productivity sites FRI varied roughly six-fold between 21-122 years across sites. The wide range of variation in FRI within BPCs indicates that wildfire risk varied markedly across sites even within a single BPC and, consequently, that FRI is only loosely correlated with predicted cumulative tree biomass. For example, sites classified as having high long-term productivity under historical dynamic equilibrium conditions could have FRIs as short as 21 years (or shorter for the extremes) or as long as 122 years (or longer for the extremes) depending on local topographic and vegetative conditions and chance. This is visually evident in the map of mean FRI for the High site BPC (**Figure 10**).

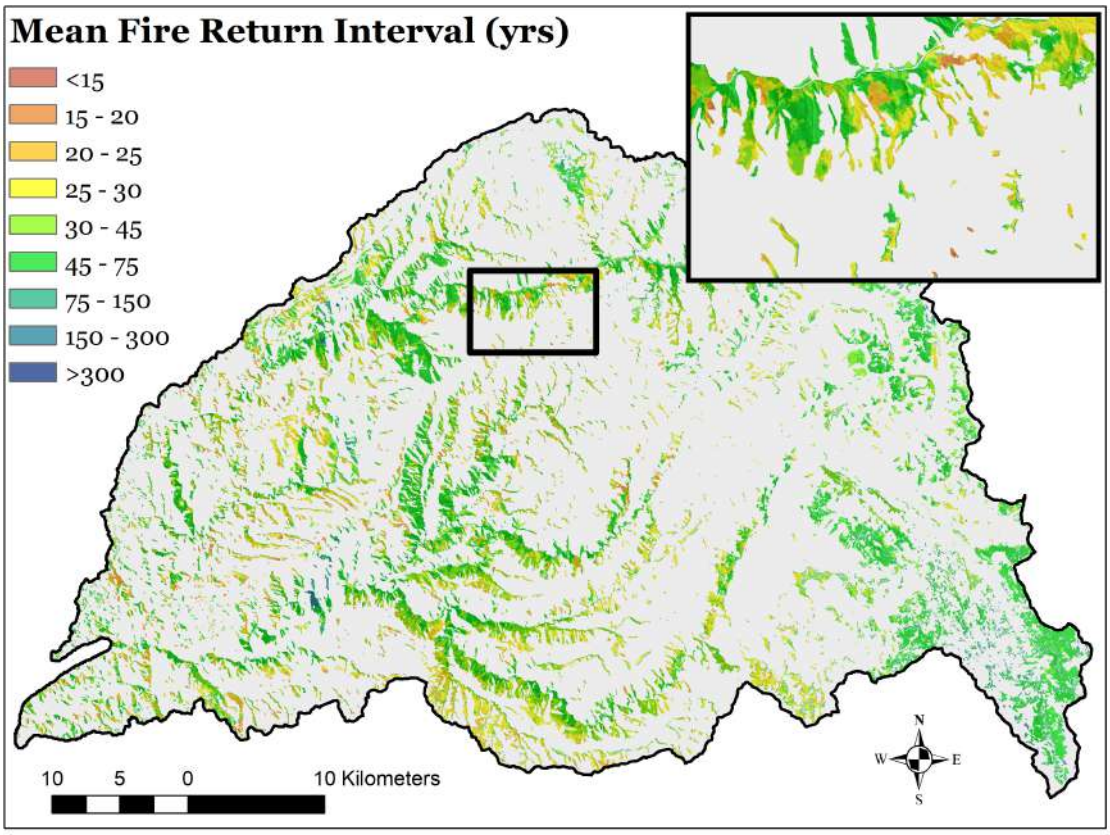

Figure 10: Simulated Fire Return Interval (FRI) (yrs) at the 5 m cell level on High productivity sites (Biophysical Class = 4) in the American North Fork River landscape.

Fire Return Interval Departure (FRID) represents the percentage deviation of the contemporary (post-settlement) mean point-specific FRI from the mean point-specific FRI under historical (i.e., pre-settlement) dynamic equilibrium conditions. Briefly, FRID measures the degree, in percent, to which contemporary fires (i.e., since 1909) are burning at frequencies similar to the frequencies that occurred prior to significant Euro-American settlement, as simulated (**Figure 11**). Positive departure indicates that the contemporary fire frequency is less than the historical fire frequency.

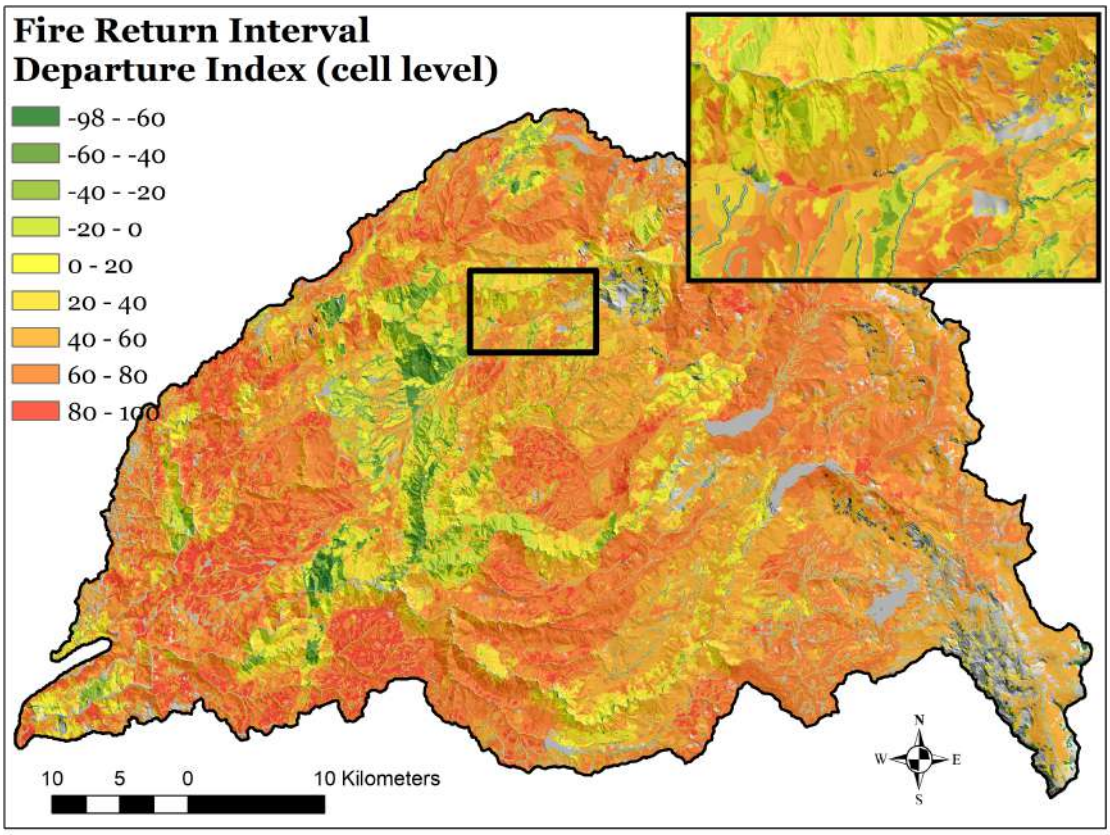

Figure 11: Fire Return Interval Departure (FRID) at the 5 m cell level in the American North Fork River landscape, representing the percent to which contemporary fires (i.e., since 1909) are burning at frequencies similar to the frequencies that occurred prior to significant Euro-American settlement, as simulated.

In addition to the cell-level map of FRID, we also summarized the mean FRID for each GPU to include in the Stewardship Atlas as a means of prioritizing units for treatment with fire (**Figure 12**).

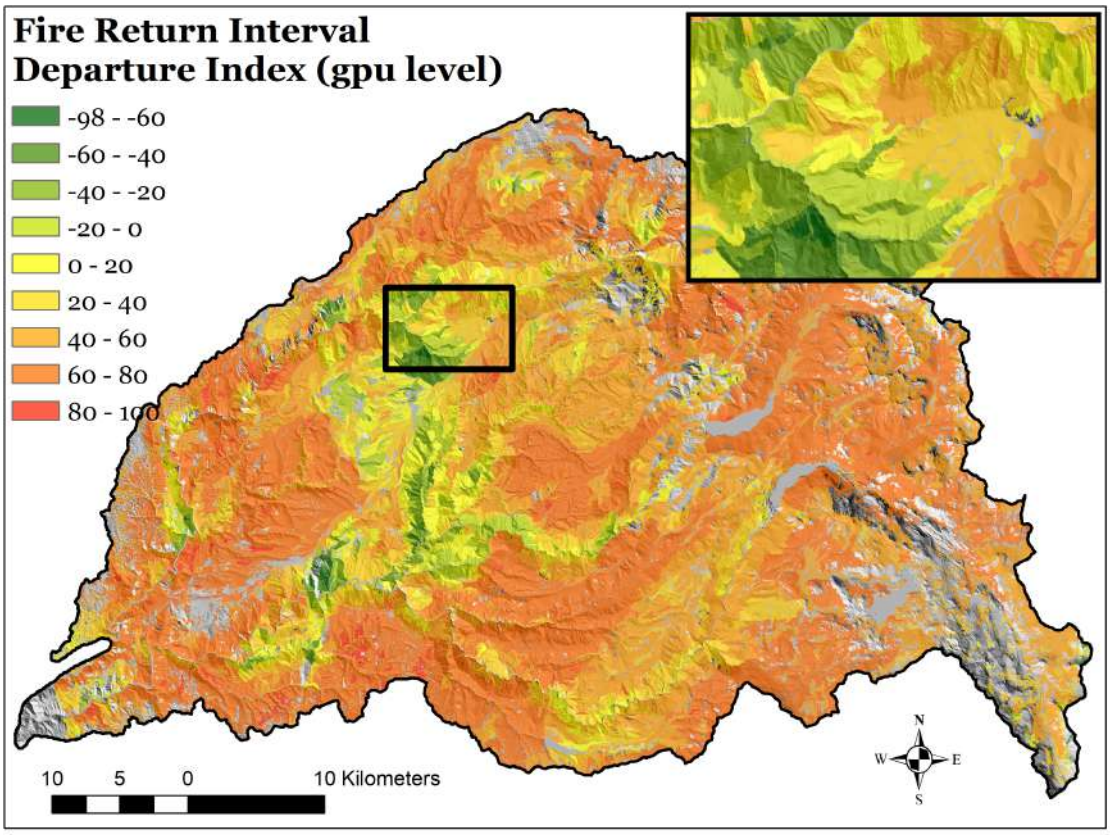

Figure 12: Geophysical Unit-level Fire Return Interval Departure (FRID) for the American North Fork River landscape, representing the average 5 m cell value in the percent to which contemporary fires (i.e., since 1909) are burning at frequencies similar to the frequencies that occurred prior to significant Euro-American settlement, as simulated.

Vegtation Persistence

We defined vegetation persistence as the likelihood of persisting in either an early- or late-seral condition at the 5 m cell level. We interpreted the observed mean FRI of high-mortality wildfires after model equilibration (N = 200 timesteps) at the cell level as a proxy for vegetation persistence, under the assumption that locations with shorter high-mortality FRIs would likely persist longer in early-seral stages and, conversely, locations with longer high-mortality FRIs would likely persist longer in late-seral stages.

Figure 13 depicts several areas with relatively long high-mortality FRIs (dark blue areas in the map) and these are sites that have a high likelihood of supporting late-seral vegetation under a natural disturbance regime. Conversely, the map depicts several areas with relatively short high-mortality FRIs (yellow and orange areas in the map) and these are sites that have a high likelihood of supporting early-seral vegetation much of the time under a natural disturbance regime. Accordingly, management objectives for these areas could be designed to capitalize on these focal areas. For example, establishing treatment objectives to maintain and enhance late-seral conditions for old forest associated species in areas with a lower likelihood of high-mortality wildfire (i.e., longer FRI) would be logical.

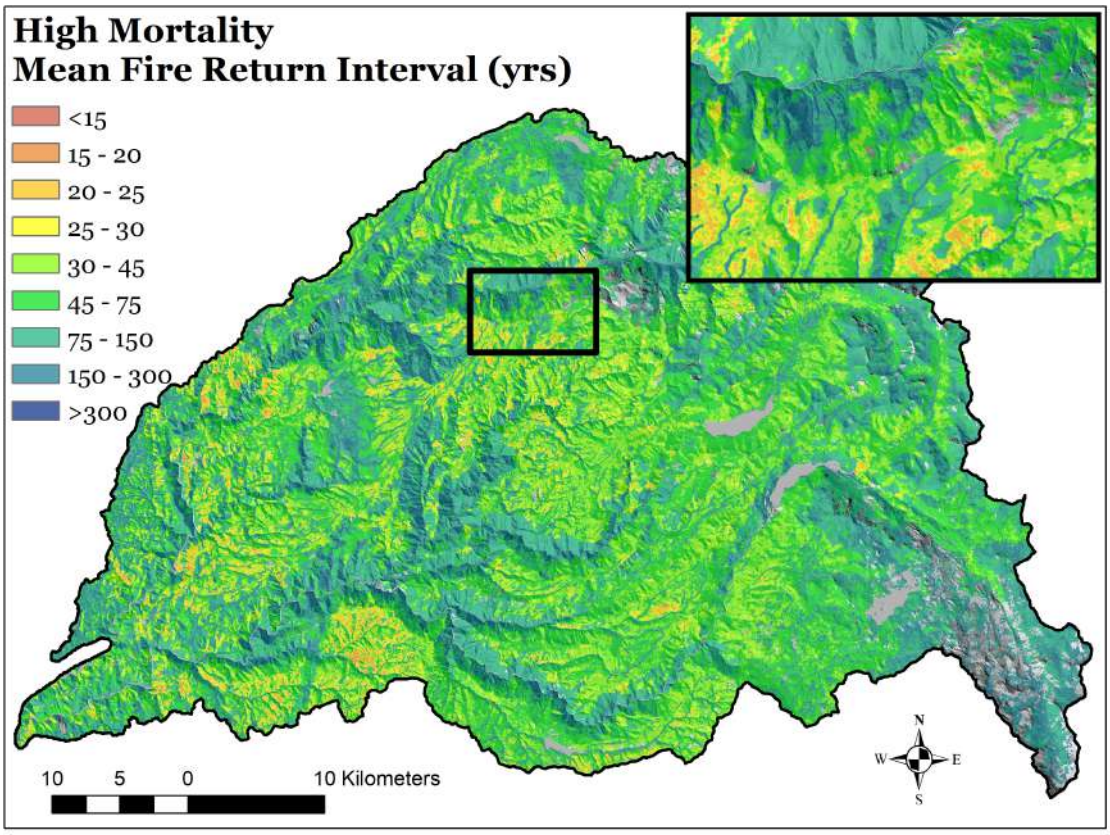

Figure 13: Simulated high-mortality Fire Return Interval (FRI) (yrs) at the 5 m cell level in the American North Fork River landscape.

Site Level HRV and Departure

The results presented in this section address landscape metrics quantified at the "Site" level. Recall from the GTR that we defined a Site as a 40-m radius window around each focal cell. Here, each Site falls within a single BPC based on the location of the focal cell and has a single value computed for each landscape metric for each point in time (i.e., snapshot). HRV represents the variation in the landscape metric across Sites and over time under historical dynamic equilibrium conditions. Further recall that the current landscape also has a range of values across Sites (CRV), rather than a single value. Thus, a comparison of the HRV and CRV distributions depicts the degree to which CRV deviates from HRV (i.e., current departure). It is important to remember that Site-level departure reflects the deviation between the CRV across Sites within the focal landscape and the HRV across Sites and over time within the focal landscape. Thus, departure for a Site is not based on a comparison of the current Site condition to its own HRV (as is the case with GPU and subbasin departure, see below); rather it is the distribution of current Site conditions across the entire landscape compared to the historical distribution across Sites that forms the basis for Site-level departure.

Recall from the GTR that we used a parsimonious suite of landscape metrics that we deemed meaningful for estimating departure at the Site-level across the focal landscape and appropriate given the available data, and computed departure as described in the GTR (and not repeated here), including the following metrics:

Developmental Stage

Developmental stage at the Site level was based on discrete stages of canopy height development. We quantified the composition of forest developmental stages at the Site level based on the percentage of the forested portion of the Site in each developmental stage. The HRV and CRV in Developmental Stage composition by BPC at the Site level is given in **Table 8** and depicted in **Figure 14**.

Table 8: Range of variability (given as quantiles) in each developmental stage class across sites (40-m radius window centered on each focal cell) by Biophysical Class (BPC) for the current range of variability (CRV) and the historical range of variability (HRV) for the American North Fork River landscape.

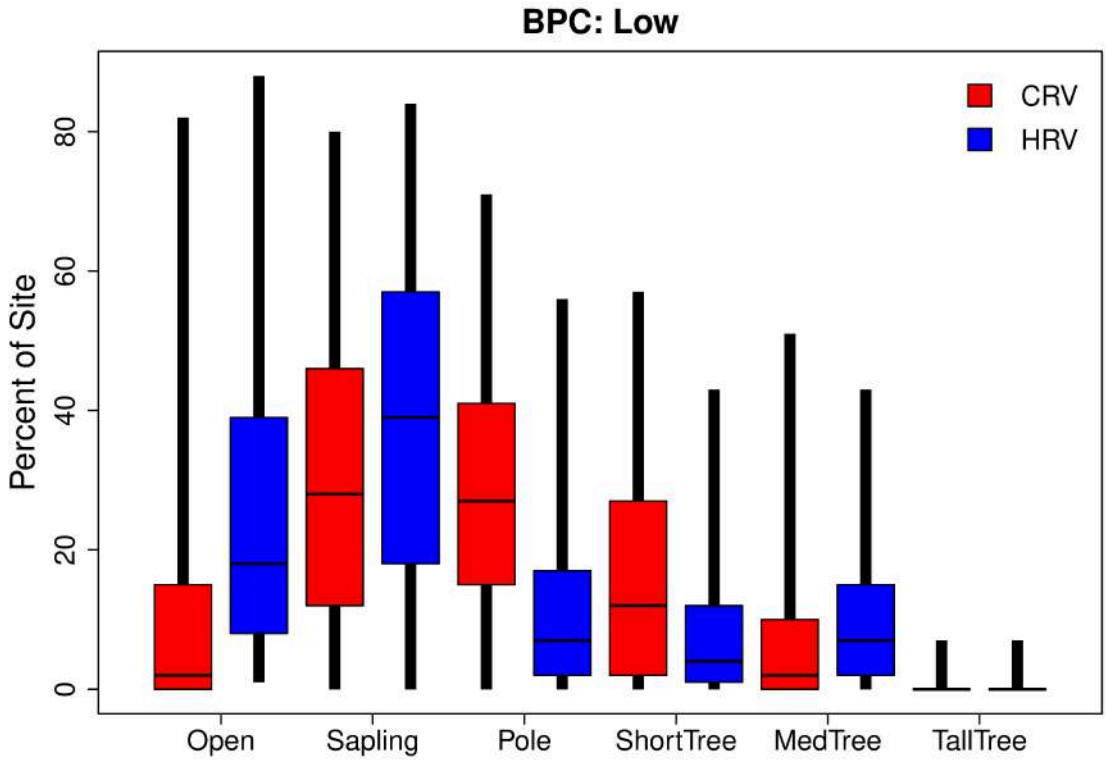

BPC	Class	Scenario	HRV 2.5%	HRV 25%	HRV 50%	HRV 75%	HRV 97.5%
Low	Open	CRV	0	0	2	15	82
Low	Open	HRV	1	8	18	39	88
Low	Sapling	CRV	0	12	28	46	80
Low	Sapling	HRV	0	18	39	57	84
Low	Pole	CRV	0	15	27	41	71
Low	Pole	HRV	0	2	7	17	56
Low	ShortTree	CRV	0	2	12	27	57
Low	ShortTree	HRV	0	1	4	12	43
Low	MedTree	CRV	0	0	2	10	51
Low	MedTree	HRV	0	2	7	15	43
Low	TallTree	CRV	0	0	0	0	7
Low	TallTree	HRV	0	0	0	0	7
ModLow	Open	CRV	0	0	3	16	84
ModLow	Open	HRV	1	6	12	26	80
ModLow	Sapling	CRV	0	11	27	44	76
ModLow	Sapling	HRV	0	16	34	52	80
ModLow	Pole	CRV	0	15	26	37	68
ModLow	Pole	HRV	0	3	9	20	59
ModLow	ShortTree	CRV	0	4	14	27	55
ModLow	ShortTree	HRV	0	2	5	13	47
ModLow	MedTree	CRV	0	0	3	14	53
ModLow	MedTree	HRV	0	5	13	23	52
ModLow	TallTree	CRV	0	0	0	0	11
ModLow	TallTree	HRV	0	0	1	3	17
ModHigh	Open	CRV	0	0	3	15	78
ModHigh	Open	HRV	1	5	9	19	71
ModHigh	Sapling	CRV	0	10	27	43	75
ModHigh	Sapling	HRV	0	11	28	46	76
ModHigh	Pole	CRV	0	15	25	36	66
ModHigh	Pole	HRV	0	4	10	22	59
ModHigh	ShortTree	CRV	0	5	15	27	57
ModHigh	ShortTree	HRV	0	2	7	15	47
ModHigh	MedTree	CRV	0	0	4	17	56
ModHigh	MedTree	HRV	1	8	17	29	57
ModHigh	TallTree	CRV	0	0	0	0	14
ModHigh	TallTree	HRV	0	0	3	7	25
High	Open	CRV	0	0	1	10	68
High	Open	HRV	1	4	7	13	60
High	Sapling	CRV	0	4	22	41	75
High	Sapling	HRV	0	4	18	36	69
High	Pole	CRV	1	14	24	37	70
High	Pole	HRV	0	4	11	23	57
High	ShortTree	CRV	0	6	17	30	61
High	ShortTree	HRV	0	3	7	15	44
High	MedTree	CRV	0	0	6	23	62
High	MedTree	HRV	1	12	22	34	61
High	TallTree	CRV	0	0	0	1	22
High	TallTree	HRV	0	3	8	17	43

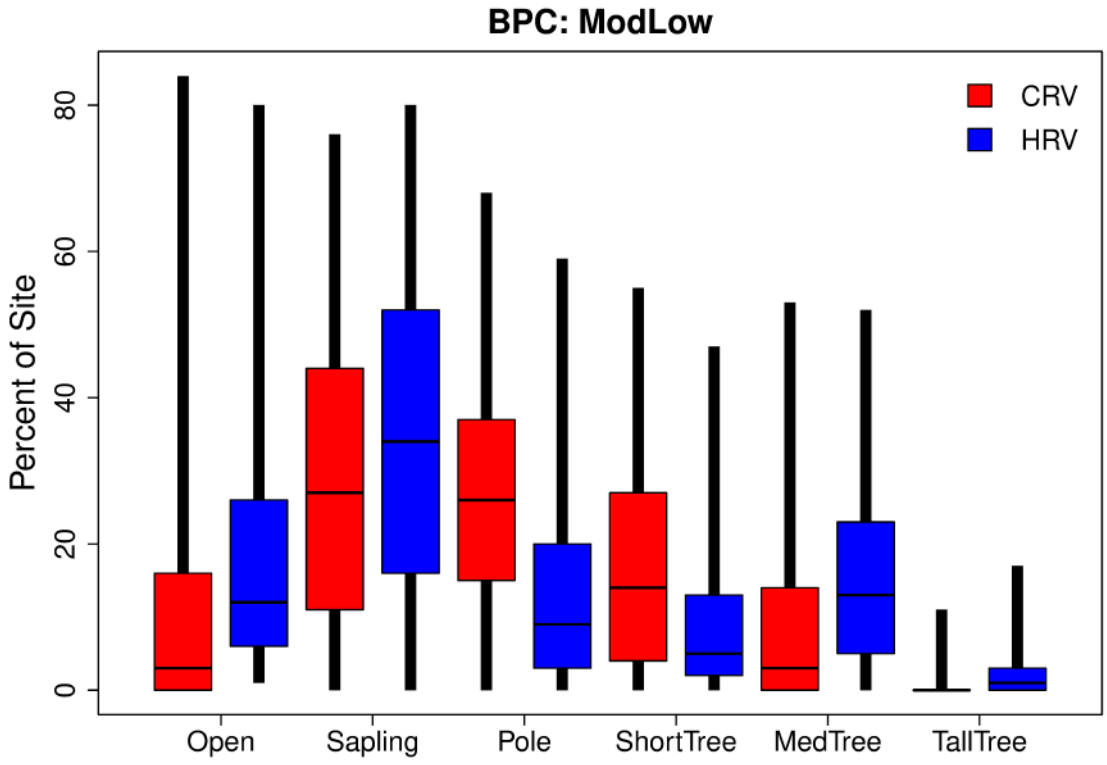
BPC: ModLow
CRV
HRV
Percent of Site
0
20
40
60
80
Open
Sapling
Pole
ShortTree
MedTree
TallTree

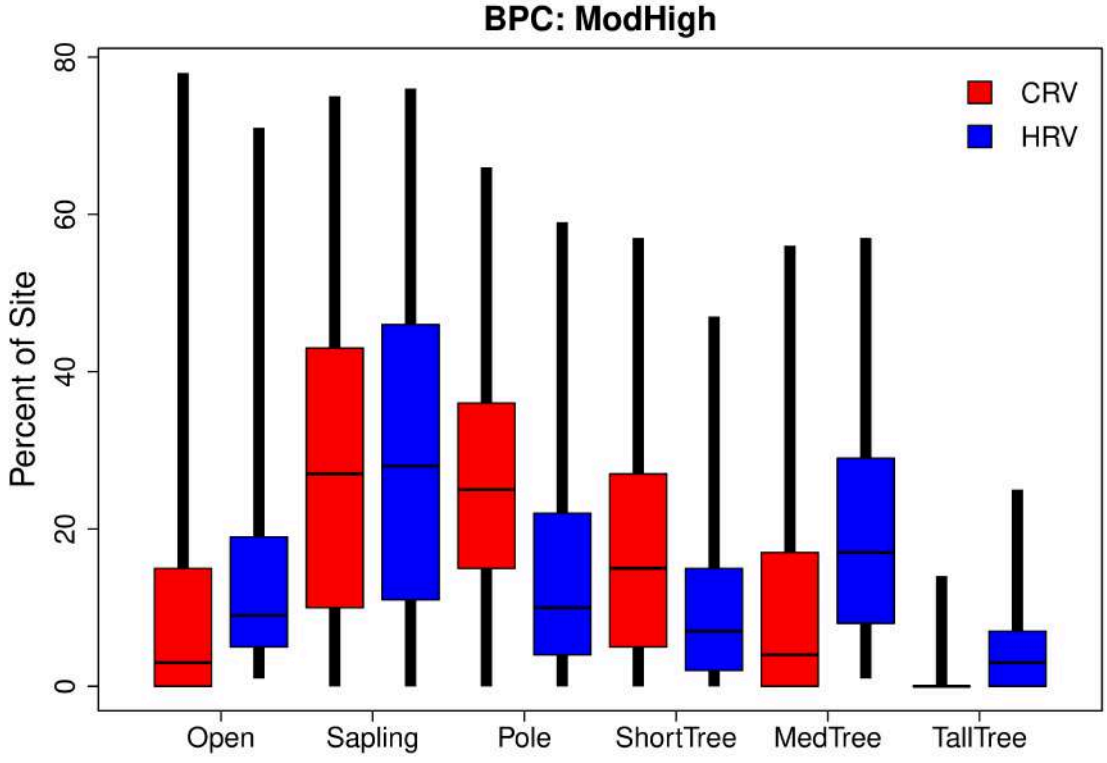
BPC: ModHigh
CRV
HRV
Percent of Site
0
20
40
60
80
Open
Sapling
Pole
ShortTree
MedTree
TallTree

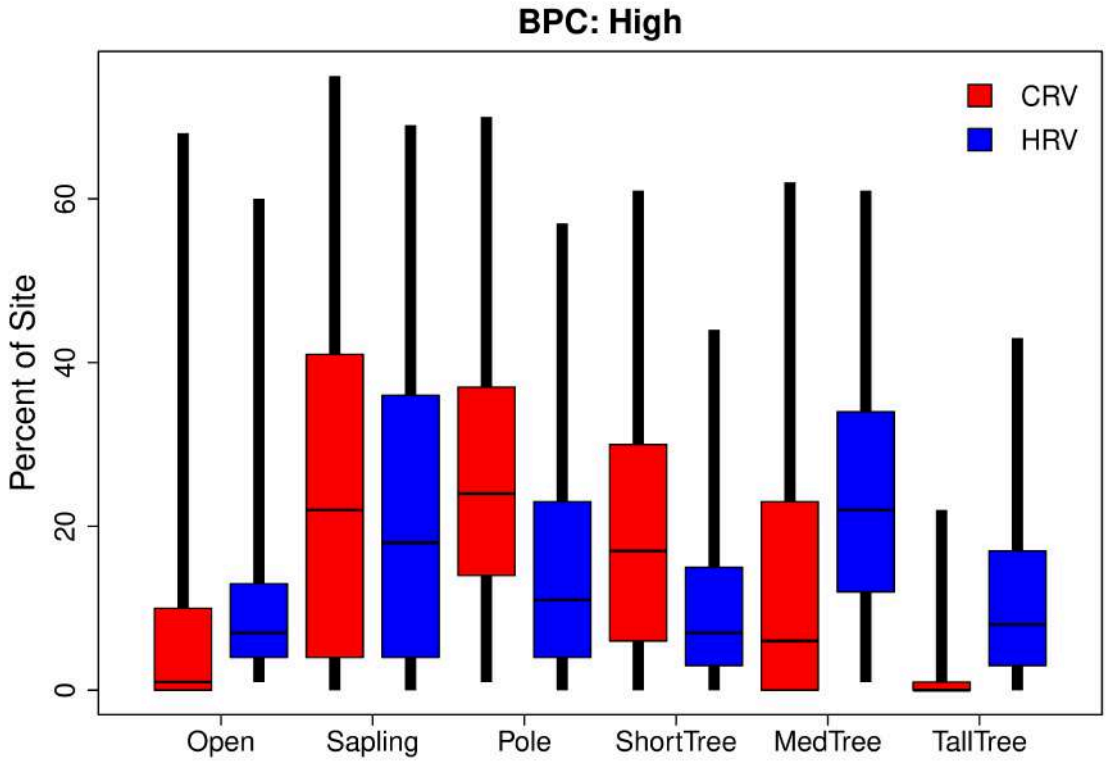

Figure 14: Historical Range of Variability (HRV) and Current range of variabiilty (CRV) among Sites (i.e., 40-m radius window) in the percent of forest in each developmental stage within the Low, Moderately Low, Moderately High and High site productivity Biophysical Classes (BPCs) in the American North Fork River landscape. Box = 25-50 percentiles; whiskers = 2.5-97.5 percentiles

Recall that current departure in the Site-level metrics provides a basis for prioritizing management at the unit level. For example, given the results above, to reduce the current departure in developmental stage composition on High productivity Sites, management could prioritize treatments that produce units with a greater percentage of Open areas intermixed with Tall trees to shift the overall developmental stage distribution across the landscape to be more aligned with the HRV distribution. The same priorities could be given to Low productivity Sites, although here the emphasis would be predominantly on increasing the proportion of Sites with a greater proportion of Open areas. Of course, aside from controlling the percentage in Open, there is only limited ability to actively manage developmental stage succession (i.e., height growth). Indeed, much of the succession required to shift the current distribution towards the later stages of development simply requires time (e.g., to allow trees in the Pole and Short Tree stages to grow into the Medium and Tall Tree stages). However, managing surface and ladder fuels to inhibit high severity wildfire and retaining current taller trees may be an effective strategy to gradually shift the CRV towards better alignment with HRV with respect to the later developmental stages.

Tree Size (QMD)

Tree Size at the Site level was based on the Quadratic Mean Diameter (QMD) of established trees within a 40-m radius of the focal cell. Recall that QMD was based on only the cells with established trees in the window. Thus, if there was a single cell with an established tree in the window, then QMD was based on that single tree and equaled the tree's diameter at breast height (DBH). Accordingly, QMD can be quite high even in relatively open areas if the few neighborhood trees are large in diameter. The HRV and CRV in Tree Size composition at the Site level by BPC is given in **Table 9** and depicted in **Figure 15**.

BPC	Scenario	HRV 2.5%	HRV 25%	HRV 50%	HRV 75%	HRV 97.5%
Low	CRV	1	4	6	9	17
Low	HRV	3	8	11	14	22
ModLow	CRV	1	5	8	11	20
ModLow	HRV	5	11	14	17	24
ModHigh	CRV	2	6	9	13	22
ModHigh	HRV	7	13	16	20	26
High	CRV	2	7	11	16	28
High	HRV	10	17	20	24	32

Table 9: Range of variability (given as quantiles) in tree size (quadratic mean diameter) across Sites (40-m radius window centered on each focal cell) by Biophysical Class (BPC) for the current range of variability (CRV) and the historical range of variability (HRV) for the American North Fork River landscape.

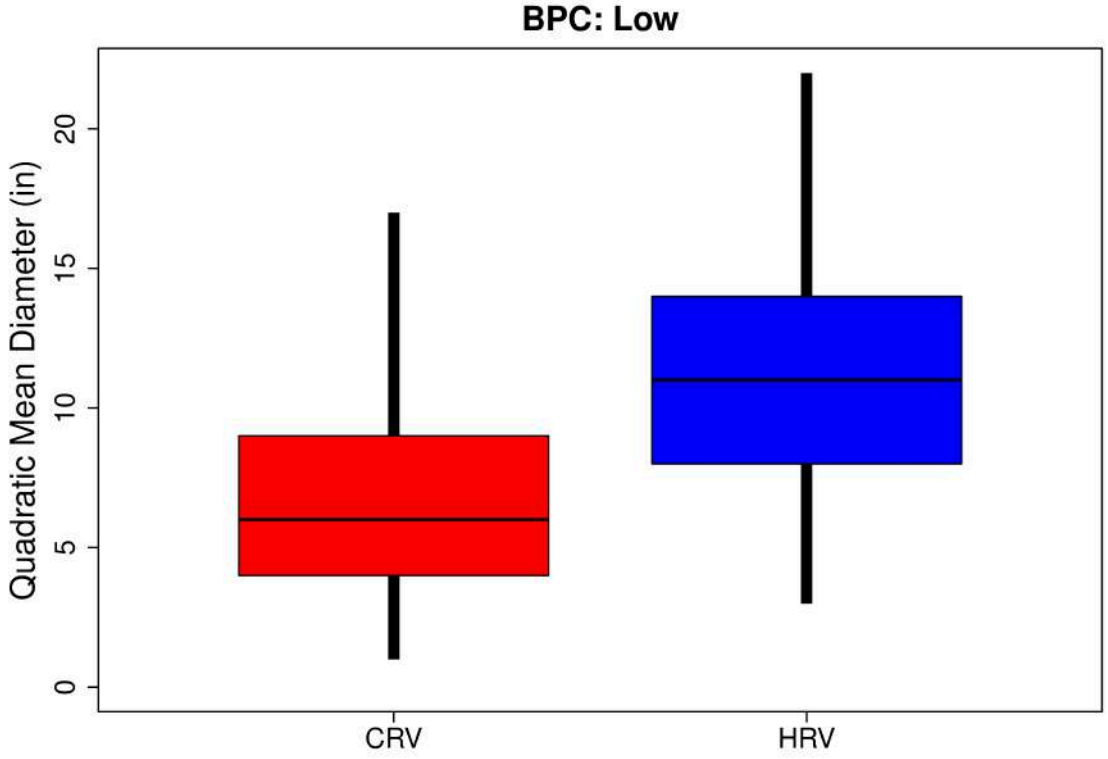

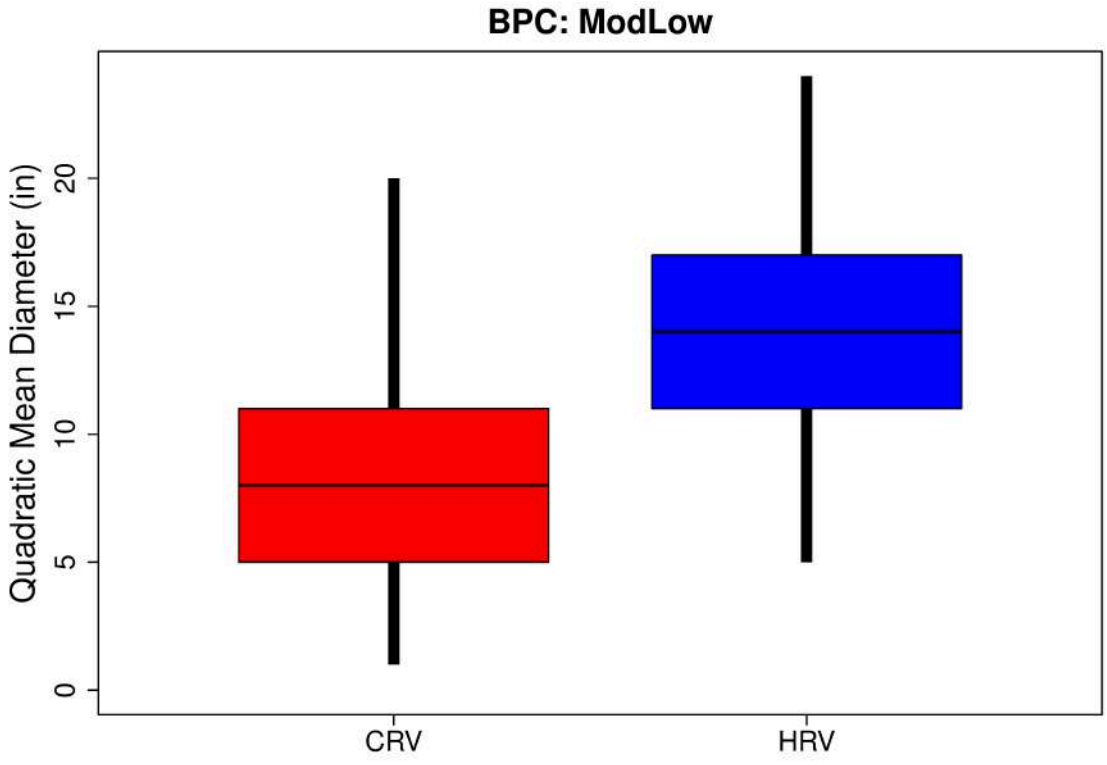
BPC: ModLow
Quadratic Mean Diameter (in)
0
5
10
15
20
CRV
HRV

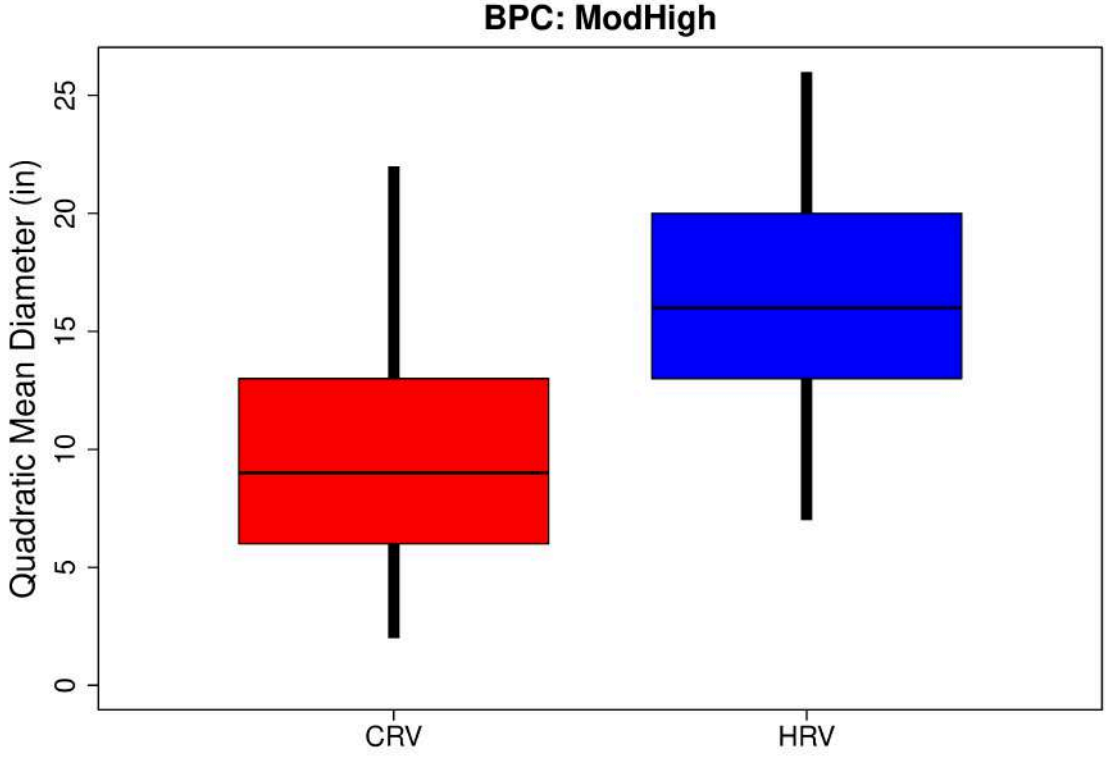
BPC: ModHigh
Quadratic Mean Diameter (in)
0
5
10
15
20
25
CRV
HRV

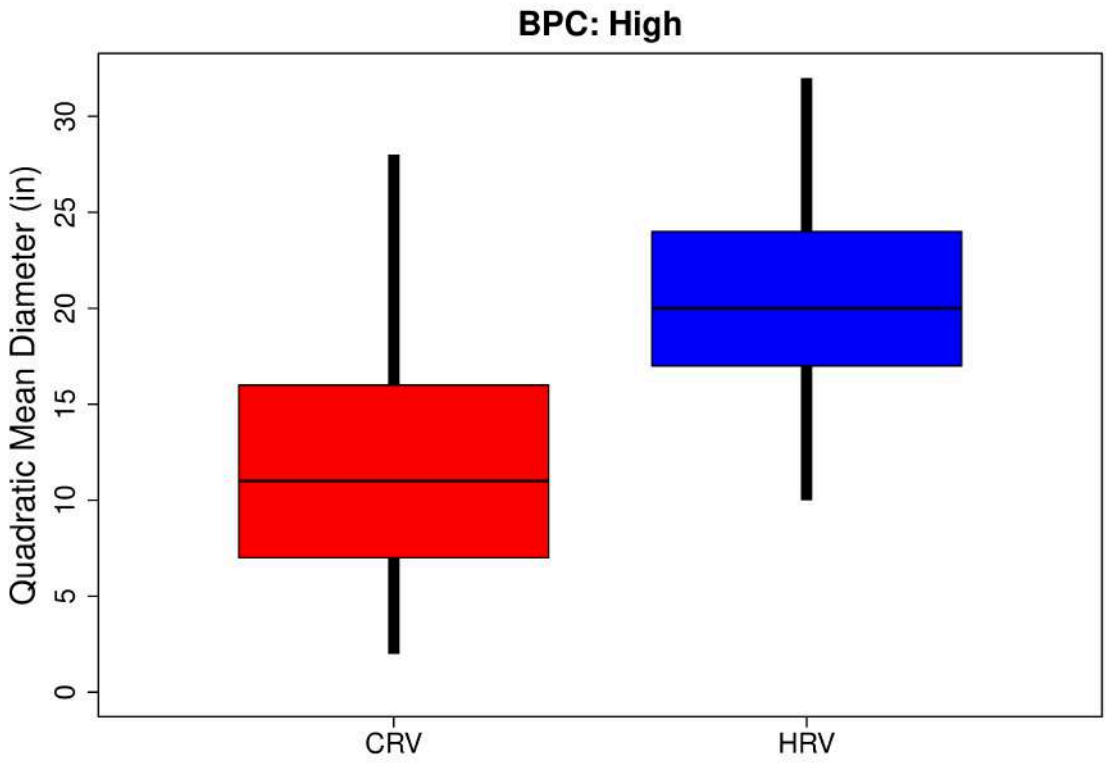

Figure 15: Historical Range of Variability (HRV) and Current range of variabiilty (CRV) among Sites (i.e., 40-m radius window) in the Quadratic Mean Diameter (QMD) of established trees to breast height within the Low, Moderately Low, Moderately High and High site productivity Biophysical Classes (BPCs) in the American North Fork River landscape. Box = 25-50 percentiles; whiskers = 2.5-97.5 percentiles

Tree Cover

Tree Cover at the Site level was based on the percentage of 5-m cells with established trees to breast height within a 40-m radius of the focal cell. Recall that even a cell in the Open developmental stage (i.e., forest cell without an established tree to breast height) has a percent tree cover > 0 % so long as there was a single established tree within 40 m of the focal cell. In addition, recall that Tree Cover, as computed here, represents the percentage of cells within 40 m containing one or more established trees to breast height, not actual tree canopy cover, and as such is biased high by an average of 16% over actual tree canopy cover (i.e., actual tree canopy cover will be less than reported here by an average of 16%). The HRV and CRV in Tree Cover composition at the Site level by BPC is given in **Table 10** and depicted in **Figure 16**.

Table 10: Range of variability (given as quantiles) in percent tree cover across Sites (40-m radius window centered on each focal cell) by Biophysical Class (BPC) for the current range of variability (CRV) and the historical range of variability (HRV) for the American North Fork River landscape.

BPC	Scenario	HRV 2.5%	HRV 25%	HRV 50%	HRV 75%	HRV 97.5%
Low	CRV	17	84	97	100	100
Low	HRV	11	60	81	91	98
ModLow	CRV	15	83	96	100	100
ModLow	HRV	19	73	87	93	98
ModHigh	CRV	21	84	96	100	100
ModHigh	HRV	28	80	90	94	98
High	CRV	31	89	98	100	100
High	HRV	39	86	92	95	98

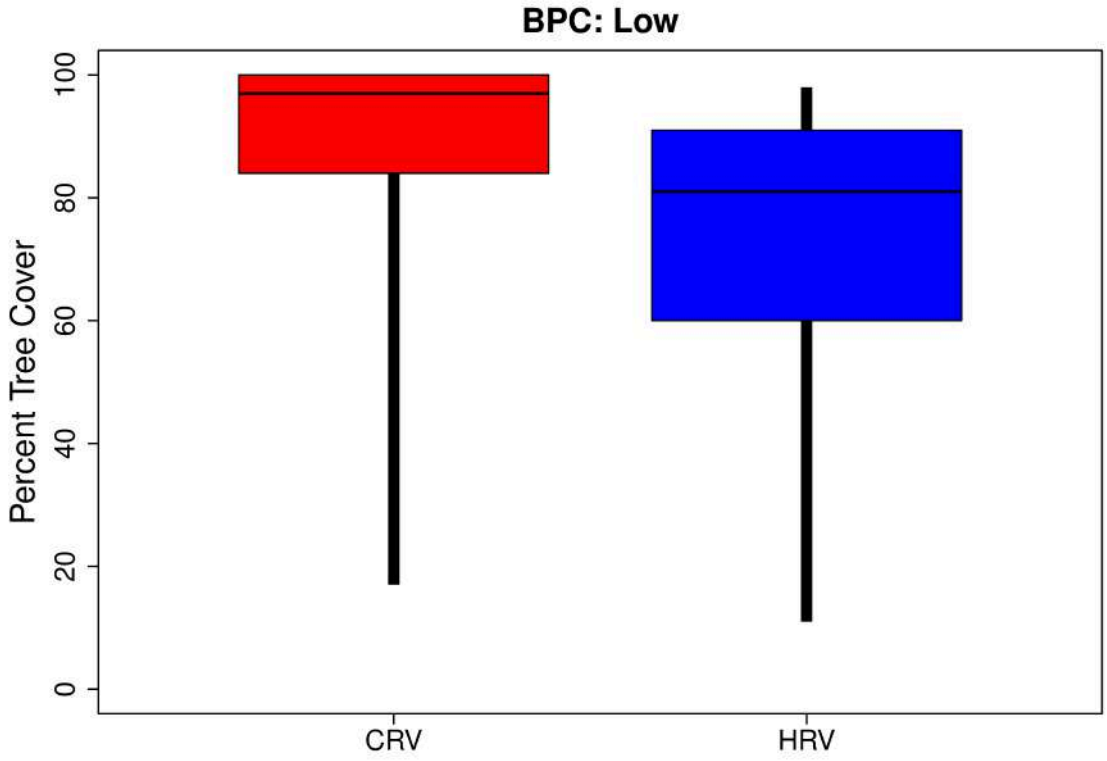

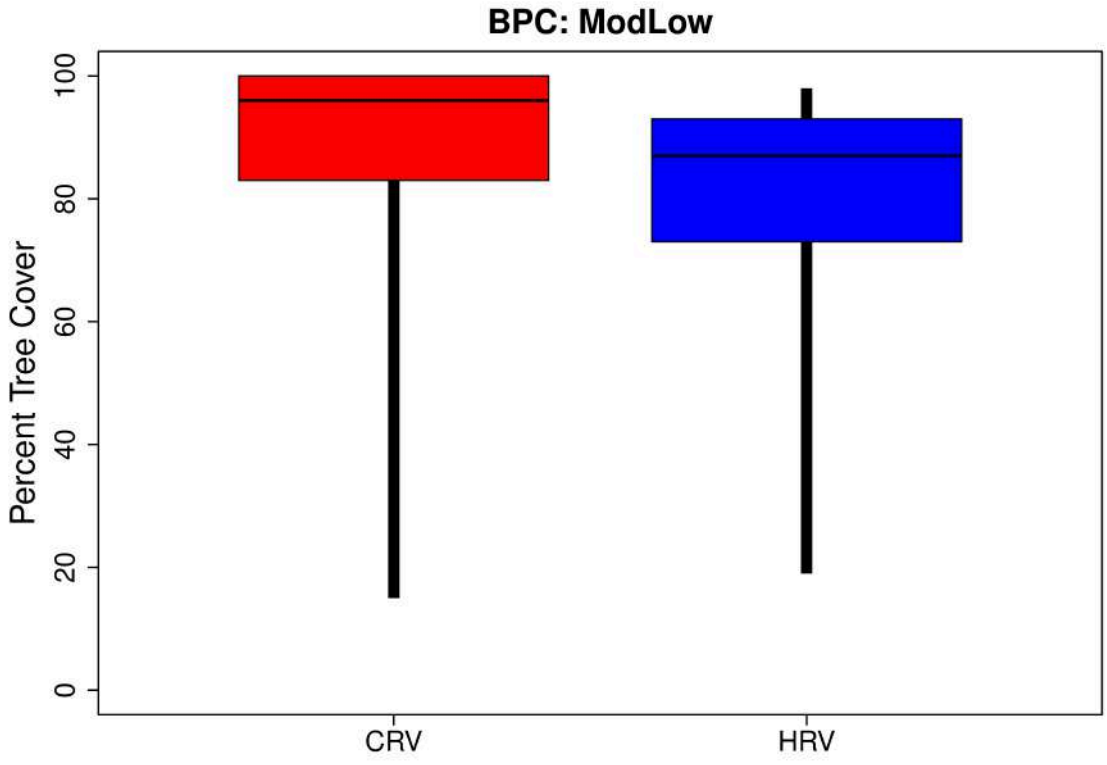
BPC: ModLow
Percent Tree Cover
0
20
40
60
80
100
CRV
HRV

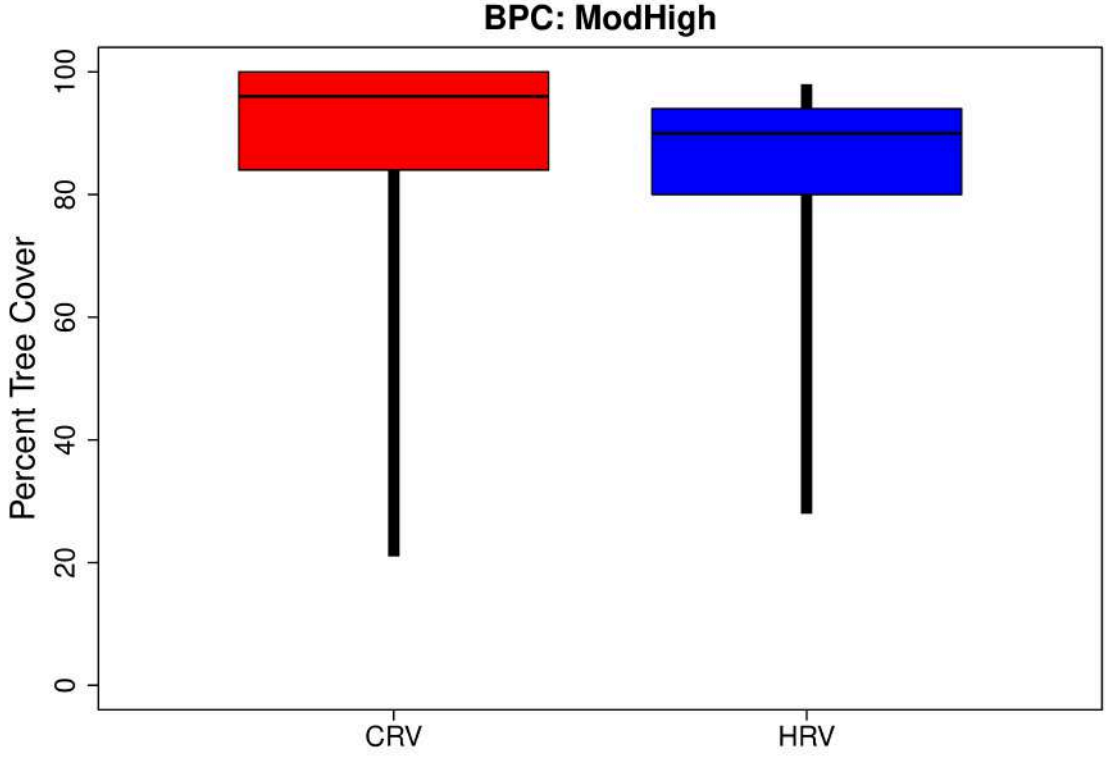
BPC: ModHigh
Percent Tree Cover
0
20
40
60
80
100
CRV
HRV

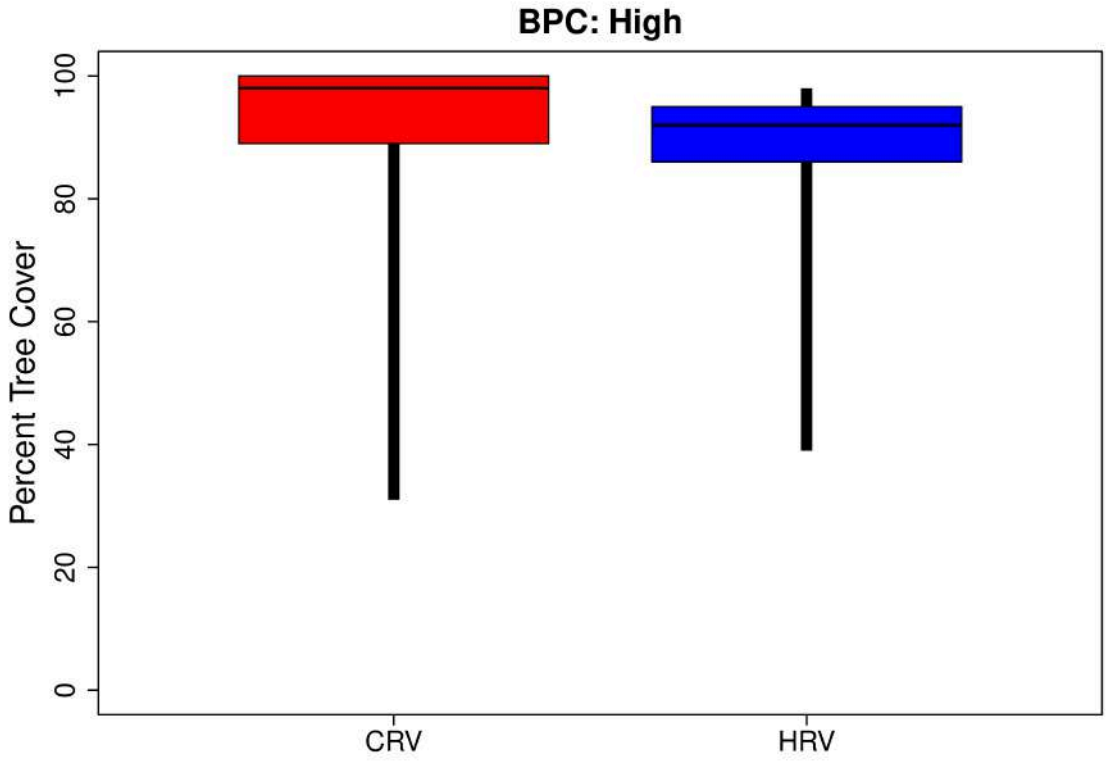

Figure 16: Historical Range of Variability (HRV) and Current range of variabiilty (CRV) among Sites (i.e., 40-m radius window) in the percent Tree Cover of established trees to breast height within the Low, Moderately Low, Moderately High and High site productivity Biophysical Classes (BPCs) in the American North Fork River landscape. Box = 25-50 percentiles; whiskers = 2.5-97.5 percentiles

Geophysical Unit Level Departure

The results presented in this section address current departure in landscape metrics quantified at the spatial extent of a single Geophysical Unit (GPU). The American North Fork River landscape was divided into 9,907 separate GPUs, which collectively encompass the area mapped as forest in the Existing Cover layer (Ecover) and within existing Lidar at the time of this analysis. Recall from the GTR that we defined GPUs based on similarity in a suite of 10 geophysical attributes and that they were defined only for the forested portion of the landscape and only where we had Lidar coverage. In addition, recall that each GPU was assessed independently; i.e., that we compared the current condition of each GPU to its own HRV in vegetation conditions. Thus, current departure of a GPU was specific to that GPU and independent of that measured for other GPUs. Lastly, recall that we used a large but parsimonious suite of landscape metrics that we deemed meaningful for estimating departure at the GPU level and appropriate given the available data, and computed departure as described in the GTR (and not repeated here), including the following:

Metric 1: Basal Area Departure

Departure in basal area of trees within the GPU was based on a metric derived by the TCSI project and adapted here for our purposes (**Figure 17**). GPUs with an increasingly positive departure have a current basal area that is greater than expected under HRV.

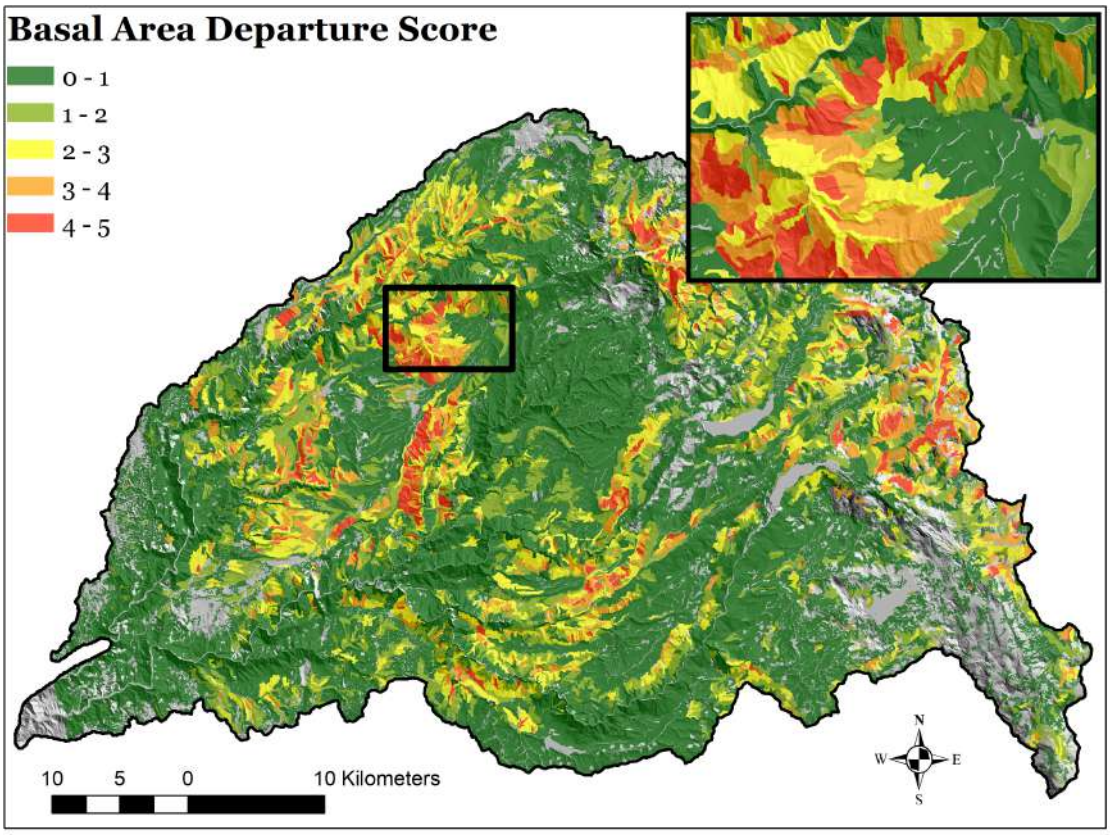

Figure 17: Geophysical Unit (GPU)-level basal area departure score for the American North Fork River landscape. The departure score (0-5) represents the deviation of the current GPU condition from its historical range of variability (HRV), as estimated from a suite of contemporary reference sites. Values increase with increasing degrees of departure.

Metric 2: Percent Open Forest

We measured departure in the percent of forested cells within the GPU in the Open developmental stage (**Figure 18**). GPUs with a departure index less than -1 have less area in the Open developmental stage than under HRV.

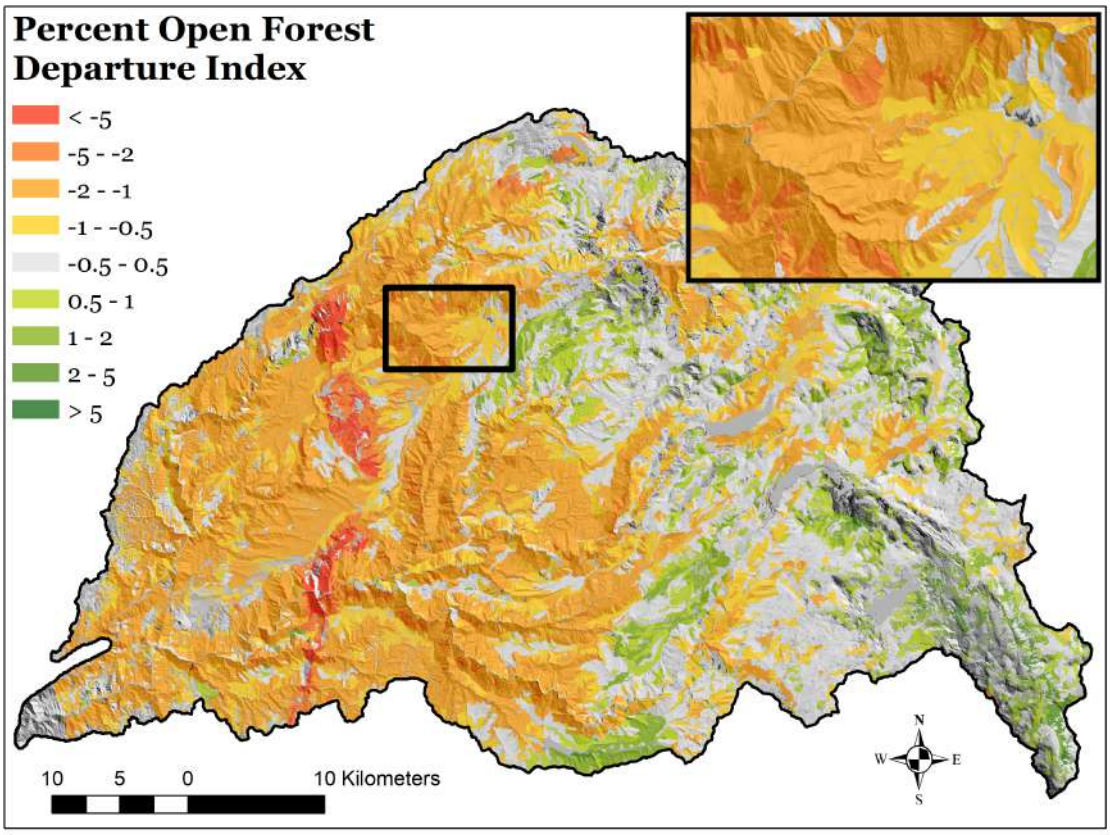

Figure 18: Geophysical Unit (GPU)-level departure index (unbounded) for the percentage of the forest within the GPU in the Open developmental stage for the American North Fork River landscape. The departure Index represents the deviation of the current GPU condition from its historical range of variability (HRV), as simulated. Values < -1 represent a current condition that is less than the HRV for the GPU, and increasingly negative values represent increasing degrees of negative departure.

Metric 3: Developmental Stage Diversity

We measured departure in the diversity of forest developmental stages within the GPU based on the Simpson's Diversity index (**Figure 19**). Here, Simpson's Diversity is defined as the probability that any two cells selected at random would be different developmental stages. The departure index for Simpson's Diversity is less than -1 if the current GPU has a diversity of developmental stages that is less than HRV.

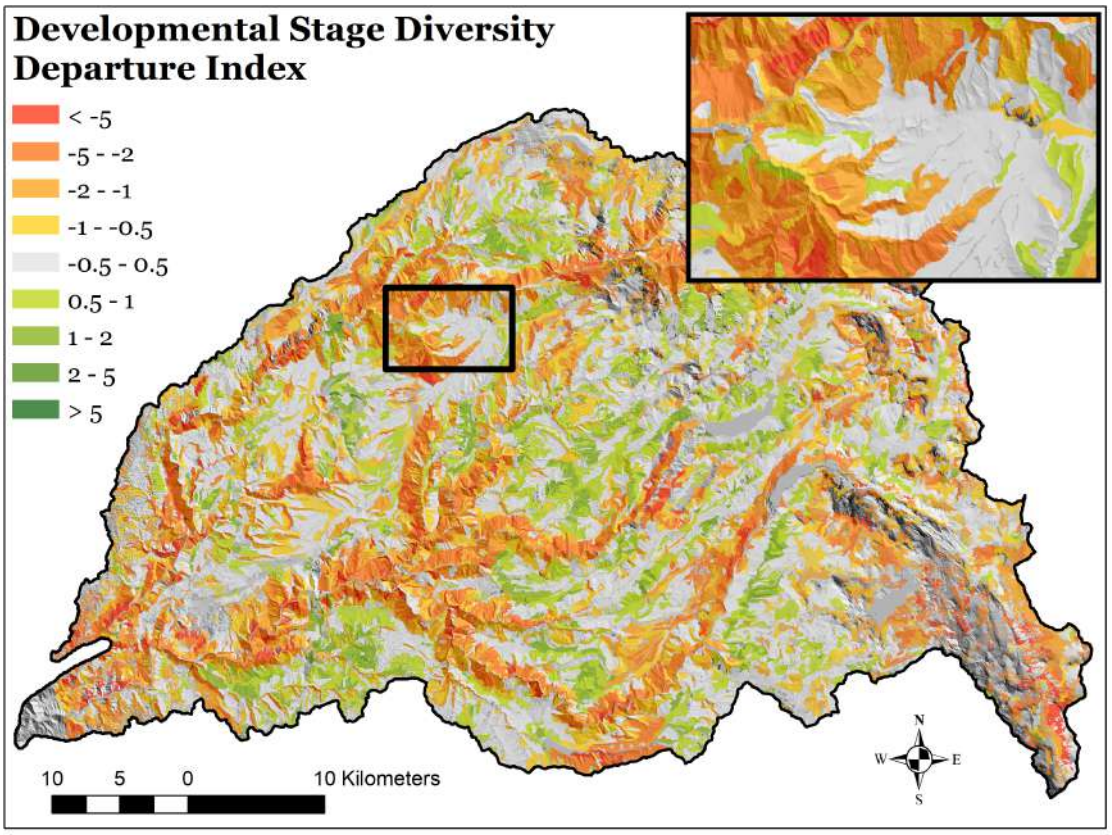

Figure 19: Geophysical Unit (GPU)-level departure index (unbounded) for the Simpson Diversity of developmental stages within the GPU for the American North Fork River landscape. The departure Index represents the deviation of the current GPU condition from its historical range of variability (HRV), as simulated. Values < -1 represent a current condition that is less than the HRV for the GPU, and increasingly negative values represent increasing degrees of negative departure.

Metric 4: Coefficient of Variation in Open Patch Size

We measured departure in the Coefficient of Variation (CV) in the size of all Open forest patches, including single cell patches, in which forest openings are defined by contiguous cells in the Open developmental stage based on the 4-neighbor rule (i.e., orthogonal neighbors)(**Figure 20**). The departure index is less than -1 if the current GPU has relatively invariant Open patch sizes compared to HRV.

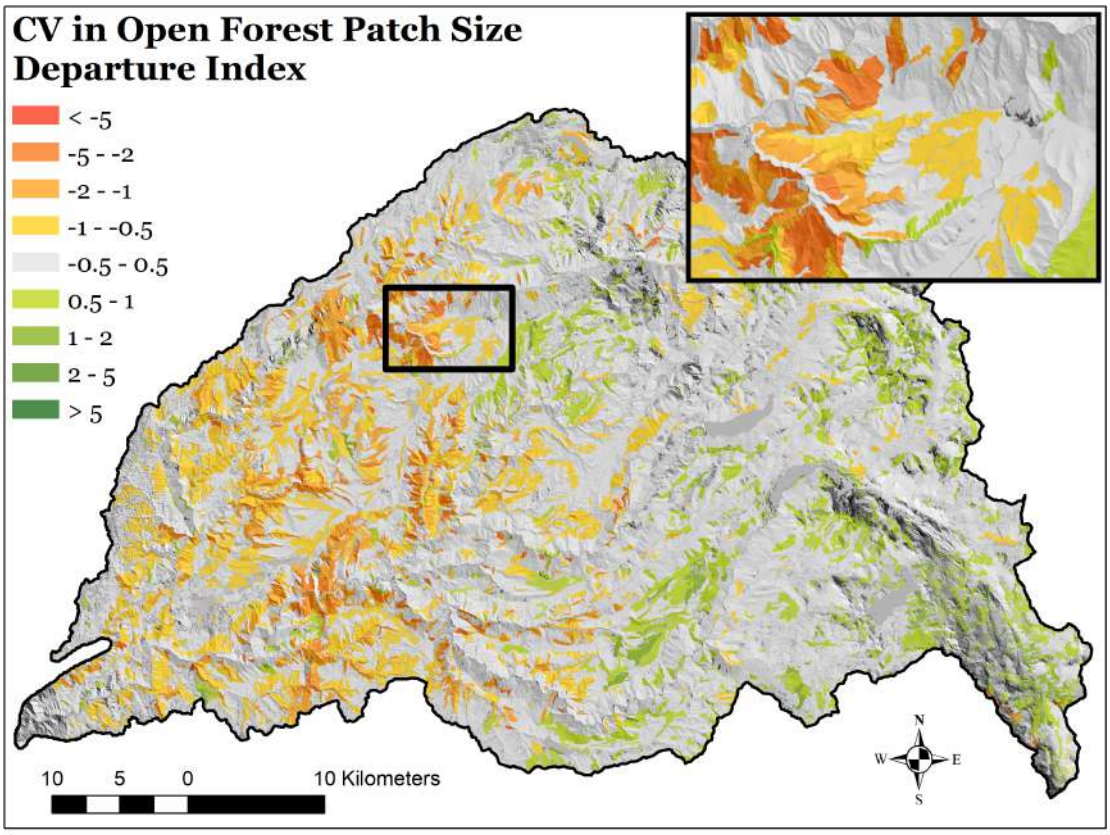

Figure 20: Geophysical Unit (GPU)-level departure index (unbounded) for the Coefficient of Variation (CV) in the size of patches in the Open developmental stage within the GPU for the American North Fork River landscape. The departure Index represents the deviation of the current GPU condition from its historical range of variability (HRV), as simulated. Values < -1 represent a current condition that is less than the HRV for the GPU, and increasingly negative values represent increasing degrees of negative departure.

Metric 5: Coefficient of Variation in Developmental Stage Patch Size

We measured departure in the CV in the size of all forest developmental stage patches, including single cell patches, in which patches are defined by contiguous cells in the same developmental stage based on the 4-neighbor rule (**Figure 21**). The departure index is less than -1 if the current GPU has relatively invariant developmental stage patch sizes compared to HRV.

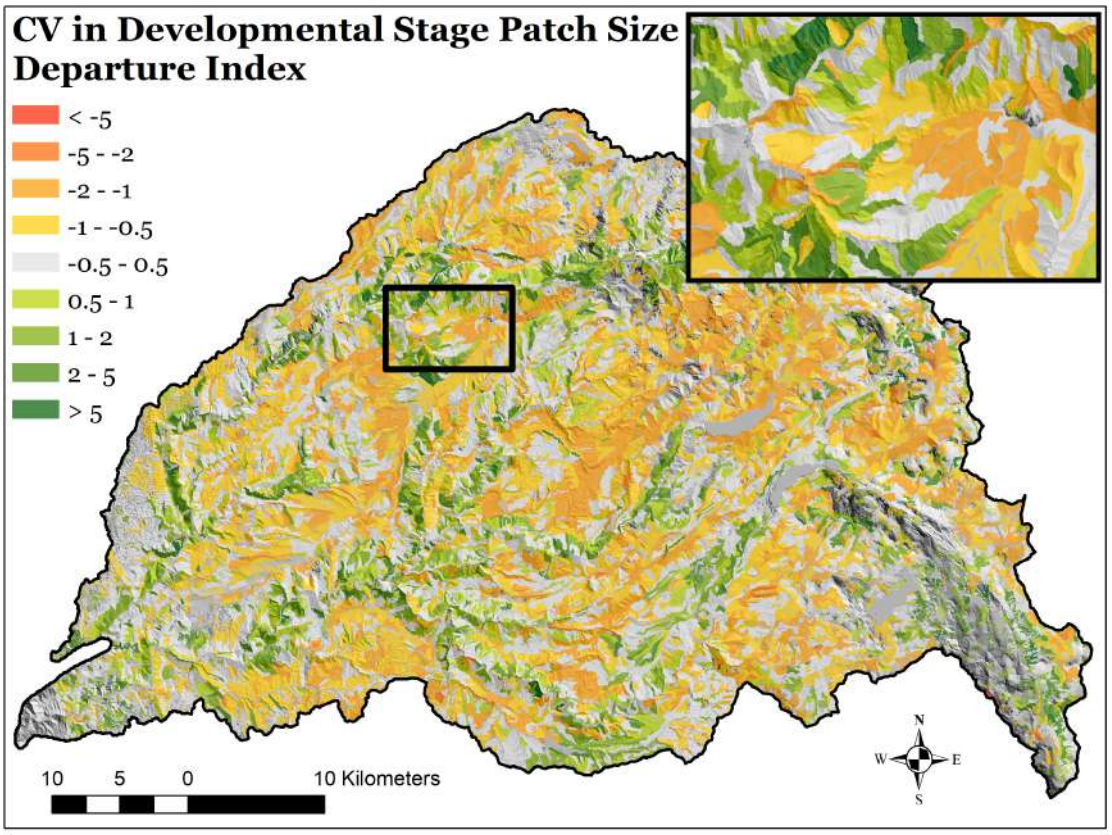

Figure 21: Geophysical Unit (GPU)-level departure index (unbounded) for the Coefficient of Variation (CV) in the size of patches based on developmental stages within the GPU for the American North Fork River landscape. The departure Index represents the deviation of the current GPU condition from its historical range of variability (HRV), as simulated. Values < -1 represent a current condition that is less than the HRV for the GPU, and increasingly negative values represent increasing degrees of negative departure.

Metric 6: Percent Large Trees

We measured departure in the percent of forested cells within the GPU in the Large tree size class (≥30 in dbh)(**Figure 22**). GPUs with a departure index less than -1 have less area in the Large tree class than under HRV.

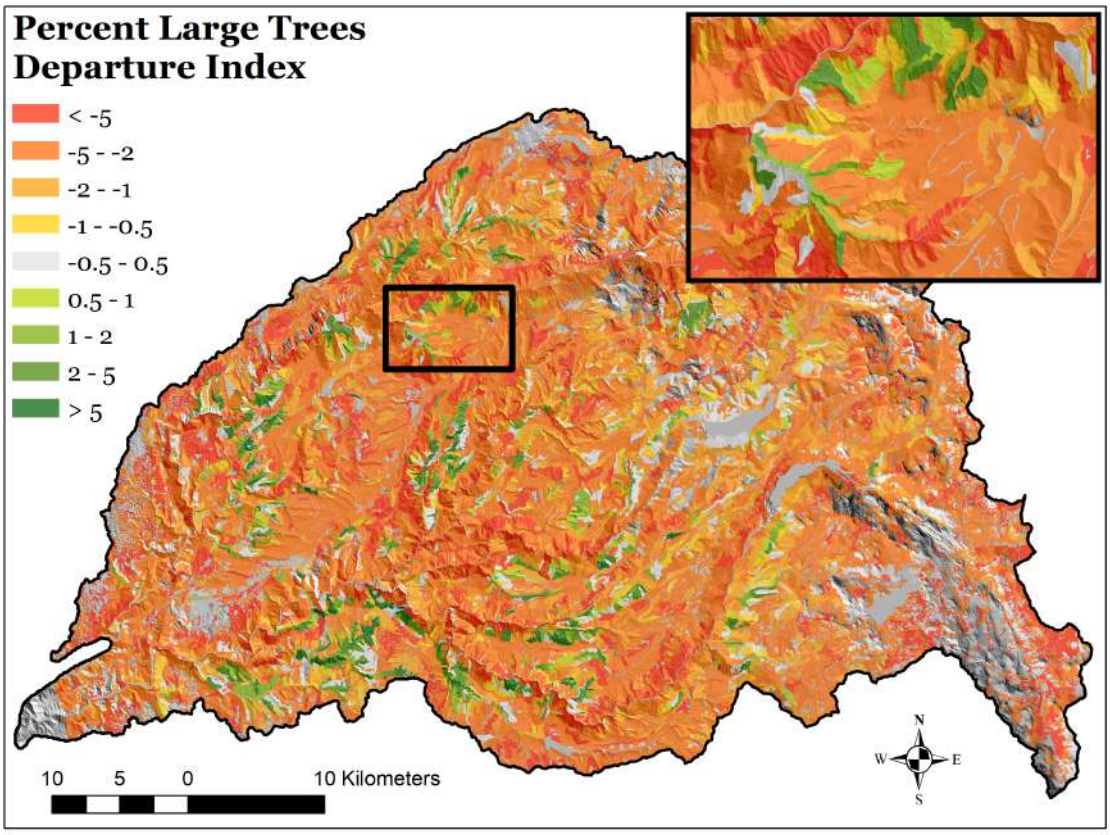

Figure 22: Geophysical Unit (GPU)-level departure index (unbounded) for the percentage of the forest in the Large tree size class (30 in dbh) within the GPU for the American North Fork River landscape. The departure Index represents the deviation of the current GPU condition from its historical range of variability (HRV), as simulated. Values < -1 represent a current condition that is less than the HRV for the GPU, and increasingly negative values represent increasing degrees of negative departure.

Metric 7: Tree Size Class Diversity

We measured departure in the diversity of tree size classes within the forested portion of the GPU based on the Simpson's Diversity index (**Figure 23**). Here, Simpson's Diversity is defined as the probability that any two cells selected at random would be from different tree size classes. The departure index for Simpson's Diversity is less than -1 if the current GPU has a diversity of tree size classes that is less than HRV.

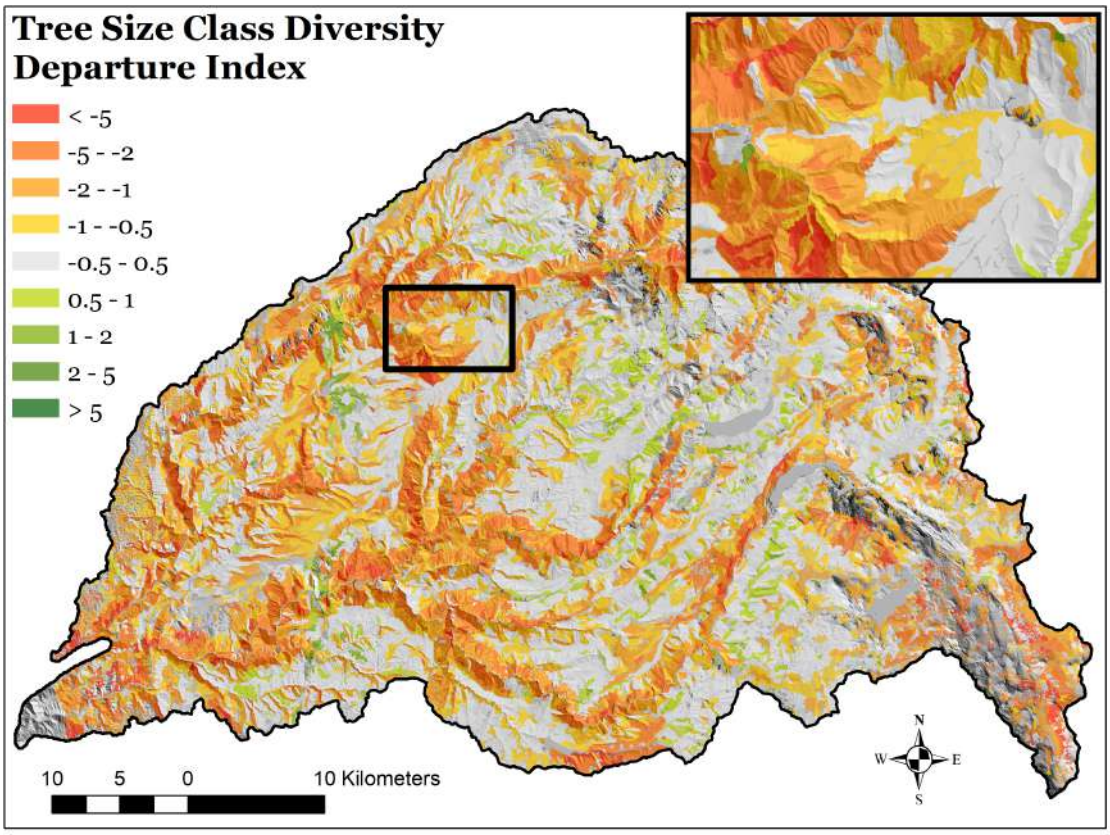

Figure 23: Geophysical Unit (GPU)-level departure index (unbounded) for the Simpson Diversity of tree size clases within the GPU for the American North Fork River landscape. The departure Index represents the deviation of the current GPU condition from its historical range of variability (HRV), as simulated. Values < -1 represent a current condition that is less than the HRV for the GPU, and increasingly negative values represent increasing degrees of negative departure.

Metric 8: Coefficient of Variation in Large Tree Patch Size

We measured departure in the CV in the size of all Large tree patches, including single cell patches, in which Large tree patches were defined by contiguous cells in the Large tree class (≥30 in dbh) based on the 4-neighbor rule (**Figure 24**). The departure index is less than -1 if the current GPU has relatively invariant Large tree patch sizes compared to HRV.

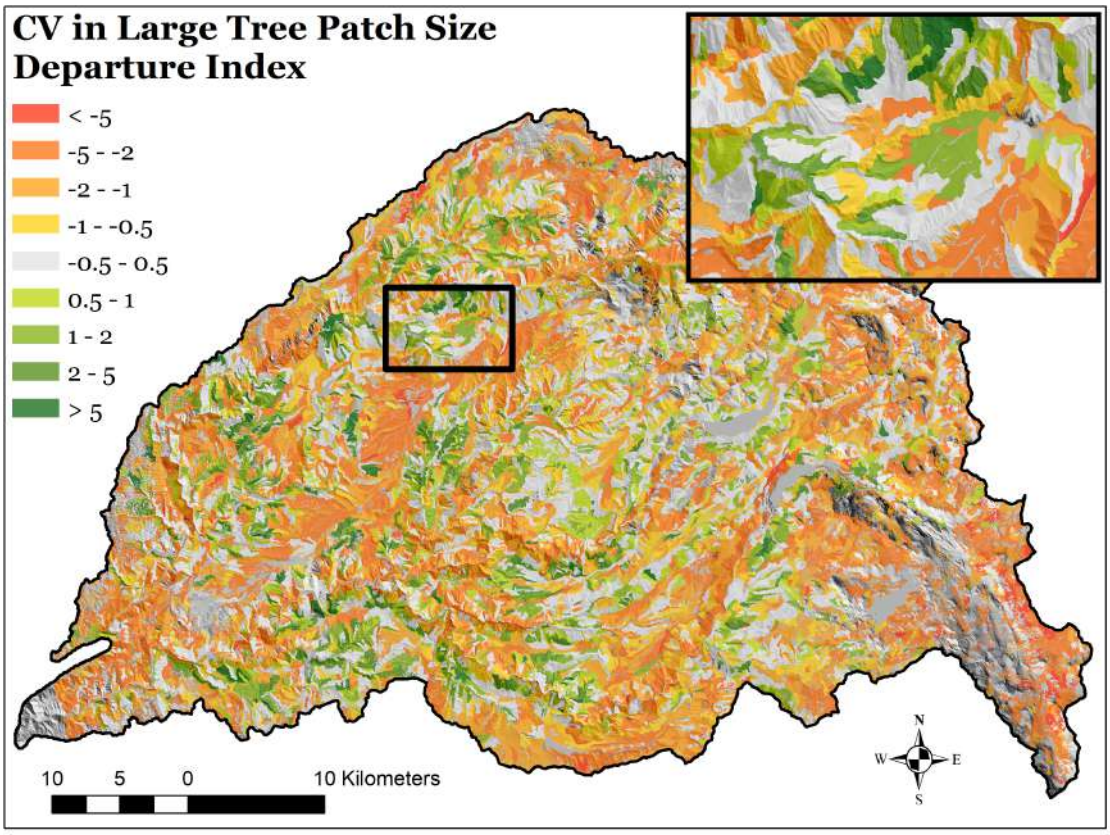

Figure 24: Geophysical Unit (GPU)-level departure index (unbounded) for the Coefficient of Variation (CV) in the size of patches in the Large tree size class (30 in dbh) within the GPU for the American North Fork River landscape. The departure Index represents the deviation of the current GPU condition from its historical range of variability (HRV), as simulated. Values < -1 represent a current condition that is less than the HRV for the GPU, and increasingly negative values represent increasing degrees of negative departure.

Metric 9: Coefficient of Variation in Tree Size Class Patch Size

We measured departure in the CV in the size of all tree size class patches, including single cell patches, in which patches were defined by contiguous cells in the same tree size class based on the 4-neighbor rule (**Figure 25**). The departure index is less than -1 if the current GPU has relatively invariant tree size class patch sizes compared to HRV.

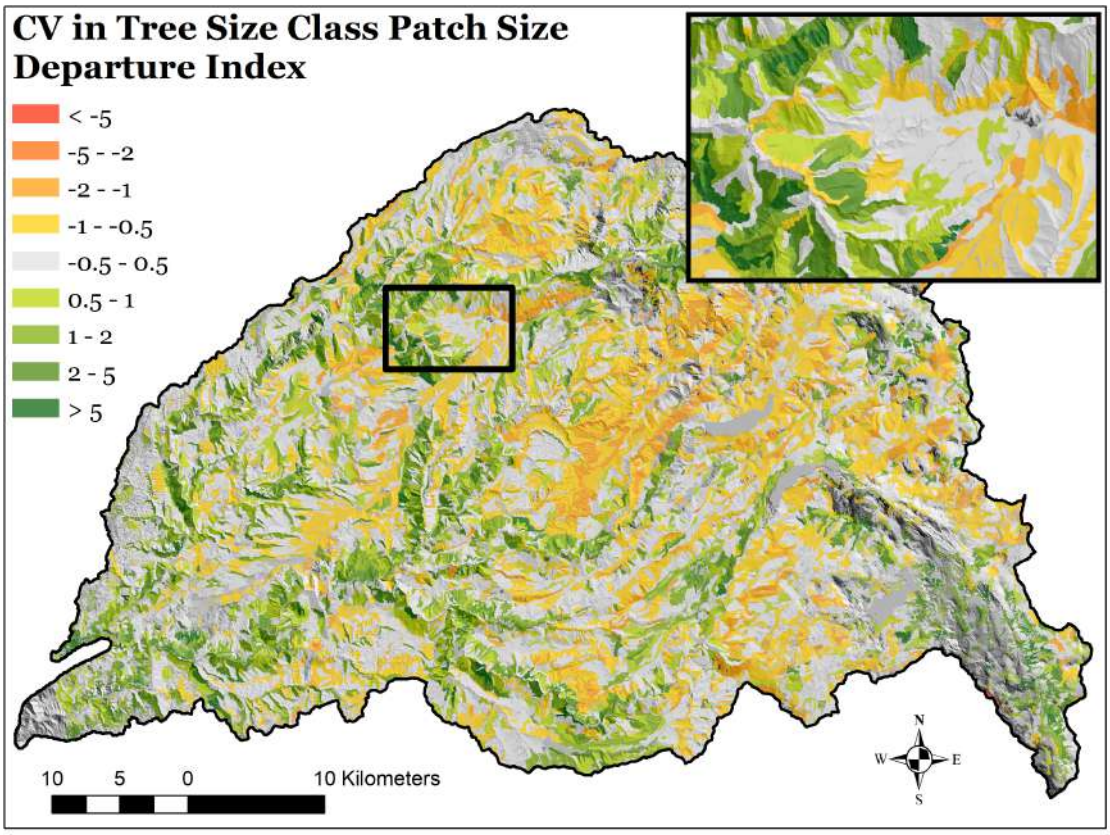

Figure 25: Geophysical Unit (GPU)-level departure index (unbounded) for the Coefficient of Variation (CV) in the size of patches based on tree size classes within the GPU for the American North Fork River landscape. The departure Index represents the deviation of the current GPU condition from its historical range of variability (HRV), as simulated. Values < -1 represent a current condition that is less than the HRV for the GPU, and increasingly negative values represent increasing degrees of negative departure.

Metric 10: Coefficient of Variation in Quadratic Mean Diameter

We measured departure in the CV in site-level Quadratic Mean Diameter (QMD) of established trees within the GPU (**Figure 26**). Recall that a site was defined as a 40-m radius window around each focal cell. Thus, QMD was computed for the site associated with each focal cell, which produced a continuous surface of QMD values, from which the CV in QMD values within the GPU was computed. The departure index is less than -1 if the current GPU has relatively homogeneous QMD compared to HRV.

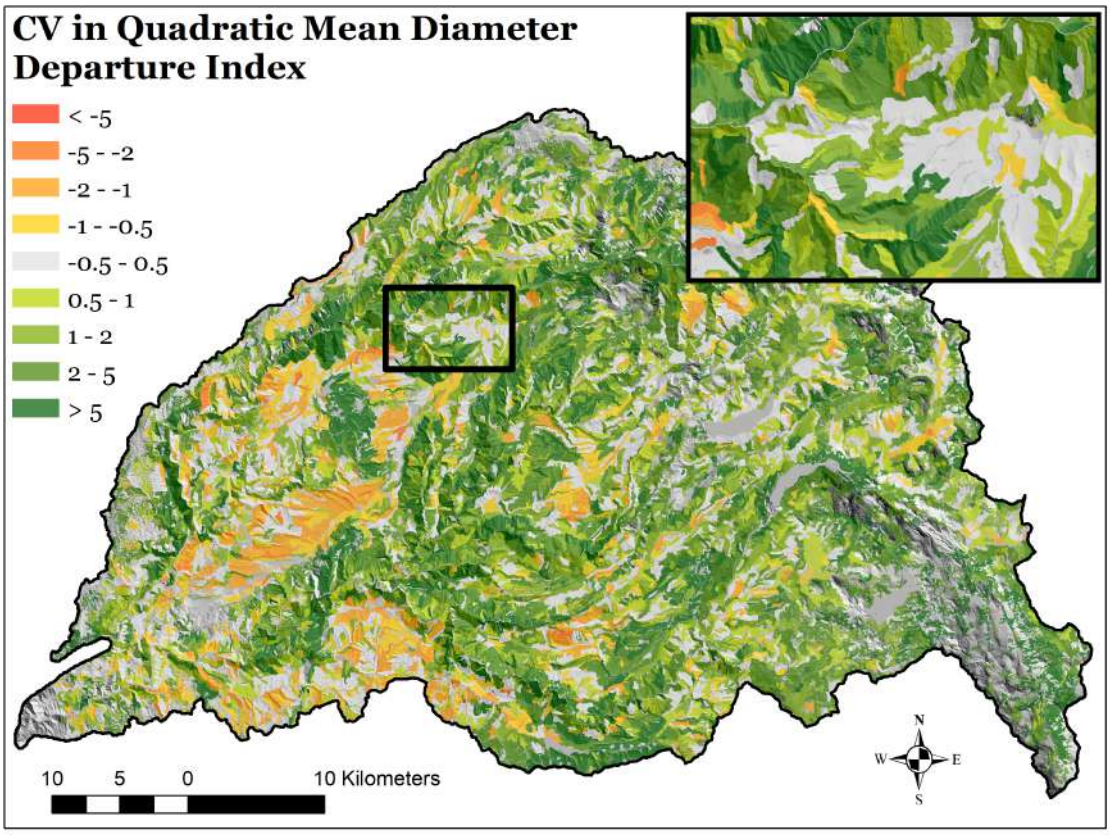

Figure 26: Geophysical Unit (GPU)-level departure index (unbounded) for the Coefficient of Variation (CV) in Site-level (i.e., 40 m radius window around each focal cell) Quadratic Mean Diameter (QMD, in inches) within the GPU for the American North Fork River landscape. The departure Index represents the deviation of the current GPU condition from its historical range of variability (HRV), as simulated. Values < -1 represent a current condition that is less than the HRV for the GPU, and increasingly negative values represent increasing degrees of negative departure.

Metric 11: Coefficient of Variation in Percent Tree Cover

We measured departure in the CV in site-level percent cover of established trees within the GPU (**Figure 27**). Again, recall that a site was defined as a 40-m radius window around each focal cell. Thus, percent tree Cover was computed for the site associated with each focal cell, which produced a continuous surface of percent tree cover values, from which the CV in tree cover within the GPU was computed. The departure index is less than -1 if the current GPU has relatively homogeneous tree cover compared to HRV.

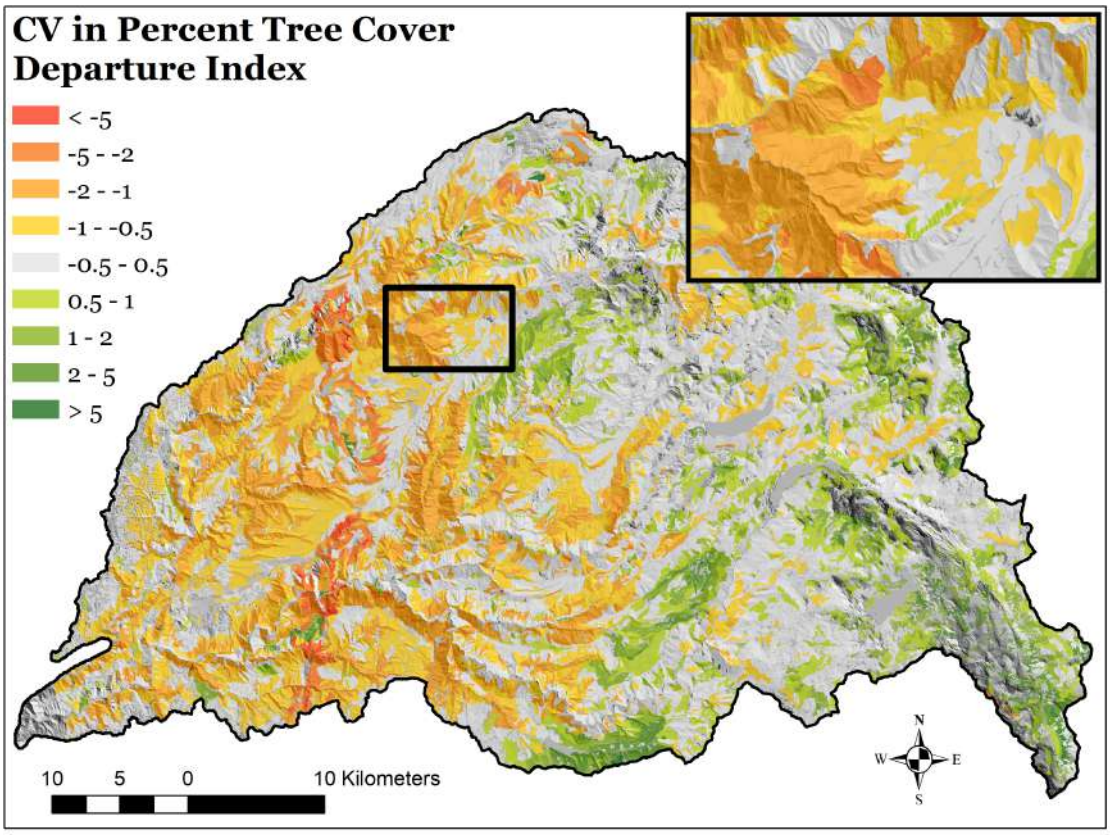

Figure 27: Geophysical Unit (GPU)-level departure index (unbounded) for the Coefficient of Variation (CV) in Site-level (i.e., 40 m radius window around each focal cell) percent tree cover within the GPU for the American North Fork River landscape. Note, percent tree cover as measured is on average 16 % greater than percent canopy cover. The departure Index represents the deviation of the current GPU condition from its historical range of variability (HRV), as simulated. Values < -1 represent a current condition that is less than the HRV for the GPU, and increasingly negative values represent increasing degrees of negative departure.

Composite Departure Index

We combined the 11 GPU-level departure indices above into two composite departure scores: 1) composite "negative" departure, and 2) composite "absolute" departure (see GTR for details). Both of these composite scores can be interpreted as a measure of overall GPU departure in vegetation composition and configuration. Increasing departure scores (given as a percent of maximum) indicate increasing degrees of departure.

Negative Departure - Maximum "negative" departure occurs when a GPU has too little Open forest area, too few Large trees, too little diversity in forest developmental stages (i.e., tree heights) and tree size classes (i.e., dbh), too little variability in the size of patches based on forest developmental stage and tree size, and too little spatial variability in percent tree cover and weighted average tree size (i.e., QMD) relative to its HRV. In other words, maximum negative departure occurs when the forest is too closed-canopy, depauperate in Large trees, and too homogeneous in vegetation composition and configuration.

The composite negative departure score is depicted in **Figure 28**. This score can be interpreted as the percent of maximum deviation in negative departure. Thus, a value of 0 represents no departure in any of the component metrics and a value of 100 represents maximum negative departure in each of the component metrics. GPUs with relatively high scores are the logical ones to prioritize for restoration treatment - should that be the goal. Importantly, this composite departure score can serve as a first stage in identifying and prioritizing GPUs for treatment, but specific objectives and treatments for each GPU requires decomposing the composite score into the component metrics to determine which aspects of the forest vegetation composition and/or configuration are most departed.

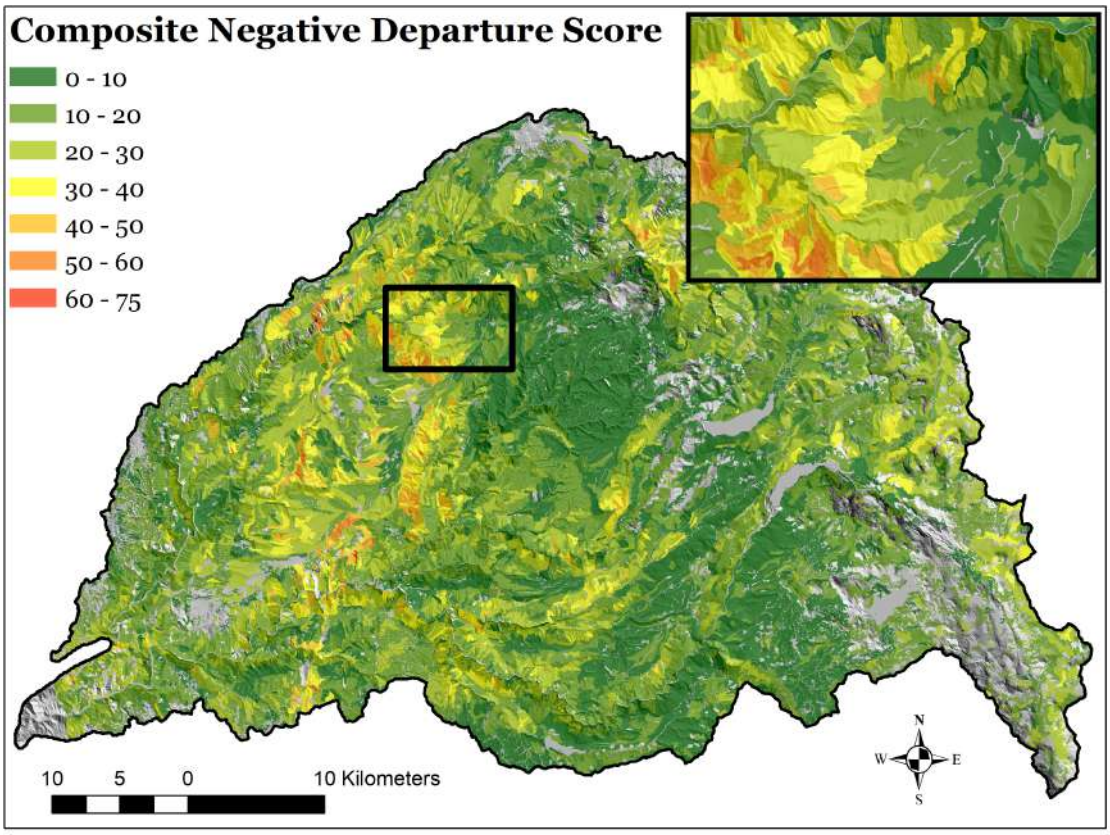

Figure 28: Geophysical Unit (GPU)-level composite negative departure score composed of a weighted combination of 11 individual departure metrics within the GPU for the American North Fork River landscape. The score represents the percentage of maximum departure of the current GPU condition from its historical range of variability (HRV), as simulated. Larger values indicate increasing degrees of departure.

Absolute Departure - Maximum "absolute" departure occurs when a GPU has either too little or too much Open forest area, too few or too many Large trees, too little or too much diversity in forest developmental stages (i.e., tree heights) and tree size classes (i.e., dbh), too little or too much variability in the size of patches based on forest developmental stage and tree size, and too little or too much spatial variability in percent tree cover and weighted average tree size (i.e., QMD) relative to HRV. In other words, maximum departure occurs when the GPU differs in any way in both composition and configuration from its HRV, as measured by this suite of metrics.

Subbasin Level Departure

The results presented in this section represent landscape metrics quantified at the subbasin-by-BPC level; i.e., each subbasin subdivided into BPCs treated as a whole unit (a.k.a. "zones"). The American North Fork River landscape was divided into 36 distinct subbasins (**Figure 29**), each of which was partitioned into the four forested BPCs for a total of 144 subbasin-by-BPC partitions or zones. Recall from the GTR that each partition was assessed independently to create a departure index; i.e., that we compared the current condition of each partition to its own HRV in vegetation conditions. In addition, recall that the final departure score reflected negative departure in the percent of the partition in large openings and large trees (i.e., in which the current landscape contains less area in large openings and large trees than expected under HRV), but was bidirectional with respect to the landscape configuration metrics; i.e., it reflected the magnitude of the absolute differences between the current and historical landscape conditions, regardless of

whether the current condition was greater or less than the historical condition. In other words, any differences between current and historical vegetation conditions with respect to landscape configuration registered as departure. Lastly, recall that we used a parsimonious suite of landscape metrics (see below) that we deemed meaningful for estimating departure at the subbasin level and appropriate given the available data, and computed departure as described in the GTR (and not repeated here), including the following metrics:

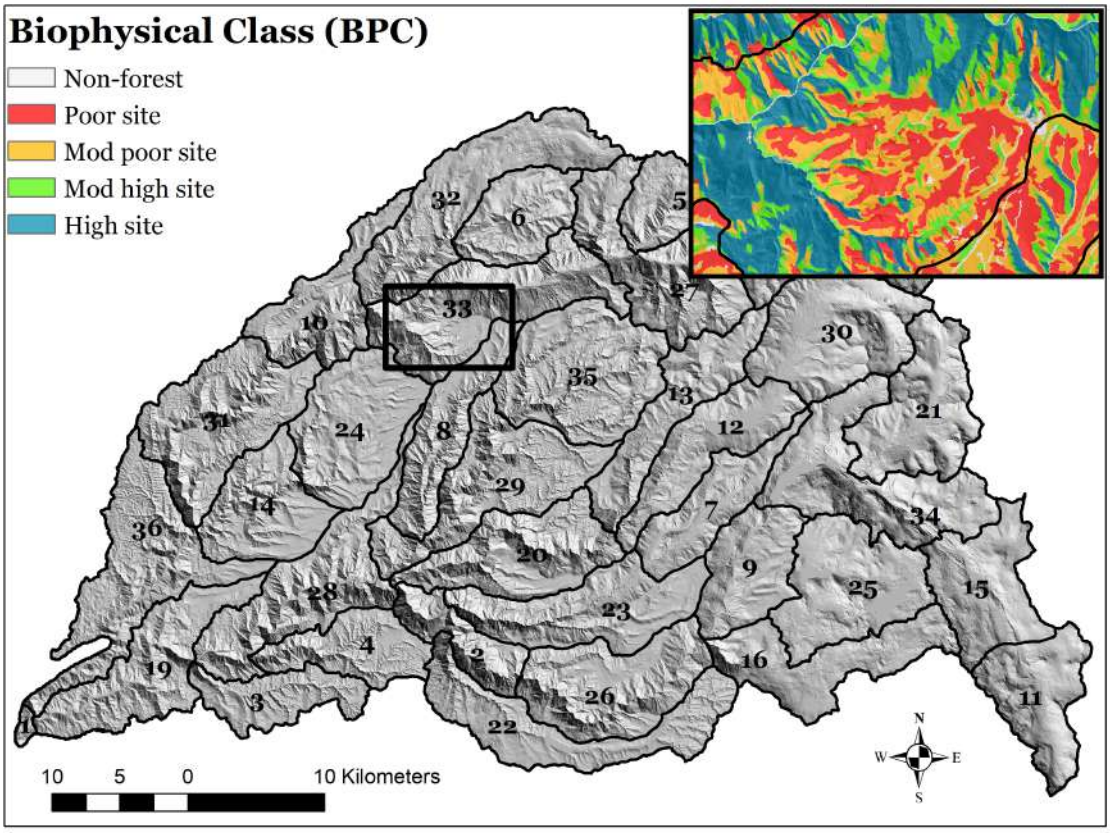

Figure 29: The American North Fork River landscape HUC12 subbasins, as modified, defined for the purpose of summarizing Historical Range of Variability (HRV) and current departure.

Metric 1: Percent Large Forest Openings

We defined large forest openings as contiguous forested cells in the Open developmental stage (i.e., no established trees to breast height) encompassing a minimum of 0.04 ha (0.1 acres). Contiguity was based on the 4-neighbor rule (i.e., orthogonal neighbors) that ensured a minimum width of 5 m for any opening. We defined Percent Large Forest Openings as the percent of the forest within the subbasin-by-BPC partition in large forest openings (as defined), and the departure index reflected whether or not the current landscape was deficient in large forest openings relative to HRV and, if so, the degree of deficiency.

The Percent Large Forest Openings departure index is depicted in **Figure 30**. Note, the departure index was assigned to each subbasin-by-BPC partition; consequently, there were 144 distinct values assigned. Thus, to better assess departure by subbasin and BPC, one needs to examine the attribute table for the departure layer.

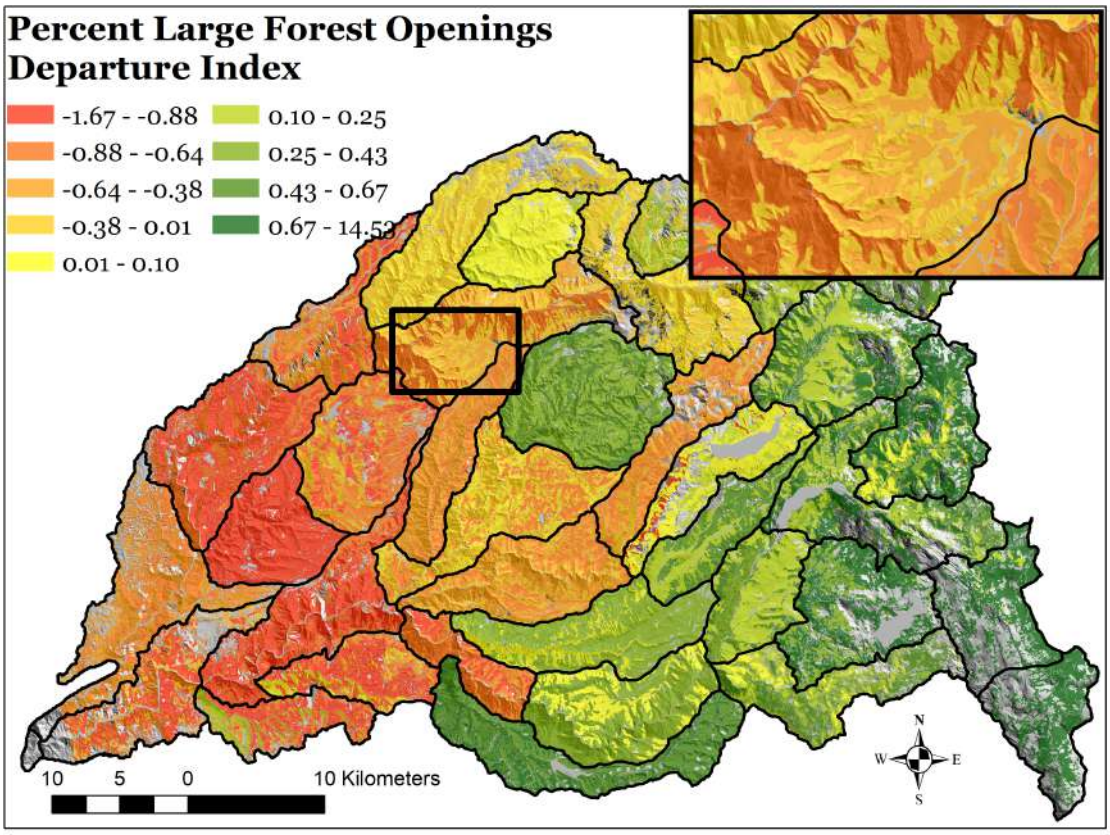

Figure 30: Subbasin-by-BPC level departure index for large forest openings (> 0.04 ha or 0.1 acres and > 5 m mininum width) for the American North Fork River landscape. The departure index represents the deviation of the current subbasin and biophsyical class (BPC) condition from its historical reference period condition, as simulated. Departure indices < -1 represent a current landscape with less total area in large forest openings than during the historical reference period, as simulated, and increasing negative values represent increasing degrees of departure.

As discussed in the GTR, the Percent Large Forest Openings Departure Index can be miss-interpreted if not understood well. As the previous figure depicts, the distribution of index values would suggest that most of the subbasin-by-BPC partitions are within the HRV given that most of the partitions have values between -1 - 1. Recall, index values within this range reflect a current landscape condition that is within the 2.5% and 97.5% HRV. This would seem to indicate that most of the partitions are within HRV. While this might technically be correct, the reality is that most of the partitions are close to the lower limit of HRV and have index values close to -1. Consequently, the distribution of index values is heavily skewed towards values on the lower limit of HRV, suggesting that the landscape as a whole is, on average, deficient in large forest openings. A alternative and more useful way to assess current departure in this metric is to compare the distribution of values representing the percentage of the partition in large forest openings between the HRV and CRV, as shown **Figure 31**.

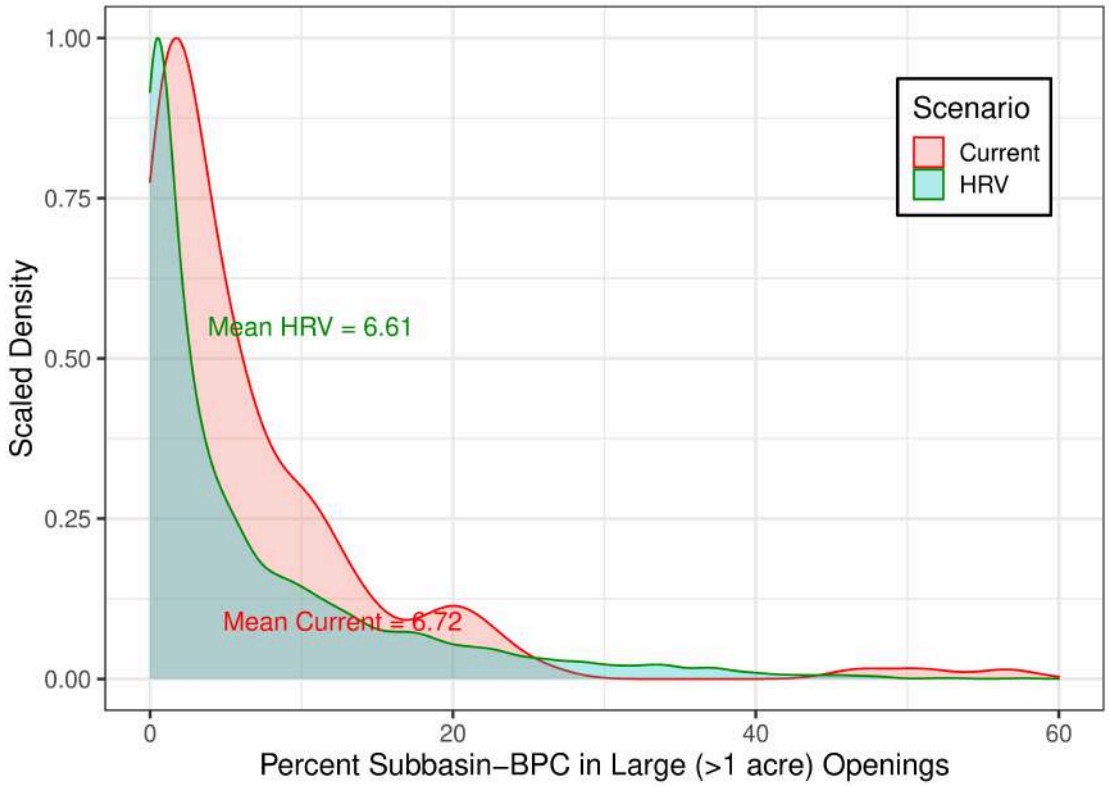

Figure 31: Current and historical distribution of Percent Large Forest Openings across the Subbasin-by-Biophysical Class (BPC) landscape partitions for the American North Fork River landscape. The comparative distributions reveal that even though the departure index for most of the partitions technically may fall with the historical range of variation (see previous figure), the overall distributions in the raw metric values differ markedly and reflect departure for the landscape as a whole

Metric 2: Large Forest Openings Patch Size Distribution

We defined large forest openings as described above. Here, we quantified the size of individual openings and determined the percent of forest within the subbasin-by-BPC partition in large openings in each of several patch size classes or bins (see GTR). The departure index reflects whether or not the current landscape has a distribution of large forest opening patch sizes that differed from HRV and, if so, the degree of differences in the two distributions.

The Large Forest Openings Patch Size Distribution departure index is depicted in **Figure 32**. As before, the departure index was assigned to each subbasin-by-BPC partition; consequently, there were 144 distinct values assigned. Thus, to better assess departure by subbasin and BPC, one needs to examine the attribute table for the departure layer.

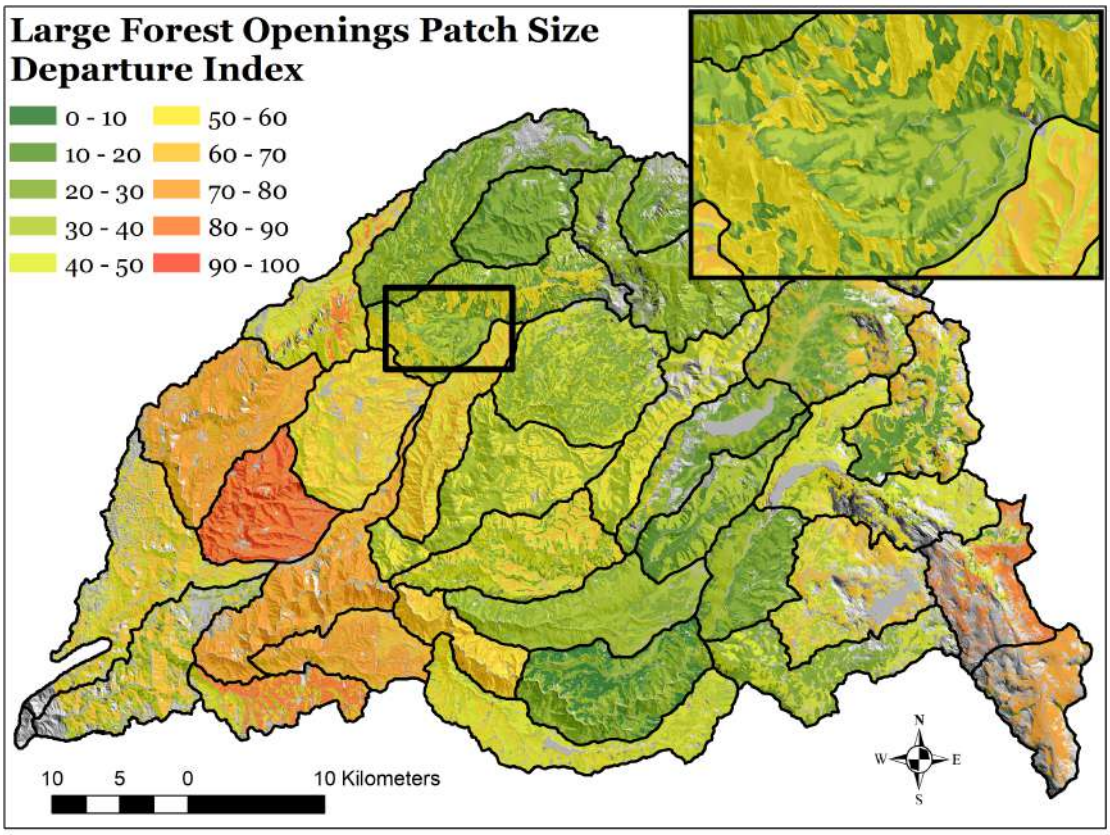

Figure 32: Subbasin-by-BPC level departure index for large forest openings (> 0.04 ha or 0.1 acres and > 5 m mininum width) patch size distribution for the American North Fork River landscape. The departure index represents the deviation of the current subbasin and biophsyical class (BPC) condition from its historical reference period condition, as simulated. Departure indices > 0 represent a current landscape with a distribution of large forest opening patch sizes that differs in some way from the historical reference period distribution, as simulated, and increasing values represent increasing degrees of departure.

To further evaluate departure in this patch size distribution metric, it is necessary to examine the CRV and HRV patch size distributions for the selected subbasin-by-BPC partition, for example as depicted in **Figure 33**.

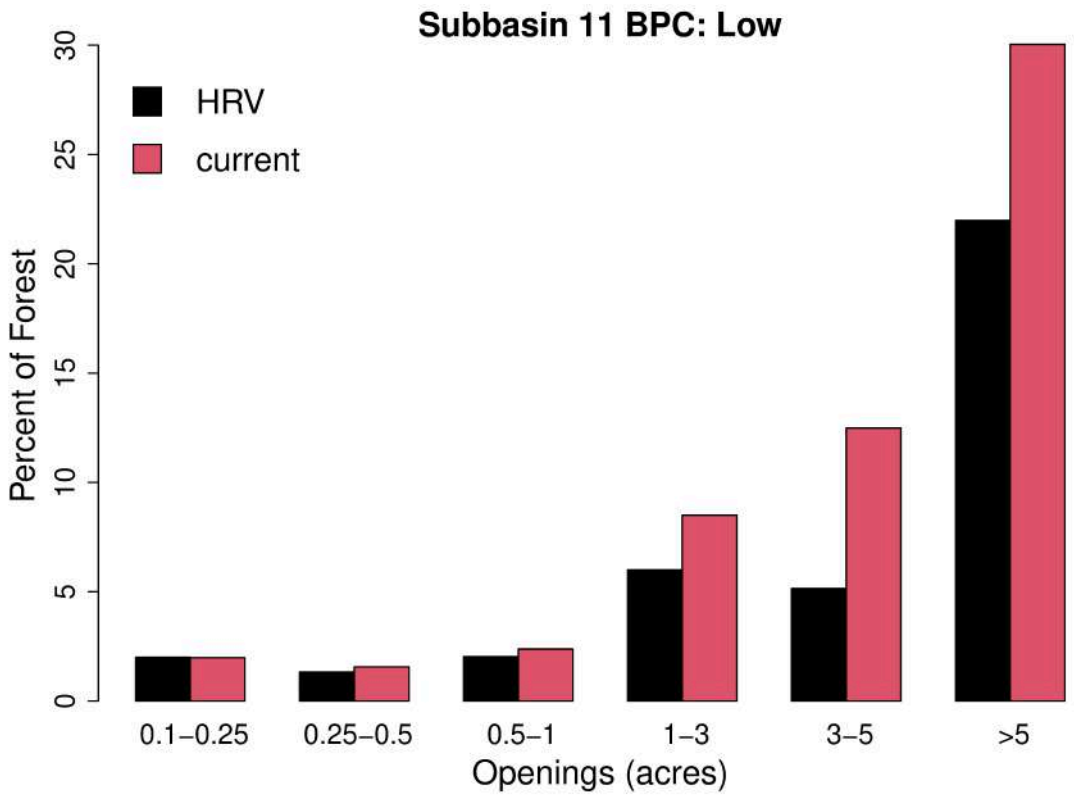

Figure 33: Barplot of the distribution of large forest openings (> 0.04 ha or 0.1 acres and > 5 m mininum width) patch sizes for the current landscape and the historical reference period (HRV) for subbasin 11 and the Low productivity Biophysical Class (BPC = 1) for the American North Fork River landscape. Each bar represents the percent of forest within the subbasin and Biophysical Class (BPC) in large forest openings of a particular patch size. The departure index represents the percentage dissimilarity between the CRV and HRV distributions. Departure indices > 0 represent a current landscape with a distribution of large forest opening patch sizes that differs in some way from the historical reference period distribution, as simulated, and increasing values represent increasing degrees of departure.

Metric 3: Developmental Stage Patch Size Distribution

We defined developmental stages based on six tree height classes, ranging from Open (< 4.5 ft) to Tall Trees (> 125 ft), as described in the GTR. Here, for each snapshot of the landscape we constructed a patch mosaic comprised of developmental stages in which patches were defined using the 4-neighbor rule. For each snapshot, we quantified the size of each developmental stage patch and determined the percent of forest within the subbasin-by-BPC partition in each of several patch size classes or bins. The departure index reflects whether or not the current landscape has a distribution of developmental stage patch sizes that differs from HRV and, if so, the degree of differences in the two distributions.

The Developmental Stage Patch Size Distribution departure index is depicted in **Figure 34**. As before, the departure index was assigned to each subbasin-by-BPC partition; consequently, there were 144 distinct values assigned. Thus, to better assess departure by subbasin and BPC, one needs to examine the attribute table for the departure layer.

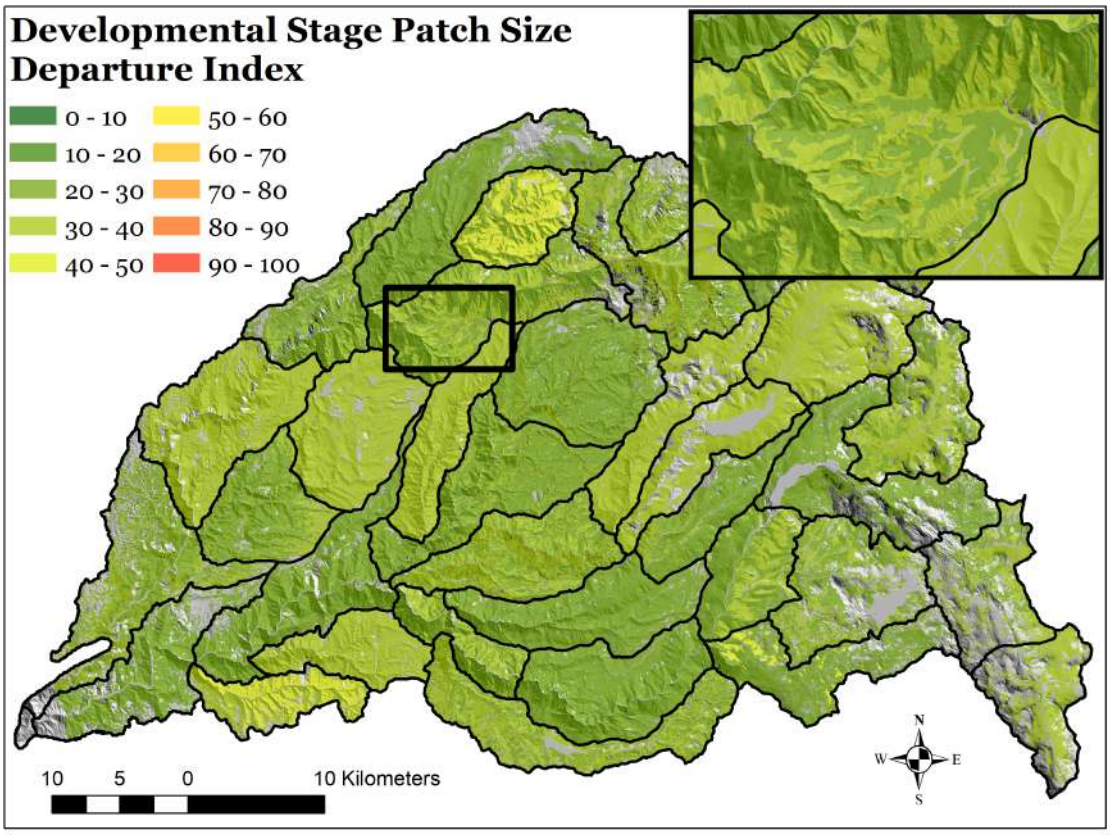

Figure 34: Subbasin-by-BPC level departure index for the developmental stage patch size distribution for the American North Fork River landscape. Developmental stages were based on tree height classes and patches were based on the 4-neighbor adjacency rule. The departure index represents the deviation of the current subbasin and biophsyical class (BPC) condition from its historical reference period condition, as simulated. Departure indices > 0 represent a current landscape with a distribution of developmental stage patch sizes that differs in some way from the historical reference period distribution, as simulated, and increasing values represent increasing degrees of departure.

To further evaluate departure in this patch size distribution metric, it is necessary to examine the CRV and HRV patch size distributions for the selected subbasin-by-BPC partition, for example as depicted in **Figure 35**.

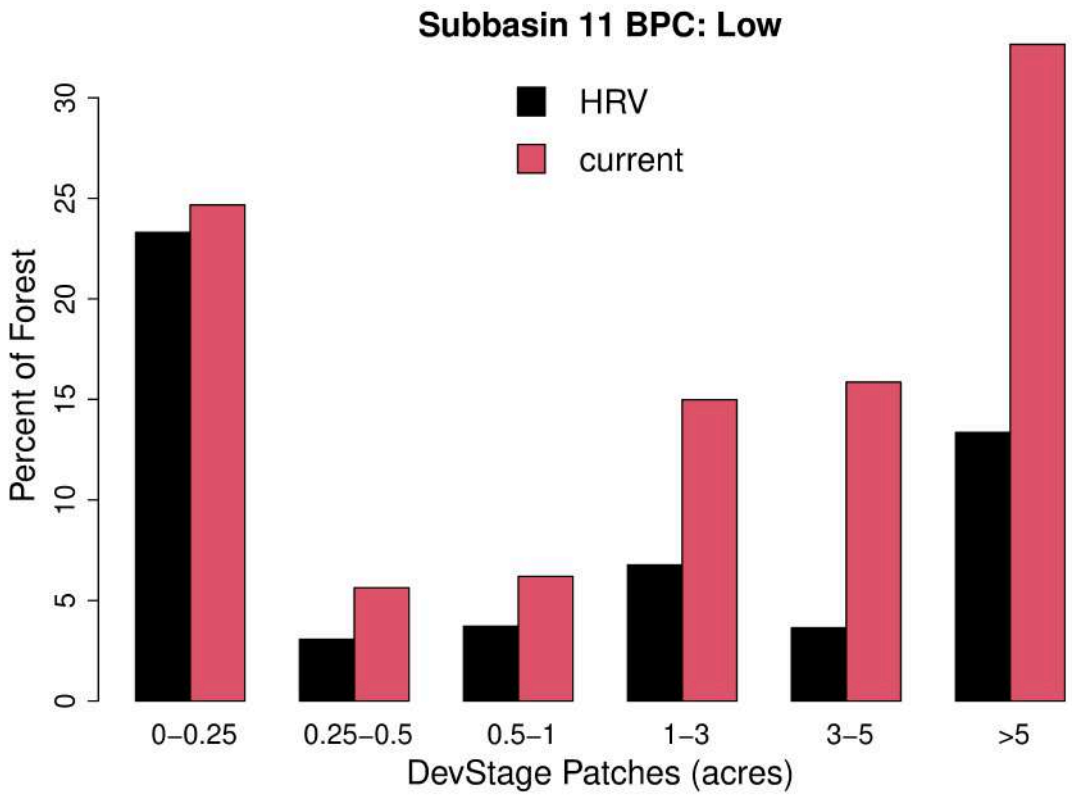

Figure 35: Barplot of the distribution of developmental stage patch sizes for the current landscape and the historical reference period (HRV) for subbasin 11 and the Low productivity Biophysical Class (BPC = 1) for the American North Fork River landscape. Developmental stages were based on tree height classes and patches were based on the 4-neighbor adjacency rule. Each bar represents the percent of forest within the subbasin and BPC in developmental stage patches of a particular size. The departure index represents the sum of the deviations between the current and HRV bars. Departure indices > 0 represent a current landscape with a distribution of developmental stage patch sizes that differs in some way from the historical reference period distribution, as simulated, and increasing values represent increasing degrees of departure.

Metric 4: Percent Large Trees

We defined large trees as > 30 inch dbh. Percent Large Trees is defined as the percent of the forest within the subbasin-by-BPC partition in large trees, as defined, and the departure index reflects whether or not the current landscape is deficient in large trees relative to HRV and, if so, the degree of deficiency. The departure index is negative if the current landscape has too little area in large trees compared to HRV.

The Percent Large Trees departure index is depicted in **Figure 36**. As before, the departure index was assigned to each subbasin-by-BPC partition; consequently, there were 144 distinct values assigned. Thus, to better assess departure by subbasin and BPC, one needs to examine the attribute table for the departure layer.

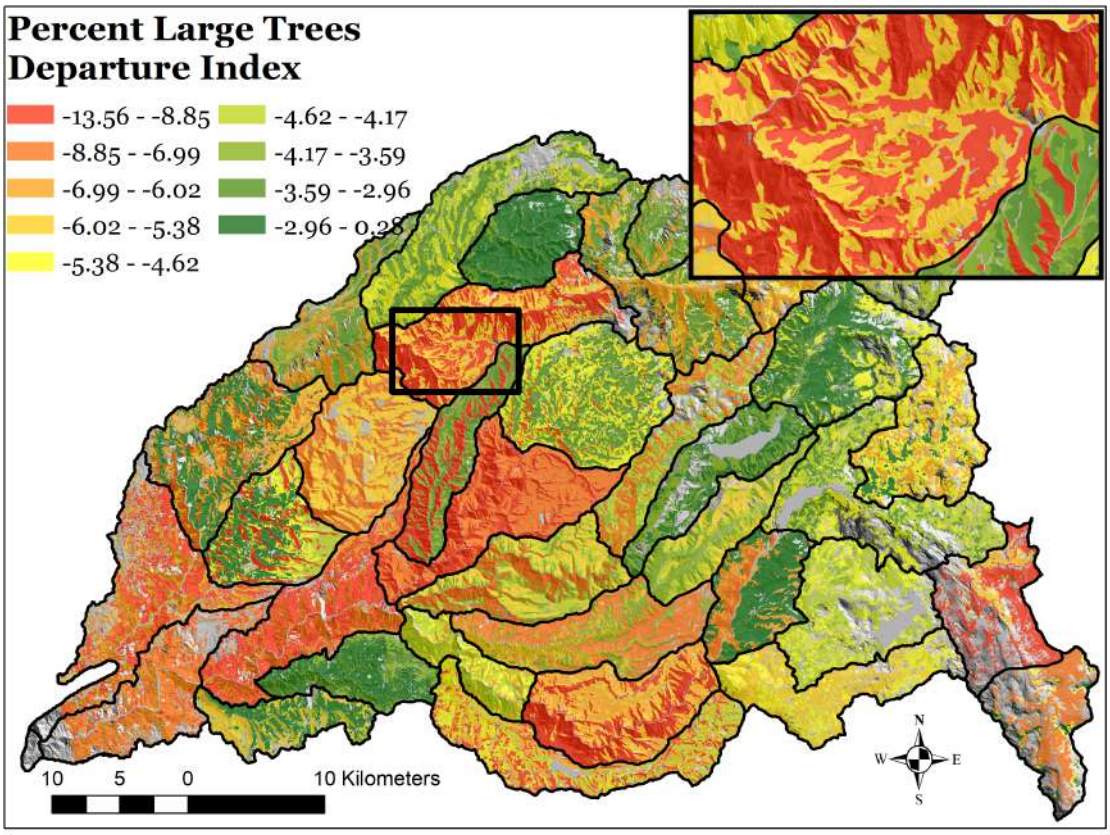

Figure 36: Subbasin-by-BPC level departure index for large trees (> 30 inch dbh) for the American North Fork River landscape. The departure index represents the deviation of the current subbasin and biophsyical class (BPC) condition from its historical reference period condition, as simulated. Departure indices < -1 represent a current landscape with less total area in large trees than during the historical reference period, as simulated, and increasing negative values represent increasing degrees of departure.

Metric 5: Large Tree Patch Size Distribution

We defined large trees as described above. Here, we quantified the size of individual patches of large trees and determined the percent of forest within the subbasin-by-BPC partition in large tree patches in each of several patch size classes or bins (see above), and compared the current and historical distributions. The departure index reflects whether or not the current landscape has a distribution of large tree patch sizes that differs from HRV and, if so, the degree of differences in the two distributions.

The Large Tree Patch Size Distribution departure index is depicted in **Figure 37**. As before, the departure index was assigned to each subbasin-by-BPC partition; consequently, there were 144 distinct values assigned. Thus, to better assess departure by subbasin and BPC, one needs to examine the attribute table for the departure layer.

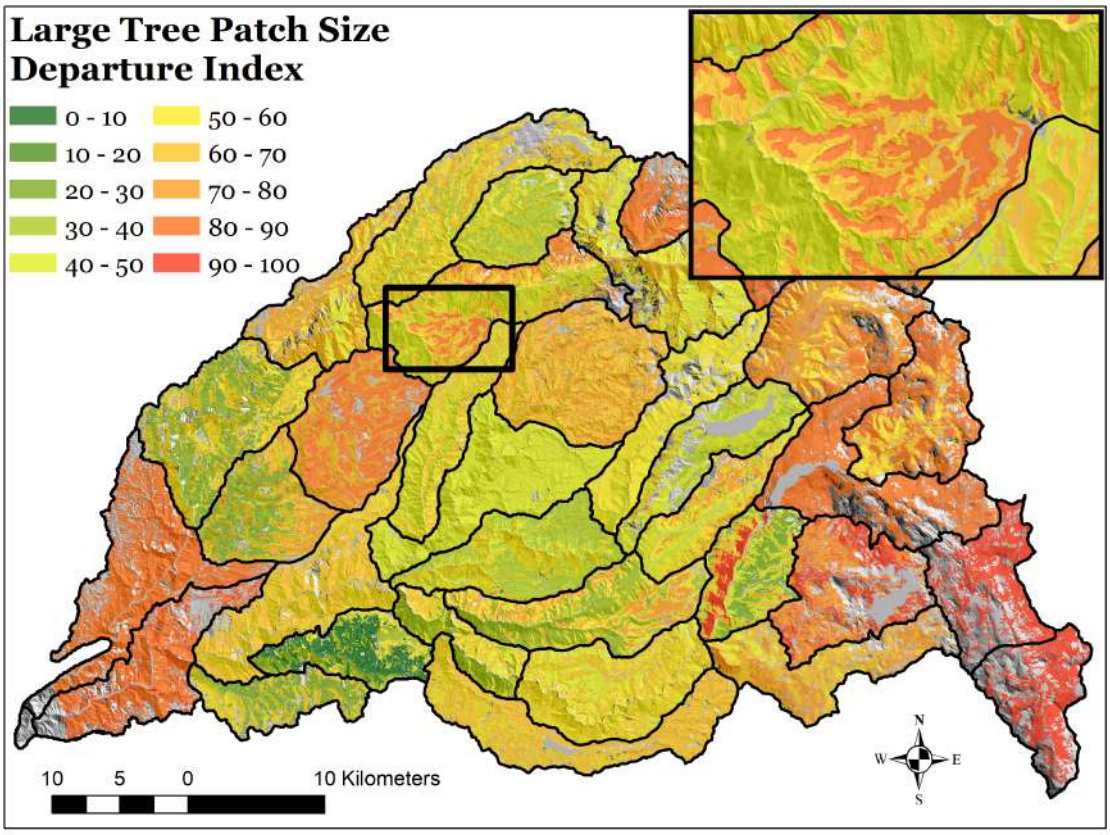

Figure 37: Subbasin-by-BPC level departure index for large tree (> 30 inch dbh) patch size distribution for the American North Fork River landscape. The departure index represents the deviation of the current subbasin and biophsyical class (BPC) condition from its historical reference period condition, as simulated. Departure indices > 0 represent a current landscape with a distribution of large tree patch sizes that differs in some way from the historical reference period distribution, as simulated, and increasing values represent increasing degrees of departure.

To further evaluate departure in this patch size distribution metric, it is necessary to examine the CRV and HRV patch size distributions for the selected subbasin-by-BPC partition, for example as depicted in **Figure 38**.

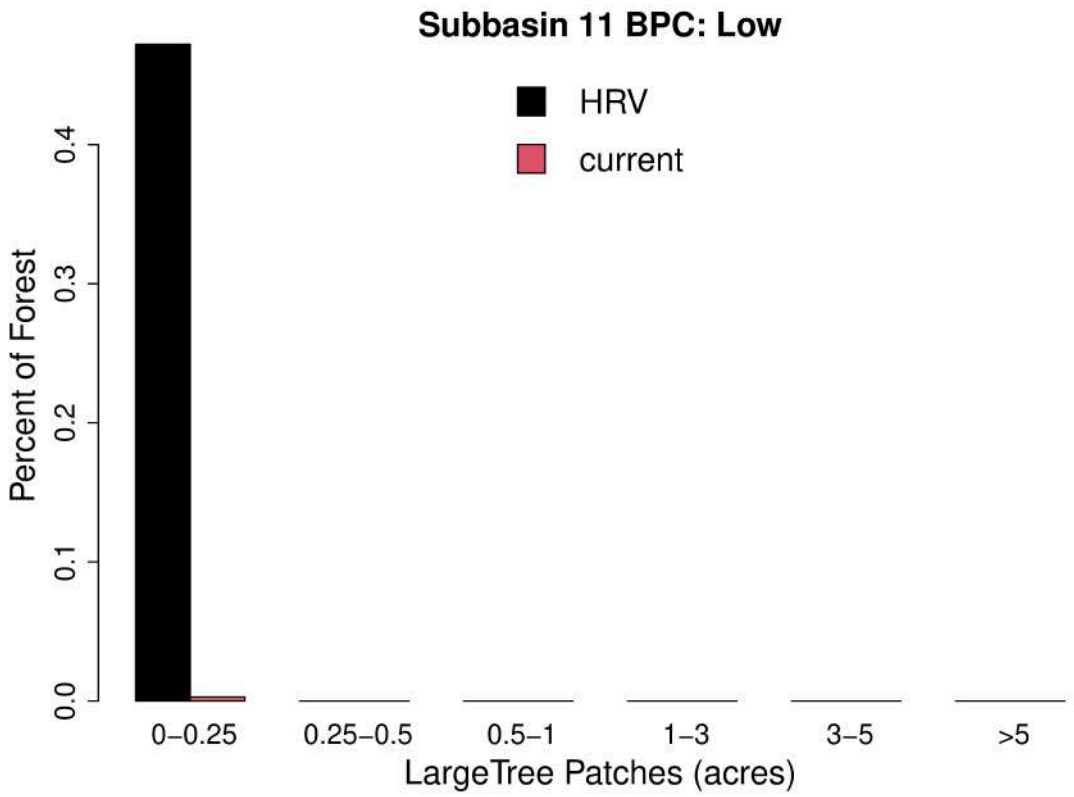

Figure 38: Barplot of the distribution of large tree (> 30 inch dbh) patch sizes for the current landscape and the historical reference period (HRV) for subbasin 11 and the Low productivity Biophysical Class (BPC = 4) for the American North Fork River landscape. See previous barplot caption for details on interpretation.

Metric 6: Tree Size Class Patch Size Distribution

We defined tree size class based on six tree diameter classes, ranging from Open (< 1 in dbh) to large Trees (> 30 in dbh), as described previously. Here, for each snapshot of the landscape we constructed a patch mosaic comprised of tree size classes in which patches were defined using the 4-neighbor rule. For each snapshot, we quantified the size of each tree size class patch and determined the percent of forest within the subbasin-by-BPC partition in each of several patch size classes or bins. The departure index reflects whether or not the current landscape has a distribution of tree size class patch sizes that differs from HRV and, if so, the degree of differences in the two distributions.

The Tree Size Class Patch Size Distribution departure index is depicted in **Figure 39**. As before, the departure index was assigned to each subbasin-by-BPC partition; consequently, there were 144 distinct values assigned. Thus, to better assess departure by subbasin and BPC, one needs to examine the attribute table for the departure layer.

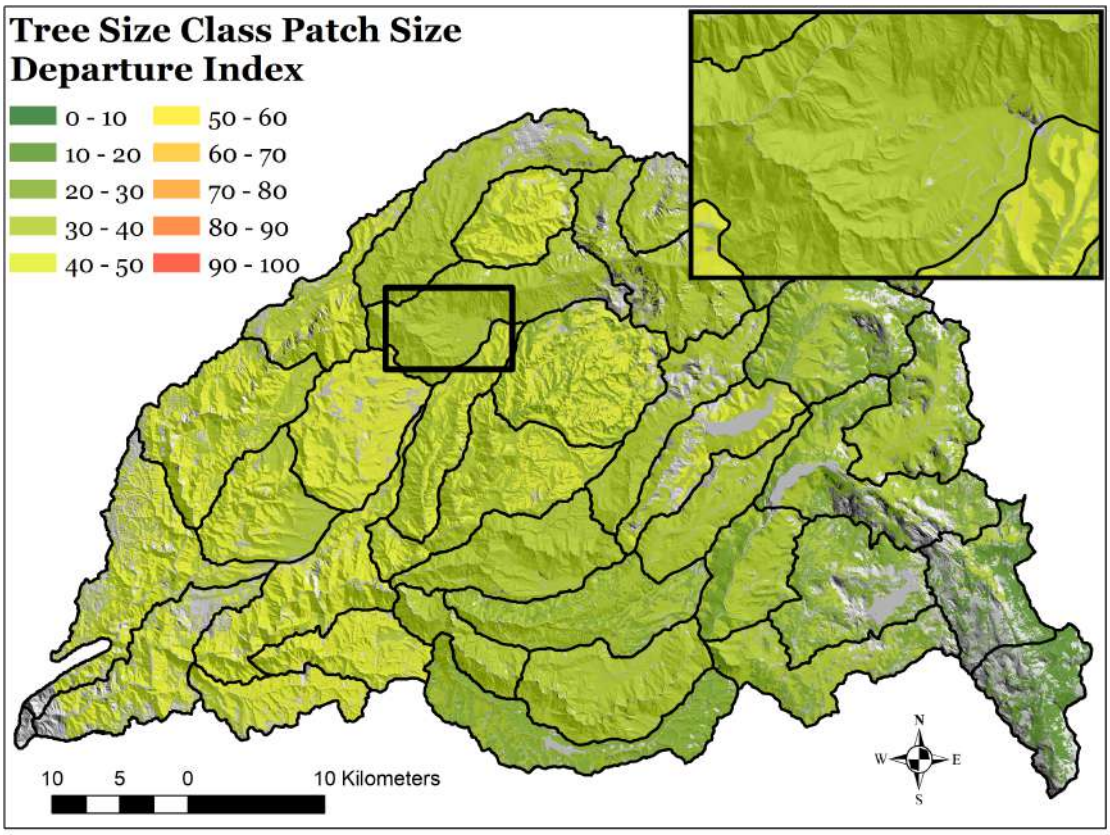

Figure 39: Subbasin-by-BPC level departure index for tree size class (based on dbh) patch size distribution for the American North Fork River landscape. The departure index represents the deviation of the current subbasin and biophsyical class (BPC) condition from its historical reference period condition, as simulated. Departure indices > 0 represent a current landscape with a distribution of tree size patch sizes that differs in some way from the historical reference period distribution, as simulated, and increasing values represent increasing degrees of departure.

To further evaluate departure in this patch size distribution metric, it is necessary to examine the CRV and HRV patch size distributions for the selected subbasin-by-BPC partition, for example as depicted in **Figure 40**.

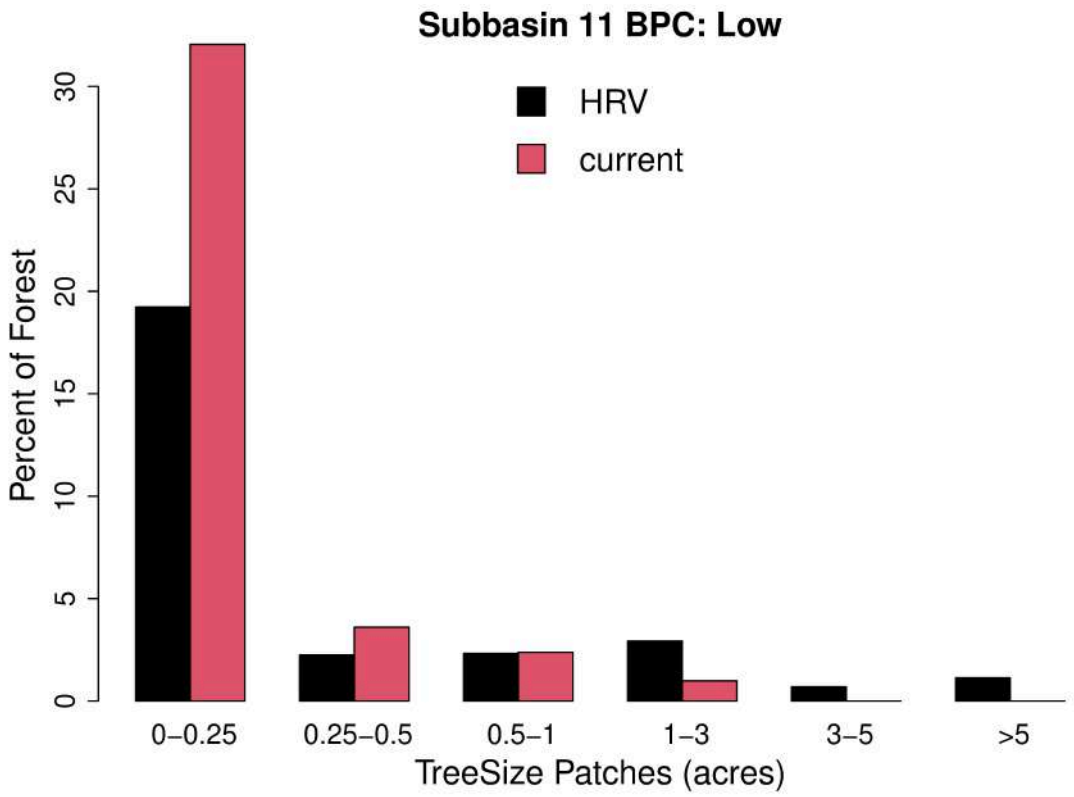

Figure 40: Barplot of the distribution of tree size class (based on dbh) patch sizes for the current landscape and the historical reference period (HRV) for subbasin 11 and the Low productivity Biophysical Class (BPC = 4) for the American North Fork River landscape. See previous barplot caption for details on interpretation.

Composite Departure Score

We combined the 6 subbasin-level departure metrics above into a single composite departure score, which can be interpreted as a measure of overall departure in vegetation composition and configuration within the subbasin-by-BPC partition. Maximum departure occurs when the forest has too little area in large forest openings and/or large trees, and/or too homogeneous or uniform a vegetation patch mosaic (i.e., too little spatial variability) defined on the basis of either developmental stages (or tree height classes) or tree size classes (or tree diameter classes).

The composite departure score is depicted in **Figure 41**. Not surprisingly, the subbasins and BPCs vary somewhat in their overall departure from HRV, and these differences provide a basis for prioritizing project locations with this landscape.

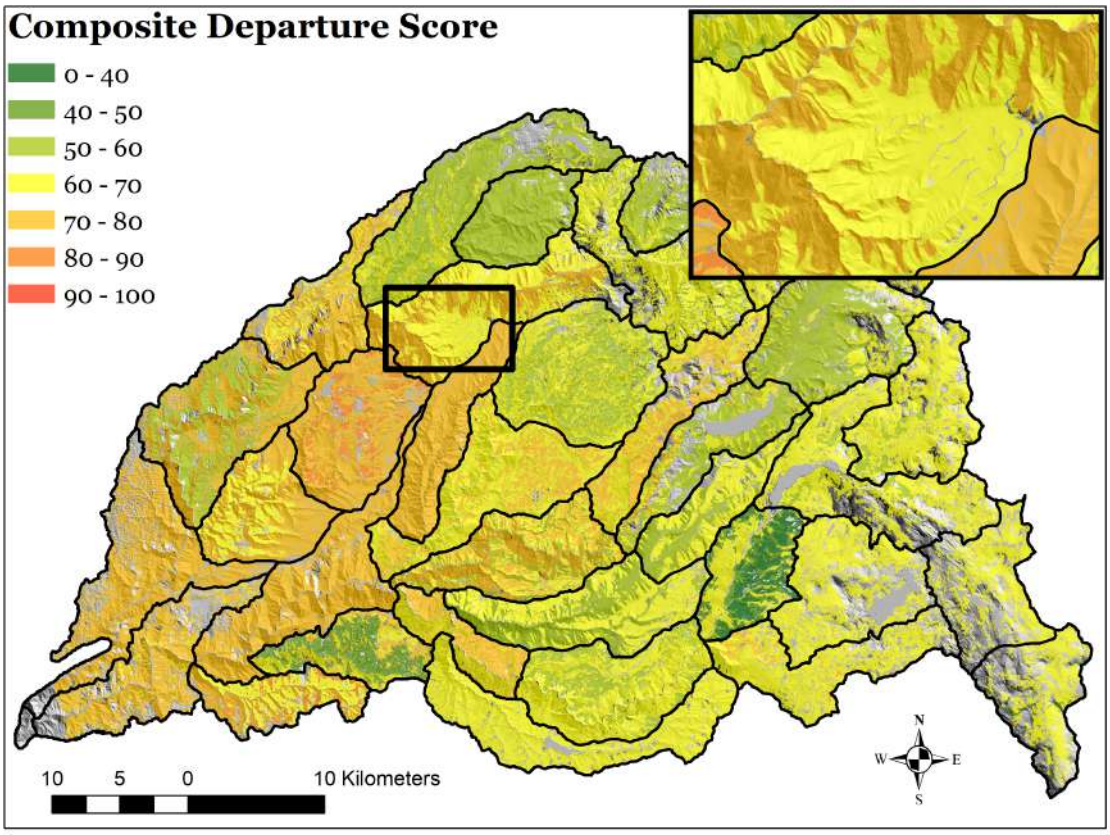

Figure 41: Subbasin-by-BPC level composite departure index derived from the average of the six component metrics for the American North Fork River landscape. The composite departure index represents the percentage of maximum departure of the current GPU condition from its historical range of variability (HRV), as simulated. Larger values indicate increasing degrees of departure.

APPENDIX E1 - Wildfire Susceptibility

As described in the text, wildfire susceptibility was modeled as a Logistic function of fuels and climate for most cover types. The fuels component was modeled as a Logistic function of the number of years since the last fire (fuelAge) and the Heat Load Index (hli). The climate component was modeled as a Logistic function of the Wildfire Climate Index which was based on the inverted and rescaled 5-year mean Palmer Modified Drought Index. The fuels and climate components were combined with a geometric mean to produce the final Wildfire Susceptibility Index. The final function included 5 beta coefficients (b_0 - b_4). We used expert opinion to specify the beta coefficients for each cover type. We varied the b_0 and b_1 coefficients among cover types to reflect differences in reported historical mean fire return intervals among cover types - shifting the response curves left or right so that the inflection point (Wildfire Susceptibility Index = 0.5) roughly equaled the target mean return interval - and held the Heat Load Index coefficient (b_2) and Climate coefficients (b_3 and b_4) the same across all cover types to reflect the global affect of topography and climate on wildfire susceptibility.

The figures below depict the final wildfire susceptibility response functions for each cover type in alphabetical order (noting that some cover types did not have response functions as noted in the text). The response functions depict the wildfire Susceptibility Index as a Logistic function of the number of years since the last fire (Years since fire). The dashed, solid and dotted lines depict the response functions for the minimum, mean and maximum Heat Load Index (hli), and the red, black and green sets of lines depict the response functions for the minimum, mean and maximum Wildfire Climate Index. The values of the Logistic parameters (b_0 - b_4) for the cover type are shown as well.

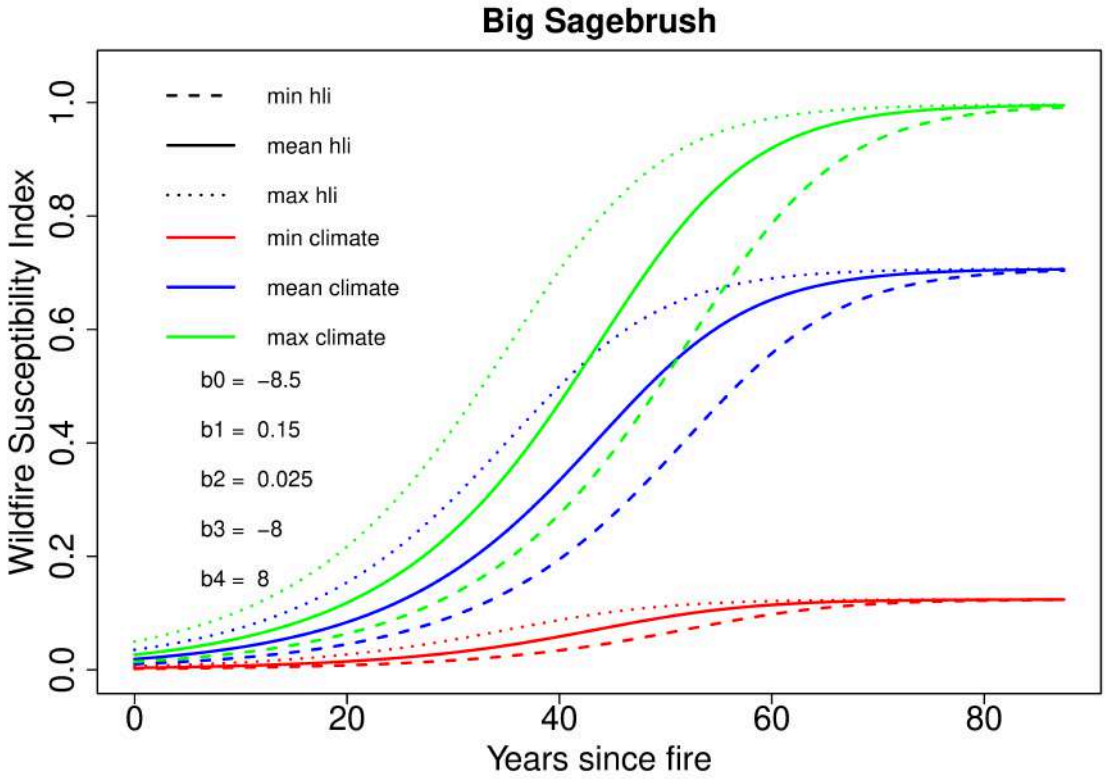

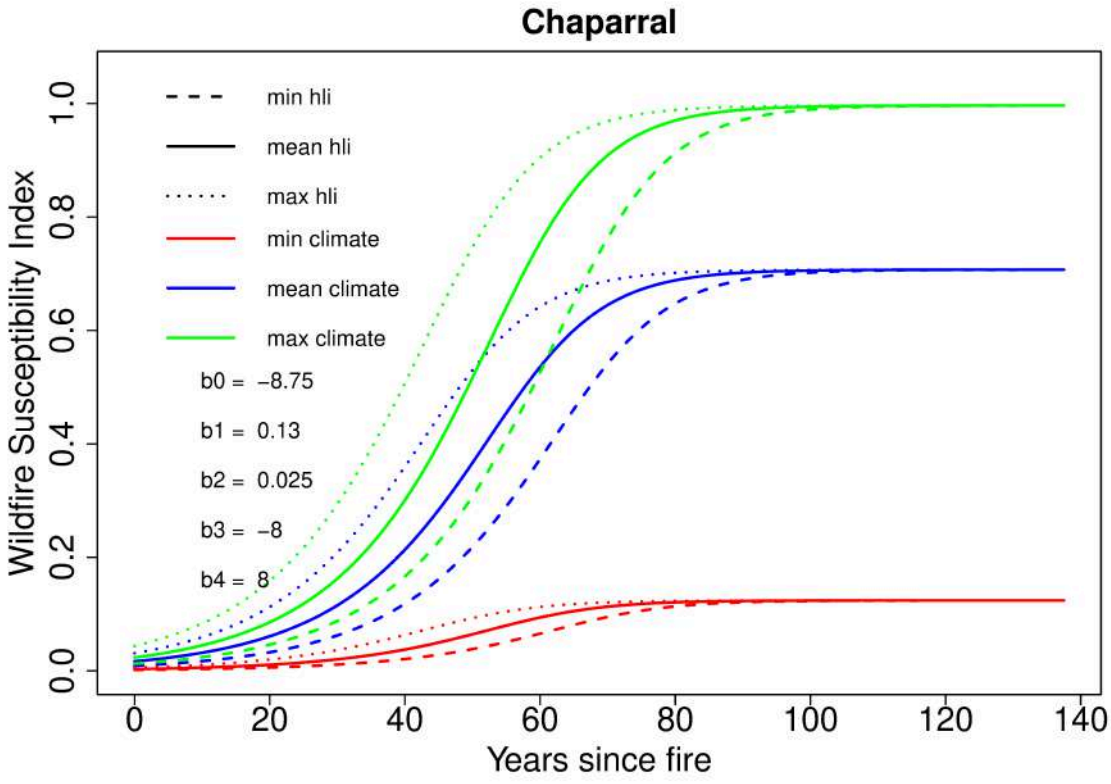
Chaparral
min hli
mean hli
max hli
min climate
mean climate
max climate
b0 = −8.75
b1 = 0.13
b2 = 0.025
b3 = −8
b4 = 8
Wildfire Susceptibility Index
0.0
0.2
0.4
0.6
0.8
1.0
0
20
40
60
80
100
120
140
Years since fire

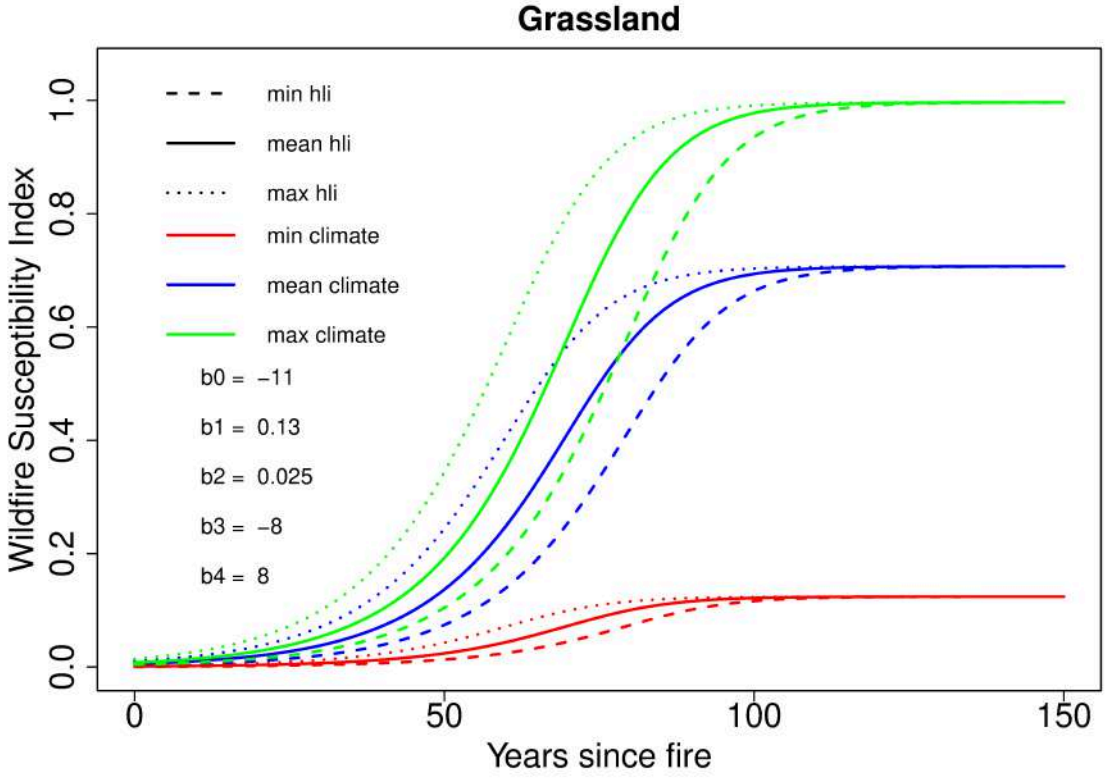
Grassland
min hli
mean hli
max hli
min climate
mean climate
max climate
b0 = −11
b1 = 0.13
b2 = 0.025
b3 = −8
b4 = 8
Wildfire Susceptibility Index
0.0
0.2
0.4
0.6
0.8
1.0
0
50
100
150
Years since fire

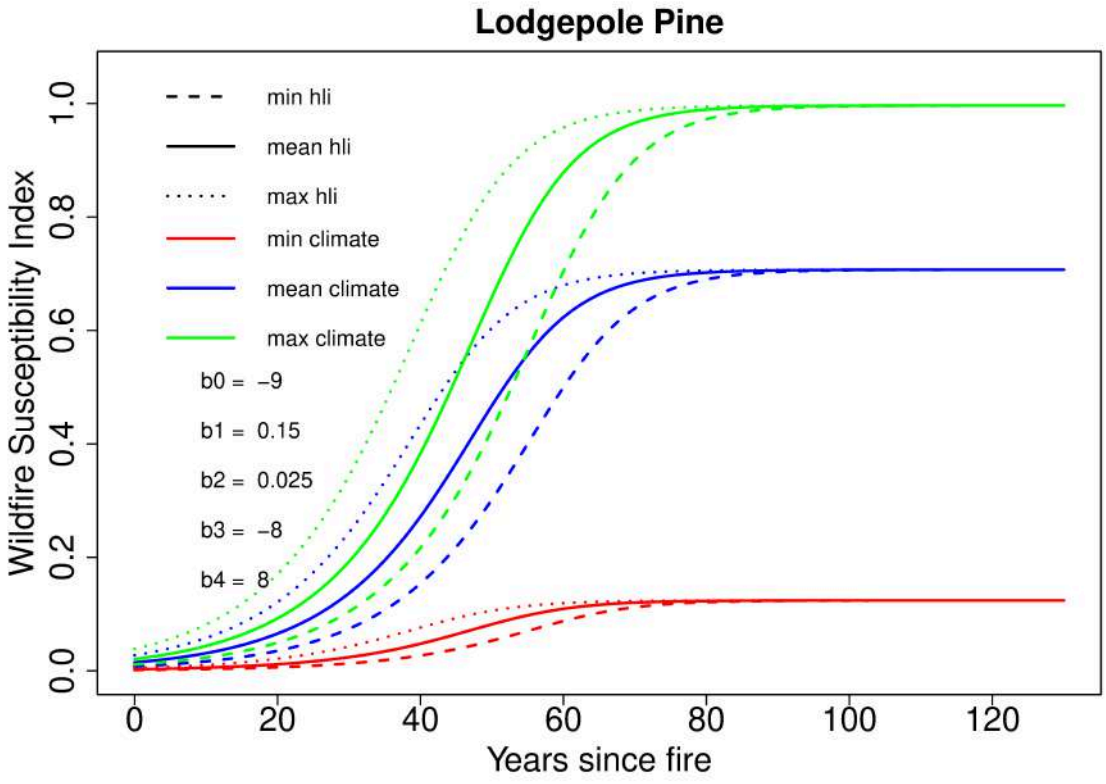
Lodgepole Pine
min hli
mean hli
max hli
min climate
mean climate
max climate
b0 = −9
b1 = 0.15
b2 = 0.025
b3 = −8
b4 = 8
Wildfire Susceptibility Index
0.0
0.2
0.4
0.6
0.8
1.0
0
20
40
60
80
100
120
Years since fire

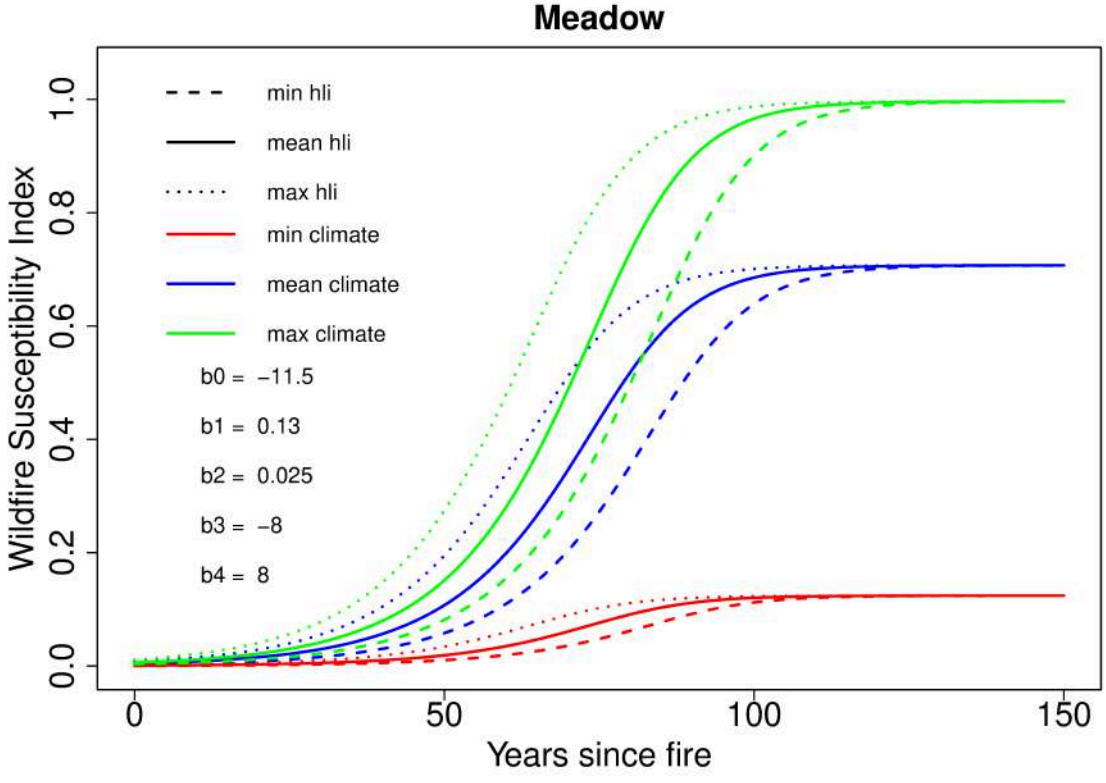
Meadow
min hli
mean hli
max hli
min climate
mean climate
max climate
b0 = −11.5
b1 = 0.13
b2 = 0.025
b3 = −8
b4 = 8
Wildfire Susceptibility Index
0.0
0.2
0.4
0.6
0.8
1.0
0
50
100
150
Years since fire

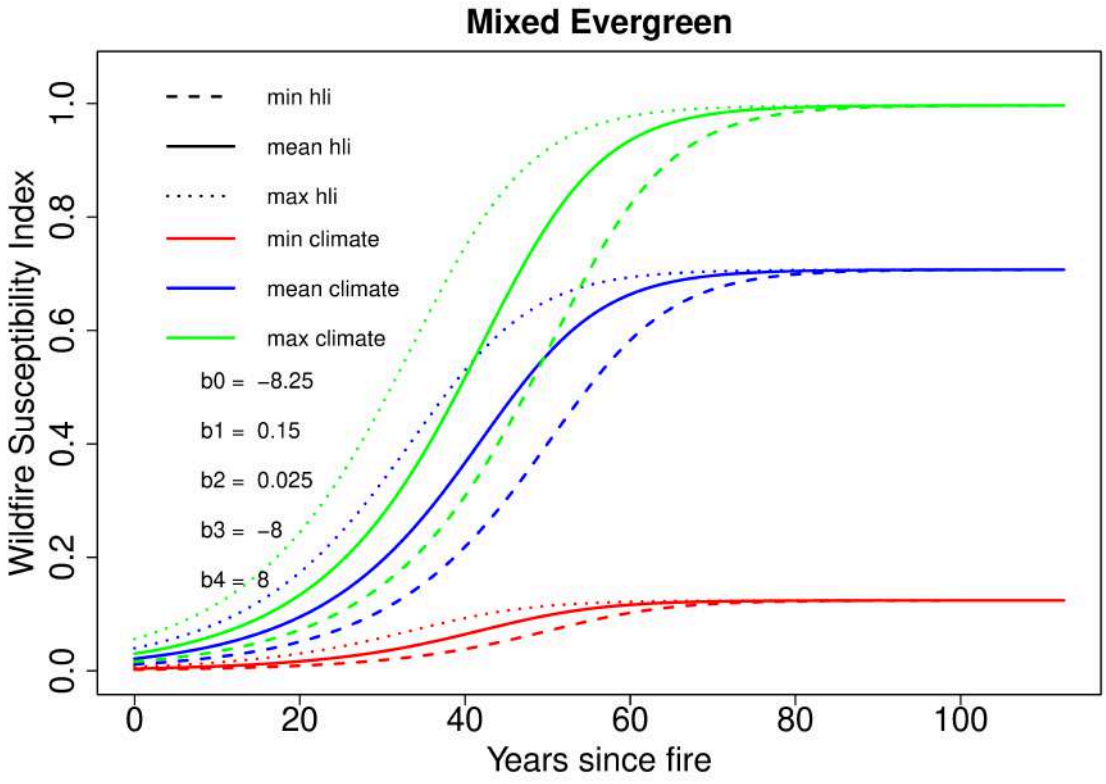
Mixed Evergreen
min hli
mean hli
max hli
min climate
mean climate
max climate
b0 = −8.25
b1 = 0.15
b2 = 0.025
b3 = −8
b4 = 8
Wildfire Susceptibility Index
0.0
0.2
0.4
0.6
0.8
1.0
0
20
40
60
80
100
Years since fire

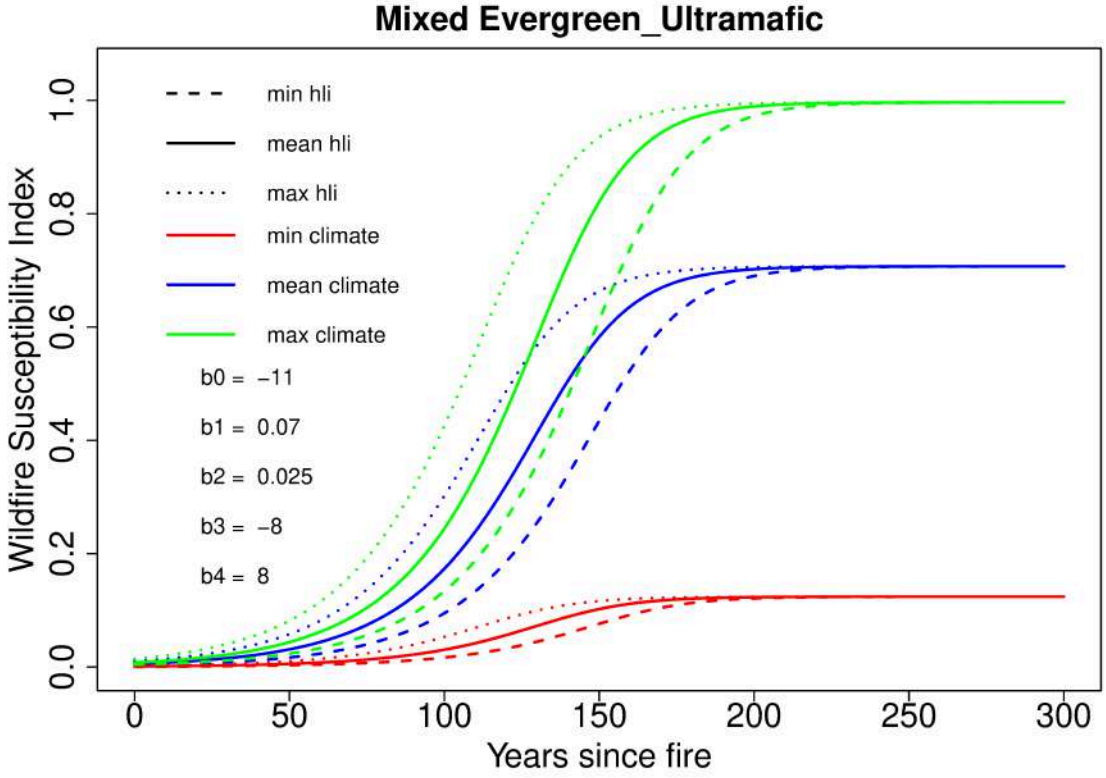
Mixed Evergreen_Ultramafic
min hli
mean hli
max hli
min climate
mean climate
max climate
b0 = −11
b1 = 0.07
b2 = 0.025
b3 = −8
b4 = 8
Wildfire Susceptibility Index
0.0
0.2
0.4
0.6
0.8
1.0
0
50
100
150
200
250
300
Years since fire

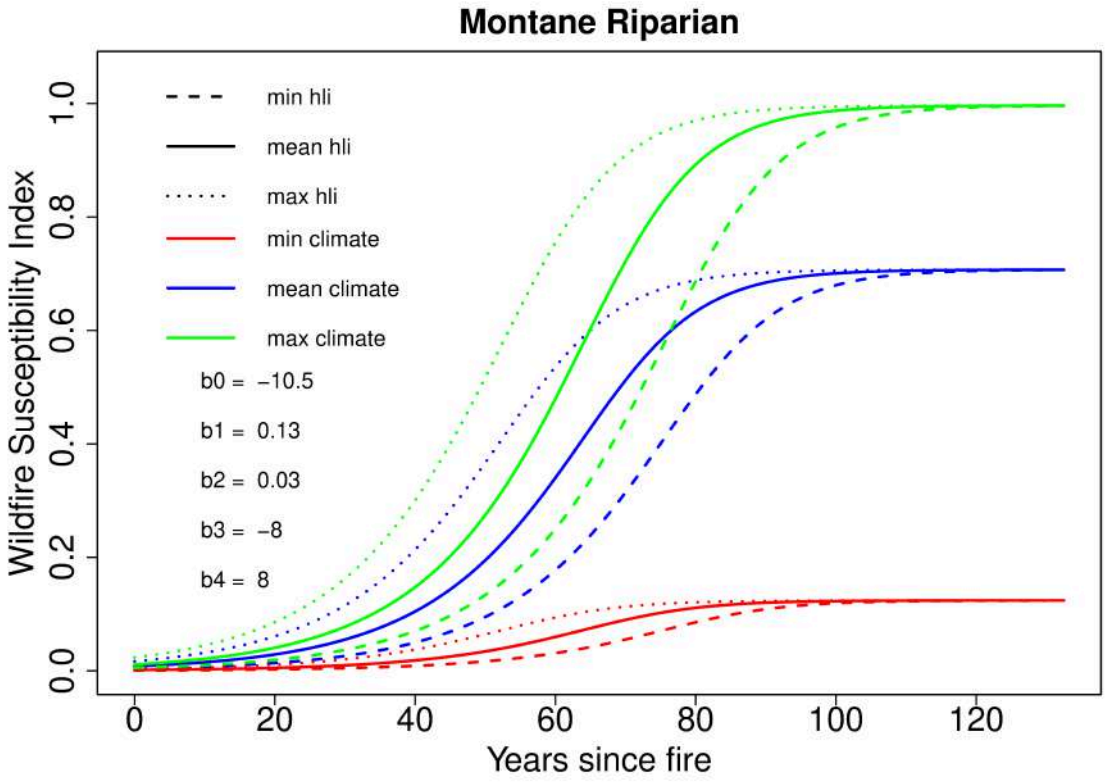
Montane Riparian
min hli
mean hli
max hli
min climate
mean climate
max climate
b0 = −10.5
b1 = 0.13
b2 = 0.03
b3 = −8
b4 = 8
Wildfire Susceptibility Index
0.0
0.2
0.4
0.6
0.8
1.0
0
20
40
60
80
100
120
Years since fire

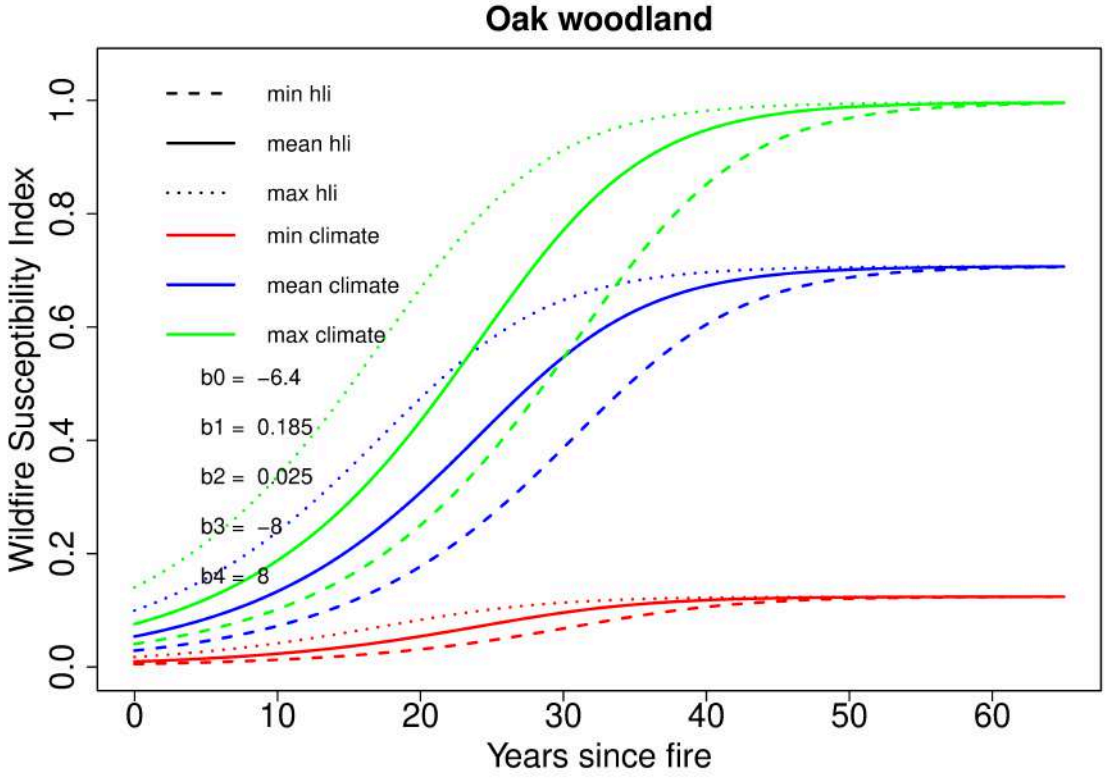
Oak woodland
min hli
mean hli
max hli
min climate
mean climate
max climate
b0 = −6.4
b1 = 0.185
b2 = 0.025
b3 = −8
b4 = 8
Wildfire Susceptibility Index
0.0
0.2
0.4
0.6
0.8
1.0
0
10
20
30
40
50
60
Years since fire

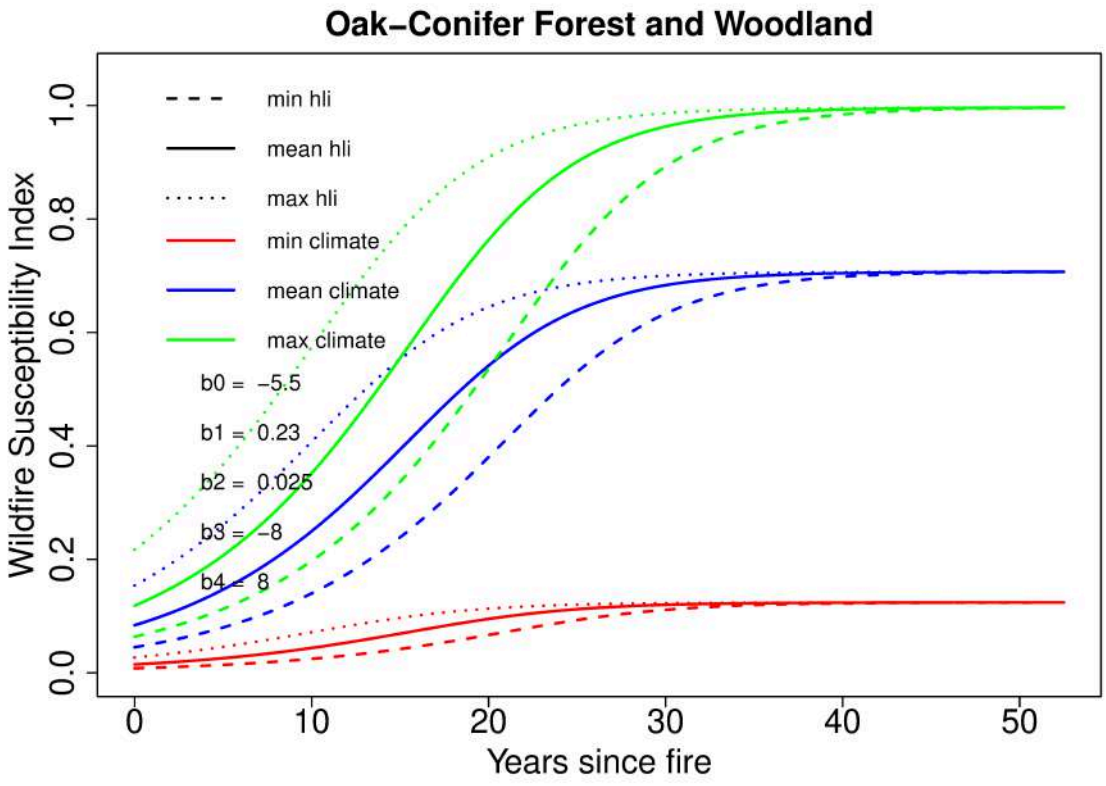
Oak–Conifer Forest and Woodland
min hli
mean hli
max hli
min climate
mean climate
max climate
b0 = −5.5
b1 = 0.23
b2 = 0.025
b3 = −8
b4 = 8
Wildfire Susceptibility Index
0.0
0.2
0.4
0.6
0.8
1.0
0
10
20
30
40
50
Years since fire

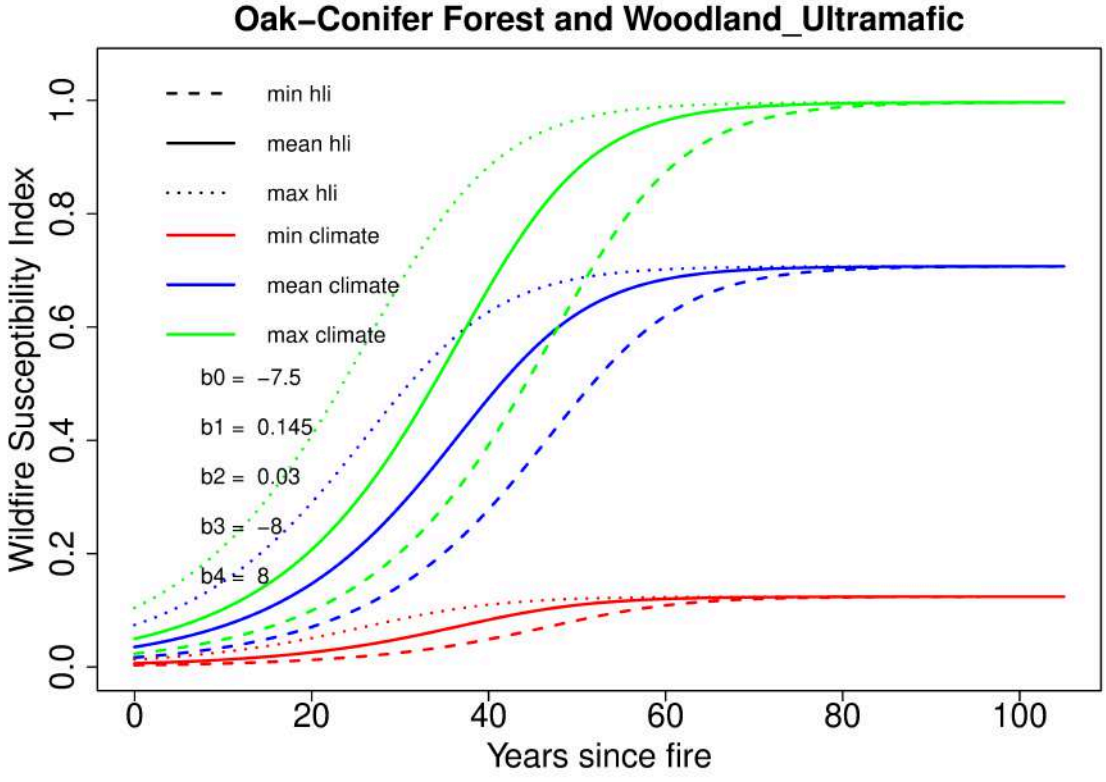
Oak–Conifer Forest and Woodland_Ultramafic
min hli
mean hli
max hli
min climate
mean climate
max climate
b0 = −7.5
b1 = 0.145
b2 = 0.03
b3 = −8
b4 = 8
Wildfire Susceptibility Index
0.0
0.2
0.4
0.6
0.8
1.0
0
20
40
60
80
100
Years since fire

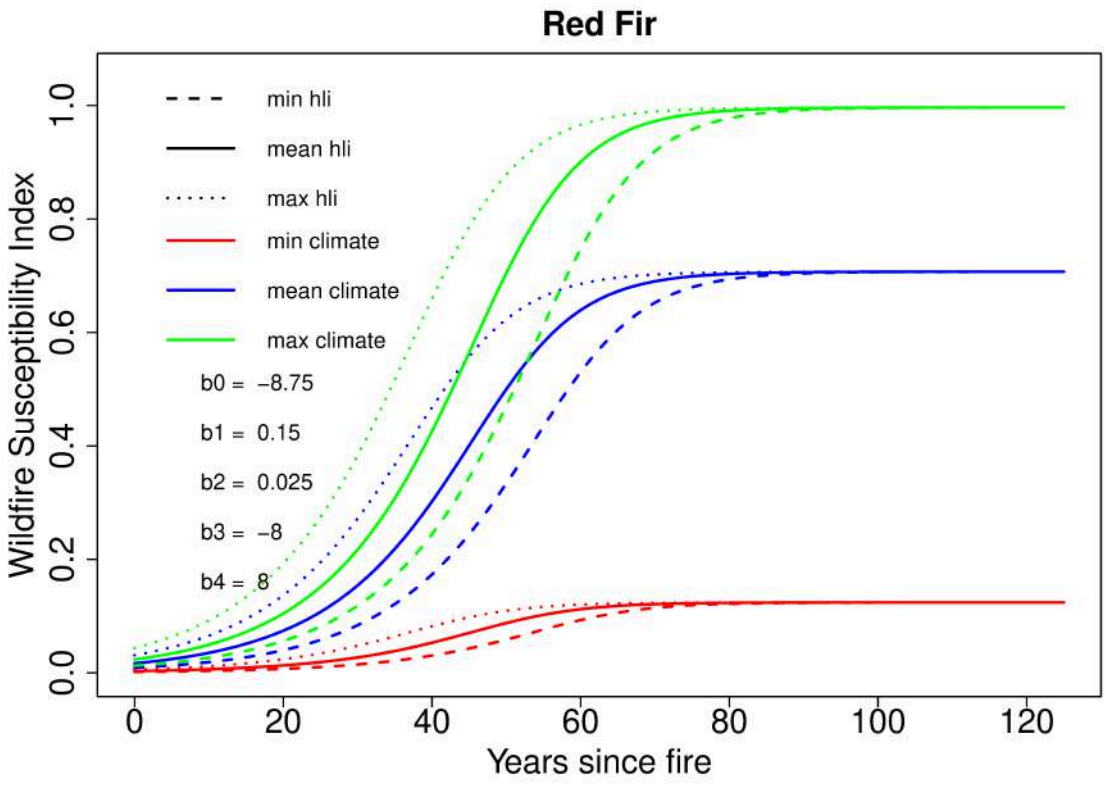
Red Fir
min hli
mean hli
max hli
min climate
mean climate
max climate
b0 = −8.75
b1 = 0.15
b2 = 0.025
b3 = −8
b4 = 8
Wildfire Susceptibility Index
0.0
0.2
0.4
0.6
0.8
1.0
0
20
40
60
80
100
120
Years since fire

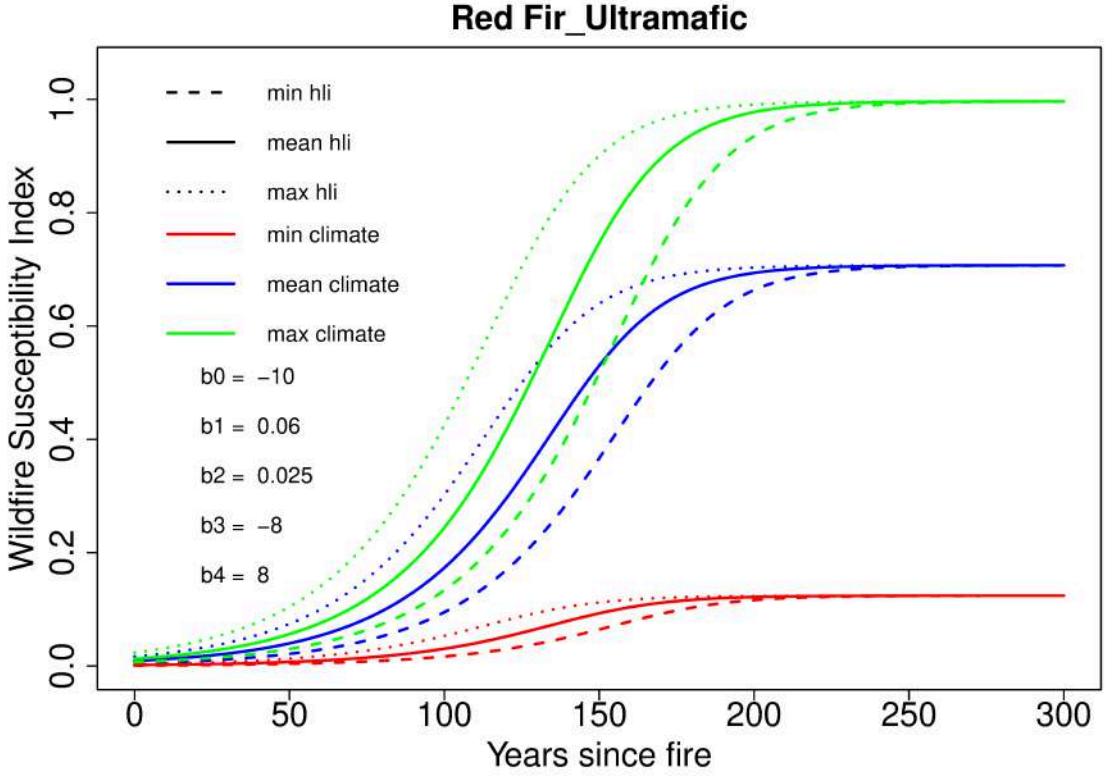
Red Fir_Ultramafic
min hli
mean hli
max hli
min climate
mean climate
max climate
b0 = −10
b1 = 0.06
b2 = 0.025
b3 = −8
b4 = 8
Wildfire Susceptibility Index
0.0
0.2
0.4
0.6
0.8
1.0
0
50
100
150
200
250
300
Years since fire

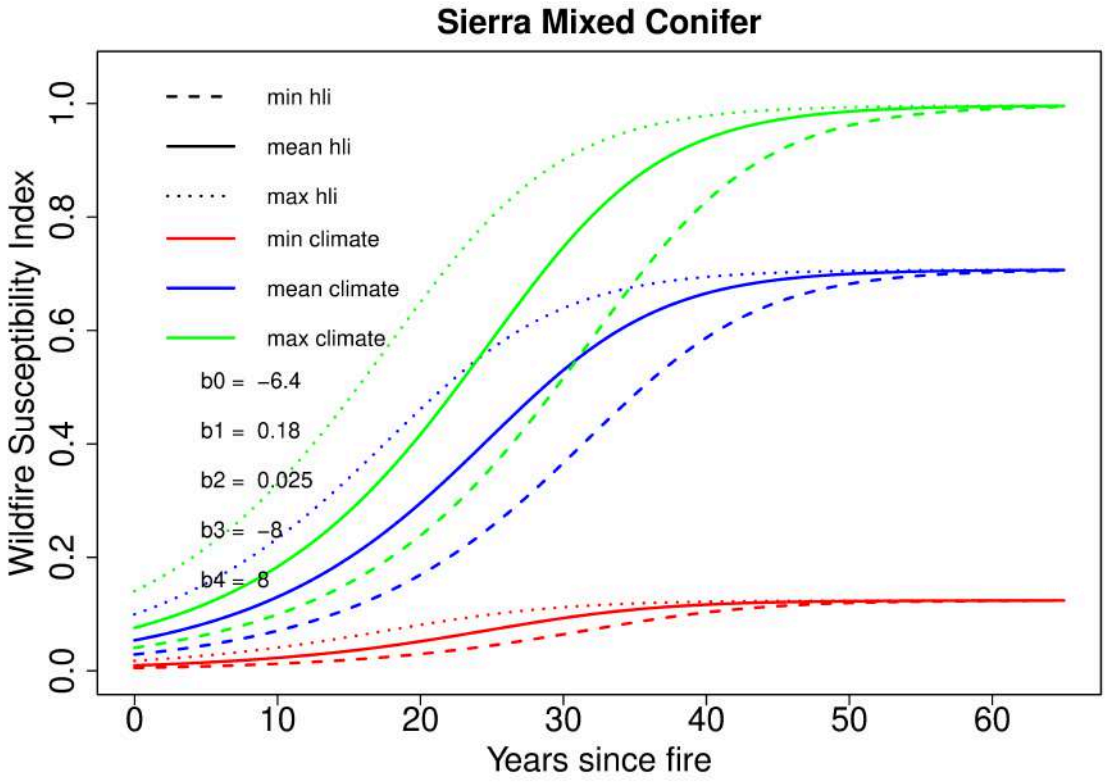
Sierra Mixed Conifer
min hli
mean hli
max hli
min climate
mean climate
max climate
b0 = −6.4
b1 = 0.18
b2 = 0.025
b3 = −8
b4 = 8
Wildfire Susceptibility Index
0.0
0.2
0.4
0.6
0.8
1.0
0
10
20
30
40
50
60
Years since fire

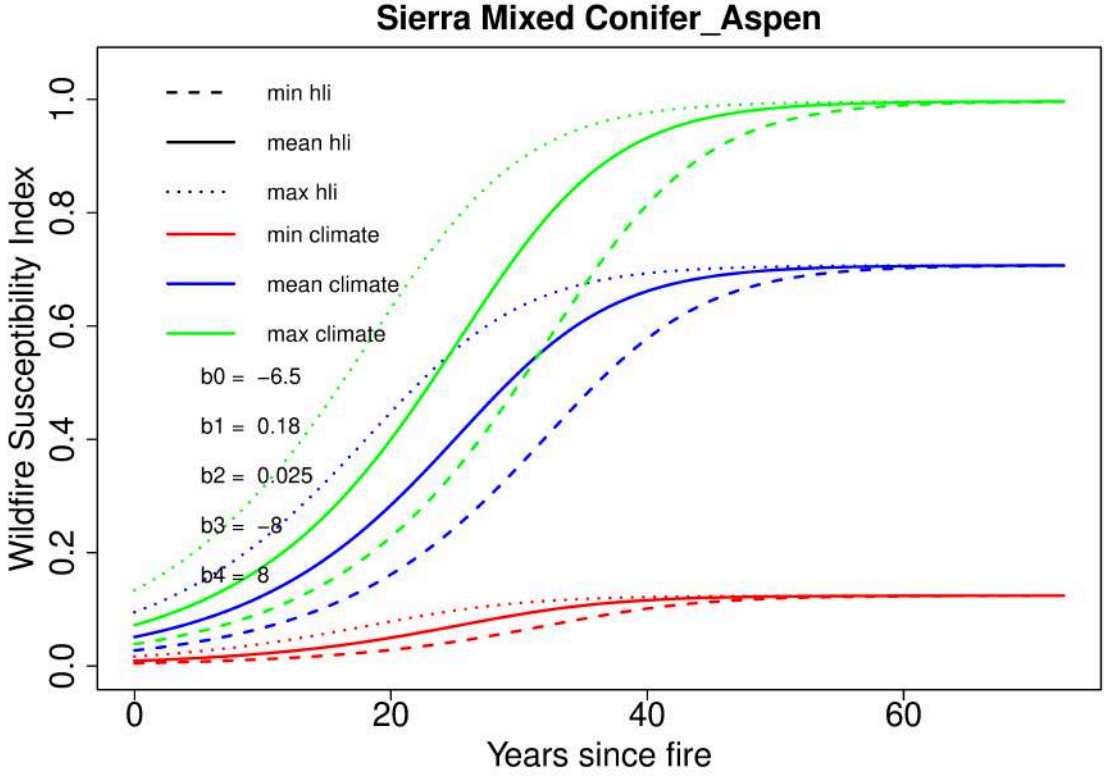
Sierra Mixed Conifer_Aspen
min hli
mean hli
max hli
min climate
mean climate
max climate
b0 = −6.5
b1 = 0.18
b2 = 0.025
b3 = −8
b4 = 8
Wildfire Susceptibility Index
0.0
0.2
0.4
0.6
0.8
1.0
0
20
40
60
Years since fire

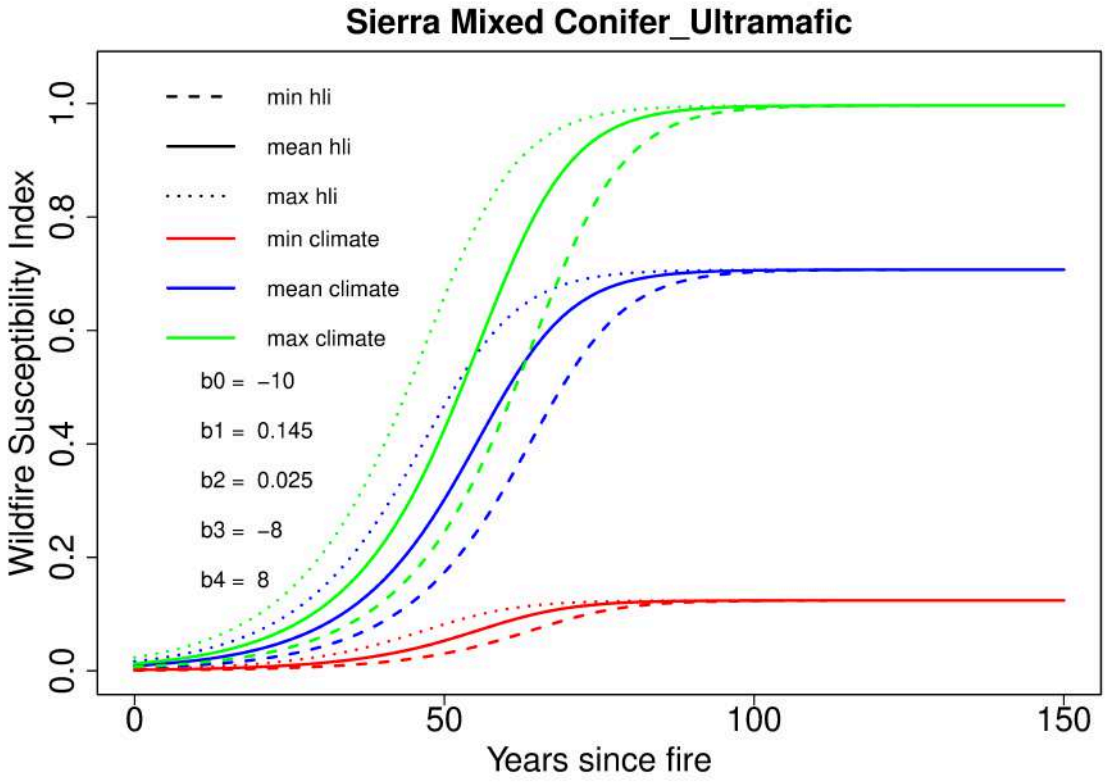
Sierra Mixed Conifer_Ultramafic
min hli
mean hli
max hli
min climate
mean climate
max climate
b0 = −10
b1 = 0.145
b2 = 0.025
b3 = −8
b4 = 8
Wildfire Susceptibility Index
0.0
0.2
0.4
0.6
0.8
1.0
0
50
100
150
Years since fire

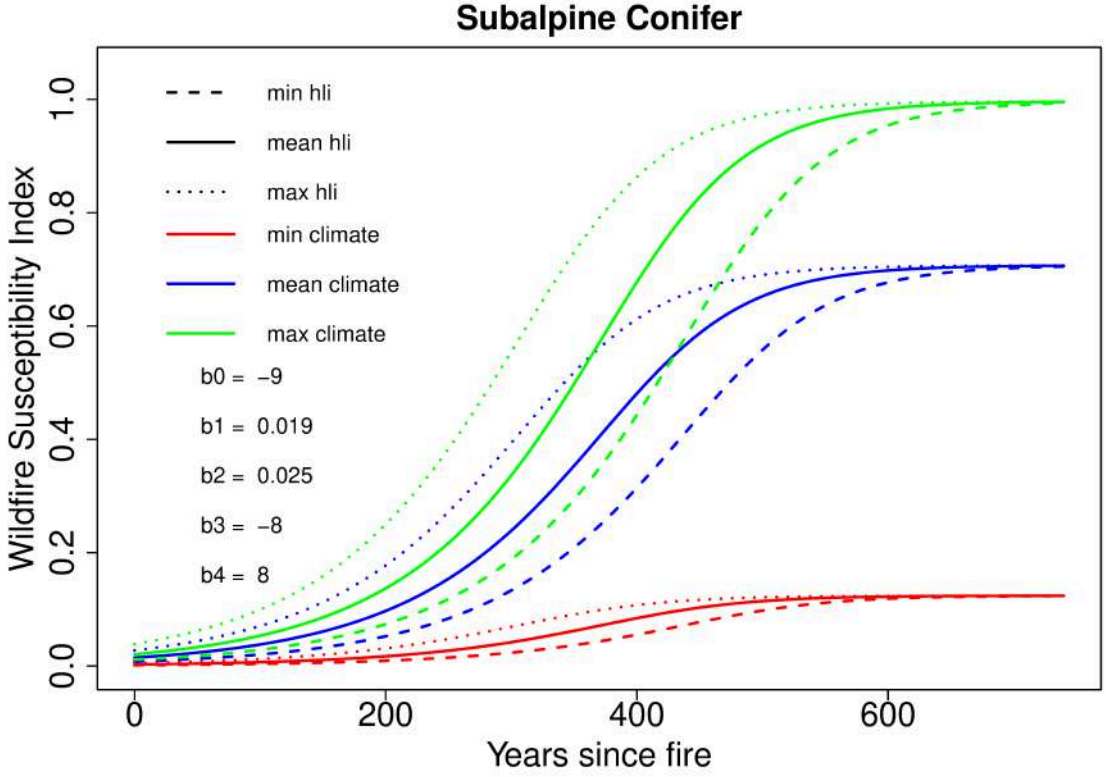
Subalpine Conifer
min hli
mean hli
max hli
min climate
mean climate
max climate
b0 = −9
b1 = 0.019
b2 = 0.025
b3 = −8
b4 = 8
Wildfire Susceptibility Index
0.0
0.2
0.4
0.6
0.8
1.0
0
200
400
600
Years since fire

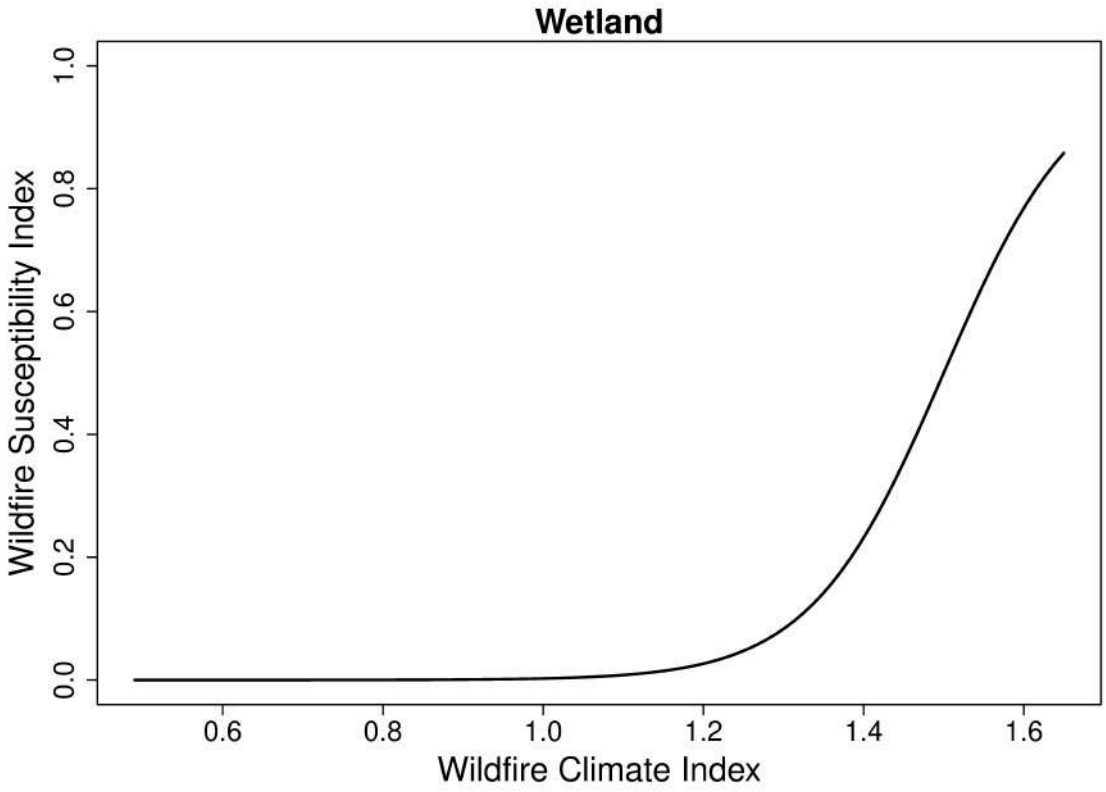
Wetland
Wildfire Susceptibility Index
0.0
0.2
0.4
0.6
0.8
1.0
0.6
0.8
1.0
1.2
1.4
1.6
Wildfire Climate Index

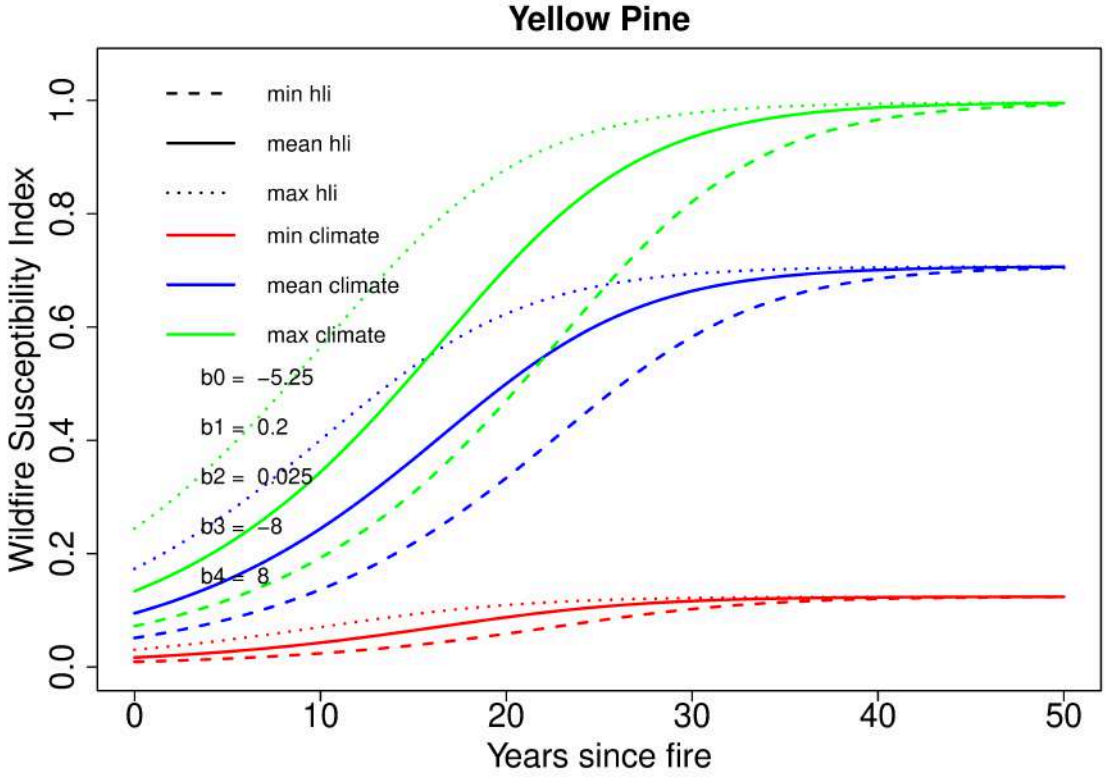
Yellow Pine
min hli
mean hli
max hli
min climate
mean climate
max climate
b0 = −5.25
b1 = 0.2
b2 = 0.025
b3 = −8
b4 = 8
Wildfire Susceptibility Index
0.0
0.2
0.4
0.6
0.8
1.0
0
10
20
30
40
50
Years since fire

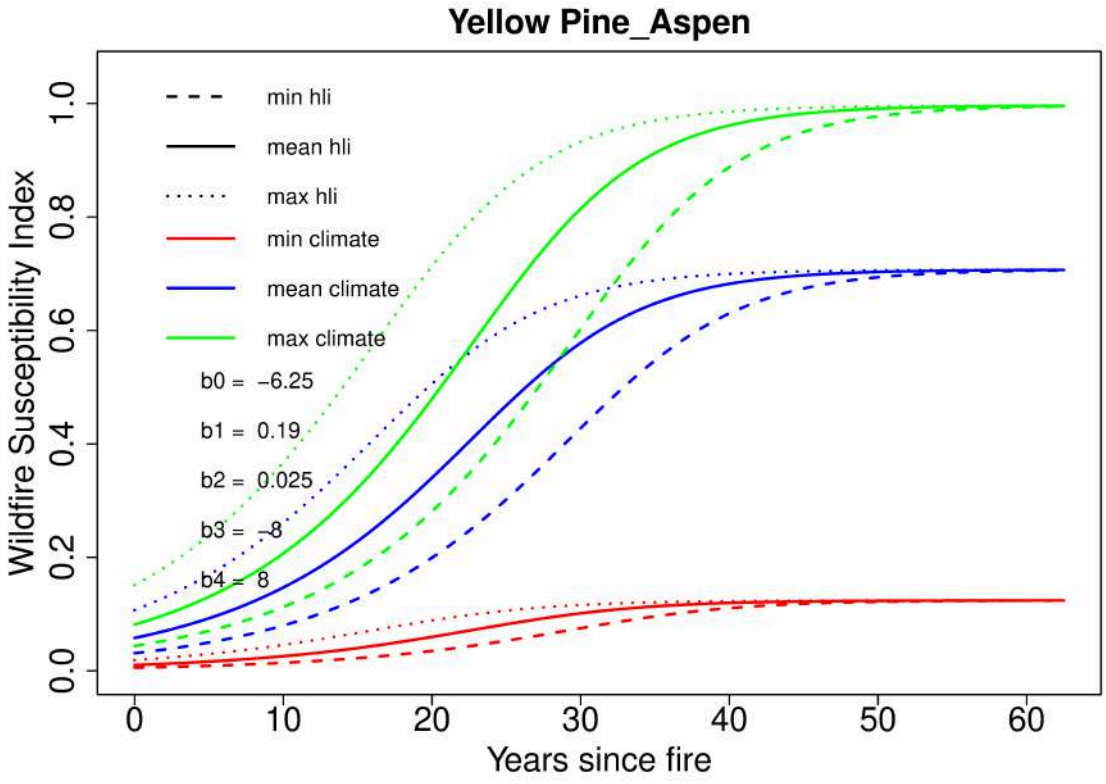
Yellow Pine_Aspen
min hli
mean hli
max hli
min climate
mean climate
max climate
b0 = −6.25
b1 = 0.19
b2 = 0.025
b3 = −8
b4 = 8
Wildfire Susceptibility Index
0.0
0.2
0.4
0.6
0.8
1.0
0
10
20
30
40
50
60
Years since fire

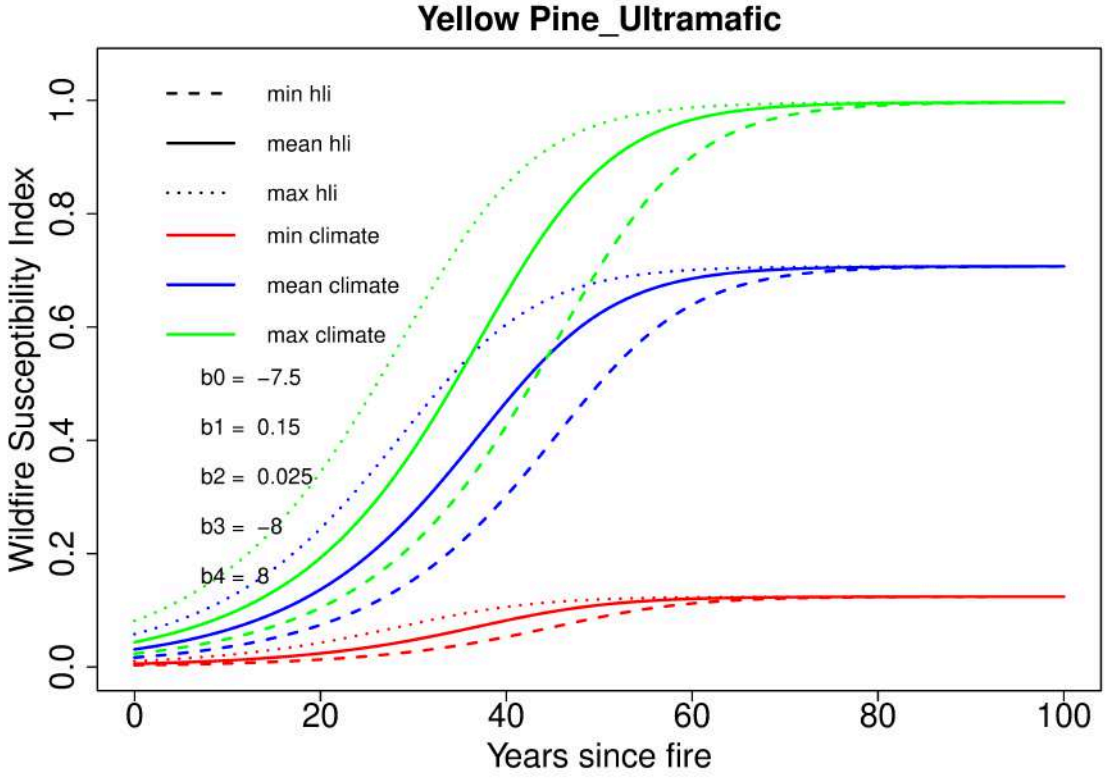
Yellow Pine_Ultramafic
min hli
mean hli
max hli
min climate
mean climate
max climate
b0 = −7.5
b1 = 0.15
b2 = 0.025
b3 = −8
b4 = 8
Wildfire Susceptibility Index
0.0
0.2
0.4
0.6
0.8
1.0
0
20
40
60
80
100
Years since fire

APPENDIX E2 - Wildfire Mortality

As described in the GTR, wildfire mortality (i.e., the probability of high mortality or death of the overstory vegetation in each 5 m cell that burned) was determined by a complex function involving two major factors: 1) fire intensity, which was a Logistic function of the fuel loads in the neighborhood of the focal cell (proxied by the age of the vegetation and time since the last fire), the topographic position of the focal cell, and the climate conditions in the current time step; and 2) the resistance of the focal cell, which was a negative exponential function of the age of the vegetation in the focal cell in which the rate of exponential decline with age decreased with increasing fire intensity (see main text for details). The complex wildfire mortality function included 6 user-specified beta coefficients. As described in the main text, b_0 - b_4 were held constant across all cover types. We varied b_5 and b_6 among cover types to reflect differences in reported historical mean fire return intervals and high mortality rates among cover types. Specifically, we varied these two beta coefficients during model calibration to either increase or decrease the rate of exponential decline in high mortality with increasing vegetation age as a function of fire intensity to achieve the target percentage of high mortality rate in each cover type.

The figures below depict the final wildfire mortality response functions for each cover type in alphabetical order. Cover types not shown either were not eligible to burn (e.g., water, barren) or were always assigned a high mortality response after burning (e.g., grassland, meadow). The response functions depict the probability of high mortality wildfire as a negative exponential function of vegetation Age (yrs) and fire intensity (as indexed). The dashed, solid and dotted lines depict the response functions for the minimum, mean and maximum Fire Intensity Index. Universally, the probability of high mortality decreased with increasing vegetation Age, but the rate of exponential decline decreased (i.e.,shallower slope) with increasing fire intensity, such that for any given Age the probability of high mortality increased with increasing fire intensity.

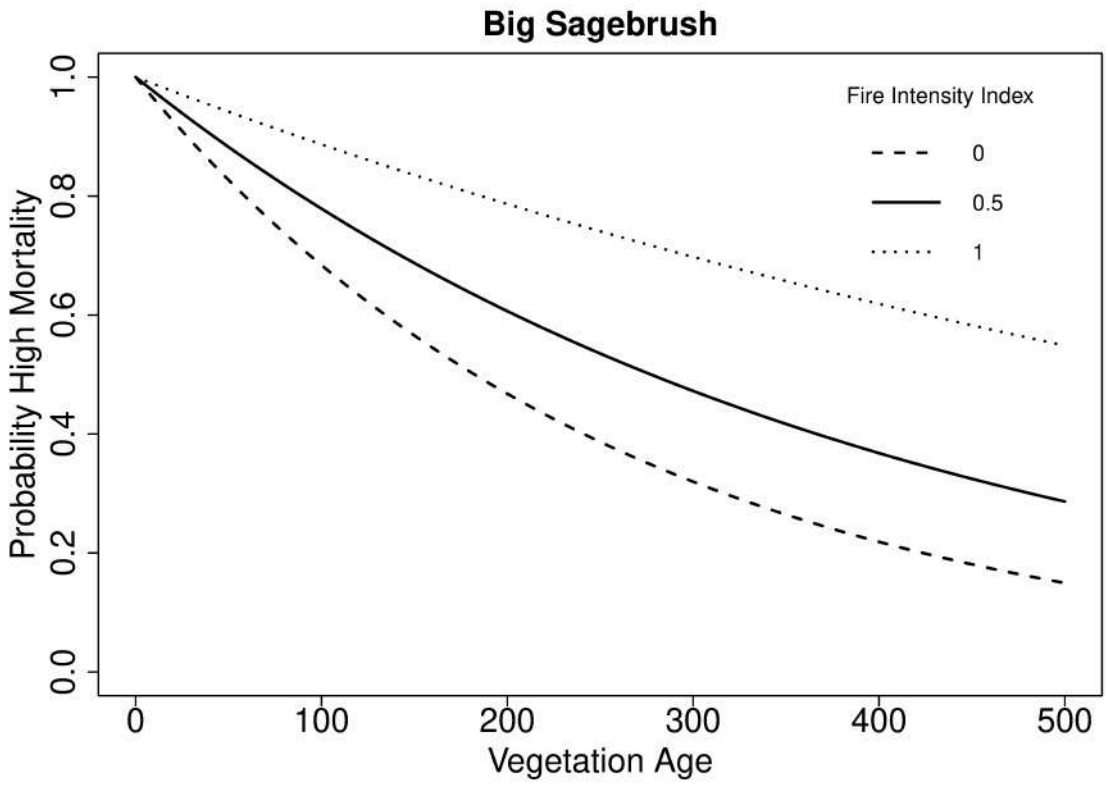

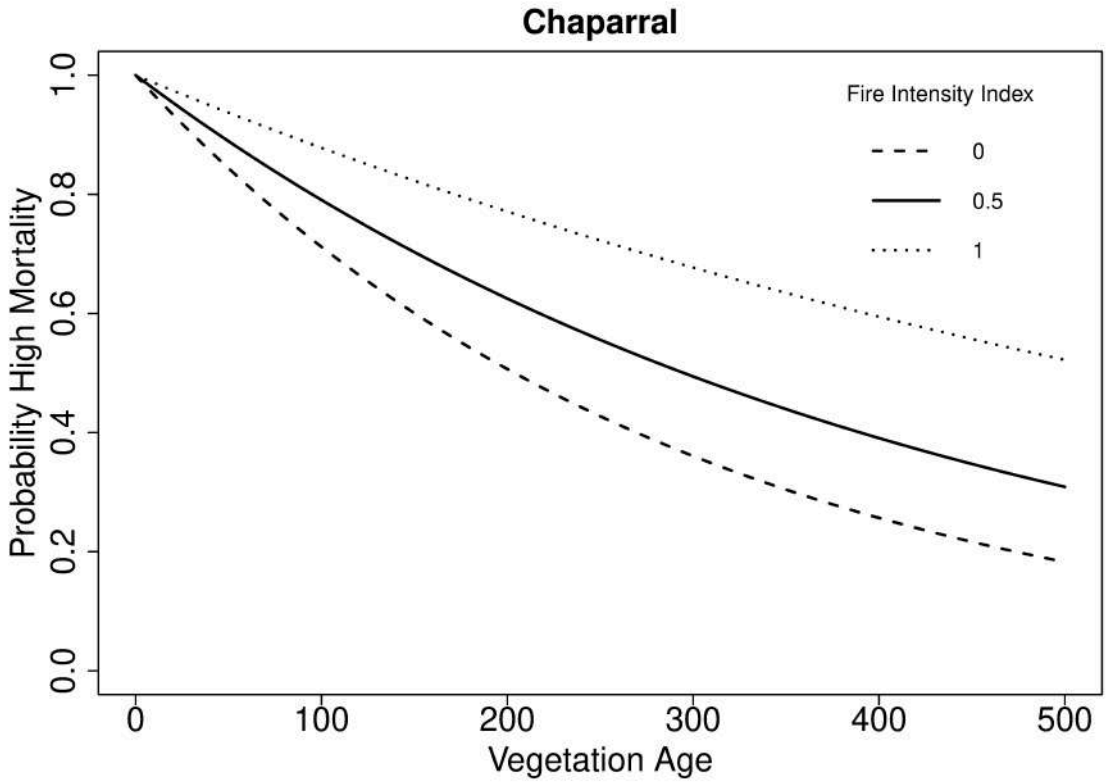
Chaparral
Probability High Mortality
0.0
0.2
0.4
0.6
0.8
1.0
0
100
200
300
400
500
Vegetation Age
Fire Intensity Index
0
0.5
1

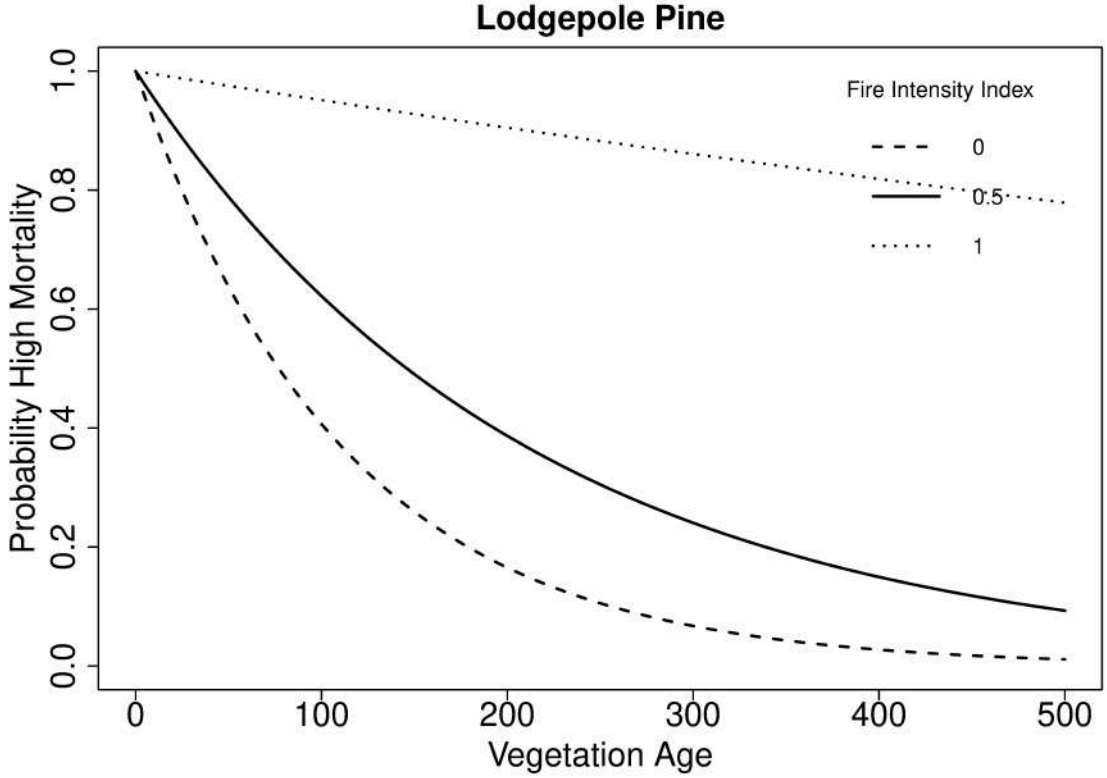
Lodgepole Pine
Probability High Mortality
0.0
0.2
0.4
0.6
0.8
1.0
0
100
200
300
400
500
Vegetation Age
Fire Intensity Index
0
0.5
1

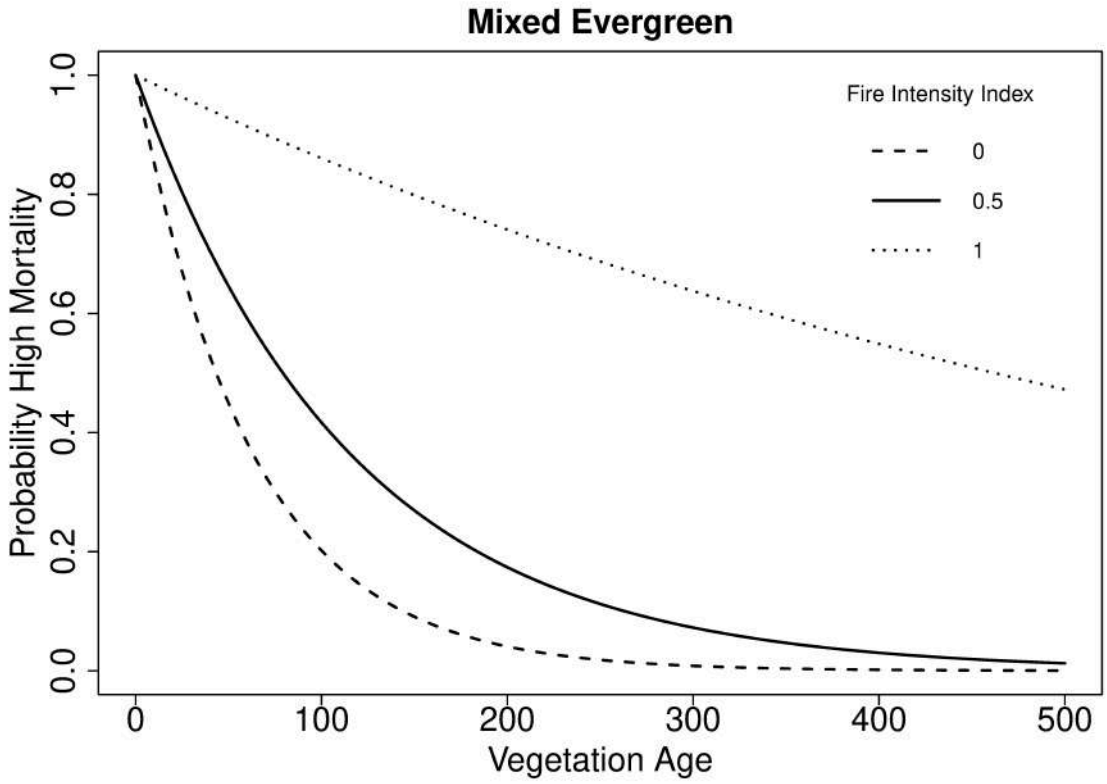
Mixed Evergreen
Fire Intensity Index
0
0.5
1
Probability High Mortality
0.0
0.2
0.4
0.6
0.8
1.0
0
100
200
300
400
500
Vegetation Age

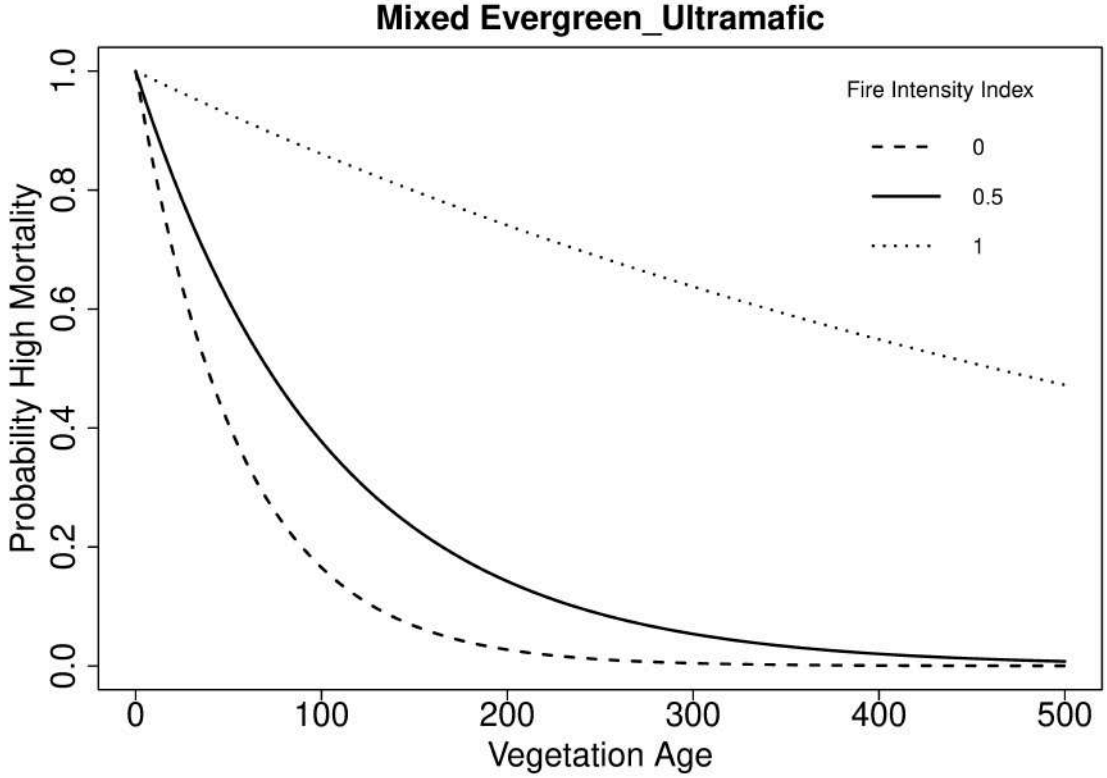
Mixed Evergreen_Ultramafic
Fire Intensity Index
0
0.5
1
Probability High Mortality
0.0
0.2
0.4
0.6
0.8
1.0
0
100
200
300
400
500
Vegetation Age

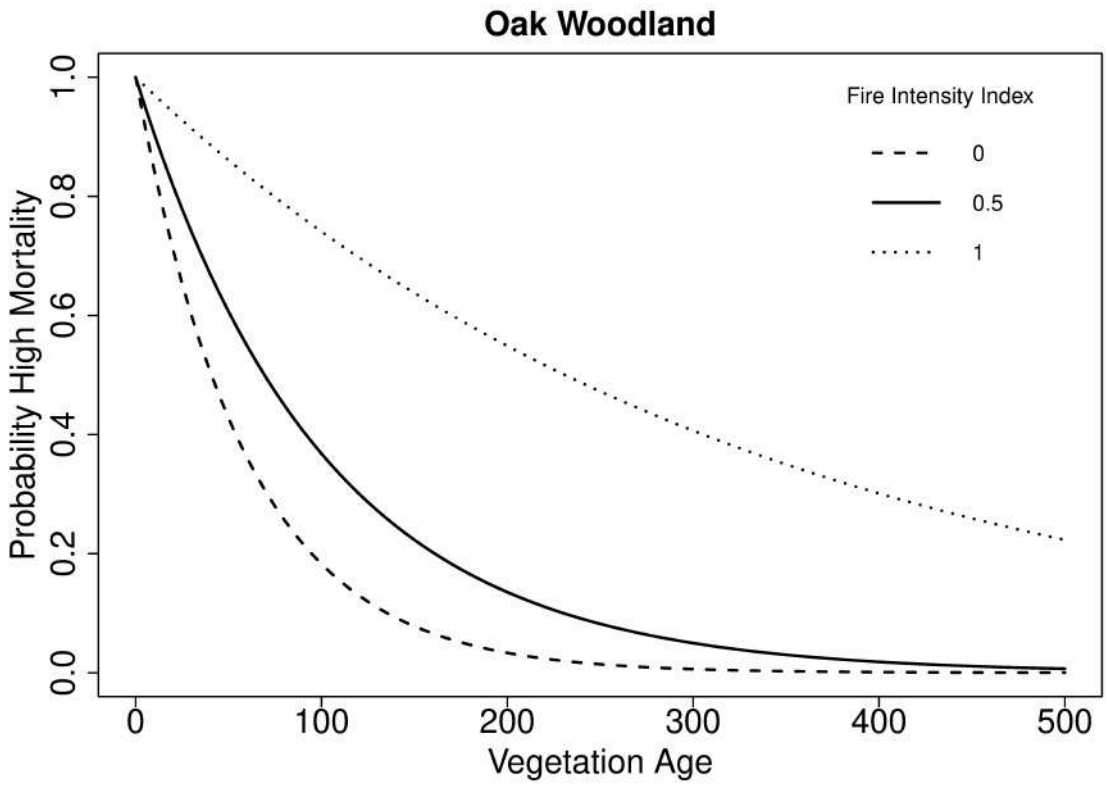
Oak Woodland
Probability High Mortality
0.0
0.2
0.4
0.6
0.8
1.0
0
100
200
300
400
500
Vegetation Age
Fire Intensity Index
0
0.5
1

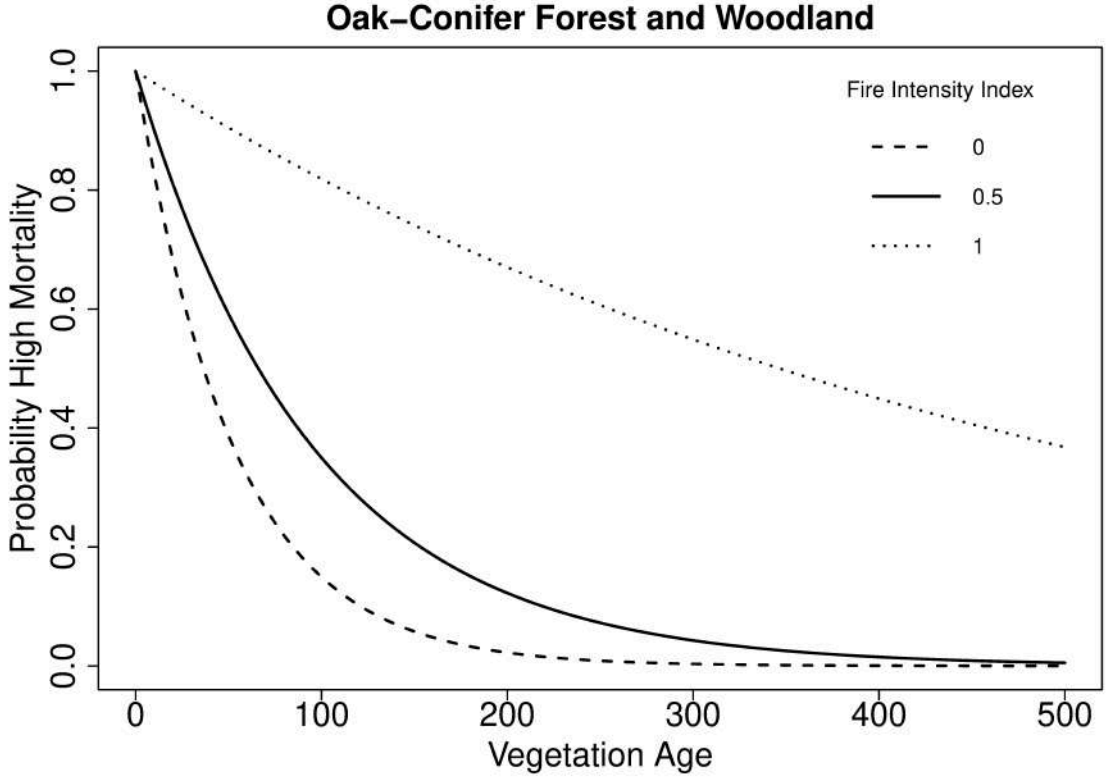
Oak–Conifer Forest and Woodland
Probability High Mortality
0.0
0.2
0.4
0.6
0.8
1.0
0
100
200
300
400
500
Vegetation Age
Fire Intensity Index
0
0.5
1

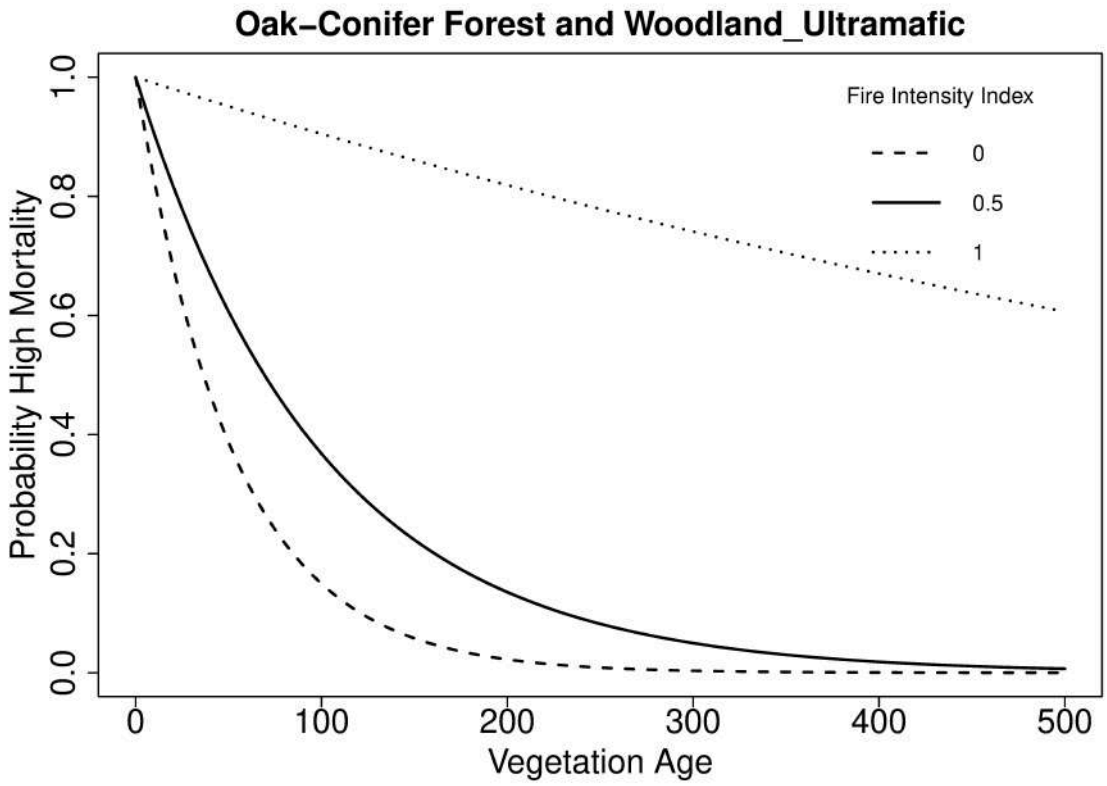
Oak–Conifer Forest and Woodland_Ultramafic
Fire Intensity Index
0
0.5
1
Probability High Mortality
0.0
0.2
0.4
0.6
0.8
1.0
0
100
200
300
400
500
Vegetation Age

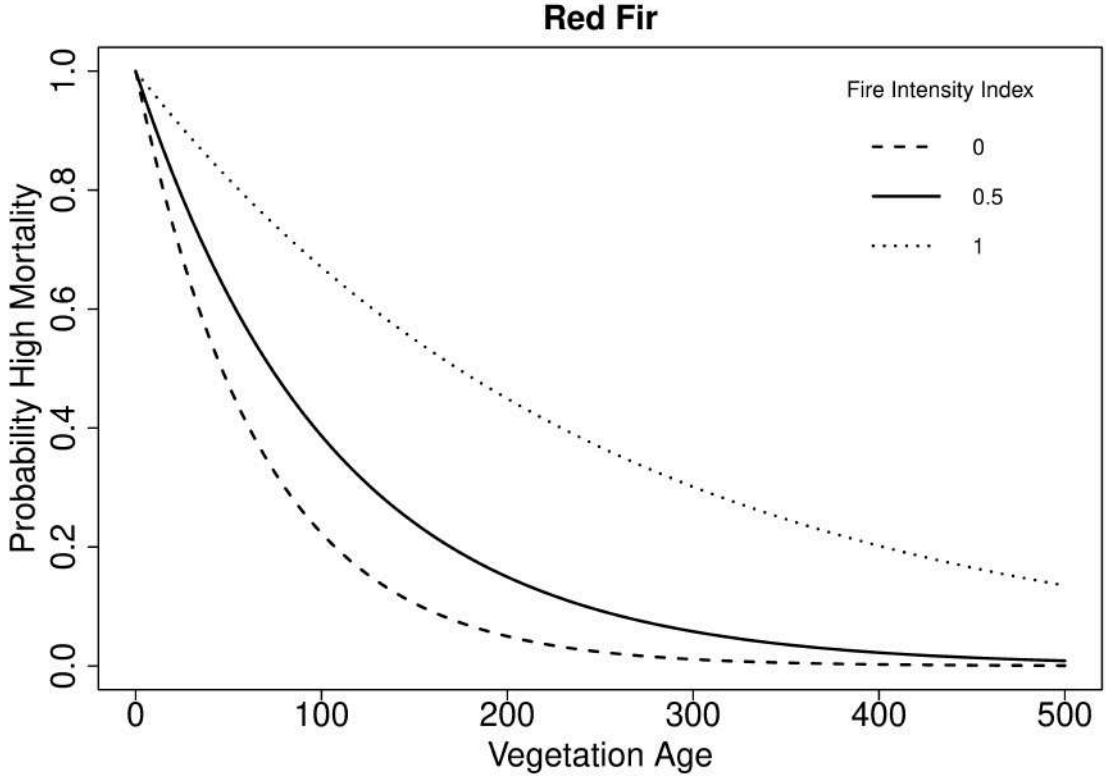
Red Fir
Fire Intensity Index
0
0.5
1
Probability High Mortality
0.0
0.2
0.4
0.6
0.8
1.0
0
100
200
300
400
500
Vegetation Age

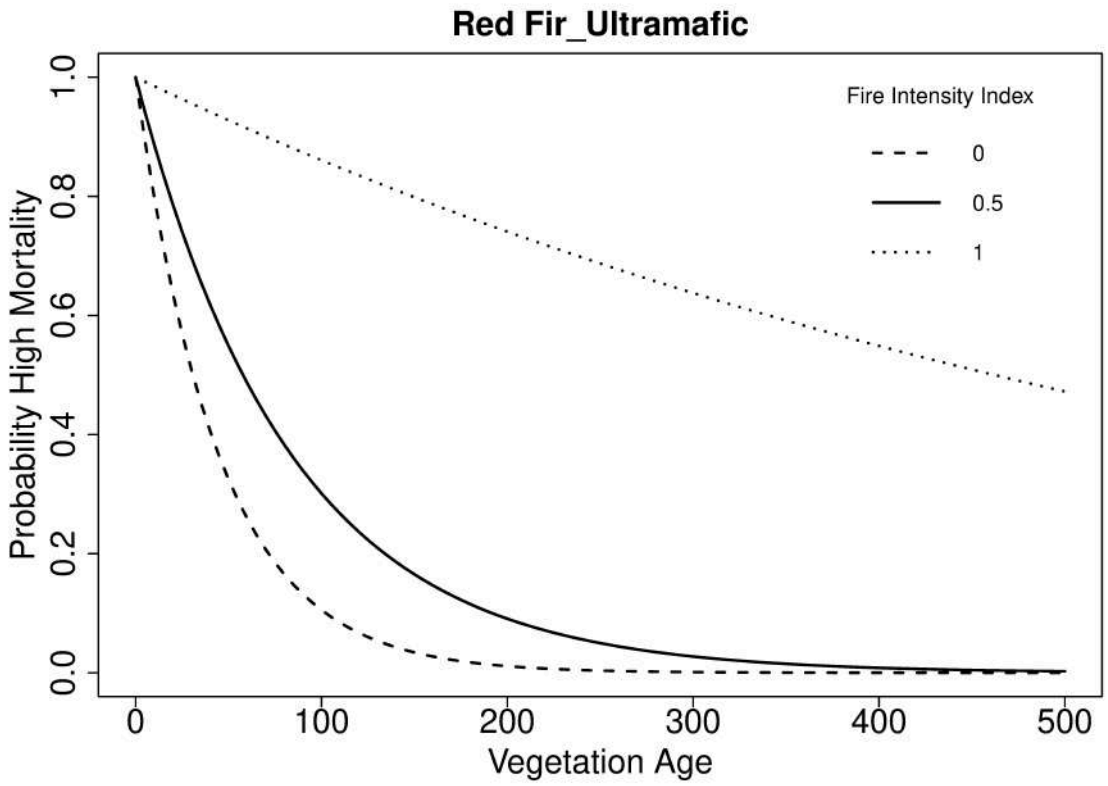
Red Fir_Ultramafic
Fire Intensity Index
0
0.5
1
Probability High Mortality
0.0
0.2
0.4
0.6
0.8
1.0
0
100
200
300
400
500
Vegetation Age

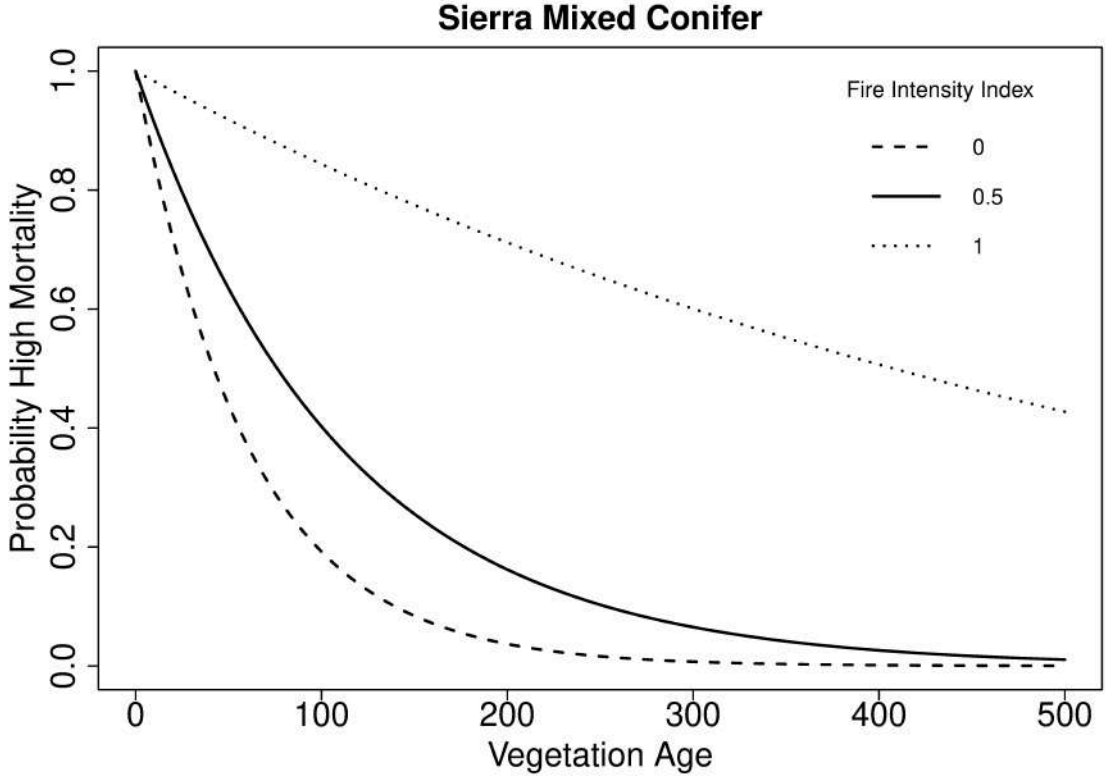
Sierra Mixed Conifer
Fire Intensity Index
0
0.5
1
Probability High Mortality
0.0
0.2
0.4
0.6
0.8
1.0
0
100
200
300
400
500
Vegetation Age

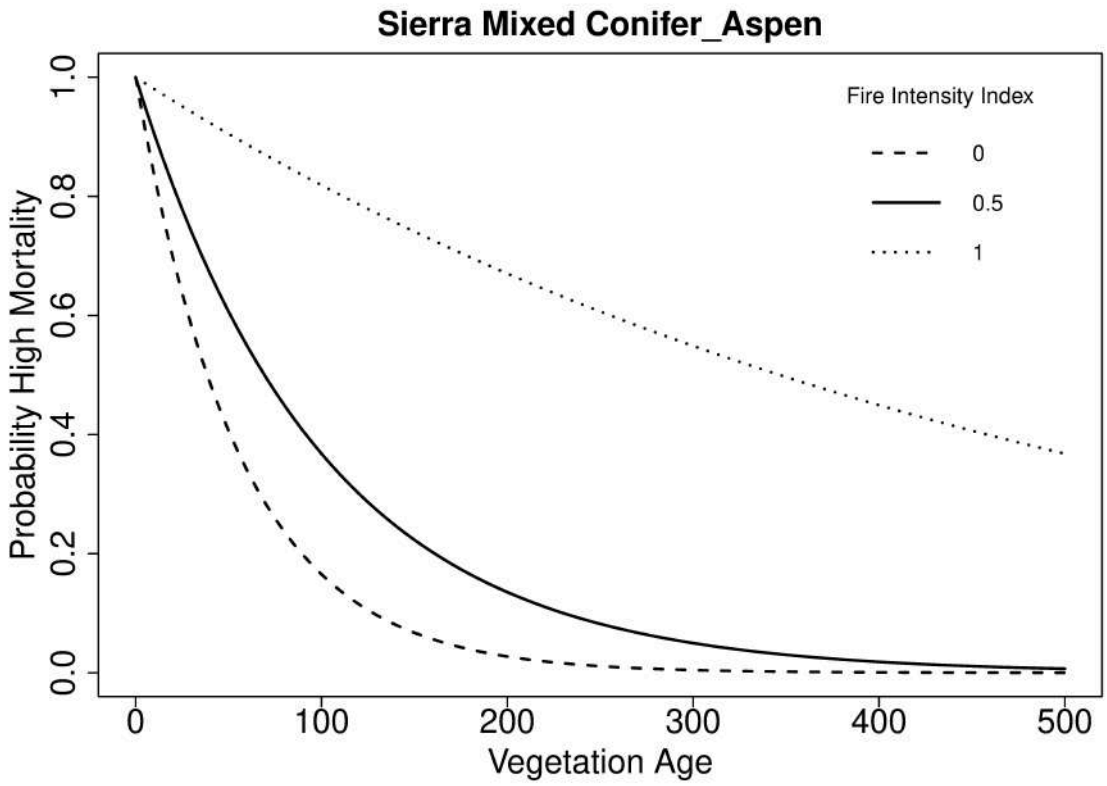
Sierra Mixed Conifer_Aspen
Fire Intensity Index
0
0.5
1
Probability High Mortality
0.0
0.2
0.4
0.6
0.8
1.0
0
100
200
300
400
500
Vegetation Age

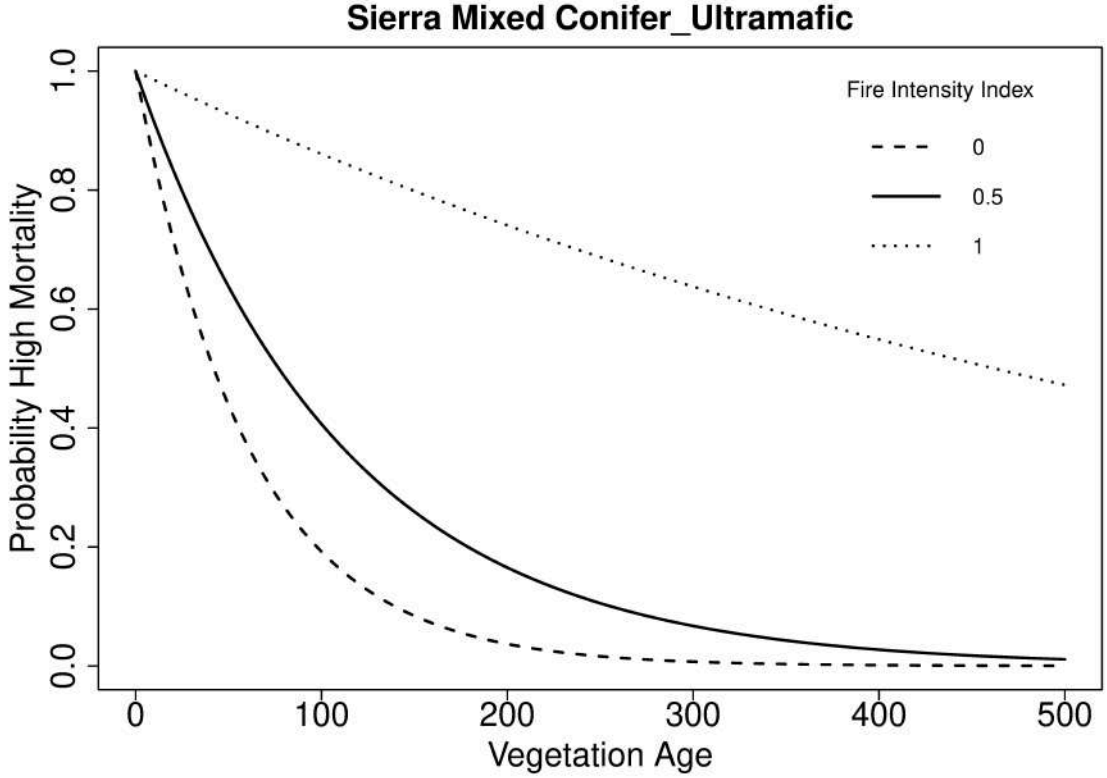
Sierra Mixed Conifer_Ultramafic
Fire Intensity Index
0
0.5
1
Probability High Mortality
0.0
0.2
0.4
0.6
0.8
1.0
0
100
200
300
400
500
Vegetation Age

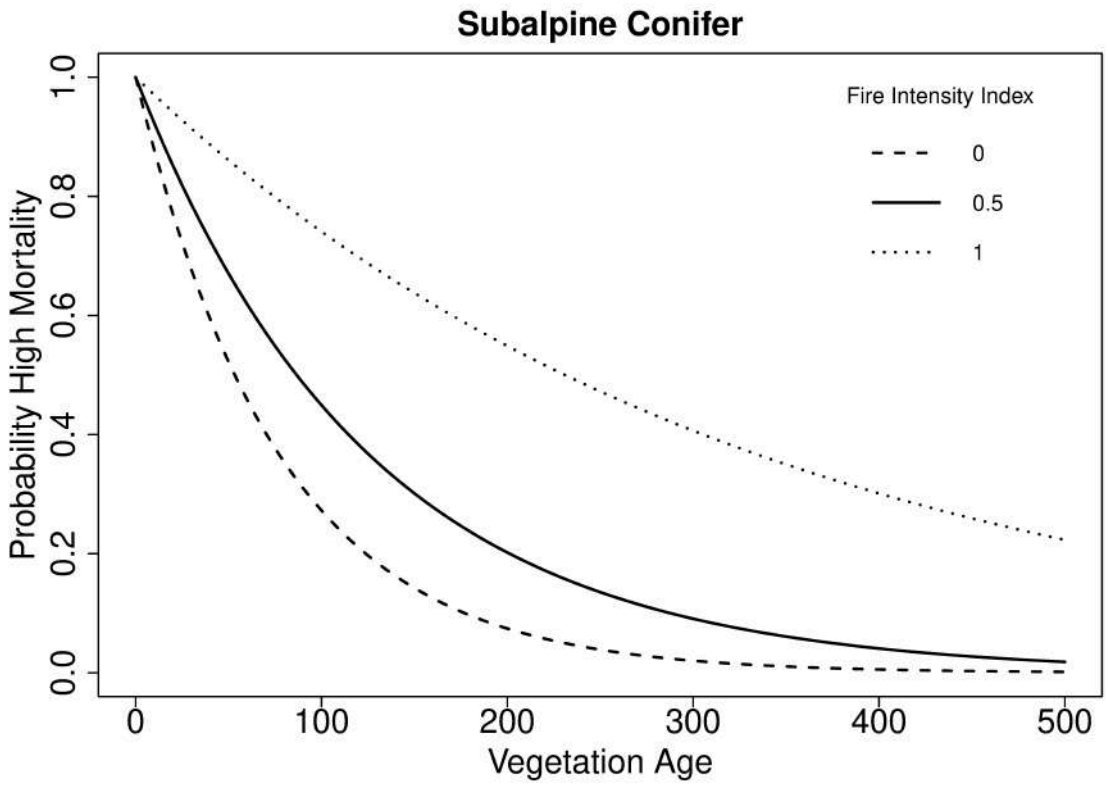
Subalpine Conifer
Fire Intensity Index
0
0.5
1
Probability High Mortality
0.0
0.2
0.4
0.6
0.8
1.0
0
100
200
300
400
500
Vegetation Age

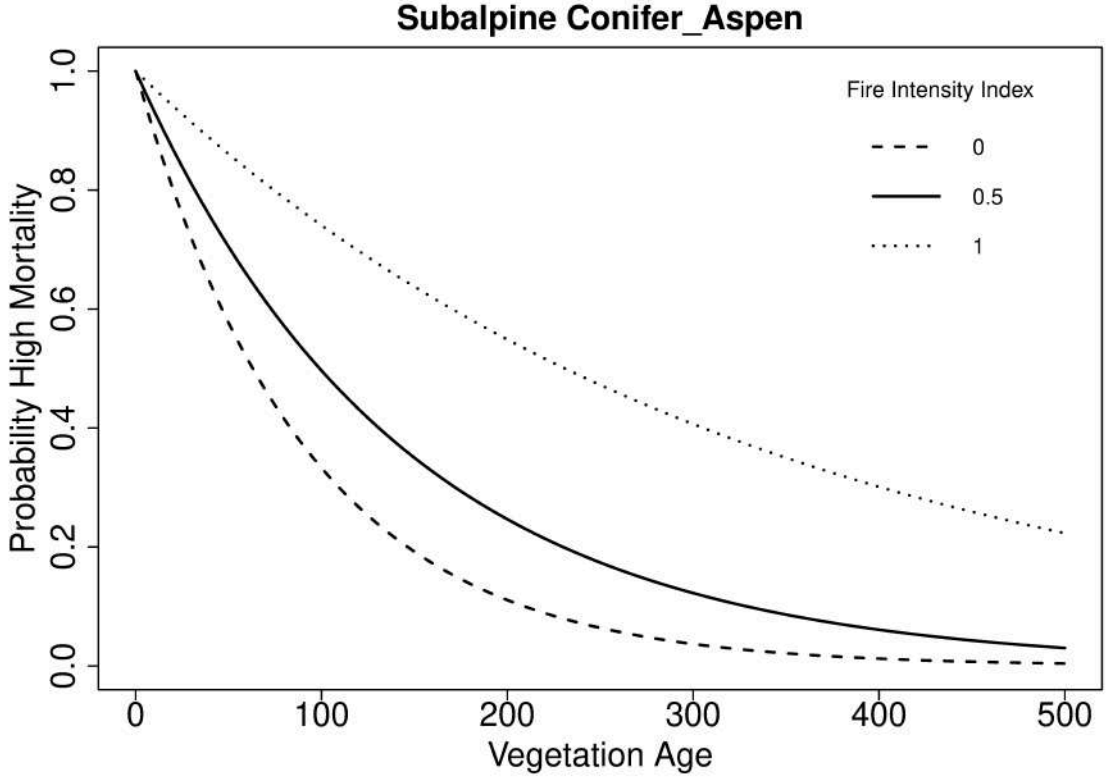
Subalpine Conifer_Aspen
Fire Intensity Index
0
0.5
1
Probability High Mortality
0.0
0.2
0.4
0.6
0.8
1.0
0
100
200
300
400
500
Vegetation Age

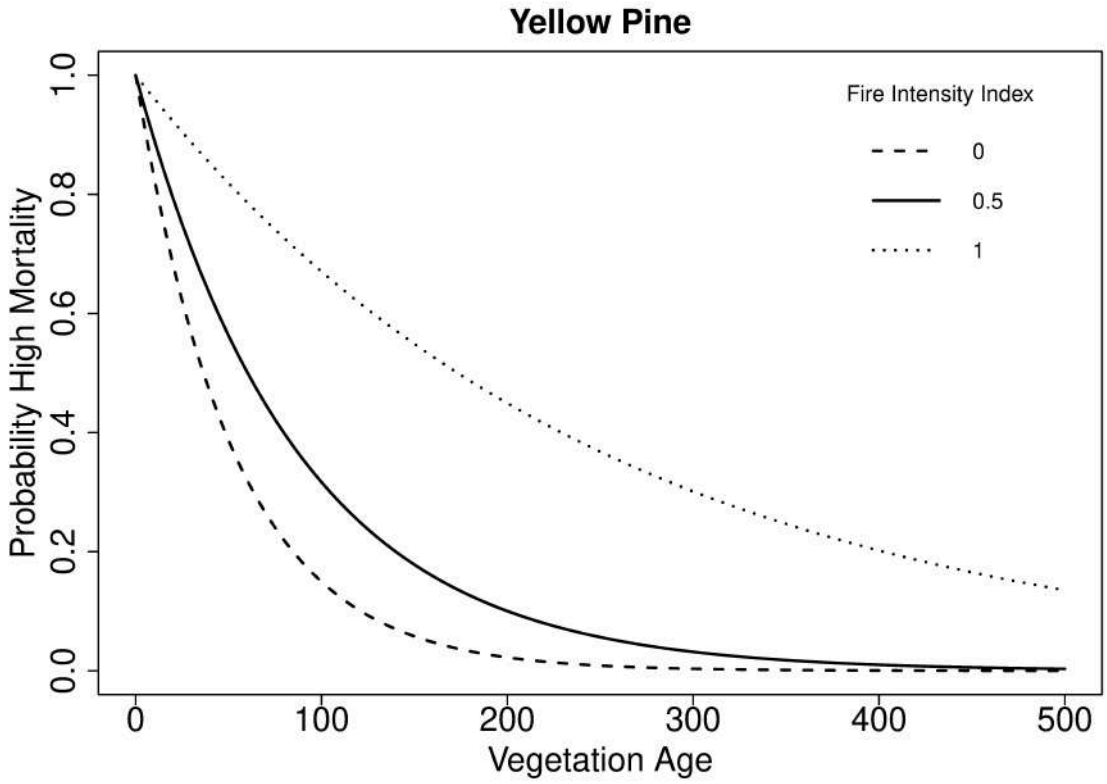
Yellow Pine
Probability High Mortality
0.0
0.2
0.4
0.6
0.8
1.0
0
100
200
300
400
500
Vegetation Age
Fire Intensity Index
0
0.5
1

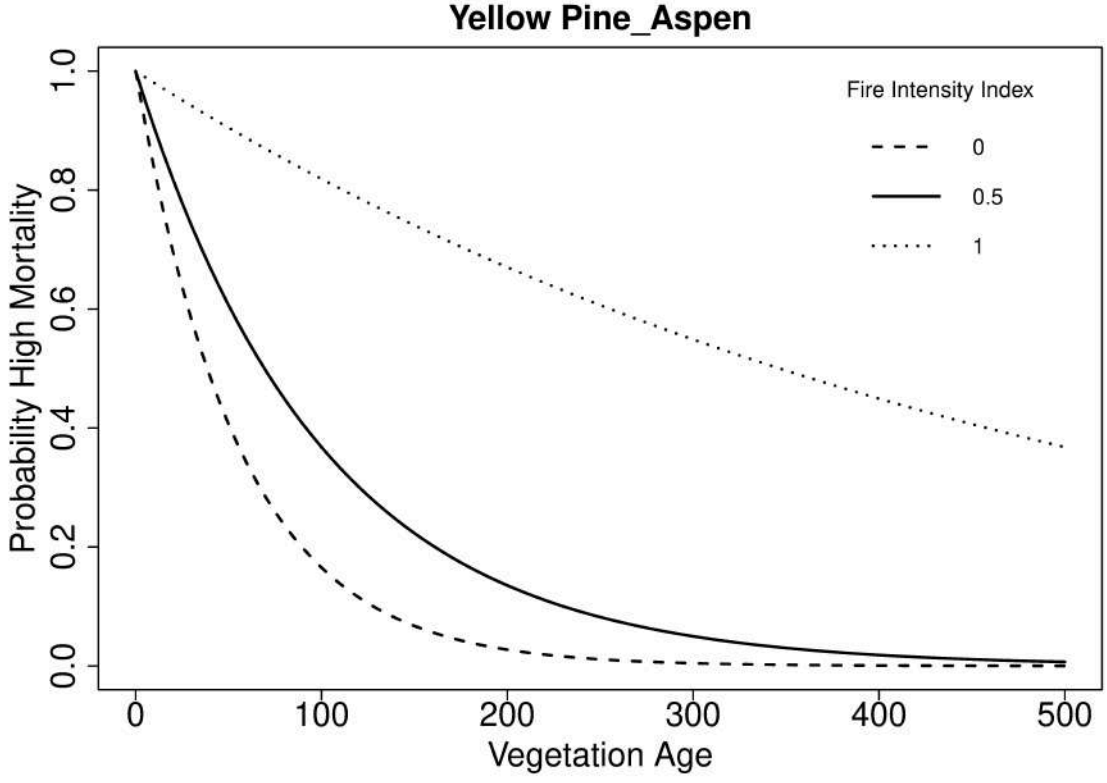
Yellow Pine_Aspen
Probability High Mortality
0.0
0.2
0.4
0.6
0.8
1.0
0
100
200
300
400
500
Vegetation Age
Fire Intensity Index
0
0.5
1

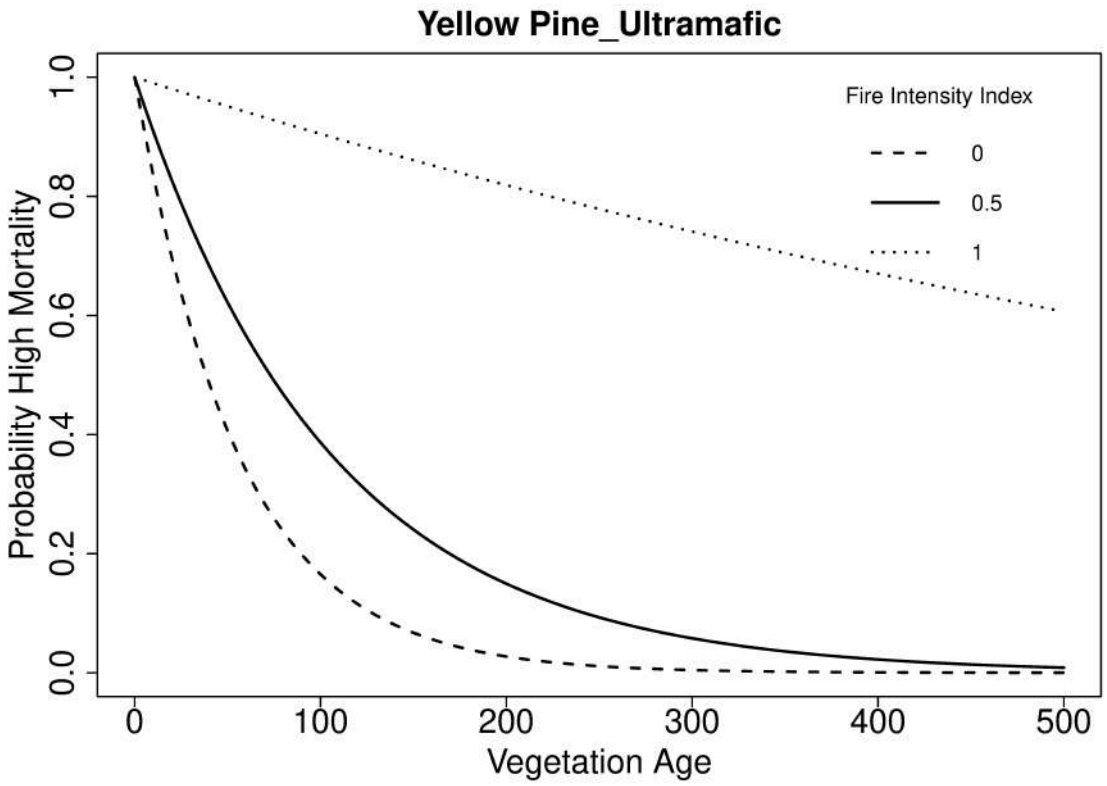
Yellow Pine_Ultramafic
Probability High Mortality
0.0
0.2
0.4
0.6
0.8
1.0
0
100
200
300
400
500
Vegetation Age
Fire Intensity Index
0
0.5
1

Appendix G - American South Fork River Landscape Historical Range of Variability and Current Landscape Departure

DRAFT Report

Kevin McGarigal Becky Estes Scott Conway Danielle Perrot
Marilyn Tierney Terri Walsh Christina Liang Laurie Perrot
Edward Smith

August, 2022

Authors

- Kevin McGarigal is a landscape ecologist with Vibrant Planet, proprietor of LandEco Consulting and retired professor of landscape ecology at the University of Massachusetts, Amherst. He received a B.S. in Forestry and Wildlife from Virginia Tech, an M.S. in Wildlife Science from Oregon State University, and a Ph.D. in Forest Science from Oregon State University.
- Becky Estes is the Central Sierra Province Ecologist (Tahoe, Eldorado, Stanislaus, and Lake Tahoe Basin Management Unit), Pacific Southwest Region, USDA Forest Service. She received a Ph.D. in Forestry from Auburn University and is a Certified Ecologist with the Ecological Society of America.
- Scott Conway is the chief resilience officer with Vibrant Planet and former forest ecologist with Pacific Southwest Region, USDA Forest Service Remote Sensing Lab and Truckee District Ranger, Tahoe National Forest, Pacific Southwest Region, USDA Forest Service. He received a B.S. in Natural Resources Management from Colorado State University.
- Danielle Perrot is an applied ecologist with Vibrant Planet. She received a B.S. in Environmental Science from University of California, Los Angeles and an M.A. in Geography from University of Colorado, Boulder.
- Marilyn Tierney is retired District Biologist for the American South Fork River Ranger District, Tahoe National Forest, Pacific Southwest Region, USDA Forest Service. She received a B.S. in Biology and an M.A. in Biology with an emphasis in Ecology and Systematics from San Francisco State University.
- Terri Walsh is silviculturist for the Tahoe National Forest, Pacific Southwest Region, USDA Forest Service. She is a certified silviculturist and studied Forestry at Cal Poly San Luis Obispo.
- Christina Liang is Forest Biologist for the Tahoe National Forest, Pacific Southwest Region, USDA Forest Service. She received a Ph.D. in Ecology from University of California, Davis.
- Laurie Perrot is Forest Environmental Coordinator for the Tahoe National Forest, Pacific Southwest Region, USDA Forest Service. She received a B.S. in forestry from the University of California, Berkeley.
- Edward Smith is Senior Forest Ecologist and Fire Manager for The Nature Conservancy in California. He received a BA in Biology from the University of California, San Diego and a MS in Forestry from Northern Arizona University.

Preface

This document[1] is an appendix to the Northern Sierra Historical Range of Variability and Current Landscape Departure General Technical Report (GTR) and includes detailed results for the American South Fork River landscape. Importantly, the background and detailed methods behind these results are presented in the GTR and not repeated here, and thus it behooves the reader to review the GTR before interpreting these results. In addition, here we present details pertaining the Landscape Disturbance-Succession Model parameterization and calibration specific to this focal landscape; all other model parameterization and calibration generalized to the Northern Sierra ecoregion is presented in the GTR. Lastly, here we present results specific to this focal landscape, but with minimal interpretation or discussion of these results or their application to management, as this was all done in the GTR. The GTR describes how to interpret the results for any of the focal landscapes and how they can be applied to management; here, we simply provide the raw results specific to this focal landscape.

Note, all datasets associated with the results for this focal landscape can be made available. Please contact Becky Estes, becky.estes@usda.gov for access.

---

[1] In accordance with Federal law and U.S. Department of Agriculture policy, this institution is prohibited from discriminating on the basis of race, color, national origin, sex, age, or disability. (Not all prohibited bases apply to all programs.) To file a complaint of discrimination, write USDA, Director, Office of Civil Rights, Room 326-W, Whitten Building, 1400 Independence Avenue, SW, Washington, DC 20250-9410 or call (202) 720-5964 (voice and TDD). USDA is an equal opportunity provider and employer.

FOCAL LANDSCAPE

The American South Fork River landscape, as we defined it, is comprised of the HUC8-level Upper American South Fork River watershed and is located on the western slopes of the Sierra Nevada Mountains in the north Sierra ecoregion (**Figure 1**). The American South Fork River landscape encompasses 167,896 ha and otherwise reflects the description of the north Sierra ecoregion presented in the GTR.

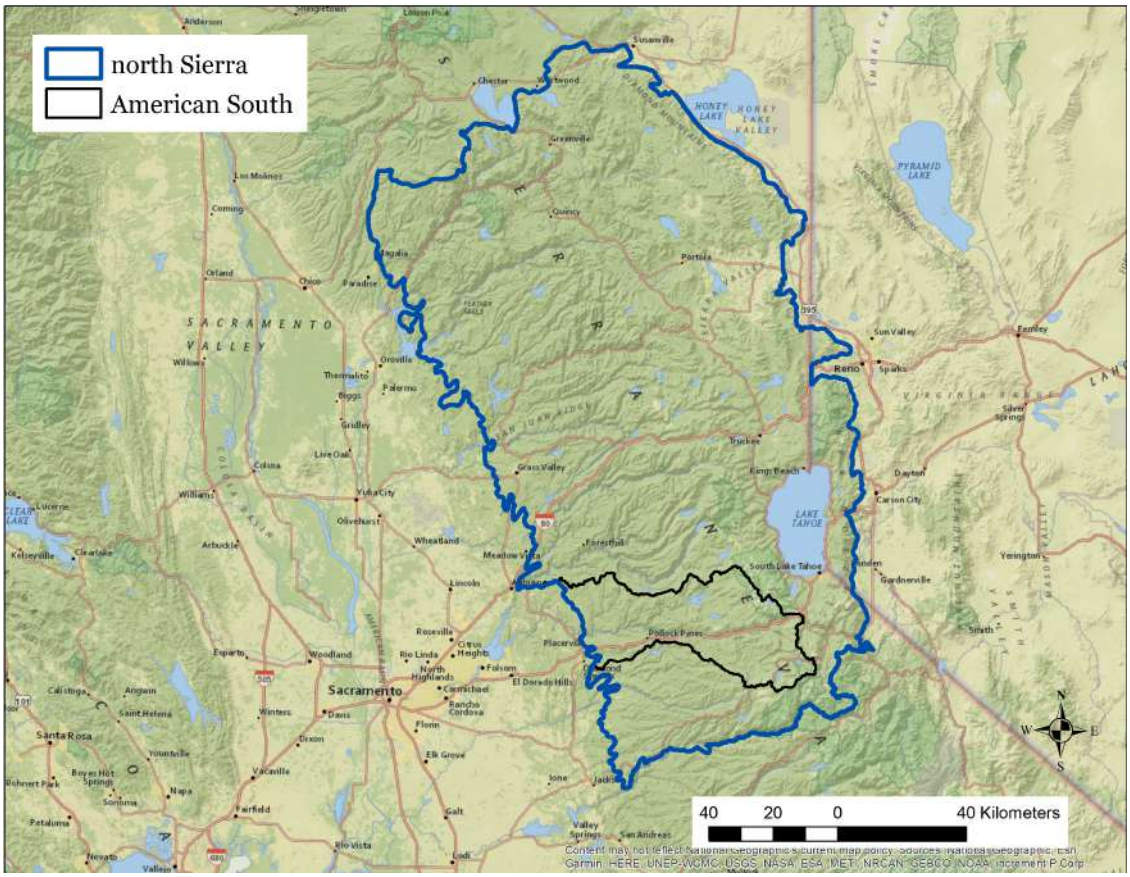

Figure 1: The American South Fork River landscape, including the middle and north forks of the American South Fork River, defined for the purpose of simulating wildfire disturbance and vegetation succession.

MODEL PARAMETERIZATION

In this section, we present only model parameters specific to this focal landscape; all north Sierra-wide parameters are discussed in the GTR. In addition, here we do not discuss in detail the methods and use of the model parameters in LDSim, as this was already done in the GTR. Please refer to the GTR for a full understanding of how the model parameters were used in LDSim.

Wildfire Climate

Climate conditions affecting wildfire disturbance during each timestep of the simulation were governed by a single global parameter, the Wildfire Climate Index based on the Palmer Modified Drought Severity Index (PMDI), in which a single coefficient was assigned to each timestep of the simulation. The final Wildfire Climate Index trajectory represented a vector of coefficients, one for each timestep, as shown in **Figure 2**.

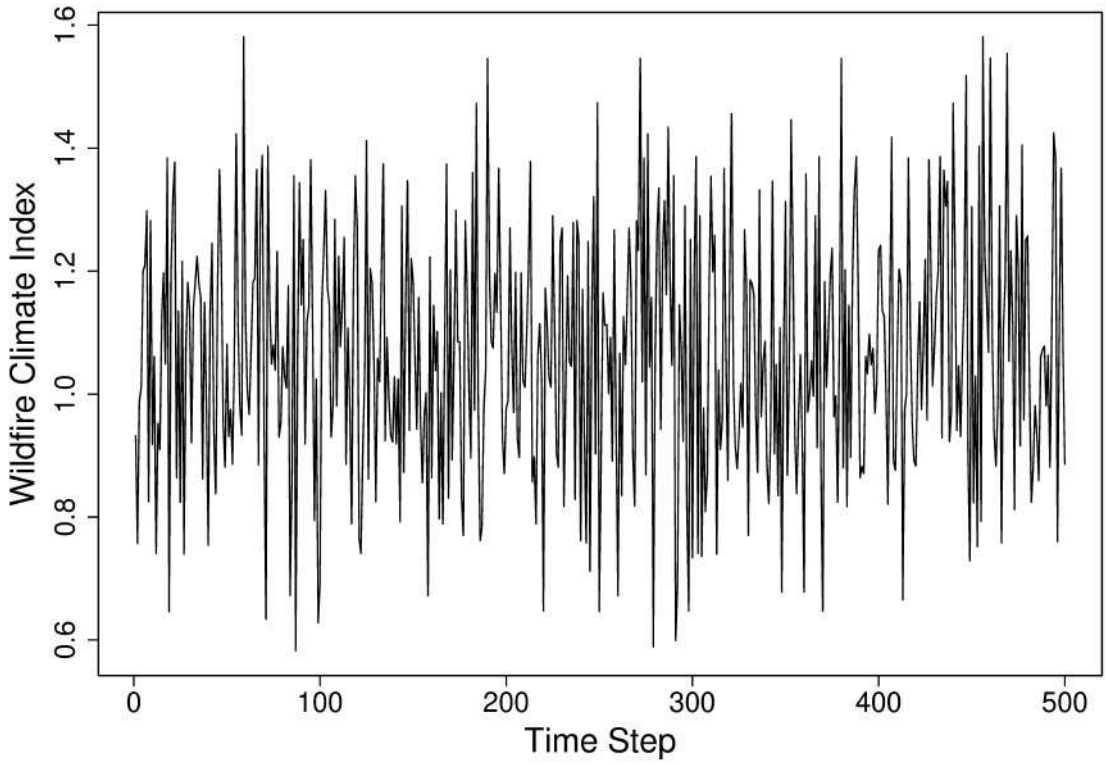

Figure 2: Wildfire Climate Index trajectory for the American South Fork River landscape corresponding to 500 5-year timesteps in the simulation. The Climate Index was based on the inverted and rescaled 5-year averaged, inverse-distance weighted mean Palmer Modified Drought Severity Index (PMDI) for the sample point locations within the north Sierra ecoregion relative to the focal landscape (American South Fork River watershed in this case). Note, here we inverted PMDI so that positive values represented drier conditions and negative values represented wetter conditions, and we also rescaled the index to have a standard deviation of 0.2 (see text for details).

Wildfire Susceptibility

Wildfire susceptibility for any given cell in each timestep was modeled as a complex function of fuels and climate, separately for each cover type, as described in the GTR. The final Wildfire Susceptibility Index on the probability scale (0-1) was used in the wildfire initiation and spread functions such that a value of 0 would prevent wildfires from initiating in or spreading into the cell, and as the value increased to 1 the probability of initiating a wildfire would increase as would the probability of a wildfire spreading to the focal cell from an adjacent burning cell, all other things being equal.

Briefly, we varied the beta coefficients of the wildfire susceptibility function for each cover type to reflect differences in reported historical mean fire return intervals among cover types - shifting the response curves left or right - as a means of calibrating the model to achieve target mean fire return intervals for each cover type (see Model Calibration). The calibrated wildfire susceptibility functions for each cover type are included in **Appendix E1**.

Wildfire Initiation

The number and spatial distribution of wildfire initiations in any given timestep was governed by: 1) a global wildfire initiation rate parameter that controlled the number of initiation attempts per unit area and

remained constant over time; 2) the current climate conditions, as represented by the Wildfire Climate Index, that varied over time but not space; and 3) the susceptibility to wildfire, as represented by the Wildfire Susceptibility Index, that varied over both space and time. We treated the global wildfire initiation rate as a calibration parameter - shifting it up or down to increase or decrease the overall amount of realized wildfire over time - and ultimately settled on a rate of 400 attempted initiations per 100,000 ha/year. Note, this parameter affected the attempted number of wildfire initiations, not the realized number of wildfires, which was considerably less due to the vegetation and climate conditions that affected whether an attempt (i.e., lightning strike) materialized into an actual wildfire. The realized number of wildfire initiations for the American South Fork River landscape is shown in **Figure 3**.

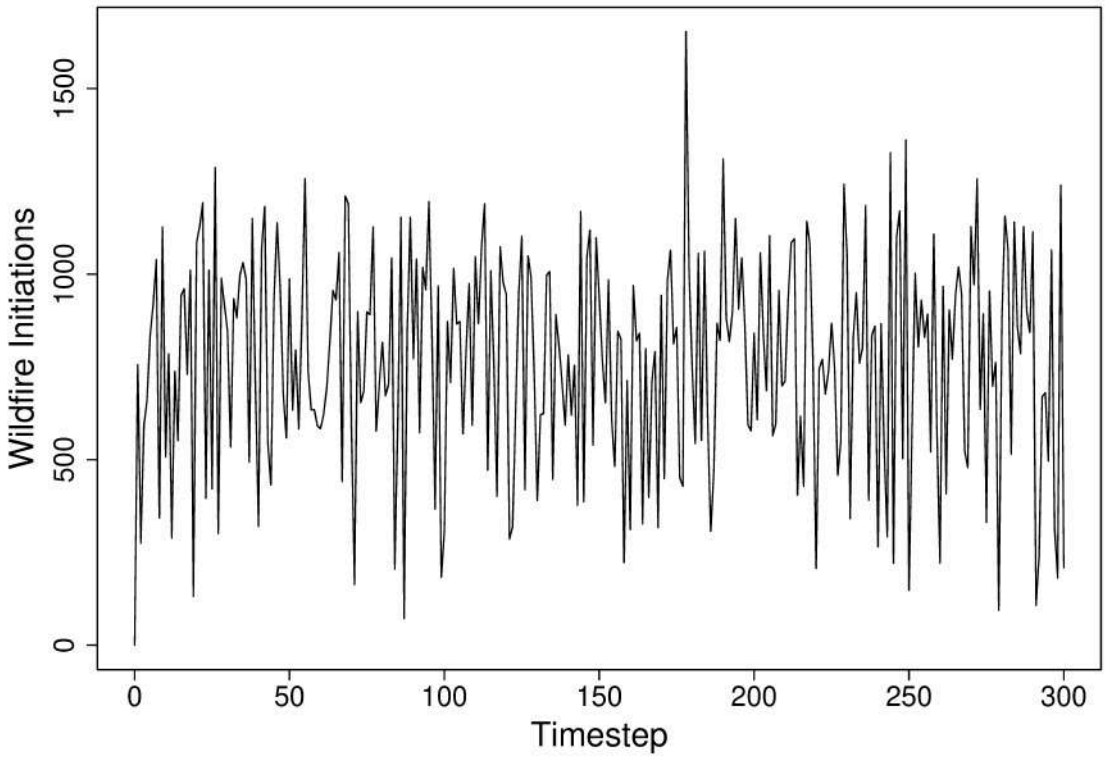

Figure 3: Realized simulated number of wildfire initiations per 5-year timestep for the American South Fork River landscape.

Wildfire Mortality

Following the termination of a wildfire event the probability of high versus low mortality of the overstory vegetation in each 5 m cell that burned was determined by two major factors combined in a complex function, as described in the GTR: 1) fire intensity, which was a function of the fuel loads in the neighborhood of the focal cell (proxied by the age of the vegetation and time since the last fire), the topographic position of the focal cell, and the climate conditions of the current timestep; and 2) the resistance of the focal cell, which was a function of the age of the vegetation in the focal cell.

Briefly, we varied the beta coefficients of the resistance component of the complex function for each cover type to reflect differences in reported historical mean fire return intervals and high mortality rates among cover types - increasing or decreasing the rate of exponential decline in high mortality with increasing vegetation ages as a function of fire intensity - as a means of calibrating the model to achieve target high mortality rates for each cover type (see Model Calibration). The calibrated wildfire mortality functions for each cover type are included in **Appendix E2**.

Succession Climate

Climate conditions affecting vegetation succession during each timestep of the simulation were governed by a single global parameter, the Succession Climate Index based on the Palmer Modified Drought Severity Index (PMDI), in which a single coefficient was assigned to each timestep of the simulation. The final Succession Climate Index trajectory represented a vector of coefficients, one for each timestep, and is shown in **Figure 4**.

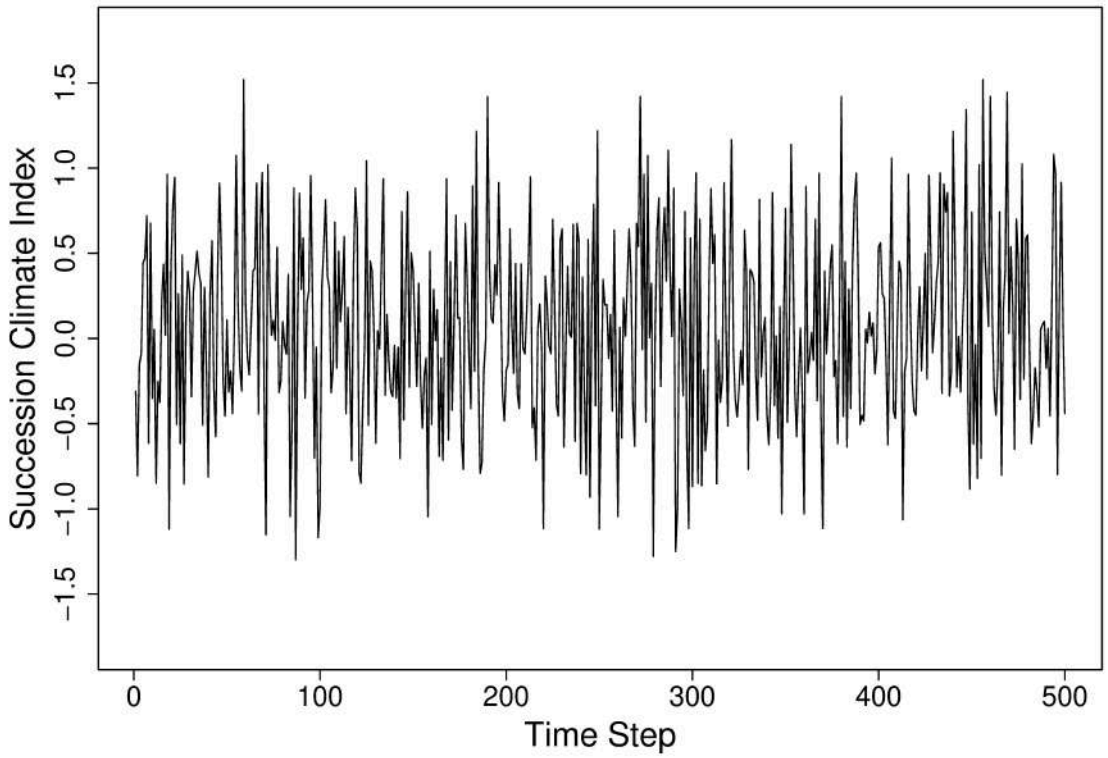

Figure 4: Succession Climate Index trajectory for the American South Fork River landscape corresponding to 500 5-year timesteps in the simulation. The Climate Index was based on the inverted 5-year averaged, inverse-distance weighted mean Palmer Modified Drought Severity Index (PMDI) for the sample point locations within the north Sierra ecoregion relative to the focal landscape (American South Fork River watershed in this case). Note, here we inverted PMDI so that positive values represented drier conditions and negative values represented wetter conditions (see text for details).

MODEL CALIBRATION

Although LDSim is a process-oriented model with individual parameters sourced either from data, literature, or expert opinion, the model outcomes reflect the complex spatio-temporal interactions of the various stochastic disturbance and succession processes. Consequently, it is necessary to calibrate the model by tuning (i.e., adjusting up or down) one or more of the model parameters to produce selected outcomes that are consistent with the data, literature and expert opinion. Importantly, in this context, we considered the parameters associated with the disturbance process to be "independent" variables and the

vegetation conditions (e.g., seral stage distribution, spatial patterns of vegetation states, etc.) to be "dependent" outcomes. Therefore, we calibrated select disturbance parameters (i.e., independent variables) to achieve the targeted disturbance regime without any attention to the vegetation response, which we treated as the dependent outcome of the disturbance regime. Importantly, we did not tune disturbance regime parameters to achieve desired vegetation outcomes. To calibrate the model, we focused on the following five disturbance regime attributes that we considered emergent properties of the disturbance regime, as discussed in detail in the GTR.

Fire Rotation Period

Fire Rotation Period (FRP) is the number of years required to burn a cumulative area equal to the extent under consideration. FRP combines fire frequency and fire size into a single integrated measure of how much fire is actually applied to a unit of ground. FRP is equivalent to the "point-specific" or "population" mean Fire Return Interval (FRI); i.e., the average number of years between fires to a single point on the ground (or cell), and is roughly equivalent to the oft reported "grand mean" FRI computed from a large sample of point-specific intervals (e.g., from a set of fire-scarred trees).

Briefly, we tuned the global wildfire initiation rate parameter, which controlled the number of wildfire initiation attempts per unit area within each timestep and remained constant over time (see Wildfire Initiation above), and two of the wildfire susceptibility coefficients (b_0 and b_1) for each cover type, which affected the susceptibility of fire initiation and spread in each cover type (see Wildfire Susceptibility above), and measured calibration success based on agreement with the pre-specified target FRP for each cover type. We set our calibration goal as within 10% of the target FRP for forested cover types with extents > 1,000 ha. We closely met our calibration target for 6 of 7 forest cover types with > 1,000 ha, and came acceptably close for the remaining cover type, as shown in **Table 1**.

Table 1: Target and simulated Fire Rotation Periods (FRP) for the American South Fork River landscape.

Cover type	**Area (ha)**	**Target FRP**	**Simulated FRP**	**%Deviation**
Sierra Mixed Conifer	63679	26	26	0
Red Fir	25597	50	50	0
Yellow Pine	24725	20	19	-5
Mixed Evergreen	12472	45	44	-2
Oak-Conifer Forest and Woodland	8084	21	21	0
Lodgepole Pine	3561	52	59	13
Subalpine Conifer	1716	296	315	6
Oak Woodland	233	26	29	12
Total	155529	30	30	0

Fire Mortality Rate

Fire mortality rate (FMR) is the percentage of burned cells that exhibit a high-mortality response (i.e., complete overstory mortality). For the purpose of model calibration, we considered the FMR only for cells in the "short", "medium" and "tall" tree developmental stages (i.e., "mature" trees) since this was the basis for specifying the target values.

Briefly, we tuned two of the wildfire mortality coefficients (b_5 and b_6) for each cover type, which affected the probability of high mortality fire as a function of age and fire intensity in each cover type (see Wildfire Mortality above), and measured calibration success based on conformity to pre-specified fire mortality targets for each cover type. We set our calibration goal as within 10% of the targets for forested cover types with > 1,000 ha in the focal landscapes. We closely met our calibration targets for all of the forested cover types, as shown in **Table 2**.

Table 2: Target and simulated Fire Mortality Rates (FMR) for the American South Fork River landscape.

Cover type	Area (ha)	Target FMR	Simulated FMR	%Deviation
Sierra Mixed Conifer	63679	7	7.36	5
Red Fir	25597	10	9.95	-1
Yellow Pine	24725	5	5.02	0
Mixed Evergreen	12472	7	6.96	-1
Oak-Conifer Forest and Woodland	8084	5	5.33	7
Lodgepole Pine	3561	24	25.68	7
Subalpine Conifer	1716	10	9.63	-4
Oak Woodland	233	6	5.77	-4

Fire Size Distribution

Fire size distribution (FSD) is the percentage of realized fire sizes across bins of increasing fire size. We opted not to tune the parameters affecting the fire size distribution as these were empirically based. Instead, we treated the realized fire size distribution as an emergent outcome of the model and measured calibration success based on agreement with the pre-specified fire distribution derived from the post-settlement period of 1908 - 1979 from which we had an empirical record. We set our calibration goal as a subjective evaluation of the realized fire size distribution compared to the target fire size distribution. We met our calibration target reasonably well, as depicted in **Figure 5**.

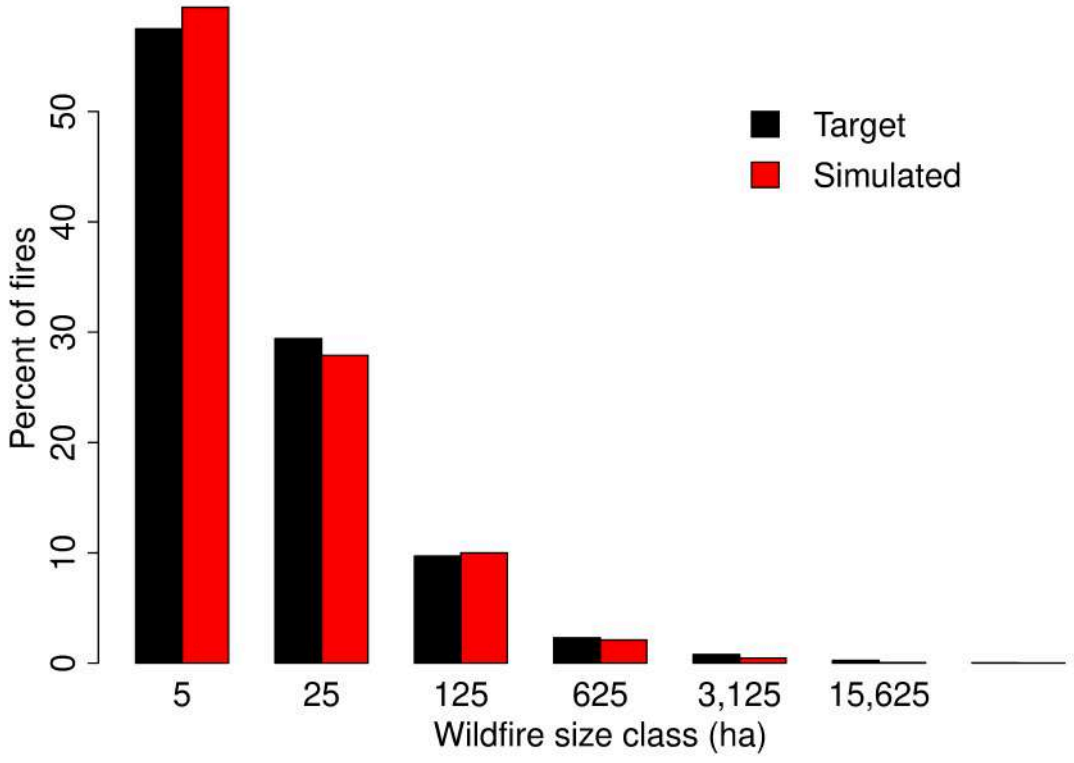

Figure 5: Target and simulated wildfire size distribution for the American South Fork River landscape.

Variability in Total Area Burned

Variability in total area burned over time is a measure of the temporal variability in the wildfire disturbance regime. We opted not to tune the primary parameter affecting the temporal variability in total area burned - the Wildfire Climate Index - as it was empirically based. Instead, we treated the variability in total area burned as an emergent outcome of the model and measured calibration success based on agreement with the observed variability in total area burned for the post-settlement period of 1908 - 1979 from which we had an empirical record. We set our calibration goal as within 10% of the target coefficient of variation (CV) in total area burned per timestep (CV = 91.8%, see GTR). We closely met our calibration target, as depicted in **Figure 6**.

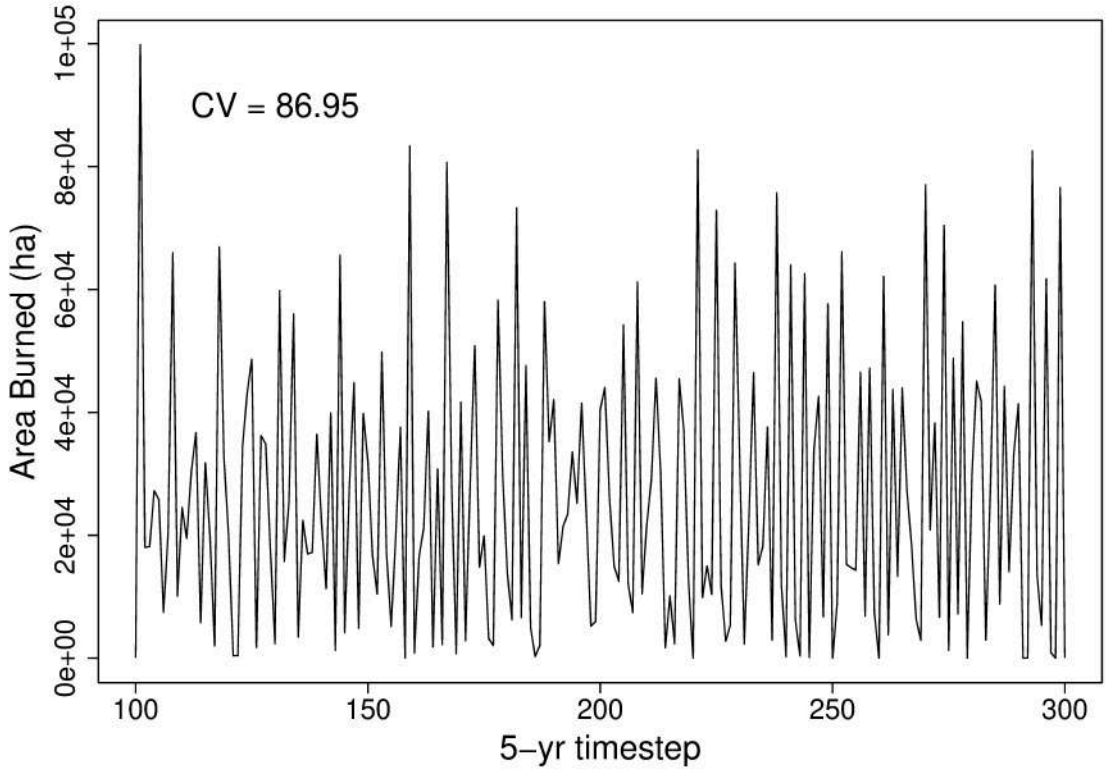

Figure 6: Total simulated area burned per 5 years in the American South Fork River landscape representing the historical reference period of 1550-1850 and the computed Coefficient of Variation (CV).

Relationship Between Total Area Burned and Climate

The relationship between total area burned and climate is a measure of the degree to which the simulated total area burned is affected by variability in the specified Wildfire Climate Index. We opted not to tune the Wildfire Climate Index, in particular, or any parameter associated with the wildfire disturbance process with regards to this calibration metric. Instead, we treated the observed relationship between total area burned and the climate index as an emergent outcome of the model and measured calibration success based on agreement with the strength of the relationship for the post-settlement period of 1908 - 1979 from which we had an empirical record. We set our calibration goal as within 10% of the target coefficient of determination (R2) in the fit of a linear regression to the target data (R2 = 0.25, see GTR). We did not met this calibration target very well, as we simulated a more closely fitting relationship between total area burned and the climate index and a relationship that was distinctly more non-linear compared to observed post-settlement observations, as depicted in **Figure 7**.

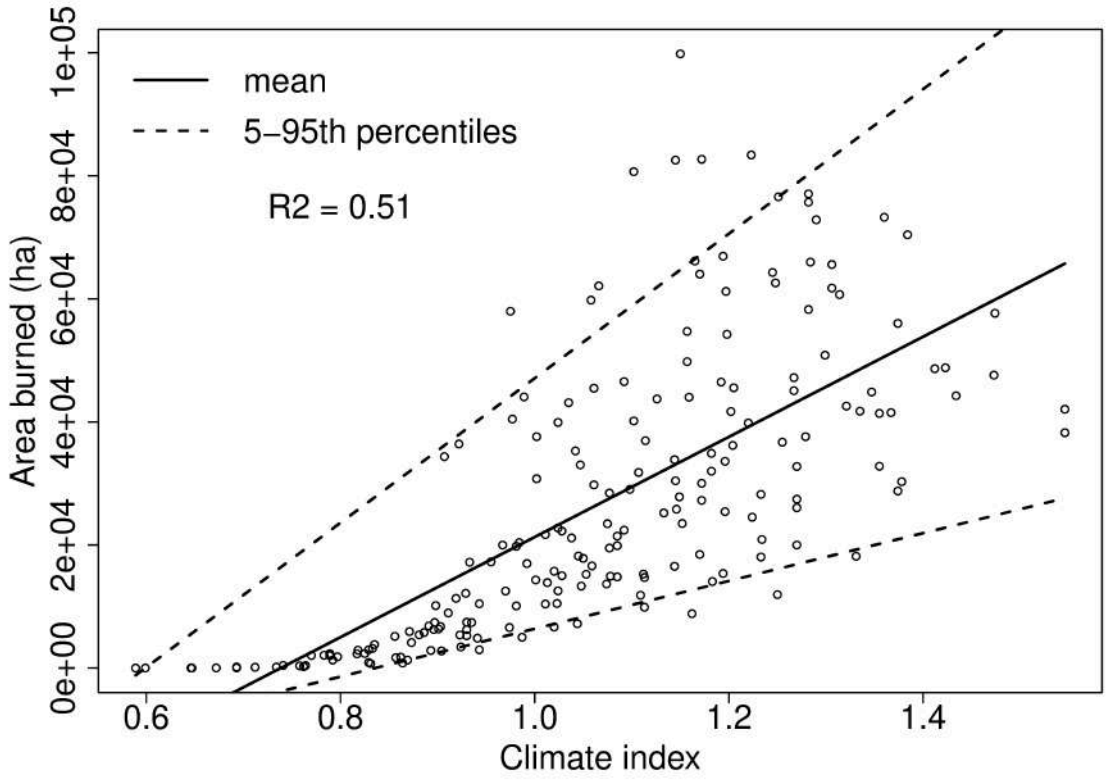

Figure 7: Scatterplot of the modified wildfire Climate Index based on the modified Palmer Drought Severity Index (see text for details) and the log of simulated total area burned per 5 years in the American South Fork River landscape representing the historical reference period of 1550-1850, and the fitted linear regression for the mean and 5-95th quantiles (see text for details) along with the Coefficient of Determination (R2) of the fit.

HISTORICAL RANGE OF VARIABILITY and CURRENT DEPARTURE

Biophysical Classes and Units

To summarize HRV and current departure in landscape structure at the Site and subbasin levels, we subdivided the landscape into a set of Biophysical Classes (BPCs), as described in detail in the GTR. Briefly, we indexed site productivity based on the cumulative tree biomass generated over the course of the simulation, after model equilibration, and then modeled tree biomass as a function of 10 geophysical variables using a Random Forest analytical framework, and lastly classified predicted Biomass into 4 equal-area classes based on quartiles of the data, plus a zero class for all non-forest cells. The final BPC layer included 4 classes ranging from the least productive to most productive sites, plus a non-forest class, as depicted in **Figure 8**.

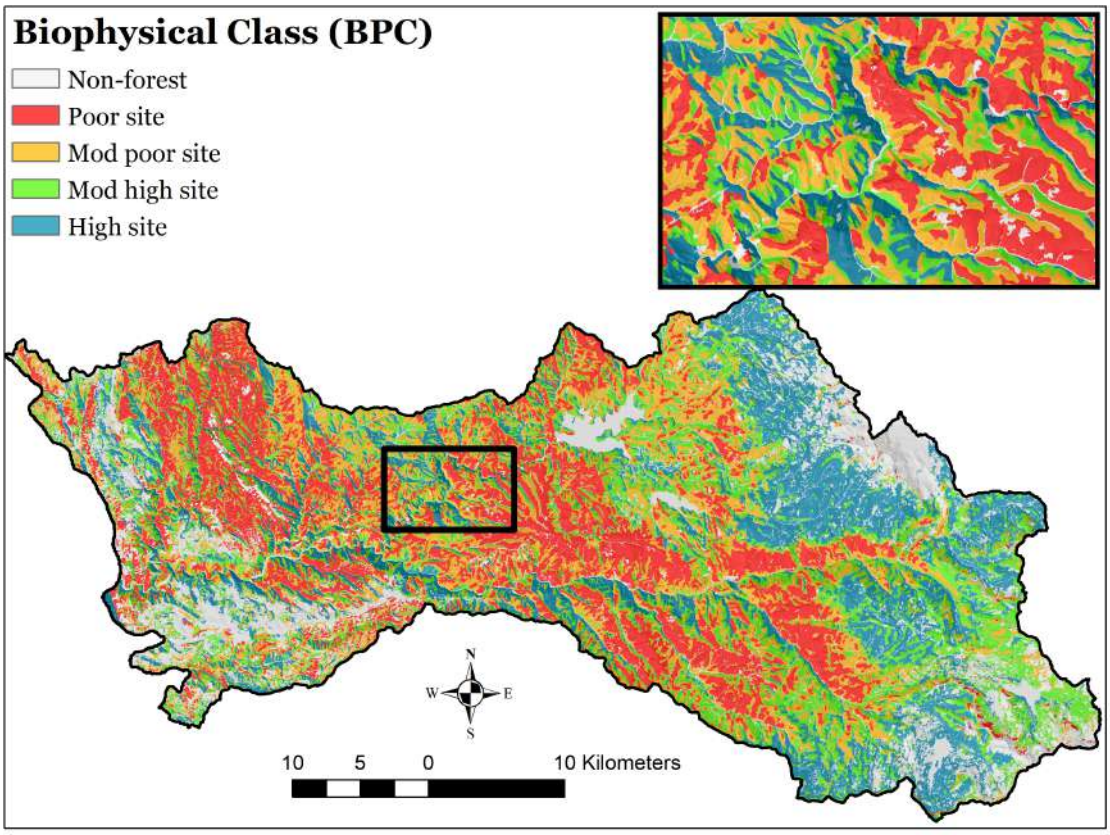

Figure 8: Biophysical Classes (BPCs) based on quartiles of predicted Biomass derived from a Random Forest model to predict Biomass (i.e., simulated cumulative tree height) from 10 biophysical variables. The Random Forest model explained ~70% of the variation in Biomass under simulated historical dynamic equilibrium conditions in the American South Fork River landscape.

The final BPCs were distinguishable on the basis of the 10 geophysical variables and cover type, although there was considerable overlap among BPCs in each of the variables, as described below for a select set of the variables.

- *Cover Type* - The distribution of each cover type among BPCs (as a percentage of the cover type), ordered roughly from low to high elevation distributions, is given in **Table 3**. Most forest types were well distributed among BPCs, suggesting that cover type was generally not a good discriminator of BPCs. However, there were some notable exceptions. For example, Lodgepole Pine and Red Fir were essentially absent from Low productivity sites; whereas, Yellow Pine was disproportionately found on lower productivity sites as was Sierra Mixed Conifer_Ultramafic. The most abundant cover type, Sierra Mixed Conifer, was broadly distributed across site productivity classes.

  Table 3: Percentage of each cover type in each Biophysical Class (BPC) for the American South Fork River landscape.

Cover type	Area (ha)	Low	ModLow	ModHigh	High
Oak Woodland	184	15.50	40.61	37.17	6.72
Yellow Pine	23777	48.61	27.59	15.45	8.35
Oak-Conifer Forest and Woodland	7031	34.29	26.29	21.63	17.79
Mixed Evergreen	11309	23.75	30.45	24.96	20.84
Mixed Evergreen_Ultramafic	154	23.44	32.10	28.66	15.80
Sierra Mixed Conifer	62882	29.06	31.28	24.87	14.79
Sierra Mixed Conifer_Ultramafic	119	48.85	16.94	18.61	15.60
Lodgepole Pine	3480	1.99	17.40	66.99	13.62
Red Fir	25492	0.61	5.35	25.58	68.46
Subalpine Conifer	1695	11.92	22.48	45.88	19.72

- *Mesic Index* - The distribution of the Mesic Index for each BPC (given as quantiles of the index) is given in **Table 4**. As expected, the Mesic Index distribution increased as the site productivity class increased from Low to High, but with considerable overlap in distributions between adjacent BPC classes. Despite the strong overlap, the BPC classes represented a gradient in expected site moisture, with the Low site class representing the driest sites and the High site class representing the wettest sites.

  Table 4: Distribution of the Mesic Index in each Biophysical Class (BPC), given as quantiles for the American South Fork River landscape.

BPC	2.5%	25%	50%	75%	97.5%
Low	20	33	39	46	66
ModLow	26	43	50	58	72
ModHigh	32	47	54	61	75
High	39	52	59	67	81

- *Topographic Position* - The distribution of the Topographic Position Index for each BPC (given as quantiles of the index) is given in **Table 5**. As expected, the Topographic Position Index distribution decreased as the site productivity class increased from Low to High, but with considerable overlap in distributions between adjacent BPC classes. Despite the strong overlap, the BPC classes represented a clear gradient in topographic position, with the Low site class found more commonly on the upper slopes and ridgetops and the High site class found more commonly on the lower slopes and valley bottoms.

  Table 5: Distribution of the Topographic Position Index each each Biophysical Class (BPC), given as quantiles for the American South Fork River landscape.

BPC	2.5%	25%	50%	75%	97.5%
Low	21	44	54	63	85
ModLow	19	41	50	59	82
ModHigh	20	41	49	58	79
High	11	37	45	52	68

- *Aspect* - The distribution of aspect classes among BPCs (as a percentage of the BPC) is given in **Table 6**. Not surprisingly, each BPC class was distributed across all aspect classes, but still exhibited a pronounced orientation, with the Low site class disproportionately occupying southwesterly aspects and the High site class disproportionately occupying northeasterly aspects.

Table 6: Percentage of each Biophysical Class (BPC) in each aspect class for the American South Fork River landscape.

Aspect	N	NE	E	SE	S	SW	W	NW	Flat
Low	2.33	1.23	1.67	9.24	20.63	28.54	18.52	16.33	1.51
ModLow	9.21	5.14	5.47	14.74	15.01	17.67	10.87	19.47	2.42
ModHigh	15.80	14.10	11.45	11.94	8.45	11.13	7.35	16.20	3.60
High	15.19	20.37	13.57	9.60	7.33	9.73	5.69	13.33	5.20

Fire Return Interval and Departure

Mean point-specific Fire Return Interval (FRI) represents the average number of years between fire events at the 5 m cell level. We interpreted the observed mean FRI after model equilibration (N = 200 timesteps) at the cell level as a single integrated (albeit not comprehensive) summary of the historical wildfire disturbance regime. The historical mean FRI varied from < 15 years to > 300 years across the landscape, with evident influences of both cover type and terrain (**Figure 9**).

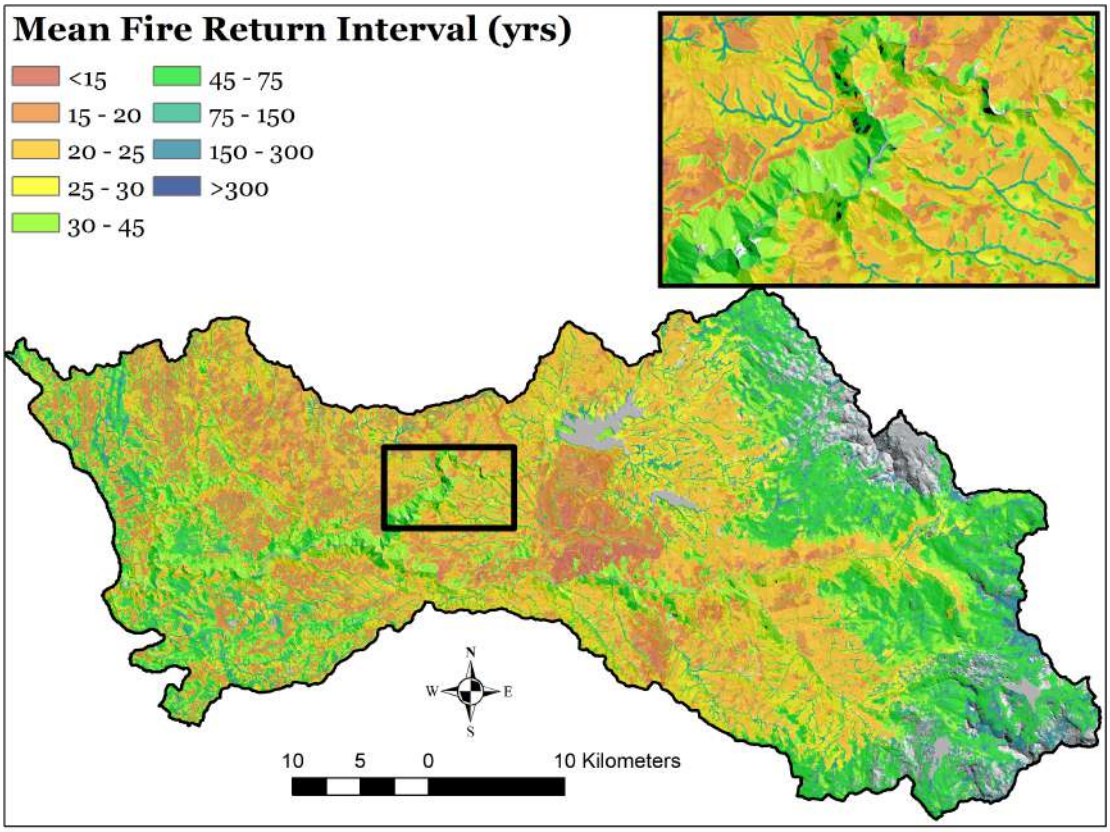

Figure 9: Simulated Fire Return Interval (FRI) (yrs) at the 5 m cell level for the American South Fork River landscape.

In addition, the historical mean FRI varied among BPCs as expected (**Table 7**). Specifically, the median FRI increased steadily from 22 to 46 years with increasing site productivity; i.e., from Low to High BPC. Low productivity sites that occurred disproportionately on upper slopes and ridgetops and southwesterly aspects were warmer and drier and thus more susceptible to wildfire, despite having less fuel build-up over

time. Conversely, High productivity sites that occurred disproportionately on lower slopes and valley bottoms and on northeasterly aspects were cooler and wetter and thus less susceptible to wildfire, despite having more fuel build-up over time. The relatively short median FRIs across all sites indicates that historically wildfires typically occurred frequently enough to keep surface and ladder fuel loads low enough to reduce the occurrence of high-severity wildfire.

Table 7: Range of variability (given as quantiles) in the mean fire return interval (FRI) by Biophysical Class (BPC) for the American South Fork River landscape.

BPC	HRV2.5%	HRV25%	HRV50%	HRV75%	HRV97.5%
Low	15	18	22	24	51
ModLow	17	22	25	31	85
ModHigh	19	26	31	48	144
High	21	31	46	52	131

These results also indicate that the HRV in mean FRI varied several-fold across sites within each BPC. For example, on High productivity sites FRI varied roughly six-fold between 21-131 years across sites. The wide range of variation in FRI within BPCs indicates that wildfire risk varied markedly across sites even within a single BPC and, consequently, that FRI is only loosely correlated with predicted cumulative tree biomass. For example, sites classified as having high long-term productivity under historical dynamic equilibrium conditions could have FRIs as short as 21 years (or shorter for the extremes) or as long as 131 years (or longer for the extremes) depending on local topographic and vegetative conditions and chance. This is visually evident in the map of mean FRI for the High site BPC (**Figure 10**).

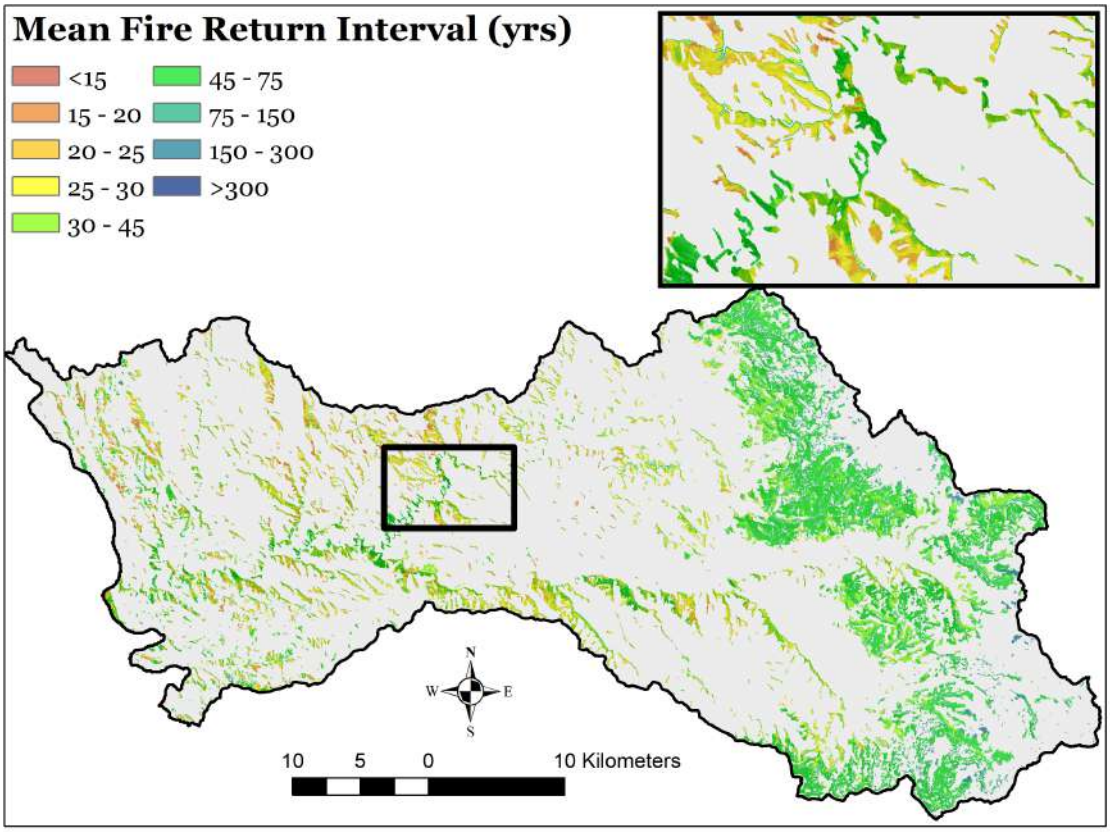

Figure 10: Simulated Fire Return Interval (FRI) (yrs) at the 5 m cell level on High productivity sites (Biophysical Class = 4) in the American South Fork River landscape.

Fire Return Interval Departure (FRID) represents the percentage deviation of the contemporary (post-settlement) mean point-specific FRI from the mean point-specific FRI under historical (i.e., pre-settlement) dynamic equilibrium conditions. Briefly, FRID measures the degree, in percent, to which contemporary fires (i.e., since 1909) are burning at frequencies similar to the frequencies that occurred prior to significant Euro-American settlement, as simulated (**Figure 11**). Positive departure indicates that the contemporary fire frequency is less than the historical fire frequency.

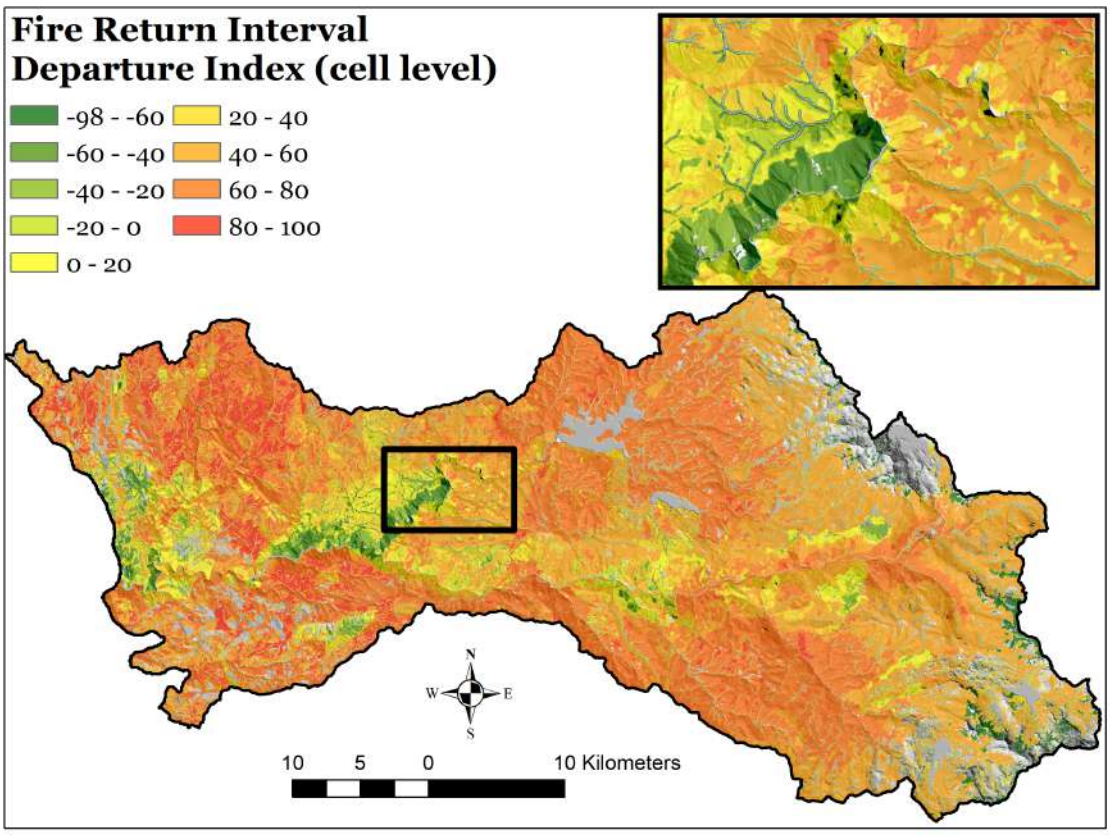

Figure 11: Fire Return Interval Departure (FRID) at the 5 m cell level in the American South Fork River landscape, representing the percent to which contemporary fires (i.e., since 1909) are burning at frequencies similar to the frequencies that occurred prior to significant Euro-American settlement, as simulated.

In addition to the cell-level map of FRID, we also summarized the mean FRID for each GPU to include in the Stewardship Atlas as a means of prioritizing units for treatment with fire (**Figure 12**).

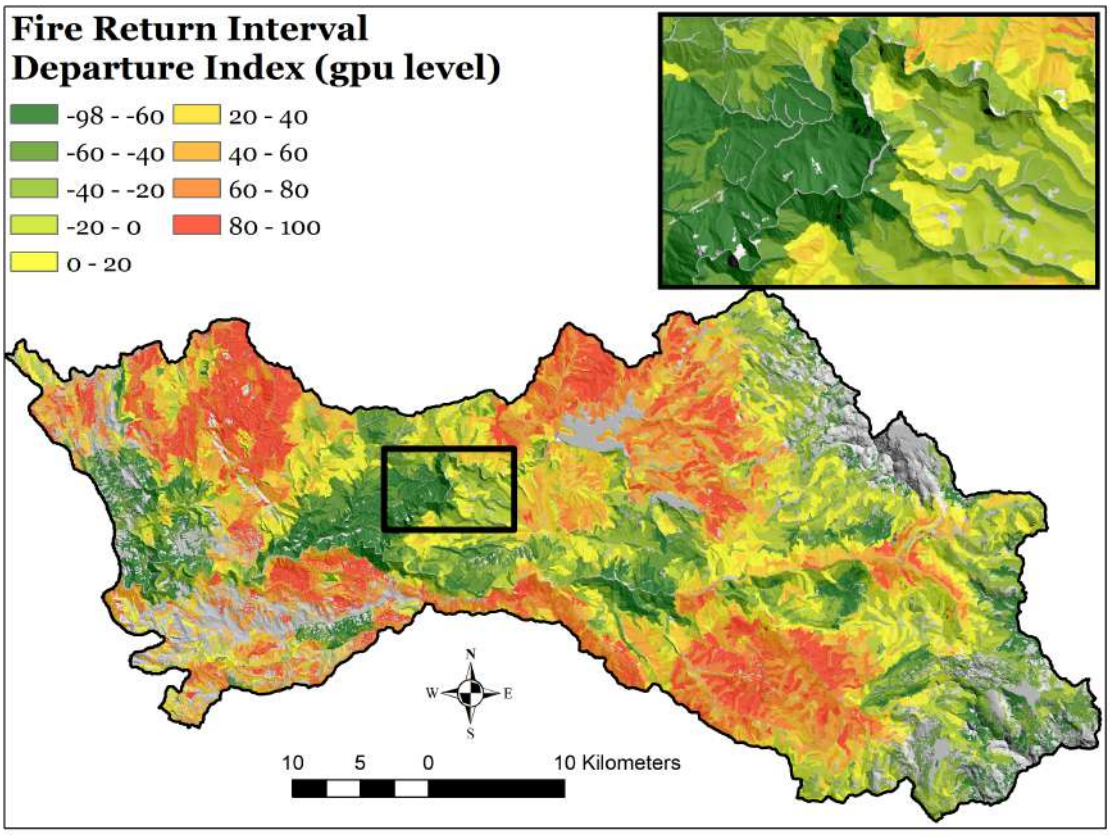

Figure 12: Geophysical Unit-level Fire Return Interval Departure (FRID) for the American South Fork River landscape, representing the average 5 m cell value in the percent to which contemporary fires (i.e., since 1909) are burning at frequencies similar to the frequencies that occurred prior to significant Euro-American settlement, as simulated.

Vegtation Persistence

We defined vegetation persistence as the likelihood of persisting in either an early- or late-seral condition at the 5 m cell level. We interpreted the observed mean FRI of high-mortality wildfires after model equilibration (N = 200 timesteps) at the cell level as a proxy for vegetation persistence, under the assumption that locations with shorter high-mortality FRIs would likely persist longer in early-seral stages and, conversely, locations with longer high-mortality FRIs would likely persist longer in late-seral stages.

Figure 13 depicts several areas with relatively long high-mortality FRIs (dark blue areas in the map) and these are sites that have a high likelihood of supporting late-seral vegetation under a natural disturbance regime. Conversely, the map depicts several areas with relatively short high-mortality FRIs (yellow and orange areas in the map) and these are sites that have a high likelihood of supporting early-seral vegetation much of the time under a natural disturbance regime. Accordingly, management objectives for these areas could be designed to capitalize on these focal areas. For example, establishing treatment objectives to maintain and enhance late-seral conditions for old forest associated species in areas with a lower likelihood of high-mortality wildfire (i.e., longer FRI) would be logical.

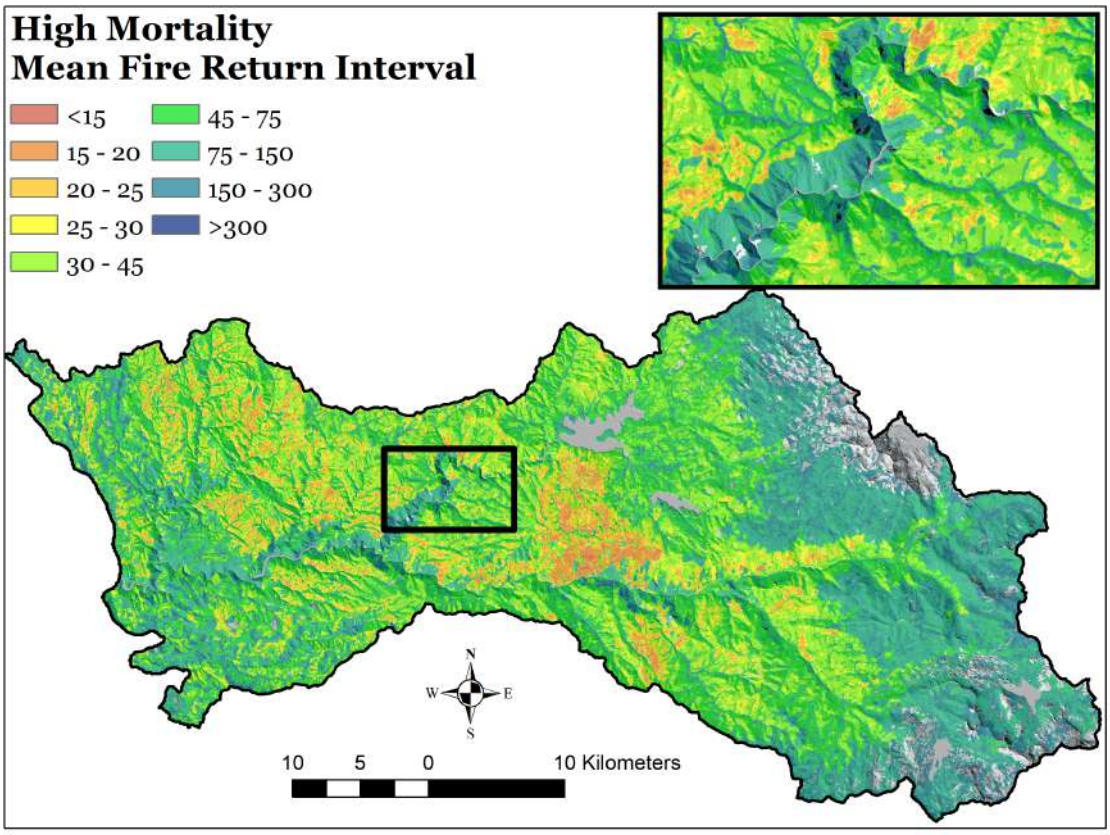

Figure 13: Simulated high-mortality Fire Return Interval (FRI) (yrs) at the 5 m cell level in the American South Fork River landscape.

Site Level HRV and Departure

The results presented in this section address landscape metrics quantified at the "Site" level. Recall from the GTR that we defined a Site as a 40-m radius window around each focal cell. Here, each Site falls within a single BPC based on the location of the focal cell and has a single value computed for each landscape metric for each point in time (i.e., snapshot). HRV represents the variation in the landscape metric across Sites and over time under historical dynamic equilibrium conditions. Further recall that the current landscape also has a range of values across Sites (CRV), rather than a single value. Thus, a comparison of the HRV and CRV distributions depicts the degree to which CRV deviates from HRV (i.e., current departure). It is important to remember that Site-level departure reflects the deviation between the CRV across Sites within the focal landscape and the HRV across Sites and over time within the focal landscape. Thus, departure for a Site is not based on a comparison of the current Site condition to its own HRV (as is the case with GPU and subbasin departure, see below); rather it is the distribution of current Site conditions across the entire landscape compared to the historical distribution across Sites that forms the basis for Site-level departure.

Recall from the GTR that we used a parsimonious suite of landscape metrics that we deemed meaningful for estimating departure at the Site-level across the focal landscape and appropriate given the available data, and computed departure as described in the GTR (and not repeated here), including the following metrics:

Developmental Stage

Developmental stage at the Site level was based on discrete stages of canopy height development. We quantified the composition of forest developmental stages at the Site level based on the percentage of the forested portion of the Site in each developmental stage. The HRV and CRV in Developmental Stage composition by BPC at the Site level is given in **Table 8** and depicted in **Figure 14**.

Table 8: Range of variability (given as quantiles) in each developmental stage class across sites (40-m radius window centered on each focal cell) by Biophysical Class (BPC) for the current range of variability (CRV) and the historical range of variability (HRV) for the American South Fork River landscape.

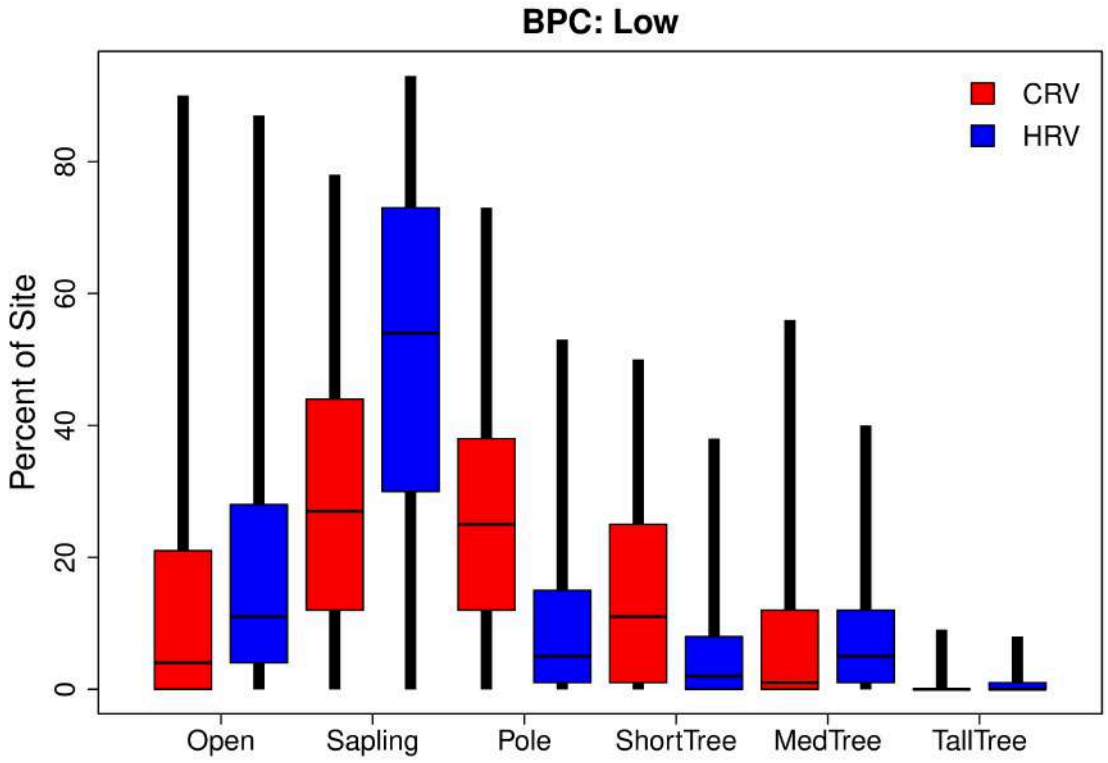

BPC	Class	Scenario	HRV 2.5%	HRV 25%	HRV 50%	HRV 75%	HRV 97.5%
Low	Open	CRV	0	0	4	21	90
Low	Open	HRV	0	4	11	28	87
Low	Sapling	CRV	0	12	27	44	78
Low	Sapling	HRV	0	30	54	73	93
Low	Pole	CRV	0	12	25	38	73
Low	Pole	HRV	0	1	5	15	53
Low	ShortTree	CRV	0	1	11	25	50
Low	ShortTree	HRV	0	0	2	8	38
Low	MedTree	CRV	0	0	1	12	56
Low	MedTree	HRV	0	1	5	12	40
Low	TallTree	CRV	0	0	0	0	9
Low	TallTree	HRV	0	0	0	1	8
ModLow	Open	CRV	0	0	6	24	96
ModLow	Open	HRV	0	3	7	18	75
ModLow	Sapling	CRV	0	12	26	42	74
ModLow	Sapling	HRV	1	21	42	62	88
ModLow	Pole	CRV	0	12	24	36	67
ModLow	Pole	HRV	0	3	9	21	60
ModLow	ShortTree	CRV	0	2	12	24	49
ModLow	ShortTree	HRV	0	1	4	12	45
ModLow	MedTree	CRV	0	0	2	13	53
ModLow	MedTree	HRV	0	4	10	20	49
ModLow	TallTree	CRV	0	0	0	0	12
ModLow	TallTree	HRV	0	0	1	3	17
ModHigh	Open	CRV	0	1	7	27	95
ModHigh	Open	HRV	0	3	6	14	64
ModHigh	Sapling	CRV	0	13	27	40	69
ModHigh	Sapling	HRV	0	14	30	50	81
ModHigh	Pole	CRV	0	13	24	34	62
ModHigh	Pole	HRV	0	5	12	25	60
ModHigh	ShortTree	CRV	0	3	12	24	49
ModHigh	ShortTree	HRV	0	2	6	15	48
ModHigh	MedTree	CRV	0	0	2	13	53
ModHigh	MedTree	HRV	1	8	16	28	56
ModHigh	TallTree	CRV	0	0	0	0	13
ModHigh	TallTree	HRV	0	0	2	6	23
High	Open	CRV	0	1	8	27	89
High	Open	HRV	0	3	6	11	51
High	Sapling	CRV	0	15	29	40	66
High	Sapling	HRV	0	7	20	37	72
High	Pole	CRV	0	13	23	32	57
High	Pole	HRV	0	5	13	26	59
High	ShortTree	CRV	0	4	13	22	48
High	ShortTree	HRV	0	3	8	16	48
High	MedTree	CRV	0	0	3	14	55
High	MedTree	HRV	2	12	23	35	62
High	TallTree	CRV	0	0	0	0	20
High	TallTree	HRV	0	1	5	12	36

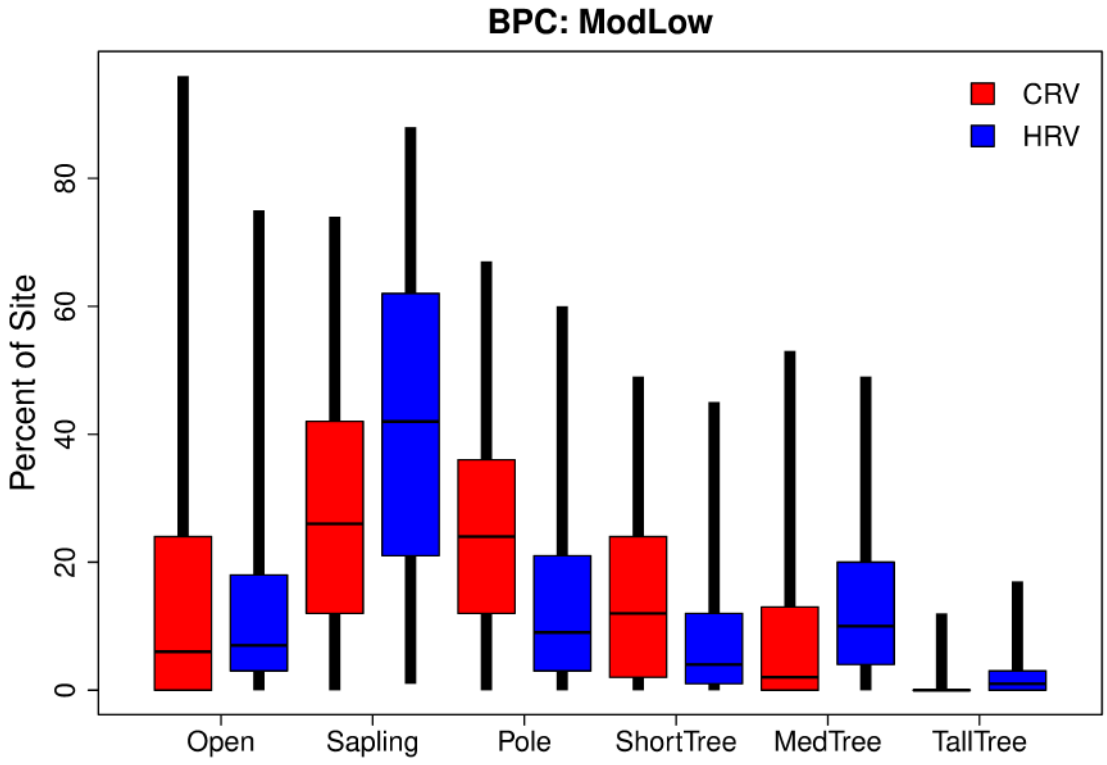
BPC: ModLow
CRV
HRV
Percent of Site
0
20
40
60
80
Open
Sapling
Pole
ShortTree
MedTree
TallTree

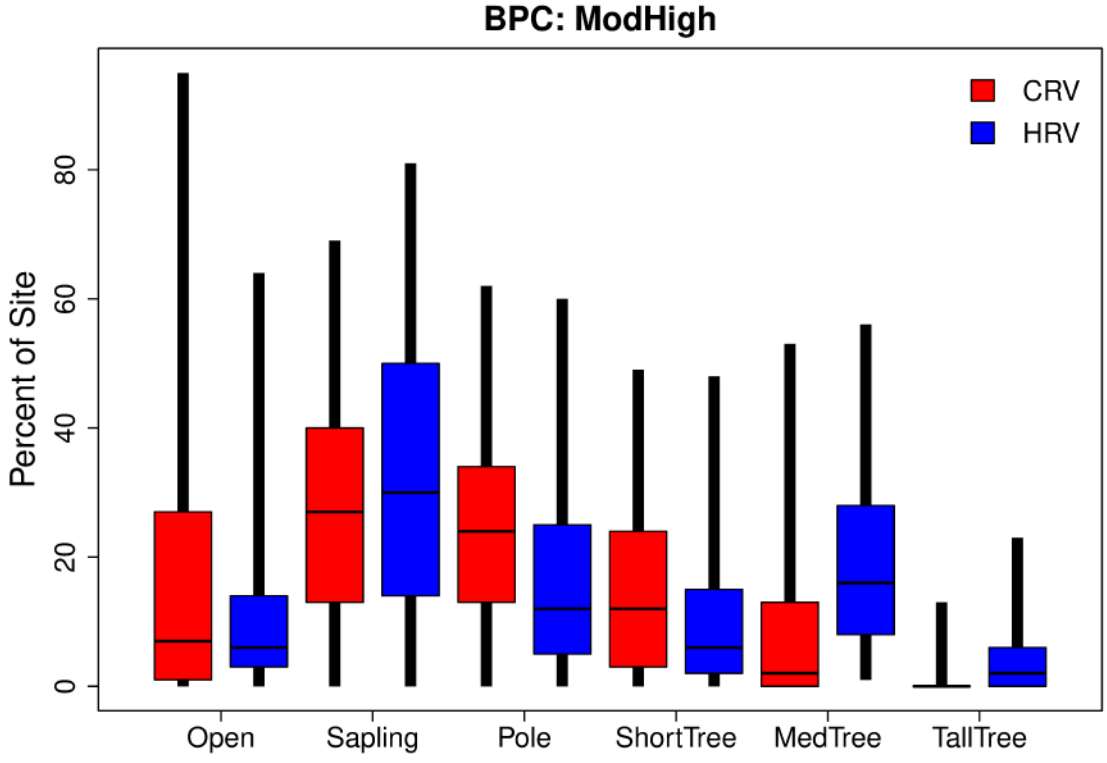
BPC: ModHigh
CRV
HRV
Percent of Site
0
20
40
60
80
Open
Sapling
Pole
ShortTree
MedTree
TallTree

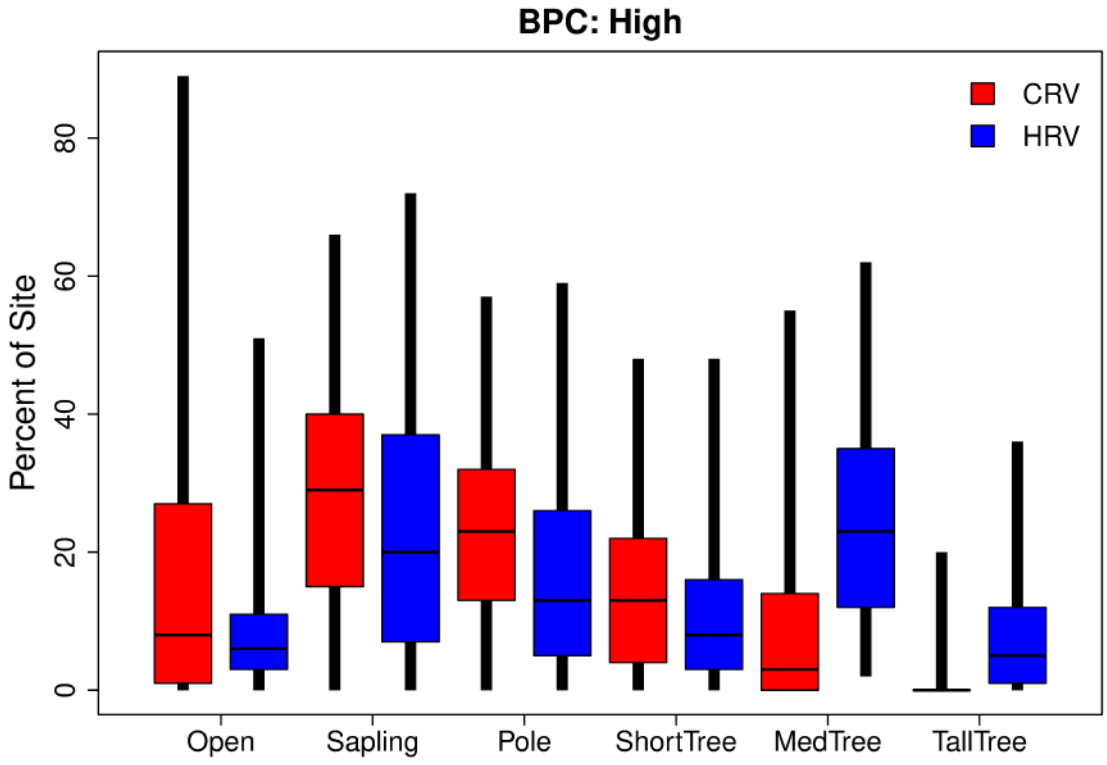

Figure 14: Historical Range of Variability (HRV) and Current range of variabiilty (CRV) among Sites (i.e., 40-m radius window) in the percent of forest in each developmental stage within the Low, Moderately Low, Moderately High and High site productivity Biophysical Classes (BPCs) in the American South Fork River landscape. Box = 25-50 percentiles; whiskers = 2.5-97.5 percentiles

Recall that current departure in the Site-level metrics provides a basis for prioritizing management at the unit level. For example, given the results above, to reduce the current departure in developmental stage composition on Low productivity Sites, management could prioritize treatments that produce units with a greater percentage of Open areas intermixed with Tall trees to shift the overall developmental stage distribution across the landscape to be more aligned with the HRV distribution. The same priorities could be given to High productivity Sites, although here the emphasis would be predominantly on increasing the proportion of Sites with a greater proportion of Tall trees. Of course, aside from controlling the percentage in Open, there is only limited ability to actively manage developmental stage succession (i.e., height growth). Indeed, much of the succession required to shift the current distribution towards the later stages of development simply requires time (e.g., to allow trees in the Pole and Short Tree stages to grow into the Medium and Tall Tree stages). However, managing surface and ladder fuels to inhibit high severity wildfire and retaining current taller trees may be an effective strategy to gradually shift the CRV towards better alignment with HRV with respect to the later developmental stages.

Tree Size (QMD)

Tree Size at the Site level was based on the Quadratic Mean Diameter (QMD) of established trees within a 40-m radius of the focal cell. Recall that QMD was based on only the cells with established trees in the window. Thus, if there was a single cell with an established tree in the window, then QMD was based on that single tree and equaled the tree's diameter at breast height (DBH). Accordingly, QMD can be quite high even in relatively open areas if the few neighborhood trees are large in diameter. The HRV and CRV in Tree Size composition at the Site level by BPC is given in **Table 9** and depicted in **Figure 15**.

BPC	Scenario	HRV 2.5%	HRV 25%	HRV 50%	HRV 75%	HRV 97.5%
Low	CRV	1	4	7	10	19
Low	HRV	2	6	9	13	21
ModLow	CRV	1	5	8	11	21
ModLow	HRV	5	10	13	16	23
ModHigh	CRV	1	5	8	12	23
ModHigh	HRV	7	13	16	19	26
High	CRV	2	6	10	14	27
High	HRV	10	17	20	23	30

Table 9: Range of variability (given as quantiles) in tree size (quadratic mean diameter) across Sites (40-m radius window centered on each focal cell) by Biophysical Class (BPC) for the current range of variability (CRV) and the historical range of variability (HRV) for the American South Fork River landscape.

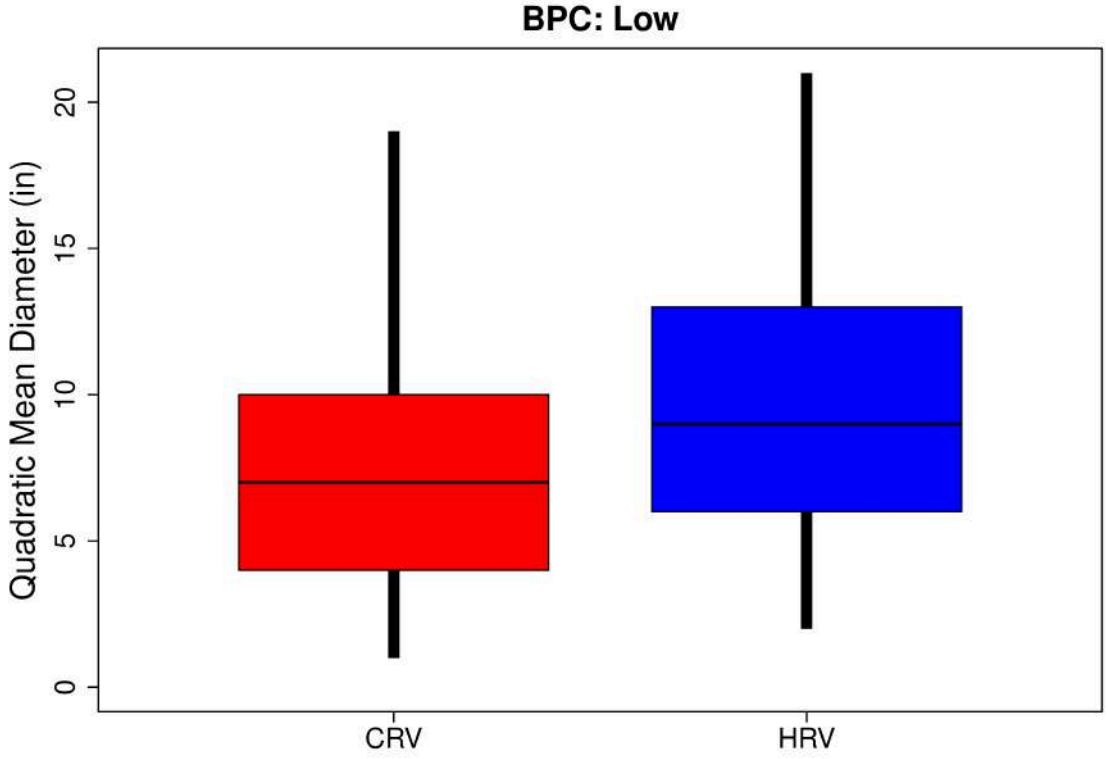

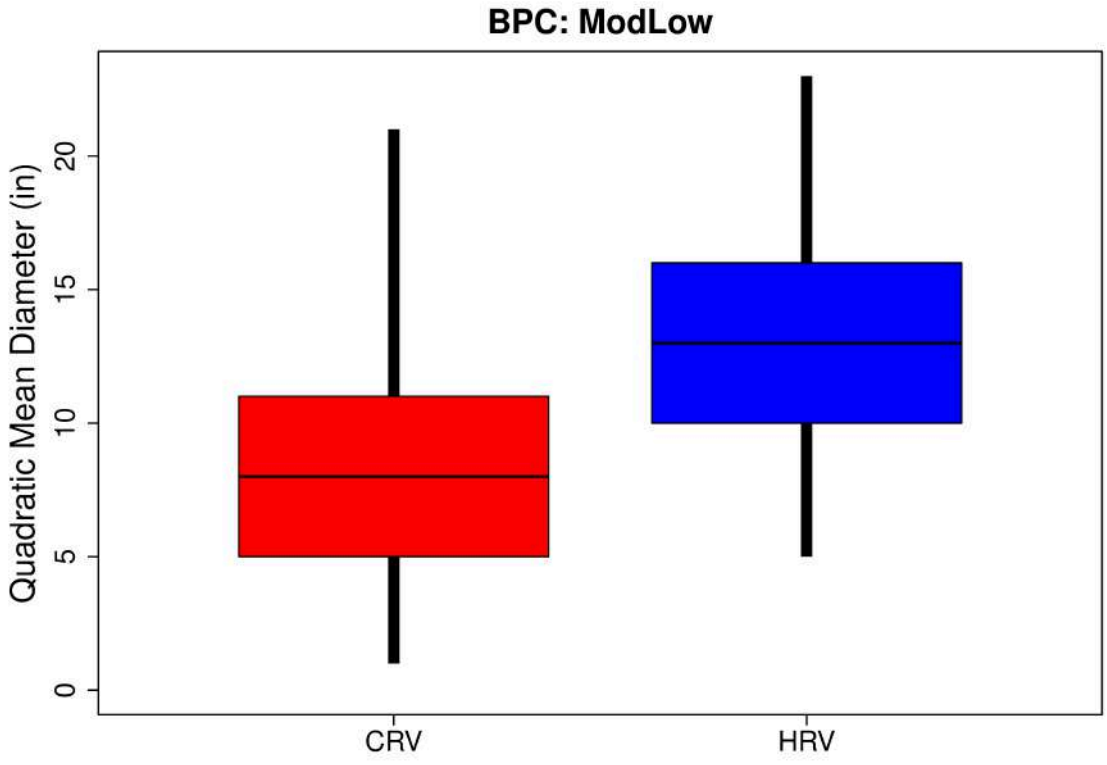
BPC: ModLow
Quadratic Mean Diameter (in)
0
5
10
15
20
CRV
HRV

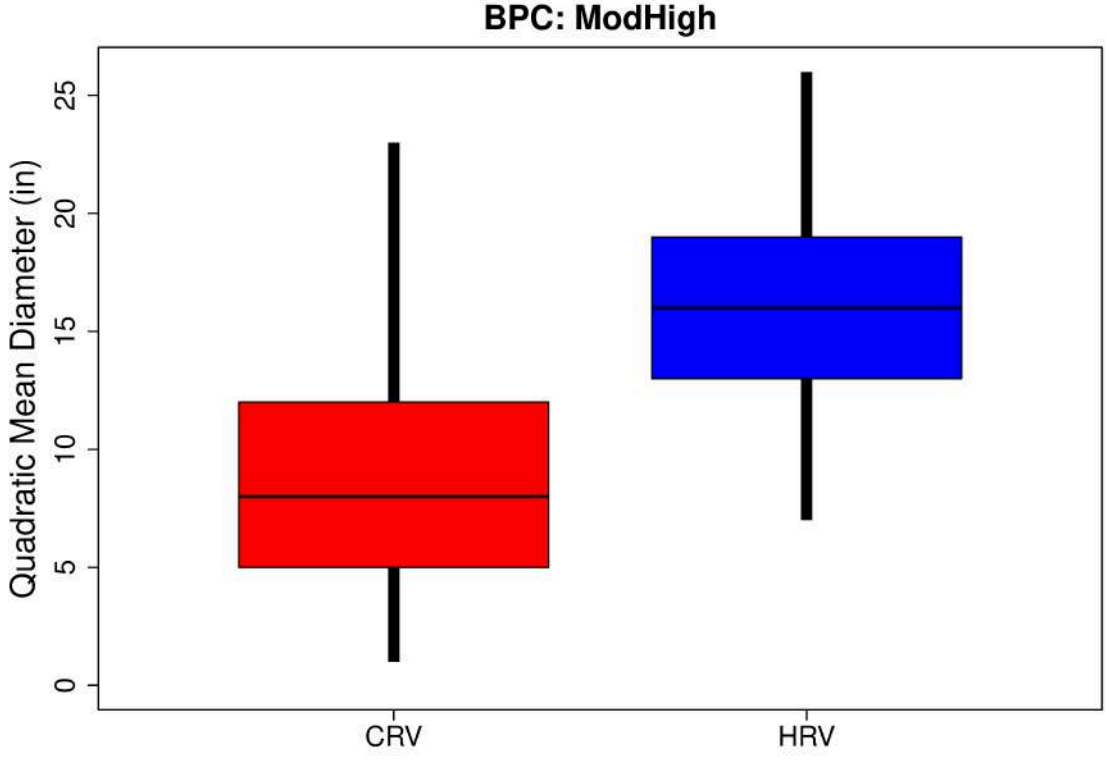
BPC: ModHigh
Quadratic Mean Diameter (in)
0
5
10
15
20
25
CRV
HRV

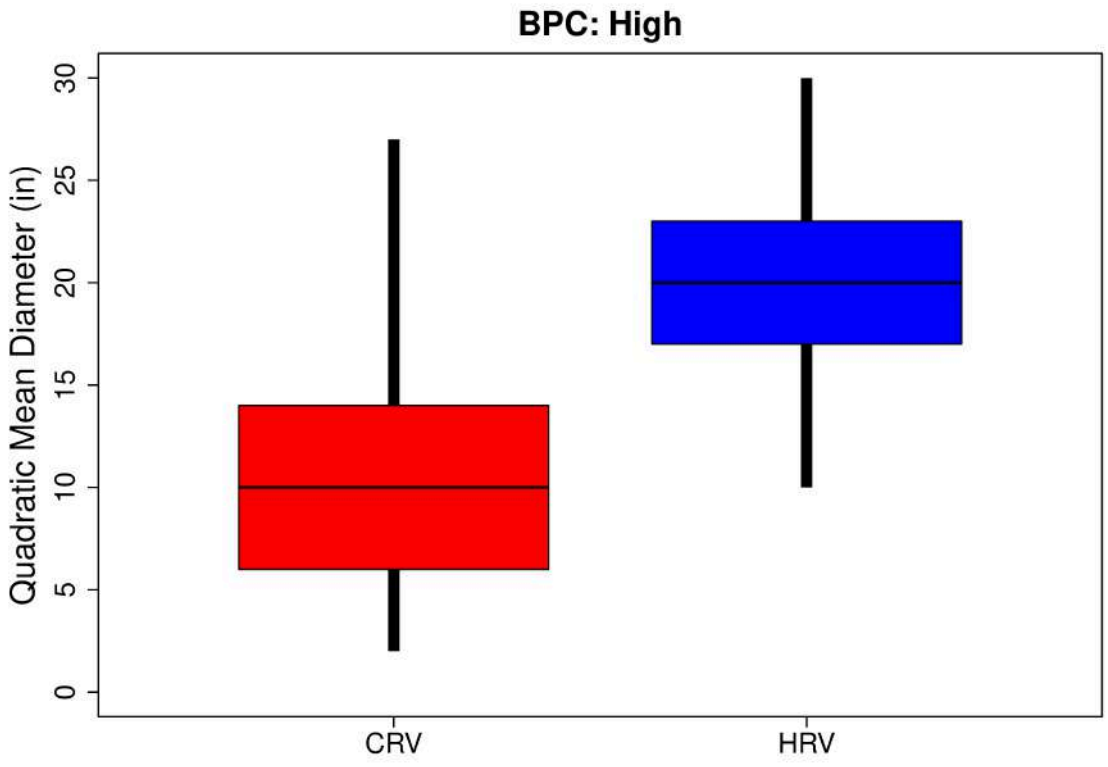

Figure 15: Historical Range of Variability (HRV) and Current range of variabiilty (CRV) among Sites (i.e., 40-m radius window) in the Quadratic Mean Diameter (QMD) of established trees to breast height within the Low, Moderately Low, Moderately High and High site productivity Biophysical Classes (BPCs) in the American South Fork River landscape. Box = 25-50 percentiles; whiskers = 2.5-97.5 percentiles

Tree Cover

Tree Cover at the Site level was based on the percentage of 5-m cells with established trees to breast height within a 40-m radius of the focal cell. Recall that even a cell in the Open developmental stage (i.e., forest cell without an established tree to breast height) has a percent tree cover > 0 % so long as there was a single established tree within 40 m of the focal cell. In addition, recall that Tree Cover, as computed here, represents the percentage of cells within 40 m containing one or more established trees to breast height, not actual tree canopy cover, and as such is biased high by an average of 16% over actual tree canopy cover (i.e., actual tree canopy cover will be less than reported here by an average of 16%). The HRV and CRV in Tree Cover composition at the Site level by BPC is given in **Table 10** and depicted in **Figure 16**.

Table 10: Range of variability (given as quantiles) in percent tree cover across Sites (40-m radius window centered on each focal cell) by Biophysical Class (BPC) for the current range of variability (CRV) and the historical range of variability (HRV) for the American South Fork River landscape.

BPC	Scenario	HRV 2.5%	HRV 25%	HRV 50%	HRV 75%	HRV 97.5%
Low	CRV	9	78	95	100	100
Low	HRV	12	71	88	95	99
ModLow	CRV	3	75	93	99	100
ModLow	HRV	24	81	92	96	99
ModHigh	CRV	4	72	92	98	100
ModHigh	HRV	35	85	93	96	99
High	CRV	10	72	91	98	100
High	HRV	48	88	93	96	99

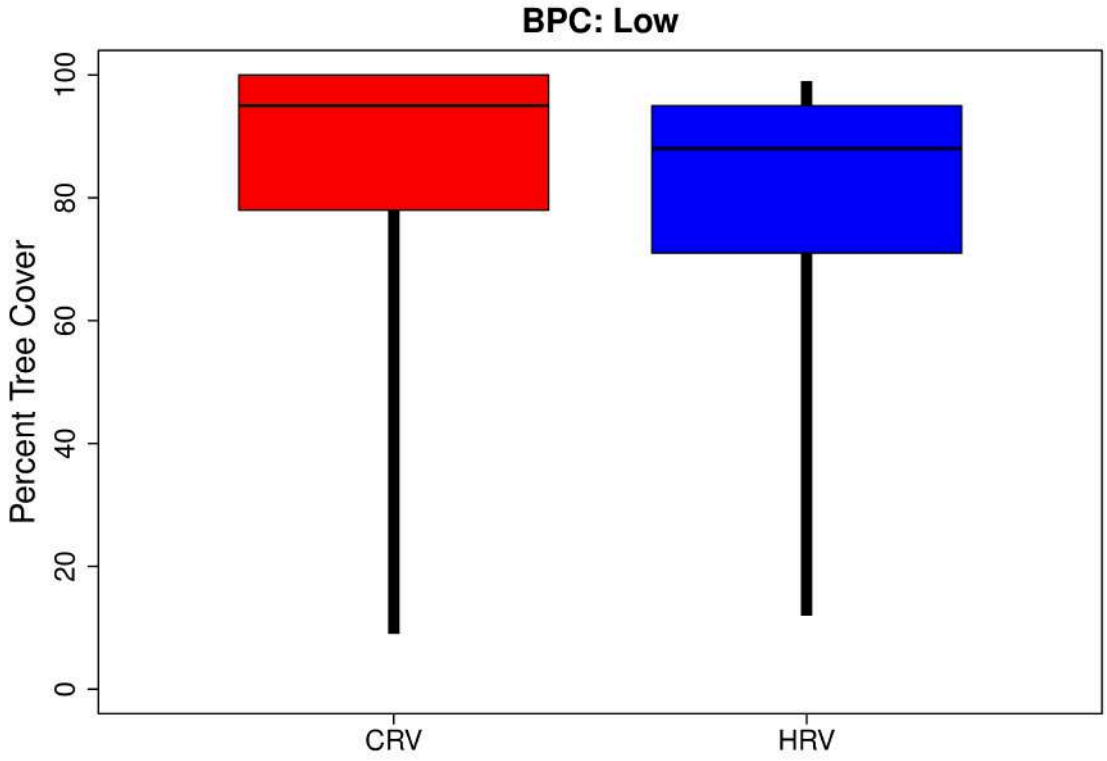

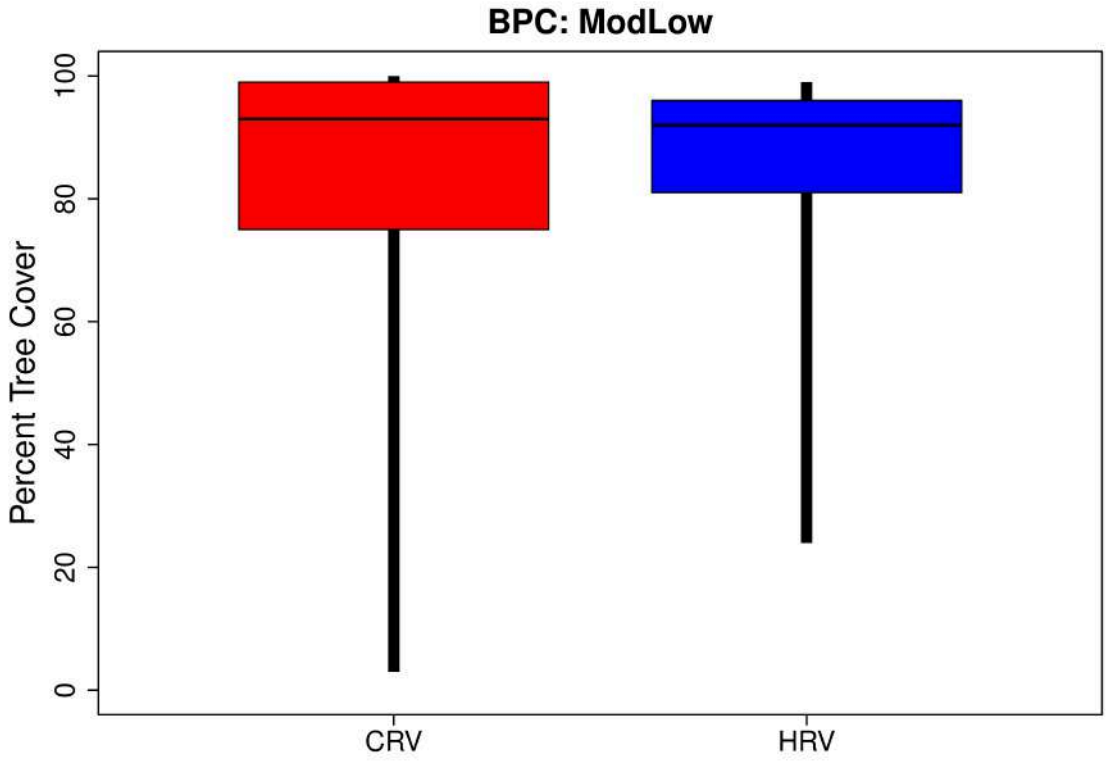
BPC: ModLow
Percent Tree Cover
0
20
40
60
80
100
CRV
HRV

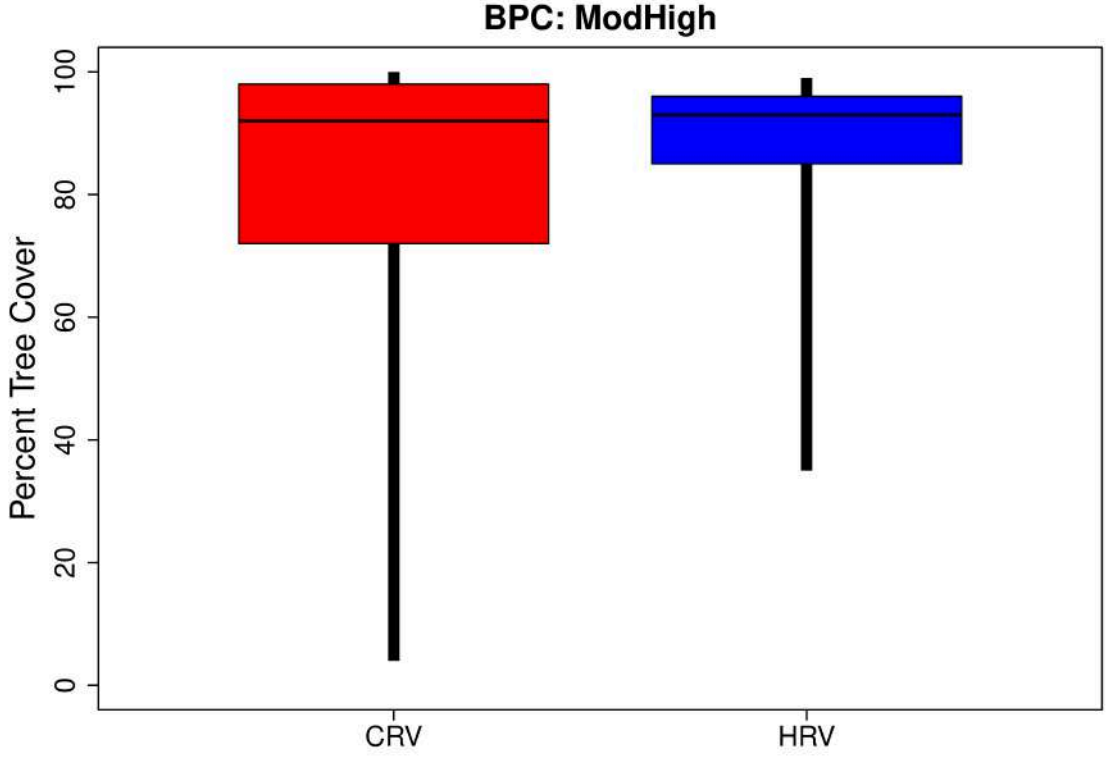
BPC: ModHigh
Percent Tree Cover
0
20
40
60
80
100
CRV
HRV

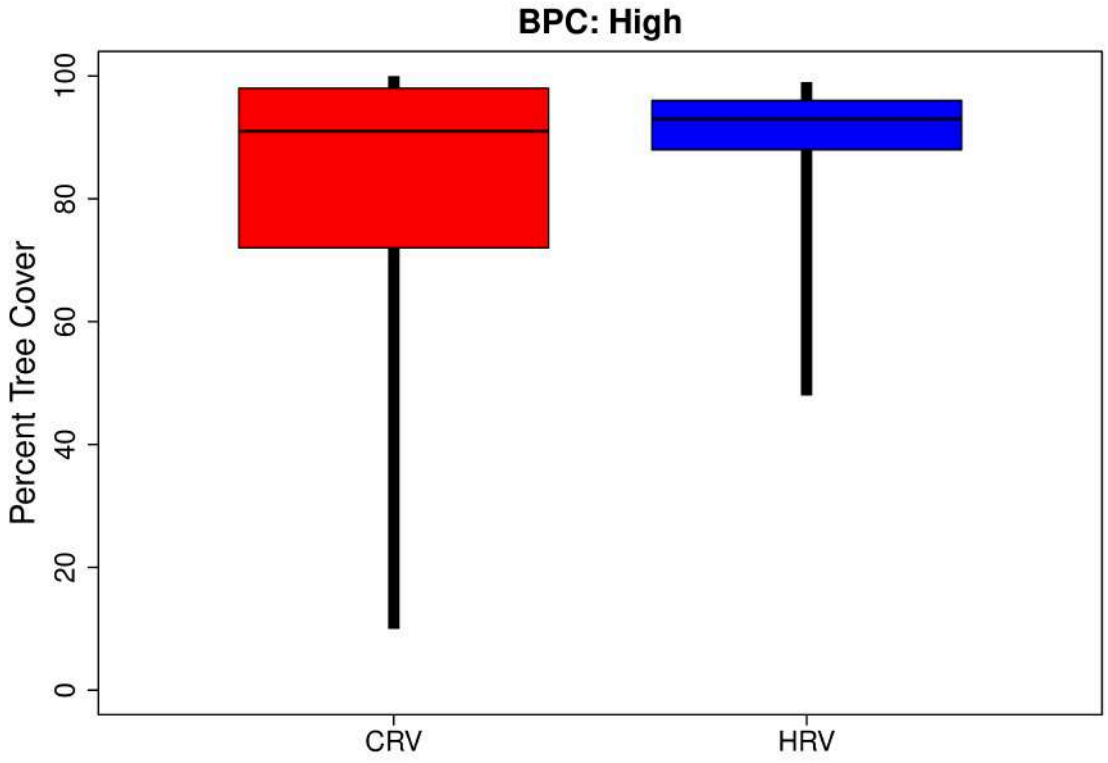

Figure 16: Historical Range of Variability (HRV) and Current range of variabiilty (CRV) among Sites (i.e., 40-m radius window) in the percent Tree Cover of established trees to breast height within the Low, Moderately Low, Moderately High and High site productivity Biophysical Classes (BPCs) in the American South Fork River landscape. Box = 25-50 percentiles; whiskers = 2.5-97.5 percentiles

Geophysical Unit Level Departure

The results presented in this section address current departure in landscape metrics quantified at the spatial extent of a single Geophysical Unit (GPU). The American South Fork River landscape was divided into 6,645 separate GPUs, which collectively encompass the area mapped as forest in the Existing Cover layer (Ecover) and within existing Lidar at the time of this analysis. Recall from the GTR that we defined GPUs based on similarity in a suite of 10 geophysical attributes and that they were defined only for the forested portion of the landscape and only where we had Lidar coverage. In addition, recall that each GPU was assessed independently; i.e., that we compared the current condition of each GPU to its own HRV in vegetation conditions. Thus, current departure of a GPU was specific to that GPU and independent of that measured for other GPUs. Lastly, recall that we used a large but parsimonious suite of landscape metrics that we deemed meaningful for estimating departure at the GPU level and appropriate given the available data, and computed departure as described in the GTR (and not repeated here), including the following:

Metric 1: Basal Area Departure

Departure in basal area of trees within the GPU was based on a metric derived by the TCSI project and adapted here for our purposes (**Figure 42**). GPUs with an increasingly positive departure have a current basal area that is greater than expected under HRV.

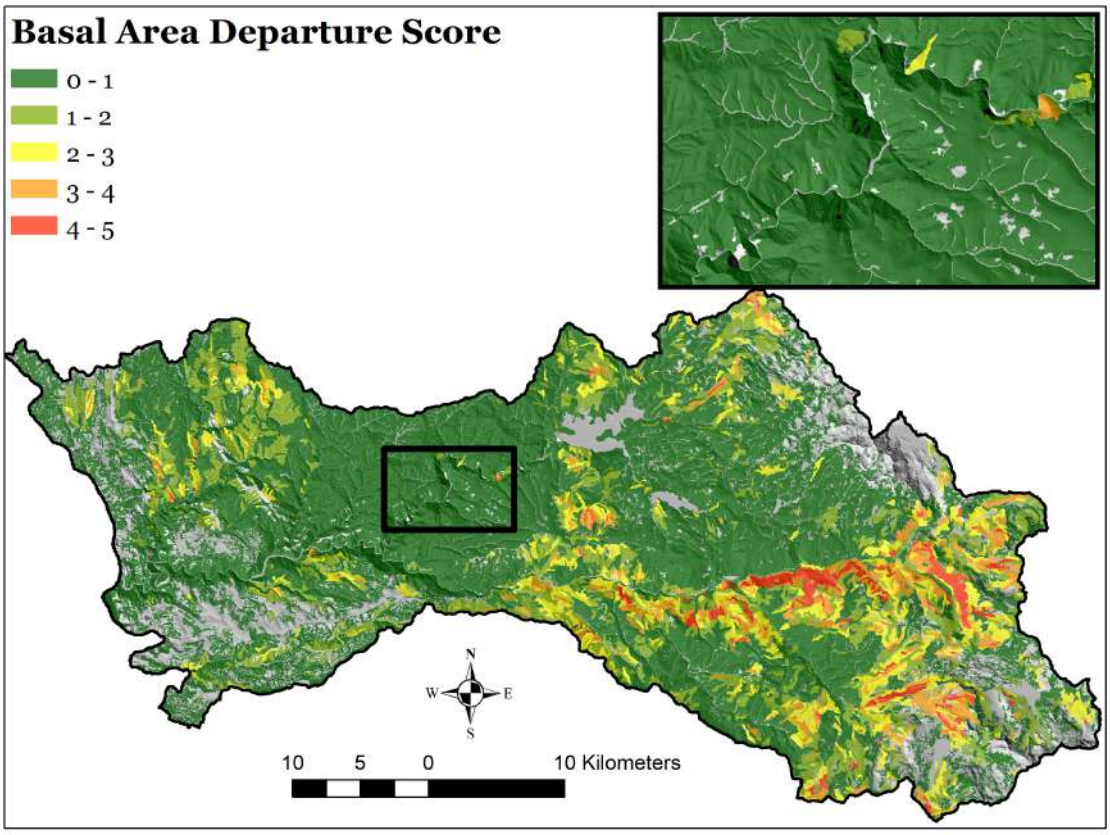

Figure 17: Geophysical Unit (GPU)-level basal area departure score for the American South Fork River landscape. The departure score (0-5) represents the deviation of the current GPU condition from its historical range of variability (HRV), as estimated from a suite of contemporary reference sites. Values increase with increasing degrees of departure.

Metric 2: Percent Open Forest

We measured departure in the percent of forested cells within the GPU in the Open developmental stage (**Figure 18**). GPUs with a departure index less than -1 have less area in the Open developmental stage than under HRV.

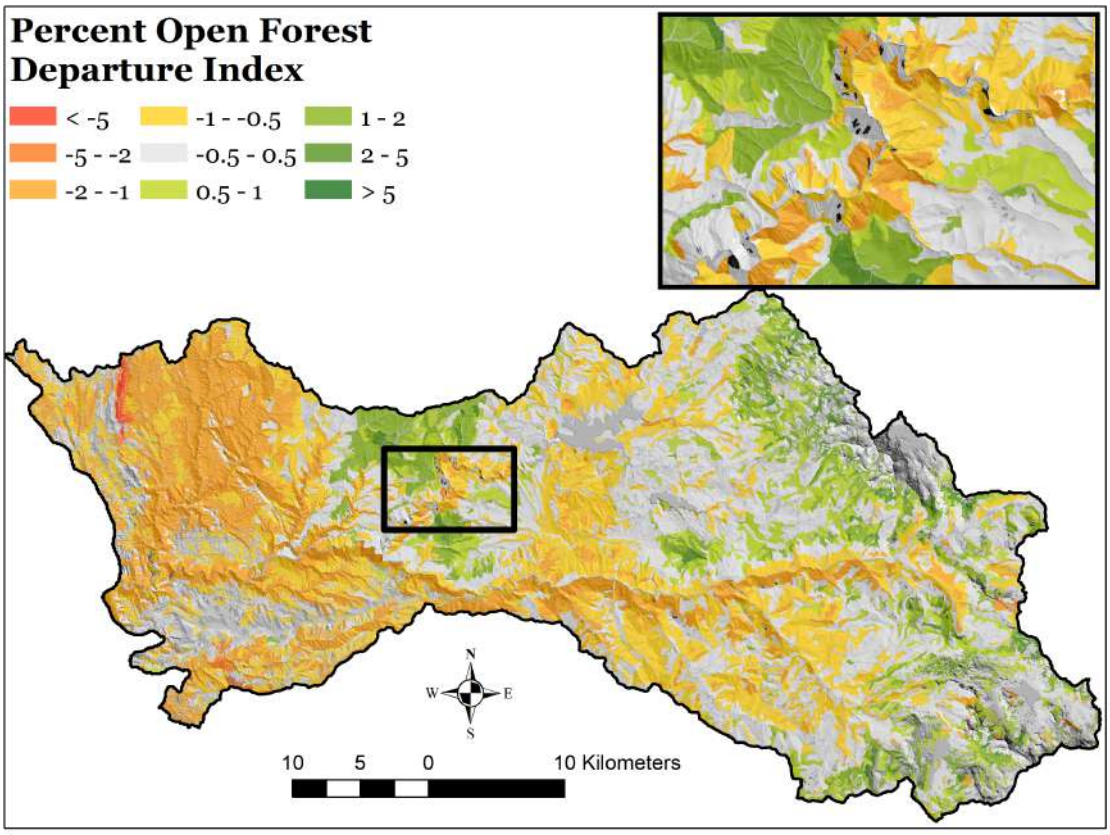

Figure 18: Geophysical Unit (GPU)-level departure index (unbounded) for the percentage of the forest within the GPU in the Open developmental stage for the American South Fork River landscape. The departure Index represents the deviation of the current GPU condition from its historical range of variability (HRV), as simulated. Values < -1 represent a current condition that is less than the HRV for the GPU, and increasingly negative values represent increasing degrees of negative departure.

Metric 3: Developmental Stage Diversity

We measured departure in the diversity of forest developmental stages within the GPU based on the Simpson's Diversity index (**Figure 19**). Here, Simpson's Diversity is defined as the probability that any two cells selected at random would be different developmental stages. The departure index for Simpson's Diversity is less than -1 if the current GPU has a diversity of developmental stages that is less than HRV.

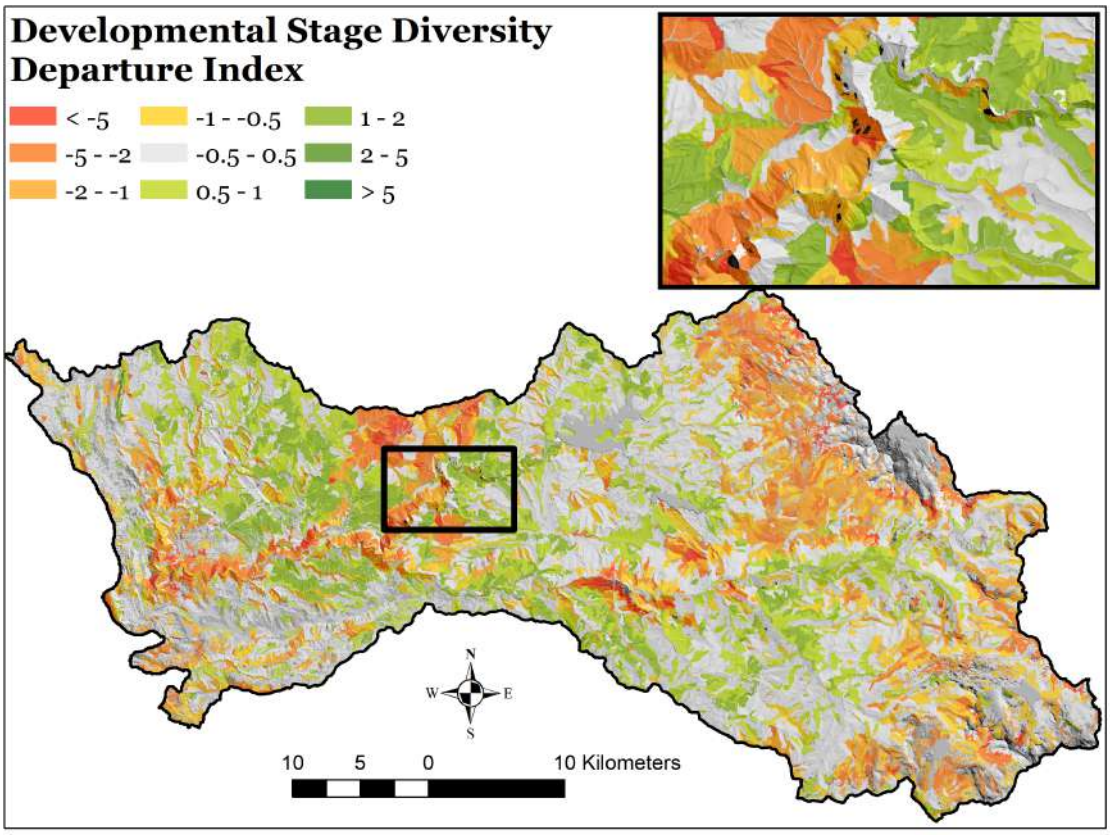

Figure 19: Geophysical Unit (GPU)-level departure index (unbounded) for the Simpson Diversity of developmental stages within the GPU for the American South Fork River landscape. The departure Index represents the deviation of the current GPU condition from its historical range of variability (HRV), as simulated. Values < -1 represent a current condition that is less than the HRV for the GPU, and increasingly negative values represent increasing degrees of negative departure.

Metric 4: Coefficient of Variation in Open Patch Size

We measured departure in the Coe icient of Variation (CV) in the size of all Open forest patches, including single cell patches, in which forest openings are defined by contiguous cells in the Open developmental stage based on the 4-neighbor rule (i.e., orthogonal neighbors)(**Figure 20**). The departure index is less than -1 if the current GPU has relatively invariant Open patch sizes compared to HRV.

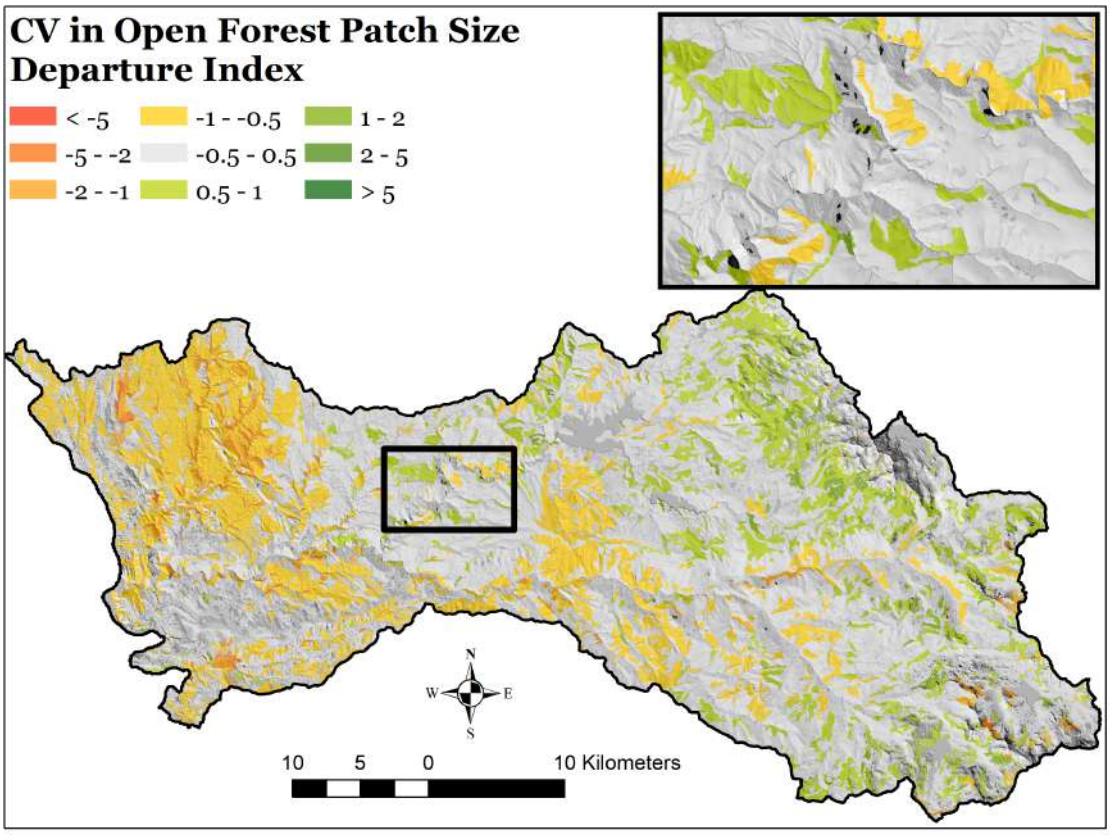

Figure 20: Geophysical Unit (GPU)-level departure index (unbounded) for the Coefficient of Variation (CV) in the size of patches in the Open developmental stage within the GPU for the American South Fork River landscape. The departure Index represents the deviation of the current GPU condition from its historical range of variability (HRV), as simulated. Values < -1 represent a current condition that is less than the HRV for the GPU, and increasingly negative values represent increasing degrees of negative departure.

Metric 5: Coefficient of Variation in Developmental Stage Patch Size

We measured departure in the CV in the size of all forest developmental stage patches, including single cell patches, in which patches are defined by contiguous cells in the same developmental stage based on the 4-neighbor rule (**Figure 21**). The departure index is less than -1 if the current GPU has relatively invariant developmental stage patch sizes compared to HRV.

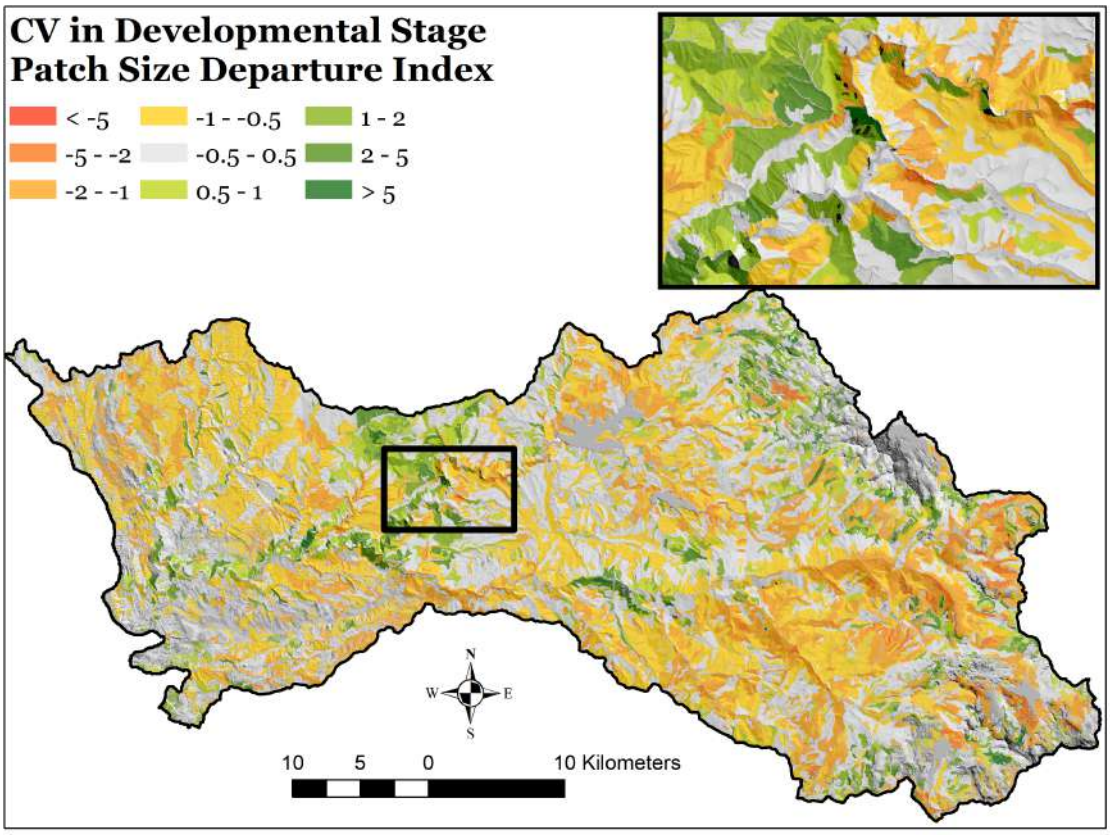

Figure 21: Geophysical Unit (GPU)-level departure index (unbounded) for the Coefficient of Variation (CV) in the size of patches based on developmental stages within the GPU for the American South Fork River landscape. The departure Index represents the deviation of the current GPU condition from its historical range of variability (HRV), as simulated. Values < -1 represent a current condition that is less than the HRV for the GPU, and increasingly negative values represent increasing degrees of negative departure.

Metric 6: Percent Large Trees

We measured departure in the percent of forested cells within the GPU in the Large tree size class (≥30 in dbh)(**Figure 22**). GPUs with a departure index less than -1 have less area in the Large tree class than under HRV.

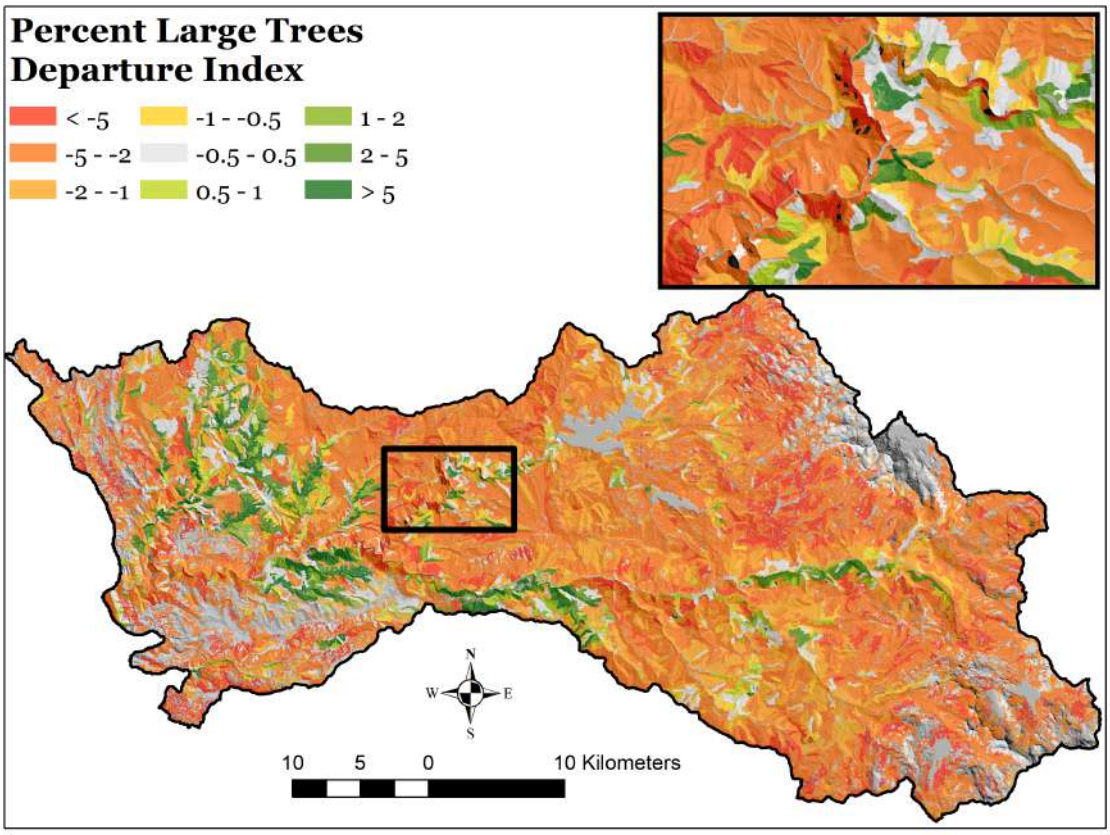

Figure 22: Geophysical Unit (GPU)-level departure index (unbounded) for the percentage of the forest in the Large tree size class (30 in dbh) within the GPU for the American South Fork River landscape. The departure Index represents the deviation of the current GPU condition from its historical range of variability (HRV), as simulated. Values < -1 represent a current condition that is less than the HRV for the GPU, and increasingly negative values represent increasing degrees of negative departure.

Metric 7: Tree Size Class Diversity

We measured departure in the diversity of tree size classes within the forested portion of the GPU based on the Simpson's Diversity index (**Figure 23**). Here, Simpson's Diversity is defined as the probability that any two cells selected at random would be from different tree size classes. The departure index for Simpson's Diversity is less than -1 if the current GPU has a diversity of tree size classes that is less than HRV.

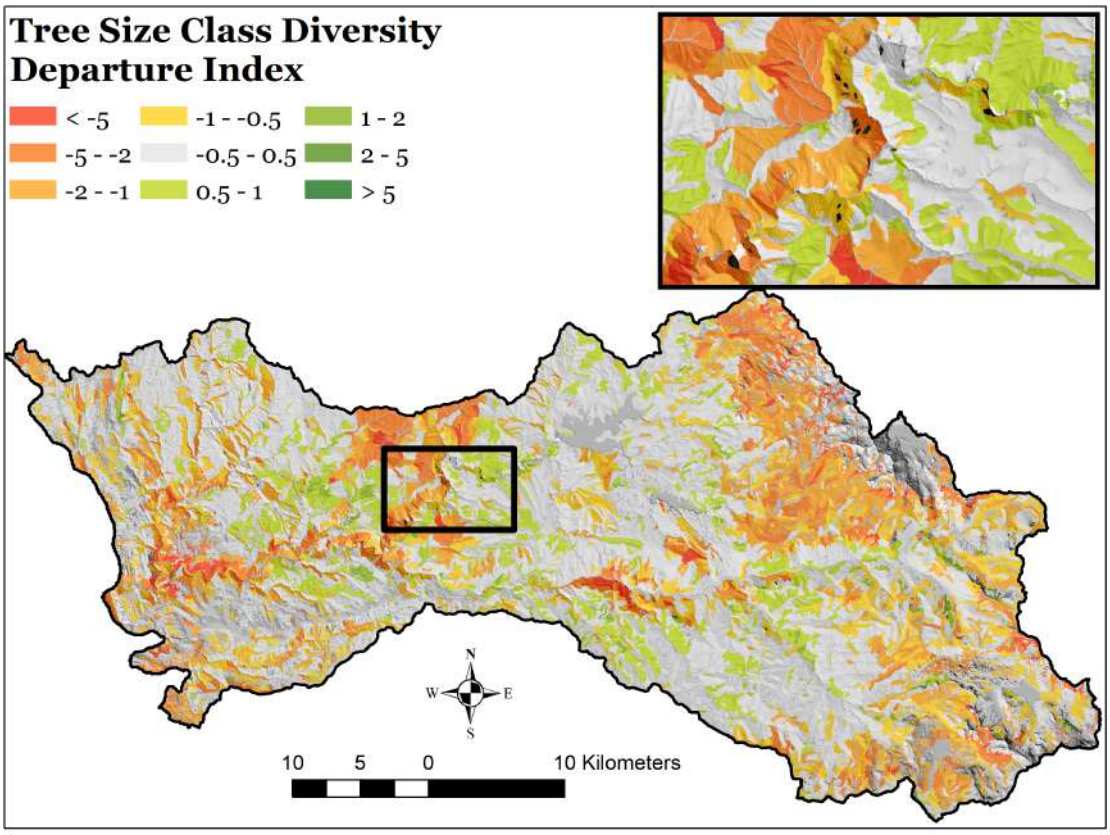

Figure 23: Geophysical Unit (GPU)-level departure index (unbounded) for the Simpson Diversity of tree size classes within the GPU for the American South Fork River landscape. The departure Index represents the deviation of the current GPU condition from its historical range of variability (HRV), as simulated. Values < -1 represent a current condition that is less than the HRV for the GPU, and increasingly negative values represent increasing degrees of negative departure.

Metric 8: **Coefficient of Variation in Large Tree Patch Size**

We measured departure in the CV in the size of all Large tree patches, including single cell patches, in which Large tree patches were defined by contiguous cells in the Large tree class (≥30 in dbh) based on the 4-neighbor rule (**Figure 49**). The departure index is less than -1 if the current GPU has relatively invariant Large tree patch sizes compared to HRV.

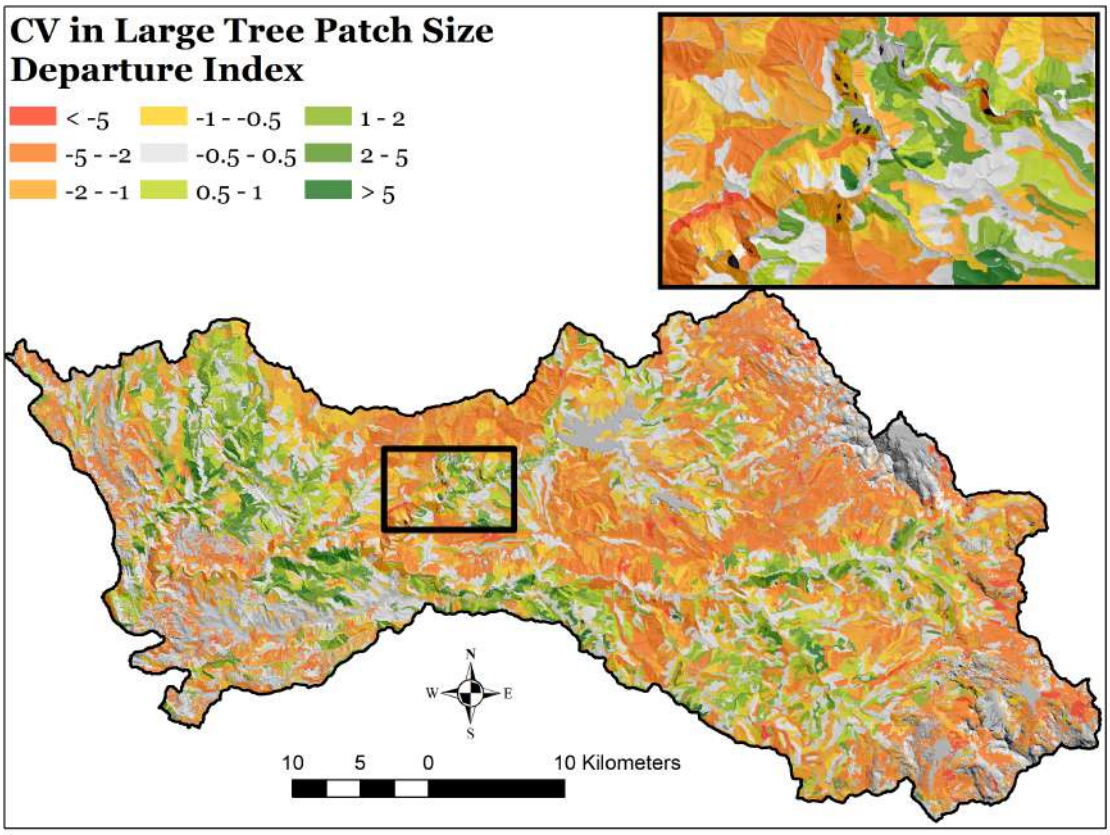

Figure 24: Geophysical Unit (GPU)-level departure index (unbounded) for the Coefficient of Variation (CV) in the size of patches in the Large tree size class (30 in dbh) within the GPU for the American South Fork River landscape. The departure Index represents the deviation of the current GPU condition from its historical range of variability (HRV), as simulated. Values < -1 represent a current condition that is less than the HRV for the GPU, and increasingly negative values represent increasing degrees of negative departure.

Metric 9: Coefficient of Variation in Tree Size Class Patch Size

We measured departure in the CV in the size of all tree size class patches, including single cell patches, in which patches were defined by contiguous cells in the same tree size class based on the 4-neighbor rule (**Figure 25**). The departure index is less than -1 if the current GPU has relatively invariant tree size class patch sizes compared to HRV.

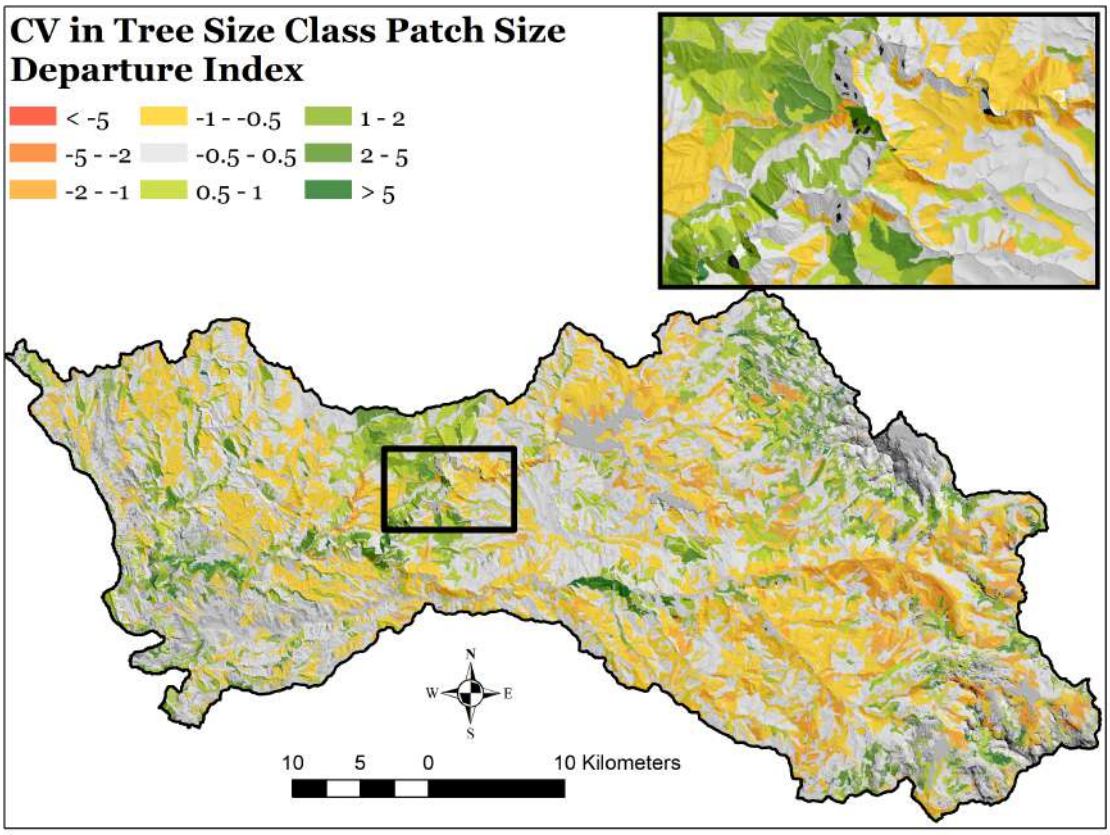

Figure 25: Geophysical Unit (GPU)-level departure index (unbounded) for the Coefficient of Variation (CV) in the size of patches based on tree size classes within the GPU for the American South Fork River landscape. The departure Index represents the deviation of the current GPU condition from its historical range of variability (HRV), as simulated. Values < -1 represent a current condition that is less than the HRV for the GPU, and increasingly negative values represent increasing degrees of negative departure.

Metric 10: Coefficient of Variation in Quadratic Mean Diameter

We measured departure in the CV in site-level Quadratic Mean Diameter (QMD) of established trees within the GPU (**Figure 26**). Recall that a site was defined as a 40-m radius window around each focal cell. Thus, QMD was computed for the site associated with each focal cell, which produced a continuous surface of QMD values, from which the CV in QMD values within the GPU was computed. The departure index is less than -1 if the current GPU has relatively homogeneous QMD compared to HRV.

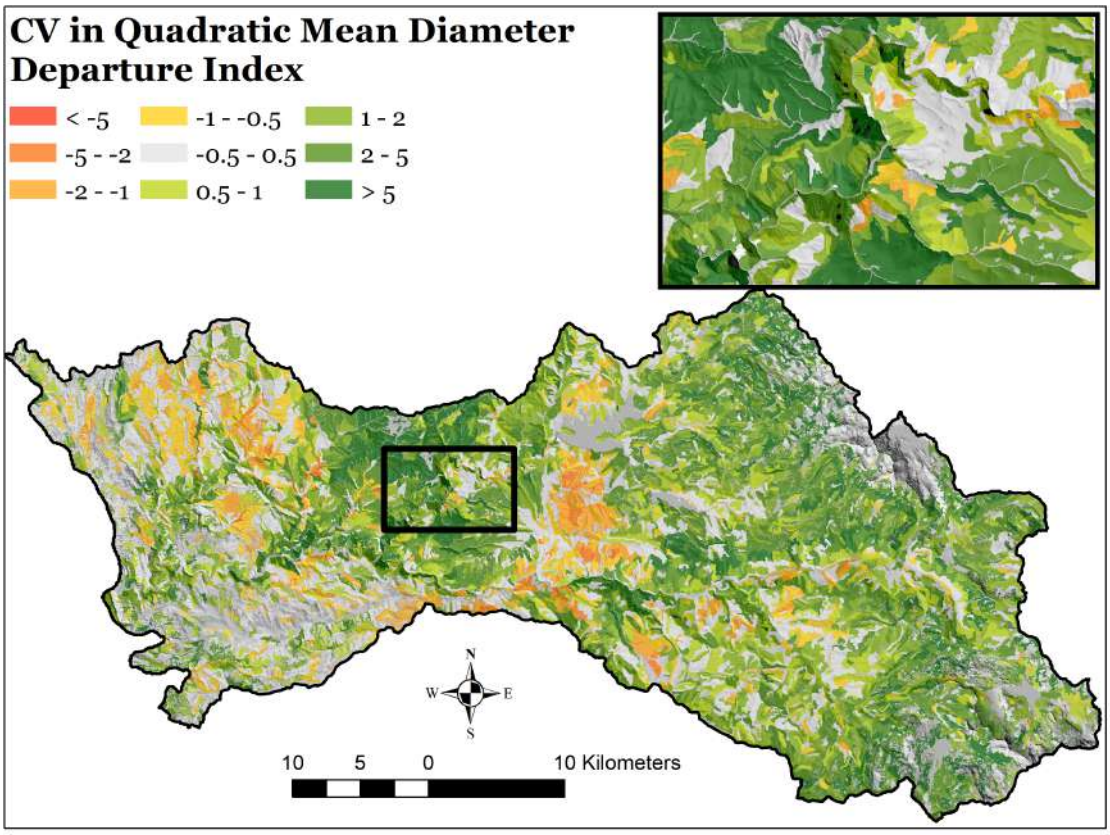

Figure 26: Geophysical Unit (GPU)-level departure index (unbounded) for the Coefficient of Variation (CV) in Site-level (i.e., 40 m radius window around each focal cell) Quadratic Mean Diameter (QMD, in inches) within the GPU for the American South Fork River landscape. The departure Index represents the deviation of the current GPU condition from its historical range of variability (HRV), as simulated. Values < -1 represent a current condition that is less than the HRV for the GPU, and increasingly negative values represent increasing degrees of negative departure.

Metric 11: Coefficient of Variation in Percent Tree Cover

We measured departure in the CV in site-level percent cover of established trees within the GPU (**Figure 27**). Again, recall that a site was defined as a 40-m radius window around each focal cell. Thus, percent tree Cover was computed for the site associated with each focal cell, which produced a continuous surface of percent tree cover values, from which the CV in tree cover within the GPU was computed. The departure index is less than -1 if the current GPU has relatively homogeneous tree cover compared to HRV.

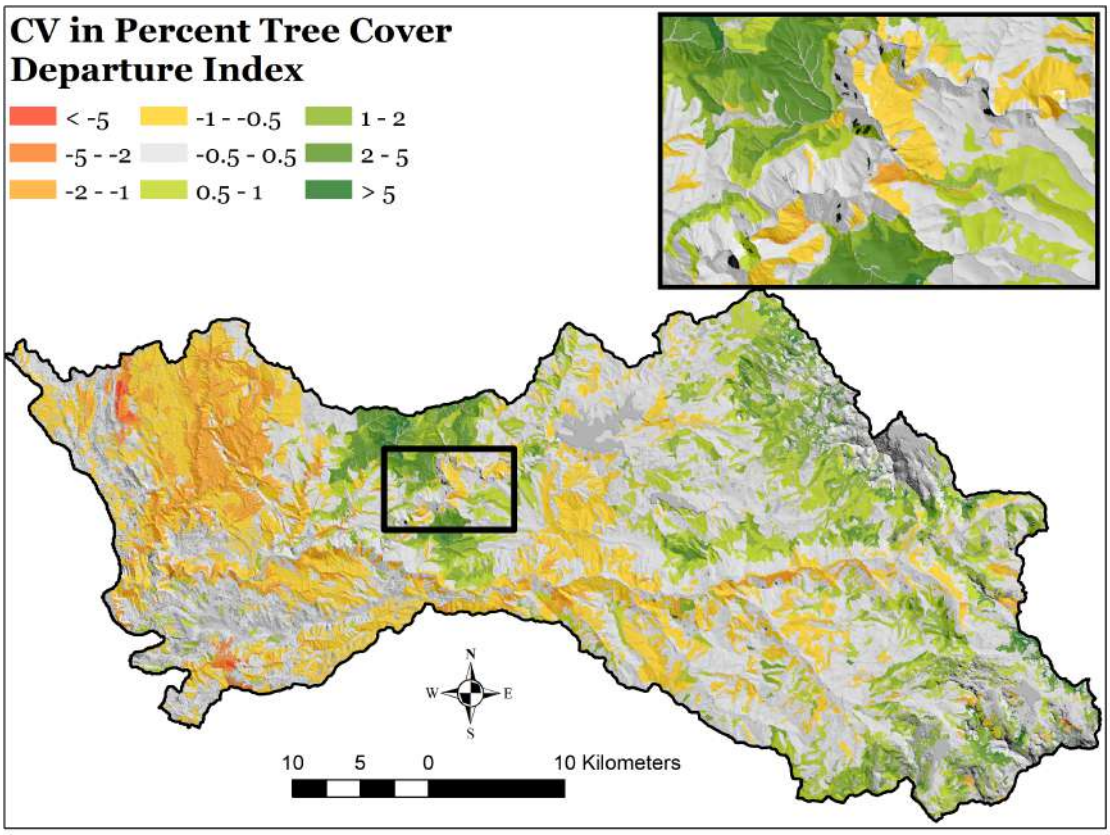

Figure 27: Geophysical Unit (GPU)-level departure index (unbounded) for the Coefficient of Variation (CV) in Site-level (i.e., 40 m radius window around each focal cell) percent tree cover within the GPU for the American South Fork River landscape. Note, percent tree cover as measured is on average 16 % greater than percent canopy cover. The departure Index represents the deviation of the current GPU condition from its historical range of variability (HRV), as simulated. Values < -1 represent a current condition that is less than the HRV for the GPU, and increasingly negative values represent increasing degrees of negative departure.

Composite Departure Index

We combined the 11 GPU-level departure indices above into two composite departure scores: 1) composite "negative" departure, and 2) composite "absolute" departure (see GTR for details). Both of these composite scores can be interpreted as a measure of overall GPU departure in vegetation composition and configuration. Increasing departure scores (given as a percent of maximum) indicate increasing degrees of departure.

Negative Departure - Maximum "negative" departure occurs when a GPU has too little Open forest area, too few Large trees, too little diversity in forest developmental stages (i.e., tree heights) and tree size classes (i.e., dbh), too little variability in the size of patches based on forest developmental stage and tree size, and too little spatial variability in percent tree cover and weighted average tree size (i.e., QMD) relative to its HRV. In other words, maximum negative departure occurs when the forest is too closed-canopy, depauperate in Large trees, and too homogeneous in vegetation composition and configuration.

The composite negative departure score is depicted in **Figure 28**. This score can be interpreted as the percent of maximum deviation in negative departure. Thus, a value of 0 represents no departure in any of the component metrics and a value of 100 represents maximum negative departure in each of the component metrics. GPUs with relatively high scores are the logical ones to prioritize for restoration treatment - should that be the goal. Importantly, this composite departure score can serve as a first stage in identifying and prioritizing GPUs for treatment, but specific objectives and treatments for each GPU requires decomposing the composite score into the component metrics to determine which aspects of the forest vegetation composition and/or configuration are most departed.

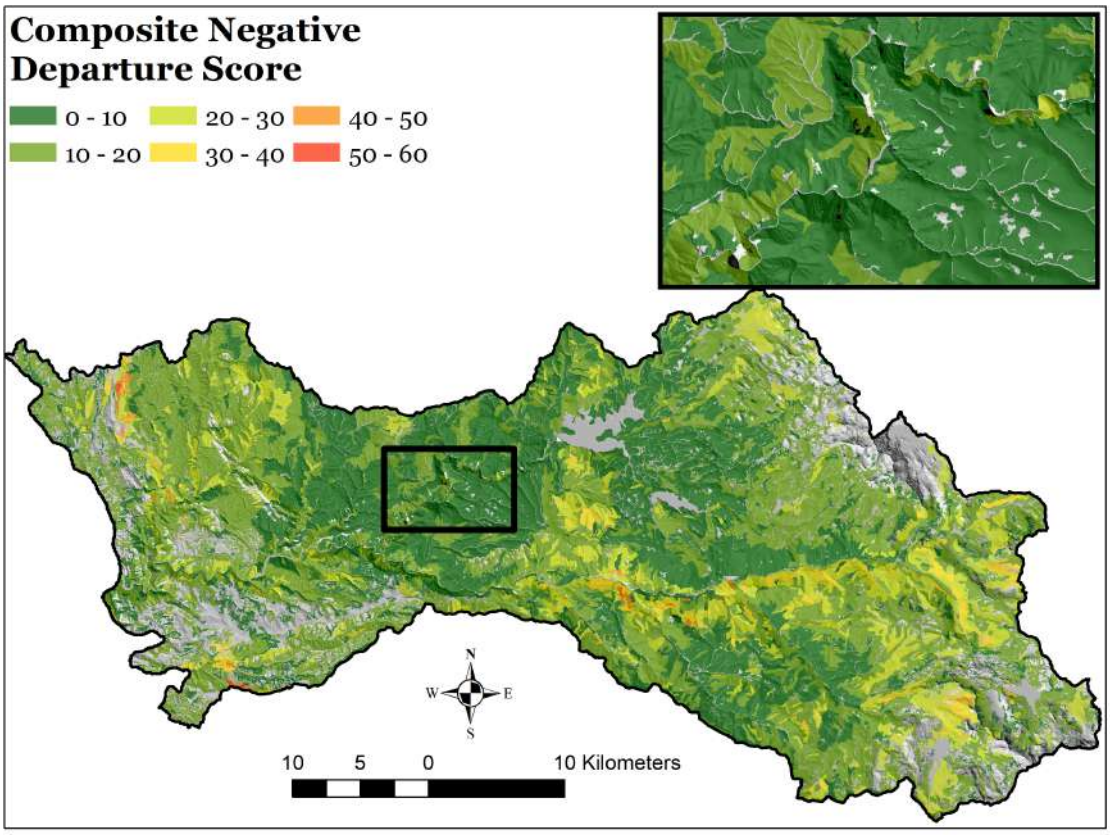

Figure 28: Geophysical Unit (GPU)-level composite negative departure score composed of a weighted combination of 11 individual departure metrics within the GPU for the American South Fork River landscape. The score represents the percentage of maximum departure of the current GPU condition from its historical range of variability (HRV), as simulated. Larger values indicate increasing degrees of departure.

Absolute Departure - Maximum "absolute" departure occurs when a GPU has either too little or too much Open forest area, too few or too many Large trees, too little or too much diversity in forest developmental stages (i.e., tree heights) and tree size classes (i.e., dbh), too little or too much variability in the size of patches based on forest developmental stage and tree size, and too little or too much spatial variability in percent tree cover and weighted average tree size (i.e., QMD) relative to HRV. In other words, maximum departure occurs when the GPU differs in any way in both composition and configuration from its HRV, as measured by this suite of metrics.

Subbasin Level Departure

The results presented in this section represent landscape metrics quantified at the subbasin-by-BPC level; i.e., each subbasin subdivided into BPCs treated as a whole unit (a.k.a. "zones"). The American South Fork River landscape was divided into 28 distinct subbasins (**Figure 29**), each of which was partitioned into the four forested BPCs for a total of 112 subbasin-by-BPC partitions or zones. Recall from the GTR that each partition was assessed independently to create a departure index; i.e., that we compared the current condition of each partition to its own HRV in vegetation conditions. In addition, recall that the final departure score reflected negative departure in the percent of the partition in large openings and large trees (i.e., in which the current landscape contains less area in large openings and large trees than expected under HRV), but was bidirectional with respect to the landscape configuration metrics; i.e., it reflected the magnitude of the absolute differences between the current and historical landscape conditions, regardless of

whether the current condition was greater or less than the historical condition. In other words, any differences between current and historical vegetation conditions with respect to landscape configuration registered as departure. Lastly, recall that we used a parsimonious suite of landscape metrics (see below) that we deemed meaningful for estimating departure at the subbasin level and appropriate given the available data, and computed departure as described in the GTR (and not repeated here), including the following metrics:

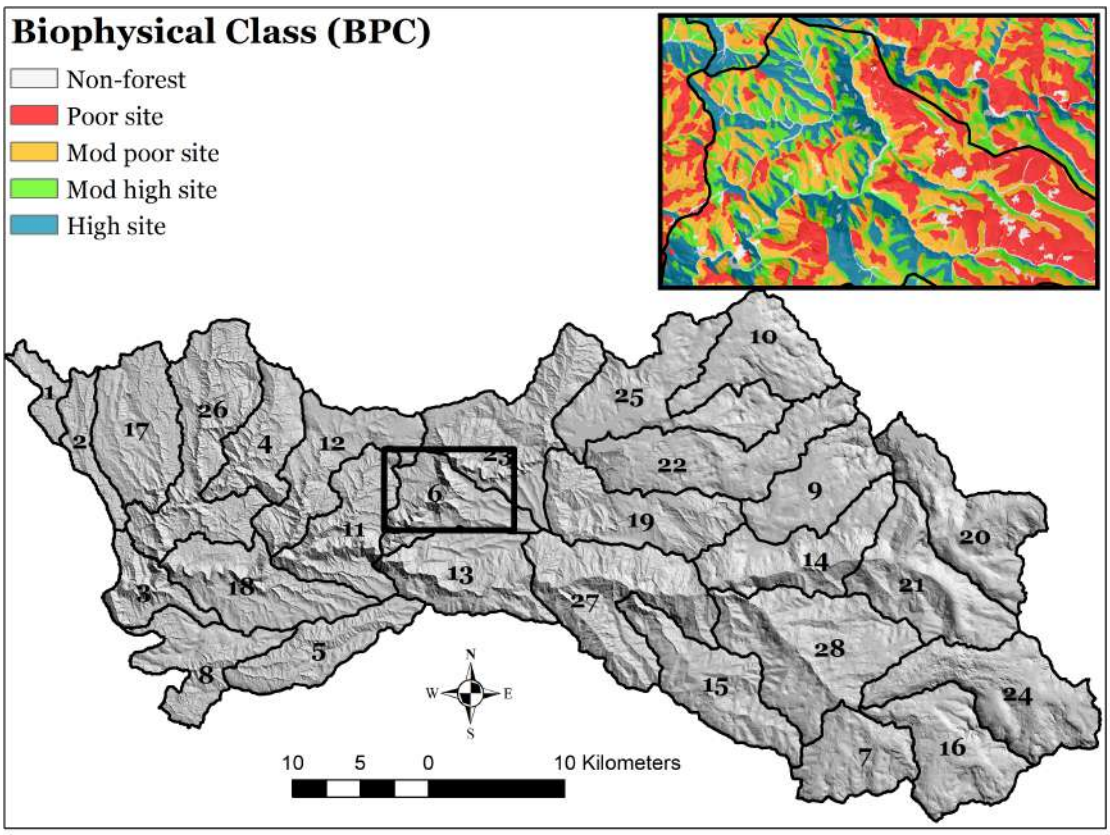

Figure 29: The American South Fork River landscape HUC12 subbasins, as modified, defined for the purpose of summarizing Historical Range of Variability (HRV) and current departure.

Metric 1: Percent Large Forest Openings

We defined large forest openings as contiguous forested cells in the Open developmental stage (i.e., no established trees to breast height) encompassing a minimum of 0.04 ha (0.1 acres). Contiguity was based on the 4-neighbor rule (i.e., orthogonal neighbors) that ensured a minimum width of 5 m for any opening. We defined Percent Large Forest Openings as the percent of the forest within the subbasin-by-BPC partition in large forest openings (as defined), and the departure index reflected whether or not the current landscape was deficient in large forest openings relative to HRV and, if so, the degree of deficiency.

The Percent Large Forest Openings departure index is depicted in **Figure 3**. Note, the departure index was assigned to each subbasin-by-BPC partition; consequently, there were 112 distinct values assigned. Thus, to better assess departure by subbasin and BPC, one needs to examine the attribute table for the departure layer.

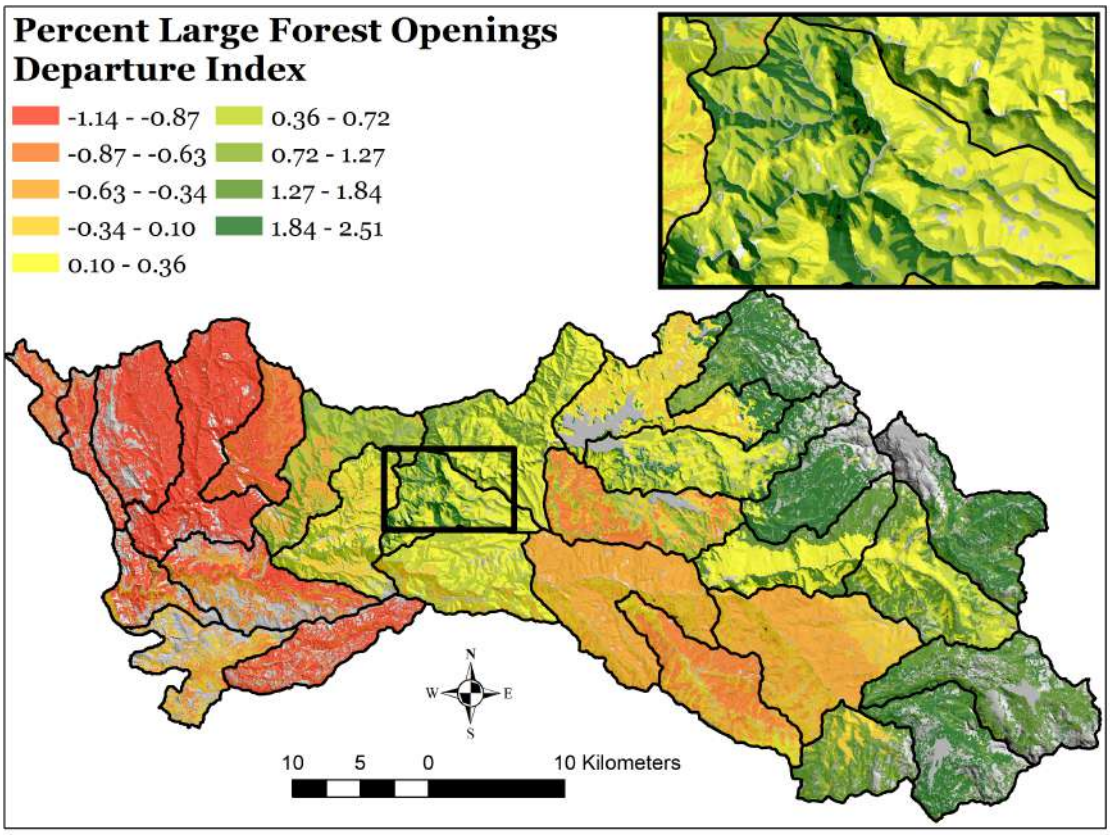

Figure 30: Subbasin-by-BPC level departure index for large forest openings (> 0.04 ha or 0.1 acres and > 5 m mininum width) for the American South Fork River landscape. The departure index represents the deviation of the current subbasin and biophsyical class (BPC) condition from its historical reference period condition, as simulated. Departure indices -1 represent a current landscape with less total area in large forest openings than during the historical reference period, as simulated, and increasing negative values represent increasing degrees of departure.

As discussed in the GTR, the Percent Large Forest Openings Departure Index can be miss-interpreted if not understood well. As the previous figure depicts, the distribution of index values would suggest that most of the subbasin-by-BPC partitions are within the HRV given that most of the partitions have values between -1 - 1. Recall, index values within this range reflect a current landscape condition that is within the 2.5% and 97.5% HRV. This would seem to indicate that most of the partitions are within HRV. While this might technically be correct, it is feasible that most of the partitions are close to the lower limit of HRV and have index values close to -1. Consequently, the distribution of index values could be skewed towards values on the lower limit of HRV, suggesting that the landscape as a whole could be, on average, deficient in large forest openings. A alternative and more useful way to assess current departure in this metric is to compare the distribution of values representing the percentage of the partition in large forest openings between the HRV and CRV, as shown **Figure 31**. In this case, interestingly, the HRV distribution is skewed towards lower values compared to the CRV, suggesting that the current landscape is not deficient in large forest openings and, in fact, has an excess of large forest openings, at least at the scale of subbasin-by-BPC partitions.

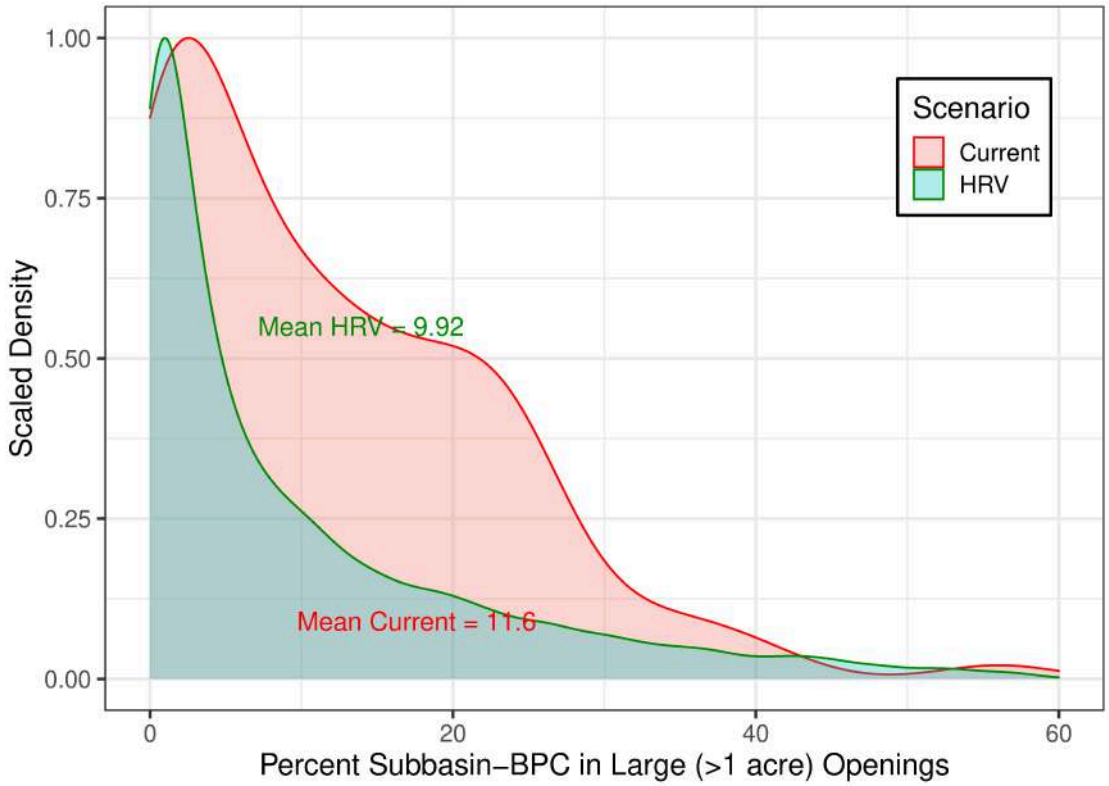

Figure 31: Current and historical distribution of Percent Large Forest Openings across the Subbasin-by-Biophysical Class (BPC) landscape partitions for the American South Fork River landscape. The comparative distributions reveal that even though the departure index for most of the partitions technically may fall with the historical range of variation (see previous figure), the overall distributions in the raw metric values differ markedly and reflect departure for the landscape as a whole

Metric 2: Large Forest Openings Patch Size Distribution

We defined large forest openings as described above. Here, we quantified the size of individual openings and determined the percent of forest within the subbasin-by-BPC partition in large openings in each of several patch size classes or bins (see GTR). The departure index reflects whether or not the current landscape has a distribution of large forest opening patch sizes that differed from HRV and, if so, the degree of differences in the two distributions.

The Large Forest Openings Patch Size Distribution departure index is depicted in **Figure 32**. As before, the departure index was assigned to each subbasin-by-BPC partition; consequently, there were 112 distinct values assigned. Thus, to better assess departure by subbasin and BPC, one needs to examine the attribute table for the departure layer.

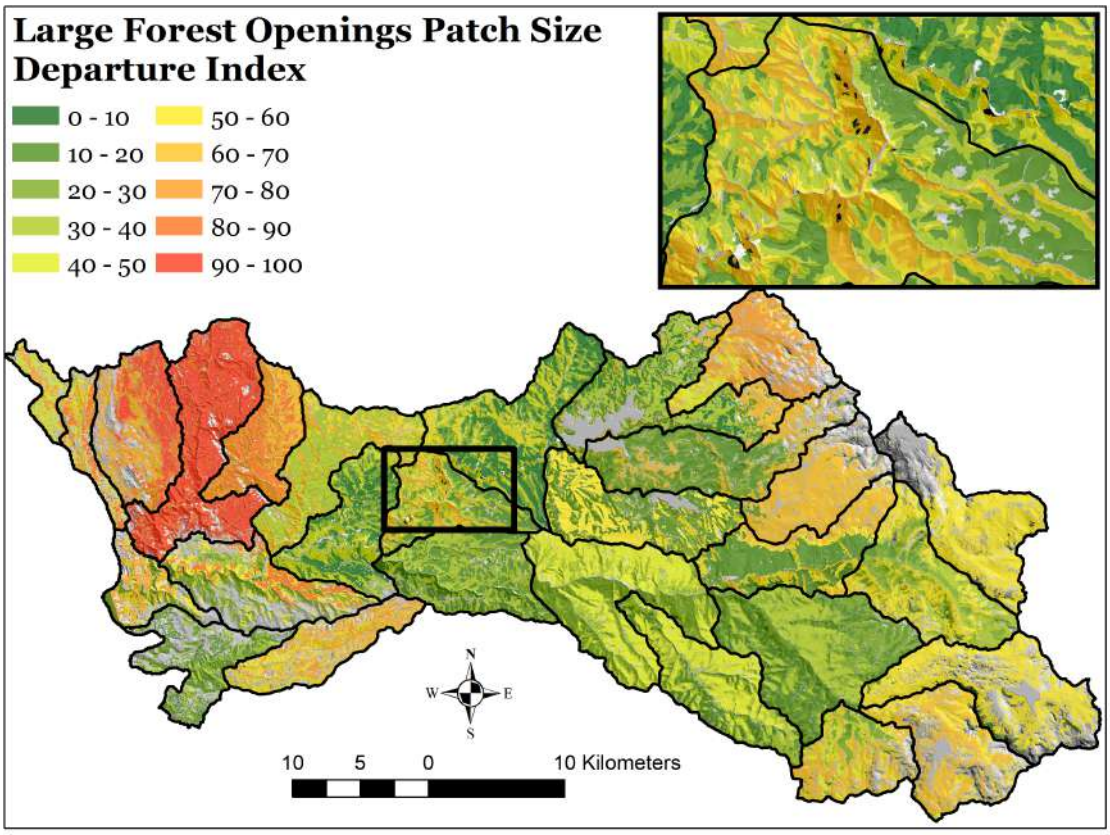

Figure 32: Subbasin-by-BPC level departure index for large forest openings (> 0.04 ha or 0.1 acres and > 5 m mininum width) patch size distribution for the American South Fork River landscape. The departure index represents the deviation of the current subbasin and biophsyical class (BPC) condition from its historical reference period condition, as simulated. Departure indices > 0 represent a current landscape with a distribution of large forest opening patch sizes that differs in some way from the historical reference period distribution, as simulated, and increasing values represent increasing degrees of departure.

To further evaluate departure in this patch size distribution metric, it is necessary to examine the CRV and HRV patch size distributions for the selected subbasin-by-BPC partition, for example as depicted in **Figure 33**.

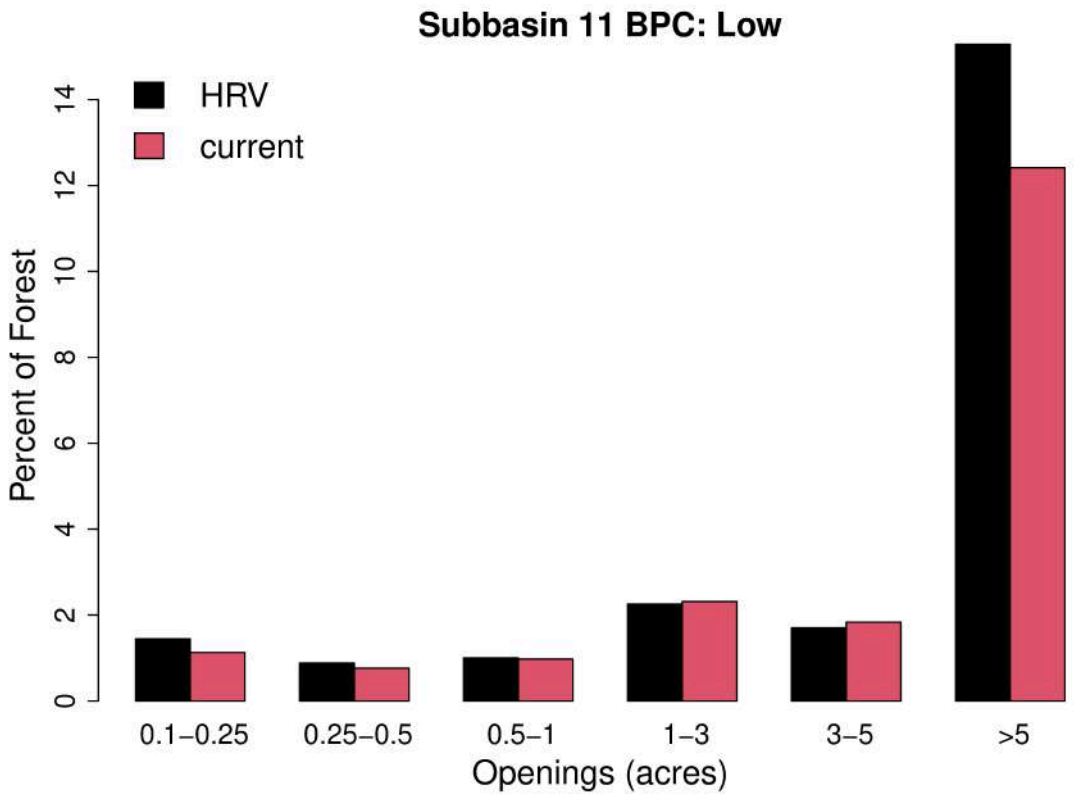

Figure 33: Barplot of the distribution of large forest openings (> 0.04 ha or 0.1 acres and > 5 m mininum width) patch sizes for the current landscape and the historical reference period (HRV) for subbasin 11 and the Low productivity Biophysical Class (BPC = 1) for the American South Fork River landscape. Each bar represents the percent of forest within the subbasin and Biophysical Class (BPC) in large forest openings of a particular patch size. The departure index represents the percentage dissimilarity between the CRV and HRV distributions. Departure indices > 0 represent a current landscape with a distribution of large forest opening patch sizes that differs in some way from the historical reference period distribution, as simulated, and increasing values represent increasing degrees of departure.

Metric 3: Developmental Stage Patch Size Distribution

We defined developmental stages based on six tree height classes, ranging from Open (4.5 ft) to Tall Trees (> 125 ft), as described in the GTR. Here, for each snapshot of the landscape we constructed a patch mosaic comprised of developmental stages in which patches were defined using the 4-neighbor rule. For each snapshot, we quantified the size of each developmental stage patch and determined the percent of forest within the subbasin-by-BPC partition in each of several patch size classes or bins. The departure index reflects whether or not the current landscape has a distribution of developmental stage patch sizes that differs from HRV and, if so, the degree of differences in the two distributions.

The Developmental Stage Patch Size Distribution departure index is depicted in **Figure 34**. As before, the departure index was assigned to each subbasin-by-BPC partition; consequently, there were 112 distinct values assigned. Thus, to better assess departure by subbasin and BPC, one needs to examine the attribute table for the departure layer.

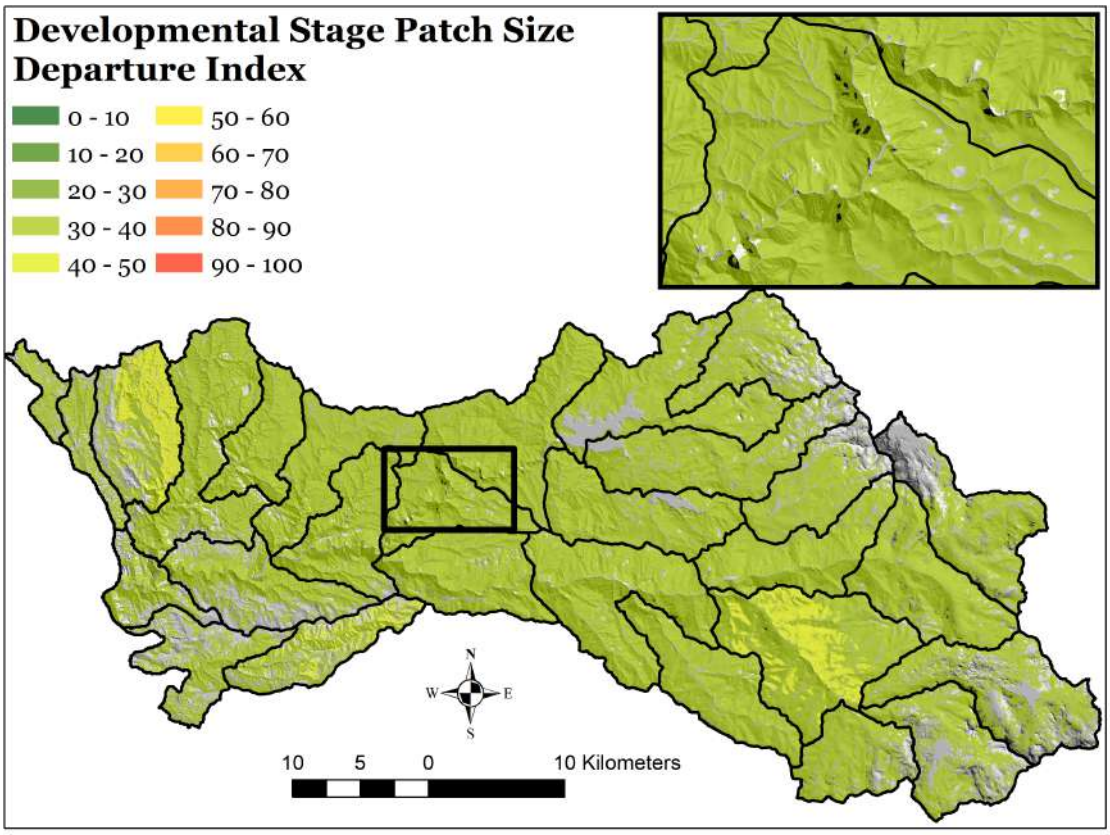

Figure 34: Subbasin-by-BPC level departure index for the developmental stage patch size distribution for the American South Fork River landscape. Developmental stages were based on tree height classes and patches were based on the 4-neighbor adjacency rule. The departure index represents the deviation of the current subbasin and biophsyical class (BPC) condition from its historical reference period condition, as simulated. Departure indices > 0 represent a current landscape with a distribution of developmental stage patch sizes that differs in some way from the historical reference period distribution, as simulated, and increasing values represent increasing degrees of departure.

To further evaluate departure in this patch size distribution metric, it is necessary to examine the CRV and HRV patch size distributions for the selected subbasin-by-BPC partition, for example as depicted in **Figure 35**.

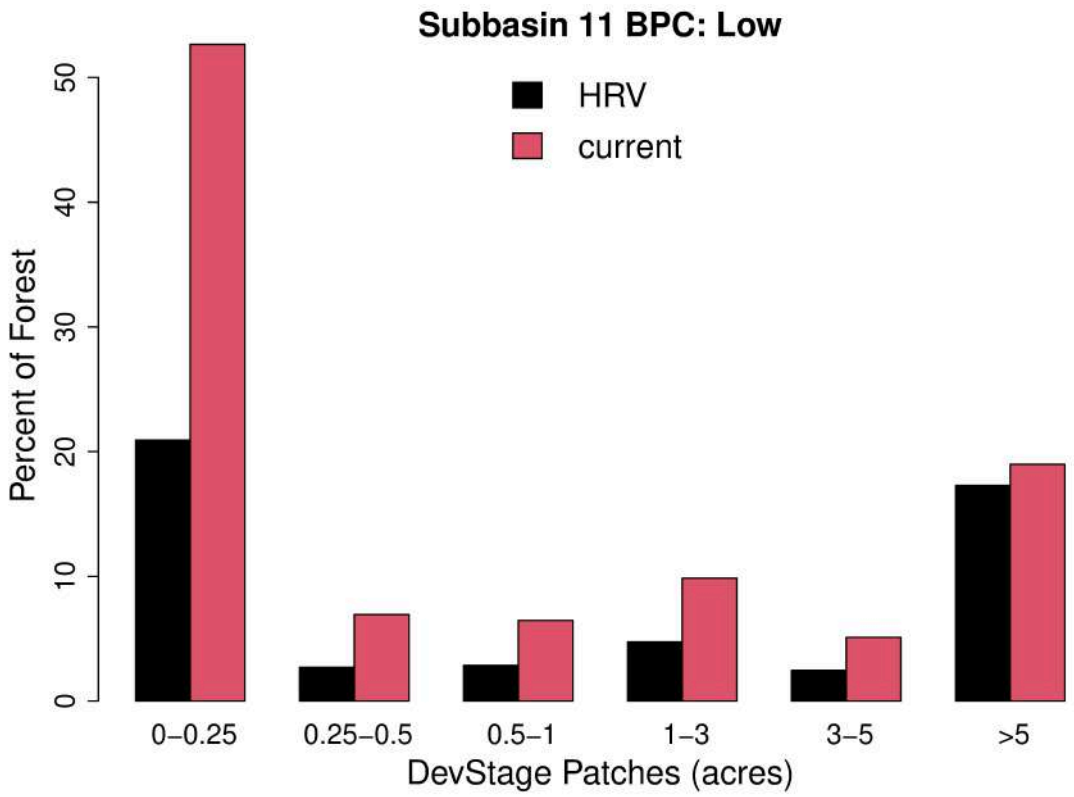

Figure 35: Barplot of the distribution of developmental stage patch sizes for the current landscape and the historical reference period (HRV) for subbasin 11 and the Low productivity Biophysical Class (BPC = 1) for the American South Fork River landscape. Developmental stages were based on tree height classes and patches were based on the 4-neighbor adjacency rule. Each bar represents the percent of forest within the subbasin and BPC in developmental stage patches of a particular size. The departure index represents the sum of the deviations between the current and HRV bars. Departure indices > 0 represent a current landscape with a distribution of developmental stage patch sizes that differs in some way from the historical reference period distribution, as simulated, and increasing values represent increasing degrees of departure.

Metric 4: Percent Large Trees

We defined large trees as > 30 inch dbh. Percent Large Trees is defined as the percent of the forest within the subbasin-by-BPC partition in large trees, as defined, and the departure index reflects whether or not the current landscape is deficient in large trees relative to HRV and, if so, the degree of deficiency. The departure index is negative if the current landscape has too little area in large trees compared to HRV.

The Percent Large Trees departure index is depicted in **Figure 36**. As before, the departure index was assigned to each subbasin-by-BPC partition; consequently, there were 112 distinct values assigned. Thus, to better assess departure by subbasin and BPC, one needs to examine the attribute table for the departure layer.

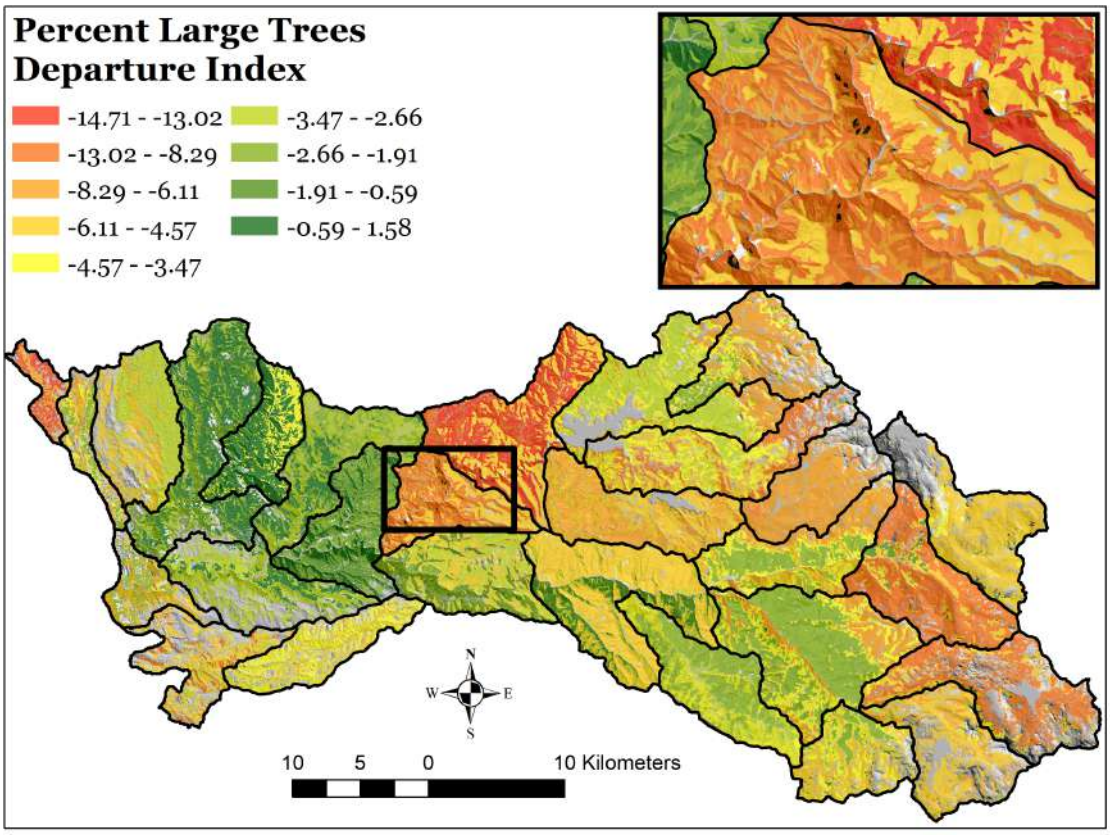

Figure 36: Subbasin-by-BPC level departure index for large trees (> 30 inch dbh) for the American South Fork River landscape. The departure index represents the deviation of the current subbasin and biophsyical class (BPC) condition from its historical reference period condition, as simulated. Departure indices -1 represent a current landscape with less total area in large trees than during the historical reference period, as simulated, and increasing negative values represent increasing degrees of departure.

Metric 5: Large Tree Patch Size Distribution

We defined large trees as described above. Here, we quantified the size of individual patches of large trees and determined the percent of forest within the subbasin-by-BPC partition in large tree patches in each of several patch size classes or bins (see above), and compared the current and historical distributions. The departure index reflects whether or not the current landscape has a distribution of large tree patch sizes that differs from HRV and, if so, the degree of differences in the two distributions.

The Large Tree Patch Size Distribution departure index is depicted in **Figure 37**. As before, the departure index was assigned to each subbasin-by-BPC partition; consequently, there were 112 distinct values assigned. Thus, to better assess departure by subbasin and BPC, one needs to examine the attribute table for the departure layer.

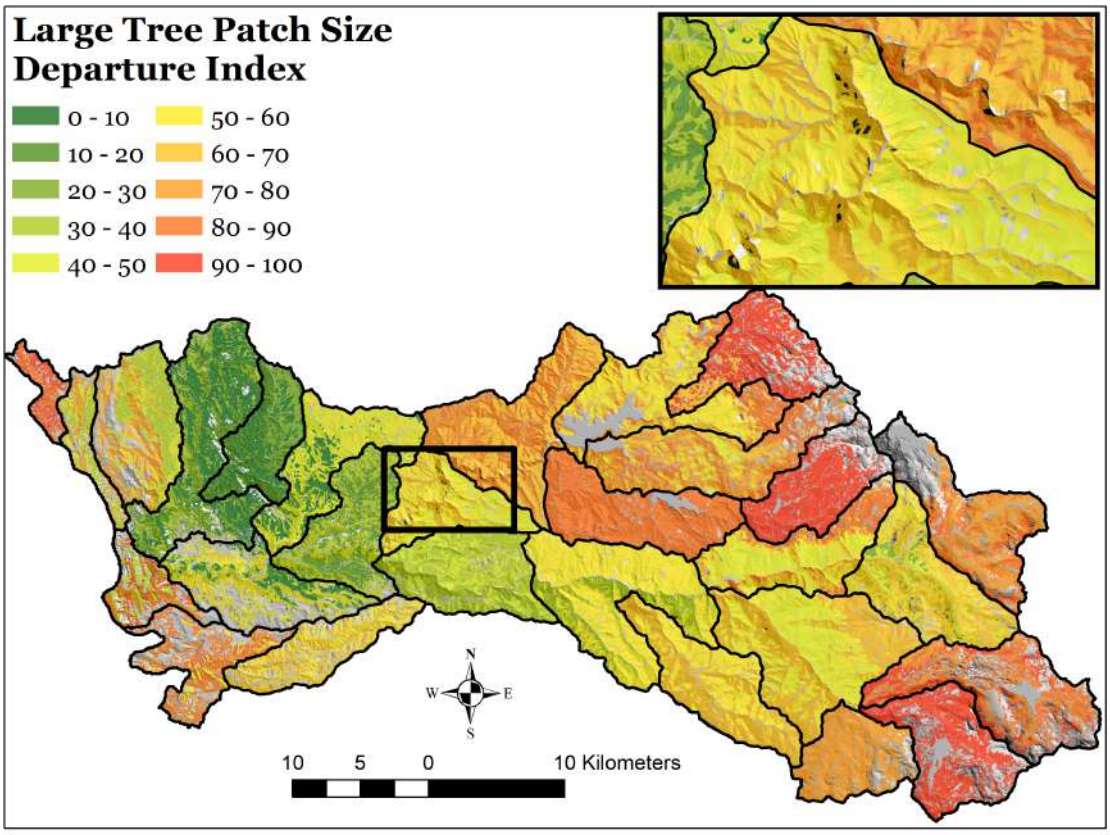

Figure 37: Subbasin-by-BPC level departure index for large tree (> 30 inch dbh) patch size distribution for the American South Fork River landscape. The departure index represents the deviation of the current subbasin and biophsyical class (BPC) condition from its historical reference period condition, as simulated. Departure indices > 0 represent a current landscape with a distribution of large tree patch sizes that differs in some way from the historical reference period distribution, as simulated, and increasing values represent increasing degrees of departure.

To further evaluate departure in this patch size distribution metric, it is necessary to examine the CRV and HRV patch size distributions for the selected subbasin-by-BPC partition, for example as depicted in **Figure 38**.

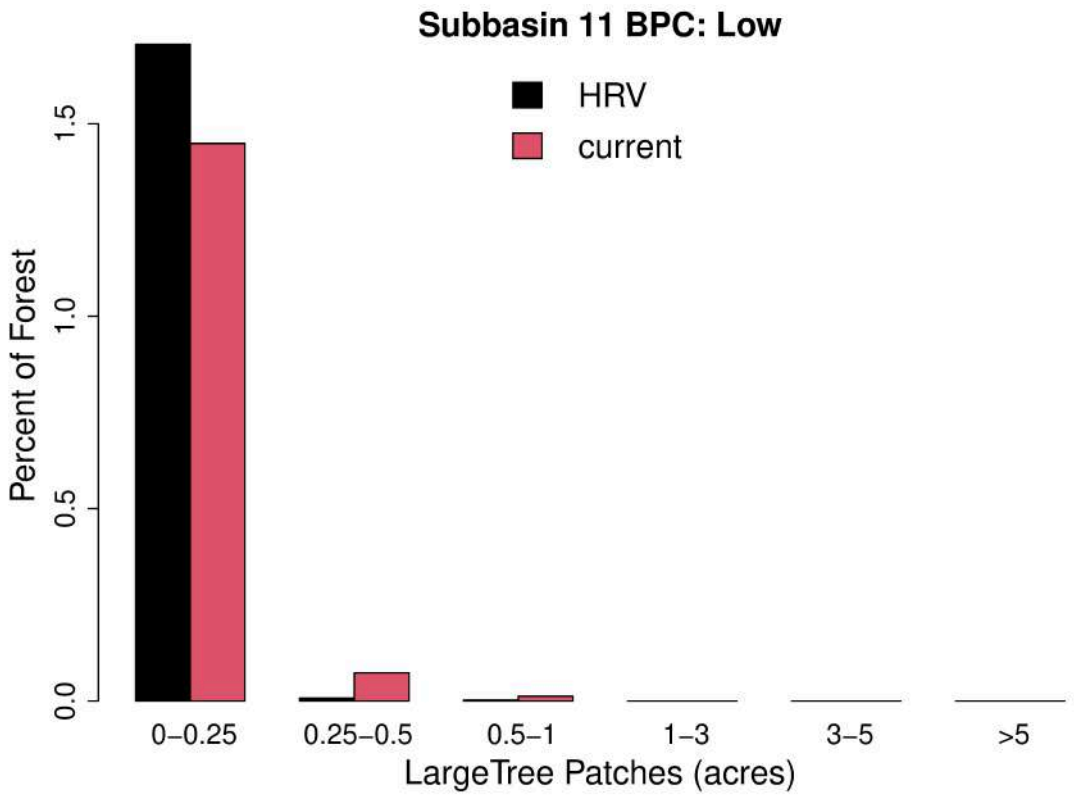

Figure 38: Barplot of the distribution of large tree (> 30 inch dbh) patch sizes for the current landscape and the historical reference period (HRV) for subbasin 11 and the Low productivity Biophysical Class (BPC = 4) for the American South Fork River landscape. See previous barplot caption for details on interpretation.

Metric 6: Tree Size Class Patch Size Distribution

We defined tree size class based on six tree diameter classes, ranging from Open (1 in dbh) to large Trees (> 30 in dbh), as described previously. Here, for each snapshot of the landscape we constructed a patch mosaic comprised of tree size classes in which patches were defined using the 4-neighbor rule. For each snapshot, we quantified the size of each tree size class patch and determined the percent of forest within the subbasin-by-BPC partition in each of several patch size classes or bins. The departure index reflects whether or not the current landscape has a distribution of tree size class patch sizes that differs from HRV and, if so, the degree of differences in the two distributions.

The Tree Size Class Patch Size Distribution departure index is depicted in **Figure 39**. As before, the departure index was assigned to each subbasin-by-BPC partition; consequently, there were 112 distinct values assigned. Thus, to better assess departure by subbasin and BPC, one needs to examine the attribute table for the departure layer.

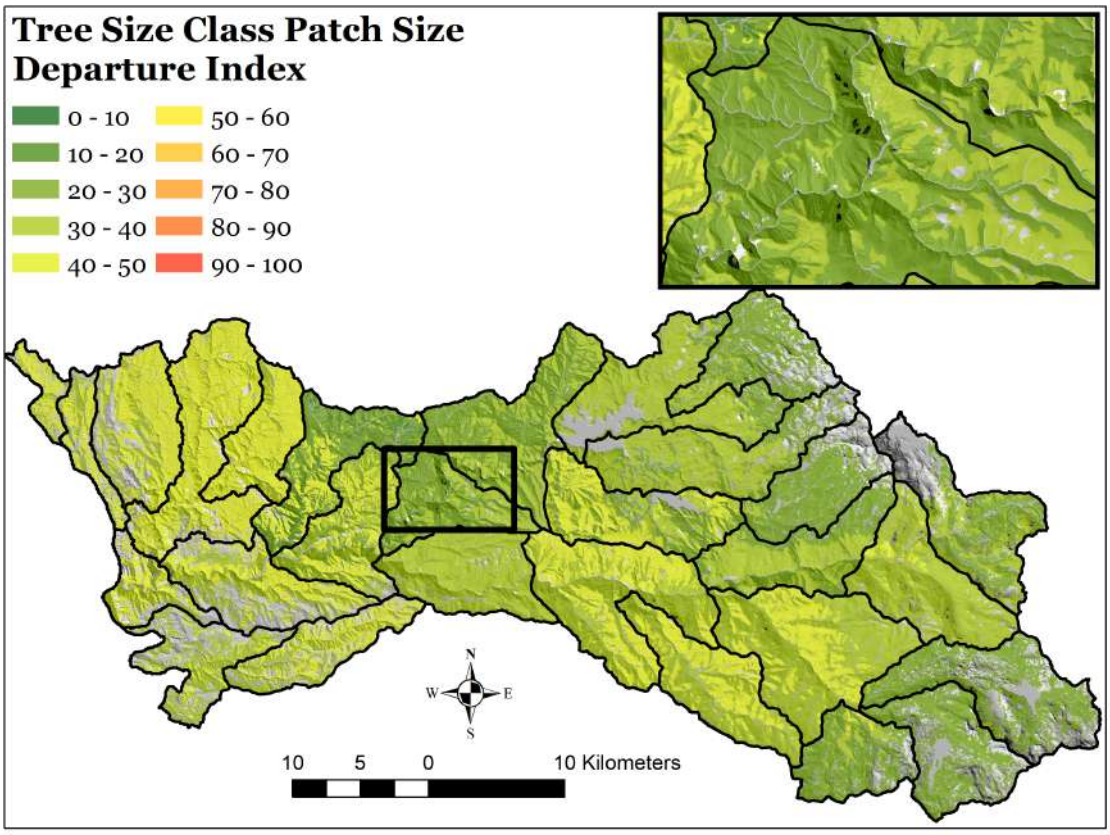

Figure 39: Subbasin-by-BPC level departure index for tree size class (based on dbh) patch size distribution for the American South Fork River landscape. The departure index represents the deviation of the current subbasin and biophsyical class (BPC) condition from its historical reference period condition, as simulated. Departure indices > 0 represent a current landscape with a distribution of tree size patch sizes that differs in some way from the historical reference period distribution, as simulated, and increasing values represent increasing degrees of departure.

To further evaluate departure in this patch size distribution metric, it is necessary to examine the CRV and HRV patch size distributions for the selected subbasin-by-BPC partition, for example as depicted in **Figure 4**.

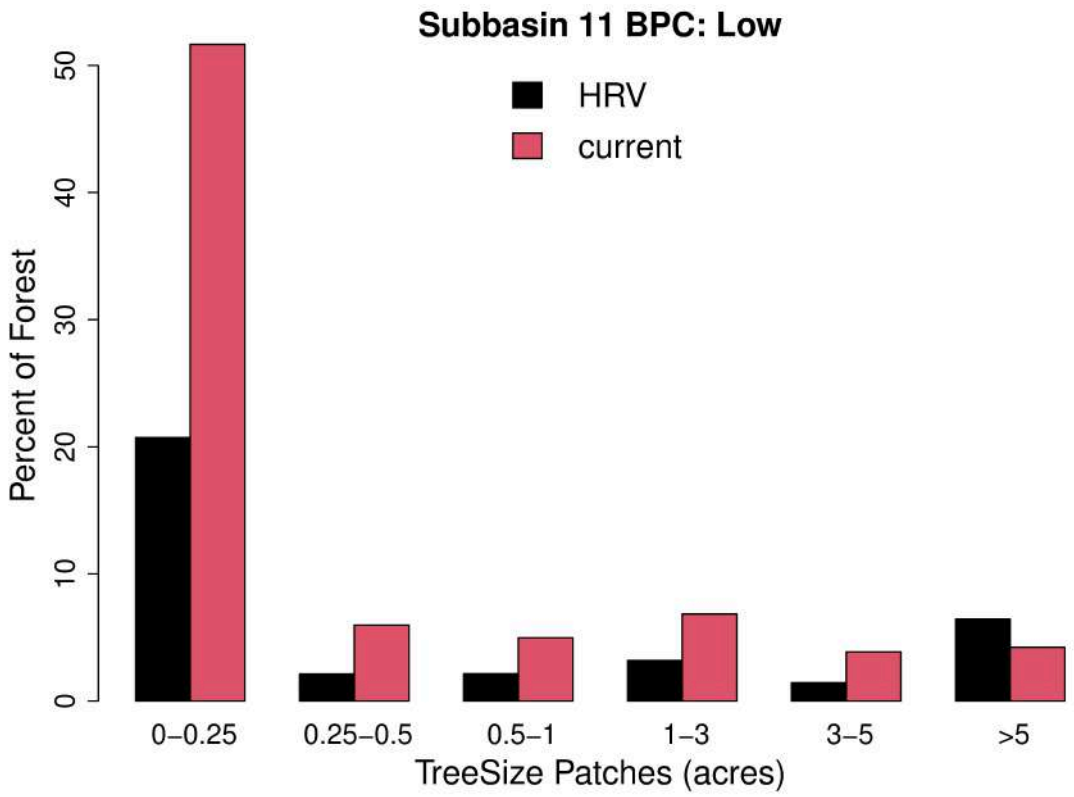

Figure 40: Barplot of the distribution of tree size class (based on dbh) patch sizes for the current landscape and the historical reference period (HRV) for subbasin 11 and the Low productivity Biophysical Class (BPC = 4) for the American South Fork River landscape. See previous barplot caption for details on interpretation.

Composite Departure Score

We combined the 6 subbasin-level departure metrics above into a single composite departure score, which can be interpreted as a measure of overall departure in vegetation composition and configuration within the subbasin-by-BPC partition. Maximum departure occurs when the forest has too little area in large forest openings and/or large trees, and/or too homogeneous or uniform a vegetation patch mosaic (i.e., too little spatial variability) defined on the basis of either developmental stages (or tree height classes) or tree size classes (or tree diameter classes).

The composite departure score is depicted in **Figure 41**. Not surprisingly, the subbasins and BPCs vary somewhat in their overall departure from HRV, and these differences provide a basis for prioritizing project locations with this landscape.

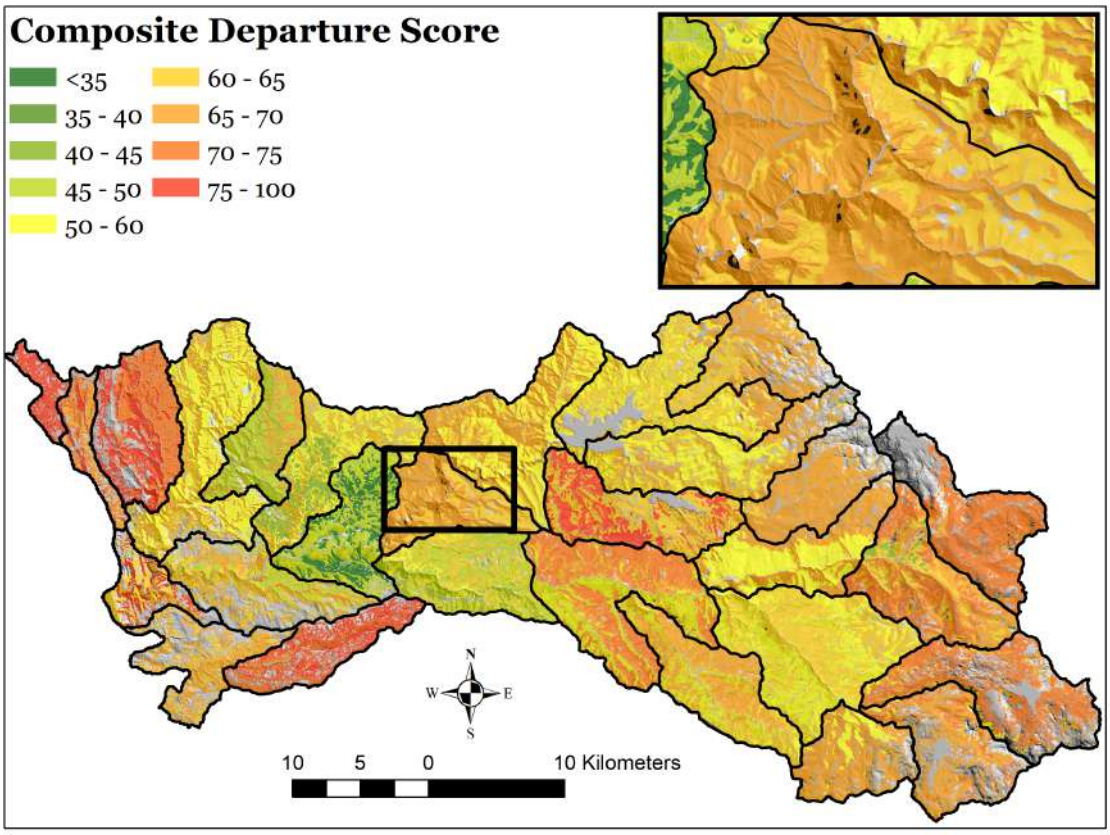

Figure 41: Subbasin-by-BPC level composite departure index derived from the average of the six component metrics for the American South Fork River landscape. The composite departure index represents the percentage of maximum departure of the current GPU condition from its historical range of variability (HRV), as simulated. Larger values indicate increasing degrees of departure.

APPENDIX E1 - Wildfire Susceptibility

As described in the text, wildfire susceptibility was modeled as a Logistic function of fuels and climate for most cover types. The fuels component was modeled as a Logistic function of the number of years since the last fire (fuelAge) and the Heat Load Index (hli). The climate component was modeled as a Logistic function of the Wildfire Climate Index which was based on the inverted and rescaled 5-year mean Palmer Modified Drought Index. The fuels and climate components were combined with a geometric mean to produce the final Wildfire Susceptibility Index. The final function included 5 beta coefficients (b_0 - b_4). We used expert opinion to specify the beta coefficients for each cover type. We varied the b_0 and b_1 coefficients among cover types to reflect differences in reported historical mean fire return intervals among cover types - shifting the response curves left or right so that the inflection point (Wildfire Susceptibility Index = 0.5) roughly equaled the target mean return interval - and held the Heat Load Index coefficient (b_2) and Climate coefficients (b_3 and b_4) the same across all cover types to reflect the global affect of topography and climate on wildfire susceptibility.

The figures below depict the final wildfire susceptibility response functions for each cover type in alphabetical order (noting that some cover types did not have response functions as noted in the text). The response functions depict the wildfire Susceptibility Index as a Logistic function of the number of years since the last fire (Years since fire). The dashed, solid and dotted lines depict the response functions for the minimum, mean and maximum Heat Load Index (hli), and the red, black and green sets of lines depict the response functions for the minimum, mean and maximum Wildfire Climate Index. The values of the Logistic parameters (b_0 - b_4) for the cover type are shown as well.

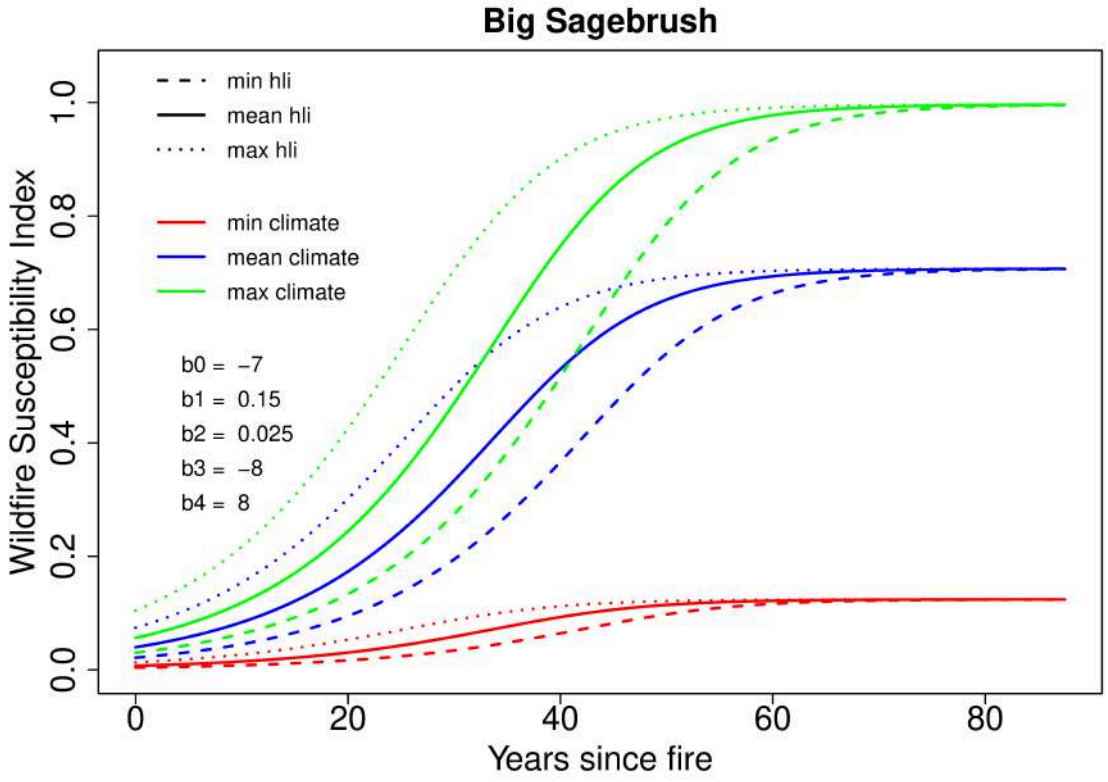

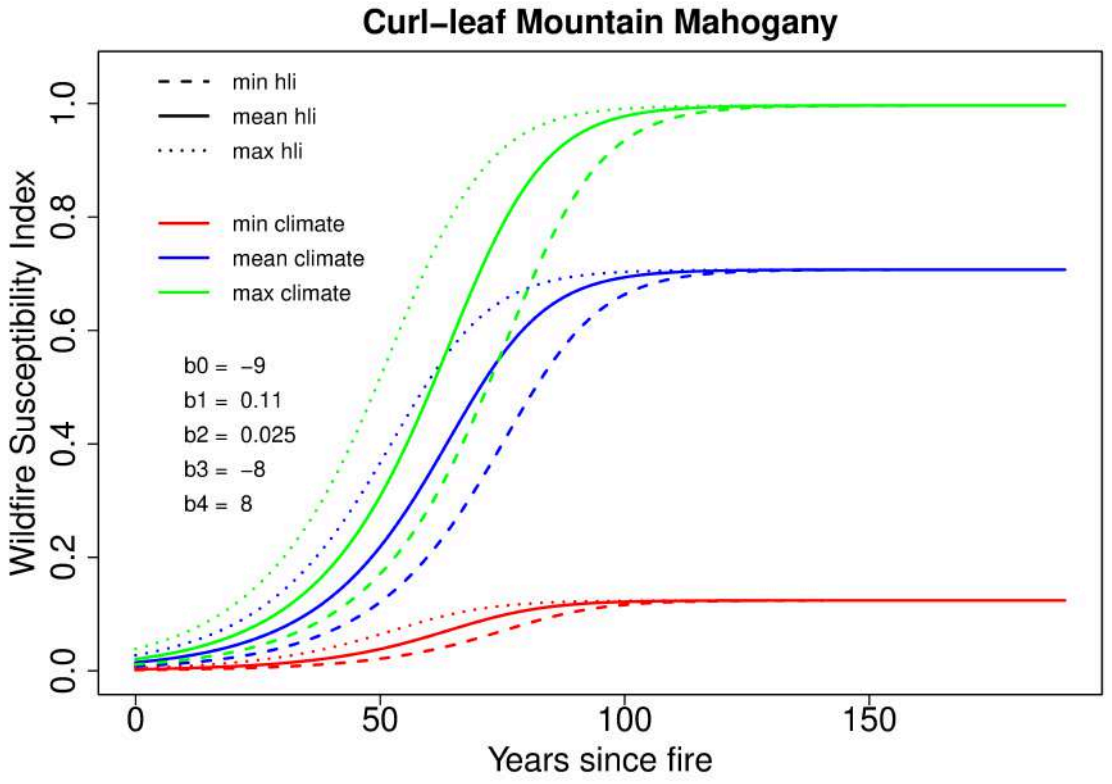
Curl−leaf Mountain Mahogany
min hli
mean hli
max hli
min climate
mean climate
max climate
b0 = −9
b1 = 0.11
b2 = 0.025
b3 = −8
b4 = 8
Wildfire Susceptibility Index
0.0
0.2
0.4
0.6
0.8
1.0
0
50
100
150
Years since fire

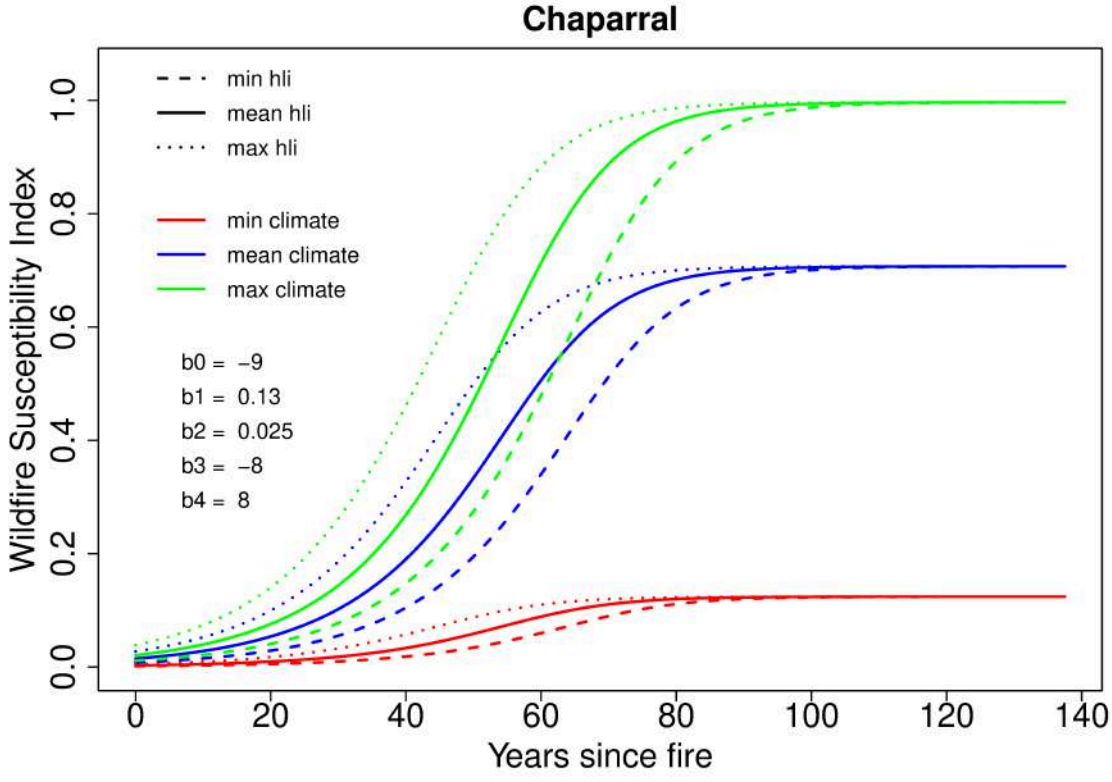
Chaparral
min hli
mean hli
max hli
min climate
mean climate
max climate
b0 = −9
b1 = 0.13
b2 = 0.025
b3 = −8
b4 = 8
Wildfire Susceptibility Index
0.0
0.2
0.4
0.6
0.8
1.0
0
20
40
60
80
100
120
140
Years since fire

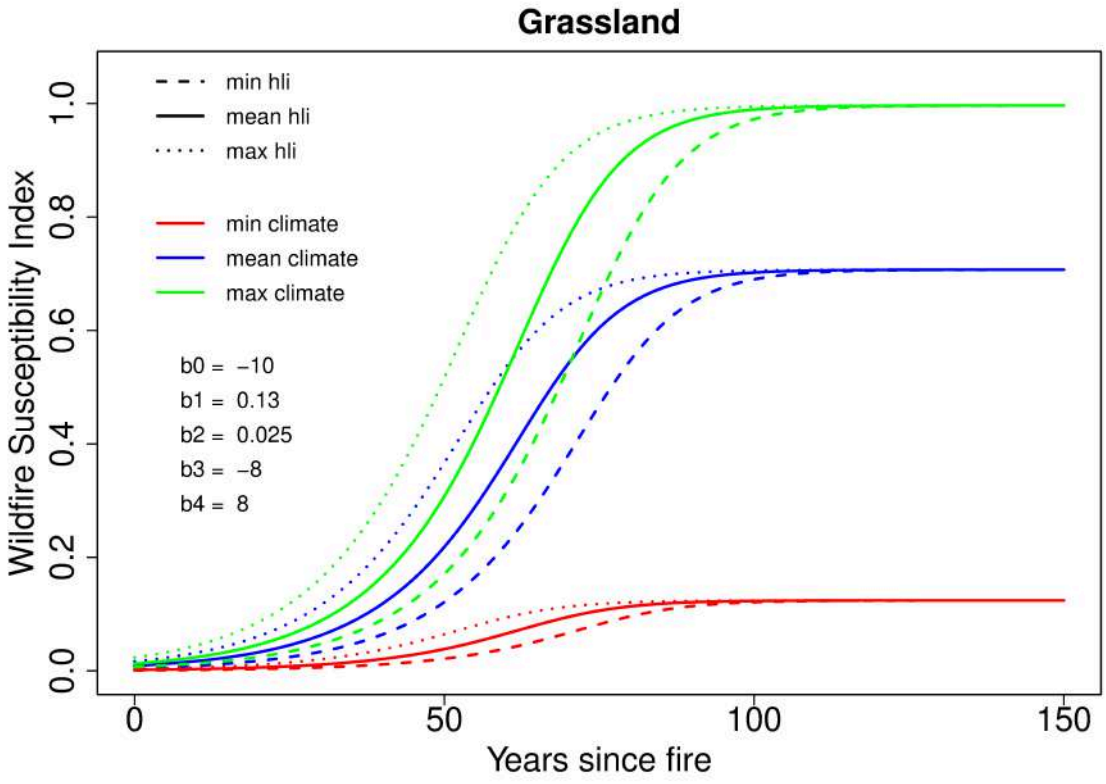
Grassland
min hli
mean hli
max hli
min climate
mean climate
max climate
b0 = −10
b1 = 0.13
b2 = 0.025
b3 = −8
b4 = 8
Wildfire Susceptibility Index
0.0
0.2
0.4
0.6
0.8
1.0
0
50
100
150
Years since fire

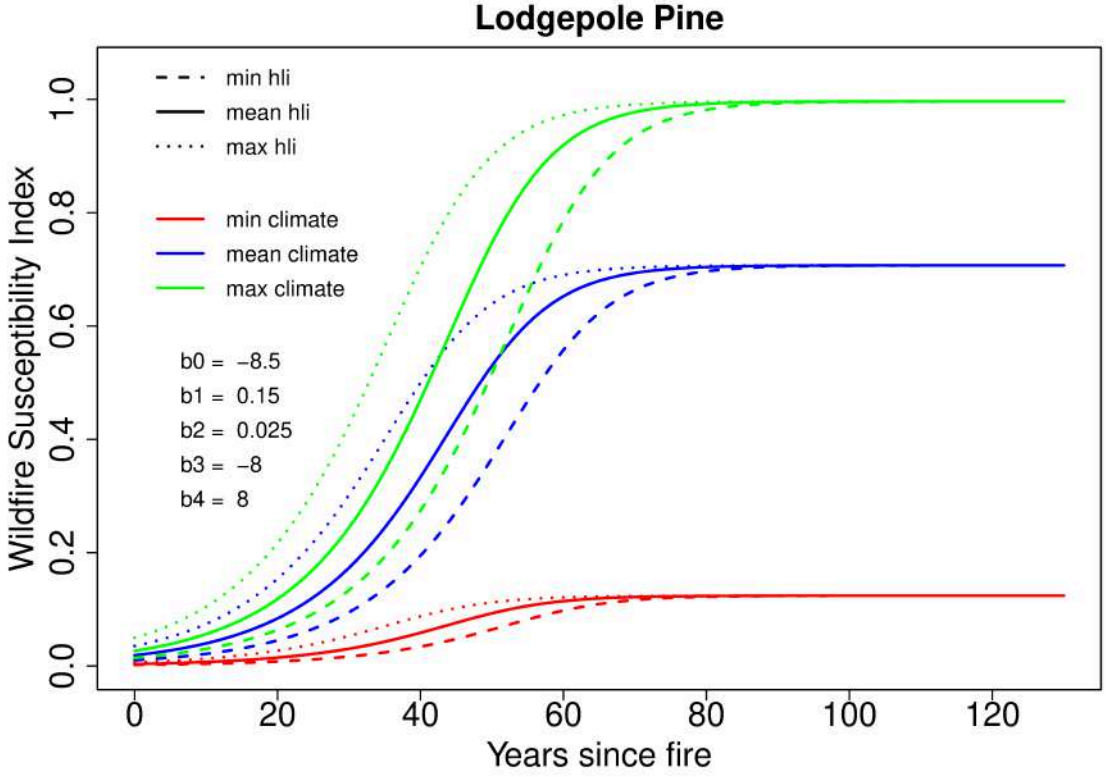
Lodgepole Pine
min hli
mean hli
max hli
min climate
mean climate
max climate
b0 = −8.5
b1 = 0.15
b2 = 0.025
b3 = −8
b4 = 8
Wildfire Susceptibility Index
0.0
0.2
0.4
0.6
0.8
1.0
0
20
40
60
80
100
120
Years since fire

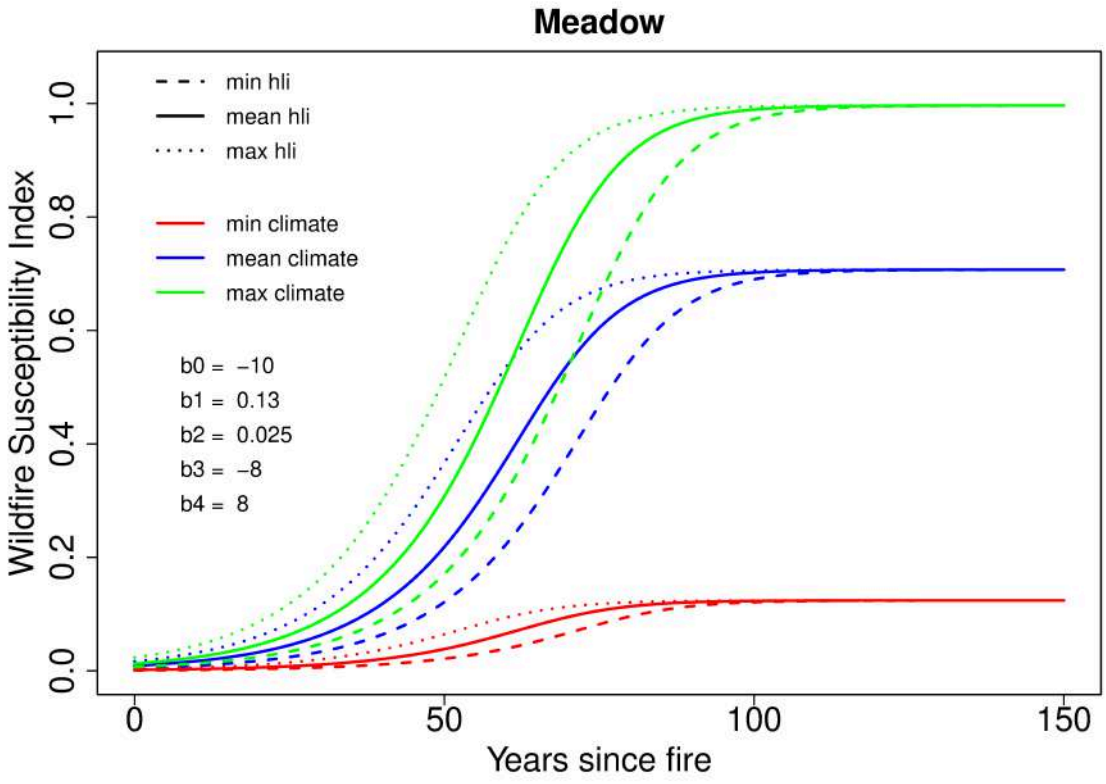
Meadow
min hli
mean hli
max hli
min climate
mean climate
max climate
b0 = −10
b1 = 0.13
b2 = 0.025
b3 = −8
b4 = 8
Wildfire Susceptibility Index
0.0
0.2
0.4
0.6
0.8
1.0
0
50
100
150
Years since fire

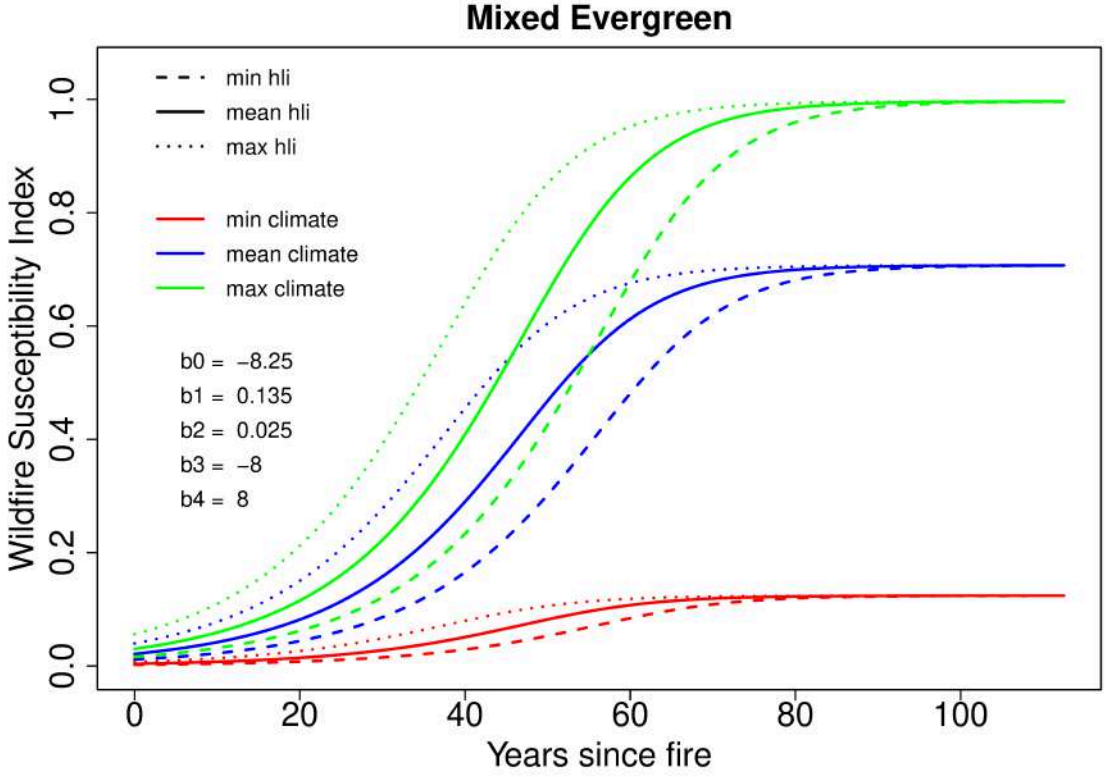
Mixed Evergreen
min hli
mean hli
max hli
min climate
mean climate
max climate
b0 = −8.25
b1 = 0.135
b2 = 0.025
b3 = −8
b4 = 8
Wildfire Susceptibility Index
0.0
0.2
0.4
0.6
0.8
1.0
0
20
40
60
80
100
Years since fire

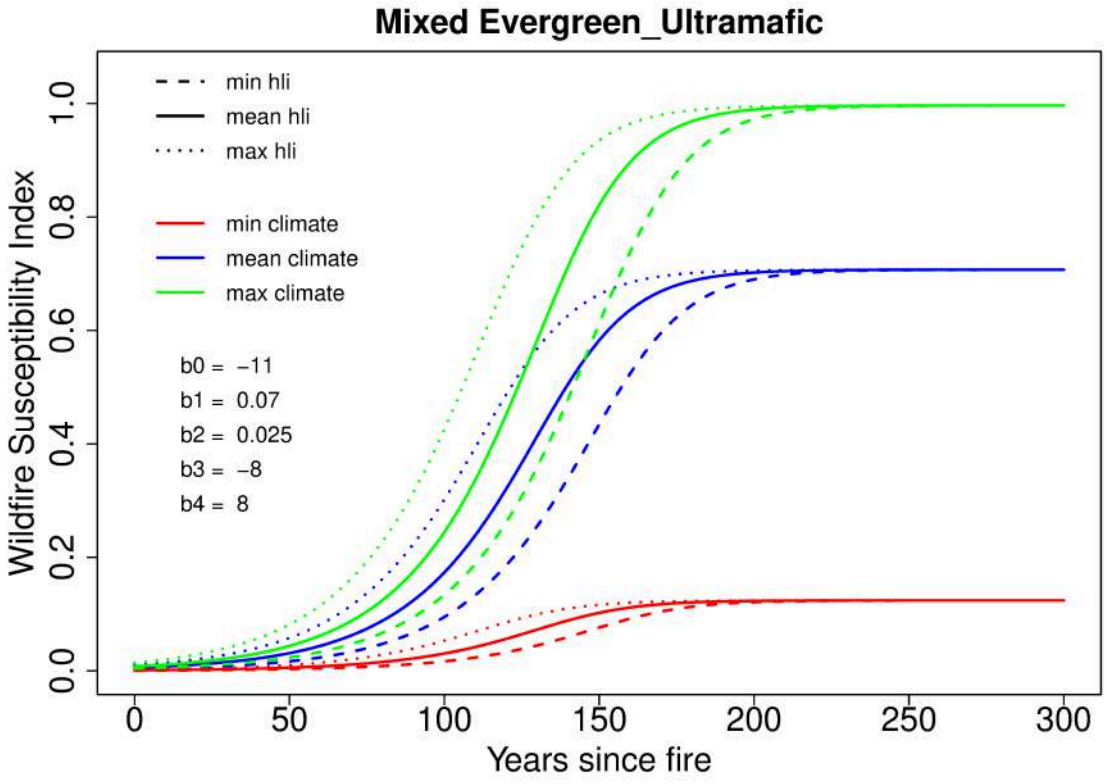
Mixed Evergreen_Ultramafic
min hli
mean hli
max hli
min climate
mean climate
max climate
b0 = −11
b1 = 0.07
b2 = 0.025
b3 = −8
b4 = 8
Wildfire Susceptibility Index
0.0
0.2
0.4
0.6
0.8
1.0
0
50
100
150
200
250
300
Years since fire

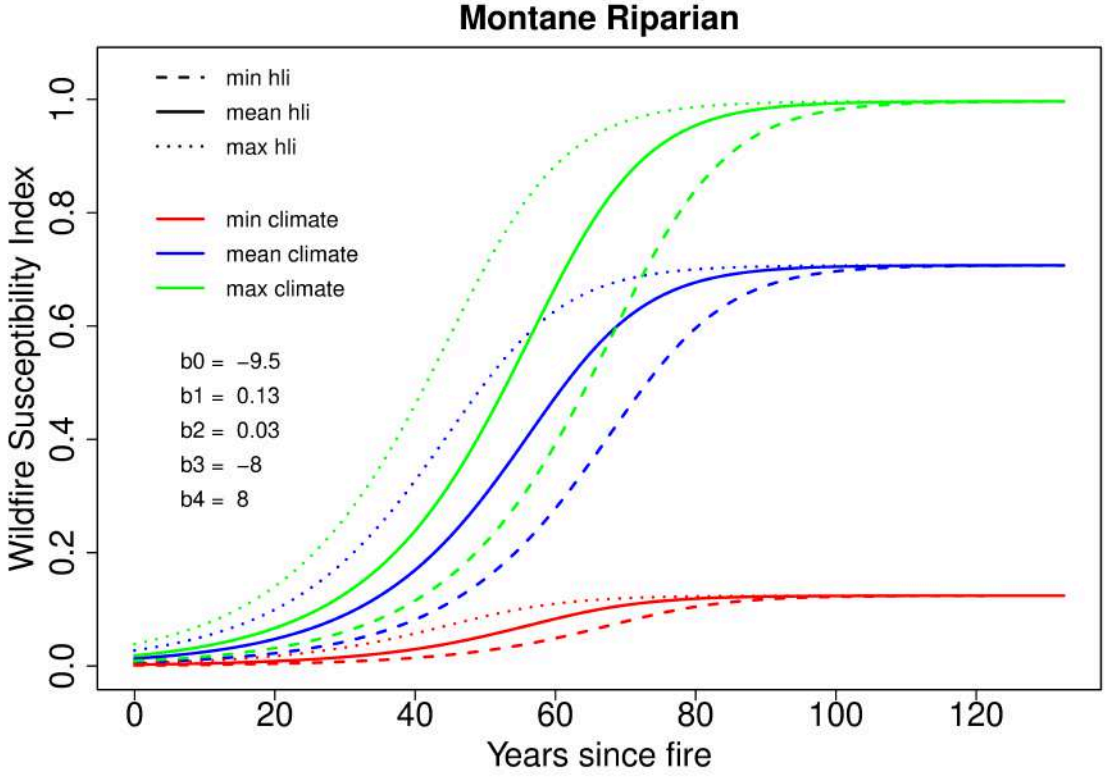
Montane Riparian
min hli
mean hli
max hli
min climate
mean climate
max climate
b0 = −9.5
b1 = 0.13
b2 = 0.03
b3 = −8
b4 = 8
Wildfire Susceptibility Index
0.0
0.2
0.4
0.6
0.8
1.0
0
20
40
60
80
100
120
Years since fire

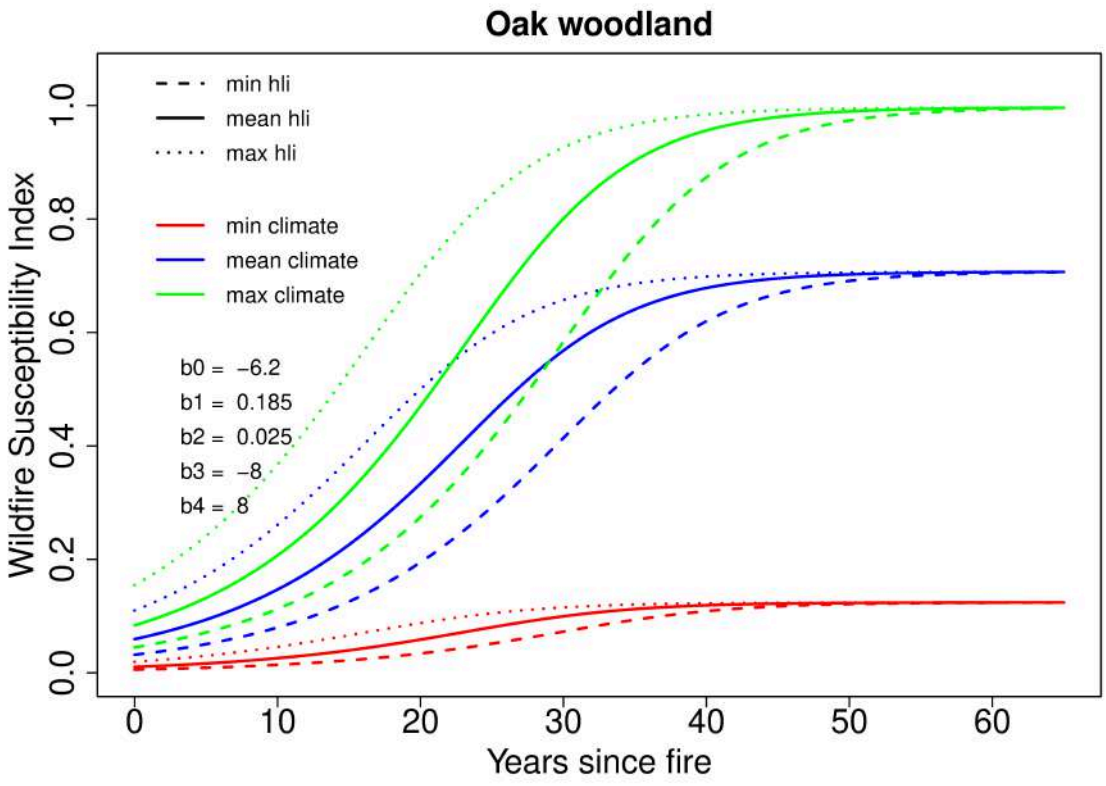
Oak woodland
min hli
mean hli
max hli
min climate
mean climate
max climate
b0 = −6.2
b1 = 0.185
b2 = 0.025
b3 = −8
b4 = .8
Wildfire Susceptibility Index
0.0
0.2
0.4
0.6
0.8
1.0
0
10
20
30
40
50
60
Years since fire

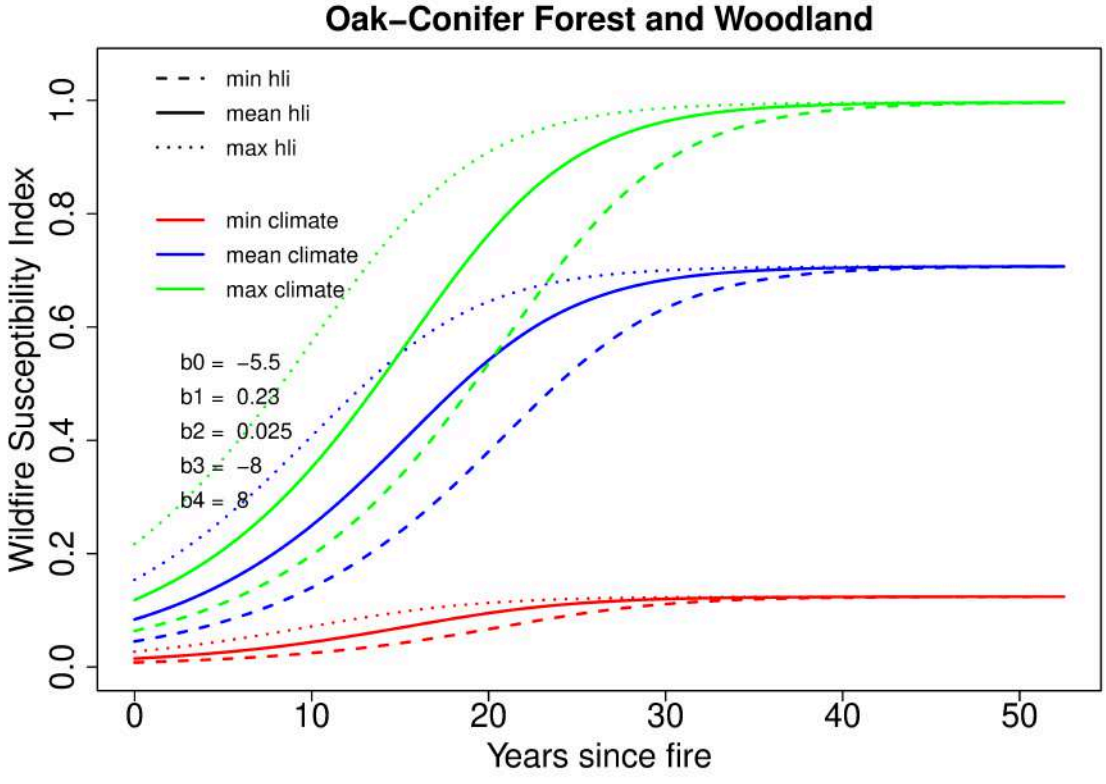
Oak–Conifer Forest and Woodland
min hli
mean hli
max hli
min climate
mean climate
max climate
b0 = −5.5
b1 = 0.23
b2 = 0.025
b3 = −8
b4 = .8
Wildfire Susceptibility Index
0.0
0.2
0.4
0.6
0.8
1.0
0
10
20
30
40
50
Years since fire

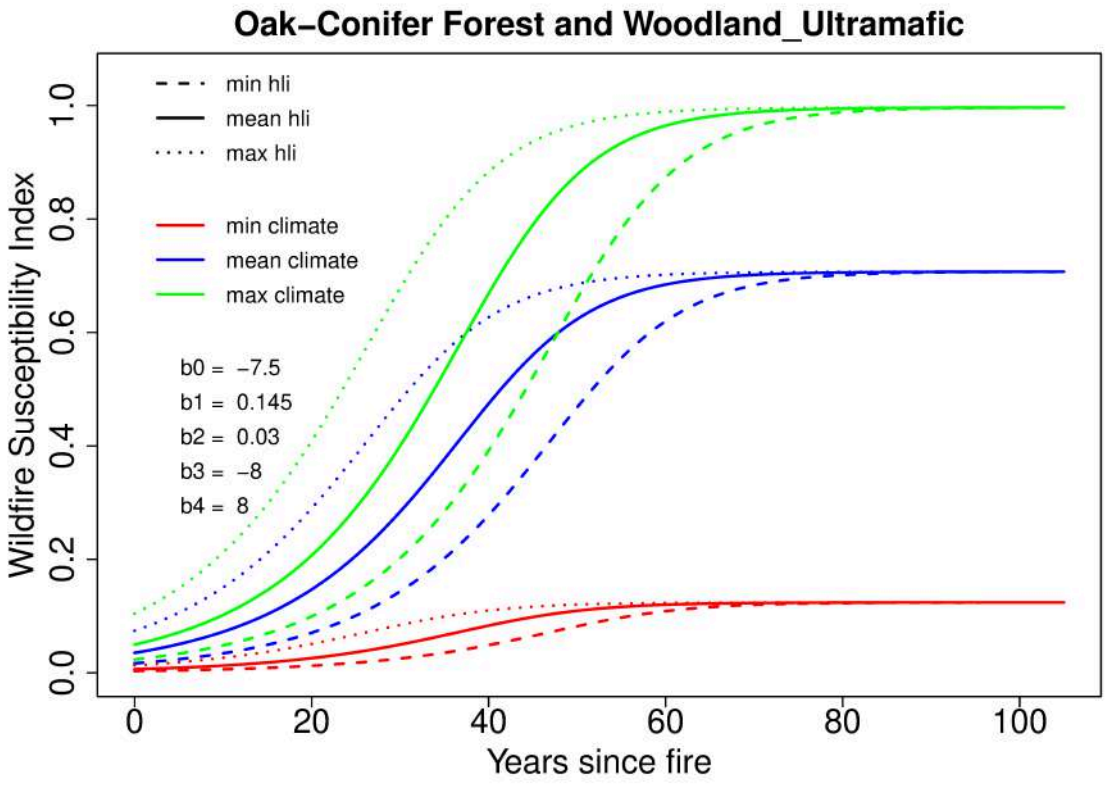
Oak–Conifer Forest and Woodland_Ultramafic
min hli
mean hli
max hli
min climate
mean climate
max climate
b0 = −7.5
b1 = 0.145
b2 = 0.03
b3 = −8
b4 = 8
Wildfire Susceptibility Index
0.0
0.2
0.4
0.6
0.8
1.0
0
20
40
60
80
100
Years since fire

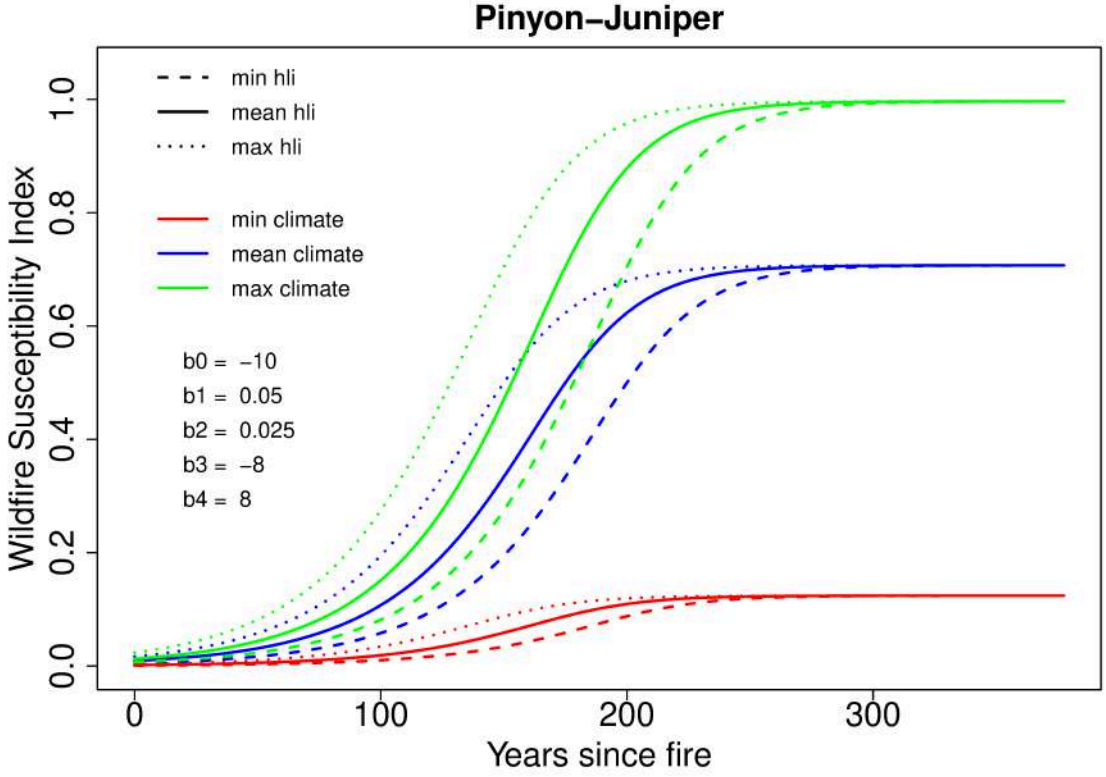
Pinyon–Juniper
min hli
mean hli
max hli
min climate
mean climate
max climate
b0 = −10
b1 = 0.05
b2 = 0.025
b3 = −8
b4 = 8
Wildfire Susceptibility Index
0.0
0.2
0.4
0.6
0.8
1.0
0
100
200
300
Years since fire

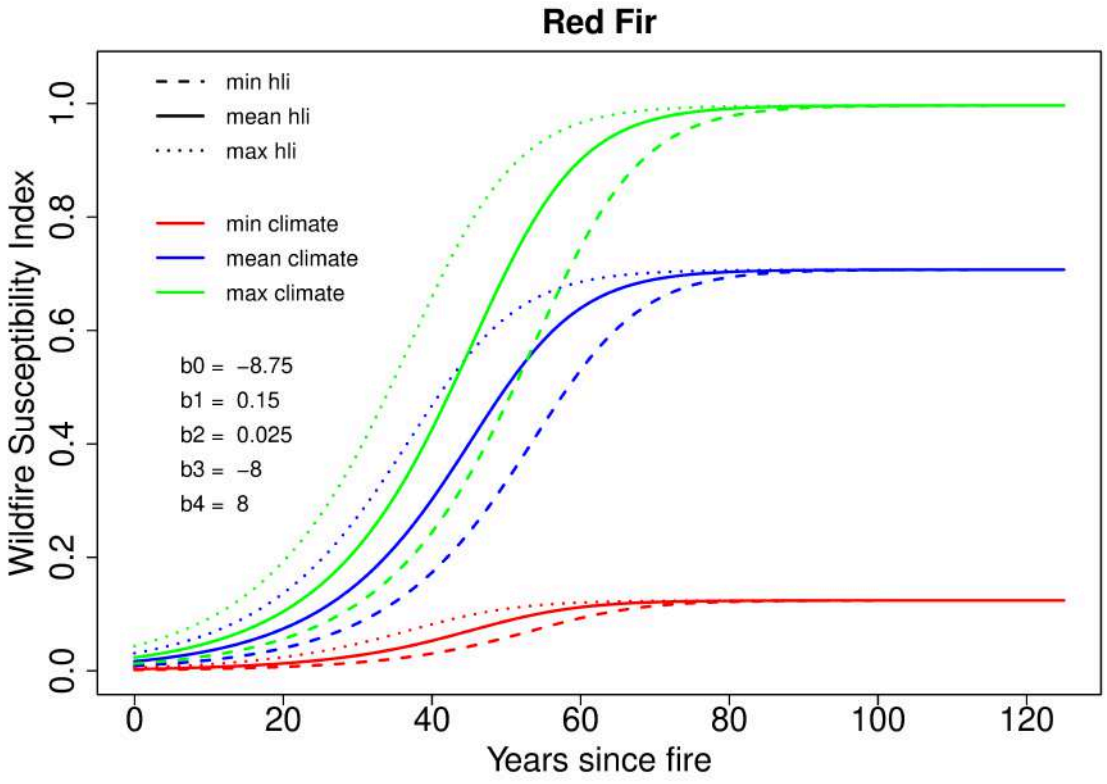
Red Fir
min hli
mean hli
max hli
min climate
mean climate
max climate
b0 = −8.75
b1 = 0.15
b2 = 0.025
b3 = −8
b4 = 8
Wildfire Susceptibility Index
0.0
0.2
0.4
0.6
0.8
1.0
0
20
40
60
80
100
120
Years since fire

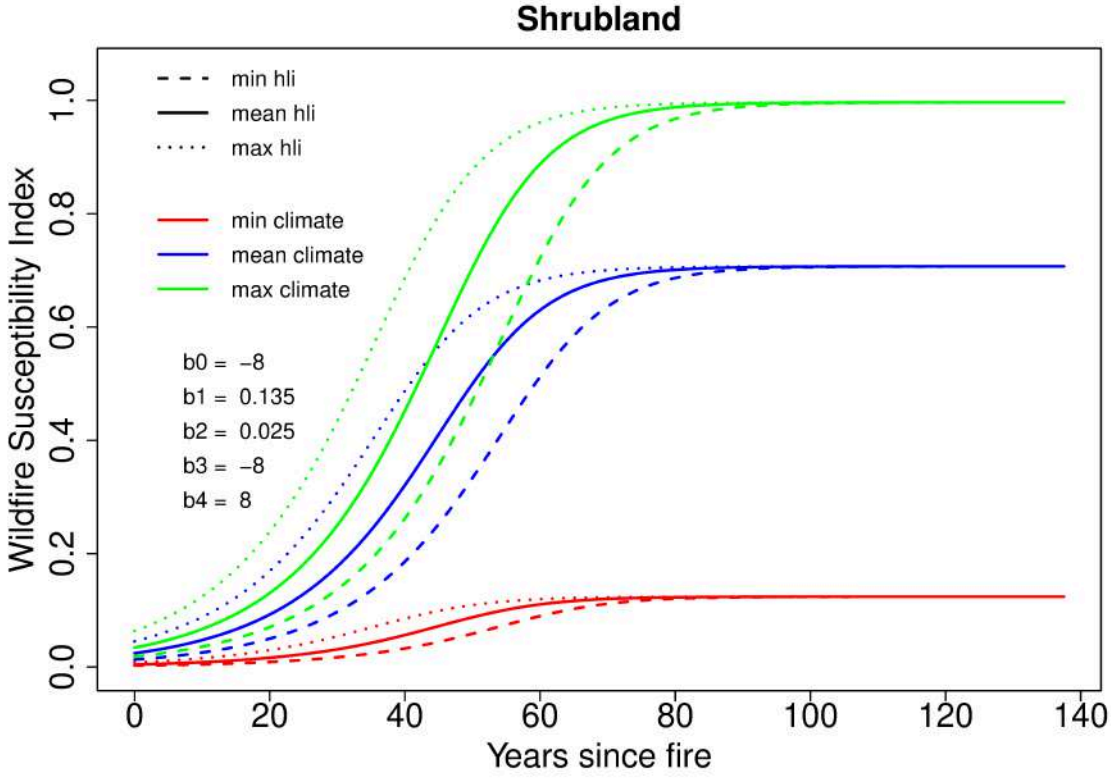
Shrubland
min hli
mean hli
max hli
min climate
mean climate
max climate
b0 = −8
b1 = 0.135
b2 = 0.025
b3 = −8
b4 = 8
Wildfire Susceptibility Index
0.0
0.2
0.4
0.6
0.8
1.0
0
20
40
60
80
100
120
140
Years since fire

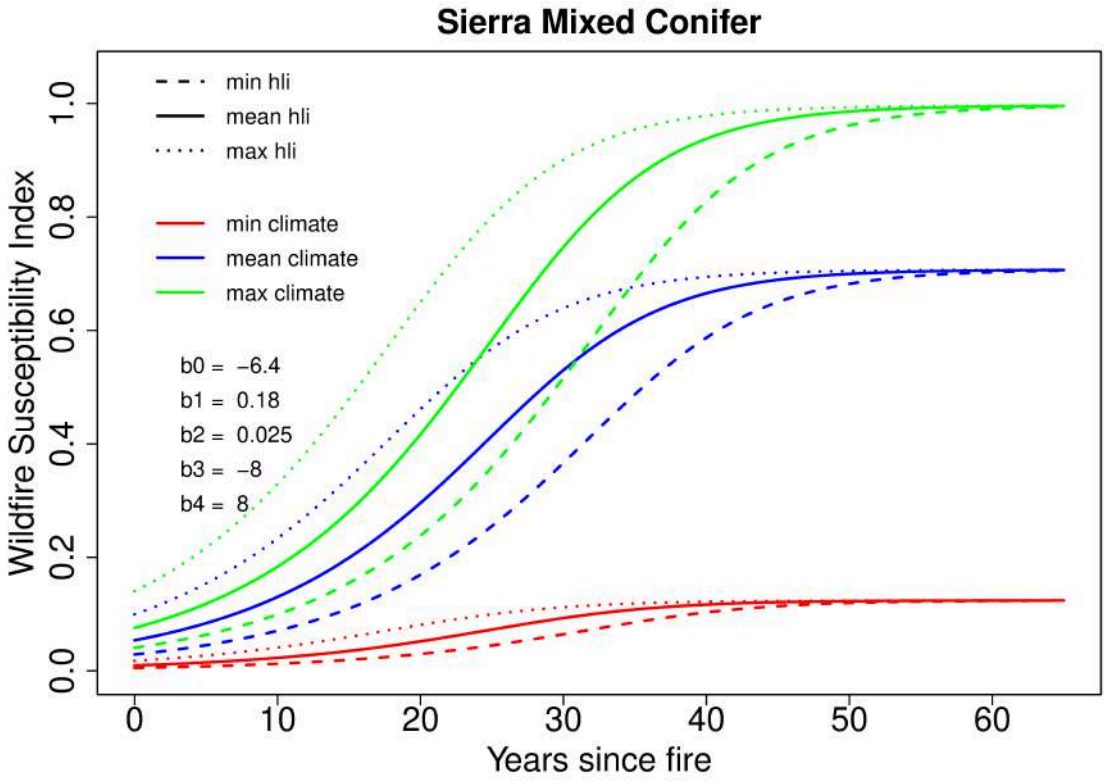
Sierra Mixed Conifer
min hli
mean hli
max hli
min climate
mean climate
max climate
b0 = −6.4
b1 = 0.18
b2 = 0.025
b3 = −8
b4 = 8
Wildfire Susceptibility Index
0.0
0.2
0.4
0.6
0.8
1.0
0
10
20
30
40
50
60
Years since fire

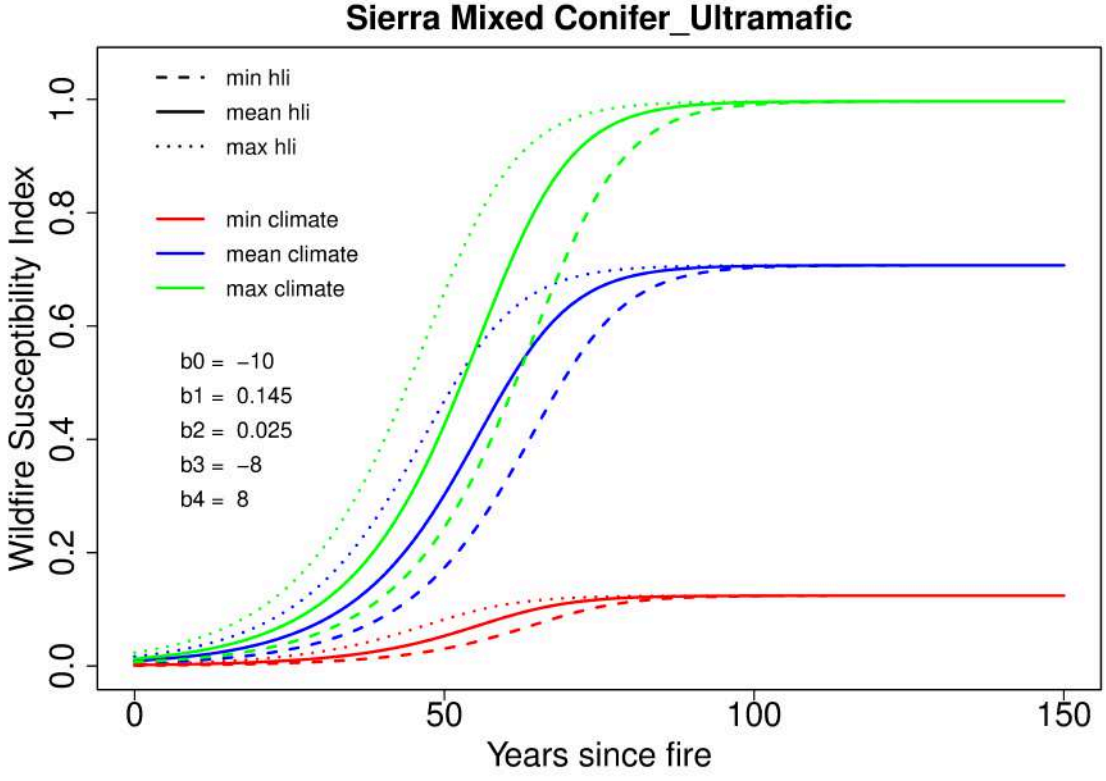
Sierra Mixed Conifer_Ultramafic
min hli
mean hli
max hli
min climate
mean climate
max climate
b0 = −10
b1 = 0.145
b2 = 0.025
b3 = −8
b4 = 8
Wildfire Susceptibility Index
0.0
0.2
0.4
0.6
0.8
1.0
0
50
100
150
Years since fire

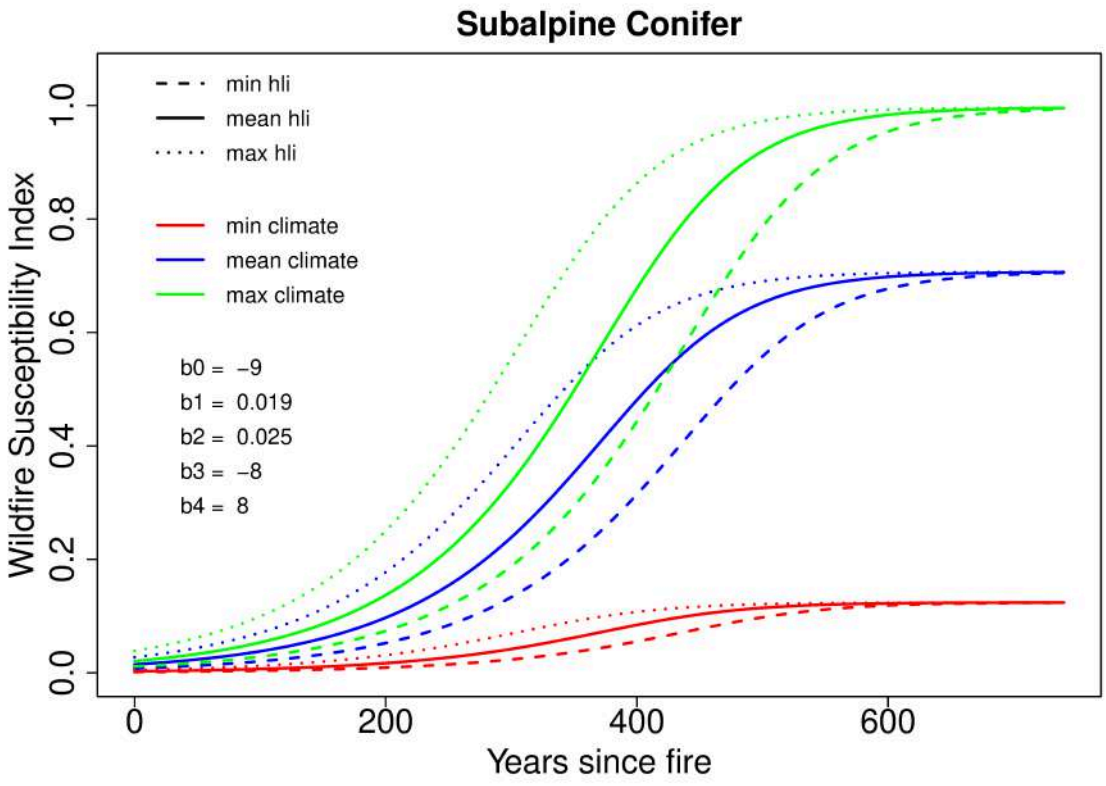
Subalpine Conifer
min hli
mean hli
max hli
min climate
mean climate
max climate
b0 = −9
b1 = 0.019
b2 = 0.025
b3 = −8
b4 = 8
Wildfire Susceptibility Index
0.0
0.2
0.4
0.6
0.8
1.0
0
200
400
600
Years since fire

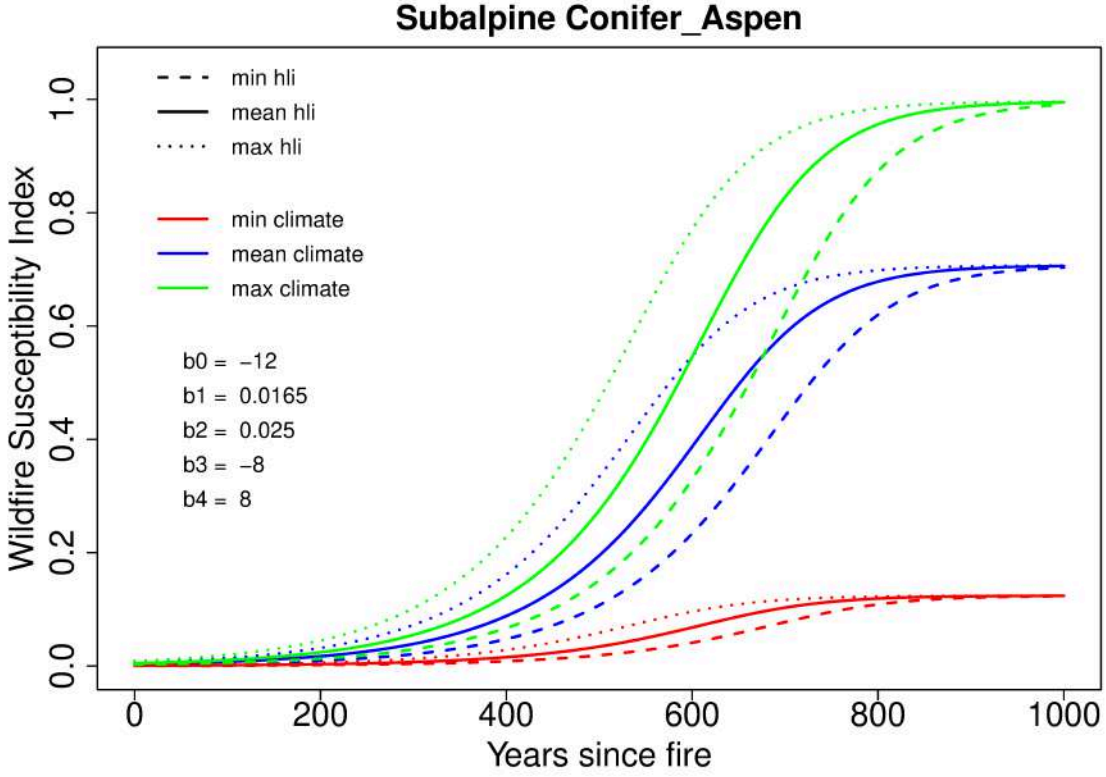
Subalpine Conifer_Aspen
min hli
mean hli
max hli
min climate
mean climate
max climate
b0 = −12
b1 = 0.0165
b2 = 0.025
b3 = −8
b4 = 8
Wildfire Susceptibility Index
0.0
0.2
0.4
0.6
0.8
1.0
0
200
400
600
800
1000
Years since fire

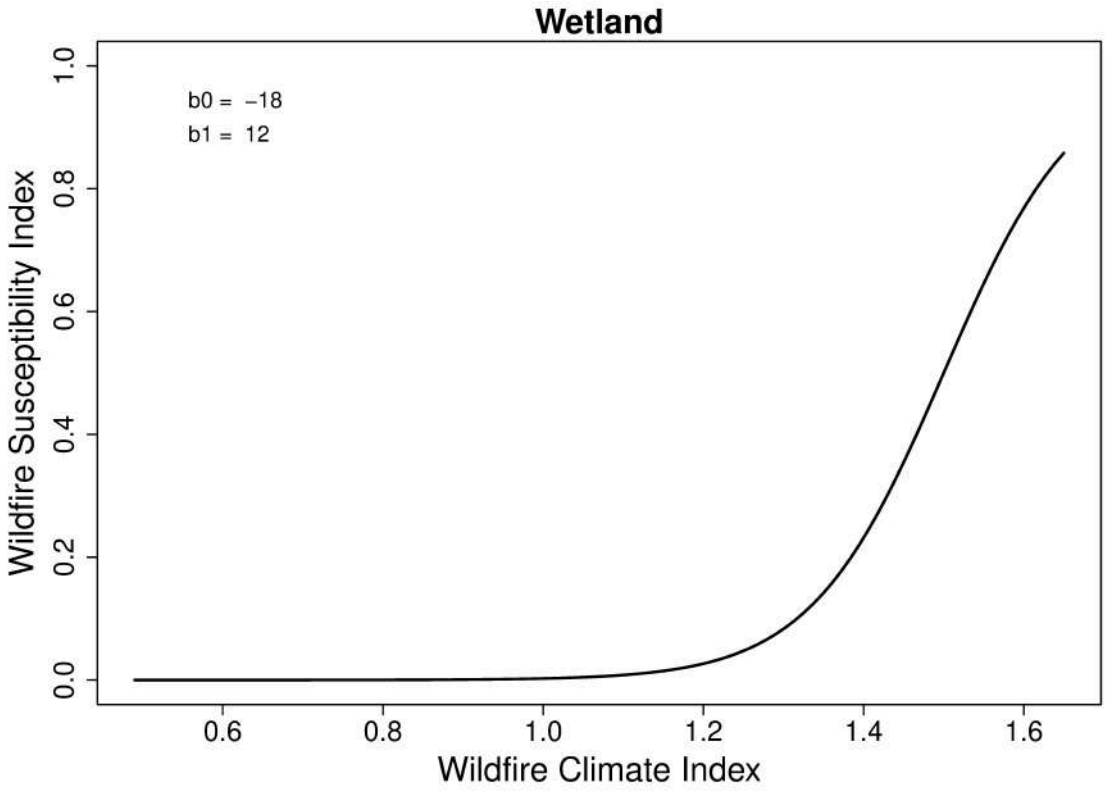
Wetland
b0 = −18
b1 = 12
Wildfire Susceptibility Index
0.0
0.2
0.4
0.6
0.8
1.0
0.6
0.8
1.0
1.2
1.4
1.6
Wildfire Climate Index

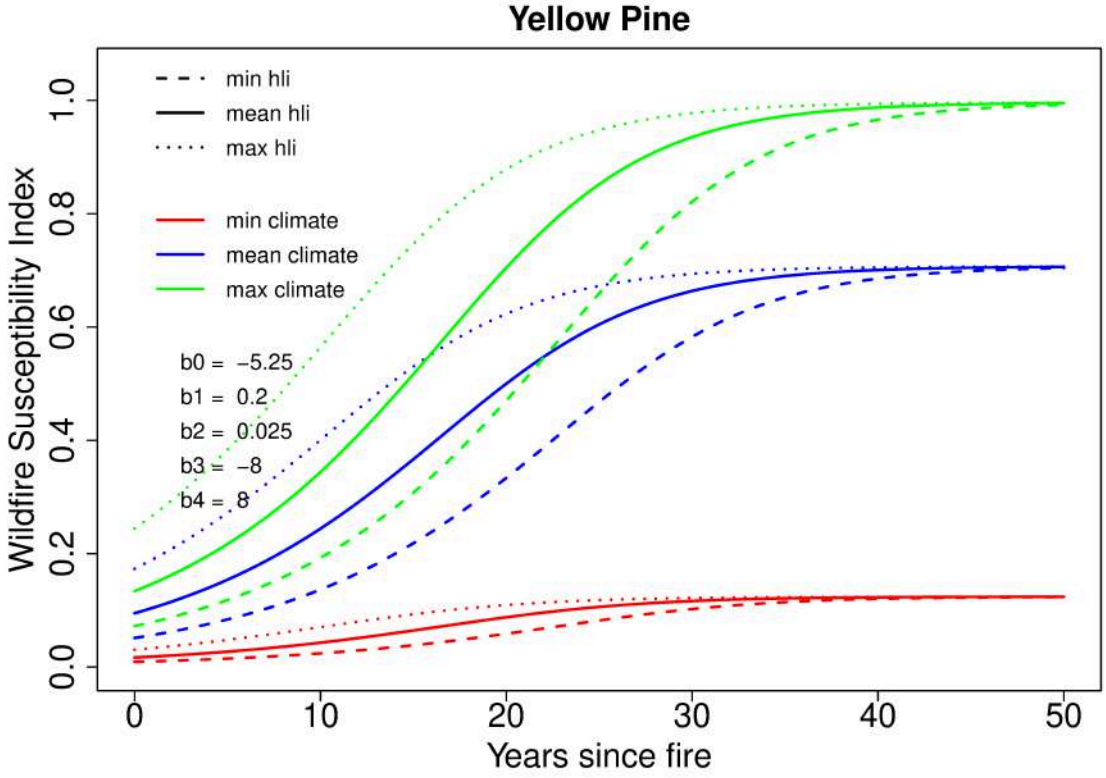
Yellow Pine
min hli
mean hli
max hli
min climate
mean climate
max climate
b0 = −5.25
b1 = 0.2
b2 = 0.025
b3 = −8
b4 = 8
Wildfire Susceptibility Index
0.0
0.2
0.4
0.6
0.8
1.0
0
10
20
30
40
50
Years since fire

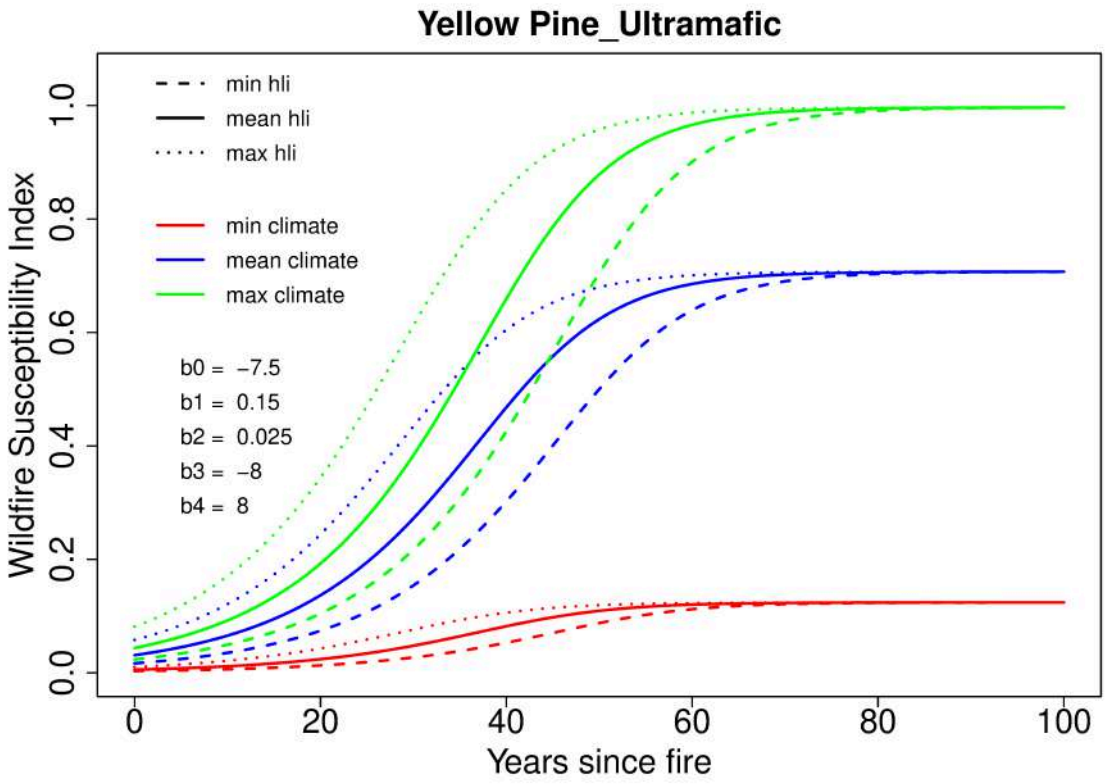
Yellow Pine_Ultramafic
min hli
mean hli
max hli
min climate
mean climate
max climate
b0 = −7.5
b1 = 0.15
b2 = 0.025
b3 = −8
b4 = 8
Wildfire Susceptibility Index
0.0
0.2
0.4
0.6
0.8
1.0
0
20
40
60
80
100
Years since fire

APPENDIX E2 - Wildfire Mortality

As described in the GTR, wildfire mortality (i.e., the probability of high mortality or death of the overstory vegetation in each 5 m cell that burned) was determined by a complex function involving two major factors: 1) fire intensity, which was a Logistic function of the fuel loads in the neighborhood of the focal cell (proxied by the age of the vegetation and time since the last fire), the topographic position of the focal cell, and the climate conditions in the current time step; and 2) the resistance of the focal cell, which was a negative exponential function of the age of the vegetation in the focal cell in which the rate of exponential decline with age decreased with increasing fire intensity (see main text for details). The complex wildfire mortality function included 6 user-specified beta coefficients. As described in the main text, b_0 - b_4 were held constant across all cover types. We varied b_5 and b_6 among cover types to reflect differences in reported historical mean fire return intervals and high mortality rates among cover types. Specifically, we varied these two beta coefficients during model calibration to either increase or decrease the rate of exponential decline in high mortality with increasing vegetation age as a function of fire intensity to achieve the target percentage of high mortality rate in each cover type.

The figures below depict the final wildfire mortality response functions for each cover type in alphabetical order. Cover types not shown either were not eligible to burn (e.g., water, barren) or were always assigned a high mortality response after burning (e.g., grassland, meadow). The response functions depict the probability of high mortality wildfire as a negative exponential function of vegetation Age (yrs) and fire intensity (as indexed). The dashed, solid and dotted lines depict the response functions for the minimum, mean and maximum Fire Intensity Index. Universally, the probability of high mortality decreased with increasing vegetation Age, but the rate of exponential decline decreased (i.e.,shallower slope) with increasing fire intensity, such that for any given Age the probability of high mortality increased with increasing fire intensity.

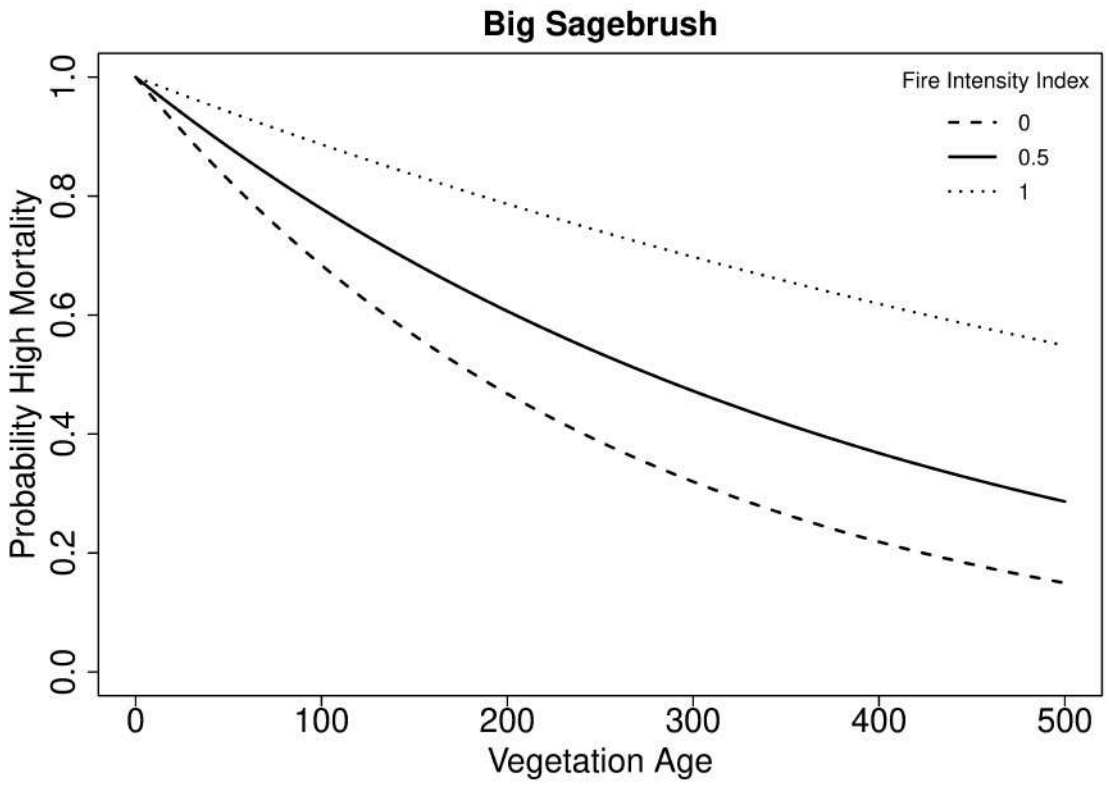

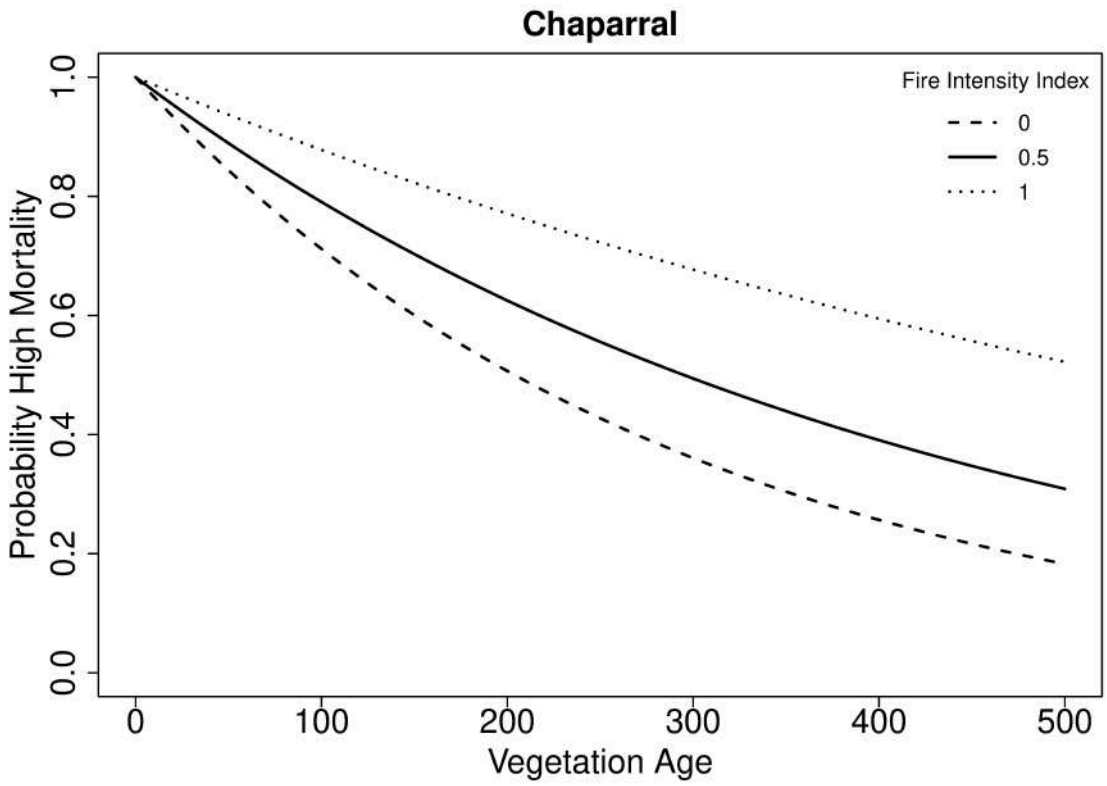
Chaparral
Fire Intensity Index
0
0.5
1
Probability High Mortality
0.0
0.2
0.4
0.6
0.8
1.0
0
100
200
300
400
500
Vegetation Age

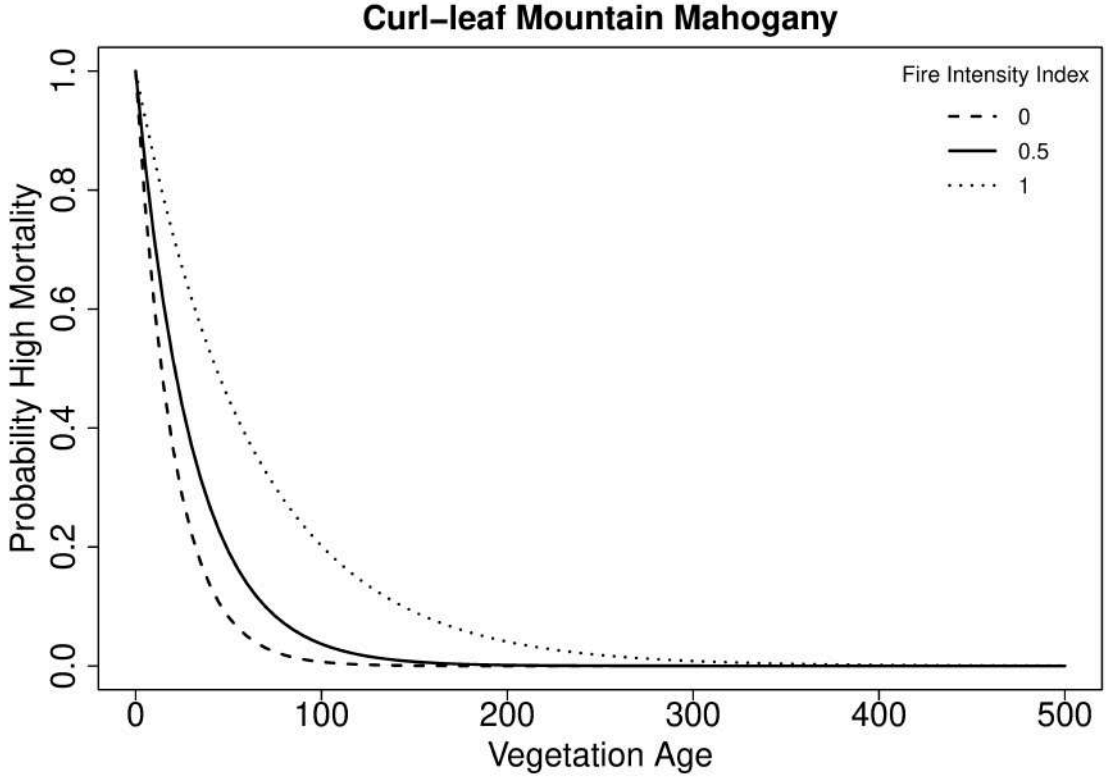
Curl−leaf Mountain Mahogany
Fire Intensity Index
0
0.5
1
Probability High Mortality
0.0
0.2
0.4
0.6
0.8
1.0
0
100
200
300
400
500
Vegetation Age

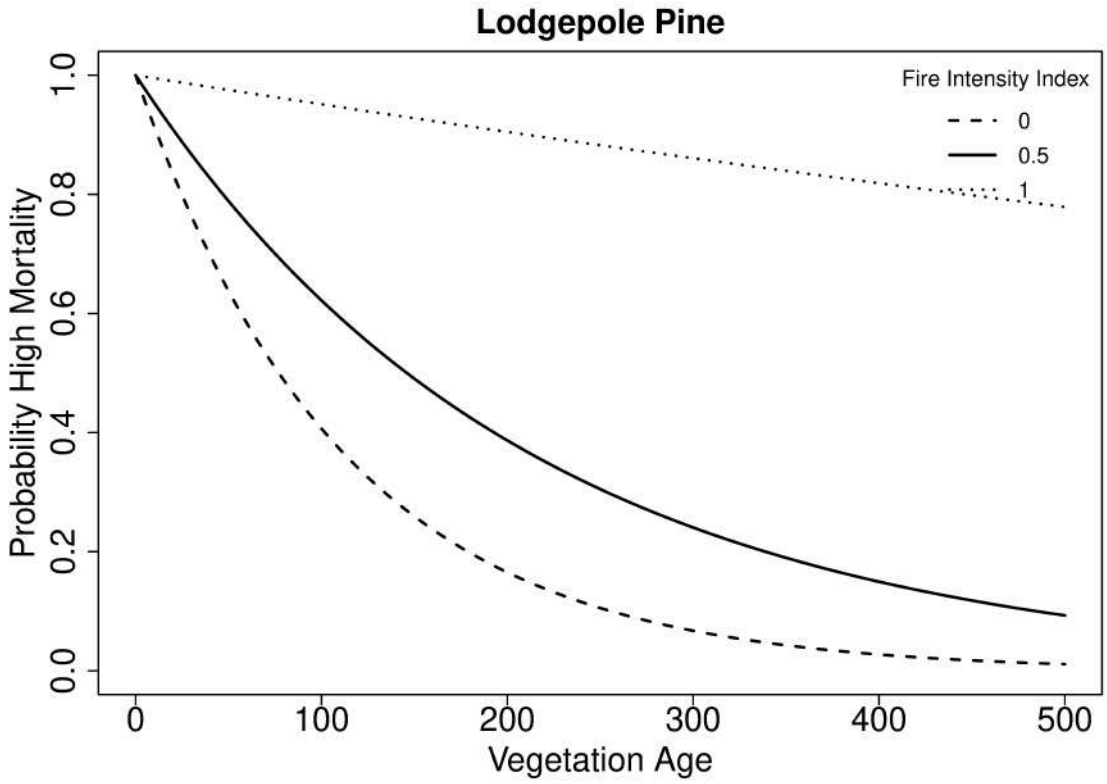
Lodgepole Pine
Fire Intensity Index
0
0.5
1
Probability High Mortality
0.0
0.2
0.4
0.6
0.8
1.0
0
100
200
300
400
500
Vegetation Age

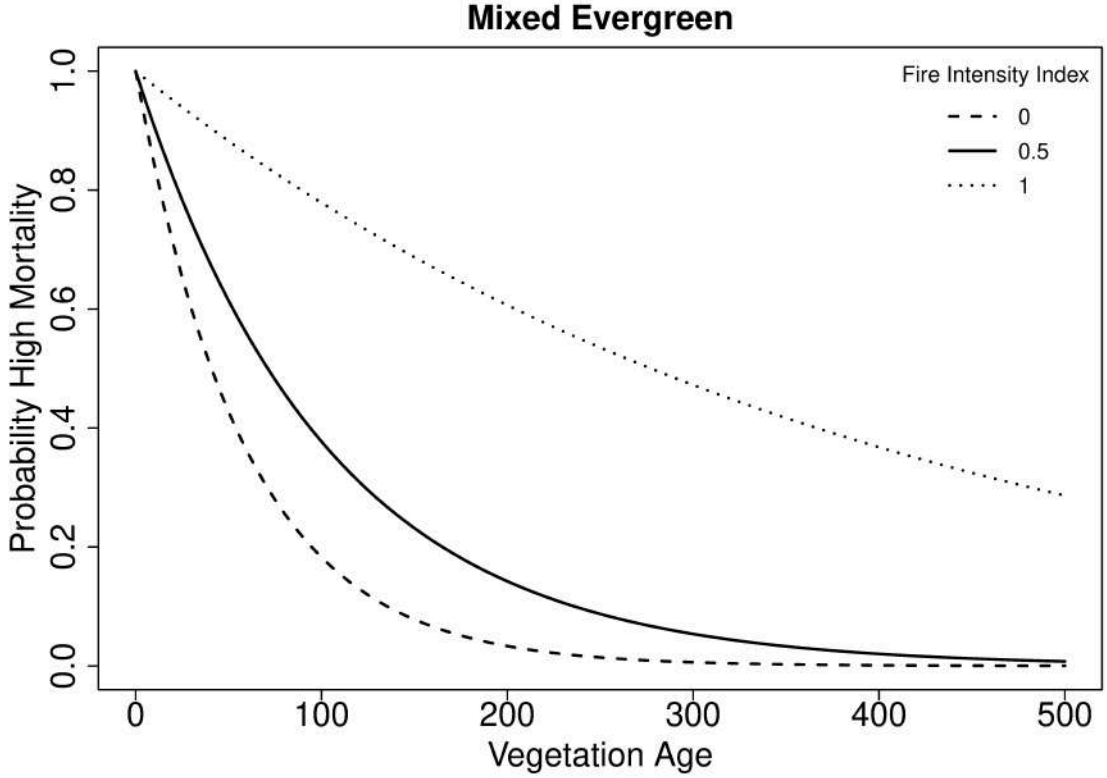
Mixed Evergreen
Fire Intensity Index
0
0.5
1
Probability High Mortality
0.0
0.2
0.4
0.6
0.8
1.0
0
100
200
300
400
500
Vegetation Age

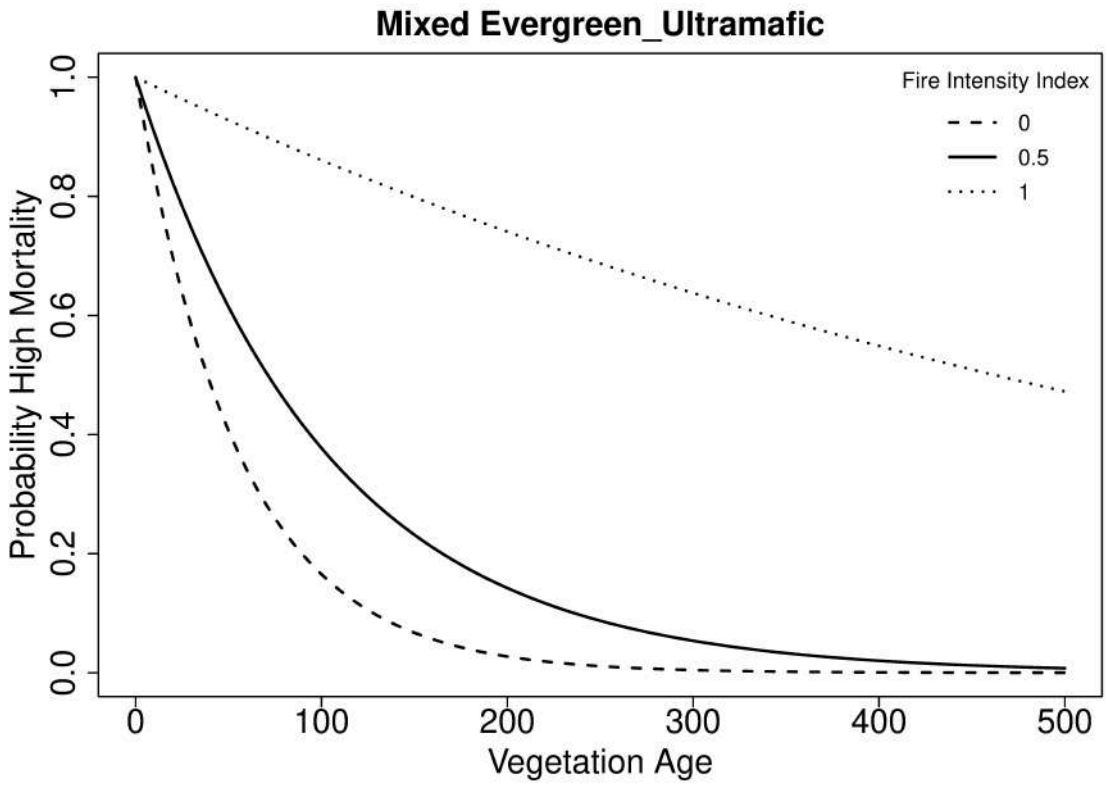
Mixed Evergreen_Ultramafic
Fire Intensity Index
0
0.5
1
Probability High Mortality
0.0
0.2
0.4
0.6
0.8
1.0
0
100
200
300
400
500
Vegetation Age

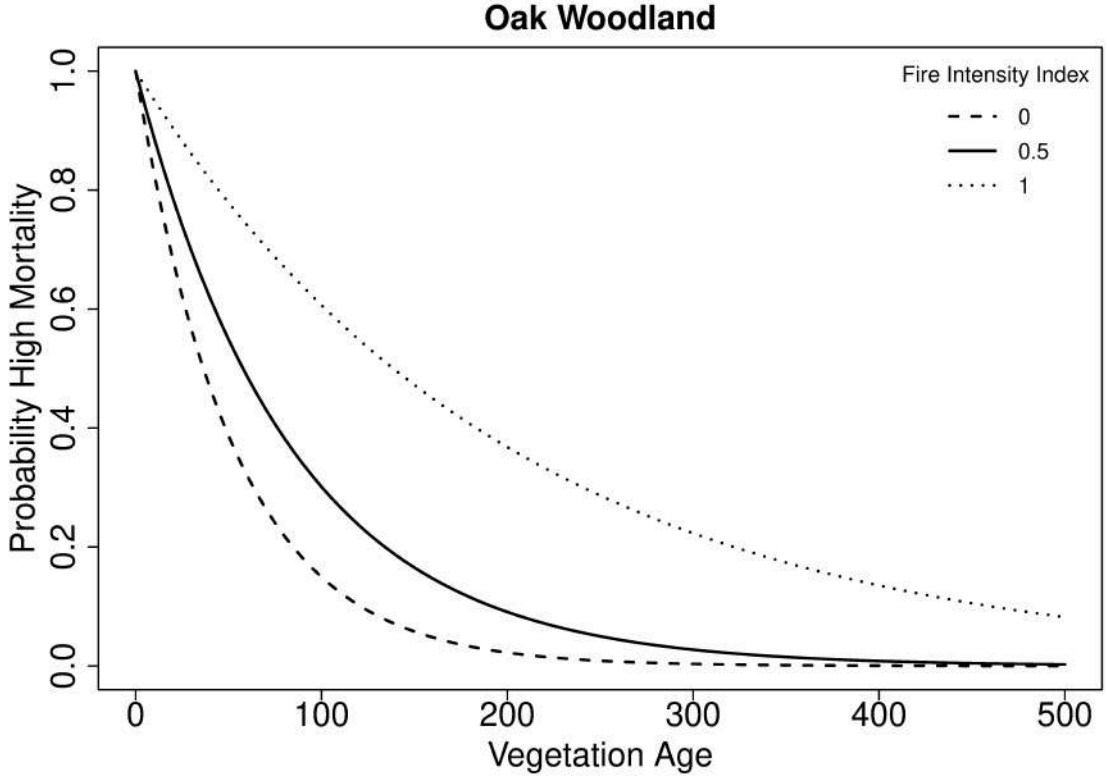
Oak Woodland
Fire Intensity Index
0
0.5
1
Probability High Mortality
0.0
0.2
0.4
0.6
0.8
1.0
0
100
200
300
400
500
Vegetation Age

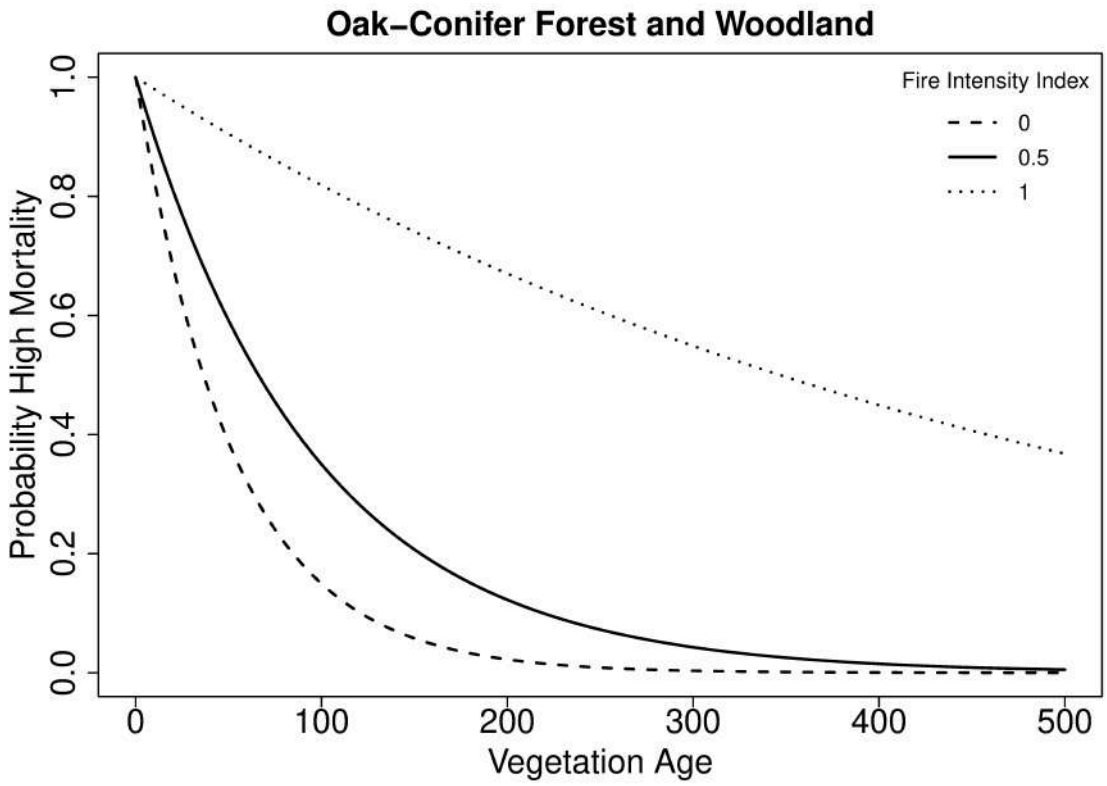
Oak–Conifer Forest and Woodland
Fire Intensity Index
0
0.5
1
Probability High Mortality
0.0
0.2
0.4
0.6
0.8
1.0
0
100
200
300
400
500
Vegetation Age

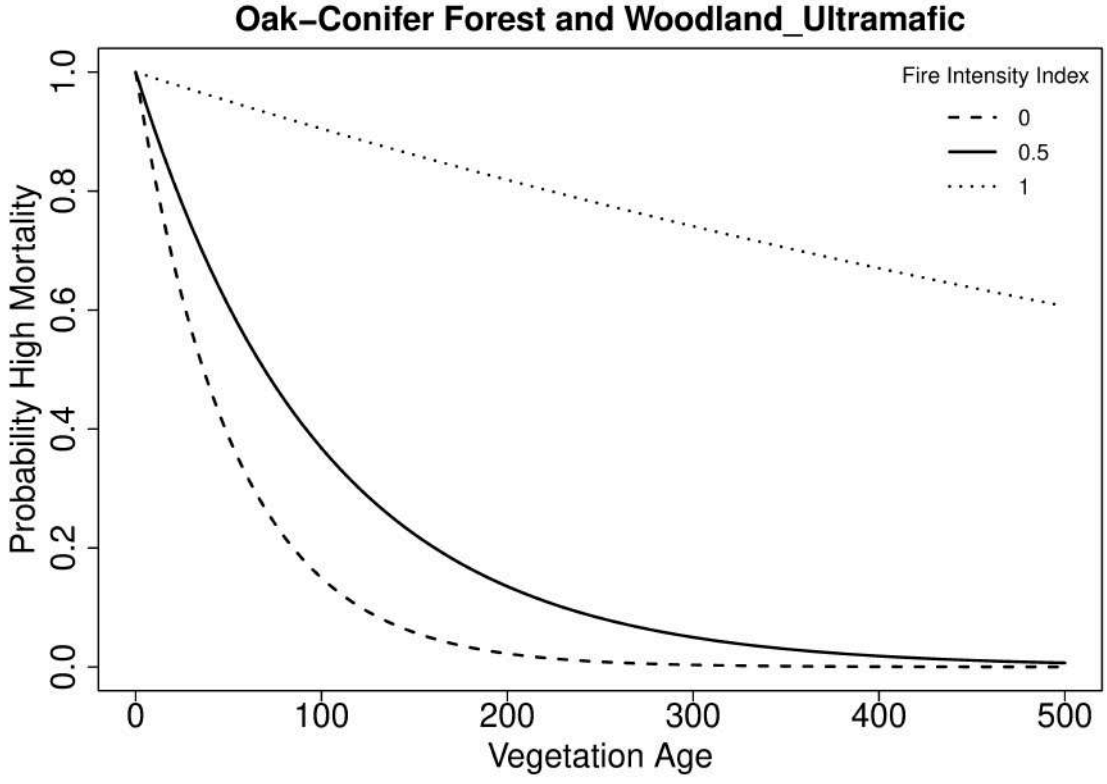
Oak–Conifer Forest and Woodland_Ultramafic
Fire Intensity Index
0
0.5
1
Probability High Mortality
0.0
0.2
0.4
0.6
0.8
1.0
0
100
200
300
400
500
Vegetation Age

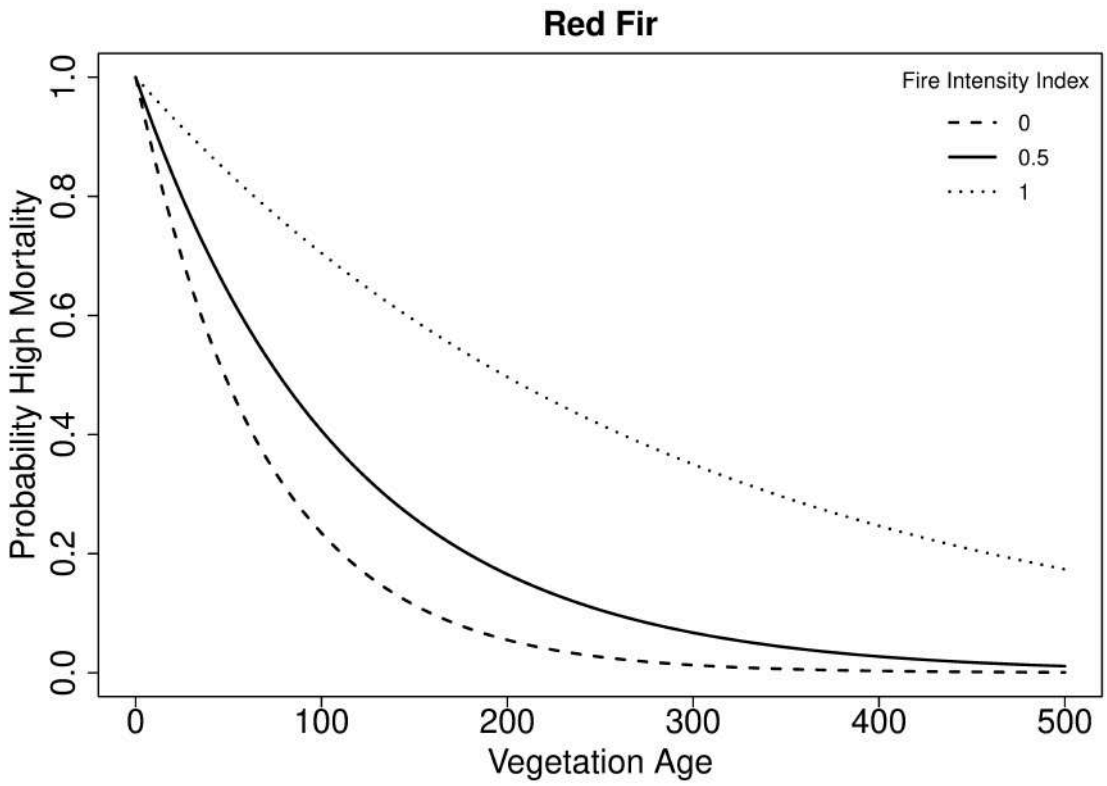
Red Fir
Fire Intensity Index
0
0.5
1
Probability High Mortality
0.0
0.2
0.4
0.6
0.8
1.0
0
100
200
300
400
500
Vegetation Age

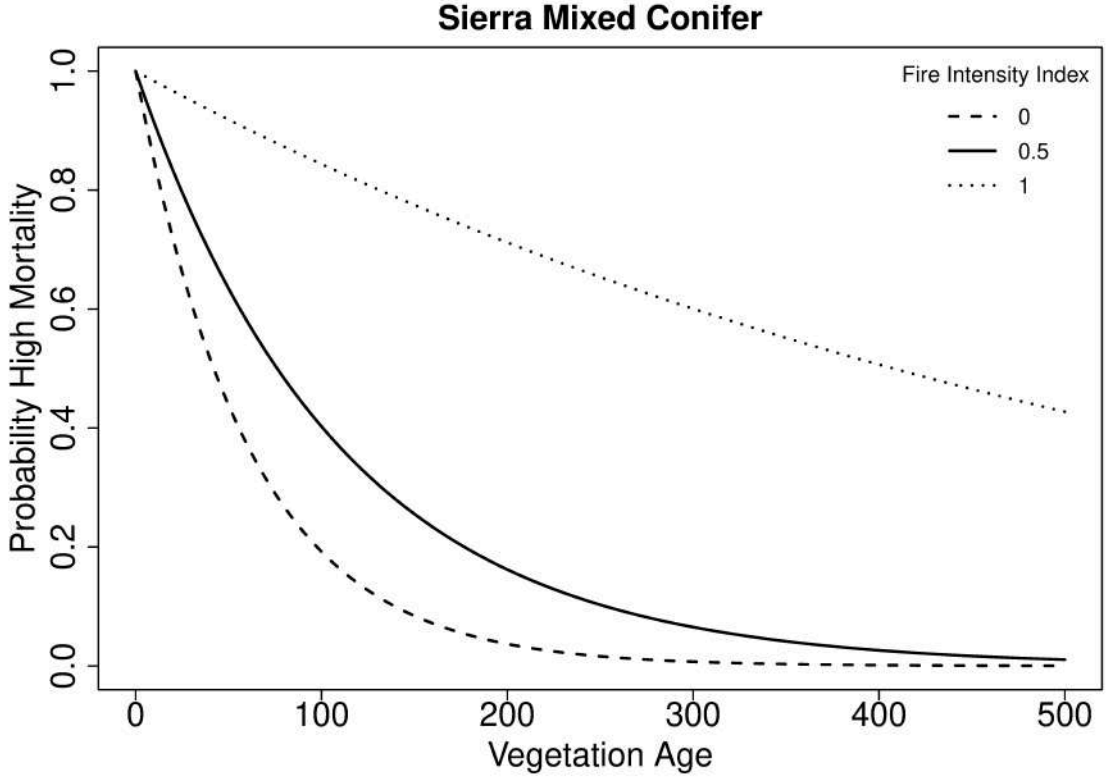
Sierra Mixed Conifer
Fire Intensity Index
0
0.5
1
Probability High Mortality
0.0
0.2
0.4
0.6
0.8
1.0
0
100
200
300
400
500
Vegetation Age

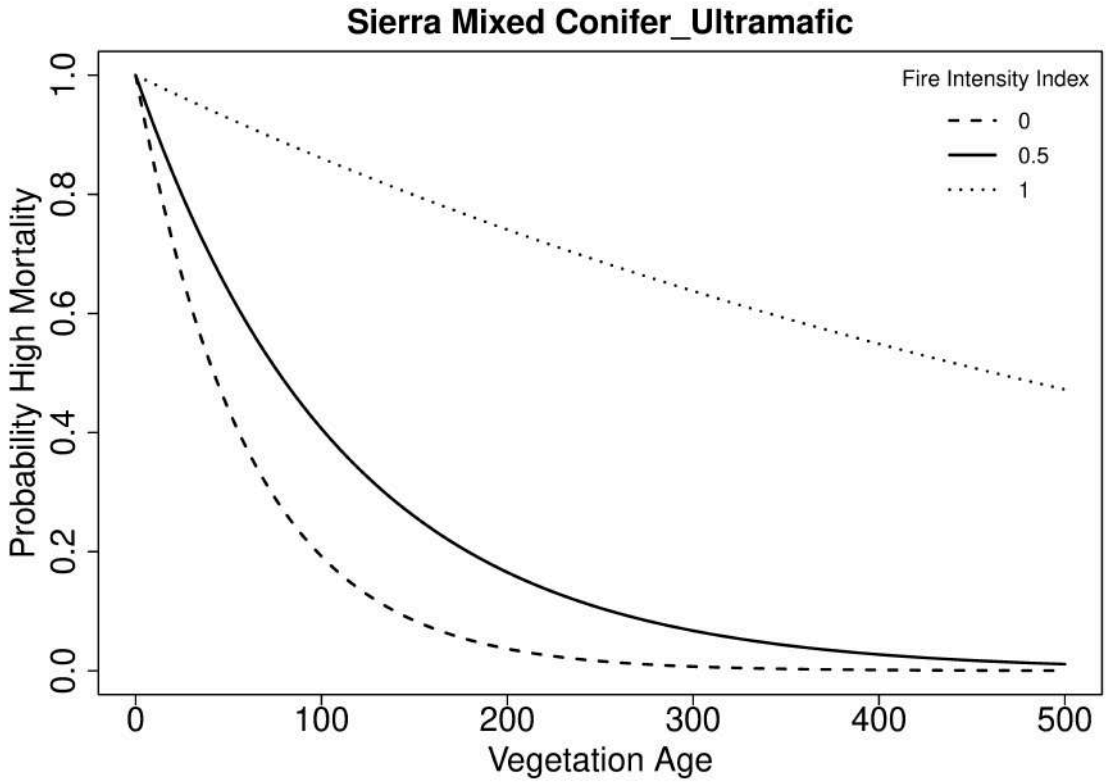
Sierra Mixed Conifer_Ultramafic
Fire Intensity Index
0
0.5
1
Probability High Mortality
0.0
0.2
0.4
0.6
0.8
1.0
0
100
200
300
400
500
Vegetation Age

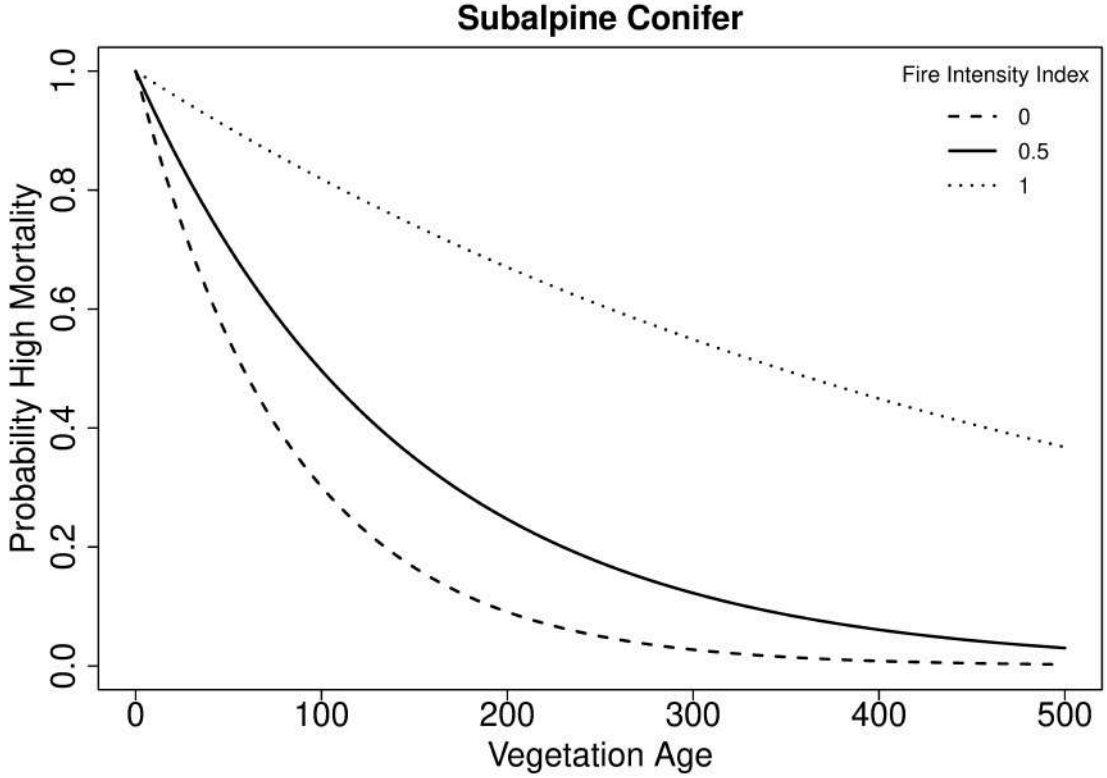
Subalpine Conifer
Fire Intensity Index
0
0.5
1
Probability High Mortality
0.0
0.2
0.4
0.6
0.8
1.0
0
100
200
300
400
500
Vegetation Age

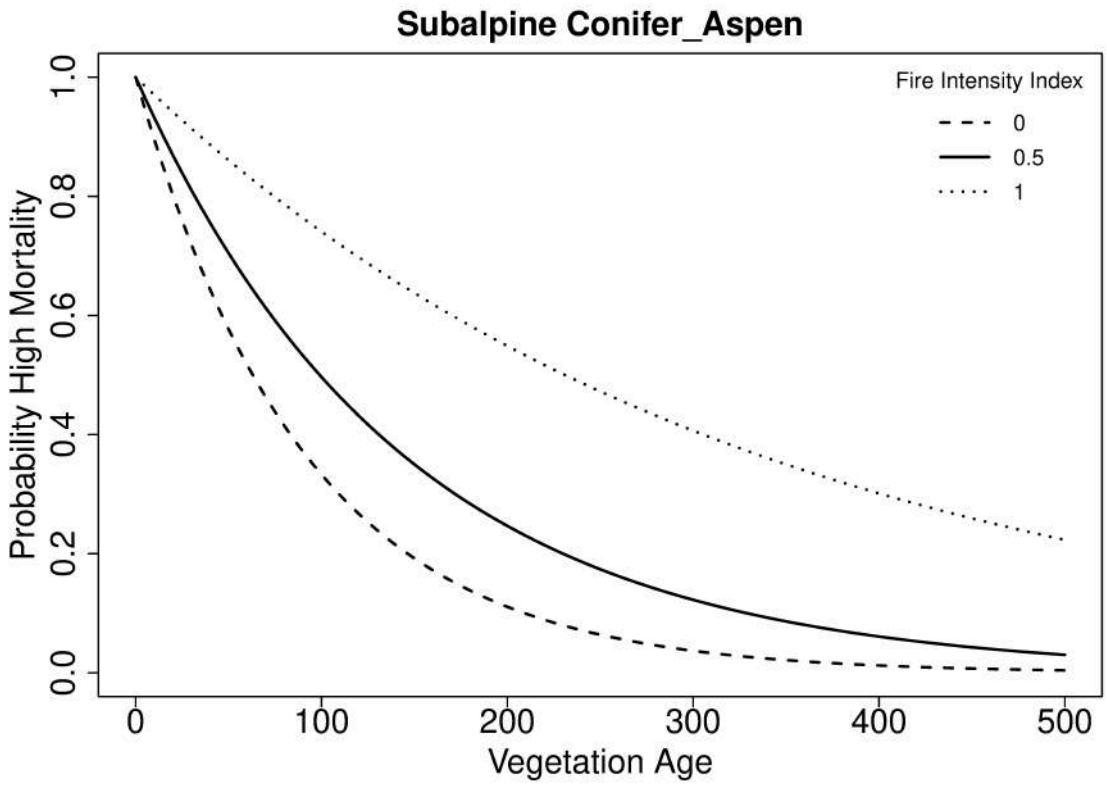
Subalpine Conifer_Aspen
Fire Intensity Index
0
0.5
1
Probability High Mortality
0.0
0.2
0.4
0.6
0.8
1.0
0
100
200
300
400
500
Vegetation Age

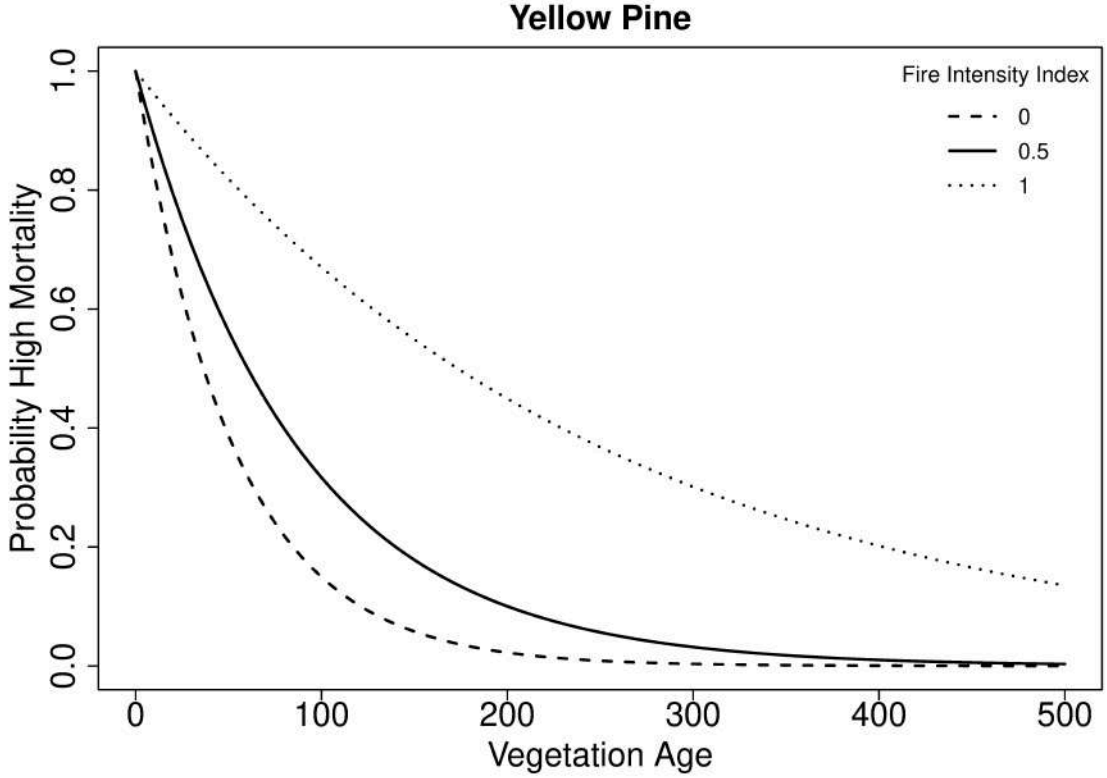
Yellow Pine
Fire Intensity Index
0
0.5
1
Probability High Mortality
0.0
0.2
0.4
0.6
0.8
1.0
0
100
200
300
400
500
Vegetation Age

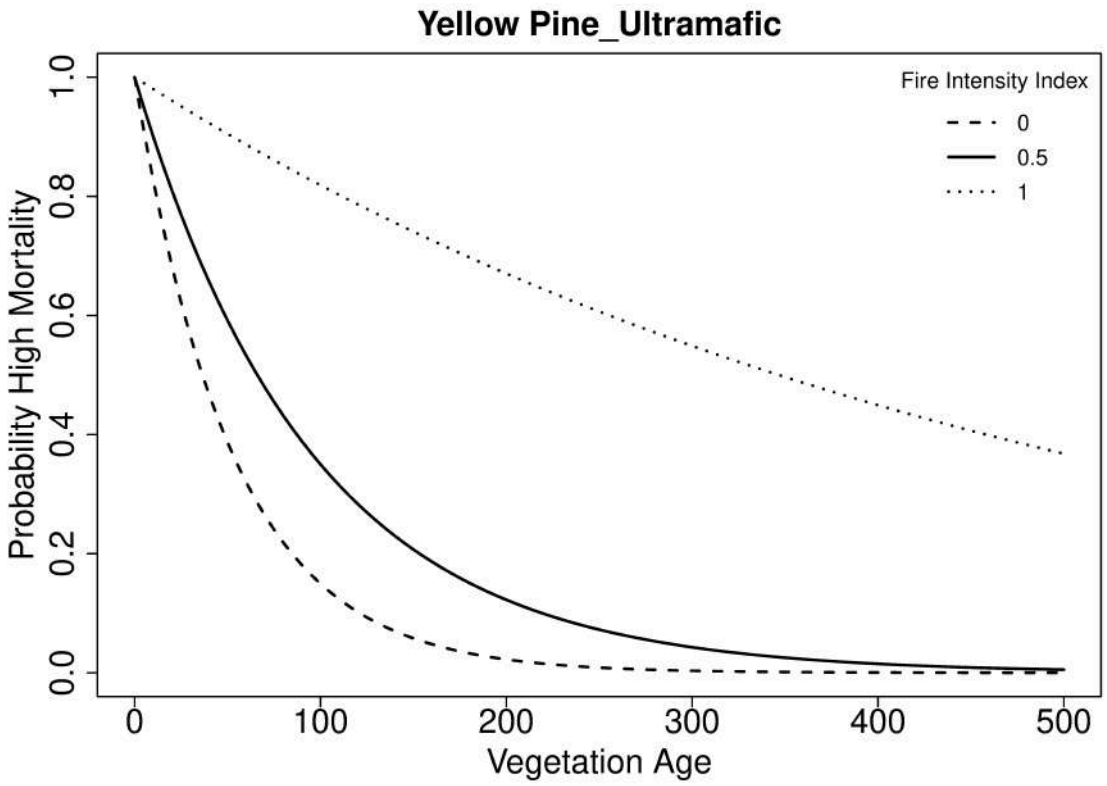
Yellow Pine_Ultramafic
Fire Intensity Index
0
0.5
1
Probability High Mortality
0.0
0.2
0.4
0.6
0.8
1.0
0
100
200
300
400
500
Vegetation Age